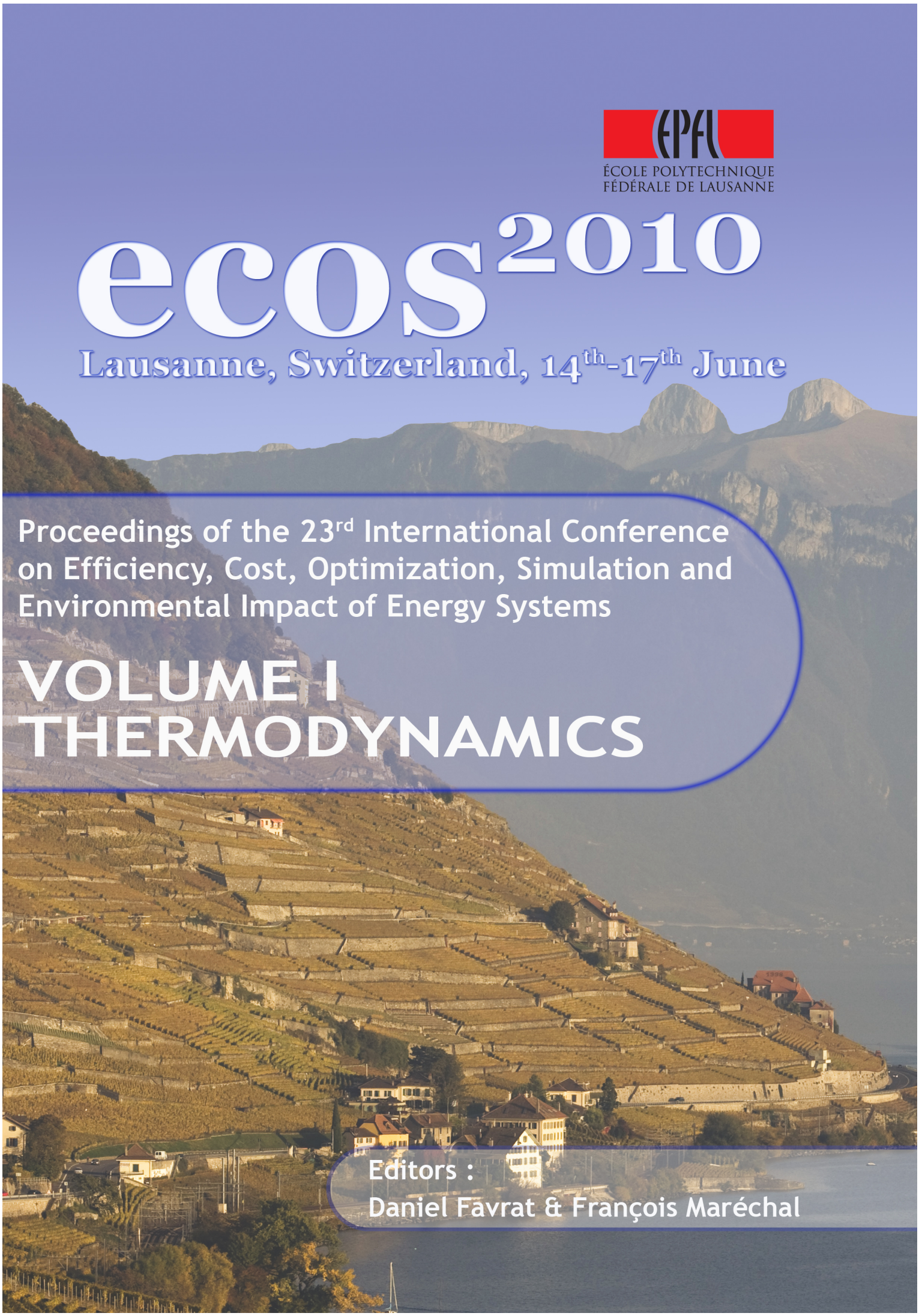
ÉCOLE POLYTECHNIQUE
FÉDÉRALE DE LAUSANNE
ecos2010
Lausanne, Switzerland, 14th-17th June
Proceedings of the 23rd International Conference on Efficiency, Cost, Optimization, Simulation and Environmental Impact of Energy Systems
VOLUME I
THERMODYNAMICS
Editors :
Daniel Favrat & François Maréchal

ecos2010

Proceedings of the 23rd International Conference on
Efficiency, Cost, Optimization, Simulation,
and Environmental Impact of Energy Systems

Lausanne, Switzerland
June 14-17, 2010

Volume I
Thermodynamics

Editors
Daniel Favrat and François Maréchal

Organised by
Laboratoire d'Énergétique Industrielle (LENI)
École Polytechnique Fédérale de Lausanne (EPFL)

Official Website of the conference
www.ecos2010.ch

Corresponding e-mail
ecos2010@epfl.ch

Corresponding address
EPFL / LENI – ISE - STI
Bat. ME A2
Station 9
CH-1015 Lausanne
Switzerland

Book creation
Nicolas BORBOËN, Yannick BRAVO

PREFACE

Energy plays a major role in human societies. The supply of energy services is also a major contributor to the global and, too often, local environmental problems the World is facing. According to the International Energy Agency, actions to target future CO_2 concentrations in atmosphere below either 550ppm, or even below 450ppm, will have to be primarily focused on efficiency. A broader use of renewable, nuclear power and perhaps carbon sequestration will also contribute. To maintain a viable economic development these actions will have to be cost effective while globally reducing all emissions and caring about energy and material resources. A systemic approach is therefore essential to get a holistic vision, design better systems and optimize money and resources utilization.

The ECOS conferences have a long tradition in fostering the key aspects and the scientific knowledge that are essential for the engineers. The organizers of this 23rd edition are proud to acknowledge one of the largest participation ever with many original and high quality papers.

Our thanks go to the authors who accepted to travel from all continents and meet in Lausanne to present and share their scientific contributions. Many thanks also to all reviewers and members of the scientific committee who contributed to the quality of these proceedings. The conference chairmen are also grateful to the local organizing team including in particular, Nicolas Borboën, Stina Zufferey, Brigitte Gabioud, Yannick Bravo, Suzanne Zahnd and Irène Laroche. Many thanks also to the other members of the Industrial Energy Systems Laboratory of EPFL, the MEDIACOM EPFL team and the sponsors who greatly helped the organization of this fruitful event.

Daniel Favrat & François Maréchal

ORGANISING COMMITTEE

Prof. Daniel Favrat (chairman)
François Maréchal (chairman)

Nicolas Borboën, Yannick Bravo, Brigitte Gabioud,
Irène Laroche, Suzanne Zahnd, Stina Zufferey

INTERNATIONAL ADVISORY BOARD

Ozer Arnas, United States
Christos A. Frangopoulos, Greece
George Tsatsaronis, Germany

SCIENTIFIC COMMITTEE

Monika Axel, Sweden
Rangan Banerjee, India
Adrian Bejan, United States
Thore Berntsson, Sweden
Asfaw Beyene, United States
Paolo Bosshard, Italy
Denis Clodic, France
Stephen R. Connors, United States
R.L Cornelissen, Netherlands
Michel Feidt, France
Carl-Johan Fogelholm, Finland
Richard Gaggioli, United States
Yalçın A. Göğüş, Turkey
Gershon Grossman, Israel
Simon Harvey, Sweden
Abel Hernandez-Guerrero, Mexico
Gerard Hirs, Netherlands
Andrew Forbes Alexander Hoadley, Australia
Koichi Ito, Japan
Hervé Jeanmart, Belgium
Signe Kjelstrup, Norway
Jiri Klemes, Hungary
Zygmunt Kolenda, Poland
Andrea Lazzaretto, Italy
Noam Lior, United States
Sylvie Lorente, France
Giampaolo Manfrida, Italy
Philippe Mathieu, Belgium
Alberto Mirandola, Italy
Michael Moran, United States
Zhang Na, China
Silvia Azucena Nebra, Brazil
Eduardo de Oliveira Fernandes, Portugal
Silvio de Oliveira Júnior, Brazil
Ricardo Rivero, Mexico
Marc A. Rosen, Canada
Dominick A. Sama, United States
Peter Schossig, Germany
Enrico Sciubba, Italy
Luis M. Serra, Spain
Samuel Stucki, Switzerland
Pascal Terrien, France
Jules Thibault, Canada
Daniel Tondeur, France
Vittorio Verda, Italy
Laura Vanoli, Italy
Michael R. von Spakovsky, United States
Carl-Jochen Winter, Germany
Li Zheng, China
Andrzej Ziębik, Poland
Ron Zevenhoven, Finland

Entropy Analysis of a TMP and Paper Mill – the Effects of Different Process Solutions and Effective Heat-Absorbing and Heat-Emitting Temperatures

Jaana Federley, Markku Lampinen

Aalto University School of Science and Technology, Department of Energy Technology, Espoo, Finland

Abstract: The purpose of this work was to study the use of entropy analysis for evaluating the energy efficiency of industrial processes. The aim was to estimate the use of entropy analysis as a tool for localizing the processes that have the greatest potential to improve the energy efficiency of the whole mill. Also the influence of the different components and process solutions on the whole mill's entropy generation was investigated. The calculations were done for a simulated pulp and paper mill model that includes a TMP plant and a paper machine. The entropy generation was calculated for different cases with slightly different secondary energy systems and vacuum systems. The method of effective heat-absorbing and heat-emitting temperatures for the system boundaries was applied in the entropy generation calculations. According to the calculations it is possible to discover most of the differences between the two cases. Results show that the main and reject refining processes generate the most entropy and have the biggest power losses (0.9 and 0.3 MWh/t_{paper}). Also the process changes in the vacuum system have a slight effect on the paper machine's entropy generation.

Keywords: Entropy, Paper machine, TMP, Energy efficiency, Process integration.

1. Introduction

Entropy analysis is based on the first and second laws of thermodynamics, and every operation that is not reversible increases the entropy generation of the system. Accordingly, entropy generation is always a positive quantity. It reveals the causes and magnitude of the imperfections in the thermal or chemical process. [1-2]

Bejan [2-4] showed that entropy minimization will improve a system's efficiency. A lot of research has been done on the topic, and entropy analysis has been applied to many fields of research and industry [5-8].

Earlier, there was no unambiguous method to define the heat transfer temperature T when calculating the entropy generation. In many papers [9-11] the temperature T is defined as an ambient temperature. That can cause errors in the results. In this paper the calculations of the entropy generation are based on the effective heat-absorbing and heat-emitting temperatures on the boundary of the system. This theory was first represented by [12]. Reference [13-14] also deals with the definition of the temperature T_0, when calculating the entropy generation or exergy loss.

The operating environment and structure of the Finnish pulp and paper industry are undergoing radical changes. The industry needs to improve its profitability in order to survive in the competitive international marketplace. To achieve a sustainable and effective process, it is crucially important to maximize the thermodynamic efficiency of the processes. Many opportunities for reducing energy usage and greenhouse gas emissions still exist in the paper industry. In [10] entropy analysis was used to examine the efficiency of a Swedish kraft pulp mill's sodium and calcium cycles. Richards and Theliander [10] found that the most entropy was generated in the recovery boiler. In their other study [9], they used entropy analysis to investigate the differences in the thermodynamic efficiency of the kraft pulp mill's three different cooking chemical recovery processes. They discovered small differences between the processes. In [15] entropy generation was calculated for multi-cylinder paper dryer sections and the results were compared for 5 different paper machines. In one paper [16] the

Corresponding Author: Jaana Federley, Email: jaana.federley@tkk.fi

best alternative for producing sodium hydroxide on a kraft pulp mill site was studied by using first and second law analyses. In [17] the entropy production of a Norwegian multi-cylinder paper drying machine was optimised.

The focus of this study was to clarify whether entropy analysis can be used as a tool to investigate energy efficiency and to improve the possibilities of a big industrial process. Also the effects of the different process solutions on the entropy generation were also studied. The processes that use the most energy at a paper mill are already well known, but the effects that the different process solutions or components have on the energy efficiency of the whole mill can be difficult to estimate due to the complexity of the processes. In this problem, entropy analysis can be a practical tool.

2. Theory

Entropy generation is defined by the second law of thermodynamics

$$\delta_{irr} = S(B) - S(A) - \int_{A;\mathcal{P}}^{B} \frac{dQ}{T} \geq 0\,, \tag{1}$$

where S is the entropy of the system and δ_{irr} is the entropy generation term. The path from A to B is taken following the process $\mathcal{P}$. T is the boundary temperature of the system and dQ is the heat flows across the system boundary.

Entropy generation can be calculated from

$$\sigma = \frac{Q_-}{T_-} - \frac{Q_+}{T_+} + \sum_{out} \dot{m} s - \sum_{in} \dot{m} s\,, \tag{2}$$

where Q_+ is the heat absorbed by the system at the effective heat-absorbing temperature T_+ and Q_- is the heat emitted by the system at the effective heat-emitting temperature T_-. [12]

T_+ and T_- are defined as follows [12]

$$\frac{Q_+}{T_+} \equiv \int_{A;\mathcal{P}}^{B} \frac{dQ_+}{T} \tag{3}$$

$$\frac{Q_-}{T_-} \equiv \int_{A;\mathcal{P}}^{B} \frac{dQ_-}{T}\,. \tag{4}$$

In this paper the effective heat-absorbing temperature T_+ and the effective heat-emitting temperature T_- for a defined system are calculated as follows

$$T_+ = \frac{\tau_+^{out} - \tau_+^{in}}{\ln \frac{\tau_+^{out}}{\tau_+^{in}}} \tag{5}$$

$$T_- = \frac{\tau_-^{in} - \tau_-^{out}}{\ln \frac{\tau_-^{in}}{\tau_-^{out}}} \tag{6}$$

where τ is the temperature of the flow. "+" refer to flows that absorb heat and "–" to flows that emit heat. [12] If the system includes many different heat flows at different temperatures, the total heat-emitting temperature T_- for the whole system, is

$$T_- = \frac{\sum_{i=1}^{n} Q_{-i}}{\sum_{i=1}^{n} \left(\frac{Q_{-i}}{T_{-i}} \right)}\,, \tag{7}$$

where Q_{-i} is the heat emitted by one sub-system at the certain effective heat-emitting temperature T_{-i} and n is the number of different sub-systems. T_+ can be calculated in the same way.

Working power made by the system can be expressed as follows [12]:

$$P = \dot{m}\left((h_{in} - T_- s_{in}) + \frac{1}{2} w_{in}^2 + g H_{in} \right) - \dot{m}\left((h_{out} - T_- s_{out}) + \frac{1}{2} w_{out}^2 + g H_{out} \right) + \phi_+ \left[1 - \frac{T_-}{T_+} \right] - T_{eff}\sigma\,. \tag{8}$$

Equation (8) can also be written as

$$P = P_{teor} - T_{eff}\sigma \tag{9}$$

where P is the real working power, P_{teor} is the theoretically maximum working power and $T_{eff}\sigma$ is the real exergy loss of the system. T_{eff} can be either T_- or T_+ depending on the process.

3. Case definitions

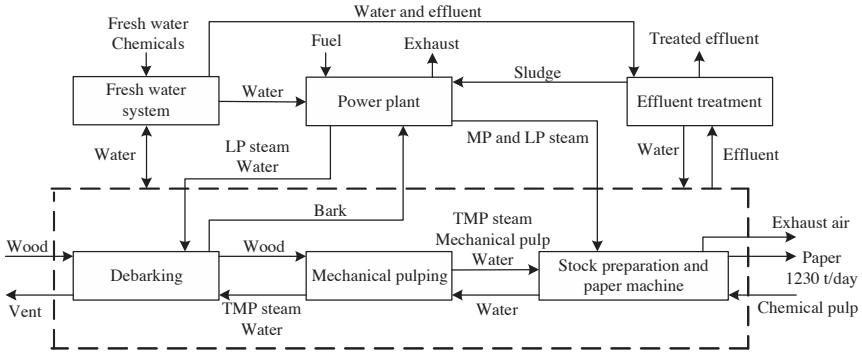

Fig. 1.The flows between the process units. TMP steam = 300 kPa, low-pressure steam = 500 kPa and middle-pressure steam = 1100

3.1. Simulation model

In this work the entropy generation was calculated for the 24 processes of the simulated pulp and paper mill. The calculations were done using a steady state simulation software application called Balas©. Information on Balas can be found in [18-20]. The model used in this study illustrates an average integrated North European pulp and paper mill that includes a TMP plant and a paper machine. The model is not based on any specific existing mill and it has been represented in [21]. The mill consists of a debarking unit, TMP mill, stock preparation, paper machine, power plant, fresh water system and effluent treatment units, as shown in Figure 1. Entropy generation was calculated only for the processes of the debarking, mechanical pulping, stock preparation and paper machine units.

The logs are defrosted and debarked at the debarking unit. The mechanical pulping process consists of main and reject refining lines, and the paper machine has cylinder and infrared dryers. The exhaust air from the paper machine's drying section is used for pre-heating the hall air, process water and drying air. TMP steam and low-pressure steam from the power plant are used for defrosting wood, drying paper and heating water, hall air and the wire pit. Middle-pressure steam is used in the paper machine's coating kitchen and supercalander.

3.2. Two different cases

The entropy generation of the paper mill was calculated for two cases that have slightly different secondary energy systems. In Case 1 the mill is quite realistic and there are some thermodynamically incorrect steam heatings and energy usages. In Case 2 the mill has a good heat recovery system and the heat losses of the mill are minimal. Table 1 and 2 present the differences between these two cases.

Table 1. Steam heating demand in the two cases.

Steam heating demand	Case 1	Case 2
Defrosting wood at the debarking plant	1 960 kW	-
Pulp heating before headbox	5 390 kW	-
Heating of the pre-dyer section's drying air	2 450 kW	1 170 kW
Heating of the after-dryer section's drying air	1 280 kW	778 kW
Warm water preparation	6 660 kW	3 830 kW
Hall air heating	2 920 kW	-

More steam is used for the heating processes in Case 1 than in Case 2 because of the different heat recovery systems. Logs can be defrosted using either steam (Case 1) or hot process water (Case 2). The temperature of the pulp before the head box is controlled by the wire pit's steam heating. In Case 1 the pulp needs to be heated by steam. Since the mill in Case 2 has a better heat recovery system, there is no need for wire pit

heating. The paper machine's heat recovery system is more effective in Case 2 than in Case 1. In Case 1 the exhaust air from the paper machine is too dry and the heat exchangers are inefficient. Warm water, ventilation air and the paper machine's drying air are all heated by the heat recovered from the exhaust air. If that is not enough, steam is used.

Table 2. Different process solutions in the two cases.

Unit	Case 1	Case 2
Paper machine's cooling tower	Thermal duty: 1 360 kW	Thermal duty: 1 740 kW
The drying section's exhaust air	Moisture: 120 g/kg	Moisture: 160 g/kg
Heat recovery between the TMP unit and the paper machine	Heat recovery: 2 380 kW	Heat recovery: 5 020 kW
Unnecessary use of process water	10 kg/s (60°C, 2500 kW)	No unnecessary use of water

The cooling water of the gear box and the hydraulic and compressed air systems is cooled down in a cooling tower. In Case 2 only the hot cooling water is directed to the tower. In Case 1, the cooling water is first mixed with the other process waters and then the whole stream is cooled down in the cooling tower. In Case 1 the exhaust air from the drying section is too dry for efficient heat recovery. Heat recovery from the TMP unit to the paper machine is also less efficient in Case 1 than in Case 2. In Case 2 no unnecessary process water is used and in Case 1 10 kg/s of water is wasted.

3.3. Vacuum system configurations

The purpose of the press and the drying section of the paper machine is to remove water from the web. The paper machine's vacuum system generates low pressure to the web and it can be done by vacuum pumps or turbo blowers. [22]

In this study there are three different possibilities for the vacuum system:

- Vacuum pumps
- Turbo blowers 1 (Exhaust air from the turbo blowers is used to preheat the drying air.)
- Turbo blowers 2 (Exhaust air from the turbo blowers is used directly as drying air.)

When vacuum pumps are used, there needs to be a water cooling system for them. The cooling water is not hot enough to be utilized after the pumps. Turbo blowers do not need water cooling. Exhaust air from the turbo blowers can be used to preheat the drying section's drying air. This system is called Turbo blowers 1 in this paper. Hot air from the turbo blowers can also be used directly as drying air in the drying section. In this case the hall air needs to be cooled down and dried before the turbo blowers. This system is called Turbo blower 2 in this paper.

4. Results

The entropy generation was calculated using the concept described in (1) – (6). All the emitting heat flows (Q_) are heat losses from the process components to the surrounding hall air. All the absorbing heat flows (Q_+) are from components that convey heat to the papermaking process. All the heat flows and effective heat transfer temperatures are presented in Tables 3, 4 and 5.

Table 3. Heat flows and effective heat-emitting temperatures for the TMP plant's components.

Process	Case 1		Case 2	
	T_ K	Q_ kW	T_ K	Q_ kW
Debarking				
Conveyor	307	581	308	658
Bark press	372	24	372	24
Dewater-1	309	4	311	4
Dewater-2	307	60	308	66
Dewater-3	306	14	307	16
Main line refining				
Refiner-1	333	976	333	976
Refiner-2	383	627	382	627
Reject refining				
Refiner-1	353	238	353	238
Refiner-2	382	238	381	238
Screening				
Tank	343	20	344	20
Heat recovery				
Reboiler	412	481	413	482
Chip washing				
Chip wash	349	59	351	61
Foul cond.	375	15	375	16
Chip screw	375	51	375	53
Reject tank	347	2	349	2
Thickening				
Disc filter	344	851	345	853

Table 4. Heat flows and effective heat-emitting temperatures for the paper machine's components.

Process	Case 1		Case 2	
	T_ K	Q_ kW	T_ K	Q_ kW
Pre-dryer				
Cylinder dyer	341	285	341	285
Chemical pulp				
Pulp refiner	334	223	337	223
After dryer				
Cylinder dyer	366	64	366	64
Infrared dryer	369	150	369	150
Wet end				
Seal pit	326	26	326	26
Press water	327	67	327	67
Coating kitchen				
Chem. mixer	332	8	332	8
Fibre recovery				
Disc filter	330	837	330	835
Stock chest	329	48	329	47
Broke handling				
Tank	329	43	329	42
Broke tank	330	9	330	9

Table 5. Heat flows and effective heat-absorbing temperatures for the TMP and paper machine's components.

Process	Case 1		Case 2	
	T+ K	Q+ kW	T+ K	Q+ kW
Debarking				
Heating comp.	282	200	282	200
Cooling & heat recovery				
Gear box	296	600	296	600
Hydraulic	297	900	297	900
Compressed air	297	600	297	600

The effective heat-emitting temperatures in Cases 1 and 2 are slightly different, as can be seen in Tables 3 and 4, due to the different process solutions. However, this does not have a significant impact on the results. At the same time the effective temperatures differ greatly between the components. For instance, the effective temperature of the dewatering systems in the debarking process is approximately 307 K, and the effective temperature for the main line refiner is 382 K. If the entropy generation of the paper mill were calculated using the average outside temperature 293.15 K for every component, entropy generation of the whole mill would increase by 220 kJ/K/t_{paper}. The heat-emitting temperatures for the processes that have heat losses to the surroundings are calculated using (7) and are presented in Table 6.

Table 6 shows the results of the entropy generation calculations. The descriptions of the different cases can be found in the previous chapters. Results show that the main and reject refining processes generate the most entropy. This is a predictable result based on the high electricity demand of these processes. The entropy generation of the approach and pre-drying processes is also moderately high.

According to the calculations it is possible to discover most of the differences between the two cases. Absolutely the biggest difference in entropy generation is in the approach system (1 100 kJ/K/t_{paper}), where the wire pit's steam heating is removed. The same effect can be seen in the debarking process, where the steam heating is replaced with warm process water. Appreciable changes in entropy generation also occur in the pre-dryer, after-dryer, warm water preparation and hall ventilation processes. This is due to the changes in the heat recovery of the paper machine and the moisture of the paper machine's exhaust air. When heat recovery is less efficient, more steam needs be used for heating processes, which increases the entropy generation of those processes.

In some processes, entropy generation is higher in Case 2 than in Case 1. This is due to the slightly higher flow temperatures in Case 2, which increases the heat losses to the surroundings. Some flow temperatures are higher in Case 2 because of the better heat recovery system.

Results show that the changes in the vacuum system have a slight effect on the paper machine's entropy generation. As expected, replacing the vacuum system's vacuum pumps with turbo blowers has the biggest impact on the wet end's entropy generation. Entropy generation also changes in the warm water preparation, pre-dryer, air ventilation and cooling and heat recovery units.

Table 6. Entropy generations of the paper machine and TMP plant in the two different cases and with the three different vacuum systems.

Process	Entropy generation (kJ/K/t_{paper})		Change (kJ/K/t_{paper})	Change (%)	Entropy generation (kJ/K/t_{paper})		
	Case 1	Case 2			Vacuum pumps	Turbo blowers 1	Turbo blowers 2
TMP							
Debarking	193	129	-64	-33	193	193	193
Main line refining	9 420	9 420	-2.0	-0.021	9 420	9 420	9 420
Reject refining	2 810	2 810	-0.32	-0.012	2 810	2 810	2 810
Screening	423	423	0.58	0.14	423	423	423
Heat recovery	211	337	130	59	211	211	211
Chip washing	37.3	84.3	47	130	37.3	37.4	37.4
Thickening	12.3	12.8	0.53	4.3	12.3	13.5	12.5
Bleaching	8.46	8.70	0.24	2.9	8.46	8.61	8.43
Total	13 100	13 200	110	0.82	13 100	13 100	13 100
Paper machine and stock prep.							
Approach system	2 670	1 620	-1 100	-39	2 670	2 680	2 680
Pre-dryer	1 470	1360	-110	-7.3	1 470	1 510	1 510
Chemical pulp	665	659	-5.5	-0.83	665	665	665
After-dryer	586	553	-33	-5.6	586	586	586
Warm water preparation	286	158	-130	-45	286	270	270
Wet end	265	265	-0.027	-0.010	265	190	190
Ventilation air	201	55.6	-150	-72	201	207	207
Cooling & heat recovery	88.5	140	51	58	88.5	100	100
Coating kitchen	79.0	79.0	0.00046	0.00059	79.0	79.1	79.1
Condensate collection	76.0	63.8	-12	-16	76.0	76.9	76.9
Headbox	25.3	25.2	-0.098	-0.39	25.3	25.3	25.3
Fibre recovery	8.21	13.6	5.4	66	8.21	8.21	8.16
Supercalander	5.50	5.50	0	0	5.50	5.50	5.50
Stock preparation	5.32	9.81	4.5	84	5.32	5.32	5.32
Broke handling	0.161	0.0296	-0.13	-82	0.161	0.0204	0.0177
Shower water system	0.00763	0.00803	0.00040	5.2	0.00763	0.00773	0.00773
Total	6 430	5 010	-1 400	-22	6 430	6 400	6 400
Total	19 500	18 200	-1300	-6.7	19 500	19 500	19 500

Table 7. Exergy losses to the surrounding.

Process	Exergy loss kWh/t_{paper}	
	Case 1	Case2
Debarking	18.5	12.3
Main refining	905	903
Reject refining	270	270
Screening	40.6	40.6
Heat recovery	20.3	32.3
Chip washing	3.58	8.09
Thickening	1.18	1.23
Pre-dryer	141	131
Chemical pulp	63.9	63.2
After-dryer	56.3	53.0
Wet end	25.4	25.4
Coating kitchen	7.59	7.58
Fibre recovery	0.789	1.30
Broke handling	0.015	0.003

The losses that are caused by the heat flows from the process to the surroundings are calculated using (8) and (9) from the entropy generation and the effective heat-emitting temperature of the process. These energy losses are presented in Table 7. As expected, the processes that have the biggest losses are the main and reject refining lines and the pre-dryer. All the processes do not have heat losses to the surroundings in this model. The effective heat-emitting temperature for the whole mill is 345 K in Case 1 and 346 K in Case 2.

5. Conclusions and discussion

Entropy analysis can be a useful tool when different processes or different configurations of the same process need to be compared. According to the calculations it is possible to discover most of the differences between the two cases. Results also reveal that a small system change has an impact on the whole process's entropy generation. Entropy generation can be calculated only for a single mill, but to get some useful results it is good idea to compare the entropy generations of the different processes' execution possibilities.

Entropy analysis can also reveal the causations of complex processes. For example, the case study of this paper shows that even when the entropy generation of some processes increases when the secondary heat system is improved, the whole mill's entropy generation still decreases. Process changes can have far-reaching and adverse effects on the heating and heat recovery systems, and understanding these causations is vital when improving the energy efficiency of the whole mill.

The entropy generation calculations of a real industrial process require accurate data on the flows and the energy usages of the process. This information is not always available. The appropriate position of the balance borders and the defining of the processes are essential when making an entropy analysis of a larger process. If the system boundaries are not purposefully set, either the calculations become disproportionally cumbersome or the results are not accurate enough to draw any conclusions.

Entropy analysis does not give any information about the economic side of the process solutions about their technical feasibility. That is why the entropy analysis could be used as a directional tool when process changes are being considered. It doesn't provide all the answers, but it does helps to focus attention on the processes that have the biggest improvement potential.

References

[1] Bejan, A., 2002, Fundamentals of Exergy Analysis, Entropy Generation Minimization, and the Generation of Flow Architecture, International Journal of Energy Research, (26), pp. 545-565.

[2] Bejan, A., 1996, Entropy Generation Minimization, the Method of Thermodynamic Optimization of Finite-size Systems and Finite-time Processes, CRC Press, Florida.

[3] Bejan, A., 1982, Entropy Generation Through Heat and Fluid Flow, Wiley, New York.

[4] Bejan, A., 1988, Advanced Engineering Thermodynamics, Wiley, USA.

[5] Kotas, T. J., 1995, The Exergy Method of Thermal Plant Analysis, Butterworth-Heinemann, Stoneham, USA.

[6] Moran, M. J., and Shapiro H. N., 1995, Fundamentals of Engineering Thermodynamics, 5th ed., Wiley, New York.

[7] Shiner J. S. ed., 1996, Entropy and Entropy Generation, Fundamentals and Applications, Kluwer Academic Publishers, Dordrecht, Netherlands.

[8] Szargut, J., 2005, Exergy Method, Technical and Ecological Applications, WIT Press, Southampton, UK.

[9] Richards, T., and Theliander, H., 2005, Process Efficiency with Entropy - The Recovery Cycle in the Kraft Pulp Process, Nordic Pulp and Paper Research Journal, 20(1), pp. 100-106.

[10] Richards, T., and Theliander, H., 2005, Second-law Analysis Applied to a Kraft Pulp Mill, Nordic Pulp and Paper Research Journal, 20(1), pp. 93-99.

[11] Struchtrup, H., and Rosen, M. A., 2002, How much work is lost in an irreversible

turbine?, Exergy, an International Journal, (2), pp. 152–158.

[12] Lampinen, M. J., and Wiksten, R., 2006, Theory of Effective Heat-absorbing and Heat-emitting Temperatures in Entropy and Exergy Analysis with Applications to Flow Systems and Combustion Processes, Journal of Non-Equilibrium Thermodynamics, 31(3), pp. 257-291.

[13] Holmberg, H., and Ruohonen, P., and Ahtila, P., 2009, Determination of the Real Power Loss for a Steam Turbine, Chemical Engineering Transactions, (18), pp. 379-384.

[14] Holmberg, H., and Ruohonen, P., and Ahtila, P., 2009, Determination of the Real Loss of Power for a Condensing and a Backpressure Turbine by Means of Second Law Analysis, Entropy, (11), pp. 702-712.

[15] Koper, G. J. M., et al., 2007, Entropy Production for Cylinder Drying of Linerboard and Newsprint, International Journal of Heat and Mass Transfer, (50), pp. 1344–1355.

[16] Richards, T., and Pavletic, C., and Pettersson, J., 2009, Efficiencies of NaOH production methods in a Kraft pulp mill, International Journal of Energy Research, (33), pp. 1341-1351.

[17] Zvolinschi, A., and Johannessen, E., and Kjelstrup, S., 2006, The second-law optimal operation of a paper drying machine, Chemical Engineering Science, (61), pp. 3653 – 3662.

[18] Kaijaluoto, S., 1984, Process Optimization by Flowsheet Simulation, PhD. Dissertation, Technical Research Center of Finland.

[19] Hakanen, J., and Hakala, J., and Manninen, J., 2006, An integrated multiobjective design tool for process design, Applied Thermal Engineering, (26), pp. 1393-1399.

[20] Balas, 2009, Balas® Process Simulation Software, VTT, http://balas.vtt.fi.

[21] Ruohonen, P., and Ahtila, P., 2009, Analysis of a thermo mechanical pulp and paper mill using advanced composite curves, 22nd International Conference on Efficiency, Cost, Optimization, Simulation and Environmental Impact of Energy Systems, August 31 – September 3, 2009. Foz do Iguaçu, Paraná, Brazil.

[22] Räisänen, K., 2007, Vacuum Systems, Paulapuro, H., Ed., Paper Making Part 1, Stock Preparation and Wet End, Book 8Paper making Science and Technology, Finnish Paper Engineers' Association, Jyväskylä, Finland.

Acknowledgements: This article is part of the TEKET research project of Aalto University School of Science and Technology and VTT. The project's aim was to study the methods by which industry could measure and improve the energy efficiency of their utility systems.

The Impact of Reference State on the Second-Law Analysis of Evaporative Cooling Processes

Constanze Bongs[a], *Hans-Martin Henning*[a]

[a] *Fraunhofer Institute for Solar Energy Systems, Freiburg, Germany*

Abstract: Evaporative cooling is a promising environmentally friendly alternative to common air-conditioning processes. Thus, there is a high interest to apply second-law analysis to improve and compare moist air processes. The applied framework of analysis is however not always the same - especially the choice of reference humidity ratio often differs. This paper shows that the choice of the reference state for the humidity ratio has no impact on the irreversibility determined by exergy analysis - however it strongly affects the exergetic efficiency. The calculated irreversibility is subject to uncertainty which is already implied in the choice of ideal gas relations to determine moist air entropy. The best application of the method is the location of irreversibility in a complex system, but using the exergetic efficiency for the comparison of completely different systems seems questionable.

Keywords: Moist Air, Entropy, Exergy, Evaporative Cooling.

1. Introduction

A rising demand for active cooling and the need to provide desired rates of ventilation leads to an increase in the energy consumption for air conditioning in buildings. Cooling technologies involving "free" evaporative cooling represent one possible alternative to common electrically driven air-conditioning technologies. With the ongoing development of these technologies the interest in second-law analysis as a) a method to identify possible process improvements and b) a method of comparison to other air-conditioning processes is rising.

Entropy and exergy analyses are widely used methods for the second-law analysis of thermal processes [3-9]. However, conducting a literature review on entropy and exergy analysis of moist air processes reveals that a common framework of second-law analysis is not always obvious. The following sources of missing clarity may be identified:

- Application of real or ideal gas models for the determination of moist air entropy
- Different moist air entropy equations based on ideal gas relations
- Different reference states for both entropic and exergetic analysis
- The use of exergetic performance figures, in particular the exergetic efficiency

This paper firstly aims to highlight where entropy and exergy analysis are not as straightforward as often assumed. It then gives explanations how to bring together seemingly different frameworks. The final objective is to outline how second-law analysis can be well applied – and when this seems critical.

2. Second law analysis of moist air processes

2.1. Moist air entropy according to the ideal gas model

In the following the relevant equations for the calculation of moist air entropy will be reviewed and discussed with respect to their dependence on reference values.

2.1.1. Reference data for entropy evaluation

As processes in air-conditioning are generally operated close to ambient pressure, the ideal gas model (IGM) is usually applied to describe moist air states. A real gas model [1] was however used for the table of thermodynamic properties given in

Corresponding Author: Constanze Bongs, Email: constanze.bongs@ise.fraunhofer.de

[2]. Reference point of zero entropy is dry air at a temperature of T_0=273.15 K and standard atmospheric pressure p_0=101325 Pa. It will be used as a benchmark for the ideal gas model relations for entropy given in the literature.

2.1.2. Ideal gas relations

Textbooks generally give two definitions for the entropy of moist air. [3] describes moist air entropy $s_{1+x(1)}$ as the sum of the entropies of the mass fractions of the two individual components, dry air $s_{A(1)}$ and water vapour $s_{V(1)}$ at their individual partial pressures. Humidity ratio x_V (and entropy) are given on a dry air base. Specific heat c_p is assumed constant in the relevant temperature range.

$$s_{1+x(1)} = s_{A(1)} + x_V \cdot s_{V(1)} \quad (1)$$

$$s_{A(1)} = c_{pA} \ln\frac{T}{T_0} - R_A \ln\frac{p_A}{p_0} \quad (2)$$

$$s_{V(1)} = c_{pV} \ln\frac{T}{T_0} + \frac{r_0}{T_0} - R_V \ln\frac{p_V}{p_s(T_0)} \quad (3)$$

The reference state is set at the temperature T_0= 273.15 K and the pressure p_0= 101325 Pa. Note that here the reference pressure for water vapour is the saturation pressure of water at the reference temperature. This first approach is highlighted by the index (1).

A second approach [4] - highlighted by the index (2) - describes the entropy of the two components dry air and water vapour with respect to the total pressure p. In accordance to the definition of moist air enthalpy, the reference state is set at the triple point (T_0=T_{triple}=273.16 K, p_0=p_{triple}=611.7Pa). The entropy of moist air is then defined as the sum of the entropies of the two individual components and the mixing entropy, taking into account the entropy production of an expansion of the individual component gases from the total pressure p to their partial pressures.

$$s_{1+x(2)} = s_{A(2)} + x_V \cdot s_{V(2)} + \Delta s_{mix(2)} \quad (4)$$

$$s_{A(2)} = c_{pA} \ln\frac{T}{T_{triple}} - R_A \ln\frac{p}{p_{triple}} \quad (5)$$

$$s_{V(2)} = c_{pV} \ln\frac{T}{T_{triple}} - R_V \ln\frac{p}{p_{triple}} + \frac{r(T_{triple})}{T_{triple}} \quad (6)$$

The mixing entropy reads (7)

$$\Delta s_{mix(2)} = R_V\left[(C + x_V)\cdot \ln(C + x_V) - C\ln C - x_V \ln x_V\right]$$

where C represents the ratio of specific gas constants of air and water vapour $C=R_A/R_V\approx0.622$.

2.1.3. Accuracy of the saturated moist air entropy based on the ideal gas model

In order to evaluate the accuracy of the specific entropy based on the ideal gas model, the entropy of saturated moist air is compared to tabulated data [2] based on a real gas model [1]. The moist air entropy is calculated by the first set of equations (1-3). As a preliminary step, the calculated saturation humidity ratio x_{sV} is evaluated. According to the ideal gas model, saturation humidity ratio is determined by equation (8):

$$x_{sV} = \frac{R_A}{R_V}\frac{p_s(T)}{p - p_s(T)} \quad (8)$$

Fig. 1 gives the relative deviation of the calculated humidity ratio from the tabulated values $\{100*(x_{sV,calc}-x_{sV,tab})/\ x_{sV,tab}\}$. The tabulated values are given up to a temperature of t=90°C. The accuracy of the ideal gas model decreases with rising temperature. Results are within a margin of +1% up to a temperature of approximately t=75°C. This is in line with [5] identifying a margin of error below 0.75% at standard atmospheric pressure for saturated air humidity ratio, enthalpy and specific volume derived from ideal gas relations.

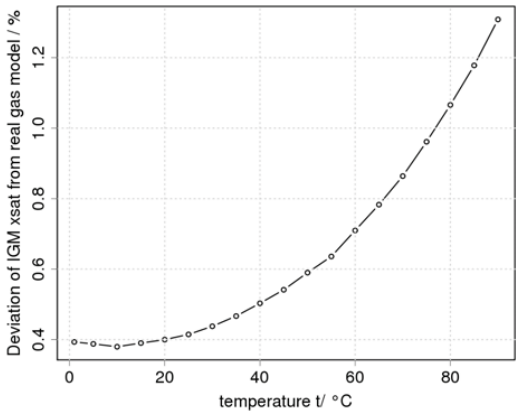

Fig. 1. Difference in saturation humidity ratio between calculated (IGM) values and tabulated values according to the real gas model [2].

Fig. 2 shows the deviation of the moist air entropy calculated by (1) applying a) the more accurate, tabulated saturation humidity ratio and b) the saturation humidity ratio calculated according to the ideal gas law (8). Again, the deviation is calculated by $\{100*(s_{sMA,calc}-s_{sMA,tab})/\ s_{sMA,tab}\}$. When applying the tabulated data for the saturation humidity ratio the resulting entropy lies

within a margin of 0.25% from the tabulated entropy – underlining the applicability of the entropy calculation via the ideal gas model (1). Lying somewhat higher but still within a margin of 1% for the second case b) the specific entropy may be applied in an ideal gas framework within the relevant temperature range (0-90°C).

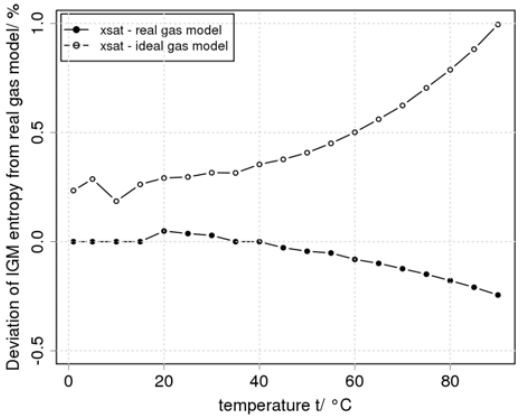

Fig. 2. Difference in the entropy of saturated moist air values calculated with IGM saturation humidity ratio and tabulated saturation humidity ratio.

2.1.4. Moist air entropy and reference state

The relation between the two above stated equations for moist air entropy {(1) and (4)} is not so obvious at first sight.

According to (4) the water vapour is assumed to be initially present at the absolute pressure (e.g. p=101325 Pa). The mixing entropy is then taking account of the expansion to the partial pressure of the individual gases. In contrast, (1) directly applies the entropy of the components at their individual partial pressures and does not explicitely account for the mixing entropy. As opposed to (1) the numerical values of (4) are non-zero at the reference point (here: triple point). However, the entropy value of a single air state is not of interest – entropy differences between air states must be evaluated. In order to compare the results of the two equations, the dry air entropy at the triple point is subtracted from the temperature dependent saturated air entropy. For the given reference states (see 2.1.2), the two equations yield exactly the same results. When trying to transform equation (4) into equation (1), the different definition of reference state is however an obstacle.

Looking at equation (4) again, the triple point temperature and pressure are given as one specific reference state for the entropies of both dry air and water vapour. It is however not directly clear how to write a generalized expression of (4).

For a better understanding, it is therefore interesting to vary the reference state. When looking at entropy differences the reference state should cancel out – it should be possible to choose the reference state arbitrarily. Two alternative ways to generalize (4) might come into mind. First, one might assume a common reference pressure (other than the triple point pressure) for both the dry air and the water vapour entropy. Second, one might assume one reference pressure for the dry air, e.g. standard atmospheric pressure, and the saturation pressure at the reference temperature for the water vapour.

The result of the first approach for two different reference pressures is given in Fig. 3. It can be clearly seen that the result depends on the reference state. However, this approach allows applying physically non-meaningful combinations of reference temperature and pressure for the water vapour term which is clearly wrong.

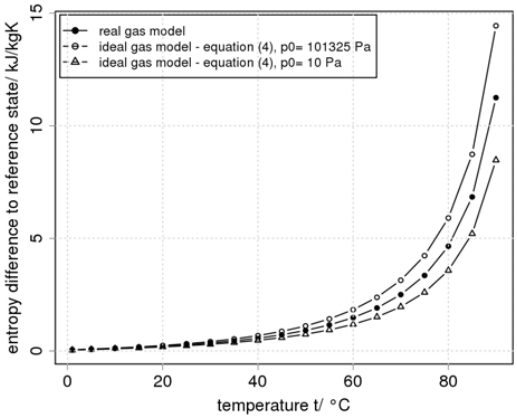

Fig. 3. Calculated entropy when assuming a common reference pressure for dry air and water vapour: the resulting entropy difference depends on the reference pressure.

The second approach fixes the moist air reference pressure to a physically meaningful value. Its results are equivalent to the results obtained applying (1). Therefore, it is the correct generalized way to express (4). Generalizing (4) according to this second approach, it is also analytically possible to transform (4) into (1).

Nonetheless, Fig 3. also shows in an exaggerated manner that the reference state does not completely vanish when calculating the entropy difference of the water-air mixture at two different humidity ratios. Calculating entropy differences between air states of single components, the logarithmic reference state terms cancel out. When applying (9) for the calculation of the discrete entropy difference between two air states, the reference terms do not completely vanish due to the multiplication of the water vapour entropy with the humidity ratio x_V.

$$\Delta s_{1+x} = (s_{A2} - s_{A1}) + (x_{V2} \cdot s_{V2} - x_{V1} \cdot s_{V1}) \quad (9)$$

The following conclusion may be drawn. Applying the reference state as described under 2.1.2, both equations give results that represent the benchmarking data derived from a real gas model with satisfying accuracy. Therefore, they represent a common framework for entropy analysis of processes involving moist air. For reasons of simplicity (1) is the favoured way of expression of moist air entropy by the authors – it can be more easily handled in the derivation of the moist air exergy equation than (4).

2.2. Exergy of moist air and liquid water

Exergy quantifies the potential of matter to perform work when brought into equilibrium with the environment. Exergy analysis may be used equivalent to entropy analysis to detect and quantify irreversibilities in a thermodynamic process. Whereas in entropy analysis irreversibility is described by entropy production S_{gen}, exergy analysis determines exergy destruction E_D. The relation between both is given by the Guoy-Stodola equation (10):

$$E_D = T_0 \cdot S_{gen} \quad (10)$$

Irreversibility may also be determined directly from exergy balances. To this purpose the flow exergy of a stream of matter must be known. For complex systems this offers the possibility to graphically represent the results of irreversibility analysis in an exergy flow chart. The definition of the specific exergy of moist air will be given in the following.

2.2.1. Derivation of moist air exergy equation

Moist air exergy is derived as the sum (11) of the individual component exergies e_i (12). The reference state is again represented by the index "0" – the numerical value may however differ from the entropy reference state discussed before.

$$e_{1+x} = e_A + x_V e_V \quad (11)$$

$$e_i = h_i - h_{i0} - T_0(s_i - s_{i0}) \quad (12)$$

The specific exergy equation (13) for the analysis of moist air processes is a summation of terms quantifying a non-equilibirium in temperature, pressure and mixture composition (so-called thermal, mechanical and chemical exergy) [6, 7].

$$e_{1+x} = (c_{pA} + x c_{pV}) \left(T - T_0 - T_0 \ln \frac{T}{T_0} \right) + \ldots \quad (13)$$

$$(1+\tilde{x}) R_A T_0 \ln \frac{p}{p_0} + R_A T_0 \left[(1+\tilde{x}) \ln \frac{(1+\tilde{x}_0)}{(1+\tilde{x})} + \tilde{x} \ln \frac{\tilde{x}}{\tilde{x}_0} \right]$$

Here, $\tilde{x}$ is the product of the humidity ratio and the ratio of molar masses of air and water (14).

$$\tilde{x} = \frac{M_A}{M_V} x \approx 1.608x \quad (14)$$

For the evaluation of processes involving water evaporation it is also necessary considering the specific exergy of liquid water (15), simplified here to a term describing the thermal exergy and a second expansion term.

$$e_W = c_{pW} \left(T - T_0 - T_0 \ln \frac{T}{T_0} \right) + R_V T_0 \ln \frac{p_s(T_0)}{p_{V0}} \quad (15)$$

This second term describes the ability to perform work by expansion of water vapour at saturation pressure to the partial pressure of water vapour in the air and depends on the reference state alone [6]. This pressure ratio is equivalent to the reciprocal of the reference relative humidity – that is with increasing reference relative humidity the specific exergy of liquid water is diminishing.

2.2.2. Numerical values of moist air exergy depending on reference state

To discuss reference states in exergy analysis of moist air processes, the numerical values for different reference states shall be shortly presented. From (10) it is already clear that the numerical value of exergy destruction depends on the reference temperature – the dependence on the reference humidity ratio is however less clear.

In the literature, mainly two different ways to choose the reference state of humidity ratio are discussed. The first and generally applied reference state is ambient humidity ratio [6,7]. The second approach presented in [8] applies the

saturation humidity ratio of moist air as reference humidity ratio. This is justified by reasoning that air at ambient air state has a potential to perform work. An air flow at ambient air state may be humidified to the wet bulb temperature (until saturation) enabling work to be performed between the reservoir at the wet bulb temperature and the ambient temperature. Fig. 4 gives the numerical values of specific exergy for an ambient state of t=35°C and x=0.014 kg/kg. Air temperature and pressure are assumed to be in equilibrium with the ambient, thus Fig. 4 is equivalent to chemical exergy alone. Assuming the saturation humidity ratio as reference the moist air exergy falls monotonously until approaching saturation.

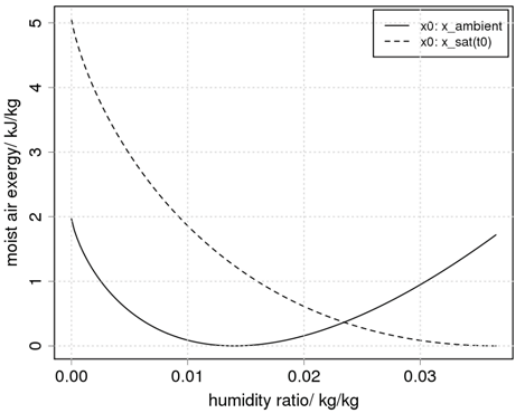

Fig. 4 Moist air specific exergy for two different reference humidity ratios.

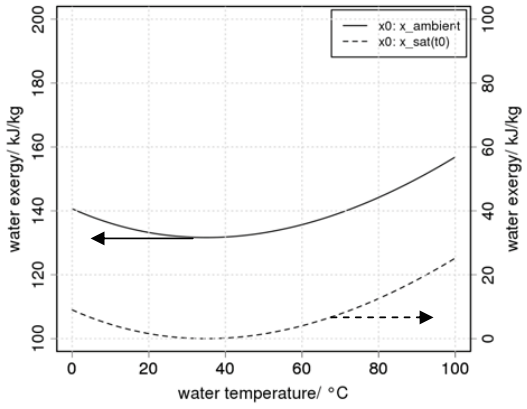

Fig. 5. Specific exergy of liquid water for two different reference humidity ratios.

Air exergy must be discussed in conjunction with the exergy of liquid water. The difference of the exergy of liquid water for the two reference states is shown in Fig. 5. Applying ambient humidity ratio as reference state, the liquid water exergy shifts up by the offset given by the pressure term in (15). The curvature is due to the thermal exergy (first term in (15)). The difference between the approaches might also be interpreted as follows. In the first approach (ambient humidity ratio), evaporation is enabled by the existence of water being the restricted resource in a system. The ability to perform work is inherent to the water rather than the air. The second approach might however represent an environment in which air is the restricted resource and water is readily available. The first approach seems to be closer to reality.

Fig. 5 illustrates one further reasoning by [8] argueing that the effluent of a small amount of water from a system (such as effluent of condensate in an air-conditioning application) would result in a high exergy loss. They further argue that this would result in an underestimation of the exergetic efficiency of the process. This will be discussed further along.

2.3. Virtual case studies

An evaporative cooling process will be evaluated with the two reference states given above. Further, difficulties with the use of measurement data for second-law analysis will be discussed.

2.3.1. Adiabatic humidification

Evaporative cooling processes can be ideally considered adiabatic. Air and water states of an exemplary process are given in Fig. 6.

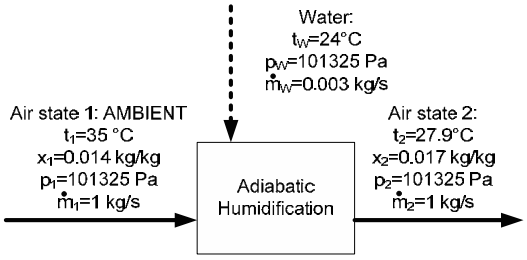

Fig. 6. Air states assumed for an adiabatic humidification process.

The entropy flow balance is shown here (16) to give an example for the order of magnitude.

$$\Delta\dot{S}_{gen} = \dot{m}_{A2}s_2 - (\dot{m}_{A1}s_1 + \dot{m}_W s_W) \qquad (16)$$

$$\Delta\dot{S}_{gen} = \left[252.40 - (250.47 + 1.06)\right]\frac{W}{K} \approx 0.87\frac{W}{K}$$

Note that the difference in air entropy between the states at inlet and outlet is already very small – it amounts to less than 1% of the absolute value of moist air specific entropy. The entropy generation of the evaporation process lies therefore within the magnitude of error that must be assumed for the entropy determination using ideal gas relations.

When assuming the ambient temperature (T_1) as the reference temperature for exergy analysis, the exergy destruction may first be determined via the Gouy-Stodola equation. The exergy destruction flow $\dot{E}_D$ then results to 267.7 W for the given example. The exergy destruction shall now be determined with an exergy balance (17) and two different reference humidity ratios.

$$\dot{E}_D = \dot{m}_{A1}e_1 + \dot{m}_W e_W - \dot{m}_{A2}e_2 \qquad (17)$$

First, ambient air humidity ratio (here x_1) is applied as the reference, second the saturation humidity ratio $x_s(T_1)$ is applied. Ambient temperature and pressure are applied as reference in both cases. This yields the following numerical values.

$$x_0 = x_1 : \dot{E}_D = (0 + 397.5 - 128.8)W = 268.7W$$

$$x_0 = x_s(T_1) : \dot{E}_D = (1243.8 + 2.5 - 977.6)W = 268.7W$$

The irreversibility derived from the Gouy-Stodola equation and from exergy flow analysis do not completely match. The difference is however small enough to assume that the Gouy-Stodola equation still holds true for adiabatic humidification. The reference state of the exergy analysis has no impact on the determination of irreversibilities.

In order to obtain such a result, entropy generation must be applied to the Gouy-Stodola equation with at least two digits. This is however more specific than the accuracy that may be assumed for applying real gas relations. Once more, this illustrates the high margin of error that is already implied in the method. Results may be interpreted for a comparative analysis of components in a complex system, the absolute numerical values should however be treated with care.

2.3.2. Figures quantifying process efficiency

In order to measure the exergetic performance of a process different types of exergetic efficiency are often defined [9]. The most commonly applied figures are the exergy destruction ratio (18), the exergy loss ratio (19) and the exergetic efficiency (20). The exergy destruction ratio is defined by the ratio of exergy destruction to the overall "fuel" exergy $\dot{E}_F$, that is the cumulative exergy of the inlet flow streams.

$$y_D = \frac{\dot{E}_D}{\dot{E}_F} \qquad (18)$$

The exergy loss ratio is the ratio of exergy losses $\dot{E}_L$ – that is the exergy content of unused effluents – to the overall "fuel" exergy.

$$y_L = \frac{\dot{E}_L}{\dot{E}_F} \qquad (19)$$

The exergetic efficiency measures the ratio of the product exergy flow $\dot{E}_P$ – that is the useful effect of the system – to the overall "fuel" exergy.

$$y_{EFF} = \frac{\dot{E}_P}{\dot{E}_F} \qquad (20)$$

Table 1 shows that the calculation of exergetic performance figures is highly dependent on reference state. For equivalent air states and performance the resulting figures vary significantly.

Table 1. Efficiency figures of adiabatic mixing and humidification for different reference states.

Reference state	y_{EFF}	y_D	y_L
$T_0=T_{amb}$, $x_0=x_{amb}$	0.32	0.68	0.00
$T_0=T_{amb}$, $x_0=x_s(T_0)$	0.78	0.22	0.00

When analysing a complex system the share of the exergy destruction ratio in each component to the total exergy destruction in the system may also be calculated. This figure directly corresponds to entropy production. According to the Gouy-Stodola equation the reference temperature cancels out – results do not vary with reference state.

It must be concluded that the meaningfulness of the exergetic performance figures (18-20) is questionable. The line of argument presented in [8] seems a somewhat arbitrary way to apply an efficiency figure giving a high performance of evaporative cooling processes. As highlighted by [9] exergetic efficiency should only be used to compare similar systems, or components e.g.

subject to incremental variations – the figure seems however often to be misused to suggest comparability of results for completely different systems. It should be clear that the main objective of exergy analysis is determining irreversibilities.

2.3.3. Discussion of the effect of measurement errors on the analysis

When conducting irreversibility analysis it might come into mind to use experimental data as a base for the analysis. Experimental data is always subject to measurement errors, thus the energy balance is usually not completely satisfied. Fig. 7 gives possible air states for two air flows exchanging sensible heat that fulfill the energy balance. All air flows are assumed to be present at ambient pressure and an air flow rate of 1 kg/s. Due to the dependence of the heat capacity on the moist air humidity ratio, the temperature difference on the hot side does not equal the one on the cold side.

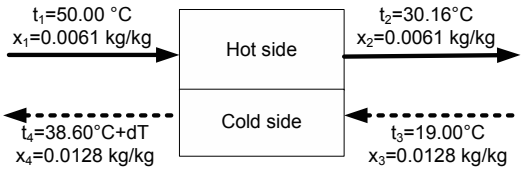

Fig. 7. Air states assumed for a sensible heat exchange process.

When applying the values that fulfill the energy balance, the irreversibility analysis via entropy balance and exergy balance yields the same result ($\dot{E}_D = 734W$).This is shown by the crossing point in Fig. 8.

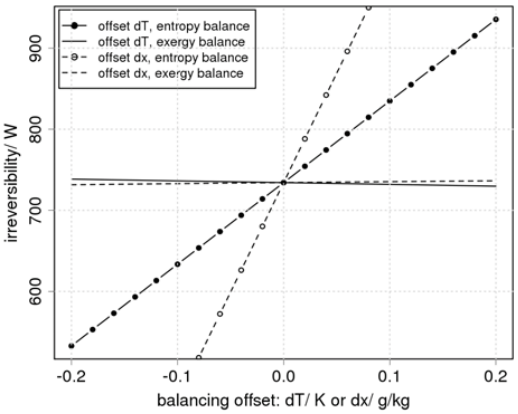

Fig. 8. Irreversibility calculated from entropy balance or exergy balance depending on the offset (dT, dx) from values fulfilling the energy balance

As in the previous example the exergy reference state is t_0=35°C and x_0=0.014 kg/kg. When assuming a measurement error on the cold side outlet temperature and applying this value directly to the entropy and exergy balances, the resulting irreversibility is however not identical any more. Fig. 8 shows the resulting irreversibility as a function of the offset (temperature and humidity ratio) of the measured air state to the value that fulfills the energy balance. This figure applies to the heat exchange process as given in Fig. 7. When calculating irreversibility from entropy analysis, the result is highly dependent on the offset whereas when applying exergy analysis the dependence is not very strong. This seems contradicting at first, but may be explained by a closer look at the analysis.

For an exemplary calculation, the offset on the cold side outlet temperature is assumed to be dT=0.2 K which would be a relatively small error for temperature measurement in an air flow. This temperature difference is to be considered as a real effect, corresponding to an additional heat input to the air flow. This heat flow amounts to $\dot{Q}_{err} = 205W$. The entropy flow associated with this heat input can be calculated by (21).

$$\dot{S}_{err} = \dot{Q}_{err} / T \qquad (21)$$

T is the thermodynamic mean temperature at which the heat is supplied to the air flow rate and here calculated as T=T_4+dT/2. Multiplication with the reference temperature T_0 yields the anergy of the heat flow which amounts to 201 W for this example. In this example, the entropy production of this heat flow (22) is however very small.

$$\dot{S}_{gen,err} = \dot{m}_3 s_{4,err} - \dot{m}_3 s_4 - \dot{S}_{err} = 2 \cdot 10^{-8} W / K \qquad (22)$$

When it is not considered as an input in the entropy balance (correctly shown in (23)), the entropy flow associated with the (virtual) heat input $\dot{S}_{err}$ is completely treated as an entropy generation term – resulting in an overestimation of irreversibility.

$$\dot{S}_{gen} = \dot{S}_{4,err} + \dot{S}_2 - \dot{S}_{err} - \dot{S}_1 - \dot{S}_3 \qquad (23)$$

The exergy of the heat flow (24) is calculated applying the thermodynamic efficiency.

$$\dot{E}_{err} = (1 - T_0 / T)\dot{Q}_{err} = \dot{Q}_{err} - T_0 \dot{S}_{err} \qquad (24)$$

In the given example, the reference state T_0 and the temperature T are very close, thus the exergy flow of the heat flow is very small ($\dot{E}_{err} = 4W$). This is

the missing term in the exergy balance. Not considering the exergy of the (virtual) heat input in the exergy balance leads to an underestimation of exergy destruction. Therefore, heat losses or gains must be clearly distinguished from measurement errors in order to conduct a reasonable analysis. Otherwise, irreversibility analysis conducted with measurement data is easily subject to error. This error might result acceptable for exergy analysis (<1% for the given example), but not for entropy analysis (<30%).

3. Conclusions

The comparison of moist air entropy derived from ideal gas relations to reference real gas data showed that the deviation is less than 1%. Two seemingly different entropy equations were shown to give equivalent results. The reference state of humidity ratio has no impact on the irreversibilities determined when applying both ambient humidity ratio and saturation humidity ratio as reference humidity to an exergy analysis of an adiabatic humidification process. Exergetic performance figures, most prominently the exergetic efficiency, are however strongly affected by the choice of reference state. The calculated irreversibility is subject to uncertainty which is implied in using ideal gas relations to determine moist air entropy. Conducting irreversibility analysis with measurement data, there is a high risk of error when measurement errors and real effects such as heat losses cannot be distinguished. The best application of the method seems to be the location of irreversibility in a complex (theoretical) system, not the comparison of highly diverse systems by exergetic performance figures.

Nomenclature

c	specific heat, J/kgK
e, E	specific exergy, J/kg, and exergy, J
h	specific enthalpy, J/kg
$\dot{m}$	mass flow rate, kg/s
p	pressure, Pa
$\dot{Q}$	heat flow rate, W
r	enthalpy of evaporation, J/kg
R	specific gas constant, J/kgK
s, S	specific entropy, J/kgK, entropy, J/K
t,T	temperature, °C and K
x	humidity ratio, kg_V/kg_A
y	ratio/ performance figure, -

Subscripts and superscripts

0	reference state
A	air
amb	ambient
D	destruction
eff	efficient
err	measurement error
F	input, “fuel”
gen	generation
L	loss
mix	mixing
s	saturation
V	water vapour
W	liquid water

References

[1] Hyland, R.W., and Wexler, A., 1983, Formulations for the thermodynamic properties of dry air from 173.15 K to 473.15 K, and of saturated moist air from 173.15 K to 372.15 K, at pressures to 5 MPa, ASHRAE Transactions, 89(2), pp.520-535.

[2] ASHRAE, 2005, *Fundamentals – ASHRAE Handbook*, Atlanta.

[3] Bosnjakovic, F., and Knoche, K.F., 1997, *Technische Thermodynamik, Teil II*, 6th ed., Steinkopff, Darmstadt.

[4] Baehr, H.D., and Kabelac, S., 2006, *Thermodynamik*, 13th ed., Springer, Berlin

[5] Kuehn, T., et al., 1998, *Thermal evironmental engineering*, 3rd ed., Prentice-Hall, Upper Saddle River, NJ.

[6] Szargut, J., and Stryrylska, T., 1969, Die exergetische Analyse von Prozessen der feuchten Luft, Heizung, Lüftung, Haustechnik, 5, pp.173-178.

[7] Wepfer, W.J., et al., 1979, Proper evaluation of available energy for HVAC, ASHRAE Transactions, 85(1), pp. 667-677.

[8] Chengqin, R., et al., 2002, Principles of exergy analysis in HVAC and evaluation of evaporative cooling schemes, Building and Environment, 37, pp. 1045-1055.

[9] Bejan, A., et al., 1996, *Thermal Design and Optimization*, John Wiley & Sons, New York.

Acknowledgments: This work was supported by a Ph.D. scholarship of the Reiner Lemoine Stiftung.

Conventional and Advanced Exergetic Analyses Applied to a Combined Cycle Power Plant

Fontina Petrakopoulou, George Tsatsaronis, Tatiana Morosuk and Anna Carassai

Institute for Energy Engineering, Technische Universität Berlin, Germany

Abstract: Conventional exergy-based methods pinpoint components and processes with high irreversibilities. However, they lack certain insight. For a given advanced technological state, there is a minimum level of exergy destruction related to technological and/or economic constrains that is *unavoidable*. Furthermore, in any interactive thermodynamic system, exergy destruction stems from both component interactions (*exogenous*) and component inefficiencies (*endogenous*). To overcome the limitations of the conventional analyses and to increase our knowledge about a plant, advanced exergy-based analyses have been developed. These analyses provide additional information about component interactions and reveal the real potential for improvement of each component constituting a system, as well as of the overall system. In this paper, a combined cycle power plant is analyzed using both conventional and advanced exergetic analyses. Except for the gas turbine and the high-pressure steam turbine of the energy conversion system, most of the exergy destruction in the plant components is unavoidable. This unavoidable part is constrained by internal technological limitations, i.e. each component's endogenous exergy destruction. High levels of endogenous exergy destruction show that component interactions do not contribute significantly to the losses. Therefore, inefficiencies that cause these irreversibilities are of secondary interest, and even more so since they are unavoidable to a large extent. Using an advanced exergetic analysis, we rank the components of a plant by decreasing significance with respect to the improvement of the overall system. Calculations related to the total avoidable exergy destruction caused by each component of the plant supplement the outcome of the conventional exergetic analysis. With the input of the advanced analysis, new improvement strategies are revealed that could not otherwise be found.

Keywords: thermodynamic inefficiencies, exergy destruction, conventional exergetic analysis, advanced exergetic analysis, combined cycle power plant.

1. INTRODUCTION

Conventional exergetic, economic and exergoeconomic analyses assist in a rigorous evaluation of energy conversion systems. A conventional exergetic analysis reveals irreversibilities within each component of a plant. The costs related to the irreversibilities are then estimated in an exergoeconomic analysis [1-5]. Advanced exergetic and exergoeconomic analyses are needed in order to determine which part of the inefficiencies and the related costs is caused by component interactions and which part can be avoided through technological improvement of a plant. Using these analyses helps to explicitly iden-tify the exergy destruction and costs and separate them into two main groups: (1) *avoidable- unavoidable exergy destruction/cost* and (2) *endogenous-exogenous exergy destruction/cost*.

More specifically, concerning the advanced exergetic analysis, the source of irreversibilities for a component is either component interactions (*exogenous exergy destruction*) or operational inefficiencies within the component (*endogenous exergy destruction*). Moreover, part of the overall irreversibilities exists due to physical, technological and economic constraints and cannot be prevented (*unavoidable exergy destruction*). Irreversibilities that can be prevented through design improvement constitute the *avoidable exergy destruction*. The exogenous and endogenous parts can be further split into avoidable and unavoidable parts facilitating the understanding of component interconnections and the estimation of the potential for improvement. In a similar way, the imposed costs can also be separated in the advanced exergoeconomic analysis. Work in this field has been conducted in recent years at the Technical University of Berlin [6-13]. Through the classifications developed in

these analyses, the components that influence the performance of the overall process are identified, and the focus lies on the avoidable part of the endogenous and exogenous exergy destruction.

The present paper focuses on the application of the advanced exergetic analysis, while the advanced exergoeconomic analysis will be considered in another study. The analysis is applied to a complex energy conversion system: a three-pressure-level combined cycle power plant. The main objective is to identify the more influential components, in order to indicate changes related to (1) the structure and (2) the operation of the plant components that will result in a more efficient performance of the overall plant.

2. METHODOLOGY

2.1 Conventional exergetic analysis

Through the exergetic analysis, the components with high irreversibilities in a system are identified. Attributes and advantages of the exergetic analysis are well established [14].

By defining the exergy of the product, $\dot{E}_{P,k}$, and the exergy of the fuel, $\dot{E}_{F,k}$, for the k^{th} component, we can determine its exergetic efficiency, $\varepsilon_k = \dot{E}_{P,k} / \dot{E}_{F,k}$. A useful variable for comparison of dissimilar components is the exergy destruction ratio defined as: $y_{D,k} = \dot{E}_{D,k} / \dot{E}_{F,tot}$, with $\dot{E}_{D,k}$ being the exergy destruction within the k^{th} component and $\dot{E}_{F,tot}$ the total exergy of the fuel provided to the plant. The ratio $y_{D,k}$ is a measure of the contribution of the exergy destruction within the k^{th} component to the reduction of the overall exergetic efficiency.

2.2 Advanced exergetic analysis

Through an advanced exergetic analysis, the exergy destruction is split into avoidable, $\dot{E}_D^{AV}$, and unavoidable, $\dot{E}_D^{UN}$, parts as well as into endogenous, $\dot{E}_D^{EN}$, and exogenous, $\dot{E}_D^{EX}$, parts. With this analysis, the effect of component interactions and technological limitations on the effectiveness of a system are estimated. A detailed description of the methodology is provided in [8] and [11], but its main principles are presented below.

2.2.1 Endogenous – exogenous exergy destruction

In a system with n components, the endogenous exergy destruction, $\dot{E}_{D,k}^{EN}$, is the exergy destruction related to the operation of the k^{th} component itself. It is determined when this component operates under real conditions and all other components of the process are considered to operate without irreversibilities (theoretically). The power output of the overall plant is kept constant in all cases. The theoretical conditions for the most important components are shown in Table 1. For the combustion chamber no theoretical conditions can be defined, due to the chemical reactions that take place. Different methods have been proposed to overcome this problem [9]. One approach, proposed in [11], is valid for more complex systems and has been applied here. After the estimation of the endogenous exergy destruction of the k^{th} component, its exogenous exergy destruction is calculated by subtracting its endogenous exergy destruction from its real exergy destruction, $\dot{E}_{D,k}^{real}$:

$$\dot{E}_{D,k}^{EX} = \dot{E}_{D,k}^{real} - \dot{E}_{D,k}^{EN} \quad (1)$$

The exogenous exergy destruction, $\dot{E}_{D,k}^{EX}$, is therefore the exergy destruction imposed on the k^{th} component through the operation of the remaining *n-1* components constituting the overall process. The $\dot{E}_D^{EX}$ of component k can also be further split, revealing the specific components that cause it. The sum of the exogenous exergy destruction terms is different than the exogenous exergy destruction of the k^{th} component. This difference, the *mexogenous exergy destruction* $\left(\dot{E}_{D,k}^{MX}\right)$, is caused by the simultaneous interconnections of all (n) components and it is calculated as in [11]:

$$\dot{E}_{D,k}^{MX} = \dot{E}_{D,k}^{EX} - \sum_{\substack{r=1 \\ r \neq k}}^{n} \dot{E}_{D,k}^{EX,r} \quad (2)$$

2.2.2 Avoidable – unavoidable exergy destruction

Technological and economic design limitations determine a minimum value of the exergy destruction. This part of the exergy destruction which cannot be avoided with technologically feasible design modifications, at least in the foreseeable future, is called the unavoidable exergy destruction, $\dot{E}_D^{UN}$. The unavoidable exergy

Table 1: Assumptions of theoretical and unavoidable conditions.

Component	Theoretical conditions	Unavoidable conditions
Compressor	η_{is} = 100%	η_{is} = 98%
	η_{mech} = 100%	η_{mech} = 100%
	Q_{loss} = 0	Q_{loss} = 0
Combustion chamber	Δp = 0	Δp = 0
	λ= 2.05	λ= 1
	ε = 100%	
Expander	η_{is} = 100%	η_{is} = 99%
	η_{mech} = 100%	η_{mech} = 100%
Generators	η_{electr} = 100%	η_{electr} = 99.5%
Superheaters, Reheater	ΔT_{min} = 0	ΔT_{min} = 4
	Δp = 0	Δp = 0
	ΔT_{min} = 0	ΔT_{min} = 1
Evaporators	Approach Temp. = 0	Approach Temp. = 0
	Δp = 0	Δp = 0
Economizers	ΔT_{min} = 0	ΔT_{min} = 1
	Δp = 0	Δp = 0
Steam Turbines	η_{is} = 100%	η_{is} = 97%
	η_{mech} = 100%	η_{mech} = 100%
Pumps	η_{is} = 100%	η_{is} = 95%
	η_{mech} = 100%	η_{mech} = 100%
Motors	η_{electr} = 100%	η_{electr} = 98%

destruction is calculated by considering each component in isolation, separated from the cycle. The assumptions taken into consideration for the calculation of the unavoidable exergy destruction are shown in Table 1. Operation with high efficiency and low losses is considered. The ratio of exergy destruction per unit of product exergy $\left(\dot{E}_D^*/\dot{E}_P\right)_k^{UN}$ is then calculated. For the k^{th} component with exergy of the product in the real process $\dot{E}_{P,k}^{real}$, the unavoidable exergy destruction $\dot{E}_{D,k}^{UN}$ is calculated as:

$$\dot{E}_{D,k}^{UN} = \dot{E}_{P,k}^{real} \times \left(\frac{\dot{E}_D^*}{\dot{E}_P}\right)_k^{UN} \quad (3)$$

When the unavoidable exergy destruction of the k^{th} component is known, the avoidable exergy destruction is obtained with Eq. (4):

$$\dot{E}_{D,k}^{AV} = \dot{E}_{D,k}^{real} - \dot{E}_{D,k}^{UN} \quad (4)$$

For the mixers, the deaerator and the condenser, no distinction between avoidable and unavoidable exergy destruction was made here.

2.2.3 Splitting avoidable and unavoidable exergy destruction into endogenous and exogenous parts

The unavoidable endogenous exergy destruction, $\dot{E}_{D,k}^{UN,EN}$, within the k^{th} component is calculated as:

$$\dot{E}_{D,k}^{UN,EN} = \dot{E}_{P,k}^{EN} \times \left(\frac{\dot{E}_D^*}{\dot{E}_P}\right)_k^{UN} \quad (5)$$

The exogenous unavoidable exergy destruction is calculated with Eq. (6).

$$\dot{E}_{D,k}^{UN,EX} = \dot{E}_{D,k}^{UN} - \dot{E}_{D,k}^{UN,EN} \quad (6)$$

The avoidable endogenous and the avoidable exogenous exergy destructions are then calculated by subtracting the unavoidable endogenous and unavoidable exogenous from the total endogenous and exogenous exergy destruction, respectively:

$$\dot{E}_{D,k}^{AV,EN} = \dot{E}_{D,k}^{EN} - \dot{E}_{D,k}^{UN,EN} \text{ and} \quad (7a)$$

$$\dot{E}_{D,k}^{AV,EX} = \dot{E}_{D,k}^{EX} - \dot{E}_{D,k}^{UN,EX} \quad (7b)$$

To identify the real potential for improving plant components, the sum of the avoidable exergy destruction caused by each component is calculated as:

$$\dot{E}_{D,k}^{AV,\Sigma} = \dot{E}_{D,k}^{AV,EN} + \sum_{\substack{r=1 \\ r\neq k}}^{n} \dot{E}_{D,r}^{AV,EX,k} \quad (8)$$

$\sum_{\substack{r=1 \\ r\neq k}}^{n} \dot{E}_{D,r}^{AV,EX,k}$ is the sum of the avoidable exogenous exergy destruction caused by component *k* within the remaining components. Each part of this sum is calculated for each component *r* separately, via the unavoidable exogenous exergy destruction, as in [11]:

$$\dot{E}_{D,r}^{UN,EN,r+k} = \dot{E}_{P,r}^{UN,EN,r+k} \left(\frac{\dot{E}_D^*}{\dot{E}_P}\right)_r^{UN} \quad (9)$$

$\dot{E}_{P,r}^{UN,EN,r+k}$ is the $\dot{E}_P$ of component *r*, when components *r* and *k* operate under real conditions and all remaining components operate under theoretical conditions.

The unavoidable exogenous exergy destruction, $\dot{E}_{D,r}^{UN,EX,k}$, in component *r* due to component *k* is calculated as:

$$\dot{E}_{D,r}^{UN,EX,k} = \dot{E}_{D,r}^{UN,EN,r+k} - \dot{E}_{D,r}^{UN,EN} \quad (10)$$

Finally, the avoidable exogenous exergy destruction of component *r* caused by component *k*, is found by subtracting its unavoidable exogenous exergy destruction from its total exogenous exergy destruction:

$$\dot{E}_{D,r}^{AV,EX,k} = \dot{E}_{D,r}^{EX} - \dot{E}_{D,r}^{UN,EX,k} \quad (11)$$

3. THE COMBINED CYCLE POWER PLANT

3.1 Process description

The power plant studied in this paper is a three-pressure-level combined cycle with one reheat stage. The plant has one product – electricity – and works with natural gas that was assumed here to be pure methane. The configuration of the process is shown in Figure 1. The thermodynamic variables for selected streams of the plant are shown in Table 2. The total exergy, $\dot{E}_{tot,j}$, includes both the chemical and physical exergy of each stream *j*.

High-temperature flue gas with a mass flow rate of 628 kg/s exits the plant's *gas turbine* (GT) and it is led to the *heat recovery steam generator* (HRSG), where it provides thermal energy to produce steam at three different pressure levels, 124, 22, and 4.1 bar. The combustion products enter the HRSG with a pressure of 1.058 bar at 580°C and are exhausted to the atmosphere at 95°C. The high-pressure steam at 560°C is expanded to 23 bar in the *high-pressure steam turbine* (HPST) and returns to the HRSG, where it is reheated to 560°C. The reheated steam is sent to the *intermediate-pressure steam turbine* (IPST), where it is expanded to 4.1 bar. This low-pressure steam is mixed with low-pressure superheated steam and it is then led to the *low-pressure steam turbine* (LPST), where it is expanded to 0.05 bar. The steam is condensed in the condenser, preheated, led to the deaerator of the plant and further conveyed to the feedwater pumps to continue the cycle.

4. RESULTS AND DISCUSSION

4.1 Exergetic analysis

Table 3, shows the main results obtained by the conventional exergetic analysis of the plant under consideration. The results of this analysis have been partly presented in previous publications [15,16]. Here, however, they are shown in a slightly different way, since the motors and generators used for pumps and turbines, respectively, are examined separately. Thus, the values presented here differ from those in the

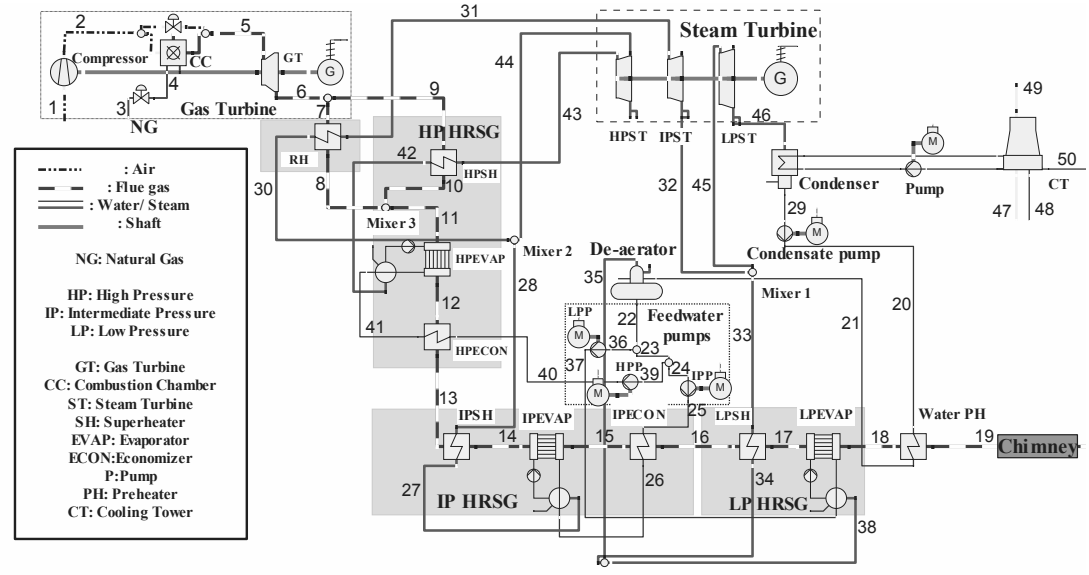

Fig. 1. Structure of the combined cycle power plant

Table 2: *Calculated variables for selected streams.*

Stream, j	$\dot{m}_j$ [kg/s]	T_j [°C]	p_j [bar]	$\dot{E}_{tot,j}$ [MW]
1	614.50	15.0	1.01	0.96
2	614.50	392.9	17.00	232.25
3	14.00	15.0	50.00	729.62
4	14.00	15.0	17.00	727.37
5	628.50	1264.0	16.49	741.01
6	628.50	580.6	1.06	189.87
7	268.50	580.6	1.06	81.11
8	268.50	447.6	1.05	54.64
9	360.00	580.6	1.06	108.75
10	360.00	449.3	1.05	73.68
11	628.50	448.6	1.05	128.33
12	628.50	341.2	1.04	84.69
13	628.50	257.9	1.04	55.77
14	628.50	257.3	1.04	55.59
15	628.50	237.6	1.04	49.49
16	628.50	234.1	1.04	48.43
17	628.50	229.3	1.04	47.01
18	628.50	156.4	1.03	27.98
19	628.50	95.3	1.03	16.49
20	94.58	32.9	3.73	0.47
21	94.58	135.6	3.62	8.18
22	95.41	140.0	3.62	8.79
23	72.43	140.0	3.62	6.67
24	7.22	140.0	3.62	0.67
25	7.22	140.5	25.13	0.68
26	7.22	216.6	24.38	1.56
27	7.22	222.6	24.38	7.23
28	7.22	237.9	23.16	7.35
29	94.58	32.9	0.05	0.44
30	72.43	305.1	23.16	79.53
31	72.43	560.6	22.00	103.42
32	72.43	317.2	4.10	66.03
33	22.15	214.1	4.10	18.01
34	22.15	146.4	4.32	16.96
35	0.83	146.4	4.32	0.63
36	22.97	140.0	3.62	2.12
37	22.97	140.0	4.32	2.12
38	22.97	146.4	4.32	17.60
39	65.21	140.0	3.62	6.01
40	65.21	141.8	134.56	6.96
41	65.21	325.2	130.53	31.88
42	65.21	331.2	130.53	71.79
43	65.21	560.6	124.00	103.51
44	65.21	313.2	23.16	72.22
45	94.58	293.0	4.10	83.86
46	94.58	32.9	0.05	12.87

Table 3. Calculated variables for selected components

Component, k	$\dot{E}_{F,k}$ [MW]	$\dot{E}_{P,k}$ [MW]	$\dot{E}_{D,k}$ [MW]	ε_k [%]	$y_{D,k}$ [%]
Compressor	242.67	231.30	11.38	95.31	1.56
CC	729.62	508.76	220.87	69.73	30.23
GT	551.15	535.06	16.09	97.08	2.20
Reheater	26.47	23.89	2.57	90.27	0.35
HPSH	35.07	31.72	3.35	90.45	0.46
HPEVAP	43.64	39.91	3.73	91.46	0.51
HPECON	28.92	24.91	4.00	86.16	0.55
IPSH	0.18	0.12	0.06	69.01	0.01
IPEVAP	6.10	5.67	0.43	92.92	0.06
IPECON	1.06	0.87	0.19	82.47	0.03
LPSH	1.43	1.04	0.38	73.27	0.05
LPEVAP	19.03	15.48	3.55	81.36	0.49
LPECON	11.49	7.71	3.78	67.07	0.52
HPST	31.29	29.62	1.67	94.67	0.23
IPST	37.39	35.75	1.65	95.60	0.23
LPST	70.99	62.29	8.71	87.73	1.19
Condensate	0.04	0.04	0.00	90.34	0.00
HP Pump	1.06	0.96	0.11	89.96	0.01
IP Pump	0.03	0.02	0.01	75.81	0.00
LP Pump	0.00	0.00	0.00	83.22	0.00
GT generator	292.38	288.00	4.39	98.50	0.60
ST generator	127.65	125.74	1.91	98.50	0.26
Condensate	0.04	0.04	0.01	87.20	0.00
HP Pump	1.12	1.06	0.06	94.80	0.01
IP Pump	0.03	0.03	0.00	86.20	0.00
LP Pump	0.00	0.00	0.00	80.70	0.00
Total	**730.58**	**412.54**	**304.01**	**56.47**	**41.61**

references. The exergy destruction ratio, $y_{D,k}$, provides information about the performance of each component and enables the comparison of dissimilar components. As shown in Table 3, the highest exergy destruction ratio is found for the components that constitute the GT system, with the *combustion chamber* (CC) having the highest value, followed by the HPHRSG, consisting of the *high-pressure superheater* (HPSH), the *high-pressure evaporator* (HPEVAP) and the *high - pressure economizer* (HPECON).

4.2 Advanced exergetic analysis

The results of the advanced exergetic analysis are shown in Table 4 and are obtained from Eqs. (1) and (3)-(7). When evaluating a plant, we mainly

focus on its avoidable exergy destruction, because it represents the potential for improvement. With the exception of the gas turbine and the HPST, the majority of the exergy destruction within the components of the plant is unavoidable. In particular, in the CC, 68% of the exergy destruction is unavoidable. Moreover, most of the overall exergy destruction of the plant is endogenous (84%). This means that component interactions, represented by the exogenous exergy destruction, do not play a significant role. Therefore, the focus should be on the improvement of internal inefficiencies of the components. Additionally, for the CC, the compressor, the IPST and LPST and the majority of the heat exchangers, most of the endogenous exergy destruction is unavoidable. In contrast, in the GT, the HPST and the generators of the plant, the avoidable part of the endogenous exergy destruction is larger than the unavoidable part. However, when the exogenous exergy destruction is split into avoidable and unavoidable parts, for most components (including the GT and the LPST), the unavoidable part is found to be larger. To determine which components should be improved first, we further split each component's exogenous exergy destruction into its source components. This separation results in a number of simulations totaling $n^2/2$, with n being the number of the components in the plant. The results for the components with the highest exogenous exergy destruction are shown in Table 5. The mexogenous exergy destruction is calculated using Eq. (2).

To better understand the improvement potential of the components, we calculate the variable $\dot{E}_{D,k}^{AV,\Sigma}$, as stated in Eq. (8) (Table 6). The total avoidable exergy destruction of component k, consists of both its avoidable endogenous exergy destruction and the avoidable exogenous exergy destruction it causes to the remaining components of the plant. The higher this value is, the higher the influence of the considered component on the overall system.

The negative values calculated for the exogenous exergy destruction (Table 4) are a result of a change in the mass flow rates when calculating the endogenous exergy destructions. For example, for the calculation of the endogenous exergy destruction of the IPSH, all other components are considered under theoretical conditions, while the superheater operates under real conditions. Due to the elimination of any pressure losses through the theoretical components, the operational pressure of the heat exchanger during the calculation of the E_D^{EN} is lower. These conditions result in an increased mass of steam flowing through the heat exchanger. Thus, the endogenous exergy destruction is found to be higher than the E_D^{real} and the E_D^{EX} negative. The negative E_D^{EX} of the GT generator is similarly justified. In the calculation of the E_D^{EN}, the power output of the steam cycle is decreased, due to the lower temperature of the combustion products entering the HRSG - a result of the high isentropic efficiency of the expander. With this lower temperature, the power of the steam turbines is reduced. To keep the overall power output of the process constant, the power output of the GT must increase. This is, however, determined by the mass flow, since the inlet temperature of the GT remains constant. With increased mass flow, the E_D^{EN} of the generator is higher than the E_D^{real}, resulting in a negative E_D^{EX}. Similar explanations can be used for the negative values of the $E_D^{UN,EX}$, since their calculation is dependent on the calculation of the $E_D^{UN,EN}$. When the exergy of the product, E_P^{EN}, increases in the simulation used for the calculation of the E_D^{EN} in comparison to the real case, the $E_D^{UN,EX}$ results in negative values. Generally, with the exception of the generators and motors that are influenced only by the components to which they are directly connected, to improve the overall system, the component with negative exergy destruction should operate with reduced performance.

The CC has the highest absolute value of exergy destruction, 68% of which cannot be avoided and only 13% of the unavoidable exergy destruction is exogenous. Thus, the remaining 87% of the unavoidable exergy destruction is due to the component itself, most of which cannot be avoided. Additionally, 51.6% of the exogenous exergy destruction in the CC stems from the GT and the compressor (Table 5), almost 33% (4.6 MW) of which is avoidable. In the GT and the compressor, the main part of the exergy destruction is also endogenous, i.e., caused internally by the operation of the components themselves, while the exogenous part is mainly imposed by the CC. However, a large part of the exogenous exergy destruction stemming from the CC is avoidable (41%).

The larger the influence of a component, the higher its improvement priority must be, if the improvement of the overall plant is considered. The CC is the component with the highest absolute value of exergy destruction, leading to the highest avoidable exergy destruction. The GT and the compressor follow in absolute values of avoidable exergy destruction.

In the first column of Table 6 the exogenous exergy destruction caused by each component is presented. As shown, the exogenous exergy destruction caused by the GT is almost double that caused by the CC. However, due to the significantly larger endogenous exergy destruction of the CC, its total avoidable exergy destruction is almost 6 times higher, when compared to that of the GT. When comparing the GT with the compressor, the GT causes double the exergy destruction in the plant, resulting in a higher absolute value of avoidable exogenous exergy destruction. Moreover, due to the doubled endogenous avoidable exergy destruction of the GT, its total avoidable exergy destruction is also almost double that of the compressor.

The results of the conventional exergetic analysis are strongly supplemented by the advanced exergetic analysis. Irreversibilities identified in the conventional exergetic analysis are split, according to their origins, in the advanced exergetic analysis. Only the part of the irreversibilities that can be avoided should be considered for the improvement of a plant with interacting processes.

Table 4. Selected results of the advanced exergetic analysis at the component level.

	$\dot{E}^{EN}_{D,k}$	$\dot{E}^{EX}_{D,k}$	$\dot{E}^{UN}_{D,k}$	$\dot{E}^{AV}_{D,k}$	$\dot{E}^{UN}_{D,k}$		$\dot{E}^{AV}_{D,k}$	
Component,					$\dot{E}^{UN,EN}_{D,k}$	$\dot{E}^{UN,EX}_{D,k}$	$\dot{E}^{AV,EN}_{D,k}$	$\dot{E}^{AV,EX}_{D,k}$
k	[MW]	[MW]	[MW]	[MW]	[MW]	[MW]	[MW]	[MW]
Compressor	6.95	4.43	6.26	5.11	3.80	2.46	3.15	1.96
CC	193.42	27.44	149.84	71.03	131.05	18.79	62.37	8.66
GT	13.55	2.54	7.77	8.32	6.25	1.52	7.30	1.02
Reheater	1.99	0.59	1.68	0.89	1.11	0.57	0.87	0.02
HPSH	1.79	1.56	2.48	0.87	1.30	1.18	0.49	0.38
HPEVAP	2.01	1.72	3.35	0.38	2.02	1.32	-0.02	0.40
HPECON	2.24	1.76	2.72	1.28	1.75	0.97	0.50	0.79
IPSH	0.09	**-0.03**	0.01	0.05	0.01	-0.01	0.07	**-0.03**
IPEVAP	0.41	0.02	0.28	0.15	0.25	0.03	0.16	**-0.01**
IPECON	0.16	0.02	0.12	0.07	0.18	-0.06	-0.01	0.08
LPSH	0.18	0.20	0.16	0.22	0.06	0.10	0.12	0.10
LPEVAP	1.69	2.05	2.98	0.76	1.66	1.32	0.03	0.73
LPECON	2.20	1.59	1.52	2.27	1.07	0.45	1.12	1.14
HPST	1.11	0.56	0.78	0.89	0.50	0.29	0.61	0.28
IPST	1.19	0.45	0.94	0.71	0.66	0.28	0.54	0.17
LPST	6.02	2.69	5.10	3.61	3.53	1.57	2.49	1.11
Condensate Pump	0.00	0.44	0.00	0.45	0.01	0.00	0.00	0.44
HP Pump	0.06	**-0.06**	0.05	**-0.05**	0.03	0.02	0.03	**-0.08**
IP Pump	0.01	0.02	0.00	0.02	0.01	0.00	0.00	0.02
LP Pump	0.00	0.11	0.00	0.10	0.00	0.00	0.00	0.10
GT generator	4.77	**-0.39**	1.45	2.94	1.57	-0.13	3.20	**-0.26**
ST generator	1.43	0.48	0.63	1.28	0.47	0.16	0.96	0.32
Condensate Pump Motor	0.00	0.01	0.00	0.00	0.00	0.00	0.00	0.01
HP Pump Motor	0.00	0.06	0.00	0.15	0.01	0.01	0.00	0.05
IP Pump Motor	0.00	0.00	0.02	0.04	0.00	0.00	**-0.01**	0.00
LP Pump Motor	0.00	0.15	0.00	0.00	0.00	0.00	0.00	0.15
Total	249.99	48.43						
Total (%)	**83.77**	**16.23**						

Table 5. Splitting of the exogenous exergy destruction.

Component, k	$\dot{E}_{D,k}^{EX}$ [MW]	*Component, r*	$\dot{E}_{D,k}^{EX,r}$ * [MW]	*Component, k*	$\dot{E}_{D,k}^{EX}$ [MW]	*Component, r*	$\dot{E}_{D,k}^{EX,r}$ [MW]
CC	27.44	GT	8.91	*LPECON*	1.59	LPEVAP	0.51
		Compressor	5.24			CC	0.25
		LPST	3.35			GT	0.12
		GT generator	2.17			Compressor	0.07
		LP EVAP	0.80			LPST	0.03
		mexo	**3.20**			**mexo**	**0.43**
Compressor	4.43	CC	3.27	*HPSH*	1.56	GT	0.92
		GT	0.29			CC	0.20
		LPST	0.11			Compressor	0.05
		GT generator	0.08			Reheater	0.03
		LP EVAP	0.03			LPST	0.03
		mexo	**0.52**			**mexo**	**0.32**
LPST	2.69	GT	1.06	*Reheater*	0.59	CC	0.23
		CC	0.70			HPSH	0.18
		Compressor	0.18			GT	0.15
		IPST	0.12			Compressor	0.06
		GT generator	0.07			IPSH	0.05
		mexo	**0.51**			**mexo**	**0.13**
GT	2.54	CC	1.12	*LPSH*	0.20	IP Evaporator	0.11
		Compressor	0.30			CC	0.02
		LPST	0.25			Reheater	0.02
		Generator GT	0.15			GT	0.02
		Generator STs	0.06			Deareator	0.01
		mexo	**0.39**			**mexo**	**0.05**
HPECON	1.76	HPEVAP	0.28	*LPEVAP*	2.05	IPEVAP	0.84
		CC	0.25			CC	0.19
		GT	0.22			GT	0.18
		Deareator	0.18			Reheater	0.14
		Compressor	0.07			IPSH	0.11
		mexo	**0.59**			**mexo**	**0.54**
HPEVAP	1.72	GT	0.85				
		CC	0.23				
		Reheater	0.11				
		IPEVAP	0.08				
		Compressor	0.06				
		mexo	**0.40**				

5. CONCLUSIONS

In this paper, a complex energy conversion system, a combined cycle power plant, has been analyzed using both conventional and advanced exergetic analyses. The exergetic analysis uses variables that reveal the components with the highest exergy destruction. More specific insight, however, about component interactions and the improvement potential of the plant is revealed by the advanced exergetic analysis.

The highest exergy destruction is caused by the CC. Almost 87% of the total exergy destruction

* $\dot{E}_{D,k}^{EX,r}$: Exogenous exergy destruction within component *k* caused by component *r*.

there results from the chemical reaction (*endogenous exergy destruction*) and 68% of the total exergy destruction cannot be avoided (*unavoidable exergy destruction*). In total, there is some improvement potential for the overall plant, most of which is related to the internal operating conditions of the components (*endogenous exergy destruction*), while component interactions (*exogenous exergy destruction*) are less significant. Considering the avoidable exergy destruction caused by each component both to itself and the remaining components of the plant, the results are well justified. Similar to the results of the conventional analysis, the advanced analysis ranks the improvement priority of the CC first, followed by the GT expander and the compressor. When considering the total avoidable exergy destruction of each component, the GT and the compressor increase in importance moving closer to the CC. This results from the high avoidable exergy destruction of these two components.

An advanced exergetic analysis is a valuable supplement to a conventional exergetic analysis. The application of the conventional and advanced exergoeconomic analyses is the next step of this study and will be presented in a subsequent paper.

Table 6. Total avoidable exergy destruction caused by component k (Eq. 8).

Component, k	$\sum_{\substack{r=1 \\ r\neq k}}^{n} \dot{E}_{D,r}^{EX,k}$ [MW]	$\sum_{\substack{r=1 \\ r\neq k}}^{n} \dot{E}_{D,r}^{EX,AV,k}$ [MW]	$\dot{E}_{D,k}^{EN,AV}$ [MW]	$\dot{E}_{D,k}^{AV,\Sigma}$ [MW]
CC	7.8	3.60 (5%)	62.37 (95%)	**65.97**
GT	14.9	4.95 (40%)	7.30 (60%)	**12.26**
Compressor	6.4	2.32 (42%)	3.15 (58%)	**5.47**
LPST	4.0	1.84 (43%)	2.49 (57%)	**4.34**
LPEVAP	1.0	0.53 (95%)	0.03 (5%)	**0.56**
HPECON	0.0	0.01 (2%)	0.49 (98%)	**0.51**
HPSH	0.5	0.20 (33%)	0.49 (67%)	**0.73**
LPSH	0.2	0.08 (32%)	0.12 (68%)	**0.18**

REFERENCES

[1] Bejan A., Tsatsaronis G., Moran M., 1996, *Thermal design and optimization*, John Wiley., USA.

[2] Tsatsaronis, G., 1999, *Design optimization using exergoeconomics* in Thermodynamic Optimization of Complex Energy Systems, Bejan A. and Mamut E., eds., Kluwer Academic Publishers, Dordrecht, Boston, London. pp. 101-115.

[3] Tsatsaronis, G., 2002, Cziesla, F., *Thermoeconomics* in Encyclopedia of Physical Science and Technology, 3rd Edition, Volume 16, Academic Press, pp. 659-680.

[4] Lazzaretto, A. and Tsatsaronis, G.**,** 2006, SPECO: a systematic and general methodology for calculating efficiencies and costs in thermal systems, Energy, 31, pp. 1257–1289.

[5] Tsatsaronis G. and Cziesla F., 2009, Six articles published in *Exergy, Energy Systems Analysis and Optimization* as part of the: Encyclopedia of Life Support Systems (EOLSS), developed under the Auspices of UNESCO, Eolss Publishers, Oxford, UK, 2009, Vol. 1, pp. 34-146.

[6] Tsatsaronis, G., Park, M.H., 2002, On avoidable and unavoidable exergy destructions and investment costs in thermal systems, Energy Conversion and Management, 43. pp. 1259–1270.

[7] Cziesla, F., Tsatsaronis, G., Gao, Z., 2006, Avoidable thermodynamic inefficiencies and costs in an externally fired combined cycle power plant, Energy – The International Journal, 31(10–11), pp. 1472–1489.

[8] Tsatsaronis, G., Kelly, S., Morosuk, T., 2006, Endogenous and exogenous exergy destruction in thermal systems, *Proceedings of the ASME IMECE*, [CD-ROM], 2006-13675 Chicago, USA.

[9] Kelly, S., 2008, Energy systems improvement based on endogenous and exogenous exergy destruction, Ph.D. Thesis, Technische Universität Berlin, Germany.

[10] Tsatsaronis, G., Morosuk, T., 2007, Advanced exergoeconomic evaluation and its application to compression refrigeration machines, *Proceedings of the ASME IMECE*, File IMECE2007-41202, Seattle, USA.

[11] Morosuk, T., Tsatsaronis, G., 2008, How to Calculate the Parts of Exergy Destruction in an Advanced Exergetic Analysis in: A. Ziebik, Z.Kolenda, W.Stanek, eds., *Proceedings ECOS 2008*, Cracow-Gliwice, Poland, pp. 185-194.

[12] Tsatsaronis, G., and Morosuk, T., 2008, A general exergy-based method for combining a cost analysis with an environmental impact analysis. Part I – Theoretical Development, *Proceedings of the ASME IMECE*, File IMECE2008-67218, Boston, USA.

[13] Tsatsaronis, G., and Morosuk, T., 2008, A general exergy-based method for combining a cost analysis with an environmental impact analysis. Part II – Application to a cogeneration system, *Proceedings of the ASME IMECE*, file IMECE2008-67219, Boston, USA.

[14] Tsatsaronis, G., 1999, Strengths and limitations of exergy analysis, *Thermodynamic optimization of complex energy systems*, Bejan, A. and Mamut, E., eds., Dordrecht: Kluwer Academic Publishers, pp. 93–100.

[15] Petrakopoulou F., Boyano A., Cabrera M., Tsatsaronis G., 2009, Exergoeconomic and exergoenvironmental analyses of the AZEP concept, a combined cycle power plant with CO_2 capture, *Proceedings of The 8th International Conference on Sustainable Energy Technologies* (SET), Aachen, Germany, CD-ROOM.

[16] Petrakopoulou F., Boyano A., Cabrera M., Tsatsaronis G., 2009, Exergoeconomic and exergoenvironmental analyses of a combined cycle power plant with chemical looping technology, *Proceedings of The 5th Trondheim Conference on CO_2 Capture, Transport and Storage*, Trondheim, Norway, CD-ROOM.

Thermodynamics and Optimization of Combined Heat and Power Systems : Comparison of various Systems

M. Feidt

LEMTA, UMR CNRS 7563, University Henri Poincaré, Nancy, France
Tél. 03.83.59.57.34, Fax 03.83.59.56.16 michel.feidt@ensem.inpl-nancy.fr

Abstract: In the present paper, we intent to compare various C.H.P. systems configurations (vapour turbine, T.V. ; gas turbine, G.T. ; Internal Combustion Engine, I.C.E. ; External Combustion Engine (Stirling, Ericsson), E.C.E. ; fuel cells, F.C…), regarding thermodynamical criterions : first law efficiency, exergy efficiency.

Thermodynamics optimization of these systems is performed relative to maximization of useful exergy, and various practical related constraints (imposed mechanical useful energy ; imposed heat demand ; imposed heat to power ratio) or main physical limitations (limited heat availability ; maximum system temperature allowed : thermomechanical constraints). A sensitivity analysis to model parameters is given. Main conclusions and recommendations are reported.

Keywords: Thermodynamics, Optimization, C.H.P. Combined Heat and Power systems.

1. Introduction

In the recent past, due to environment impact considerations and energy efficient uses purposes, a renewal and development of combined heat and power systems is growing up [1, 2, 3] ; even for small scale C.H.P. systems. New configurations of C.H.P. systems are studied : among them PV/T configuration [4] ; fuel cells C.H.P. systems [2, 3]. Also the fuel disposal is considered, mainly various biomass availabilities [5]. The question is to validate the various proposed alternatives ; for that purpose a lot of criterions exist. Multicriteria evaluations according to weighting methodologies have been proposed recently [6] . Economic analysis of three micro C.H.P. applications (engine ; gas turbine ; Fuel Cell) has been performed [7]. More recently heat production by cogeneration or heat pump were compared [8] according to the first law efficiency criterion. Exergy optimization has been also performed in the recent past [9], but for a vapour turbine configuration.

Perspectives of the proposed Thermodynamics approach are finally given in direction of cold cogeneration systems, trigenerations system, and also extension to polygeneration systems. These concepts and methodologies could help to a better design, management and integration of these systems in the future, regarding also environmental and economical concerns.

2. Modeling of various CHP systems

We consider here exclusively combined hot Heat and Power systems. But even in this particular case various processes are possible, characterized by systems or cycles referring to different technics [10]. The first one to be developed was with vapour turbines ; it appears that this engine is externally fired (by a boiler or generator). Other kind of external combustion engines will be considered hereafter, like Ericsson and Stirling ones.

C.H.H.P. systems well developed today are also composed of internal combustion engines from various size starting from 1 kw_{elec} to more than 1 MW for industrial or urban applications.

The third main systems category used is based on gas turbines ; in that case postcombustion could be used.

To these categories have been added some more recent ones using Fuel Cells, or Solar photovoltaïcs arrays for example. We deliberately limit, at first, to the main categories, Vapour Turbines V.T., External Combustion Engines E.C.E., Internal Combustion Engines I.C.E., and Gas Turbines G.T. All these systems are thermomechanical systems ; each system consist of a hot heat source. The heat is obtained burning a fuel, whatever is the fuel. Mechanical and

electrical power is produced inside an engine (the machine). According to second law, the machine gives back heat to a cold sink (U.E., useful energy), before rejecting the remaining heat to the ambiance at T_0, reference temperature.

We intent to compare hereafter the performances of the 4 main engines acting as C.H.H.P. machines. They are represented respectively by the Carnot, Stirling (Ericsson), Otto or Diesel, and finally Brayton-Joule cycle [11], but we develop the model starting from equilibrium Thermodynamics, to go to more insight in the representation of the C.H.H.P. system (heat losses; irreversibilities) and in also various possible performances criterions (section 3.), and constraints associated to the objective function to optimize (section 4.)

3. Criterions and optimizations

The proposed models are subject to steady state (nominal) hypothesis : the two useful effects of C.H.H.P. systems are $\dot{w}$, the mechanical power (negative with the proposed sign convention) and $\dot{q}_U$, the useful hot flux (negative too). The convention is : each quantity entering the machine is a positive one, and the opposite (negative one) for each leaving quantity.

However the machines are non adiabatic. There are thermal losses. As a first attempt lumped analysis implies that these losses can be represented as an equivalent one between the hottest point of the system, and the coldest one. They are summarized as $\dot{q}_L$, heat flux loss between the hot and cold side (positive quantity).

3.1. First law criterion, $\eta_{I\,CHP}$

Whatever is the engine, the energy balance corresponds to :

$$\dot{q}_H + \dot{w} + \dot{q}_U + \dot{q}_L = 0 \qquad (1)$$

$\dot{q}_{SH}$, hot heat flux consumed (E.C., energy consumption, $\dot{q}_{SH} = \dot{q}_H + \dot{q}_L$).

$\dot{q}_H$, hot heat flux entering the converter.

The first law efficiency $\eta_{I\,CHP}$ is given by the ratio of U.E. useful energy divided by E.C. ; so, it comes :

$$\eta_{I\,CHP} = -\frac{\dot{w} + \dot{q}_U}{\dot{q}_{SH}} = 1 - \frac{\dot{q}_L}{\dot{q}_{SH}} \qquad (2)$$

The consequence is, that the first law implies only an “adiabaticity efficiency” whatever is the thermomechanical C.H. P. system. If the system is without loss, the limit $\eta_{I\,CHP}$ is one, whatever is the system ; but it is to note that if it could be for external combustion engines (see Fig. 1 a, b),

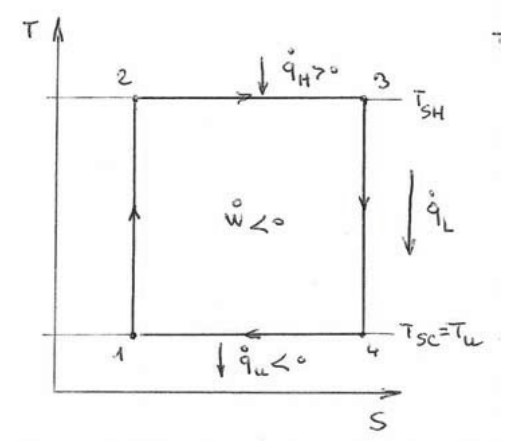

(a) Carnot cycle

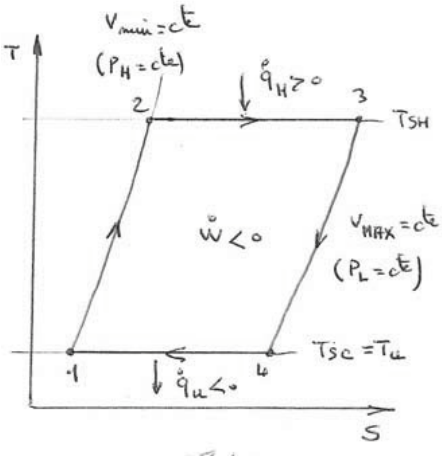

(b) Stirling (Ericsson) cycle

Fig. 1. Equilibrium Thermodynamics of C.H.H.P. Thermomechanical (E.C.E.)

it is not the case of internal combustion engines (see Fig. 1 c, d), due to the fact that corresponding engines are open systems and $T_U > T_0$; so that heat

losses to ambient appear : these dissimilarities are due to the fact that in case a and b useful heat could be delivered at constant temperature (T_{SC} = T_U) ; that is not the case for c and d (finite heat source effect).

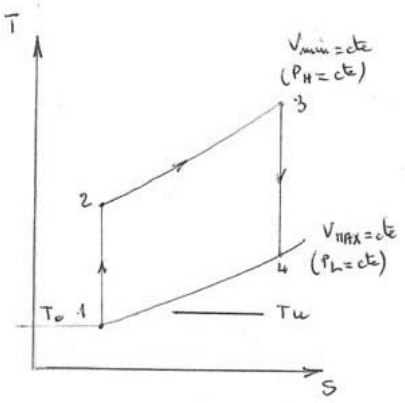

(c) Otto (Diesel) cycle

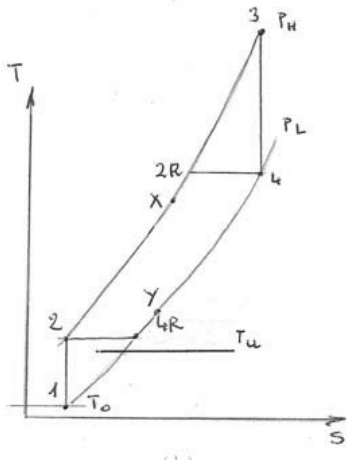

(d) Joule cycle

Fig. 1. Equilibrium Thermodynamics of C.H.H.P. thermomechanical engines (I.C.E.)

To conclude the temperature level of the useful heat appears important ; it is why exergetic criterions have to be considered :

3.2. Exergetic criterions η_{ex}

Whatever is the engine, the useful exergy flux is :

$$\dot{E}x_U = \dot{w} + \left(1 - \frac{T_0}{T_U}\right)\dot{q}_U \qquad (3)$$

This corresponds to useful thermal exergy from the point of view of external utility (and not the cycled fluid). This remark confirms the difference between E.C.E. and I.C.E. as said in section 3.1

We intent hereafter to precise the difference between the machine (engine) and the system from the exergetic point of view. To explicit this difference in case of endoirreversible thermodynamic approach, we write the two entropy balances. For the two E.C.E. it comes :

- For the engine :

$$\frac{\dot{q}_H}{T_{SH}} + \frac{\dot{q}_U}{T_U} + \dot{s}_i = 0 \qquad (4)$$

- For the non adiabatic system :

$$\frac{\dot{q}_{SH}}{T_{SH}} + \frac{\dot{q}_U - \dot{q}_L}{T_0} + \dot{s}_t = 0 \qquad (5)$$

$\dot{s}_i$, internal created entropy flux of the engine.

$\dot{s}_t$, total created entropy flux of the system including source and sink (the hypothesis is that the useful heat is at the end delivered to the environment).

Combining (4) –(5) it results after some simple calculations the s_t value of the C.H.H.P. system :

$$\dot{s}_t = \dot{s}_i + \dot{q}_L\left(\frac{1}{T_0} - \frac{1}{T_{SH}}\right) - \dot{q}_u\left(\frac{1}{T_0} - \frac{1}{T_u}\right)$$

With $\dot{E}x_C$, the exergy flux consumed = $\dot{q}_{SH}\left(1 - \frac{T_0}{T_{SH}}\right)$.

This result confirms that irreversibilities $\dot{I}_i = T_0\,\dot{s}_i$ have a negative impact on the exergy efficiency of the system.

The exergy efficiency of the engine differs slightly due to the fact that $\dot{E}x_C$ moves from the preceding value to $\dot{E}x_C = \dot{q}_H\left(1 - \frac{T_0}{T_{SH}}\right)$. The same methodology will be applied to I.C.E. hereafter.

3.3. General optimization procedure

With the same hypothesis as adopted in section 2., we develop here a two heat conductances model

corresponding to the one proposed by B. Sahin et A. Kodal [12].

In place of the irreversibility ratio method used, we report the endoreversible case, and basic configuration of the C.H.H.P. vapour turbine system without losses, to examplify. External Heat transfer irreversibilities appears at source and engine contact, and at engine and sink contact (Fig. 2).

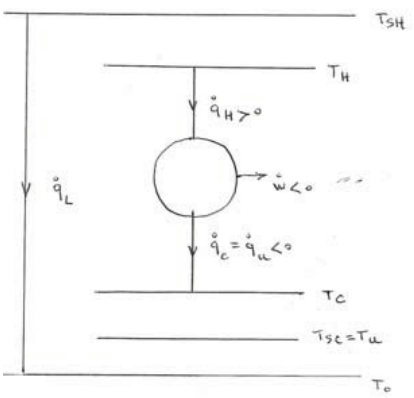

Fig. 2. Schematic of the temperature distribution in a C.H.H.P. Carnot system

It comes for the engine entropy balance :

$$\frac{\dot{q}_H}{T_H}+\frac{\dot{q}_U}{T_C}=0 \qquad (6)$$

It is clear that energy efficiency (equal to one) does not depend on T_U, nor T_H, T_C, but system exergy efficiency becomes (combining 1, 3, 6) :

$$\eta_{exCHPS}=\left(1-\frac{T_0\,T_C}{T_U\,T_H}\right)/\left(1-\frac{T_0}{T_{SH}}\right) \qquad (7)$$

If $\dot{q}_H=\dot{q}_{SH}$ is imposed, the maximum of efficiency gives back the equilibrium case ($T_C = T_{SC}$; $T_H = T_{SH}$). But the necessary finite rate heat transfer imposes through the entropy balance a constraint between the two degrees of freedom (T_C, T_H).

If we suppose as an example the linear law heat transfer case

$$(\dot{q}_H=K_H\,(T_{SH}-T_H)\,;\dot{q}_C=K_C\,(T_U-T_C)) \quad ,$$

optimization with respect to T_C, T_H gives using lagrangian method (variational calculus see 14 and 17 for details) :

$$\frac{T_C}{T_U}=\frac{T_H}{\sqrt{T_{SH}\,T_0}} \qquad (8)$$

$$T_{H\,opt}=\frac{\sqrt{T_{SH}\,T_0}+\frac{K_H}{K_C}T_{SH}}{1+\frac{K_H}{K_C}} \qquad (9)$$

K_H, K_C parameters associated to a given design.

Consequently we obtain :

$$\left|\dot{E}\,x_{U\,opt}\right|=\frac{K_H\,K_C}{K_H+K_C}\left(\sqrt{T_{SH}}-\sqrt{T_0}\right)^2 \qquad (10)$$

Optimal exergy does not depend on the level of T_U.

If we impose a constrained dimension for the system : $K_H + K_C = K_T$, a maximum of useful exergy is obtained at equipartition of the heat transfer conductances (endoreversible case) :

$$K_H{}^*=K_C{}^*=\frac{K_T}{2}$$

$$MAX\left|\dot{E}\,x_{U\,opt}\right|=\frac{K_T}{4}\left(\sqrt{T_{SH}}-\sqrt{T_0}\right)^2 \qquad (11)$$

Remark : if lim $T_C = T_U$ is considered (Chambadal – Novikov limit), K_C tends to infinity, $T_H{}^* = \sqrt{T_0\,T_{SH}}$ whatever is K_H ; numerically we suppose T_{SH} = 2000 K, T_0 = 300 K, so $T_H{}^*$ = 100 $\sqrt{60}$ ≈ 775 K, near of the common values used today.

4. Optimization with constraints

The use and design of a C.H.H.P. system is characterized by the ratio of useful heat flux, to useful power $R=\dot{q}_U/\dot{w}$. Two other parameters can be added to this one corresponding to the two possible priorities, the needed power, $\dot{w}_0$, or the needed useful heat $\dot{q}_{U0}$. The last more significant case could be the hot source heat flux availability limited to $\dot{q}_{SH0}$.

All these situations correspond to one technical added constraints that suppresses one degree of freedom for the optimization.

We consider hereafter, these four situations, and give new corresponding results for the Carnot endoreversible C.H.H.P. system without heat losses.

4.1. Carnot C.H.H.P. system with R imposed

From a general point of view optimizing energy C.H.H.P. efficiency is the same as optimizing engine efficiency. After some simple calculations, it comes for the endoreversible system :

$$\frac{T_C}{T_H} = \frac{R_0}{1+R_0} \tag{12}$$

R_0 imposed value of the R ratio whatever is the heat transfer law, and the available heat flux at hot source. In the limit of equilibrium thermodynamics relation (12) becomes :

$$\frac{T_U}{T_{SH}} = \frac{R_0}{1+R_0} \tag{13}$$

So the ratio R_0 is fundamentally related, to the Carnot efficiency of the engine according to

$$R_0 = 1 - 1/\eta_C$$

If we consider again linear heat transfer law (K_H, K_C, parameters), the corresponding useful exergy flux becomes :

$$\dot{E}x_U = -\frac{K_H K_C}{K_H + K_C}\left(T_{SH} - T_U.X_0\right)\left(1 - \frac{T_0}{T_U.X_0}\right) \tag{14}$$

with $X = \dfrac{1+R_0}{R_0}$

It is easy to demonstrate that optimum optimorum of useful effect is again given by (11), but that at the optimum R_0, T_U, T_{SH} are interrelated by :

$$\frac{1+R_0}{R_0} T_U = \sqrt{T_{SH}\, T_0} \tag{15}$$

This important relation means that :

T_{SH} being parameter, R_{0opt} satisfies relation (15) for a chosen T_U or T_{Uopt} satisfies (15) for an imposed R_0.

4.2. Carnot C.H.H.P. system with $\dot{w}$ imposed

Here we use the same methodology as for engine optimization [13], but adding the constraint $w = \dot{w}_0$, it appears the intermediate variable α

$$\alpha = \frac{X_H}{T_H} = \frac{T_{SH} - T_H}{T_H} = \frac{T_C - T_U}{T_C} \tag{16}$$

The optimum of $\dot{E}x_U$ corresponds to equipartition of heat transfer conductances, and α_{opt} satisfies the following equation :

$$\alpha^2\left[K_T\left(T_{SH} + T_U\right) + 2\dot{w}_0\right] - \alpha\left[K_T\left(T_{SH} - T_U\right)\right] - 2\dot{w}_0 = 0 \tag{17}$$

The equilibrium thermodynamics limit is straight forward ($\dot{w}_0 = 0$) : the corresponding limit of energy and exergy efficiency tends to one, with adiabaticity and reversibility.

If $\dot{w}_0 << K_T(T_{SH} + T_U)$, an interesting limit appears:

$$\alpha_{opt} \approx \frac{-2\dot{w}_0}{K_T\left(T_{SH} - T_U\right)} \tag{18}$$

And the corresponding approximated $\dot{E}_{X\,U\,opt}$:

$$\dot{E}x_{U\,opt} \approx \dot{w}_0 \frac{T_{SH} - T_0}{T_{SC} - T_U} \tag{19}$$

We conclude that the optimized useful exergy is proportional to the imposed power $\dot{w}_0$, but nearly amplified by the temperature ratio $(T_{SH} - T_0)/(T_{SH} - T_U)$.

4.3. Useful heat flux imposed

Here, priority is to the heat utility such that $\dot{q}_U = \dot{q}_{U0}$. Using the same way as in section 4.2., the optimum of $\dot{E}x_u$ corresponds always to equipartition of heat transfer conductances, but α_{opt} becomes :

$$\alpha_{opt} = \frac{-2\dot{q}_{U0}}{K_T T_U - 2\dot{q}_{U0}} \quad (20)$$

The corresponding $\dot{E}x_{U\,opt}$ is equal to :

$$\dot{E}x_{U\,opt} = \dot{q}_{U0} \cdot \frac{K_T (T_{SH} - T_0) + 4\dot{q}_{U0} T_0 / T_U}{K_T T_U - 4\dot{q}_{U0}} \quad (21)$$

It is easy to show that, it exists an optimum optimorum, that imposes :

$$\dot{q}_{U0\,opt} = \frac{K_T T_U}{4}\left(\sqrt{\frac{T_{SH}}{T_0}} - 1\right) \quad (22)$$

It gives again the relation (11) for $MAX\left|\dot{E}x_{U\,opt}\right|$

4.4 Energy consumption imposed

The consumed heat flux is $\dot{q}_{SH} = \dot{q}_{SH0}$. The useful flux associated is at conductances equipartition :

$$\left|\dot{E}x_{U\,opt}\right| = \dot{q}_{SH0}\left(1 - \frac{T_0}{T_{SH} - 4\dot{q}_{SH0}/K_T}\right) \quad (23)$$

Here again a maximum maximorum exists and corresponds to

$$\dot{q}_{SH0\,opt} = \frac{K_T}{4}\left(\sqrt{T_{SH}} - \sqrt{T_0}\right)\sqrt{T_{SH}} \quad (24)$$

It restitutes always the relation (11) for $MAX\left|\dot{E}x_{U\,opt}\right|$.

4.5. Partial conclusion

The conclusion with the section 4 is that in presence of constraints the optimum of the useful exergy function is given by specific relations (14), (21), (23), and that the optimum optimorum corresponds to special values of the constrained parameters giving back relation (11) ; $MAX\left|\dot{E}x_{U\,opt}\right|$ does not depend on T_U, but is proportional to K_T related to the size of the system. Lastly an interesting constraint is $T_{SH} = T_{MAX}$ (due to material limitation). We have seen that $MAX\left|\dot{E}x_{U\,opt}\right|$ is increasing of T_{SH}, in the limit T_{MAX} imposed by materials. However for a non adiabatic system, a new optimum exists, limited by the stagnation temperature of the system [14].

These extensions will be summarized hereafter (section 5).

5 Discussion – Comparisons

Due to lack of place, we examplify the results with some tables given hereafter, and corresponding comments.

Extensive examination of C.H.H.P. configurations using thermo-equilibrium thermodynamics does not exhibits optima for the studied systems ; moreover first law efficiencies are not appropriate to qualify performance of these systems : exergetic efficiencies are recommended.

5.1 Thermodynamic optimization of CARNOT C.H.H.P. systems

Contrarily, if we consider the Finite Dimensions of the systems, and use the preconized criterions, optimum configurations exist, relative to temperature distribution and design variables of the system (heat transfer conductances ; heat flux rate ; heat exchanger effectiveness).

The proposed model include heat losses from the system to ambiance, and also internal irreversibilities of the converter. Two ways are possible, through entropy flux created inside the system $\dot{s}_i$, or through an irreversibility ratio, the most used irreversibility representation. Reference [14] reports on these extensions for Carnot C.H.P. system.

Table 1 gives the obtained results for the Carnot adiabatic C.H.H.P. system and considering I, the irreversibility ratio, under various proposed added constraints. It comes from this Table that the optimal allocation of heat transfer conductances does not depend on the added constraints. In every case, the results differs from equipartition :

$$K_{H\,opt} = \frac{K_T}{\sqrt{I+1}} < K_{C\,opt} = \frac{K_T\sqrt{I}}{\sqrt{I}+1} \quad (25)$$

The optimal internal temperature of the cycled fluid depends on the added constraint ; $T_{H\,opt}$ is non dependent of T_U, except when the ratio $R = R_0$ is imposed.

The objective function studied is logically the useful exergy flux $\dot{E}\,x_U$, whose optimal value is depending on the studied case, as given in Table 1.

Table 1. Carnot C.H.H.P. system optimization, with added constraint, and irreversibility ratio method

optimum / added constraint	$T_{H\,opt}$	$T_{C\,opt}$	$\left\lvert \dot{E}\,x_U \right\rvert_{opt}$
without	$\sqrt{IT_{SH}}\sqrt{\frac{\sqrt{T_{SH}}+\sqrt{T_0}}{\sqrt{I}+1}}$	$\frac{T_U}{\sqrt{T_0}}\cdot\frac{\sqrt{T_{SH}}+\sqrt{T_0}}{\sqrt{I}+1}$	$\frac{K_T}{\left(\sqrt{I}+1\right)^2}\left(\sqrt{T_{SH}}-\sqrt{IT_0}\right)$
$\dot{q}_H=\dot{q}_{H0}$	$T_{SH}-\frac{\dot{q}_{H0}}{K_H}$	$T_U\frac{1}{1-I\frac{\dot{q}_{H0}}{K_C T_H}}$	$\dot{q}_{H0}\left[1-\frac{IT_0}{T_{SH}-\frac{\dot{q}_{H0}\left(1+\sqrt{I}\right)^2}{K_T}}\right]$
$R=R_0$	$\frac{\sqrt{I}}{1+\sqrt{I}}\left(T_{SH}+T_U\sqrt{I}\frac{1+R_0}{R_0}\right)$	$\frac{1}{1+\sqrt{I}}\left[\frac{R_0}{(1+R_0)\sqrt{I}}T_{SH}+T_U\right]$	$\frac{K_T}{\left(\sqrt{I}+1\right)^2}\left[T_{SH}-I\frac{1+R_0}{R_0}T_U\right]\left[1-\frac{R_0T_0}{(1+R_0)T_U}\right]$
$\dot{w}=\dot{w}_0$	$\frac{T_{SH}}{1+\frac{\alpha_{opt}}{\sqrt{I}}}$	$\frac{T_U}{1-\alpha_{opt}}$	$-\dot{w}_0+\frac{K_TT_U\sqrt{I}}{1+\sqrt{I}}\left(1-\frac{T_0}{T_U}\right)\cdot\frac{\alpha_{opt}}{1-\alpha_{opt}}$
$\dot{q}_U=\dot{q}_{U0}$	$\frac{T_{SH}}{1+\frac{\alpha_{opt}}{\sqrt{I}}}$	$\frac{T_U}{1-\alpha_{opt}}$	$\frac{K_TT_{SH}}{1+\sqrt{I}}\cdot\frac{\alpha_{opt}}{\sqrt{I}+\alpha_{opt}}+\dot{q}_{U0}\frac{T_0}{T_U}$

The maximum maximorum of $\left\lvert \dot{E}\,x_U \right\rvert$ corresponds to :

$$\left\lvert \dot{E}\,x_U \right\rvert = \frac{K_T}{\left(\sqrt{I}+1\right)^2}\left(\sqrt{T_{SH}}-\sqrt{IT_0}\right)^2 \qquad (26)$$

It is to be noted, that this value does not depend on T_U, the useful temperature level of the heat ; the same conclusion holds, if we choose the entropy flux method

$$\left\lvert \dot{E}\,x_U \right\rvert = \left[K_T-\dot{s}_i\frac{\sqrt{T_{SH}}+\sqrt{T_0}}{\sqrt{T_{SH}}-\sqrt{T_0}}\right]\frac{\left(\sqrt{T_{SH}}+\sqrt{T_0}\right)^2}{4} - \sqrt{T_0}\,\dot{s}_i\frac{\sqrt{T_{SH}}+\sqrt{T_0}}{2} \qquad (27)$$

Complementary results have been published, when the C.H.H.P. system is a non adiabatic ones. In that case, the maximum attainable temperature of the system, the stagnation temperatureT_S is a useful quantity to be introduced : a new compromise between the heat transfer conductances and the heat losses has been defined (see reference [14] for some details).

5.2 Other C.H.H.P. configurations optimization

As can be seen figure 1, Stirling or Ericsson C.H.H.P. system are also externally fired ; so results have great similarity with the previous examined ones (section 4). Complementary results could be find in a recent report [15].

Contrarily Otto (Diesel) C.H.H.P. systems, as well as Joule C.H.H.P. systems are internally fired. Due to this similarity, we give hereafter an insight to a combustion turbine C.H.H.P. system, to be optimized with the added constraint of T_{MAX}, maximum temperature imposed : it is well known, that this condition is actually the more limiting one for gas turbines, in order to preserve material properties.

Details of the model could be find in a recent published paper [16]. The heat exchangers model used is the (NTU, effectiveness) model : the corresponding effectiveness are ε_R for recuperator and ε_U for the useful heat exchanger.

It comes the following relation for optimal temperatures according to figure 1.d :

$$T_X = \varepsilon_R.T_4 + (1-\varepsilon_R).T_2$$

$$T_Y = T_4.(1-\varepsilon_R) + \varepsilon_R T_2$$

$$T_2 = \frac{T_{MAX}.T_0}{kT_4}$$

With $k = \exp\left[-\dot{s}_i/\dot{C}\right]$

$$T_{4opt} = T_0\sqrt{\frac{1-\varepsilon_R\varepsilon_U\left(t_U-1\right)}{1+\varepsilon_U\left(1-\frac{1}{t_U}\right)\left(\varepsilon_R-1\right)}\cdot\frac{t_{MAX}}{k}}$$

The corresponding $MAX\left\lvert \dot{E}\,x_U \right\rvert$ is :

$$MAX\left\lvert \dot{E}\,x_U \right\rvert = \frac{\dot{C}}{e}(e-1)\left(T_{MAX}-T_0\right)$$

With

$$e = \sqrt{\left[1 - \varepsilon_R \varepsilon_u \left(t_U - 1\right)\right]\left[1 + \varepsilon_U \left(1 - \frac{1}{t_U}\right)\left(\varepsilon_R - 1\right)\right]}$$

The figures 2 and 3, illustrate the influence of T_U level on the optimum T_4 optimum temperature at the turbine exit : if T_U increases, the optimal T_4 temperature diminishes. $T_{4\ opt}$ otherwise increases with the allowed T_{MAX} (figure 2), and decreases significantly with the internal irreversibility of the turbine (figure 3).

These models are presently in due course of development.

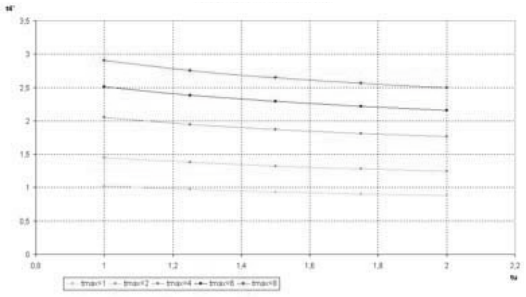

Fig.3. Evolution of t_4^* in function of t_U for t_{MAX} variable

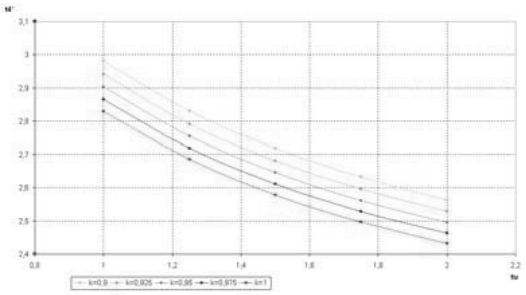

Fig.4. Evolution of t_4^* in function of t_U for k variable

6. Conclusion

6.1. Thermodynamics of Combined Heat and Power Systems has been reviewed, with a focus on C.H.H.P. (Combined Hot Heat and Power Systems) and particularly the most common one to say thermomechanical ones : two main categories are proposed :

- E.C.E., External Combustion Engine
- I.C.E., Internal Combustion Engine

6.2. Optimization criterions for these systems are reviewed. It is confirmed that first law efficiency criterion are only representative of the adiabaticity of the system (thermal losses). So it is preconized to prefer exergy efficiencies, that takes account of the heat quality, and qualify too the irreversibilities of the converter (engine), or of the system depending on the model used (section 3.2).

6.3. Optimization could be performed only if the finite size of the system is considered ; equilibrium thermodynamics don't furnish optima. The finite size optima obtained are coherent with the observed one.

6.4. Various significant added constraints have been proposed, that are useful for the design of specific systems and allows to precise the influence on design of model main parameters ; the main constraints are imposed ratio R, imposed useful power $\dot{w}_0$ (electrical or mechanical priority), imposed useful heat flux $\dot{q}_{U0}$ (heat demand priority), lastly imposed available source heat flux $\dot{q}_{SH0}$. Main tendencies for Carnot C.H.H.P. system are given (Table 1).

The maximum maximorum useful energy flux, for the Carnot C.H.H.P. system has been obtained as :

$$MAX\left|\dot{E}\,x_{U\,opt}\right| = \frac{K_T}{4}\left(\sqrt{T_{SH}} - \sqrt{T_0}\right)^2$$

6.5. Other C.H.H.P. system have been examined : the Joule Combustion Turbine is considered the more representative of Internal Combustion Engine C.H.H.P. system. The corresponding optimum has been proposed in the case where maximum temperature T_{MAX} is fixed. This case is the most significant for the present state of the art of combustion turbine.

6.5. A model of trigeneration systems has been examined recently [17]. All these models are presently completed in order to compare all constrained cases for the various existing systems.

Appendix

This annex gives the α_{opt} value announced in Table 1 :

If $\dot{w} = \dot{w}_0 < 0$

α_{opt} , solution of the equation :

$$a\alpha^2 - b\alpha - c = 0$$

with $a = \left[1 + \frac{T_U}{T_{SH}}\sqrt{I} + \frac{\dot{w}_0}{K_T T_{SC}}\left(\sqrt{I}+1\right)\right]$

$$b = -\left[1 - \frac{T_U}{T_{SH}}\sqrt{I} + (1-I)\frac{\dot{w}_0}{K_T T_{SH}}\right]$$

$$c = -\frac{\dot{w}_0}{K_T T_{SH}}\sqrt{I}\left(\sqrt{I}+1\right)$$

If $\dot{q}_U = \dot{q}_{U0} < 0$

$$\alpha_{opt} = \frac{d}{1+d}$$

with $d = \frac{1+\sqrt{I}}{\sqrt{I}} \cdot \frac{\dot{q}_{U0}}{K_T T_U}$

Nomenclature

$\dot{q}$	heat flux
$\dot{w}$	mechanical power
T	temperature
$\dot{s}$	entropy flux
$\dot{E}_X$	exergy flux
K	heat transfer conductance
X	temperature difference

Greek symbols

η	efficiency
α	intermediate variable

Subscripts and superscripts

U	useful
L	loss
I	first law
C.H.P.	combined heat and power
C.H.H.P.	combined hot heat and power
PV	photovoltaic system
SH	hot source
SC	cold sink
ex	exergetic
i	irreversible
o	ambient
t	total
c	consumed or Carnot

References

[1] *Proc. Of ECOS'07, ECOS'08, ECOS'09* (special sessions devoted to cogeneration).

[2] Radulescu, M., 2006, Systèmes de cogénération d'électricité et de chaleur avec piles à combustible de type PEMFC ou SOFC et vaporeformage interne, Ph. D thesis, University Henri Poincaré, Nancy, France.

[3] Descieux, D., 2007, Modélisations et comparaisons énergétiques de systèmes de cogénération, Ph. D. thesis, University Henri Poincaré, Nancy, France.

[4] Ji, J., et al., 2007, Thermal analysis of PV/T evaporator of a solar assisted heat pump, *Int. J. Energy Res.*, 31, pp. 525-545.

[5] Obernberger, I., et al., 2003, State of the art and future developments regarding small scale biomass CHP systems with a special focus on ORC and Stirling engine technologies, *communication International Nordic Bioenergy Conference*.

[6] Wang, J.J., et al., 2009, Weighting methodologies in multicriteria evaluations of CHP systems, *Int. J. Energy Res.*, 33, pp. 1023-1039.

[7] Iannone, F., et al., 2005, Economic analysis of micro CHP urban applications, *Proc. CIEM'2005*, Bucuresti, Romania, pp. 7-19.

[8] Lallemand, A., et al., 2009, Comparative study of heat production by cogeneration or heat pump; presented to CIEM'2009, Bucuresti, Romania, to be published in UPB Sci. Bull. Series.

[9] Erdil, A., 2005, Exergy optimization for an irreversible combined cogeneration cycle, *J. Energy Inst.*, 78(1), pp. 27-31.

[10] Lévy, C., Les techniques de cogénération, in *Techniques de l'Ingénieur*, Traité de Génie Energétique c, B8910, 24 pages.

[11] Feidt, M., 2006, *Energétique*, Dunod Editor, Paris, France, chap. 19.

[12] Sahin, B., and Kodal, A., 1999, *Recent advances in Finite Time Thermodynamics*, Wu C. et al Editors, Nova Science Publ.

[13] Feidt, M., Costea, M., Petré, C., Petrescu, S., 2007, Optimization of direct Carnot cycle, *Applied Thermal Engineering*, 27(5-6), pp. 829-839.

[14] Feidt, M., 2009, Optimal thermodynamics – New upperbounds, *Entropy*, 11, doi: 10.3390/e11040529, pp. 529-547.

[15] Samba, A., 2010, Microcogénération : optimisation thermodynamique et adaptabilité à divers combustibles, Master thesis, Ecole des Mines, Nancy, France.

[16] Feidt, M., Costéa, M., and Postelnicu, V., 2006, Comparaison entre le cycle simple de Brayton avec apport thermique impose et avec contrainte de temperature maximale, *OGST revue de l'IFP*, 61(2), pp. 237-247.

[17] Feidt M. and Lang S., 2002, Conception optimale de systèmes combinés à génération de puissance, chaleur et froid, *Entropie*, 242, pp. 2-11.

Second Law Efficiency Optimization of a Regenerative Gas Turbine Power Plant

Y. Haseli, J. A. van Oijen

Department of Mechanical Engineering, Eindhoven University of Technology, Eindhoven, The Netherlands

Abstract: The idea is to find out whether 2nd law efficiency optimization may be a suitable trade-off between maximum work output and maximum 1st law efficiency designs for a regenerator gas turbine engine operating on the basis of an open Brayton cycle. It is shown that an ideal Brayton-type engine with or without a regenerator cannot operate at fully reversible limit; regime of zero entropy generation. Hence, the 2nd law efficiency of the power cycle is defined as the ratio of the 1st law efficiency to the efficiency of the ideal power cycle. For an ideal cycle, minimization of entropy production is equivalent to maximization of the system thermal efficiency. Except at regenerator effectiveness of 50 percent, at which maximum work output, maximum 1st law efficiency, and minimum entropy generation become identical, no relation is observed between these three optimization criteria for an irreversible engine. A design region is established within which pressure ratio of a real engine must lie between optimum pressure ratios corresponding to maximum work output and maximum 1st law efficiency, respectively, as the upper and the lower limits of this region. The results indicate that the 2nd law efficiency optimization is approximately equivalent to maximum work output design when regenerator effectiveness is between 0.78 and 0.82. For the regenerator effectiveness beyond 0.82, the 2nd law efficiency optimization may be considered as a trade-off between optimized work output and 1st law efficiency. However, if the effectiveness value happens to be less than 0.78, the 2nd law efficiency optimization may give no useful design information.

Keywords: Regenerative Gas Turbine cycle, Optimization, Second law efficiency, Optimum Pressure Ratio

1. Introduction

Optimization of gas turbine power engines has received remarkable attention from numerous researchers during the past few decades. In principle, a design of a gas turbine engine operating on Brayton cycle can be carried out either by maximizing the power output or maximizing the thermal efficiency. Whether the optimization should be performed according to maximum power or maximum efficiency depends on the problem constrains; the relative prices of power and fuel. At one extreme we operate the engine to deliver as much power as possible without regard to how much fuel we waste. At the other extreme we try to get the maximum work out of the fuel without regard to how long it takes [1]. In general, a real engine must operate in a region imposed by maximum work output and maximum thermal efficiency designs. Within this region the thermal efficiency would be greater than the efficiency at maximum work and less than the maximum possible efficiency, whereas the work output would be greater than the work at maximum efficiency and less than the maximum possible work output [2]. Typical design regime of a regenerative Brayton engine at three values of the cycle highest-to-lowest temperature ratio, r_T, is depicted in Fig. 1. When the temperature ratio is higher, the allowable operational region becomes

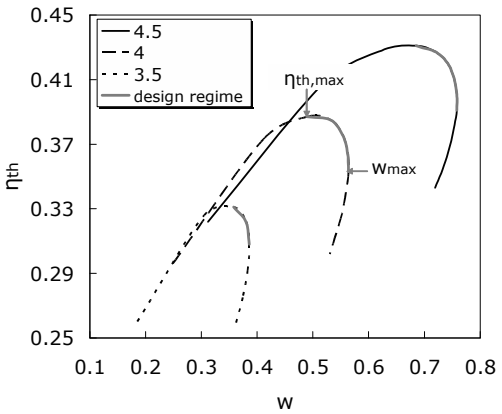

Fig. 1. Illustration of operational region of a regenerative gas turbine engine on the efficiency-work output curve at three highest-to-lowest temperature ratios

Corresponding Author: Yousef Haseli, Email: y.haseli@tue.nl

wider. Also, a higher r_T results in a better performance of the engine from both efficiency and work output perspectives. As a matter of fact, design of a power engine would basically require selection of only one point from the design area imposed by maximum work output and maximum thermal efficiency designs. On what basis this best design point must be chosen depends, practically, on economical parameters such as capital costs, fuel and power prices, and operational and maintenance costs.

In this paper, 2nd law efficiency optimization of a regenerative gas turbine power plant is studied. The idea is to find out whether this method may be considered as a proper trade-off between maximum work output and maximum 1st law efficiency designs. One important message of this article is that an ideal Brayton cycle, as described in standard thermodynamics textbooks; e. g. [3], cannot operate at zero entropy generation regime. In other words, entropy production (system plus surrounding) is an essential requirement to make an ideal Brayton cycle operate as a heat engine. It will be shown that it is incorrect to consider the Carnot engine as the ultimate limit of a Brayton-type engine. So, maximum attainable limit of the thermal/1st law efficiency of a real engine is the 1st law efficiency of the ideal cycle.

2. Ideal Cycle Analysis

In any heat engine that operates between two heat reservoirs maintained at constant temperatures T_H (heat source temperature) and T_L (heat sink temperature), work and entropy are produced due to heat exchange between the working substance and the heat reservoirs. Hence,

$$W = Q_H - Q_L \tag{1}$$

$$S_{Gen} = \frac{Q_L}{T_L} - \frac{Q_H}{T_H} \tag{2}$$

Consider an ideal open Brayton cycle whose T-S diagram is depicted in Fig. 2. Notice that a simple Brayton engine operates through path 1-2-3-4, whereas the process path in a plant with a regenerator would be 1-2-2a-3-4-4a. Due to the second law, only some portion of the combustion heat is converted into mechanical work and the rest is dumped into the ambient through discharging exhaust stream of turbine. Hence, the 1st law (thermal) efficiency of the power cycle is [3]

$$\eta_I = 1 - r_P^{-\alpha} \qquad \text{(simple)} \tag{3a}$$

$$\eta_I = 1 - \frac{r_P^{\alpha}}{r_T} \qquad \text{(regenerative)} \tag{3b}$$

where r_P is pressure ratio across the compressor, and $\alpha = (\gamma - 1)/\gamma$ with γ representing specific heats ratio. The 1st law efficiency of a simple ideal Brayton cycle increases consistently with the pressure ratio, but the thermal efficiency of an ideal regenerative Brayton engine decreases monotonically with the pressure ratio.

From the models of components, one may derive the following relationships for dimensionless work output and entropy production of the engine.

$$w = \left(r_T - r_P^{\alpha}\right)\left(1 - r_P^{-\alpha}\right) \tag{4}$$

$$N_{Gen} = r_T (r_P)^{-\alpha} + \pi r_P^{\alpha} - (r_T \pi + 1) \quad \text{(simple)} \tag{5a}$$

$$N_{Gen} = r_T \pi (r_P)^{-\alpha} + r_P^{\alpha} - (r_T \pi + 1) \quad \text{(regenerative)} \tag{5b}$$

where $\pi = T_L / T_H$.

In fact, work and entropy production defined in (1) and (2) are divided by heat capacitance of the working fluid to give the dimensionless parameters. Figure 3 illustrates graphical trends of the 1st law efficiency and the entropy generation number for an ideal Brayton cycle with/without a regenerator. In the case of the simple cycle, the entropy generation decreases, and the 1st law efficiency increases monotonically with pressure ratio, whereas for the case of the regenerative Brayton cycle the trends of the entropy generation and the 1st law efficiency are opposite. An

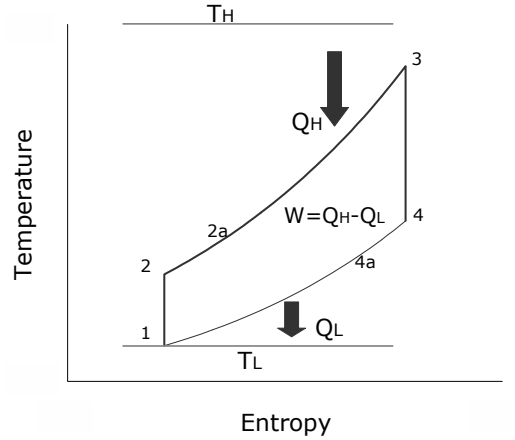

Fig. 2. T-S diagram of an ideal open Brayton Cycle operating between two heat reservoirs maintained at constant temperatures T_H and T_L. Note that process path 1-2-3-4 represents a simple cycle, and path 1-2-2a-3-4-4a shows a regenerative engine.

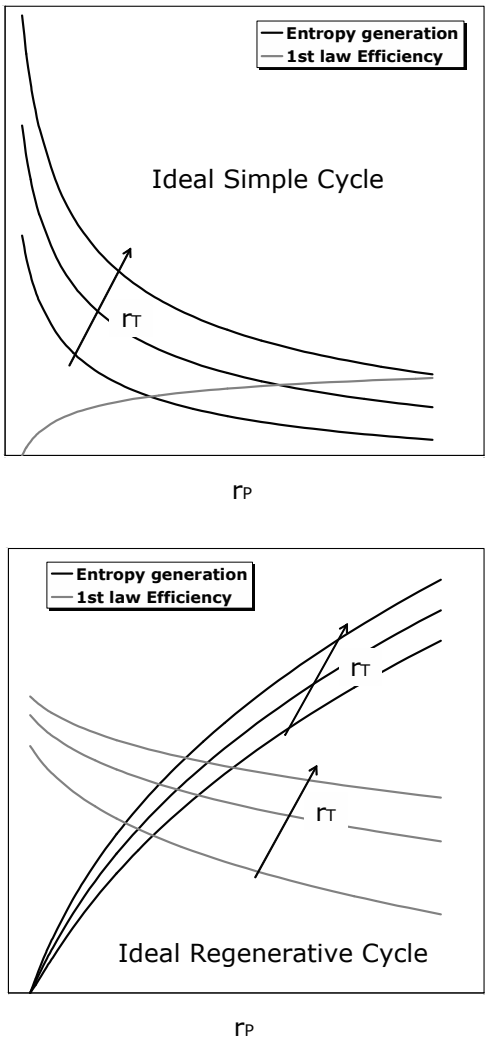

Fig. 3. Illustration of the trends of the 1st law efficiency and the entropy generation number versus pressure ratio for an ideal simple Brayton cycle (top), and an ideal regenerative Brayton cycle (bottom)

interesting observation from Fig. 3 is that the ideal simple Brayton cycle operating at a given efficiency may experience different entropy productions depending upon the cycle temperature ratio.

One important task is to examine the work output of the heat engine at fully reversible conditions, when the efficiency of the engine reaches the Carnot efficiency, η_{Ca}. To fulfill this task, the analysis proceeds by setting the entropy generation numbers equal to zero in (5a) and (5b). This allows one to obtain the overall pressure ratio at fully reversible condition. For the case of a regenerative ideal Brayton cycle, we get two roots as follows: $r_P = 1$, and $r_P^\alpha = r_T \pi = T_4/T_H$. At the pressure ratio of unity, in fact, no work is required to derive the compressor, nor would the turbine produce power; thereby resulting in an engine with zero work output. On the other hand, inserting the second root, $r_P^\alpha = r_T \pi$, in (4) yields a negative work output for the power cycle, which is impossible.

Likewise, for the case of a simple ideal Brayton cycle, two roots with respect to the pressure ratio may lead to zero entropy generation, which are: $r_P^\alpha = r_T$ and $r_P^\alpha = \pi^{-1}$. Similar results are obtained; zero work output at $r_P^\alpha = r_T$, and negative work output at $r_P^\alpha = \pi^{-1}$.

As a result, an ideal Brayton cycle with or without a regenerator operating at fully reversible limit, which corresponds to the regime of Carnot efficiency, would have zero net work output. The fully reversible condition implies $Q_H / T_H = Q_L / T_L$, and zero work output corresponds to $Q_H = Q_L$, whereby resulting in $T_H = T_L$, or $\eta_{Ca} = 0$; no engine at all! The main conclusion is that it is impossible for an ideal open Brayton cycle to operate at fully reversible limit. Thus, the generation of entropy is necessarily a basic requirement to drive a Brayton cycle. This implies that it is incorrect to consider the Carnot efficiency as the upper limit of the thermal efficiency of the power cycle.

3. Irreversible Cycle Analysis

Now we extend the analysis to an irreversible regenerative Brayton cycle. Energy is degraded due to components inefficiencies and pressure drop throughout the cycle. The energy degradation is taken into consideration by introducing compressor, turbine and regenerator efficiencies represented, respectively, by η_C, η_T and η_R, and pressure drop factor, P_F. This latter parameter is a factor with a maximum value of 1, which represents the total pressure drop within the power cycle. Hence, dimensionless work output, 1st law efficiency and entropy generation number for an irreversible cycle are given by

$$w = \eta_T r_T \left[1 - \left(r_P P_F\right)^{-\alpha}\right] - \frac{r_P^\alpha - 1}{\eta_C} \qquad (6)$$

$$\eta_I = \left[\eta_T r_T\left[1-\left(r_P P_F\right)^{-\alpha}\right]-\frac{r_P^{\alpha}-1}{\eta_C}\right]\times \frac{1}{r_T-\left(1+\frac{r_P^{\alpha}-1}{\eta_C}\right)(1-\eta_R)-\eta_R r_T\left\{1-\eta_T\left[1-\left(r_P P_F\right)^{-\alpha}\right]\right\}} \quad (7)$$

$$N_{Gen} = r_T\left\{1-\eta_T\left[1-\left(r_P P_F\right)^{-\alpha}\right]\right\}\left[(1-\eta_R)+\eta_R\pi\right] + \left(1+\frac{r_P^{\alpha}-1}{\eta_C}\right)\left[\eta_R+(1-\eta_R)\pi\right]-\left(r_T\pi+1\right) \quad (8)$$

Typical trends of the above three parameters versus the system pressure ratio are illustrated in Fig. 4 at some practical values of the components efficiencies; e. g., η_C = 0.85, η_T =0.9 and η_R = 0.80. As seen, the work output and the thermal efficiency have both optimums with respect to r_P but at different points. Typical values of $r_P(\eta_{I,max})$ and $r_P(w_{max})$ corresponding to Fig. 4 are 5 and 9, respectively. A past study by Roco et al. [4] revealed that when the regenerator effectiveness is less than 0.5, the optimum pressure ratio corresponding to maximum work output, $r_P(w_{max})$, is lower than the optimum pressure ratio obtained by maximizing the thermal efficiency, $r_P(\eta_{I,max})$. This trend would be opposite when $\eta_R > 0.5$. In a practical design, of course, the regenerator effectiveness must be much higher than 0.5, and the graphical trend of the system 1st law efficiency and its work output is similar to those depicted in Fig. 4. This figure in fact offers a design region in terms of the pressure ratio. In other words, a real engine pressure ratio must lie between $r_P(\eta_{I,max})$ and $r_P(w_{max})$.

Another important observation in Fig. 4 is that entropy generation consistently increases with pressure ratio. It does have an optimal point with respect to the pressure ratio, which happens to be less than 2. Bejan has pointed out in several papers that maximum work output design is equivalent to minimum entropy generation design; e. g., see Ref [5] p. 1216 and Refs [6, 7]. However, the results of the present study indicate that his statement is not a general theorem, as it does not hold for a regenerative gas turbine engine.

Explicit relationships can be derived to determine optimum pressure ratio leading to a maximum 1st law efficiency, maximum work output, or minimum entropy generation. Optimal pressure ratio leading to a maximum 1st law efficiency is computed through an equation obtained from $\partial\eta_I / \partial r_P = 0$; which gives

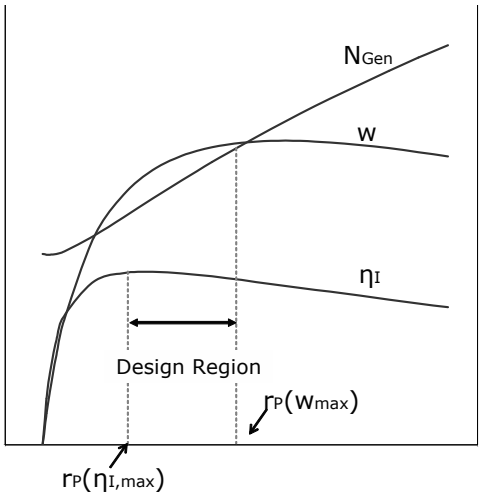

Fig. 4. General trends of dimensionless work output, 1st law efficiency, and entropy generation number of a regenerative gas turbine power plant

$$C_2\left[r_P\left(\eta_{I,max}\right)\right]^{2\alpha}+C_1\left[r_P\left(\eta_{I,max}\right)\right]^{\alpha}+C_0=0 \quad (9)$$

where

$$C_0 = \eta_T r_T P_F^{-\alpha}\left[(1-2\eta_R)+\eta_C(r_T-1)(1-\eta_R)\right]$$

$$C_1 = 2\eta_T r_T P_F^{-\alpha}(2\eta_R-1)$$

$$C_2 = \eta_T r_T(1-2\eta_R)-(r_T-1)(1-\eta_R)$$

Notice that if we could design a perfect heat exchanger with 100 percent effectiveness, equation (9) would reduce to $\left[r_P\left(\eta_{I,max}\right)\right]^{2\alpha}-2P_F^{-\alpha}\left[r_P\left(\eta_{I,max}\right)\right]^{\alpha}+P_F^{-\alpha}=0$, which means that the optimum pressure ratio subject to maximization of the 1st law efficiency would be a function of only pressure drop factor.

Likewise, optimum pressure ratios corresponding to maximum work output and minimum entropy production are obtained from $\partial w / \partial r_P = 0$ and $\partial N_{Gen} / \partial r_P = 0$, respectively.

$$r_P\left(w_{max}\right)=\left(\eta_C\eta_T r_T P_F^{-\alpha}\right)^{\frac{1}{2\alpha}} \quad (10)$$

$$r_P\left(N_{Gen,min}\right)=\left(\eta_C\eta_T r_T P_F^{-\alpha}\right)^{\frac{1}{2\alpha}}.C \quad (11)$$

where *C* is defined as below.

$$C=\left\{\frac{(1-\eta_R)+\eta_R\pi}{\eta_R+(1-\eta_R)\pi}\right\}^{\frac{1}{2\alpha}} \quad (12)$$

It is seen that maximization of work output and minimization of entropy generation have led to different results for optimal pressure ratio of the cycle, emphasizing that maximization of work output of a power plant is not necessarily identical to minimizing the entropy generation associated with the power plant, and they may be equivalent under special circumstances. For the case of a regenerative gas turbine engine, these two optimization strategies would come up with identical result only if the effectiveness of the regenerator were 50 percent. However, in practice, the thermal effectiveness of regenerative heat exchangers is much higher than 50 percent. This means that the constant *C* has a value of less than 1, with a typical value of 0.12, for instance; that is, the optimum r_P obtained from maximizing the work would be over 8 times greater than that resulted from minimizing the entropy generation.

Worthy of noting is that the regenerator effectiveness of 50 percent is an interesting case as Roco et al. [4] and Hernandez et al. [8] reported, based on their numerical results, that maximum efficiency and maximum power operating points became coincident at $\eta_R = 0.5$. One may also show it analytically by solving the quadratic equation (9) with $\eta_R = 0.5$, which would lead to the same result given in (10). As a conclusion, all the above optimization approaches are equivalent at the regenerator effectiveness of 50 percent for a regenerative gas turbine power plant.

The effect of the regenerator effectiveness on optimum pressure ratios corresponding to maximum 1st law efficiency, maximum work output and minimum entropy generation is illustrated in Fig. 5. Both $r_P(\eta_{I,max})$ and $r_P(N_{Gen,min})$ decrease consistently as η_R increases from zero to one, given that $r_P(w_{max})$ remains unaltered according to (10). Note that curves of $r_P(\eta_{I,max})$, $r_P(w_{max})$ and $r_P(N_{Gen,min})$ cross each other at η_R = 0.5. Figure 5 clearly indicates that $r_P(\eta_{I,max})$ is less than $r_P(w_{max})$ for practical values of η_R (typically greater than 0.7), and $r_P(N_{Gen,min})$ is much less than $r_P(\eta_{I,max})$ and $r_P(w_{max})$. As mentioned previously, design value of the system pressure ratio must lie between $r_P(\eta_{I,max})$ and $r_P(w_{max})$.

Based on the results of Figs. 5, a useful criterion can be maintained as the operating regime of the power cycle, which should satisfy the following inequality.

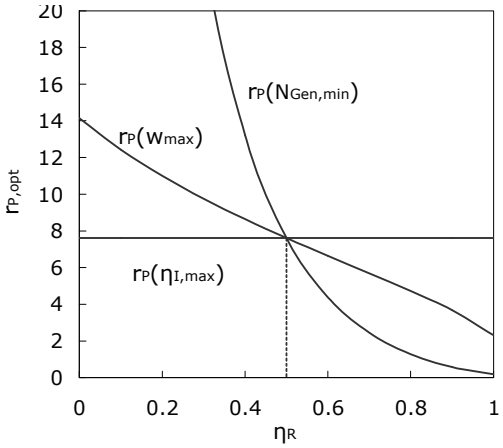

Fig. 5. Illustrative example representing the influence of the regenerator effectiveness on optimum pressure ratios subject to maximum 1st law efficiency, maximum work output, and minimum entropy generation

$$r_P(\eta_{I,max}) < r_{P,opt} < r_P(w_{max}) \quad (13)$$

Yet, no criterion has been proposed to establish a conceptual trade-off between the maximum 1st law efficiency and the maximum work output designs. The upcoming section is devoted to examine whether the 2nd law efficiency optimization may be considered as an appropriate design trade-off.

4. Second Law Efficiency Optimization

Taking into account the results of section 2, the 2nd law efficiency of the Brayton-type engine should be defined as $\eta_{II} = \eta_I / \eta_i$, where η_I and η_i (irreversible and ideal 1st law efficiencies) are determined from (7) and (3), respectively. The ideal 1st law efficiency of the power cycle, η_i, corresponds to a condition that no entropy, due to degradation of energy, would be generated in the plant, whereas a real engine suffers from energy degradation within its components. So, the ratio η_I / η_i indicates the inefficiencies within the real engine due to production of entropy resulted from degradation of energy compared to the ideal situation.

Hence, with the aid of (7) and (3), the 2nd law efficiency of a regenerative gas turbine power plant is described as follows,

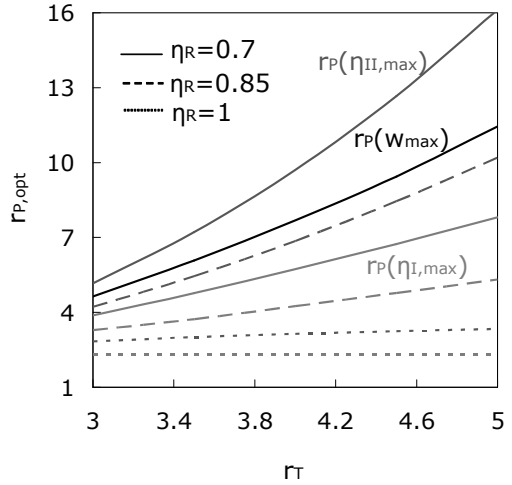

Fig. 6. Variations of optimum pressure ratios with the temperature ratio at three values of regenerator effectiveness. Note that $r_P(w_{max})$ is identical at all effectiveness cases ($P_F = 0.85$, $\eta_C = 0.85$, $\eta_T = 0.9$).

$$\eta_{II} = \left[\eta_T r_T\left[1-(r_P P_F)^{-\alpha}\right]-\frac{r_P^{\alpha}-1}{\eta_C}\right]\times\frac{r_T}{r_T-r_P^{\alpha}}\times \frac{1}{r_T-\left(1+\frac{r_P^{\alpha}-1}{\eta_C}\right)(1-\eta_R)-\eta_R r_T\left\{1-\eta_T\left[1-(r_P P_F)^{-\alpha}\right]\right\}} \quad (14)$$

Notice that η_{II} is always greater than η_I at a given process conditions. For the condition of Fig. 4, as an example, η_I may reach to a maximum value of 43% when $r_T = 4.5$ and $P_F = 0.85$, whereas η_{II} can increase up to 69%.

Maximizing η_{II} with respect to r_P results in a more complicated equation compared to those obtained for optimum pressure ratios in (9) – (11).

$$C_4'(r_P)^4 + C_3'(r_P)^3 + C_2'(r_P)^2 + C_1' r_P + C_0' = 0 \quad (15)$$

where $C_0'...C_4'$ are complex functions of the process independent parameters.

Figure 6 reveals that depending on the value of η_R the optimum pressure ratio resulted from maximizing the 2nd law efficiency may lie between $r_P(\eta_{I,max})$ and $r_P(w_{max})$, or stand upper than $r_P(w_{max})$. Notice that the curve of $r_P(w_{max})$ versus r_T is identical for all regenerator effectiveness values. At $\eta_R = 1$, the results of both efficiencies optimization are quiet close. By decreasing η_R, both $r_P(\eta_{I,max})$ and $r_P(\eta_{II,max})$ increase; this latter one with a higher rate, such that it reaches $r_P(w_{max})$ at

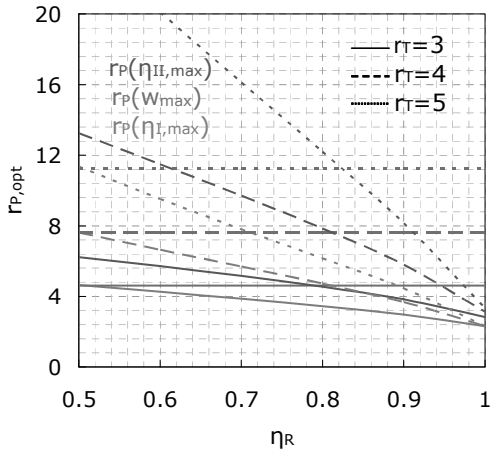

Fig. 7. The effect of the regenerator effectiveness on optimum pressure ratios at three different temperature ratios ($P_F = 0.85$, $\eta_C = 0.85$, $\eta_T = 0.9$)

around $\eta_R = 0.8$. Further reduction of η_R leads to a higher $r_P(\eta_{II,max})$ than $r_P(w_{max})$.

The trends of optimum pressure ratios varying with the regenerator effectiveness at different temperature ratios, pressure drop factors, and turbo-compressor efficiencies are also investigated; the results are depicted in Figs. 7 – 10. Shown in Fig. 7 are the graphs of the optimum pressure ratios versus η_R at three values of the temperature ratio. As seen, $r_P(\eta_{II,max})$ crosses $r_P(w_{max})$ somewhere between $\eta_R = 0.8$ and $\eta_R = 0.82$ depending upon the value of r_T. Thus, the 2nd law efficiency optimization method cannot be a good design method for $\eta_R < 0.80$ since inequality (13) is not satisfied, whereas for efficient heat exchangers having effectiveness of higher than 0.8, it can be employed as a compromise between the maximum work output and maximum 1st law efficiency designs.

Figure 8 illustrates the effect of the pressure drop factor on the trends of $r_{P,opt} - \eta_R$ curves. From this figure, $r_P(\eta_{II,max})$ happens to lie between $r_P(\eta_{I,max})$ and $r_P(w_{max})$ for $\eta_R > 0.81$, and the curves of $r_P(\eta_{II,max}) - \eta_R$ cross those of $r_P(w_{max}) - \eta_R$ at $\eta_R = 0.81$ regardless of the value of the pressure drop factor.

Lastly, the effects of the turbine and the compressor efficiencies on the optimum pressure ratios varying with the regenerator effectiveness are studied. Figure 9 shows that by varying the turbine efficiency in the range of 0.8 – 0.9, $r_P(w_{max})$ and $r_P(\eta_{II,max})$ become identical at $0.77 \le \eta_R \le 0.8$. Worthy of noting is that for

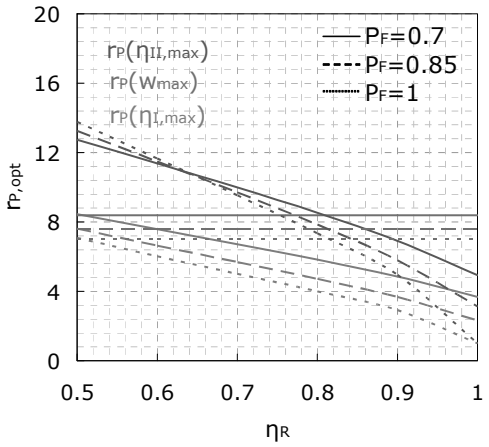

Fig. 8. The effect of the regenerator effectiveness on optimum pressure ratios at three different pressure drop factors (r_T = 4, η_C = 0.85, η_T = 0.9)

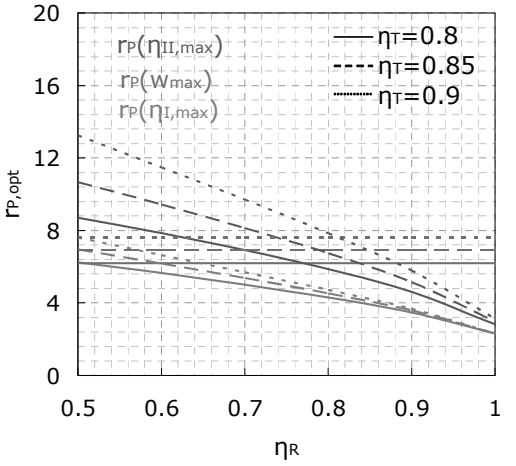

Fig. 9. The effect of the regenerator effectiveness on optimum pressure ratios at three different values of the trubine efficiency (r_T = 4, P_F = 0.85, η_C = 0.85)

$\eta_R \geq 0.85$, $r_P(\eta_{I,max})$ is almost independent of the turbine efficiency. The effect of the compressor efficiency on the optimum pressure ratios is illustrated in Fig. 10. Unlike other process parameters, a significant displacement in the crossing point of $r_P(\eta_{II,max})$ - η_R and $r_P(w_{max})$ - η_R is evident when changing the compressor efficiency. From Fig. 10, the location of this crossing point corresponds to $0.78 \leq \eta_R \leq 0.84$ for the compressor efficiency varying between 0.8 and 0.9.

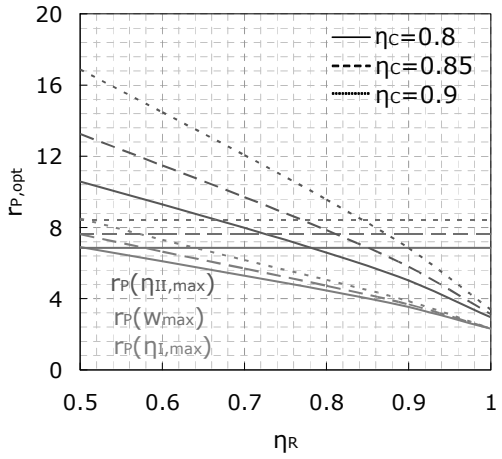

Fig. 10. The effect of the regenerator effectiveness on optimum pressure ratios at three different values of the compressor efficiency (r_T = 4, P_F = 0.85, η_T = 0.9)

5. Conclusions

The results of this study reveal that the upper limit of the 1st law (thermal) efficiency of a heat engine operating on an open Brayton cycle with or without a regenerator, cannot be the Carnot efficiency. Indeed, the 1st law efficiency of such an engine may ultimately reach the efficiency of the ideal cycle; i. e., (3). Hence, the 2nd law efficiency of a regenerative gas turbine power plant is defined as the ratio of the thermal efficiency of the irreversible plant to the thermal efficiency of the ideal power cycle. Various optimization criteria were considered. The results indicate that a regenerative Brayton cycle can operate simultaneously at maximum work output, maximum 1st law efficiency and minimum entropy generation rate at the regenerator effectiveness of 50 percent. A real engine must operate in the region imposed by maximum work output and maximum 1st law efficiency designs. Thus, the real engine pressure ratio must satisfy inequality (13). The possibility of employing the 2nd law efficiency optimization as a trade-off between the optimized work output and the 1st law efficiency was examined. It was found out that if the regenerator effectiveness lies between 0.78 and 0.82, a design based on the 2nd law efficiency maximization would be almost equivalent to the maximum work output design. For the regenerator effectiveness

greater than 0.82, the 2nd law efficiency may be considered as a trade-off between the maximum work and maximum 1st law efficiency designs. However, if a regenerator operates at efficiency less than 0.78, the 2nd law efficiency optimization is not recommended as a design criterion.

Nomenclature

C	Parameter defined in (12)
C_0, C_1, C_2	Parameters defined in (9)
N_{Gen}	Entropy generation number
P_F	Pressure drop factor
Q_H	Heat transfer in combustor, J
Q_L	Heat rejection to ambient, J
r_p	Pressure ratio
$r_P(N_{Gen,min})$	Optimum pressure ratio leading to minimum entropy generation
$r_P(w_{max})$	Optimum pressure ratio leading to maximum work output
$r_P(\eta_{I,max})$	Optimum pressure ratio leading to maximum 1st law efficiency
$r_P(\eta_{II,max})$	Optimum pressure ratio leading to maximum 2nd law efficiency
r_T	Cycle highest-to-lowest temperature ratio
S_{Gen}	Entropy generation, J/K
T_H	Heat source temperature, K
T_L	Heat sink temperature, K
W	Work output, J
w	Dimensionless work output

Greek Letters

α	$= (\gamma-1)/\gamma$
γ	Ratio of specific heats
η	Efficiency
π	$= T_L/T_H$

Subscripts

C	Compressor
I	1st law
II	2nd law
i	Ideal
opt	Optimum
R	Regenerator
th	Thermal
T	Turbine

References

[1] Salamon, P., Hoffmann, K. H., Schubert, S., Berry, R. S., Andresen, B., 2001, What Conditions Make Minimum Entropy Production Equivalent to Maximum Power Production, Journal of Non-Equilibrium Thermodynamics, 26, pp. 73-83.

[2] Hernandez, A. C., Roco, J. M. M., Medina, A., 1996, Power and Efficiency in a Regenerative Gas-Turbine Cycle with Multiple Reheating and Intercooling Stages, Journal of Physics D: Applied Physics, 29, pp. 1462–1468.

[3] Razak, A. M. Y., 2007, Industrial Gas Turbines: Performance and Operability, Taylor & Francis Group, LLC, Chap. 2.

[4] Roco, J. M. M., Velasco, S., Medina, A., Hernandez, A. C., 1997, Optimum Performance of a Regenerative Brayton Thermal Cycle, Journal of Applied Physics, 82(6), pp. 2735-2741.

[5] Bejan, A., 1988, Theory of Heat Transfer-Irreversible Power Plants, International Journal of Heat and Mass Transfer, 31(6), pp. 1211-1219.

[6] Bejan, A., 1995, Models of Power Plant That Generates Minimum Entropy While Operating at Maximum Power, American Journal of Physics, 64(8), pp. 1054-1058.

[7] Bejan, A., 1996, The Equivalence of Maximum Power and Minimum Entropy Generation Rate in the Optimization of Power Plants, Journal of Energy Resources Technology, Transactions of the ASME, 118(2), pp. 98-101.

[8] Hernandez, A. C., Medina, A., Roco, J. M. M., 1995, Power and Efficiency in a Regenerative Gas Turbine Cycle, Journal of Physics D: Applied Physics, 28, pp. 2020-2023.

Thermodynamic Estimation of the Pollution Prevention and Control Regulations and Measures in the Nitrogen Fertilizer Industry

Zornitza Kirova – Yordanova[a]

[a]*University "Prof. Assen Zlatarov", Bourgas, Bulgaria*

Abstract: In the last decade the Integrated Pollution Prevention and Control (IPPC) Directive was the key law on industrial emissions in the European Union, aiming to achieve a high level of environmental protection in the major industrial activities. The Best Available Techniques (BAT) were recommended for each industrial branch, especially in the process industry, with the purpose to prevent and reduce the pollution and to use energy more effective. This prompted the development and application of new methods for the production processes improvements and emissions minimization.
In some chemical processes the emissions minimization is achieved simultaneously with the reduction of energy and feedstock consumption. However, in most cases the emissions reduction requires additional energy and chemicals to be consumed. Also, as a rule, the stronger emission limits are required, the more energy and non-energy resources have to be consumed additionally.
In this work a thermodynamic estimation of the emissions abatement methods, recommended as BAT for the major production processes in nitrogen fertilizers industry is made. The exergy method and the cumulative exergy concept are used in order to estimate the total and the additional natural resources consumption in the production of ammonia, nitric acid, ammonium nitrate and urea, based on recommended BAT processes and emission limits.

Keywords: Nitrogen fertilizers, Emissions, Pollutants, Exergy analysis, Urea, Nitric acid, Ammonia

1. Introduction

The European industry is subject to a range of industrial emissions legislations, first of them the Integrated Pollution Prevention and Control (IPPC) Directive (Directive 96/61/EC, codified in 2008 as Directive 2008/1/EC) with about 52000 industrial installations covered [1]. The deadlines for the full implementation of the IPPC Directive for new plants were 30 October 1999 and for existing plants 30 October 2007 [1].

From December 2007, a recast procedure of the IPPC Directive is in progress and a new Industrial Emissions Directive (IED) is now close to finalizing [2].

The concept of the Best Available Techniques (BAT) is one of the basic principles of the IPPC Directive. The emissions limit values (ELVs), which are mandatory according to the IPPC and IED Directives, should be determined on the basis of the emissions values for new and existing plants, recommended in the BAT Reference Documents (BREFs) for each industrial sector. Especially for chemical industry, a BREF document for each sub-sector is now adopted by the EC. The Second Draft Reference Document on Best Available Techniques in the Large Volume Inorganic Chemicals, Ammonia, Acids and Fertilizers Industries (LVIC-AAF) was published in 2004, and the final BREF Document – in August 2007 [3,4]. It is clear that the BREF Documents have been adopted long after the deadlines for the IPPC Directive implementation.

However, the BAT processes and emission levels for the fertilizers industry have been recommended earlier by the European Fertilizers Manufacturers Association (EFMA) in 1995 and then in 2000 in two sets of 8 booklets covering all nitrogen, phosphorous and complex fertilizers production processes, including production of intermediates. Some of these booklets concerning nitrogen fertilizers production processes are referred in [5].

The BREF documents [3,4] for fertilizers industry are based to a great extent on the EFMA BAT recommendations.

However, a comparison of these two sets of documents shows that for some production processes (e.g. for urea and nitric acid plants) significant differences exist between the values of

the emissions determined as BAT and a tendency to tighter BAT emission values for existing as well as for new plants is apparent in BREF documents. It is rather strange, that in the same time for other processes (e.g. ammonium nitrate plants) the BAT emission values recommended in the EFMA booklets [5] for existing and for new plants are equal; moreover, no values are determined as BAT in both BREF Documents [3,4] (Table 1).

Table 1. Concentrations and mass flow rates of the pollutants, emitted to the air and to water from existing and new BAT nitrogen fertilizers production plants [3-5]

Pollutants	Existing BAT plants.				New BAT plants			
	EFMA 2000		BREF 2004-2007		EFMA 2000		BREF 2004-2007	
	Concentration	Quantity kg/t	Concentration	Quantity kg/t	Concentration	Quantity kg/t	Concentration	Quantity kg/t
Ammonia plants								
CO_2 from ammonia plant in: Vent gas (99% CO_2) Flue gas from reforming furnace		 1200 500				 1200 500		
NO_x (as NO_2) in flue gas from reforming furnace	mg/Nm^3 200-400	 0.90	mg/Nm^3 230	 0.32	mg/Nm^3 150	 0.45	mg/Nm^3 90	 0.29
Total into air	-	**1700**				**1700**		
Process condensate to water: ▪ NH_3		 **0.1**				 **0.1**		
Total from ammonia plants	-	**1701**	-		-	**1701**	-	
Nitric acid plants								
Tail gas from nitric acid plant: **NO_x** (as NO_2): **N_2O**	mg/Nm^3 400 -	 1.4 -	mg/Nm^3 10-180 40-600	 0.03-0.55 0.12-1.85	mg/Nm^3 200 -	0.65 -	mg/Nm^3 10-150 40-200	 0.03-0.45 0.12-0.60
Total from nitric acid plants	-	-	-	**0.15-2.40**	-	-	-	**0.15-1.05**
Ammonium nitrate (AN) plants								
Process condensate after treatment: NH_4NO_3 (as N)	mg N/ l 100	 0.20	-	-	mg N/ l 100	 0.20	-	-
Total to water (as N)	**100**	**0.20**	-	-	**100**	**0.20**	-	-
Air from prilling: ▪ NH_3 ▪ AN dust Other emission points: ▪ NH_3 ▪ AN dust	mg/Nm^3 10 15 50 30	 0.12 0.18 - -	- - - -	- - - -	mg/Nm^3 10 15 50 30	 0.12 0.18 0.08 0.32	- - - -	- - - -
Total to air: ▪ NH_3 ▪ AN dust **Total to air as N**	-	 **0.2** **0.5** **0.34**	- - -	 - - -	 - - -	 **0.2** **0.5** **0.34**	 - - -	 - - -
Total from AN plants (as N)	-	**0.54**	-	-	-	**0.54**	-	-
Urea plants								
Waste water after treatment: ▪ NH_3 ▪ Urea	mg/l 150.0 150.0	 0.100 0.100	mg/l 10.0 5.0	 0.0050 0.0025	mg/l 5.0 1.0	 0.0025 0.0005	mg/l 1.0 1.0	 0.0005 0.0005
Total to water	**300.0**	**0.200**	**15.0**	**0.0075**	**6.0**	**0.0030**	**2.0**	**0.0010**
Total to water (as N)	**193**	**0.130**	**10.6**	**0.0053**	**4.6**	**0.0023**	**1.3**	**0.0006**
Air from prilling: ▪ NH_3 ▪ Urea dust ▪ NH_3 in vents	mg/Nm^3 65-100 100-150 -	 0.65-1.0 1.0-1.5 0.75	mg/Nm^3 3-35 15-55 -	 0.03-0.35 0.15-0.55 0.004-0.008	mg/Nm^3 50.0 50.0 -	 0.5000 0.5000 0.0600	mg/Nm^3 3-35 15-55 -	 0.03-0.35 0.15-0.55 0.002
Total to air	-	**2.40-3.25**	-	**0.18-0.91**	-	**1.0600**	-	**0.18-0.90**
Total from urea plants	-	**2.60-3.45**	-	**0.19-0.92**	-	**1.0630**	-	**0.18-0.90**
Total from urea plants (as N)	-	**1.60-2.14**	-	**0.10-0.56**	-	**0.7000**	-	**0.10-0.55**

The Best Available Techniques (BAT) were recommended with the purpose to prompt the development and application of new methods for the production processes improvements and emissions minimization.

In some chemical processes the emissions minimization is achieved simultaneously with the reduction of energy and feedstock consumption. However, in most cases the emissions reduction requires additional energy and chemicals to be consumed. Also, as a rule, the stronger emission limits are required, the more energy and non-energy resources have to be consumed additionally.

As it is pointed in [6], sustainable environmental protection can only be successful if seen as a whole. Therefore, the Industrial Emissions Directive should allow not only emissions reduction to be taken in consideration, but also all its aspects as well as possible side effects. Indeed, it would be useless to decrease some pollutants if this was to lead to unbalanced production of other emissions in particular associated with increased energy consumption [6].

The aim of this work is to make an attempt to estimate the overall net effect from the reduction of the emission values, recommended as BAT with respect not only to the emissions from the analysed process itself, but also of the pollutants and GHGs, emitted from the overall technological chain from feedstock and primary energy input through the intermediates production processes to the final product output. Also the net effect from the reduction of the emission values on the overall natural resources consumption reduction or increase is taken into account. A set of various Second-Law based indices is used in order to compare and estimate the thermodynamic cost and benefits from emission values tightening. Two basic nitrogen fertilizers production processes (urea and nitric acid) representing the most significant reduction of the BAT emission values are analysed as examples applying the exergy method and the cumulative exergy concept [7].

2. Methodology

The overall net effect from a waste flow treatment process includes both positive and negative effects with respect to the emissions of pollutants and GHGs, as well as to natural resources consumption.

The problem is what effect is more significant, i.e., is the net overall effect positive or negative.

In order to estimate the overall effects from the treatment processes building block models and a top-down approach are used [8,9].

This approach not only analyzes the emissions from the studied process but also the emissions from all the preceding processes in which intermediates are produced, as well as the emissions from the utilities (power plant and/or separate steam boiler) in the production site. As the emissions from these processes are rather different, the total mass rate of the emissions (incl. pollutants and GHGs) may not give a real picture of their impact on the environment; also the application of some weight coefficients is not well-grounded. The total chemical exergy of the emissions and GHGs would be a more acceptable criterion, because the potential of the emissions to damage the environment, depends mainly on their chemical composition and especially, on the concentrations and properties of the pollutants. However, in most cases there is no direct correlation between the chemical exergy of the pollutants and their impact on the various components of the environment. Therefore, the most useful information could be obtained by comparing the exergy consumption and the cumulative exergy consumption in the analyzed processes for emissions abatement, including all the preceding processes in which intermediates and utilities are produced. In two recent papers [10,11] this approach was applied to the ammonium nitrate and nitric acid production processes and was used to compare different processes for waste flows treatment and pollutions abatement.

The structure of the building block models of both analyzed systems includes production of ammonia as an intermediate, and also a steam and power plant (Figs. 1 and 2).

The accumulated reduction and rise of the emissions are calculated by tracing out from the urea plant or from the nitric acid plant back down to the ammonia unit and also to the steam and power plant.

The data, used in the building block models, about feedstock and fuel consumption in ammonia and power plants and about emissions from these units, are extracted from EFMA and EC publications for BAT plants [3-5].

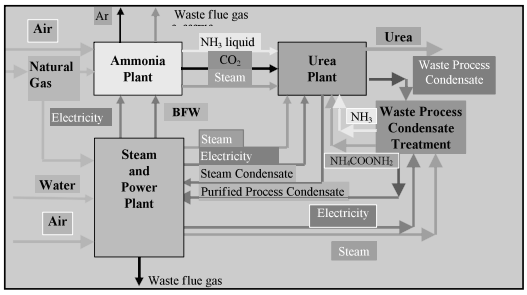

Fig. 1. Block flow diagram of an urea production site

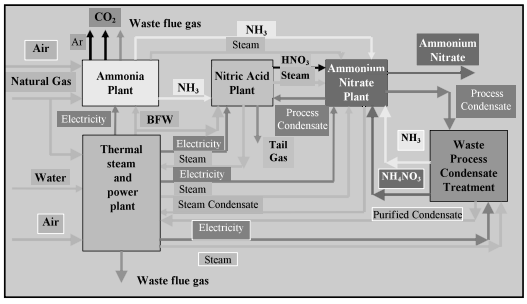

Fig. 2. Block flow diagram of an ammonium nitrate production site

3. Results and discussion

3.1. Reduction of BAT values of the emissions from urea production plants

As is clear from Table 1, the tightening of the values recommended as BAT is the greatest for the emissions from urea plants and concerns existing as well as new plants.

The BAT values of the emissions to water for existing plants recommended in the EFMA Booklet No. 5 in 2000 [5] were rather high (150 mg/l for both ammonia and urea, equivalent to total 193 mg N/l). This value was higher than the BAT value for existing ammonium nitrate (AN) plants, recommended also in 2000 from EFMA in Booklet No. 6 [5]. However the total mass of the nitrogen emissions to water from urea plants (0.13 kg as N/t) was lower than from AN plants (0.20 kg as N/t) (Table 1).

All these values are rather high and are specific for the older urea plants, designed in 70th and 80th. In last two decades the methods for treatment of waste water from urea plants have been strongly improved [3-5] and now extremely low urea and ammonia concentrations are achieved in the liquid effluent from urea plants. In the new generation of urea plants also the mass flow rate of the waste water have been reduced.

Thus in the new generation urea plants the concentrations of the pollutants as well as the total mass of the nitrogen emitted into water are strongly reduced. For the existing plants the concentrations and the total mass of the emissions are reduced more than 10 times, and the difference between exiting and new plants is more than 100 times (Table 1).

As the ammonia and urea are recycled back into the urea production process, the decreasing of the emissions has a very positive result: some reduction of the feedstock and power consumption in ammonia and urea production, and thus some reduction of fuel consumption for power generation. An additional positive effect is some reduction of the emissions from ammonia and from power plant.

However, the new more precise waste water treatment methods are more energy intensive; the quantity and the parameters of the consumed steam are higher. As the steam is generated in a utility boiler or in a steam power station in the same site, the additional fuel is consumed and some additional emissions arise.

In order to estimate the effects from the most significant tightening of the BAT emissions values for urea plants, the analysis included:

- The effect from the decreasing of the recommended emissions values for existing BAT plants from 2000 [5] to 2007 [4];
- The effect from the decreasing of the recommended emissions values for existing BAT plants to new BAT plants in the final 2007 BREF document [4].

The results from analysis of the effect of the decreasing of the emissions values on the overall mass flow and exergy of the emissions from urea, ammonia and power plants are shown in Table 2. The results concerning the overall reduction and the overall additional consumption of exergy, Cumulative Energy Consumption (CEnC) and Cumulative Exergy Consumption (CExC) are shown in Table 3. A comparison of all indices is shown in Figures 3 –5.

Table 2. Reduction of the emissions as a result from the waste water treatment in BAT urea plants

Reduction of the emissions	In existing BAT urea plants from 2000 to 2007 [4,5]					From existing to new BAT urea plants in 2007 [4]				
	NH_3 to water	urea to water	CO_2 to air	NOx to air	Total	NH_3 to water	urea to water	CO_2 to air	NOx to air	Total
Reduction of the mass of the emissions (kg/t urea)										
Emissions reduction	0.095	0.0975	0.2903	0.0001	0.4829	0.0045	0.0020	0.0108	<0.0001	0.0173
Additional emissions	-	-	14.941	0.012	14.953	-	-	4.606	0.0039	4.6099
Net reduction	**0.095**	**0.0975**	**-14.6507**	**-0.0119**	**-14.470**	**0.0045**	**0.0020**	**-4.5952**	**-0.0039**	**-4.5926**
Reduction of the exergy of the emissions (MJ/t urea)										
Emissions reduction	1.902	1.109	0.1328	0.0001	3.1438	0.090	0.023	0.005	<0.0001	0.118
Additional emissions	-	-	6.837	0.0151	6.8521	-	-	2.108	0.005	2.113
Net reduction	**1.902**	**1.109**	**-6.704**	**-0.015**	**-3.7083**	**0.090**	**0.0023**	**-2.103**	**-0.005**	**-1.995**

Table 3. Reduction of the exergy, Cumulative energy (CEnC) and Cumulative exergy (CExC) consumption for waste water treatment in BAT urea plants

Reduction of the exergy, Cumulative energy (CEnC) and Cumulative exergy (CExC) consumption	In existing BAT urea plants from 2000 to 2007 [4,5]				From existing to new BAT urea plants in 2007 [4]			
	Natural gas Nm^3/ t urea	CEnC MJ/t urea	Exergy MJ/t urea	CExC MJ/t urea	Natural gas Nm^3/ t urea	CEnC MJ/t urea	Exergy MJ/t urea	CExC MJ/t urea
Consumption reduction	0.148	5,294	5,571	6,367	0.0055	0,197	0,207	0,237
Additional consumption	7,606	272,43	286,72	327,68	2,345	83,990	88,391	101,019
Net reduction	**-7,4582**	**-267,136**	**-281.149**	**-321,313**	**-2,3395**	**-83,793**	**-88.184**	**-100,782**

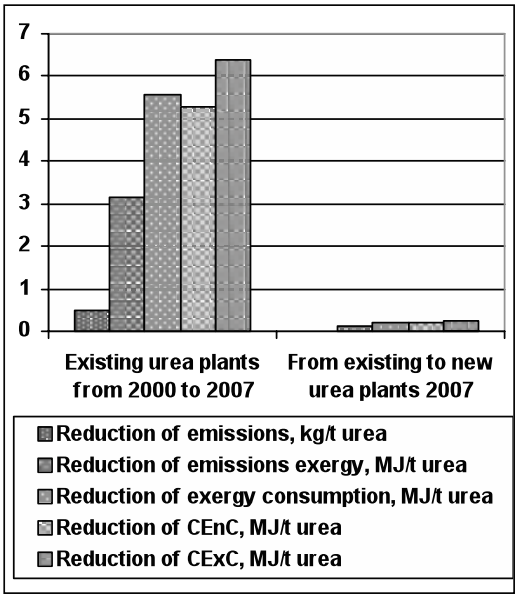

Fig. 3. Some positive effects from reduction of the emissions into water from BAT urea plants

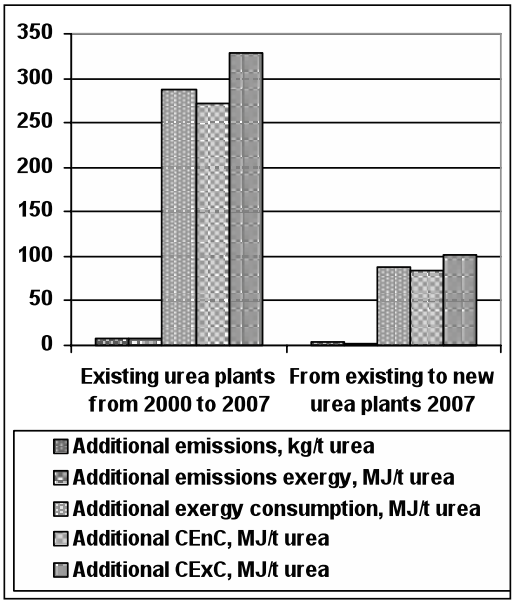

Fig. 4. Some negative effects from reduction of the emissions into water from urea plants

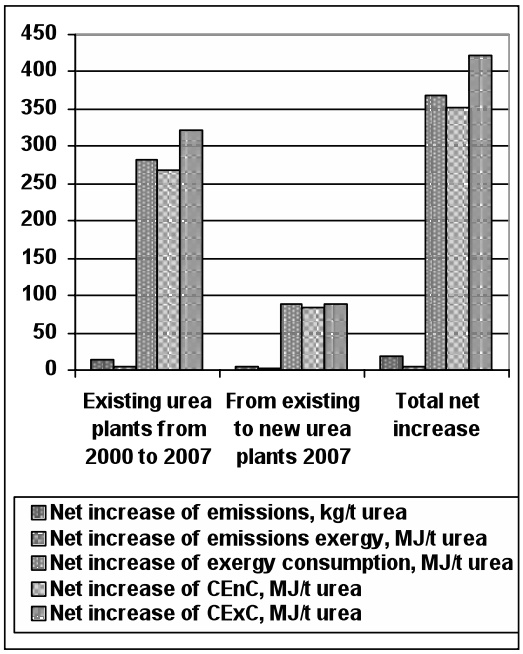

Fig. 5. Overall effects from reduction of the emissions into water from urea plants

The results show that in both cases the mass rate of the additional emissions is higher than the value of the reduced emissions and the net effect is negative: the mass rate of the total emissions increases in both analyzed cases. The exergy of the additional emissions (mainly CO_2) is lower than the exergy of the reduced emissions (ammonia and urea) and the total net effect is also negative, but rather small. However, the additional consumption of exergy, as well as the additional consumption of cumulative energy (CEnC) and cumulative exergy (CExC) are many times higher then their reduction. As a result, the overall net effect is a significant increase of the natural energy resources consumption (Tables 2 and 3 and Fig. 5). The total increase is about 0.3-0.42 GJ/t urea. As the exergy of urea is 11.4 GJ/t, and the total CExC for urea in new BAT plants is about 30 GJ/t, the effect of the reduction of the emissions to water is a CExC increase by about 1-1.5%.

3.2. Reduction of BAT values of the emissions from nitric acid plants

The NOx abatement methods from the tail gas released to the air from nitric acid plants are improved strongly in the last decade [3-5]. New better catalysts for the SCR and NSCR, improved absorption column internals have been introduced. On this basis in 2000 the recommended values of NOx for BAT new plants (200 ppmv or 400 mg/Nm^3) were half as much than these for BAT existing plants (100 ppmv or 200 mg/Nm^3) [5]. However, in the final BREF 2007 document [3] the recommended values for both kinds of plants are strongly reduced and extremely low values are recommended as lower limits (Table 1). As these lower limits are technically not applicable, the upper limits for both existing and new plants are used in this work as a basis of the analysis. The effects from the reduction of NOx in the tail gas from 2000 [5] to 2007 [3] are analyzed for existing and for new nitric acid plants.

The results are shown in Tables 4 and 5 and in Figures 6-8.

Two from all three NOx abatement methods recommended as BAT, are subject of the analysis: extended absorption (EA) and selective catalytic reduction (SCR). The 3rd method - non-selective catalytic reduction (NSCR) is not included, as it is not an end-of-pipe method.

The results show that extended absorption is preferable from both criteria: the overall net reduction of the emissions as well as of the natural resources consumption are positive. The SCR gives a reverse effect: the values of all overall net indices are slightly negative. The reason is that in the extended absorption NOx is recycled back into the process and in the SCR NOx is reduced to the elemental nitrogen.

However, the EA requires lower temperatures in the absorption column. The values of NOx in the tail gas down to 200 ppmv (400 mg/Nm^3) are achievable if the fresh cooling water temperature is 10-15^{0}C. If the colder fresh water is available, the NOx values down to the 90 ppmv (180 mg/Nm^3) could be achieved [3]. Another way, the recommended lower NOx values (75-90 ppmv) require some additional energy consumption for refrigeration. As the results in this work are obtained by the assumption, that no refrigeration is used, the only applicable method for satisfy the BREF 2007 regulations as for existing as well as for new plants is the SCR, despite the negative values of all indices.

*Table 4. Reduction of the emissions as a result of the tail gas treatment in **existing** and **new** BAT nitric acid plants from 2000 [5] to 2007 [4]*

Tail gas treatment method in BAT plants	Extended Absorption				Selective Catalytic Reduction of NOx			
	Existing BAT plants		New BAT plants		Existing BAT plants		New BAT plants	
Emissions concentration reduction, mg NOx/Nm^3	From 400 to 180		From 200 to 150		From 400 to 180		From 200 to 150	
Reduction of the emissions	Quantity kg/t HNO_3	Exergy MJ/t HNO_3	Quantity kg/t HNO_3	Exergy MJ/t HNO_3	Quantity kg/t HNO_3	Exergy MJ/t HNO_3	Quantity kg/t HNO_3	Exergy MJ/t HNO_3
Total emissions reduction	1.1782	1.0729	0.2670	0.2444	0.2971	0.1361	0.0696	0.0319
Additional emissions	0.0803	0.0368	0.0181	0.0083	0.6313	0.2893	0.1423	0.0652
Net emissions reduction	**1.0979**	**1.0361**	**0.2497**	**0.2361**	**-0.3342**	**-0.1532**	**-0.0727**	**-0.0333**

*Table 5. Reduction of the Exergy Consumption, Cumulative energy consumption (CEnC) and Cumulative exergy consumption (CExC) for tail gas treatment in **existing** and **new** BAT nitric acid plants from 2000 [5] to 2007 43]*

Reduction of the energy and exergy consumption	**Energy and exergy indices**					
	Extended Absorption			Selective Catalytic Reduction of NOx		
	Exergy MJ/t HNO_3	CEnC MJ/t HNO_3	CExC MJ/t HNO_3	Exergy MJ/t HNO_3	CEnC MJ/t HNO_3	CExC MJ/t HNO_3
Existing BAT nitric acid plants from 2000 [5] (400 mg NOx/Nm^3) to 2007 (180 mg NOx/Nm^3) [4]						
Total consumption reduction	5.306	8.704	10.468	1.972	5.415	6.512
Additional consumption	0.532	1.465	1.776	7.013	11.504	13.836
Net consumption reduction	**4.774**	**7.239**	**8.692**	**-5.041**	**-5.789**	**-7.324**
New BAT nitric acid plants from 2000 [5] (200 mg NOx/Nm^3) to 2007 (150 mg NOx/Nm^3) [4]						
Total consumption reduction	1.200	1.970	2.369	0.464	1.274	1.532
Additional consumption	0.120	0.330	0.397	1.582	2.593	3.119
Net consumption reduction	**1.080**	**1.640**	**1.972**	**-1.118**	**-1.319**	**-1.587**

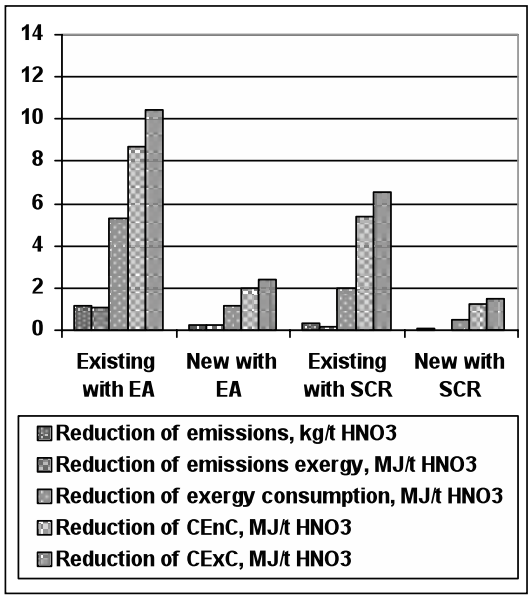

Fig. 6. Some positive effects from reduction of the emissions into air from BAT nitric acid plants

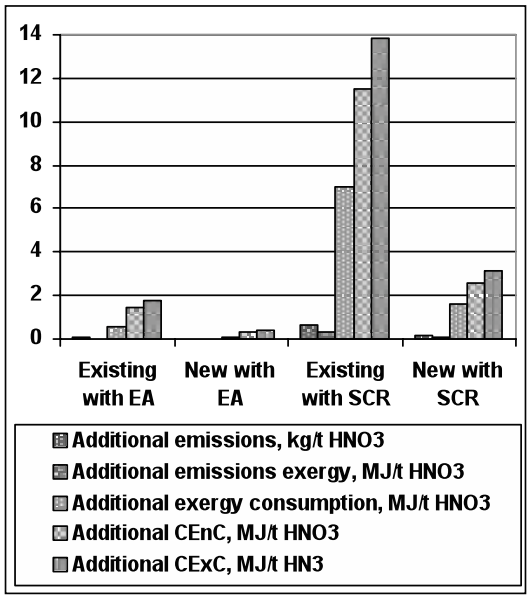

Fig. 7. Some negative effects from reduction of the emissions into air from BAT nitric acid plants

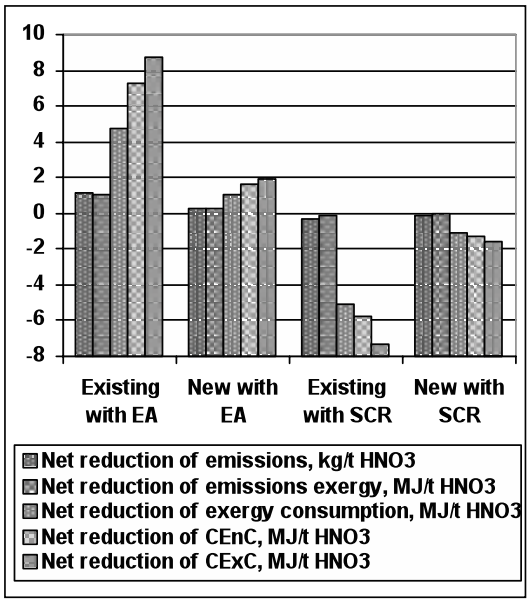

Fig. 8. Overall net effects from reduction of the emissions into air from BAT nitric acid plants

Conclusions

The exergy method and Cumulative Exergy concept are used in order to estimate the overall effects from the reduction of the emissions, recommended for existing and new BAT urea and nitric acid plants.

- The reduction of the ammonia and urea emissions into water from urea plants for existing and new plant from 2000 to 2007 has a large negative overall environmental effect, expressed as by an increase of the total emissions from the overall production site, as well as by a large increase of the overall consumption of natural resources (natural gas).

- The reduction of the NOx emissions into air for existing and new nitric acid plants from 2000 to 2007 shows positive values of all overall net emissions and natural resources consumption indices if the extended absorption is used and negative values if SCR is used. However, if low temperature fresh cooling water is not available at the site and a refrigeration unit is necessary, the only SCR method is capable to satisfy the BREF 2007 regulations, especially as an end-of pipe method for existing plants.

References

[1] Integrated pollution prevention and control: IPPC Directive http://europa.eu/legislation_summaries/environment/waste_management/l28045_en.htm

[2] The IPPC Directive: New Proposal for a Directive on Industrial emissions http://ec.europa.eu/environment/air/pollutants/stationary/ippc/proposal.htm

[3] Integrated Pollution Prevention and Control. Draft Reference Document on Best Available Techniques in the Large Volume Inorganic Chemicals, Ammonia, Acids and Fertilizers Industries. Second Draft. 2004. European Commission, Directorate-General JRC.

[4] Integrated Pollution Prevention and Control. Reference Document on Best Available Techniques for the Manufacture of Large Volume Inorganic Chemicals - Ammonia, Acids and Fertilizers, 2007, European Commission, Directorate-General JRC. Available at: ftp://ftp.jrc.es/pub/eippcb/doc/lvic_bref_0907.pdf

[5] Best Available Techniques for Pollution Prevention and Control in the European Fertilizer Industry: Booklet N 1: Production of Ammonia. Booklet N 2: Production of Nitric Acid. Booklet N 5: Production of Urea and Urea Ammonium Nitrate. Booklet N 6: Production of Ammonium Nitrate and Calcium Ammonium Nitrate. 2000, EFMA, Brussels, Belgium. Available at: http://www.efma.org/subcontent.asp?id=6&sid=31&ssid=31

[6] Sustainable environmental protection through the Industrial Emissions Directive http://www.cefic.be/_files/downloads/Leaflet-IED-Web.pdf

[7] Szargut, J., Morris, D. R., and Steward, F. R., 1988, *Exergy Analysis of Thermal, Chemical and Metallurgical Processes,* Hemisphere Publ.Co.,NY

[8] Isherwood,K.F., Mineral Fertilizer Production and Environment. Part 1. The Fertilizer Industry's Manufacturing Processes and Environmental Issues. 1999. UNEP/ UNIDO/ IFA Technical Report No 26, Paris.

[9] Kongshaug G. Energy Consumption and Greenhouse Gas Emissions in Fertilizer Production. IFA Technical Conference, Marrakech, Morocco, 1998. See also: http://www.fertilizer.org/ifa/Home-page/LIBRARY/Publication-database.html/Energy-Consumption-and-Greenhouse-Gas-Emissions-in-Fertilizer-Production.html

[10] Kirova-Yordanova, Z., Application of the Exergy Method to the Environmental Impact Estimation: the Ammonium Nitrate Production as a Case Study, Energy (2010), doi:10.1016/j.energy.2010.03.063.

[11] Kirova-Yordanova, Z., 2009, Application of the Exergy Method to the Environmental Impact Estimation: the Nitric Acid Production as a Case Study, *Proc. of the ECOS 2009*, Foz do Iguacu, Brazil, S. Nebra, S.de Oliveira Jr., E.Bazzo, eds., pp.1019-1029.

EXERGOECONOMIC ANALYSIS of TETRA-COMBINED TRIGENERATION SYSTEMS

Juan Carlos Burbano[a], Luiz Felipe Pellegrini[b], Silvio de Oliveira Jr.[c]

[a] *Technological University of Pereira, Pereira, Colombia*
[b] *University of São Paulo, São Paulo, Brazil*
[c] *University of São Paulo, São Paulo, Brazil*

Abstract: The present work intends to contribute to the efficient and rational use of a primary energy source, like natural gas, looking for alternative models of trigeneration systems. The economy of energy can be for industry or tertiary sector, a way to keep the production with less expense. So, the necessity of reduction in the production costs has been stimulating the development of this type of systems. A trigeneration system can be divided in two parts: the CHP unit (Combined Heat and Power) that produces electricity and heat and the refrigeration system (chiller) of vapor compression or absorption, which produces the cooling effect using electricity or heat available from CHP unit. Different trigeneration schemes are developed in this paper doing emphasis on trigeneration systems using absorption chillers. The study of absorption refrigeration systems has gained more importance in the last years since the primary energy that is used in an absorption system may come from heat available from a residual source or, even, a renewable one. Therefore, these systems not only use energy that would be rejected to environment, but also they avoid consumption of expensive fossil fuels. Thus, the use of these systems reduces the anthropogenic impact on the environment by decreasing the emission of CO_2. This paper intends to evaluate the performance of different trigeneration system configurations, including one using a hybrid absorption ejecto-compression chiller, by means of an exergetic and exergoeconomic analysis of these configurations in order to calculate the exergy-based cost of the final products. The trigeneration systems are applied to satisfy the energy requirements of a dairy industry.

Keywords: Trigeneration, absorption ejecto-compression chiller, exergoeconomic analysis

1. Introduction

Trigeneration, the combined production of power, heat and cold (generally, cold water for air conditioned purposes) from a single energy source, is a very effective way of utilizing the primary energy of a fuel more efficiently, economically, reliably and with less harm to the environment than centralized, dedicated electric production [1,2]. A trigeneration system can be divided into two parts: the CHP (Combined Heat and Power) unit, which produces electricity and heat, and the second part, the chiller (compression or absorption type), which produces refrigerating effect using electricity and/or heat from the CHP unit. Combined heating and power (CHP) technology has been in use in industrial applications from the end of 19th century. However, the rapid development of the technologies involved through the last decades, made easier the penetration of CHP technology in buildings, hotels, hospitals, schools, community heating or waste treatment sites. Most recent advances incorporate the use of alternative fuels such as hydrogen or biomass, or the exploitation of excess heat converting it to cooling power, that is used in air conditioning or in various industrial processes [3]. Trigeneration plant has become economically viable due to the commercial spread of absorption chillers [3, 4]. Absorption chillers are generally classified as direct or indirect-fired, and as single, double or triple-effect. In direct-fired units, the heat source can be gas or some other fuel that is burned in the unit. Indirect-fired units use steam or some other heat transfer fluid that brings in heat from a separate source, such as a boiler or heat recovered from an industrial process.

Low-pressure, steam-driven absorption chillers are available in capacities ranging from 100 to 1500 TR. Absorption chillers come in two commercially available designs: single-effect and double-effect. Single-effect machines provide a thermal COP of 0.7 and require about 8,2 kg of steam at 2,0 bar (abs) per TR of cooling. Double-effect machines are about 40% more efficient, but require a higher grade of thermal input, using about 4,5 kg of steam at 6.9-10.3 bar (abs) per TR [5].

In short, absorption cooling may fit when a source of free or low-cost heat is available, or if restrictions related to using conventional refrigeration exist. Essentially, the low-cost heat source displaces higher-cost electricity in a conventional chiller.

Trigeneration includes various technologies like: gas turbines, steam turbines, combined cycles, internal combustion engines, fuel cells and Stirling engines. Some works show diverse applications of the trigeneration systems: [6] in supermarkets, [7] in the petrochemical industry, [8] in the food industry, [9] in hospitals or the work of [10] that proposes a conceptual system of trigeneration based on gas turbine.

Exergy analysis predicts the thermodynamic performance of an energy system and the efficiency of the system components by accurately quantifying the entropy-generation of the components [11]. Exergy analysis of energy conversion plants allows characterizing how the available exergy (e.g. a fuel, employed as energy source) is used and destroyed in the existent processes of energy conversion in the plant, by means of a quantitative evaluation of the destruction and loss of exergy associated to the system. The basis of exergoeconomic approach is the consideration that exergy is an objective measure of the thermodynamic value of an energy carrier. Furthermore, it is considered that it is closely related to the economic value of the energy carrier. Hence, when a cost is attributed to an energy carrier, exergy is taken as the basis for allocating costs. In this paper an exergetic and exergoeconomic comparison of different trigeneration systems, including a tetra-combined one is carried out in order to calculate the efficiencies and exergy based cost of electricity, steam and exergy transferred to chilled water.

2. System Description

The trigeneration system analyzed in this work and here called tetra-combined trigeneration system is formed by three subsystems in thermal cascade: gas turbine, a cogeneration system based on a steam cycle and a hybrid absorption ejecto-compression chiller that was proposed by [12]. The expression tetra-combined is derived from the fact of this system to be based on two power cycles (Brayton and Rankine) and two refrigeration technologies (absorption and ejecto-compression). The performance of this system is compared with the performance of different conventional trigeneration systems, analyzed in [13], for the same operation conditions.

In Tetra-combined trigeneration system, the gas turbine produces power and it uses natural gas as energy source. The cogeneration subsystem, based on a steam cycle, uses the rejected gases from the gas turbine to produce superheated steam in a HRSG. The superheated steam feeds an extraction /condensation steam turbine. The steam turbine produces power and has three steam extractions. The first extraction is to feed the ejectors of the hybrid absorption ejecto-compression chiller; the second one is imposed by the process. This process steam is highly superheated and in certain applications saturated steam is needed, so it is necessary include a desuperheater to take the superheated steam down to the saturated state. In the desuperheater a mixture of superheated steam and water is produced and therefore the saturated steam is obtained. The third steam extraction in turbine is used as heat source to feed the generator of hybrid absorption ejecto-compression chiller. The remaining steam goes out from turbine and enters in the condenser to be recovered like feed water for boiler.

Figure 1 shows a schematic diagram of the tetra-combined trigeneration system.

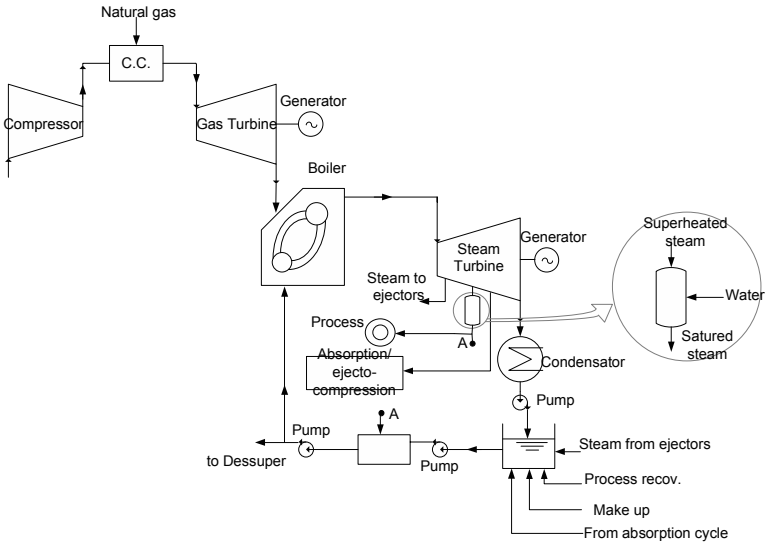

Fig. 1. Schematic diagram of the tetra-combined trigeneration system.

2.1. Hybrid Absorption ejecto-compression chiller

The absorption ejecto-compression refrigeration system had its origin in the works of [14] and [15]. The system is characterized by having ejectors between the evaporator and absorber. The operation is similar to the single-effect absorption system, with the variation of using ejectors. The number of ejectors depends on the steam pressure decrease required in the evaporator and the steam pressure increase required in the absorber. Each ejector operates with a pressure ratio of approximately of 2. The ejector exhaust is discharged to the absorber, causing the absorber pressure to be at a higher level than that in the evaporator. Therefore, the solution within the absorber can be kept away from crystallization when the system is needed to operate with low evaporator temperature or with high absorber temperature such as an air-cooled unit.

Figure 2 shows a water/lithium-bromide absorption ejecto-compression refrigeration system. Configurations of absorption refrigeration systems using ejectors are described in [16].

An ejector works as follow in Fig. 3: the refrigerant vapor at low pressure enters to ejector at point (1), and it is drawn by means of the expansion of the high pressure steam at point (B) that produces a vacuum when it enters in the ejector at point (2) and goes out in the point (A), so it lifts up the refrigerant vapor pressure in two times at the exit of ejector (point 3). This steam at the exit of the first ejector is used by a second ejector to lift up the refrigerant vapor pressure up to the absorber pressure. The motive steam then is absorbed by the strong solution coming from the generator. The refrigerant steam flow that is not vaporized remains in concentrated solution that is sent to generator where again the water steam is separated from the solution to flow up to the condenser and to continue the cycle.

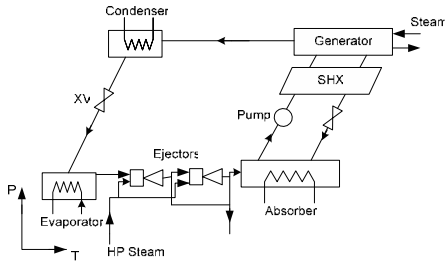

Fig. 2. Absorption-ejecto compression refrigeration system Dühring chart schematic.

Figure 3 shows the evolution of motive steam and the refrigerant drawn vapour throughout ejector.

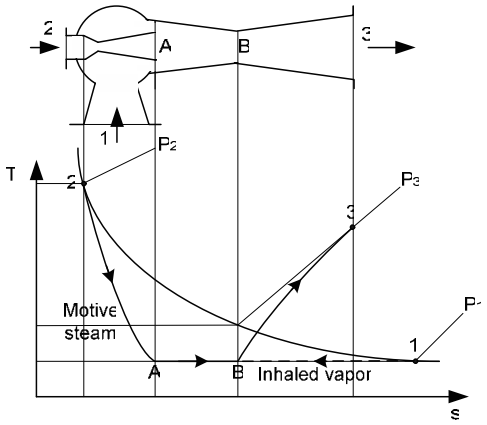

Fig. 3. Evolution of motive steam and drawn vapor throughout ejector (Oliveira Jr., 1991).

To reduce the motive steam consumption, in each ejector exit there is a mass flowrate deviation that is sent again to the boiler, or used in another process, if the pressure conditions allow.

3. Modelling and Simulation

The tetra-combined trigeneration system was developed to satisfy the energy requirement of a dairy industry [17], thus it's possible to compare it with the performance of trigeneration systems described, developed and analyzed in [13]:

i. Steam turbines and vapour-compression refrigeration.
ii. Steam turbines and single effect absorption refrigeration.
iii. Gas turbine and single effect absorption refrigeration.
iv. Combined cycle with single effect absorption refrigeration system.

Some assumed parameters used to simulate the trigeneration systems are shown in Table 1.

Table 1. Assumed parameters used to simulate the trigeneration system

Parameter	Value
Turbine inlet temperature (TIT) (°C)	1200
Compressor Isentropic Efficiency (%)	85
Gas Turbine Isentropic Efficiency (%)	87
Saturated Steam Pressure (bar)	10
HRSG heat losses (%)	2
HRSG Pinch (°C)	10
HRSG Approach (°C)	5
Pump Isentropic Efficiency (%)	70

In addition, the parameters shown in Table 2, are also considered.

Table 2. Additional assumed parameters to simulate the trigeneration systems

Parameter	Value
Electric Generator Efficiency (%)	95
Steam Pressure (bar)	42
Steam Temperature (°C)	420
Turbine (condensing-extraction) Isentropic Efficiency (%)	78-80
Pump Isentropic Efficiency (%)	70

For the purpose of analysis of absorption refrigeration systems, the following assumptions are made:

- The analysis is made under steady state conditions.
- The refrigerant at the outlet of the condenser is saturated liquid.
- The refrigerant at the outlet of the evaporator is saturated vapor.
- The outlet temperatures from the absorber and from generators correspond to equilibrium conditions of the mixing and separation, respectively.
- Pressure losses in the pipelines and in heat exchangers are negligible.
- Heat exchanges between the system and surroundings, other than the prescribed at the generator, high temperature generator (in double-effect absorption system), evaporator, condenser and absorber, are negligible.
- The reference environmental state for systems is water at an environment temperature of 25 °C (T_0) and 1 bar pressure (p_0).

In hybrid absorption ejecto-compression chiller, the following assumptions were considered for ejectors energy balance:

- Adiabatic flow.
- The kinetic energy in different points of ejector is negligible.
- One dimensional flow.
- Steady state condition.

- The thermodynamic state of drawn vapor does not change when going from point 1 to point A (Fig. 3).
- The vapor pressure at the mixing region of vapors (point A to point B of Fig. 3) is constant.

Thus, according to hypothesis assumed above, and applying the energy balance, the high-pressure steam flow entering into the ejector (based on Fig. 3, can be written by (1):

$$\dot{m}_{HPsteam} = \dot{m}\frac{(h_1 - h_3)}{(h_3 - h_2)} \quad (1)$$

The calculation of energy and exergy consumed by ejector can be made according to operational condition. Thus, considering output steam of each stage, which is not used by absorption system, it can be used by another process and the expressions for specific energy and exergy are respectively given by (2) and (3) [14]:

$$e_{ej} = \sum_{i=1}^{k}[\alpha(i)(h_2 - h_{3i})] \quad (2)$$

$$b_{ej} = \sum_{i=1}^{k}[\alpha(i)(h_2 - h_{3i}) - T_0(s_2 - s_{3i})] \quad (3)$$

Where k is the number of ejectors and $\alpha(i)$ is defined by (4):

$$\alpha(i) = \frac{\dot{m}_{HP\,steam}}{m_1} \quad (4)$$

The hybrid absorption ejecto-compression refrigeration system was modeled with two ejectors connected in series flow arrangement and using a pressure ratio of 1.8 for each one.

The models presented above were implemented in the Engineering Equation Solver [18], and simulated considering a steady-state operation.

For evaluating the costs, the idea is the development of cost balances for each component in the system. Considering the exergy-based cost for fuel equal to 1 kJ/kJ, it is possible to calculate the cost of the different plant flows. For distribution costs in control volumes with more than one product, the equality criterion was adopted. That is, each product has the same importance and consequently their exergy based cost were set equal (i.e. electricity and process steam, in cogeneration systems). Thus, the cost associated to the irreversibilities in the control volume is distributed equally among the exergy content of the outlet product flows.

4. Results

The results are presented and discussed for three scenarios, as done in [13]: the first one, for steam turbine configurations satisfying the plant requirements: 2.3 MW of electric power, 25 kg/s of chilled water at 5°C and 2 kg/s of saturated steam at 5 bar for process. The second one includes a gas turbine with HRSG and absorption refrigeration system capable to generate 1800 kW of electricity surplus under modelling parameters and the last one, including a combined cycle with absorption refrigeration system and the tetra-combined trigeneration system generating 7500 kW of electricity surplus.

According to [19] the only variable that unequivocally characterizes the performance of a component, from a thermodynamic point of view, is the exergy efficiency. Thus, for the described configurations above, the energetic and exergetic efficiencies were calculated and the results are presented in Tables 3 to 5.

Table 3. Energetic and exergetic efficiency for trigeneration system based in steam turbine.

Trigeneration System	Energetic Efficiency (%)	Exergetic Efficiency (%)
Steam turbine with compression refrigeration system.	56.88	26.64
Steam turbine with absorption refrigeration system.	57.37	26.87

Table 4. Energetic and exergetic efficiency for trigeneration system with 1800 kW excess electricity.

Trigeneration system	Energetic efficiency (%)	Exergetic efficiency (%)
Steam turbine with compression refrigeration system.	44.89	25.23
Steam turbine with absorption refrigeration system.	45.28	25.45
Gas turbine and HRSG with absorption refrigeration system.	79.12	44.65

Table 5. Energetic and exergetic efficiency for trigeneration system with 7500 kW excess electricity.

Trigeneration system	Energy Efficiency (%)	Exergy Efficiency (%)
Steam turbine with compression refrigeration system.	33.53	23.9
Steam turbine with absorption refrigeration system.	33.82	24.11
Combined cycle with absorption refrigeration system.	65.45	46.21
Tetra-combined cycle	65.79	46.45

In order to show the results of exergoeconomic study for the trigeneration systems, the fuel exergy rate, exergy destruction rate and exergy-based costs for each configuration were calculated and discussed below.

Figure 4 shows fuel exergy rate (kW) of each studied configuration for the analyzed scenarios: without and with electricity surplus.

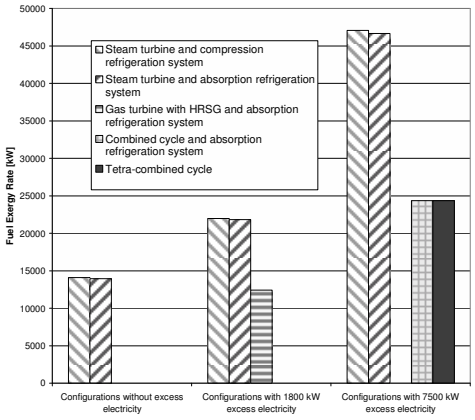

Fig. 4. Fuel exergy rate comparison for the analyzed systems.

As Fig. 4 shows, fuel exergy rate for configuration using steam turbines systems is very similar, in all cases, with a small advantage for the cycle with absorption refrigeration system and for 1800 kW excess electricity, gas turbine with HRSG and absorption refrigeration system presents a reduction in fuel exergy rate around 44% with respect to steam turbine configurations as was analyzed in [13].

For 7500 kW excess electricity, combined cycle with absorption refrigeration system and tetra-combined cycle present important reduction (around 48%) of fuel exergy rate with respect to steam turbine with compression and absorption refrigeration systems respectively.

Figure 5 shows the exergy destruction (in kW) caused by systems for all studied cases.

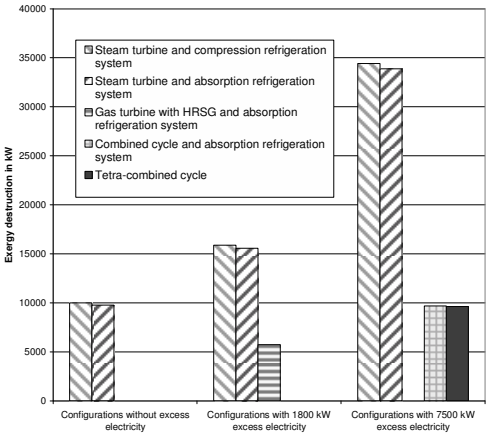

Fig. 5. Exergy destruction for the different systems.

As Fig. 5 shows that the exergy destroyed by steam turbine with compression refrigeration system is slightly higher than steam turbine with absorption refrigeration system, for all analyzed cases. For 1800 kW of electricity surplus, gas turbine with HRSG and absorption refrigeration system presents a reduction in exergy destruction of around 63% with respect to steam turbine configurations. For 7500 kW of electricity surplus, the exergy destroyed by tetra-combined cycle is a slightly lower than combined cycle with absorption refrigeration system and presenting a reduction of exergy destruction around of 71% with respect to steam turbine with compression and absorption refrigeration systems.

The figure 6 shows a comparison of the exergy-based costs (kJ/kJ) of electricity, process steam and exergy transferred to chilled water for the studied configurations under the three scenarios.

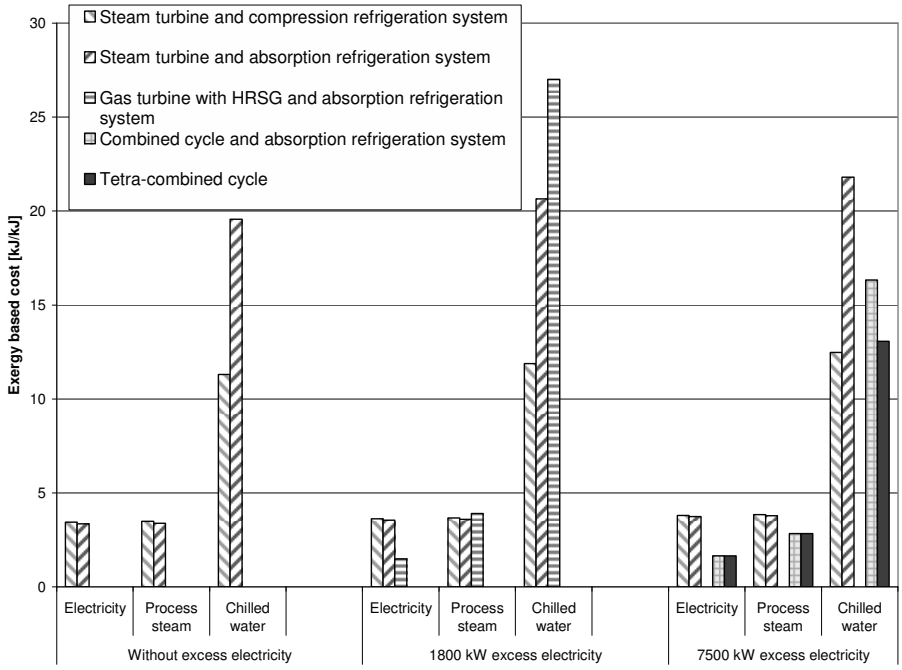

Fig. 6. Exergy-based costs (kJ/kJ) of electricity, process steam and chilled water for studied configurations.

As Fig. 6 shows, without electricity surplus scenario, the exergy-based cost of electricity and process steam are similar in steam turbine configurations, being slightly higher in system with compression refrigeration system. Comparison for chilled water cost among two configurations is interesting, since in the first case, exergy based cost is 11.3 kJ/kJ, whereas with absorption cycle it is 19.55 kJ/kJ. The reason for this difference is because the coefficient of performance (COP) for compression refrigeration system is 4.874 and its exergetic efficiency is 30.41% versus a COP of the absorption refrigeration system of 0.67, and exergetic efficiency of 17.14%.

The results also show, in the 1800 kW electricity surplus scenario, the gas turbine with HRSG and absorption refrigeration system results in lower electricity exergy based cost in comparison with steam turbine configurations. For process steam the exergy based cost is very similar for the three analyzed configuration. Regarding the exergy transferred to chilled water exergy based cost, the highest one is for gas turbine configuration. This happens because the steam exergy based cost entering the generator of absorption refrigeration system has an exergy based cost of 5.4 kJ/kJ and a chiller exergetic efficiency of 17.14%. However, the gas turbine with HRSG and absorption refrigeration system presents higher global plant exergetic efficiency as can be seen in Table 4.

In the last scenario, 7500 kW of electricity surplus, the combined cycle with absorption refrigeration system and tetra-combined cycle, have two kinds of electricity exergy based costs: one from gas turbine and another one from steam turbine. The results showed in Fig. 6 for these scenario, are an average, calculated taking into account the power developed by each turbine. The combined cycle and Tetra-combined cycle present considerable reduction in electricity and process steam exergy based costs in comparison with steam turbine configuration. In this scenario, the biggest reduction in the exergy-based cost of chilled water is presented in the Tetra-combined cycle, as consequence of having an exergy efficiency in the hybrid absorption ejecto-compression chiller of 21.24 %, in contrast with the exergy efficiency of

the single effect absorption chiller of combined cycle of 17.14 %, showing an advantage of including ejectors between the evaporator and absorber.

Tables 6 to 8 show the average exergy-based cost of products for the different studied configurations.

In general, observing the impact in the formation of energy conversion costs for the proposed configurations, the minor impact in exergy-based costs of products (electricity, process steam and exergy transferred to chilled water) is for Tetra-combined cycle, as it is possible to appreciate looking at the average exergy-based costs of the different configurations on Tables 6 to 8.

Table 6. Average exergy-based cost of products for trigeneration system based in steam turbine.

Trigeneration System	**Average Exergy Cost (kJ/kJ)**
Steam turbine with compression refrigeration system.	3.75
Steam turbine with absorption refrigeration system.	3.72

Table 7. Average exergy-based cost of products for trigeneration system with 1800 kW excess electricity.

Trigeneration system	**Average Exergy Cost (kJ/kJ)**
Steam turbine with compression refrigeration system.	3.96
Steam turbine with absorption refrigeration system.	3.93
Gas turbine and HRSG with absorption refrigeration system.	2.24

Table 8. Average exergy-based cost of products for trigeneration system with 7500 kW excess electricity.

Trigeneration system	Average Exergy Cost (kJ/kJ)
Steam turbine with compression refrigeration system.	4.18
Steam turbine with absorption refrigeration system.	4.14
Combined cycle with absorption refrigeration system.	2.17
Tetra-combined cycle	2.15

Finally, fuel consumption and exergy destruction for the different systems are reflected in exergy based costs as Fig. 6 shows. Nevertheless, to choose an alternative or another, it is also necessary to take in consideration technical and financial aspects, since better efficiency means minor fuel consumption and higher investment costs.

5. Conclusions

The trigeneration represents a quite interesting alternative of producing electricity and reducing the production costs of utilities. In this work an analysis of different trigeneration systems was done, including a tetra-combined system, by means of the use of exergoeconomic analysis to quantify its energetic and exergetic efficiency and the impact in the production of electricity, process steam and chilled water for air conditioning purpose. The preliminary performance results of the studied trigeneration systems show the viability of tetra-combined cycle. This system has a higher exergetic efficiency than the single effect absorption chiller. This configuration also presents a bigger impact in the exergetic based cost of chilled water in comparison with other analyzed systems.

Nomenclature

h specific enthalpy, kJ/kg

$\dot{m}$ mass flowrate, kg/s

s specific entropy, kJ/(kg K)

T temperature, K

Subscripts and superscripts

0 Standard environmental state

References

[1] Wu, D.W., Wang, R.Z., 2006, Combined cooling, heating and power: A review, Progress in Energy and Combustion Science, 32, pp. 459-495.

[2] Hernandez-Santoyo, J., Sanchez-Cifuentes, A., 2003, Trigeneration: an alternative for energy savings, Applied Energy, 76, pp. 219-227.

[3] Kavvadias, K.C., Tosios, A.P., Maroulis, Z.B., 2010, Design of a combined heating, cooling and power system: Sizing, operation strategy selection and parametric analysis, Energy Conversion and Management, 51, pp. 833–845.

[4] Cardona, E., Piacentino, A., 2003, A methodology for sizing a trigeneration plant in Mediterranean areas, Applied Thermal Engineering, 23, pp. 1665-1680.

[5] Absorption Chillers. 2010. Available in: http://www.absorptionchillers.com/. Accessed in January of 2010.

[6] Maidment, G.G., Tozer, R.M., Missenden, J.F., 2001. Combined Cooling, Heat and Power (CCHP) in Supermarkets. H*eat Powered Cycles Conference,* Conservatoire national des arts et métiers, Paris. pp. 277-284.

[7] Colonna, P., Gabrielli, S., 2003, Industrial trigeneration using ammonia-water absorption refrigeration systems (AAR). Applied Thermal Engineering, 23, pp. 381-396.

[8] Bassols, J., Kuckelkorn, B., Langreck, J., Schneider, R., Veelken H., 2002, Trigeneration in the food industry. Applied Thermal Engineering, 22, pp. 595-602.

[9] Ziher, D., Poredos, A., 2006, Economics of trigenerationsystem in a hospital. Applied Thermal Engineering. 26, pp. 680-687.

[10] Khaliq, A., 2009, Exergy analysis of gas turbine trigeneration system for combined production of power heat and refrigeration. International Journal of Refrigeration, 32, pp. 534-545.

[11] Kwak, H.Y., Kim, D.Y., Jeon, J.S., 2003, Exergetic and thermoeconomics analyses for power plant, Energy, 28, pp. 343–360.

[12] Garagatti Arriola, D. W., Oliveira Jr., S., 2003, Tetra-combined Trigeneration System. Exergy and Thermoeconomic Analysis. *Proceedings of the ECOS'2003 Efficiency, Costs, Optimization, Simulation and Environmental Impact of Energy Systems*, 1, pp 137-144.

[13] Burbano, J. C., Pellegrini, L. F., Oliveira Jr., 2009, Comparative exergoeconomic analysis of trigeneration systems for a dairy industry. *Proceedings of the 21st International Conference on Efficiency, Costs, Optimization, Simulation and Environmental Impact of Energy Systems.* Foz de Iguaçú, v. 4, pp. 513-524.

[14] Oliveira Jr., S., 1991, Upgrading industrial thermal effluents – exergetic, entropic and economic analysis, In French. Ph.D. Dissertation. Polytechnic National Institute of Lorraine, France.

[15] Oliveira Jr., S., Le Goff, P., 1993, Hybrid systems absorption-compression to upgrade industrial waste heat. *Energy Systems and Ecology Proceedings of the international conference*. Krakow, 2, pp. 651-658.

[16] Srikhirin, P., Aphornratana, S., Chungpaibulpatana, S., 2001, A review of absorption refrigeration technologies, Renewable and Sustainable Energy Reviews, 5 pp. 343–372.

[17] Larrazábal, M. L., Oliveira Jr., S., 2002, Thermoeconomic Evaluation of Cogeneration Systems for a Dairy Industry, *Proceedings of ECOS'2002 - Efficiency, Costs, Optimization, Simulation and Environmental Impact of Energy Systems*, Berlin. pp. 1409-1416.

[18] F-Chart, 2009, EES® Engineering Equation Solver.

[19] Tsatsaronis, G., 1999. Strengths and limitation on exergy analysis in Bejan, A., Mamut, E., *Thermodynamic Optimization of Complex Energy Systems*. NATO Science series. Springel Ed.

A New and General Methodology for Calculating Efficiency and Cost in Thermoeconomics

José Santos[a], José Escobar Palacio[b], Julio Mendes da Silva[c] and Hugo Moreira[d]

[a] *Federal University of Espírito Santo, Vitória-ES, Brazil*
[b] *Federal University of Itajubá, Itajubá-MG, Brazil*
[c] *University of São Paulo, São Paulo-SP, Brazil*
[d] *Federal University of Rio Grande do Norte, Natal-RN, Brazil*

Abstract: The inclusion of the negentropy in thermoeconomics represented, indeed, a great advance in the discipline, since it allowed one to quantify the condenser product in a steam cycle plant and to allocate explicitly the cost of the residues to the final products of the systems. However, by using the negentropy joined up with the exergy, the product of the condenser (negentropy) is always greater than its fuel (exergy), which seems that the condenser efficiency is greater than 100 percent. Therefore, this paper presents a new methodology for calculating efficiencies and related costs in thermal systems. In this new methodology, called H&S Model, the fuels and the products of each component are defined by taking into account all enthalpy, entropy and also chemical exergy additions to and removals from all the streams. Consequently, a direct link between the definition of fuel and product for a component and the corresponding costing equations is established. In particular, this paper shows that by using the H&S Model, the efficiency of each component (including the dissipative ones, such as the condenser) ranges from zero (for a totally irreversible process) to 100 percent (for a totally reversible process).

Keywords: Efficiency, Cost, Exergy Components, H&S Model, Thermoeconomics.

1. Introduction

The thermoeconomic methodologies have been searching for productive structures that represent the process of cost formation in the thermal systems. Generally, the productive structures defines the productive propose of the subsystems (products and fuels), using thermodynamic magnitudes. The way in which we define the productive structure is the key point of the thermoeconomic analysis [1]. The products and the fuels are defined by considering the desired result produced by the component and the resources expended to generate this result, respectively. The efficiency of a component is defined as the ratio between products and fuels.

Most analysts agree that exergy, instead of enthalpy only, is the most adequate thermodynamic property to define the fuels and the products of the subsystems since it contains information from the second law of thermodynamics and accounts for energy quality. Sometimes, under a thermoeconomic analysis point of view, it is necessary to consider a mass or an energy flow rate consisting of several components, for example thermal, mechanical or chemical exergy, or even to include fictitious flows (negentropy) [2]. The inclusion of the negentropy in thermoeconomics represented, indeed, a great advance in the discipline, since it allowed one to quantify the condenser product in a steam cycle plant, which was not possible before once that it is a dissipative component, whose product cannot be expressed in terms of exergy.

Although the use of the negentropy concept to define the productive structure is good in order to apportion the cost of the condenser and residues to the productive components of the system, the product of the condenser (negentropy) is always greater than its fuel (exergy), which seems that the condenser efficiency is greater than 100 percent.

Therefore, this paper proposes a new and general methodology for calculating efficiencies and related costs in thermal systems, by systematically defining a productive structure in which the efficiency (the ratio between products and fuels) of all components (including the dissipative one) ranges from zero (for a totally irreversible process) to 100 percent (for a totally reversible process).

By using two different applications, this paper shows that this new methodology is easily applicable to any thermodynamic cycle whose processes can be represented in the h-s plane.

Corresponding Author: José Santos, Email: jjcssantos@yahoo.com.br

2. The H&S Model

This methodology is called H&S Model because it is based on the disaggregation of physical exergy into enthalpic ($m.\Delta h$) and entropic ($m.T_0.\Delta s$) components. Thus, in the productive structure of the H&S Model, the fuels and the products of each component are defined by taking into account all enthalpy, entropy and also chemical exergy additions to and removals from all the streams.

The entropic component of physical exergy and the negentropy are the same magnitude ($m.T_0.\Delta s$). However, the negentropy is a fictitious flow running parallel to the exergy flow [3,4] and the entropic component is a part of the exergy flow, i.e., it is a physical exergy component flow.

In previous works, the words negentropy [5-8] and syntropy [9-11] were used to describe this exergy component ($m.T_0.\Delta s$). To avoid misunderstanding, in this paper, we use entropic component only.

The H&S approach consist of the following steps:

- Representation of the thermodynamic cycle in the h,s plane.
- Definition and representation of the productive structure using the functional diagram.
- Calculation of the productive flow values.
- Formulation of the cost equations.

The solution of the set of cost equations allows the attainment of the unit cost of each internal flow and final product.

The efficiency of the overall system and subsystems is obtained by calculating the ratio between their products and their fuels.

2.1. The h,s Plane

In agreement with [12], efficiency, cost and behaviour of the system are based in the trajectory in the h,s plane any flow performs when it works for the specific purpose of the plant.

Therefore, in order to apply the H&S Model the plant must be represented in the h,s plane.

The products and the fuels of each subsystem, in terms of enthalpic and chemical exergy component, are defined based on the quantity of these magnitudes added to and removed from the working fluid, respectively. On the other hand, the entropic component flows are the products of the subsystems that decrease the working fluid entropy, and subsystems that increase the working fluid entropy are entropic components consumers.

2.2. The Productive Structure

According to [1], perhaps the fundamental limitation of the Theory of Exergetic Cost, as it was originally formulated, consisted of defining the productive structure in relation to the same flows and components present in the physical structure. The resulting difficulties lie mainly in the adequate treatment of the dissipative units and of the residues.

Therefore, in order to carry out a thermoeconomic analysis, the H&S Model defines the productive purpose of the subsystems (fuels and products), as well as the distribution of the external resources and internal products throughout the system. The productive structure could be represented by means of a functional diagram, as proposed by [3] and used by [1] and [4].

The functional diagram represents graphically the cost formation process of the system. The rectangles are the real units (or subsystems) that represent the actual equipments of the system. The rhombus and the circles are fictitious units called junction and bifurcations, respectively. Each productive units has inlet and outlet arrows, that represent its fuel (or resource) and products, respectively. There are productive units that have small junction to indicate that they have more than one fuels, and/or a small bifurcation to indicate that they have more than one product.

2.3. The Productive Flow Values

The flows of the functional diagram are productive flows. The only limitation which must be imposed is that it must be possible to evaluate all these flows in relation to the state of the plant as defined by the physical structure. The productive flows that represent power and external fuel are the same flows presented in the physical structure. These flows are total exergy. The remaining productive flows are the variation of an exergy component between two different states of the physical structure. For example, the productive flows expressed in terms of physical exergy ($E^{PH}_{j:k}$) are variations of physical exergy between two state (j and k) of the physical structure, as explained in (1).

$$E^{PH}_{j:k} = m \cdot [h_j - h_k - T_0 \cdot (s_j - s_k)] \quad (1)$$

The productive flows representing the enthalpic ($E^{H}_{j:k}$) and the entropic ($E^{S}_{j:k}$) components of the physical exergy are calculated using, respectively, (2) and (3), for water, steam and refrigerants, or (4) and (5) for fluids considered as ideal gas.

$$E^{H}_{j:k} = m \cdot (h_j - h_k) \quad (2)$$

$$E^{S}_{j:k} = m \cdot T_0 \cdot (s_j - s_k) \quad (3)$$

$$E^{H}_{j:k} = m \cdot \int_{T_k}^{T_j} Cp \cdot dT \quad (4)$$

$$E^{S}_{j:k} = m \cdot T_0 \cdot \left[\int_{T_k}^{T_j} \frac{Cp}{T} \cdot dT - R \cdot \ln\left(\frac{p_j}{p_k} \right) \right] \quad (5)$$

The chemical exergy ($E^{CH}_{j:k}$) is considered as fuels and/or product of subsystems when the working fluid changes its chemical composition between the inlet and the outlet (j and k), as shown in (6).

$$E^{CH}_{j:k} = E^{CH}_{j} - E^{CH}_{k} \quad (6)$$

The procedures to calculate the chemical exergy of the streams (E^{CH}_{j} and E^{CH}_{k}) can be found in [13].

2.4. The Cost Equations

The mathematical model for cost allocation is obtained by formulating the cost equations balance in each actual and fictitious units of the functional diagram, as shown in (7), where c is the monetary unit cost of each flow of the productive structure (unknown variable) and Y is a generical way to represent the flows of the functional diagram, which can be power (P) and external fuel (Q), or enthalpic (E^{H}), entropic (E^{S}), physical (E^{PH}) and chemical (E^{CH}) exergy added to and removed from the working fluid. The monetary unit cost of a flow is the amount of monetary unit required to obtain one unit of this flow. The variable Z is the hourly cost of each unit due to the capital cost, operation and maintenance. Note that the monetary unit cost of the external fuel is a known variable.

$$c_{ufd} \cdot \sum Y_{out} - \sum (c_{in} \cdot Y_{in}) = Z \quad (7)$$

As shown in (7), the H&S Model attributes the same monetary unit cost (c_{ufd}) to all of the flows leaving the same productive unit or leaving the same bifurcation (Y_{out}).

By modifying (7) in order to formulate the cost balances to provide the exergetic unit cost (k) of each flow of the productive structure, we obtain (8). The exergetic unit cost of a flow is the amount of exergy required to obtain one unit of this flow. This cost is a measure of the thermodynamic efficiency of the production process generating this flow [12]. In this case, the hourly cost of the subsystem due to the capital cost, operation and maintenance must be equals zero ($Z = 0$) and the monetary unit cost of the external fuel is replaced by the exergetic unit cost of an external resource, which is equal 1.00 kW/kW, because there is no exergy destruction before the productive process is performed [12]. The auxiliary equations are the same as used to obtain the monetary unit cost.

$$k_{ufd} \cdot \sum Y_{out} - \sum (k_{in} \cdot Y_{in}) = 0 \quad (8)$$

The solution of the sets of cost equations obtained by applying (7) and (8) in each device of the productive structure allows the attainment of the monetary and exergetic unit cost of each internal flow and final product, respectively.

3. Applications of the H&S Model

The beauty of a theory is usually shown in the simplicity of its forms and the generality of its message, but its power resides in its capacity to solve practical cases [4]. Two simple examples of thermal systems are used, in this paper, to illustrate the application of the H&S Model: a Rankine cycle power plant (RCPP) and a Brayton cycle cogeneration plant (BCCP). By using these plants, this paper shows the capacity of the H&S Model to treat two important points in discussion related to the thermoeconomic methodologies: the dissipative components (e. g., the condenser) and the residues (e. g., the exhaust gases), respectively.

3.1. Rankine Cycle Power Plant

The physical structure of the Rankine cycle power plant (RCPP) represented in Fig. 1 essentially coincides with the one used by [3] and [4]. The plant (system) is considered made up of four components (subsystems): boiler (B), turbine and generator (T-G), condenser and cooling water pump (C), and boiler feeding pump (P).

The representation of the plant in the h,s plane is shown in Fig. 2. The functional diagram is shown in Fig. 3. We can see that the enthalpy of the working fluid is increased as much in the pump as in the boiler. The turbine consumes part of this enthalpy. The operation of these productive units (pump, boiler and turbine) increases the entropy of the working fluid. The condenser consumes the remaining part of enthalpy while it decreases the entropy of the working fluid. In other words, the condenser product is entropic exergy component flow, and its fuel is enthalpic exergy component flow. Therefore, the cost of the condenser must be charged to all the productive units responsible

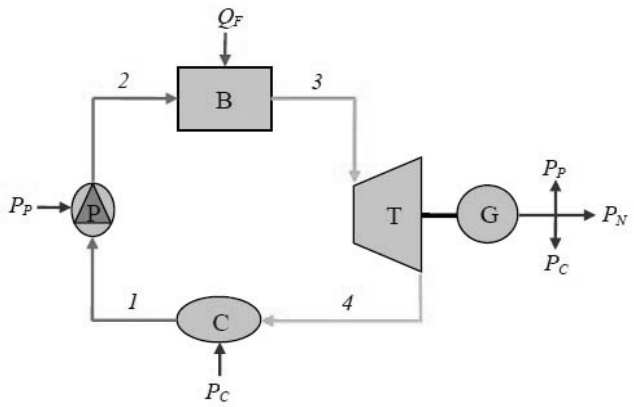

Fig. 1. Physical Structure of the Rankine Cycle Power Plant

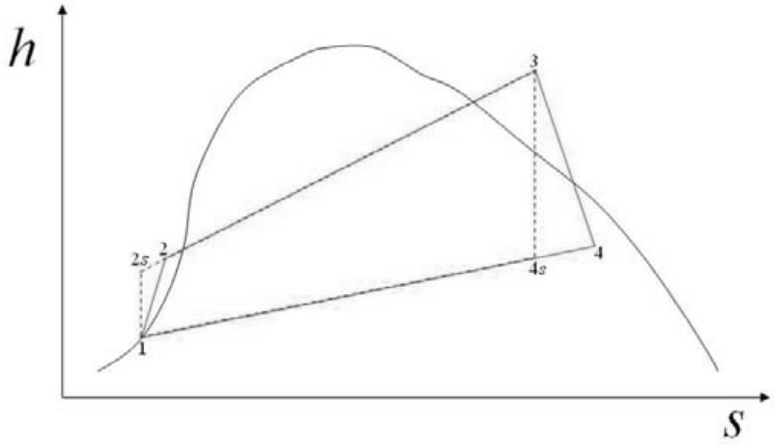

Fig. 2. Rankine Cycle Power Plant represented in the h,s Plane

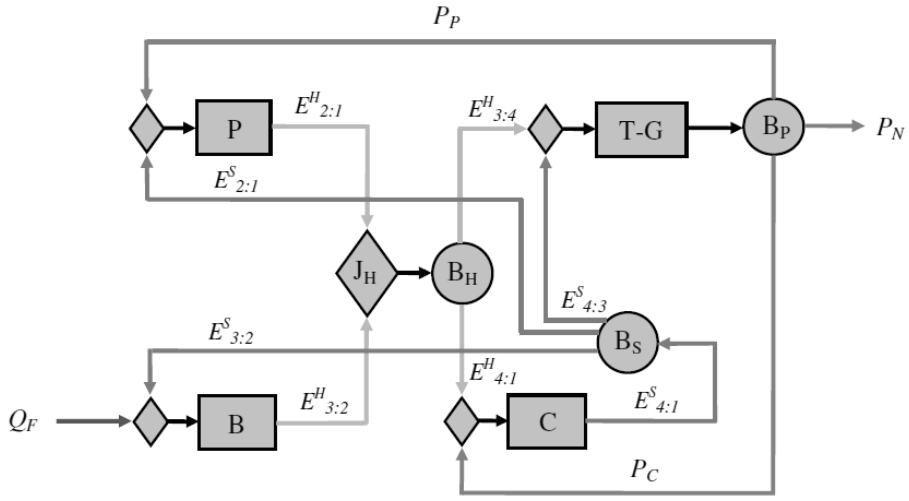

Fig. 3. Productive Structure of the Rankine Cycle Power Plant

for the increase of the working fluid entropy (pump, boiler and turbine), proportionally to the working fluid entropy increased by each of them.

3.2. Brayton Cycle Cogeneration Plant

Figure 4 shows the physical structure of the Brayton cycle cogeneration plant (BCCP). The system is considered made up of four subsystems: air compressor (AC), combustion chamber (CC), gas turbine (GT) and recovery boiler (RB). Figure 5 shows the processes of the Brayton cycle in the h,s plane. The functional diagram of the Brayton cycle cogeneration plant is shown in Fig. 6.

In this case, the residual enthalpy of the gases which abandon the plant through the chimney of the recovery boiler can be explained by the increase of the working fluid entropy in the compressor, in the combustor and in the turbine. The recovery boiler has a negative contribution. Thus, the recovery boiler produces entropic exergy flow. The other part of entropic exergy is produced by the environment (E), an imaginary dissipative unit, where residual enthalpy and chemical exergy of the gases is charged. This entropic exergy flow, plus that produced by the recovery boiler are given to the units that increase the working fluid entropy.

Once the residues must be allocated where they have been originated, the chemical component of the residue is allocated to the combustion chamber. Thus, the enthalpic component of the residue is charged to the productive units that increase de working fluid entropy in the cycle.

4. Cost and Efficiency

Table 1 shows the productive flows, its exergy values and its respective exergetic unit costs, considering the two kind of plant: the Rankine cycle power plant (RCPP) and the Brayton cycle cogeneration plant (BCCP). These plants were analyzed in details in [9] and [11], respectively.

According to [12], irreversibility is the magnitude generating the costs. Consequently, in any irreversible cycle plant, the exergetic unit cost should be increased along the productive structure. Bearing this in mind, the exergetic unit costs of the internal flows and final products obtained by the H&S Model are consistent because they are greater than one, once that the exergetic unit cost of the external fuel is equals one.

In H&S Model, the fuels and products used in the functional diagram in order to calculate the costs coincide with the fuels and product which is used for calculating efficiency for both productive and dissipative units, as shown in (9). This equation under any condition, for any subsystem, can be interpreted as, or coincide with the classical and well-known product-fuel definition of efficiency.

$$\eta_{tufd} = \frac{\sum Y_{out}}{\sum Y_{in}} \tag{9}$$

The formula and the value of efficiency for each unit or subsystem of the functional diagram of the Rankine cycle power plant and the Brayton cycle cogeneration plant are shown in Table 2 and 3, respectively. In Table 2, the efficiency of the turbine and generator was calculated as a single unit, but the efficiencies of the turbine and generator, separately, are 85.56% and 94.96%, respectively. We can see that the efficiency of each unit (subsystem or component) is lower than 100%, including that of the dissipative ones. The efficiency of the condenser and cooling water pump (Table 2) is 95.33%, but the efficiency of the condenser, alone, is 95.50%. By using the H&S Model, the condenser efficiency in an actual steam power cycle will always be less than 100%, and this efficiency would only be 100% in case it were possible to transfer heat in the condenser at the same temperature, i. e., if the condensation temperature and the reference temperature were the same (in a reversible steam power cycle [9]). In other words, by using the H&S Model, the efficiency of each component (including the dissipative one, such as the condenser) ranges from zero (for a totally irreversible process) to 100 percent (for a totally reversible process).

5. Closure

This paper presented the H&S Model, which is a new and general methodology for calculating efficiency and cost in thermoeconomics, in which a direct link between (i) the definition of fuel and product, (ii) the corresponding costing equations and (iii) the efficiency calculation is established.

The H&S Model is a new methodology since it is the first disaggregating the physical exergy into enthalpic and entropic component, in which the fuels and products of the components are defined by considering all enthalpy, entropy and chemical exergy additions to and removals from all streams.

The H&S is a general methodology because it can be applied to any component, unit or subsystem, including the dissipative ones. Furthermore, it can

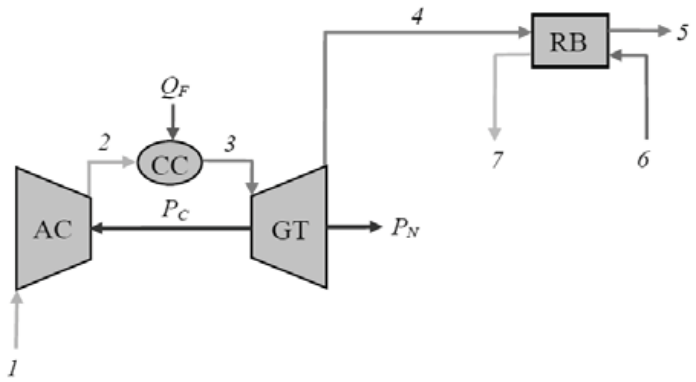

Fig. 4. Physical Structure of the Brayton Cycle Cogeneration Plant

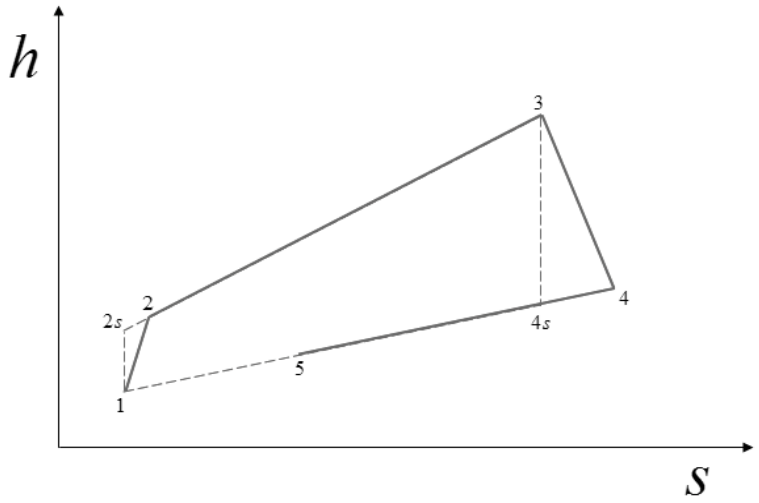

Fig. 5. Brayton Cycle Cogeneration Plant represented in the h,s Plane

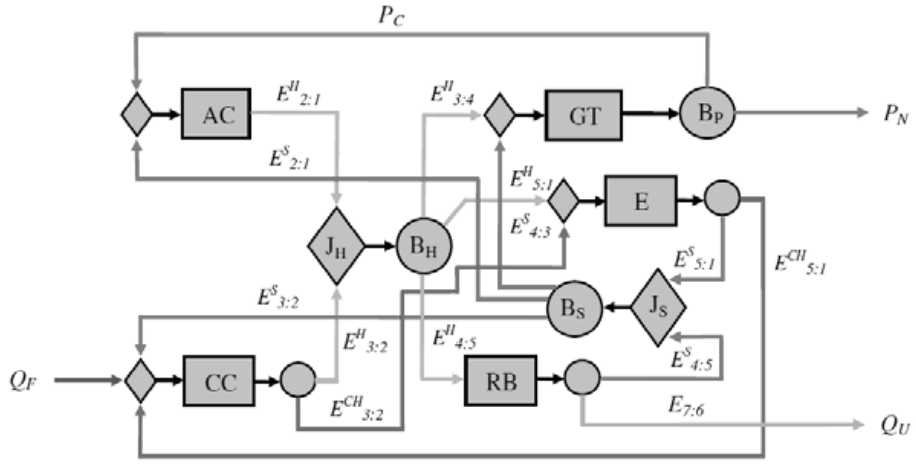

Fig. 6. Productive Structure of the Brayton Cycle Cogeneration Plant

Table 1. The Productive Flows and theirs Exergetic Unit Cost obtained by using the H&S Model

Productive Flow	Value (kW)		Exergetic Unit Cost (kW/kW)	
	RCPP	BCCP	RCPP	BCCP
Q_F	70,000.00	11,630.96	1.00	1.00
$E^H_{2:1}$	146.22	3,113.03	4.15	2.63
$E^H_{3:2}$	63,406.09	10,806.96	2.82	2.10
$E^H_{3:4}$	21,304.58	5,546.50	2.82	2.22
$E^H_{4:1}$	42,247.73	----------	2.82	-----
$E^H_{4:5}$ / $E^H_{5:1}$	----------	6,389.87 / 1,983.62	-----	2.22
$E^S_{2:1}$ / $E^S_{3:2}$ / $E^S_{4:3}$	21.70 / 36,731.52 / 3,594.51	313.90 / 4,202.19 / 307.13	2.96	2.61
$E^S_{4:1}$	40,347.73	----------	2.96	-----
$E^S_{4:5}$	----------	3,170.04	-----	2.62
$E^S_{5:1}$	----------	1,653.19	-----	2.60
$E^{CH}_{3:2}$	----------	189.67	-----	2.10
$E^{CH}_{5:1}$	----------	189.67	-----	2.60
P_N / P_C / P_P	20,000.00 / 75.00 / 155.00	--------	3.50	-----
P_N / P_C	----------	2,433.47 / 3,113.03	-----	2.36
$Q_U = E_{7:6}$	----------	2,246.32	-----	2.62

be applied to any thermodynamic cycle whose processes can be represented in the h-s plane, including to a reversible steam power cycle [9].

Table 2. Efficiency of Productive Units in RCPP

Productive Unit	Efficiency	
	Formula	Value (%)
Pump (P)	$\frac{E^H_{2:1}}{E^S_{2:1} + P_P}$	82.75
Boiler (B)	$\frac{E^H_{3:2}}{E^S_{3:2} + Q_F}$	59.41
Turbine and Generator (T-G)	$\frac{P_N + P_P + P_C}{E^H_{3:4} + E^S_{4:3}}$	81.25
Condenser and pump (C)	$\frac{E^S_{4:1}}{E^H_{4:1} + P_C}$	95.33
Power Plant (RCPP)	$\frac{P_N}{Q_F}$	28.57

The H&S Model establishes a direct link between the definition of fuel and product, the costing equations and the efficiency calculation because the fuels and the products used in the functional diagram to calculate costs coincide with the fuels and products which are used for calculating the efficiency of both productive and dissipative units.

Table 3. Efficiency of Productive Units in BCCP

Productive Unit	Efficiency	
	Formula	Value (%)
Air Compressor (AC)	$\frac{E^H_{2:1}}{E^S_{2:1} + P_C}$	90.84
Combustion Chamber (CC)	$\frac{E^H_{3:2} + E^{CH}_{3:2}}{Q_F + E^{CH}_{5:1}}$	68.63
Gas Turbine (GT)	$\frac{P_N + P_C}{E^H_{3:4} + E^S_{4:3}}$	94.75
Recovery Boiler (RB)	$\frac{E^S_{4:5} + Q_U}{E^H_{4:5}}$	84.76
Environment (E)	$\frac{E^S_{5:1} + E^{CH}_{5:1}}{E^H_{5:1} + E^{CH}_{3:2}}$	84.80
Cogeneration Plant (BCCP)	$\frac{P_N + Q_U}{Q_F}$	40.24

Nomenclature

c monetary unit cost, $/kWh
Cp specific heat, kJ/(kmol.K)
E exergy flow, kW
h specific enthalpy, kJ/kg
k exergetic unit cost, kW/kW
M molecular weight, kg/kmol
m mass flow, kg/s
p pressure, kPa
R constant of gases, kJ/(kg.K)
s specific entropy, kJ/(kg.K)
T temperature, ^{o}C
Y generic productive flow, kW
Z hourly cost of the subsystem, $/h

Greek symbols

η efficiency

Superscripts

CH chemical component only
H enthalpic component only
PH physical component only
S entropic component only

Subscripts

in inlet flow
j physical stream
j:k from stream *k* to stream *j*
k physical stream
o environment or reference
out environment or reference
ufd subsystem or unit of the functional diagram

References

[1] Lozano, M. A., and Valero, A., 1993, Thermoeconomic Analysis of a Gas Turbine Cogeneration System, *ASME Book no. H00874, WAM 1993, AES*, Vol. 30, p. 312-20.

[2] Torres, C., et al., 1996, The Productive Structure and Thermoeconomic Theories of System Optimization, *ME'96: International Mechanical Engineering Congress & Exposition (ASME WAN' 96)*.

[3] Frangopoulos, C. A., 1987, Thermo-Economic Functional Analysis and Optimization, Energy, 12(7), pp. 563-571.

[4] Lozano, M.A., et al., 1993, Theory of Exergetic Cost and Thermoeconomic Optimization, Energy Systems and Ecology, Eds. J. Szargut, Z. Kolenda, G. Tsatsaronis and A. Ziebik. Vol. 1, pp. 339-350, July 5-9, Cracow, Poland.

[5] Santos, J., et al., 2006, On The Thermoeconomic Modeling for Cost Allocation in a Dual-Purpose Power and Desalination Plant, *In Proceedings of ECOS 2006*, Volume 1, pp. 441-448, Aghia Pelagia, Crete, Greece.

[6] Santos, J., et al., 2008, On The Productive Structure for the Residues Cost Allocation in a Gas Turbine Cogeneration Plant, *In Proceedings of ECOS 2008*, Volume 2, pp. 641-648. Cracow, Poland.

[7] Santos, J., et al., 2008, On The Negentropy Application in Thermoeconomics: a fictitious or an exergy component flow?, *In Proceedings of ECOS 2008*, Volume 1, pp. 253-260. Cracow, Poland.

[8] Santos, J., et al., 2009, On The Negentropy Application in Thermoeconomics: a fictitious or an exergy component flow?, Int. J. of Thermodynamics, 12(3), pp. 163-176.

[9] Santos, J., et al., 2009, On The Consistency of the Thermoeconomic Approaches regarding a Reversible Steam Power Cycle, *In Proceedings of ECOS 2009*, Foz do Iguaçu, Paraná, Brazil.

[10] Santos, J., et al., 2009, On The Treatment of Dissipative Components and Residues in Thermoeconomic Modeling, *In Proceedings of ECOS 2009*, Foz do Iguaçu, Paraná, Brazil.

[11] Santos, J., et al., 2010, On The Disaggregation of Exergy regarding the Accuracy Improvements in Thermoeconomics, *In Proceedings of ECOS 2010*, Lausanne, Switzerland.

[12] Valero, A., et al., 2006, Fundamentals of Exergy Cost Accounting and Thermoeconomics. Part I: Theory, Journal of Energy Resources Technology, Vol. 128, pp. 1-8.

[13] Moran, M. J., and Shapiro, H. N., 2004, *Fundamentals of Engineering Thermodynamics*, 5th ed, John Wiley & Sons, New York.

Acknowledgments: The three first authors of this paper would like to tank ANP, CAPES and CNPq, respectively, for the financial supports.

Distribution of resources and allocation of environmental loads applied to trigeneration systems

Monica Carvalho[a], Volker Wohlgemuth[b], Miguel A. Lozano[c] and Luis M. Serra[d]

[a, c, d] *GITSE-I3A, University of Zaragoza, Zaragoza, Spain*
[b] *University of Applied Sciences (HTW Berlin),Industrial Environmental Informatics Unit, Berlin, Germany*

Abstract: Thermoeconomic analysis techniques and Life Cycle Assessment are both based on accounting as well as on distribution, of the resources required for producing several goods and/or services. Both methodologies can be combined providing an integrated energy, economic, and environmental analysis with a global perspective of a system. Umberto software is specifically designed for analyzing the distribution of material and energy resources throughout a productive system. Environmental information associated with the usage and consumption of natural resources can be also implemented. The allocation of environmental loads in multiproduct processes is a very important and controversial issue when carrying out a Life Cycle Inventory. This is the case when analyzing, for example, trigeneration systems, where heat, cooling and power are produced in the system. In this work the Umberto software has been used to model a trigeneration system. The system was built with the flexibility to purchase/sell electricity from/to the electric grid, waste heat, and operate with an auxiliary boiler. The distribution of resources and allocation of environmental loads throughout the internal flows and final products of the trigeneration system is performed with the help of Umberto software and the application of thermoeconomic analysis background.

Keywords: Allocation, Environmental loads, Trigeneration, Software Umberto.

1. Introduction

Environmental impacts are a growing concern, e.g. one of the most important environmental challenges of our time is climate change. Changes in lifestyle and behavior patterns can contribute to reduce the environmental burden across all sectors. Management practices can also have a positive role, as for example, the use of technologies that can result in considerable reduction of environmental impacts related to energy use in buildings [1]. According to the EU Directive on Energy Performance of Buildings [2], the buildings sector accounts for 40% of the EU's energy requirements. Substantial reductions in environmental loads from energy use in buildings can be achieved using energy-efficient technologies that already exist, such as trigeneration, where significant savings in primary energy are possible [3, 4]. Furthermore, changes in lifestyle and behavior require the provision of appropriate information to consumers, regarding the environmental burden and consequences of using different products and services.

Accurate environmental assessment becomes increasingly important. It provides an evaluation of the environmental implications of decisions taken by governments, industries and consumers. Thus, environmental consequences of decisions can be estimated before they are made. In this context, public decision-making is being progressively supported by the explicit consideration of the life cycle concept [5].

According to ISO 14040 standard [6]: "LCA is a technique for assessing the environmental aspects and potential impacts associated with a product by compiling an inventory of relevant inputs and outputs of a product system, evaluating the potential environmental impacts associated with those inputs and outputs, interpreting the results of the inventory analysis and impact assessment phases in relation to the objectives of the study".

Thermoeconomic analysis combines economic and thermodynamic analysis by implementing the concept of cost, an economic property, to a thermodynamic analysis. The basic tool of thermoeconomic analysis is the cost, understood as the amount of resources consumed for obtaining a piece of equipment, a flow or a commodity. Hence, the cost of a flow in a plant represents the amount of resources that have to be supplied to the

overall system to produce this flow. In agreement with Sciubba and Wall [7] thermoeconomics traces the exergetic history of a good or commodity, i.e., to some extent it takes a life time perspective. Thermoeconomic methodologies are usually based on the costs of the mass and energy flows of the plant evaluated on an exergy basis. However, they can also be expressed in monetary or other units [8].

The inventory phase of the LCA methodology basically consists of an accounting of the amount of natural resources required for obtaining, maintaining and operating such product or service during its life cycle.

Both thermoeconomic analysis techniques and LCA are based on the accounting of the resources required for producing a good or service. Thermoeconomics is usually applied to industrial plants and the limits of the system are those of the plant. There is no constraint that impedes the widening of the limits of analysis to the well or the mine from where the natural resources were extracted. Thus, both methodologies could be combined providing an integrated energy, economic and environmental analysis with a global perspective of a complex system. Some authors have already proposed and developed research in exergy-life cycle assessment [9, 10] and others have already proposed the combination of thermoeconomic analysis with Life Cycle Assessment [11, 12].

A particularly flexible and efficient approach to represent substance and energy flows of a system is the application of Material Flow Networks (MFN) [13]. The term "material" refers to substances and energy; in MFN there is virtually no distinction between substances and energy. MFN can be applied to systems of any size or even to a specific stage of production. The Umberto software [14] is specifically designed for analyzing the distribution of material and energy resources throughout a productive system. By incorporating environmental information on the usage and consumption of resources into Umberto software, the approach of MFN will give insight on the environmental loads associated with each flow of the system.

This study is a continuation of a previous work [15, 16] where the operation of a simple trigeneration system was analyzed from a thermoeconomic point of view. The same trigeneration system was modeled with the Umberto software, with the incorporation of environmental information, obtained by applying the LCA technique on the consumption of resources. Typically, analysis of environmental loads is based on a black-box approach and as a consequence concentrates on the input and output of energy and materials of a system. Usually no analysis of the internal operations/processes takes place. This study also addresses the issue of allocation of the environmental loads to the internal operations/processes and final products of the trigeneration system, applying a set of rules that are similar to those of the thermoeconomic analysis for the evaluation of internal costs.

As a result, the flow analysis of individual production steps specific to operation takes the work presented in [15, 16] a step further, making it possible to study the operational activities more precisely by implementing environmental information. Thus, the consumers of the trigeneration system will know the environmental loads associated with the consumption of each energy service (electricity, heat, and cooling), as well as the contribution of every internal physical mass and energy flowstreams to the environmental impact of the analyzed trigeneration system.

2. Trigeneration System

The purpose of the trigeneration system shown in Fig. 1 is to meet the demand of different energy services (electricity, E_d; heating, Q_d; and cooling, R_d) of a consumer center.

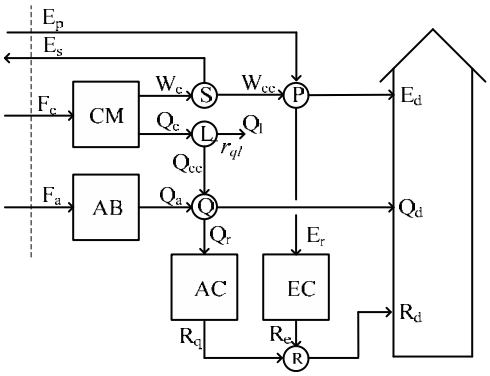

Fig. 1. Diagram of the simple trigeneration system.

The trigeneration system consists of the following productive units: a cogeneration module CM (providing heat, Q_c, and work, W_c), an auxiliary boiler AB (providing heat, Q_a), an absorption

chiller AC (providing cooling, R_q, and driven by heat, Q_r) and a vapor compression chiller EC (providing cooling, R_e, and driven by electricity, E_r). Demands will always be met either by the productive units of the trigeneration system or with the help of purchased electricity from the electric grid (E_p). There is also the possibility of selling electricity (E_s) to the market. F_c and F_a are, respectively, the fuel required for the cogeneration module and the auxiliary boiler. Here it was considered that both equipments operate on natural gas. A fraction (Q_l) of the cogenerated heat could be wasted, allowing the operation of the cogeneration module to match the demand of the consumer center or to realize profit by selling surplus electricity produced to the market.

Table 1 shows the technical data of the trigeneration system productive units. Units can operate either at part load or full load, assuming constant values of efficiency coefficients.

Table 1. Technical parameters.

Unit	Efficiency coefficient	Nominal capacity [kW]
CM	$\alpha_w \equiv W_c/F_c = 0.35$ $\alpha_q \equiv Q_c/F_c = 0.40$	$W_{c\,nom} = 350$
AB	$\eta_q \equiv Q_a/F_a = 0.80$	$Q_{a\,nom} = 400$
AC	$COP_q \equiv R_q/Q_r = 0.625$	$R_{q\,nom} = 250$
EC	$COP_e \equiv R_e/E_r = 5.0$	$R_{e\,nom} = 250$

The consideration of all possible values of purchased electricity (E_p), sold electricity (E_s), auxiliary heat (Q_a) and waste heat (Q_l) yielded a group of operation states, classified in 9 different operation modes,. These operation modes are shown in Table 2.

Table 2. Operation modes.

	Ep > 0 Es = 0	Ep = 0 Es = 0	Ep = 0 Es > 0
Qa > 0 Ql = 0	**C1**	C4	C7
Qa = 0 Ql = 0	C2	C5	C8
Qa = 0 Ql > 0	C3	C6	C9

The optimal operation for the simple trigeneration system was obtained by solving a linear programming model [15, 16], minimizing the hourly operation variable cost (€/h). Examples of optimal operation states corresponding to operation modes C1, C3, C7 and C9 are shown in Table 3.

Table 3. Examples of optimal operation states.

		C1	C3	C7	C9
E_d	kW	400	400	200	200
Q_d	kW	400	100	600	100
R_d	kW	400	100	100	100
E_p	kW	100	50	0	0
E_s	kW	0	0	130	150
F_c	kW	1000	1000	1000	1000
F_a	kW	300	0	250	0
W_c	kW	350	350	350	350
Q_c	kW	400	400	400	400
W_{cc}	kW	350	350	220	200
E_r	kW	50	0	20	0
Q_l	kW	0	140	0	140
Q_{cc}	kW	400	260	400	260
Q_a	kW	240	0	200	0
Q_r	kW	240	160	0	160
R_q	kW	150	100	0	100
R_e	kW	250	0	100	0
CH	€/h	41.00	30.00	19.60	13.00

3. Material Flow Networks (MFN)

MFN is a particularly flexible and efficient approach to represent substance and energy flows of a system. It can be applied to systems of any size or even to a specific stage of production.

According to Wohlgemuth *et al.* [17], the most attractive feature of MFN is the possibility to combine the compilation of eco-balances for a company, industrial plant, or production process with an analysis of material flows associated with given products or services. The concept of Petri nets utilized by the Umberto software ensures that material flow networks are clearly setup. The model of the resource distribution during the operation of the simple trigeneration system is shown in Fig. 2. Squares represent each piece of equipment (CM, AB, AC, EC) and branching points (S, L, P, Q, R). Inputs (E_p, F_c, F_a) and outputs (E_d, Q_d, R_d, Environmental loads) were represented by circles. As a direct connection between two similar elements is not permitted, two concentric circles were utilized, in which direct

throughput without storage occurs. Arrows specify the direction of the flows.

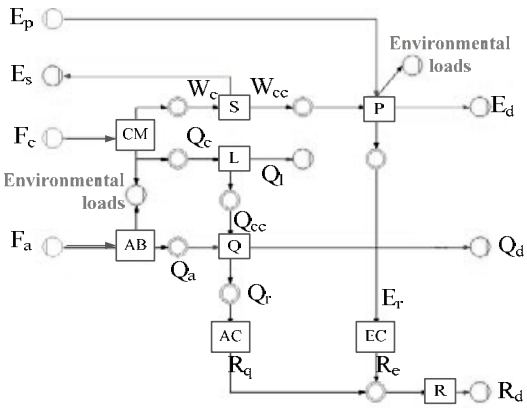

Fig. 2. Resource distribution with Umberto software.

4. Environmental evaluation

Two environmental criteria were chosen to carry out the analysis of the operation of the trigeneration system. Firstly, the Eco-indicator 99 (EI-99) Single Score, which is an environmental indicator that encompasses several impact categories and gives a global environmental perspective [18]. And secondly, the CO_2 emissions, as they accounted for 77% of total global anthropogenic GHG emissions in 2004 (being principally responsible for global climate change) [19].

There are different available impact assessment methods that utilize different environmental criteria and therefore evaluate and assess different environmental aspects. EI-99 was selected because it is widely used in LCA, incorporating relevant environmental burdens into different impact categories, which in turn allow the evaluation of damages to human health, ecosystem quality, and resources. Furthermore, the LCA results of EI-99 are aggregated into an easily understandable number, the Single Score.

The EI-99 method (utilized for the Life Cycle Inventory Analysis, LCIA) considers the values of eleven impact categories, which are added into three damage categories (Fig. 3), weighted, and then aggregated into an index, the Single Score, which represents the overall environmental load in points. One point (pt) can be interpreted as one thousandth of the annual environmental load of one average European inhabitant.

In order to account for the subjectivity of the impact assessment procedure, EI-99 presents three different perspectives, with different impact perceptions, different normalizing factors and weights and thus, leading to different results. The Hierarchist version of the damage model was selected for its balanced time perspective [18].

The environmental loads (CO_2 emissions and EI-99 Single Score) were obtained for the consumption of electricity from the grid and natural gas. Data were obtained utilizing SimaPro [20], a specialized LCA tool that includes several inventory databases with thousands of processes.

The CO_2 emissions associated with the Spanish electricity mix were calculated considering the proportions (25.8% Coal; 24.4% Natural gas in combined cycle; 19.7% Nuclear; 10.4% Others: biomass, cogeneration, minihydraulic, 9.4% Eolic; 9.4% Hydraulic; and 0.9% Fuel-gas) to produce the electricity consumed in 2007 [21]. The average CO_2 emissions associated with electricity in Spain in 2007 were EM_{epCO2} = 0.385 kg CO_2 per kWh consumed. The CO_2 emissions associated with the consumption of natural gas in Spain were EM_{gCO2} = 0.272 kg CO_2 per kWh consumed. The IDEMAT [22] and Ecoinvent [23] databases were utilized to specify the emissions.

The EI-99 Single Score associated with the consumption of electricity from the grid in Spain, evaluated by the Eco Indicator-99 method, was EM_{epEI99} = 0.0226 points per kWh consumed.

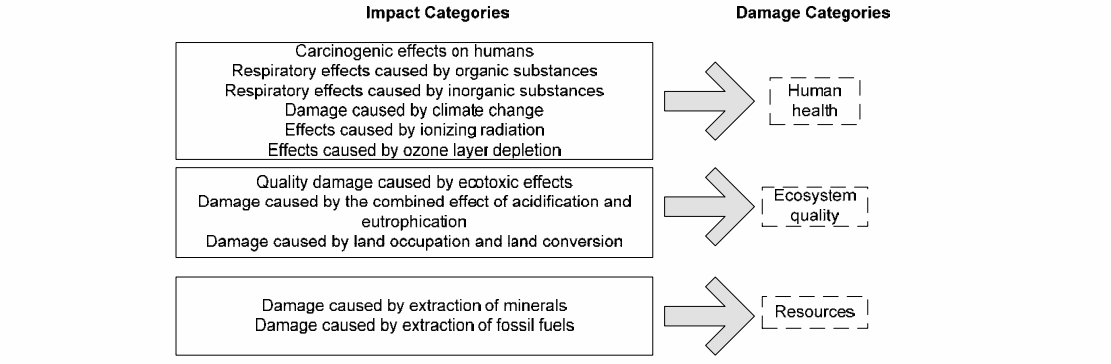

Fig. 3 Impact and damage categories for EI-99

In the case of natural gas, the single score obtained when utilizing the EI-99 method was EM_{gEI99} = 0.0378 points per kWh consumed.

Environmental data were incorporated into the trigeneration model to verify the share of environmental loads associated with the consumption of each energy service.

5. Allocation of environmental loads

The allocation of energy and other environmental interventions is a key issue. Many companies, government agencies, and researchers have struggled with the question of how to allocate emissions and environmental impacts for a system that has multiple products and multiple inputs [24, 25]. In this paper the allocation of environmental loads to the internal flows and final products of the trigeneration system is made by applying algebra and rules similar to those used in thermoeconomic analysis for the evaluation of internal costs. Thermoeconomic analysis allows the cost formation process to be transparent throughout the system, from energy resources to final products. Similarly, it is possible to evaluate the process of formation of the environmental impact associated with the consumption of natural resources and generation of emissions throughout the system, from the input of natural resources to the output of the final products and emissions.

Balances are explicitly formulated and external resources used in the production process are valued by the environmental burden caused. An assistant was created and implemented in the Umberto software to evaluate the environmental loads of internal flows and products, after the network calculation. The balance equations were:

$$\text{CM: } EM_g \bullet F_c = EM_{wc} \bullet W_c + EM_{qc} \bullet Q_c \quad (1)$$

$$\text{AB: } EM_g \bullet F_a = EM_{qa} \bullet Q_a \quad (2)$$

$$\text{AC: } EM_{qr} \bullet Q_r = EM_{rq} \bullet R_q \quad (3)$$

$$\text{EC: } EM_{er} \bullet E_r = EM_{re} \bullet R_e \quad (4)$$

$$\text{S: } EM_{wc} \bullet W_c = EM_{wcc} \bullet W_{cc} + EM_{es} \bullet E_s \quad (5)$$

$$\text{P: } EM_{wcc} \bullet W_{cc} + EM_{ep} \bullet E_p = EM_{er} \bullet E_r + EM_{ed} \bullet E_d \quad (6)$$

$$\text{L: } EM_{qc} \bullet Q_c + EM_{ql} \bullet Q_l = EM_{qcc} \bullet Q_{cc} \quad (7)$$

$$\text{Q: } EM_{qcc} \bullet Q_{cc} + EM_{qa} \bullet Q_a = EM_{qr} \bullet Q_r + EM_{qd} \bullet Q_d \quad (8)$$

$$\text{R: } EM_{rq} \bullet R_q + EM_{re} \bullet R_e = EM_{rd} \bullet R_d \quad (9)$$

EM represents the unit environmental loads associated with each mass and energy flowstream of the analyzed trigeneration system (Fig. 2).

In operation mode C1, $E_s = 0$ and $Q_l = 0$. Thus, $W_{cc} = W_c$ and $Q_{cc} = Q_c$.

Therefore, the balance equations are simplified to:

$$\text{CM: } EM_g \bullet F_c = EM_{wc} \bullet W_c + EM_{qc} \bullet Q_c \quad (10)$$

$$\text{AB: } EM_g \bullet F_a = EM_{qa} \bullet Q_a \quad (11)$$

$$\text{AC: } EM_{qr} \bullet Q_r = EM_{rq} \bullet R_q \quad (12)$$

$$\text{EC: } EM_{er} \bullet E_r = EM_{re} \bullet R_e \quad (13)$$

$$\text{P: } EM_{wc} \bullet W_c + EM_{ep} \bullet E_p = EM_{er} \bullet E_r + EM_{ed} \bullet E_d \quad (14)$$

$$\text{Q: } EM_{qc} \bullet Q_c + EM_{qa} \bullet Q_a = EM_{qr} \bullet Q_r + EM_{qd} \bullet Q_d \quad (15)$$

$$\text{R: } EM_{rq} \bullet R_q + EM_{re} \bullet R_e = EM_{rd} \bullet R_d \quad (16)$$

The unit environmental loads of the consumed resources (EM_g, EM_{ep}) are known. As the system is described using 7 equations with 10 unknowns (EM_{wc}, EM_{qc}, EM_{qa}, EM_{qr}, EM_{rq}, EM_{er}, EM_{re}, EM_{ed}, EM_{qd}, EM_{rd}), 3 auxiliary assessment equations are needed. Considering that the unit environmental load of several flows obtained from homogeneous flows is the same, then for branching points P and Q it yields:

$$\text{P: } EM_{ed} = EM_{er} \quad (17)$$

$$\text{Q: } EM_{qd} = EM_{qr} \quad (18)$$

The third auxiliary assessment equation must define how environmental loads of the cogeneration module should be attributed to its products: heat and power.

Different allocation proposals of environmental loads to electricity and heat products are found in literature [26]. A few are presented next:

A Allocation based on energy. The fractions of the environmental loads allocated to electrical and heat productions are assessed in proportion to the energy content of the cogenerated work and heat:

$$EM_{qc} / EM_{wc} = 1 \quad (19A)$$

B Allocation based on exergy. The fractions of the environmental loads allocated to electrical and heat productions are assessed in proportion to the exergy content of the cogenerated work and heat:

$$EM_{qc} / EM_{wc} = \beta_{qc} \quad (19B)$$

β_{qc} is the Carnot factor $(1 - T_0/T_c)$ corresponding to the cogenerated heat. In this work a value equal to 0.25 was considered.

C Allocation based on economic value. The fractions of the environmental loads allocated to electrical and heat productions are assessed in proportion to their market value:

$$EM_{qc} / EM_{wc} = p_{qc} / p_{wc} \quad (19C)$$

where p_{qc} and p_{wc} are, respectively, the unit economic values of the electrical product and the thermal product of the cogeneration system. The market prices considered were p_{qc} = 0.100 €/kWh and p_{wc} = 0.030 €/kWh.

D Fuel Chargeable to Power. Many consultants in the cogeneration area utilize this "Fuel Chargeable to Power" method, in which it is considered that the heat is produced in a conventional manner and the fuel demand is allocated to this energy carrier accordingly. The remainder of the fuel is allocated to electricity. The fractions of the environmental loads allocated to electrical and heat productions are assessed in proportion to the fuel allocated:

$$EM_{qc} / EM_{wc} = W_c / (\eta_B F_c - Q_c) \quad (19D)$$

where η_B is the thermal efficiency of the hypothetical boiler that would have been used in the production of heat energy. A reference boiler with η_B = 0.85 was considered.

Our thesis is that a rational distribution of costs or environmental loads toward the products of the cogeneration module must consider the nature of the operation mode [15,27]. This implies that different operation modes, as shown in Table 2, require different auxiliary equations. In operation mode C1 (electricity purchased/auxiliary boiler in service) our proposal is:

E to assign unit environmental loads to the products of the cogeneration module in proportion to the unit environmental load of their separate production:

$$EM_{qc} / EM_{wc} = EM_{qa} / EM_{ep} \quad (19E)$$

EM_{ep} being the environmental loads corresponding to electricity purchased from the Spanish electricity mix, and EM_{qa} the environmental loads associated with the heat produced in the auxiliary boiler.

Tables 4 and 5 show the results obtained for the example of optimal operation state C1 (energy flow values in Table 3). The unit environmental loads allocated to the internal flows and final products are shown in Table 4 and the distribution of environmental loads (kg CO_2 emissions and EI-99 Single Score points) throughout the internal mass and energy flows are shown in Table 5. This information allows the detailed evaluation of the contribution of each piece of equipment and the different operation modes, from an environmental viewpoint.

Table 4a. Unit environmental CO_2 emissions ($kgCO_2/kWh$) in operation mode C1

	A	B	C	D	E
E_d	0.3676	0.5557	0.5357	0.4056	0.3864
Q_d	0.3542	0.2219	0.2360	0.3275	0.3410
R_d	0.2585	0.2026	0.2086	0.2472	0.2529
E_p	0.3850	0.3850	0.3850	0.3850	0.3850
F_c	0.2720	0.2720	0.2720	0.2720	0.2720
F_a	0.2720	0.2720	0.2720	0.2720	0.2720
W_c	0.3627	0.6064	0.5787	0.4114	0.3868
Q_c	0.3627	0.1511	0.1736	0.3200	0.3416
E_r	0.3676	0.5557	0.5357	0.4056	0.3864
Q_a	0.3400	0.3400	0.3400	0.3400	0.3400
Q_r	0.3542	0.2219	0.2360	0.3275	0.3410
R_q	0.5667	0.3551	0.3776	0.5240	0.5456
R_e	0.0735	0.1111	0.1071	0.0811	0.0773

Table 4b. Unit environmental EI-99 loads (points/kWh) in operation mode C1

	A	B	C	D	E
E_d	0.0442	0.0704	0.0676	0.0495	0.0298
Q_d	0.0492	0.0308	0.0328	0.0455	0.0594
R_d	0.0351	0.0273	0.0281	0.0335	0.0393
E_p	0.0226	0.0226	0.0226	0.0226	0.0226
F_c	0.0378	0.0378	0.0378	0.0378	0.0378
F_a	0.0378	0.0378	0.0378	0.0378	0.0378
W_c	0.0504	0.0840	0.0804	0.0572	0.0319
Q_c	0.0504	0.0210	0.0241	0.0445	0.0666
E_r	0.0442	0.0704	0.0676	0.0495	0.0298
Q_a	0.0473	0.0473	0.0473	0.0473	0.0473
Q_r	0.0492	0.0308	0.0328	0.0455	0.0594
R_q	0.0788	0.0494	0.0525	0.0728	0.0950
R_e	0.0088	0.0141	0.0135	0.0099	0.0060

Table 5a. Allocation of CO_2 (kg CO_2/h) emissions to final products in operation mode C1.

	A	B	C	D	E
Ed	147.05	222.27	214.27	162.22	154.56
Qd	141.67	88.78	94.40	131.00	136.40
Rd	103.38	81.05	83.43	98.88	101.16
Total	392.10	392.10	392.10	392.10	392.12

Table 5b. Allocation of EI-99 Single Score (points/h) to final products in operation mode C1.

	A	B	C	D	E
Ed	17,69	28.14	27.03	19.80	11.92
Qd	19.69	12.34	13.12	18.21	23.76
Rd	14.02	10.92	11.25	13.40	15.72
Total	51.40	51.40	51.40	51.41	51.40

For the three products of the trigeneration system (example C1), Table 6 shows the fractions of fuel that constitute each output and total CO_2 emissions and EI-99 Single Score obtained with allocation based on exergy. For all cases the operation of the system during one hour was considered.

Table 6: Exergy allocation. Fractions of fuel that constitute each output and total CO_2 emissions and EI-99 Single Score.

	Ep (kWh/h)	Fc (kWh/h)	Fa (kWh/h)	CO_2 (kg CO_2/h)	EI-99 (points/h)
Ed	88.89	691.36	-	222.27	28.14
Qd	-	138.89	187.50	88.78	12.34
Rd	11.11	169.75	112.50	81.05	10.92
Total	100.00	1000.00	300.00	392.10	51.40

For each allocation method it is also possible to evaluate how the emissions of each final product are apportioned throughout the productive system. Figures 3, 4 and 5 show, respectively, the share of environmental loads based on the exergy allocation method for the trigeneration system for the example C1. Each figure corresponds to an output (E_d, Q_d, R_d).

Figure 3 shows the contributors to the environmental loads of the electricity demand (E_d), which is satisfied by the generation of electricity in the cogeneration module (operating with fuel F_c), and is complemented by the purchase of electricity from the grid (E_p).

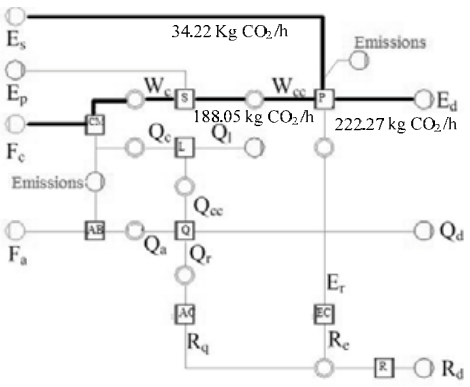

Fig. 3. Contribution of flows to output Ed in operation mode C1 (allocation method: exergy).

Figure 4 shows the contributors to the environmental loads of the heat demand (Q_d). The cogeneration module generates heat (operating with fuel F_c) and is complemented by heat produced by the auxiliary boiler Q_a (which operates with fuel F_a).

Figure 5 shows the contributors to the environmental loads of the cooling demand R_d. Electricity purchased E_p from the grid and electricity generated W_c by the cogeneration module contribute to operate the electrical chiller. The auxiliary boiler operates on heat produced by the cogeneration module (Q_c) plus heat produced by the auxiliary boiler (Q_a).

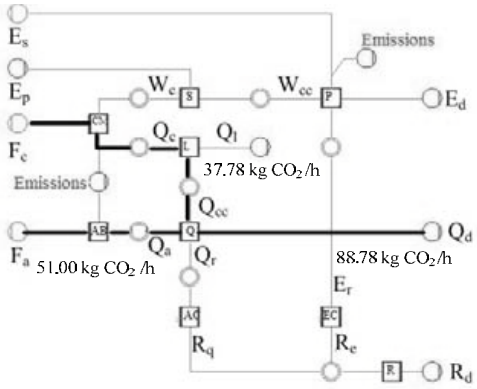

Fig. 4. Contribution of flows to output Qd in operation mode C1 (allocation method: exergy).

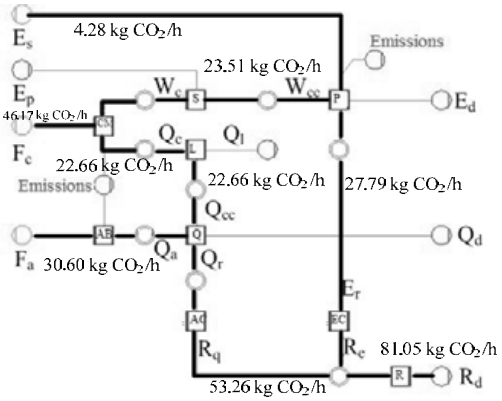

Fig. 5. Contribution of flows to output Rd in operation mode C1 (allocation method: exergy).

The Environmental Management Information System (EMIS) Umberto software efficiently supported data management, modeling of material flows, and proved to be a useful tool, allowing the tracking of environmental impacts associated with each output. Umberto software successfully

answered the question on what emissions were caused by the current inventory strategy for the trigeneration system, while considering different approaches to the allocation issue.

5. Closure

The combination of Environmental Management Information Systems (EMIS) such as the Umberto material analysis tool with LCA databases and thermoconomic analysis can provide a solution for the owner of a trigeneration system that wishes to inform its consumers of the environmental loads associated with the consumption of each energy service (electricity, heat, cooling).

A simple trigeneration system was modeled using Umberto software, with the flexibility to purchase/sell electricity from/to the grid. The possibilities of wasting part of the cogenerated heat and operating an auxiliary boiler also existed. The model was calculated for specific energy service demands, identifying where emissions were generated, and allowing the possibility of tracking the emissions throughout the system. A greater sophistication of the model (using non linear production restrictions and binary variables limiting both the minimum load of the productive units and on/off status) would provide more precise results but, generally, the same conclusions would still prevail.

The allocation of environmental loads (CO_2 emissions and Eco-Indicator 99 Single Score) to the internal flows and final products of a simple trigeneration system was carried out by applying algebra and rules similar to those used in thermoeconomic analysis for the evaluation of internal costs. Thermoeconomic analysis allows the cost formation process to be transparent throughout the system, from energy resources to final products. Similarly, it is possible to evaluate the process of formation of the environmental impact associated with the consumption of natural resources and generation of emissions throughout the system, from the input of natural resources to the output of final products and emissions.

Different allocation methods were utilized to apportion the emissions to each product, analyzing the breakdown of fuel usage attributable to each product. Future work by the authors will present a detailed analysis specifically focused on the analysis of environmental allocation rules. Research on allocation of emissions and environmental burden will allow the environmental benefits of properly designed and operated cogeneration technologies to be better understood and exploited [28, 29].

Effective environmental related strategies connect the reduction of emissions with a system's operational strategy (consumption of resources). Therefore the usage of EMIS and LCA tools could be promoted to i) analyze the distribution of material and energy resources throughout a productive system, ii) allow an emission-efficient economy to develop; iii) identify the most beneficial among competing technologies, and iv) serve the numerical registration and interpretation of environmental effects.

References

[1] IPCC: Summary for Policymakers, 2007. In: Climate Change 2007: Mitigation, Cambridge University Press, Cambridge, United Kingdom and New York, NY, USA.

[2] Directive 2002/91/EC on the energy performance of buildings, 2002, Official Journal of the European Communities, 4.1.2003, L1, pp. 65-71.

[3] Serra LM, Lozano MA, Ramos J, Ensinas AV, Nebra SA, 2009, Polygeneration and efficient use of natural resources, Energy, 34(5):575-586.

[4] Lozano MA, Ramos JC, Carvalho M, Serra LM, 2009, Structure optimization of energy supply systems in tertiary sector buildings. Energy and Buildings, 41(10):1063-1075.

[5] Miettinen, P. and Hämäläinen, R. P., 1997, How to benefit from decision analysis in environmental life cycle assessment (LCA), European Journal of Operational Research, 102 (2), pp. 279-294.

[6] ISO 14040. *Environmental Management. Life cycle assessment. Principles and framework*. Geneva. Switzerland, 2006.

[7] Sciubba, E., Wall, G., 2004, A brief commented history of exergy from the beginnings to 2004. International Journal of Thermodynamics, Vol. 10 (nº 1), pp. 1-26.

[8] Lozano MA, Valero A, 1993, Theory of the exergetic cost, Energy, 18(9): 939-960.

[9] Cornelissen, R.L., Hirs, G.G., 2002, The value of the exergetic life cycle assessment besides the LCA, Energy Conversion and Management, Vol. 43, pp. 1417-1424.

[10] Hau, J.L., 2002, *Integrating Life Cycle Assessment, Exergy and Emergy Analyses*. M.Sc. Thesis. Department of Chemical Engineering. Ohio State University.

[11] Tsatsaronis, G., Exergoeconomics and Exergoenvironmental Evaluation of Energy Systems. Presented in 4th International Conference on Sustainable Development of Energy, Water and Environment Systems (Special Session: Thermodynamics and the Destruction of Resources), Dubrovnik, Croatia, June 4-8, 2007.

[12] Serra, L.M., Uche, J., Raluy, R.G., 2007, Integrated Energy, Economic and Environmental Analysis of Combined Power and Desalination Plants, Symposium Towards Innovative Desalination and Power Generation in Kuwait, KFAS, Kuwait, December 2007. pp. 134-148.

[13] Möller, A., Rolf, A., Page, B., Wohlgemuth, V, Foundations and Applications of Computer Based Material Flow Networks for Environmental Management. In: C. Rautenstrauch; S. Patig (Eds.) Environmental Information Systems in Industry und Public Administration. Hershey, PA USA 2001, pp. 379-396.

[14] Umberto, 2006, version 5.0, ifu Hamburg GmbH and ifeu GmbH, Hamburg, Germany. <http://www.umberto.de/en/>.

[15] Lozano MA, Carvalho M, Ramos J, Serra LM, 2009, Thermoeconomic analysis of simple trigeneration systems, International Journal of Thermodynamics, 12 (3), pp. 147-153.

[16] Lozano MA, Carvalho M, Serra LM, 2009, Operational strategy and marginal costs in simple trigeneration systems, Energy, 34(11): 2001-2008.

[17] Wohlgemuth, V., Page, B., Kreutzer, W., 2006, Combining discrete event simulation and material flow analysis in a component-based approach to industrial environmental protection, Environmental Modelling & Software, 21 (11), pp. 1607-1617.

[18] Goedkoop M, Effting S, Collignon M. The Eco-indicator 99. PRé Consultants B.V., Amersfoot, 2000.

[19] Rogner, H.-H. *et al.*, 2007, Introduction. In Climate Change 2007: Mitigation, Cambridge University Press, Cambridge, United Kingdom and New York, NY, USA.

[20] SIMAPRO - Life cycle assessment software, 2008, PRé Consultants, Amersfoort, The Netherlands. <http://www.pre.nl/simapro>.

[21] REE – Red Eléctrica Española (Spanish electric power network), 2007, El sistema eléctrico español, Technical Report, <http://www.ree.es/sistema_electrico/pdf/infosis/Inf_Sis_Elec_REE_2007_ElSectorElectrico_v2.pdf>.

[22] IDEMAT Database, 2005, Section for Environmental Product Development, Faculty of Industrial Design, Delft University of Technology. Delft, The Netherlands. http://www.idemat.nl/

[23] Ecoinvent v2.0 Database, 2007, Swiss Centre for Life Cycle Inventories. Dübendorf, Switzerland.

[24] Rosen, M., 2008, Allocating carbon dioxide emissions from cogeneration systems: descriptions of selected output-based methods, *Journal of Cleaner Production*, 16 (2), pp. 171-177.

[25] Huppes, G. and Schneider, F. (eds), 1994, *Proc. European Workshop on Allocation in LCA*, Leiden.

[26] Phylipsen, G., Blok, K., Worrell, E., 1998, *Handbook on international comparisons of energy efficiency in the manufacturing industry*, Utrecht University Press, the Netherlands.

[27] Lozano MA, Serra LM, Carvalho M, Energy cost analysis of simple trigeneration systems under variable operation conditions. Proceedings of the 22nd International Conference on Efficiency, Cost, Optimization, Simulation and Environmental Impact of Energy Systems, Foz do Iguaçu, Brazil, 2009.

[28] Abusoglu, A. and Kanoglu, M., 2009, Allocation of Emissions for Power and Steam Production Based on Energy and Exergy in Diesel Engine Powered Cogeneration, Energy & Fuels, 23, pp. 1526–1533.

[29] Rosen, M. A. and Dincer, I., 2001, Exergy as the confluence of energy, environment and sustainable development, Exergy, an International Journal, 1 (1), pp. 3-13.

Acknowledgments: This work was developed within the framework of research project ENE2007-67122, funded in part by the Spanish Government (Energy program) and the European Union (FEDER program). Special thanks are extended to the Department of Industrial Environmental Informatics at HTW Berlin for the support given to Monica Carvalho during her research stay.

Exergoeconomic Analysis of a Cryogenic Process to Purify Natural Gas

R. Rivero, J. M. Santos

Posgrado en Ingeniería, Universidad Nacional Autonoma de Mexico, Mexico City, Mexico

Abstract: In order to have more energy efficient processes for obtaining purified natural gas (PNG) it is important to improve the cryogenic processes needed to separate this non-renewable natural resource. In this paper a typical turbo-expansion cryogenic process is analyzed in which hydrocarbons are separated by a demethanizer column, previously cooling the dry sweet gas. An exergy analysis has been conducted in order to obtain three relevant exergy performance parameters: the Irreversible exergy losses (Irr), the Effectiveness (e) and the Exergy Improvement Potential (Pot). Thermodynamic properties have been obtained using the simulation of the cryogenic process with the HYSYS simulation code. For the exergoeconomic analysis, the estimation of the equipment costs was obtained from different data bases and empirical correlations. For chemical exergy the Szargut's reference model was corrected to reference conditions. The results show that one of the most energy intensive equipment of the process is the demethanizer tower, including its reboiler, but the turbo-expander, the feed tank and feed cooler are very important; also, a mixer and a valve present important values of the exergy improvement potential. From this, new technology could be developed to improve these equipment items and the overall process.

Keywords: Cryogenic Process, Exergy, Exergoeconomic Analysis, Irreversibility, Natural Gas.

1. Introduction

Exergoeconomic analysis is a quantitative and qualitative method to determine losses of energy. Knowledge of useful energy (exergy) is important to improve and design processes. It is important to realize an exergy analysis previously in order to get useful information. The exergy analysis consists basically in obtaining three relevant exergy performance parameters: the Irreversible exergy losses (Irr), the Effectiveness (ε) and the Exergy Improvement Potential (Pot) of every block, Rivero, R. [1]. These thermodynamic parameters are useful to know where and how energy is degraded.

Exergoeconomic analysis consists in the integration of economic issues with thermodynamics properties to obtain the exergy cost of all streams, Tsatsaronis [2]. This analysis is useful to determine the price of products taking into account production costs and other expenditures. The results of exergy and exergoeconomic analysis are used to improve processes later on.

In order to have a more efficient process to purify natural gas (NG), in this paper a typical cryogenic process with an exergoeconomic is analyzed. NG is a non-renewable gas extracted from wells. It is made up C_1 to C_7 hydrocarbons, CO_2, S, H_2O and other impurities in different concentrations. The objective of purify NG consists basically in separating heavier hydrocarbons that lighter ones. As higher the methane concentration in the NG, the higher its purify. The benefits of obtaining purified natural gas (PNG) are multiple: it has a clean combustion; it is more valuable and produces more energy. It is clear that the advantages are: ecologic, economic and energetic. In this form, PNG can be used in many industry and domestic applications, if the efficiency of PNG production process is increased, then this will go under the direction of a sustainable result, optimizing ecology, economic and energy aspects at the same time, Rivero, R. [3].

1.1. Process description

One way for obtaining PNG is a Cryogenic Process using a single stage expander [4]. The raw material is a dry sweet gas, with the composition shown in Table 1. At the following conditions: 37.78 ºC and 38.93 bar. This gas comes from a sweetener unit and a dehydrator unit where sulfur and H_2O have been removed previously.

The cryogenic process, shown in Fig. 1 consists in the following steps: reception, cooling, expansion, separation and output. Reception receives the dry

R. Rivero: Ricardo Rivero, Email: rrivero@exergia.com.mx; Web: http://www.exergia.com.mx
J. M. Santos: José María Santos, Email: filuoque@yahoo.com.mx

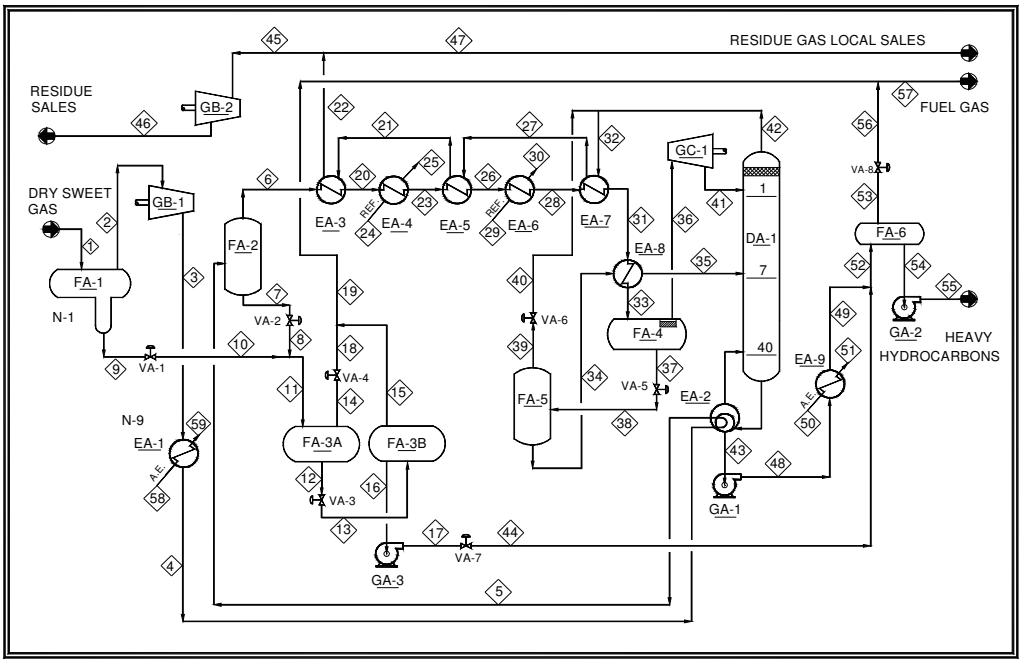

Fig. 1. Flow diagram of the Cryogenic process

sweet gas and sends it to the compressor of turbo-expander. Cooling is carrying out with an interchange train that uses the energy of the cooling steams. Expansion uses the expander of turbo-expander that received the gas, and expand it to a demethanizer column where is achieved the separation of hydrocarbons. Heavier components go to the bottom of the column and lighter ones to the top. The efficiency of this process increases if more light hydrocarbons are obtained.

The ideal gas would consist in pure methane; nevertheless there are some problems [5], such as the CO_2 contamination that requires to be removed avoiding the solids formation (freezing) in the cold section of the processing plant, thus incrusting the equipment. Other undesirable component is water, for the same reason of the CO_2; therefore the gas used as raw material is dried previously. The operating obstacles to avoid that amount of ethane or propane go away with the methane is other inconvenience. The efficiency of the process depends on the flexibility of the operation to get PNG with traces of heaviest hydrocarbons regardless of the composition of raw material, always caring of the dray sweet gas inlet composition.

Table 1. Composition of dry sweet gas.

compound	composition
N_2	0.0062
CH_4	0.7945
CO_2	0.0025
C_2H_6	0.1065
C_3H_8	0.0551
i-C_4H_{10}	0.0084
n-C_4H_{11}	0.0136
i-C_5H_{12}	0.0032
n-C_5H_{13}	0.0037
n-C_6H_{14}	0.0029
C_7H_{16}+	0.0034
Total	1.0000

In the analysis exergy it is important the reference state, that is 33ºC and 1 bar. These conditions are obtained considering the pressure and temperature annual average for the location where the process is performed, in a warm weather. Table 2 shows concentration of compounds at environmental conditions used as reference reactions, as later will be mentioned.

2. Exergy analysis

Scope of this analysis is to determine the irreversibility and optimization parameters for each equipment of the process. In this way it will be possible to have a structural vision and to know where and how energy is degraded. Comparison of these parameters will help to determine improvement decisions.

2.1. Block diagram

The block diagram of the process is shown in Fig. 2, where all equipment and process have been delimited. Aggregation grade of this diagram is the number of blocks, that`s 34. In the case of turbo-expander it is formed by two items (compressor GB-1 and expander GC-1) but it is considered as a single block. Mixers and other equipments area considered alone.

2.2. Evaluation of exergy

Exergy is defined as "the maximum work output attainable in the natural environment, or as the minimum work input necessary to realize the reversible process" Rant, Z. [6]. Exergy can be calculated in different forms, according to the different forms of energy [1]. Exergy can be associated to matter as a state function or as a transfer function. In this work exergy physical is evaluated with

$$Ex_f = (H - H_0) - T_0(S - S_0), \qquad (1)$$

where T_0 is the environment temperature. All properties with subscript 0 are evaluated at the reference state. This is considered as the environment temperature. That indicates that exergy is zero at this point. Enthalpy difference between the reference state and process state is the given energy to the system while the second term represents losses of exergy. Physical exergy has pressure and temperature contribution of the exergy into the system and is evaluated keeping the composition constant.

Every physical property is evaluated at pressure and temperature for every stream at process conditions. These data were obtained from the simulation code with the Peng-Robinson equation-of-state. Every stream was evaluated for the same composition at pressure and temperature of the environment, mentioned in process description.

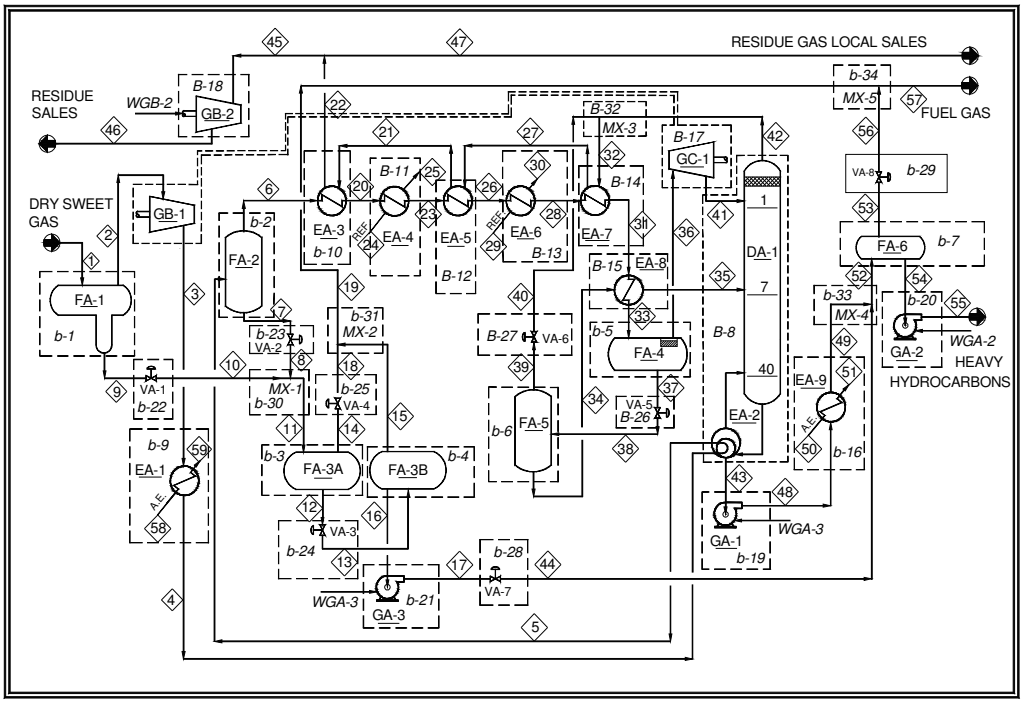

Fig. 2. Block diagram of the Cryogenic proces

In this process there are no chemical reactions, only compositional changes, and such chemical exergy has only this contribution. Compositional exergy is the difference between compositional exergy at reference state and the process keeping temperature and pressure constant:

$$Ex_{ch} = \sum_i x_i Ex^0_{ch_i} + RT_0 \sum_i x_i \ln x_i \,, \qquad (2)$$

Standard chemical exergy, Ex_{ch}, for each component has been corrected from values reported in [7]. It was made following a methodology cited by [8]; considering temperature, pressure and composition at process environment state respect to the reported values. In Table 2 reference conditions correspond to values reported in [8] and the process conditions.

Table 2. Conditions of reference and process.

Condition	Reference	Process
composition		
O2	0.207200	0.203500
CO2	0.000300	0.000300
H2O	0.008900	0.031967
pressure (bar)	1.01325	1.00000
temperature (K)	298.15	306.15

Into the methodology to correct standard chemical exergy it is necessary to propose a reference reaction for each compound of the NG mixing, Table 3.

Table 3. Reference reactions to correct standard chemical exergy.

Methane:	$CH_4 + 2O_2 \rightarrow CO_2 + 2H_2O$
Ethane:	$CH_4 + 3.5O_2 \rightarrow 2CO_2 + 3H_2O$
Propane:	$CH_4 + 5O_2 \rightarrow 3CO_2 + 4H_2O$
i-Butane,n-Butane:	$CH_4 + 6.5O_2 \rightarrow 4CO_2 + 5H_2O$
i-Pentane, n-Pentane:	$CH_4 + 8O_2 \rightarrow 5CO_2 + 6H_2O$
n-Hexane:	$CH_4 + 9.5O_2 \rightarrow 6CO_2 + 7H_2O$
n-Heptane:	$CH_4 + 11O_2 \rightarrow 7CO_2 + 8H_2O$

Once this is made, correction of standard exergy was made with (3) [8].

$$Ex^0_{ch_c} = Ex^0_{ch} + W_1 + (q_2 + q_3)\theta + W_4 + W_5 \,, \qquad (3)$$

2.3. Exergy balance and optimization parameters

Exergy looses represent the irreversibility of the process. An irreversible process is one that has inefficiencies; such as a reversible process is totally efficient and doesn´t have exergy looses. A general form to obtain irreversibility is with an exergy balance through the theorem of Gouy-Stodola

$$Irr = T_0 S_{gen} \,, \qquad (4)$$

S_{gen} represents the degradation of energy. This term is useful to know quantitatively how much energy is used. Irreversibility is equal to the input exergy, Ex_{tte}, less the exergy output, Ex_{tts}, in the system:

$$Irr = Ex_{tte} - Ex_{tts} \,, \qquad (5)$$

Another approach is to consider the system as a donor-acceptor exergy converter [1]. Supplied exergy, Ex_{nts}, is the part of system that gives exergy while produced exergy, Ex_{ntp}, is the result of the use of supplied exergy. The difference of these terms is the irreversibility:

$$Irr = Ex_{nts} - Ex_{ntp} \,, \qquad (6)$$

Exergy total looses have two contributions: internal and external. Internal exergy looses are irreversibility and external are streams rejected to the environment, *Efl*. The addition of these is evaluated with

$$Pex = Irr + Efl \,, \qquad (7)$$

Input and output exergy of each block have two contributions: physical and chemical exergy. The addition of these terms is called substantial exergy for each stream.

Optimization parameters are: qualitative, quantitative and a combination of these two. Efficiency (η) is a quantitative relation between input exergy and output exergy. This parameter doesn´t indicate how energy is utilized for the original purpose. To evaluate this is necessary to use the effectiveness (ε) that is a qualitative parameter [9].

$$\varepsilon = Ex_{ntp} / Ex_{ntp} \,, \qquad (8)$$

Effectiveness determines the capacity of a system to produce work and is evaluated as a relation of produced exergy to supplied exergy.

Improvement potential (*Pot*) has both quantitative and qualitative aspects. It shows how much the process could be improved; the higher *Pot* represents higher possibilities to improve the system. *Pot* is evaluated with (9), as a function of: absolute potential, *Irr*, relative potential, (1-ε), and environment potential, *Efl*.

$$Pot = Irr(1-\varepsilon) + Efl\,, \tag{9}$$

2.4. Exergy results

The process does not present external exergy looses (*Efl*=0), so total looses are only due to internal irreversibility in equipment. This irreversibility was evaluated through an exergy balance evaluating substantial exergy of each stream. Total irreversibly of the system is 4,929.8 kWe.

2.4.1. Block results

The irreversibility of each block is shown in Fig. 3 where Block 8, demethanizer column with reboiler (DA-1/EA-2) presents maximum irreversibility. Demethanizer column has a change of composition, obtaining PNG with an increment of chemical exergy in top section. That is because NG is more pure. That increment is a result of a decrease in physical exergy of the outlet streams of this. This apparatus has thermal contribution because reboiler gives energy to the column.

Block 17, turbo-expander (GB-1/GC-1) occupied second place in irreversibility. This is a mechanical device that uses exergy of stream inlet to operate and expand NG that is sent to the demethanizeer column. Both Blocks, 8 and 17, are very important to the process as indicated by their irreversibilities.

In third place of irreversibility is Block 14, exchanger EA-7. Valves have low irreversibility except Block 26 (VA-5). Mixers have low irreversibility except MX-3 and MX-4, this is due to the different levels of exergy in the streams mixed.

The effectiveness of the blocks is shown in Fig. 4. Valves have an effectiveness equal to zero because these do not produce any work. Equipment like pumps and separators have higher effectiveness. Block 1 (FA-1) and Block 7 (FA-6) have effectiveness equal to zero because these equipment operate in steady state. Blocks 9 and 16 (exchangers EA-1 and EA-9) present lower effectiveness because there is a very high temperature difference in their streams. Blocks 31 and 33 (mixers MX-2 and MX-4) also present lower effectiveness that is due for a very high composition difference in the mixers streams.

Improvement potential for each block is shown in Fig. 5. Block 8, the demethanizer column and its reboiler have the most important *Pot*, so this is the first equipment to be improved. Then Block 17, turbo-expander (GB-1/GC-1) has a high *Pot*. In third place Block 9, exchanger EA-1; in fourth Block 1, tank FA-1; in fifth, Block 26, valve VA-5. In order to improve the process changes are needed. These changes could be structural that are expensive except for Block 26, because it is a valve, cheaper than the other items. In another

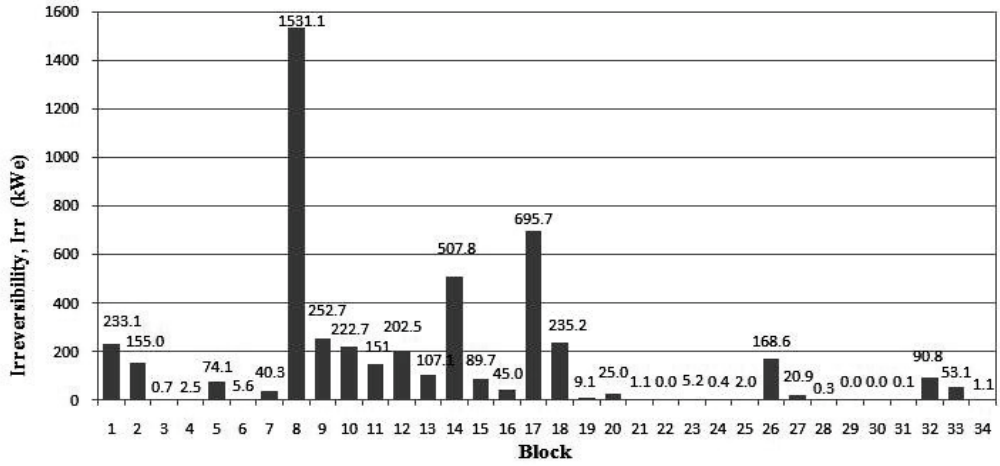

Fig. 3. Irreversibility of each block

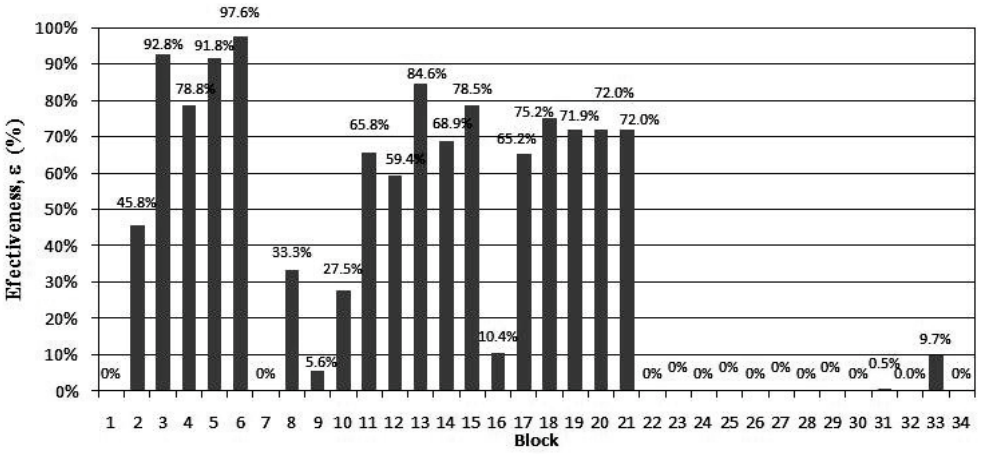

Fig. 4. Effectiveness of each block

hand if operation changes are conducted it would represent cheaper costs. Decisions to improve the process depend of many factors, especially economic ones. That is the reason why exergoeconomic analysis has to be done.

3. Exergoeconomic analysis

3.1. Exergoeconomic balance and costs

The purpose of an exergoeconomic analysis is to obtain the production exergy costs. These costs are obtained for each block proposing an exergy balance that involves the exergy of each stream and economic issues. The general balance for each block is shown in equation (10), Rivero, R[10].

$$\sum_{i=1}^{IN} Ex_{bi}\phi_i + F_b = \sum_{j=1}^{OUT} Ex_{bj}\phi_j \,, \qquad (10)$$

The additional cost (F_b) in the balance of equation (10) plus the input exergy is equal to output exergy. The cost of each item to realize its function depends on the equipment cost and expenditures that each block has. Consideration for balance exergoeconomic were proposed for 34 blocks based on the purpose of each item [2]. Then a numerical system has been solved obtaining the exergy specific cost of all the streams. The cost of each stream, Φ, is the exegy specific cost multiplied for the mass flow.

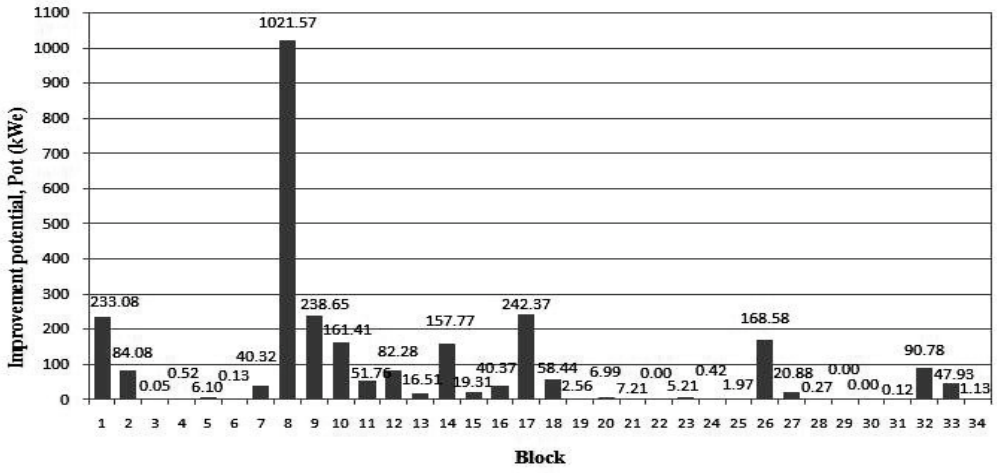

Fig. 5. Improvement potential of each block

Capital cost is the total equipment cost for each block, shown in Table 4. It was obtained depending of equipment item, for mechanical equipment it was made calculating the power and for pressure tanks it was necessary to calculate the weight; and exchangers with their duty. Capital costs were obtained from correlations of historical data and adjusting with an expected inflation of 6% to get the real cost when this plant is to be built. Each equipment considers supplied and installation Concepts considered are: pipe lines, concrete, steel, instrumentation, electric items, isolating and painting.

Table 4. Production cost.

Service	Cost	
Cool water	0.1	USD/m^3
Electricity	0.05923	USD/kWh
Dry sweet gas	0.011028	USD/ft^3
Propane	12.504	USD/ft^3

Operation cost is made up of: transformation cost, salaries, administration and maintenance. Transformation cost contemplates raw material and utilities used as services as shown in Table 4. Separator FA-1 receives the main raw material and some exchangers that are cooled (Fig. 1). This gas comes from other facilities as well as electricity. So each item has its own transformation cost.

Administration and salaries costs were obtained using a planning and control project methodology. Engineering activities were listed and programmed having the requested time for each activity as same as construction and having the total cost for this concepts. Maintenance was obtained assigning a percentage. The salaries, administration and maintenances costs were weighted for each item according to their Irreversibility.

Total additional cost is equal to the capital cost plus operation and they were levelized considering 20 years of amortization for the plant.

The exergy costs are shown in Table 5 where streams 24 and 29 (of refrigerant) are higher. After these, streams: 21, 22 and 32 and 42 are the highest, they are used in the demethanizerer tower

Table 5. Cost of streams

No.	ϕ (USD/kJ)	Φ (USD/h)	No.	ϕ (USD/kJ)	Φ (USD/h)	No.	ϕ (USD/kJ)	Φ (USD/h)
1	1.047E-08	93.97	**22**	6.714E-06	42789.45	**43**	6.653E-06	15349.69
2	1.047E-08	93.96	**23**	1.220E-06	10607.80	**44**	1.102E-06	287.27
3	1.047E-08	94.01	**24**	7.250E-05	2048502.12	**45**	6.714E-06	21394.73
4	3.909E-07	3509.81	**25**	7.250E-05	2048386.68	**46**	7.754E-06	24726.15
5	3.909E-07	3508.90	**26**	1.536E-06	13357.52	**47**	6.714E-06	21394.73
6	6.245E-07	5428.29	**27**	6.714E-06	42808.93	**48**	6.707E-06	15474.67
7	6.245E-07	176.43	**28**	1.723E-06	14987.01	**49**	7.019E-06	16194.96
8	8.737E-07	246.83	**29**	7.250E-05	1059488.39	**50**	8.241E-08	350.62
9	0.000E+00	0.00	**30**	7.250E-05	1059307.12	**51**	8.241E-08	350.60
10	0.000E+00	0.00	**31**	2.516E-06	21889.48	**52**	6.846E-06	17578.63
11	8.737E-07	246.83	**32**	6.714E-06	42848.43	**53**	0.000E+00	0.00
12	9.064E-07	246.36	**33**	2.656E-06	23108.45	**54**	6.846E-06	17578.53
13	9.064E-07	246.36	**34**	3.587E-06	9047.98	**55**	6.979E-06	17921.47
14	9.064E-07	9.70	**35**	3.587E-06	9042.60	**56**	0.000E+00	0.00
15	1.030E-06	11.39	**36**	2.771E-06	16107.47	**57**	2.267E-06	49.30
16	1.030E-06	268.57	**37**	2.771E-06	8003.52	**58**	8.241E-08	0.09
17	1.088E-06	283.62	**38**	3.560E-06	10281.74	**59**	8.241E-08	0.09
18	3.395E-06	36.31	**39**	3.587E-06	1309.95	**WGB2**	1.646E-05	56.08
19	2.267E-06	49.31	**40**	4.360E-06	1592.16	**WGA1**	1.646E-05	1.92
20	9.717E-07	8446.70	**41**	4.416E-06	25639.72	**WGA2**	1.646E-05	5.29
21	6.714E-06	42796.88	**42**	6.653E-06	40029.42	**WGA3**	1.646E-05	0.23

and output streams of the exchanger train.

4. Conclusions

Exergoeconomic analysis is very necessary to get production costs. Through this analysis, cost of streams and irreversibilities are determined. In terms of irreversibility and improvement potential the demethanizer column and the turbo-expander are very intensive. There are operative changes that are not expensive as the mixer MX-3 that is a part of the demethanizer column outlet. Economically, the outlet of the heat exchanger train and the refrigerant represent the higher costs as well as streams of the demethanizer column. This equipment is the most important to be improved. Structural changes could be expensive, but this can be necessary.

Nomenclature

Ex exergy, kWe
Efl effluent, kWe
F additional cost,USD
H enthalpy, J/kg
Irr irreversibility, kWe
M mega
p pressure, psia
Pex total exergy losses, kWe
Pot exergy improvement potential, kWe
q thermal flow
S entropy, J/kg °C
T temperature, °C
x mole fraction
W Work

Greek symbols

ε effectiveness
θ Carnot factor
ϕ average exergy cost, USD/kJ
Φ cost of stream, USD/h
1-5 number of stage

Subscripts and superscripts

gen generate
c corrected
ch chemical
f physical
b block
i, j *i*-th and *j*-th componente
tte input total
tts output total
nts supplied total
ntp produced total
0 reference state

References

[1] Rivero, R.; Anaya, A. *Exergy Analysis of Industrial Processes. Energy - Economy - Ecology.* Latin American Applied Research (ISSN: 0327-0793). Vol. 27, No. 4, 1997. pp. 191-205.

[2] Bejan A., Tsatsaronis, G., Moran, M.; *Thermal Design and optimization*; John Wiley and sons, inc. New York,1996.

[3] Rivero, R.; *Exergia. en: El IMP, la Sociedad y el Medio Ambiente"* (ISBN: 968-489-015-X). Instituto Mexicano del Petróleo México, 2003, pp. 78-89.

[4] Lynch, J.; Pitman, R. *Retrofitting the Williams energy services Ignacio Plant for higher throughput and recovery* presented at the 78th annual convention of the Gas Processors Association; ORTLOFF, Nashville, Tennessee, 1999.

[5] Pitman, R.., Hudson, H., Wilkinson, J.; *Next generation processes for NGL/LPG recovery* presented at the 77th annual convention of the Gas Processors Association; ORTLOFF, Houston, Texas, 1998.

[6] Rant, Z.; Exergy*, a new word for "technical available work*" (in German). Forsch, Ing,-Wes. 22(1), pp. 36-37, 1956.

[7] Rivero, R.; Garfias, M. *Standard chemical exergy of elements updated*; Energy (ISSN: 0360-5442). Vol 31, 2006, pp. 3310-3326.

[8] Montero G.; Rivero, R. *Corrección de exergias estándar para diferentes condiciones de referencia.* Revista del IMIQ (ISSN: 0188-73 19) Año XL, Vol. 7-9, Julio 1999 pp. 15-20

[9] Rivero, R; Application of the exergy concept in the petroleum refining and petrochemical industry, Energy Conversion and Management, 43, 1199-1220; 2002

*[10]*Rivero, R.; Rendon, C.; Gallegos, S.; *Exergy and exergoeconómic analysis of a crude oil destilation unit*, Energy (29), 2004, 1909-1927

Composite Curves in Direct and Indirect Heat Exchange Network for Simultaneous Heat and Mass Transfer System: Analysis and Applications

Martínez-Patiño J.[a], Verda V.[b], Serra L.M. [c], Picón-Núñez M.[a], Hernández-Figueroa M. A. [a]

[a] *University of Guanajuato, Mexico*
[b] *Department of Energy, Politecnico di Torino, Italy*
[c] *Group of Thermal Engineering and Energy Systems (GITSE), Aragon Institute of Engineering Research (I3A), Department of Mechanical Engineering, University of Zaragoza. CPS Ingenieros (Ed. Betancourt), María de Luna 3, 50018 Zaragoza (Spain)*

Abstract: In many industrial processes such as, pulp and paper, foods and oil industry there is need for direct and indirect heat and mass exchange networks for energy recovery and removal of contaminants. These networks make up a Simultaneous Heat and Mass Transfer System for the optimization of water and energy consumption in industrial processes. These systems are constituted by three networks: Heat and mass transfer network, direct heat exchange network and indirect heat exchange network. In a previous work, a heuristic procedure for the optimal integration of these three networks has been proposed. The optimal design is driven by rules that allow to avoid penalties which are identified by the analysis of the composite curves. In this work are presented alternatives for composite curves design considering the penalties in the direct heat transfer zone.

Keywords: Process integration; Combined Heat and Mass Transfer, Thermal Pinch, Simultaneous heat and mass transfer system.

1. Introduction

Water is largely used in industrial plants in processes as diluting, cleaning, heating and cooling etc. As the request of this resource is very high in many areas, it is important to rationalize its use. Similarly, the use of primary energy must be rationalized. In industrial plants primary energy is often directly converted into thermal energy, which leave the door open to improvements.

In recent years, the importance of water and energy has brought the development of methodologies [1-8] that simultaneously reduce these two inputs. These methodologies are based on the concept of process integration, for example: Thermal Pinch Analysis and Water Pinch Analysis. Heat recovery is achieved through a network of heat exchangers, and the fresh water consumption is minimized by reusing water streams.

Some of these methodologies [1,2,3,4,7,8] use a Simultaneous Heat and Mass Transfer System (Fig. 1). These systems are constituted by three networks: Heat and mass transfer network (Fig. 2), direct heat exchange network and indirect heat exchange network (Fig. 3). This system is designed using the composite curves of the cold and hot streams. These composite curves are subdivided in two zones: Direct heat transfer zone (non-isothermal mixing) and indirect heat transfer zone (to determine the heat exchangers) (Fig. 3).

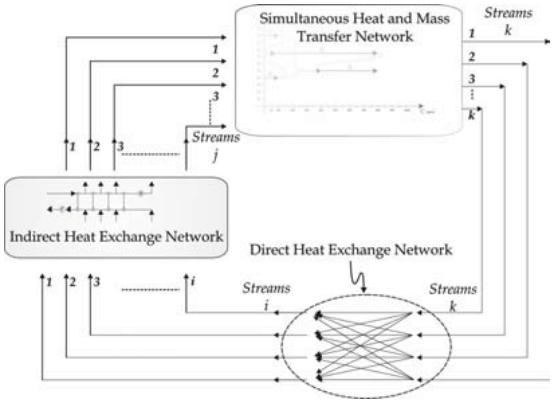

Fig 1 . Simultaneous heat and mass transfer system [7].

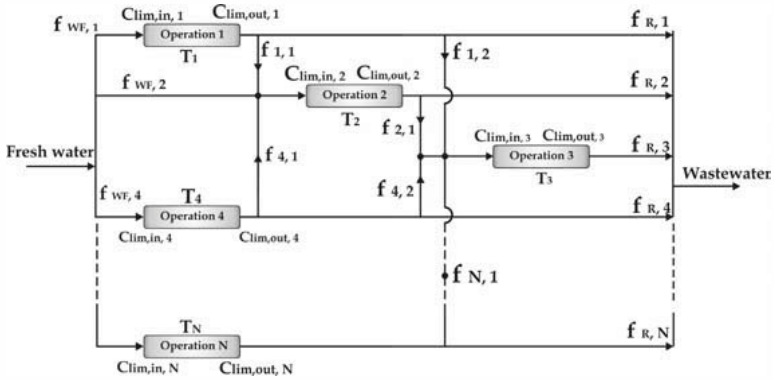

Fig 2 . Simultaneous Heat and Mass Transfer Network [7]..

In this work new considerations oriented to build the composite curves to design Simultaneous Heat and Mass Transfer System are presented.

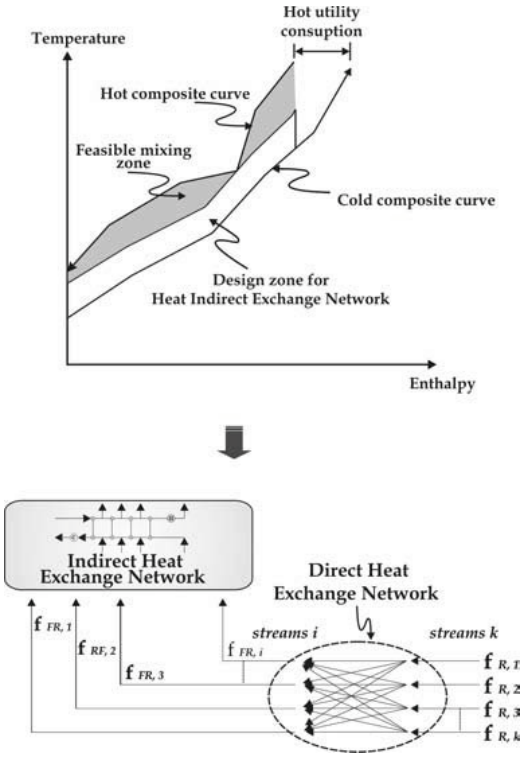

Fig. 3. Composite curve for design of Indirect Heat Exchange Network and Direct Heat Exchange Network. Case: Mixing taking place on cold streams

2. Simultaneous water and energy minimization

Various methodologies derived from process integration have been proposed with the aim of simultaneous minimization of energy and water consumption. The application of Pinch Analysis [9-11] has brought the Water Pinch methods [12-14] to reduce water utilization.

Most of the methodologies for simultaneous energy and water minimization start by applying the Water Pinch Analysis. In analogy with the Thermal Pinch Analysis, water pinch uses composite curves to minimize the water consumption. These curves represent concentration of contaminants versus removed mass. The inlet and outlet concentrations for each operation are very important for the design the networks conforming the Simultaneous Heat and Mass Transfer System.

These systems are constituted by three networks: Heat and mass transfer network, direct heat exchange network and indirect heat exchange network.

- Direct Heat Exchange Network: Is a network of water streams where the target temperatures are reached by direct mixing between them.
- Indirect Heat Exchange Network: It is a network of water streams where heat is transferred indirectly through heat exchangers.
- Simultaneous Heat and Mass Transfer Network: It is a network of water streams that come out of various operations where heat and mass are transferred simultaneously. The mass

of contaminant that is eliminated from the various operations is exchanged from stream to stream in order to reach the required concentration at the entrance of a downstream operation. At the same time, heat exchange takes place for the target temperatures to be achieved.

The way these sub-networks are linked is shown in Figure 1. To build the system, it is needed first to design the Simultaneous Heat and Mass Transfer Network (Fig. 2), the composite curve is built from the incoming and out coming flows of this network, and splits the zones mentioned before: Direct heat transfer zone and Indirect heat transfer zone, thus to build the two remaining networks of the Simultaneous Heat and Mass Transfer System: Direct Heat Exchange Network and Indirect Heat Exchange Network (Figure 3). Sorin M. et al. [1] introduces the concepts of the networks mentioned above, while Martinez-Patiño [4,7,8] links the three networks in a single system, in the heuristic methodology, minimizing the water and energy consumption in industrial processes.

3. Case study

The case studied is taken from Savulescu's (Table 1) [2,3]former work, in which four operations for the whole process are considered. For each operation, two concentration limits for the stream of water are proposed, one for the inlet, and one for the outlet, there is also a temperature at which the flow must enter and leave the system (Figure 4).

By applying the Water Pinch Analysis for the study case, a consumption of 90 kg/s (applying reuse) [12] is presented in the process for different combinations of the mixture to accomplish the removal of pollutants in the operations Inlet cold water temperature is 20 ºC, and the waste water outlet temperature coincides with the minimum temperature of the various processes (40ºC). The heat consumption shown in the composite curves is 7560 KW, with a temperature difference (ΔT) of 21.5ºC. (Fig. 4)

In order to build the composite curve, it is necessary to design first the Simultaneous Heat and Mass transfer Network. This design must satisfy the concentration requirements (C_{lim}) to remove the quantity of CML (Contaminant Mass Load) from every operation and temperature (T_n) (Table 1), where LWF is Limiting Water Flowrate. The Simultaneous Heat and Mass Transfer Network will provide the cold flows ($f_{WF,N}$) and the hot flows ($f_{R,N}$) (Fig. 2) for the design of the composite curve according to the different combinations that can exist in the exchange and mixing of flows for each operation of the process. The temperatures of fresh water and waste water are also important.

Table 1. Process data for case study. [2,3]

Op (No.)	C_{in} (ppm)	C_{out} (ppm)	$T_{op,\,in}$ (ºC)	$T_{op,\,out}$ (ºC)	LWF (kg/s)	CML (g/s)
1	50	100	100	100	100	5
2	50	800	75	75	40	30
3	400	800	50	50	10	4
4	0	100	40	40	20	2

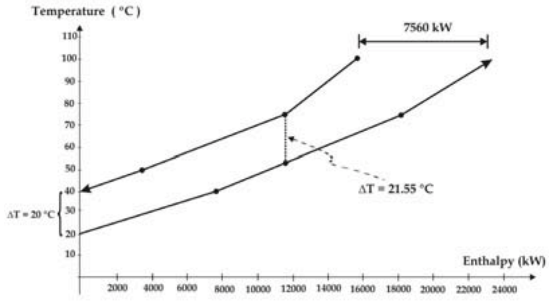

Fig. 4. Composite curves for T_{out} = 40ºC

For the case study, two different methodologies are presented: Savulescu et al. [2,3] (Case 1) and Martinez-Patiño et al. [7,8](Case 2). The difference between the two methodologies is on the construction of the Simultaneous Heat and Mass Transfer Network, obtaining different consumption of heat and cooling. For example: considered that the cold water enters the process at 20 ºC and the wastewater at 30ºC, Savulescu´s methodology [2,3] (Case 1) (Fig. 5) the heat consumption is 4265 kW and 485 kW for cold and Martinez-Patiño´s methodology [7,8](Case 2), (Fig. 6) the heat consumption is 4165 kW and 385 kW for cold.

By considering the two cases mentioned before, the composite curves are designed for each methodology and taking into account that the flow of waste water is at 30 ºC. In other words, the Simultaneous Heat and Mass Transfer System is designed by finding the ΔT_{min} where the Non-isothermal streams mixing area brings a temperature of 30ºC at the exit of the process. For the case 1 (Savulescu et al. [2,3]) the ΔT_{min} is 8.35ºC (Fig. 7) and for the case 2 (Martinez-Patiño et al. [7,8]) the ΔT_{min} is 8.69ºC (Fig. 8).

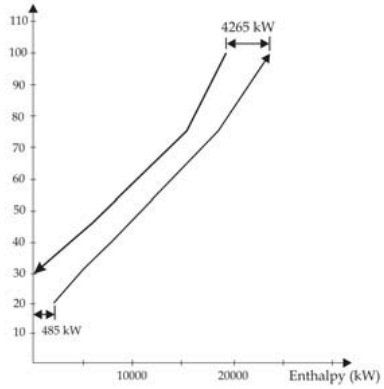

Fig. 5. Composite curves for case 1. [2,3]

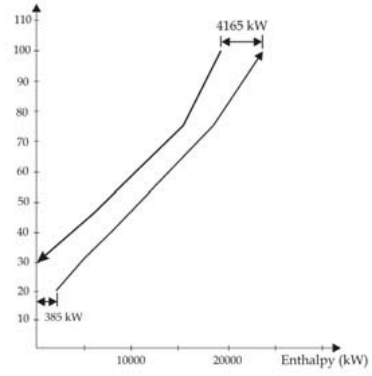

Fig. 6. Composite curves for case 2. [7,8]

In Figure 7 and Figure 8, it can be seen that on the cold side of the composite curves, the Direct Heat transfer zone (non-isothermal mixing) has a penalty by the mixture, i.e., the ΔT_{min} is not the same between the composite curves as the ΔT_{min} of Indirect Heat transfer zone; i.e., for the case 1 the ΔT_{min} always has to be 8.35 ºC, while on the left side (cold side) of the composite curves is of 10ºC, it is the same condition for the case 2, the ΔT_{min} always has to be 8.69 ºC while on the left side of the composite curves (cold side) is of 10ºC.

This work presents alternatives and considerations to manage this penalty in the composite curves, the Direct Heat transfer zone and Indirect Heat transfer zone.

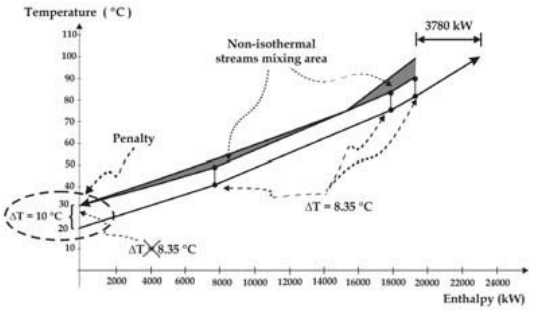

Fig. 7. Composite curves for case 1 (ΔT_{min} = 8.35ºC) [2, 3].

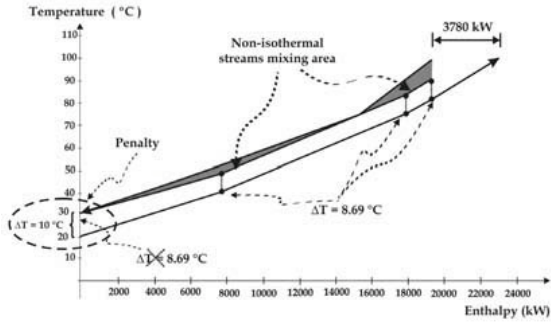

Fig. 8. Composite curves for case 2(ΔT_{min} =8.69ºC). [4]

4. Conceptual insights

Direct heat transfer zone in the hot part of the curve

The composite curves are built from the cold stream entering to the process and the warm streams leaving the process. Considering the temperature of the flow stream, two zones are defined between the hot composite curve and the cold composite curve that will define the direct heat exchange zone (mixture of streams), and the indirect heat exchange zone (heat exchangers).

Therefore, it is possible to design two sub-networks of the system: Direct and Indirect Heat Exchange Networks. There are two alternatives to set zones of stream mixture: combining cold streams (Fig. 9) or hot streams (Fig. 10).

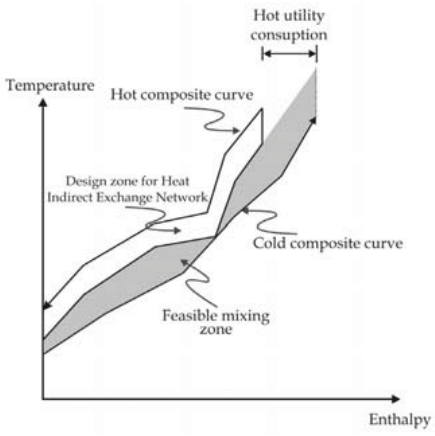

Fig. 9. Mixing taking place on cold streams

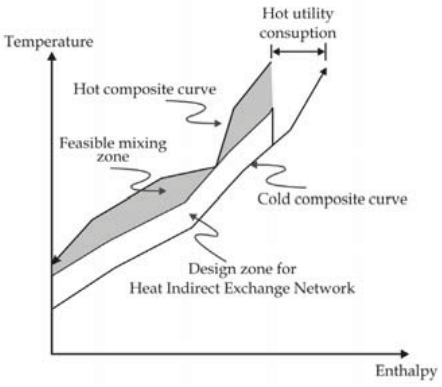

Fig. 10. Mixing taking place on hot streams.

Depending on the location of the mixture of streams, the quantity of energy transmission can be modified by reducing or increasing the average temperature of the hot and cold streams, and thus affecting the dimensions of the heat exchangers needed for the transfer of indirect heat.

Analyzing the two zones of mixture obtained [4] (hot and cold stream zone) it can be established that the cold stream zone affects the heat transfer zone between streams of external services and the process, and reduces the driving force of the average temperature that exists between the two streams. Consequently, the dimensions of the necessary equipment for heat transfer are bigger.

Design of heat and mass transfer Network

Depending on how the water streams are distributed within the heat and mass transfer Network, the profile of the composite curves change, affecting the temperature differences for heat recovery and therefore energy consumption, as shown in Figure 11.

The objective of a Heat and Mass Transfer Network is to satisfy the requirements of temperature and concentration at the inlet of each of the operations that comprise a process. This objective can be achieved through a variety of possible combinations of supply-streams. The temperature and composition of the effluent at the exit will be dependent on the selected combination of flowstreams, which in turn will determine the profiles of the composite curves, and the consumption of energy. These cases have been reviewed by Martinez-Patiño [7,8] and Leewongtanawit [9].

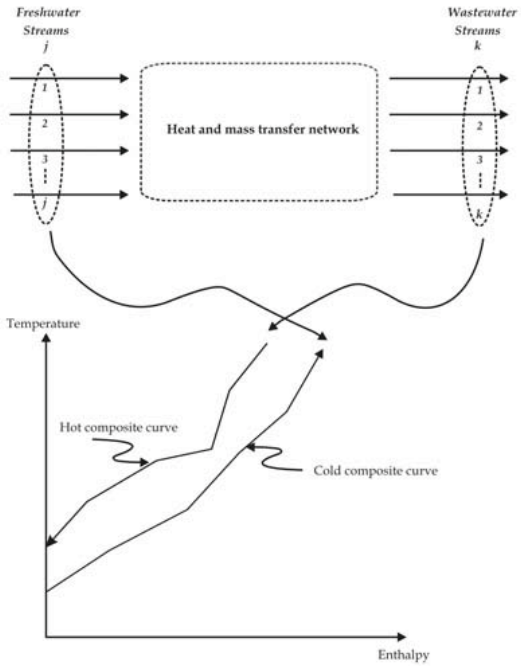

Fig. 11. Relationship between composite curve and heat and mass transfer network.

Level of heat recovery

For a given stream of cold water and a distribution of water streams within the subnet of direct heat and mass transfer, the energy consumption varies with the level of heat recovery (related to the $\Delta T_{mín}$ of the process). The maximum level of heat recovery is presented where the cooling process is zero. This can be seen in the case where the cold composite curve is displaced to the left and contrary if it moves parallel to the right, the mean temperature difference ($\Delta T_{mín}$) for indirect heat transfer increases, affecting directly the cost of heat exchangers (reduced by decreasing the exchange surface necessary for heat transfer) but at the expense of the increment of the energy consumed.

In Figure 7 and Figure 8 it is observed that the calculated $\Delta T_{mín}$ between the composite curves is 8.35 ºC and 8.69 ºC; when the mixing of streams is performed, a $\Delta T_{cold\text{-}side}$ of 10ºC is obtained in the cold side of the composite curves. Therefore, to know the minimal energy consumption in the process, the $\Delta T_{mín}$ from the colds side of the composite curves must be considered; the Figure 7 and Figure 8 show a $\Delta T_{cold\text{-}side}$ =10 ºC. Using the equation (1) [15] an energy consumption of 3780kW.

$$Q = M \cdot c_p \cdot \left(T_{dis} - T_{\sup ply}\right) \quad (1)$$

This consideration is important to know the real minimal energy consumption that can be achieved for the Simultaneous Heat and Mass Transfer System.

5. New conceptual insight

As seen in the previous paragraph, several considerations for the design of Simultaneous Heat and Mass Transfer System should be taken into consideration. In the design of the Direct Heat Exchange Network it is very important not provoke any penalty when blending different streams that could impact on the cold side ΔT. The new conceptual insight proposes to the designer to be careful in the different mixtures in the Direct Heat Transfer Zone (Non-isothermal streams mixing area) to accomplish the requisites of temperature in the Indirect Heat exchange Network (Heat exchangers zone) and the requisites of discharge temperature of wastewater.

For the case of study it is necessary that the discharge temperature of wastewater equals 30ºC, so the $\Delta T_{cold\text{-}side}$=10ºC in the cold side of the composite curves, obtaining an energy consumption of 3780 kW and a $\Delta T_{mín}$ of 8.35ºC (case 1) and a $\Delta T_{mín}$ of 8.69ºC (case 2).

As mentioned before, and with thee requisites of discharge temperature of wastewater in the process, a question comes out: Will it be the only way to guarantee a $\Delta T_{cold\text{-}side}$ =10ºC in the cold side of the composite curves? The answer is negative; the direct heat transfer zone allows the modification of the different mixtures to achieve the required $\Delta T_{mín}$, using the *penalty* of stream mixing in the Direct heat Transfer Zone, as explained next in the two cases for the same $\Delta T_{cold\text{-}side}$ =10ºC in the cold side of the composite curves: for the case 1 (Fig. 12), an energy consumption of 4265kW is obtained with a $\Delta T_{mín}$=11.28ºC between the composite curves, and for the case 2 (Fig. 13), an energy consumption of 4165 kW is obtained with a $\Delta T_{mín}$=11.02ºC between the composite curves. In the results shown it is observed that the energy consumption augments in relation with the increment of the $\Delta T_{mín}$ between the composite curves.

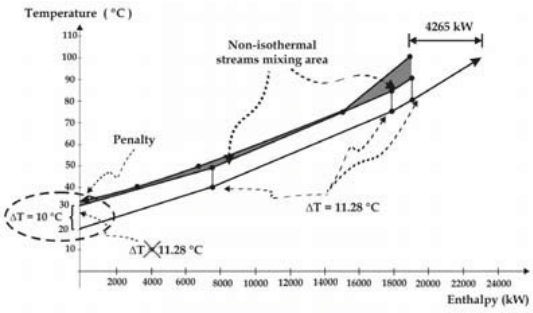

Fig. 12. Composite curves for case 1 (ΔT_{min} =11.28ºC)

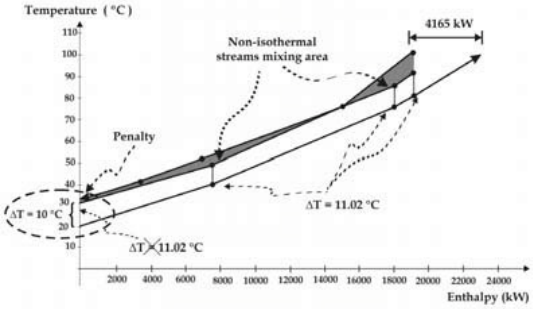

Fig. 13. Composite curves for case 2. (ΔT_{min} =11.02 ºC)

For the case in which there was not a requisite of discharge temperature of the wastewater in the process, a $\Delta T_{min} = \Delta T_{cold\text{-}side}$ could be calculated between the composite curves in the cold side, obtaining the next results for the cases of study of this work: for the case 1, an energy consumption of 5963kW was obtained with a $\Delta T_{min} = \Delta T_{cold\text{-}side}$ =15.77ºC (Fig. 14), while fo the case 2, an energy consumption of 5513kW was obtained with a $\Delta T_{min} = \Delta T_{cold\text{-}side}$ =14.58ºC.(Fig. 15)

The new conceptual insight allows choosing the design alternatives to accomplish the requisite of discharge temperature of wastewater, and not having the stream mixture fouling of the Direct Heat Transfer Zone.

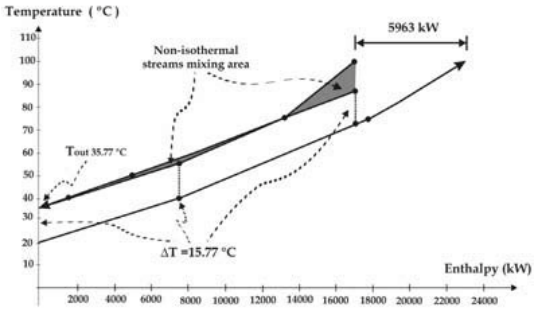

Fig. 14. Composite curves for case 1 (ΔT_{min} =15.77ºC).

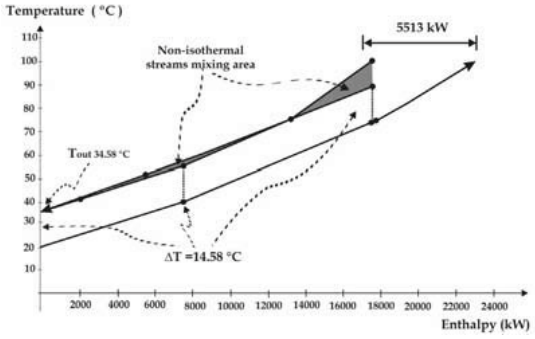

Fig. 15. Composite curves for case 2 (ΔT_{min} =14.58 ºC).

6. Conclusions

For a better design of Simultaneous Heat and Mass Transfer System, it is important to consider the relations of the three networks: Heat and mass transfer network, direct heat exchange network and indirect heat exchange network. This paper presented a number of insights of several previous works, and proposes a new insight to consider in the design of these systems, focusing on the penalty caused by Direct Heat Transfer Zone (Non-isothermal mixing area streams).

In addition, this work demonstrates the differences that can be obtained for the ΔT_{min} between the composite curves and the $\Delta T_{cold\text{-}side}$ from the cold side of the composite curves a due to the mixing of streams in the Direct Heat Transfer Zone, and proposes alternatives to handle these temperature differences, and ensuring that the fouling inflicted by these mixtures do not affect the requisite of temperature for the discharge wastewater.

The optimal design of Simultaneous Heat and Mass Transfer System is identified by the analysis of the composite curves with the support of the insights proposed in this paper.

Nomenclature

C_{in}	Limiting inlet concentration,	[ppm]
C_{out}	Limiting outlet concentration	[ppm]
CML	Contaminant mass load	[g/s]
CP	Flowrate capacity	[kW/ºC]
Cp	Heat capacity at constant pressure	[kJ/kgºC]
LWF	Limiting water flowrate	[kg/s]
f	Water flowrate	[kg/s]
f_i	Water flowrate in each operation *i*	[kg/s]
$f_{WF,i}$	Fresh water flowrate, flowrate number *i*	[kg/s]
$f_{FR,i}$	Watewater flowrate (outlet), flowrate number *i*	[kg/s]
$f_{R,i}$	Watewater flowrate (inlet), flowrate number *i*	[kg/s]
T_{dis}	Temperature of discharge wastewater	[ºC]
T_{supply}	Temperature of supply	[ºC]
$T_{op,in}$	Temperature of supply in the operation,	[ºC]
$T_{op,out}$	Temperature of discharge in the operation	[ºC]
ΔT	Difference of temperature	[ºC]
ΔT_{min}	Minimum temperature approach	[ºC]

$\Delta T_{cold\text{-}side}$	Minimum temperature for the cold side of the composite curves	[ºC]
M	Mass flow rate	[kg/s]
Op	Operation	
Q	Hot utility	[kW]
T	Temperature	[ºC]
T_{in}	Temperature of freshwater	[ºC]
T_{out}	Discharge temperature of wastewater	[ºC]

References

[1] Sorin, M. and L. Savulescu (2004). "On minimization of the number of heat exchangers in water networks." Heat Transfer Engineering 25(5), pp 30 - 38.

[2] Savulescu, L., J.-K. Kim, et al. (2005 a). "Studies on simultaneous energy and water minimisation- Part I: Systems with no water re-use." Chemical Engineering Science 60, pp. 3279 - 3290.

[3] Savulescu, L., J.-K. Kim, et al. (2005b). "Studies on simultaneous energy and water minimisation- Part II: Systems with maximum re-use of water." Chemical Engineering Science 60, pp. 3291 - 3308.

[4] Martinez-Patiño J., (2008). Combined method for the minimization of water and energy in pulp and paper processes. PhD. Thesis. University of Zaragoza.

[5] Leewongtanawit, B. and J.-K. Kim (2008). "Synthesis and optimisation of heat-integrated multiple-contaminant water systems." Chemical Engineering and Processing: Process Intensification 47(4), pp 670-694.

[6] Leewongtanawit, B. and J.-K. Kim (2009). "Improving energy recovery for water minimisation." Energy 34(7), pp 880-893.

[7] Martinez-Patiño J., et al. 2009, Integrated Optimization of Water and Energy Consumption. Part I: Studies and Considerations on Simultaneous Energy and Water Minimization, *Proc. of ECOS 2009,* pp 1413-1422

[8] Martinez-Patiño J., et al. 2009, Integrated Optimization of Water and Energy Consumption. Part II: Systematic Approach, *Proc. of ECOS 2009*, pp 1423-1430

[9] Linnhoff B. Townsend, D.W., Boland, D., Hewitt, D.F., Thomas, B.E.A., Guy, A.R. and Marsland RH. (1982)User Guide on Process Integration for the Efficient Use of Energy, Institution of Chemical Engineers. IchemE.

[10] Kemp, I. C. (1990). Process integration: process change and batch processes. ESDU Data Item 90033. Available by subscription from ESDU International plc, 27 Corsham Street, LONDON N1 6UA.

[11] Kemp I. C. (2007).Pinch Analysis Process Integration. Second Edition, IChemE.

[12] Wang Y. P. and Smith R. (1994). Wastewater Minimization. Chemical Engineering Science, Volume 49, Issue 7 , April 1994, pp. 981-1006.

[13] Olesen, S. G. and G. T. Polley (1997). "A simple methodology for the design of water networks handling single contaminants." Chemical Engineering Research and Design.

[14] Tripathi, P. (Nov 1996). Pinch Technology Reduces Wastewater; Mass exchange integration maximizes water recycling at a paper mill. Chemical Engineering. Vol. 103, Iss. 11; p. 87

[15] Polley G. and Picon-Nunez M., (2009),Design of water and heat recovery networks for the simultaneous minimization of water and energy consumption, Chemical Engineering Transactions, Vol. 18, pp 899-904. DOI: 10.3303/CET0918147.

Design & Optimization of Indirect Heat Integration of Batch Processes Using Genetic Algorithms

Pierre Krummenacher[a], Daniel Favrat[b], Blaise Renaud[c]

[a] *BG Consulting Engineers, Lausanne, Switzerland*
[b] *Industrial Energy Systems Lab., Ecole Polytechnique Fédérale de Lausanne (EPFL), Switzerland*
[c] *OptWare CH, Lussy-sur-Morges, Switzerland*

Abstract: Indirect heat integration – resorting to intermediate heat storage – is known for safeguarding the flexibility of the batch mode of production. This paper describes a framework to design & optimize indirect heat recovery schemes using evolutionary algorithms. It uses fixed temperature / variable mass heat storage units (HSUs). Given a number of HSUs, a superstructure is defined, incorporating all possible heat exchange matches between process streams and HSUs. A mathematical model is set up; its decisions variables (DVs) are defined to fit the specificities of the evolutionary algorithm used (*Struggle*). The resulting model is explicit, i.e. its computation doesn't require iterations. A two-levels, two-stages optimization scheme is implemented: the upper level addresses the structural optimization (binary DVs: streams to be integrated), while the lower level achieves the parametric optimization (real DVs: operating temperature of HSUs & heat load of heat exchange matches). The first stage aims at maximizing the heat recovery, while the second minimizes the total costs. An open heat storage model, attractive e.g. for processes consuming large amounts of hot process water, is also proposed. Using *Struggle*, the framework is validated on a brewing process.

Keywords: Batch process, Heat integration, Heat storage, Evolutionary algorithm, Food industry.

1. Introduction

The heat integration of batch processes involves both temperature and time constraints. Direct heat integration sets heat exchangers (HEXs) between process streams coexisting in time (as for continuous processes), while indirect heat integration resorts to intermediate heat storage to recover heat from hot process streams before supplying heat to cold process streams when needed.

Among the early pioneering methods, the time-dependent Cascade Analysis [1] is the first methodology specifically developed for batch processes. Assuming a single ΔT_{min}, the Cascade Analysis provides energy targets corresponding to various ways of cascading heat in both temperature and time dimensions. Rescheduling opportunities to increase the direct heat exchange targets may be identified. Direct heat exchange networks (HENs) are designed using the Pinch Design Method for each time slice, followed by merging them together for a maximum reuse of heat exchangers (HEXs). Heat storage between any pair of time slices may be determined.

A review of the methods and tools developed since the late 80's, based either on Pinch Analysis, on combinatorial approaches or on Mathematical Programming, may be found in [2].

The flexibility of operation is a major benefit of the batch processing mode. Owing to the intermediate heat storage avoiding the schedule constraints associated with direct HENs, the indirect heat integration doesn't induce detrimental effect on the flexibility, providing the indirect heat integration with a higher acceptability in practice.

1.1. Indirect heat integration

This paper addresses purely indirect heat integration, using fixed temperature / variable mass (FTVM) heat storage units (HSUs). The heat integration system, consisting essentially of HSUs and HEXs matches (hot streams to heat storage fluid, and heat storage fluid to cold streams), is named an indirect heat recovery scheme (IHRS). A storage sub-system (SSs) represents a set of two adjacent HSUs (when ordered by operating temperature). Figure 1 exemplifies such IHRSs.

Earlier contributors [3] developed methods for predicting the maximum heat integration potential between a number of tanks which require heating or cooling, in co-current, counter-current, and combinations of the two. Heuristics and a multi-

Corresponding Author: Krummenacher Pierre, Email: pierre.krummenacher@bg-21.com

period MILP formulation were applied to solve the optimal matching problem. The time schedule of the process was not taken into account (it was assumed that all tanks were available for matching at the same time).

In a purely indirect heat integration, the operating temperatures of FTVM HSUs are constrained by the supply temperature of streams, as [4] suggests, based on a Time Average Model composites representation. Opportunities for rescheduling to reduce the capacity of HSUs are considered, as well as unsteady state heat storage systems.

The Permutation Method (PM) [5] is a combinatorial approach to the design of IHRSs. The PM searches, among a set of feasible operating temperatures of FTVM HSUs and a sub-set of process streams to be heat integrated, the most cost-effective configuration of process streams–HSU matches. To achieve the HSU mass balance at the end of a batch cycle, mixing of storage fluid, followed by utility supply (if need be), is used. The set of feasible operating temperatures of HSUs is based on the supply and target temperatures of process streams. Within the restricted solution domain resulting from heuristic rules, the search is exhaustive. The PM has been further developed [6], but the proposed post-optimization stage for fine-tuning the real (continuous) variables remains difficult to apply.

A IHRS targeting method [7] enables the determination of the minimum number of HSUs as a function of the amount of heat recovery (HR) (basing on the Time Average Model composites, and on schedule and supply temperatures of the streams). It provides an insight into issues such as the set of streams to be integrated and the temperature range for each HSU, and produces feasible IHRSs of acceptable quality. But it fails to efficiently address the degrees of freedom of IHRS, featuring complex economic trade-off effects between HEX areas and HSU capacities.

This paper describes additional methodological developments proposed for the design and optimization of IHRSs, and presents application results for a brewing process.

1.2. Genetic algorithm pathway

A genetic algorithm (GA), or evolutionary algorithm, mimics, in a computational manner, the natural evolution of living species, where the fittest individuals of a population (i.e. the ones which are best suited to the constraints of their environment), have more chances to survive and reproduce. Evolutionary algorithms are now commonly used for optimization purposes.

Three reasons motivated the choice of the GA optimization pathway for IHRSs:

- the positive feedback with GAs reported for complex non-linear optimization problems (e.g. [8], using *Struggle* GA [9]), for both the structural and parametric optimizations;
- the capability to manage real life problems involving e.g. highly non-linear as well as discontinuous costs functions, and requiring *if ... then ... else …* decisions;
- the fact that GA based approaches deliver several good solutions in various respects (instead of only "the best one").

Struggle is a multimodal GA providing an improved niching method, efficient in searching multiple optima of functions of continuous (real) variables. *Struggle* does not resort to binary coding of real decision variables (DVs); real DVs are treated using a so-called *blend crossover* operator.

Since any GA optimization is intensive in evaluations of the objective function (OF) (requiring the largest share of computing time), these guidelines apply when setting up the model:

- as far as possible, avoid the need to solve implicit equations requiring iterations;
- whenever manageable, include the constraints in the definition of the DVs so as to minimize the number of generated infeasible solutions.

2. Proposed design methodology

Refer to Appendix A for the definition of the heat recovery (*HR*) and of the total batch costs (*TBCs*).

2.1. Closed heat storage system

A closed storage means the standard IHRS, i.e. using a separate, intermediate heat storage fluid in a closed system (no mass transfer to or from the process streams).

2.1.1. Superstructure

The IHRS superstructure depicted in Fig. 1 embeds all possible IHRS structures. It includes:

- a heat transfer match from each hot process stream to each SSs, and from each SSs to each cold process stream;

- utility coolers on hot process streams and utility heaters on cold streams;
- utility coolers or heaters between HSUs, to enable the mass rebalance, over a batch cycle, of HSUs in any case, whatever the mass transfers set by the DVs during the GA optimization process.

The heat losses of HSUs to the environment are neglected (but could be taken into account).

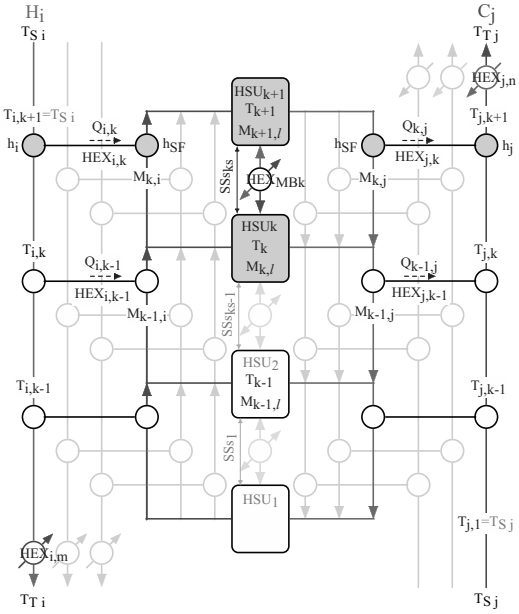

Fig. 1. Superstructure of a closed storage IHRS, including 4 HSUs.

Figure 1 also illustrates the nomenclature:

- subscript i: hot process streams ($i = 1 .. I$);
- subscript j: cold process streams ($j = 1 .. J$);
- subscript k: HSU ($k = 1 .. K$);
- subscript ks: SSs ($ks = 1 .. K$-1);
- subscript l: time slice of batch cycle ($l = 1 .. L$);
- $M_{k,i}$: mass of storage fluid (SF) heated, over a batch cycle, by stream i and moved from HSU_k into HSU_{k+1} as a result of $Q_{i,k}$;
- $M_{k,j}$: mass of SF cooled, over a batch cycle, by stream j and moved from HSU_{k+1} into HSU_k as a result of $Q_{k,j}$;
- $M_{k,l}$: mass of SF in HSU_k at end of time slice l.

2.1.2. Problem statement

Considering the above superstructure, the problem of optimal IHRS synthesis is stated as follows:

Given:

- a batch process, operated in a cyclic manner (whose schedule is considered "as is");
- a number of HSUs specified by the user;

determine:

- the operating temperature of each HSU;
- the heat exchanged by each process – heat storage streams match;

which minimize the total batch costs (*TBCs*) of the IHRS,

subject to the following set of constraints:

2.1.3. Constraints

Referring to Fig. 1, the constraints are:

1. monotonically increasing temperature of HSUs:

$$T_k > T_{k\text{-}1} \qquad (k : 2 .. K), \qquad (1)$$

$$\text{while } T_{HSUmin} \le T_k \le T_{HSUmax} \qquad (k : 1 .. K), \qquad (2)$$

where T_{HSUmin} and T_{HSUmax}: lower bound and upper bounds of the operating temperature of HSUs;

2. decreasing (increasing) cut-off temperatures of hot (cold) process streams :

$$T_{i,k} \le T_{i,k+1} \qquad (k : 1 .. K\text{-}1), \qquad (3)$$

$$\text{while } T_{T\,i} \le T_{i,k} \le T_{S\,i} \qquad (k : 1 .. K\text{-}1); \qquad (4)$$

$$T_{j,k+1} \ge T_{j,k} \qquad (k : 1 .. K\text{-}1), \qquad (5)$$

$$\text{while } T_{T\,j} \ge T_{j,k} \ge T_{S\,j} \qquad (k : 2 .. K); \qquad (6)$$

3. feasibility of HEX match between hot process stream i (cold process stream j) and SSs_{ks}:

$$T_{i,k+1} > T_{k+1} \text{ and } T_{i,k} > T_k \qquad (k : 1 .. K\text{-}1), \qquad (7)$$

$$T_{j,k+1} < T_{k+1} \text{ and } T_{j,k} < T_k \qquad (k : 1 .. K\text{-}1); \qquad (8)$$

4. K-1 mass balances of HSUs over a batch cycle:

$$\left(\sum_j M_{k,j} - \sum_i M_{k,i} - MBB_k\right) - \left(\sum_j M_{k-1,j} - \sum_i M_{k-1,i} - MBB_{k-1}\right) = 0 \qquad (9)$$

where $-MBB_k$: required mass to close the balance of HSU_k (MBB_k being the excess of mass cumulated in HSU_k during a batch cycle due to the contributions of process streams only).

Note: the T_{HSUmin} and T_{HSUmax} bounds depend on the set of streams to be integrated [7] and on the range of safe operation of the SF used.

2.1.4. Decision variables

The decisions variables (DVs) of the model are:

- $\boldsymbol{Y} = \{y_s\}$ (of size $S=I+J$) binary DVs, defining which stream should be integrated ($y_s=1$) and which must not be integrated ($y_s=0$);
- $\boldsymbol{X} = \{x_k ; x_{i,k} ; x_{j,k}\}$ (of size $K+I\cdot(K-1)+J\cdot(K-1)$) real, dimensionless DVs (with fixed bounds $0 < x_k < 1$, $0 \le x_{i,k} < 1$, $0 \le x_{j,k} < 1$) defining the operating temperature of HSU_k, the cut-off temperature of stream i after heat exchange with HSU_k, and the cut-off temperature of stream j after heat exchange with HSU_{k-1}, respectively.

The temperatures T_k, $T_{i,k}$, and $T_{j,k}$ are related to the x_k, $x_{i,k}$, and $x_{j,k}$ DVs as follows:

$$T_k = (1 - x_k)\cdot T_{k-1} + x_k \cdot T_{HSUmax} \,, \qquad (10)$$

Eq. (10) is applied from $k=1$ ($T_0=T_{HSUmin}$) to $k=K$;

$$T_{i,k} = (1 - x_{i,k})\cdot T_{i,k+1} + x_{i,k} \cdot T_{lim\,i,k} \,, \qquad (11)$$

where $T_{lim\,i,k} = max[T_k ; T_{T\,i} ; T(pinch_{i,k})]$,

Eq. (11) is successively applied to all feasible matches on stream i from $T_{S\,i}$ down to $T_{T\,i}$;

$$T_{j,k+1} = (1 - x_{j,k})\cdot T_{j,k} + x_{j,k} \cdot T_{lim\,j,k+1} \,, \qquad (12)$$

where $T_{lim\,j,k+1} = min[T_{k+1} ; T_{T\,j} ; T(pinch_{j,k+1})]$,

Eq. (12) is successively applied to all feasible matches on stream j from $T_{S\,j}$ up to $T_{T\,j}$.

The third term in the *max*[..] and *min*[..] accounts for the possible existence of an internal pinch as a result of a process stream undergoing phase change (or condensation of hot humid air, etc.).

Applying (10) to (12) to calculate T_k, $T_{i,k}$ and $T_{j,k}$ is called decoding of $\boldsymbol{X}$ DVs. The definition of the $\boldsymbol{X}$ DVs ensures that the constraints 1. to 3. ((1) through (8), responsible for the variable bounds) are automatically met. Any individual described by x_k, $x_{i,k}$, and $x_{j,k}$ DVs (within their fixed bounds) is a feasible individual (maybe performing bad, but feasible anyway !). This prevents the optimization from spending time generating and evaluating infeasible individuals. However, as (10) through (12) indicate, there aren't one-to-one relationships between the x_k, $x_{i,k}$, and $x_{j,k}$ DVs and T_k, $T_{i,k}$ and $T_{j,k}$, since any change of, say, $x_{k=1}$ propagates and induces changes of every T_k (for $k>1$) of HSUs downwards in the propagation chain (even without any change of x_k (for $k>1$). Although a matter of concern when setting up the model, negative effects of these dependency links on the efficiency of the GA optimization could be identified.

Further, whenever a stream has reached its target temperature, any match downstream becomes independent of its corresponding x variable.

The HSUs mass balance constraints 4. are much more difficult to account, since these equality constraints link a large number of DVs together. In fact there is no way meeting these constraints at the onset by a clever choice of $\boldsymbol{X}$. Instead, a procedure (see below) determines the minimum utility costs penalty needed to rebalance the HSUs; this penalty is a measure of the fitness of the generated individual.

The HSUs temperatures T_k determine which process-storage streams matches are actually feasible. $k_{max\,i}$ and $k_{min\,j}$ are introduced to define the feasible part of the superstructure:

$k_{max\,i}$: largest k still satisfying $T_{S\,i} > T_k$, (13)

matches with i are feasible up to $SSs_{kmax\,i-1}$;

$k_{min\,j}$: smallest k still satisfying $T_{S\,j} < T_k$, (14)

matches with j are feasible down to $SSs_{kmin\,j}$.

Note: $x_{i,k}$ and $x_{j,k}$ DVs corresponding to infeasible matches are ignored during decoding.

2.1.5. Mass balance of heat storage units

Opportunities for mixing of storage fluid prior to mass rebalancing by utilities may exist in IHRSs including at least three HSUs. Utility mass rebalancing costs are minimized by sequentially calculating (refer to [2], Appendix C, for details):

- the mass before balance MBB_k defined by (9);
- the cumulated mass before balance $CMBB_k$ (kg) starting from HSU_K (highest temperature):

  $$CMBB_k = CMBB_{k+1} + MBB_k \,; \qquad (15)$$

- the imbalance heat load cascade IQC (kJ):

  $$IQC_k = IQC_{k+1} + CMBB_{k+1}\cdot c_{pSF}\cdot(T_{k+1} - T_k) \,; \qquad (16)$$

- the imbalance heat load cascade without pocket $IQCWP$ (kJ) (pocket = mixing opportunity);
- the cumulated mass before utility balance $CMBUB_k$ (kg):

  $$CMBUB_k = \frac{IQCWP_{k-1} - IQCWP_k}{c_{pSF}\cdot(T_k - T_{k-1})} \,; \qquad (16)$$

- the mass before utility balance $MBUB_k$ (kg):

  $$MBUB_k = CMBUB_k - CMBUB_{k+1} \,; \qquad (17)$$

- the overall mixing mass contribution $M_{M\,k}$ (kg):

  $M_{M\,k} = MBUB_k - MBB_k$, (18)

  $M_{M\,k} > 0$: incoming balancing mixing mass,

  $MBUB_k > 0$: incoming rebalancing utility mass.

The overall mixing mass contributions may be decomposed into a set of elementary and independent mixing steps, each involving only mixing of SF from two adjoining HSUs. The schedule of the elementary mixing steps could be optimized to minimize the capacities of HSUs, but this issue is not addressed so far.

2.1.6. Model calculation flowsheet

Given $\boldsymbol{X}$ a vector of DVs, *TBCs* are calculated as shown on Fig. 2 (where $x_{i,k}$ and $x_{j,k}$ variables of streams not selected by $\boldsymbol{Y}$ (i.e. y_s=0) are ignored).

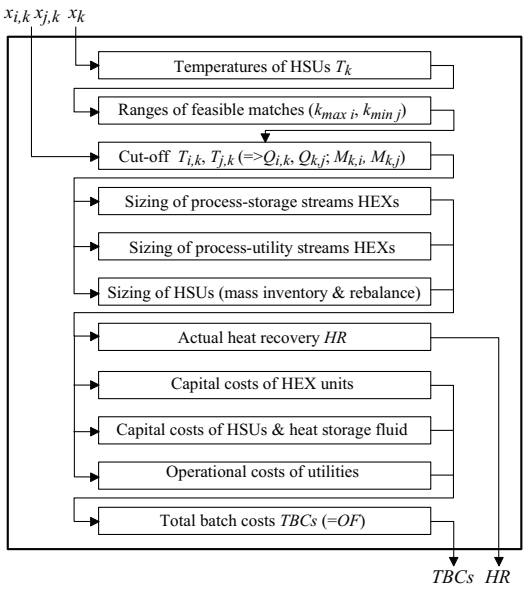

*Fig. 2. Flowsheet of the model to calculate OF(**X**,**Y**).*

2.1.7. Optimization issues

Keeping the population diversity is tricky. A suitable distance function (DF) and a two-levels, two-stages optimization, solve this issue.

Defining the DF based on the x DVs is not recommended (refer to 2.1.4). Instead, DF is defined as a combination of a structural distance D_K (effect of T_k on feasible matches) and of a parametric distance D_T (with A, B: individuals):

$$D(A,B) = \sqrt[2]{\left[D_K(A,B)\right]^2 + \left[D_T(A,B)\right]^2} \quad , \qquad (19)$$

where:

$$D_K(A,B) = w_k \left\{ \sum_{i,k} \left[q_i \left(k_{\max i\,a} - k_{\max i\,b} \right) \right]^2 + \sum_{j,k} \left[q_j \left(k_{\min j\,a} - k_{\min j\,b} \right) \right]^2 \right\}^{1/2} \quad , \qquad (20)$$

$$D_T(A,B) = \left\{ \sum_{i,k} \left[q_i \left(T_{i,k\,a} - T_{i,k\,b} \right) \right]^2 + \sum_{j,k} \left[q_j \left(T_{j,k\,a} - T_{j,k\,b} \right) \right]^2 \right\}^{1/2} \quad , \qquad (21)$$

- q_i (q_j) : ratio of the potential heat contribution of hot (cold) process stream i (j) over the overall heat recovery potential;
- w_k : weighting factor, chosen so that a single difference in k_{max} or k_{min} results in a contribution larger than that arising from a significant difference in the $T_{i,k}$ and $T_{j,k}$.

Early optimization runs were scarcely able to develop individuals featuring large *HR*. Owing to the *Struggle* replacement strategy, individuals potentially achieving a large *HR* but whose $\boldsymbol{X}$ DVs are not fine-tuned yet to achieve an acceptable mass balance (hence utility and costs penalty), are prematurely rejected before they can improve and develop their full capability.

To bypass this shortcoming, the *HR* is maximized during a first phase to allow for individuals featuring large *HR* to develop, before *OF=TBCs*.

2.2. Open heat storage system

Food and beverage industries use large amounts of hot process water and are good candidates for cost-efficient IHRSs. Therefore, an open storage IHRS model has been set up. The benefits include HEX unit & area savings, potential for reducing the number of HSUs and/or achieving a larger *HR*.

2.2.1. Superstructure

Compared to the closed storage superstructure, the open storage superstructure (Fig. 3) highlights two additional features: a so-called PW HSU and mixers to prepare the PW streams.

The PW HSU represents the supply network of process water. The process water at supply temperature $T_{S\,PW}$ is transferred to the adjoining HSU(s) by process-storage streams matches, i.e. in

the same way the storage fluid is transferred between the standard HSUs.

Depending on the temperature of the HSUs (i.e. on the x_k DVs of the individual being evaluated), the PW HSU may be intermediate in the row of HSUs as on Fig. 4, or be located at one end of the row.

Unlike "standard" cold process streams, heated up by storage-process HEXs (e.g. Cj), PW streams Ca and Cb are prepared by mixing of storage fluid from (potentially) all HSUs above, and including, the PW HSU. The $x_{j,k}$ DVs determine the proportion of the PW stream mass flow rate to be extracted from the corresponding HSU.

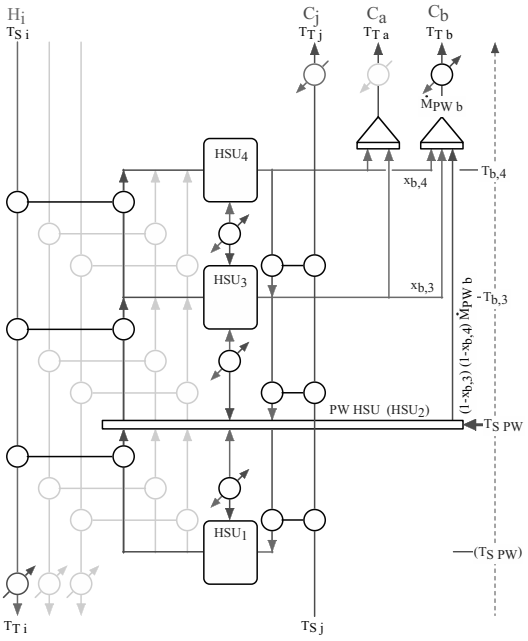

Fig. 3. Superstructure of an open storage IHRS including 3 HSUs & 1 PW HSU.

2.2.2. Changes to the IHRS model

The "standard" closed storage IHRS model must be modified with respect to:

- the mass balance of the special PW HSU,
- the meaning of $x_{j,k}$ DVs for PW streams,
- and the definition of cut-off temperature of PW streams to be taken into account in the DF.

The PW HSU is a special HSU in that it has a "single way capacity". The supplied mass flow rate must be $\dot{M}^{-}_{PW\,l} \geq 0$ whatever the time slice l, i.e. it can only supply (at any time). In addition, over a batch cycle, the total mass M_{PW} supplied by the PW HSU is equal to the sum of masses of the PW streams. Hence, the open storage IHRS model features l–1 additional constraints. A systematic procedure is proposed. The costs to meet these constraints (utility operation costs, capital costs of required HEXs) are minimized by a staged use of:

- the mixing mass contributions (the cheapest),
- the balancing utility mass contributions (more expensive),
- and finally of the additional utility mass contributions (the most expensive).

The mixing contributions are scheduled according to a peak shaving / hollow filling strategy, to allow a minimum heat rate strategy for the rebalancing utility contributions to minimize the costs of the related HEXs.

This procedure is applied once the HSU overall mass rebalancing calculations (as for the closed storage IHRS model) have been achieved.

Regarding the preparation (heating) of PW streams by mixing, the mass flow rate contributions of the HSUs are calculated, from the hottest down to the HSU just above the PW HSU, by:

$$\dot{M}_{PW\,j,k} = x_{j,k} \cdot \left(\dot{M}_{PW\,j} - \sum_{n=k+1}^{K+1} \dot{M}_{PW\,j,n} \right). \qquad (22)$$

The PW HSU supplies the remaining flow rate:

$$\dot{M}_{PW\,j,k_{PW}} = \dot{M}_{PW\,j} - \sum_{n=k_{PW}+1}^{K+1} \dot{M}_{PW\,j,n}\,. \qquad (23)$$

The mass flow rate of the PW stream j is met in any case. The resulting mixing temperature $T_{mix\,PW\,j}$ can be lower or higher than the target temperature $T_{T\,PW\,j}$. In the latter case, reverse utility (cold utility on cold stream) is applied, until the GA adjusts the $x_{j,k}$ so as to avoid this penalty. The above general strategy holds for Cb, while a deterministic mixing of PW from surrounding HSUs is assumed for Ca.

To express the contributions of PW streams to the DF in equivalent cut-off temperatures as for "standard" process streams, the following conversion is applied (from k_{PW+1} up to K+1):

$$T_{j,k} = T_{j,k-1} + \frac{\dot{M}_{PW\,j,k}}{\dot{M}_{PW\,j}} \cdot \left(T_k - T_{S\,PW} \right). \qquad (24)$$

$T_{j,k}$–$T_{j,k-1}$ is the equivalent temperature increase of the total flow rate $\dot{M}_{PW\,j}$ due to the PW flow rate

$\dot{M}_{PW\,j,k}$ out of HSU_k. By convention, the temperatures $T_{j,k}$ up to k_{PW} remain at $T_{S\,PW}$.

Note: choosing an open storage system or a closed one is a user's decision. An optimization run may be achieved for both cases and results compared.

3. Case study

Process EP-3 (refer to Appendix B) is a brewing process, extensively analyzed in [6]. The resulting optimal IHRSs (applying the Permutation Method followed by the Post-Optimization) are used as reference for validating the GA based framework.

EP-3 features 12 process streams, while the resulting optimal IHRSs of [6] include 3 HSUs. Hence, the required number of DVs is:

- 12 binary DVs to address the full structural optimization;
- 27 real DVs (3+12x(3-1)) for the parametric optimization of a closed storage IHRS model;
- 39 real DVs (3+12x(4-1)) for the parametric optimization of an open storage IHRS model.

Owing to computing time constraints, the results presented below have been obtained with a single level (real DVs) optimization, while the binary DVs defining the streams to be integrated were set. The streams have been selected using the targeting methodology [7], which helps restricting the search domain and the computational burden; but this is not a requirement of the model. The two-levels optimization scheme has been successfully tested, yet with fewer generations and smaller populations for both upper and lower levels.

Note: the proposed model may include the start-up and shut-down phases of a repeated batch operation in the optimization problem as well.

3.1. Closed heat storage system

The best solution reported by [6] and depicted in Fig. 4 integrates C1, C4, C7, C13, H9, H11/12. The GA optimization settings are: N_{Pop}=100; N_{Gen}=1000; OF=*HR* for first 300 generations; 3 HSUs; same set of selected streams; $x_{j,2}$=1 for C1, C4, C7 and C13 to avoid HU on these streams and speed up the search. Table 1 summarizes the results obtained by both approaches.

Both solutions achieve the same HR, but the utility costs of the GA solution are slightly higher, owing to 35 kWh/batch of CU, needed for mass rebalance after 35 kWh/batch of excess heat being recovered on stream H11 (a heat recovery stream).

The GA based IHRS model uses a HEX cost function (refer to Appendix B) including a fixed cost $C_{0X\,circ}$ to account for the costs of an intermediate connection to a HSU. The penalty for the N_{circ}=5 intermediate connections contributes to 1/3 of the difference between the two solutions (i.e 0.34 % of the *TBCs*).

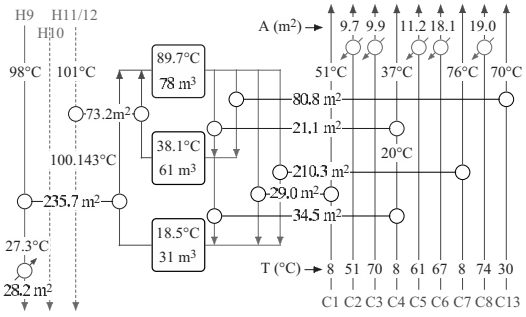

Fig. 4. Best IHRS solution of [6] (for a closed heat storage system) integrating 6 streams.

Table 1. GA based vs [6] IHRS optimization results.

COSTS	HEXs	HSUs	UTIL.	TBCs	ΔTBCs
Method	DKK/b	DKK/b	DKK/b	DKK/b	%
Optim [6]	507.2	136.2	632.7	1276.1	100
GA Optim	515.9	133.5	639.3	1288.7	101.0

SIZES	HR	HEXs	HSUs	HU	CU
Method	kWh/b	m^2	m^3	kWh/b	kWh/b
Optim [6]	14510	780.8	170.0	5766	1931
GA Optim	14510	783.4	166.3	5766	1966

HSUs	HSU1		HSU2		HSU3	
Method	°C	m^3	°C	m^3	°C	m^3
Optim [6]	18.5	31.0	38.1	61.0	89.7	78.0
GA Optim	19.2	27.7	39.4	58.4	88.6	80.2

3.2. Open heat storage system

3.2.1. IHRS integrating 9 streams

C7 is specified as a PW stream. The GA optimization settings are: N_{Pop}=200; N_{Gen}=2000; OF=*HR* for first 300 generations; 3 HSUs & 1 PW HSU; set of selected streams: C1, C2, C4, C7, C8, C13, H9, H11/12. The resulting best IHRS is represented on Fig. 5.

Table 2 summarizes the results and compares them to those of the closed storage system of [6]. The open storage IHRS is 13 % cheaper while achieving a 12 % larger *HR*. The *HR* is significantly increased by the integration of C2 and C8; these streams require an intermediate HSU (HSU3) at a temperature T3 > 51 °C (for

C2), and T3 > 74 °C (for C8); this condition is met by the open storage IHRS because the PW HSU sets one HSU free to match this temperature condition, relaxing the conflicting conditions which prevail for closed storage system.

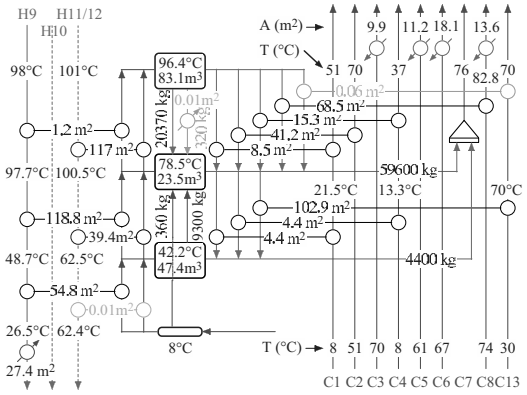

Fig. 5. GA-optimized open storage IHRS.

Table 2. Open storage (GA) vs Closed [6] best IHRSs.

Storage	HR	HEXs		HSUs		UTIL.	TBCs
model	kWh/b	m²	DKK/b	m³	DKK/b	DKK/b	DKK/b
Closed [6]	14510	781	507.2	170	136.2	632.7	1276.1
Open	16185	656	505.9	154	124.9	477.0	1107.8

3.2.2. IHRS potentially integrating all streams

Figure 6 displays the *TBCs vs HR* curve obtained for an IHRS potentially integrating all streams (same optimization parameters as under 3.2.1.). The points keep track of the min *TBCs* individuals within each [*HR*–d*HR* ; *HR*+d*HR*] interval. Local minimums corresponding to different sets of $k_{max\,i}$ & $k_{min\,j}$ exist in the range 14'000 to 18'000 kWh/b.

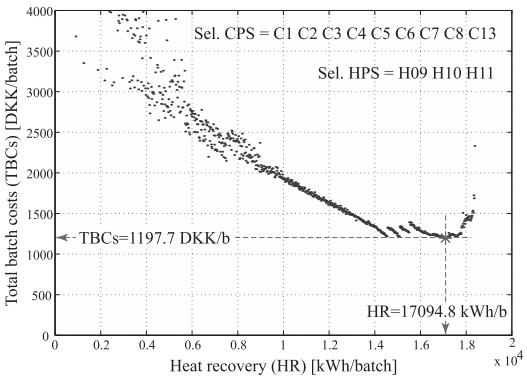

Fig. 6. Least TBCs curve of all individuals generated during a GA optimization of an open storage IHRS potentially integrating all streams.

The envelope curve is the smoothest in the region featuring low *TBCs* & large *HR*, while the scattering of points (= best generated individuals in each *HR* interval) increases as *HR* decreases below 9'000 kWh/b. This highlights the effect of the preliminary stage with OF=*HR* to explore and focus on large *HR* regions and of the subsequent phase achieving a fine parametric optimization.

4. Conclusion and outlook

A IHRS synthesis framework suitable for a GA based optimization has been developed and successfully tested with the *Struggle* GA. A two-levels, two-stages optimization scheme (1st stage: *max(HR)*, 2nd stage: *min(TBCs)*), an appropriate definition of the decision variables, and a distance function keeping population diversity, are used to achieve adequate optimization performances.

IHRSs designed by the proposed approach compete well with best IHRS of [6]. This structured approach requires less user's decisions to be made than that of [5,6]. It improves the mass rebalancing calculations of the latter by proposing a systematic calculation strategy. Test cases further demonstrate the practice relevance and the benefits of the proposed open storage system.

Nonetheless, a significant scope for improvement does exist in terms of:

- Computing time: speed-up factors ≥ 1000 are expected by optimization of the Matlab code, its compilation and the use of more up-to-date processor frequencies, compared to the mixed code used (IHRS model in interpreted Matlab, linked to the GA in compiled C++);
- Optimization scheme: going for recently developed evolutionary multi-objective optimization approaches may spare the two-stages strategy;
- Engineering practice relevance of the IHRSs: the models may be extended to additional capabilities (e.g. the way utilities are supplied and scheduled, the control over the intermediate connections to HSUs, accounting of other costs factors, several heat storage fluids, latent heat storage, heat losses, etc.).

Nomenclature

A heat exchange area, m²

a_B pay-off factor per batch

BCD batch cycle duration, s (min)

c_p specific heat, kJ/(kg K)
CU cold utility
DF distance function (dimensionless)
DKK Danish Crown (monetary unit)
DV decision variable
FTVM fixed temperature / variable mass
GA genetic (or evolutionary) algorithm
h heat transfer coefficient, W/(m^2 K)
HEX heat exchanger
HR heat recovery (per batch), kWh
HSU heat storage unit
HU hot utility
I number of hot process streams
IHRS indirect heat recovery scheme
IR interest rate
J number of cold process streams
K number of heat storage units
k_{max} highest HSU index ensuring feasible heat exchange with a hot process stream
k_{min} lowest HSU index ensuring feasible heat exchange with a cold process stream
L number of time slices in a batch cycle
M mass, kg
$\dot{M}$ mass flow rate, kg/s
$max()$ Maximum function
$min()$ Minimum function
N_{BPY} number of batches per year
N_{Gen} number of generations
N_{Pop} number of individuals in a population
OF objective function
POP pay-off period, year
Q heat, kJ (kWh)
$\dot{Q}$ heat rate (heat duty), kW
S number of process streams (S=I+J)
SSs storage sub-system
T temperature, °C
T_S supply temperature of stream, °C
T_T target temperature of stream, °C
t time, s (min)
V volume (useful capacity of HSU), m^3
$\boldsymbol{X}$ vector of real DVs of one individual
x dimensionless real DV
$\boldsymbol{Y}$ vector of binary DVs of one individual
y binary DV

Greek symbols

ρ density, kg/m^3
ΔT_{LM} logarithmic mean temperature difference, K

Subscripts and superscripts

C cold stream
H hot stream
i hot process stream (i = 1 .. I)
j cold process stream (j = 1 .. J)
k heat storage unit (k = 1 .. K)
ks storage sub-system (ks = 1 .. K-1)
l time slice (l = 1 .. L)
n_{gen} generation (n_{gen} = 1 .. N_{Gen})
PW process water
S heat storage
s process stream (s = 1 .. S)
SF storage fluid (heat storage material)
X heat exchanger (in HEX cost function context)

References

[1] Kemp I.C., and Deakin A.W., 1989, The Cascade Analysis for Energy and Process Integration of Batch Processes (Part 1: Calculation of Energy Targets; Part 2: Network Design and Process Scheduling; Part 3: a Case Study), Chem. Eng. Res. & Des., 67, pp. 495-525.

[2] Krummenacher P., 2001, Contribution to the Heat Integration of Batch Processes (with or without Heat Storage), Ph.D. Dissertation (URL: http://library.epfl.ch/theses/?nr=2480), EPFL, Lausanne, Switzerland.

[3] Vaselenak J.A., et al., 1986, Heat Integration in Batch Processing", I & EC Proc. Des. Dev., 21, pp. 79-86.

[4] Sadr-Kazemi N., and Polley G.T., 1996, Design of Energy Storage Systems for Batch Process Plants, Trans IChemE, 74(A), pp. 584-596.

[5] Stoltze S., et al., 1995, Waste Heat Recovery in Batch Processes Using Heat Storage, J. of Energy Res. Tech. (Trans. of ASME), 117(2), pp. 142-149.

[6] Mikkelsen J.B., 1998, Thermal-Energy Storage Systems in Batch Processing, Ph.D. Dissertation, DTU, Copenhagen, Denmark.

[7] Krummenacher P., and Favrat D., 2001, Indirect and Mixed Direct-Indirect Heat Integration of Batch Processes Based on Pinch Analysis, Int. J. Applied Thermodynamics, 4(3), pp. 135-143.

[8] Olsommer B., Favrat D., 1999, An Approach for the Time-Dependent Thermoeconomic Modeling and Optimization of Energy System Synthesis, Design and Operation Part I: Methodology and Results, Int. J. Applied Thermodynamics, 2(3), pp. 97-114.

[9] Senin N., et al., 1999, Object-based Design Modeling and Optimization with Genetic Algorithms, *Proc. of the Genetic and Evolutionary Computation Conf.*, Orlando, USA

Acknowledgments: This work has been partially funded by the Swiss Federal Office of Energy (BFE/OFEN) under grant 77863. Thanks to MIT-CADLAB too, for making the GALib library (including *Struggle*) available.

Appendix A

The *HR* of an IHRS is defined as the actually useful heat transferred, over a batch cycle, from hot process streams to cold process streams through the heat storage system. The heat balance of the heat storage system as a whole must hold:

$$HR = Q_{H-S} - Q_{S-CU} = Q_{S-C} - Q_{HU-S}, \qquad (A.1)$$

where $Q_{H\text{-}S}$: overall heat transferred from hot process streams to storage system; $Q_{S\text{-}CU}$: overall heat extracted by cold utility from the storage system; $Q_{S\text{-}C}$: overall heat transferred from storage system to cold process streams; $Q_{HU\text{-}S}$: overall heat supplied by hot utility to storage system.

The Total Batch Costs (*TBCs*) represent the overall energy related costs to produce one batch:

$$TBCs = a_B \cdot \sum_p C_{cap\,p} + \sum_d C_{oper\,d}, \qquad (A.2)$$

- $a_B = \frac{1}{N_{BPY}} \cdot \frac{IR}{1-(1+IR)^{-POP}}$,
- $C_{cap\,p}$, capital cost of part p (HEX, HSU, control valves, piping, heat storage fluid, etc.),
- $C_{oper\,d}$, operation cost of duty d (HU, CU, cleaning of HEXs, etc.).

Appendix B

Table B1. Data of process EP-3.

Process streams: (h = 4000 W/(m^2 K) for every stream)

Stream name	T_S °C	T_T °C	M kg	c_p kJ/(kg K)	t_{start} min	t_{stop} min
C1	8	51	30000	3.5	0	60
C2	51	70	30000	3.5	60	75
C3	70	100	30000	3.5	90	120
C4	8	37	38000	3.8	75	105
C5	61	67	67200	3.7	120	130
C6	67	76	67200	3.7	190	200
C7	8	76	64000	4.186	345	405
C8	74	100	117200	3.9	345	405
C13	30	70	151200	4.186	0	200
H9	98	11	105200	3.9	540	660
H10	101	100	800	2257	120	140
H11	101	100	12000	2257	405	495
H12	100	30	12000	4.186	405	495

Utilities: (h = 4000 W/(m^2 K) for both utilities)

Utility name	T_{in} °C	T_{out} °C	Unit cost DKK/kWh
HU	175	174	0.09
CU	1	2	0.0612

Heat storage: (h = 4000 W/(m^2 K) for all heat storage streams)

Storage fluid	$T_{SF\,min}$ °C	$T_{SF\,max}$ °C	c_p kJ/(kg K)	ρ kg/m^3
Water	2	100	4.186	1000

Economic parameters:

BCD min	N_{BPY} batch/year	POP year	IR -
200	1500	10	0.05

HEX cost: $C_X = C_{0X} + C_{0X\,circ} \cdot N_{circ} + C_{rX} \cdot \left(\frac{A}{A_r}\right)^{m_X}$

A m^2	C_{0X} DKK	$C_{0X\,circ}$ DKK	C_{rX} DKK	A_r m^2	m_X -
Cost parameters used in [6]:					
< 20	75600	0	10224	1	1
≥ 20	180000	0	4968	1	1
Cost parameters used in this work:					
< 20	65600	10000	10224	1	1
≥ 20	170000	10000	4968	1	1

HSU cost: $C_S = C_{0S} + C_{rS} \cdot \left(\frac{V}{V_r}\right)^{m_S}$

V m^3	C_{0S} DKK	C_{rS} DKK	V_r m^3	m_S -
< 100	0	22800	1	0.78
≥ 100	0	63000	1	0.5593

H10, H11 and H12 are heat recovery streams (i.e. their target temperature is soft, no utility needed).

An improved Process of the Crude Oil Atmospheric Distillation for Energy Integration

Tahar Benali, Daniel Tondeur, Jean Noël Jaubert

Laboratoire Réactions et Génie des Procédés, ENSIC-INPL, Nancy, France.

Abstract: This paper describes a specific application of the Exergy analysis method in order to modify the flowsheet of the crude oil atmospheric distillation process by a preliminary separation of the partly vaporized components in the pre-heating train. This pre-separation avoids unnecessary overheating of these organics in the furnace. As a result, a significant reduction of the fuel consumption and the carbon dioxide emissions in this process are achieved.

Keywords: Energy saving, Exergy analysis, Multi-component distillation, Process simulation.

1. Introduction

In order to face the decline of fossil fuel raw materials and the increase of green house gases, scientists are favoring the renewable energy research path over the optimization of already existing processes. However, many optimization methods can be applied to reduce energy consumption in these processes and slow down this tendency. In many cases, small and cheap modifications in the flowsheet of energy intensive processes like those in petroleum refining and petrochemicals can generate an important improvement in terms of energy savings.

As for example, classic crude oil distillation processes range from a simple distillation column with a furnace and racking end products to a distillation column with strippers, end product conditioners as well as lateral pumparounds used to stabilize the column temperature profile. As a result, an important amount of heat is retrieved and carried to preheat the partly vaporized charge. This charge will be vaporized in a furnace and then fed to the distillation column over its wash zone.

In a preliminary study, this process has been simulated and an exergy analysis has been performed. The exergy balance around the column shows a high amount of irreversibilities and the first step was dedicated to understand the phenomena responsible of this exergy destruction by defining different kinds of exergies involved and the corresponding column profiles.

No significant effect was noticed on the decrease of irrevesibilies by dividing the stripping steam throughout the column in order to spread irreversibilities on all the trays instead of feeding it only at the bottom of the column. On the other hand it is important to consider that the crude oil, prior to its introduction to the furnace and to the column, undergoes a continuous vaporization. This is due to the heat exchange with the condenser, the end products and the pumparounds of the column in the pre-heating train. So we understand that this vaporized part is unnecessarily fed to the furnace and then to the bottom of the column.

An important improvement is reached by implementing a preliminary separation of the vaporized components in flashes installed throughout the pre-heating train and by sending the resulting vapors directly to the distillation column at the tray with the same temperature as each flash. As a result, an improved crude oil distillation process is proposed and a complete study has been performed to quantify energy savings.

2. Exergy analysis of a simplified crude oil distillation unit

2.1. Description of the process

Basically, the crude oil atmospheric distillation process, Fig. 1, consists in a pre-heating train where crude oil is fed from the holding tank. Then this oil is vaporized in the furnace where the combustion of a fuel (commonly

Corresponding Author: Tahar Benali, Email: tahar.benali@ensic.inpl-nancy.fr

methane) is taking place. Finally it is fed to the bottom of the distillation column just above its wash zone (1).

The distillation column is considered to be the master unit since all different cuts like light and heavy naphtha, kerosene, light and heavy gas oils and atmospheric residue are separated and purified. A large amount of heat is carried out to the preheating train from the condenser, the end products, the strippers and the pumparounds. This also means a high amount of energy degradation and it is worth studying the performances of the process in terms of exergy destruction.

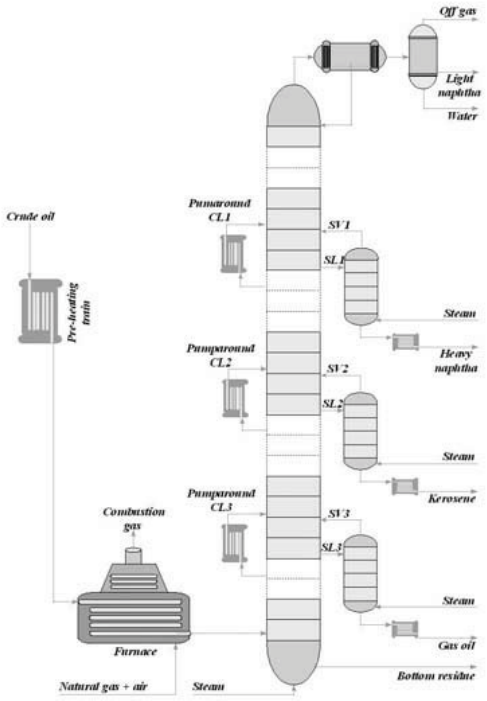

Fig. 1. A simplified crude oil distillation process.

2.2. Exergy profile of multi-component distillation column

2.2.1. Exergy destruction around a simple multi-component tray

The exergy of a mixture, E, is a function of its enthalpy H and its entropy S in operating conditions and its enthalpy H_0 and its entropy S_0 at surrounding temperature T_0 and it is defined as (1):

$$E = (H - H_0) - T_0 \cdot (S - S_0) \quad (1)$$

In the case of the simple multi-component distillation tray, Fig. 2, the contact between vapor V_{i+1} fed from tray $i + 1$ and the liquid L_i falling from the tray i produces an amount of exergy destruction that can be classified into two classes and six parts (2):

Exergy destruction due to mass transfer resulting from the evaporation, the condensation and the mixing in vapor and liquid phases.

Exergy destruction due to the liquid heating and the vapor cooling.

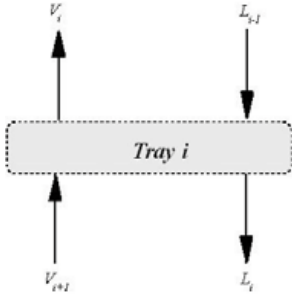

Fig. 2. A model of a simple multi-component distillation tray.

We designate by $\overline{\overline{\Xi}}_i$ the amount of exergy destroyed around the distillation tray i and we decompose it as follows:

$$\overline{\overline{\Xi}}_i = \Xi_{\theta_i} + \Xi_{\varphi_i} + \Xi_{\mu_i} \quad (2)$$

Where:

is the exergy destruction by the liquid heating and the vapor cooling over the tray i:

$$\Xi_{\theta_i} = V_{i+1} \sum_{j=1}^{n} y_{i+1,j} \begin{pmatrix} h_{i+1,j} - T_0 s_{i+1,j} \\ - h_{i,j} + T_0 s_{i,j} \end{pmatrix} - L_{i-1} \sum x_{i-1,j} \begin{pmatrix} h_{i,j} - T_0 s_{i,j} \\ - h_{i-1,j} + T_0 s_{i-1,j} \end{pmatrix} \quad (3)$$

The summations (on index j) apply to the n components.

is the exergy destruction by phase change in the liquid vaporization and the vapor condensation on the tray i:

$$\Xi_{\varphi_i} = \sum_{j=1}^{n_c} n_{c_{i,j}} \Delta_c H_{i,j} - T_0 \sum_{j=1}^{n_c} n_{c_{i,j}} \Delta_c S_{i,j} - \sum_{j=1}^{n_v} n_{V_{i,j}} \Delta_{vap} H_{i,j} + T_0 \sum_{j=1}^{n_v} n_{V_{i,j}} \Delta_{vap} S_{i,j} \quad (4)$$

n_c and n_v are respectively the number of condensed and the number of vaporized

components, and $_cH$, $_cS$, $_{vap}H$ and $_{vap}S$ are there corresponding enthalpies and entropies.

$_{\mu i}$ is the exergy destruction due to the mixing of the vapor from the tray $i+1$ with the one from the tray i and the mixing of the liquid from the tray $i-1$ with the one from the tray i:

$$\Xi_{\mu_i} = RT_0\left(\left(L_{i-1}\sum_{j=1}^{n} x_{i-1,j}\ln x_{i-1,j}\right) - \left(L_i\sum_{j=1}^{n} x_{i,j}\ln x_{i,j}\right)\right) - RT_0\left(\left(V_{i+1}\sum_{j=1}^{n} y_{i+1,j}\ln y_{i+1,j}\right) - \left(V_i\sum_{j=1}^{n} y_{i,j}\ln y_{i,j}\right)\right) \quad (5)$$

The expression above implies the assumption that liquid and gas phases are ideal mixtures.

2.2.2. Exergy destruction around a general crude oil distillation tray

Figure 3 represents a general tray i of oil distillation where all kinds of feeds and products to and from this tray are taken into account. It shows the washed up vapor V_{i+1} coming into contact with the liquid L_{i-1} where a part of the vapor will condense in order to vaporize a part of the liquid to generate the vapor flux V_i and the liquid flux L_i that leave the tray i. Vaporized crude oil F_i, pumparound exit LP_i and return PR_i streams as well as strippers feeds LS_i and returns FS_i fluxes can take place on this tray i.

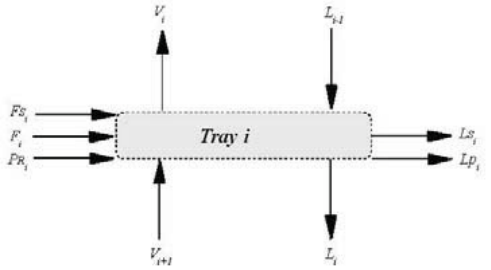

Fig. 3. A model of a general crude oil tray.

In order to simplify the calculation of irreversibilities around this tray, new fluxes are defined in order to have the same development for the simple tray:

$$\begin{cases} \overline{V}_i = V_i \\ \overline{V}_{i+1} = V_{i+1} + FS_i + x_v F_i \\ \overline{L}_{i-1} = L_{i-1} + PR_i + (1 - x_v) F_i \\ \overline{L}_i = L_i + LP_i + LS_i \end{cases} \quad (6)$$

x_v is the vapor fraction in the feed F_i.

The reasoning to define the different kinds of exergy destructions is similar to the simple case. It is sufficient to add exergy destruction due to mixing, heating and cooling of fluxes feeding and leaving the column.

2.2.3. Exergy destruction throughout a multi-component distillation column

We can also use arrays to introduce individual exergy destruction amounts (per tray and per component) in the column by considering:

$$\overline{\overline{\Xi}} = \sum_{i=1}^{N}\sum_{j=1}^{n}\Xi_{i,j} \quad (7)$$

$_{i,j}$ is the exergy destruction at the tray i of a column with N trays associated with the component j of a flux of n components :

$$\overline{\overline{\Xi}} = \begin{bmatrix} \Xi_{1,1} & \Xi_{i-1,1} & \Xi_{i,1} & \Xi_{N,1} \\ \Xi_{1,2} & \Xi_{i-1,2} & \Xi_{i,2} & \Xi_{N,2} \\ \Xi_{1,j} & \Xi_{i-1,j} & \Xi_{i,j} & \Xi_{N,j} \\ \Xi_{1,j+1} & \Xi_{i-1,j+1} & \Xi_{i,j+1} & \Xi_{N,J+1} \\ \Xi_{1,n-1} & \Xi_{i-1,n-1} & \Xi_{i,n-1} & \Xi_{N,n-1} \\ \Xi_{1,n} & \Xi_{i-1,n} & \Xi_{i,n} & \Xi_{N,n} \end{bmatrix} \quad (8)$$

2.3. Hypothesis for exergy destruction minimization in the crude oil atmospheric distillation column

It is interesting to mention three observations when the array (8) in the section 2.2.3 is analyzed:

Intuitively, it is clear that the amount of exergy destroyed is increasing from the top to the bottom of the column because the number of components is increasing and the temperature gap between trays is also increasing.

The bottom left coefficients correspond to heavy species in the upper part of the column. These coefficients are insignificant or non-existent.

The top right coefficients correspond to light species that are located in the bottom part of the column. These species are not negligible since all the crude is fed to this zone and they have to cross the whole column till the corresponding tray of extraction. Remembering that these species are already partially or totally vaporized before the crude enters the furnace, one may express the following conjecture:

If these light species are separated before the vaporizer by an adiabatic flash, for example, and sent directly to the column, their contribution to the exergy destruction in the bottom of the column will be insignificant. These species have to be fed to the tray having the same temperature as the flash.

With a single flash, a new scheme of the simplified process is then that of Fig. 4. It is designated below as "Improved process".

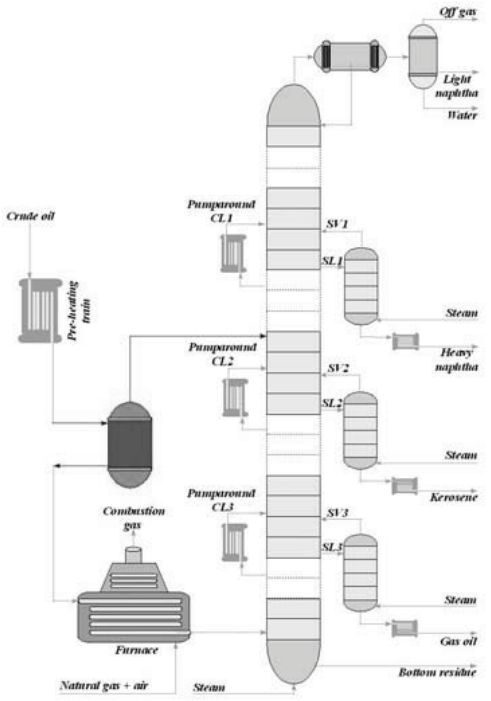

Fig. 4. Improved multi-component distillation process.

The exergy destruction array of this process is represented in equation (9):

$$\|\Xi\| = \begin{bmatrix} \Xi_{1,1} & \Xi_{1,2} & & & \Xi_{1,j+1} & & \Xi_{1,n-1} & \Xi_{1,n} \\ \Xi_{2,1} & \Xi_{2,2} & & & \Xi_{2,j+1} & & \Xi_{2,n-1} & \Xi_{2,n} \\ & & & & & & & \\ \Xi_{i-1,1} & \Xi_{i-1,2} & & & \Xi_{i-1,j+1} & & \Xi_{i-1,n-1} & \Xi_{i-1,n} \\ \Xi_{i,1} & \Xi_{i,2} & & & \Xi_{i,j+1} & & \Xi_{i,n-1} & \Xi_{i,n} \\ & & & & & & & \\ \Xi_{N-1,1} & \Xi_{N-1,2} & & & \Xi_{N-1,j+1} & & \Xi_{N-1,n-1} & \Xi_{N-1,n} \\ \Xi_{N,1} & \Xi_{N,2} & & & \Xi_{N,j+1} & & \Xi_{N,n-1} & \Xi_{N,n} \end{bmatrix} \quad \begin{matrix} \Xi_{2,1} & 0 & 0 & 0 & 0 & 0 \\ \Xi_{2,2} & 0 & 0 & 0 & 0 & 0 \\ & 0 & 0 & & & 0 \\ & 0 & & 0 & & 0 \\ & 0 & & & 0 & 0 \\ \Xi_{2,j+1} & 0 & 0 & 0 & 0 & 0 \\ & & & & & \\ \Xi_{N-1,j+1} & & & & & \Xi_{N-1,J+1} \\ \Xi_{N,j+1} & & & & & \Xi_{N,J+1} \\ & & & & & \\ \Xi_{N-1,n-1} & & & & & \Xi_{N-1,n-1} \\ \Xi_{N-1,n} & & & & & \Xi_{N,n} \end{matrix} \tag{9}$$

3. Application

3.1. Process data and conditions

In the simplified process described in Fig.1 in section 2.1., a flux of 21000 tonsm/day is fed from the oil holding tank at 15 °C and 1 atm. It is preheated to 250 °C in one heat exchanger representing the complete pre-heating train and then fed to the furnace where heat is obtained by fuel combustion. Finally it is fed at 358 °C to the bottom of a 30 tray column provided with a condenser, three pumparounds and three strippers. The final products are: Sour gas, water, light and heavy naphtha, kerosene, gas oil and bottom residue.

3.2. Process simulation

PRO/II from SIMSCI (3) was used to perform the simulation of this process. The Arabic light and heavy fuels characterization is based on their True Boiling Point, Fig. 5, and their specific gravity versus temperature curves (4).

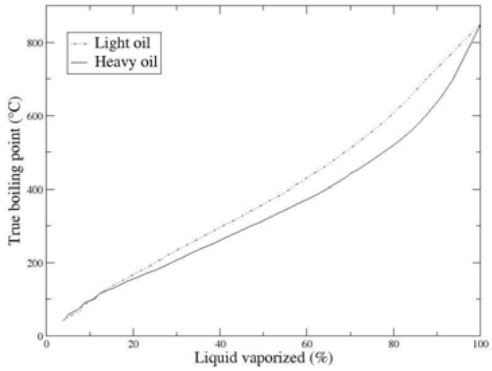

Fig.5. True boiling point of light and heavy crude oil characterization curves.

Raking end products are defined as oil cuts and their characterization is shown in Fig. 6 where their ASTM D80 temperature versus their ideal boiling point curves are plotted.

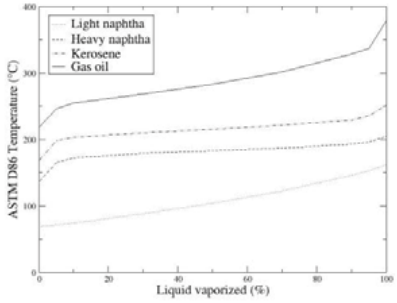

Fig. 6. ASTM D80 temperature versus ideal boiling point of oil cuts.

The Grayson Streed equation of state (5) is commonly used to evaluate thermodynamic properties of oil distillation but Braun K10 can provide good results too. Moreover, a recent study (4) shows insignificant differences between both equations of state in this kind of processes.

In order to maintain the same operating conditions throughout the column in the improved process, the heat condenser and the column temperature profile are maintained identical to those of the classical process and pumparound flows are decreased (Fig. 7 and Table 1).

3.3. Results

The exergy analysis is calculated for both simple and improved processes and their performances are compared in terms of mass and energy.

In the classical process, and beside the top condenser, the column is cooled by sending a part of it is internal liquid reflux to the pre-heating train in order to lower its return temperature. In the improved process, this operation is largely replaced by the already cool vapors carried directly inside the column from the flash.

To make sure that temperature profiles of the column are kept similar, Fig. 7, and that the heat recovery from the condenser and the temperature in the top of the column are equal to those in the improved process, the pumparound flows are adjusted as shown in Table 1.

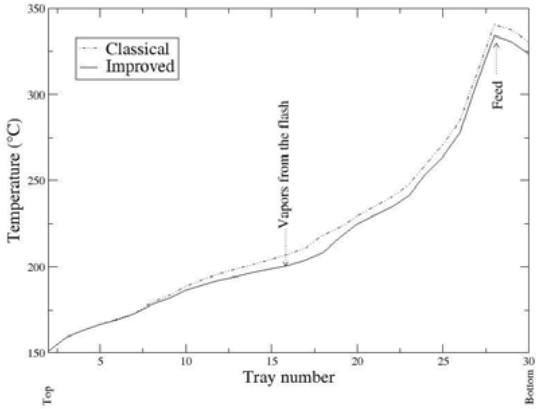

Fig. 7. Temperature profiles of the column in classical and improved process.

Table 1. Input operating data for classical and improved processes.

	Classical process	Improved process
Q Condenser (MW)	20.5	20.5
T. Condenser (°C)	151	151
Pumparound 1 (T/hr)	380	260
Pumparound 2 (T/hr)	400	270
Pumparound 3 (T/hr)	345	270

As a result, the comparison of racking end products flows shows no significant difference, Table 2, but the energy consumption in the furnace is decreased from 73.5 MW to 58.1 MW that is almost 21% of the initial consumption.

Table 2. Racking end products in classical and improved processes.

Products (Tonsm/day)	Classical process	Improved Process	Gap (%)
Light naphtha	3315	3321	0.2
Heavy naphtha	1264	1280	1.3
Kerosene	870	839	-4.3
Gas oil	3516	3497	-0.5
Residue	12081	12224	+1.1
Column feed	21000	17955	-14.5

Figures 8 and 9 show the exergy destructions in the four units of both classical and improved processes. They remain equal for the pre-heater and the condenser since one of the specifications is dictated to maintain the same amount of heat exchange in these two units. Half of these destructions is located in the furnace.

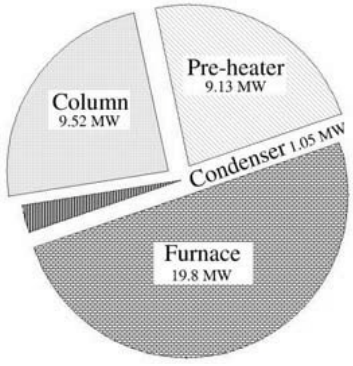

Fig.8. The exergy destruction in a classical crude oil distillation process.

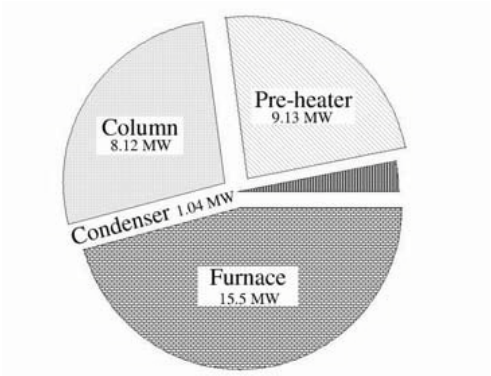

Fig. 9. Exergy destruction in the improved process.

The total exergy destruction, Fig. 10, is decreased by 14.5% from 40 MW in the classical process to 33.8 MW in the improved one. The best improvement is achieved in the furnace and it is about 4.5 MW or up to 21% of the exergy destroyed in this unit. It is followed by the distillation column with 1.4 MW or 14.5%.

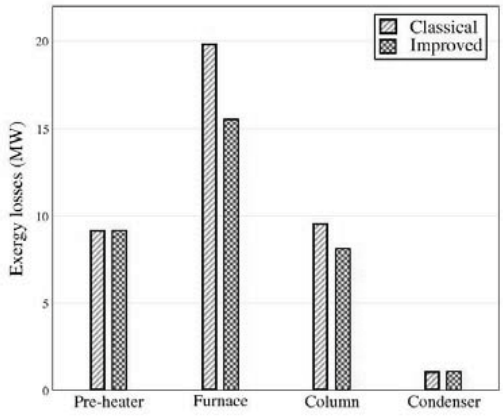

Fig.10. Comparison of the exergy destruction between classical and improved crude oil distillation processes.

4. Conclusions

An improved process for crude oil atmospheric distillation is proposed in this paper. It is based on the observation that light species are continuously vaporized in the pre-heating train, unnecessarily overheated in the furnace and then fed to the bottom of the distillation column.

The conjecture, expressed here, states that these lights have to be separated in the pre-heating train previous to the furnace by the installation of adiabatic flashes and to be fed directly to the column. The tray having the same temperature as the flash is a suitable position to feed these lights to the column.

This process was simulated and compared to the classical one. The temperature profile was kept similar in both processes by lowering the pumparound flows and maintaining the same heat recovery in the condenser and the same temperature profile in the column.

The amount of the end products is approximately the same while the exergy destruction is decreased by up to 14% in the whole process and by more than 21% in the furnace.

This improvement is combined with a reduction of up to 20% of fossil fuel consumption and green house gas.

In a more detailed paper, a complete comparison between these two processes will be performed. It will include the whole pre-heating train where end products are conditioned and pumparounds are cooled. Grassmann diagrams (6) and enthalpy versus temperature curves (7) will graphically demonstrate the improvement. The performances of two processes fed respectively with light and heavy oil will be compared as well.

References

[1] Charles D. Holland, 1981, Fundamentals of Multi-Component Distillation, McGraw Hill Book Company.

[2] Dr. Y. Demirel, 2004, Thermodynamic Analysis of Separation Systems, Chemical and Bimolecular Engineering Research and Publications, pp. 3896–3942.

[3] SIMSCI-ESSCOR, Process Engineering Suite, URL: www.scimci.com

[4] Dr. Jungho Cho, 2001, Crude Distillation Unit Simulation Using PRO/II with Provision for FPCC, URL: www.cheric.org/ippage/e/ipdata /2001/14/file/e200114-12.ppt.

[5] John E. Edwards, Process Modeling Selection of Thermodynamic Methods, URL:http://www. chemstations.com/content/documents/ TechnicalArticles/thermo.pdf.

[6] Masaru Ishida and Ruchira Taprap, 1996, Graphic Exergy Analysis of Processes in Distillation Column by Energy Utilization Diagrams, AIChE Journal 42, pp. 1633–1641.

[7] Linnhoff March, 1998, A Guide to Pinch Technology: Introduction to Pinch Technology, Linnhoff March, UK.

Control and Modelling of Multi-source Renewable Energy Systems

S.H.Lee[a] , S.M.Begg[b] and R.J.Howlett[c]

[a] Centre for SMART Systems, School of Environment and Technology, University of Brighton, Cockcroft Building, BN2 4GJ, U.K

[b] Sir Harry Ricardo Laboratories, School of Environment and Technology, University of Brighton, Cockcroft Building, BN2 4GJ, U.K.

[c] Bournemouth University, U.K.

Abstract: A primary aim in power and energy research is centred upon improving efficiency whilst reducing carbon emissions developed by the conventional generation of electricity from fossil fuels. Furthermore, future legislation will increasingly require that alternative methods of supplementing power generation by renewable means are implemented. In the UK, as in much of Europe, the Department for Energy and Climate Change's policies are central to delivering 20% of the total energy demand from renewable sources by 2020. It is proposed to take the micro-generation combined heat and power (micro-CHP) concept of generating power near to the point of use a stage further, by combining micro-CHP with several other low-carbon-impact energy generation mechanisms to provide space heating and domestic hot water. However, these systems are dependent on local weather conditions and therefore conventional gas and electricity, an internal combustion engine and generator, battery or other, renewable energy sources, will be required to cope with any shortfall in supply. In such multi-source, local energy generation systems, it is important to understand the flow of energy and how that can be used to achieve optimum efficiency from each of the components and performance of the system as a whole. In this study, an Intelligent Energy Management System (IEMS) approach, based upon artificial neural networks, was proposed to capture the characteristics of the energy flow. A simulation model was devised in the Simulink environment that takes into account the dynamic performance of the system as well as the individual components of a domestic type micro-CHP system over a long time period. Training data, such as local weather station information, was used to formulate algorithms for the most efficient combination of energy sources and the optimum control and scheduling for a given application and environmental condition. The model advisor was then used to optimise the system in a predictive manner. Finally, the study demonstrated the benefits of managing the use of energy, from multiple, modular, renewable and sustainable energy sources, by means of an intelligent systems approach. Future work is concentrating on the establishment of a Neuro-fuzzy paradigm for adaptive, fast, accurate and optimised energy management system.

Keywords: Intelligent systems, CHP, Hybrid energy management, Simulation.

1. Introduction

Most electricity is generated from fossil fuel resources causing large quantities of CO_2 to be released into the atmosphere that has a detrimental impact upon our environment. Around one third of the UK's CO_2 emissions are generated by households. Carbon emissions from conventional fossil fuel electricity generation are increased significantly by the inefficiency of the generation process. Centralised electricity generation incurs significant energy wastage due to losses during the transmission of power. Local electricity generation is possible using photovoltaic panels, and small roof-mounted wind turbines. However, they are not reliable, being dependent on weather conditions.

Micro-Combined Heat and Power (Micro-CHP) is the use of a heat engine or a thermal power unit to simultaneously generate both electrical power and useful heat. Novel low-cost systems that generate power locally and also achieve increased efficiency by the use of "waste" heat for water and space heating can produce a considerable reduction in fuel use, resulting in an appreciable reduction in CO_2 emissions. The combined systems generate electricity from the power of the wind and sun. The average annual amount of CO_2 emissions is reduced significantly, contributing to the UK Government's energy goals; a reduction in

Corresponding Author: Shaun Lee, Email: s.h.lee@brighton.ac.uk

the CO_2 emissions by 60% by 2050 [1]. Governments in the UK, the EU and the rest of the world, are striving to increase the proportion of energy that is produced through CHP by incorporating renewable energy sources. The EU target is 20% electricity from renewable energy by 2020 [2]. At present, industries and households are not prepared to invest in these systems because the benefits are not yet apparent. However, the UK government will implement a feed-in-tariff in April 2010, in line with other EU countries. This will mean that homeowners can earn money from generating their own electricity. However, the pay-back time for a typical investment could still be nearer to 10 years [3].

It has been proposed to take the micro-generation CHP concept of generating power near to the point of use a stage further, by combining several other low-carbon-impact energy generation mechanisms to provide space heating and domestic hot water. During times when sunlight is intense, electricity and hot water can be generated by photovoltaic and solar water panels. At times of appreciable wind speed, electricity can be generated by a wind turbine. At times of low solar gain, low wind, or when demand is high, the micro-generation CHP system will be called into play.

The aim of this project was to develop a demonstrator software package that could model micro-generation CHP systems that incorporate a range of renewable and sustainable energy sources. The project involved an investigation into the mathematical simulation of poly-generation CHP systems, where photovoltaic, wind turbine, and solar panel energy sources are supplemented by a micro-generation CHP system. The package could enable the most efficient combination of energy sources to be devised, and the optimum control and scheduling algorithms to be developed. Significant savings could be achieved both in terms of running costs and the reduction of carbon dioxide emissions.

2. Background

The Smart Systems research group at the University of Brighton have a broad range of electronics and software expertise. Their research focuses on the development of practical, applied systems exploiting the power of applied artificial intelligence. Research areas include; condition monitoring, data analysis, fault diagnosis, intelligent control, web-based systems and innovative magnetic materials, which are applied to industrial and commercial problems. The group is currently developing simulation model for multi-source, renewable energy systems including optimal control and scheduling algorithms for hybrid energy systems.

In this study, several types of renewable energy sources were considered that contribute to the overall sustainability of a system and the ability to reduce its environmental impact. The intelligent energy management system was used to determine and optimise the amount of power needed to satisfy the demand and manage the quantity input to storage. Consideration of the system status, (e.g. desired temperature) and predicted demands, (based upon prior history) were matched to the current operating conditions. If the storage (battery) needed to be charged, for example, 'negative' power was assigned; the energy from one (or a combination) of CHP, photovoltaic and wind-turbine sources would provide enough power to satisfy the demands and at the same time charge up the storage. During the course of the development, a number of renewable energy sources were investigated, such as photovoltaic panels, hot water storage and battery banks. These were considered in the form of building blocks. Transient energy transfers between the blocks were examined. The variation of ambient air temperature and solar radiation, over a period of time, was included in the analyses. An intelligent control strategy and scheduling algorithm was developed; such schemes are considered pivotal in achieving the move towards hybrid local-generation systems. Such highly efficient intelligent energy controllers could substantially benefit the micro-CHP companies, system designers and integrators, components manufacturers and their clients.

3. Framework for Modelling and Simulations

The Simulink Modelling Environment in the Matlab software package, provided by Mathworks, was chosen for this project. The package has a wide selection of dynamic systems for modelling, analysis and simulation. It offers a user interface for creating block diagram models. An example of the hot water block diagram model is shown in Figure 1. A system can be constructed from a

number of configurable blocks taken from a library of standard or custom components. During the course of the simulation, algorithms and parameters can be changed to fine tune 'intuitive' results. The user has a readily accessible tool for simulating many of the operational problems found in the real world.

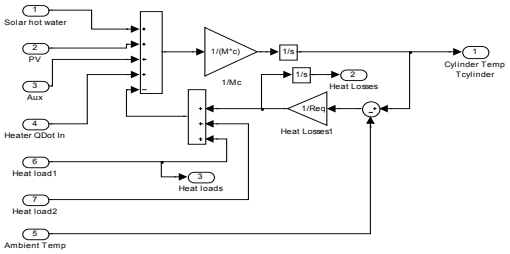

Figure 1: Graphical Simulink representation of the hot water storage block

4. Modelling the Hybrid Energy System

The thermal energy generation and storage strategies were devised based upon first order thermodynamic models. Figure 2 shows an overview of the IEMS simulation model, together with the key energy components presented as subsystems. These can be summarised as follows:

- Solar thermal hot water system
- Photovoltaic panel
- Battery system
- Wind turbine
- Heat and power controller

Each of these energy components has been mathematically represented and their performance was evaluated using the principles of conservation (thermodynamic and electrical) with a step time short enough to capture the plant dynamics.

A set of subsystems was devised at the same time to analyse available weather data. Each model accessed a database of historical, ambient air temperature, wind speed and direction and solar radiation. Parameters for each energy source, such as maximum output, efficiency, cost and operational constraints that influenced the plant output were considered. The results were written back to the database and represented in a graphical format. The results of the simulation can be made accessible to other models for further processing.

Initially, the wind turbine and solar panel models were created using a simple linear correlation. This was improved as further knowledge of the underlying technology was added, such as manufacturer data relating to system dynamics, historical wind strength measurements and real-world electrical wind production data. A data file was used to store all system data and constants.

The wind turbine subsystem is illustrated in Figure 3. . The model was constructed in such a way that operating parameters could be changed easily and directly before or during the simulation. This not only facilitated real-time testing of a particular design idea but also provided an improved understanding of the interaction between components in energy system.

5. Controller

The system exhibited strong non-linear and discontinuous behaviour. The sequence control of the start-up procedure ran through several states in which heat and power flowed through the system; for example, the interactions taking place between the diesel-generator set and the battery bank.

Given the complexity of the electrical and the hot water systems, a decision was taken to develop these controller in stages, focusing on the individual subsystems and then merging them using essential control elements. The control system included three functional groups, namely:

- Status machine
- Closed-loop controls
- Open-loop controls

The electrical and thermal subsystem operated in many different states. The operating state was determined by the nature of the energy flow (either in or out of the system), by load conditions, and by the operating mode such as timed, adaptive or automatic. Figures 4 and 5 show the thermal (temperature driven) and electrical power controller subsystems, respectively.

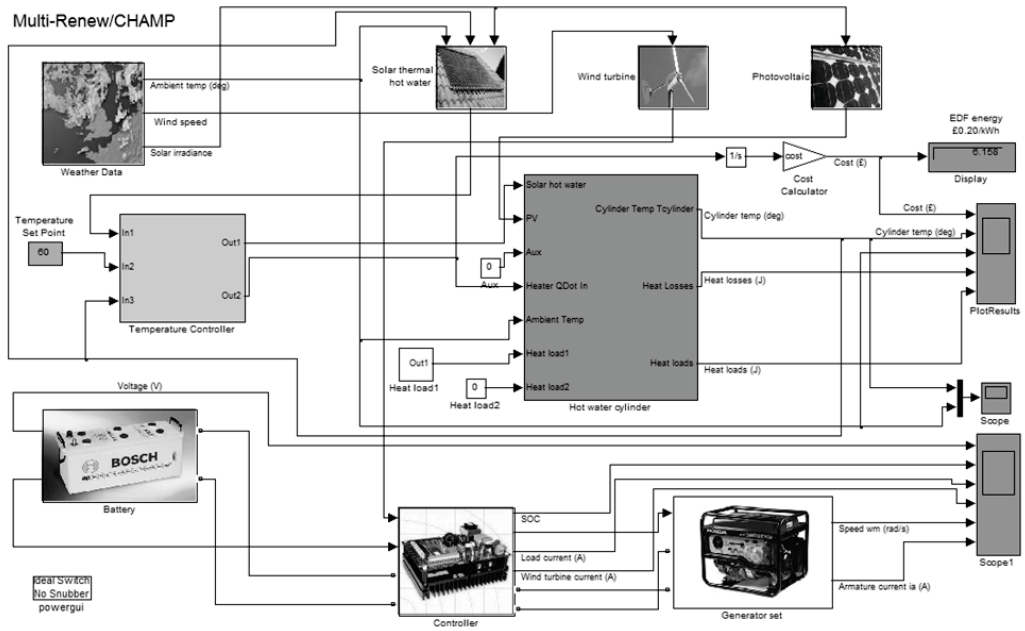

Figure 2: An overview of the Intelligent Energy Management System (IEMS) simulation model

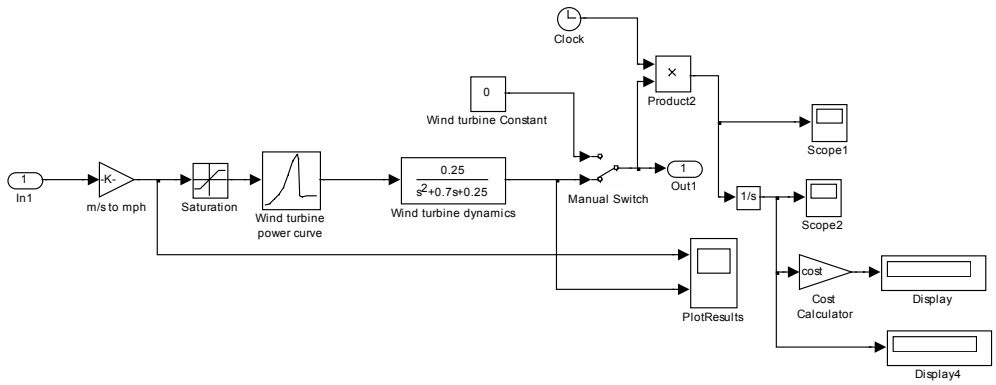

Figure 3: Wind turbine subsystem

Since the system exhibits a pronounced non-linear behaviour, classical PID controllers are not suitable. Therefore, in the future, a Neuro-fuzzy controller is likely to be implemented to resolve some of the practical tuning requirements.

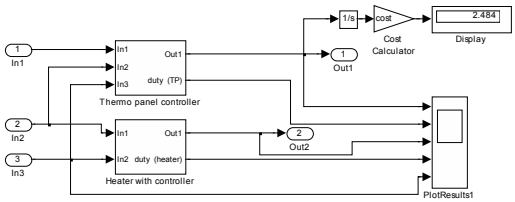

Figure 4: Temperature controller subsystem

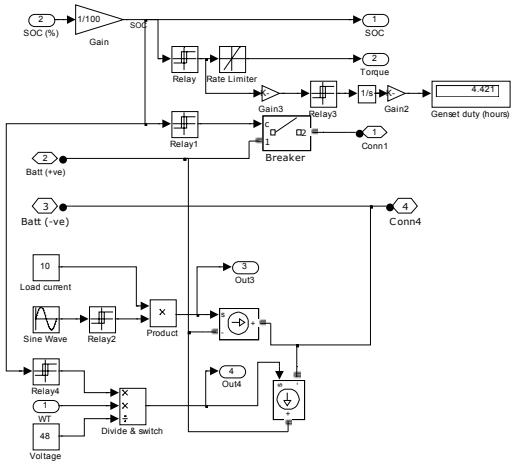

Figure 5: Power controller subsystem

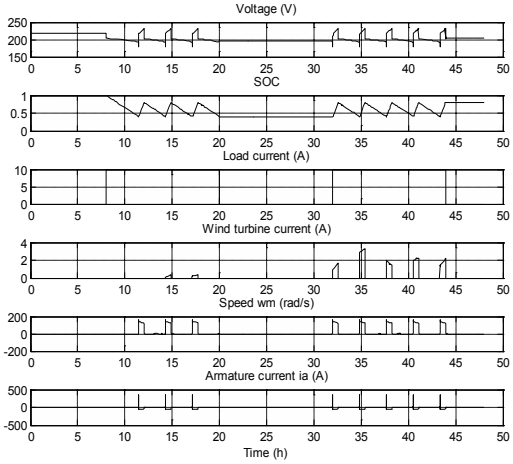

Figure 7: Electrical energy simulation results

6. Simulation Results

After building and installing the pre-executable programme on the system, testing the software and its controller was initiated by running a batch file. The simulation time was initially set for 2 days. The software routine automatically computed each parameters in a given time step of 1 second, and then stored the result in a file which could be used for off-line analysis.

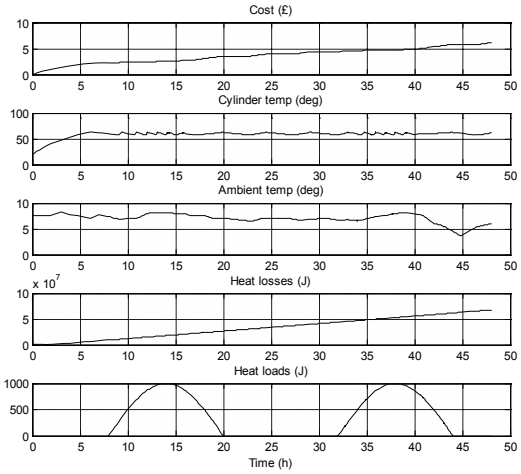

Figure 6: Thermal energy simulation results

The results of a typical simulation are shown in Figures 6 and 7 for the thermal and electrical model responses respectively. Monitored parameters include, for example water cylinder temperature and battery 'State-of-Charge' (SOC), and operating status.

7. Conclusions and Future Work

Greater use of renewable energy systems is a key-driver influencing the strategies of energy companies, builders of the housing stock, offices and factory units. Planning of optimal combinations of multiple energy sources and devising optimal control and scheduling algorithms, as can be accomplished with the IEMS package, will be pivotal in achieving the move towards hybrid local-generation systems. However, the design, control and optimisation of such a system can be very complex.

This study reviewed the most relevant developments in the design, simulation, control and optimisation of hybrid systems. A typical energy system, consisting of a photovoltaic generator, wind turbine and/or Diesel generator with energy storage in lead-acid batteries was investigated. Design and simulation tools were developed. The system dynamics, simulation, and the design of the controller were taken into consideration. A system based in Simulink was used to determine its sensitivity and response to varying inputs. The simulation results demonstrated how efficiently the power and

temperature were controlled under highly varying conditions.

The application of intelligent techniques to energy systems has become a realistic research proposition. Previous work by the authors has demonstrated the effectiveness of a Neuro-fuzzy system applied in control and modelling of non-linear systems [e.g. 10]. The optimal energy control parameters of the IEMS controller can be determined by using intelligent methodologies. Further test and evaluation will be performed to validate its adaptation between different weather conditions and load changes. The optimal intelligent controller should be inexpensive to set up and computationally efficient. This technique is likely to be highly beneficial in future hybrid energy systems design.

References

[1] Meeting the Energy Challenge, A White Paper on Energy 2007, Department of Trade and Industry, UK

[2] The EU's Target for Renewable Energy, 27th Report Session 2007-08 Volume 1 Report, Authority of the House of Lords, London.

[3] Draisey, I., 2009, Solar's dividend for homeowners, Dulas Engineering, UK.

[4] Jose, L., Bernal-Agustin and Rodolfo, D., Simulation and optimization of stand-alone hybrid renewable energy systems, Journal of Renewable and Sustainable Energy Reviews 13 (2009), pp.2111-2118.

[5] Muselli, M., Notton, G. and Louche, A., 1999, Design of hybrid-photovoltaic power generator with optimization of energy management. Journal of Solar Energy, 65(3), pp. 130-157.

[6] Deshmukh, M.K. and Deshmukh, S.S., 2008, Modeling of hybrid renewable energy systems, Journal of Renewable and Sustainable Energy Reviews, 12, pp. 235–249.

[7] Tremblay, O., Dessaint, L.-A. And Dekkiche, A.-I., 2007, A Generic Battery Model for the Dynamic Simulation of Hybrid Electric Vehicles, Vehicle Power and Propulsion Conference, 2007. VPPC 2007. IEEE 9-12, pp. 284-289.

[8] Shepherd, C. M., 1965, Design of Primary and Secondary Cells - Part 2. An equation describing battery discharge, Journal of Electrochemical Society, Volume 112, pp. 657-664.

[9] White, A., 2009, Thermodynamic analysis of the reverse Joule–Brayton cycle heat pump for domestic heating, Journal of Applied Energy 86, pp. 2443–2450.

[10] Lee, S.H., et al., 2007, Fuzzy logic and neuro-fuzzy modelling of diesel spray penetration: a comparative study. Journal of Intelligent and Fuzzy Systems, 18 (1). pp. 43-56.

[11] Kalogirou, S.A., 2000, Applications of artificial neural-networks for energy systems, Journal of Apply Energy 67, pp.17–35.

[12] Jang, J., 1993, ANFIS: Adaptive network-based fuzzy inference systems, IEEE Transactions on Systems, Man, and Cybernetics 23, pp.665-685.

[13] Harris, C.J., et al., 1996, Advances in Neurofuzzy Algorithms for Real-time Modelling and Control, Engineering Applications of Artificial Intelligence, Vol.9, Issue 1, pp.1-16.

[14] CIBSE guide, 2002, Weather, solar and illuminance data, The Chartered Institution of Building Services Engineers, London.

[15] HOMER (The Hybrid Optimization Model for Electric Renewables), URL: http://www.homerenergy.com/

[16] British Standard Document: Solar Thermal Test Methods, Part 2, 2006, BS EN 12975-2: 2006.

[17] Khan, M.J., and Iqbal, M.T., 2005, Dynamic modeling and simulation of a small wind–fuel cell hybrid energy system, An International Journal Renewable Energy 30, pp. 421–439.

[18] Baring-Gould, I., 1998, The Hybrid System Simulation Model: Hybrid 2, National Renewable Energy Laboratory, U.S. Department of Energy.

[19] Toyota Motor Corporation, Public Affair Division, Toyota Hybrid System THSII, 2009 URL: http://www2.toyota.co.jp/en/tech/environment/ths2/index.html.

[20] Solar domestic hot water systems, data sheet, Vaillant, UK.

[21] Makrides, G., et al., 2009, Temperature behaviour of different photovoltaic systems installed in Cyprus and Germany, Journal of Solar Energy Materials & Solar Cells 9, pp. 1095–1099.

[22] Krause et al., Analysis of Electric Machinery, pp. 89-92.

[23] Perez-Blanco, H., 2009, The Dynamics of Energy, CRC Press, London.

Acknowledgments: This work is co-funded by the European Union under the Interreg IVa Programme of the European Regional Development Fund. Project number 1880 – Low-Carbon Hybrid Advanced Motive Power - CHAMP.

Pinch Analysis of Time Dependent Processes in Yeast and Ethyl Alcohol Production Plant

Predrag Rašković[a], Aleksandar Anastasovski[b], and Svetislav Cvetković[a]

[a] *Faculty of Technology, University of Niš, Niš, Republic of Serbia*
[b] *Technical Faculty, International Balkan University, Skopje, Republic of Macedonia (FYROM)*

Abstract: Process integration study of yeast and ethyl alcohol plant is accomplished by heat recovery system for capturing and utilization of the waste heat. Heat recovery task is realized by Pinch Analysis for two different models, continuous and batch, depending of production scheduling. In the case of batch model pinch procedure employed the Time Slice Model approach which considers the heat recovery by direct heat exchange. Final design of heat recovery system are presented in the form of heat exchanger networks and evaluated by different economic criteria.

Keywords: Process integration, Pinch analysis, Yeast and ethyl alcohol plant.

1. Introduction

Technological trends toward the manufacture of specialty chemicals, growing requirement for high value biochemical products, and global emphasis on emissions reduction recently initiate the considerable attention on batch processing plants. Batch plants belong to the group of non-continuous (or discontinuous) processing plants, which operations and properties may vary, either in a discrete or a continuous manner over time. Generally, non-continuous processes involving batch processing operations (characterized by a processing time) and semi continuous processing operations (characterized a processing rate).

From engineering point of view the increased popularity of batch plants is mainly caused due to their higher flexibility and adaptability. Flexibility is recognizing as unique feature to accomplish several operations within the only one process unit. Adaptability enables the manufacture under regime with low capacities, complex reaction paths and seasonal demands.

Today about 50% of chemical plants worldwide are batch processing plants [1]. Batch plants are mostly suited in food processing, biotechnology, pharmaceutical and in all other industry where efficient continuous mode of operation is not feasible or economically impractical.

During the last few decades, the number of studies concerning the energy saving in batch plants has been less presented in the literature than studies of continuous plants. In the comprehensive review about heat exchanger network synthesis in 20th century [2] only 5 % of the paper investigated the batch processes.

Such situation can be explained by a few reasons. Batch plants are usually energy non-intensive with small share of energy costs (about 5-10% in total production costs [3]), and since that with small opportunities for sizeable energy savings. Next, a wider range of conditions in batch processes, adjusted the new, more rigorous, process models which lead to extra complexity in the design and operation of the plant. However, recently some authors have reported respectable energy savings [4,5] and CO_2 reduction possibilities [6] in detailed case studies.

Study presented in this paper is the part of comprehensive energy project which considers the energy efficiency opportunities in the *Yeast* and *Ethyl Alcohol* (Y&EA) plant. Considering the technology limits of Y&EA production, it was found that capturing and utilization of the waste heat is the most promising option for energy savings. Research strategy was limited on *Process Integration* (PI) approach and the use of *Pinch Analysis* (PA), certainly the most widely used method for design of cost-optimal heat recovery system.

The first stage of research [7] was dedicated to detail descriptions of the processes, physical and mathematical models of the process units/ subsystems and flow-sheet simulations of the plant. In that stage of research, heat recovery task considered only the process streams which operate in continuous mode. The results defined a process

Corresponding Author: Predrag Rašković, Email: pr.raskovic@sezampro.rs

streams set which enable the design of heat recovery system for significant energy savings.

In this paper heat recovery task is upgrade on two ways. First, the set of process stream suitable for heat recovery task involved two new sours streams; also additional increase of heat recovery is enabled by different target temperature of other source streams. Second, task is extended to the full period of the production, and as a consequence mode of plant operation was changed from continuous to batch.

These changes enable the definition of two new research models, continuous and batch model, in which the time-varying operations are accommodated by *Time Slice Model* (TSM) and direct heat exchange approach.

The results of the study are presented in the form of *Heat Exchanger Networks* (HENs) and evaluated by some of economic criteria.

2. Process design and heat integration of batch plants

Design task of batch plants, concerning the efficient use of energy and material in production practice, is commonly addressed to the problems of scheduling and heat integration.

Scheduling of batch plant [8] involves the optimal determination of the order and detailed timing of different process operation. These operations can be carried out on the different or the same process units. According to the time horizon scheduling of batch plant can be classified on *short-term scheduling*, which spans a horizon of few days; and *planning* which horizon extends to few months or a year. Short-term scheduling define the detailed operating conditions and disturbing events in plant operation, while planning involves consideration of financial and business decisions over extended periods.

Heat Integration (HI) is a part of PI which deals with global allocation, generation, and exchange of energy, throughout the process [9]. The objective of heat integration is maximum energy savings which can be obtained by design of HEN. This objective can be achieved on direct or indirect way, considering the heat exchange between process streams.

Direct heat integration is encountered when both, sink and source process streams, are active over a common time interval, while indirect heat integration allows heat exchange between process streams regardless of the time interval (but only in the period when source stream takes place before the sink stream). Direct heat integration enables the use of HENs for heat recovery task. Result of indirect integration is the surplus energy which can be stored in *Heat Storage System* for later use. In practice *indirect heat integration* implies higher capital costs, and very often process of *rescheduling* is considered to increase the potential of direct heat exchanges.

The methodologies for optimal design of batch plants are performing by *simultaneous* and *sequential* approach [10]. The simultaneous approach is characterized by integrated mathematical model comprising of scheduling and heat integration and solving simultaneously for maximum economic benefit. [11,12]. In the sequential approach problem is first decomposed; next the scheduling part is determined by mathematical modeling and optimization; on the end the HI task is solved, either by mathematical methods or by PA as unique conceptual approach.

Mathematical methods for HI are effective in the case of large-scale systems with complex constraints and additional considerations, like scheduling, multi-product plant, etc. Main disadvantage of these methods lies in the small opportunities for interactive work during the design of heat recovery network. It should be noted that these method are used in the first paper addressing HI for batch processes [13].

2.1. Pinch analysis of batch processes

In the last few decades PA has been widely accepted as the most effective heat integration tool. Generally speaking, PA in the framework of batch processes (in the following text *Batch Pinch Analysis*-BPA) is based on the pinch concept for continuous plants [14], which had been modified in order to accommodate the time-varying operation.

The early BPA methods were based on pseudo continuous approach, which considered the temperature as primary, and time as secondary constrain. Model proposed by *Clayton* [15], *Time Average Model* – TAM, ignored the time schedule and assumed that heating or cooling of the streams took place in the entire batch period. In practice, this model does not fit with real behavior of batch production, and its final accomplishment is only to indicate the absolute maximum heat recovery that

can be obtained, if all time constraints were removed.

The first appropriate time-dependent model for BPA, with fixed production scheduling, was proposed by *Kemp* and *Macdonald* [16], and named as the *Time Slice Model* – TSM. The entire batch period is divided into "time intervals" analogous to the "temperature intervals" in conventional problem table analysis. Time intervals are identified by start and finish times for all process streams involved in heating or cooling. Finally heat recovery options are investigated separately for each slice.

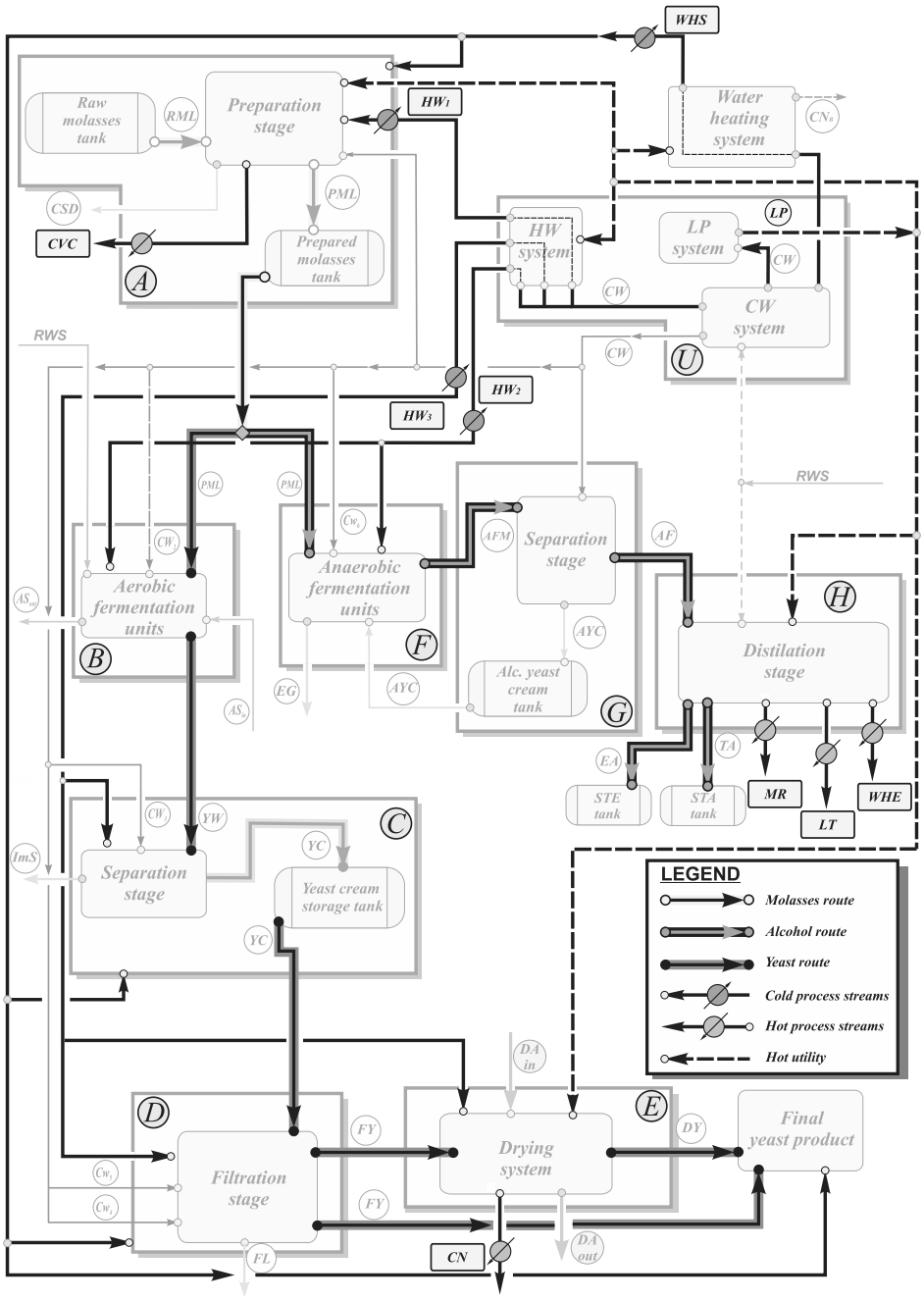

Fig. 1. Mapping of flowing and heat recovery streams in the physical model of Y&EA plant.

Two years later, TSM model is upgraded [17,18] by *Time Dependent Heat Cascade Analysis* (TDHCA) Tabular methods is used to calculate the energy targets and to identify the heat storage, direct heat exchange and rescheduling opportunities. Another upgrade, graphical diagram so-called *Batch Utility Curves* [19], used the idea of the *Total Site Sink/Source Profiles* to consider the indirect heat exchange through heat storage systems.

In 1995 *Wang* and *Smith* [20] initiate the *Time Pinch Analysis* (TPA), a new approach for heat integration of batch processes. In TPA approach the role of temperature and time are reversed. Heat duties, as function of time, are presented in *Time Composite Curves* and *Time Grand Composite Curve* which are used to identify the heat recovery potential for both direct and indirect heat integration. Differently than TAM and TSL methods, TPA treats time as the primary and temperature as secondary constraint.

3. Heat recovery in yeast and ethyl alcohol plant

The Y&EA plant under study can be classified as multiproduct batch plant, which main products are fresh baker's yeast (1200 t/year in the active dry form and 6000 t/year in the compressed form) and ethyl alcohol–ethanol (5×106 m^3 of ethanol per year). Beside these two, there are also a wide range of by-products like: technical alcohol (mixture of ethanol, aldehydes and other less volatile components), wine and selenium yeast, baker`s additives, bee food, etc.

Physical model of the plant (Fig. 1) is presented in the form of inter-connected subsystems. Here, the subsystem comprises a set of process units which accomplish one of the technology operations. Production process is divided in three main routes.

First, *Molasses route* fulfill only one technology operation: preparation of feeding material (*subsystem A*). Second, *Yeast route* comprises the technology operations of: aerobic fermentation (*subsystem B*), centrifugal separation (*subsystem E*), filtration (*subsystem F*), drying (*subsystem G*) and yeast storage and packaging. Third, *Alcohol route* comprises: anaerobic fermentation (*subsystem H*), separation of alcoholic wort and yeast cream (*subsystem C*), distillation of alcoholic wort (*subsystem D*) and alcohol storage.

For the purpose of production, energy system of plant provides some utilities from *subsystem U*:

- Law pressure steam (LP) – saturated steam (p = 8 bar, T = 172.57 °C).
- Ice water, a solution of ethanol/water at temperature range between −2 °C and −4 °C.
- Cooling water, obtained from regional water supply system.

Streams that are considered as suitable candidates for heat recovery task are classified as:

- *Flowing streams*; sink/cold streams which are characterized by fixed and time-independent thermodynamic parameters, during the period of stream's existence. Flowing streams are:
  - Hot water streams HW_1, HW_2 and HW_3, used for process improvements, temperature regulation and washing purpose in subsystems A, B, C, D, E, and F. In the current practice these streams are provided by direct steam injection.
  - WHE stream used for space heating in the subsystem A, C, D and E.
- *Heat recovery streams*; sour/hot streams, characterized by considerable capacity for heat exchange, unalterable composition and "soft" target temperatures. In the current production practice these streams are discharged to the environment beside their great opportunity for heat recovery. Heat recovery streams are: molasses residues (MR), organic acid water solution known as Luter (LT), discharged cooling water from heat exchangers (WHE) and cooled volatile components (CVC).

Heat recovery task consider all streams as a part of semi-continuous operation e.g. heat exchange during the transfer between subsystems.

3.1. Pinch analysis of yeast and ethyl alcohol plant

Gantt chart of Y&EA production which corresponds to the physical model of the plant is presented on Fig. 2a. Process streams involved in PA are presented in the time event chart in Fig. 2b (parallel arrangement with Gant chart) and grid diagram (Fig. 2c). The entire batch period is divided in four time intervals, limited by starting and finishing time of the streams. Other necessary data are presented in the legend of Fig. 2. Position of the streams in time event chart initiated the research on two different models:

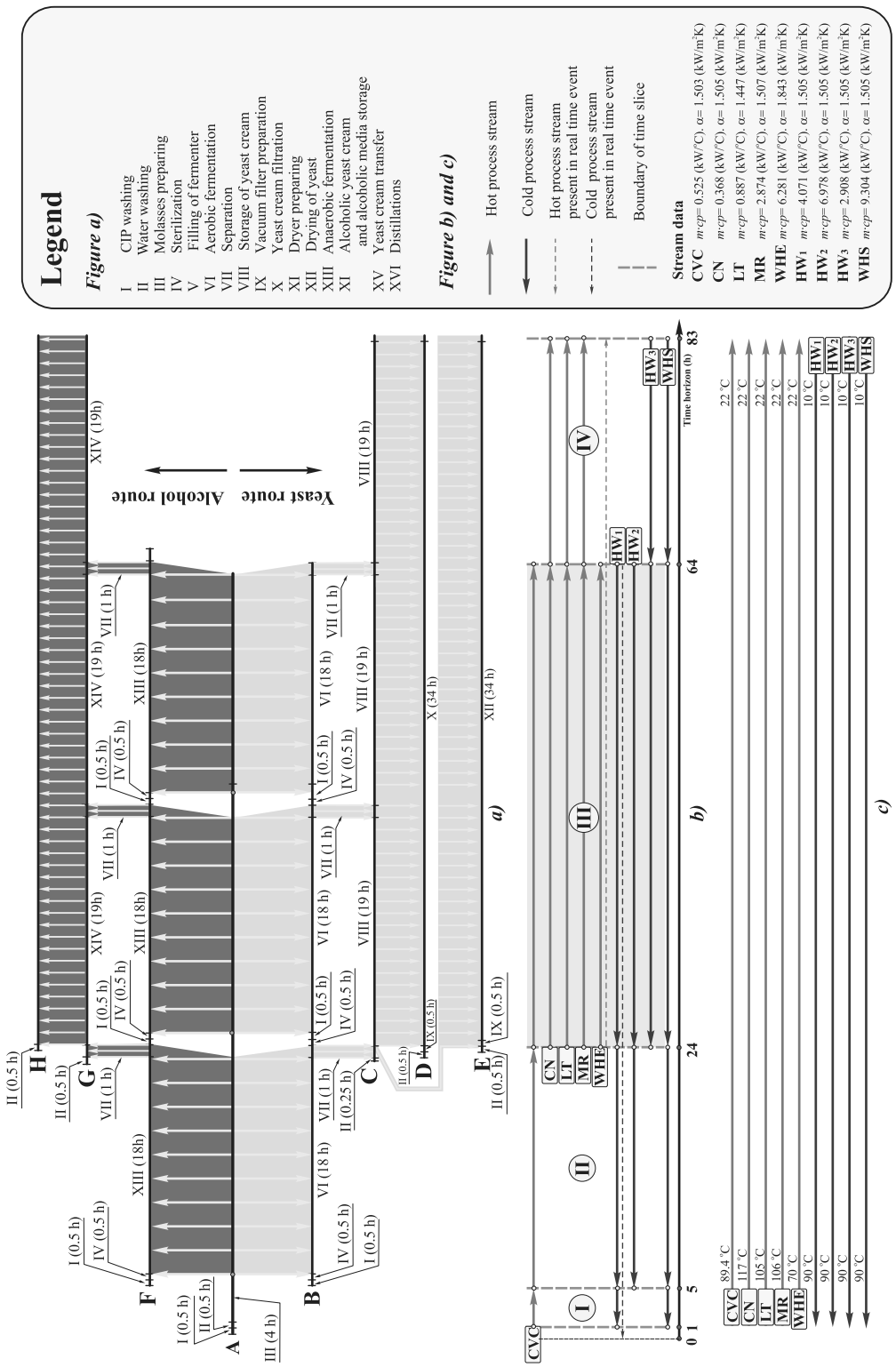

Fig. 2. a) Gantt chart of Y&EA production; b) Time event chart of process streams; c) Grid diagram of process streams.

- Continuous model, which considered parameters of process streams only in the time interval III. During this period (from 24 h to 64 h) the existence of all process streams creates the opportunity for continuous HENS problem.
- Batch model, which considered parameters of process streams during the full time of production (from 1 h to 83 h). In the case of this model, the TSM method is used for HENS task. Research was limited to the direct heat integration, with same ΔT_{min} for every time interval.

The operating cost (CO) for external heating is obtained by estimating the price of hot utilities at 6.38 $/GJ. Energy saving in models are expressed in the money value (CO_S) and calculated as a difference between:

- Operating cost without HEN (CO_{WOH}) – the cost of external heating when process stream (which are involved in pinch task) do not exchange the heat between them.
- Operating cost with the HEN (CO_{WH}) – cost of external heating when process streams exchange the heat by the heat recovery system.

Capital cost (CC) of HEN is calculated as in [7], while total cost of HEN (TC) present the sum of CO_{WH} and CC.

4. Results and discussion

The first results of PA are obtained in targeting phase. Energy and economic performance of both models were investigated in the range from ΔT_{min}= 12 °C (minimum allowable) to 20 °C. During the targeting, composite curves are moved in the position which indicates the threshold pinch problem for every predefined ΔT_{min}. This operation eliminates the need for additional cooling, since all heat recovery streams have a soft target temperature. Economic parameters on annual level are obtained estimating the manufacture with maximum number of production cycles per year– 90 cycles. This number of cycles corresponds to the operating period of about 7200 h for Batch model and 3600 h for Continuous model.

The results of targeting are presented in the Fig. 3. Lines in the graph connected the values of percentage difference between the economic parameters calculated for ΔT_{min}=12 °C and parameters calculated for other ΔT_{min} (from predefined range). Position of the curves identify ΔT_{min}=12 °C as a good starting point for design of cost-effective HEN in both models.

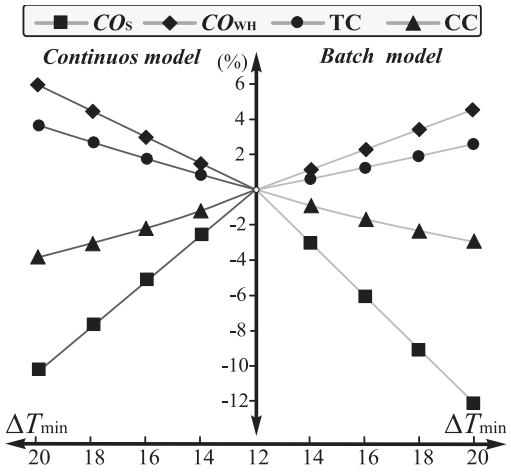

Fig. 3. Economic analysis of results obtained from targeting phase in pinch analysis.

Figure 4 and Fig. 5 shows initial and optimized design of HENs. In the case of Batch model initial network is established by combining the networks of all individual time intervals.

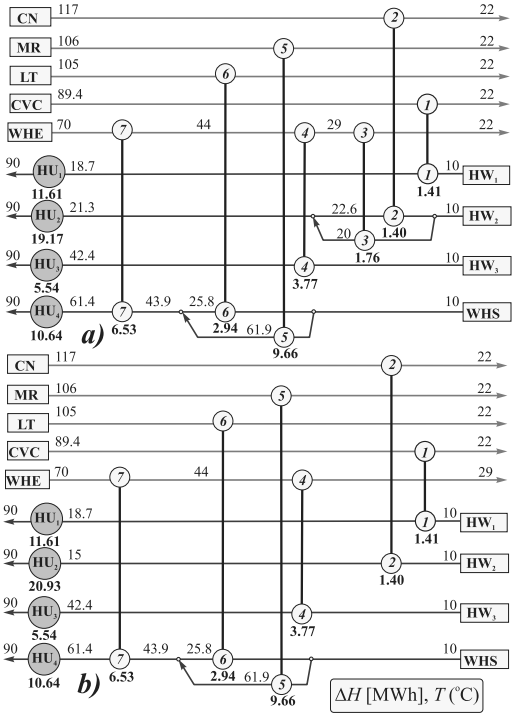

Fig. 4. Initial and optimized HENs; continuous model.

Networks optimization is done on two levels. First solutions are obtained by the conventional methods which utilized heat load loops and paths.

In the next level networks are additionally simplified by removing the two heat exchangers, with minimal heat load and transfer area (1 and 2 on the Fig. 4b and Fig. 5b). Beside a lot of interesting design solutions (which will be presented in the following papers) the results of optimization and simplifications did not made a significant improvements of HENs economic. Since that the following analysis will be focused on initial network solutions for batch and continuous models.

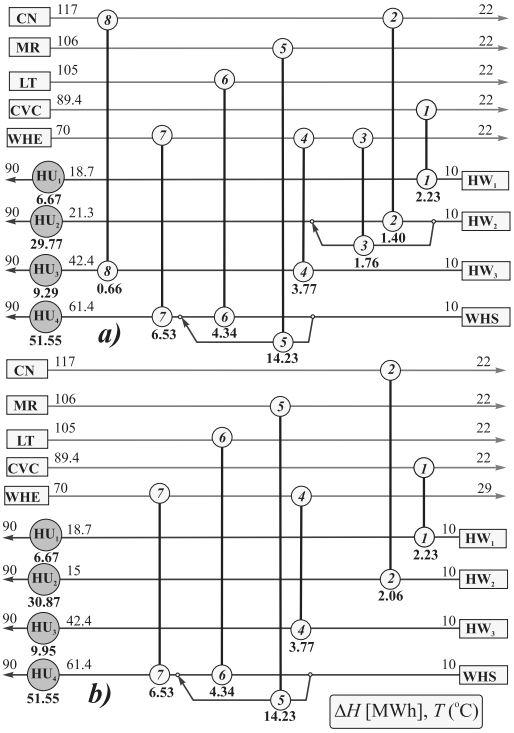

Fig. 5. Initial and optimized HENs; batch model.

The most important economic parameters of HENs are presented on Fig. 6. Values put in the upper part of the graph express the parameters obtained during the one production cycle. Values presented in the under part of the graph (also with positive sign) are obtained by dividing the corresponding parameters from upper part with the number of operating hours. According to the time event chart (Fig. 3b) operating time per cycle for continuous model is 40 hours and for batch model 82 hours.

Economic evaluation shows that batch model enables the 21 % more energy savings during the one production cycle. This savings are followed by small increase of capital cost (batch model is 6.7 % more expensive), and considerable difference in operating cost (batch model has about 51 % bigger CO). Finally, total cost of batch model is 42% higher for one production cycle.

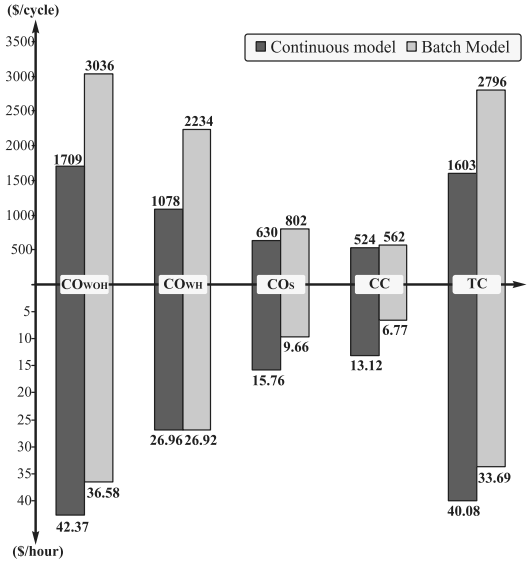

Fig. 6. Economic parameters of HENs for continuous and batch models.

In the case of analysis per operating hour continuous model has 38% higher energy savings and only 15 % higher total cost. Obviously the effectiveness of continuous model is quite better considering the time of its operation.

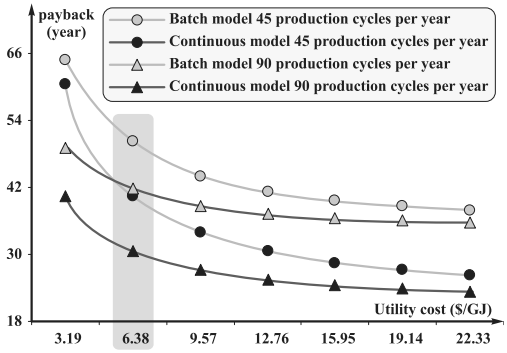

Fig. 7. Payback period of heat recovery systems in relation of estimated utility cost.

Such conclusion can be reviewed by calculation of payback period. Payback period, for adopted cost of hot utility (6.38 $/GJ) and maximum number of production cycles during the year (90), is almost 13 months shorter for continuous model. Similar

trends can be expected with different utility costs and different number of production cycles as it can be seen in Fig. 7.

5. Conclusion

Economic evaluation of HI solutions revealed the advantage of heat recovery system based on continuous model vs. batch model. The main reason for that lay in the chosen methodology for batch model – TSM by direct heat integration. On this way, batch model involved in the task time intervals where heat exchange between the process streams are not so intensive like in the third time interval, which correspond to the continuous model. This conclusion should be the right direction for future improvements based on rescheduling and indirect heat exchange opportunities.

REFERENCES

[1] Bieler, P.S., et al., 2004, Modeling the Energy Consumption of Chemical Batch Plants: Bottom-Up Approach, Ind. Eng. Chem. Res., 43, pp. 7785-7795.

[2] Furman, K.C., and Sahinidis, N.V., 2002, A critical review and annotated bibliography for heat exchanger network synthesis in the 20th Century, Ind. Eng. Chem. Res., 41(10), pp. 2335–2370.

[3] Vaklieva-Bancheva, N., et al., 1996, Heat Exchanger Network Design for Multipurpose Batch Plants, Comput. Chem. Eng., 20, pp. 989-1001.

[4] Ashton, G., 1993, *Design of Energy Efficient Batch Processes*, In Energy Efficiency in Process Technology, Pilavachi, P.A., Editor, Elsevier Applied Science, London.

[5] Krummenacher, P., et al., 2002, Diskontinuierlich Energie Sparen, ENET-News 2002, pp. 35-36.

[6] Rumazo, C.A., et al., 2000, Cleaner Production in the Chemical Industry, Water Sci. Technol., 42, pp. 1-7.

[7] Rašković, P., et al., 2010, Process Integration in Bioprocess Industry: Waste Heat Recovery in Yeast and Ethyl Alcohol Plant, Energy, 35(2), pp. 704-717.

[8] Floudas, C.A., and Lin, X., 2004, Continuous-time Versus Discrete-time Approaches for Scheduling of Chemical Processes, A Review. Comput. Chem. Eng., 28, pp. 2109.

[9] Dunn, R.F., and El-Halwagi, M.M., 2003, Process Integration Technology Review: Background and Applications in the Chemical Process Industry, J. Chem. Technol. Biotechnol., 78, pp. 1011-1021.

[10] Iskandar, H., and Rajagopalan, S., 2009, Sequential Methodology for Scheduling of Heat-Integrated Batch Plants, Ind. Eng. Chem. Res., 48, pp. 8551–8565.

[11] Majozi, T., 2006, Heat Integration of Multipurpose Batch Plants Using a Continuous-time Framework, Appl. Therm. Eng., 26, pp. 1369-1377.

[12] Adonyi, R., et al., 2003, Incorporating Heat Integration in Batch Process Scheduling, Appl. Therm. Eng., 23, pp. 1743-1762.

[13] Vaselenak J.A., et al., 1986, Heat Integration In Batch Processing, Ind. Eng. Chem. Process Des. Dev., 25, pp. 357–366.

[14] Linnhoff, B., 1982, *User Guide on Process Integration for the Efficient Use of Energy*, IchemE, Rugby, UK.

[15] Clayton, R.W., 1986, Report Nr RD 14/14, Technical Report, Harwell Laboratory, United Kingdom.

[16] Kemp, I.C., and MacDonald, E.K., 1987, Energy and process integration in continuous and batch processes, IChemE Symposium Series, 105, pp. 185–200.

[17] Kemp, I.C., and Deakin, A.W., 1989, The Cascade Analysis for Energy and Process Integration of Batch Processes - Part I. Calculation of Energy Targets, Chem. Eng. Res. Des., 67, pp. 495-509.

[18] Obeng, E.D.A., and Ashton, G. J., 1988, On Pinch Technology Based Procedures for Design of Batch Processes, Chem. Eng. Res. Des., 66, pp. 255-259

[19] Gremouti, I.D., Integration of Batch Processes for Energy Savings and Debottlenecking, M.Sc. Thesis, UMIST, Dept. of Process Integration, Manchester, UK.

[20] Wang, Y.P., and Smith, R., 1995, Time Pinch Analysis, Trans. of IChemE, 73, pp. 905-914.

PinCH: An Analysis Tool for the Process Industries

Don Olsen[a], Armin Egli[a] and Beat Wellig[a]

[a] *Lucerne School of Engineering and Architecture, Horw, Switzerland*

Abstract: This paper describes a newly developed software application called PinCH. The software is designed to support the application of process integration through the use of the pinch method. The project has been developed in cooperation with several partners from industry and has been funded by the Swiss Federal Office of Energy (SFOE). The product is a replacement of the original PinchLENI application developed in early 1990's at the Swiss Federal Institute of Technology Lausanne (EPFL). A key goal in this project has been to continue to provide and extend the foundation for the teaching and the transfer of skills and knowledge of process integration to industry. Therefore, the target group of users includes both students and teachers in academia as well as design engineers in the praxis. An overview of the project methodology, application design and several of the main visualization components are presented.

Keywords: Process Integration, Pinch Analysis, Process Optimization, Heat Exchanger Network, Software.

1. Introduction

Energy use in the world today is important for the world's economic and innovation progress. However, the increasing cost of energy and stricter environmental legislation require industrial firms to seek ways to reduce their energy needs. Process integration has played an important role in seeking ways to improve resource utilization. A mature but somewhat under utilized method used in process integration studies is pinch analysis [1, 2]. This method provides a relatively practical interpretation of the second law of thermodynamics and seeks to determine energy targets that distinguish between the inevitable and avoidable exergetic losses. To help promote the use of the pinch analysis method, a software tool called PinCH (CH stands for the Latin name "Confoederatio Helvetica", i.e. Switzerland) is being developed to provide a sound basis for the application and support of the pinch method.

2. Project Description

The project has been supported by the Swiss Federal Office of Energy SFOE to replace and provide additional features to the PinchLENI software developed at Swiss Federal Institute of Technology Lausanne (EPFL) in the early 1990's [3]. This software tool allowed students and practicing engineers to learn and apply the pinch method in the praxis successfully. However, it was requested to upgrade the code base and implement additional features and algorithms that have since matured. Information exchange and support from present and previous academic staff at the EPFL was initiated in order to ensure appropriate knowledge transfer of the existing PinchLENI program implementation as well as associated literature available within the department.

Inherent in the overall project goals is the need to continue to provide a user friendly foundation for the teaching of the pinch method and for the easy application in industry. In addition, the internal structure is to provide the flexibility to allow further development and extension of more advanced algorithms and techniques. Finally, the present specific improvements are as follows:

1. Dynamic stream table data specification
2. Humid air auto-segmentation
3. Scenario management of targeting and heat exchanger design results
4. Soft stream handling in targeting and heat exchanger network design
5. Stream merging in heat exchanger network design
6. Split grand composite curve visualization
7. Driving force plot visualization

Compared to existing commercially or scientifically available software, the project goals are limited primarily to the implementation of the

Corresponding Author: Beat Wellig, Email: beat.wellig@hslu.ch

classical pinch method for the targeting and design of heat exchanger networks. There are no present plans for implementing automated heat exchange network optimization design algorithms outside batch and multiple base case optimization.

Notwithstanding the importance of the software product, a fundamental initiative of the project is to support the transfer of skills based on the principles of process integration and the pinch method to industry through teaching and application. A key distinction is the recognized importance of enhancing the skill of new engineers in the analysis procedures and thinking processes of overall system design along side the development of skills in process engineering and unit operation design and optimization. This foundation building is important for continued improvements in industrial energy system optimization providing a basis for the application of more advanced techniques.

3. Methodology

The application of the pinch method is manual in nature; however, it provides a systematic and structured approach to the difficult problem of overall system design [4]. The method places a considerable amount of responsibility on the user to fully understand the process they are focused on optimizing. However, this action in itself provides a strong benefit as the design engineer speaks in terms of his or her process on a practical concrete level of understanding. Figure 1 shows the project flow diagram for a typical pinch study in industry [5]. The flow involves 3 major phases 1) mass and energy balance validation, 2) pinch method calculations and 3) new design change recommendations. The PinCH software mainly focuses on supporting the second phase involving targeting and heat exchanger network design calculations. The skills involved in the first and third steps can only be minimally supported and require the design engineer to develop the necessary skills in process engineering and unit operation design through learning and experience.

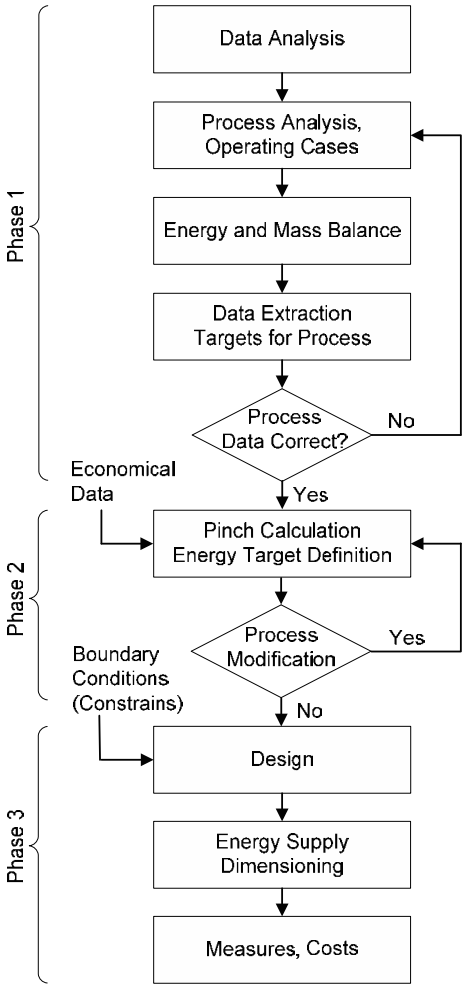

Fig.1. Pinch Study Process [5]

However, within the context of the pinch study calculations, ten major processing steps were identified that are typically done and are directly supported in the PinCH software. They are as follows:

1. Entering Stream Data
2. Creating Processes
3. Assigning Streams to Processes
4. Setting Economic Data (Global and Utility Stream Specific)
5. Creating an Operating Cases Schedule
6. Creating a Target Group
7. Calculating a Target Result (e.g. Separate Design or Time Average Model (TAM) Design)

8. Calculating Target Results Based on Variations of ΔTmin Values or other parameters (e.g. economic data and scheduling data)
9. Adding Energy Conversion Units
10. Creating Heat Exchanger Network (HEN) Designs for Specific Target Results

Each of these steps is managed within PinCH through the use of graphical user interface object visualizers. The key features include the ability to create complex plant design scenarios for the analysis of single continuous, multiple base case and single product batch processes. Once standard targeting calculations are complete detailed heat exchanger network grid diagrams can be created to produce minimum energy or relaxed designs.

4. Visualization Components

In order to support the ten steps identified for completing a pinch study, user interface visualizer components were created. These components represent individual objects encapsulated to provide separate and enclosed feature behaviour. To manage these components, the overall system architecture was based on the well established n-tier design. The implementation specifically used the Model-View-ViewModel pattern [6], but with the addition of controllers to separate out specific visual controlling behaviour. This design provides the necessary flexibility for future extensions. An event notification system has been implemented that is used to handle communication between the different layers as well as the different visualizers.

Each of the visualizer components are dynamically displayed and managed on the main application user interface Workbench (Fig. 2). The details of the major visualization components are presented next.

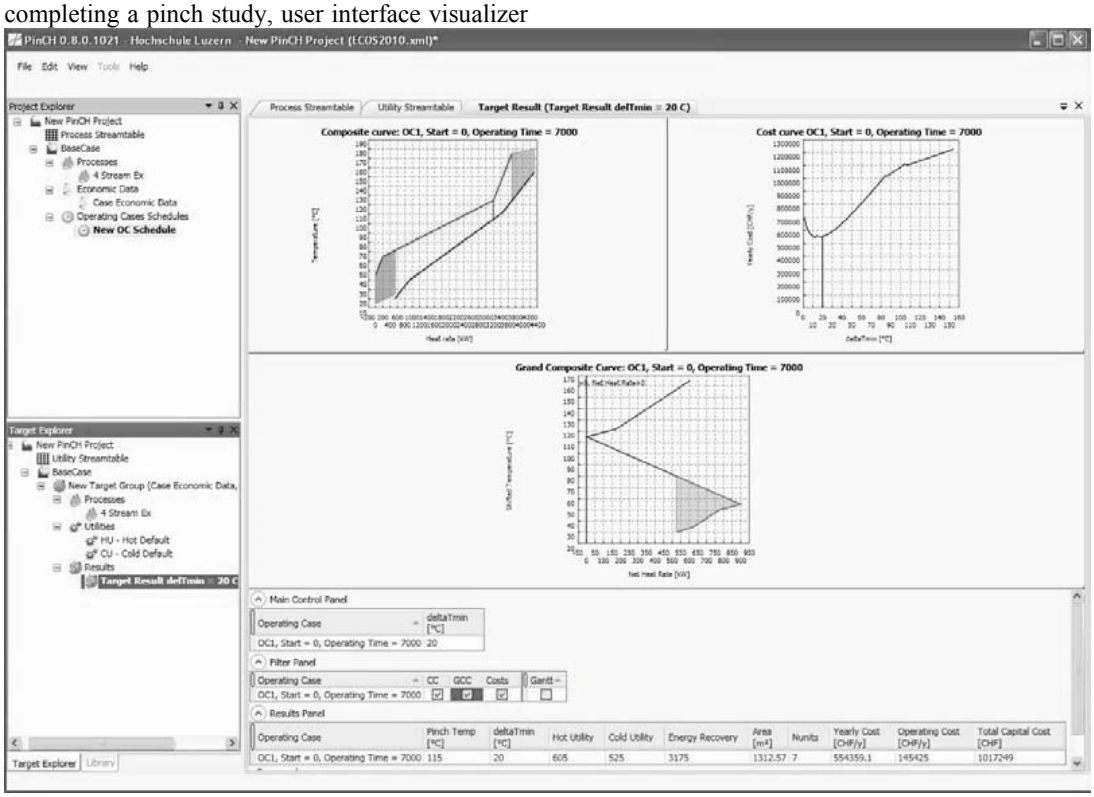

Fig.2. Workbench User Interface of PinCH

4.1 Project Scenario Management

The management of project scenarios is done within the project explorer (Fig 3). This visualizer provides configuration capabilities necessary to define continuous, batch and multiple base case processes. The configuration

features include the steps 1 to 5 of the major processing steps and are linked to the project explorer through additional interface objects. The user is able to import and export data to and from the stream table. The stream table supports simple streams as well as standard refrigerants based on rigorously calculated physical property data using [7]. The steam table and the humid air models are also supported allowing the automatic segmentation of streams. Once the stream table information is imported, the streams can be grouped into processes or areas based on any logical separation the design engineer requires.

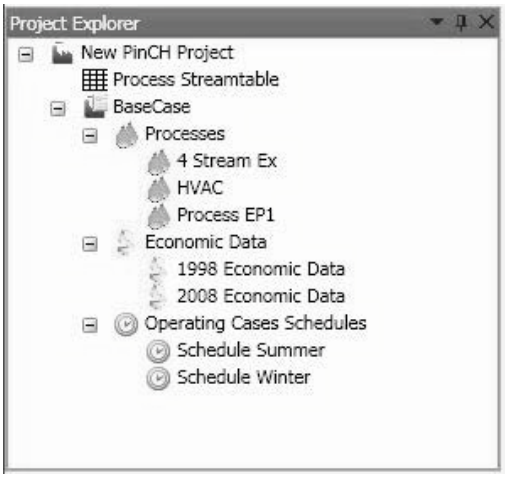

Fig.3.PinCH Project Explorer for Managing Static Scenarios

To complete the static configuration of the project, global economic data and process operating case schedule information must be provided. Versions of each type of data can be managed on the project explorer as shown in Fig. 3.

Economic data can be defined on a global, HEN or utility stream basis. Separate heat exchanger costs can be defined in order to provide a separate breakdown of cold and hot utility exchanger costs as well as process to process exchanger costs. Scheduling information can be used to define overlapping batches, number of batches in a cycle and number of repeat batch sequences. Finally, utility costs are defined separately for each utility stream providing the ability to explore the cost effects of multiple utilities.

4.2 Targeting Scenario Management

Targeting result creation and management is made possible using the target explorer (Fig. 4). This visualizer is the main location to configure new targeting groups involved in the more dynamic processing steps 6 to 9. Each target group requires the assignment of a process, an economic data and an operating case schedule configured on the project explorer. In addition, as a minimum, a default cold and hot utility must be assigned before a target result can be calculated. Multiple processes can be selected to facilitate zonal targeting analysis when compared to the processes on an individual basis.

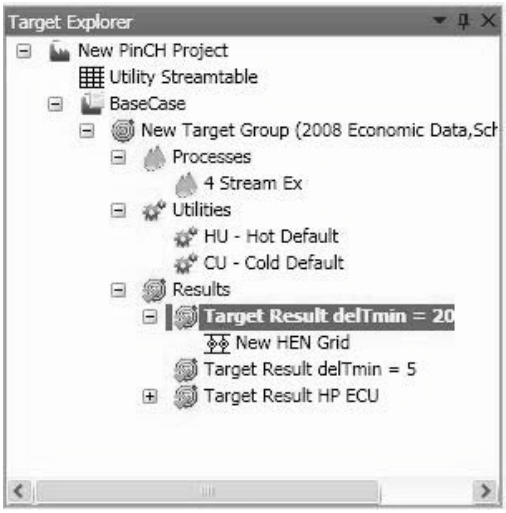

Fig.4.PinCH Target Explorer for Dynamic Targeting Scenario Management Visualization

The target result can be created using either the separate design tool or the TAM tool. The separate design tool decomposes the time data to create operating cases based on the process schedules and the individual stream existence times for pure batch streams. A Gantt chart is available to illustrate both the process and stream existence time dependencies (Fig. 5). Once the tool has completed calculation, the results are viewed in a targeting result visualizer. In this location the user can view and interact with the composite curve (CC), grand composite curve (GCC), balanced composite curve (BCC), and the cost curves (Fig. 2).

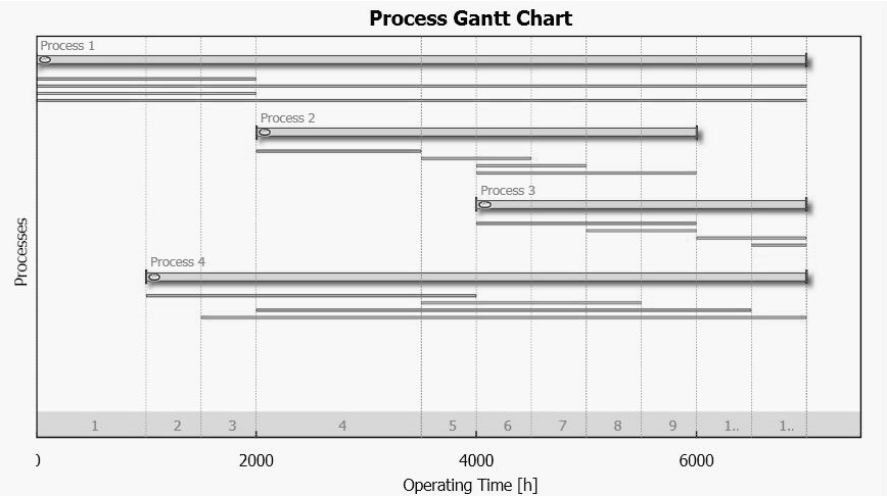

Fig.5.Gantt Chart Illustrating Process Schedules and Individual Stream Existence Times

Further analysis can be done through the use of additional features such as integrating energy conversion units (ECU), designating soft-stream segments and performing continuous targeting based on the cold composite curve shifting. In addition, creation of additional targeting results for specific ΔTmin values can also be made and saved in the scenario manager of the explorer. The BCC is created based on predefined utilities and sized using the GCC. A split grand composite curve is also available to display an extracted process mirrored against a background process.

Details of several of these features mentioned features are presented next.

4.2.1 Energy Conversion Units

The energy conversion units (ECU) are unit operating models that can be integrated into the stream table population to investigate the effects of additional utility streams. The implemented ECUs include a standard Heat Pump, Mechanical Vapour Recompression (MVR) unit, Organic Rankine Cycle (ORC) and a standard combined heat and power (CHP) engine. Each ECU thermodynamic cycle is solved based on input sizing information such as energy loads fitted to the grand composite curve or the required electrical power generation. The algorithm calculates the necessary refrigerant or waste heat streams and automatically integrates them into the stream table. The targeting result is recalculated to see the effects on energy and cost targets which can be compared with a base case result.

4.2.2 Area Calculation

The targeting area calculation produces a breakdown of the area on a match-wise basis [8] as shown in (1) and (2).

$$A\min, L = \sum_{k=1}^{Ni} \frac{1}{LMTD, k} * \sum_{i=1}^{NH_L} \sum_{j=1}^{NC_L} Q_{(i,j)k,L} \left(\frac{1}{\alpha_{i,j}} + \frac{1}{\alpha_{j,i}}\right) \quad (1)$$

$$A\min = \sum_{L=1}^{NE} A\min, L \quad (2)$$

This approach gives the flexibility to calculate the area distribution based on either a single stream or a particular heat exchanger specification match. The flexibility provides the ability to calculate the area distribution for different heat exchanger specifications such as the individual utility exchanger costs. The unit distribution for different heat exchanger designs is also calculated individually [8].

4.2.3 Continuous Graphical Targeting Technique

The ability to shift the composite curves relative to one another was implemented using a digital form of the graphical technique. The technique was originally developed in the predecessor PinchLENI [3] application and the same procedure is used internally. Each composite curve interval is stored internally and simply

CkP,(H ’vv2x. Plq (2 (kH2,,CH{ L(PbR) xHTLBxH ,2x ’ qP*Hl t [Pl “’bLH bb c2L1. (’xuqH{ xHCLb(“’bLHC CLvk ’C ’xH v2C(’1. L1R(C ’xH .)1’[Rv’bb) L].’(H ’1.]b2((H (2 Ck2” (kH H,,Hv(C2, CLvk [2“H{ Hl(Pl (kHv2b v2[ ]2CR(H vLx“HxHb’(P*H(2 (kHk2(v2[ ]2CR(HvLx“Ha m

4.2.4 Operating Cases Decomposition

t kRC ,L1v(P21’bR() RC LCH Pl vxH’(Plq (kH 2]Hk’(Plq v’CHC (k’(HSRC(Pl c’(vk 2x [Lb(P]bH c’CH v’CH GvkH LbPlq GvHl’xl2C t kH Pl(Hkl’b ’bq2xR(k[LCHC (kH GvkH LbH ’1. C(xH’[Pl,2x[’(P21 ,2x c’(vk]x2vHCCHC 2x v21(Pl L2LC]x2vHCC(2 .Hv2[ ]2CH(kH(P{ H. H]Hl. Hl([2. Hb Pl(2 CH]’x’(H 2]Hk’(Plq v’CHC ’vk 2]Hk’(Plq v’CH v’1 (kHl cH ’1’b)j H Pl. P*P. L’bb) 2x (2qH(kHk (2]x2“P. HPlCRqk(Pl(2 (kH y .HCRq1 2](H{ P}’(P21 2]]2x(L1R(HCcH(” HHl (P{ H]Hk12. C

4.2.5 Soft Stream Integration

t kRC ,H’(LxH P{]bH{ Hl(’(P21 ’bb2” C (kH .H,Pl R(P21 2, C2,(C(xH’[CHq[Hl(2(k]x2vHCC ’1. L(PbR) C(xH’[C v’1 cH[’xAH ’C C2,(,x2[” kRvk (kH LCHk v’1 C]bR((kHC(xH’[Pl(2 k’x ’1. C2,( ]’x(C El(Hkl’bb) (kH C2,( ]’x(C ’xH ’L(2[’(Rv’bb) HSvbL. H ,x2[(kH CL]Hk(’x(Plq v’bvLb’(P21 ’1. (kH RC L].’(H (2 xH}bHv((kH 1H’ 2](P{ L[t kH LCHk RC’cbH(2 CHH(kH H,,Hv(C 21 (kH]Plvk (H{]Hk’(LxH ’1. .H(Hk[Pl H k2” [Lvk 2,’C(xH’[v’1 cH LCH Pl kH’(HSvk’1qH ’1. k2” [Lvk v’1 cH Rq12xH bb. H]Hl. Hl((’xuqH(Plq “RCL’bB}HkC ’xH L].’(H .)1’[Rv’bb) 2” H‘Hk Pl (kH y xP. (kH LCHk RC qP*Hl (kH 2]]2x(L1R) (2 Rq12xH(kHC2,(Hl Hkq)]’x(C2x LCH (kH] 22b2, C2,(Hl Hkq) Pl 2x. Hk(2 HSvk’1qH” R(k 2(kHk]x2vHCC(xH’[C

4.2.6 Cost Calculation

t kH v2C(v’bvLb’(P21 RC c’CH 21 (kH ” Hbb HC(’cbRCkH v2C(,2x[Lb’ (k’(’CCL[HC HTL’b .RC(xRcL(P21 2, ’xH 2“Hk (kH 1L[cHk 2, L1R(C P,,HkHl(C{]bH v2C(b’” C v’1 cH LCHk ,2x]x2vHCC]x2vHCC2x L(PbR)]x2vHCCkH’(HSvk’1qH . . R(P21’bv2C(CCLvk ’C]HkC211Hb [’Pl(Hl’1vH ’1. Pl. H]Hl. Hl(v2C(Cv’1 ’bC2 cH Plvb L. H t kH 2]Hk’(Plq v2C(C ’xH ’CCRq1H 21 ’ L(PbR) c’CRC ’1. ’xHPlvbL. H Pl (kH2“Hk’bb2]Hk’(Plq v2C(,2x ’ qP*Hl c’b’1vH v2[ ]2CR(HvLx“H

4.4 Heat Exchanger Network Design Scenario Management

t kHvxH’(P21 2, kH’(HSvk’1qHk 1H{” 2xAC y RC [’1’qH ” R(kPl (kH (’xuqH(Plq HS]b2xHk “RCL’bB}Hk ’vk y RC c2L1. (2 ’]’x(RvLb’x (’xuqH{ xHCLb(t [Pl ’1. RC(kHkH,2xH. RC]b’)H Pl ’1 ’((’vkH [’11Hk(2 (kH(’xuqH{ xHCLb(Rq t kH. H{’PbH . HCRq1 2,’ y RC. 21HLCPlq (kH y qxP. . HCRq1 “RCL’bB}Hk Rq t kRC qx’]kRv’b “RCL’bB}Hk ’bb2” C(kH LCHk (2 cLPb (kH [Pl P[L[HlHkq) xHTLBxH{ Hl(g s 1H{” 2xA Pl R(P bB}H ,x2[(kH ’CC2vP(H (’xuqH(Plq xHCLb(t kH]Plvk . HCRq1 xLbHC’xHHl,2xvH HlCLxPlq (kH (’xuqH(Plq v21C(x’Pl(C ’xH [’Pl(’Pl H ’b21q ” R(k (kH qx’]kRv’b Pl. Rv’(P21 ” kHlH‘Hk (kH v21CHk“’(P21 2, HlHkq)]xPlvP]bHRC“P2b’(H

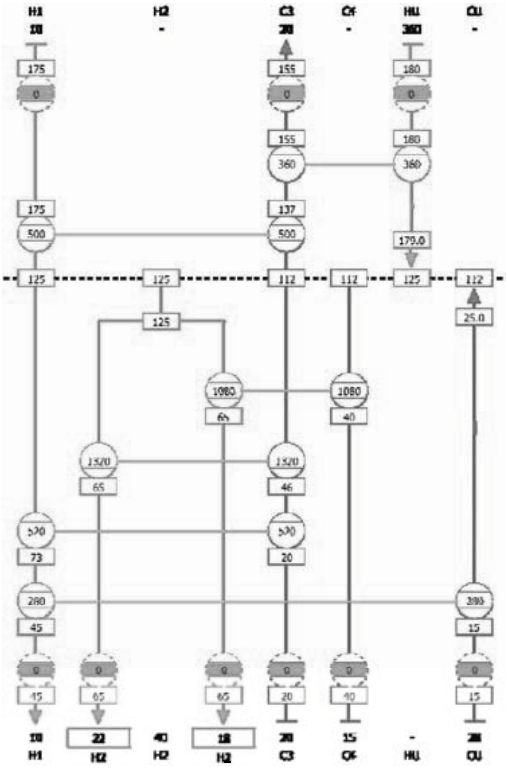

Fig.6.PinCH Heat Exchanger Design Visualization

t kH y qxP. ’bb2” C(kHLCHk (2 C]bR(2x [HkqH C(xH’[C Pl 2x. Hk (2 v2[ ]bH(H ’ g s . HCRq1 i H‘Hk’b “HkCP21C2, (kH . HCRq1 v’1 cH vxH’(H ’1. v2[ ]’xH (2 21H’12(kHk ’C” Hbb ’C” R(k 2(kHk “HkCP21C,x2[2(kHk (’xuqH(Plq xHCLb(C t kH 1H{” 2xA v’1 ’bC2 cH xHb’SH Pl 2x. Hk (2 Pl“HC(Rq’(H]2CCRc PbR(PHC (2 xH LvH(kH 1L[cHk 2, L1R(C2x (2 CHH(kHH,,Hv(C2, b2v’bkH’(HSvk’1qHk ’]]x2’vk (H{]Hk’(LxHC (k’(.P,,Hk ,x2[(kH qb2c’b t [Pl g Lb(P]bH c’CH v’CHC’1. [Lb(P]bH c’(vk 2]Hk’(Plq v’CHC’xH’L(2[’(Rv’bb) vxH’(H

and can be viewed and compared directly with the HEN Grid visualizer. This capability aids in the design of an optimum network valid over all time periods.

5. Conclusion

A software tool PinCH has been built to provide a foundation for the continued transfer of skills in process integration and in particular the pinch method. The software is a user friendly application designed to help and support new and experienced design engineers in academia and industry to apply the principles of pinch analysis. The project plans are for a version 1.0 release middle of 2010. Future plans include advancements in extensibility, MBC/Batch super-targeting, and remaining problem analysis techniques.

Nomenclature

Amin minimum area target for a entire network, m^2

Amin,L minimum area contribution of exchanger specification, m^2

i hot stream

j cold stream

k enthalpy interval

L exchanger specification

Ni number of enthalpy intervals

NE number of different exchanger specifications

NH_L number of hot streams with exchanger specification L

NC_L number of cold streams with exchanger specification L

$Q_{(i,j)}$ heat load between hot stream i and cold stream j

α heat transfer coefficient, $W/(m^2 K)$

References

[1] Linhoff, B., 1993, Pinch Analysis – A state-of-the-art overview, Trans. IChemE, Vol. 71, Part A, 503-522.

[2] Kemp, I., 2007, Pinch Analysis and Process Integration – A User Guide on Process Integration for the Efficient Use of Energy, Second Edition, Elsevier Ltd., Oxford, UK.

[3] Staine, F., Logiciel PinchLeni – version 2.0 PC Windows, Bundesamt für Energiewirtschaft 1995, ENETArt. 30374.

[4] Shenoy, U., Heat Exchanger Network Synthesis – Process Optimization by Energy and Resource Analysis, Gulf Publishing Company, Houston, USA, 1995.

[5] Morand, R., et al, Prozessintegration Mit Der Pinch-Methode – Handbuch Zum BFE-Einführungskurs, Bundesamt für Energie BFE, 2006, [online handbuch], URL: http://www.bfe.admin.ch/energie/00572/00870/index.html?lang=en&dossier_id=01259.

[6] Block, G., Patterns For Building Composite Applications With WPF, MSDN Magazine, [online article], 2008, URL: http://msdn.microsoft.com/en-gb/magazine/cc785479.aspx

[7] Lee, B.Y., Kesler, M.G., 1975, A generalized thermodynamic correlation based on three-parameter corresponding states, AIChE Journal, 21, 3, 510-527.

[8] Jegede, F.O., Polley, G.T., 1991, Capital cost targets for networks with non-uniform heat exchanger specifications, Computers & Chemical Engineering, 16, 5, 477-495.

[9] Krummenacher, P., 2001, Contribution to The Heat Integration Of Batch Processes (With or Without Heat Storage), Thèse No .2480, École Polytechnique Fédérale de Lausanne, Switzerland.

Acknowledgments: The authours would like to thank the Swiss Federal Office of Energy (SFOE) for funding the development of PinCH (Martin Stettler) and the following companies who worked in collaboration on the project: Helbling Beratung + Bauplanung (Florian Brunner, Raymond Morand), BG Bonnard & Gardel, Ingénieurs Conseils SA (Pierre Krummenacher) and Thomas Bürki GmbH (Thomas Bürki).

Thermal Integration Of Heat Pumps In Cheese Factory

Rabih Murr[a], Assaad Zoughaib[a], Denis Clodic[a]

[a] *Center For Energy and Processes, MINES ParisTech, Palaiseau, France*

Abstract: This paper presents the study of hot water generation at several levels of temperatures by heat pumps that recover heat from different effluents. The cheese production process is described by the Pinch method in order to define the overall energy gains of heat pump integration. The effluents used as cold source are available at 51°C and 33°C.
Comparisons are made between the pure refrigerants, especially R-134a and R-1234yf, and zeotropic refrigerant blends using the second law of thermodynamics, and other criteria such as: compressor discharge temperature, condensing pressure, GWP, flammability, and swept volume of the compressor.
Experimental investigations on a heat pump prototype are used to validate the thermodynamic calculations. Results show that the designed zeotropic mixtures reduce the temperature difference between the refrigerant and the heated liquid for counter-current heat exchangers, which leads to minimization of entropy generation and higher COPs.

Keywords: Heat Pump, Pinch, Refrigerant, Temperature Glide, Exergy, Selection Criteria.

1. Introduction

Environmental impact of industrial processes including cheese processes and their energy consumption are increasing. Exergy analysis and process integration can be applied on the processes to optimize them and to limit their footprint. These methodologies have been developed during the last 15 years by many scientists like Linnhoff [1], Berntsson [2] and Gourlia [3]. The Pinch method is used to represent the internal heat exchanges between process streams (hot and cold streams) and to establish the minimum energy consumption targets for the process. It allows the best method of integration of heat exchangers and thermodynamic systems (e.g. heat pumps) in the process. This methodology has many advantages like reducing operating cost, improving efficiency and reducing investment cost. It is based on the drawing of the composite curves from the heat demands called cold flux and heat availabilities called hot flux in a temperature, heat diagram. To obtain the minimum energy consumption target, the composite curves should be moved horizontally to reach the minimum temperature difference. This distance is called the pinch temperature (ΔT_{min}). These curves are obtained from Equation (1).

$$\dot{Q} = \dot{m}.C_p.\Delta T, \qquad (1)$$

Where:

$\dot{Q}$ Is the enthalpy variation (kW), $\dot{m}$ is the mass flow (kg/s), C_p is the specific heat of the product (kJ/kg.K), and ΔT is the temperature variation (K).
In some processes, multiple utility levels can be used. The use of the cheaper utility should be maximized. It is possible to optimize the uses of utilities by using the grand composite curve. It is simply drawn by increasing and decreasing respectively the cold composite temperature and hot composite temperature by $1/2\Delta T_{min}$ and by subtracting enthalpies at a constant temperature.
In the studied cheese production process, hot water is used in many process steps and at several levels of temperatures (60°C, 70°C, 85°C, and 90°C). Effluents are available at two levels of temperature (33°C and 51°C). The amount of energy for each process can be estimated once the hot water volume, the inlet water temperature, and the outlet water temperature are known.

Both sources of effluents are available at two different sites. For environmental hygiene conditions, it is forbidden to circulate the effluents in the factory. Processes 1, 2, 3, and 5 represented in Table 1 are close to the source of effluents at 51°C and Process 4 is close to the source at 33°C.
The parameters of hot water and effluents are presented in Table 1 for each process.

Corresponding Author: Rabih Murr, Email: rabih.murr@ensmp.fr

Table 1: inlet and outlet temperatures and mass flow rates of hot water needed and effluents for each process.

Pr	Effluents			Hot water		
	Inlet T	Outlet T	$\dot{m}$	Inlet T	Outlet T	$\dot{m}$
1	51	24	1.67	10	60	0.97
2	51	30	0.44	60	70	1.27
3	51	34	1.46	70	85	2.5
4	33	13	0.8	70	85	1.72
5	51	25	0.1	85	90	0.71

To study the possibility of integration of heat exchangers and heat pumps in the factory, the Pinch method is applied for each process. The heat pump is used when Q_{Hmin} and Q_{Cmin} are respectively above and under the pinch point. For this type of systems, a pinch of 5 K is usually considered. This parameter may be optimized by thermo-economic optimization techniques but it is not done in this study which focuses more on the heat pump design. The composite curves and the Grand Composite Curve (GCC) of process 1 are represented in Figure 1.

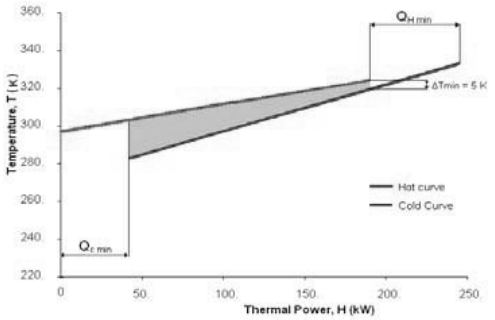

Fig. 1-a: Composite curves for process 1.

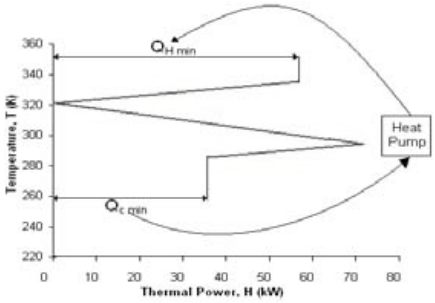

Fig. 1-b: Grand Composite curve for process 1.

In Fig. 1 the composite curves (grey zone) and the GCC show that a heat exchanger called PHX can be installed in addition to the heat pump to produce the needed energy. The PHX should be placed upstream the heat pump evaporator [5]; the city water is preheated before the condenser inlet. Fig. 2 shows the heat pump with the PHX for process 1.

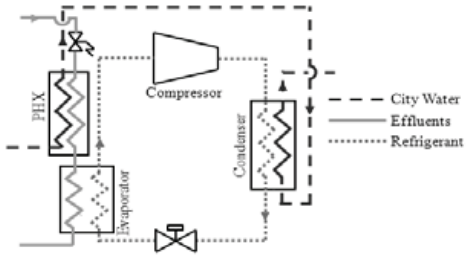

Fig. 2: Heat pump with PHX for process 1.

The use of the PHX influences the system performance represented by the COP, which is the ratio of the total heating capacity to the total electrical energy consumption.

$$COP = \frac{\text{total heating capacity}}{\text{total energy consumption}}, \quad (2)$$

In a normal case, the total heating capacity (kW) is represented by the heat delivered at the condenser of the heat pump and the total energy consumption (kW) is equal to the sum of powers absorbed by the heat pump compressor and the auxiliary electric components. In this case the total heating capacity is equal to the heat delivered at the condenser of the heat pump and the heating capacity transferred by the PHX. Table 2 presents the inlet and outlet temperatures of the hot water and effluents for process 1 with the PHX.

Table 2: Inlet and outlet temperatures (°C) for process 1 with PHX.

	PHX		Heat pump	
	Inlet T	Outlet T	Inlet T	Outlet T
Effluents	51	30	30	24
Hot water	10	46	46	60

For processes 2, 3, 4 and 5, there is no possibility to install PHXs because effluents are available at 51°C and 33°C which are lower than the temperatures of hot water that must be heated from 60°C to 70°C for Process 2, from 70°C to 85°C for Process 3, from 70°C to 85°C for process 4 and from 85°C to 90°C for Process 5.
Table 3 shows the inlet and outlet temperatures and the mass flow rates of the hot water and effluents at the condensers and evaporators of heat pumps for all processes. For Processes 4 and 5,

heat pumps are two-stage heat pumps. Furthermore, it shows that the temperature glide at the evaporator and the condenser of each process is significant. Thus the interest of using blends of refrigerants with glide matching to reduce the exergy losses in the heat exchangers and allow improving the system performance.

Table 3: Inlet and outlet temperatures and mass flow rates at the evaporators and condensers of heat pumps.

Pr	Evaporator			Condenser		
	Inlet T	Outlet T	$\dot{m}$	Inlet T	Outlet T	$\dot{m}$
1	30	24	1.67	46	60	0.97
2	51	30	0.44	60	70	1.27
3	51	34	1.46	70	85	2.5
4	33	13	0.8	70	85	1.72
5	51	25	0.1	85	90	0.71

Liu Nanxi et al. [6] tested the performance of a heat pump using a near-azeotropic blend for high condensing temperature (near to 90°C). Miyara et al. [7] tested the performance of a heat pump using a binary blend with condenser inlet and outlet temperatures of 40°C and 60°C.
In this study, refrigerant blends are tested for each level of temperature in order to choose the suitable one and these choices are validated experimentally by testing the blends on a prototype heat pump.

2. Comparisons between pure refrigerants and mixtures for each process

The refrigerant used in a heat pump can be either a pure fluid or a blend of fluids. The last one is divided into three groups: azeotropic mixtures, near azeotropic, and zeotropic mixtures. Zeotropic mixtures offer several advantages compared to pure refrigerants and azeotropic blends. They offer the possibility to reduce irreversibilities at the evaporator and the condenser. When designing a refrigerant or a blend, it is important to control properties such as flammability and GWP. In addition, the operating pressure at the condenser has to be limited by choosing the suitable composition.

2.1. Working fluid selection criteria

As introduced in the previous section, the methodology of fluid design is a multi-objective and multi-constraint optimization process:

Environmental criteria: the working fluid has to have a low environmental impact represented by the GWP.
Safety criteria: it concerns either the toxicity or the flammability of the refrigerant. To distinguish a flammable fluid from a non-flammable one, a coefficient called *RF-number* defined by Kondo [4] is used.

$$RF = \frac{(LFLxUFL)^{1/2} - LFL}{LFL} x \frac{P_c}{M_m}, \quad (3)$$

Where:
RF = RF-number (J/g); UFL = Upper Flammability Level (%); LFL = Lower Flammability Level (%); P_c = heat of combustion of the fluid (J/mol); M_m = molar mass of the fluid (g/mol). For this evaluation, fluids are considered moderately flammable if their RF-number is less than 30 and highly flammable if their RF-number is greater than 30 (Kondo [4]).

Compressor discharge temperature: this temperature should be less than 130°C in order to use the usual lubricants. It is directly related to the , $_p / C_v$).

Condensing pressure: this pressure should be less than 3 MPa to limit the tubing cost. High-pressure levels (> 3 MPa) require non-standard elements.

Swept volume of the compressor: minimizing the swept volume of the compressor reduces the investment costs.

Exergy destruction (irreversibility): minimizing the exergy destruction minimizes the operating costs.

2.2. Working fluids for the five processes

The pure fluids that may be used as components of a refrigerant blend are presented in Table 3.

Table 3: Properties of the selected fluids.

Symbol	M_m (g/mol)	T_{crit} (°C)	P_{crit} (MPa)	NBT (°C)	GWP (kgeq CO_2)
R-134a	102.03	101.06	4.06	-26.1	1300
R-152a	66.05	113.26	4.52	-24	120
R-1234yf	114.04	94.8	3.26	-29.2	4
R-245fa	134.05	154.1	4.43	15.1	950
R-32	52.02	78.1	3.64	-51.7	120
R-125	120.02	66.02	3.45	-48.09	3500
R-744	44.01	30.97	7.38	-78.4	1

The saturation curves and operation pressures are the crucial characteristics of a working fluid. They affect the fluid applicability and the overall efficiency of the heat pump. Figures 3 and 4 present the operation pressure and saturated curve respectively.

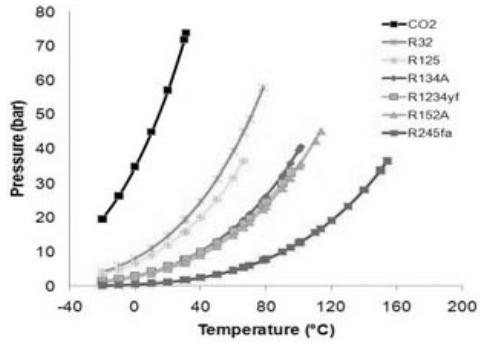

Fig. 3: Operation pressure of different fluids.

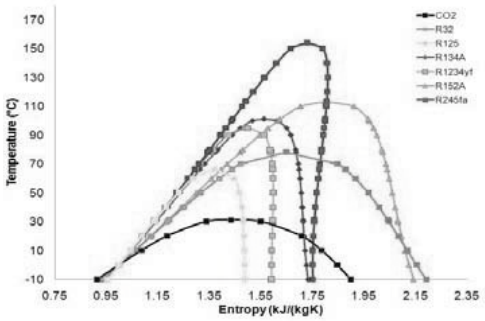

Fig. 4: Saturation curves of different fluids.

It had been verified [5] that CO_2 does not mix with other fluids due to its high volatility. This leads to decrease the temperature glide of the working fluid and to increase the condensing pressure.

From figures 3 and 4, we notice that R-32 and R-125 have similar properties with a big difference of GWP; then, R-32 will be used as component of the blend.

R-1234yf, R-134a and R-152a also have similar properties; then, we can use one of them with other pure fluids.

Method of selection of mixtures from the pure fluids for the 5 processes is based on the triangle method represented in figures 5, 6 and 7 for the processes 5 only (high temperature level), and the same method is applied to other processes.

The comparison between refrigerants is based on considering the same functioning regime at the condenser and the evaporator (same inlet and outlet temperatures and mass flow rate of water) and the same pinch at the heat exchangers (5K). The heat transfer coefficient and the heat transfer surface will depend on the refrigerant.

The dark grey areas represent the admissible areas where the mixtures respond to all criteria.

The thermodynamic cycle properties and the characteristics of the heat pumps are calculated by considering a constant pinch at the heat exchangers.

Blends are created using five pure fluids (R-134a, R-1234yf, R-152a, R-245fa, and R-32) presenting good thermodynamic properties at temperature levels of the 5 processes and blends obtained from the above simulations.

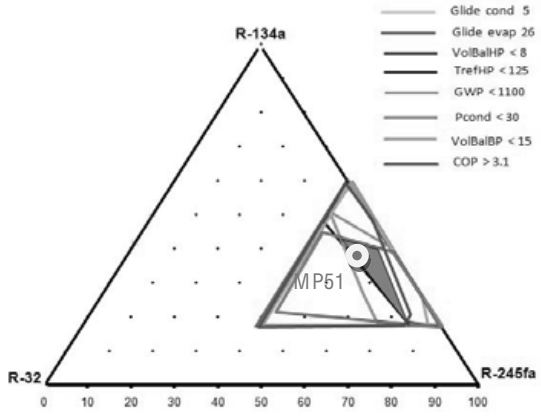

Fig. 5: Concentration diagram for R-134a, R-245fa, R-32 for Process 5.

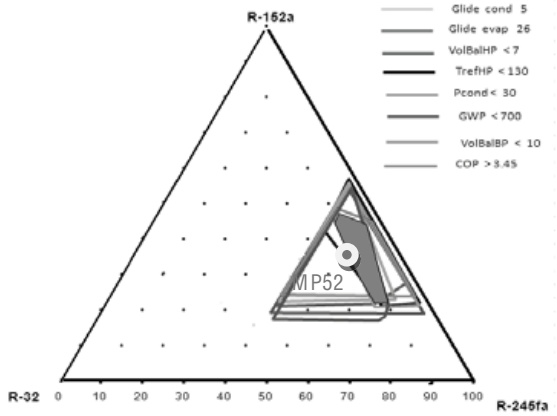

Fig. 6: Concentration diagram for R-152a, R-245fa, R-32 for Process 5.

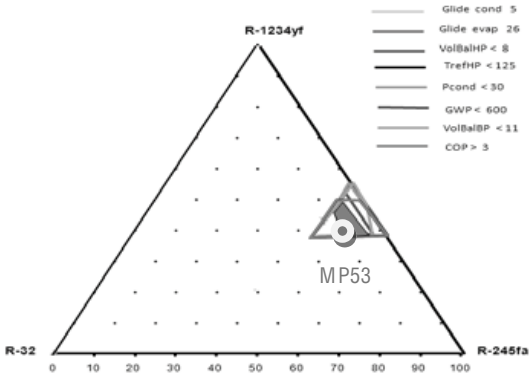

Fig. 7: Concentration diagram for R-1234yf, R-245fa, R-32 for Process 5.

Several blends are compared for each processes in terms of condensing pressure, GWP, COP, compressor discharge temperature, swept volume of the compressor, and exergy destruction. One should notice that R-152a is the more flammable than R-1234yf; then if two blends have the same composition as their components, and one contains R-152a and the other contains R-1234yf, it is obvious to say that the blend containing R-152a is more flammable than one containing R-1234yf.

Table 4 shows a comparison between three blends that can be used for process 5.
Tables 5, 6, and 7 are a comparison between the selected blends for each process and four pure fluids.

Table 4: Comparison between three blends for Process 5.

Refrigerant	MP51	MP52	MP53
Mass composition (%)	45% R-134a, 50% R-245fa, 5% R-32	40% R-152a, 50% R-245fa, 10% R-32	45% R-1234yf, 45% R-245fa, 10% R-32
$T_{we\ i,\ o}$ (°C)	51 25	51 25	51 25
$T_{wc\ i,o}$ (°C)	85 90	85 90	85 90
P_{cond} (MPa)	2.7	2.86	2.83
$COP_{heat\ pump}$	3.06	3.09	2.96
SV LP (m^3/h)	14	12.6	13.23
SV HP (m^3/h)	7.8	7	7.88
$T_{outcomp\ HP}$ (°C)	123	130	120
GWP	1087.5	578	504
Ex gain (kW)	2.27	2.2	2.3
Evap glide (K)	14	13	16
Cond glide (K)	11	10	11

Table 5: Thermodynamic properties of selected blends and pure fluids for Processes 1 and 2.

Process	Process 1					Process 2				
Refrigerant	MP13	R-134a	R-152a	R-1234yf	R-245fa	MP24	R-134a	R-152a	R-1234yf	R-245fa
Mass composition (%)	85% R-1234yf, 10% R-245fa, 5% R-32	100	100	100	100	75% R-1234yf, 15% R-245fa, 10% R-32	100	100	100	100
P_{cond} (MPa)	1.79	1.8	1.6	1.73	0.52	2.51	2.27	2.0	2.15	0.68
$COP_{heat\ pump}$	4.75	3.8	4	3.6	3.97	3.66	3.43	3.56	3.19	3.55
SV (m^3/h)	51	56.4	58.4	63.21	196	40	47.4	48	55	156
$T_{outcomp}$ (°C)	77	83	93	75	76	93.25	93	104	85	84
GWP	126	1300	120	4	950	200	1300	120	4	950
Ex gain (kW)	4.7	4.62	4.25	4	3.9	4.4	4.3	4.1	4.35	4.1
Evap glide (K)	7.28	0	0	0	0	7.7	0	0	0	0
Cond glide (K)	5.26	0	0	0	0	8.9	0	0	0	0

Table 6: Thermodynamic properties of selected blends and pure fluids for Processes 3 and 4.

Process	Process 3					Process 4				
Refrigerant	MP33	R-134a	R-152a	R-1234yf	R-245fa	MP43	R-134a	R-152a	R-1234yf	R-245fa
Mass composition (%)	50% R-1234yf, 40% R-245fa, 10% R-32	100	100	100	100	35% R-152a, 50% R-245fa, 15% R-32	100	100	100	100
P_{cond} (MPa)	2.65	2.99	2.67	2.79	0.98	2.36	2.98	2.64	2.8	0.98
$COP_{heat\ pump}$	3.26	2.75	3	2.5	2.96	2.75	2.32	2.39	2.18	2.37
SV LP(m^3/h)	130	141	137	172	437	120	108	119	111	437
SV HP(m^3/h)	--	--	--	--	98	60	64	61	80	190
$T_{outcomp}$ (°C)	111	107	119	98	950	127	109	122	98	99
GWP	437	1300	120	4	49	600	1300	120	4	950
Ex gain (kW)	18.87	18.34	18.27	18.1	18.3	17.5	17.3	17	17.2	17.2
Evap glide (K)	13.6	0	0	0	0	17	0	0	0	0
Cond glide (K)	14.1	0	0	0	0	14.4	0	0	0	0

Table 7: Thermodynamic properties of selected blends and pure fluids for Process 5.

Refrigerant	MP51	R-134a	R-152a	R-245fa
Mass composition (%)	45% R-134a, 50% R-245fa, 5% R-32	100	100	100
P_{cond} (MPa)	2.7	3.5	3.1	1.12
$COP_{heat\ pump}$	3.06	2.76	2.95	3.01
SV LP(m^3/h)	14	11	12	39
SV HP(m^3/h)	7.8	7	7	20
$T_{outcomp\ HP}$ (°C)	123	112	127	103
GWP	1087.5	1300	120	950
$_{cycle}$	51	48	50	51
Ex gain (kW)	2.27	2.2	2.1	2.22
Evap glide (K)	14	0	0	0
Cond glide (K)	11	0	0	0

2.3. Interpretation of results

According to the previous study, the following points can be observed.

- Using pure fluids in the heat pumps leads to lower COP and higher compressor swept volume.
- In the refrigerant blends, R-32 decreases the swept volume of compressors.

- Based essentially on the COP of heat pumps, the swept volume of compressors, and the GWP of refrigerants, the following conclusions have been reached:
  - For process 1, MP13 (85% R-1234yf, 10% R-245fa, 5% R-32) seems to be the best blend.
  - For process 2, MP24 (75% R-1234yf, 15% R-245fa, 10% R-32) seems to be the best blend.
  - For process 3, MP33 (50% R-1234yf, 40% R-245fa, 10% R-32) seems to be the best blend.
  - For process 4, MP43 (35% R-152a, 50% R-245fa, 15% R-32) seems to be the best blend.
  - For process 5, MP51 (45% R-134a, 50% R-245fa, 5% R-32) seems to be the best blend.

2.4. Experimental investigations using a reduced scale prototype of heat pump

Series of experiments have been investigated to verify the previous optimization study using a single / two-stage heat pump prototype. This prototype had been designed to produce hot water up to 90°C.

Due to time constraint, the only operating conditions used to compare pure fluids and refrigerant mixtures are process 5 conditions (85°C 90°C at the condenser, high temperature level) and the optimal mixture refrigerant named MP51 is compared to R-134a. Results are presented in Table 8.

Calculations showed that it is impossible to reach this regime with R-134a because of the high-condensing pressure. That is why experiments were limited to show the possibility of use of MP51 and results are compared to R-134a calculations. Also, experiments showed that there is a difference between experimental and simulation values obtained with MP51. This difference is due to the compressor efficiency (experimental efficiency is lower than the simulation one).

Table 8: Comparison between refrigerant mixture MP51 and R-134a for process 5.

	MP51 Experimental	MP51 Simulation	R-134a Simulation
Mass composition (%)	45% R-134a, 50% R-245fa, 5% R-32	45% R-134a, 50% R-245fa, 5% R-32	
$T_{we\ i,\ o}$ (°C)	51 32	51 25	51 25
$T_{wc\ i,o}$ (°C)	85 90	85 90	85 90
P_{cond} (MPa)	2.76	2.69	3.8
Heat capacity (kW)	13.1	15.4	19
$COP_{heat\ pump}$	2.4	2.96	2.35
SV LP(m^3/h)	14.37	14.37	14.37
SV HP(m^3/h)	7.31	7.31	7.31
$T_{outcomp\ HP}$ (°C)	126	123	118
GWP	1087.5	1087.5	1300
$_g$ LP	49	68.7	69
$_v$ LP	72	92	92
$_g$ HP	55	61	59
$_v$ HP	81	95	95
KS	1	1	1
KS	1.85	1.85	1.85

3. Conclusion

The application of the Pinch method and the exergy analysis together with the economic and environmental analysis show the interest of heat pump integration in industrial processes.

The development of refrigerant blends that respond to several criteria like flammability gives economic and environmental gains represented by higher COPs, lower GWP, and lower swept volumes of the compressors, especially in case of large temperature glide at the evaporator and condenser.

New tertiary blends have been developed for multi-temperature levels water-water heat pumps using the triangle method. Tests with 15 kW heat pump system showed the gains obtained when using the tertiary blend named MP51 compared to R-134a for process 5 while the inlet and outlet water temperatures at the condenser are 85°C and

90°C respectively, which is a non-conventional level for heat pumps.

4. Perspectives

All tests with the same 15 kW heat pump system will be done in order to compare blends to pure fluids and to show the gains obtained by using mixtures at the different temperature levels.
The efficiency difference of compressors between experiments and simulations has to be analyzed especially at high temperature levels. This difference is shown in Table 8.

Nomenclature

Cp	Specific heat at constant pressure, kJ /kg.K
Cv	Specific heat at constant pressure, kJ/ kg.K
H	Thermal power, kW
$\dot{m}$	Mass flow rate (kg/s)
P	Pressure, MPa
$Q_{C\ min}$	Minimum cold utility requirement, kW
$Q_{H\ min}$	Minimum hot utility requirement, kW
SV	Swept Volume, m^3/h
T	Temperature, °C
$T_{we\ i,o}$	Inlet and outlet water temperature at the evaporator, °C
$T_{outcomp}$	Discharge compressor temperature, °C
ΔT_{min}	Pinch temperature, K

Greek symbols

η	Efficiency

Subscripts and superscripts

Cond	Condenser
Comp	Compressor
Evap	Evaporator
Ex	Exergy
Exp	Experimental
G	Global
HP	High pressure
LP	Low pressure
PHX	Preheat Exchanger
Pr	Process
Theo	Theoretical
V	Volumetric

Abbreviations

COP	Coefficient Of Performance
GWP	Global Warming Potential
LMTD	Log Mean Temperature Difference, K
NBT	Normal Boiling Temperature

References

[1] B. Linnhoff et al., A User's Guide on Process Integration for the Efficient Use of Energy. IChemE, UK (1982).

[2] K. M. Berntsonn et al., An introduction to pinch technology. Heat Transformers in Industrial Processes. CADDET Analyses Series No. 2.

[3] J. P. Gourlia, la methode de pincement ou exploitation des diagrammes température / enthalpie, Revue générale de Thermique, No. 327 (1989).

[4] Kondo S. et al., RF-number as a new index for assessing combustion hazard of flammable gases, Journal of Hazardous Materials, A93: 259-267 (2002).

[5] Nehme G., Etude Et Conception D'une Pompe A Chaleur A Haute Efficacité Energétique Utilisant Les Eaux Grises Comme Source De Chaleur Pour Produire De L'eau Chaude Sanitaire, thèse à l'école de mines de Paris, 2009.

[6] Liu Nanxi et al., Moderately high temperature water source heat pumps using a near-azeotropic refrigerant mixture, Department of Thermal Engineering, China, 2004.

[7] Miyara et al., Consideration of the performance of a vapor-compression heat pump cycle using non-azeotropic mixtures. Int J Refrig 1992; 15 (1):35-40.

"Thermal penalty factors" accounting for site topological characteristics in pinch design of Heat Exchanger Networks

Antonio Piacentino[a], *Raffaele Imperato*

[a] *Dpt of Energetic and Environmental Researches, University of Palermo, Palermo, Italy*

Abstract: Pinch analysis allows to determine targets and solutions for minimum energy requirements in process plants, basing on innovative tools like composite curves and table problem formulation, which ultimately allow generating an optimized heat exchanger network design. On another hand, this technique does not account directly for a number of factors which could play a primary role for the practical feasibility of the network. What if, for instance, once identified an optimal lay-out, we realize that some matches are hardly feasible in practice? Could we adapt the conventional pinch approach to keep into account site topological features since the preliminary design phase? In this paper the authors attempt answering these questions by introducing "Thermal Penalty Factors", to be calculated for any match by accounting for the capital cost needed to realize it. Appropriate expressions for these penalty factors (in kW) are firstly obtained; successively, these factors are integrated into the composite curves, so as to enable the analyst to account for them since the design phase. A simple case study is adopted to highlight the potential of thermal penalty factors in contributing to achieve more reliable targets.

Keywords: pinch analysis, heat exchanger network, thermal penalty factors, energy saving, topology

1. Introduction

Pinch analysis certainly represents an effective approach to achieve maximum energy savings in heat exchanger networks (HENs) design.

Despite of the large potential for energy and money saving in the process industry, heat recovery solutions derived by pinch techniques are rarely implemented, being such approaches often perceived as "hard to apply in real world cases".

In order to generate a new heat exchanger network covering all the required matches between fluid flows, large investments are usually required to purchase the new heat exchangers and piping connections. Both in large and small plants top-down approaches based on generating a Maximum Energy Recovery (MER) design and relaxing it to exclude inconvenient matches might lead to positive results. Besides of chemical compatibility issues, which have already been considered in literature, we could ask: what if some matches are hardly feasible, due to the excessive distance between the matching streams and the consequently excessive cost for purchasing pipes-connections and operating the network (pumping- and heat losses-related costs)?

What if the match between two streams is unfeasible due to the presence of an obstacle or a physical barrier (removable at a non-null cost) to their connection? It is necessary to consider all these problems, related to the application of the technology in practice, since the design phase.

In case of retrofit of existing HENs, it is alternatively possible to follow a bottom-up approach oriented to gradually improve the existing network with different topology changes, having the MER design as a final, possible target. In such cases we could ask which matches should be preferred among a set of possible alternatives.

In this paper the authors attempt answering the above questions by introducing the "Thermal Penalty Factors" (TPF), to be calculated through simple analytical expressions involving, for each match, economical variables and details on the topological characteristics of the site, so as to recognize eventual priorities for preferential matches that lead to reductions in the total cost.

An Excel sheet was developed, allowing for proper inclusion of the required data and for automatic evaluation of the "Penalty Table", synthesizing the TPFs for the available matches.

Corresponding Author: Antonio Piacentino, Email: piacentino@dream.unipa.it

A simple case study will be considered to show the potential of the approach, which essentially represents an inverse perspective to the problem of *supertargeting*. In particular, a TPF-based HEN design will be compared with a MER design, finally revealing more effective as concerns its capability to suggest simple lay-outs.

2. Case study

The examined case study is not a real plant, but a simple small plant, defined for explanatory purposes. With respect to the set of data usually needed to perform a pinch study, topological data on the plant should be also included; for the sake of simplicity let us assume that the hot and cold fluids are located in small areas, identified by numbers and small circles in Fig. 1. In the same figure several barriers to the feasible paths for fluid distribution are shown.

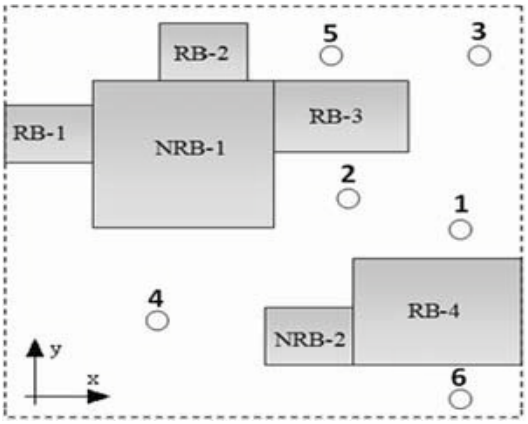

Fig. 1. View of the plant and fluxes disposition

Such barriers could represent either physical or functional (for normative provisions, safety, etc.) obstacles; they are classified as:

- Non Removable Barriers (NRBs);
- Barriers removable (RBs) at a non null cost.

A sketch of the input data for the improved pinch approach proposed ahead in this paper is provided in Tab. 1. Let us leave aside, for a moment, the analysis of the last column, which has not been described yet.

Table 1: Input data table

Flux number	Flow rate (kg/s)	Specific heat (kJ/kg°C)	CP (kW/°C)	Tin (°C)	Ttarget (°C)	X (m)	Y (m)	Diameter band
1	2,00	2,50	5,00	120	80	85,0	45,0	1
2	5,00	2,00	10,00	90	50	65,0	50,0	2
3	1,00	12,00	12,00	70	30	90,0	85,0	1
4	8,00	1,00	8,00	20	50	30,0	20,0	2
5	5,00	2,00	10,00	30	80	60,0	85,0	2
6	11,00	1,00	11,00	50	80	85,0	5,0	3

3. How to calculate "Thermal Penalty Factors"

As anticipated in section 1, in order to calculate the TPF associated with a match we must evaluate all the contributes to the total capital cost associated with the match. Let us analyze separately the two main contributes, that are the cost related to the piping connections and the cost of heat exchangers. Extrapolating reliable cost figures for both "components" would be a very complex task; hence, in the next subsections we will refer to simplificative cost scenarios.

3.1. Piping capital cost

Piping capital costs could be immediately evaluated for every match once the path of each stream has been specified in detail. The following variables mostly influence the capital costs:

- Nominal piping lengths [m]: minimum distance covered by piping connections, assuming any path as composed of branches oriented alternatively along the x and y axis;
- Additional piping length to move around the barriers [m]: unavoidable for non removable barriers, while this cost should be traded off with respect to cost for barriers' removal (see next item listed) in case of removable barriers;
- Additional cost due to removing impediments [€];
- Unit piping cost, expressed in [€/m], which is supposed to assume a discrete number of values, depending on the "diameter band".

Let us assume to collocate any heat exchanger as close as possible to the matching stream with the higher heat capacity rate, CP; this assumption often allows to reduce the pumping costs and leads to less restrictive margins for pipes' thermal insulation (since the stream with the higher ΔT is transported). With reference to the case study, for instance, whether a match between streams n. 4 and n. 5 should be included, the heat exchanger would be positioned approximately at (x_4, y_4), position A in Fig. 2.

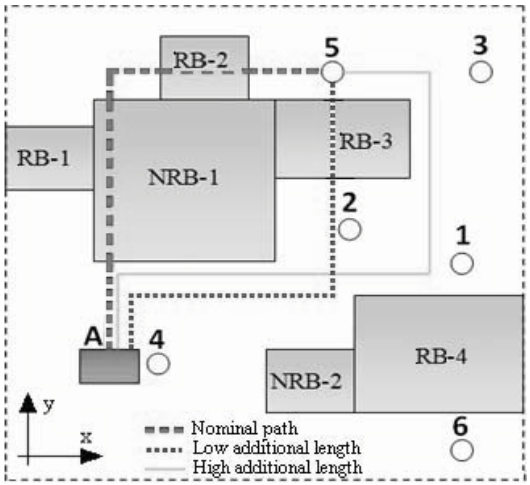

Fig.2. Possible paths for the 4-5 match

With reference to Fig. 2, the red hatched line represents the nominal path (associated with the nominal piping length); the green (dotted) and the yellow (continuous) lines are associated with additional piping lengths, which assume a lower value for the green path (where an additional cost for barrier's removal must be included) and a higher one for the yellow path (where stream 5 is moved around the barriers).

It is now evident that the piping nominal length represents the minimum distance between the streams (under the constraint of branches oriented along the x and y axes), with no regard to any barrier.

For each feasible match, whose path has been fixed, it is now possible to calculate the piping cost.

Assuming a fixed 0.9-1.6 m/s range for fluid velocity and neglecting the variations in fluid density, the higher is the mass flow rate of a stream, the higher the pipe diameter and the associated purchase cost (for underground pipes, the additional cost associated with civil works should be accounted for).

Let us assume to have identified only 3 different diameter bands, each characterized by a specific unit cost as indicated in Tab. 2. In this particular case it was supposed all the streams to be represented by liquid, with a density in the range $0.7 \div 1.3 \cdot 10^3$ kg/m^3; it was then possible to provide the diameter bands directly in terms of flow rate range. More generally, when both liquids and gases are concerned, the limits for the diameters' bands could be indicated in mm.

The Excel sheet identifies the diameter band associated with each stream and adopts the correct unit cost when evaluating the TPFs.

Table 2: Unit pipe cost for the examined HEN

Flow rate limits	Diameter band	Unit pipe cost [€/m]
0 < G ≤ 4 kg/s	Band 1	500
4 < G ≤ 10 kg/s	Band 2	600
G > 10 kg/s	Band 3	700

3.2 Heat exchangers's capital cost

Heat exchangers' capital cost depends on different factors like the type of exchanger, its configuration and efficiency and its heat exchange area. Assuming, as usual, to adopt a unique type of heat exchanger, with a pre-fixed configuration, the most relevant variable is the heat transfer area. Several cost figures have been provided in literature [1,3], most of them expressed according to the following equation:

$$HEC = a + bA^c \quad (1)$$

with HEC representing the heat exchanger cost and a, b and c that are constant to evaluate. In the following of this study a=10,000 €, b=1.14 €/m^{1,9} and c=0.95 were assumed.

In Eq. 1 A is the heat exchange area, that can be evaluated by the following expression:

$$A = \frac{Q}{F\,U\,\Delta T_{lm}} \quad (2)$$

where:

- Q represents the heat transfer rate between the two streams, expressed in kW
- U (kW/m^2°C) is the global heat transfer coefficient, that depends essentially on the heat transfer coefficient on the tube and the shell side, being usually neglected the tube wall resistance
- ΔT_{lm} is the log mean temperature difference [°C], that can be calculated only once matches are decided and opportunely sized
- F is the ΔT_{lm} correction factor for non-purely countercurrent stream flows

3.3 Converting a capital cost into a thermal penalty factor

The main objective of pinch analysis is to maximize heat recovery by process integration, i.e. by designing an appropriate HEN. This will lead to minimize, at the meantime, both the cooling utility required to lead hot fluids to their target temperature and, more important, the hot utility needed to lead cold streams to their target temperature. The cost related to the cold utility is usually in the order of 3÷6 €/kW (for 3,500-7,000 hours per year operation), much lower that the 50÷100 €/kW unit cost associated with natural gas or diesel oil fed hot utilities.

If a match between two streams is included an heat flow rate Q will be saved (both from the hot and the cold utility), with an additional cost related to purchasing, installing and operating the new pipe connections and heat exchangers; these opposite effects should evidently be traded off, to identify optimal recovery targets.

Trading off these quantities requires them to have been expressed into homogeneous terms; as said in section 1, we intend converting capital costs into a TPF. This capital cost should be preliminarily converted into an annual cost, by introducing a capital recovery factor that is, in our example, evaluated under the following assumptions:

- The amortization period n, expressed in years, is set equal to 2. With respect to the values tipically assumed in other fields, in process plants a very short payback time is expected;
- The interest rate r is assumed equal to 5%.

Now let us pose the problem of the conversion, into "equivalent energetic units", of an amount of money. How much fuel could have been acquired with an amount of money equal to the piping's and heat exchangers' cost? At a fixed annual operation, imposed by the process, what is the heat rate that could have been supplied with the aforementioned quantity of fuel?

Let us consider a methane boiler and indicate by PC_Y the piping cost per year [€], obtained by multiplying the piping purchase and installation cost by the capital recovery factor. The amount of fuel can be calculated by the following expression:

$$PC_Y = FQ \cdot c_F \quad (3)$$

where:

- FQ is the aforementioned amount of fuel [Nm^3]
- c_F is the fuel cost [€/Nm^3]

Assuming the plant to have an unique load condition, the rated heat supplied by a methane boiler fed with the aforementioned amount of fuel is given by:

$$TPF = \frac{FQ \cdot LHV_F \cdot \eta_B}{\tau_{op}} \quad (4)$$

where:

- TPF is the rated heat supplied by the boiler [kW]
- τ_{op} is the annual operation time [h/year]
- FQ is the amount of fuel derived by Eq. 3
- LHV is the Lower Heat Value of fuel [kWh/Nm^3]
- η_B is the boiler efficiency

In Tab. 3 the main data adopted in this paper for the analysis of the case study are indicated.

Table 3: Reference values for the main variables

Variables	Values
Functioning hours per year	5,000 h
Methane LHV	9.72 kWh/Nm^3
Boiler efficiency	0.9
Methane cost	0.50 €/Nm^3

The rated heat capacity of the boiler represents the thermal penalty factor, accounting for the capital costs for pipes and heat exchangers, converted into energetic units.

When evaluating the convenience in introducing a match between two streams, A and B, we should consider both the heat recovery potential, Q^{AB} and the penalty associated with the cost for connecting the streams and purchasing the heat exchanger, "$TPF^{AB} = TPF^{AB}_{piping} + TPF^{AB}_{h.exch.}$"; a match is convenient when:

$$Q^{AB} > TPF^{AB} \quad (5)$$

and the quantity "Q-TPF" is a figure of merit for the possible matches, which can be used to define hierarchies between the feasible options, whenever degrees of freedom exist in HEN's design. When Eq. 5 is not fulfilled, matching streams A and B is inconvenient, because the marginal costs for

piping and for the heat exchanger exceed the energetic benefit associated with heat recovery.

The above analysis was extensively applied to the streams of our case study; for each stream, matching with all other streams the TPS was evaluated. In Tab. 4 the results are shown for the hot stream n. 1, which was hypothesized to be matched against all the cold streams.

Table 4: TPF table for stream n. 1

Match with	Nominal length	Add. length	Add. costs	Piping cost	PC_Y [k€]	TPF [kW]
4	80	0	0	40000	20.50	71,8
5	65	0	0	32500	16.66	58,3
6	40	10	9000	34000	17.43	61,0

4. Including "Thermal Penalty Factors" into composite curves

Composite curves are a main theoretic instrument of pinch analysis, aiming at determining energy recovery targets. A composite curve is a single broken line, in a temperature-heat load diagram, that resumes the heat available from hot streams or the heat required from cold fluxes, at different temperatures.

In Fig. 3 the composite curves for the examined 6-streams case study are presented; below each curve and for each specific temperature range, the involved streams are indicated.

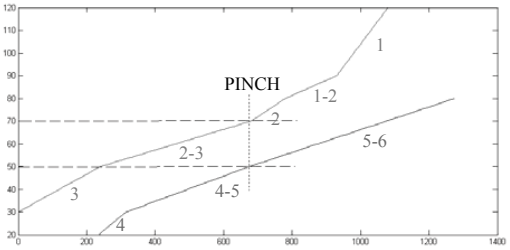

Fig.3. Composite curves for the case study

In order to properly include thermal penalty factors into composite curves, it should be possible to identify, for each temperature interval, the hot streams that could release heat and the cold fluids requiring it; in other words, we should be able to plot, for each interval, all the feasible matches and evaluate their "Q-TPF".

Let us focus, for instance, on the region immediately above pinch (the most constrained), where the only hot fluid, n. 2, could release 100 kW to either the cold streams n. 5 and n. 6, which both require 100 kW; the situation is represented in Fig. 4.

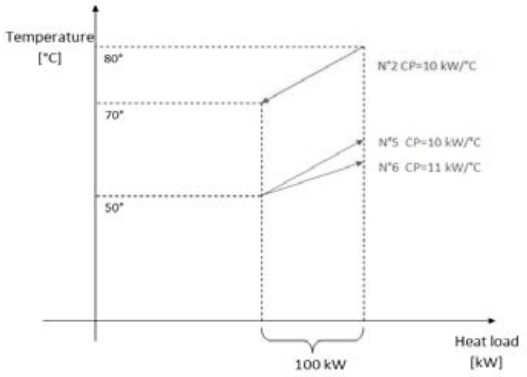

Fig. 4. Zoom on immediately above pinch zone

The so-called "*golden rules of MER design*" provide us with suggestions on the feasible matches. In order to preclude ΔT_{pinch} violations, immediately above the pinch the feasible matches should fulfill the following condition, relating the heat capacity rates:

$$CP_{cold} \geq CP_{hot} \quad (6)$$

In Eq. 6 CP_{cold} and CP_{hot} are respectively the heat capacity flow rate of the cold and the hot matching streams. In our example both the match 2-5 and 2-6 fulfil Eq. 6; the fundamentals of MER design suggest us to prefer the match with the higher CP difference between the streams, in order to minimize heat exchange areas; according to this principle, the match 2-6 should be selected.

Can we rely upon the aforementioned criterion to select the matches to prioritize, with no regard to any secondary implications?

Actually, once the inlet and outlet temperatures of each stream at any match are known, an analytical study for each match can be performed, based on ΔT_{lm}, on a predicted overall heat transfer coefficient U and keeping into account specific design parameters such as the number of shells and the ΔT_{lm} correction factor F; the heat transfer area can be consequently calculated and, basing on Eq. 1, the purchase cost is finally determined and converted into a $TPF_{h.\ exch.}$. A global TPF for each match is calculated by summing up TPF_{piping} and $TPF_{h.\ exch.}$; the values obtained for the examined 2-5 and 2-6 matches are presented in Tab. 5. Because of the small size of the heat exchangers

(areas ≤ 50 m^2), according to Eq. 1 the heat exchangers provided an almost constant 18 kW contribute to the TPF. Consequently, in the following of the analysis the fraction $TPF_{h.exch}$ will not be further analyzed, the attention being focused only on the TPF fraction associated with piping costs.

Table 5. Piping TPF for matches 2-5 and 2-6.

Match	Piping TPF
2-5	50 kW
2-6	70 kW

These penalties could be included into the T-H diagram.

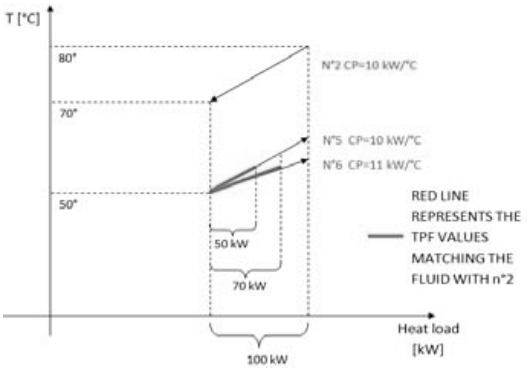

Fig. 5. TPF values immediately above the pinch

In Fig. 5 the TPF values are represented, associated with matching stream n. 2 with both the cold streams n. 5 and n. 6 available immediately above pinch. We may observe that once these values have been represented, the useful "overlap" between the hot and cold streams is fictitiously reduced, thus providing a graphical idea about the most convenient match.

Immediately below the pinch golden rules for MER design suggest to not use heating utilities, thus being needed to match all the cold fluxes with hot fluxes leading them to the target temperature. The CP condition is here expressed as follows:

$$CP_{hot} \geq CP_{cold} \quad (7)$$

Looking at the composite curves plotted in Fig. 3, it is evident that the cold streams n. 4 and n. 5, with a CP respectively equal to 8.0 and 10.0 kW/°C, could lead to different matches with the hot streams n. 2 and n. 3, respectively with a CP equal to 10.0 and 12.0 kW/°C. Both the solutions "match 2-4 and match 3-5" and the solution "match 3-4 and match 2-5" fulfill Eq. 7, being impossible to identify, a priori, the best option; in few words, we have a degree of freedom in network design. Let us now introduce the TPFs and verify whether they allow to introduce a hierarchic order between the feasible designs; the global TPFs are shown in Tab. 6.

Considering the two alternative designs, we get:

- Design 1: adopting the matches 3-4 and 2-5 the TPF is 150 kW;
- Design 2: if we choose matches 2-4 and 3-5 the TPF is 80 kW.

When two alternative designs achieve the same energy saving Q, the objective to *maximize "Q-TPF"* can be intended as *minimize TPF*.

Table 6. Piping TPF for the feasible matches immediately below the pinch.

Match	Piping TPF	Match	Piping TPF
4-2	60 kW	**5-2**	50 kW
4-3	100 kW	**5-3**	20 kW

This is not the case: adopting the match 3-4 would increase the energy recovery by 40 kW (240 kW saved, instead of 200 achieved by Design 2); however, passing from Design 2 to Design 1 the total TPF would increase much more. The Design 2 can be therefore identified as a preferable option, as will be seen in section 5. In Fig. 6 the quantities "Q-TPF" are graphically compared for both the examined options.

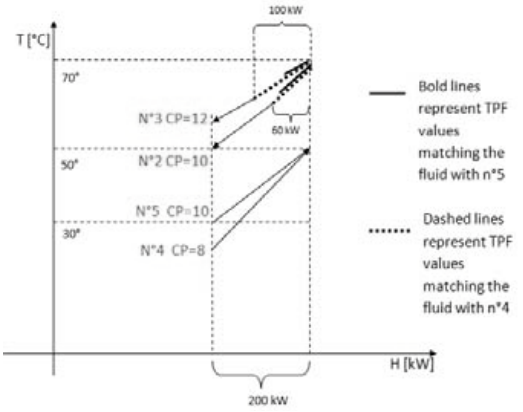

Fig. 6. Piping TPF values immediately below the pinch

5. MER design vs TPF design

Let us now compare the results obtained by the proposed TPF-based approach with those that might have been achieved by a conventional MER design; a 20°C ΔT_{pinch} was assumed in both cases. We could expect the MER design to lead to maximum energy savings, but to a much more complex topology of the physical network.

5.1. MER design for the case study

For such a simple problem, the MER design can be easily obtained by applying the so-called golden rules and the tick-off heuristics, oriented to minimize the number of units. The final lay-out is presented in Fig. 7.

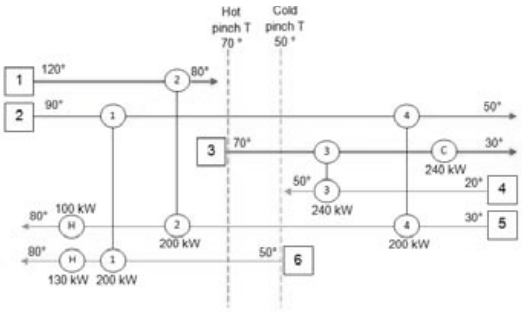

Fig. 7. MER lay-out for the case study.

MER rules below the pinch suggest to match the stream n. 4 with the n. 3, to save 240 kW (by the match 4-2 only 200 kW could have been recovered). A complete simulation of the MER design led to calculate the values in Tab. 7; in Fig. 8 the stream paths along the plant area are plotted.

Tab.7: Results for MER design

Heat recovery	840 kW
Hot utilities	230 kW
Cold utilities	240 kW
Heat exchanger 1 area	48 m^2
Heat exchanger 2 area	26 m^2
Heat exchanger 3 area	49 m^2
Heat exchanger 4 area	50 m^2
Total area	173 m^2
Total Thermal Penalty Factor	294 kW

5.2 TPF design for the case study

As observed in the previous sections, the final objective of a TPF-based pinch analysis consists of finding the optimal compromise between the marginal energy savings and capital costs (related to piping connections and heat exchangers) between two or more alternatives. Again design is split in two subproblems at the pinch.

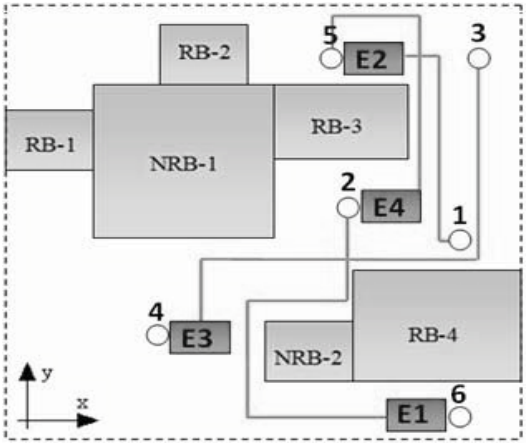

Fig. 8. Executive lay-out for MER design.

With reference to the case study, above the pinch the solution “match 2-5 and match 1-6” achieves a 400 kW energy saving with a 135.6 global TPF; it is then preferred to the alternative solution “match 2-6 and match 1-5”, which would have achieved the same energy saving with a 143.8 kW TPF.

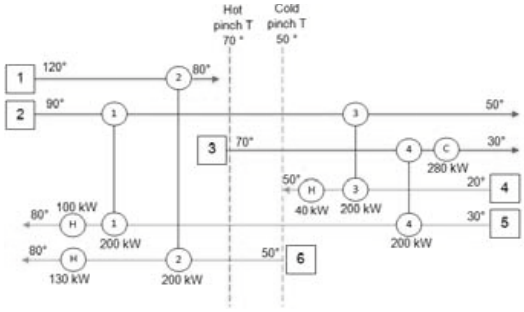

Fig. 9. TPF lay-out for the case study.

Similarly, below the pinch the solution “match 3-4 and match 2-5” achieves a 440 kW energy recovery, with a 150 kW global TPF; then, it is worse than the alternative solution “match 2-4 and match 3-5”, which although achieves a lower energy recovery target, 400 kW, lead us to a much

lower value of the global TPF (i.e. 80 kW). Then a supertargeting approach induces us to prefer this latter option, being the lay-out topology more cost-influencing than the energy recovery target. The grid diagram for the TPF-based design is presented in Fig. 9, while the associated results are shown in Tab. 8.

Table 8: Results for the TPF-based design

Heat recovery	800 kW
Hot utilities	270 kW
Cold utilities	280 kW
Heat exchanger 1 area	50 m^2
Heat exchanger 2 area	25 m^2
Heat exchanger 3 area	37 m^2
Heat exchanger 4 area	47 m^2
Total area	159 m^2
Total Thermal Penalty Factor	230 kW

Fig. 10 shows that the executive lay-out obtained with a TPF-based supertargeting method results much less complex than the design achievable through a simple pinch analysis. In "real world" applications it is expected the simplification of the HEN design to be highly appreciable also due to unquantifiable objectives.

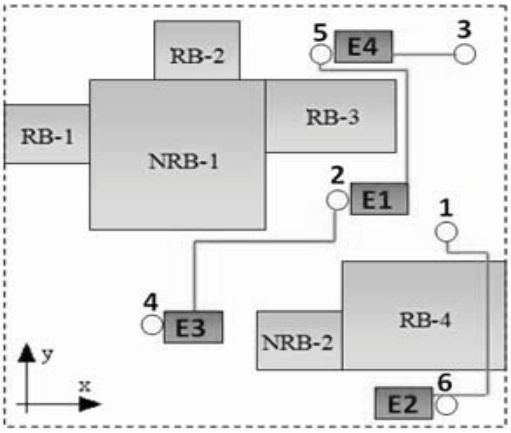

Fig.10 Executive lay-out for TPF design

6. Conclusions

An innovative approach was proposed to internalize cost-influencing topological variables in the heat exchanger network optimization process. The method represents an extended supertargeting, where the cost of piping-connections is summed up with heat exchangers' cost. Streams far on the site map are thus assigned a "thermal penalty", enabling the analyst to take more accurate decisions whenever some freedom degrees exist. With reference to the case study examined in this paper, the method led to relevant simplifications in the resulting HEN lay-out. Further efforts will be needed in the future to fully extend the integration between the traditional pinch techniques and the use of thermal penalty factors.

Nomenclature

A heat transfer area, m^2
CP heat capacity flow rate, kW/°C
F ΔT_{LM} correction factor
FQ fuel quantity, Nm^3
c_F fuel cost, €/Nm^3
HEC heat exchanger cost, €
HEN heat exchanger network
HP_B boiler heat power, kW
LHV lower heat value, kWh/m^3
NRB non removable barrier
MER maximum energy recovery
PC_Y piping cost per year, €
Q heat load, kW
RB removable barrier
TPF thermal penalty factor
U global heat transfer coefficient, kW/m^2°C
ΔT_{LM} log mean difference of temperature
η_B boiler efficiency
τ_{op} functioning hours per year

References

[1] Kemp, I. C., 2007, *Pinch Analysis and Process Integration*, Butterworth-Imprint of Elsevier, Oxford, UK.

[2] Asante, N. D. K., and Zhu, X. X., 1997, An automated and interactive approach for heat exchanger network retrofit, Trans. IChemE, 75(3), pp. 349-360.

[3] Serth, R. W., 2007, *Process Heat Transfer – Principles and Applications*, C Academic Press – Imprint of Elsevier, Oxford, UK.

Retrofit Model with Relocation for Heat Exchanger Network Design

Noppanat Rueangul[a], *Kitipat Siemanond*[a], *Sira Nukulkit*[b]

[a] *The Petroleum and Petrochemical College, Chulalongkorn University, Thailand*
[b] *The Department of Civil Engineering, Chulalongkorn University, Thailand.*

Abstract: This paper proposes a solution method based upon mathematical programming for Heat Exchanger Network (HENs) retrofit. Retrofit of HENs is among the common projects to reduce the plant operational cost including utility cost. Retrofit design consists of four features such as additional or removal heat exchanger area, adding new heat exchanger, repiping and splitting. Four features were used to retrofit heat exchanger network in retrofit by GAMS and Visual C++. This research consists of two steps (retrofit and relocation). Stage model (MILP) by Yee and Grossmann (1990) was used to develop the model. Not only minimization of utility cost, but also minimization of exchanger area are concerned. Example problems from literatures are used to demonstrate the effectiveness of the approach in terms of the solution quality and time.

Keywords: Retrofit, Heat Exchanger Network Design.

1. Introduction

Heat exchanger networks (HENs) are widely used in many process industries for the purpose of maximizing heat recovery and reducing utility consumption and investment cost.

Retrofit studies are still actively pursued to further improve energy recovery. It was reported that 70% of the projects conducted in the industry involved process retrofit. There are two main streams of the research regarding heat exchanger network (HEN) retrofit. One is based on thermodynamic analysis, namely Pinch Analysis and the other is relied on Mathematical Programming.

Using mathematical programming for HENs retrofit does not require too much expertise and this method can optimize the problem by handling different kinds of constraints simultaneously. HEN retrofit problem is basically a Mixed Integer Non–Linear Programming (MINLP) problem of the non–linearity of the exchanger area equations.

Many researches tried to get the best solution by solving one single MINLP model and this method has still not yet succeeded. Because of this, the problem is normally simplified as a Mixed Integer Linear (MILP) model by imposing some assumption.

The purpose of this work is to avoid nonlinear equation and develop a model using GAMS (General Algebraic Modeling System) to minimize utility cost, number of heat exchanger and investment. GAMS is the main tool for developing model. Stage model by Yee and Grossmann (1990) is developed by GAMS. The whole set of equations were modeled using GAMS and solved by using the MILP solver. The retrofit solution provides the additional area required for the base case HEN.

2. Mathematical Software

Ma et al. **[5]** proposed an MILP model that can solve the HEN retrofit in one single step. The model adopted the stage-wise superstructure from Yee and Grossmann (1990), which takes into account the energy consumption; network structural modifications as well as new exchanger areas were considered implicitly by setting a minimum approach temperature in order to remove the non-linearity of exchanger area calculation. With this simple model, good alternative design are quickly determined. The drawback of this approach was

that exchanger areas were not considered explicitly inside the model; therefore, further optimization was required for the selected network. The details of the formation are presented as follows:

2.1 Overall heat balance for each stream:

$$(Tout_j - Tin_j)F_j = \sum_{k\in ST}\sum_{i\in HP} q_{ijk} + qhu_j \quad j\in CP \quad .....(1)$$

$$(Tin_i - Tout_i)F_i = \sum_{k\in ST}\sum_{j\in CP} q_{ijk} + qcu_i \quad i\in HP \quad .....(2)$$

2.2 Heat balance of each stream at each stage:

$$(t_{j,k} - t_{j,k+1})F_j = \sum_{i\in HP} q_{ijk} \quad j\in CP,\ k\in ST \quad .....(3)$$

$$(t_{i,k} - t_{i,k+1})Fi = \sum_{j\in CP} q_{ijk} \quad i\in HP,\ k\in ST \quad .....(4)$$

2.3 Assignment of superstructure inlet temperature:

$$Tin_j = t_{j,N+1} \quad j\in CP \quad .....(5)$$

$$Tin_i = t_{i,1} \quad i\in HP \quad .....(6)$$

2.4 Feasibility of temperature

$$t_{j,k} \geq t_{j,k+1} \quad j\in CP\ k\in ST \quad .....(7)$$

$$Tout_j \geq t_{j,1} \quad j\in CP \quad .....(8)$$

$$t_{i,k} \geq t_{i,k+1} \quad i\in HP\ k\in ST \quad .....(9)$$

$$Tout_i \leq t_{i,N+1} \quad i\in HP \quad .....(10)$$

2.5 Hot and cold utility load:

$$(Tout_j - t_{j,1})F_j = qhu_j \quad j\in CP \quad .....(11)$$

$$(t_{i,N} - Tout_i)F_i = qcu_i \quad i\in HP \quad .....(12)$$

2.6 Logical constraints:

$$q_{ijk} - \Omega_p Y_{ijk} \leq 0 \quad i\in HP\ j\in CP\ k\in ST \quad .....(13)$$

$$qhu_j - \Omega_p Y_{hj} \leq 0 \quad j\in CP \quad .....(14)$$

$$qcu_i - \Omega_c Y_{ic} \leq 0 \quad i\in HP \quad .....(15)$$

Y_{ijk}, Y_{hj}, Y_{ic} are binary variables.

2.7 Feasible driving force:

$$dt_{ijk} \leq t_{i,k} - t_{j,k} + \Gamma_{ij}(1 - Y_{ijk}) \quad i\in HP, j\in CP, k\in ST \quad .....(16)$$

$$dt_{ijk} \leq t_{i,k+1} - t_{j,k+1} + \Gamma_{ij}(1 - Y_{ijk}) \quad i\in HP, j\in CP, k\in ST \quad .....(17)$$

$$dt_{ijk+1},\ dthu_j \text{ and } dtcu_i \geq EMAT \quad i\in HP, j\in CP, k\in ST \quad .....(18)$$

The above constraints are used to model the heat flows of stage-wise superstructure and restricted all heat exchange approach temperatures of the required matches to be larger or equal to the Exchanger Minimum Approach Temperature (EMAT).

2.1 Objective function

Finally, the objective function is defined as minimizing the total cost for the network. The total cost involves the utility cost, and the fixed charges for the exchangers,

The objective function is defined as follows:

$$\sum C_{CU} \cdot qcu_i + \sum C_{HU} \cdot qhu_j + \sum\sum\sum C_{ijk} \cdot z_{ijk} + \sum C_{i,CU} \cdot zcu_{ijk} + \sum C_{j,HU} \cdot zhu_j$$

$$i\in HP, j\in CP, k\in ST \quad .....(19)$$

Nomenclature

Indices

i hot process stream in retrofit network

j cold process stream in retrofit network

k stage in retrofit network 1,…,N and temperature location 1,…,N+1

h hot utility

c cold utility

Sets

HP i|i is a hot process stream

HU hot utility. s

CP j|j is a hot process stream

CU cold utility, s

ST k|k is the stage in superstructure, k=1,…,N

Parameters

Tin inlet temperature of stream (C)

Tout outlet temperature of stream (C)

A heat exchanger area (m^2)

F heat capacity flow rate (kW/ C)

N total number of stages

C.CU cold utility cost ($/ kw)

C.HU hot utility cost ($/ kw)

$C.F_{i,CU}$ constant fixed cost of cooler ($/ exchanger unit)

$C.F_{i,HU}$ constant fixed cost of heater ($/ exchanger unit)

$C.F_{i,j}$ constant fixed cost of exchanger ($/ exchanger unit)

Ω upper bound for heat exchanged

Γij upper bound for temperature difference between stream i and j

Γhj upper bound for temperature difference between hot utility h and stream j

Γic upper bound for temperature difference between stream i and cold utility c

Binary Variables

Y_{ijk} required process match (i,j,k) in retrofit network

Y_{hj} required hot utility match (h,j) in retrofit network

Y_{ic} required cold utility match (i,c) in retrofit network

Variables

dt_{ijk} temperature approach for match (i,j) at temperature location k

q_{ijk} heat exchanged for match (i,j) in stage k (kw)

qhu_j heat exchanged for hot utility match (h,j) (kw)

qcu_i heat exchanged for cold utility match (i,c) (kw)

$t_{i,k}$ temperature of hot stream i at temperature location k (C)

$t_{j,k}$ temperature of cold stream j at temperature location k (C)

z_{ijk} a binary variable of existing of exchanger matches between hot (i) and cold (j) streams at stage k .

zcu_{ik} cold utility matching at stream i at stage k

zhu_{jk} hot utility matching at stream j at stage k

3. Retrofit Procedure for HEN Design

The procedure for HENs retrofit consists of two steps, retrofit step, and relocation step as shown in Figure 3.1

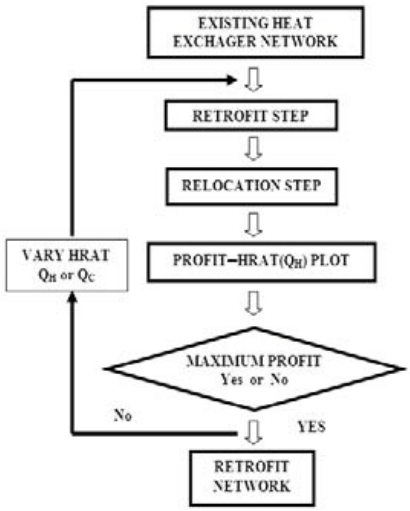

Fig. 3.1 Flow chart to fund optimal retrofitted HEN.

Heat exchanger network design has four features including additional or removal area, add new heat exchanger, moving heat exchanger to other matching (repiping) and splitting.

3.1 Retrofit Step

Retrofit step is the procedure including additional or removal area, new heat exchanger and splitting. This step reduces the HRAT or overall hot/cold utility and generates the retrofit design HEN structure using stage model with MILP (Mixed integer linear programming). This step also finds the best HEN structure for minimum utility cost and fixed cost of exchanger with a constraint of fixing the position of heat exchanger, as shown in equation 20.

Retrofit constraint using the base-case exchangers for the retrofit case

$$Zijk \geq 1 \qquad \ldots\ldots\ldots(20)$$

Where Zijk is a binary variable of existing of exchanger matches between hot(i) and cold(j) streams at stage k .

3.2 Relocation Step

For relocation, it shows where the base case exchanger are used or relocated in the retrofit case.

3.2.1 Relocation with Concept 1

(based on minimum area difference between the base case and the retrofit exchangers)

The relocation of the base-case exchanger to the new location of the retrofit occurs when the minimum area difference between the base-case exchanger and one from the retrofit case is found. The relocation procedure will be applied to the rest of base-case exchangers for moving them to new location of retrofit case. This technique is trying to reuse all base-case exchangers with additional or removal area algorithm for the retrofit case. The relocation is done by using Microsoft Visual C++ and a flow diagram of this concept is shown in Figure 3.2.

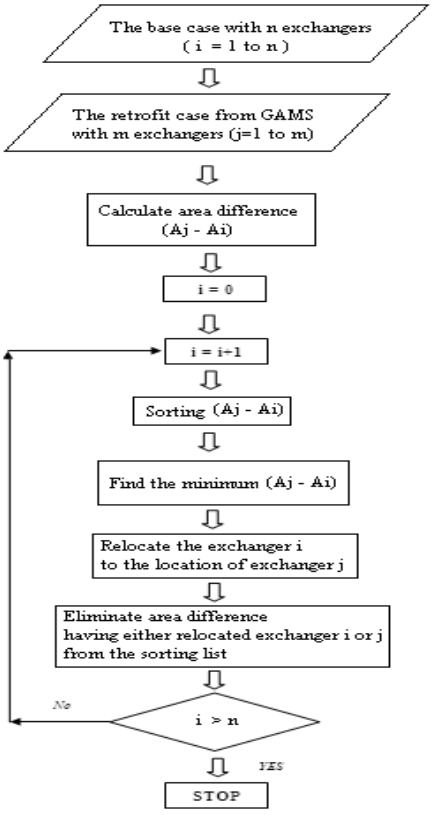

Fig. 3.2 Flow chart of relocation concept 1.

where

(Ai =Exchanger no. i of the base case

Aj = Exchanger no. j of the retrofit case)

3.2.2 Relocation with Concept 2

(based on fixed exchanger matches of the base-case exchangers)

Relocating the base-case exchanger to the new match between hot and cold streams has costs to pay. In this concept, the base-case exchangers with their matches are reused in the retrofit case to save the relocation cost. Flow diagram of this concept is shown in Figure. 3.3

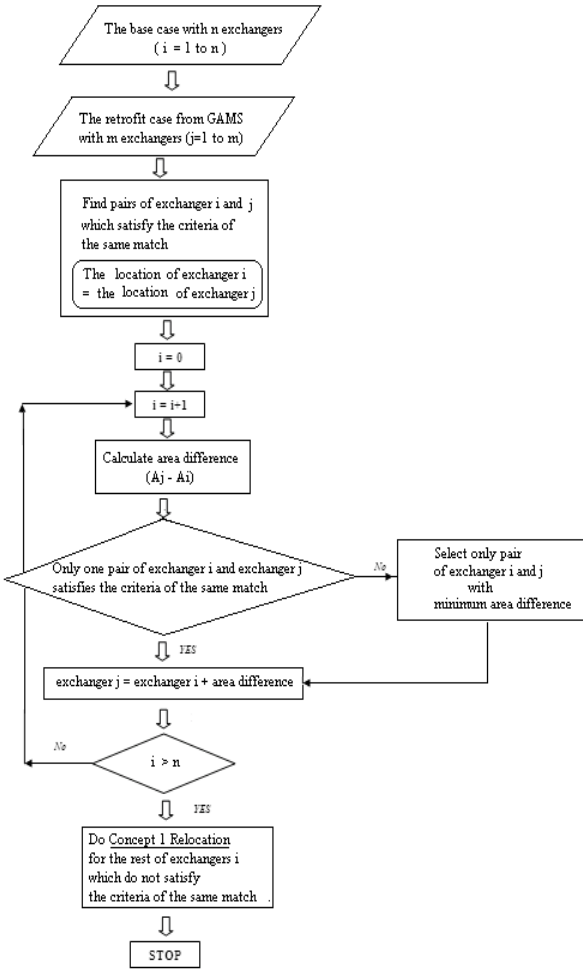

Fig. 3.3 Flow chart of relocation concept 2.

4. Result and Discussion

This example is to do retrofit the base-case HEN from the research of Abdelbagi Osman, M.I. Abdul Mutalib, M. Shuhaimi and K.A. Amminudin **[6]**. They studied the retrofit design by paths combination method. The base-case

HEN consists of two hot and three cold streams, as shown in Figure 4.1. The hot and cold utility consumptions of the existing network are 11,275 kW and 9,267 kW, respectively, as shown composite curves of Figure 4.2, corresponding to heat recovery approach temperature (HRAT) = 27 C and exchanger minimum approach temperature (EMAT) = 7.7 C. Detail information of the base-case; such as heat exchanger area, heat load, etc is shown in Table 4.1 and 4.2.

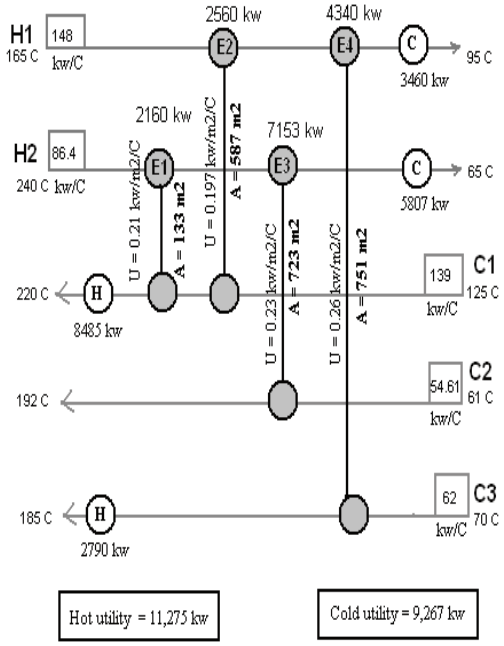

Fig. 4.1 Grid diagram of the base-case HEN..

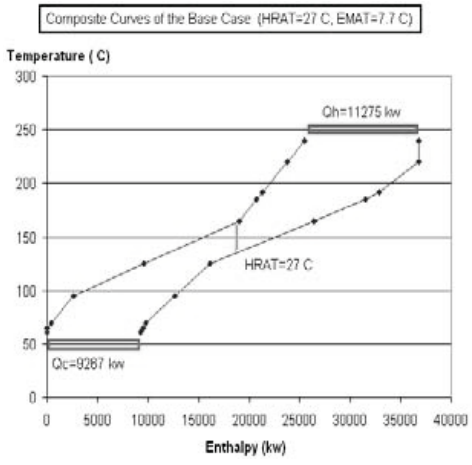

Fig. 4.2 Composite curves of the base-case HEN.

Table 4.1. Information of the base-case exchangers.

UNIT	Heat Exchanger Area(m^2)	Heat Load (kW)
E1	133	2160
E2	587	2560
E3	723	7153
E4	751	4340

Table 4.2 Data of hot and cold streams.

Stream	TIN (°C)	TOUT (°C)	FCp (kW/°C)	h (kW/m^2°C)
H1	165	95	148	0.45
H2	240	65	86.4	0.55
C1	125	220	139	0.35
C2	61	192	54.6	0.40
C3	70	185	62	0.64

The economic data used for calculating profit of the retrofitted HEN are shown below;

- *Cost ($) = 6,600+670(Area)$^{0.83}$* for all new exchanger, *Area in m^2*
- *Cost ($) = 670(ΔArea)$^{0.83}$* for addition of area in existing heat exchanger
- Life time = 2.5 years
  (from economic analysis of the project)
- % annual interest = 0
- Hot utility cost = 120 $/kW/year
- Cold utility cost = 20 $/kW/year

The profit of the retrofit case is calculated by eq. 21:

Profit=Utility saving cost - New exchanger cost-Added area cost .....(21)

The base-case HEN is retrofitted by using retrofit model of GAMS with MILP (Mixed Integer Linear Programming) and the relocation program with concept 1 and 2 using Visual C++. The retrofitted HEN at different HRAT are generated by the retrofit model. Applying the program of the relocation concept 1, the profit of retrofitted HEN at different HRAT (or hot utility) are plotted as shown in Figure 4.3. And the

optimal retrofitted HEN with relocation concept 1 is found as shown in Figure 4.4, giving the maximum profit of $ 1,000,000 in 2.5 years.

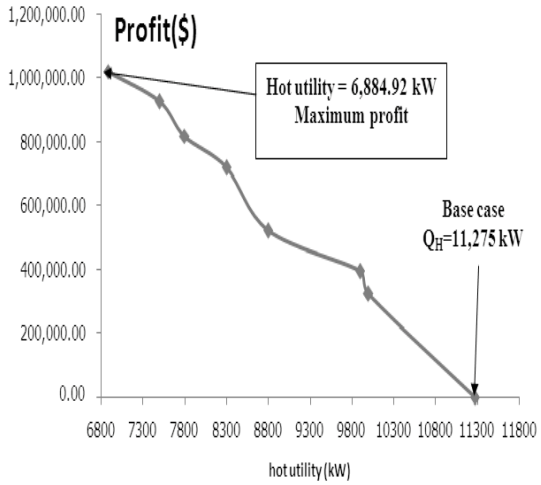

Fig. 4.3 Total profit as a function of hot utility of the retrofit cases with relocation concept 1.

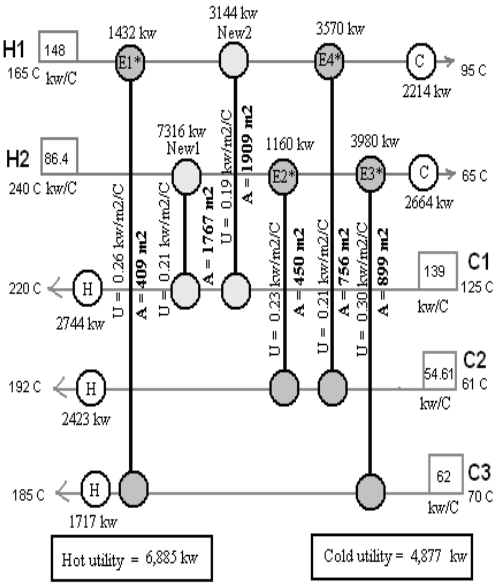

Fig. 4.4 Grid diagram of the optimal retrofit case with relocation concept 1.

The optimal retrofit case consumes hot and cold utilities of 6,885 and 4,877 kw, respectively, with HRAT = 7.7 C, as shown in the composite curves of Figure 4.5.

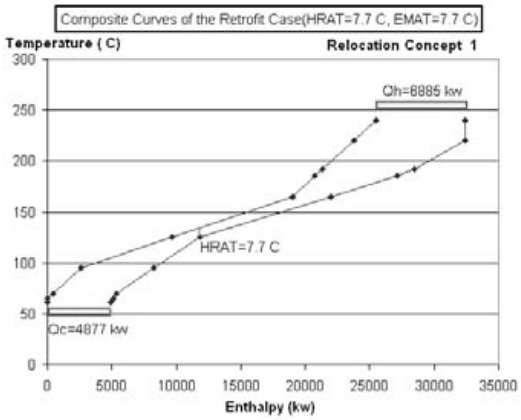

Fig. 4.5 Composite curves of the optimal retrofit case with relocation concept 1.

The relocated and new exchangers of the retrofit case with relocation concept 1 is shown in Table 4.3.

Table 4.3 Result of the optimal retrofit case with relocation concept 1.

.UNIT	Heat Exchanger Area (m^2)	Heat Load (kw)	Area Cost ($)
E1*=E1+276 m^2	409	1,432.507	71,126.156
E2*=E2-138 m^2	450	1,159.994	-
E3*E3+175 m^2	899	3,980.093	48,730
E4*=E4+14 m^2	756	3,569.507	5,989.09
New1	1,767	3,144.305	338,709.38
New2	1,909	7,316.274	360,714.51

** = relocated exchanger, New = new exchanger*

For the retrofit case with relocation concept 2, the retrofitted HEN at different HRAT are generated by the retrofit model. Applying the program of the relocation concept 2, the profit of retrofitted HEN at different HRAT (or hot utility) are plotted as shown in Figure 4.6. And the optimal retrofitted HEN with relocation concept 2 is found as shown in Figure 4.7, giving the maximum profit of $ 900,000 in 2.5 years.

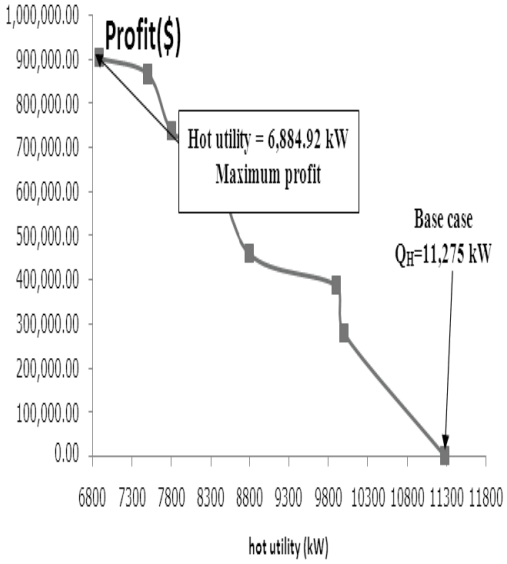

Fig. 4.6 Total profit as a function of hot utility of the retrofit cases with relocation concept 2.

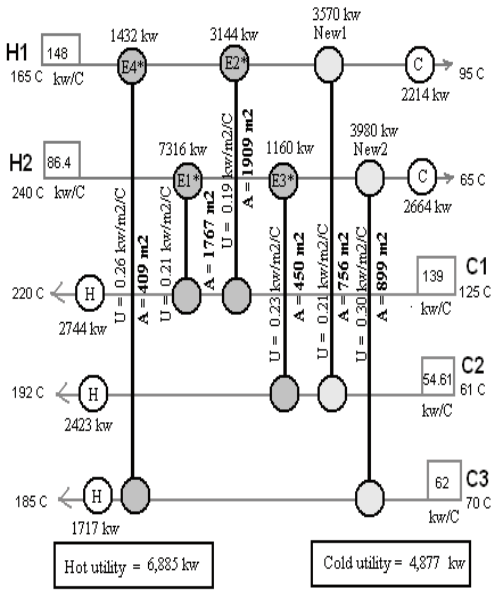

Fig. 4.7 Grid diagram of the optimal retrofit case with relocation concept 2.

The optimal retrofit case consumes hot and cold utilities of 6,885 and 4,877 kw, respectively, with HRAT = 7.7 C, as shown in the composite curves of Figure 4.8.

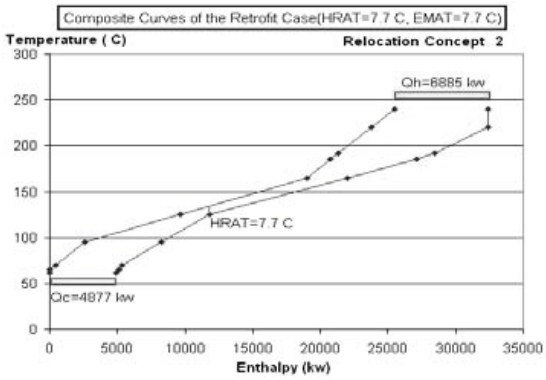

Fig. 4.8. Composite curves of the optimal retrofit case with relocation concept 2.

The relocated and new exchangers of the retrofit case with relocation concept 2 is shown in Table 4.4.

Table 4.4 Result of optimal retrofit case with relocation concept 2.

UNIT	Heat Exchanger Area (m^2)	Heat Load (kw)	Area Cost ($)
E1*=E1+1635m^2	1,767	1,432.507	311,382.74
E2*=E2+1321 m^2	1,909	1,159.994	260,870
E3*E3-273 m^2	450	3,980.093	-
E4*=E4-343 m^2	409	3,569.507	-
New1	756	7,316.274	172,552.84
New2	899	3,144.305	196,487.50

** = relocated exchanger, New = new exchanger*

5. Conclusion

In this work, an MILP model is formulated for HEN retrofit. This model simultaneously considers the utility saving cost, structural modification, new area cost and additional area cost. To overcome the nonlinear problems, a two−step approach is presented. In the first step; retrofit step, it finds the retrofitted network and the second step; relocation step, it indicates where the base-case heat exchangers are relocated. It consists of relocation concept 1 and 2. For this example, the concept 1 is quite better than concept 2 because it gives more profit, as shown in Table 4.5.

Table 4.5 Comparison of the retrofit results between optimal retrofit case with relocation concept 1 and 2.

Options	Hot Utility		Cold Utility		
Retrofit with relocation	Q_H	saving (%)	Q_C	saving (%)	Profit ($)
Concept1 (Fig. 4.4)	6,884.92	38.94	4,877.32	47.37	1,000,000
Concept2 (Fig. 4.7)	6,884.92	38.94	4,877.32	47.37	900,000

Options	Additional area requirement [m^2]						Total Area (m^2)
Retrofit with relocation	E1	E2	E3	E4	New1	New2	
Concept1 (Fig. 4.4)	276	-138	175	14	1,767	1,909	6,190
Concept2 (Fig. 4.7)	1,767	1,909	450	409	756	899	6,190

6. References

[1]. T.N. Tjoe, B. Linnhoff, Using pinch technology for peocess retrofit, Chemical Engineering 93 (1986) 47-60.

[2]. A.R. Ciric, C.A. Floudas, A retrofit approach for heat exchanger networks, Comput. & Chem. Eng. 13 (6) (1989) 703-715.

[3]. A.R. Ciric, C.A. Floudas, A mixed integer nonlinear programming model for retrofitting heat–exchanger networks, Ind. Eng. Chem. Research 29 (2) (1990) 239–251.

[4]. T.F. Yee and I.E. Grossmann., (1990). Simultaneous Optimization Models for Heat Integration−II. Heat Exchanger Network Synthesis. Computers chem. Eng, Vol.14, No.10, pp.1165−1184, 1990.

[5]. R. Ma, T.F. Yee, C.W. Hui, A simultaneously method for heat exchanger network retrofit, in: Proceedings of the 1st Conference on Process Integration, Modeling and Optimization for Energy Saving and Pollution Reduction (PRES'98), Praha, Czech Republic, 23–28 August, 1998.

[6]. Abdelbagi Osman, M.I. Abdul Mutalib, M. Shuhaimi and K.A. Amminudin. Paths combination for HENs retrofit. Applied Thermal Engineering 29 (2009) 3103–3109.

Acknowledgments: Authors would like to express our gratitude to the Government Budget, the Petroleum and Petrochemical College, Chulalongkorn University, and Center for Petroleum, Petrochemical, and Advanced Materials for funding support. In addition, we would like to acknowledge with thanks the valuable contribution of Prof. Miguel Bagajewicz in educating us mathematical programming, GAMS.

Supertargeting-based hierarchic evaluation for setting paths in relaxation of retrofitted Heat Exchanger Networks

Antonio Piacentino[a], Raffaele Imperato

[a] *Dpt. of Energetic and Environmental Researches, University of Palermo, Palermo, Italy*

Abstract: The application of pinch analysis to the retrofit of existing heat exchanger networks is a complex task, which can be hardly standardised due to the large number of unquantifiable design considerations. Top-down and bottom-up approaches have been usually pursued, respectively oriented to relax a Maximum Energy Recovery (MER) configuration and to improve the existing network by removing network pinches. In this paper the bottom-up approach is critically examined, considering a well known case study represented by an aromatics plant; a MER design is also obtained and evaluated, to represent a target for process improvement. The final objective of researches in this sector is the identification of preferential routes for the improvement of the existing network. In this paper several retrofit routes are investigated, identifying six solutions that lead to a small number of topology changes. For each solution, a detailed thermal analysis provided the size, the number of shells and the temperature profiles associated with the operation of any heat exchanger; the solutions were relaxed to reduce the number of new units and the relaxed configurations were also evaluated. An analysis of the payback time associated with any retrofit option let us recognize that preferential routes could be identified by a preliminary evaluation of marginal costs.

Keywords: pinch analysis, heat recovery network, retrofit, relaxation, optimization

1. Introduction

Pinch technology represents a comprehensive approach to the optimization of heat exchanger networks (HENs), aiming at determining energy recovery targets and assessing qualitatively and quantitatively the hot and cold utilities. Basic instruments are represented by the Composite Curves (CCs), the problem table and the Grand Composite Curve (GCC). With respect to mathematical programming techniques, pinch analysis preserves the valuable role of analyst's expertise, through a highly interactive procedure; once identified the targets, in fact, the extrapolation of a feasible network design requires a someway "manual" procedure which offers to the analyst some freedom degrees.

Even when the ΔT_{min} is evaluated through super-targeting (i.e. minimization of a total cost associated with the heat exchange area and the energy consumption), the Maximum Energy Recovery (MER) network is usually an inconvenient solution for practical reasons [1]. It could eventually include very small exchangers or non-feasible exchanges; hence, relaxing the MER network, thus renouncing to achieve the heat recovery targets, is usually convenient.

In the case of retrofit of existing networks, this phase is very delicate; revolutioning completely the network topology and dismissing all or most of the existing heat exchangers could dramatically affect the economic viability of the project, with respect to more conservative solutions. Bottom-up and top-down strategies, respectively moving in the "Existing HEN→MER design" and in "MER design→ Existing HEN" directions, have been widely explored in literature [2]; search algorithms for optimal paths are required [3].

As shown in [4], the retrofit of existing systems requires optimizing the number $n^{\Delta top}$ of topology changes; at a fixed $n^{\Delta top}$, a "retrofit curve" can be plotted, providing the energy consumption (or, equivalently, the energy saving) versus the heat transfer area A. The retrofit curve also provides an energy saving target $Sav_{max}(n^{\Delta top})$, which obviously increases with $n^{\Delta top}$; two main problems remain:

1. For complex lay-outs the retrofit curve is not easy to determine. Once fixed, for instance, $n^{\Delta top}=2$, depending on the two particular changes made, the representative point can either lie or not on the "$n^{\Delta top}=2$ retrofit curve";
2. If minimization of the total cost (i.e. sum of the cost fractions associated with energy consumption by the utilities and capital cost of

Corresponding Author: Antonio Piacentino, Email: piacentino@dream.unipa.it

plant retrofit) is pursued, according to an approach usually named as supertargeting, an optimal $n^{\Delta top}$ will exist, which might be determined by trading off capital and energy costs.

In few words, the above problems pose us the following questions:

- How to identify the optimal network, at a given $n^{\Delta top}$?
- How to select $n^{\Delta top}$?

In this paper the authors attempt answering these questions by an inductive approach, i.e. starting from the analysis of a case study. A hierarchic evaluation of a number of retrofit solutions will be made, based on cost supertargeting, on accurate expressions for the investment cost and the real number of shells, N_s, and on detailed area targeting [5]. Although this article is focused on a bottom-up approach, in Section 3 a detailed diagnosis of a MER design will be performed to recognize margins for relaxation. In Section 4 the focus will be entirely posed on the feasible routes for the improvement of the existing network.

2. Case study: an aromatics plant

A large number of facilities have been analysed in literature by pinch analysis, revealing the large efforts of researchers as concerns one of the most delicate phase of pinch study, i.e. data extraction. Being this paper devoted to the analysis of retrofit criteria, referring to a well known and complex case study first presented in [6] seemed convenient. The examined aromatics plant is schematically presented in Fig. 1, with the associated grid diagram of the existing heat recovery network in Fig. 2. In [1] an accurate description of the plant is provided.

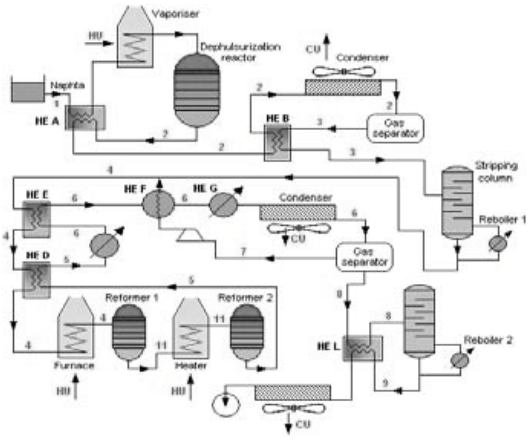

Fig. 1. Schematic of the aromatics plant.

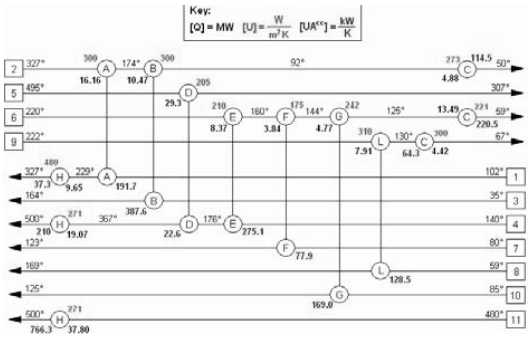

Fig. 2. Grid diagram of the existing HEN.

Some streams undergo phase change and significant changes of the rated heat capacity along their evolution; in the following of this paper we will refer to the data disaggregation level emerging from the existing HEN. The column reboilers are not included in the analysis because modifications in the fractioning process at the columns are not considered, thus leading to constant heat loads on these specific hot utilities.

3. Maximum energy recovery design

The minimum ΔT (10°C) in the existing HEN occurs at the hot side of Heat Exchanger (HE) B. As observed in [1], assuming a ΔT_{pinch}=10 °C there is scope for a 12.44 MW saving; this result can be immediately obtained by any simple worksheet like [7].

3.1. Determining a MER configuration

MER design can be easily obtained by applying well established rules and methods. Starting at the pinch, i.e. the most constrained point, we move toward the "far from pinch" regions, always fulfilling the so-called *golden rules*, i.e. avoiding to use cold utilities above pinch or hot utilities below pinch and to transfer heat across pinch. In order to minimize the number of units, the so-called "*tick-off heuristics*" is applied. In our case, pinch is located at 145 °C (i.e. at 150 °C on the hot streams side and at 140 °C on the cold stream side). The obtained MER design is presented in Fig. 3.a,b, respectively for the above and below pinch regions.

3.1. Diagnosis of the MER solution

In order to assess whether the obtained MER configuration represents a good solution, we should compare it with the feasible targets. The main risk is to have achieved a system with a

number of units higher than the minimum feasible, because the examined plant has a large near pinch region, which often did not allow the application of the "tick-off heuristics".

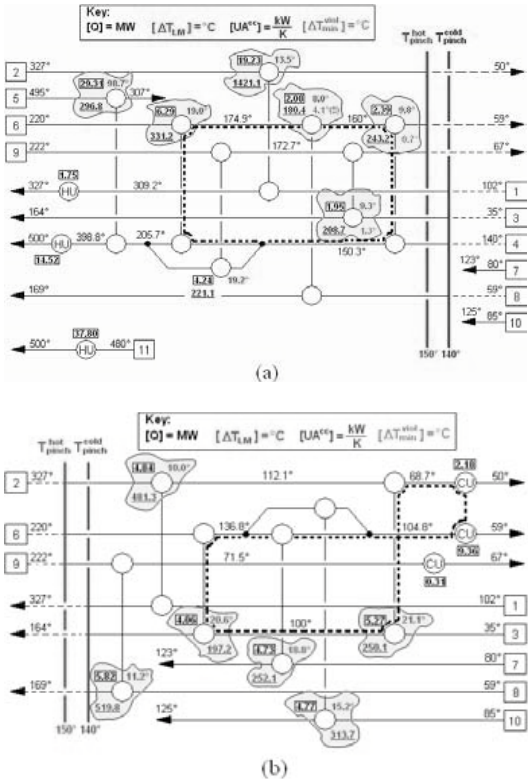

Fig. 3. MER design: a) above pinch, b) below pinch.

Actually, we get:

$$U_{network} = U_{HE} + U_{he-u} = 19 \quad (1)$$

$$U_{min,MER} = (l-1)_{above\ pinch} + (l-1)_{below\ pinch} = 17 \quad (2)$$

with an "$U_{network}$-$U_{min,MER}$=2" redundancy, related to the presence of the two loops indicated in bold hatched line in Fig. 3.a,b. A clear diagnosis, however, requires also comparing the heat transfer area and the number of shells of the MER design with the relative targets.

Setting up the targets requires the implementation of two procedures, clearly described in [8]. The minimum number of shells, N_s^{min}, is here determined by the so-called analytical method, consisting of a procedure in three phases:

1. The composite curves are divided into enthalpy intervals, as shown in Fig. 4, and, for each interval, the terminal temperatures are used;
2. The N_s for each interval is determined by assuming that the ΔT_{lm} correction factor, F, maintains higher than 0.8. Assuming TEMA E-type shells connected in series and the hot fluid in the shell side, we must ensure values of P and R, defined as:

$$P = \frac{T_{c,o} - T_{c,i}}{T_{h,i} - T_{c,i}} \qquad R = \frac{T_{h,i} - T_{h,o}}{T_{c,o} - T_{c,i}} \quad (3.a,b)$$

such that F≥0.8, that occurs when:

$$X_P = 0.5P \cdot \left(R + 1 + \sqrt{R^2 + 1} \right) \geq 0.85 \quad (4)$$

The following expressions are then adopted:

$$W = \frac{R + 1 + \sqrt{R^2 + 1} - 2RX_P}{R + 1 + \sqrt{R^2 + 1} + 2RX_P} \quad (5)$$

$$N_S = \frac{\ln\left(\frac{1 - RP}{1 - P}\right)}{\ln W}, \ \forall R \neq 1 \quad (6)$$

3. Once calculated N_s for each interval, the minimum number of shells is:

$$N_s^{min} = \sum_{j \in \{streams\}} (N_s)_{stream\ j} - \sum_{i \in \{intervals\}} (N_s)_{interval\ i} \quad (7)$$

In this case, we obtained N_s^{min} =59; a detailed simulation of the thermal behaviour of the heat exchangers included in the MER design allowed us to calculate N_s^{MER} =60.

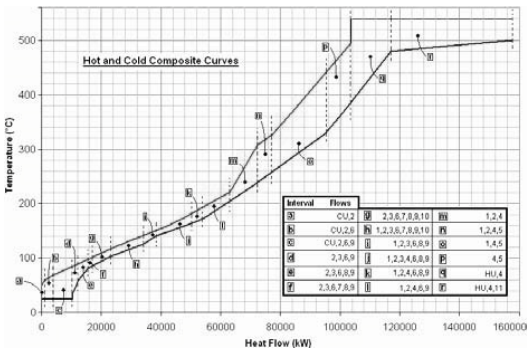

Fig. 4. Composite curves and enthalpy intervals.

Let us now focus on the area targets, that are calculated by summing the minimum heat transfer area for each interval identified in Fig. 4. The conventional approach, based on neglecting tube wall resistances and assuming the area ratio

A_{out}/A_{int} equal to unity, cannot be applied to gas-liquid finned tube exchangers. The typical expression:

$$A_{\text{interval i}} = \frac{1}{F_i(\Delta T_{lm})_i}\sum_j\left(\frac{q_j}{h_j}\right)_i \quad (8)$$

is modified into the more general:

$$A_{\text{interval i}} = \frac{1}{F_i(\Delta T_{lm})_i}\sum_j\left(\frac{q_j}{h_{j\text{-}k}}\right)_i \quad (9)$$

where $h_{j\text{-}k}$ represents either the heat transfer coefficient of stream j or that of the stream k, which transfer/receives heat to/from j. In particular:

$$\begin{cases} h_{j-k} = h_j \text{ when } (OM)_{h_j} \geq (OM)_{h_k} \\ h_{j-k} = h_k \text{ when } (OM)_{h_j} < (OM)_{h_k} \end{cases} \quad (10)$$

having being indicated with OM_h the order of magnitude of the heat transfer coefficient. Equations 9-10 relies on the assumption that, for finned heat exchangers where $(OM)_{h_j} \neq (OM)_{h_k}$, $h_j A_{j-side} \cong h_k A_{k-side}$. Equations 9-10 are of immediate use only when matches are someway predictable or, for instance, we have all liquid streams on either the hot or the cold composite curve. F is calculated by:

$$F = \frac{\sqrt{R^2+1}\cdot\ln\left(\frac{1-S}{1-RS}\right)}{(R-1)\ln\left[\frac{2-S\left(R+1-\sqrt{R^2+1}\right)}{2-S\left(R+1+\sqrt{R^2+1}\right)}\right]} \quad (11)$$

where:

$$S = \frac{\alpha-1}{\alpha-R} \qquad \alpha = \left(\frac{1-RP}{1-P}\right)^{\frac{1}{N_S}} \quad (12.a,b)$$

This analytical approach, implemented into a worksheet, allowed us to determine a target area for MER designs $A^{min}_{MER} = 23.35\cdot10^3\,m^2$. In Fig. 5 the specific heat transfer area (in m^2/kW) is plotted versus the intervals; relevant increases may be observed in the large near pinch region. The problem includes so tighten thermodynamic constraints that we can predict any MER design to achieve just a slightly higher heat transfer area than the target; a complete solution of the MER design provided in Fig. 3, in fact, leads to an $A_{MER} = 24.32\cdot10^5\,m^2$, just 4.1% higher than A^{min}_{MER}. We may conclude that the identified MER design represents a very suitable solution; whether or not it is economically viable, however, remains to be assessed.

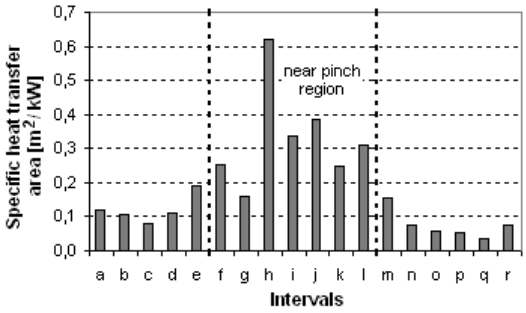

Fig. 5: specific heat transfer area in different intervals

4. Bottom-up approach to plant retrofit

Although in the previous Section an interesting MER solution was determined, it is likely that renouncing to some energy saving more advantageous lay-outs could be identified. Let us attempt to improve the efficiency of the existing HEN by introducing some modifications in its lay-out; let us indicate with $n^{\Delta top}$ the number of topology changes needed to generate each design option, starting from the existing heat recovery network. Topology changes could essentially consist of:

a. Resequencing, i.e. reversing the order of two exchangers;
b. Repiping, i.e. changing one of the matching streams in an exchanger;
c. Adding a new match;
d. Splitting a stream, thus reducing the load on a stream involved in the pinching match (the match where the so-called *network pinch* is located).

Let us identify a number of topologies, basing essentially on the first three topology changes in the above list; stream splitting, in fact, largely increases the number of feasible topologies and introduces additional uncertainties, being difficult to reliably predict the associated cost. The examined changes, represented in Fig. 6.a-e, are here briefly described:

– Solution no. 1 ($n^{\Delta top}$=0): increase the surface of HE E, so as to achieve a ΔT_{min}=10°C. HE

E then preheats stream 4 to a higher temperature and the load on HU-4 is reduced. The cold inlet temperature to HE D will be increased, reducing the driving force; then, the area of HE D is also increased;

- Solution no. 2 ($n^{\Delta top}$=1): add a new 9-4 match, limited by the ΔT=10°C on the cold side;
- Solution no. 3 ($n^{\Delta top}$=2): repipe HE B to match stream 3 with stream 9, rather than with stream 2. The surface of HE A is increased and the load on HU-1 reduces. A new 6-3 match is needed to preheat stream 3 up to 117°C;
- Solution no. 4 ($n^{\Delta top}$=2): add a new 9-4 match, limited by the need to lead stream 8 to its target temperature. Stream 8 is preheated by a new 2-8 match; small ΔT_{min} violations are allowed;
- Solution no. 5 ($n^{\Delta top}$=2): similar to solution no. 4, but with stream 8 preheated by a new match with stream 6. The higher heat capacity rate of stream 6 allows for a higher preheating temperature;
- Solution no. 6 ($n^{\Delta top}$=1): add a new 9-3 match, shift to a lower temperature range HE B and increase the area of HE A, thus reducing the load on HU-1.

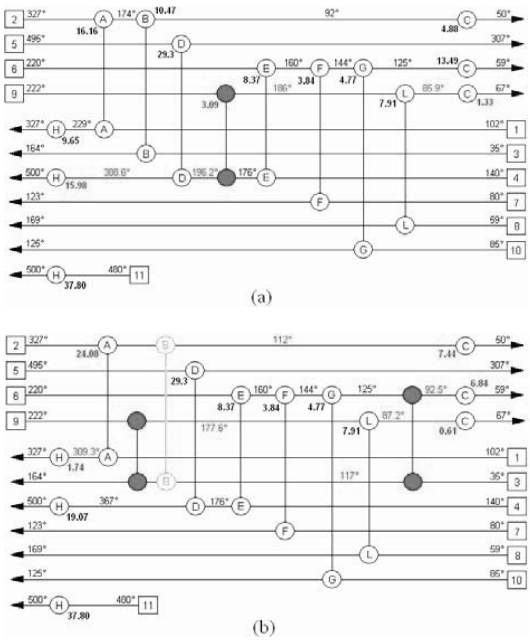

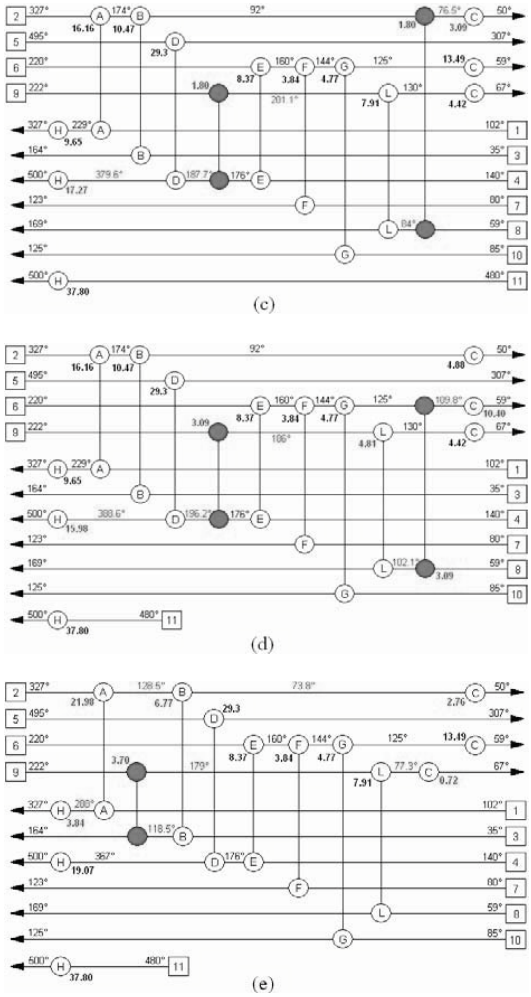

Fig. 6. Grid diagram of the examined topology changes: a)solution no. 2, b)solution no. 3, c) solution no. 4, d) solution no. 5, e) solution no. 6.

The six designs produced offer us an occasion to reflect on the need for peculiar analyses in case of retrofit of an existing HEN, with respect to those usually performed for new plants. Let us compare the results associated with these 6 designs under the "new plant" restriction, i.e. assuming that no heat recovery solutions had been previously implemented. Then, all the heat exchangers are new components, that must be purchased at a cost calculated according to the following expression:

$$Z_{HE} = a + b\, N_s \left(A / N_s\right)^c \qquad (12)$$

with a=5,000 € for utility exchangers and a=10,000 € for heat recovery units, b=340 and

c=0.8; let us also assume an 80 €/kW year cost for the hot utility and a 6 €/kW year for the cold one.

The scope for this analysis is to point out, in the following of the paper, at what extent a good topology for a "new plant" case can be sub-optimal for a retrofit analysis,

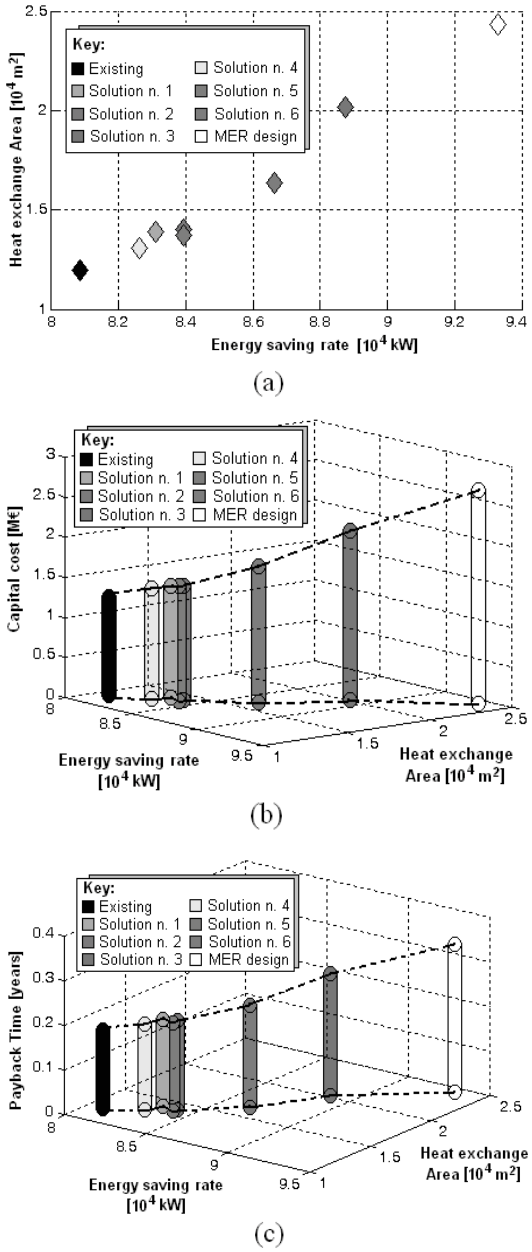

Fig. 7. a)Heat transfer area vs. energy saving rate, b)capital "new plant" cost associated with the examined solutions, c) payback time

The obtained results are shown in Fig. 7.a-c: the energy saving increases almost linearly with the heat transfer area, while the payback time increases less than linearly. In all cases the payback time is extremely short; considering that the reference case is the "no heat recovery" conditions (since we are under the assumption of "new plant"), Fig. 7.c suggests that some fraction of the total heat recovery potential can be achieved very easily.

Let us pose now the attention on retrofitting the existing HEN, which possibly already exploits the most convenient fraction of the heat recovery potential. In Fig. 8 the identified solutions 1-6 are marked with a circle; these points were determined by adjusting, for each topology, the area of all heat exchangers so as to maximize the energy saving (the values comply with the temperatures shown in Fig. 6.a-e).

Grouping these solutions basing on their $n^{\Delta top}$, we may observe that the solutions approximately lie on curves whose shape reflects the shape postulated by Asante and Zhu in [4]. Actually the dotted retrofit curve corresponding to $n^{\Delta top}=2$ was plotted with a slight translation on the left side with respect to the convolution of the representative points for solutions n. 3, n. 4 and n. 5 since, for such low number of representative points, we cannot predict whether they actually lie on the optimal "Area-Energy consumption" frontier.

The solutions n. 1÷6 have been identified regardless of the size of the heat exchangers in the existing HEN; hence, in order to exactly obtain these solutions, the heat exchangers involved in the topology changes should be *fully replaced*. Let us now attempt to relax these solutions, by determining a number of auxiliary configurations; the following relaxations are investigated and the relative lay-outs are indicated in Fig. 8 in the same colour of the associated topology:

a. Solution n. 2:
   - 1st relaxation: assume KA(HE D)=constant. Due to the reduced ΔT_{lm}, the transferred heat rate Q_D will slightly reduce, thus reducing the energy saving at HU-4;
   - 2nd relaxation: since the solution n. 2 led to an N_s(HE L)=5, let us increase $T_{9,o}$ at the new 9-4 match, so as to reduce the number of shells of HE L;

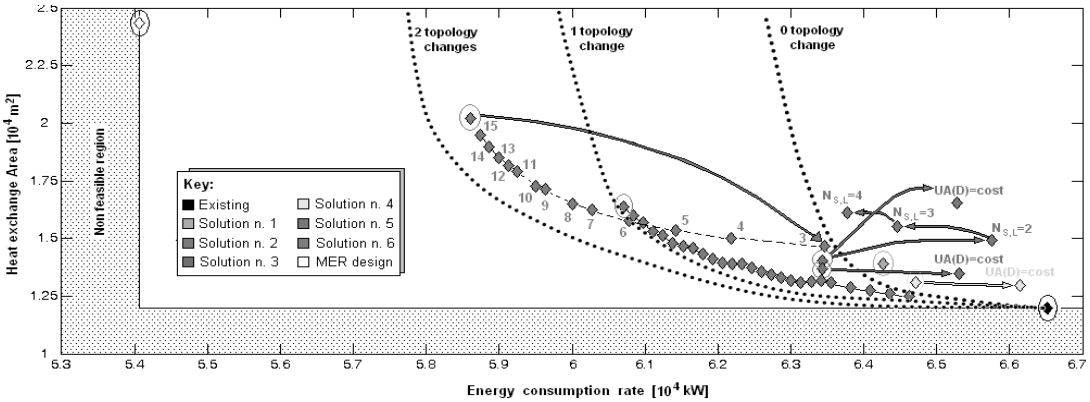

Fig. 8. Heat transfer area vs. energy consumption for the examined retrofit solutions and their relaxed lay-outs.

b. Solution n. 3: this configuration includes very tighten constraints on the new 9-3 match and on HE-L. Due to the increased capacity of HE-A, it needs to have 16 shells: let us assume to slightly increase $T_{2,o}$ so as to reduce the number of shells of A down to 3 (N_s for each option is indicated in Fig. 8);

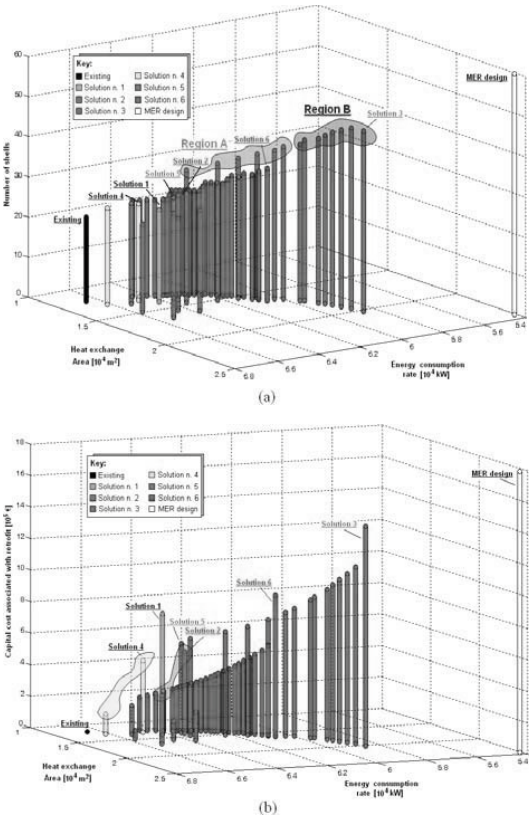

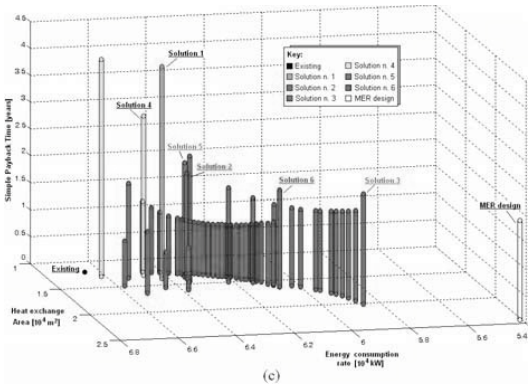

Fig. 9. Comparative results in terms of: a)Number of shells, b) retrofit cost, c) payback time

c. Solutions n. 4 and n. 5: assume KA(HE D)=constant, again reductions in the energy saving at HU-4 being expected;
d. Solution n. 6: let us increase $T_{9,o}$ of the new 9-3 match, so as to reduce the heat transfer area and the N_s of HE A and HE L.

Complete simulations were performed referring to the same economic data adopted earlier in this Section; here, however, the possibility to acquire the marginal capacity by eventually adding one or more shells to an existing heat exchanger is taken into account; this assumption leads us to privilege the options more conservative with respect to the existing HEN. The results are presented in Fig. 9.a-c. We may immediately observe that:

– Most of the original retrofit solutions have a much higher payback time than the relaxed lay-outs;

– In order to compare the benefits associated with a same "relaxation path", when adopted for different topologies, let us consider the two shaded areas in Fig. 9.b, both referring to the relaxation path oriented to save the current HE D (i.e. under the restriction "UA(D)=const"). Relaxing solution n. 4 (yellow area in Fig. 9.b) leads to a 230 €/$kW_{penalty}$ saving index, approximately twice the capital saving achieved by relaxing solution n. 2 (magenta area in Fig. 9.b); each relaxation path should be consequently analysed in depth being aware of the topological structure where it is adopted;
– In order to understand at what extent relaxation should be pursued, local values of design or cost variables should be used. For instance, from Fig. 9.a we recognize that relaxing solution 3 is very convenient in the "Region B" (dark blue area in the figure), where $\frac{\mathrm{d\,Sav}}{\mathrm{d\,N_s}} \approx 153 \frac{\mathrm{kW}}{\mathrm{shell}}$ (slight energetic penalty for relaxation), while it is less convenient in the "Region A" (light blue area in the figure), where $\frac{\mathrm{d\,Sav}}{\mathrm{d\,N_s}} \approx 638 \frac{\mathrm{kW}}{\mathrm{shell}}$ (high energetic penalty). In this particular case, such an analysis allows us to recognize that the large temperature crossing for heat exchanger A is associated with a great potential for reductions in N_s.

The proposed analysis made us realize that in the relaxation of existing HENs large asymmetries could exist between apparently similar solutions; the presence of integer variables like N_s, the hardly predictable position changes of network pinch and the influence of energy unit cost suggest to the analyst to widely explore the space of feasible solutions, eventually mapping the local trends of N_s, heat transfer areas, capital and energy costs to be able to detect optimality and local minima.

5. Conclusions

In this paper the retrofit of an existing heat recovery network for a process plant was discussed. After having identified and diagnosed a Maximum Energy Recovery configuration, a bottom-up approach was pursued by examining several topology modifications for the improvement of the existing network. An accurate thermal simulation of the heat exchangers included in the network allowed us to properly map the local sensitiveness of each topology to the heat transfer area distribution and to put into evidence the need for detailed analyses oriented to maximise the economical benefits.

Nomenclature

A heat transfer area, m^2
CU,HU cold and hot utility, respectively
F correction factor of ΔT_{lm}
h heat transfer coefficient, $W/(m^2\,K)$
HE heat recovery exchanger
HEN heat exchanger network
l number of flows, dimensionless
MER maximum energy recovery
$n^{\Delta top}$ number of topology changes
N_s number of shells
OM_h order of magnitude of h
P,R,S Indices for the thermal simulation of heat exchangers
q heat transfer rate, kW
Sav Energy saving rate, kW
T temperature, °C
U number of units
K overall heat transfer coefficient, $kW/m^2°C$
Z capital cost, €

Subscripts and superscripts

c/h,i inlet of the cold/hot fluid
c/h,o outlet of the cold/hot fluid
he-u heat exchanger with utility
int internal tube wall surface
lm log mean
out outer tube wall surface

References

[1] Kemp, I. C., 2007, *Pinch Analysis and Process Integration*, Butterworth-Imprint of Elsevier, Oxford, UK.

[2] Al-Riyami, B. A., et al., 2001, Heat integration retrofit analysis of a heat exchanger network of a fluid catalytic cracking plant, Applied Thermal Engineering, 21(13-14), pp. 1449-1487.

[3] Nordman, R., and Berntsson, T., 2009, Use of advanced composite curves for assessing cost-effective HEN retrofit I: Theory and concepts,

Applied Thermal Engineering, 29(2-3), pp. 275-281.

[4] Asante, N. D. K., and Zhu, X. X., 1997, An automated and interactive approach for heat exchanger network retrofit, Trans. IChemE, 75(3), pp. 349-360.

[5] Serth, R. W., 2007, *Process Heat Transfer – Principles and Applications*, C Academic Press – Imprint of Elsevier, Oxford, UK.

[6] Linnhoff, B., Townsend, D. W., Boland, D., A user guide, 1982, *A User Guide on Process Integration for the Efficient Use of Energy*, IChemE, Rugby, UK.

[7] Pinch spreadsheet NOV06 FINAL, URL: http://books.elsevier.com/companions

[8] Ahmad, S., et al., 1988, Design of multipass heat exchangers: an alternative approach, Journal of Heat Transfer, 110(2), pp. 304-3091487.

Molecular dynamics simulation of ozone destruction by bromine ions on the boundary of water clusters

A.E. Galashev and O.R. Rakhmanova

Institute of industrial ecology UB RAS, Yekaterinburg, Russia
rahmanova@ecko.uran.ru

Abstract: The interaction of $(Br^-)_i(H_2O)_{50-i}$, $0 \le i \le 6$ clusters with oxygen and ozone molecules is investigated by the method of molecular dynamics with the use of flexible molecules model. The ability of cluster to absorb the infrared (IR) radiation is reduced in a frequency range of $0 \le \omega \le 3500$ cm^{-1} when the number of bromine ions in cluster containing molecular oxygen grows. Ozone molecules are absorbed by cluster and do not leave it as well as bromine ions during calculation of 25 ps. The intensity of Raman spectra does not change significantly when Br^- ions are added to the system containing ozone. However, when the number of bromine ions is six the sharp reduction of integral intensity of Raman spectrum is occurred. Bromine ions influence on absorbed ozone molecules much longer than chlorine ones.

Keywords: Water cluster, Bromine ions, Ozone, Infrared and Raman spectra

1. Introduction

The decay of freon molecules causes the extraction of free chlorine and bromine atoms which participate directly in destruction of ozone molecules in the atmosphere. Because of cyclicity of these chemical processes each chlorine and bromine atom can destruct up to several hundred thousand of ozone molecules. These processes are most intensive in polar areas, especially in the Antarctica, because there are many long periods of time with very low temperature of air (-70° C) and because of particularities of atmospheric circulation in these areas. A lot of time (from several ten years up to several ones) can pass from the moment of getting into the atmosphere of freon molecules up to the moment of their decay.

In spite of the fact that bromine is less distributed in the atmosphere than chlorine, it gives in 45-69 times more effective depletion of ozone [1]. The reactions including bromine determine about half a season losses of polar ozone. Recently attention was brought to the influence of bromine on the stratosphere. The observations on BrO have shown that the amount of inorganic bromine filling the stratosphere (Br_y) makes about 21 pptv (parts on trillion) [2]. It was shown that the amount of the stratospheric bromine surpasses the amount of bromine brought by long living organic gaseous sources by 4-8 pptv [3]. This distinction can be explained by contributions from short living (with life time less than half a year) gas sources of bromine. The short living components containing bromine have basically an oceanic origin [4].

The goal of the present work is to study the interaction of bromine with "cold" water clusters being in close contact with ozone and oxygen molecules, to determine the influence of bromine on infrared absorption spectra and on Raman spectra of cluster systems and to investigate the mechanisms of ozone destruction. The choice of bromine ions is connected with the fact that heterogeneous reactions with ions take place on a surface; in our case it's a cluster surface.

2. Molecular dynamics model

In the present work the polarizable variant of advanced TIP4P model of water is used [5]. In this case parameters of Lennard-Jones (LD) parts of potential and the site of localization of negative charge are essentially changed. As a result the permanent dipole moment of water molecule corresponds to the experimental value of that quantity in a gas phase (1.848 D). The linear oxygen molecule is formed by two atoms taking place on a distance of 0.12074 nm from each other [6]. The geometry of ozone molecules is determined by an isosceles triangle, the length of equal sides is 0.12074 nm and the angle between them is 116.8°. The total energy was represented as a sum of kinetic, potential and polarization energy. In the case of water-water interactions the pair part of the potential was the sum of Lennard-Jones and Coulomb contributions. Noncoulomb part of water-oxygen (ozone) and oxygen (ozone) - oxygen (ozone) interactions was represented as a sum of repulsive and dispersive contributions [7, 8]

$$\Phi(r_{ij}) = b_i b_j \exp[-(c_i + c_j) r_{ij}] - a_i a_j r_{ij}^{-6} \quad (1)$$

where a_i, b_i, c_i are potential parameters describing these interactions. They are taken from work [9].

Coulomb interaction of Br^- ion with water was taken into account due to its electric charge $q_{Br^-} = -1\,e$, where e is an elementary charge. The noncoulomb Br^-–H_2O interaction was determined as Lennard-Jones one with parameters of work [10]. Between Br^- ions and also between ions and atoms of O_2 or O_3 molecules besides Coulomb interaction the atom-atom interaction determined by formula (1) with parameters of work [9] was also taken into account. The central atom of ozone molecule had a positive electric charge $q_{cen} = 0.19\,e$ and side atoms of this molecule carried a negative charge $q_{side} = -0.095\,e$. Atoms of O_2 molecule had no electric charges.

Flexible models of molecules were considered. The flexibility of molecules was created using the procedure developed within the framework of Hamiltonian dynamics [11, 12]. We consider the diatomic molecule. Let atoms a and b in a molecule be separated by the distance

$$q = \|\mathbf{r}_a - \mathbf{r}_b\|, \quad (2)$$

where $\mathbf{r}_a$ and $\mathbf{r}_b$ are vectors that determine the positions of atoms. Corresponding velocities are denoted by $\mathbf{v}_a$ and $\mathbf{v}_b$, and the reduced mass is written as

$$\mu = \frac{m_a m_b}{m_a + m_b} \quad (3)$$

The size of molecule presented by atoms a and b is determined from the equality condition by the values of potential $\mathbf{f}(\mathbf{q}) = -\frac{\partial \mathbf{r}}{\partial \mathbf{q}} \nabla \Phi(\mathbf{r}))$ and centrifugal $-\mu q \omega^2$ forces so that

$$-\mu q \omega^2 - \mathbf{f}(\mathbf{r}) \frac{\partial \mathbf{r}}{\partial \mathbf{q}} = 0, \quad (4)$$

where $\omega = \|\mathbf{v}_a - \mathbf{v}_b\| / q$ is the angular velocity. From the condition of the minimal contributions to potential U from each generalized coordinate, we have

$$\frac{\partial}{\partial q_i} H(\mathbf{r}, \mathbf{v}) = \frac{\partial}{\partial q_i} \left(\frac{1}{2} \mu_i q_i^2 \omega_i^2 + U(\mathbf{r}) \right) = 0 \quad (5)$$

This method is generalized to molecules of any composition [13].

Simulation of interaction of $(Br^-)_i (H_2O)_{50-i}$ clusters with gas environment containing i H_2O molecules and six O_2 or O_3 molecules began with the creation of configuration from equilibrium $(H_2O)_{50}$ water cluster in molecular dynam-

ics calculation with the kinetic energy corresponding to the temperature of 233 K. Further $(Br^-)_i(H_2O)_{50-i}$ cluster was created. The coordinate system connected with the cluster centre of mass was used to determine the position of bromine ions in cluster. The virtual sphere around water cluster was drown. Water molecules which were closer than other ones to points of an exit from sphere of coordinate axes were found. Each of these molecules (from 1 up to 6) moved outside along the appropriate coordinate axis on distance of 0.7 nm from former position of its centre of mass. The Br^- ion was placed instead of displaced molecule. The number of ions corresponded to the number of replaced molecules. The interaction of formed $(Br^-)_i(H_2O)_{50-i}$ cluster with water, ozone or oxygen molecules was investigated in ensemble with external thermostat [13] at temperature of 233 K. The cut-off radius of molecular interactions in model was 0.9 nm. Six O_2 or O_3 molecules were placed close the bottom part of cluster. The time step of molecular dynamics calculation was $\Delta t = 10^{-17} c$. Calculation of spectral characteristics began from the moment of time $t = 10^5 \Delta t$ (1 ps). The full duration of calculation was made of $2.1 \cdot 10^6 \Delta t$ time steps.

The motion equations for the centers of mass of the molecules were integrated by the Gear fourth-order method [14]. Equations for the rotational motion of molecules were analytically solved using the Rodrig–Hamilton parameters [15]. The integration scheme for rotational motion equations corresponded to the approach proposed by Sonnenschein [16].

3. The dielectric properties

It is possible to calculate Raman and infrared spectra of clusters through the autocorrelation functions of polarizability and dipole moment correspondently. The polar molecule is characterized by $\mathbf{d}_{i,0}$ permanent (gas phase) dipole moment and by $\boldsymbol{\alpha}_{i,0}$ polarizability tensor. The induced dipole moment and polarizability of i molecule create the interaction with the neighboring molecules. In model each molecule can be considered as a polarizable dot dipole taking place in the molecule centre of mass. The $\mathbf{d}_i$ dipole moment of i molecule and its $\boldsymbol{\alpha}_i$ polarizability are connected due to the interaction with surrounded molecules [17]

$$\mathbf{d}_i = \mathbf{d}_{i,0} + \boldsymbol{\alpha}_{i,0} \sum_{j \neq i} \mathbf{T}_{ij} \mathbf{d}_j , \qquad (6)$$

$$\boldsymbol{\alpha}_i = \boldsymbol{\alpha}_{i,0} + \boldsymbol{\alpha}_{i,0} \sum_{j \neq i} \mathbf{T}_{ij} \boldsymbol{\alpha}_j . \qquad (7)$$

Here $\mathbf{d}_{ij}$ is a tensor of dipole-dipole interaction.

$$\mathbf{T}_{ij} = \frac{1}{\left| r_{ij} \right|^3} \left(3 \hat{\mathbf{r}}_{ij} \hat{\mathbf{r}}_{ij} - \mathbf{1} \right). \qquad (8)$$

In equation (8) $\hat{\mathbf{r}}_{ij}$ is a unit vector in $\mathbf{r}_i - \mathbf{r}_j$ direction, where $\mathbf{r}_i$ and $\mathbf{r}_j$ are positions of i and j molecules centers of mass, $\mathbf{1}$ is a unit 3×3 tensor. For water molecule the anisotropic gas phase tensor of polarizability $\alpha_{xx,yy,zz} = \{1.495, 1.626, 1.286\}$ Å^3 was used [17]. Ozone molecules were characterized by izotropic experimental value of polarizability of 2.85 Å^3 [18]. Bromine ions had polarizability of 4.53 Å^3 [19]. For the calculation of induced dipole moments the standard iterative procedure was used on each time step [5]. Accuracy of $\mathbf{d}_i$ definition is set in a range of $10^{-5} \div 10^{-4}$ D.

The infrared absorption signal was given in the form [20]

$$\sigma(\omega) = \left(\frac{2}{\varepsilon_0 c \hbar n} \right) \omega \tanh\left(\frac{\hbar \omega}{2kT} \right) \times \times \mathrm{Re} \int_0^\infty dt e^{i\omega t} \left\langle \mathbf{M}(t) \cdot \mathbf{M}(0) \right\rangle \qquad (9)$$

where ε_0 is the vacuum permittivity, c is the velocity of light, $\hbar = h / 2\pi$, h is Planck's constant, n is a non dependant on

frequency ω refractive index, $\mathbf{M}(t)$ is a normalized autocorrelation function of the total dipole moment of cluster.

In the case of depolarized light Raman spectrum is set by the equation [17]

$$J(\omega) = \frac{\omega}{(\omega_L - \omega)^4}\left(1 - e^{-\hbar\omega/kT}\right) \times \times \mathrm{Re}\int_0^\infty dt e^{i\omega t}\left\langle \Pi_{xz}(t)\Pi_{xz}(0)\right\rangle, \quad (10)$$

where

$$\Pi(t) \equiv \sum_{j=1}^{N}\left[\boldsymbol{\alpha}_j(t) - \left\langle \boldsymbol{\alpha}_j \right\rangle\right], \quad (11)$$

ω_L is a frequency of exciting laser, Π_{xz} is xz component of $\Pi(t)$ quantity, axes x is directed along a molecular dipole, and xy is a molecular plane. We used the quantity of ω_L = 19436.3 cm^{-1} (green line of argon laser, λ = 514.5 nm).

4. The results of calculation

The configurations of $(Br^-)_6(H_2O)_{44} + 6O_2 + 6H_2O$ system corresponding to the moments of time 1 and 25 ps are shown in fig. 1. The Br^- ions were displaced outside from water core by the moment of time 1 ps. On the contrary, water molecules surrounding cluster came closer to the core. As a result a complete cluster in which 50 H_2O molecules contact with 6 O_2 molecules and 6 Br^- ions was formed. However, O_2 molecules and Br^- ions leave the cluster with the time being. Finally $(Br^-)_6(H_2O)_{50}(O_2)_6$ cluster has lost 2 O_2 molecules and 3 Br^- ions by the moment of time 25 ps. One of the evaporating bromine ions is shown in the bottom part of fig. 1b.

Absorption spectra of IR radiation of cluster systems containing oxygen molecules are shown in fig. 2. The intensities of IR spectra decrease when the number of bromine ions increases in the system. The integral intensities of IR spectra with O_2 molecules correlate as: 1 : 0.71 : 0.71 : 0.56 : 0.42 : 0.52 : 0.42. The location of principal maximum of IR spectrum is not changed significantly with the growth of number of Br^- ions number in the system. It is displaced to the high frequencies relatively to the location of the principal maximum of the appropriate experimental spectrum of liquid water [21].

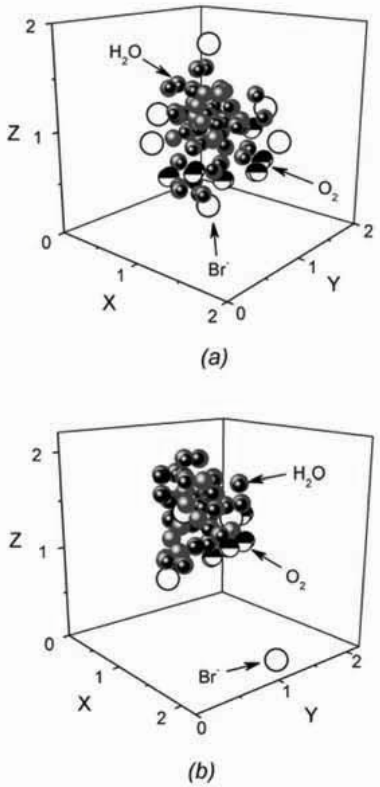

Fig. 1. Configurations of $6O_2 + (H_2O)_n + 6Br^-$ *system corresponding to the moments of time: a – 1 ps b – 25 ps. Coordinates of molecules are in nm.*

On the contrary, the wide first peak locating at $\omega = 1858$ cm^{-1} for $(H_2O)_{50} + 6O_2$ system has blue shift ~ 50 cm^{-1} for IR spectrum of $(Br^-)_2(H_2O)_{50} + 6O_2$ system, and it is transformed to a shoulder for

$(Br^-)_4(H_2O)_{50} + 6O_2$ and $(Br^-)_6(H_2O)_{50} + 6O_2$ systems. The growth of intensity of calculated IR spectra in a vicinity of frequency $\omega = 1000$ cm^{-1} correlates with a location of the principal maximum of the experimental IR spectrum of $O_2 + O_3$ gaseous mixture [22]. The relative decrease of IR spectra intensity in a vicinity of frequency $\omega = 2500$ cm^{-1} results in disappearing of the first peak. It correlates with the location of high intensity in experimental spectrum of gaseous bromine hydride [23]. Nonpolar O_2 molecules create effect "dilution" owing to the decrease of the total dipole moment magnitude. Br^- ions perturb an internal electric field of cluster, accelerating attenuation of autocorrelation function of d_{cl} magnitude. As a result the intensity of the IR spectrum decreases with growth of number of bromine ions.

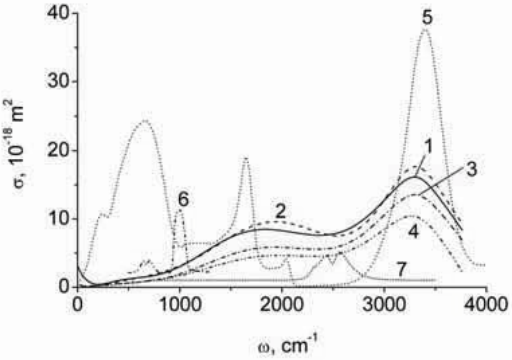

Fig. 2. Infrared absorption spectra of systems: 1 – $(H_2O)_{50} + 6O_2$, 2 – $(Br^-)_2(H_2O)_{50} + 6O_2$, 3 – $(Br^-)_4(H_2O)_{50} + 6O_2$, 4 – $(Br^-)_6(H_2O)_{50} + 6O_2$; 5 – $\sigma(\omega)$ function of bulk water, experiment [21]; 6 – experimental spectrum for $O_2 + O_3$ gas phase mixture [22]; 7 – experimental spectrum of gas phase bromine hydride [23].

The Raman $J(\omega)$ spectra of $(H_2O)_{50} + 6O_3$ and $(Br^-)_6(H_2O)_{50} + 6O_3$ systems containing ozone molecules together with the appropriate experimental spectra of liquid water [24], gaseous ozone [25] and clathrate hydrate of crystal bromine [26] are shown in fig. 3. Raman spectra of $(Br^-)_i(H_2O)_{50} + 6O_3$, $1 \le i \le 5$, systems differ a little from the appropriate spectrum

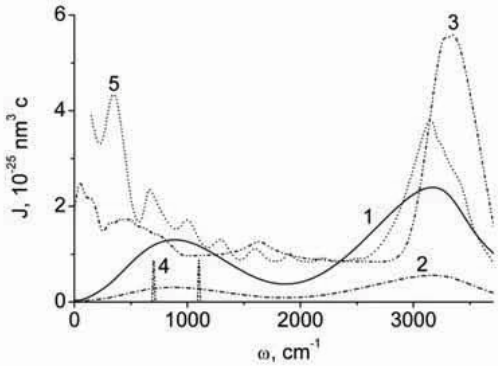

Fig. 3. Raman spectrum for system: 1 – $(H_2O)_{50} + 6O_3$, 2 – $(Br^-)_6(H_2O)_{50} + 6O_3$ 3 – bulk water at T = 293 K, experiment [24], 4 – gas phase ozone, experiment [25], 5 – bromine clathrate hydrate at 266 K, experiment [26].

of $(H_2O)_{50} + 6O_3$ system. The integral intensity of $J(\omega)$ spectrum for system having 6 Br^- ions is lower by factor 4.3 than that for system without bromine ions. The location of the principal maximum of Raman spectrum for ozone-containing systems is displaced toward high frequencies concerning the peak location of the appropriate spectrum for bromine clathrate hydrat and toward low frequencies concerning the location of the principal maximum of experimental spectrum for liquid water. The first peak of $J(\omega)$ spectra for $(Br^-)_i(H_2O)_{50} + 6O_3$, $0 \le i \le 6$, systems is in a frequency range determined by location of peaks for gaseous ozone. Polar molecules

of ozone have higher polarizability (α_p = 2.7 Å^3) than water ones. Therefore the $\overline{\alpha}_p$ magnitude here is higher than α_p for water cluster. Disordering of the dipole moments amplifies with increase in the number of Br^- ions and values of polarizability are smoothly reduced. Here fluctuations of α_p magnitude are lower than that for systems with oxygen. As a result the intensity of $J(\omega)$ spectrum for systems containing ozone is reduced in process of increase of Br^- ions number.

The destruction of ozone molecule goes easily. The length of ozone molecule is longer than that of oxygen one. The bond energy (52 kJ/mol) between the third oxygen atom is almost in five times less than that between two other oxygen atoms in O_3 molecule. As a result the strength of O_3 molecule is less than that of oxygen molecule. Intramolecular bond in oxygen is much stronger than that in ozone. In all states (gaseous, liquid and solid) O_2 is a paramagnetic substance and its dissociation energy is 496 kJ/mol. The disintegration energy of water to simple substances is equal to 484 kJ/mol. The dissociation energy of nitrogen N_2 (the most widespread molecule in the atmosphere) is 945 kJ/mol. The oxygen molecule has more significant chemical activity than nitrogen one. The high energy collisions of Br^- ions with O_2 and O_3 molecules were recorded in calculations. The ozone destruction takes place when cluster has 3 and more bromine ions. Three easily dissociated molecules break up when there are 3 Br^- ions in the system and only 2 ones in the other cases.

5. Conclusion

The important role of bromine in chemistry of troposphere is defined first of all by its influence upon the contents of ozone. Destruction of ozone begins with photolysis of molecular compound containing Br^-. As a result atomic bromine is formed. Bromine destroys ozone according to the well known cycle including BrO_x and HO_x components. The process of ozone destruction can be caused not only by chlorine components, fluorine and bromine, but also by microparticles of water and ice which activate this process. Atomic oxygen is an initial product of ozone destruction. At the same time O_2 molecule is considerably stronger and it is not exposed to destruction under action of UF radiation in the stratosphere.

It is shown in the present work that water clusters can keep bromine ions interacting with environmental molecular oxygen and ozone. During the whole MD calculation by duration of 25 ps Br^- ions contacted with water and ozone molecules. The bromine ions show low desorption even at high concentration. It helps them to be in water cluster during time exceeding by order the average life time of the same amount of Cl^- ions in water clusters of similar size [27]. It testifies that in disperse water medium Br^- ions influence considerably stronger (owing to increase of contact time) to ozone destruction than Cl^- ones. Water cluster can make a high concentration of Br^- ions around itself. In this case bromine ions get high kinetic energy because of electrostatic repulsive. The high energy bromine ion colliding with an oxygen molecule can remove it easily from system. The absorption intensity of IR radiation decreases consistently during addition of Br^- ions to water cluster. The bromine ions in water clusters absorbing oxygen molecules have considerably more long setting life than chlorine ones.

The presence of bromine ions in water clusters with ozone results in week sensitivity of Raman spectra of investigated system with ozone molecules to containing of bromine ions. But the strong decrease of Raman spectrum intensity of disperse system is observed at high concentration of bromine ions. Infrared absorption spectra of disperse water systems with ozone molecules considerably increase its intensity at presence of Br^- ions. However, the more the number of bromine ions in clusters, the weaker the in-

tensity grows. At high concentration of Br^- ions the growth stops at all.

Acknowledgments: This work was supported by Russian Foundation of Basic Research, project No. 08-08-00136-a.

References

1. Sinnhuber B.-M., et al., 2006, The contribution of anthropogenic bromine emissions to past stratospheric ozone trends: a modelling study, Atmos. Chem. Phys. Discuss, 6, pp. 6497–6524.
2. Sinnhuber B.-M., et al., 2005, Large decadal scale changes of polar ozone suggest solar influence, Atmos. Chem. Phys. Discuss, 5, pp. 12103–12117.
3. Salawitch R.J., et al., 2005, Sensitivity of ozone to bromine in the lower stratosphere, Geophys. Res. Lett, 32, pp. L05811–L05818.
4. Chuck A.L., Turner S.M., Liss P.S., 2005, Oceanic distributions and air-sea fluxes of biogenic halocarbons in the open ocean, J. Geophys. Res, 110, pp. C10022–C10030.
5. Dang L.X., Chang T.M., 1997, Molecular dynamics study of water clusters, liquid and liquid – vapor interface of water with many-body potentials, J. Chem. Phys, 106, pp. 8149–8159.
6. *The Chemists book*, 1971, Nikolskyi B.P. (Ed.), Himiya, Leningrad.
7. Galashev A.E., Rakhmanova O.R., Chukanov V.N., 2005, Molecular dynamics simulation of spectral characteristic and dielectric properties of water clusters, Rus. J. Chem. Phys. B, 24, pp. 90–97.
8. Spackman M.A., 1986, Atom-atom potentials via electron gas theory, J. Chem. Phys, 85, pp. 6579–6582.
9. Spackman M.A., 1986, A simple quantitative model of hydrogen bonding, J. Chem. Phys, 85, pp. 6587–6591.
10. Perera L., Berkowitz M.L., 1991, Many-body effects in molecular dynamics simulations of $Na^+(H_2O)_n$ and $Cl^-(H_2O)_n$ clusters, J. Chem. Phys, 95, pp. 1954–1962.
11. Lemberg H.L., Stillinger F.H., 1975, Central-force model for liquid water, J. Chem. Phys, 62, pp. 1677–1682.
12. Rahman A., Stillinger F.H., Lemberg H.L., 1975, Study of a central force model for liquid water by molecular dynamics, J. Chem. Phys, 63, pp. 5223–5232.
13. Berendsen H.J.C., et al., 1984, Molecular dynamics with coupling to an external bath, J. Chem. Phys, 81, pp. 3684–3690.
14. Haile J.M., 1992, *Molecular Dynamics Simulation. Elementary Methods*, New York: John Wiley & Sons.
15. Koshlaykov V.N., 1985, *Problems of solid body dynamics and applied theory of gyroscopes*, Nauka, Moscow.
16. Sonnenschein R., 1985, An improved algorithm for molecular dynamics simulation of rigid molecules, J. Comp. Phys 59, pp. 347–350.
17. Bosma W.B., Fried L.E., Mukamel S., 1993, Simulation of the intermolecular vibrational spectra of liquid water and water clusters, J. Chem. Phys, 98, pp. 4413–4421.
18. Huiszoon C., 1986, Ab initio calculations of multipole moments, polarizabilities and isotropic long range interaction coefficients for dimethylether, methanol, methane and water, Mol. Phys, 58, pp. 865-885.
19. Hunt S.W. 2004, Formation of Molecular Bromine from the Reaction of Ozone with Deliquesced NaBr Aerosol: Evidence for Interface Chemistry, J. Phys. Chem. A, 108, pp. 11559–11572.
20. Neumann M., 1986, Dielectric relaxation in water. Computer simulations with the TIP4P potential, J. Chem. Phys, 85. pp. 1567–1580.
21. Goggin P.L., Carr C., 1986, Far infrared spectroscopy and aqueous solutions, in: Neilson G.W., Enderby J.E. (Eds.), *Water and aqueous solutions*, Adam Hilger, Boston, pp. 149–161.
22. Potapova G.F., et al., 2005, Abstracts, The first Russian Conference «Ozone and other ecologically pure oxidants. Science and technology», Moscow State University, Moscow.

23. Kozintzev V.I., Belov M.L., Gorodnichev V.A., Fedotov U.V., 2003, Laser optical acoustic analysis of multicomponent gas mixtures. MSTU named N.E. Bauman, Moscow.
24. Vallee P., et al., 2003, Raman scattering of water and photoluminescence of pollutants arising from solid-water interaction, J. Molec. Struct, 651–653, pp. 371–379.
25. Andrews L., Spiker R.C. Jr., 1972, Argon matrix Raman and infrared spectra and vibrational analysis of ozone and the oxygen-18 substituted ozone molecules, J. Phys. Chem, 76, pp. 3208–3213.
26. Goldschleger I. U., Kerenskaya G., Janda K. C., Apkarian V. A., 2008. Polymorphism in Br_2 Clathrate Hydrates, J. Phys. Chem. A, 112, pp. 787–790.
27. Galashev A. E., Rakhmanova O. R., Novruzova O. A., 2009, Molecular dynamics calculation of spectral characteristics of water clusters in the presence of ozone molecules and chlorine ions, Russian Journal of General Chemistry, 79, pp. 1675–1772.

TESTING the COMPLIANCE of the EUROPEAN WATER FRAMEWORK DIRECTIVE in the HUERVA RIVER from the EXERGY APROACH

Beatriz Carrasquer, Javier Uche, Amaya Martínez and Antonio Valero

CIRCE Institute, University of Zaragoza, Spain

Abstract: The European Water Framework Directive (WFD), which came into force in 2000, constitutes a key point to get degraded waters bodies up to a good natural status by 2015. In this way, adequate and cost-effective restoration environmental measures should be entirely written by competent Authorities, by 2009. Physical Hydronomics (PH) was presented in previous ECOS Conferences as an objective tool to calculate and allocate among users the restoration costs of water bodies through the exergy analysis. In this paper, the whole analysis of the Huerva River, a tributary of the Ebro River, the most plentiful stream in Spain, is presented. It was modelled with a specific hydraulic simulation software called AQUATOOL for the period 2002-2007. That software includes both quantitative and qualitative aspects and guarantees a comprehensive study of physico-chemical behaviour of the river, what assure the precise calculation of those above mentioned costs. In addition, an important novelty is presented in this work: the testing of the Programme of Measures proposed for the Huerva River. Results show that the proposed restoration measures are enough to reach the desired objective state of the Huerva waters by 2015. Similar global figures are found by conventional and PH approaches; however, PH presents some relevant advantages such the simplicity of using an only unit (exergy), or allowing to charge the users restoration costs according to degradation on the river provoked by them, as well as providing a more disaggregated and detailed information.

Keywords: Exergy approach, Programme of measures, Physical Hydronomics, Water Framework Directive

1. Introduction

An increasing demand for cleaner World fresh water resources has been confirmed. In Europe, a more and more environmentally-concern water policy is arising. It led to the publication of the Water Framework Directive (WFD) in 2000, with the main purpose of establishing a framework for the protection of inland surface waters, transitional waters, coastal waters and ground-waters. Specifically, the objective of achieving good water status involves a set of measures in all areas related to the water environment, from the natural aspects to its economic and social nature.

In this sense, the WFD defines the methods, procedures and indicator parameters necessary for characterising the condition of water, and the strategies and instruments needed to protect this condition and to regenerate it (if necessary) [1]. In this context, the most important aspects of the WFD are:

- Evaluating the condition of all water bodies, using quantitative and qualitative parameters.
- Determining the ecological status of these water bodies, and identifying the associated pressures, impacts and risks conditioning that status.
- Creating economic instruments for a good water management, based on the principle of recovery of costs.
- Promoting public participation in decisions related to water management.
- Drawing up river basin water plans including the programmes of measures to achieve the environmental objectives already mentioned, and all the exceptions or difficulties to get the compliance.

In consequence, according to the WFD road map, new River Basin Plans (RBP) should be finished by 2009 by the corresponding competent organism. In particular, the WFD in its Article 11, states that *"...each RBP must contain a detailed Plan of Measures (PM) to apply in order to reach the ecological objectives pursued for each water body of a given basin"* [1]. The development of the PM includes diverse actions such as control of water regimes, water demand management,

Corresponding author. Beatriz Carrasquer, *E-mail:* becarras@unizar.es

economic instruments -incentives and taxes-, or river restoration strategies, among others.
The study and analysis of that PM from the exergy approach is the main target of this work, based on Physical Hydronomics (PH), and was already presented as an accounting tool for the WFD [2-4]. PH is defined as the specific application of Thermodynamics to physically characterize the degradation and further restoration of water bodies, through the exergy loss calculation. The final objective of PH is to use those calculated physical costs as a guide to allocate the environmental and resource costs proposed by the WFD.

Along the PH development, the diverse river statuses proposed by the Directive were defined in exergy terms by means of their quantity and quality characterization. From the quantity and quality measurements in the river (they give the exergy value to water bodies), the exergy profiles of the river at different statuses defined by the WFD were obtained [2,3]. Then, the environmental cost (EC) of water was obtained as the exergy needed to cover the gap between the current state of the river and the good ecological state (GES) of the water bodies in a given area, also included in the PH spectrum. Then, the effectiveness of such a Plan could be easily tested, as well as the additional cost of non compliance of the PM initially developed when measures do not reach the GES. This is the new approach presented in this paper.

2. Methodology

Any river state can be characterized by its exergy value (B, given in KWh), defined as the product of its flow (Q, given in m^3/s) and its specific exergy (b, given in kJ/kg of water) [2,3]. Then, the exergy profile of a river could be created by a set of Q and b pairs along the river course. Diverse profiles could be analyzed depending on the WFD effectiveness, as it follows:

- Future State (FS) of the river is understood as the probable state of the river by 2015, starting from present state (PS) of the water stream but introducing the projected pressures (as an example, the three percent of increase in water demands).
- Objective State (OS) is that state proposed by authorities as the good status of the river in order to fulfill with the WFD requirements.
- Measures State (MS) is defined as the resulting state after applying the specific Plan of Measures (PM) proposed for that river.

The exergy difference among the diverse river profiles gives an idea about how far is the Future State (FS) of the river, from the Objective State (OS). In addition, the comparison between the state of the river after implementing the PM and the OS, makes possible to analyse the effectiveness of that PM.

Afterwards, those explained differences are translated to real energy and economic values. Then, the conventional costs concept arises. According to the WFD, the environmental cost (EC) of water regards the alteration of the physical and biological aspects of water bodies due to human activities and represents the average cost damage that water uses impose on the environment and ecosystems. Then, connecting this description to the exergy concept, the EC was defined within the PH methodology, as the difference between the real state and the objective states of the river, by 2015, as indicated in (1). It can be disaggregated in the corresponding quantity and quality terms.

$$EC = \Delta B_{OS-FS} = B_{OS} - B_{FS} = b_{FS}\Delta Q + Q_{OS}\Delta b = \Delta B_m + \Delta B_q \quad (1)$$

Where ΔQ and Δb are the flow and specific exergy gaps, respectively, between the FS and the OS; m and q stands for quantity and quality exergy components, respectively.

In order to analyze the implications of PM, the new defined river state (MS) makes possible to define an additional cost, the non-compliance cost (NCC) which, as mentioned, informs about the accuracy of the implemented measures in the water body. Specifically, the NCC is determined by the difference between the OS and the MS according to (2). A positive value of the NCC indicates that the PM within the watershed is not good enough because the OS has not been reached. A negative value, however, leads to the conclusion that the PM projected to that river has been oversized.

$$NCC = \Delta B_{OS-MS} = B_{OS} - B_{MS} = b_{MS}\Delta Q + Q_{OS}\Delta b \quad (2)$$

Additionally, the measures cost (MC) can be defined as the necessary cost to implement the PM presented by the competent authority, that is, the

difference between the FS of the river and the MS. Since the present state of the river, and this Future State by 2015 are really different status, a transition cost (TC), whose values are generally quite low, can be defined

These previously mentioned exergy states and costs are summarized graphically in Fig. 1.

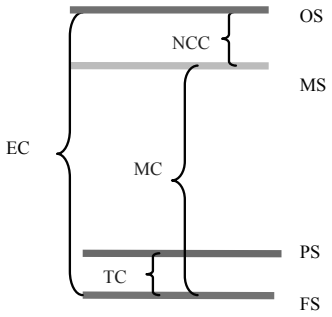

Fig. 1. New PH States defined in WFD framework

2.1. Distribution of restoration costs among users

The above developed methodology was used to carry out the calculation of restoration costs, and to allocate them among the different river users. Three water scenarios were studied; they were defined as follows:

- Without Users State (WUS) of the river is understood as the state of the river without any demand.
- Urban Users State (UUS) is the state in which only the contribution of urban demands is considered.
- Agriculture Users State (AUS) is defined as the resulting state by taking into account only the agriculture demands.

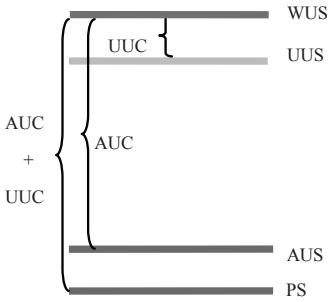

Fig. 2. New PH States to distribute restoration costs among users

As it can be seen in Fig. 2, two new costs can be considered:

- Urban Users Cost (UUC) is defined by the gap between Without Users State and Urban Users State.
- Agriculture Users Cost (AUC) is defined by the gap between WUS and Agriculture Users State.

These exergy costs were used to calculate the contribution of each user to the total exergy gap because of the water uses within the river. Additionally, quantity and quality exergy components were calculated for different users, and then translated into monetary terms, as stated in [2], by using the unitary exergy costs defined by operation data for different technologies [2] and the current prize of energy.

With the aim of illustrating the applicability of the above mentioned methodology, the case study of the Huerva river (a tributary of the Ebro, the most plentiful river in Spain) is developed by using a specific hydraulic simulation software. A brief overview of the case study is included in section three. Then, main software characteristics and the methodology are included in section four. According to simulation obtained results and PH methodology, restoration costs based on physical degradation of water, defined in quantity and quality terms were calculated by applying (1). Final figures and main conclusions are summarized in sections five and six, respectively.

3. The Huerva River basin: case study

The Huerva basin is a small tributary of the Medium Ebro river, in Aragón, Spain. It is characterized by scarce precipitation, being especially low in summer [5-7]. The Huerva average contribution is small, around 47 hm^3 per year, so it is quite vulnerable to any anthropogenic pressure.

3.1. Main water uses in the Huerva basin

The Huerva basin is divided in three main areas which are delimitated by two dams: Las Torcas (7 hm^3) and Mezalocha (3 hm^3) [6,7]. Important quality variations are found along the river course. The river header is located at 1220 m high, in Fonfría. Its total length is about 133 km, with very low pressures for both point and non-point pollution sources. In consequence, the stretch

comprised between the header to Las Torcas Dam, and even the village of Villanueva de Huerva, can be assumed to be quite close to its Natural State. Therefore, the water quality is identified as good enough [6]. Then, some urban demands (included some industrial ones) return close to the irrigation diffuse loads coming from Villanueva, at the end of the medium river course (before Mezalocha dam). Then, lower course is quite polluted up to its dead at Zaragoza (200 m height). Industrial returns from the lower Huerva are collected by the municipal waste water network of Zaragoza.

The Huerva Basin can be seen in Fig. 3. It was finally divided into thirteen stretches, containing two dams and five external water inputs (including runoff) of their corresponding five draining areas. This scheme includes also seven consumptive demands: four of them for irrigation, which constitute about the 98 percent of the water demand in an average year [7].

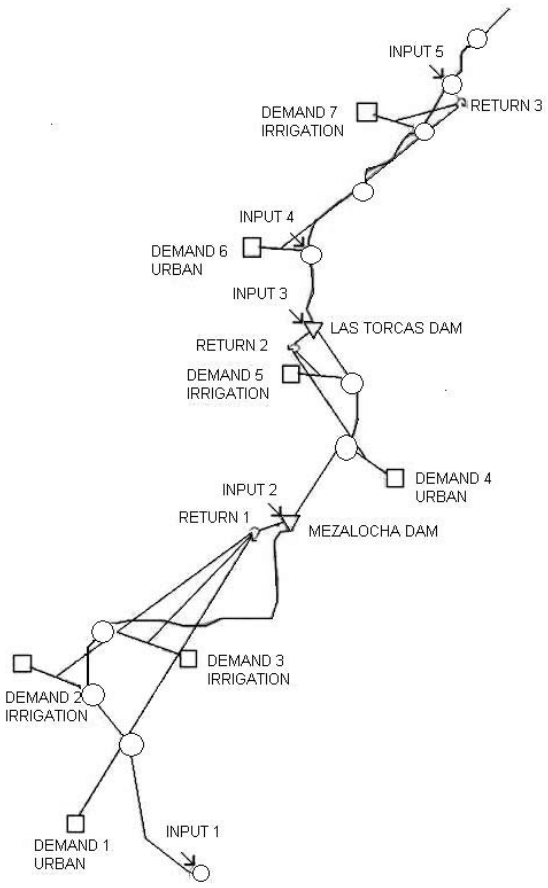

Fig. 3. The Huerva river basin

3.2. The case study Plan of Measures definition: important considerations

According to the preliminary ideas provided by the report elaborated by the Confederación Hidrográfica del Ebro [8] concerning to the future Plans of Measures in the whole watershed, it was considered that the Huerva river PM should mainly include by 2015:

- The modernization of existing irrigation systems, that implies, in the case of Huerva basin, a lower abstraction and also a lower but more concentrated return [9-11]. However, modernization is nowadays an unclear issue and is still complicated to state general characteristic figures. Unlike basins in which small irrigation systems exists (such as the case of the Huerva river), more water consumer crops and higher evapo-transpiration provoked by new irrigation systems usually imply a increment in water consumption.
- The construction of a new waste water treatment plant (WWTP) located in Villanueva de Huerva [12].

An increase of a three percent in water demands with respect to present water status is frequently considered in a future scenario. Nevertheless, the enlargement of the storage capacity in Las Torcas Dam proposed by [8] implies an increment in consumptive demands of about 3 hm^3 per year, according to the PS. Then, it is not really a measure to reach the OS, since it increases water consumption. This is why it was considered in a FS scenario, independent of any applied measure. In consequence, for this case study, present state and future state are quite different, and the obtained TC is high.

4. River modeling

The simulation software [13], developed by the Polytechnic University of Valencia, contains two independent modules to simulate flow (SIMGES) and quality (GESCAL) patterns, respectively, of a river basin. This specific quality module makes possible to take into account, for several hydrologic years, aquifers, dams, diffuse returns, dangerous substances, or hydroelectric plants. Finally, its capacity of linking and editing GIS data fields, assure a flexible and reliable simulation tool.

4.1. Input data treatment

Input monthly flows data for each year within the 2002-2007 period, were introduced in the Aquatool-GESCAL interface. In particular, the modelled quality inputs parameters were sulphates, alkalinity, calcium, sodium, magnesium, chlorine, organic matter, nitrates, ammonium (in kg component/m^3), and the conductivity (µs/cm). The calibration of these input flow data constituted an important but not so easy task to be solved. Mass balances were carried out with the different water flows, by using the SIMGES program module, with deals with quantity figures. Quality data given by quality control stations along the river course [7] were used to structure quality water inflows in river stretches. Water deterioration provoked by its use was considered starting from the return ratios for different kind of users, eighty and twenty percent for urban and agriculture users, respectively [14], as well as from the elimination ratios of the existing Wastewater Treatment Plant of Cuarte [14-16], and the pollution ones for different users [16]. Additionally, monthly evolution of temperature, and dam related data as evapo-transpiration as well as level-capacity curves found in [7] were used.

4.2. Simulator outputs

Quantity and quality flow data were obtained, monthly, per simulated year and stretch. Then, exergy profiles could be calculated. By using (1), the quantity and quality components could be studied individually. Different exergy contributions were calculated [3-5], has follows: the Inorganic Matter (IM), which stands for inorganic salts and water; and the Nitrogen-Phosphorous (NP) component, which accounts for the nitrogen and phosphor in the water flow, in form of nitrates, nitrites, ammonia and phosphates. Organic Matter, thermal and potential components were also calculated.

5. Results discussion

A brief summary of the most important obtained results is included here. Figure 4 shows that only the PS flow evolution along the river differs from the other three stages flow values. It is due to Las Torcas Dam enlargement considered in the FS. The evolution along the river course of IM, OM and NP quality components is represented in Figs.5 to 7, for a given simulated month.

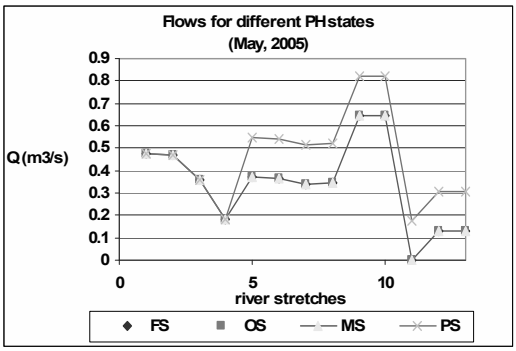

Fig. 4. Flow along the river course for different PH states

Figure 5 shows the evolution of IM quality contribution for one of the most cold and rainy months of the year. This is why the storing effect by Las Torcas Dam can be specially observed in the stretch five.

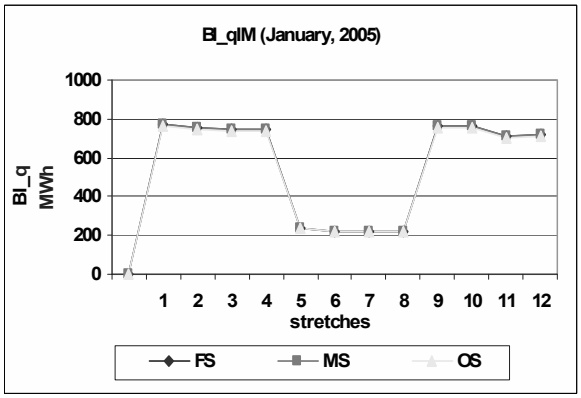

Fig . 5. IM quality component along the Huerva course

On the other hand, Figs 6 to 7 represent the evolution of NP and OM quality contribution for summer months. An exergy increment due to returns, mainly coming from agriculture, can be observed (see stretches five, nine and twelve).

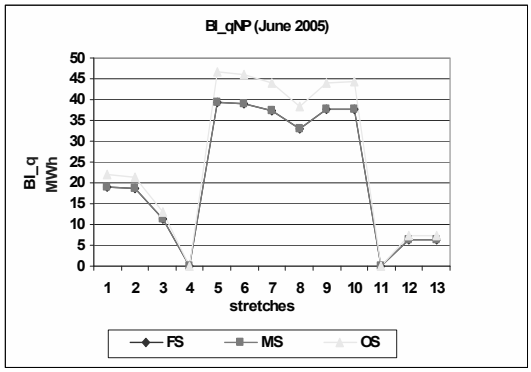

Fig.6. NP quality component along the Huerva course

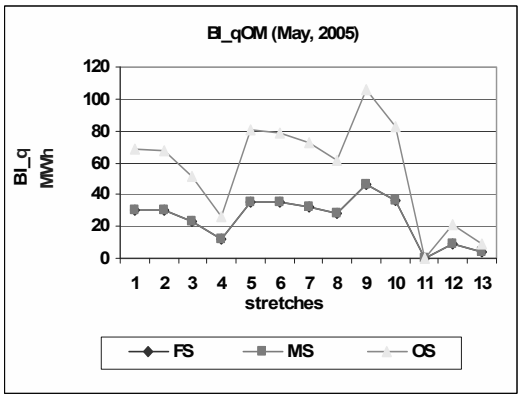

Fig.7. OM quality component along the Huerva course

As it can be seen in previous figures, measures are enough to fulfil with OS objectives. Then, MS water composition is far below the OS maximum required level, in spite of the almost imperceptible change of future state by measures. However, the TC values must be also analyzed. The component which is more easy to understand, its potential component (given by the product of the flow gap between PS and FS and altitude), is represented for two hydrologic years in Fig. 8. They were very different, not only due to the quantity of precipitations, but also for its distribution during the year. The hydrologic year 2005-2006 shows lower water storage, but it was high in some months in which lower water was stored during the previous hydrologic year 2004-2005. It shows the alternation of precipitations and runoffs quantities between two consecutive years, which is typical of the Mediterranean weather.

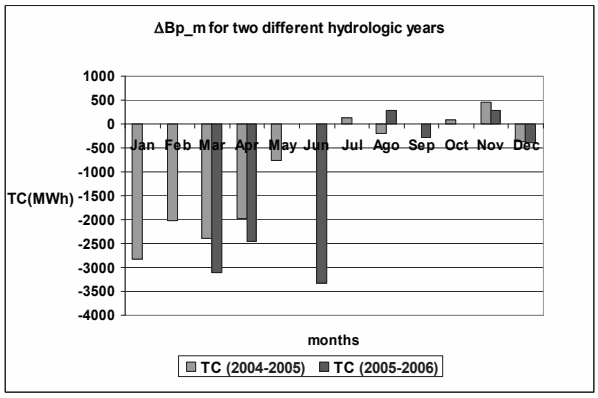

Fig. 8. Potential component during two Hydrologic years.

Finally, results of water pollution loads distribution among users and water restoration monetary charges are summarized in Tables 1 and 2, respectively. Higher pollution loads have been found for agriculture users (see Tables 1 and 2).

Table 1. Water pollution loads distribution among users

ΔB	URBAN use (%)	AGRICULTURE use (%)
ΔBq_IM	**0.63**	**99.37**
ΔBq_OM	**0.42**	**99.58**
ΔBq_NP	**0.49**	**99.95**
ΔBm_IM	**0.73**	**99.27**
ΔBm_OM	**0.22**	**99.78**
ΔBm_NP	**1.31**	**98.69**
AVERAGE	**0.63**	**99.37**

Table 2. Monetary water restoration costs for different users

ΔB	URBAN use (€/yr)	AGRICULTURE use (€/yr)
ΔBq_IM	**675**	**111,898**
ΔBq_OM	**3,150**	**521,865**
ΔBq_NP	**1,359**	**225,104**
ΔBm_IM	**914**	**124,280**
ΔBm_OM	**1,355**	**614,400**
ΔBm_NP	**32**	**234,723**

Note that, although Huerva river flows through Zaragoza, the main urban area in the Ebro Basin, figures do not shown this contribution due to the water sewage network. The urban pollution loads coming from this area are directed to the WWTP thought a pipe fed some kilometres upstream the

last quality reference station into the Huerva river, and poured downstream this quality station.

6. Conclusions

The main fulfilled goal in this paper consisted on applying PH to a river case study in Aragón, Spain. A new perspective which includes a new state named MS was added to PH methodology. Then, the effectiveness of PM proposed by water authorities, included in the WFD road map, was studied. In this way, the EC, calculated in previous works, was here divided in two contributions: the MC and the NCC, highlighting the variability of the PM effectiveness depending on the hydrologic year. It is possible that, in some years, MS could be good enough, even oversized, but, in others, they could not be adequate to reach the OS proposed by authorities.

This methodology was applied to the Huerva River, where the contribution of measures to reach the objective state (MC) is quite low. Nevertheless, since a future real state of the river by 2015 different from the current real state was considered, this TC contribution defined by the difference between both states gets more importance to lead on the fulfilment of the proposed Environmental Objectives.

Additionally, the contribution to river degradation due to users was divided among them, making possible the distribution of water restoration costs monetary charges. Main contribution to the quality and quantity river deterioration comes from agriculture. Higher abstractions, despite of the lower returns ratios, and the absence of WWTP for that use, contribute to higher river diffuse contamination charges. On the other hand, it must be underlined that urban pollution coming from the city of Zaragoza is not considered in the accounting of the urban users pollution loads, since it is directed to the WTP thought a pipe, and poured downriver to the Huerva death.

Finally, the simulation with an specific hydraulic software (here Aquatool) was a key point in this work, since it allows obtaining different water scenarios, making possible the calculation of exergy gaps between them, and even the diversion of them among users, taking into account the WFD road map.

Nomenclature

AUC: Agriculture Users Cost

AUS: Agriculture Users State

b: Specific exergy (kJ/kg water)

B: Exergy (KWh)

BP: Basins Plan

EC: Environmental costs

FS: Future State

GES: Good Ecological Status

Q: Flow (m^3/s)

MC: Measures Cost

MS: Measures State

NCC: Not Compliance Cost

OS: Objective State

PS: Present State

PH: Physical Hydronomics

PM: Plan of Measures

PS: Present state

TC: Transition Cost

UUC: Urban Users Cost

UUS: Urban Users State

WUS: Without Users State

WWTP: Waste Water Treatment Plant

Subscripts and superscripts

IM: Inorganic Matter

m: quantity

NP: Nitrogen-Phosphorous

OM: Organic Matter

q: quality

References

[1] The European Commission, 2009, *Report from the Commission to the European Parliament and the Council in accordance with article 18.3 of the Water Framework Directive 2000/60/CE on programmes for monitoring water status*, Technical report, [SEC(2009)415], Commission of the European Communities, Brussels.

[2] Martínez, A., 2009, *Exergy costs assessment of water bodies: Physical Hydronomics*, Ph.D Dissertation, University of Zaragoza, Aragón, Spain.

[3] Valero, A., et al, 2009, *Physical Hydronomics: Application of the exergy analysis to the assessment of environmental costs of water bodies. The case of the inland*

basins of Catalonia, Energy 34 (12), pp. 2101-2107.

[4] Martínez, A; Uche, J; Valero, A. and Valero, Al., 2010, *Environmental costs of a river watershed within the European water framework directive: Results from Physical Hydronomics*, Energy, 35 (2), pp. 1008-1016.

[5] Martínez, A. and Uche, J., 2010, *Exergy of organic matter in a water flow*, Energy 35 (1), pp. 77-84.

[6] Del Valle, J., el at, 2009, *Atlas de los ríos en Aragón,* Prames Ediciones, Gobierno de Aragón, Zaragoza, Spain [in Spanish].

[7] Confederación Hidrográfica del Ebro, 2009, *datos de la Oficina de Planificación Hidrológica,* Ministerio de Medio Ambiente [available online], URL: http://oph.chebro.es/

[8] Confederación Hidrográfica del Ebro*, 2006, Plan Hidrológico Piloto del río Huerva*, Technical report, Ministerio de Medioambiente, Confederación hidrográfica del Ebro, Zaragoza, Spain [in Spanish].

[9] Lecina, S, et al, 2009, *Efecto de la modernización de los regadíos sobre la cantidad y calidad de las aguas: la cuenca del Ebro como caso de estudio,* Instituto Nacional de Investigación y Tecnología agraria y alimentaria, Ministerio de Ciencia e Innovación, Madrid, Spain [in Spanish].

[10] Lecina, S., et al, 2008, *Modernización de los regadíos en al Cuenca del Ebro: Efectos sobre la Cantidad y Calidad del agua,* Technical Report, Instituto Nacional de Investigación y Tecnología agraria y alimentaria, Ministerio de Ciencia e Innovación, Madrid, Spain [in Spanish].

[11] Bielsa, J. and Duarte, R., 2000, La eficiencia técnica de riego: Análisis de las conexiones y la utilidad de sus diversas definiciones, *Estudios Agro-sociales y pesqueros*, nº 189, pp 103-118 [in Spanish].

[12] Red Aragón, 2009, *Nueva depuradora y mejor Iluminación*, La crónica, Campo Cariñena, nº 119, [online journal], URL: http://www.redaragon.com/cronicas/carinena

[13] Aquatool-DMA, quantity and quality water masses simulation software, October 2009, Software Package. Universidad Politécnica de Valencia. IIAMA. Spain.

[14] Hernández, A., 2001, *Saneamiento y alcantarillado. Vertidos Residuales*, Colegio de Ingenieros de Caminos, Canales y Puertos, Universidad de Zaragoza, Zaragoza, Spain [in Spanish].

[15] Instituto Nacional de Estadística (INE), 2007; Informe INE, datos 2007, Technical Report, INE, Madrid, Spain [in Spanish].

[16] Instituto Aragonés del Agua (IAA), 2005, *Medio Ambiente Aragón 2004-2005*, IAA, [online report], URL: http://portal.aragon.es

Acknowledgments: The authors greatly acknowledge, firstly, the financial support given to this paper, which is under the framework of the IDERE R+D+I project (ENE2007-067191), financed by the Spanish Ministry of Education and Science. Additionally, authors are very pleased for the helpful given by the Confederación Hidrográfica del Ebro organism belonging to the Spanish Ministry of Environment.

Energetic efficiency in Waste Water Treatments Plants: Optimization of activated sludge process coupled with anaerobic digestion.

Descoins Nicolas[a], Deleris Stephane[b], Lestienne Remi[b] and Maréchal François[a]

[a] *Ecole Polytechnique Fédérale de Lausanne, LENI, Switzerland*
[b] *Veolia Environnement, Anjou Recherche, France*

Abstract: This paper presents a study concerning the energetic optimization of a process for Waste Water Treatment including activated sludge reactors coupled with an anaerobic digestion reactor. The process deals with carbon and azote removal, by nitrification and de-nitrification, caused by heterotrophs and autotrophs micro-organisms biological activity. Starting from the [CEIT] approach, rigorous Plant-Wide models have been constructed and represent the bio-chemical transformations occurring inside the bio-reactors. The energetic consumption for Each Physical unit Operation involved in the flow-sheet is evaluated, and a full link is made between the biological activity and the electrical demand or production. Rigorous steady-state mathematical optimizations are then computed, and the influence of primary settling efficiency on electrical autonomy is quantified and demonstrated. The ammonium return from digestion to activated sludge reactors is also demonstrated to be a limiting factor for the overall energetic efficiency, as well as the C-substrate availability for denitrifying.

Keywords: WWTP, plant-wide, steady-state, optimization, modeling, energetic efficiency.

1. Introduction and general context

Wastewater treatment consists mainly in three major processes: biochemical treatments, liquid/solid separations operation and thermal processes for sludge treatment and valorization. The Figure 1 is an overview of a classical Waste Water Treatment Plant (WWTP), each unit representing a Physical Unit Operation (PUO). The wastewater is treated by mean of biochemical and settling processes in the water line. This water line finally results in two streams: the "purified" water, and a "sludge" stream, concentrated in biomass. The sludge line processes consist then in treating the sludge, by stabilizing and valorize it, before the remaining matter is released to the environment. Biological treatments are made inside different kind of reactors, and consist very basically in supplying oxygen (for aerobic treatment) inside the reactors in order to maintain and grow micro-organisms, which use the pollutants presents in raw wastewater as nutrients. The liquid/solids separation process step consists in separating the water (and soluble species) with the solid or pseudo-solid matter, called "particles". To achieve this step, different technologies exist. The most used is the settling process. Under gravity effect, the particles settles down and finally two streams are produced: a particle clarified stream and a particle concentrated stream. The sludge has also to be stabilized and reduced both in volume and pollutants concentration. Anaerobic digestion is a biological phenomenon that appears when oxygen and nitrate sludge concentrations are very low. Under specific temperature and for long residence time, specialized micro-organisms become active, using the remaining organic matter present in the sludge as nutrient and partially convert it into a mix of methane and carbon dioxide (gaseous phase).

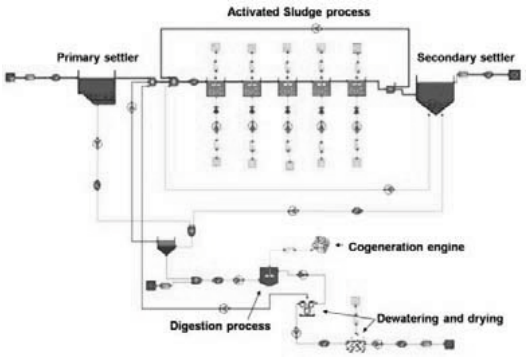

Figure 1 WWTP under study

This process (combined to dewatering and drying) leads to reduced and stabilized sludge volume. The

Corresponding author: Descoins Nicolas, nicolas.descoins@epfl.ch

biogas produced can be burned inside a cogeneration engine, and so heat and electricity is produced locally, reducing the energetic costs.

Up to now the scientific community involved in the field of waste water treatment has focused mainly on the water quality and associated modelling aspects. In our opinion, efforts must be done to link water quality and WWTP pollutants removal efficiency with energetic aspects, because future industrial practice in the context of global warming and fossil resource rarefaction will be greatly impacted by the energetic costs. Mathematical models and rigorous optimization algorithms are really helpful in this context, as they capture the main features of each Physical Unit Operation. Furthermore, they bring a deep understanding of the physical mechanisms and there interactions. All the models used in this work are implemented on gPROMS® platform, and the equations are solved using the numerical solvers provided by Process System Enterprise.

2. Modeling methodology

This section introduces the main mathematical models used in this work to run steady-state optimizations. Some equations are skipped as they are classical models available in the extensive literature concerning WWTP modeling. This is the case for the settling processes, including one-dimensional models and point models; which are in fact the basis for all the liquid/solid separation processes included on the flow-sheet studied in this paper. The biochemical modeling has been the subject of special attention, and the models developed for this study are conservative in terms of mass. The matter composition is also homogeneous in all the different PUO (plant-wide models) and therefore no special interfaces are needed to connect the Activated Sludge part and the Anaerobic digestion part. These models are based on the CEIT methodology [1]. The reactors models as well as the compressors and pumps models to evaluate the energetic consumption of the flow-sheet under study are also introduced.

2.1. Plant-wide biochemical modeling

The plant-wide models used for computations are presented under the form of a Petersen matrix and a kinetic vector, similarly to the ASM [2] and ADM [3] models. They are called PW AS (Plant wide Activated Sludge) and PW AD (Plant Wide Anaerobic Digestion) models, and are able to reproduce all the features of ASM and ADM models. The full details and the methodology used to develop these models will be given in a dedicated paper. The models have been compared successfully with literature benchmarks.

2.1.1. Defining a set of common species

The first step to build the models consists in defining the set of species that will be used in the plant wide models. This set must be able to reproduce all the features of ASM and ADM models. A particular effort has been made to avoid the use of lumped components, and all species, including each acids and bases, are taken into account. The plant-wide model will include 39 species (except water), divided into 25 soluble species and 14 particulate species. Each component include in the model is characterized in term of C, H, O, N, P, charge and equivalent Theoretical Oxygen Demand (ThOD). The elemental compositions for each compound are the same as those reported in [1]. Chemical equilibriums are also included, by describing corresponding acid/base reactions and kinetics. Some species are considered to be aqueous, and will be subject to mass transfer with a gaseous phase. Inerts are represented both in soluble and particulate forms, and these fractions are supposed to be common to the different biological models. Looking to the particulates components, some are considered as substrates, and others as groups of micro-organisms that degrade and transform the organic matter, releasing minerals and gaseous species. Concerning composites (organic particles and macromolecules), only one specie is taken into account. More composites could be included, as suggested in [1], and added to the stoichiometry matrices, if necessary.

2.1.2. Petersen matrix and kinetics vector for PW AS and PW AD models

The next step to build the AS and AD plant-wide models consists in writing the stoichiometry matrices and the kinetics vectors. The behavior of the different kinds of micro-organisms considered in the aerobic/anoxic and anaerobic reactors is described, assuming that the different groups are fully differentiated. The matrices are balanced for each element: C, H, O, N, P and ThOD. This is done by computing correct values for the sink or sources coefficients in the matrices (noted θ_j, C_j, N_j, P_j, H_j, O_j). The species chosen to fulfill the elemental balances are mineral ones: dissolved

oxygen, ammonium, phosphates, water and dissolved carbon dioxide or alkalinity.

Each biochemical process introduced in the PW matrices needs to be linked to kinetics expressions that follow general rules concerning the modeling of micro-organisms growth (Monod kinetics form). Generally-speaking and for a biological process corresponding to a growth referred by index j, the kinetic mathematical form is:

$$\rho_j = k_m \frac{S_{sub}}{H_{sub} S_{sub}} \frac{S_{sub}}{S_{tot}} A_{NH_4} A_{HPO_4} \ldots I_1 I_{pH} \ldots X_{bio} \quad (1)$$

The terms noted $A_{NH_4} A_{HPO_4} \ldots$ are called activation terms, and are related to the sink/source terms used to balance the stoichiometry matrix. The terms $I_1 I_{pH} \ldots$ are inhibition terms related to chemicals compounds or pH. Each process corresponding to a growth includes a rate kinetic parameter named k_m which is corresponding to a substrate uptake. The macro substrates (particles) are first hydrolyzed by enzymes to become available to the micro-organisms. Corresponding disintegration and hydrolysis rates expressions are functions of the ratio between the hydrolyzed substrate concentration and the total micro-organisms concentration [2]. The full expressions for the AS and AD kinetics vector are written following these rules. The source term involved in mass balance equations for each specie i is then deduced by the following relationship:

$$r_i = \sum_{j=1}^{N_{pro}} (\nu_{ij} \rho_j) \quad (2)$$

ν_{ij} are the matrix coefficients, ρ_j the kinetics rates and N_{pro} the number of chemical processes included in the biological model.

2.2. Completely Stirred Tank Reactors (CSTR) models

Activated sludge processes are usually operated in aerated tank reactors and channels, the mixing is ensured for a part by mechanical work (impellers) and the other part by aerators. Concerning Anaerobic Digestion, more sophisticated reactors exist, and could involved particles separation from water (membranes) and/or settling effects. The reactors involved in this work are modeled using the CSTR hypothesis. Each reactor model include two phases, a liquid and a gaseous phase, mainly because all the energetic aspects involved in Waste Water Treatment are strongly associated to gaseous mass transfer (oxygen transfer to activated sludge and methane production by digestion).

2.2.1. Liquid phase mass balances

The mass conservation equations for the liquid phase are written under the following form for each compound i, C_i is a concentration referring to one of the soluble or particulate components include in the plant-wide models.

$$\frac{dC_i}{dt} = \frac{Q_{liq}}{V_{liq}} (C_i^{in} - C_i^{out}) + r_i = k_l a_i (C_i^{sat} - C_i^{out}) \quad (3)$$

Some compounds are subjected to mass transfer with the gas phase (but not all the compounds). The Henry law coupled with an experimental law for computing the liquid gas exchange coefficient will describe the mass transfer phenomenon for the activated sludge reactors. The exchange $k_l a$ coefficient is then a function of gas flow rate, gas composition and diffusers characteristics. For the digester, the exchange coefficient is set to the value indicated in [3]. Combined with plant-wide models, 40 equations must be solved for each reactor if the water compound is included.

2.2.2. Gas phase mass balances

The use of mole per liter (noted n) as the unit for gases is convenient, and mass balances equations for gaseous components could be deduced from general mass balance equation:

$$\frac{dn_i^{out}}{dt} = \frac{\dot{V}_{gas}^{in} n_i^{in} - \dot{V}_{gas}^{out} n_i^{out}}{V_{gas}} + k_l a_i \frac{V_{liq}}{V_{gas}} \left(\frac{C_i^{sat}}{M_i} - \frac{C_i}{M_i} \right) \quad (4)$$

No chemistry is considered to occur in the gas phase, and so no source terms appear in the equation(4). The mass transfer between liquid and gas is still taken into account by mean of the $k_l a_i$ coefficient and associated term involving saturation constants for aqueous compound. The total gas flow rate is then deduced from the perfect gas law, including the mass transfer from the liquid phase to the gaseous phase:

$$\dot{V}_{gas}^{out} = \frac{P_{gas}^{in}}{P_{gas}^{out}} \frac{T_{gas}^{out}}{T_{gas}^{in}} \dot{V}_{gas}^{in} + R \frac{T_{gas}^{out}}{P_{gas}^{out}} V_{liq} \sum_{k=1}^{N_{gas}} k_l a_k \left(\frac{C_k^{sat}}{M_k} - \frac{C_k^{out}}{M_k} \right) \quad (5)$$

The gas pressure at the entry (the bottom of the reactor) is corresponding to the pressure required to compensate the pressure surrounding the bubbles, which is caused by the diffusers submergence (water column above the diffusers), the tension surface of water that must be broken to form bubbles. The inlet pressure P_{gas}^{in} is then given

by, where H_{aer} is the height of the water column above the diffuser:

$$P_{gas}^{in} \quad P_{atm} \quad)_{liq} g H_{aer} \quad P_{bubbles} \qquad (6)$$

Consequently, the aeration system (usually compressors) must pressurized the gas to the required pressure P_{gas}^{in} to form bubbles inside the reactor, but it also need to compensate the head losses due to the network distribution pipes and diffusers, which are taken into account.

2.3. Pumps and compressor modeling

Waste Water treatment plants involve many different liquid and gases flow through pipes monitored by pumps and compressors. Even if the main water stream is powered by gravity only (caused by altitude differences), the electric consumption caused by pumping and pressurizing is the main plant energy consumer. Actually, pumps counts for 25 percent of the total electrical consumption, while compressors used for aeration counts for almost 70 percent. The head losses insides the pipes are quantified by mathematical expressions. For example we use the following semi-empirical relationship, (Lechapt-Calmon formulae):

$$P \quad)_{liq} g \; 0.0011 \quad \dot{m}_{liq}^{1.89} D_{pipe}^{5.01} L \quad Z \qquad (7)$$

The pipe diameter and length are taken into account, as well the altitude difference between the (,)) (,) . ,))) s upon the liquid mass flow rate and the pipe diameter could be identified from experiments if necessary. The energy requirement for pumping the liquid through the pipe considered is then deduced from the following law (assuming incompressible flow):

$$\dot{E}_{pumps} \quad \frac{100}{} \dot{V}_{liq} \quad P \qquad (8)$$

The diameter and the length of the pipe must be specified, as well as the altitude difference, corresponding to the flow. $\dot{E}_{pumps}$ is expressed in kWh.day (,))) lly ranged within 60 and 85 percent.

The oxygen is supplied to the micro-organisms in the reactors by mean of a pressurized gas (usually air), distributed by a pipe network and diffusers placed on the bottom of the tanks. Only subsurface aeration is considered in this work, as it is the most efficient way from an energetic point of view to blow air into the reactors [5]. The gas must be pressurized to the required pressure (deduced from equation(6)) in order to produce a gas flow through the reactor liquid phase and to transfer oxygen in a sufficient quantity to let the micro-organisms grown. Compressors are generally employed to blow the gas, and a simple model is used in this work to estimate the corresponding energy consumption. The model is based on the assumption of a polytropic flow, the corresponding law is given by equation(9):

$$PV^{n_p} \quad cste \qquad (9)$$

The polytropic head H_p (in J.mol) is deduced from equation (9) and represent the energy required to pressurize one mole of gas:

$$H_p \quad \frac{n_p}{n_p \quad 1} \quad RT^{in} \quad \left(\frac{P^{out}}{P^{in}} \quad P\right)^{\frac{n_p}{n_p \quad 1}} \quad 1 \qquad (10)$$

,)))) ,)) . .) inside the pipe network linked to the diffusers and used to distribute the gas to the aerated reactor surface. It is calculated using the singular head losses relationship corresponding to equation(7). The power $\dot{E}_{comp}$ consumed to pressurize from P^{in} to P^{out} is given by equation(11), where the pressure are expressed in Pa and the volumetric flow rate in m day :

$$\dot{E}_{comp} \quad \frac{100}{} H_p \frac{\dot{V}^{in} P^{in}}{RT^{in}} \qquad (11)$$

$\dot{E}_{comp}$ is expressed in J.day , it is further converted to kWh.day to be coherent with the pump model.

3. Steady-state optimizations

The PUO models could be linked on flow-sheets to reproduce the Activated Sludge process combined with the Anaerobic digestion process. The resulting model is a set of equations that could be solved both for dynamic or steady-state cases. The WWTP configuration studied is reproduced on Figure 1.

3.1. Initialization and steady-state

To compute a steady-state, an influent to the process is first specified, by defining the inlet temperature, the volumetric flow rate of water and the concentration of the different species considered in the PW models. A complete set of parameters is also required, and we use the ASM1 benchmark (BSM1) [4] and the ADM1 [3] as references for the biochemical, aeration and

settlers models. The influent to the WWTP was also specified similarly to the BSM1, corresponding to dry weather. The energetic consumption of each pumps and compressors is deduced from the energetic data available in the BSM1 [4] or in the OFEN Report [5].

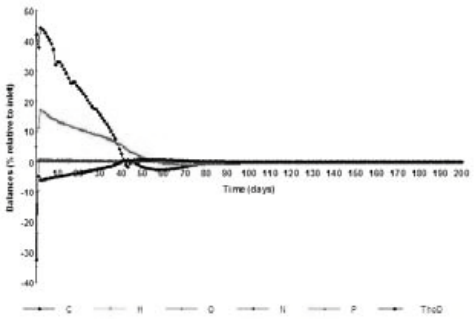

Figure 2 Mass balances during initialization

The models are then solved for the corresponding steady-state by an initialization procedure, and the mass balances are systematically checked to ensure that a steady-state is effectively reached (see Figure 2).

3.2. Optimal point and parametric procedure

To optimize the WWTP, some variables are set as decision variables and the optimization algorithm will compute them (within a predefined range) to minimize or maximize a predefined objective function, satisfying in the same all the constraints imposed to the system. This optimal set of variables is corresponding to a minimum or a maximum of the objective function from a mathematical point of view. If one (or more) constraint is modified, a new set of decision variables is obtained. This procedure is called parametric optimization, and a special algorithm is used to obtain a complete range of optimal points corresponding to different constraints on water quality. The procedure used in this work is resumed on Figure 3. Each steady-state optimal point is recomputed by the initialization procedure and the result is saved as a text file (including all the models variables), by using the optimal set of decision variables, solution of the optimization problem. The main decision variables are reported in the Table 1. The optimisation problem must also be constrained correctly, in order to obtain realistic results. The constraints define the water quality, by specifying indexes on Chemical Oxygen Demand (COD) and azotes at the exit of the WWTP, in the clarified and treated water. The values are expressed by cubic meter of water incoming to the WWTP.

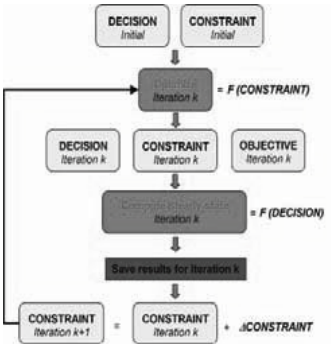

Figure 3 Optimization algorithm

Table 1 Main decision variables

Q_1	Q_2	Q_3	Q_4	Q_5	R_d	Q_W	Q_N	Q_R	p
Air flow rate in AS reactor n°1	Air flow rate in AS reactor n°2	Air flow rate in AS reactor n°3	Air flow rate in AS reactor n°4	Air flow rate in AS reactor n°5	Digester radius	Secondary settler wastage	Nitrate recycle	Secondary settler recycle	Primary settler efficiency
m^3/day	m^3/day	m^3/day	m^3/day	m^3/day	m	m^3/day	m^3/day	m^3/day	-

A constraint is also specified for the sludge age, corresponding to an acceptable range. The sludge age is representing the residence time of particles in the Activated Sludge process. Constraints are also imposed for the residence time in digester, for Total Solids Suspended (TSS) in Activated Sludge reactors and at the inlet of the digester reactor (noted TSS_{dig}). The Table 2 resumes the constraints and the associated units and range. The constraint on NH_4 is varying and it is the object of the parametric optimization procedure, as the removal of ammonium is known to be a strong limiting factor to the overall energetic efficiency of WWTP. The constraint on NO_3^- is also varied, and set to predefined values (8, 12 and 20 gN/m^3).

Table 2 Constraints imposed to the system

	out COD	out NH_4	out NO_3	sludge	meso	TSS_{AS}	TSS_{dig}
	$gCOD/m^3$	gN/m^3	gN/m^3	days	days	g/l	g/l
min	0	0	0	5	10	1	50
max	60	Var*	8,12,20	35	50	9	50

3.3. Results

The parametric optimization procedure has been applied to the flow-sheet reported on Figure 1. The objective function to maximize was define as the electrical autonomy of the WWTP, E_{auto}:

$$E_{auto} \quad \frac{\sum_{k=1}^{N_{comp}} \dot{E}^{k}_{comp} + \sum_{n=1}^{N_{pump}} \dot{E}^{n}_{pump} + \sum_{m=1}^{N_{puo}} \dot{E}^{m}_{mix}}{\dot{E}_{cogen}} \qquad (12)$$

Where $\dot{E}^{m}_{mix}$ is the electrical consumption for mixing and operate the PUO indexed by m. N_{comp}, N_{pump} and N_{puo} are respectively the numbers of compressors, pumps and Physical Unit Operation involved in the process. Consequently, the optimizer algorithm will try to find optimal configuration corresponding to a minimal operating electrical consumption and maximal biogas production (or maximal electricity production by the co generation engine). The cogeneration engine is assumed to be efficient to 30 percent concerning the electricity production.

3.3.1. Primary settling efficiency as parameter

The first computations presented have been done by considering the primary settler efficiency as a parameter, varying between 0% and 100 %. 0% efficiency means that the particles incoming to the WWTP are not segregated by the primary settler, and the concentration of particles in the main water flux and in the primary sludge flux (which is not really a sludge in this case) are the same. 100% efficiency means that all the particles incoming to the WWTP are going to the primary sludge and consequently in the digester. The pre-settling before the digester reactor ensures that the mix of secondary and primary sludge is sufficiently concentrated in all the cases (TSS_{dig} constrained to 50 g/l). The results corresponding to $^{out}_{NO_3}$ = 8 gN/m^3 are presented on Figure 4. As we can see, the electrical autonomy is strongly dependent on the water quality at the exit of the WWTP (in the clarified water stream). Usually, WWTP are removing azote from waste water, and work in a range for the exit ammonium concentration lower than 10 gN/m^3. Consequently, it is important to optimize the process and understand the limiting mechanisms in this range. The more efficient is the primary settler, the more available particulate organic substrates are sent to the digester (the primary sludge is in this case richer in C-substrate), and the more biogas is produced. This is why the electrical autonomy is increased when the primary settler efficiency is increased, but this tendency tends to reverse for efficiency superior to 50% and for high NH_4^+ removal.

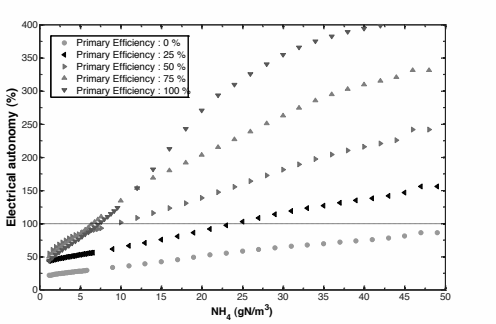

Figure 4 Optimal electrical autonomy for $^{out}_{NO_3}$ = 8 gN/m^3

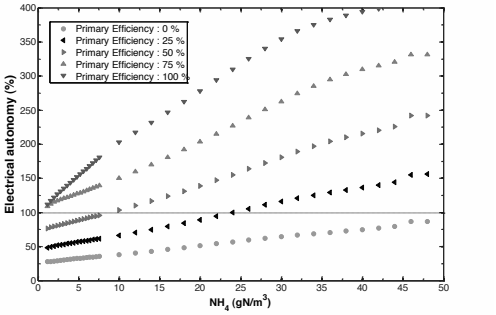

Figure 5 Optimal electrical autonomy for $^{out}_{NO_3}$ = 20 gN/m^3

The same calculations have been done for $^{out}_{NO_3}$ = 20 gN/m^3 and the corresponding results are reported on Figure 5. The same kind of observations can be made, but an increase of the electrical autonomy is noticed, corresponding to a primary settler efficiency superior to 25%. For 75% and 100% primary efficiency, the electrical autonomy is more than 100 %. Consequently, we can say that the de-nitrification process by heterotrophs (removal of NO_3^-) is limiting the overall efficiency of the system, together with the nitrification process by autotrophs (transforming the NH_4^+ ions into nitrate NO_3^-). To visualise the intensity of nitrification / de-nitrification in the activated sludge reactors and the ammonium production in the digester for optimal points, the corresponding production or consumption of NH_4^+ and NO_3^- ionic species are plotted on Figure 6.

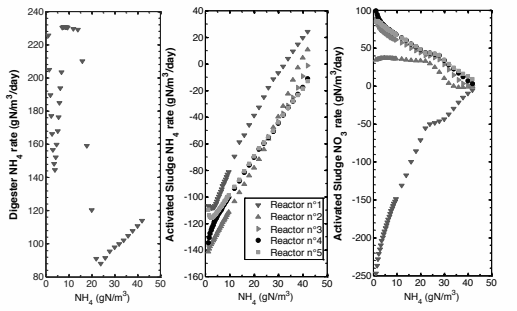

Figure 6 Ammonium and nitrate rates (primary settler efficiency = 100% and $I_{NO_3}^{out}$ = 8 gN/m³)

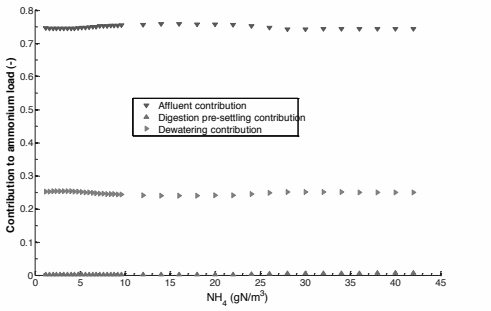

Figure 7 Contributions to ammonium load incoming to the Activated Sludge reactors (primary settler efficiency = 100% and $I_{NO_3}^{out}$ = 8 gN/m3)

As expected, when the primary sludge is richer in available C-substrate (corresponding to 100 % efficiency), the more biogas is produced but also the more ammonium is produced by the digester. This ammonium production is caused by the hydrolysis of the proteins present in the primary sludge sent to the digester, which contains both C and N elements. The ammonium produced is then returned at the entry of the activated sludge process when the sludge outgoing from the digester is dewatered, as shown on Figure 7. As the liquid return from dewatering is highly concentrated in ammonium, the contribution to the total load is quite important (up to 25%) and it can be noticed that the optimal solutions consist in limiting the size of the digestion reactor in order to maintain the production of NH_4^+ to reasonable level (accounting for no more than 25% percent of the total load). This is easily checked by plotting for example the optimal residence time in the digestion reactor (Figure 8).

The lack of Carbon in the anoxic reactors for denitrifying also strongly limits the efficiency of the whole plant, because more particulate substrate must be maintained in the Activated Sludge reactors in order to produce available C-substrates, which leads to an increase in the oxygen demand and consequently on the electrical energy required to blow air inside the liquid phase.

The optimal sludge age is plotted on Figure 9 and confirms this trend. The sludge age increase with the quantity of particulate substrates sent to the digester (the primary efficiency increase in this case). The requirements on C-substrate for denitrifying are still important, and the quantity of particulate matter hydrolyzed in the activated sludge reactors is then increased, leading to the formation of available C-substrate for denitrifying.

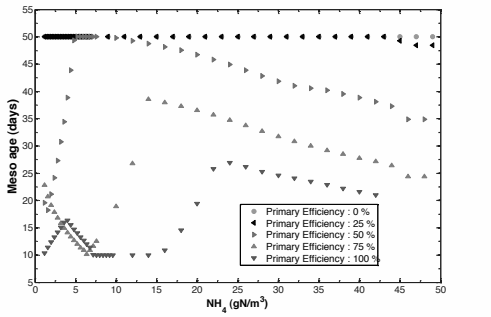

Figure 8 Optimal residence time in the mesophile digester ($I_{NO_3}^{out}$ = 8 gN/m³)

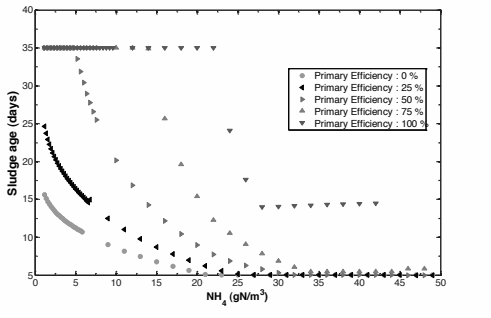

Figure 9 Optimal sludge age ($I_{NO_3}^{out}$ = 8 gN/m³)

3.3.2. Primary settling efficiency as decision variable

The results presented in the previous section demonstrate the importance of the primary settling on the energetic efficiency for the whole process, and we set in the next computations the primary settling efficiency as a decision variable. The optimizer can now estimate optimal values for this efficiency. The others decision variables and constraints are identical. The maximal electrical autonomy is computed for three values of NO_3^- concentration at the exit of the WWTP, the results are reported on Figure 10.

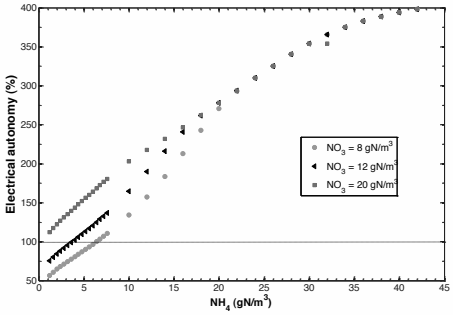

Figure 10 Optimal electrical autonomy with primary efficiency as decision variable

Compared to the case where the efficiency of the primary settler is fixed a priori, the electrical autonomy is slightly increased (superior for all cases to 50%). The optimal values for the primary settler efficiency are reported on the Figure 11.

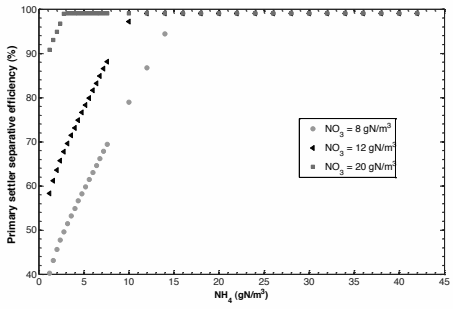

Figure 11 Optimal primary settler efficiency

As shown, optimal values for the primary settling efficiency exists, and the more ammonium and nitrate removal is requested, the less particulate substrates are sent to the digester. Both the ammonium production by the digester and the carbon requirement for denitrifying are limiting the overall energetic efficiency of the system.

4. Conclusions and perspectives

Mathematical models for most of the Physical Unit Operation involved in WWTP have been developed and implemented on gPROMS platform. The resulting sets of equations are solved to compute optimal steady-state configurations. The results presented focus on electrical efficiency, but others studies are possible, for example by including economic costs. Two mechanisms have been demonstrated to be limiting factors to the overall energetic efficiency, the production of ammonium by the digestion process, and the lack of available C-substrate for denitrifying in the Activated Sludge reactors. The interest of specialized treatment for ammonium highly concentrated streams is highlighted, as well as the interest to provide carbon substrates form external sources. Future work will focus on including Sharon-Annamox [6] process to the models library. A rigorous methodology to identify models parameters from a real pilot plant is also planned, by using the identification parameters and experiments design methodology available on gPROMS software.

References

[1] P. Grau, M. de Gracia, P.A. Vanrolleghem, E. Ayesa, 2007. *A new plant-wide modelling methodology for WWTPs.* Water Research 41 4357-4372.

[2] Henze M., Gujer, Mino, T. and van Loosdrecht M. *Activated Sludge Models ASM1, ASM2, ASM2d and ASM3.* IWA Scientific and Technical Report, London.

[3] Batstone, D.J., Keller, J., Angelikadi, R.I., Kalyuzhnyi, S.V., Pavlostathis, S.G., Rozzi, A., Sanders, W.T.M., Siegrist, H., Vavilin, *Anaerobic digestion model n°1. V.A.* 2002, Scientific and Technical Report n°13, IWA publishing London.

[4] *Benchmark Simulation Model n°1*, http://www.iea.lth.se/publications/Reports/

[5] *L'énergie dans les stations d'épurations*, Office Fédéral de l'Energie, Berne, Suisse.

[6] U. van Dongen, M.S.M. Jetten and M.C.M. van Loosdrecht, *The SHARON®-Anammox® process for treatment of ammonium rich wastewater.* Water Science and Technology: Vol 44 No1 pp 153–160.

The hidden value of water flows: the chemical exergy of rivers

Antonio Valero, Javier Uche, Amaya Martínez[*]
CIRCE – University of Zaragoza, Zaragoza, Spain

Abstract: The hydroelectricity potential of rivers is a very well-know parameter used to characterize the availability of a river as a function of its flow and its altitude. However, the chemical potential of water flowing through the rivers is commonly ignored. In its source, water presents high quality and, therefore, it owns an important availability that can be expressed through its chemical exergy value. On the opposite, when it flows into the sea and reaches the thermodynamic equilibrium, it can not be further used and it is converted into a null exergy value. Within these two limit values, the exergy state of the river at its different stages can be assessed. On the other hand, water availability for specific uses depends on its quality.
In this way, the almost always hidden value of water, its chemical potential, is highlighted and can be compared to the potential component, since they are expressed in the same units (energy units). In this paper, it is shown that potential and chemical exergy values of rivers rise up with values with the same order of magnitude. That is, the chemical value of a river is, from a thermodynamic perspective, as much as its potential value. The main difference lies in the current available technologies to take advantage of those physical disequilibrium: while hydro-power turbines are a completely proved technology, there are not yet commercial devices to take advantage of the hydro-chemical potential.
Results of those estimations for a small Spanish river, the Muga river, are presented in this paper in order to prove the accuracy of the methodology. It is shown that the potential exergy of that river ranges from 2.37 to 7.15 MW, while its chemical exergy is comprised between 2.30 and 8.78 MW for the present state of the river. In addition, several exergy indexes are defined as basic parameters to provide information about the advantage taken from the river, that is, about the water uses within the watershed.

Keywords: exergy of water, chemical exergy, water potential

1. Introduction

The energy of moving water has been used for thousands of years to power flour mills and irrigation systems. Water wheels were set within a flowing river, and the rotation generated movement was transformed into shaft work. In fact, water was the primary energy source for industrial applications during the 19th Century, when mill buildings appeared along the rivers throughout the Europe and United States [1].
This way of producing electricity has been improved along the years and it is nowadays a well proved technology despite of its inconvenient consequences such as those associated to the construction of reservoirs.
Hydroelectric power is then one of the oldest power generation methods and a critical part of world power generation (15% of the share of world global electricity). It is expected to continue expanding due to its non-reliance on fossil fuels, especially in developing countries with high potential.
The operating costs of hydro-power utilities represent only a small fraction of the initial capital cost. Hydroelectricity is a compelling partner to ensure security in mixed power systems as well and the multi-purpose reservoirs can be associated to security of water supply as well as power [2]. As far as hydropower resources are concerned, the IHA [3] estimates that only one-third of the realistic potential has been developed.
Just like mass flows spontaneously from a position of high gravitational potential to a position of low gravitational potential, it is also well-known that matter flows from a region of high chemical potential to a region of low chemical potential. The chemical potential can therefore be used to determine whether or not a system is in equilibrium. That chemical imbalance in the river streams flowing to the sea is pointed out in this paper. If our technology were able to take advantage of the available energy coming from chemical potential of water, an important amount of energy could be obtained.
The associated physical phenomenon is the osmosis effect. As it is well known, it is the net movement of water across a selectively permeable membrane driven by a difference in osmotic pressure across the membrane. Present-day applications of the osmosis phenomenon extend from water treatment and food processing to power generation and novel methods for controlled drug release [4]. In the field of water

* Corresponding author: amayamg@unizar.es

treatment, reverse osmosis is generally a more familiar process than osmosis.

Osmosis is also named as forward osmosis (FO) or direct osmosis. This phenomenon has been used at bench-scale to treat industrial wastewaters and to treat liquid foods in the food industry; and to concentrate landfill leachate at pilot- and full-scale. FO is also being evaluated for reclaiming wastewater for potable reuse in life support systems (at demonstration-scale), for desalinating seawater, and for purifying water in emergency relief situations [4]. Recent developments in materials science have also allowed the use of FO in controlled drug release in the body. Nevertheless, there are few publications in literature on the use of osmosis for water treatment and/or engineering applications. In any case, the reported initiatives regarding the state of the art of the FO make clear that it is still an immature technology when the attention is focused on a large scale, that is, for instance, on taking advantage of the chemical potential of rivers.

In order to assess such a chemical value, our proposal is to include the quality and degradation aspects in the analysis of water bodies. A river is something further from altitude and flow. It is the core of the fluvial ecosystem that embodies life and it chemical composition and chemical potential are therefore a fundamental aspect in its characterization.

From a physical perspective, this means to include the second law of thermodynamics i.e. [5]. i.e. exergy as the working tool.

2. Thermoeconomic basis

Many authors have contributed to the development of exergy and thermoeconomic accounting, completing the existing theories and even opening new research lines [6-15]. As it is well known, the exergy balance accounts for the degradation of energy. Eq. (1) quantifies the irreversibilities of a process as the difference between the input and the output flows.

$$B_{input} - B_{output} = \sum I \qquad (1)$$

Within thermoeconomics, each flow or some purposive combination of flows are identified either as fuel, product or residual (waste). Then Eq. (1) becomes for pro-energy devices, those whose aim is to increase the exergy of the product(s):

$$F - P = R + I > 0 \qquad (2)$$

And, for anti-energy devices, those whose aim is to deliberately decrease the exergy of the residual(s):

$$R + F_R = I_R \qquad (3)$$

Where F_R is the additional fuel needed to get rid of the residual and I_R the additional irreversibility caused for such an abatement. Equations (2) and (3) are of utmost importance because they place *purpose* in the heart of thermodynamics. The desire to produce a certain product is external to the system, and must be defined beforehand. This information is not implicit in the second law and is the most important conceptual leap separating and at the same time joining Physics and Economics.

As a summary, it can be said that in any flow, a product and a waste or residual component can be identified. This idea is applied in the following.

In addition, the analogy between the availability of a natural resource and its exergy helps us to relate each resource parameter with its exergy components. These parameters are physical and also chemical and will be explained in section 3.

Exergoecology is defined as the application of the second law of thermodynamics and thermoeconomics for the assessment of natural fluxes and resources on the Earth [7]. The consumption of natural resources implies destruction of organized systems and dispersion, which is in fact generation of entropy or exergy destruction. This is why the exergy analysis can describe perfectly the depletion of natural capital and, specifically, the degradation of water bodies.

The application of the explained theory to a watershed can be faced from to different boundary systems:

i) Water-related technology plants

ii) The whole river

2.1 Water plant approach

First, the water-related plants operating in the river basin can be studied. The eventual type of technologies would be:

2.1.1) Potential exergy device or conventional Dam, where the potential energy of water is converted into electricity.

2.1.2) Chemical exergy device (CED). Although they do not currently exist, they would be based on forward osmosis phenomena.

Both devices could be represented by the general schema shown in Fig. 1 and analyzed according to Eq. (4), where it can be identified the exergy as fuel in the input (i) and output points (o), the

obtained product (P) and the irreversibility of the process (I). It is directly obtained from Eq. (2).

$$F_i - F_o = P + I \qquad (4)$$

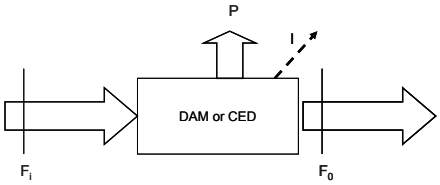

Figure 1. Dam or CED diagram

2.1.3) Waste water treatment plant (WWTP). They are located close to the water use areas and they are the most common quality-restoration technologies in any watershed.

Before representing the plant diagram, as in the two previous technologies, it may be convenient to state that, from the previous analysis, any water flow can be interpreted as an exergy flow carrying some valuable exergy, the product P, and some exergy that needs to be eliminate, the residual R. The stated final objective in a WWTP would be then eliminating that R. To achieve the final state, external exergy sources need to be implemented. F_R represents the expended exergy to clean-up or produce quality water. In particular, the idea can be summarized as Figure 2 indicates. Each part of the water flow, the product P and the waste R, can be characterized by it chemical exergy, which is separately given for its inorganic matter and organic matter components. This separation is commonly used in Physical Hydronomics [16], since the measures to restore them are different.

The exergy of the product is defined by the exergy in the objective or aimed state of the river (OS) in a given location. However, in order to reach such a state, the waste R (accounting for the difference between the present state, PS, and the OS) has to be eliminated.

The waste R may show a negative or a positive value depending on the considered parameter, but it does not affect the concept of being a residual that needs to be eliminated from the water flow.

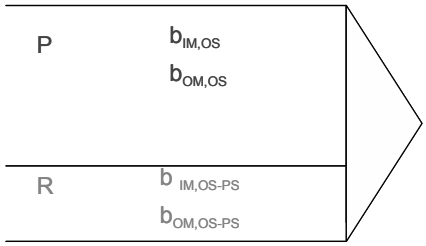

Figure 2. Water stream as an exergy flow

The irreversibility in the system is then given by the waste and the exergy that is needed to expend in order to eliminate it (Eq. 3). In the considered water flow, a part of the residuals to be eliminated is organic matter, OM, mainly coming from the urban domestic uses, and the other one is inorganic matter, IM, accounting for the excess of different salts (Eq. 5).

$$R_{OM} + R_{IM} + F_{R,OM} + F_{R,IM} = I_R \qquad (5)$$

In consequence, the simplified diagram of a WWTP according to the Thermoeconomics theory is as shown in Fig. 3. The irreversibility I and the residue R (R_{OM}+R_{IM}) comprise the I_R term in Eq. (5).

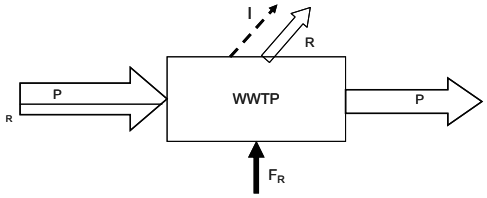

Fig. 3 WWTP diagram

An index related to this dissipative process can be defined. The residuals in the treatment plant index (RTPI) is the ratio between the residuals and the fuel used to eliminate that waste (Eq. 6). Nowadays, the OM is the factor determining the value of this index because it is the most representative parameter being eliminated in the waste water treatment plants (WWTPs).

$$RTPI = -\frac{R}{F_R} \qquad (6)$$

The value of this index in the studied cases is, in general, lower than one because of the amount of exergy required to clean the river. However, its theoretical limit value is infinite when the river were restored without using any external exergy source.

2.2 Whole river approach

By making wider the boundaries of the system the whole river can be studied from an exergy perspective. Two approaches are considered: the productive (pro-energy) approach and the dissipative (anti-energy) one.

2.2.1) Pro-energy river approach. The river can be seen as a fuel (F_{pot} and F_{chem}) flowing to the sea from which different products (P_{pot} and P_{chem}) can be obtained. Within the basin, several dams (ΣDam) and chemical exergy devices (ΣCED)

may exist. The conceptual diagram is shown in Fig. 4.

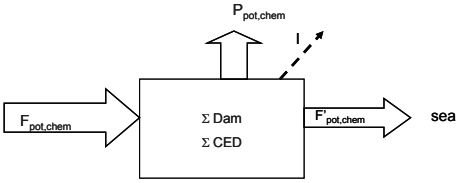

Fig. 4 Productive (pro-energy) overall vision of the river

Going further in this idea, some pure thermoeconomic index may be defined. Remember that there exist two basic exergy values for any given location of the river: the potential and the chemical potential. As said before, only the potential component is exploited in hydro-electrical utilities. The chemical potential, although important and existing, is commonly ignored.

In this way, the index of potential use of the river (PURI, Eq. 7) and the index of chemical use of the river (CURI, Eq. 8) may be defined. They can be both understood as indices of the productive process naturally related to water.

$$PURI = \frac{P_{pot}}{F_{pot}} \qquad (7)$$

Where P_{pot} represents the energy obtained from the facilities along the river course, in MWh/yr, and F_{pot} stands for the existing potential in the watershed (potential exergy component of a water flow) due to the height differences. Conventionally it is named as the gross theoretical capability of hydropower in the watershed. This index, therefore, gives an idea about how much of the height potential is being used and its maximum value is one.

In parallel to the potential coming from the altitude, the chemical potential is relevant as well.

$$CURI = \frac{P_{ch}}{F_{ch}} \qquad (8)$$

Where P_{ch} is the energy obtained from the facilities using the chemical potential of the water and F_{ch} stands for the existing potential in the watershed. Currently, there is not any utility able to take advantage of the chemical exergy of the river at large scale and, in consequence, P_{ch} is equal to zero in any river. Then, the chemical use index of rivers is, at the current technology state, null.

2.2.1) Anti-energy river approach. Here, all the WWTPs contributing to the maintenance of the river with an adequate quality are accounted for. The required exergy to operate all of them (ΣF_R) is compared to the chemical exergy of the river, given by F_{chem}. The considered flows are schematized in Fig. 5.

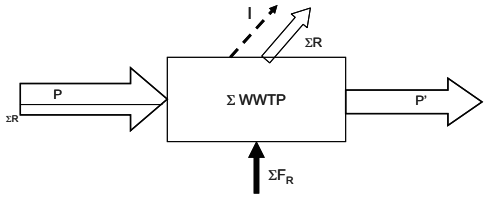

Fig. 5 Dissipative (anti-energy) overall vision of the river

A third index can be additionally defined in order to obtain information about the fuel consumed to keep clean the whole river waters, in relation to the overall chemical potential in the river. That is the fuel-residuals river index (F_RRI), as Eq. 9 indicates.

$$F_R RI = \frac{F_R}{F_{ch}} \qquad (9)$$

The analysis of this index is very interesting, since it allows the comparison between the exergy that could be potentially obtained from the chemical disequilibrium in the river and the exergy that is currently being invested to return the water flow with a good enough quality. It could happen that more resources were needed to maintain water with the required quality than the real exergy contained in the stream.

3. Methodology

When using a resource, it must be changed chemically and physically to the required conditions (e.g., for human consumption, water must be extracted from a river or sea, must be purified and finally sent to end users). In consequence, the exergy of a system gives an idea of its potential for not being in thermodynamic equilibrium with the Environment or, what is the same, for not being in a dead state related to the Reference Environment, RE.

The most important features of the exergy components of water have been studied in the literature [15, 16]. Potential, chemical and, in

some cases, thermal components are concluded to be the more relevant parameters to be studied in general water bodies analyses, which makes them differ from the surroundings.

The proposed assessment methodology starts with a deep knowledge of the watershed. First, a set of gauging stations and chemical measurements are identified and filtered with the final target of getting measures of flow and quality coinciding in space and time. Since they do not generally cover the whole river area, a simulation software is implemented to complete the input data for the exergy calculations. Afterwards, from the exergy values along the water flow, the exergy profile of the river is obtained by integrating the exergy values along the course, according to Eq. (10) and Eq. (11) . These calculations are developed separately for each of the exergy components because of their different nature and order of magnitude.

Finally, the comparison of the physical exergy values of the river with those real values being used within the basin is carried out through the defined indexes.

$$B_p = \int gQ(h)dh \approx g\sum_i \left(Q(h)\cdot \Delta h\right)_i \qquad (10)$$

$$B_{ch} = \int Q(b)db \approx \sum_i \left(Q(b)\cdot \Delta b\right)_i \qquad (11)$$

3.1 Exergy value of a water flow

The exergy value of a water body has, in general, five components: thermal, mechanical, chemical, kinetic and potential [15]. As already said we have two main basic components: its composition (chemical exergy), which makes it useful for different urban, industrial and agricultural uses, and its altitude (potential exergy), that can be used to produce shaft work and electricity.

Therefore, and starting from these components, it is possible to evaluate in quantitative (flow, Q) and qualitative (specific exergy, b) terms a water body and any water resource characterised by its exergy components. The proposed model considers temperature, pressure, height, velocity, concentration and composition. The model assumes the approximation to an incompressible liquid [17].

$$\underbrace{b_{H_2O}(kJ/kg)}_{Total\,specific\,exergy\,b} = \underbrace{c_{p,H_2O}\left[T - T_0 - T_0 \ln\left(\frac{T}{T_0}\right)\right]}_{Thermal\,Ex\,b_t} + \underbrace{v_{H_2O}(p - p_0)}_{Mechanical\,Ex\,b_{mech}} + \qquad (12)$$

$$\underbrace{\left[\sum_i y_i\left(\Delta G_{f_i} + \sum_e n_e b_{ch,n_e}\right)_i\right]_p}_{Chemical\,Ex\,b_{ch,c}} + \underbrace{RT_0\sum_i x_i \ln\frac{a_i}{a_0}}_{Concentration\,Ex\,b_{ch,f}} + \underbrace{\frac{1}{2}\left(\frac{C^2 - C_0^2}{1000}\right)}_{Kinetic\,Ex\,b_k} + \underbrace{g(z - z_0)}_{Potential\,Ex\,b_p}$$

where subindex *o* denotes the water properties of the reference. C_p stands for the specific heat at constant pressure; y represents the moles of the substance i divided by the total mass of the dissolution (it can assumed equal to the molality); ΔG_f is the Gibbs free energy; n_e is the moles number of the elements (e) forming a compound (i) and $b_{ch,ne}$ its corresponding specific chemical exergy; x_i is the molar fraction and *a* is the activity.

Each component in Eq. (12) should be separately calculated. The sum of all components expresses the exergy of the given water resource and can be understood as the minimum energy required to restore the resource from its RE.

The reference environment for this analysis is, clearly, the ocean. An idealized ocean without organic matter and the typical salts composition of the corresponding seawater is considered as the reference state for the natural water cycle. Its main features are altitude equal to zero and chemical composition equal to the average oceans composition. Then, when a water flow reaches its mouth after being used, and mixes into the seawater, it has zero chemical exergy as well. Additionally, this means that a significant loss of exergy occurs by mixing river and seawaters in the river mouth.

In other words, it could be said that the exergy in the source and in the mouth of the river is null. From the general expression of the total exergy as product of the flow times the specific exergy, it can be easily understood the null value from the null flow at the spring, and also the exergy equal to zero when it mixed with the ocean. However, that statement has to be correctly understood, keeping in mind the importance of the nutrients that the river provides to its mouth area. Such a contribution is fundamental for the maintenance of the biological life in the area. In this sense, the null value of the exergy is achived some kilometres far from the coast, when the equilibrium with the ocean water has been reached.

Only the two mentioned and more representative exergy components of water are commonly considered for fresh water analyses: chemical quality and geopotential [18, 19]. The first one is the minimum energy needed to return the quality characteristics to water and could be obtained by desalination and depuration techniques. The second one is the minimum energy needed to return the resource to its condition of potential disequilibrium as delivered by the hydrological

cycle. In the following, a brief description and practical considerations of those exergy components is provided.

3.1.1 Potential exergy component

As it is well-known, the potential exergy term - Eq. (13)- is calculated from the height z (m) where the measurement is taken. Q stands for the flow, g represents the gravitational force of the Earth (9.81 m/s^2) and z the altitude (z_0=0 at sea level).

$$B_p = Q \cdot g\left(z - z_0\right) \quad (13)$$

Although this term is quite important in the river source of a basin, it should be considered with special attention the case of reservoirs with installed hydropower utilities: this potential exergy will be converted successively into kinetic, mechanical and electrical energy within the power station.

No matter the disaggregation level, this potential component will be present in any water analysis related to energy. It can be calculated from the flow and altitude figures, but there is also a different alternative to obtain the potential exergy component of a river. It is suggested from the point of view of the second law of thermodynamics: the minimum energy to elevate water (potential exergy) coincides with the maximum energy obtained when it is turbinated using a reversible machine. Therefore, available figures from the inventory of the world's hydropower capacity can be used to calculate the minimum energy required for pumping (or restoring potential exergy component).

Hydropower generation is measured on a large scale in TWh/year and different associated parameters are defined. The *gross theoretical capability* (GTC) expresses the total amount of electricity which could potentially be generated, if all available water resources were turned to this use. Those figures are estimated on the basis of atmospheric precipitation and water run-off. The *technically exploitable capability* (TEC) means the hydropower capability which is attractive and readily available with existing technology. The *economically exploitable capability* (EEC) is that amount of hydropower generating capacity which could be built, after carrying out a feasibility study on each site at current prices, and producing a positive outcome [2].

3.1.2 Chemical exergy component

The intrinsic chemical exergy of any element is easily found in any chemical exergy table [6] and its expression is given in the $b_{ch,f}$ component in Eq. (14). In addition to the chemical exergy, the concentration of the substance in the water body has to be compared with its concentration in the RE. This term, defined by the second part of Eq. (14), $b_{ch,c}$, is the most complex term to calculate since three different contributions have to be considered: the concentration of pure water and the contributions corresponding to the dissolved inorganic and organic substances.

$$B_{ch} = Q \cdot (b_{ch,f} + b_{ch,c}) = Q \cdot \left[\sum_i y_i \left(\Delta G_{f_i} + \sum_e n_e b_{ch,n_e} \right) + R\, T_0 \sum x_i \ln \frac{a_i}{a_{0\,i}} \right] \quad (14)$$

where ΔG_f is the formation Gibbs energy, n_e is the amount of kmol of the element e and b_{chne} is the standard chemical exergy of the element. This component gives an idea about the energy required to form a molecule from the existing substances in the RE. If the molecule takes part of the RE, its formation exergy component is equal to zero (since it already exists in that RE). x_i is the molar concentration and a_i is the activity coefficient of substance i on water. Activities are rather used than molar concentrations, since we are dealing with solutions.

Attending to the chosen RE (an idealized seawater with average salts composition and without any organic matter), it is important to analyze how the chemical exergy component is going to be obtained. The IM chemical component will be assessed by calculating the second component in Eq. (14). The chemical exergy coming from the OM, however, will be calculated with the first term in Eq. (14), where the formation energy is accounted for.

Once the tool to assess the value of a river has been explained, the attention is focused on the river to be analyzed.

Exergoecology has been repeatedly applied during the last years to calculate the degradation costs of water bodies due to the anthropogenic presence. Special attention has been devoted to the comparison of the exergy difference between two given states of the river. Such a difference is obtained through the total exergy profiles of water courses under present or any other objective conditions. Each river exergy profile represents one of the statuses of the river.

In particular, several works related to the European Water Framework Directive (WFD) implementation through the branch of

exergoecology called Physical Hydronomics, have been published by the authors [5, 19, 20].

Physical Hydronomics is the specific application of thermodynamics to physically characterize the degradation and correction of water bodies. i.e., the physical application to European Water Framework Directive,WFD. The final objective of PH is to use those calculated physical costs as a guide to allocate the environmental and resource costs proposed by the WFD.

In this paper, some of the river states defined by the PH are going to be used in order to illustrate the starting hypothesis: the huge importance of the chemical potential of rivers. This river profiles are the present state (PS), the objective state (OS) and the natural state (NS) of the river. The former is understood as current state of the river, defined by its pressures and natural conditions. The OS comes from the objectives established by the WFD regarding to the required state of the rivers by 2015 (in flow and quality) according to the type of river or water mass that is being considered. Finally, the NS of the river is characterized as if the water stream were unaffected by any anthropogenic presence.

4. Case Study

The methodology can be carried out for any water body. It is only after studying the obtained figures when the theoretical hypothesis take shape and the scope of the ideas can be tested. The proposed methodology to highlight the relevance of the chemical component of rivers is going to be applied in this section to a Spanish river basin. The Muga Watershed (Figure 6) is located in the l'Alt Empordà region, northeast Catalonia, in the eastern Spain. Its surface is 758 km^2 (2.3% of Catalonia), with an average annual rainfall of 612 hm^3 (807 mm) and an average yearly contribution under natural regime conditions of 147.76 hm^3 [21]. There are 34 villages in the watershed area and the population rise to 65,756 inhabitants.

The *Muga* river is born in the Pirenees and it flows along 65 km until its mouth close to the Natural Park *Aiguamolls de l'Empordà* [4]. The upper stretch of the Muga river, upstream of the Boadella reservoir, flows trough a mountainous area where several particular spurious irrigation lands are located [23].

Figure 6. La Muga Basin (Source: Institut Cartogràfic de Catalunya, 1995)

The dam is devoted to supply water to *Figueres* and to irrigate wide agricultural lands downstream. It has also permission for nautical sailing activities. In the dam there is also a hydroelectric power plant (3.6 MW). Hydropower generation is subordinated to the irrigation demands, that is, only the water flowing to irrigation canals is turbinated. So, *Figueres* supply catchment and the maintenance flows are independent from the central derivation and those flows are not turbined. Downstream the dam there is a canal to regulate the drainage from the hydropower and, in this way, to be able to favour the plant operation: when the irrigation demand decreases, a water volume higher than the demand is turbined and regulated in that canal.

4.1 Results. Exergy value of La Muga river.

The potential content of water is commonly used in hydroelectricity issues, what leads to the PURI index definition. Nowadays, the chemical content of the river is not used to produce energy and, as a result, the CURI index is always zero. In addition, two additional indices related to the fuel used to maintain clean the river waters are defined (see section 2.1).

At this point, it is worth to remember that the chemical potential is defined by the exergy of water b_{H2O}. This value generally appears aggregated with the b_{salts} in the term b_{IM}. Because of the small value of the salts exergy, b_{H2O} and b_{IM} are similar (Table 1). However, the salts contribution is fundamental because the increase of salts dissolved in the river water indicates a decrease in the water exergy value.

B_{H2O}(MW)	Min	Max
PS	2.30	8.78
OS	2.62	9.71
NS	2.51	9.40

B_{chem} (MW)	Min	Max
PS	2.30	8.78
OS	2.36	8.85
NS	2.38	8.91

Table 1.Comparison of B_{H2O} and B_{IM} for the PS, OS and NS in the Muga river

Table 2 summarizes the results obtained for the potential and the IM component. The study was carried out for each month in an average year. Here, for the sake of clarity, only the values range (minimum and maximum), have been reproduced.

B_{pot} (MW)	Min	Max
PS	2.37	7.15
OS	2.44	7.16
NS	2.64	8.05

B_{chem} (MW)	Min	Max
PS	2.30	8.78
OS	2.36	8.85
NS	2.38	8.91

Table 2.Minimum and maximum exergy values of the Muga river

The maximum chemical exergy value of water is, as expected, obtained for the Natural State of the river and rises up until 8.91 MW. Since the altitude is constant, independently of the considered state of the river, this value is determined by the flow and the flow in the natural state of the river is in general the highest one.

Table 3 summarizes the average exergy values for the Muga watershed. As it can be seen, the order of magnitude of the pot and IM components is the same. The potential of the NS of the river is higher than the potential in the PS and in the OS.

	$B_{av,pot}$ (MW)	$B_{av,chem}$ (MW)
PS	4.83	5.10
OS	4.97	5.58
NS	5.76	6.01

Table 3.Average exergy values of the Muga river

Assuming that the Natural State of the river stands for the maximum exergy potential (100%), the present state represents its 84% and 85% for the potential and chemical component, respectively. The figures obtained for the Objective State are about 86% for the potential and 93% for the chemical.

On average, the exergy value of the Muga river, is about 5 MW (potential) and 5 MW (chemical) in the Present State (PS) of the river. It perfectly fits with the known data of the hydroelectricity power installed in the Boadella Dam (close to the river source), which is 3.6 MW.

In addition to that, looking at the monthly figures, it can be observed that the resulting power is higher in those months when the river flow is higher, as expected.

An additional interesting figure was obtained when these global exergy chemical values were compared with the power that is currently being used to clean the Muga river waters. In the Muga area, there are several waste water treatment plants; the most important, attending to its capacity, is the *Figueres* one. In the last stretch, the *Peralada*, the *Castelló d' Empuries* and the *Empuriabrava* WWTPs are located. The total power accounts for all those utilities and it is about 4 MW, almost the same as the calculated chemical exergy of the river.

Finally, the indices related to the potential and chemical use of the river can be calculated by applying the definitions provided in section 2.1. The input figures for the calculation are given in Table 4. There, it can be seen that the current use of the potential component of the river is quantified in 3.6 MW (from a total potential of 4.83 MW), while there is not any technology taking advantage of the 5.1 MW of chemical potential. Moreover, the exergy content of the residuals within the water flow in the Muga river is 0.71 MW and the fuel required to clean it is 3.92 MW. This last figure is calculated after analyzing the efficiency of the WWTPs running in the area.

P_{pot}	P_{chem}	F_{pot}	F_{chem}	R	F_R
3.60	0.00	4.83	5.10	0.71	3.92

Table 4.Index Refining the exergy value of the Muga river in its PS.

As a result, the potential of the river coming from the geopotential exergy is currently exploited at 75% of its capacity, according to the value of PURI indicated in Table 5. The chemical potential, as already explained, is not being used and, therefore, the CURI value is equal to zero.

Plant index	Whole river indices		
RTPI	PURI	CURI	F_RRI
0.18	0.75	0.00	0.77

Table 5.Index Refining the exergy value of the Muga river in its present state.

The Residuals in the Treatment Plant Index (RTPI) results 0.18, which indicates that the

water treatment plants within the watershed are working far from taking full profit of the exergy of these residues to clean up the river, or in other words, we need 5 times more exergy to get rid of these waste than its contained exergy. A technological objective for waste treatment plants could be to reach self-sufficiency. In other words, that the exergy needed to clean up the water would be equal to the exergy of its organic waste. Finally, the Fuel-Residuals River Index (F_RRI) indicates that the fuel required to eliminate the waste is about 77% of the chemical potential exergy of the water flowing through the Muga river. At this point, the comparison leads to think that the exergy required to maintain the quality of the river water could be, in specific cases, even higher than the chemical potential of the stream.

5. Conclusions

The main thermodynamic value of a river comes, if none special thermal phenomena are detected, from its potential and chemical features. The global potential and chemical value of a water body can be given from a thermodynamic perspective attending to the evolution of them along the time and space.

It has been explained along the work that it is possible to use to assess the exergy difference between two given states and, in this way, analyzing how much of the potential of the river is being used.

The obtained figures give an idea about the exergy value of the considered river and allows its comparison with other parameters such as the power consumed by the currently installed waste water treatment plants along its course.

The exergy content in the water flow is given by F_{pot}. It decreases as the altitude does, until the river mouth. The chemical potential is represented by F_{ch}, which gives idea about the amount of exergy dispersed into the sea although, as mentioned, it is used by the biodiversity in the shore.

In this paper, it has been shown the chemical value of a river is, from a thermodynamic perspective, as much as its potential value. Obtained values are both about 5 MW for the Muga river. This result is the most relevant contribution of this paper: the chemical value of the river is as much as its well-known and exploited potential value.

An elementary and mistaken conclusion could be obtained from our analysis: if our technology were able to take advantage of the chemical exergy potential of water, an energy source similar to hydropower could be developed. So let´s develop it. However, if we would accept such a statement, it would mean that Nature is nothing but an inventory of resources for human purposes. Thus denying a wide-ranging perspective.

The important amount of chemical exergy that continuously goes into the see in the river mouths constitute the natural irreversibility in the estuaries that maintain and develop the diverse fishes and plants in those areas. That is, life exists because of that exergy and its associated irreversibility.

If our reflection after examining the numbers for F_{pot} and F_{ch} is limited to the idea of installing a huge forward osmosis plant in each water stream, we are loosing the most important guideline: we are just a part of the ecosystem.

Our planet is plenty of resources and those resources are for the *Life* (in its most general sense), not for the humans settled in the considered watershed. There is then, effectively, a hidden chemical value of water. It is far from being null and it is not a value for the future at expenses of the technological development. It is already a fundamental value that is being used by the biodiversity living in the estuaries, the richest places within the oceans.

All in all, Physical Hydronomics may help to bring up to light that hidden value of water flows, their chemical exergy.

Nomenclature

B: Exergy
b: specific exergy
CURI: Chemical Use of River Index
F: Fuel
F_R: required fuel to eliminate the waste R
FO: Forward Osmosis
IM: Inorganic Matter
NS: Natural State
OM: Organic Matter
OS: Objective State
P: Product
PS: Present State
PURI: Potential Use of River Index
R: Residuals/waste
WWTP: Waster Water Treatment Plant
Subscripts

ch: chemical
pot: potential

References

[1] Delli Priscoli, J. 2000. Water and civilization: using history to reframe water policy debates and to build a new ecological realism. Water Policy, 1 (6): 623-636.
[2] WEC, 2007. *Survey of Energy Resources 2007*. World Energy Council.
[3] IHA, 2008. *The contribution of hydropower. Factsheets.* International Hydropower Association. Available at: www.hydropower.org
[4] Cath T.Y., Childress A.E., Elimelech M, 2006. *Forward osmosis: Principles, applications, and recent developments.* Journal of Membrane Science, 281 (1-2): 70-87.
[5] Valero, A., et al, 2009, Physical Hydronomics: Application of the exergy analysis to the assessment of environmental costs of water bodies. The case of the inland basins of Catalonia, Energy 34 (12), pp. 2101-2107.
[6] Szargut,J.; Morris, D.R; and Steward, F.R. 1988. *Exergy analysis of thermal, chemical and metallurgical processes*. New York: Hemisphere.
[7] Valero, A. 1998. *Thermoeconomics as a conceptual basis for energy ecological analysis.* Proceedings of the 1st International workshop Advances in Energy Studies. Pp. 415-444. SG Editoriali Padova.
[8] Wall, G. 1986. *Exergy -A useful concept*. Physical Resource Theory Group. Chalmers Bibliot. Trick. University of Technology, Göteborg, Sweden 3,4 EOLSS Publisher.
[9] Jørgensen, S.E. 2006. *Eco - Exergy as Sustainabilit*y. WIT Press Southampton, Boston.
[10] Rosen, M.A. and Dincer, I. 2001. *Exergy as the confluence of energy, environment and sustainable development*. Exergy, an International Journal, 1 pp. 3-13. Elsevier.
[11] Gong, M. and Wall, G. 2001. *On exergy and sustainable development, Part-2*. Exergy, an International Journal 4, pp-217-233. Elsevier.
[12] Chen, G.Q. 2006. *Scarcity of exergy and ecological evaluation based on embodied exergy*. Nonlinear Science and Numerical Simulation 11, pp. 531-552. Elsevier.
[13] Chen, G.Q. and Ji, X. 2007. *Chemical exergy based evaluation of water quality*. Ecological Modelling. Pp. 259-268. Elsevier.
[14] Valero, A.; Lozano, M.A. and Muñoz, M. 1986. *A general theory of exergy saving, I, II and III.* Computed Aided Engineering and Energy Systems: Second Law Analysis and Modelling, AES. Vol 2-3 Vol. 2-3, ASME Book H0341C. New York.
[15] Zaleta-Aguilar, A.; Ranz, L. and Valero, A. 1998. Towards a Unified measure of renewable resources availability: The exergy method applied to the water of a river. Energy Conversion Management, 39 (16-18): 1911-1917.
[16] Valero, A; Uche, J; Valero, Al; Martínez, A; Naredo, J. and Escriu, J. 2009. *The Fundamentals of Physical Hydronomics: a novel approach for physico-chemical water valuation*. In "Water, Agriculture, and Sustainable Well-Being" Chapter 5, pp. 97-118. Oxford University Press.
[17] Martínez, A. and Uche, J., 2010, *Exergy of organic matter in a water flow*, Energy 35 (1), pp. 77-84.
[18] Botero, E., 2000. *Valoración exergética de recursos naturales, minerales, agua y combustibles fósiles*. Tesis doctoral. Departamento de Ingeniería Mecánica. Universidad de Zaragoza. [In Spanish].
[19] Martínez, A., 2009, *Exergy costs assessment of water bodies: Physical Hydronomics*, Ph.D Dissertation, University of Zaragoza. Spain.
[20] Martínez, A; Uche, J; Valero, A. and Valero, Al., 2010, Environmental costs of a river watershed within the European water framework directive: Results from Physical Hydronomics, Energy, 35 (2), pp. 1008-1016.
[21] CWA, 2004. *Recull de dades. Els recursos hidrics en regim natural a les conques internes de catalunya (1940-200).* Agéncia Catalana de l´Aigua. Generalitat de Catalunya, Departament de Medi Ambient i Habitatge. [In Catalan].
[22] Ventura, M.; Ribas, A. and Sauri, D. 2000. *Gestión del agua y conflictividad social en la Cuenca del Río Muga*. Geographicalia, 38 pp. 55-70. [In Spanish].
[23] CWA, 2008. *Análisi Económica per a la planificació hidrológica. Catalunya: L´experiéncia pilot a la Conca de la Muga*.Agéncia Catalana de l´Aigua.Generalitat de Catalunya. Departament de Medi Ambient i Habitatge. [In Catalan].

Acknowledgements

The authors greatly acknowledge the financial support given to this paper, which is under the framework of the IDERE R+D+I project (ENE2007-067191), financed by the Spanish Ministry of Education and Science.

Optimization of Hybrid Renewable Energy Systems Powered Reverse Osmosis Desalination Plants

Prof. A. Hossam-Eldin[a] , Prof. A. M. El-Nashar[b], and A.Ismaiel[c]
[a]*Alexandria University, Egypt*
[b]*Alexandria University, Egypt*
[c]*Alexandria University, Egypt*

Abstract:This paper investigates the use of Hybrid renewable energy systems (HRES) in Reverse Osmosis (RO) desalination. Mathematical model aided with a newly developed computer program for sizing (HRES) components. The study evaluates the individual and total expenses needed as well as the amount of excess renewable energy production. An optimization program was developed to select the best (HRES) combination that can produce desalinated water in a relatively economic cost. It demonstrates an investigated optimization approach based on minimization of the excess energy. it presents the impact of the considered optimization technique on the unit cost of energy and consequently unit cost of desalinated water. Unit production costs of both energy and desalinated water for two existing small and medium (RO) plants powered with conventional electricity grid are compared with the generated electricity from optimized (HRES). Cost sensitivity evaluation for (HRES) components to estimate the most economical price of (HRES) for desalination is presented.

Keywords: Optimization; Hybrid Renewable Energy System; Reverse Osmosis desalination; Sensitivity Analysis.

1. Introduction

Hybrid Renewable Energy Sources (HRES) is defined as a combination of one or more resources of renewable energy. it represents one of the promising options for the considerable energy needs of desalination processes especially in remote and arid regions, where the use of conventional energy (fossil fuels, electricity) is costly or not available. (HRES) powered desalination plants may be an attractive alternative option. In most cases, fresh water scarcity co-exists with abundant renewable energy (RE) resources. (RO) desalination processes have been the technology of choice as a result of recent technological developments in the process engineering. The average costs of product water have decreased significantly [1, 2].

The main desirable features for renewable Energy Systems (RES) are low cost. The selection of the optimum combination of RES and desalination technologies for a specific location is based on resource availability and the technical compatibility [2]. Numerous RES –RO combinations have been identified by several researches [3–8]. Economic aspects of these technologies are sufficiently promising to include them in developing power generation capacity for developing countries and there is still need for more effort to be done so that the system can be optimized. Several studies have been done demonstrating the ability to optimize hybrid configurations of renewable energy systems in order to maximize performance while minimizing cost [9-14]. However while the results of these optimization processes show the optimum sizing and appropriate Combination of components for the system, but the problem of maximum component capacity must be taken in consideration in order to overcoming the existence of high excess energy [9]. This paper discusses the importance of reducing excess energy in minimizing the cost of energy (C_E) for RES which defined as the ratio of total annualized cost and annual load served by the renewable energy hybrid system. Suggestion of maximizing load reserve for two case studies is considered to meet this optimization objective, consequently produce both energy and water at reasonable cost.

2. Methodology

The proposed (HRES) as shown in Fig.1 it is consisted of a wind turbine (WT) and solar photovoltaic panels (PV). Diesel generator (G), battery (Batt.) and inverter (Inv.) are added as part of back-up and storage system

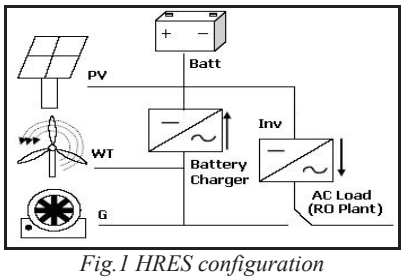

Fig.1 HRES configuration

3. Mathematical modeling

The developed computer program algorithms are based on the following equations:

3.1 Energy consumption (Load demand):

The pump Delivered power:

$$P_{Pumb} = 0.02278 * P * Q / \%\eta_{Pumb} \quad (1)$$

The RO plant power:

$$P_{RO} = [P_{FP} + P_{HPP} + \sum P_{DP}] * N_{URO} \quad (2)$$

The RO plant Energy:

$$E_{RO} = P_{RO} * time \quad (3)$$

Specific Energy Consumption:

$$SE_{RO} = E_{RO} / Q_{P} \quad (4)$$

Annual Consumption Energy:

$$E_{A.RO} = P_{RO} * \Phi * 365 \quad (5)$$

3.2 (HRES) Production:

The wind power:

$$P_{WT} = N_{WT} * [\frac{\eta_W * \eta_g * \rho_a * C_p * A_S * V_W^3}{2*1000}] \quad (6)$$

Annual Wind Energy:

$$E_{WT} = P_{WT} * 8760 \quad (7)$$

The PV power:

$$P_{PV} = N_{Pan.} * [\frac{\eta_{Pan.} * Pan._{kW}}{1000}] \quad (8)$$

Annual PV Energy

$$E_{PV} = P_{PV} * 12 * 365 \quad (9)$$

Annual Total Renewable Energy:

$$RE_T = E_{WT} + E_{PV} \quad (10)$$

Annual Diesel Generator Energy

$$E_G = E_{RO} - RE_T \quad (11)$$

Annual Diesel Generator operating hours

$$G_{oh} = E_G / G_{P_r} \quad (12)$$

Annual Total Energy Production:

$$E_{A.Tot} = RE_T + E_G \quad (13)$$

Annual Excess Energy:

$$E_{A.exc} = E_{A.Tot} - E_{A.RO} \quad (14)$$

3.3 Sizing Battery system and Inverter:

Total Daily Load:

$$I_D = \frac{P_{RO} * \Phi * 1000}{\sqrt{3} * V_{AC} * \cos\varphi * \eta_{Inv}} \quad (15)$$

Total Battery capacity

$$I_{Batt.} = I_D * DOA * DF \quad (16)$$

Required Number of batteries:

$$N_{Batt.} = ROUND[\frac{I_{Batt.}}{UI_{Batt.}}] \quad (17)$$

Number of series batteries:

$$N_{SB_{att.}} = ROUND[\frac{V_{AC}}{V_{Batt.}}] \quad (18)$$

3.4 Cost Estimation:

Annual capital Cost:

$$C_{A.cap} = C_{cap} * CRF \quad (19)$$

$$CRF = \frac{i*(1+i)^n}{(1+i)^n - 1} \quad (20)$$

Annual replacement Cost:

$$C_{A.rep} = \frac{C_{rep} * N_{rep}}{n} \quad (21)$$

$$N_{rep} = \frac{n - N_{comp.}}{N_{comp.}} \quad (22)$$

Annual Operation and Maintenance Cost:

Annual Operation and Maintenance (O&M) Cost is defined as the following:

$$C_{O_{WT}} = N_{WT} * C_{O/WT},$$

$$C_{O_{PV}} = 0,$$

$$C_{O_G} = C_{O/G} * G_{Oh},$$

$$C_{O_{Batt}} = N_{Batt} * C_{O/Batt}, \text{and}$$

$$C_{O_{Inv.}} = N_{Inv.} * C_{O/Inv.} \quad (23)$$

Annual Fuel Cost:

$$C_{A.Fu} = Fu_{Sur} * E_G * C_{Fu} \quad (24)$$

Annual Total Cost:

$$C_{A.Tot} = C_{A.cap} + C_{A.rep} + C_{A.O} + C_{A.Fu} \quad (25)$$

Cost of Energy:

$$C_E = C_{A.Tot} / E_{A.Tot} \quad (26)$$

Cost of water

$$C_W = SE_{RO} * C_E \quad (27)$$

4. CASE STUDIES

The software has been used to identify and design most appropriate (RES) powered (RO) desalination plant for two case studies of existing small and medium size plants powered with conventional grid supply. Four alternative combinations of (RES) have been evaluated for each case. The optimum combination that gives minimum unit cost of energy is optimized in order to minimize its excess energy. Necessary cost comparing and sensitivity is performed.

4.1 RO Plants Data

Plants specifications are shown in table 1.

4.2 (HRES) Data

4.2.1 Wind turbine

The used wind turbine kind is FL 250, has a Rotor diameter 96.8 m [14].The average wind speed for the plants location is 5.3m/s[22]. Air density, coefficient of performance, generator efficiency and gearbox-bearings efficiency are about 1.2 kg/m3, 0.25, 50%, 50% respectively. Turbine capital cost is$100,000 and its replacement at $100,000. Annual (O&M) cost is 2% of capital cost, life time is 20 years.

4.2.2 Solar PV Panels

The PV Panel power is 1kW, panel efficiency is about 90%. The monthly average daily solar radiation is 5kWh/m2/day [22]. The monthly average daily sunshine duration is assumed 12 h. Panel efficiency is 90%. life time is 20 years.
Panel capital cost is $4,000 and its replacement at $4,000. Annual (O&M) cost is neglected.

4.2.3 Diesel Generator

The AC generator capital cost is 400$/kW and its replacement cost is 400$/kW. The (O&M) cost is 0.005$/kW of operating hour. The lifetime of the generator is estimated at 15000 operating hours. Its efficiency is about 75%. Diesel is priced at 0.3$ per liter.

4.2.4 Battery system

The valve regulated lead acid battery is rated at 12 V and has a capacity 305 Ah. Battery capital cost is $450. The replacement cost is $450. The annually (O&M) cost about 1% of capital cost. Design Factor, Days of Autonomy is 1.25 and 5 respectively. life time is 4 years.

4.2.5 Inverter

The Inverter capital cost is 750$/kW and its replacement cost is 700$/kW. The (O&M) is 20% of capital cost. Its efficiency is about 80%. Lifetime is 20 years.

4.2.6 Economics and Constraints

The calculations take into account the annual interest rate at 6% and the (HRES) lifetime is 20 years. The operating reserve is set at 10%, 15 %and 25% of the load demands, out put wind and solar power respectively.

5. RESULTS &DISSCUSIONS

For case I, the optimum combination consists of 4 wind turbines, 125kW diesel generator, 160 batteries and 125 kW inverter have the lowest costs of energy, water at 0.1023$/kWh and 1.787$/m3 which are about 62% and 19% higher if compared with the current electricity tariff set by Egypt government at 0.0631$/kWh [21], and unit cost of desalinated water at 1.6$/m3. This combination can provide annually 1.207*106 kWh of energy with amount of excess energy about 33% of product energy. For case II, the optimum combination consists of 8 wind turbines, 125 PV Panels, 300kW diesel generator, 416 batteries and 300 kW inverter have the lowest costs of energy, water at 0.1135$/kWh and 1.403$/m3 which are about 40% and 12% higher if compared with the current electricity tariff at 0.0807$/kWh and unit cost of desalinated water at 1.25$/m3. This combination can provide annually2.963*106 kWh of energy with amount of excess energy about 30% of produced energy. Table 2 lists the Optimum (HRES) component sizing.
For case I components, WT, generator, battery and inverter costs contribute about 44%, 19%, 26% and 11% respectively of the total annual cost of $82,202.23. while case II components, WT, PV , generator, battery and inverter costs contribute about 30%, 19%,17%, 24% and 10% respectively of the total annual cost of $232,010.00.The costs of WT and Battery play important part in determining cost of energy due to the fact that WT

is the main power component in the system which directly affects the capital cost. Batteries need to be replaced after predetermined time which mean that certain number of batteries has to be replaced which directly affects the replacement cost. Figure.2 shows the annualized cost analysis for optimum (HRES).

Figure 3 shows the optimization approach by increasing the load demand in order to minimize the amount of excess energy; for each case optimum (HRES) subjected to the excess energy must not less than 10% of total energy production (which represents a reserve) to insure that there is no unmeet load in system. have a load demand increase 35% and 30% respectively, the excess energy will decrease by about 23% and 21% respectively (of the total energy production) and the cost of energy is reduced to be \$0.0756 and \$0.0871 which indicate an improvement of 42.3% and 32.7% respectively. Consequently the cost of water is reduced to \$1.591and \$1.279 which illustrate a cost reduction of 13% and 9.9 % of the initial cost. It is clear that case II is more economical than case I. This is due to the fact that case II is medium scale RO plant while case I is a small one

The Sensitivity of the components costs for case II is shown in Figure 4. If (due to the effort of researches) a reduction of 10% in the cost of WT and, keeping the cost of other components constants the cost of energy unit will be \$0.083 while a more reduction of 20% will result in the cost of energy unit will be \$0.0803 which much better than initial unit cost of energy. A more reduction in WT cost of 30% will cause more reduction to reach \$0.0769/kWh. Repeating the same procedures for PV, Battery, WT plus PV, it is clear that a general reduction will occur but it still not economical. On the contrary the (HRES) with WT, PV and Battery will prove to be economical. If the calculation were repeated for a reduction of 20% ,(HRES)will be much more economical. The more reduction in cost of 30% will show that all systems are economical with the HRES (PV+BAtt+WT) is effectively economical than all other cases. For this reason we are urging the scientists to work hard on the research to reduce the cost of RES. If presumably, the electricity cost has been increased by 10% over its current prices, as it may be forecasted now days, the developed hybrid renewable energy systems will show superiority in its cost and less pollution which reflects on a drastic improve in environmental conditions.

6. CONCLUSIONS

- From a techno economic point of view, sizing (RES) power supply options in combination with RO depends on several conditions such as renewable energy sources, available components well as the design constraints considerations. From that point of view, it is hardly define straightforward way to select the favorable system design for general application and an iterative approach is most probable to be followed, involving careful assessment of available options in meeting water demand and the economic viability of the selected solution

Title	case I (small Scale Plant)					Case II (Medium Scale Plant)				
Product water flow,m^3/h	7.5					15				
Pumps and Energy Recovery	No.	Q, m^3/h	P, bar	η, %	P,kW	No.	Q, m^3/h	P, bar	η, %	P,kW
Feed Pump	1	25	3	80	2.60	1	50	3	80	5.2
High Pressure Pump	1	25	55.39	80	48.08	1	50	35	80	60.76
Energy Recovery	0	0	0	0	0	1	35	55	90	0
Dosing Pump	5	0.015	5	80	0.013	10	0.015	5	80	0.026
Product water pump	1	15	3	80	1.562	2	30	3	80	3.12
Power Consumption, kW	110					280				
Specific Energy Consump., kWh/m^3	7.3					4.6				
Unit Cost of product water,$\$/m^3$	1.6					1.25				
Unit Cost of Energy,\$/kWh	0.0631					0.0807				
Specific Unit Cost of Energy,$\$/m^3$	0.463					0.376				

Table1: Case studies RO plants Techno-Economic and meteorological

Table: 2 Optimum (HRES) component sizing

	PV, kW	WT	G, kW	Batt	Inv, kW	E_{Exces}, %	C_E, $/kWh	C_W, $/m^3$
case I	0	4	125	160	125	33.48	0.1023	1.787
	1	4	125	160	125	33.702	0.1028	1.790
	0	0	125	0	0	16.66	0.18	2.356
	110	0	125	160	125	25.77	0.208	2.562
case II	125	8	300	416	300	30.994	0.1135	1.403
	0	8	300	416	300	27.431	0.1163	1.416
	0	0	300	0	0	16.66	0.1727	1.679
	280	0	300	416	300	25.776	0.203	1.820

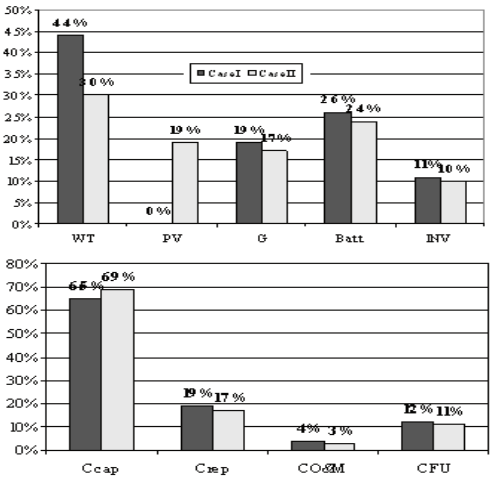

Fig .2 cost analysis

- Wind energy is a best choice in the present days however, solar energy is essential for the future.
- In order to reduce the cost of energy production using (HRES) it is important to minimize the amount of excess energy the system produce. As a result depicts, reduction of 20% excess energy would have about 30% decreasing on the cost of produced energy.
- The use of (HRES) is more appropriate for medium scale RO Plants than small scale ones in countries with same Egyptian conditions.
- For medium scale (RO) plants, elementary reduction of 20%, 25% and 30% or gathering one with 10% of WT, Battery` and PV panel prices would give (RES) the economic priority in comparison with conventional grid supply. The same result can be achieved with 10% increase of electrical energy tariff.
- Due to advances in renewable energy technologies to drive the prices down, subsequent rise in prices of petroleum products and depleting reserves. Economic aspects of these technologies are sufficiently promising to include them in power and water production for developing countries.

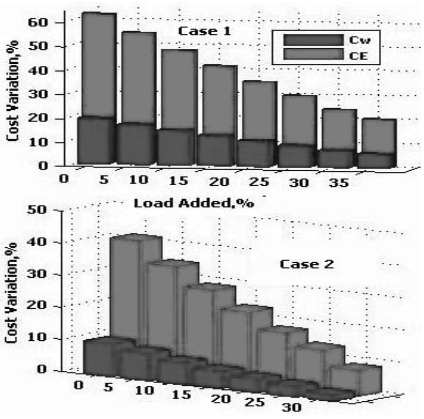

Fig. 3 optimization results for load demand increasing

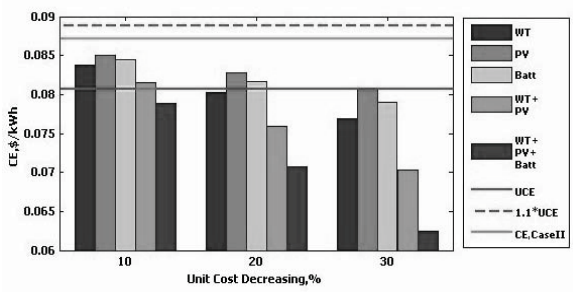

Fig.4 Sensitivity of components Cost for caseII

- In spite of cost and technological development of (HRES) in recent years has been encouraging, they remain an expensive source of power and mainly used for remote area power applications and are now a days cost-effective where extension of grid supply is expensive.

References

[1] A. Hossam-Eldin and A.Ismaiel, "An Investigation into Economic Desalination Using Solar/Wind Energy System", Tenth International Water Technology Conference, IWTC10 2006, Alexandria, Egypt, 733-743.

[2] D.Voivontas, K. Misirlis, E.Manoli, G. Arampatzis, D. Assimacopoulos, "A Tool for the Design of Desalination Plants Powered by Renewable Energies", Desalination 133 (2001) 175-198.

[3] L. García-Rodríguez, and C.Gómez Camacho, "Econoic analysis of wind-powered desalination", Desalination 137 (2001), 259–265

[4] S. Abdallah, W.abu-Hilal and M.S. Mohsen," Performance of a photovoltaic Powered Reverse Osmosis System under Local Climate Conditions", Desalination 183(2005), 95-104.
[5]MEDRC Series of R&D Reports, Project: 98-BS-033, " PV Powered Desalination ", 2003.
[6]International Atomic Energy Agency, IAEA, VIENNA, "Desalination Economic Evaluation Program", (DEEP-3.0), 2006
[7]A.M. Helal, S.A. Al-Malek, E.S. Al-Katheeri,"Economic Feasibility of Alternative Designs of a PV-RO Desalination Unit for Remote Areas in the United Arab Emirates", Desalination 221 (2008) 1–16
[8]Sing-Foong Cheah, "Photovoltaic Reverse Osmosis Desalination System", U.S. Department of the Interior Report No. 104, May 2004.
[9]Juhari Ab. Razak, Kamaruzzaman Sopian and Yusoff Ali, "Optimization of Renewable Energy Hybrid System by Minimizing Excess Capacity", International Journal of Energy, Issue 3, Vol. 1, 2007, 77 – 81.
[10]Kellog, W., Nehrir, M.H., Venkataramanan, G.and Gerez,V.," Optimal Unit Sizing for a Hybrid Wind / Photovoltaic Generating System", Electric Power Systems Research, Vol 39, 1996, 35 38.
[11]Borowy, B.S. & Salameh, Z.M., "Optimum Photovoltaic Array Size for a Hybrid Wind/PV System", IEEE Transaction on Energy Conversion, Vol. 9, No. 3, 1994, 482 488.
[12]Kamel, S and Dahl, C., "The Economics of Hybrid Power Systems for Sustainable Desert Agriculture in Egypt", Energy, Vol. 30, 2005, 1271 1281.
[13]Khan, M.J., & Iqbal, M.T., "Pre Feasibility Study of Stand Alone Hybrid Energy Systems for Applications in Newfoundland", Renewable Energy, Vol. 30, 2005, 835 854.
[14]National Renewable Energy Laboratory, "HOMER", Getting Started Guide Version 2.1, NREL, 2005.http://www.nrel.gov.
[15]Annual Report 2007/2008, New and Renewable Energy Authority, Egypt.
[16]Lotfi KRICHEN, "Modeling and Control of a Hybrid Renewable Energy Production Unit", ICGST-ACSE Journal, Volume 7, Issue 1, May 2007
[17] M.K. Deshmukha, S.S. Deshmukh, "Modeling of hybrid renewable energy systems", Renewable and Sustainable Energy Reviews,12 (2008) 235–249
[18]Ashok, S. "Optimized Model for Community Based Hybrid Energy System", Renewable Energy, Vol. 32, No. 7, 2007,1155 1164.
[19] Authority of the House of Lords, London, "The Economics of Renewable Energy", 4th Report of Session 2007–08
[20] Severin Borenstein, " The Market Value and Cost of Solar Photovoltaic Electricity Production ", CSEM WP 176, January 2008
[21] Annual Report 2007/2008, Ministry of Electricity and Energy, Egypt.
[22] NASA Surface meteorology and Solar Energy, www. nasa.gov.

Nomenclature

Notation	Explanation
Ann	Annual
As	Swept area,(m2)
CA.Cap	Ann. capital cost,($/y)
CA.Fu	Ann Fuel cost,($/y)
CA.O	Ann O & M cost,($/y)
CA.rep	Ann replacement cost,($/y)
CA.Tot	Ann Total cost,($/y)
Ccap	Capital Cost,($)
CE	Cost of energy,($/kWh)
CFu	Fuel cost,($/L)
CO/Batt	Ann battery O&M cost,($/y)
CO/G	Ann Generator O&M cost,($/y)
CO/Inv	Ann Inverter O&M cost,($/y)
CO/WT	Ann WT O&M cost,($/y)
COBatt	Total Battery O&M cost,($/y)
COG	Total Generator O&M cost,($/y)
COInv	Total Inverter O&M cost,($/y)
COPV	Total PV O&M cost,($/y)
COWT	Total WT O&M cost,($/y)
Cp	Coefficient of performance
Crep	replacement cost,($)
Cw	Cost of product water,($/m3)
EA.Exc	Ann Excess Energy,(kWh/y)
EA.RO	Ann Consump.Energy,(kWh/y)
EA.Tot	Ann Total Energy,(kWh/y)
EPV	Ann PV Energy,(kWh/y)
ERO	Ann RO plant Energy,(kWh/y)
EWT	Ann Wind Energy,(kWh/y)
FUSur	Specific Fu. usage rate,(L/kWh)
GOh	Ann Generator operating hours,(h)
GP	Generator rated Power, (kW)
i	Interest rate
IBatt	Total Battery capacity,(Ah)
ID	Total Daily Load ,(Ah)
n	Number of years
NBatt	Required Number of battery
Ncomp	Number of Components
NInv	Required Number of Inverters
Npan	Required Number of PV Panels

Nrep	Number of replacements
NSBatt	Number of Battery in series
NURO	Number of RO Units
NWT	Number of WT's
P	Pressure (bar), Power (kW)
Pan.kW	PV Panel Power in kilowatt
PDP	Dosing chemicals pump power,(kW)
PFP	Feed water pump power,(kW)
PHPP	High Pressure pump power,(kW)
Ppumb	pump Delivered power,(kW)
PPV	PV power,(kW)
PRO	RO plant power,(kW)
PWT	wind power,(kW)
Qp	Product water Flow rate,(m3/h)
RET	Annual Total RE,(kWh/y)
SERO	Spec. Energy Consumption, (kWh/m3)
UIBatt	Unit Battery Capacity,(Ah)
Vbatt	Battery DC Voltage, (volt)
Vw	Average Wind Velocity,(m/s)
ρa	Air density,(kg/m3)
ηg	WT generator efficiency
ηPan	PV Panel efficiency
ηPumb	Pump efficiency
ηWT	WT efficiency
Batt	Battery
COSφ	Power Factor
CRF	Capital Recovery Factor
DF	Design Factor
DOA	Days of Autonomy
Φ	daily operating hours,(h)

Developing a Novel Graphical Method Based On Pinch Technology for Optimizing Of Water Distribution Network From Energy Consumption Point Of View

Majid Amidpour[a], *Abazar Vahdat Azad*[b]

[a] *Department of Mechanical Engineering, K.N. Toosi University of Technology, Tehran, Iran*
[b] *Department of Mechanical Engineering, K.N. Toosi University of Technology, Tehran, Iran*

Abstract: In this paper a new graphical method as "Hydraulic Pinch" has been proposed for optimal design of water distribution network point of view of energy consumption. Name Pinch technology for researchers and scientists active in the field of Energy is the known and familiar. This technology, first were used for analysis and optimizing of Heat exchanger network to reduce energy consumption. Then researcher developed this approach as optimization method in different engineering field such as Hydrogen Pinch in order to reduce the required hydrogen in refinery industry, Oxygen Pinch in water treatment field, Water pinch in water reuse systems and etc. we have developed a new application of pinch method. This approach is used for Factories and plants, cities, regions and countries that have considerable resources of water for transfer to consumers. The Proposed Method determines the minimum number of equipment and lowest necessary energy to the pumping operation. In the first phase innovative Pinch method suggests transferring of water from resources to consumers by using the gravity force. Then optimal position and head of required pumps that transfer the remaining water needed to be used in consumers are discovered by using graphical decision maker of Hydraulic Pinch. In this way, the height differences between water resources and consumers are the important key parameter. The investigation conducted in this article, over 80 percent of the water needed by consumers has been transferred by gravity force and the remaining 20 percent have transferred by using the pumping devices that have optimal position and characterization of energy consumption viewpoint. The results of this analysis introduce the Hydraulic Pinch as efficient and suitable method for optimal designing of water distribution network

Keywords: Pinch Technology, Energy, pumping power, water distribution networks, optimization

1. Introduction

Name Pinch for technology researchers and scientists active in the field of Energy is the known and familiar. This technology was used first by Linnhoff and Turner [1] for analysis and assessment of Heat exchanger network to reduce energy consumption. They investigate the composite curve as an important tool in energy recovery. Their Emphasize on Pinch point as a key point in energy recovery due to select the phrase Pinch technology for this method. They search for minimizing the required number of Heat exchanger network Linnhoff and Flow [2] and minimizing the required level Heat exchanger network Linnhoff and Townsend [3], Linnhoff and Ahmad [4]. The first report of application of Pinch technology related to ICI which 30 percent reduction in energy consumption of petrochemical and chemical processes was achieved. Then Union Carbide reported that 50 percent of average energy consumption has decreased. Pinch technology has many improvements in optimization of Heat exchanger networks, distillation towers, and furnace and etc. Parallel with researches in pinch technology for optimization of heat exchanger network, Wang And Smith used this method for the reuse of water resources [11,12]. In 1999 Alves [13] and Towler [14] considered the Hydrogen Pinch method in order to reduce the hydrogen request, especially in refineries. The research in water treatment by Zhelev And Bhaw [15], Zhelev And Ntlhakana [16] led to the introduction the Oxygen Pinch.

Since the water distribution networks are crucial and need a significant cost making, their cost optimization are considered from different perspectives such as cost of investment, operating costs and maintenance costs in last 30 years. Different techniques have been used to optimize water distribution networks include the linear programming [17,18,19,20,21], dynamic programming [22], and nonlinear programming [23,24]. Evolutionary optimization methods such

as genetic algorithms (GA) [25,26], simulated annealing (SA) [27] and ant colony (ACO) [28,29] has been used for optimization problems. But the use of graphical methods such as Pinch technology has not been used for optimization of water distribution networks. This article has been developed graphical method based Pinch technologies for optimizing the water distribution networks from operational cost (energy cost) point of view. This development of pinch application is innovative method that is very efficient and powerful tools for assessment and optimization of design of water distribution network.

2. Problem representation

In water distribution networks, large part to costs due of pumping costs. Pumping costs due to investment costs and costs related to purchase of pumping equipment, repair and maintenance costs and energy costs. According to research [30] conducted that more than 50 percent of the cost of water pumping station is cost of investment for buying equipment of station. More than 30 percent of the total cost of water pumping station is the Energy consumption costs. Therefore, the pumps can be used less as a suitable solution to reduce the cost of water pumping. Also reduction of energy consumption in pumping stations lead to reduction of most of the costs. In this article a new application of Pinch analysis is recommended as hydraulic pinch to optimize the cost of pumping of water distribution network in which minimum number of pumping stations and reduction of energy consumption in each station are achieved by using optimum positioning of pumping station.

3. Hydraulic Pinch method

All real fluids have Adhesion and viscosity. However, there are many states in which, regardless of the adhesion is logical work. Equation of frictionless current, the Euler equation, can be achieved from the general movement equation. Since there is not shear stress in frictionless fluids and vertical tension is equal with negative thermodynamic pressure, movement Equation of frictionless flow can be expressed as follow:

$$\rho g - \nabla p = \rho \frac{Dv}{Dt} \tag{1}$$

Euler equation for steady state flow along a stream line is given by the following relation:

$$-\frac{1}{\rho}\frac{\partial P}{\partial s} - g\frac{\partial z}{\partial s} = v\frac{\partial v}{\partial s} \tag{2}$$

The P, v, g,, z, s, and ρ respectively represent the Thermodynamic pressure, velocity, acceleration of gravity, the height from the base level, flow direction and fluid density. If Flow is stable, the following equation is written.

$$\frac{dP}{\rho} + gdz + vdv = 0 \tag{3}$$

Above equation is based on three suppose.
1–Fluid flow is frictionless.
2–Fluid flow is along the streamline.
3 – If density is not a function of pressure, can be integral from Euler equation. When the ρ is constant, the Bernoulli equation is obtained. Bernoulli relationship during non-compressible fluid is established as follow

$$\frac{P}{\rho} + \frac{V^2}{2} + gz = cte \tag{4}$$

By simplification of Bernoulli equation the equation (5) is obtained:

$$\frac{P}{\gamma} + \frac{V^2}{2g} + z = cte \tag{5}$$

Equation (5) can be wrote between two consecutive points on the stream path.

$$\frac{P_1}{\gamma} + \frac{V_1^2}{2g} + z_1 = \frac{P_2}{\gamma} + \frac{V_2^2}{2g} + z_2 \tag{6}$$

The index 1 indicates the beginning point and the index 2 indicates any point after it along the current direction. If the flow velocity in the point 1 ,starting point, is taken zero, and Thermodynamic pressure is the constant value along the path, we have the equation(7):

$$h = z_1 - z_2 = \frac{V_2^2}{2g} \tag{7}$$

If stream pressure drop causing from pipes length, pipes diameter, bends fitting and other parameter are considered, we will have:

$$h_t = z_1 - z_2 - h_{loss} = \frac{V_2^2}{2g} \tag{8}$$

Impact of pressure loss (h_{loss}) will be described in computing of the " Minimum Allowable Pseudo Height Difference " and will be applied. Relation

between the speed and flow rate of the water is as follow.

$$V.A = Q \tag{9}$$

Q, A and V respectively are the flow rate, area of stream cross section and velocity of fluid. By placement V of the equation (9) in relation (7) we have:

$$h = \frac{(Q/A)^2}{2g} \tag{10}$$

In this article is defined an important and key parameter, named "pseudo height" as follow.

$$h' = \sqrt{h} \tag{11}$$

Also the parameter "m" is defined in relation (12).

$$\mathrm{m} = \frac{1}{\mathrm{A}\sqrt{2\mathrm{g}}} \tag{12}$$

As a result, the relation (10) can be written as follow.

$$\mathrm{h}' = m.\mathrm{Q} \tag{13}$$

Plotting of h' against Q for a water source and a consumer is shown in the figure (1).

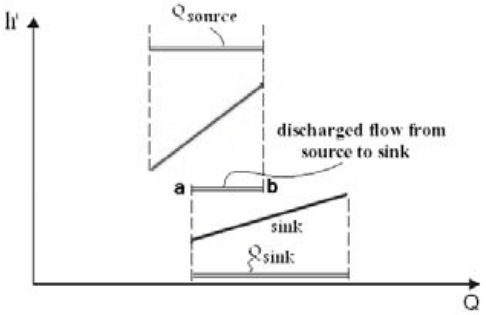

Fig. 1. plotting h' against Q for a water source and a consumer

It is observed from figure 1 that the Curve of water source has Flow rate Q_{source} which set between the two up and down values of the pseudo height. For illustratation of this case, take a river as water source that Flow rate Q_{source} can be achieved from it. Pseudo Height of river in the range which Q_{source} achived has two up and down limits. This case is true for water Consumers. For example, consider a city as a consumer that needs to the Flow rate Q_{sink}. Height above sea level of City has two high and low limit. Therefore, the pseudo height curve of city placed between high and low limit.

As mentioned in previous sections of this article Gravitational transition of water and the use of gravity force is an important objective. In the above example, if the height above sea level of river is upper than height above sea level of the city its water can be transferred to consumer (the city). In other words only the part of the water source that has more height than the height of the city can be delivered to consumers, by earth gravity driven force.

For identifying the Amount of water source that can be transferred only by using gravity force and without using the pumping, the two curves source and sink (consumer) must shift horizontally toward each other as intersect each other at the one point. This point named as point P (Figure (2)). Point P has a physical sense and concept. Point P on the source curve indicate the pseudo height limit that if the water source has pseudo height value less than it, can not discharge the water towards the consumer by using gravity force.

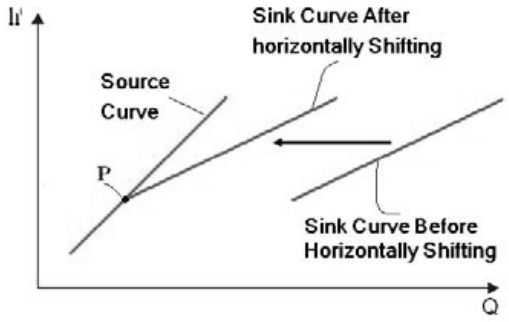

Fig. 2. shifting the water source curve to the water sink curve for identifying the pinch point

Part of the project of source and sink curve on Q axis that are overlapped with each other (line a-b in Figure (3)) represent the amount of water that can Flow from the source to consumer by using weight force. Obviously, the increase of the section which two curves are overlapped with each other, cause to increase of amount of water that can be transferred by gravity force from the source to the consumer. Therefore there isn't any request to energy for pumping the water to the consumer. Use of Geomagnetism for water transition is called Gravitational water transition. Gravitational water transition is conventional

method in water distribution networks and water transmitting between the source and the consumer. In this article the intersection point of two curves source and consumer (P point), is called the Pinch point. In the proposed method we are trying to increase the overlapped section, which the source and the consumer are cover each other.

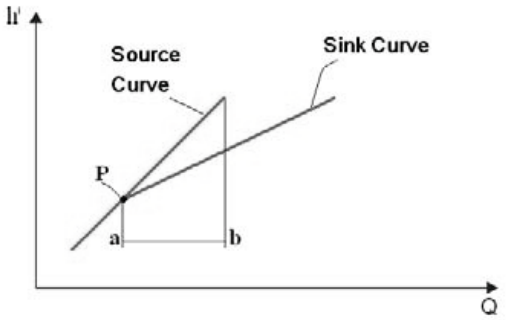

Fig. 3. identifying the amount of water source that can be transferred to water sink with gravity driven force

4. Minimum allowable pseudo height difference

By considering to the explanation that presented about the P point or Pinch point it resulted that there is not driven force for water source with the pseudo height equal with the pseudo of water consumer for water transition. The points of source curve that have little pseudo height upper than pseudo height of Pinch point have very little energy to transfer the water to consumers. In the design of water networks always a specific value for the desired velocity and pressure of water is defined in position consumer. Therefore, in this article an appropriate solution is considered in which fluid source curve has suitable pseudo height differences to consumer curve at pinch point and driven force, as the water consumers can receive water with appropriate specification.

It also is known that head loss due pressure losses suppose must be considered. For this purpose, a pseudo height difference between the source and consumer curves is calculated and is defined in which gravitational driven force from it lead to the desired velocity and pressure on consumption position and pass over head losses. The amount of pseudo height difference between sources and sinks are defined as $\Delta h'_{\min}$ or $h'_{\min}$. For considering to $h'_{\min}$ value at Pinch point, before horizontally shifting of the curves toward each other, each curve is shifted vertically with the size $\frac{h'_{\min}}{2}$ together. Then they are shifted horizontally until cross each other at pinch point. In fact, we know that between water source and consumer curves at intersection point (pinch point), there are the pseudo height difference $h'_{\min}$ that necessary velocity and pressure conditions of corresponding consumer at pinch point are satisfied and driving force to overcome the head loss is provided. Here the new diagram that source and consumer curves have been shifted vertically towards each is named as “Shifted composite Curves”.

When the number of water source or water sink are more than one we use the other curve as Composite Curve. Composite Curves (curve of water sources or consumers) is combination of all consumers or resources curves. To make the Composite curve we perform as follows. Here making of water source composite curves are explained. Composite Curve of consumers is similarly obtained.

1 – At First layout all of the up and down limit of pseudo height of resources respectively from smallest to largest value. In this case, district intervals of pseudo heights are obtained. We assume that the number successive interval is n. for each interval should be drawn a curve in which the starting point of each interval curve is end of previous interval curve. Slope of each interval Curve is obtained by using the following correlation.

$$m_j = (\quad 1/m_i)^{-1} \qquad j = 1,2,...,n \qquad (14)$$

2 - in the above equation the index j related to each interval from one to n, and index i indicates each of the curve is located at the jth interval. In other words the slope of jth curve interval is reverse of sum of reverse value of slope of the all curves located in j interval. For example, in the figure (4) the slope of source composite curve in m-n interval is obtained from the following relation.

$$m = 1/(1/a + 1/b) \qquad (15)$$

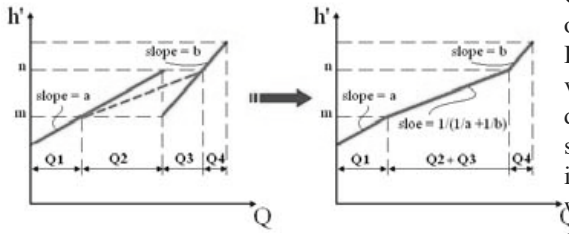

Fig .4. making the source composite curve

The above-illustrated Methods can also be used to obtaining for consumer as Sink Composite Curve. Curves of the source and the consumer can be plotted as Shifted Composite Curves. For this purpose, each of the consumer and resource curves can be vertically shifted in the size $\frac{h'_{\min}}{2}$ toward each other. Now consumer and source composite curve can be shifted horizontally toward each other to cross two curves in Pinch point. The section which two Shifted Composite Curves are overlapped with each other indicate Flow rate value of water source in which can be transferred to consumer without pumping and only by using gravity force.

What was expressed to this stage is to feature of graphical method based Pinch technology (Hydraulic Pinch) in water distribution using the gravity force. In the next steps, the purpose of this new and innovative method is providing driven force for transition of the residual required water to consumers by using the pumps so they related Positions, numbers, and energy consumption of pumps are optimized. The hydraulic Pinch determines Position of pumps in way that requirement to them employment is the minimum amount as possible. For this purpose, Pinch points are considered at the Shifted Composite Curve as the key point because they are very important. By Analysis of Pinch points in the shifted composite curve are identified the source or sources that cause to limitation the overlapped section.

In Figure (5) Source stream A, B are on the right and sources stream A, B and C are on left side of Pinch point. Pinch point prevent from horizontal movement of water sink curve to the left side. Therefore, to increase the overlapped section of curves, position of the Pinch point must be changed. If the height of Pinch point is increased, sink curve can move toward the left. Increasing of pseudo height of source C leads to raise the pseudo height of pinch point. So consumers and source Curve can be moved horizontally towards each other in order to increase the overlapped section. In this method the critical source are determined very fast and easily. The graphical and conceptual decision maker determine the key limiting source stream (Source C) in Pinch point, and by introducing the appropriate and best Position of water pumping station the lowest demanded energy to pumping found out.

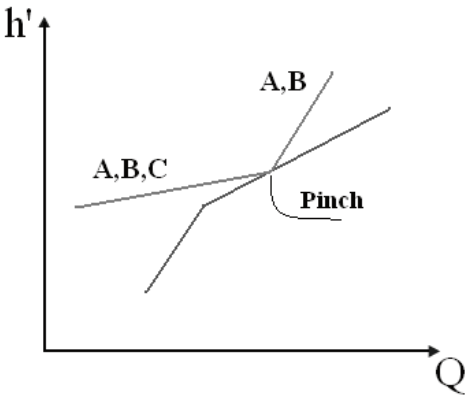

Fig. 5. determining the key and the critical water source in point Pinch

By considering to above mentioned description the instruction for optimization of water distribution network by using the proposed method (Hydraulic Pinch) is as follow.

1 - Extract data and information of water sources and consumer (up and down level of pseudo height, steam flow rate, pressure loss between sources and sinks).
2 - Define the minimum allowable amount of pseudo height difference by considering to maximum pressure loss between sources and consumers and the velocity and pressure requirements of consumers in water deliveration position.
3 – Make Composite Curve for source and consumer.
4 – Plot the resources and consumers Composite Curve in a common diagram so the consumer Composite Curve is in the right side of sources Composite Curve.
5 – Make Shifted Composite Curves with vertically displacement of two curves to each other.
6 - Shift horizontally the Composite curves toward each other until cross each other at Pinch point.
7 – Determine the key source or sources at Pinch

point.
8 - Change the pseudo height of the key water source or sources at Pinch point with pumping operations.
By using the above scenario water transition with maximum using of Gravitational driven force and minimum using of water pumping and energy cost is obtained. In the next section by analysis of an example, performance of hydraulic Pinch method will be investigated.

5. An example of optimization of water distribution network

In this section, an example of water distribution that has the common water resources and consumers is analyzed. Data and information of water sources and consumer are showed in table (1). River No. 1 and 2 (First and Second River), Lake, Origin Storage (Reservoir), Swamp and Pond are water resources in problem. Consumer applications are including urban water (Municipal), agriculture (Agricultural), Industry (Industrial), Rural, and special tourism province (Tourism). Minimum allowable pseudo height calculated by considering to desired pressure and velocity in position of water delivery to consumer and pressure loss. As see in table (2) maximum value of pressure loss between sources and sinks relate to water flow from Second River to municipal consumer. This value is 0.59m. Pseudo height in its stream is 0.77 m1/2. Minimum desired velocity in consumers is 2.7 m/s. corresponding pseudo height for this velocity is 0.63 m1/2. There for minimum allowable pseudo height calculated as follow.

$$h_{\min} = 0.63^2 + 0.77^2 = 1m$$
$$h'_{\min} = \sqrt{h_{\min}} = \sqrt{1} = 1m^{1/2}$$

Therefore, the minimum head difference between resources and consumer should not be less than 1 meter.

For the design of optimal water distribution network from perspective of pumping energy consumption the scenarios of hydraulic Pinch method are employed. At First Composite Curve of sinks and sources are created with regard to the minimum allowable pseudo height $h'_{\min}$ (Figure (6)).

Table 1. Data of water sources and sinks

water source			
Name	upper head bond($m^{1/2}$)	lower head bond($m^{1/2}$)	Flow (m^3/s) × 1000
Reservoir	10	8	57
First River	8	4	54
Second River	7	3	200
Swamps	5	3	1.5406
lake	4.5	2	406
Pond	6	3	5
water sink			
Name	Lower head bond($m^{1/2}$)	upper head bond($m^{1/2}$)	Flow (m^3/s) × 1000
Municipal	2	6	70
Agriculture	2	5	460
Rural	3	4	7
Industry	2	5	12
Tourism	1	3	5

Table 2. head loss(m) of water flow between sources and sinks

	Reservoir	First River	Second River	Swamps	lake	Pond
Municipal	0.36	0.28	0.59	0.44	0.16	0.4
Agriculture	0.47	0.24	0.36	0.38	0.3	0.1
Rural	0.12	0.17	0.3	0.22	0.36	0.4
Industry	0.21	0.23	0.16	0.52	0.41	0.1
Tourism	0.2	0.4	0.27	0.41	0.21	0.1

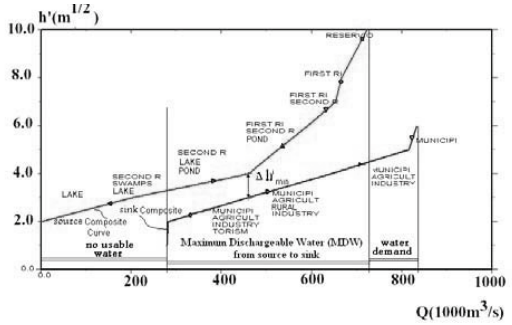

Fig. 6. Setting the $h'_{\min}$ for resources and consumers composite curves

Table 3. Pseudo head loss($m^{1/2}$) of water flow between sources and sink

	Reservoir	First River	Second River	Swamps	lake	Pond
Municipal	0.6	0.53	0.77	0.66	0.4	0.65
Agriculture	0.69	0.49	0.6	0.62	0.55	0.39
Rural	0.35	0.41	0.55	0.47	0.6	0.65
Industry	0.46	0.48	0.4	0.72	0.64	0.37
Tourism	0.45	0.63	0.52	0.64	0.46	0.39

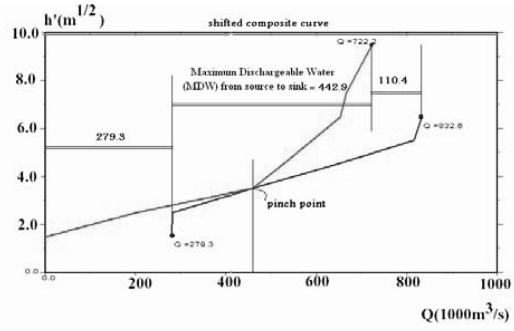

Fig. 7. Chart shifted composite curves

Composite Curve of source and consumer are shifted vertically towards each other with size $\frac{h'_{\min}}{2}$. Then two curves are moved horizontally until cross each other at the pinch point (figure 7)). As can be seen the maximum water transmitted by gravitational driven force is equal with horizontal section that two curve overlap with each other $442.9\times10^3\ m^3/s$. In other words by using hydraulic Pinch maximum amount of water that can be distributed in network only by using earth gravity force and without the use of pumping, was determined. Remaining required water for consumers that can not be transferred by gravitational force is equal with $110.4\times10^3\ m^3/s$. This amount should be transferred by pumping operations.

in the design of water networks Optimum position of pumping station and the optimal required driven force for providing remaining demanded water for consumer is answer of a complex problem, but the innovative hydraulic pinch method determined them fast and easily. By considering what was said in the previous section, if look at Pinch point it understand that the Lake is the critical and key source, which cause to making Pinch point. Therefore must be performed necessary changes in pseudo height of this resource, so that the point Pinch as restrictive point is removed or moved horizontally toward left side of source composite curve. As result sources and consumers can transfer toward each other. The Pseudo height of Lake is between 2 ~ 4.5 m1 / 2. By Using the pumping operation upper Pseudo height limit of Lake is increased to 5 m1/ 2. In this case, Shifted Composite Curves will be as the figure (8). As we see in this figure total required water demand for consumer are satisfied.

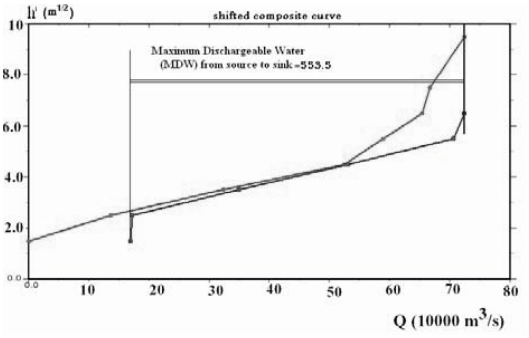

Fig. 8. Increasing the head of lake cause to change Pinch point position and increase the overlapped section

In the studied example, hydraulic Pinch method allocates water to consumer using earth gravity driven force and without any pumping employment. Then hydraulic Pinch method determined the optimal position and specification of pumping stations by graphical tools and decision makers. As was noted, improved and optimum management of water resources from energy consumption point of view is feasible and possible by proposed method.

Discussion

Hydraulic Pinch method is a graphical method based on Pinch technology that uses the graphical and conceptual scenario for optimal design of water distribution network from pumping energy point of view and costs due to its. This method determined minimum amount of power and energy required for water pumping.
In the example studied in this article pseudo height of water source increased as 0.5m1/2, which caused to supply total demanded water for consumers. Thus, the lowest using of pumps and suitable them location are determined. Equipment purchase costs due to pumps, valves and controling instrument, safety and other equipment and energy costs ,which are very significant and important, are Minimized in this method. The operating costs resulting from repair and maintenance of pumps and related equipment are reduced.
The method given in this article is a very efficient way, and still easy to design the distribution network. This method provide 80% of the required water through gravity driven force for consumer and the remaining 20% through the pumps that are selected in optimum state. Therefore, by the lowest energy consumption in pumps distribution operations is performed. Other methods may also be proposed for design of distribution network. Mathematical methods such as Super Structure is very high accuracy. But these methods need to very high computational time. They are more sophisticated methods than graphical methods and because lack of user control and proficiency on solution process, local optimal point may be obtained from optimization. But in graphical methods such as methods based on Pinch technology because all of the diagram, visual and conceptual control, optimization process is directed toward the golobal optimal point. Visual and conceptual decision-maker is capability of this noval method to optimization of large and sophisticated problem. Even with improved graphical techniques based on Tabular Method [19,20] accuracy of graphical methods can be increased.

Conclusion

In this paper was developed a new graphical method based on Pinch technology as Hydraulic Pinch for optimizing the water distribution networks form pumping energy vision. This method proposes the largest using of gravity force to transfer water from resources to consumers and then uses pumps to provide the remaining needed water for consumer in the lowest possible cost of pumps, related equipment, and energy consumption. Minimum use of pumps, electric energy and power leads to reduced maintenance and investment costs and energy costs. Hydraulic pinch by using graphical and conceptual decision makers provides better strategies for problem solving than the Mathematical methods. Controling and leading of optimization process toward the global optimum state is possible. This method is presented as a noval and efficient method for scientifics, researchers, and designers of water distribution network.

References

[1] Linnhoff, B. and Turner, J. A. “Pinch technology” Chem.E. December, pp742-746, 1980

[2] Linnhoff And Flower, J. R. , “ A Thermodynamic Approach To Practical Process Network Design”, Aich 72nd Annual Meeting, November 25-29, San Francisco, Paper No 28b, 1979.

[3] Towmsend, D. W. and Linnhoff, B., "Surface Area Targets Heat Exchanger Networks" t I Chem..e 11th Annual Res. Metting, April, Bath, U. K, 1984.

[4] Linnhoff, B. And Ahmad, S., "Cost Optimization Heat Exchanger Networks 1. Minimum Energy And Capital Using Simple Models Capital Cost", Comp And Chem.E 14(7). 729-750.1990.

[5] Panjeh Shahi, M. H., "PRESSURE Drop Consideration In Process Integration',Ph.D Thesis. University of Manchester Institute of Science and Technology, 1992.

[6] Polly, G. T., Panjeh Shahi, M. H. And Jagede F. O., "Pressure Drop Consideration in the Retrofit of the HEN", Trans.I.Chem.E. 68A,pp. 211-220, 1990.

[7] Polly, G. T., Panjeh Shahi, M. H. "process integration retrofit subject to pressure drop constraint", process technology proceedings, vol. 9,pp. 31-36,1990.

[8] Polley, G. T., Athie, R. And Gough, M., "Use Of Heat Transfer Enhancement in Process Integration." Heat Recovery System, Chp Vol. 12, No. 3, pp 191-202, 1992.

[9] Polley, G. T., Jafari Nasr, M. R. And Terranova, A., "Determiation And Application Of Benefits Of Heat Transfer Enhancement.". Trans.Icheme. Vol. 72, Part A, Sept.,pp. 616-620, 1994.

[10] Jafari Nasr, M. R. and Polley, G. T., "Should You Use Enhanced Tubes?", Chem.E.Prog.(Cep),pp.44-50,April,2002.

[11] Wang Y.-P, Smith R. Wastewater minimization, Chem. Eng. Sci. 49 (7) (1994) 9811006.

[12] Alves J.J., Towler G.P. Analysis of refinery hydrogen distribution systems, Ind. Eng. Chem. Res. 41 (23) (2002) 57595769.

[13] Zhelev T.K., Bhaw N. Combined water oxygen pinch analysis for better wastewater treatment management, Wastewater Manag. 20 (8)(2000) 665670.

[14] Foo DCY., manan ZA., Tan YL. Synthesis of maximum water recovery network for batch process systems. J Cleaner prod 2005; 13:1381-94.

[15] towler GP., menn R., serriere AJ-L., Gabaude CMD. Refinery hydrogen management: cost analysis of chemically integrated facilities. Ir.d Eng Chem Res 1996;3:2378-88.

[16] Zhelev TK., Ntlhakana JL. Energy environment closed-loop through oxygen pinch. Compute Chem Eng 1996; 23:S79-83

[17] E. Alperovits, U. Shamir, Design of optimal water distribution systems, Water Resour. Res. 13 (6) (1977) 885–900. Eng. Optim. 7 (2) (1984) 143–155.

[18] O. Fujiwara, B. Jenchaimahakoon, N.C.P. Edirisinghe, Modified linear programming gradient method for optimal design of looped water distribution networks, Water Resour. Res. 23 (6) (1987) 977–982.

[19] A. Kessler, U. Shamir, Analsis of the linear programming gradient method for optimal design of water supply networks, Water Resour. Res. 25 (7) (1989) 1469–1480.

[20] P.R. Bhave, V.V. Sonak, A critical study of the linear programming gradient method for optimal design of water supply networks, Water Resour. Res.

[21] G. Eiger, U. Shamir, A. Ben-Tal, Optimal design of water distribution networks, Water Resour. Res. 30 (9) (1994) 2637–2646.

[22] J.C. Schaake, D. Lai, Linear programming and dynamic programming applied to water ptimization network design, MIT Hydrodynamics Lab Report 116, 1969.

[23] O. Fujiwara, D.B. Khang, A two-phase decomposition method for optimal design of looped water distribution networks, Water Resour. Res. 26 (4). (1990) 539–549. 28 (6) (1992) 1577–1584.

[24] K.V.K. Varma, N. Shankar, S.M. Bhallamudi, Optimal design of water distribution systems using an NLP method, J. Environ. Eng. 123 (4) (1997) 381–388.

[25] A.R. Simpson, G.C. Dandy, L.J. Murphy, Genetic algorithms compared to other techniques for pipe optimization, J. Water Resour. Plan. Manage.-ASCE 120 (4) (1994) 423–443.

[26] D.A. Savic, G.A. Walters, Genetic algorithms for least-cost design of water distribution networks, J. Water Resour. Plan. Manage.-ASCE 123 (2) (1997) 67–77.

[27] M.D.C. Cunha, J. Sousa, Water distribution network design optimization: Simulated annealing approach, J. Water Resour. Plan. Manage.-ASCE 125 (4) (1999) 215–221.

[28] A.C. Zecchin, A.R. Simpson, H.R. Maier, M. Leonard, A.J. Roberts, M.J. Berrisford, Application of two ant colony ptimization algorithms to waterdistribution system ptimization, Math. Comput. Modeling 44 (5–6) (2006) 451–468.

[29] H.R. Maier, A.R. Simpson, A.C. Zecchin, W.K. Foong, K.Y. Phang, H.Y. Seah, C.L. Tan, Ant colony optimization for design of water distribution systems, J. Water Resour. Plan. Manage.-ASCE 129 (3) (2003) 200–209.

[30] M .Cieslak, Life cycle costs of pumping stations, J. World Pumps, Volume 2008, Issue 505, October 2008, Pages 30-33

On the Nature of the Heat Transfer Feasibility Constraint in the Optimal Synthesis/Design of Complex Energy Systems

Andrea Toffolo[a], Andrea Lazzaretto[a] and Michael R. von Spakovsky[b]

[a] *University of Padova, Padua, Italy*
[b] *Virginia Polytechnic Institute and State University, Blacksburg (VA), USA*

Abstract: In this paper, the formulation of the constraint on heat transfer feasibility in the synthesis/design optimization of complex energy systems is discussed, with particular emphasis on the case for which the matching among the hot and cold thermal streams within the system is not defined a priori. The mathematical nature of the set of inequality constraints expressing the internal availability of thermal power at different temperature levels is examined and some examples are shown illustrating the way these constraints bound the feasible region of the search space and affect the hypersurface of the so-called optimum response surface, which results from considering a reduced number of degrees of freedom of the optimization problem. A brief discussion is also proposed about the choice of the algorithm and the variables for the optimization process.

Keywords: Heat transfer feasibility, complex energy systems, synthesis/design optimization.

1. Introduction

Optimization of the synthesis/design of complex energy systems is perhaps the most challenging problem in the field of energy systems and many issues are still to be resolved. One of the most significant contributions to system efficiency enhancement is given by the recovery of internal heat in order to lower the requirement from external hot sources. To this end, the heat transfer section of the system may even be considered as a "black box", the attention being focused on optimizing the design parameters that affect its boundaries instead of defining its configuration [1,2]. In so doing, the feasibility of the heat transfer among the thermal streams involved in the black box plays a crucial role in the integration of system components. This paper is aimed at exploring the nature and the effects of this constraint, and is organized as follows. The formulation of the constraint is first discussed and then its effects are shown on four cases of the same example application. Finally, some suggestions are given about the optimization algorithms and the decision variables to be chosen.

2. The heat transfer feasibility constraint

Imposing constraints about heat transfer feasibility is commonly perceived as the application of a corollary to the Second Law of Thermodynamics (i.e. the Clausius statement) according to which heat cannot be transferred from a lower temperature source to a higher temperature sink without the expenditure of work. This is apparent in the design parameter optimization of energy systems for which the configuration has already been defined. The inequality constraints usually imposed simply check that the temperatures of the hot flows at the ends of the heat transfer devices are higher than those of the corresponding cold flows, using a preset minimum temperature difference ΔT_{min}. In fact, this formulation focuses on temperature only, and implies an underlying "vertical" perspective in which heat flows from higher to lower temperatures.

However, the synthesis/design optimization of energy systems requires a more complex formulation of the heat transfer feasibility constraint (HTFC). When both the configuration of the heat transfer section inside the system and the temperatures and the mass flow rates at the boundaries of this section are unknown and must be optimized, the availability of thermal power for internal heat transfer integration becomes critical (this may be true even if external hot utilities are considered, since their availability may be limited in terms of thermal power and/or temperature level). In addition, heat transfer feasibility cannot be checked anyway by simply comparing the end temperatures of thermal stream couples, since the configuration of the system's heat transfer section

Corresponding Author: Andrea Toffolo, Email: andrea.toffolo@unipd.it

remains undefined and the matching between the hot and cold streams is unknown.

In general, heat transfer feasibility is checked every time a candidate solution to the synthesis/design optimization problem is evaluated. To do this, the mass flow rates and the initial/final temperatures and enthalpies of the thermal streams involved in the heat transfer section of the system must be obtained from the decision variables. Two temperature profiles merging the contributions of all hot and all cold streams are then built, the so-called hot and cold composite curves [3]. These contributions are evaluated in terms of initial/final temperature range and thermal power and are cumulated from the highest to the lowest temperature. The initial/final temperature range of each stream can also be modified in advance to take into account the minimum temperature difference allowed ΔT_{min} (the temperature ranges of hot streams are lowered by $\Delta T_{min}/2$, while the temperature ranges of cold streams are increased by half of $\Delta T_{min}/2$; different values of ΔT_{min} can be associated with different streams). The composite curves are represented in a diagram with thermal power P_{th} on the abscissas and temperature T on the ordinates (Fig. 1). At any temperature level, the abscissas of the two curves return the thermal power made available (hot composite curve, HCC) and required (cold composite curve, CCC) above that temperature level by all the thermal streams in the system's heat transfer section. When the configuration of this section is still undefined, heat transfer is implicitly assumed to occur from higher temperature hot streams to lower temperature cold streams, i.e. almost "vertically" in the diagram in Fig. 1 and without violating the corollary to the Second Law of Thermodynamics. Accordingly, the condition that ensures heat transfer feasibility is equivalent to searching for the temperature level at which the difference between the cumulated thermal power made available and required is minimum and verifying whether this minimum difference is greater than zero:

$$\min\left({}^{h}_{th}(\ ) \quad {}^{c}_{th}(T)\right) \geq 0 P. \qquad T- \qquad P \qquad (1)$$

This can be assessed by building the Pinch Technology Problem Table according to the procedure illustrated in [3]. The rows of the table refer to the temperature levels corresponding to the initial and final temperatures of thermal streams, ordered from the highest to the lowest, while one column of the table indicates the surplus or the deficit (the excess or the lack) of the cumulated thermal power made available at each temperature level with respect to the cumulated thermal power requirement. As mentioned above, the heat transfer feasibility constraint states that no deficit (no lack) is allowed, and the temperature level at which the surplus (the excess) is strictly zero is called a "pinch point".

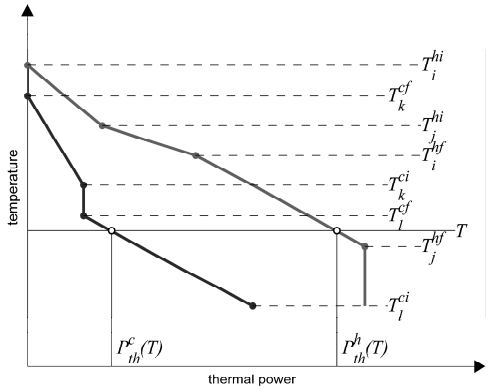

Fig. 1. Hot (red) and cold (blue) composite curves and heat transfer feasibility condition.

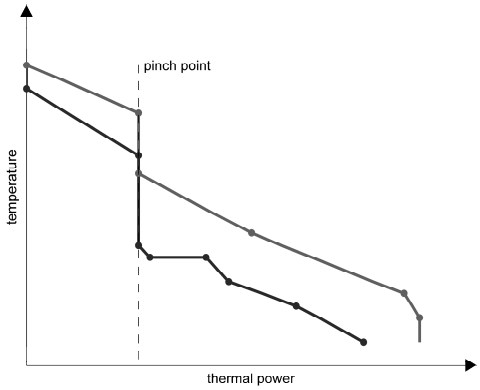

Fig. 2. Example of a "horizontal" pinch point.

Please note that this formulation of the HTFC is often considered as another "vertical" condition related to the minimum temperature difference allowed. In fact, a pinch point is usually seen as the point at which the vertical distance (the temperature difference) between the hot and cold composite curves is equal to the minimum value allowed. Actually, this is a "horizontal" condition related to a difference that is measured on the abscissas of the temperature vs. thermal power diagram. There may be cases in which the surplus

of thermal power is zero at a given temperature (or in a given temperature range) but the temperature difference between the hot and cold curves is always greater than the minimum allowed (Fig. 2). This is nevertheless a critical situation for the feasibility of the internal heat transfer within the system. This is also the reason why the composite curves should be "integrated" with vertical traits in the temperature ranges in which no thermal stream contributes, as is shown in Figs 1 and 2.

It is not advisable, in this "horizontal" perspective, to formulate the HTFC as a single inequality constraint (1) associated with the temperature level at which the minimum surplus is found in the Problem Table. In fact, during the optimization process, the temperature level at which the minimum surplus is found may change, and this is likely to mislead the search for the optimum. It is suggested, therefore, to impose an inequality constraint *at each temperature level associated with the initial and final temperatures of the thermal streams, without exceptions* (the only exception could be the highest temperature level at which the thermal power made available/required is zero by definition; however, this temperature might be surpassed by the initial/final temperature of another thermal stream during the optimization process). The inequality constraint at the generic temperature level T can be expressed as:

$$\sum \dot{m}_i^h \left(h_i(T_i^{hi}) - h_i(T_i^{hf})\right) + \sum \dot{m}_j^h \left(h_j(T_j^{hi}) - h_j(T)\right) - \sum \dot{m}_k^c \left(h_k(T_k^{cf}) - h_k(T_k^{ci})\right) + \sum \dot{m}_l^h \left(h_l(T_l^{cf}) - h_l(T)\right) \geq 0 \quad (2)$$

where i and k are the indices of the hot and cold streams, respectively, for which the temperature ranges are completely above T ($T \leq T_i^{hf} \leq T_i^{hi}$ or $T \leq T_j^{ci} \leq T_j^{cf}$); and j and l are the indices of the hot and cold streams, respectively, for which the temperature ranges are only partially above T ($T_k^{hf} \leq T \leq T_k^{hi}$ or $T_l^{ci} \leq T \leq T_l^{cf}$). The thermal streams for which the temperature ranges are completely below T do not appear in (2). Heat transfer feasibility is therefore guaranteed by a set of these inequality constraints.

The design variables that directly affect heat transfer feasibility are the mass flow rates and the initial/final temperatures of the thermal streams, as is apparent in (2). If the mass flow rate of the generic i-th thermal stream is varied, the slope of the composite curve within the temperature range of that thermal stream [T_i^i, T_i^f] changes. If the mass flow rate $\dot{m}_i$ is decreased, the composite curve will become steeper between T_i^i and T_i^f , whereas if $\dot{m}_i$ is increased, the composite curve will become flatter (Fig. 3). The slope of the composite curve above and below the range [T_i^i, T_i^f] is unaltered, but the portion of the curve below the range is shifted horizontally towards a higher or a lower thermal power if $\dot{m}_i$ is increased or diminished, respectively, because the contributions of the single thermal streams to the composite curve are cumulated.

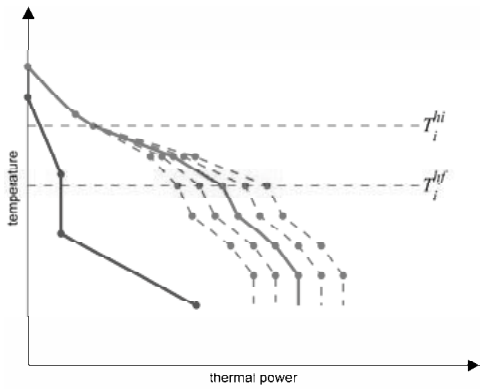

Fig. 3. The modification to a composite curve as the mass flow rate of a thermal stream is varied.

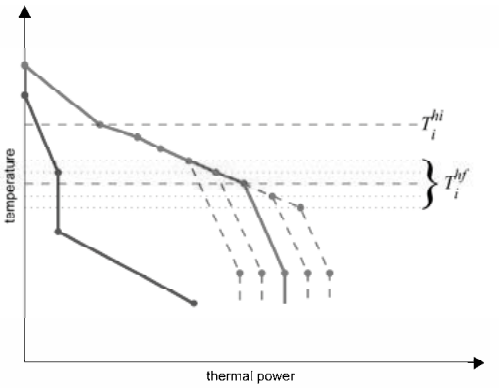

Fig. 4. The modification to a composite curve as the end temperature of a thermal stream is varied.

On the other hand, if the initial or the final temperature of a thermal stream is varied, the contribution of that thermal stream to the composite curve in terms of thermal power increases or decreases when the temperature range expands or shrinks, respectively (Fig. 4). As a

result, the slope of the composite curve remains unaltered while, again, the portion of the curve below the modified range is shifted horizontally towards a higher or a lower thermal power if the temperature range expands or shrinks, respectively.

Other design variables such as stream pressures and mass fractions play an indirect role in the set of inequality constraints, since they affect the enthalpy calculations. The role of pressure is almost negligible if the behavior of the fluid can be approximated by an ideal gas (enthalpy is a function of temperature only) but is important for real fluids, particularly when they undergo phase changes as, for instance, in water/steam cycles. Mass fractions affect the specific heat of multi-component fluids, so they can affect the slope of the composite curve in the same way as the mass flow rate does.

It is worth noting that the set of inequality constraints in (2) is valid if each thermal stream is assumed to contribute to the temperature profile of the composite curve with linear segments, so that the composite curve itself is formed by linear traits. If the temperature profile of a thermal stream is far from linear, it can be approximated with linear segments in order to keep the aforementioned formulation of the HTFC valid.

3. The impact on the search space and the optimum response surface

The general formulation of a constrained optimization problem is:

$$\begin{array}{lll} \text{minimize} & f(\boldsymbol{x}) & \text{with respect to } \boldsymbol{x} \in \Re^n \\ \text{and subject to} & g_i(\boldsymbol{x}) \geq 0 & 1 \leq i \leq p \\ & h_i(\boldsymbol{x}) = 0 & 1 \leq i \leq q \ , \end{array}$$

where $\boldsymbol{x}$ is the vector of the n decision variables (thus, n is the dimension of the space of candidate solutions), f is the objective function, g_i and h_i are the functions expressing the p inequality and the q equality constraints, respectively.

Being that the feasible region F of the search space is defined as the subset of candidate solutions which satisfy all the imposed constraints, it is apparent that any constraint tends to restrict F. In particular, each of the inequality constraints defines a hypersurface $g_i(\boldsymbol{x})=0$ (which is usually smooth) cutting the search space into two subspaces: the subspace F_i in which the candidate solutions satisfy the i-th inequality constraint and the complementary subspace ($\Re^n - F_i$) in which the candidate solutions do not satisfy that constraint. If a candidate solution $\boldsymbol{x}$' lies on this hypersurface (i.e. $g_i(\boldsymbol{x}')=0$) the i-th inequality constraint is said to be active for the corresponding set of decision variable values ($x_1'\ldots x_n'$). As a consequence, the feasible region is the intersection of all the subspaces F_i ($F=F_1\cap\ldots\cap F_p$); and it is bounded by portions of the hypersurfaces $g_i(\boldsymbol{x})=0$. These hypersurface portions are bounded by (hyper)edges shared with other hypersurfaces. For the candidate solutions belonging to these hyperedges, two or more of the inequality constraints are active at the same time. In general, the common hyperedges make the frontier of the feasible region non-smooth.

The set of inequality constraints used to ensure heat transfer feasibility (2) is a paradigmatic example of how inequality constraints affect the feasible region of the search space. Each of the inequality constraints, expressing the excess of available thermal power at a given temperature level, subtracts an unfeasible subspace (in which this excess is negative, i.e. it represents a lack) to the search space. The candidate solutions that lie on the hypersurface defined by the i-th inequality constraint have a pinch point active (the excess is zero) at the corresponding temperature level, and those that belong to a hyperedge shared by m hypersurfaces have m pinch points active at the corresponding temperature levels. The frontier of the feasible region exhibits ever higher numbers of non-smooth features as the number of involved thermal streams increases.

Such non-smooth features on the frontier of the feasible region of the search space do not affect the smoothness of the objective function but are likely to affect the smoothness of the so-called optimum response (hyper)surface (ORS), i.e. the mapping from the values assigned to a set of degrees of freedom of the optimization problem (which do not necessarily coincide with the decision variables[1]) to the optimum value of the objective function corresponding to those values. In fact, if the set comprising all the decision variables is considered as the set of degrees of freedom, this mapping coincides with the one operative for the objective function. However, if a

[1]The degrees of freedom referred to here are the "coupling functions" (see Section 3.3), which may or may not appear in the single-level optimization problem, i.e. when no physical decomposition is used.

reduced number of degrees of freedom is considered (e.g., simply for a clearer visualization or following the application of mathematical techniques to lower the computational effort of the optimization process), a projection of the optimal objective function values is made along the dimensions associated with the degrees of freedom that have been ignored. The non-smooth features on the frontier of the feasible region are inevitably involved when the optimum value to be projected lies on such features, and, thus, these features are transferred to the ORS.

3.1. The example application

In order to show the impact of the HTFC on the search space and the ORS, four cases are presented with respect to the model of a dual pressure level combined cycle power plant found in [4].

The structure of the model (Fig. 5) highlights the three thermodynamic cycles operating in the plant: a gas Brayton cycle (B) and two steam Rankine cycles (R1 and R2, at low and high pressure, respectively). The model equations are summarized in Table 1.

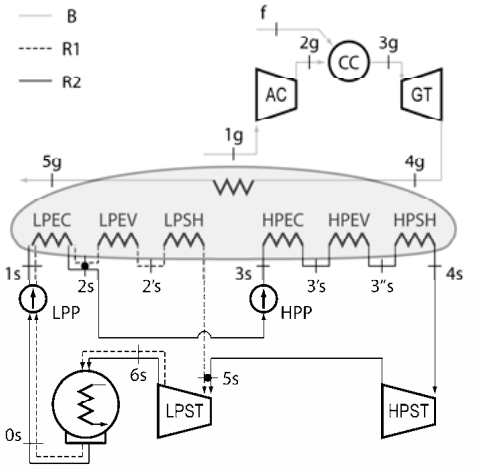

Fig. 5. Flow diagram of the dual pressure level combined cycle power plant used as the example application.

The numerical values of the model constants are

$\dot{m}_f = 1.5$ kg/s, $LHV = 50000$ kJ/kg, $\eta_{cb}^{CC} = 0.95$;
$\eta_{is}^{AC} = 0.8$, $\eta_{is}^{GT} = 0.9$; $f_p^{CC} = 0.97$, $f_p^{HRSG} = 1$;
$p_{1g} = 1.013$ bar, $T_{1g} = 288.15$ K, $T_{5g} = 378.15$ K;
$p_{0s} = 0.1$ bar, $\eta_{is}^{LPP} = \eta_{is}^{HPP} = 0.9$, $\eta_{is}^{LPST} = \eta_{is}^{HPST} = 0.9$;

and the minimum temperature difference allowed (ΔT_{min}) is set at 10 K.

The thermodynamic properties of water/steam are evaluated using routines that reproduce the Mollier diagram, whereas the air and flue gases are assumed to be ideal gases with constant ratios of specific heats (1.4 and 1.33, respectively) and constant specific heats at constant pressure (1.004 kJ/kgK and 1.17 kJ/kgK, respectively), so that each specific enthalpy difference is evaluated as the product of the specific heat and the temperature difference (although less accurate, it is sufficient for our purpose).

Table 1. Combined cycle power plant model.

model equations
$p_{2g} = r_c\, p_{1g}$
$p_{3g} = f_p^{CC}\, p_{2g}$
$p_{5g} = p_{1g} = f_p^{HRSG}\, p_{4g}$
$T_{2g} = T_{2g}(T_{1g}, p_{1g}, p_{2g}, \eta_{is}^{AC})$
$\dot{m}_g = \dot{m}_a + \dot{m}_f$
$\dot{m}_a h_{2g}(T_{2g}) + \eta_{cb}^{CC} \dot{m}_f LHV = \dot{m}_g h_{3g}(T_{3g})$
$T_{4g} = T_{4g}(T_{3g}, p_{3g}, p_{4g}, \eta_{is}^{GT})$
$h_{0s}, s_{0s} = h_{0s}, T_{0s}(p_{0s}, q_{0s} = 0)$
$h_{1s} = h_{1s}(p_{1s}, p_{0s}, s_{0s}, \eta_{is}^{LPP})$
$h_{2s}, T_{2s} = h_{2s}, T_{2s}(p_{1s}, q_{2s} = 0)$
$h_{2's}, T_{2's} = h_{2's}, T_{2's}(p_{1s}, q_{2's} = 1)$
$h_{3s} = h_{3s}(p_{3s}, p_{1s}, s_{2s}, \eta_{is}^{HPP})$
$h_{3's}, T_{3's} = h_{3's}, T_{3's}(p_{3s}, q_{3's} = 0)$
$h_{3"s}, T_{3"s} = h_{3"s}, T_{3"s}(p_{3s}, q_{3"s} = 1)$
$h_{4s}, s_{4s} = h_{4s}, s_{4s}(p_{3s}, T_{4s})$
$h_{5s} = h_{5s}(p_{3s}, p_{1s}, s_{4s}, \eta_{is}^{HPST})$
$h_{6s} = h_{6s}(p_{1s}, p_{0s}, s_{5s}, \eta_{is}^{LPST})$
model constants:
$\dot{m}_f, \eta_{is}^{AC}, \eta_{is}^{GT}, \eta_{cb}^{CC}, f_p^{CC}, f_p^{HRSG}, p_{1g}, T_{1g}, T_{5g}$
$p_{0s}, \eta_{is}^{LPP}, \eta_{is}^{HPP}, \eta_{is}^{LPST}, \eta_{is}^{HPST}$
objective function:
$f(x) = P_{NET} = \dot{m}_g(h_{3g} - h_{4g}) - \dot{m}_a(h_{2g} - h_{1g})$
$+ \dot{m}_{R1}(h_{5s} - h_{6s} - h_{1s} + h_{0s})$
$+ \dot{m}_{R2}(h_{4s} - h_{6s} - h_{3s} + h_{2s} - h_{1s} + h_{0s})$
decision variables:
$x = \{r_c, \dot{m}_a, p_{1s}, \dot{m}_{R1}, p_{3s}, \dot{m}_{R2}, T_{4s}\}$
inequality constraints (other than HTFC):
$T_{3g} \le 1500$K
$q_{6s} \ge 0.88$

The synthesis/design optimization problem considered using this model has seven decision variables (Table 1) and a thermodynamic objective (the net power generated by the plant must be maximized for a fixed fuel mass flow rate). Note that the configuration of the heat recovery steam generator is not defined a priori in the model.

Accordingly, four possible pinch points may affect heat transfer feasibility at different temperature levels (Fig. 6):

- At the maximum temperature T_{4s} of the high pressure Rankine cycle R2 (A in Fig. 6). This pinch point is equivalent to the condition $T_{4g} \geq T_{4s} + \Delta T_{min}$.
- At the evaporation temperature $T_{3's}$ of the high pressure Rankine cycle R2 (B in Fig. 6).
- At the evaporation temperature T_{2s} of the low pressure Rankine cycle R1 (C in Fig. 6).
- At the lowest temperature of the cold streams T_{1s} (D in Fig. 6). This pinch point represents the overall availability of thermal power in the heat transfer section.

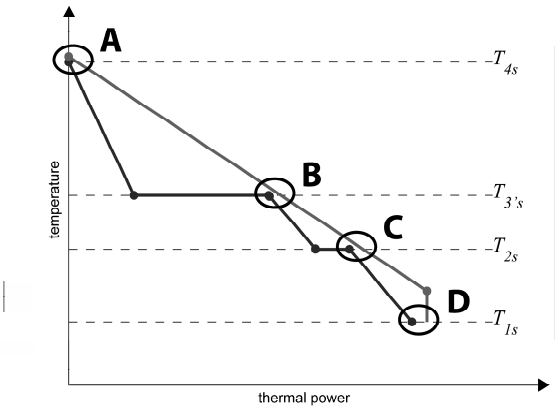

Fig. 6. The four possible pinch points in the example application.

The solution to the problem is [4]:

$P_{NET} = 38.5798$ MW; $r_c = 17.128$; $\dot{m}_a = 71.753$ kg/s; $\dot{m}_{R1} = 2.231$ kg/s; $p_{1s} = 7.097$ bar; $\dot{m}_{R2} = 9.689$ kg/s; $p_{3s} = 71.949$ bar; $T_{4s} = 811.15$ K (upper bound).

3.2. A simple case

In this first case (case I), the number of decision variables is reduced from seven to three (r_c, p_{1s} and $\dot{m}_{R2}$) in order to show the non-smooth frontier of the feasible region of the search space in a 3D diagram. To this end, constant values are assigned to $\dot{m}_{R1}$ (1.8 kg/s), p_{3s} (70 bar) and T_{4s} (811.15 K), while the value of $\dot{m}_a$ is obtained by converting the inequality constraint on T_{3g} into an equality constraint (T_{3g}=1500 K). Of course, these modifications to the original optimization problem alter the optimum solution as well, i.e. it is not the one specified in Section 3.1.

The search space is a hexahedron delimited by the following ranges of the decision variable values: $r_c \in [10,18]$, $p_{1s} \in [2,20]$ bar and $\dot{m}_{R2} \in [8,12]$ kg/s. The feasible region of the search space is shown in Fig. 7. Each of the four inequality constraints associated with the four different possible pinch points (designated with the letters A to D as in Fig. 6) cuts a portion of the search space out relative to the surface on which that particular pinch point is active. The edges (points) shared by two (three) of these surfaces are non-smooth features of the frontier of the feasible region of the search space. The optimal solution (shown with a white circle in Fig. 7) belongs to the edge along which pinch points B and C are simultaneously active.

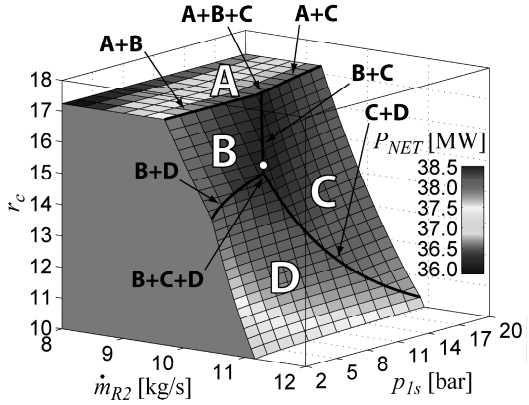

Fig. 7. Case I: the feasible region of the search space with the objective function values shown on the surfaces corresponding to active pinch points.

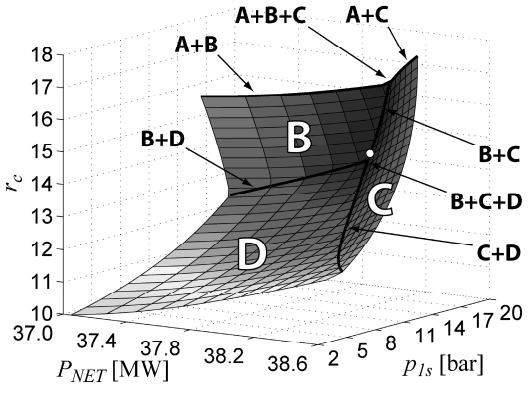

Fig. 8. Case I: the ORS with respect to r_c and p_{1s}.

The objective function is still smooth on the non-smooth frontier of the search space. On the other hand, it appears that $\dot{m}_{R2}$ gives a trivial contribution to the objective function (the higher the mass flow rate, the higher the net power). This suggests that only the objective function values corresponding to the maximum value of $\dot{m}_{R2}$ for any couple of values of r_c and p_{1s} should be considered. In this way, the ORS with respect to r_c and p_{1s} is obtained (Fig. 8). This surface is obviously non-smooth, because the non-smooth features on the frontier of the search space in Fig. 7 are directly projected onto the ORS along the $\dot{m}_{R2}$ coordinate as shown in Fig. 8.

3.3. Three more complex cases

Optimization problems with a high number of decision variables can be physically decomposed under specific hypotheses to reduce the computational effort of the optimization process. Physical decomposition can be hierarchical or non-hierarchical.

Nested optimization (see, e.g., [5]) is an example of hierarchical decomposition according to which decision variables are divided into top- and bottom-level variables. Bottom-level variables are optimized while keeping the top-level variables constant. The optimized value of the objective function is then used to calculate new guess values for the top-level variables.

Iterative local/global optimization (ILGO) [6-9] is an example of non-hierarchical decomposition proposed to optimize complex systems. The overall system is physically decomposed into local subsystems that share some quantities, named "coupling functions" (because they can be expressed as functions of the decision variables of the local subsystems), to take into account the functional links among the subsystems.

In both decomposition strategies, the optimization process exploits a reduced number of degrees of freedom of the original problem (top-level variables/coupling functions) as coordinates along which the search for the optimum is performed. According to this change of perspective, the objective function is now seen as the ORS with respect to the chosen degrees of freedom. The following three cases show that the smoothness of the ORS is deeply affected by the HTFC.

Case II presents a physical decomposition of the combined cycle power plant into two subsystems, according to the thermal coupling approach proposed in [4]. The first subsystem comprises the Brayton cycle (its local decision variables are r_c and $\dot{m}_a$), whereas the second one encloses the two Rankine cycles (its local decision variables are $\dot{m}_{R1}$, p_{1s}, $\dot{m}_{R2}$, p_{3s} and T_{4s}). The HTFC is formulated in the local optimization problem of the second subsystem, but the first subsystem must pass information about the hot flue gas stream to the second subsystem so that the HTFC can be evaluated. This information depends on both of the local decision variables of the first subsystem; and, therefore, r_c and $\dot{m}_a$ are chosen as the coupling functions linking the two subsystems (please note that this choice of a reduced number of degrees of freedom is equivalent to the choice of r_c and $\dot{m}_a$ as top-level variables in a nested optimization, i.e. the resulting ORS is the same).

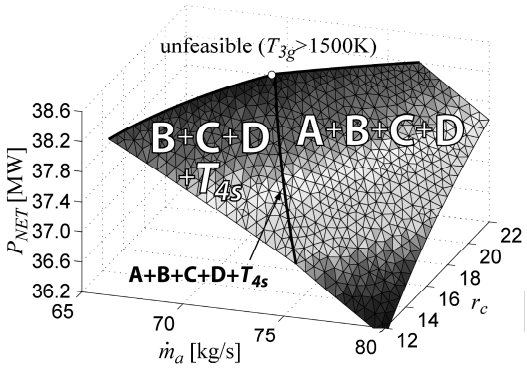

Fig. 9. Case II: the ORS with respect to r_c and $\dot{m}_a$.

The ORS of the original problem with respect to r_c and $\dot{m}_a$ is shown in Fig. 9. It appears that a large portion of the (r_c, $\dot{m}_a$) plane is unfeasible (this not because of the HTFC, since T_{3g} is greater than 1500 K) and a slightly non-smooth edge divides the ORS into two zones. In one zone all the four possible pinch points are simultaneously active (but T_{4s} is lower than its upper bound of 811.15 K), whereas in the other zone with T_{4s} equal to 811.15 K only pinch points B, C and D are simultaneously active (pinch point A is not active in this zone because T_{4g} is higher than 811.15+10 K, and T_{4s} cannot exceed its upper bound). The optimal solution (shown with a white circle) belongs to this second zone and lies on the frontier of the feasible region (this means that T_{3g}=1500 K at the optimum).

Case III presents another physical decomposition of the combined cycle power plant in which three subsystems are isolated according to the cycle superimposition coupling approach proposed in [4]. Subsystem 1 comprises the Brayton cycle while subsystems 2 and 3 comprise the low and high pressure Rankine cycles, respectively. For sake of simplicity, some modifications are made to the original optimization problem: constant values are assigned to $\dot{m}_{R1}$ (2.231 kg/s) and T_{4s} (811.15 K) and the two inequality constraints in Table 1 are converted into equality constraints. In this way, the local decision variables of the three subsystem are respectively: $\{r_c\}$, $\{p_{1s}\}$ and $\{\dot{m}_{R2}, p_{3s}\}$. The HTFC is formulated in the local optimization problem of subsystem 3, and subsystems 1 and 2 must pass information about their thermal streams to subsystem 3 in order that the HTFC can be evaluated. This information depends on the local decision variables of subsystems 1 and 2, and, therefore, r_c and p_{1s} are chosen as the coupling functions linking the three subsystems (again, this is equivalent to choosing r_c and p_{1s} as top-level variables in a nested optimization).

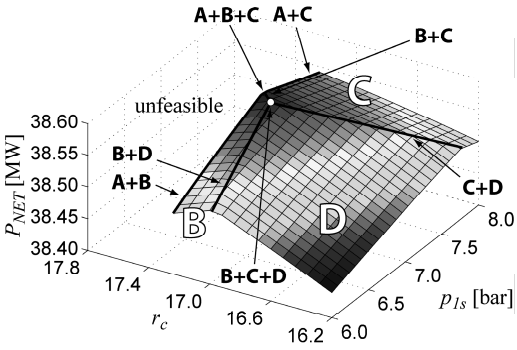

Fig. 10. Case III: the ORS with respect to r_c and p_{1s}.

The ORS of this simplified version of the optimization problem with respect to r_c and p_{1s} is shown in Fig. 10. No feasible solution is found for r_c >17.2378 (note that pinch point A is active for r_c=17.2378) because the imposition of constant values on both T_{4s} and T_{3g} becomes incompatible. Similarly to case I, the ORS is divided into three zones in which pinch points B, C and D are active one at a time. The optimal solution (shown with a white circle) is found at the junction of the three sharp edges shared by the three zones.

Finally, case IV presents a nested optimization having r_c, p_{1s} and p_{3s} as top level variables (these are probably the most significant variables of the seven as will be discussed in Section 4). The three-dimensional ORS is visualized in Fig. 11 by sectioning it at constant r_c planes (a portion of the space defined by the three top-level variables is unfeasible at high values of p_{3s} because of the constraint on q_{6s}). In the neighbourhood of the optimal solution (shown with a white circle) there are four subspaces in which different combinations of the four possible pinch points are active. Looking at the coloured contours in each plane, it appears that the behaviour of the ORS is clearly non-smooth at the surfaces shared by these four subspaces.

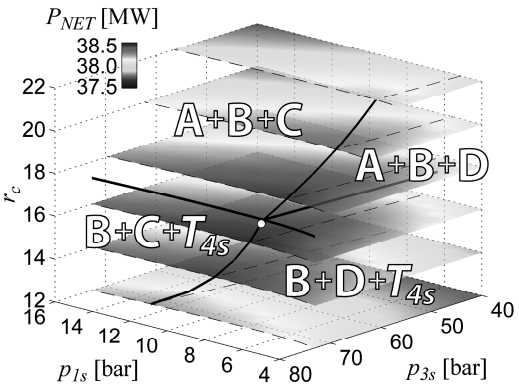

Fig. 11. Case IV: the ORS with respect to r_c, p_{1s} and p_{3s}.

4. Concluding remarks

In general, the imposition of the feasibility constraint to the undefined heat transfer section in the synthesis/design optimization of a complex energy system is expected to generate a non-smooth ORS on which the optimal solution must be found. The question which arises is what kind of optimization algorithms are able to deal with such a situation? Traditional direct search methods for constrained optimization are based on the information gathered from the derivatives of the ORS, and so they are likely to be deceived by the sharp edges generated by the (de)activation of pinch points. In fact, when a linear or quadratic model of the ORS built on one side of the edge indicates that the next guess is on the other side, the algorithm may get stuck going back and forth between the two guesses. One possible solution is to use a restricted search step, i.e. verifying that

the next guess suggested by the algorithm performs better than the current guess. Other non-traditional methods, such as evolutionary algorithms, are of great help in overcoming this problem, since they are specifically designed to deal with non-smooth objective functions. They are particularly suitable for the top level of a nested optimization, although they should be provided with a proper constraint handling technique to quickly converge to the frontier of the feasibility region if necessary.

Another important question is what variables are most suitable to be chosen as top-level variables/coupling functions? This largely depends on the specific problem at hand; but looking at the formulation of the HTFC given in (2), a general statement can be made about the role played by mass flow rates. It has already been mentioned (see Section 3.1) that mass flow rates may give trivial contributions to the objective function, but it is more important to point out that they give trivial (and linear) contributions to the activation of pinch points as well, i.e. pinch points are activated when a threshold value (corresponding to the frontier of the feasible region of the search space) is reached. Thus, if mass flow rates are not chosen as top-level variables/coupling functions, the optimization process can benefit by the two following advantages:

- The behavior of the optimal objective function values along the coordinates considered in building the ORS is not predictable in advance (i.e. is non-trivial) and, therefore, more interesting.
- If mass flow rates are the only bottom-level/local decision variables, the inequalities of the HTFC (and in some cases the objective function itself) become linear (see, e.g., [10]).

In contrast, important parameters of the thermodynamic cycles involved in energy systems (e.g., pressure levels, maximum temperatures) are the most obvious candidates for the choice of top-level variables/coupling functions.

Nomenclature

f_p pressure loss factor
LHV fuel lower heating value, kJ/kg
h specific enthalpy, kJ/kg
$\dot{m}$ mass flow rate, kg/s
p pressure, bar
P power, MW
q steam quality
r_c pressure ratio
s specific entropy, kJ/(kg K)
T temperature, K

Greek symbols

η efficiency

Subscripts and superscripts

a air
c/f cold/hot (superscripts)
cb combustion
f fuel
g gas
i/f initial/final (superscripts)
i,j,k,l stream indices (subscripts)
is isentropic
NET net
R1 low pressure Rankine cycle
R2 high pressure Rankine cycle
s water/steam
th thermal

References

[1] Lazzaretto, A., and Toffolo, A., 2008, A Method to Separate the Problem of Heat Transfer Interactions in the Synthesis of Thermal Systems. Energy, 33, pp. 163-170.

[2] Toffolo, A., Lazzaretto, A., and Morandin, M., 2009, The HEATSEP Method for the Synthesis of Thermal Systems: an Application to the S-Graz Cycle, Energy, In press.

[3] Linhoff, B., et al., 1994, *A User Guide on Process Integration for the Efficient Use of Energy,* Institution of Chemical Engineers, Rugby, UK.

[4] Lazzaretto, A., et al., 2009, Criteria for the Decomposition of Energy Systems in Local/Global Optimizations, Energy, In press.

[5] Dimopoulos, G. G., Kougioufas, and A. V., Frangopoulos, C. A., 2008, Synthesis, Design and Operation Optimization of a Marine Energy System, Energy, 33, pp. 180-188.

[6] Muñoz, J. R., and von Spakovsky, M. R., 2001, A Decomposition Approach for the Large Scale Synthesis/Design Optimization of Highly Coupled, Highly Dynamic Energy

Systems, International Journal of Applied Thermodynamics, 4(1), pp. 1-17.

[7] Muñoz, J. R., and von Spakovsky, M. R., 2001, The Application of Decomposition to the Large Scale Synthesis/Design Optimization of Aircraft Energy Systems. International Journal of Applied Thermodynamics, 4(2), pp. 61-76.

[8] Rancruel, D. F., and von Spakovsky, M.R., 2005, Development and Application of a Dynamic Decomposition Strategy for the Optimal Synthesis/Design and Operational/Control of a SOFC Based APU under Transient Conditions. *Proc. of ASME IMECE 2005*, ASME paper IMECE2005-82986.

[9] Rancruel D.F., and von Spakovsky, M.R., 2006, A Decomposition Strategy Based on Thermo-economic Isolation Applied to the Optimal Synthesis/Design and Operation of an Advanced Tactical Aircraft System. Energy, 31, pp. 3327-3341.

[10] Maréchal,. F., and Kalitventzeff, B., 1999, Targeting the Optimal Integration of Steam Networks: Mathematical Tools and Methodology, Computers and Chemical Engineering, Supplement, pp. Sl33-S136.

Using Optimization under Uncertainty to Study Different Aspects of Process Integration Investment Decisions – The Example of Lock-in Effects

Elin Svensson[a], Thore Berntsson[a]

[a] *Department of Energy and Environment, Chalmers University of Technology, Gothenburg, Sweden*

Abstract: New climate and energy policy instruments and the changed energy market conditions that follow call for the pulp and paper industry to improve their energy efficiency and reduce their CO_2 emissions. However, through the concept of the forest biorefinery, these changes also offer an interesting opportunity for the industry to diversify and potentially grow their revenues. When considering uncertainties regarding the future prices of energy and wood-based products, a systematic methodology is needed to make better informed investment decisions. Our previous research in this field has focused primarily on development of such a methodology based on stochastic programming, process integration tools, and energy market scenario models. The aim of this paper is to apply the methodology to study one important aspect of the process integration investment decision, namely the risks associated with lock-in situations. Lock-in effects are expected when investment decisions in conventional technology today are made without considering the competitiveness of emerging technologies that might enable a pathway to the forest biorefinery through manufacturing of value-added products. This is illustrated with the example of district heating co-operations and lignin extraction. The systematic approach enables quantitative assessment of the importance of lock-in effects in the decision-making process.

Keywords: Forest biorefinery, Investment planning, Lock-in situations, Optimization under uncertainty, Process integration.

1. Introduction

Following the increased climate concern in society, the energy market is bound to change. Highly probable changes include increased electricity and fuel prices, cap and trade systems for CO_2 emissions with gradually tightened caps, and intensified subsidies to renewable energy technology.

These conditions will – as intended – make it necessary for energy-intensive industries such as pulp and paper mills to make investments to improve their energy efficiency and reduce their CO_2 emissions. For the pulp and paper industry, improved process integration is a way to meet these demands, while at the same time offering interesting opportunities to diversify and potentially increase revenues.

These opportunities includes not only traditional products such as green electricity, wood fuels, and district heating, but also the transformation of the pulp mill into a forest biorefinery with production of green transportation fuels, new specialty chemicals and biomaterials in addition to pulp and paper, see e.g. [1, 2].

Biorefinery implementation can serve many goals, on both a short and long term. This can be described as a three-phase transformation, where focus is gradually changed from just lowering operating costs to value creation through a complete transformation of the core business strategy [3].

To identify the most appropriate forest biorefinery products, important aspects to consider are, for example, the competitiveness and market opportunities for the new products, the overall company business strategy, and the possibility for co-operations and partnerships [4].

The uncertainties regarding the future prices of the biorefinery products complicate, however, the choice between different promising pathways for a specific pulp mill. A systematic methodology is therefore needed to narrow down the possibly large set of promising biorefinery process/-product designs, valuing flexibility, robustness, and timing issues.

1.1. Aims and objectives

This paper seeks to describe what new and improved information can be obtained by applying

Corresponding Author: Elin Svensson, Email: elin.svensson@chalmers.se

a systematic optimization methodology for investment planning of process integration measures under uncertainty. The methodology has previously been described with focus on modelling assumptions and methodology development [5, 6].

The objective and new contribution of this paper is the suggested approach for assessment and illustration of one important aspect of the process integration investment decision. We illustrate the approach for a simple example with one set of assumptions and input data.

More explicitly, we have chosen to study the effect of lock-in situations when investments in conventional technology today are made without considering the possibility that emerging technologies will be more competitive in a near future. Here, we have assumed that the competitiveness of the emerging technology depends on whether or not it will enable the production of value-added products, thereby opening up a pathway to the forest biorefinery.

In the work presented in this paper an improved and extended energy price scenario model is also suggested.

2. Methodology

The work presented in this paper follows a methodology previously described by the authors [6, 7]. The methodology is a systematic approach for optimization of process integration investments under energy market uncertainty.

The objective of the optimization model is to maximize the expected net present value of the investments in the mill. For consistency with previous studies, we assume a strategic view on the analyzed investments, and therefore assume a discount rate of 9.3% which, over the 30 year long planning horizon corresponds to a capital recovery factor of 0.1 (For a discussion on the choice of these parameters, see [5]).

We have applied the methodology to a Swedish market pulp mill, and modelled the investment optimization problem using AMPL [8] and solved it using CPLEX [9]. The optimality criterion was set to 0.1% for the objective function.

3. Mill description

The studied pulp mill has previously been analyzed for energy-saving opportunities and the influence of short-term and seasonal variations [10]. The mill produces 425,000 ADt (air-dried metric tonnes) per year of bleached Kraft pulp from both softwood and hardwood. The total steam consumption of the mill is 230 MW. The mill delivers excess heat to a district heating system nearby. The reader is referred to the above cited article for a more detailed description of the mill.

In this mill, we have studied the risks of lock-in effects if the mill commits to increased district heating deliveries through connection to an additional district heating system. This well-proven approach to utilize excess heat competes with the emerging technology of lignin extraction and refining, which might become very profitable in the near future by providing means to produce value-added products.

3.1. Steam-saving opportunities

Theoretically, 16.5 MW of steam could be saved in the hot and warm water system (HWWS). Taking into account the seasonal variations, 13.3 MW of low-pressure steam can be saved at an investment cost of €87/kW [10]. This retrofit simultaneously enables extraction of 24.4 MW of excess heat at a temperature high enough for deliveries to, e.g., a district heating network [10].

In addition to this, steam savings should be possible to accomplish through process integration measures not connected to the HWWS. Waiting for a continuation of the process integration study at the mill, the mill is assumed to be typical for a Scandinavian mill today and the savings are estimated based on experience from an earlier study [11], but scaled with the pulp production rate.

Steam savings could, for example, be achieved in the evaporation plant, which today has six effects in two lines. Upgrading the evaporation plant to seven effects, but assuming that the stripper is not available for integration with the evaporation plant should then make it possible to save about 20 MW of low-pressure steam. Alternatively, some of the excess heat extracted trough the heat exchanger network retrofit could replace steam in the evaporation plant, enabling steam savings of 32 MW.

The investment model used in [11] to estimate the cost of the evaporation plant was developed in 2002. Since then, the price of raw material, and especially that of steel has gone up (compare e.g. with costs reported in [12]). Here, the costs according to [11] have therefore been doubled and estimated to €15 million and €20 million for the conventional plant and for the plant using excess

heat respectively. However, if investment has already been made in a conventional plant, the cost for further upgrading to use excess heat is assumed to be €10 million.

Finally, utilization of heat from flue gases for process integration is estimated to give about 6 MW at a cost of €1 million.

3.3. Internal or external use of heat

As mentioned above, the retrofit of the hot and warm water system enables extraction of excess heat at a temperature sufficiently high for deliveries to, for example, a district heating system.

Due to the seasonal variations of the district heating demand, not all excess heat can be delivered during all parts of the year. Based on the assumption that it is possible to connect the mill to an additional small district heating system [13], we have estimated the potential increase of annual average deliveries to 13.8 MW.

There is, however, a trade-off between using the heat externally for district heating and using it internally at the mill to decrease the steam demand, see Fig. 1. The heat could, for example, be used in the evaporation plant. Alternatively, excess heat could be used for integration of the pulping process with a new process for further refining of extracted lignin.

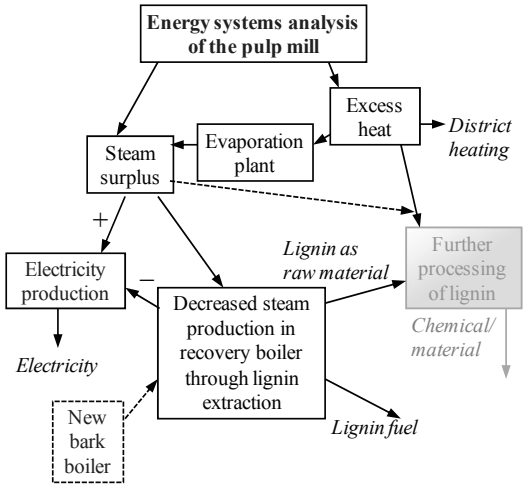

Fig. 1. Effects on the overall energy balance of the mill after steam savings and extraction of excess heat.

3.4. Steam production

With steam savings, less steam needs to be produced at the mill. In addition to the recovery boiler which covers most of the steam demand of the mill, there is a power boiler that is fired with bark. Because of large seasonal variations in the steam load of this bark boiler, it runs at minimum load during a large part of the year, but at maximum load during times of peak district heating demand. Neither increased nor decreased load will therefore be possible uniformly over the year.

Here, we have assumed that the bark boiler must be kept at the same average load as today in order to meet the large variations, but the aim is to further investigate the impact of the seasonal variations in relation to the bark boiler load in future studies.

With the assumption of a constant load on the bark boiler, the only possibility to decrease the steam production at the mill is to decrease the fuel input to the recovery boiler. The recovery boiler is, however, fuelled with black liquor containing chemicals that must be recovered in the boiler. Decreasing the load of the boiler can therefore only be accomplished through separation of lignin from the black liquor, see also Section 3.6. Decreasing the steam production will decrease the electricity production in the back-pressure turbine as shown in Fig. 2.

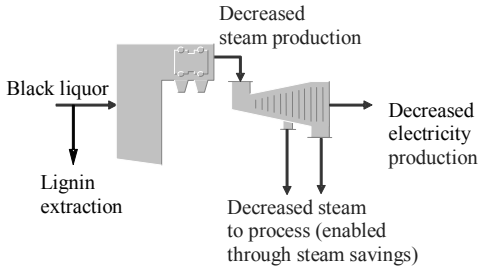

Fig. 2. Lignin extraction enabled through steam savings, but at the expense of decreased electricity production.

The model also includes the option to invest in a new bark boiler to compensate for a very high lignin extraction rate and decreased steam production in the recovery boiler, see Fig. 1.

3.5. Electricity production

The existing back-pressure turbine is assumed to be run at maximum load. To increase the electricity production, investment would therefore be needed in a new turbine. This investment option is not included in the model, since we do not consider any measures to increase the steam pro-

duction except for a new bark boiler. The new bark boiler will, however, only be of interest when the steam production from the recovery boiler is reduced.

The option to invest in a condensing turbine is included as a way to produce electricity from low-pressure steam.

3.6. Further processing of lignin

Lignin extracted from the mill can be used as a wood fuel, which is also the main assumption for lignin use today in the model. In the future, however, it is assumed that lignin can be further processed at the mill and sold for use as a specialty chemical or biomaterial. This would substantially increase the value of lignin. Processes are under development today, and if successful, this could be a competitive advantage for lignin extraction.

Further refining of lignin would require investment in a new process which, optimally, should be integrated with the existing pulping process. Since neither data for the lignin refining process nor product prices are available, we choose not to model this in detail. Instead, we simply assume that if this new process becomes available, lignin will be valued higher. Here, we further assume that it will be known in five years if this higher value can be obtained or not.

In our example, we assume the lignin price to be equal to the oil price plus a fixed value of €10/MWh. Valuing lignin compared to oil is reasonable since the lignin could be seen as a substitute for oil, for example, as a raw material for petrochemical products. The constant, €10/MWh, represents both the value of the product being renewable and the difference in costs between the lignin-based process and the oil-based process. The differences might involve, for example, different operating costs and annualized investment costs between the two process routes.

To illustrate the integration aspects, we assume a heat demand of the new process at about 80°C, which can be covered with excess heat from the pulping process. If excess heat is used for district heating or in the evaporation plant, steam is needed to cover this heat demand, see Fig. 1.

3.7. Summary of investment options

Except for the steam-saving measures, we have thus included a lignin separation plant, a new condensing turbine, a new bark boiler, and heat exchangers and piping for district heating as possible investments in the optimization model.

The energy conversion data is based on calculations and data used in previous studies [5-7, 13-15] with only slight adjustments for enthalpies and efficiencies at the mill studied here. Investment costs are shown in Table 1.

Table 1. Investment costs for new or increased capacity of technology in the pulp mill.

Technology	Investment cost (M€)
Lignin extraction	1.02 $Q^{0.6}$, Q: lignin extraction (MW)
Condensing turbine	2.38 $Q^{0.6}$, Q: generated power (MW)
Bark boiler	1.64 $Q^{0.76}$, Q: fuel capacity (MW)
District heating	0.5

4. Scenario model

The energy market model which is an important foundation of the optimization model has, in this work, been subject to new contributions compared to previous studies.

4.1. Construction of the scenario model

Consistent energy market scenarios have been achieved by using the ENPAC tool [16] where different energy market parameters are related to each other, see Fig. 3.

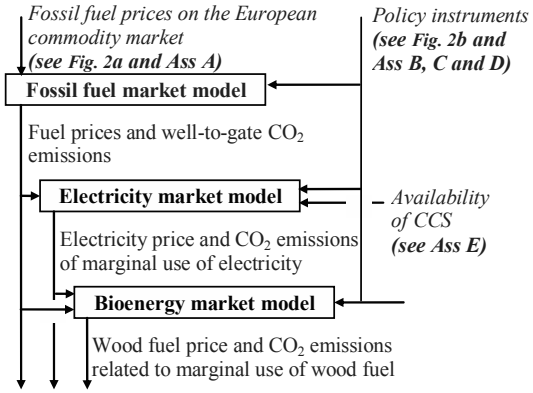

Fig. 3. Overview of the calculation tool for generation of consistent energy market parameter sets (Based on [16, p. 5, Fig. 2]). Ass A-D refer to assumptions described in Table 2.

Input data is based on the original ENPAC scenarios, but adjusted to fit to a tree structure with 5-year-intervals. Table 2 shows the main assumptions used for inputs to the scenario tool. Standard input refers to input described in [16].

Table 2. Assumptions for the scenario tool [16].

	Input	Assumption made
A	Fossil fuel prices	Standard input complemented by two scenarios and slightly adjusted to obtain branching. Prices of coal and natural gas are derived in the same way as oil prices.
B	CO2 emissions charge	Standard input, excluding the lowest and changing to exponential increase for the highest CO2 price scenario. Complementary scenarios added to obtain branching.
C	Green electricity certificates	Assumed constant at €20/MWh. Given during 15 years after investment to green electricity production.
D	Support for biofuels	Standard input.
E	CCS as build margin	Earliest 5 years after becoming the most cost-effective electricity production alternative.

Figures 4 and 5 show examples of fossil fuel price and policy instrument input to the scenario tool.

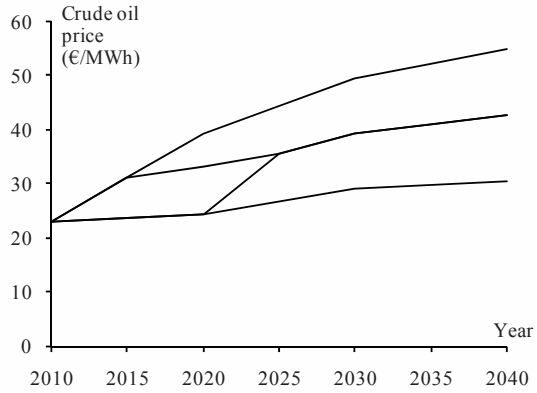

Fig. 4. Fossil fuel price scenarios exemplified by the crude oil price.

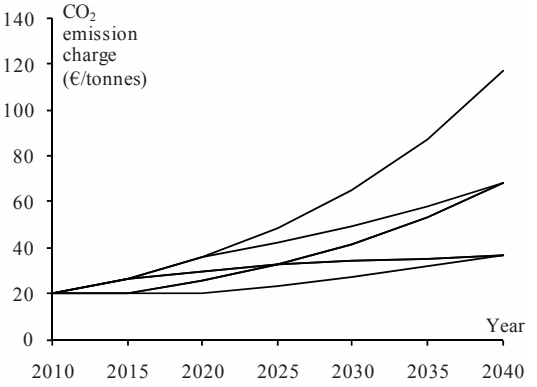

Fig. 5. Scenarios for the cost of emitting CO_2, i.e., the price of EU ETS permits.

By combining the four fossil fuel price paths with the seven paths for CO_2 price, 28 different scenarios are obtained. Using the scenario tool, market electricity and fuel prices are calculated for these 28 scenarios.

We also add to the scenario model a set of scenarios with the same main assumptions as for the original set, but with the higher lignin price (based on the oil price instead of the wood fuel price) after year 2015.

All in all, the scenario model will have 56 different scenarios and 240 nodes. For simplicity, we have assumed the same probability for all scenarios. This assumption would have to be checked in a sensitivity analysis.

4.2. Resulting energy market scenarios

For our scenario model, we need prices of electricity, district heating, lignin, and bark.

4.2.1. Electricity price

The resulting electricity price paths are shown in Fig. 6. To this value is added the price of green electricity certificates during the first 15 years after the turbine investment.

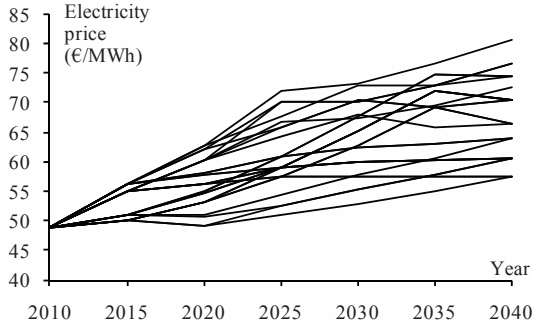

Fig. 6. Electricity price scenarios (not including the value of the green certificates).

4.2.2. District heating price

The price of the delivered heat is set to 75% of the alternative production cost of district heating, which here is assumed to be a biomass CHP plant (see [13]).

4.2.3. Lignin price

In half of the scenarios, the price of lignin is set to 1.35 times the price of wood by-products [17]. In the other scenarios, the lignin price will – after five years – be set equal to the price of oil + €10/MWh. The resulting lignin price paths are shown in Fig. 7.

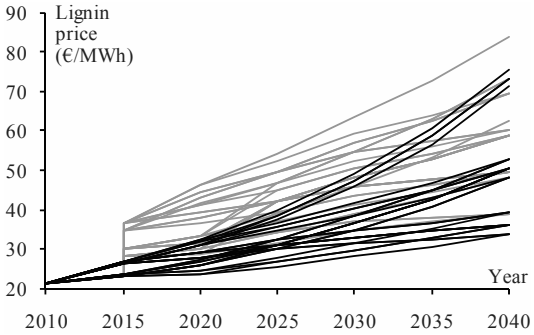

Fig. 7. Lignin price scenarios: Grey lines: Lignin priced as oil raw material, Black lines: Lignin priced as wood fuel.

4.2.4. Bark price

The price of bark (wood by-product) is given directly from the scenario tool. (See Fig. 7, Black lines, which shows the wood by-product price multiplied by 1.35).

5. Results

5.1. Reference investment plan

We first ran the optimization model without the scenarios with the higher lignin price. This represents making the investment decision today, without considering the possibility that a new process for lignin refining will become available.

The optimal investment plan is then to go for the condensing turbine and district heating, and if lignin prices later start to rise, invest in a lignin separation plant and abandon the condensing turbine. District heating deliveries are favourable and are kept at maximum throughout the planning horizon.

These results suggest that district heating is a robust solution. Hence it is reasonable to assume that a long-term contract on district heating cooperation with a municipal energy company could be established based on the results.

5.2. Lock-in effects

The next step was then to run the optimization model with all scenarios, including the ones where lignin is assumed to have a higher value.

We then compared the results obtained with and without lock-in into a district heating contract. A 15-year-contract was modelled as a constraint requiring district heating deliveries of 13.8 MW from 2010 until 2025.

The expected net present value of the investments decreased from €49.6 million to €45.8 million (or by 7.7%) when avoiding this lock-in situation. Considering that for half of the scenarios – when lignin is valued as a wood fuel – the investment plan will be the same, the cost of the lock-in situation in the other half of the scenarios is substantial.

Figure 8 illustrates the difference in annual net profit (using a capital recovery factor of 0.1) with and without the lock-in situation for the periods 2015–2020 and 2020–2025. The figure only shows the scenarios where the new biorefinery process becomes available and lignin can be upgraded to a higher added value. For the remaining scenarios the difference is zero.

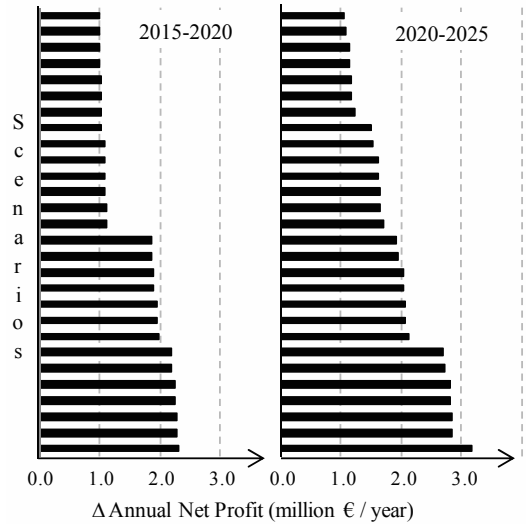

Fig. 8. Increase in annual net profit during two time periods for the scenarios with higher lignin price when district heating lock-in is avoided.

As can be seen from Fig. 8, the increase in annual net profit when there is no district heating contract (that is, the cost of the lock-in situation) varies between about one million up to over three million Euros per year in 2020–2025. This is a significant amount which can be seen by comparing it to the actual annual net profit which varies between €5.2 million/year and €11.5 million/year under the same assumptions.

After 2025 some small differences remain in some of the scenarios, but since district heating deliveries are no longer required, these are negligible in comparison.

It could be noticed that there is no difference in bark boiler investment between the cases of district heating lock-in and the ones without. In a few scenarios a new bark boiler should be built to enable a larger lignin separation plant. The size of this bark boiler, however, will be the same both with and without the lock-in. Investing in extra capacity in the case of district heating lock-in is simply not profitable, even though it would enable a higher rate of lignin upgrading.

The cost of the lock-in effects is therefore explained solely by the lower rate of lignin extraction and upgrading when excess heat is used externally for district heating instead of internally to enable more steam savings.

Finally, the optimal investment plans, both with and without district heating lock-in suggest investment in a condensing turbine today. This turbine should then be abandoned if lignin extraction becomes more competitive.

6. Discussion

6.1. Robustness of results

The assumptions used in this optimization model are, to some extent, fictitious, but nevertheless reasonable. These include, for example, the heat demand of the lignin refining process, and the value of lignin. The assumptions made serve well, however, the purpose of illustrating how the methodology for optimization under uncertainty can be used to study the effects and costs of lock-in situations.

A number of sensitivity analyses are needed to evaluate the robustness of the results. One set of parameters that are important to vary are the scenario probabilities. We have shown in previous studies how this kind of sensitivity analysis can be carried out in a straightforward way within the framework of the methodology [5, 7]. The sensitivity analysis is not presented here, however, due to the limited space.

Further work is also needed to evaluate the effect of seasonal variations for the existing bark boiler. Consideration of these variations might affect the competitiveness of the bark boiler compared to new technology at the mill, since the bark boiler is limited by its minimum load requirements.

The value of lignin is, naturally, one of the large uncertainties in this model. It depends not only on the alternative raw material for the value-added product that is produced from lignin, but also on whether efficient processes are developed. The value could also become higher if incentives to renewable materials similar to incentives to renewable fuels are introduced. Here we have assumed that the value will be high enough to offer competitiveness for lignin extraction, but only with a 50% probability. Still, the effect on the solution is noticeable.

An important aspect here is that, theoretically, there is no cost to avoid the lock-in situation. In scenarios further processing of lignin does not become available, district heating deliveries are continued. The initial investment is the same for all modelling assumptions. With this in mind, the exact cost of the lock-in is of less importance.

6.2. Competitiveness of emerging technology

Emerging technology is often placed in competition to conventional technology. Here, even if lignin extraction becomes competitive in a near future, the results show that it is beneficial to invest in a new condensing turbine today. This conventional technology is profitable enough to be paid back in a few years and could be abandoned if and when lignin extraction becomes an interesting alternative. The results therefore show that the time of investment is important to consider. Although it is important to consider future opportunities, there is no reason to postpone investments with short payback time today.

In this context, there are, however, improvements that could be implemented to the model. For example, it should be possible to consider long lead times between decision and investments.

7. Conclusions

In this paper we have illustrated how a systematic optimization methodology for investment planning of process integration measures under uncertainty can be used to assess the effect of lock-in situations on the investment decision.

We have shown that the suggested approach enables quantitative assessment of the importance of a certain aspect in the decision-making process.

We illustrated that consideration of lock-in effects can affect the optimal investment plan and the value of the investments, since lock-in might prevent later investments with probability of being profitable in the near future. The importance of considering future opportunities for emerging technologies already today was also highlighted.

In the example presented in the article, the cost of district heating lock-in was between one and three million Euros per year in scenarios where heat would be more competitively used for production of value-added chemicals.

References

[1] Towers, M., et al., 2007, Biorefinery Opportunities for the Canadian Pulp and Paper Industry, Pulp & Paper Canada, 108(6), pp. 26-29.

[2] Van Heiningen, A., 2006, Converting a Kraft Pulp Mill into an Integrated Forest Biorefinery, Pulp & Paper Canada, 107(6), pp. 38-43.

[3] Chambost, V., et al., 2009, Partnerships for Successful Enterprise Transformation of Forest Industry Companies Implementing the Forest Biorefinery, Pulp & Paper Canada, 110(5-6), pp. 19-24.

[4] Chambost, V., and Stuart, P., 2007, Selecting the Most Appropriate Products for the Forest Biorefinery, Industrial Biotechnology, 3(2), pp. 112-119.

[5] Svensson, E., et al., 2009, Benefits of Using an Optimization Methodology for Identifying Robust Process Integration Investments under Uncertainty – a Pulp Mill Example, Energy Policy, 37(3), pp. 813-824.

[6] Svensson, E., et al., 2009, An Optimization Methodology for Identifying Robust Process Integration Investments under Uncertainty, Energy Policy, 37(2), pp. 680-685.

[7] Svensson, E., et al., 2008, A Scenario-Based Stochastic Programming Model for the Optimization of Process Integration Opportunities in a Pulp Mill, Technical report, ISSN 1652-9715, no 2008:29, Chalmers University of Technology, Göteborg, Sweden.

[8] Fourer, R., et al., 2003, AMPL: A Modeling Language for Mathematical Programming, 2nd Edition. Duxbury Press & Brooks/Cole Publishing Company, Pacific Grove, CA.

[9] CPLEX: High-Performance Software for Mathematical Programming and Optimization, 2006, Software Package, Ver. 10.1, ILOG, Gentilly, France.

[10] Persson, J., and Berntsson, T., 2009, Influence of Seasonal Variations on Energy-Saving Opportunities in a Pulp Mill, Energy, 34(10), pp. 1705-1714.

[11] Axelsson, E., et al., 2006, Heat Integration Opportunities in Average Scandinavian Kraft Pulp Mills: Pinch Analyses of Model Mills, Nordic Pulp and Paper Research Journal, 21(4), pp. 466-475.

[12] Olsson, M., and Berntsson, T., 2009, Simulations Comparing Conventional Evaporation Plants with Plants Using Excess Heat, Bioresources [online journal], 4(4), pp. 1555-1571.

[13] Jönsson, J., et al., 2008, Excess Heat from Kraft Pulp Mills: Trade-Offs between Internal and External Use in the Case of Sweden – Part 2: Results for Future Energy Market Scenarios, Energy Policy, 36(11), pp. 4186-4197.

[14] Hektor, E., and Berntsson, T., 2007, Future CO_2 Removal from Pulp Mills - Process Integration Consequences, Energy Convers. Manage., 48(11), pp. 3025-3033.

[15] Olsson, M., et al., 2006, Exporting Lignin or Power from Heat-Integrated Kraft Pulp Mills: A Techno-Economic Comparison Using Model Mills, Nordic Pulp and Paper Research Journal, 21(4), pp. 476-484.

[16] Axelsson, E., and Harvey, S., 2010, Scenarios for Assessing Profitability and Carbon Balances of Energy Investments in Industry, Technical Report, 2010:EU1, Pathways to Sustainable European Energy Systems, AGS The Alliance for Global Sustainability, Göteborg, Sweden, URL: http://www.energy-pathways.org/reports.

[17] Axelsson, E., and Berntsson, T., 2008, Profitability and Off-Site CO_2-Emission Reduction from Energy Savings in the Pulp and Paper Industry in Different Future Energy Markets, In: Axelsson, E., Energy Export Opportunities from Kraft Pulp and Paper Mills and Resulting Reductions in Global CO_2 Emissions, PhD Thesis, Chalmers University of Technology, Göteborg, Sweden.

Acknowledgments: This work was financed by the Swedish Energy Agency and the Södra Foundation for Research, Development and Education.

Particle Swarm algorithm with Fuzzy decision making for a multi-objective economic and environmental optimization of design of a thermal system

Meisam Babaie[a], Hoseyn Sayyaad[a], Mohammad Reza Farmani[b] and Alireza Novinzadeh[b]

[a] *Mechanical Engineering Department K.N. Toosi University of Technology, Tehran, Iran*
[b] *Aero Space Engineering Department K.N. Toosi University of Technology, Tehran, Iran*

Abstract: Multi-Objective optimization for designing of a benchmark cogeneration system known as CGAM cogeneration system has been performed. In optimization approach, the thermoeconomic and Environmental aspects have been considered, simultaneously. The environmental objective function has been defined and expressed in cost terms. One of the most suitable optimization techniques developed using a particular class of search algorithms known as; Multi-Objective Particle Swarm Optimization (MOPSO) algorithm has been used here. This approach has been applied to find the set of Pareto optimal solutions with respect to the aforementioned objective functions. An example of fuzzy decision-making with the aid of Bellman-Zadeh approach has been presented and a final optimal solution has been introduced.

Keywords: Cogeneration, Thermoeconomics, Environmental aspects, Multi-Objective Particle Swarm Optimization, Fuzzy decision making, Bellman-Zadeh approach.

1. Introduction

The supply of our world with useful energy occurs through energy conversion processes. In order to minimize the environmental impact from energy supply, a primary target is to increase the efficiency of energy conversion processes and, thus, decrease the amount of fuel and the related overall environmental impact, especially the release of carbon dioxide, and NOx which are two of the main components of greenhouse gases. Cogeneration or CHP (Combined Heat and Power) continues to gain importance in Power Production because of its high efficiency, environmental friendliness, and flexibility. It is important for numerous reasons. The first is that capturing the waste heat from power generation can result in an increase in efficiency. This offers significant potential savings in energy costs. Moreover higher stack temperature means a higher energy loss from stack and more air pollution; with applying a cogeneration system these affects will be limited, hence, Cogeneration is more advantageous in terms of energy savings and environmental considerations.

Cogeneration is also more environmentally friendly than traditional fossil fuel power plants. First, CHP is more efficient, reducing total fossil fuel consumption and thereby reducing emissions to the atmosphere. Second, natural gas (a clean burning fossil fuel) is often used in cogeneration with steam injection to minimize emissions.

There are numerous requirements and objectives for design of an energy system. The system should for instance be efficient, have a low or no negative environmental impact, be safe, have high controllability, be easy to maintain and be profitable from an economic perspective, so the term Optimization in thermal systems is one of the most important subjects in the energy engineering field.

In general, objectives involved in the design optimization process are [1]: thermodynamic (e.g., maximum efficiency, minimum fuel consumption, minimum irreversibility and so on), economic (e.g., minimum cost per unit of time, maximum profit per unit of production) and environmental (e.g., limited emissions, minimum environmental impact). It is clear that improving a system thermodynamically without considering economics and environment is misleading. Hence, in design of thermal systems an integrated procedure should be performed to consider all

these aspects. Many researchers have started to develop links between exergy and economics. As a result, a new area called thermoeconomics or exergoeconomics has been formed . The aim of the thermoeconomic analysis is to calculate the cost of each product of the systems and investigate the cost formation process in the systems. A simple cogeneration system (CGAM) serves as an example to illustrate the application of thermoeconomic methods for evaluating and optimizing complex energy systems. In all primary works, mathematical approaches were used for optimization process. When multi-modal fitness landscapes are involved, evolutionary algorithms are more suitable than conventional approaches for both single- and (in particular) multi-objective optimization problems.

Application of multi-objective optimization method in thermal systems is not very old. In 2002, Toffolo et al [3], considered two-objective, energetic and economic, in optimization of CGAM problem. They used evolutionary algorithms (MOEAs) with a MATLAB Simulink model and presented a Pareto optimum frontier instead of the single optimum solution of the conventional single objective optimization. They improved their work by adding the environmental impact and introduced a three objectives optimization problem [4].

However their work still suffers from some shortcoming arose from the simplification in selecting decision variable and constraint. To reduce the number of non-feasible solutions that their optimization algorithm may be faced during the optimization procedure, variable ε_{ap} was preferred to the exit temperature on the air side of the Air-Preheater T_3 (the variable used in the original CGAM problem). Furthermore during the optimization process among the five decision variables in original CGAM problem, they chose three of them ($r_{cp}, T_4, \varepsilon_{ap}$) inconstant while the other two were held constant.

In 2008, Sayyaadi [5], used a more suitable method for economic modeling of the CGAM problem (TRR method). He added the environment with cost and introduced a Thermoenvironomic objective and utilized it with exergetic objective function in multi-objective optimization approach.

In this paper we consider two objective functions: thermoeconomic and environmental aspects. In comparison with previous studies in this field ([3, 4, and 5]), this work utilizes the faster and more confidant algorithm in optimization procedure (MOPSO) without any simplifications with five decisions variables. This algorithm can overcome the problem of non feasible solution which has been faced in previous studies. No decision variables are changed or fixed, and all variables and constraints are in accordance with the original CGAM problem. These improvements lead to results that have a more general validity than the corresponding results obtained before. Additionally In application of multi-objective optimization for CGAM problem, after introducing the Pareto front in previous works, there was not a systematic approach to decision making process for selecting one point as the final optimal solution. Here, after suggesting the Pareto front, Bellman-Zadeh approach is employed for decision making process and an example of fuzzy decision making is presented and discussed.

2. Particle Swarm Optimization

It is common when working with design of energy systems to have situations with more than one objective. These problems are referred to as multi objective Mathematical programming problems. Equation (1) shows how a multi objective optimization problem can be formulated mathematically:

$$\min F_j(X) \forall j \in \{1,2,3,....k\} \; subject \; to \; X \in L \qquad (1)$$

Where we have $k \geq 2$ objective functions.

In this work we develop a Multi-Objective Particle Swarm Optimizer with a dynamic fitness inheritance technique [6] to decrease the computational cost dealing with some Multi-objective optimization test problems taken from literature. An external archive is used in this method to store the non-dominated solutions which are found along the process of optimization. The leaders of other particles that guide them to the Pareto-front are selected from the top portion of this archive in each iteration. Moreover, the concept of non-dominated sorting and crowding distance is applied as NSPSO approach [7] to improve the convergence and diversity of the Pareto-optimal solutions. The comparison among the particles and their pbests is based on fully connected approach [8] to increase the selection

pressure toward the true Pareto-front. In order to reduce the cost of computation during the process, we use a dynamic fitness inheritance technique which is proposed in [9]. The following formula calculates the new position of a particle in the objective space using fitness inheritance technique:

$$F_i(t) = F_i(t-1) + VF_i(t) \tag{2}$$

$$VF_i(t) = c_1 r_1 (F_{pbest-i}(t-1) - F_i(t)) + c_2 r_2 (F_{gbest-i}(t-1) - F_i(t))$$

Where $F_i(t)$, $F_{pbest-i}$ and $F_{gbest-i}$ are $i-th$ objective function value for the current particle, and its pbest and gbest objective function values, respectively. The parameter p_i , called inheritance or approximation proportion, indicates the proportion of particles that their objective function values must be inherited or approximated instead of evaluation in each iteration. As the Pareto-optimal solutions at the end of the optimization process must be true values of the objective functions, no inherited objective values can enter into the final external archive. To determine the amount of p_i , following nonlinear function is used:

$$p_i = f(x) = x^2 \ ; \ x = \frac{gen}{Gen} \tag{3}$$

Where gen is the number of current iteration and Gen is the total number of iterations.

3. Bellman-Zadeh approach

When using the Bellman–Zadeh approach[10], each $F_j(X)$ of (1) is replaced by a fuzzy objective function or a fuzzy set:

$$A_j = \{X, \mu_{A_j}(X)\} \qquad X \in L, j = 1,2,...k \tag{4}$$

Where $\mu_{A_j}(X)$ is a membership function of A_j .

A final decision is defined by the Bellman and Zadeh model as the intersection of all fuzzy criteria and constraints and is represented by its membership function.

$$\mu_D(X) = \cap_{j=1}^{k} \mu_{A_j}(x) = \min_{j=1,...,k} \mu_{A_j}(x) \tag{5}$$

$$X \in L$$

Using (5), it is possible to obtain the solution proving the maximum degree:

$$\max \mu_D(X) = \max_{X \in L} \min_{j=1,...,k} \mu_{A_j}(x) \tag{6}$$

Of belonging to D and problem (6) is reduced to

$$X^0 = \arg \max_{X \in L} \min_{j=1,...,k} \mu_{A_j}(x) \tag{7}$$

To obtain (7), it is necessary to build membership functions $\mu_{A_j(X)}$, j = 1, ..., k reflecting a degree of achieving "own" optimas by the corresponding $F_j(X), X \in L$, j = 1, . . . , k. This is satisfied by the use of the membership functions. The membership function of the objectives and constraints, linear or nonlinear, can be chosen depending on the context of problem. One of possible fuzzy convolution schemes is presented below. [11]

- Initial approximation X-vector is chosen. Maximum (minimum) values for each criterion $F_j(X)$ are established via scalar maximization (minimization). Results are denoted as ''ideal'' points $\{X_j^0, j = 1,...,m\}$.
- The matrix table {T}, where the diagonal elements are ''ideal'' points, is defined as follows:

$$\{T\} = \begin{bmatrix} F_1(X_1^0) & F_2(X_1^0)... & F_n(X_1^0) \\ F_1(X_2^0) & F_2(X_2^0)... & F_n(X_2^0) \\ . & & \\ . & & \\ . & & \\ F_1(X_n^0) & F_2(X_n^0)... & F_n(X_n^0) \end{bmatrix} \tag{8}$$

- Maximum and minimum bounds for the criteria are defined:

$$F_i^{\min} = \min_j F_j(X_j^0) \ , \ i = 1,....,n \tag{9}$$

$$F_i^{\max} = \max_j F_j(X_j^0) \ , \ i = 1,....,n$$

- The membership functions are assumed for all fuzzy goals as follows.

$$\mu_{Fi}(X) = \begin{cases} 0 & if \quad F_i(x) > F_i^{\max} \ , \\ \dfrac{F_i^{\max} - F_i}{F_i^{\max} - F_i^{\min}} & if \quad F_i^{\min} < F_i \le F_i^{\max} \ , \\ 1 & if \quad F_i(x) \le F_i^{\min} \end{cases} \tag{10}$$

- Fuzzy constraints are formulated:

$$\mu_{Gi}(X)=\begin{cases}0 & if\ \ G_i(x)>G_i^{\max}\\ 1-\dfrac{G_j(x)-G_j^{\max}}{d_j} & if\ G_i^{\max}<G_i(X)\le G_i^{\max}+d_j\\ 1 & if\ \ G_i(x)\le G_i^{\max}\end{cases} \quad (10)$$

Where d_j is a subjective parameter that denotes a distance of admissible displacement for the bound $G_j^{\max}$ j of the j-constraint. Corresponding membership functions are defined in following manner:

$$G_j(X)\le G_j^{\max}+d_j,\quad j=1,2,....,k \quad (11)$$

- A final decision is determined as the intersection of all fuzzy criteria and constraints represented by its membership functions. This problem is reduced to the standard nonlinear programming problems: to find the such values of X and k that maximize k subject to

$$\lambda\le\mu_{F_i},\quad i=1,2,....,n \quad (12)$$

$$\lambda\le\mu_{G_j},\ j=1,2,....,k$$

The solution of the multi-criteria problem discloses the meaning of the optimality operator and depends on the decision-maker's experience and problem understanding

4. Application of algorithm to CGAM problem

4.1. Definition

A simple cogeneration system serves as an example to illustrate the application of thermoeconomic methods for evaluating and optimizing complex energy systems. The foremost professors and/or researchers of the thermoeconomic field discussed their approaches through this problem. It assumes ideal gas behavior and constant heat capacities. The CGAM Problem designs a cogeneration plant which delivers 30 MW of electricity and 14 kg/s of saturated steam at 20 bars. The installation consists of an air compressor (AC), air preheater (APH), combustion chamber (CC), gas turbine (GT), and HRSG. The structure of the cogeneration plant is shown in Figure 1. The HRSG is composed of an economizer (EC) section where the feed water is heated and an evaporator (EV) section where the heated water is vaporized into steam. Other specifications and operating condition of the CGAM problem for the base case design are [1]:

T1=298.15K, P1=1.01325bar; T8=298.15K, P8=20bar; T10=298.15K, P10=12bar; T3=850K; T4=1520K; P2/P1=10; ηsc=0.86; ηst=0.86

4.2. The thermodynamic model

The utilized thermodynamic model is developed based on the following basic assumptions [1, 3, and 4]:

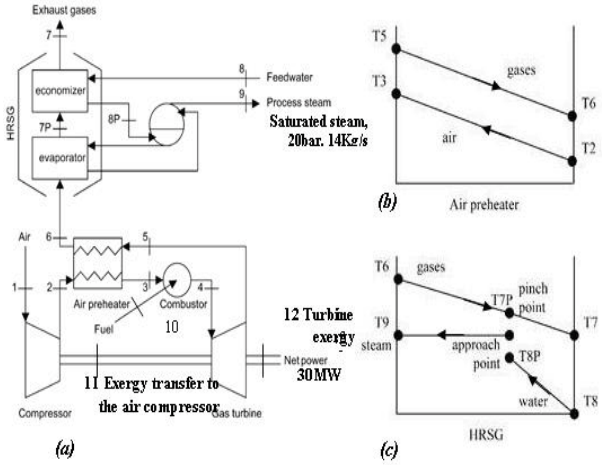

Fig. 1.Schematic flow diagram of the CGAM [1, 3].

- All processes are steady state.
- The principle of ideal-gas mixture is applied for the air and the combustion products.
- The fuel is natural gas and it is assumed to be 100% methane. The methane is an ideal gas.
- Heat loss from the combustion chamber is considered to be 2% of the fuel lower heating value. All other components are considered adiabatic.
- Constant pressure loss ratios are considered in the components.
- The restricted dead state is P0=1.013 bar and T0=25°C.
- 3% and 5% pressure losses are assumed for the air and gases in the air preheater, respectively.
- 5% pressure losses are assumed for the gases in HRSG and combustion chamber.

4.3. The thermoeconomic model

The economic model takes into account the cost of the components, including amortization and maintenance, and the cost of fuel consumption. In order to define a cost function which depends on the optimization parameters of interest, component costs have to be expressed as functions of thermodynamic variables [1and 2]. In the CGAM problem, the purchase cost functions for each plant component are already supplied. In this research, these equations with their related constants have been considered in accordance with [1 and 2].

The governing equation of thermoeconomic model for the cost balancing of a component of an energy system is as follow [1]:

$$\sum_{j=1}^{n}(c_j\dot{E}_j)_{k,in}+\dot{Z}_k^{CI}+\dot{Z}_k^{OM}=\sum_{j=1}^{m}(c_j\dot{E}_j)_{k,o} \quad (13)$$

Where cj is the unit cost of exergy for the jth stream to/from the component, $\dot{E}_j$ is exergy flow for the jth stream to/from the component and $\dot{Z}_k^{CI}$ and $\dot{Z}_k^{OM}$ are the related cost of capital investment and operating and maintenance for the component kth. Developing Eq. (13) for each component of CGAM problem along with auxiliary costing equations (according to P and F rules, see [1]) leads to the following system of equations:

$$\begin{bmatrix}
1 & 0 & 0 & 0 & 0 & 0 & 0 & 0 & 0 & 0 & 0 & 0\\
1 & -1 & 0 & 0 & 0 & 0 & 0 & 0 & 0 & 0 & 1 & 0\\
0 & 1 & -1 & 0 & 1 & -1 & 0 & 0 & 0 & 0 & 0 & 0\\
0 & 0 & 0 & 0 & \frac{1}{\dot{E}_5} & \frac{-1}{\dot{E}_6} & 0 & 0 & 0 & 0 & 0 & 0\\
0 & 0 & 1 & -1 & 0 & 0 & 0 & 0 & 0 & 1 & 0 & 0\\
0 & 0 & 0 & 0 & 0 & 0 & 0 & 0 & 0 & 1 & 0 & 0\\
0 & 0 & 0 & 1 & -1 & 0 & 0 & 0 & 0 & 0 & -1 & -1\\
0 & 0 & 0 & \frac{1}{\dot{E}_4} & \frac{-1}{\dot{E}_5} & 0 & 0 & 0 & 0 & 0 & 0 & 0\\
0 & 0 & 0 & 0 & 0 & 0 & 0 & 0 & 0 & 0 & \frac{1}{\dot{E}_{11}} & \frac{-1}{\dot{E}_{12}}\\
0 & 0 & 0 & 0 & 0 & 1 & -1 & 1 & -1 & 0 & 0 & 0\\
0 & 0 & 0 & 0 & 0 & \frac{1}{\dot{E}_6} & \frac{-1}{\dot{E}_7} & 0 & 0 & 0 & 0 & 0\\
0 & 0 & 0 & 0 & 0 & 0 & 0 & 1 & 0 & 0 & 0 & 0
\end{bmatrix}
\begin{bmatrix}\dot{C}_1\\ \dot{C}_2\\ \dot{C}_3\\ \dot{C}_4\\ \dot{C}_5\\ \dot{C}_6\\ \dot{C}_7\\ \dot{C}_8\\ \dot{C}_9\\ \dot{C}_{10}\\ \dot{C}_{11}\\ \dot{C}_{12}\end{bmatrix}=
\begin{bmatrix}0\\ -\dot{Z}_{AC}\\ -\dot{Z}_{APH}\\ 0\\ -\dot{Z}_{CC}\\ \frac{FC_L}{\tau}\\ -\dot{Z}_{GT}\\ 0\\ 0\\ -\dot{Z}_{HRSG}\\ 0\\ 0\end{bmatrix} \quad (14)$$

The system of 12 equations and 12 unknowns as indicated by Eq. 9 is solved to obtain the cost of streams 1 to 12 for CGAM problem.

4.4. The combustion pollutants

The original CGAM problem does not perform calculations on the formation of pollutants within the combustion chamber. A simple model, based on semi-analytical correlations [12], is added here to determine pollutant emissions.

The adiabatic flame temperature in the primary zone of the combustion chamber is derived from the expression by Gulder [13]:

$$T_{pz}=A\sigma^{\alpha}\exp(\beta(\sigma+\lambda)^2)\pi^x\theta^y\psi^z \quad (15)$$

where π is a dimensionless pressure p/pref (p being the combustion pressure p3, and pref = 101325 Pa); θ is a dimensionless temperature T/Tref (T being the inlet temperature T3, and Tref = 300 K); ψ is the H/C atomic ratio ($\psi=4$, the fuel being pure methane); $\sigma=\phi$ for $\phi\le1$ (ϕ being the fuel to air equivalence ratio) and $\sigma=\phi-0.7$ for $\phi>1$. φ is equivalent fuel to air ratio that is considered equal 0.64 in this work[4]. x, y and z are quadratic functions of σ in accordance with the following equations [13]:

$$x=a_1+b_1\sigma+c_1\sigma^2 \quad (16)$$

$$y=a_2+b_2\sigma+c_2\sigma^2 \quad (17)$$

$$z=a_3+b_3\sigma+c_3\sigma^2 \quad (18)$$

In Eq. (15) to (18) parameters denoted as A, α, β, λ, a_i, b_i and c_i are constants presented in [13]. In order to have an accurate prediction, four sets of constants have been determined for the following ranges [12]:

$$\begin{aligned}
&0.3\le\phi\le1.0 \text{ and } 0.92\le\theta<2.0\\
&0.3\le\phi\le1.0 \text{ and } 2.0\le\theta\le3.2\\
&1.0<\phi\le1.6 \text{ and } 0.92\le\theta<2.0\\
&1.0<\phi\le1.6 \text{ and } 2.0\le\theta\le3.2
\end{aligned} \quad (19)$$

The values of constants for each range classification are listed in [12].

The adiabatic flame temperature is used in the semi-analytical correlations proposed by Rizk and Mongia [12] to determine the pollutant emissions in grams per kilogram of fuel. With applying these assumptions the following equations for NOx emission and CO2 emission will be obtained and use for environmental pollutant modelling:

$$NO_x=\frac{0.15E16\tau^{0.5}\exp(-71100/T_{pz})}{p_3^{0.05}(\Delta p_3/p_3)^{0.5}} \quad (20)$$

$$CO=\frac{0.179E9\exp(7800/T_{pz})}{p_3^2\tau(\Delta p_3/p_3)^{0.5}} \quad (21)$$

Where τ is the residence time in the combustion zone (τ is assumed constant and is equal to 0.002 s); Tpz is the primary zone combustion temperature; p3 is the combustor inlet pressure; Δp3/p3 is the non-dimensional pressure drop in the combustor (Δp3/p3 = 0.05 as in the CGAM problem [2]).

Note that the primary zone temperature is used in the NOx correlation instead of the stochiometric temperature, since the maximum attainable temperature in premixed flames is Tpz, as pointed out by Lefebvre [13].

5. Optimization process

5.1. Definition of objective functions

The two objective functions are the "total exergetic cost rate of products" and the ''environmental impact''. The second objective function expresses the environmental impact as the total pollution damage cost ($/s) due to CO2 and NOx emissions by multiplying their respective flow rates by their corresponding unit damage cost [14] (c_{CO_2} and c_{NO_x} are equal to 0.02086 $/kgCO2 and 6.853 $/kgNOx, respectively [4]). The mathematical formulation of objective functions is as following;

Thermoeconomic:

$$\dot{C}_{P,tot} = \dot{C}_{F,tot} + \dot{Z}_{tot}^{CI} + \dot{Z}_{tot}^{OM} \quad (22)$$

Environmental [4]:

$$\dot{C}_{env} = c_{CO2}\dot{m}_{CO_2} + c_{NO_X}\dot{m}_{NO_X} \quad (23)$$

5.2. Decision variables

Withemploying this algorithm there is no need to change of the decision variables for overcoming the occurrence of non feasible solutions, as previous works do.

Decision variables are:

- The compressor pressure ratio p2/p1.
- Isentropic efficiency of the compressor ηsc.
- Isentropic efficiency of the turbine ηst.
- Temperature of the air entering the combustion chamber T3.
- Temperature of the combustion products entering the gas turbine T4.

5.3. Constraints

Although the decision variables may be varied in optimization procedure, each decision variable is normally required to be within a given range as follow:

$$6 \le p_2/\ p_1 \le 16 \quad (24)$$

$$0.6 \le \eta_{sc} \le 0.9 \quad (25)$$

$$0.6 \le \eta_{st} \le 0.92 \quad (26)$$

$$700 \le T_3 \le 1000K \quad (27)$$

$$1200 \le T_4 \le 1550K \quad (28)$$

Air preheater:

$$T5 > T3 \quad (29)$$

$$T6 > T2 \quad (30)$$

HRSG:

$$\Delta TP = T7P - T9 > 0 \quad (31)$$

$$T6 \ge T9 + \Delta TP \quad (32)$$

$$T7 \ge T8 + \Delta TP \quad (33)$$

$$T7P > T8P \quad (34)$$

$$T7 \ge 378.15K \quad (35)$$

The last constraint is an additional constraint with respect to the original CGAM problem imposed on the exhaust gases temperature. This limitation is considered to prevent the condensation of the water vapour exist in the combustion products at the outlet section of economizer.

6. Results and Discussion

MOPSO is used for the thermoeconomic and environmental design optimization of CGAM problems. Fig. 2 presents the Pareto optimum solutions for CGAM problem with the objective function indicated in Eq. (22) and (23) and constraints represented in Eq. (24) to (35).

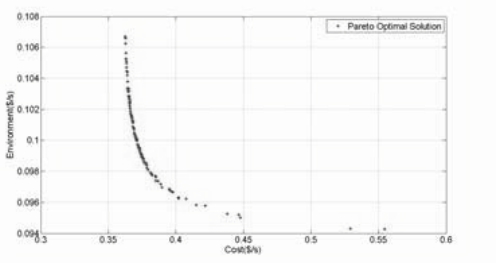

Fig. 2. The set of Pareto optimal solutions.

As shown in this figure, while the total cost rate of the plant is increased to about 0.55$/s the total cost rate of environmental damages decrease very slightly. Increasing of the total cost rate of product form 0.36$/s to 0.55$/s is corresponding to the moderate decrease in the cost rate of environmental aspect. The left most point of

diagram has the minimum cost rate equal to 0.362 $/s and it is in accordance with the optimal solution found in the original CGAM problem [2]. This point corresponds to highest environmental damage cost with the value of 0.107 $/s, on the other hand, while the thermoeconomic objective rises to 0.554 $/s environment reach to its minimum on 0.0943$/s.

Table 1.Comparison of results

Objective function, decision variables, costing and operating parameters	Conventional optimization approaches presented in [2]	Left most point of Pareto front via MOPSO Algorithms presented in this work
Product Cost Rate ($/s)	0.362009	0.362489
$T_3(K)$	914.28	835.20
$T_4(K)$	1492.63	1487.53
η_{sc}	0.8468	0.8748
η_{st}	0.8786	0. 9004
p_2 / p_1	8.52	11.88

In order to evaluate advantages and robustness of the MOPSO optimization approach, the minimum cost point compared to the original CGAM problem [2] solved using conventional mathematical optimization approach.

By using fuzzy decision maker which regards the restraints of design and manufacturing processes, one can choose the best solutions along the Pareto optimal fronts to optimize cost and environment. To visualize decision making process, the intersection point which is maintained by the concept of previous section is shown in Fig. 2 by red point. This point is the best among the possible optimal trade offs according to the parameters implemented (by someone) in the fuzzy decision maker.

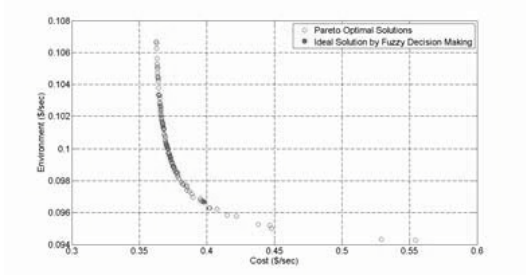

Fig. 3. The set of Pareto optimal solutions and ideal solution by fuzzy decision making

Information related to this point is summarized in table below:

Table 2.selected point among the Pareto front by Fuzzy decision making method

Selected point via fuzzy decision making information	Values
T3(k)	815.18
T4(k)	1465.2
η_{ac}	0.88057
η_{gt}	0.90743
P2/P1	11.572
Product cost rate($/s)	0.39788
Environmental damage cost rate	0.0 96661

The environmental damage cost related to cost optimum in original CGAM problem, is near to 0.11, as can be seen by using fuzzy decision making a point with more reasonable values in both environmental and thermoeconomic cost will be selected.

Conclusion

This work considered environmental aspects with thermoeconomic objective function simultaneously and introduced a fuzzy decision

making. After detailed thermodynamic and thermoeconimic modeling, environmental objective function was introduced and with employing a powerful and fast algorithm (MOPSO) the Pareto front is introduced. Finally the capability of Bellman-Zadeh approach in fuzzy decision making was shown.

References

[1] Bejan A, Tsatsaronis G, Moran M. Thermal and design optimization. New York: John Wiley and Sons Inc;1996.

[2] Valero A, Lozano MA, Serra L, Tsatsaronis G, Pisa J, Frangopoulos CA, von Spakovsky MR. CGAM problem: definition and conventional solution. Energy 1994; 19(3):279–86.

[3] Toffolo A, Lazzaretto A. Evolutionary algorithms for multi-objective energetic and economic optimization in thermal system design. Energy 2002; 27:549-67.

[4] Toffolo A, Lazzaretto A. Energy, economy and environment as objectives in multi-criteria optimization of thermal system design. Energy 2004; 29: 1139-1157.

[5] Sayyaadi H. Multi -objective approach in thermoenvironomic optimization of a benchmark cogeneration system. Applied Energy, Volume 86, Issue 6, June 2009, Pages 867-879.

[6] Konstantinos E. Parsopoulos and Michael N. Vrahatis. Particle swarm optimization method in multiobjective problems. In Proceedings of the 2002 ACM Symposium on Applied Computing (SAC'2002), pages 603–607, Madrid, Spain, 2002. ACM Press.

[7] Xiaodong Li. A non-dominated sorting particle swarm optimizer for multiobjective optimization. In Erick Cant´u-Paz et al., editor, Proceedings of the Genetic and Evolutionary Computation Conference (GECCO'2003), pages 37–48. Springer. Lecture Notes in Computer Science Vol. 2723, July 2003.

[8] Andries P. Engelbrecht, editor. Computational Intelligence: An Introduction. John Wiley & Sons, England, 2002.

[9] Reyes-Sierra, M.; Coello, C.A.C. Fitness inheritance in multi-objective particle swarm optimization, Swarm Intelligence Symposium, 2005. SIS 2005. Proceedings 2005 IEEE Volume , Issue , 8-10 June 2005 Page(s): 116 – 123.

[10] R. Bellman, L.A. Zadeh, Decision making in a fuzzy environment, Management Sci 17 (1970) 141–164.

[11] V. Mazur, Fuzzy thermoeconomic optimization of energy-transforming systems, Applied Energy 84 (2007) 749–762.

[12] Rizk NK, Mongia HC. Semianalytical correlations for NOx, CO and UHC emissions. Journal of Engineering for Gas Turbine and Power 1993; 115(3):612–9.

[13] Gülder Ö. L. Flame temperature estimation of conventional and future jet fuels. Journal of Engineering for Gas Turbine and Power 1986; 108(2):376–80.

[14] Lefebvre AH. Gas Turbine Combustion. Ann Arbor (MI): Edwards Brothers; 1998.

Increasing Conversion Efficiency in Fuel Ethanol Production from Lignocellulosic Biomass by Polygeneration – and a Paradoxon between Energy and Exergy in Process Integration

Martin Gassner and François Maréchal

Laboratory for Industrial Energy Systems, Ecole Polytechnique Fédérale de Lausanne, Switzerland

Abstract: In the public and scientific debate on biofuels, ethanol from lignocellulosic biomass is generally the most popular alternative that may allow for a sustainable production. Compared to thermochemical processing of biomass which assures a complete conversion of the feedstock, it yet suffers from an inherently lower fuel yield due to the resistance of lignin to biological degradation. Based on a recently developed process model for fuel ethanol production from lignocellulosic biomass, this paper discussed the cogeneration alternatives for the conversion of the residual lignin. Whereas an integrated gasification combined cycle (IGCC) increase the power cogeneration efficiency compared to the conventional combustion and power generation in a steam Rankine cycle, it is shown that alternative gasification and methanation to Synthetic Natural Gas (SNG) allows for roughly doubling the fuel yield from biomass.

The paper further demonstrates the paradox situation that conventional energy recovery is limited by the available energy, and not, as usually, the available exergy from the waste heat. In order to overcome this limitation, a more general energy integration approach that allows for increasing the cogeneration efficiency in this kind of situations is proposed.

Keywords: biofuels, energy integration, ethanol, exergy, process integration, SNG

1. Introduction

In the public and scientific debate on biofuels, ethanol from lignocellulosic biomass is one of the most popular alternatives that may allow for a sustainable production. Since lignin resists to biological degradation and hemicellulose can only be partially hydrolysed, ethanol fermentation yet suffers from a relatively low fuel yield. The process efficiency is therefore essentially dependent on the valorisation of the residues and the quality of the process integration. Compared to the conventional intention of drying and burning the residual lignin slurry to provide heat for ethanol distillation and power cogeneration [1], thermochemical processing is a promising alternative for substantially increase the fuel yield since it assures a complete conversion of the feedstock.

This paper discusses the prospects for increasing the efficiency of biomass-to-fuel conversion by polygeneration and demonstrates shortcomings of a conventional energy integration approach for a complete recovery of the process' exergy potential.

2. Process description

Following the systematic process design methodology outlined in [2], Zhang et al. [3] recently developed a process model for fuel ethanol production from lignocellulosic biomass based on double acid hydrolysis, whose principal process steps are depicted in the block flow diagram of Figure 1(a). In this model, the biomass is first hydrolysed in two stages at 155-165°C with conversion yields of 80%, 70% and 10% for the degration of cellulose to glucose, hemicellulose to xylose and further to furfural, respectively. After removing the suspended solids, glucose and xylose are then fermented to ethanol and CO_2 at conversion yields of 95% and 60%, respectively. The distillation is carried out in three columns, where ethanol is subsequently concentrated from 2.7%wt to 40% and further to the azeotrope at 95%wt, from which it is rectified with cyclohexane as entrainer to 99.5%wt. After recovery of the residual ethanol and cyclohexane by stripping, 90% of the organic matter in the wastewater is recovered as biogas by anaerobic digestion. For these conversions, the composite curve in Fig-

Corresponding author: Martin Gassner, Email: martin.gassner@epfl.ch

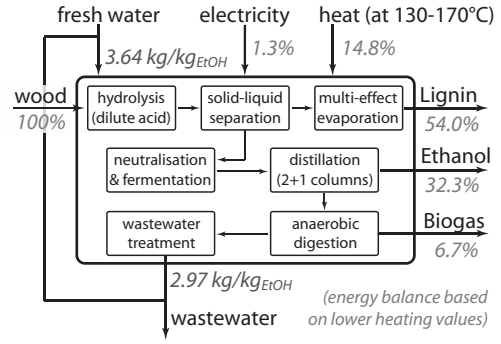

(a) Block flow diagram.

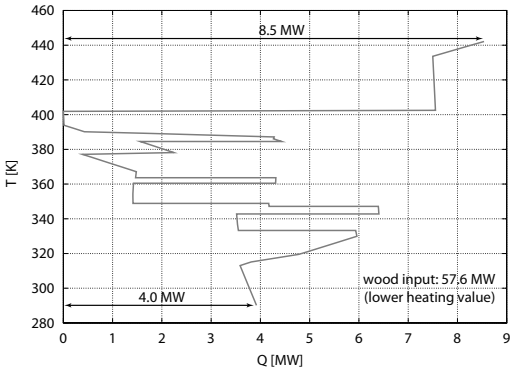

(b) Composite curve of the process streams.

Figure 1: Principal mass and energy balances of ethanol production according to the model of [3].

ure 1(b) assesses a minimum energy requirement (MER) at 130-170°C of roughly 15% of the biomass input, which also includes the multi-effect evaporation from 75 to 35%wt humidity of the lignin-rich slurry recovered from hydrolysis. With a dry biochemical composition of 12.3%wt hemicellulose, 25.9%wt cellulose and 61.8%wt lignin, this residue represents more than 50% of the feedstock's chemical energy due to the modest yields assumed in hydrolysis and fermentation.

3. Process integration

3.1. Methodology

As detailed in the applied methodology [2], the energy integration of the process is formulated as a mixed integer linear programming problem in which the mass balances between the subsystems and the heat cascade of the corrected temperature-enthalpy profiles act as constraints. Once the MER of the conversion process determined, appropriate technologies for the heat supply and energy recovery can be chosen. By considering the depleted residuals and, if required, intermediate product streams as fuels for this purpose, the optimal process integration that minimises the exergy depletion – or maximises the combined production of fuel, heat and power – is then determined.

3.2. Performance indicators

In order to characterise the relative outputs of a polygeneration plant, it is convenient to normalise the net yields of useful products as partial efficiencies of the biomass input. Accordingly, partial fuel and electric efficiencies ϵ_{f_i} and ϵ_{el} are defined as:

$$\epsilon_{f_i} = \frac{\Delta h^0_{f_i} \dot{m}^-_{f_i}}{\Delta h^0_{biomass} \dot{m}^+_{biomass}} \quad (1)$$

$$\epsilon_{el} = \frac{\dot{E}^- - \dot{E}^+}{\Delta h^0_{biomass} \dot{m}^+_{biomass}} \quad (2)$$

in which Δh^0 represents the lower heating value of a fuel f_i or biomass, $\dot{m}$ its mass flow and $\dot{E}$ electrical power. The superscripts $^-$ and $^+$ refer to net output and input flows, and one of the terms $\dot{E}^-$ and $\dot{E}^+$ thus cancels out since only the net balance is of interest.

The overall performance of the conversion can be expressed by the total energy and exergy efficiencies ϵ and η:

$$\epsilon = \frac{\sum \Delta h^0_{f_i} \dot{m}^-_{f_i} + \dot{E}^-}{\Delta h^0_{biomass} \dot{m}^+_{biomass} + \dot{E}^+} \quad (3)$$

$$\eta = \frac{\sum \Delta k^0_{f_i} \dot{m}^-_{f_i} + \dot{E}^-}{\Delta k^0_{biomass} \dot{m}^+_{biomass} + \dot{E}^+} \quad (4)$$

in which Δk^0 refers to the exergy value of a material stream. Although providing a strictly physical measure of the energy conversion and its quality degradation, ϵ and η do yet not satisfactorily assess the value of the fuel products with respect to the technical feasibility of their further conversion into final energy services. For this purpose, it is convenient to define an efficiency based on the substitution of fuel-equivalents for the consumed or by-produced power. A consistent weighting is thereby obtained if electricity is represented by the equivalent amount of fuel required for its generation in a (synthetic) natural gas combined cycle (NGCC) at an exergy efficiency η_{NGCC} of 55%:

$$\epsilon_{chem} = \frac{\sum \Delta h^0_{f_i} \dot{m}^-_{f_i} + \frac{1}{\eta_{NGCC}} \frac{\Delta h^0_{SNG}}{\Delta k^0_{SNG}} (\dot{E}^- - \dot{E}^+)}{\Delta h^0_{biomass} \dot{m}^+_{biomass}} \quad (5)$$

3.3. Results and discussion

3.3.1. Combustion and power cogeneration

The most straightforward use of the residual lignin slurry and biogas is to supply the process MER by combustion and cogenerate power from the excess heat in a steam Rankine cycle, which is the solution proposed in NREL's reference design [1]. Despite the considerable heat demand of distillation, the exergy composite curve of Figure 2(a) highlights that combustion of the residues generates a lot of excess heat which is recovered at a very modest efficiency. Assuming a single steam production level at 80 bar (295°C), superheating to 550°C, steam utilisation at 14.9 bar (198°C) and 3.6 bar (140°C) and condensation at 0.02 bar (20°C), the energy balance of Table 1 assesses a net partial electric efficiency of 17.1% based on the overall plant input, which corresponds to an electricity yield of roughly 34% from the residuals. In this configuration, the Rankine cycle operates largely independent of the ethanol plant and an important amount of energy is lost in the cooling water due the exergy losses in the heat recovery. Benefits from process integration are small.

3.3.2. Gasification alternatives

Compared to the chemical energy potential of the residuals, the process heat demand is relative small and cogeneration technologies with a low heat share are thus preferable. For this purpose, the use of an integrated gasification combined cycle (IGCC) has been investigated by Hamelinck et al. [4] and later also Laser et al. [5]. By generating power from the producer gas in a gas turbine, the exergy losses at high temperature are reduced and the total power output thus increased (cf. Fig. 2(b)). With a topping cycle design similar to the one proposed by Brown et al. [6], IGCC based on pressurised, oxygen blown gasification allows for increasing the power cogeneration from 17.1% to 21.5% of the total biomass input compared to a simple steam Rankine cycle.

In order to increase the overall fuel yield, a second alternative would be to thermochemically convert the residual lignin slurry to other liquid or gaseous products. Compared to the power generation options discussed in the previous sections, the share of excess heat of this processes is generally lower, and less exergy losses are thus expected in the conversion. While Laser et al. [7] discuss scenarios for the coproduction of Fischer-Tropsch fuels, dimethyl ether or hydrogen, we explored the suitability of

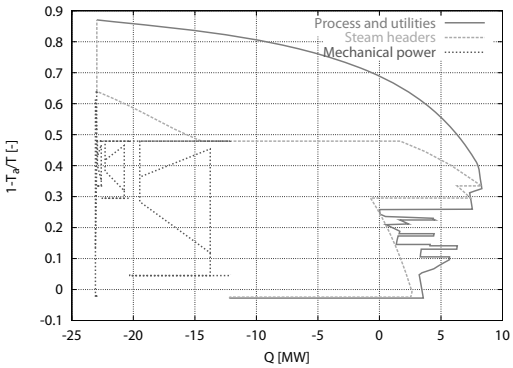

(a) Combustion and steam cycle.

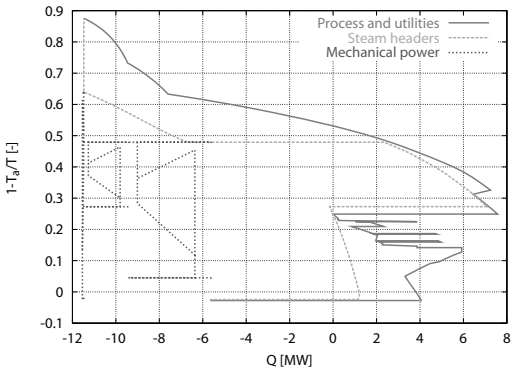

(b) IGCC (gasification, gas turbine and steam cycle).

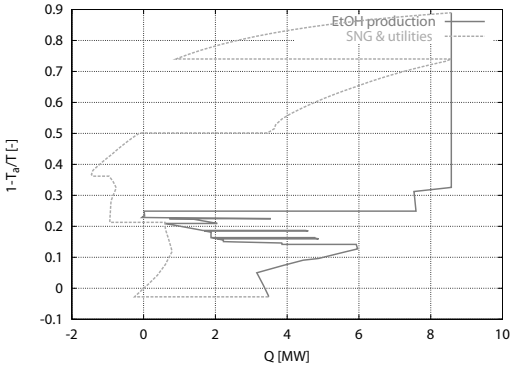

(c) SNG production (gasification and methanation).

Figure 2: Balanced exergy composite curves for different alternatives of lignin valorisation in the production of ethanol from wood (biogas is combusted in all cases).

SNG production at a case based on conventional indirectly heated gasification with the model of [8]. As illustrated by the balance exergy composite curve of Figure 2(c), the excess heat available from the conversion of the residual lignin slurry into SNG matches well with the requirement for ethanol

Lignin conversion	combustion	gasification	SNG (gasification and methanation)		
Power cogeneration	steam cycle	IGCC	-	steam cycle	& heat pumps
Composite curve	2(a)	2(b)	2(c)	3(b)	3(c)
ϵ_{EtOH}	32.3%	32.3%	32.3%	32.3%	32.3%
ϵ_{SNG}	-	-	40.3%	35.2%	41.9%
ϵ_{el}	17.1%	21.5%	-3.0%	1.9%	-0.5%
ϵ	49.4%	53.8%	70.5%	69.4%	73.6%
ϵ_{chem}	62.3%	70.0%	67.3%	70.8%	73.2%
η	52.5%	56.9%	74.9%	73.8%	78.5%

Table 1: Screening of partial and total efficiencies defined by (1) *to* (5) *for different lignin valorisation and process integration options (without any optimisation).*

distillation. Together with the sensible heat of the producer gas and fumes, the excess heat from the exothermal methane synthesis just balances with the demand for ethanol production, and the total cooling requirement equals the strict MER assessed in Figure 1(a). In this setup, SNG production allows for increasing the combined fuel yield to over 70%. However, no excess excess heat is available for power cogeneration and an equivalent net amount of 3% of the biomass input is consumed by the process (Table 1).

4. A paradox of energy and exergy

Transforming the section composite curves of Figure 2(c) into a single grand composite curve of Figure 3(a) reveals a paradoxal situation in waste heat recovery: Although valuable exergy is potentially available below the high temperature process pinch at 875°C, there is no heat excess in the system for its extraction as mechanical power. The exergy loss in the heat transfer – represented by the surface area between the hot and cold streams – cannot be prevented without supplying additional energy. Electricity cogeneration is thus limited by the first law of thermodynamics and not, as in the usual waste heat recovery problem, by the second. In order to overcome this limitation and valorise the exergy potential at high temperature, energy must be supplied to the system above the low temperature process pinch at 104°C.

One alternative is the combustion of additional producer gas to not only satisfy the pinch at gasification temperature, but also provide supplementary energy for power cogeneration from the available exergy. Such a solution is illustrated in Figure 3(b). As just as much energy to extract the exergy potential of the high-temperature streams is supplied, a marginal electric efficiency $\Delta\epsilon_{el}/\Delta\epsilon_{SNG}$ of 96% is obtained since no thermodynamic, but only thermal and mechanical losses in the boiler and turbomachinery occur. The according energy balances of Table 1 highlight that this allows for a gross power generation of roughly 5% of the total biomass input and results in an overall positive balance of the integrated plant.

Another, thermodynamically more promising alternative is to supply the required energy not by combustion of producer gas, but by heat pumping across the low temperature pinch. While combustion only transforms the chemical energy of an intermediate product without second-law losses into power, heat pumping adds more energy from below the process pinch – or the environment – above the process pinch. As illustrated in Figures 3(b) and (c), the exergy available below the pinch at 104°C is valorised and losses at high temperature are prevented. This allows for generating a net supplement of useful energy in the form of power, and not just the conversion of chemical into mechanical energy. The prevailing temperature profiles enable water as working fluid of two heat pump cycles from 68 to 107°C (0.28 to 1.29 bar) and 91 to 128°C (0.72 to 2.53 bar). With a combined shaft power of only 560 kW_{el}, these cycles provide 3.9 MW_{th} above the pinch, which allows the power cycle to extract 2.0 MW_{el} of the available high-temperature exergy. In this situation, heat pumping thus paradoxically allows for generating a net supplement of 1.4 MW_{el} of power that almost balances the overall electricity demand of the biomass conversion plant. At the same time, the SNG yield is not only constant but even increased, since the heat pumps also substitute heat that has previously been transferred across the high temperature pinch by only partially preheating the combustion air.

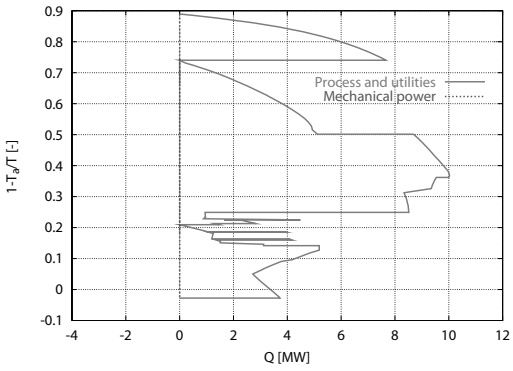

(a) Without exergy recovery (identical to Fig. 2(c)).

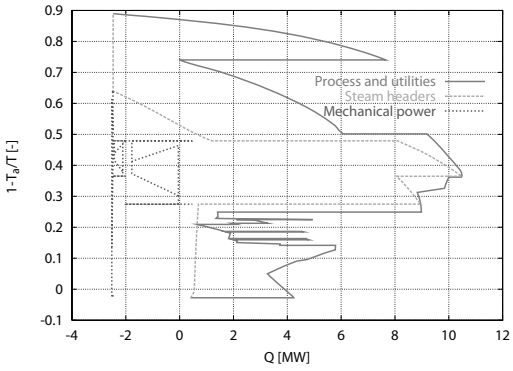

(b) Steam cycle with partial producer gas combustion.

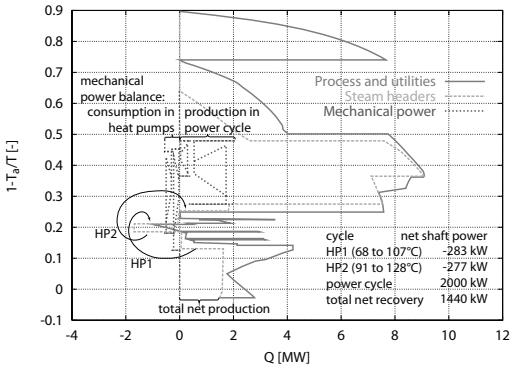

(c) Steam cycle with heat pumping.

Figure 3: Exergy recovery alternatives in combined ethanol and SNG production.

5. Conclusions

Table 1 summarises the benefit of designing site-scale integrated processes. Starting from an overall energy efficiency of 49.4% for the conventional process design, the combined production of SNG and ethanol from lignocellulosic resources allows for increasing the efficiency to up to 73.6%.

This brief outlook thus detects substantial potential in the polygeneration of fuels by exploiting the synergies between complementary conversion processes. The proper, overall-site integration of mass and energy is thereby a necessary condition to fully exploit the resource, which can only be realised by a systematic approach. In this regard, the findings with respect to thermal exergy recovery are not restricted to applications in the biofuel sector. Instead of addressing a waste heat recovery problem from the process streams' energy excess, it should be formulated as a problem of exergy minimisation, in which energy and exergy conversion technologies symmetrically allow for exchanges between all process streams and the environment.

Acknowledgments: The authors acknowledge funding provided by the Competence Centre for Energy and Mobility (CCEM), Erdgas Ostschweiz AG, Gasverbund Mittelland AG and Gaznat SA (all Switzerland).

Nomenclature

Abbreviations

HP Heat pump

IGCC Integrated gasification combined cycle

MER Minimum energy requirements

NGCC Natural gas combined cycle

SNG Synthetic natural gas

Roman Letters

$\dot{E}$ Electricity, MW

$\dot{m}$ Mass flow, kg s^{-1}

T Temperature, K

Greek Letters

Δh^0 Lower heating value, MJ kg^{-1}

Δk^0 Exergy value, MJ kg^{-1}

ϵ Energy efficiency, %

η Exergy efficiency, %

Subscripts and superscripts

$_a$ atmosphere

$_{el}$ electric

$_{th}$ thermal

$^+$ net input

$^-$ net output

References

[1] A. Aden, M. Ruth, K. Ibsen, J. Jechura, K. Neeves, J. Sheehan, and B. Wallace. Lignocellulosic biomass to ethanol process design and economics utilizing co-current dilute acid prehydrolysis and enzymatic hydrolysis for corn stover. Technical report, NREL, Colorado, USA, 2002.

[2] M. Gassner and F. Maréchal. Methodology for the optimal thermo-economic, multi-objective design of thermochemical fuel production from biomass. *Computers and Chemical Engineering*, 33:769–781, 2009.

[3] S. Zhang, F. Maréchal, M. Gassner, Z. Périn-Levasseur, W. Qi, Z. Ren, Y. Yan, and D. Favrat. Process modeling and integration of fuel ethanol production from lignocellulosic biomass based on double acid hydrolysis. *Energy and Fuels*, 23:1759–1765, 2009.

[4] C. N. Hamelinck, G. van Hooijdonk, and A. P. C. Faaij. Ethanol from lignocellulosic biomass: Techno-economic performance in short-, middle- and long-term. *Biomass and Bioenergy*, 28(4):384–410, 2005.

[5] M. Laser, H. Jin, K. Jayawardhana, and L. R. Lynd. Coproduction of ethanonl and power from switchgrass. *Biofuels, Bioproducts and Biorefining*, 3(2):195–218, 2009.

[6] D. Brown, M. Gassner, T. Fuchino, and F. Maréchal. Thermo-economic analysis for the optimal conceptual design of biomass gasification energy conversion systems. *Applied Thermal Engineering*, 29:2137–2152, 2009.

[7] M. Laser, E. Larson, B. Dale, M. Wang, N. Greene, and L. R. Lynd. Comparative analysis of efficiency, environmental impact, and process economics for mature biomass refining scenarios. *Biofuels, Bioproducts and Biorefining*, 3(2):247–270, 2009.

[8] M. Gassner and F. Maréchal. Thermo-economic process model for thermochemical production of Synthetic Natural Gas (SNG) from lignocellulosic biomass. *Biomass and Bioenergy*, 33: 1587–1604, 2009.

A Dual-gas Sourced Integrated Methanol/DME/DMC Catalysis Approach to Polygeneration Energy Systems Design and an Exergoeconomic Analysis

Zheng Li[a,b], Pei Liu[a], Fen He[a] and Minghua Wang[a]

[a] *Department of Thermal Engineering, Tsinghua University, Beijing 100084, China*
[b] *State Key Laboratory of Power Systems, Beijing 100084, China*

Abstract: Recent decades have seen a growing concern about ever-increasing green house gas (GHG) emissions and depletion of fossil fuels. Polygeneration, a multi-input multi-output energy system, provides huge opportunities to tackle these problems due to its superior performances over conventional energy systems in terms of energy conversion efficiency and GHG emissions. Many approaches have been made in process design and analysis of polygeneration energy systems, but most of them focus on using coal gasification as the only way to provide gas for downstream utilization. Coke oven gas, another gas source with huge capacity, however, has not received enough attention in polygeneration process design, and researches in this field are still rather limited.

In this paper, we present a dual-gas sourced polygeneration process design which uses both gasification gas and coke oven gas and produces methanol, dimethyl ether (DME), and dimethyl carbonate (DMC) in an integrated catalysis procedure. Gasification gas and coke oven gas are converted to synthesis gas, or syngas, via a catalytic reforming procedure, where the ratio between carbon monoxide and hydrogen in the syngas is carefully adjusted according to specific requirements of downstream chemical synthesis reactions. An integrated catalysis procedure follows, where DME is synthesized from the fresh syngas first, unconverted syngas is then sent to a methanol synthesis unit to produce methanol, and part of the methanol is further converted to DMC in a DMC synthesis unit. Based on the proposed process design, an exergoeconomic analysis and an exergy cost distribution diagram are presented, from which the production cost of a product over each functional block of the process can be easily obtained. Analysis results show that the largest exergy loss occurs in an exothermic reformer, accounting 60.4 percent of the total exergy loss. The exergy cost distribution diagram indicates that DMC has the highest exergy cost, followed by DME and methanol, and it is economically favorable to use the exhaust gas from the chemical synthesis block for power generation.

Keywords: polygeneration, dual-gas source, integrated catalysis, process design, exergoeconomic analysis.

1. Introduction

Fast increasing green house gas (GHG) emissions and depletion of fossil fuels have drawn more and more concerns in recent decades. Polygeneration is considered a promising option to tackle these challenges due to increased energy utilization efficiency and minimum environmental impacts.

A polygeneration process integrates chemical production with power generation and produces chemicals, usually synthetic liquid fuels, and electricity as main products. A typical polygeneration process starts from gasification of feedstock, usually coal or biomass, where crude synthesis gas, or syngas is produce. The crude syngas, consisting primarily of carbon monoxide and hydrogen, first goes through a series of cleanup units, where sulphur compounds, ash and other hazardous components are removed. The clean syngas is then split into two streams. One stream goes to a chemical synthesis process to produce chemical products, and the flue gas, together with the other stream of clean syngas, is fed to a power generation process to produce electricity.

Polygeneration has many advantages over conventional stand-alone processes. Firstly, due to tight integration between power generation and chemical synthesis processes, the energy utilization efficiency of a polygeneration plant is higher than a combination of stand-alone plants producing the same products. Secondly, the power generation process and the chemical synthesis process within a polygeneration plant use the same

Corresponding Author: Zheng Li, Email: lz-dte@tsinghua.edu.cn

gasifier, and the effect of economy of scale helps to further reduce the investment costs of the plant.

The configuration of a polygeneration plant may differ from one another depending on the specific types of feedstock available to the polygeneration plant and chemicals to produce [1, 2]. A number of process configurations have been proposed with significant improvement in energy utilization and cost savings [3-10].

Despite of the aforementioned approaches on configurations of gasification based polygeneration energy systems, gasification is not the only way to provide syngas. However, researches on polygeneration energy systems using different means of syngas production other than gasification are still rather limited. In this paper, we propose a polygeneration process configuration which uses coke oven gas (COG) and coal gasification as syngas sources.

Coke over gas, primarily consisting of methane and hydrogen, is a major by-product of the coking process. More than half of the world's coke oven gas production is in China, and the annual product rate is approximately 140 billion cubic meters per year [11]. However, coke oven gas is not used in an efficient way currently. Only half of the coke oven gas is recycled to supply heat for the coking process. The other half is emitted to the atmosphere either directly or via a simple burning process. This inefficient way of coke oven gas utilization leads to almost complete loss of the chemical energy of coke oven gas, and also produces a large amount of GHG emissions.

In this paper, we present a novel configuration of a coke oven gas and coal based polygeneration system which uses coke oven gas in a more efficient and clean way. Its major feature is the employment of a CO_2/CH_4 catalytic reforming procedure to produce syngas from coke oven gas and coal-derived syngas (CG). One advantage of this catalytic reforming procedure is that it can make good use of the abundant methane in coke oven gas and abundant carbon dioxide in coal-derived syngas. Another advantage is that it can precisely adjust the composition of the product syngas according to specific requirements of downstream chemical synthesis procedures, thus increases the flexibility in selecting the types of chemical products. To further illustrate the improved flexibility, three types of chemical products of large market demands, namely methanol (MeOH), dimethyl ether (DME), and dimethyl carbonate (DMC), are selected in the proposed process configuration.

This paper is organized as follows. First, the process configuration of an integrated catalysis synthesis polygeneration plant is presented, together with a systematic analysis to illustrate its advances. Secondly, key design parameters of the proposed polygeneration process are provided, based on which a process simulation is performed and simulation results are presented. Then, results of an exergy analysis of the proposed process are provided, illustrating the efficiency of the proposed process in energy utilization. Finally, an exergoeconomic analysis and an exergy cost distribution diagram are provided, indicating the economic loss occurred in each functional block on an exergy basis.

2. Process configuration

An illustrative process flow sheet of a polygeneration plant with integrated MeOH-DME-DMC catalytic synthesis is depicted in Fig. 1. The system consists of five major functional blocks, as follows:

- a COG-CG-oxygen reformer with a desulphurization process
- DME synthesis and distillation
- MeOH synthesis and distillation
- Pressure Swing Adsorption (PAS)
- DMC synthesis and distillation

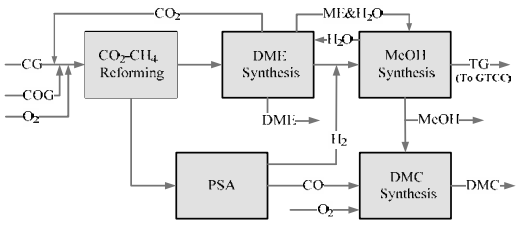

Fig. 1. Illustration of MEOH-DME-DMC integrative catalytic synthesis

In this process, coal-derived syngas, coke oven gas, and oxygen goes to a reformer first, which is operated at 1273 K and 3 MPa, producing syngas with a H_2/CO ratio of one to satisfy the requirement of DME synthesis. The syngas leaving the reformer enters a cleanup unit for desulphurization, then part of the syngas enters a compressor and the rest goes to the PSA block. The pressurized syngas exiting the compressor

flows into a DME synthesis unit operated at 6 MPa, and DME of high purity is obtained after the synthesis reaction, absorption and rectification. Tail gas leaving the DME synthesis reactor, with a H_2/CO ratio of less than one, goes to the MeOH synthesis unit. In the PSA pathway, carbon monoxide with a concentration between 96 percent and 99.9% percent is produced for DMC synthesis. Gas leaving the PSA unit is highly concentrated in hydrogen, and this is particularly beneficial to the methanol synthesis unit. It is then compressed and fed to the MeOH synthesis unit. The unreacted gas exited from the MeOH synthesis unit is sent to a gas turbine combined cycle unit to generate electricity. Part of the methanol produced is further rectified by three columns, and a part of it is sent to produce DMC.

The idea of the MeOH-DME-DMC integrated catalytic synthesis is based on the composition of coal-derived syngas and coke oven gas and the requirements of MeOH, DME and DMC synthesis with respect to pressure, temperature, and mole ratio of hydrogen to carbon monoxide, shown in Table 1.

Table 1. Composition of coke-oven gas and coal gas (volume %)

	H_2	CH_4	CO	CO_2	N_2+Ar
COG	58.10	24.90	5.86	2.35	3.90
CG	39.73	1.70	29.46	21.59	7.42

The exothermic reformer shown in Fig. 1 then converts methane in the coal oven gas to carbon monoxide and hydrogen. An appropriate H_2/CO ratio of the syngas product is carefully adjusted so that the requirements of downstream chemical synthesis are satisfied.

The main reactions occurring in the reforming process are:

$$CH_4 + 0.5O_2 = CO + 2H_2 \quad (\Delta H_0 = -35.5 \text{ kJ/mol}) \quad (1)$$

$$CH_4 + CO_2 = 2CO + 2H_2 \quad (\Delta H_0 = 247 \text{ kJ/mol}) \quad (2)$$

The reforming block produces syngas with appropriate H_2/CO ratio based on the facts that coke oven gas is rich in hydrogen and coal-derived syngas is rich in carbon dioxide. Therefore, a water gas shift reactor which would otherwise be installed in a traditional polygeneration plant is not necessary here. As a result, it avoids a significant exergy destruction that usually occurs in a water shift reaction in coal gasification based chemical synthesis processes.

Main features of the proposed polygeneration system are summarized as follows:

- For each synthesis unit, unconverted syngas is not recycled in order to minimize the energy consumption of compression and to simplify the process. The unconverted syngas can either be sent to a downstream synthesis unit or directed to the gas turbine combined cycle unit to generate electricity.
- The DME synthesis unit is placed before the MeOH and DMC units. The unconverted syngas from DME unit is directed to the methanol synthesis unit, and the methanol produced in this unit can be used for the downstream DMC synthesis.
- To make good use of the methane in the coke oven gas and increase the chemical production, the conversion ratio of methane in the reformer is set to above 99 percent. The methane content of the produced syngas can be controlled by the oxygen feedstock, and the H_2/CO ratio is mainly dependant of the ratio of coke oven gas, coal-derived gas, oxygen, and the reformer temperature. The ratio of mole flow rates of hydrogen and carbon monoxide is set to 1:1 for the DME synthesis. A high CG/COG ratio is required at the reformer entrance.
- The PSA unit has two major functions: one is to produce high purity carbon monoxide as a raw material for the DMC synthesis. The other is to obtain hydrogen-rich syngas, which helps to raise the H_2/CO ratio of the syngas entering the methanol synthesis unit.
- Due to the pressure drop through the process, syngas should firstly be compressed to a relatively high pressure level before entering the DME unit, making the DME discharge pressure high enough for the methanol synthesis unit. Therefore, it avoids extra boosters between these two synthesis units, simplifies the system and reduces investment costs of corresponding equipment.
- The mixture of alcohol and water rectified from the DME unit is sent to a methanol rectification unit without further separation, aiming at simplifying the separation system and saving energy for the rectification. The water separated from methanol rectification sector can be used as absorbent for DME production.

3. Process simulation and exergy analysis

The proposed polygeneration system is simulated using Aspen Plus. The CO/COG reformer is simulated by a Gibbis reactor. Kinetics subroutines of the MeOH/DME/DMC catalytic synthesis reactions are developed and integrated into Aspen Plus. The macro kinetic equations of the DME, MeOH and DMC synthesis reactions are taken from literature [12-14] respectively. Based on this, the synthesis reactors are simulated using the RCSTR module in Aspen Plus with the developed subroutines of reaction kinetics.

Simulation results show that the optimal mole ratio of coal-derived syngas, coke oven gas, and oxygen is 18:12.5:1, and the mass ratio of DME/MeOH/DMC products is 25:29:2. In the DME synthesis unit, the once-through conversion ratio of syngas reaches 27.8 percent and the selectivity of DME is 82.4 percent. In the DME absorption and rectification units, the purity of DME is 96.9 percent. The MeOH synthesis unit has a once-through conversion ratio of 36.4 percent, and the purity of the methanol product is 99.6 percent. In the DMC synthesis unit, the mole ratio of MeOH/CO/Oxygen is 11.23:3.16:1, the conversion ratio of methanol is 68.2 percent. The final product DMC has a purity of 99.5 percent.

Based on the process simulation results, exergy analysis has been conducted to the following five functional blocks in the process, namely the reformer, the DME synthesis block, the methanol synthesis block, the DMC synthesis block, and the PSA block. For each block, exergy of the inlet and outlet streams and exergy losses are calculated, shown in Table 2.

The total exergy loss in the chemical synthesis blocks is 20.5 percent. The largest exergy destruction occurs in the COG/CG exothermal reformer, accounting for 12.4 percent of the exergy input or 60.4 percent of the total exergy loss, mainly due to the irreversible loss during combustion and the heat exchange. In an energy viewpoint, the reformer unit has the largest potential for further efficiency improvement. In DME and MeOH synthesis units, however, although the once-through conversion rates of DME and MeOH are low, the exergy loss is not large, only accounting for 3.9 percent and 4.1 percent of the exergy input, respectively. Partial recycle can be adopted to increase the once-through conversion rates, but the benefit would be offset by the increased auxiliary power consumption of the compressors.

Table 2. Exergy distribution by functional blocks (unit : kJ/s)

Block	Input	Products	Output	Exergy loss
COG/CG reformer	94.8	73.0		11.758
DME synthesis	85.8	18.7	21.5	3.75
Methanol synthesis	47.0	16.8	17.7	3.90
PSA	0.441	0.437		0.002
DMC synthesis	1.000	0.294		0.047

4. Exergoeconomic analysis

For a polygeneration system that produces multiple products, it is necessary to rationally allocate cost amongst different products. Purely energy based allocation methods are not satisfactory, because they usually cannot take energy quality into account. When the energy criterion is applied, the cost of downstream products is inclined to be overestimated since the degradation of the energy quality along the process is simply ignored.

An exergoeconomic analysis has been performed to indicate the economic loss occurred in each functional block on an exergy basis. Methods applied in this study are obtained from the literature [15-21].

The first step of exergoeconomic analysis is to divide the system under study into several key units or clusters. The chemical synthesis process of the proposed polygeneration plant is thus divided into five units as shown in Fig. 1. Other information regarding the exergy streams and non-energy streams flowing through the system are as follows:

- external exergy streams entering the system, including coal-derived syngas, coke oven gas, and oxygen
- exergy loss during each conversion process
- the monetary cost flows, including equipment costs, utility stream costs, and O&M costs.

A system with n units and m streams, can be represented by an incidence matrix, denoted as $A_{n\times m}$. Its element $a_{i,j}$ takes the value of 1 if flow j enters unit I, -1 if flow j leaves unit i, and 0 if no direct physical relations exist between them. By introducing the incident matrix A, the system of the exergy balance can be written as:

$$A \times E = I \tag{3}$$

where E is an $n \times l$ vector representing exergy flows, and I is an $m \times l$ vector representing exergy losses in each subsystem. For any subsystem k, supposing there are e streams of exergy input, s streams of exergy output, its non-energy costs (such as depreciation costs, management fees), denoted as Z_k, unit exergy costs of input streams, denoted as E_i, and unit exergy costs of output streams, denoted as E_j, establish the following cash balance:

$$\sum_{i=1}^{e} C_i E_i + Z_k = \sum_{j=1}^{s} C_j E_j \tag{4}$$

Suppose the system has m sub-systems, there are m corresponding cash balance equations, which can be represented using the following matrix:

$$A \times E_D \times C + Z = 0 \tag{5}$$

where E_D is a $n \times n$ diagonal matrix, C is an n dimensional vector of unit exergy costs, Z is an m dimensional vector of non-energy costs of each subsystem. For any system where the number of subsystems n is greater than the number of streams m, it is necessary to have n-m supplementary equations, expressed as a matrix:

$$A' \times E_D \times C = w \tag{6}$$

where A' is a matrix containing n-m rows and n columns, and w is an n-m dimensional vector.

The complementary equations follow the following rules:

- For external exergy flow into the system, the unit exergy cost can be considered to be the market price
- If the product of a unit comprises of two or more streams, then the unit costs of those streams are equal
- If the feedstock of a unit includes a stream that goes through a unit and is utilized in another one, (e.g. syngas flows into the DME synthesis reactor and then unconverted syngas flows out of it), then the exergetic costs of the stream flowing into and out of the unit are equal to each other

With Equation (5) and Equation (6), we get:

$$\overline{A} \times E_D \times C + \overline{Z} = 0 \tag{7}$$

The unit exergetic cost can be obtained as:

$$C = -E_D^{-1} \times \overline{A}^{-1} \times \overline{Z} \tag{8}$$

Non-energy costs mainly consist of the capital cost of each unit and O&M costs. The annualized cost method is used here. The present value of capital investment is converted to an annualized cost by using the capital recovery factor, denoted as *CRF*. The annualized cost of equipment i is obtained as follows:

$$C_{\text{equip,i,an}} = \text{PV} \times \text{CRF} \tag{9}$$

$$\text{CRF} = \frac{i}{1-(1+i)^{-n}} \tag{10}$$

where $C_{equip,i,an}$ is the annualized cost of total capital investment, PV is the present value of investment, i is the discount rate, and n is the length of operating horizon, taken as 20 years for this study.

Dividing the annualized cost by 8000 annual operating hours, we obtain the following capital cost rate for the component i of the plant:

$$C_{\text{equip,i}} = \frac{C_{\text{equip,i,an}}}{8000 \times 3600} \tag{11}$$

Equipment costs and O&M costs are estimated using the following equation:

$$C_{Vy} = C_{Vx} \times \left(\frac{f_{Vy}}{f_{Vx}}\right) \times \left(\frac{V_y}{V_x}\right)^{\alpha} \tag{12}$$

where C_{Vx} is the reference cost of the equipment, f_{Vx}, f_{Vy} are plant cost indices, V_x, V_y are the sizes of equipment, α is a scaling factor ranging between 0.6 and 0.7. The cost of the CG/COG reformer is estimated based on the cost of a conventional natural gas exothermic reforming reactor.

Based on the results of the exergoeconomic analysis, an exergy cost distribution diagram is obtained and shown in Fig. 2, where the exergy cost of each product stream is highlighted with exergy flow value in brackets. It can be seen from Fig. 2 that DMC has the highest exergy cost, followed by DME, and methanol has the lowest

exergy cost. It also shows that the exergy cost of the syngas increases along the process, which suggests the fact that non-energy cost and the exergy destruction during the energy conversion process would lead to an increase of the exergy cost of the products. In methanol synthesis process, the exergetic cost of unconverted syngas is higher than that of the syngas discharged from DME reactor, but both syngas streams has a lower exergy cost than the fresh syngas. Considering the heating value of the unconverted syngas is similar to that of the fresh syngas, it is more cost effective to use the unconverted syngas for power generation than to use the fresh syngas.

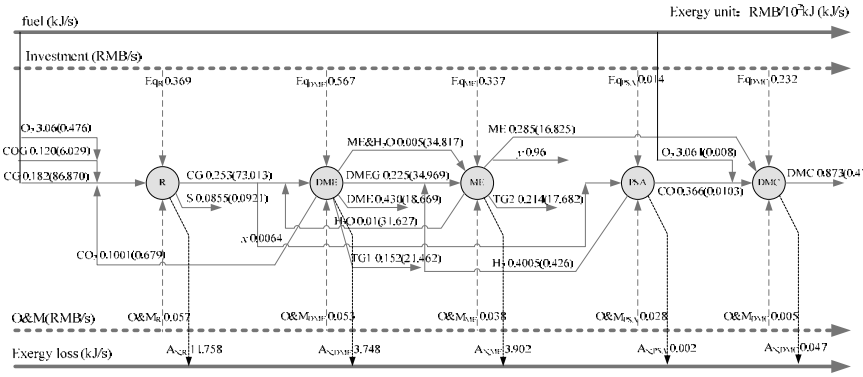

Fig. 2. Exergy cost distribution diagram of integrative catalytic synthesis system

5. Conclusions

A process configuration of a polygeneration system is proposed in this chapter, featuring utilization of coal-derived syngas and coke oven gas, and production of methanol, DME, and DMC via an integrated catalytic synthesis procedure. The proposed polygeneration system provides a great opportunity for more efficient and cleaner utilization of coke oven gas.

According to the exergy analysis, unconverted syngas used for power generation carries the largest part of exergy input, whilst most of the exergy destruction occurs in the exothermic reformer, accounting for 60.4 percent of the total exergy loss in the whole chemical synthesis process. Improvements in these parts have the greatest potential for further efficiency increase.

An exergy cost distribution diagram is obtained via exergoeconomic analysis to illustrate the cost allocation. Result show DMC has the highest exergy cost, followed by DME and MEOH. Moreover, although the heating value of the unconverted syngas discharged by the methanol synthesis reactor is close to that of fresh syngas, its exergy cost is remarkably lower, indicating that it is economically favorable to use the exhaust gas to generate electricity. These results provide a solid basis where different chemical products can be priced.

References

[1] Li, Z., Ni, W., Zheng, H., and Ma, L., *Polygeneration energy system based on coal gasification.* Energy for Sustainable Development, 2003. **7**(4): p. 57-62.

[2] Yamashita, K. and Barreto, L., *Energyplexes for the 21st century: Coal gasification for co-producing hydrogen, electricity and liquid fuels.* Energy, 2005. **30**(13): p. 2453-2473.

[3] Zheng, H., Li, Z., Ni, W., Larson, E.D., and Ren, T., *Case-study of a coal gasification-based energy supply system for China.* Energy for Sustainable Development, 2003. **7**(4): p. 63-78.

[4] Liu, P., Pistikopoulos, E.N., and Li, Z., *A mixed-integer optimization approach for polygeneration energy systems design.* Computers & Chemical Engineering, 2009. **33**(3): p. 759-768.

[5] Chiesa, P., Consonni, S., Kreutz, T., and Robert, W., *Co-production of hydrogen, electricity and CO2 from coal with commercially ready technology. Part A: Performance and emissions.* International Journal of Hydrogen Energy, 2005. **30**(7): p. 747-767.

[6] Cicconardi, S.P., Perna, A., and Spazzafumo, G., *Combined power and hydrogen production from coal. Part B: Comparison between the IGHP and CPH systems.* International Journal of Hydrogen Energy, 2008. **33**(16): p. 4397-4404.

[7] Gao, L., Li, H., Chen, B., Jin, H., Lin, R., et al., *Proposal of a natural gas-based polygeneration system for power and methanol production.* Energy, 2008. **33**(2): p. 206-212.

[8] Liu, P., Gerogiorgis, D.I., and Pistikopoulos, E.N., *Modeling and optimization of polygeneration energy systems.* Catalysis Today, 2007. **127**(1-4): p. 347-359.

[9] Liu, P., Pistikopoulos, E.N., and Li, Z., *A multi-objective optimization approach to polygeneration energy systems design.* AIChE Journal, 2010. **In press**.

[10] Liu, P., Pistikopoulos, E.N., and Li, Z., *Decomposition based stochastic programming approach for polygeneration energy systems design under uncertainty.* Industrial & Engineering Chemistry Research, 2010. **49** (7): p. 3295-3305.

[11] Sun, S., Jin, H., Gao, L., and Han, W., *Study on a multifunctional energy system producing coking heat, methanol and electricity.* Fuel, 2010. **In Press**.

[12] Ng, K.L., Chadwick, D., and Toseland, B.A., *Kinetics and modelling of dimethyl ether synthesis from synthesis gas.* Chemical Engineering Science, 1999(54): p. 3587-3592.

[13] Wang, C.W.B.D.H., *Study on Three-phase Methanol Synthesis I. The Global Kinetics of Methanol Synthesis for CO-rich Synthesis Gas in Slurry Reactor.* Journal of east China University of science and technology, 2000. **26**(4): p. 329-333.

[14] Fang, D., Cao, F., and Liu, D., *Reaction Kinetics of Methanol Oxidation and Carbonylation in Vapor Phase for DMC Production Catalyzed by CuCl2/C.* Journal of chemical engineering of Chinese universities, 1997. **11**(2): p. 212-216.

[15] Lozano, M.A. and Valero, A., *Theory of the exergetic cost.* Energy, 1993. **18**(9): p. 939-960.

[16] Valero, A., Lozano, M.A., Serra, L., and Torres, C., *Application of the exergetic cost theory to the CGAM problem.* Energy, 1994. **19**(3): p. 365-381.

[17] Alvarado, S. and Gherardelli, C., *Exergoeconomic optimization of a cogeneration plant.* Energy, 1994. **19**(12): p. 1225-1233.

[18] Kwon, Y.-H., Kwak, H.-Y., and Oh, S.-D., *Exergoeconomic analysis of gas turbine cogeneration systems.* Exergy, An International Journal, 2001. **1**(1): p. 31-40.

[19] Abusoglu, A. and Kanoglu, M., *Exergoeconomic analysis and optimization of combined heat and power production: A review.* Renewable and Sustainable Energy Reviews, 2009. **13**(9): p. 2295-2308.

[20] Kim, S.-M., Oh, S.-D., Kwon, Y.-H., and Kwak, H.-Y., *Exergoeconomic analysis of thermal systems* Fuel and Energy Abstracts, 1998. **23**(5): p. 393-406.

[21] Rosen, M.A. and Dincer, I., *Exergoeconomic analysis of power plants operating on various fuels.* Applied Thermal Engineering, 2003. **23**(6): p. 643-658.

Acknowledgments: National Basic Research Program of China (2005CB221207) is gratefully acknowledged for providing financial support for this study.

Exergy-based Comparison of the Nuclear Fuel Cycles of Light Water and Generation IV Reactors

Filippo Tani[a], Pierre-André Haldi[b], Daniel Favrat[a]

[a] *Ecole Polytechnique Fédérale de Lausanne, LENI, Switzerland*
[b] *Ecole Polytechnique Fédérale de Lausanne, Energy Center, Switzerland*

Abstract: Assessing the performance of the nuclear fuel cycles and plants on an exergy basis should provide a coherent framework to compare, from an energy efficiency viewpoint, nuclear power systems between themselves as well as with other energy systems. The energy efficiency of modern nuclear power plants is assumed to be the standard First Law thermodynamic efficiency but this paper demonstrates that this assumption is misleading because it does not take into account the effective utilisation of the nuclear fuel in the whole fuel cycle. In the once-through fuel cycle currently adopted in most light water reactors worldwide, not even 1% of the exergy introduced into the fuel cycle as uranium fuel is effectively converted into electrical energy. Only the closed nuclear fuel cycles seem to assure an efficient utilisation of the exergy content of the uranium fuel although they are still at the research stage. In this paper the closed fuel cycle for molten salt reactors is compared on an exergy basis to the once-through fuel cycle of the light water reactors. The exergy analysis of these cycles suggests that the current cycle for light water reactors is the least efficient while the closed cycles have the potential of improving by two orders of magnitude the exergy efficiency in the utilisation of uranium as well as thorium nuclear fuels.

Keywords: Exergy efficiency, Nuclear Energy, Nuclear Fuel Cycle, Generation III and IV Reactors

Nomenclature

E	exergy, J
U	internal energy, J
P_0	pressure of the environment, N/m^2
V	volume, m^3
T_0	temperature of the environment, K
S	entropy, J/K
${}_0n^1$	neutron
${}_ZN^A$	nuclide of atomic number Z and mass number A
A	energy, J
m	mass, kg
N	natural uranium feed, kg
P	enriched uranium product, kg
T	depleted uranium tail, kg
x	mass fraction of U^{235}, %
P_e	power plant electrical power, GWe
L_F	power plant annual load factor, %
B	nuclear fuel burn-up rate, GWd/t
$P_{NPP,a}$	annual enriched uranium demand, t/y
$N_{NPP,a}$	annual natural uranium demand, t/y
SW	isotopic separation work, kg SWU
V_I	isotopic potential
c	speed of light in vacuum = 3.00 x 10^8 m/s
eV	electronvolt = 1.602 x 10^{-19} J
GWd	Gigawattday = 86.4 x 10^{12}J

Greek symbols

Σ	thermodynamic system
Σ_0	environment
ε	1st Law (energy) efficiency
η	2nd Law (exergy) efficiency
ν	average number of neutrons emitted per fission

Corresponding Author: Tani Filippo, filippotani@gmail.com

1. Introduction

Exergy analysis in the field of nuclear energy analysis has been so far limited to the classical nuclear thermodynamic cycle [1,2,3]. We considered interesting to extend this approach to the analysis of the whole fuel cycle and not only to the thermodynamic conversion stage inside the nuclear reactor.

Several nuclear fuel cycles have reached maturity, in particular the open cycle for light

water reactors (LWR), the open cycle for heavy water reactors (HWR) and the cycle with reprocessing and recycling of the plutonium (for LWR).

Among the three cited cycles, the first one is chosen as reference for our study, because it is today the most commonly used nuclear fuel cycle worldwide. Unfortunately, although it represents the culmination of 50 years of technological developments, this cycle remains very inefficient in terms of the use of uranium resources.

Typically, in light water reactors less than 1% of the extracted uranium is actually "burned" while the rest is stored either as depleted uranium (front-end part of the cycle) or as used fuel (back-end part of the cycle). The potential for improving the efficiency of the use of uranium ores remains thus huge, not mentioning the potential utilization of the even more abundant thorium resources.

Among the many nuclear fuel cycles likely to make a better use of the uranium/thorium resources that could be implemented in the next 25-50 years (so-called "generation IV reactors"), we selected the cycle of molten salt reactor (MSR), a very efficient cycle from a thermodynamic viewpoint and moreover able to greatly increase the utilization yield of the nuclear ore resources.

MSR cycle could burn either uranium or thorium with a burn-up rate that could significantly approach the theoretical maximum and, in addition, thermodynamic cycle temperatures reaching 700-850 ° C.

The exergy approach opted for in this study allows us to compare the two selected nuclear fuel cycles on a coherent basis independent of the technologies used, and thus assess the actual world theoretical potential of the uranium and thorium resources.

2. The exergy concept

The concept of exergy is extremely powerful because it incorporates both the First and the Second Laws of thermodynamics in a coherent way. In fact, the exergy allows us to actually evaluate the energy degradation associated with any process.

It explicitly quantifies the thermodynamic losses (loss of potential to do work or electricity) in a given environment [4]. We remind here that the First Law of thermodynamics is unable to distinguish between different forms of energy (all are considered of equal value), while the Second Law shows that heat and work for example do not have the same potential to provide energy services. Similarly, two equal quantities of heat available at different temperatures have different thermodynamic values (in terms of the potential work that can be produced with them).

If we consider a system Σ surrounded by an environment Σ_0 (assumed of infinite size, that is much larger than the system Σ so that its properties remain unchanged when interacting with Σ), the exergy can be defined by the following relationship [5]:

$$E = U + P_0V - T_0S \qquad (2.1)$$

where U, V and S respectively represent the internal energy, the volume and the entropy (extensive state properties of the system). P_0 and T_0 are respectively the pressure and temperature (intensive state properties, often also designated by P_a and T_a) that characterize the Σ_0 environment.

By definition, the exergy E expresses the maximum theoretical work that the system Σ is able of providing relative to a reference state Σ_0. It is generally assumed that the exergy of the reference state (environment) is equal to zero when this reference state is in thermal, mechanical and physicochemical equilibrium (no chemical reactions between the different components of the system).

Exergy, contrary to energy, is partly destroyed during real transformations, due to the presence of inevitable irreversibilities (it is conserved only in the case of ideal processes).

This property of the exergy allows us to define an exergy efficiency η that is appropriate to characterize the thermodynamic quality of a technical system converting energy.

By opposition to the classical energy efficiency ε, the exergy efficiency η always takes numerical values between 0 and 1 (this last value being reached only in the case of a perfectly reversible system).

2.1. Nuclear exergy

Fission is a nuclear reaction induced by the interaction of a neutron with an atomic nucleus that results in the split up of the hit nucleus, with the formation of two fission products. A nuclear fission reaction may thus be expressed by the following relation:

$$ {}_0n^1 + {}_{Zc}N^{Ac} \rightarrow {}_{Zfp1}N^{Afp1} + {}_{Zfp2}N^{Afp2} + \nu\ {}_0n^1 + A_F \quad (2.2) $$

where A_F is the energy released by the fission, ${}_0n^1$ is the symbol of the neutron, with ν neutrons emitted by the ${}_{Zc}N^{Ac}$ nucleus that undergoes fission, and ${}_{Zfp1}N^{Afp1}$ and ${}_{Zfp2}N^{Afp2}$ the two fission products [6].

The A_F energy generated by the nuclear fission reaction can be calculated using the classical Einstein relation:

$$ A_F = \Delta m \cdot c^2 \quad (2.3) $$

where Δm represents the mass defect of the reaction, that is the difference between the mass of the nucleus that undergoes fission (including that of the neutron that triggers the reaction) and the sum of the masses of the reaction products (fission products + ν neutrons).

The most important part (80%) of the fission energy ends up in the form of kinetic energy of the fission products, the remainder being associated with β radiation (4%), γ radiation (4%) fast neutrons (3%), neutron capture reactions (4%) and emitted neutrinos (5%) [6].

The only part of the fission energy that cannot be retrieved (in the form of heat) in the reactor is the one associated with the emitted neutrinos because the likelihood of these particles to interact with matter is virtually zero.

We can therefore conclude, in agreement with [7], that the exergy of nuclear fission is given by the following relation:

$$ E = \Delta m \cdot c^2 - A_{neutrinos} \quad (2.4) $$

where $A_{neutrinos}$ represents the energy associated with the emitted neutrinos.

In nuclear physics the usual measurement unit of energy is the electronvolt (eV), which represents the energy acquired by an electron subject to a 1V voltage. It is therefore worth 1.602 x 10^{-19} J. Its multiple, the Megaelectronvolt (MeV), is thus equivalent to 1.602 x 10^{-13} J.

Table 2.1. Fission energies and exergies (in MeV) with corresponding specific exergies (in TJ/kg) [6]

Nuclide	Fission energy [MeV]	Fission exergy [MeV]	Mass exergy (TJ/kg)
U^{233}	200.0	190.0	78.7
U^{235}	203.0	192.9	79.2
U^{238}	*208.9**	*198.5**	80.4
Th^{232}	*200.0**	*190.0**	79.0
Pu^{239}	208.9	198.5	80.1
Pu^{241}	210.8	200.3	80.2

** The fission energies/exergies attributed to fertile isotopes - U^{238}, Th^{232} - are those corresponding to the fissile isotopes - respectively Pu^{239}, U^{233} - that can be produced from them by neutron capture. It is therefore assumed that the energy potential of a nuclear fuel including fertile material is the one obtained by entirely transmuting the latter in fissile material that is then burned in the reactor itself or in another reactor.*

Table 2.1 shows the typical values of the nuclear fission exergy of the nuclides that are most important for nuclear applications. It can be observed that the fission exergy for uranium-235 (U^{235}) is typically of the order of 193 MeV, while for plutonium-241 (Pu^{241}) the fission exergy exceeds 200 MeV.

The values of fission exergies shown in the above table have been used to calculate the specific exergy of natural uranium (e_U) and thorium (e_{Th}). The specific exergy of natural uranium can be defined as the maximum theoretical work that could be obtained in splitting up (fission) all the U^{235} nuclei and Pu^{239} nuclei resulting from the conversion of the U^{238} nuclei that are present in 1 kg of natural uranium.

Taking into account the mass isotopic fraction of natural uranium (99.284% U^{238}, 0.711% U^{235} and 0.005% U^{234}), the calculated specific exergy of natural uranium becomes 80.4 TJ/kg.

Following the same approach, the specific exergy of natural thorium (composed entirely of isotope Th^{232}) is found to be 79.0 TJ/kg.

The specific exergy values for uranium and natural thorium calculated this way are in good agreement with the values that can be found in the international literature [7].

In the nuclear domain, the energy released by a nuclear fuel during its stay in the reactor is often

measured in Gigawattday (GWd; 1 GWd = 86.4 TJ).

The interest of this measuring unit lies in the fact that the complete fission of one kg of natural uranium (under the above assumptions) liberates 0.93 GWd, a quantity of energy very close to 1 GWd.

2.2. Global nuclear exergy resources

The concept of exergy allows us to assess the global nuclear resources in a consistent manner, independently of the technology chosen for the exploitation of these resources. It is thus possible to estimate more correctly the potential work that could theoretically be obtained from a specific resource.

Specific exergy values calculated in the previous paragraph are therefore used to assess the global resources of uranium and thorium from an exergy perspective. It is worth noting in this context that nuclear fuels, contrary to fossil resources, have no other valuable use than for electricity production.

According to [8], identified resources of uranium that could be extracted at a cost below 130 $/kg amount to 5.47 millions of tons, representing a total exergy of about 0.44 10^{12} TJ.

If not yet discovered uranium resources (but that may reasonably be suspected to exist) are considered, the amount of resources raises up to 10.54 millions of tons, representing approximately an exergy of $0.85 \cdot 10^{12}$ TJ.

According to [9], unconventional uranium resources (mainly uranium contained in phosphate) amount to approximately 22 millions of tons, representing an additional total exergy of $1.77 \cdot 10^{12}$ TJ. If one takes into account the uranium contained in ocean waters (approximately 3 ppm concentration), the theoretical resources of uranium could take up to 4 Gt, which corresponds to $321.7 \cdot 10^{12}$ TJ.

As far as natural thorium is concerned, according to [8], the total resources, including those who have not yet been discovered, amount to 6.08 millions of tons, representing a total exergy of $0.48 \cdot 10^{12}$ TJ.

Table 2.2 summarizes the above values of World uranium and thorium exergy resources.

Table 2.2 Uranium and thorium World exergy resources.

URANIUM	
Identified resources	$0.44 \cdot 10^{12}$ TJ
Not yet discovered resources	$0.85 \cdot 10^{12}$ TJ
Unconventional resources	$1.77 \cdot 10^{12}$ TJ
Oceans	$321.7 \cdot 10^{12}$ TJ
THORIUM	
Total resources	$0.48 \cdot 10^{12}$ TJ

3. Open cycle for light water reactors

The open ('once-through') cycle for light water reactors (LWR) is the reference fuel cycle that is operated in most countries of the world today. This cycle has reached full commercial maturity in all its major steps. Among the other nuclear fuel cycles that have also reached commercial maturity, we can mention the LWR cycle with mono-recycling of plutonium and the fuel cycle for heavy water reactors (HWR).

In the LWR open cycle, three main phases can be distinguished: fuel cycle front-end, combustion in the nuclear reactor, and fuel cycle back-end.

The fuel cycle front end consists of the uranium extraction step (ore: uraninite, pitchblende), the treatment and chemical conversion of the "yellow cake" (U_3O_8), the enrichment in fissile isotopes and the manufacture of fuel elements ready to use in the reactor core.

The fuel cycle back-end comprises the temporary spent fuel storage, spent fuel reprocessing, and permanent storage of radioactive waste. Figure 3.1 schematically shows the main steps of the open cycle of a LWR.

Uranium is generally found in nature as uranium oxides (combined UO_2 and UO_3; 50-85 percent U_3O_8), but it must first be extracted from the ore. Uranium is usually extracted, using techniques similar to those employed in underground or open cast mining. The uranium extracted from mines is weakly concentrated. It must therefore be treated in a specialized plant (mining & milling steps). The uranium leaving the treatment plant is in the form of a powder of sodium or ammonium biuranate ('yellow cake') containing approximately 96 weight % of U_3O_8

oxide. The 'yellow cake', must be purified and above all transformed into a gaseous compound - uranium hexafluoride (UF_6) - that is necessary for the next enrichment step. This conversion is performed by chemical processes.

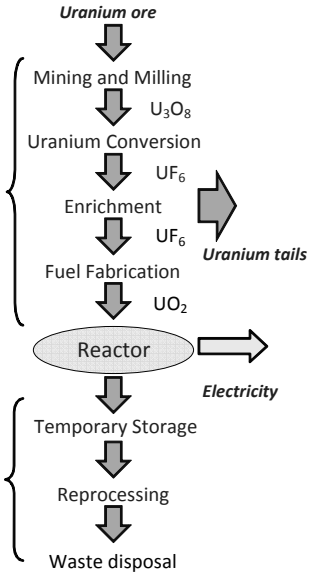

Figure 3.1. Open cycle for light water reactors.

At the only exception of heavy water reactors, all other reactors in service today require uranium enriched in its fissile component (i.e. uranium-235 in the case where uranium is used as fuel).

Enriching uranium requires separating the two isotopes, U^{235} and U^{238}. Because these isotopes are chemically identical, this cannot be done using chemical processes. The two main industrial processes that are used today to enrich uranium are the gaseous diffusion and the gaseous centrifugation.

The centrifugation enrichment technique requires an amount of energy of an order of magnitude lower than for gaseous diffusion and is thus becoming increasingly widespread [10].

In the LWR, uranium is used in the form of uranium dioxide (UO_2). With this oxide it is possible to reach temperatures significantly higher than with the uranium metal form. The manufacture of fuel elements consists of three major phases: chemical conversion of the enriched uranium hexafluoride in UO_2 oxide powder, manufacture of UO_2 pellets, and manufacture and assembly of the fuel rods.

The fuel unloaded from a reactor is highly radioactive, due essentially to the fission products and minor actinides. After its extraction from the reactor core, the spent fuel is stored in situ for a period of around one year in a fuel-cooling pool and then routed to the reprocessing plant (if this step is planned) or to another external temporary storage site (pending final storage in a stable geological formation)

4. Exergy analysis of the open cycle for LWR

The approach followed in this study is based on the calculation of material and energy fluxes associated with the main steps of the open cycle. Analysis of these fluxes helped to evaluate the corresponding exergy flows that are finally used to establish the exergy balance of the cycle.

4.1 Mass balance of LWR open cycle

The assessment of the quantity of uranium ore to extract and process in the phase of "mining & milling" has been made based on a natural U^{235} mass fraction of 0.176 %, which represents the average fraction found in U.S. mines, and on a muck/ore ratio of 5:1 [11]. Uranium losses in these two steps are estimated at 5%.

Uranium losses in the chemical conversion step are assumed to be equal to 0.5%.

A particular attention has been focused on the enrichment step because it produces a considerable amount of "waste" in the form of depleted uranium ("Uranium tails" in figure 3.1).

Increasing the mass fraction of U^{235} (which is 0.711% in natural uranium) is an indispensable step when ordinary water is used as neutron moderator. The enrichment leads to a considerable improvement of the neutron economy of a thermal reactor with obvious advantages in terms of the reactor design, operations and choice of the structure materials.

Regardless of the isotope separation technique used to enrich the uranium (see previous

paragraph), a stream (N) of natural uranium hexafluoride enters the separation cascade and two streams leave it, one of uranium hexafluoride enriched in U^{235} (P), and the other of depleted uranium hexafluoride (T) (see figure 4.1).

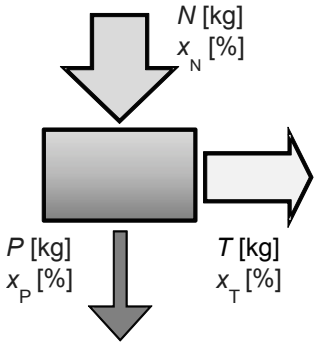

Figure 4.1.Mass balance for nuclear fuel enrichment.

If x_N, x_P and x_T respectively denote the corresponding fractions of U^{235} in these different streams, the two following uranium mass balances can be written:

$$N = P + T \quad (4.1)$$

$$x_N N = x_P P + x_T T \quad (4.2)$$

Therefore:

$$N = P \frac{x_P - x_T}{x_N - x_T} \quad (4.3)$$

As an illustration, using the formula (4.3) it can be calculated that the production of 1 kg of uranium enriched at 4% requires the processing of approximately 8 kg of natural uranium (with a residual enrichment in the depleted stream of 0.25%).

In order to calculate the needs in enriched uranium of a pressurized water reactor (PWR), we need to know the burn-up rate, that is the heat released by fission during the stay of the fuel in the reactor core. The burn-up rate is typically expressed in the nuclear domain in GWd/ton of enriched uranium.

Based on a known average burn-up rate, the annual need in enriched uranium for a nuclear power plant of given power can be calculated by the following relation [12]:

$$P_{NPP,\,a} = \frac{P_e \cdot L_F \cdot 365}{\varepsilon \cdot B} \quad (\mathrm{tU_{enriched}/yr}) \quad (4.4)$$

where P_e is the installed electrical power (GWe) of the nuclear plant, L_F its annual load factor, ε its average thermal conversion, and B the average burn-up rate of the fuel unloaded from the reactor core.

By substituting relation (4.4) in relation (4.3), we get a very useful formula for our study, which allows us to calculate the annual needs in natural uranium of a reactor of known enrichment and burn-up rate:

$$N_{NPP,\,a} = \frac{x_P - x_T}{x_N - x_T} \cdot \frac{P_e \cdot L_F \cdot 365}{\varepsilon \cdot B} \quad (\mathrm{tU_{nat}/yr}) \quad (4.5)$$

As a guideline, a PWR of the third generation such as the European Pressurized Reactor (EPR), with a net installed power of 1.65 GWe, a load factor of 0.92, a thermal efficiency of 36.7% and a burn-up rate of 65 GWd/tU [13] will theoretically require 239.5 t of natural uranium per year (under the assumption of a 5% fuel enrichment and a residual U^{235} content fraction in the tails of 0.25%).

With the same assumptions, the production of 1 TWh of electric power will require an installed power of 124.1 MWe (with a load factor of 0.92) and therefore a theoretical annual need of 18.0 t of natural uranium, not taking into account the uranium losses in the different purification/transformation processes. If we consider typical values [10] for losses during the steps of extraction and processing of uranium ores (5%), conversion (0.5%), enrichment (0.5%) and manufacturing of fuel elements (1%), we arrive at a need of 19.4 t of natural uranium/TWhe.

The burn-up rate is limited by technical and nuclear reactor safety constraints. After reaching the chosen burn-up level, the nuclear fuel is unloaded from the reactor core. The content in U^{235} of the irradiated fuel is of course lower than that of the freshly loaded fuel, but still close to the natural enrichment, or even slightly higher (the U^{235} fraction in irradiated fuel is typically of the order of 0.7%).

But part of the U^{238} has been transmuted in Pu^{239} and successively burnt in the reactor core (conversion process). The thermal reactor

conversion factor is the ratio between the Pu^{239} nuclei that are produced and the U^{235} nuclei that are splitted-up in the nuclear fuel. This factor is typically of the order of 0.75 for a PWR (between 0.7 and 0.8 for modern PWR). With this value of the conversion factor, and taking into account the residual enrichment of the spent fuel (0.7%), a simple mass balance gives us the final composition of the spent fuel: to produce 1 TWhe, 123.3 kg of nuclear fuel must be burned, i.e. 75.2 kg of U^{235} and 48.1kg of Pu^{239}.

Table 4.1. Mass balance of an EPR open cycle (for a production of 1 TWh_e).

	Phase	Quantity	t U
1	Mining	65'952 t rocks 10'992 t U ore 54'960 t waste	19.35
2	Milling	21.67 t U_3O_8	18.38
3	Conversion	27.05 t UF_6	18.29
4	Enrichment	2.61 t UF_6 (enr.) 24.30 t UF_6 (tails)	1.77 16.43
5	Fuel fabr.	1.98 t UO_2	1.75
6	Power Plant	1.98 t UO_2	1.75
7	Waste disp.	1.84 t UO_2	1.62

The spent fuel therefore contains around 1.6 t of uranium and plutonium (in first approximation), the remainder being transuranic elements and fission products.

Table 4.1 shows the mass balance of an EPR open cycle under the above assumptions.

4.2 Energy balance of LWR open cycle

Based on the mass balance established in the previous paragraph, the energy balance of the EPR open cycle was calculated using data available in the international literature [10,11,14].

For the front-end steps of the open cycle, the values supplied in the study of Chapman were adopted, except for the fuel enrichment step, for which the ORNL values contained in the [10] study have been considered as more representative of the current status of the technology (centrifugation).

For the back-end part of the fuel cycle, the energy requirements were estimated on the basis of the [11] study.

A very important parameter for our study, because it is directly linked to the energy needed for the enrichment, is the isotopic separation work (*SW*). The prime interest of the separation work concept is the fact that it is independent of the enrichment process used.

Without going into the details of the definition of the isotopic potential, the isotopic separation work is given by the following relation [15]:

$$SW = P\cdot V_I(x_P)+T\cdot V_I(x_T)- N\cdot V_I(x_N) \qquad (4.6)$$

where $V_I(x_P)$, $V_I(x_T)$ and $V_I(x_N)$ are the isotopic potentials associated to the enriched, depleted and natural uranium streams respectively.

The general expression of the isotopic potential is the following:

$$V_I(x) = (2x-1)\ln\left(\frac{x}{1-x}\right) \qquad (4.7)$$

The isotopic separation work is expressed in Separation Work Units (SWU). If *P*, *T* and *N* are given in kg, the isotopic separation work is expressed in 'kg SWU' (or simply SWU).

Under the assumptions of a fuel enrichment of 5% and a residual U^{235} content fraction of 0.25% in the tails, and taking into account the streams of uranium found in the previous paragraph, one can calculate that the isotope separation work required to meet the amount of enriched uranium needed to produce 1 TWhe is equal to 13'992 kg SWU.

Table 4.2 shows the electric and thermal energies required for the different steps of a PWR open cycle.

Table 4.2 Electric and thermal energy needs for the open cycle of a PWR [10,14].

	Phase	Unit	Electricity [GJ]	Fuels [GJ]
1	Mining	t ore		1.21
2	Milling	t ore	0.099	0.828
3	Conversion	tU	57.6	194.4
4	Enrichment	SWU	0.936	0.021
5	Fuel fabr.	tU	173	115
6	Waste disp.	tU	6.92	4.6

4.3 Exergy balance of LWR open cycle

The exergy balance of a PWR open cycle is established by applying to the calculated mass streams the values of the specific exergies listed in Table 2.1. For the different stages of the fuel cycle, it is assumed that the exergy needs are equal to the energy ones. This assumption implies that Carnot factors are supposed to be equal to 1 for both the electrical and fossil energies (it is a rough approximation for fossil fuels but its impact on the cycle exergy streams is negligible as demonstrated below).

Figure 4.2 shows the exergy requirements for an EPR open cycle.

The exergy that is introduced in the cycle in the form of natural uranium is about $1.56 \cdot 10^6$ TJ. The total exergy associated with the various processes of the nuclear fuel cycle (and considered destroyed in these processes) is however much lower, i.e. 42 TJ. It is thus clear that the processes of the cycle have only a negligible impact on the global exergy streams. However, it is important to emphasize that the exergy stream associated with the depleted uranium is the largest exergy output stream of the cycle, with a value of $1.32 \cdot 10^6$ TJ.

The exergy efficiency of LWR has already been studied in detail and several articles can be found on the subject in the scientific literature, in particular for a boiling water reactor [1] and, above all, for a pressurized water reactor [2] with a reactor exergy efficiency evaluated at 34.4%. These analyses have however been limited to the calculation of the exergy value of the heat generated in the reactor core. This article suggests that, considering the global exergy stream of the whole fuel cycle, the exergy efficiency of such reactors is much lower than the one calculated so far.

According to figure 4.2, it is clear that there are different ways to define the PWR exergy efficiency. This issue was already exposed and analyzed in detail in [16].

The approach that is defined below is a general approach that can be applied to any nuclear fuel cycle.

In the definitions of the exergy efficiency that will be discussed below, the exergy associated with the uranium losses in the various processes of the fuel cycle have been subtracted.

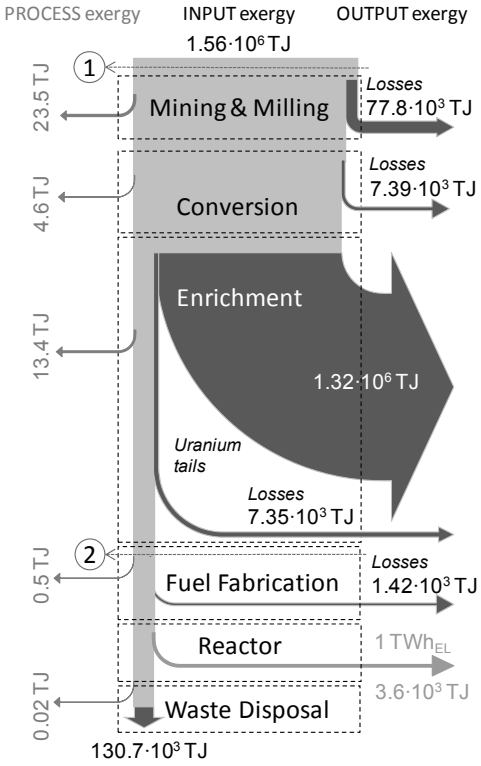

Figure 4.2. Exergy balance of a PWR open cycle (not at scale).

A first definition of the exergy efficiency of a nuclear fuel cycle is that considering the useful exergy coming out of the system (minus the one required by the processes of the cycle itself) reported to the total exergy that enters the system in the form of the specific exergy of the fuel. The efficiency thus defined may be calculated by the following formula:

$$\eta^I = \frac{E_{el,OUT} - E_P}{E_{1,IN}} \tag{4.8}$$

where $E_{el,OUT}$ is the exergy coming out of the reactor in the form of electrical energy, E_P is the exergy that is consumed by the processes of the cycle itself, and $E_{1,IN}$ the exergy associated with the natural uranium necessary for the cycle.

With the data shown in figure 4.2, η^I takes the value 0.23%.In the above approach, the depleted uranium resulting from the enrichment step is

implicitly treated as "waste" but figure 4.2 clearly shows that the associated outgoing exergy stream is the most important of the cycle. Actually, this depleted uranium could be used as fuel in fast reactors or, what is most interesting in the context of this article, in molten salt reactors (MSR).

If the depleted uranium is considered as recoverable fuel, a second definition of the exergy efficiency is the one considering as exergy input only the exergy associated with the nuclear fuel after the enrichment step (number 2 in figure 4.2). The expression of the exergy efficiency corresponding to this second definition becomes:

$$\eta^{II} = \frac{E_{el,\,OUT} - E_P}{E_{2,IN}} \tag{4.9}$$

where $E_{2,IN}$ is the exergy associated with the nuclear fuel after the enrichment step.

With the data shown in figure 4.2, η^{II} takes the value of 2.51%. In the two approaches presented above, the exergy content of the irradiated fuel is also considered unrecoverable. In fact, the uranium and plutonium of the irradiated fuel can be recovered and reused for the manufacture of MOX fuel, a mixed nuclear fuel containing both enriched uranium and plutonium [10].

The mono-recycling of the plutonium of the irradiated fuel makes it possible to reduce the needs of a PWR by 12.2% according to [17], but at the cost of a considerable increase in the complexity of the fuel cycle. In addition, the exergy cost of the reprocessing of the irradiated fuel is not well-known yet. Given this uncertainty, it has been decided not to consider this possible recovery in the context of this article.

The definition of the exergy efficiency most representative of the way the uranium resources is efficiently use is the first of the two given above, because it provides a consistent frame-work for comparing the different nuclear fuel cycles. It will be seen in the next paragraph that it is possible to achieve an exergy efficiency of the order of 40-45% with the closed fuel cycle of the molten salt reactors.

5. Generation IV selected fuel cycle

To assess the real exergy potential of the uranium and thorium resources, we chose to analyze the nuclear fuel cycle of the molten salt reactors (MSR).

5.1 Molten salt reactors

The MSR had been studied during the 1960s and 1970s. A 8 MWth reactor prototype had been in service for several years in the United States [17]. Figure 5.1 shows a simplified schematic drawing of a MSR as it is developed as part of the 'Generation IV' international reactor development program [18].

The main thermodynamic characteristics of the selected MSR can be summarized as follows: power of 1000 MWe and thermal efficiency in a range of 44-50% with a temperature of the molten salts at the output of the reactor core of 700 ° C (can be raised up to 850 ° C to produce hydrogen through thermo-chemical processes). The heat transfer fluid is helium used in a classic Brayton cycle. From a neutron point of view, it is a thermal, or epithermal, spectrum reactor moderated with graphite.

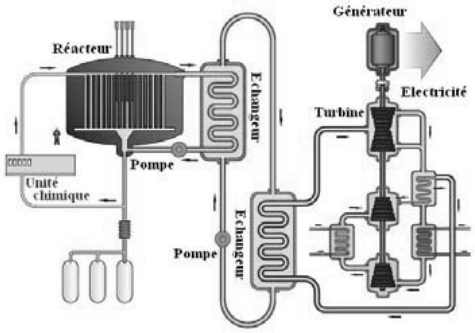

Figure 5.1. Simplified schematic drawing of a molten salt reactor (ref. [18]).

The MSR are extremely interesting especially with regard to their associated fuel cycle. In fact, they could theoretically be used in the context of a completely closed fuel cycle that could be fed either by uranium or by thorium (therefore optimal from the viewpoint of a better use of the totality of the world nuclear resources). This

closed fuel cycle can moreover be tailored to the efficient burn-up of plutonium and minor actinides.

A very innovative molten salt reactor concept is being developed by EdF under the name 'AMSTER' [19]. This is a MSR designed to minimize the quantity of very high activity waste (especially transuranic elements, with a production rate of the order of a few grams per produced TWhe). This reactor can use both uranium (in the form of depleted uranium) and thorium as nuclear fuel.

An interesting aspect of the MSR in general, and of the AMSTER concept in particular, is that it allows to encompass most of the operations of the front-end and back-end steps of the fuel cycle in the nuclear plant itself (resulting in a considerable simplification of the fuel cycle). The online chemical processing unit actually enables to cover part of the front-end operations (uranium salt enrichment) of the fuel cycle and at the same time, of the back-end step of the same cycle (extraction of the fission products and transuranic elements with in situ vitrification). This means that the reactor can be fed directly with natural uranium (in the form of UF_6 uranium hexafluoride), without prior enrichment.

A MSR such as AMSTER would require a mixture of 50 kg of natural or depleted uranium and 50 kg of thorium to produce 1 TWhe (once loaded into the reactor core and without taking into account the fuel cycle losses). This represents a huge gain in terms of efficiency of use of these natural resources.

To better quantify this gain using the exergy efficiency definitions proposed in the preceding paragraph, the following assumptions were made.

For the extraction, processing and chemical conversion steps of the uranium and thorium ores, the same values of the specific needs in electrical energy and fossil fuels as for the open cycle of the EPR are used. For all the other stages of the fuel cycle there are no data available in the literature, due to the fact that this concept of reactor has not been realized yet. Given their low importance, we chose to ignore in the present study the exergy needs for the in situ reprocessing of uranium and thorium (only the conversion exergy needs are explicitly calculated).

As far as the thermal efficiency is concerned, a value between 45% and 47% has been considered reasonable taking into account the temperatures that could be reached in the Brayton cycle (of the order of 700-850 °C),

The mass balance is established making the assumption that the mass fractions of uranium and thorium in the corresponding ores are identical (0.176 %), with a muck/ore ratio of 5.

Exergy losses associated with the extraction and ore processing steps are taken equal to 5%.

Exergy losses associated with the in situ reprocessing operations are estimated at 2%. This represents exergy losses due to the unavoidable losses of uranium and thorium in the cycle operations.

Figure 5.2 shows the exergy balance for the closed cycle of a MSR of AMSTER type.

According to this figure, the exergy efficiency (as firstly defined in the previous paragraph) takes a value of 42.0%.

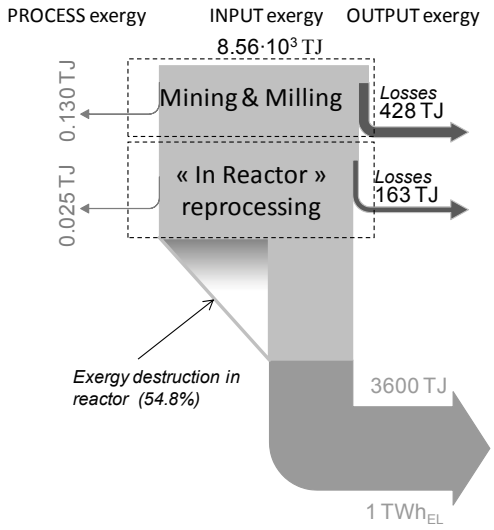

Figure 5.2 Exergy balance of the AMSTER reactor concept.

A closed cycle used in the context of a MSR of the AMSTER type can thus use the exergy potential of the uranium and thorium resources with an efficiency that exceeds 40%. This represents a considerable improvement

compared to the exergy performance obtained with the EPR open cycle (0.23%, see above).

Conclusions

The exergy approach in nuclear fuel cycle analyses allows the evaluation of the true exergy potential of the nuclear fuels, and the use made of it in different types of nuclear facilities, in a coherent way independent of the reactor technologies used. Thanks to this approach, we have demonstrated that the open cycle of PWR does not exceed an efficiency of 0.23% in the use of the exergy potential of the uranium ore. There exist however innovative cycles (such as the closed cycle of MSR of the AMSTER type) that could reach much higher efficiency values in the utilization of the uranium and thorium resources. Such cycles could utilize up to 42% of the exergy potential of the nuclear fuels. The analysis performed and presented in this article is only a first step towards a systematic exergy assessment of the nuclear fuel cycles. The preliminary results presented allow a first evaluation of the exergy potentials of uranium and thorium. Future analyses will better quantify the exergy streams in the different phases of the various nuclear fuel cycles and thus refine the results of this study, extending it to other fuel cycles.

References

[1] Dunbar, W., Moody, S., and Lior, N., 1995, Exergy analysis of an operating boiling-water-reactor nuclear power station, Energy Conversion and Management, 36(3), pp. 149-159.

[2] Durmayaz, A. and Yavuz, H., 2001, Exergy analysis of a pressurized-water-reactor nuclear power plant, Applied Energy, 69(1), pp. 39-57.

[3] Rosen, M. A., 2001, Energy- and exergy-based comparison of coal-fired and nuclear steam power plants, Exergy, 1(3), pp. 180-192.

[4] Borel, L., and Favrat, D., 2010, Thermodynamics and Energy systems analysis, Vol.1, EPFL Press, Lausanne.

[5] Cleveland, C.J., 2004, Encyclopedia of Energy, Vol.2, pp. 593-606, Elsevier, Boston.

[6] Duderstadt, J.J. and Hamilton, L.J., 1976, Nuclear Reactor Analysis, John Wiley & Sons, New York, Chapter 2.

[7] Hermann, W., 2006, Quantifying global exergy resources, Energy, 31(12), pp. 1685-1702.

[8] OECD/NEA-IAEA, 2008, Uranium 2007: Resources, Production and Demand', Nea No. 6345, Paris.

[9] OECD/NEA-IAEA, 2006, Uranium 2005: Resources, Production and Demand', Nea No. 6098, Paris.

[10] Dones, R., 2003, Ecoinvent-Bericht No.6 - Teil VII: Kernenergie, Paul Scherrer Institut, Villigen, Switzerland.

[11] Spreng, D.T., 1988, Net-Energy Analysis and the energy requirements of energy systems, Praeger, New York.

[12] Deutch, J. and Moniz, E., 2003, The future of nuclear power: an interdisciplinary MIT study, Massachusetts Institute of Technology, Cambridge, USA.

[13] Kay, J., EPR design description, 2005, Framatome ANP Inc., USA.

[14] Chapman, P.F., 1975, Energy Analysis of nuclear power stations, Energy Policy, 3(4), pp. 285-298.

[15] Ligou, J., 1986, Elements of nuclear engineering, Harwood Academic Publishers, Chur, Switzerland.

[16] Haldi, P.A., and Favrat, D., 2006, Methodological Aspects of the definition of a 2 kW society, Energy 31 (15), pp. 3159-3170.

[17] OECD/NEA-IAEA, 2001, Trends in the Nuclear Fuel Cycle', Paris.

[18] 'A Technology Roadmap for Generation IV Nuclear Systems', U.S. NERAC/GIF 2002 report.

[19] Vergnes, J, and Lecarpentier, D., 2002, The AMSTER Concept (Actinide Molten Salt TransmutER), Nuclear Engineering and Design, 216(1), pp. 43-67.

Exergy Life-Cycle Analysis of the Uranium Cycle. Part 1: from Uranium Ore to Nuclear Fuel

Giuseppe Orsini, Enrico Sciubba

Mechanical and Aeronautical Engineering Department, University of Roma 1 La Sapienza, Italy

Abstract: This paper presents an exergy analysis spanning the upstream processes of the Uranium cycle, describing the production of the nuclear fuel used in commercial *light water reactor* (*LWR*) for electricity generation. Starting from the calculation of the specific exergy content of the pristine ore extracted from the mine, the exergy consumption in every step of the entire cycle, from Uranium ore to nuclear fuel, is computed. The cumulative exergy content of a unit of nuclear fuel is calculated by accounting for the direct exergy consumption (thermal or electrical exergy delivered from sources external to the cycle), for the exergy used for the construction and installation of the equipment and for the exergy associated with process materials (for example chemicals). The analysis follows step by step the exergy destruction of the process that takes the Uranium mineral through the phases of mining, milling, refining of yellow cake, conversion to UF_6, enrichment, fuel fabrication, reclamation of the mining area and reconversion of depleted Uranium. Currently, the environmental remediation processes analyzed in this paper (reclamation of the mined area to green field condition and reconversion of the depleted Uranium) are not included in the normal operational practice. Since they are though included in any "sustainable" nuclear scenario, they are considered here as well. The exergy analysis performed in this study leads to the identification and quantification of some critical steps of the upstream part of the Uranium cycle (i. e. mining operations dependence on deposit grade, or enrichment processes), and measures the exergy "cost" related to the production of nuclear fuel. The results are extensively discussed and the conclusions indicate that a re-evaluation of the degree of sustainability of nuclear fission technology is in order.

Keywords: Uranium, Exergy Life-Cycle, Nuclear exergy, Fuel cycle, Cumulative Exergy Consumption.

1. Introduction

This study deals with the fuel cycle of the most common type of nuclear technology, representing about the 86% of the actual installed power [7], namely, the *light water reactor* (*LWR*). Since only 27% of the spent fuel is reprocessed worldwide, the *once-through* mode strategy is considered here (Fig. 1.). The first part of this paper reports a literature review about the energy requirements of the upstream processes of the Uranium cycle, i. e. the production of nuclear fuel. Subsequently, a model for the evaluation of the specific exergy of Uranium, including its nuclear term, is presented. These data are the starting point for the exergy analysis and the evaluation of the *cumulative exergy consumption* related to the production of a unit of nuclear fuel.

2. Upstream processes of the Uranium cycle

Fig. 1. shows the upstream processes of the Uranium cycle that are analyzed in this paper (mining, milling, refining yellowcake, conversion, enrichment, fuel fabrication). With the goal of evaluating the degree of sustainability of commercial nuclear chains, environmental remediations related to the management of mining tails and depleted Uranium are also presented here.

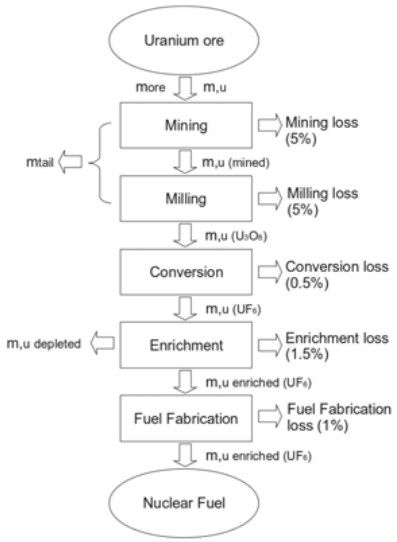

Fig. 1. Uranium mass balance for the upstream processes for a LWR in once-trough mode.

Corresponding Author: Giuseppe Orsini, Email: giuseppe.orsini@uniroma1.it

Currently, these processes are only theoretical, since no industrial practice is enforced to isolate the upstream waste from the biosphere.

2.1. Uranium mining and milling

Uranium is extracted from either surface (*open pit*) or underground mines, depending on the depth at which the vein is found. In 2007, Uranium production was for 37.7% by underground, 23.7% open pit, 27.7% In-Situ Leaching and 8,4% co-product/by-product mining techniques [8]. The raw ore is sent to a milling plant in which it is crushed, ground and leached (usually by Sulfuric Acid) to separate the precipitated Uranium from the waste rock. The output of this process is a solid with a concentration of about 80% of *Triuranium Octoxide* (U_3O_8), which is called *yellowcake* because of its characteristic color.

The mass of mineral that must be extracted in a mine and treated in milling plant to obtain 1 kg of Uranium depends obviously on the *ore grade* (*G*) of the pristine ore, usually expressed as weight percent of U_3O_8. Fig. 2 shows the distribution of the world *Reasonably Assured Resources* (*RAR*) [8] and of the main Uranium deposits classified by exporting country [9], as a function of the ore grade: the world-average value is about 0.150%.

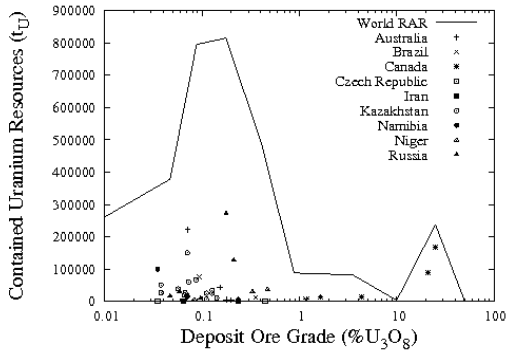

Fig. 2. Distribution of known Uranium resources as a function of ore grade.

The *extraction yield* (*Y*), defined as the ratio between the mass of Uranium actually extracted and the mass of Uranium in the treated rock, does not depend linearly on the ore grade for several reasons: the mining losses increase and the milling and extraction efficiencies decrease for lower grade mineral. As shown in Fig. 3, the relationship between *Y* and *G* used in this study [11] seems to be globally more conservative than the actual values related to 41 mines published in the "*Uranium Red Book*" [9].

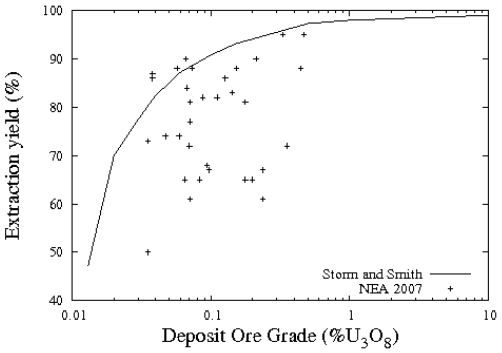

Fig. 3. Uranium extraction yield as a function of the ore grade.

The mass of ore (m_{ore}) that must be extracted to obtain the Uranium required in the upstream part of the nuclear cycle (m_U) can be calculated if the mine characteristics are known:

$$m_{ore} = \frac{m_U}{0.848 \cdot Y \cdot G}, \qquad (1)$$

where 0.848 is the mass ratio between Uranium and Triuranium Octoxide.

Energy requirement for Uranium mining and milling processes are available from an input/output based hybrid life cycle assessment for the US [10]: 1055 MJ for mining and 1065 MJ for milling one tonne of Uranium ore. These values are in sufficient agreement with other life-cycle analyses reported in the available literature [1,4,10,11], and represent the most conservative values (see Table 1).

Table 1: Review of literature data for mining and milling energy requirements.

Reference	E_{mining} (GJ/t_{ore})	$E_{milling}$ (GJ/t_{ore})
[10]	1.06	1.06
[1]	1.21	1.22
[4]	1.06	1.06
[11]	1.06	1.27

The energy requirements shown in Table 1, expressed as energy per tonne of ore, are in practice independent from mine type and Uranium ore characteristics. If energy needs are instead reported to the Uranium mass actually treated in mining process, the dependence on the grade *G* of the pristine ore is given by (1), as shown in Fig. 4. Reference [10] also distinguishes between energy used for direct consumption (58%), materials (29%) and construction (13%), and reports electricity and fossil fuel consumptions for each item.

2.1.1 Reclamation of the mined area

Mill tails contain the Uranium not extracted due to technical limitations and Uranium decay daughters that pose long term radiological and environmental risk. Reference [11] proposes a theoretical process for restoring the mined area to green field conditions and isolating the mill tailings from the biosphere. The energy requirements of this environmental remediation are estimated to be four times those of mining (4220 MJ/$t_{tailings}$).

Neglecting the mass of chemicals used in the leaching phase of the milling process (about 9%), the mass of the tails that must be neutralized and disposed of can be derived from (1):

$$m_{tail} = m_U \cdot \left(\frac{1}{0.848 \cdot Y \cdot G} - 1 \right). \quad (2)$$

Fig. 4. shows the energy expenditure of mining, milling and reclamation process as a function of the ore grade: low ore grade causes an increase of the energy needs, due to the larger amount of rock mined and milled to obtain the mass of U_3O_8 required by the remaining part of the nuclear cycle.

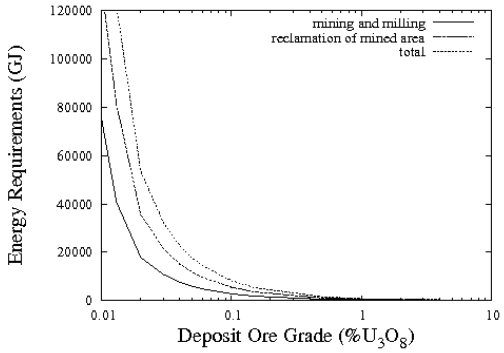

Fig. 4. Energy requirements for mining, milling and reclamation of the mined area per tonne of Uranium leaving the mill, as a function of the ore grade.

2.2 Conversion of yellowcake to UF_6

Uranium in yellowcake (U_3O_8) must be converted through a multi-step chemical process into gaseous *Uranium Hexafluoride* (UF_6) before it can be enriched. Reference [10] considers for this process an energy intensity of 1478 GJ/t_U, in agreement with literature data [1,4,10,11].

In this case, direct consumption is predominant (about 90%), as natural gas represent the main contributor to energy requirements.

2.3 Enrichment

Only a small number of nuclear reactors (i. e. *pressurized heavy water reactor* as the Canadian *CANDU, boiling heavy water reactor* as the Italian *CIRENE or gas-cooled graphite-moderated reactor* as the British *MAGNOX*) use natural Uranium as fuel. Typical light water reactors require enriched Uranium in which the proportion of the fissile ^{235}U isotope is raised to about 3.5%. At present, the main enrichment techniques are *gaseous diffusion* (mainly in the US) and *gas centrifuge* (in Europe and Russia), since *Electromagnetic isotope separation*, *jet nozzle* method and *laser enrichment* methods are still at research stage.

In a simple enrichment process, the feed F of natural Uranium is separated into the product fraction P (*enriched Uranium*) and the waste fraction W (*depleted Uranium*). If x_f is the weight fraction of ^{235}U in the feed (0.71%, for natural Uranium), x_p the weight fraction of ^{235}U in the product flow and x_t the weight fraction of ^{235}U in the waste flow (*tails*), the mass ratio between feed and product and the *separative work unit* (*SWU*) required can be calculated through the following equations:

$$\frac{F}{P} = \frac{x_p - x_t}{x_f - x_t}, \quad (3)$$

$$V_x = (2x - 1) \cdot \log\left(\frac{x}{1-x} \right), \quad (4)$$

$$\frac{SWU}{P} = V_{x_p} - V_{x_t} - \frac{F}{P}\left[V_{x_f} - V_{x_t} \right]. \quad (5)$$

In this study, the most conservative values of the direct energy needs available in the literature have been adopted: 8742 MJ/SWU for gaseous diffusion [10] and 493 MJ/SWU for centrifuge enrichment [5]. Gaseous diffusion has higher direct energy requirements (mainly electricity) than centrifuge enrichment, because this process includes an energy intensive compression of UF_6. Assuming for both types of plant a value of material and construction input of 537 MJ/SWU [10], a world-averaged energy requirement of 4096 MJ/SWU is obtained (gaseous diffusion and centrifuge representing respectively 63% and 37% of the world enrichment capacity).

2.3.1 Conditioning and disposal of depleted UF_6

Depleted Uranium is a waste product of the enrichment process. It contains mainly Uranium isotopes (^{238}U and ^{235}U in a concentration smaller

than in the natural mineral) and it is stored as UF_6 in metal containers placed in underground or surface repositories. Due to the radiological and chemical toxicity of the Uranium, its decay progeny and the health hazard posed by accidental UF_6 leaches, in a nuclear "sustainable" scenario depleted Uranium ought to be removed from the biosphere. Reference [11] describes a theoretical process for the reconversion of the depleted UF_6 (an extremely volatile and reactive gas) into U_3O_8. The energy consumption of this environmental remediation is assumed to be equal to the conversion process requirements (1478 $GJ/t_{Udepleted}$) plus the energy expenditure for conditioning, packaging (102 $GJ/t_{Udepleted}$) and disposal (103 $GJ/t_{Udepleted}$) of the depleted Uranium, for an overall energy demand of about 1683 $GJ/t_{Udepleted}$.

2.4 Fuel Fabrication

After the enrichment process, UF_6 is transported to the fabrication plant where it is converted to *Uranium Dioxide* (UO_2) powder and pressed into small pellets. These pellets are inserted into thin tubes, usually of Zirconium Alloy, to form fuel rods of about 4 m. The rods are then sealed and assembled in clusters of about 100 elements to form assemblies for use in the core of nuclear reactors. Energy requirements from several *LCA* studies for typical light water reactors related to the fuel fabrication process, with or without Plutonium recycling, are shown in Table 2. Data from [1] are expressed in $GJ/t_{Unatural}$, for converting this value to $GJ/t_{Uenriched}$, an enrichment grade of 3-4% of ^{235}U was assumed here.

Table 2: Review of literature data for fuel fabrication energy requirements.

Reference	$E_{fabrication}$ ($GJ/t_{Uenriched}$)	Note
[10]	3789	without Pu recycling
[10]	4461	with Pu recycling
[1]	7200-9600	-
[4]	3791	without Pu recycling
[11]	3791	without Pu recycling

3. Energy analysis of nuclear fuel production

In this paper a typical 1600 MW_e *Generation III*$^+$ light water reactor operating in once-through mode, with a plant efficiency of 33%, fuelled by Uranium enriched to 3.87% (0.20% of ^{235}U in the depleted Uranium) and a nominal *burn-up* of 45 GW_d/t_U (average data for European production, approximated by the *UCTE* - zone as reference [2]), is assumed as a case study. If such a reactor operates for about 32 *full power - years* (i. e. operational lifetime of 40 years with a load factor of 0.80%), its lifetime gross thermal production amounts to 4893 PJ and its fuel requirements to 1258 t_U.

From (3) it is possible to evaluate the *feed/product* ratio for the enrichment phase (*F/P*=7.20) and consequently the mass flow rates in the previously described processes (assumptions about specific mass losses are reported in Fig. 1.). Fig. 5. shows the Uranium mass balance related to the production of nuclear fuel: 1 kg of Uranium in nuclear fuel involves the extraction of about 8.17 kg of Uranium.

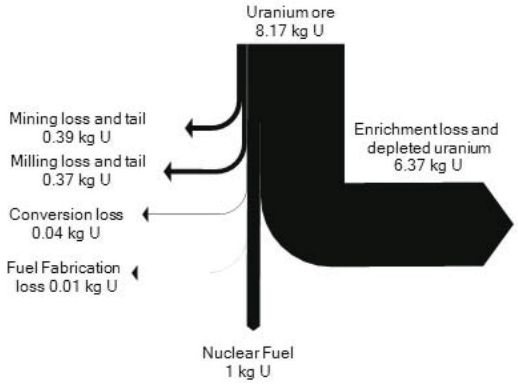

Fig. 5. Uranium mass balance of the upstream part of the Uranium cycle: mass requirements for 1 kg of Uranium in nuclear fuel.

The amount of Uranium extracted in the mining process throughout the life of the nuclear power plant is about 10286 t (the mass of the rock treated is 8686154 kg for *G=0.150%*). Since the lifetime gross electricity production of the reactor is 1615 PJ (1283 GJ_{el}/kg of enriched Uranium in the nuclear fuel), the gross energy content of Uranium *in situ* is about 157 GJ_{el}/kg_U (the values reported in the literature are in the range of 125–149 GJ_{el}/kg_U [1,4,10,11]).

The lifetime energy consumption associated with each process, classified as direct use, materials and construction requirements, are shown in Fig. 6. The enrichment process represents the main culprit for Uranium loss and energy intensity (essentially direct electricity consumption). The overall lifetime energy requirements of the upstream part of the Uranium cycle (including the above described environmental remediation) are therefore 121 PJ, a mere 8% of the lifetime electricity production of the reactor (varying ore grade *G* from 0.02% to 10%, this ratio varies from 38% to 4%).

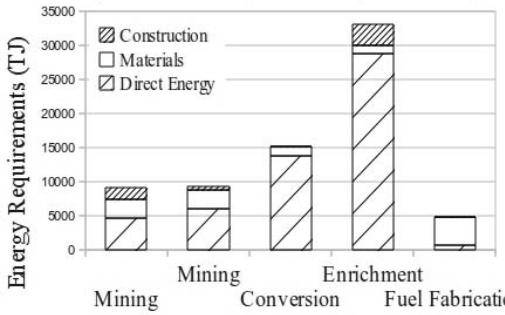

Fig. 6. Lifetime energy consumptions related to the upstream processes of Uranium cycle. Mining and milling values are calculated for ore grade G=0.150% and recovery yield Y=0.931.

4. Exergy of nuclear fuel

The classical definition of exergy is usually obtained neglecting nuclear effects. Obviously, when the purpose is that of calculating the total exergy of nuclear fuel, it is impossible to accept this omission. In this study only the nuclear *fission* cycle is analyzed, and therefore only the exergy of natural *fissile* and *fissionable* elements will be evaluated. Nuclear fission is a reaction in which the nucleus of an atom splits into lighter nuclei (eventually β or γ emitters) and free neutrons, releasing energy both as kinetic energy of the fragments (heating the bulk material where fission takes place) and as electromagnetic radiation. According to [14], the nuclear exergy of fuel is:

$$E^{Nu} = E^{P} + \sum_i E_i^{Ch} + \sum_i E_i^{Rd}, \qquad (6)$$

where E^P is the *nuclear partition exergy*, E_i^{Ch} and E_i^{Rd} are respectively the *chemical* and the *radioactive decay exergy* of the *i*-th fission fragment. In order to estimate the value of E^P for the nuclides involved in nuclear cycles, it is necessary to identify representative nuclear reactions and to evaluate the maximum work obtainable. Due to the high temperature of fission fragments ($650 \cdot 10^9$ K, according to Maxwell - Boltzmann equation, assuming the fission fragment as a perfect gas at thermodynamic equilibrium), the specific nuclear partition exergy of an isotope can be approximated by the fission energy [3]. Fission of the fissile isotope ^{235}U and of the ^{239}Pu product after fast neutron capture by ^{238}U are considered here, obtaining the following values of specific exergy: 75 TJ/kg of ^{235}U and 77 TJ/kg of ^{238}U [6].

The standard chemical exergies of Caesium and Rubidium, two of the main fission fragments, are respectively 3 MJ/kg and 4 MJ/kg [12]. Moreover, the exergy (here conservatively approximated by energy) released by the radioactive decay of a fission fragment during its lifetime τ, with a fission product yield N_0 (ratio between the mass of fission fragment product and the mass of isotope fissioned) and a decay energy Q (keV/decay event) is:

$$e^{Rd} = QN_0[1 - e^{-\lambda\tau}] = QN_0[1 - e^{-6.93}], \qquad (7)$$

Where the lifetime is approximated as 10 half-life: $\tau = 10 \cdot T_{1/2} = 6.93/\lambda$, [14]. For example, ^{137}Cs is a β - γ emitter with a fission product yield of 6.34% and a Q-value of 1176 keV: the decay exergy released is only 5 MJ for 1 kg of fissioned ^{235}U. The chemical exergy and the radioactive decay exergy of fission fragment are therefore negligible if compared to nuclear partition exergy of the fissile or fissionable nuclei.

Since the main Uranium isotopes (^{238}U and ^{235}U) are in a ratio of about 1:140 in the pristine ore and 1:25 in the nuclear fuel, the same value of 77 TJ/kg is considered for both natural and enriched Uranium. For comparison, Uranium standard chemical exergy (about 5 MJ/kg) is much more smaller than its nuclear exergy content [13]. The raw material exergy input of the Uranium cycle can therefore be considered as consisting solely of the nuclear term of the Uranium specific exergy. It is worth recalling that Uranium with more fissile isotopes does not possess a higher nuclear exergy content than natural Uranium. The enrichment of Uranium is therefore a technological need, and moreover it represents the most energy-intensive step in the fuel cycle as well as the most mass-depleting one (see Fig. 5. and Fig. 6.). Theoretically the energy quality of enriched Uranium, considered as the ability to provide useful work, is not higher than that of natural Uranium.

5. Exergy analysis of nuclear fuel production

Reference [10] illustrates the direct consumptions of each process, expressed as the energy contents of the fuels used. If the higher heating values of the energy sources used in the cycle are known, the amount of each fossil fuel can be calculated. The evaluation of the consumed fuel exergy can be done using the values reported in the first column of Table 3 [12-13] and leads to the results shown in Table 4. The production of 1 kg of Uranium in Nuclear Fuel needs an exergy of about 44584 MJ as direct consumption of electricity and fossil fuel.

Table 3: Exergy and Cumulative Exergy Consumption of the energy sources utilized for the production of nuclear fuel [12-13], as a function of the low heating value.

-	Ex/LHV	CExC/LHV
Electricity[1]	1.00	3.400
Heavy Fuel Oil	1.09	1.311
Diesel & Light fuel Oil	1.04	1.248
Gasoline	1.07	1.325
Other Petroleum[2]	1.09	1.311
Natural Gas	1.04	1.060
Propane	1.06	1.331
Bituminous Coal	1.09	1.120

[1] *From bituminous coal, energy efficiency 36%, at place of consumption.*

[2] *The same values of Heavy Fuel Oil is assumed.*

In addition to direct consumption, [10] reports the value of energy requirements for materials and construction (Fig. 6.), divided into electrical and fossil fuel input. In this case, the exergy input are obtained from the energy consumption using the average coefficient of 1.07, representative of the fossil fuels mix shown in Table 3.

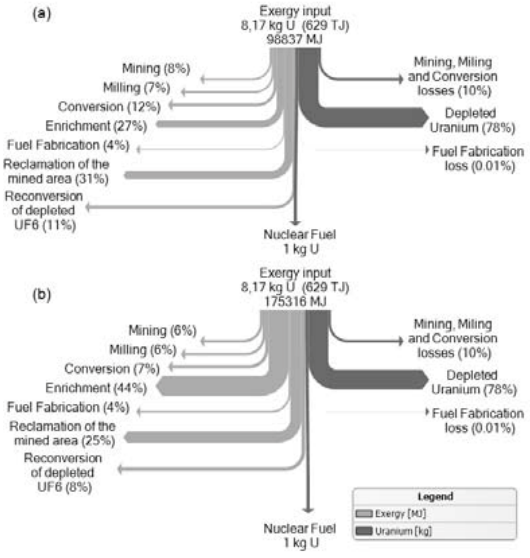

Fig. 7. Grassmann diagram of the exergy needs (a) and the Cumulative Exergy Consumption (b) for the production of 1 kg of Uranium in the nuclear fuel: direct consumptions, materials and construction requirements. Mining and milling values are calculated assuming an ore grade G=0.150% and a recovery yield Y=0.931. The exergy scale for Uranium is shrunk 10^4 times.

Including in this exergy analysis also materials and construction requirements, an overall electricity and fossil fuel exergy input of 98837 MJ per kg of Uranium in nuclear fuel is obtained (see Fig. 7.a.).

6. CExC of Nuclear fuel

The *Cumulative Exergy Consumption* (*CExC*) is defined as the sum of the exergy of natural resources consumed in all the steps of a specific production process [12-13]. In the previous part of this paper the energy and exergy values related to overall electricity and fossil fuel inputs (direct consumptions, materials and construction requirements) are calculated. Electricity and fossil fuel can be considered in turn as intermediate products of their own cradle-to-grave cycle: the amount of exergy spent for their production is certainly higher than their respective exergy contents. CExC-values for the main energy sources directly used in the production of nuclear fuel can be calculated from the second column of Table 3, leading to the results shown in Table 4.

Table 4: Energy, Exergy and CexC-values for electricity and fossil fuel directly consumed during the production of 1 kg of Uranium in nuclear fuel.

-	Energy (MJ)	Exergy (MJ)	CExC (MJ)
Electricity	25029	25029	85097
Heavy Fuel Oil	347	352	425
Diesel & Light fuel Oil	3424	3336	3997
Gasoline	189	193	239
Other Petroleum	228	232	280
Natural Gas	13979	13123	13375
Propane	2.00	1.95	2.46
Coal	2219	2317	2381
Other Energy	0.04	0.04	0.04
TOTAL (MJ)	45416	44584	105798

The exergy input for material and construction is obtained from the values of energy consumption using an average coefficient of 3.40 for electricity [13] and 1.24 for the fossil fuels mix. For a complete determination of the CExC-value related to materials production and construction, an evaluation of the exergy of the non-energetic raw material must be done. Due to lack of data this contribution has been neglected here, also considering that the exergy of non-energetic raw material is usually relatively small in comparison with the fuel exergy input. The cumulative exergy consumption for the production of nuclear fuel, calculated as the sum of specific

input (see Table 5), is about 629560 GJ per kg of Uranium. A Grassmann diagram representing the CExC balance of the upstream processes is shown in Fig. 7.b: because of the high value of nuclear energy, the flow of Uranium has been represented with a different scale than the other exergy inputs.

Table 5: Energy, Exergy and CExC-values for the production of 1 kg of Uranium in nuclear fuel. Mining and milling values are calculated assuming an ore grade G=0.150% and recovery yield Y=0.931.

-	Energy (MJ)	Exergy (MJ)	CExC (MJ)
Uranium in ore	-	629388335	629388335
Mining	7285	7441	10578
Milling	7348	7378	10198
Conversion	12077	11493	12894
Enrichment	26208	26515	77084
Fuel Fabrication	3827	3981	7053
Reclamation of the mined area	29105	30837	43169
Reconversion of depleted UF_6	10527	11192	14341
TOTAL (MJ)	96377	629487172	629563651

On the basis of the above reported calculations, and neglecting other forms of exergy (e.g. physical or chemical exergy), 1 kg of Uranium in nuclear fuel has an exergy content of about 77 TJ. It follows that the CExC index *r*, defined as the ratio between the sum of the exergy of natural resources delivered to the system in all the steps of the production cycle and the net exergy of the output of the system under consideration (Ex_p) can be written as:

$$r = \frac{\sum_i Ex_i}{Ex_p} = \frac{629563651\,MJ}{77 \cdot 10^6\,MJ} = 8.176 \cdot \qquad (8)$$

The result of (8) demonstrates that to obtain 1 Joule of useful exergy from nuclear fuel, about 8.176 J of primary exergy were spent. For comparison, traditional fossil fuels are instead characterized by a cumulative exergy consumption of about $1.06 - 1.33$ times their energy content (in this case, *LHV*), as shown in Table 3.

7. Conclusions

The relatively high value of the Nuclear Fuel CExC index *r*, almost proportional to the Uranium mass requirements, implies the under-utilization of the exergy content of the natural Uranium resource.

Fig. 8 shows the specific exergy cost of the nuclear fuel as a function of the ore grade: in three decades of constantly decreasing *G*, the CExC index *r* has increased only 0.2%.

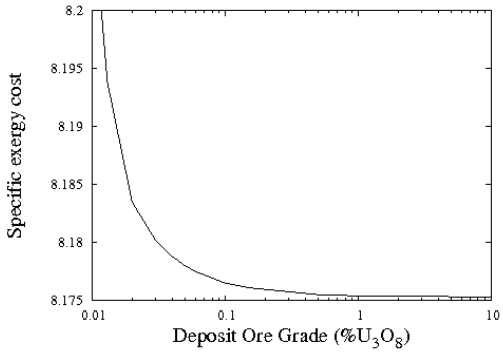

Fig. 8. Specific exergy cost (r) for nuclear fuel production, as a function of the ore grade.

This small variation in the specific exergy cost determines an extra-consumption of exergy of about 1456 GJ/kg_U. Uranium is indeed an *exergy intensive* but also very *exergy expensive* source, due to the need of transforming it from pristine ore to the enriched Uranium fuel rods. Enrichment is the most critical phase of the upstream part of the Uranium cycle, causing about 27% of the overall exergy consumption and 78% of the Uranium loss.

With the aim of improving the utilization of the Uranium resource, reactors with a higher fuel economy must be considered. While the CANDU, one of the most efficient thermal reactors, uses only 1% of the fuel, the Fast Breeder Reactor can utilize 50 - 60% of the Uranium feed. Unfortunately, this technology is not expected to be ready in the next future due to technical and economical problems (as for example safety requirements and security against nuclear proliferation or international terrorism).

At present, increasing Uranium and Plutonium recycle from traditional fuel cycle could improve the efficiency of the nuclear industry: in order to evaluate the benefits of this technological choice from a thermodynamic point of view, the mass balance for a simple reprocessing scheme is shown in Fig. 9 (data of mass flows are taken from reference [2]). Since the CExC-index *r* is almost proportional to the mass of Uranium required by the overall cycle, the reduction of specific natural Uranium consumption from 8.17 kg_U to 7.27 kg_U does not change significantly the conclusions on the depletion of natural resources related to the nuclear industry. It is important to emphasize that the high

value of the index is obtained here by considering depleted Uranium as a waste stream rather than by-product: in this case all mass losses are allocated as exergy "cost" of the main product, the nuclear fuel. If the nuclear industry adopts technologies that use depleted Uranium for commercial power generation (i. e. fast breeder reactor), the value of cumulative exergy consumption will be set to decrease significantly.

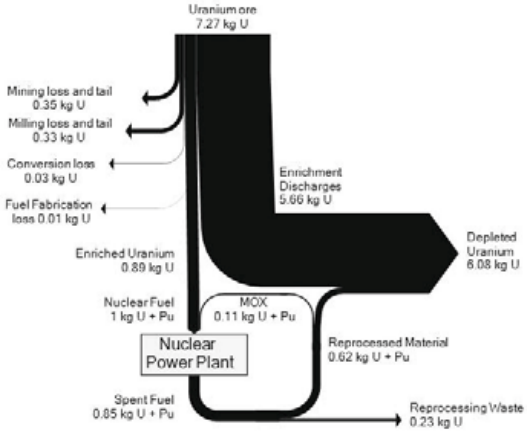

Fig. 9. Uranium and Plutonium balance for a cycle with reprocessing of burnt fuel, mass requirements for 1 kg of fissile in nuclear fuel.

However, even excluding Uranium consumption, the nuclear fuel production consumes more exergy than the other conventional fuels: the production of the Uranium required to generate 1 J of electricity implies an expenditure of about 1.10 J of exergy from fossil fuels (0.70 - 9.84 J, depending on the ore grade). If the demand for nuclear power plants increase in the next future without the discovery of new Uranium deposits, the exhaustion of available cheap resources will lead to the exploitation of low-grade Uranium. It is therefore hardly possible for nuclear energy to deliver a significant contribution to the world energy demand without increase natural resource consumption and, as a result, life-cycle emission of greenhouse gases.

Finally, in order to achieve a "sustainable" nuclear cycle, environmental remediation costs (reclamation of the mined area and reconversion of depleted Uranium) should be fully internalized. The theoretical remediation process proposed here implies an extra-consumption of about 20 - 60% over the nuclear power plant electricity production, depending on the ore grade of the Uranium deposits.

References

[1] Chapman, P., 1975, Energy analysis of nuclear power stations, Energy Policy, 3(4), pp. 285-298.

[2] Dewulf, J., et al., 2007, Cumulative exergy extraction from the natural environment (CEENE): A comprehensive life cycle impact assessment method for resource accounting, Environmental Science & Technology, 41(24), pp. 8477-8483.

[3] Durmayas, A., and Yavuz, H., 2001, Exergy analysis of a pressurized-water reactor nuclear-power plant, Applied Energy, 69(1), pp. 39-57.

[4] ERDA, 1976, A National Plan for Energy Research, Development & Demonstration: Creating Energy Choices for the Future. Volume 1: The Plan, Technical Report, ERDA-76-1, Energy Research & Development Administration, USA.

[5] Fthenakis, V. M., and Kim, H.C., 2007, Greenhouse-gas emissions from solar electric and nuclear power: A life-cycle study, Energy Policy, 35(4), pp. 2549–2557.

[6] Hermann, W., 2006, Quantifying global exergy resources, Energy, 31(12), pp. 1349-1366.

[7] IAEA, 2006, Nuclear power reactors in the world, Reference Data Series No. 2, IAEA-RDS-2/26, Vienna.

[8] IAEA, 2009, World Distribution of Uranium Deposits (UDEPO) with Uranium Deposit Classification, Technical Report, IAEA-TECDOC-1629, Vienna.

[9] OECD/NEA, and IAEA, Uranium 2007: Resources, Production and Demand, Technical Report, NEA No. 6345, Paris-Vienna.

[10] Rotty, R.M., and Perry, A.M., 1975, Net energy from nuclear power, IEA Report, IEA-75-3, Oak Ridge Associated Universities, USA.

[11] Storm van Leeuwen, J. W., and Smith P, 2008, Nuclear power – the energy balance, URL: http://www.stormsmith.nl

[12] Szargut, J., and Morris, D., and Steward, F., 1988, *Exergy analysis of thermal, chemical, and metallurgical processes*, Hemisphere, USA.

[13] Szargut, J., 2005, *Exergy Method: Technical and Ecological application*, Wit Press, UK.

[14] Verkhiver, G., and Kosoy, B., 2001, On the exergy analysis of power plants, Energy Conversion and Management, 42(18), pp. 2053-2059.

Thermoeconomics Meets Industrial Ecology

César Torres[a], *Sergio Usón*[a], *Antonio Valero*[a] *and Alicia Valero*[a]

[a] *CIRCE. Centro de Investigación de Recursos y Consumos Energéticos Universidad de Zaragoza, Zaragoza, Spain*

Abstract: Industrial Ecology involves the transformation of industrial processes from linear to closed loop systems: matter and energy flows which were initially considered as wastes become now resources for existing or new processes. In this paper, Thermoeconomics is presented as a systematic and general approach for the analysis of waste flow integration, which characterizes Industrial Ecology. The formulation is based on extending the thermoeconomic process of wastes cost formation in order to consider their use as input for other processes. Consequently, it can be applied to important Industrial Ecology issues such as identification of integration possibilities and efficiency improvement, quantification of benefits obtained by integration, or determination of fair prices based on physical roots. The capability of the methodology is demonstrated by means of a case study based on the integration of a power plant, a cement kiln and a gas-fired boiler.

Keywords: Exergy, Thermoeconomics, Industrial Ecology, Waste Treatment.

1. Introduction

Industrial Ecology (IE) offers promising opportunities for attaining sustainable industrial development. IE essentially aims at achieving a more rational and balanced industrial organization, trying to imitate the structure and operation of natural ecosystems. Like natural organisms, industrial ecosystems consume material, energy and water flows, transforming them into products and wastes. However there is one important difference among the two: the wastes produced by natural organisms are used as feedstock for other natural systems. As a result of this cyclic process, the net production of wastes in nature is zero. Wastes are a consequence of lack of knowledge. The challenge of industrial systems is thus to identify opportunities for waste reduction by imitating nature (industrial biocenosis). Instead of the *Zoo paradigm* in which any industry must be fed and cleaned up separately, the *Savannah paradigm* must prevail. In the latter, every facility feeds products and wastes from someone else and the natural surroundings act as another active member of the industrial community. In industrial ecology, the conventional linear productivity chain approach is shifted into a materials cycle approach [1]. Unfortunately, the dominant industrial conception has been so far that of the Zoo paradigm, constituting a fundamental factor in the current environmental crisis.

Industrial Ecology principles are materialized through the establishment of eco-industrial parks. These are defined as: "*A community of businesses that cooperate with each other and with the local community to efficiently share resources (information, materials, water, energy, infrastructure and natural habitat), leading to economic gains, gains in environmental quality, and equitable enhancement of human resources for the business and local community*." [2].

Some of the economic and environmental advantages are the following:

- The input costs of raw materials are reduced as waste products from one industry are provided as inputs for another.
- Wastes are converted into products with an associated economic value.
- The waste streams are reduced and hence the disposal costs.
- Enhancement of long-term resource security by increasing the availability of critical resources such as water, energy or particular raw materials through contracts.

Although theoretically IE represents a win-win situation, the associated benefits are difficult to evaluate and have seldom been carefully measured. A critical barrier commonly encountered when promoting eco-industrial parks is in encouraging companies for

Corresponding author: César Torres, Email: cesar.torres@endesa.es

pursuing industrial symbiosis. The most obvious motivations are conventional business reasons; for example, resource sharing can reduce costs and/or increase revenues [3]. But companies will unlikely act with mere qualitative statements no matter how promising they are. Companies need numbers and these numbers should be as objective and accurate as possible.

The integration of industrial systems with mutual exchanges of resources, products and wastes implies energy savings. And the most objective way to analyze the magnitude of those savings is through the laws of Thermodynamics. In this context, exergy rather than energy is the unit of measure to be used [4]. In every material and energy transformation, neither matter, nor energy disappear, it is always exergy what is lost. Each step in the manufacturing process involves the generation of irreversibilities and hence of exergy losses. The most important contribution of the exergy concept is in its ability to objectify all the physical manifestations in energy units, independently of their economic value. Any product, natural or artificial resource, productive process or polluting emission can be valued from an exergy point of view with a single unit of measure.

Unfortunately, exergy analysis is necessary but not sufficient to determine the origin of losses and the potential for energy saving. However Thermoeconomics (TE), takes a step further, including in this equation the concept of purpose by means of the definition of efficiency. This information is not implicit in the Second Law and is the most important conceptual leap separating and at the same time unifying Physics with Economics. On this way, the exergy balance is written as:

$$F - P - R = I > 0, \tag{1}$$

where F are the resources required to carry out the production P, meanwhile R are the residues generated and I is the irreversibility of the process.

Furthermore, all mass and energy streams of a production chain have an exergy cost, and the more irreversible a process is the more resources are consumed. The concept of exergy cost is still within Thermodynamics, but it already shares many of the cost accounting methodologies borrowed from Economics. It was proposed by Valero et al. [5] and almost simultaneously Szargut and Morris [6] proposed the *Cumulative exergy consumption*. Both concepts represent in fact embodied exergy.

Thermoeconomics has been largely used for the diagnosis of single production plants, allowing the identification of inefficiencies and the potential for energy savings [7]. Now, it is the time to open the approach to industrial networks under the industrial ecology paradigm. The versatility of TE allows its application to complex systems, providing a systematic and general approach for the analysis of waste flow integration.

On the other hand, Input-Output Analysis [8] has been used to address environmental issues related to Industrial Ecology [9]. However, it has been traditionally used with different quantity units for accounting for all energy and material streams coming into play, what complicates the analysis. Similarly, if monetary units are used to assign costs, arbitrariness is introduced into the analysis. As it has been argued before, exergy is a suitable physical unit to which costs should be allocated. In fact, the exergy cost methodology is isomorphous with the cost model of the Input Output Analysis (IO) using the exergy as the quantity of measure. To the same conclusion have come Hau and Bakshi [10], who applied exergy and cumulative exergy consumption to IO in a sample of industrial and ecological systems.

Thermoeconomic Input-Output Analysis, (see Appendix A) formerly Symbolic Thermoeconomics [11], is an extension of the Exergy Cost Theory that applied the IO methodology to the analysis of the cost formation process of products and wastes, which can help to rationalize the general problem of energy saving achieved through waste integration.

2. Application of Thermoeconomics to System Integration Analysis

The aim of this section is to show how Thermoeconomic Input-Output Analysis could be applied to objectively assess the costs of the primary products interchanged in eco-industrial parks, providing decision tools for process integration.

2.1. Physical structure description

We considered as a case study three installations: a coal-fired power plant, a cement plant and a gas-fired boiler producing steam. Besides, two integrations are analyzed: use of steam bleeding instead of steam produced by the gas-fired boiler, and use of part of fly ashes for substituting clinker within the cement industry.

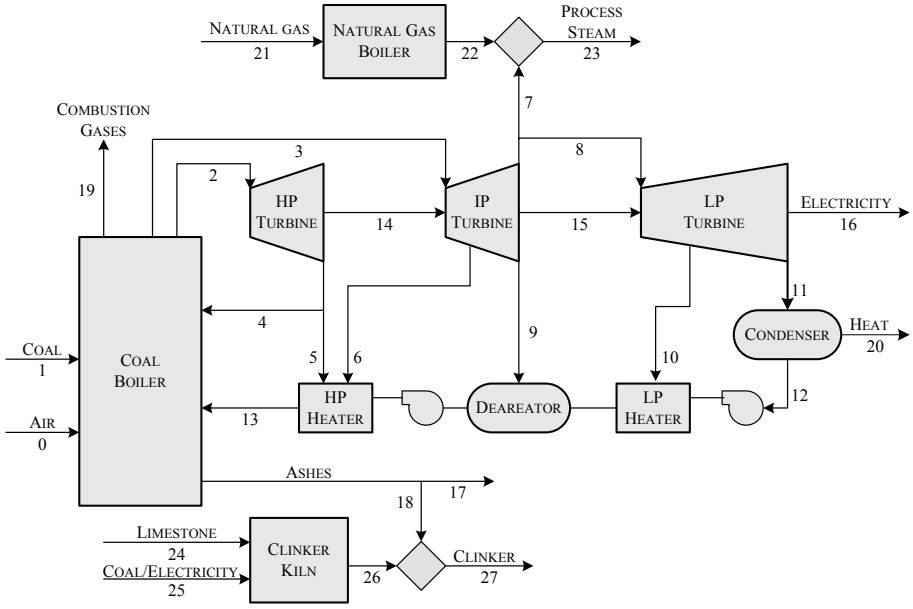

Figure 1: Eco-industrial park, integrating a power plant, a steam generator and a cement factory

A simplified physical structure of the system has been depicted in Figure 1. The main facility is a power plant producing 350 MW at design conditions. In addition to superheated and reheated steam, the coal-fired boiler produces ash and a flow of flue gases. The steam cycle is composed of high pressure, medium pressure and low pressure steam turbines. Steam leaving the last turbine is condensed and then compressed and heated by both low pressure and high pressure heaters and a deaerator prior to enter the boiler to close the cycle.

The cement factory considered has a capacity of 650000 ton/year operating 8000 hours/year. The cement manufacturing process can be divided into two parts: clinker production taking place in a kiln and grinding and mixing of this clinker with other constituents. The clinker production process begins with the calcination of limestone (mainly $CaCO_3$) at about 900 ^oC to form calcium oxide (CaO, lime). This is followed by the clinkering process in which the calcium oxide reacts at high temperature (typically 1400-1500 ^oC) with silica, alumina, and ferrous oxide to form clinker. The clinker is then milled with gypsum and other additives to produce cement.

Finally, the gas-fired boiler produces a flow of 10 kg/s of steam at 8.5 bar and 310 ^oC, and consumes 0.69 kg/s of natural gas.

Exergy flows of the power plant have been adapted from [12] and correspond to an actual operation state of the plant. In these conditions, it requires 1014.8 MW of coal to produce 351.6 MW of electricity. The exergy of the ash flow has been obtained by considering a coal heating value of 16912 kJ/kg, a coal ash content of 23.16% and an ash composition of 49% SiO_2, 26% Al_2O_3, 15% CaO and 10% Fe_2O_3, which results in an exergy value of 454.0 kJ/kg. Values of exergy related to the gas-fired boiler have been calculated by considering an energy efficiency of 90%. In the case of the cement kiln, it has been considered that each kg of clinker needs 1.54 kg of raw material (mainly limestone) and 4195 kJ of fuel (including a small part of electricity) [13]. Specific exergy of raw material and clinker are 220 kJ/kg and 1240 kJ/kg respectively, see reference [14].

In the integrated plant, steam flow produced by the natural-gas boiler is completely replaced by an equivalent flow from the steam cycle, while the power plant production is kept constant. Besides, 10% of the mass flow rate of clinker produced in the kiln is substituted by fly ashes imported from the power plant.

2.2. Productive Structure Definition

In order to perform the thermoeconomic analysis, a productive structure, see reference [15], comprising

a power plant, a cement kiln and a gas-fired boiler must be defined defined. Since this structure focuses on the purpose of the processes, it contains not only actual devices appearing in the physical structure but mainly groups of them as well as fictitious components for joining and distributing flows.

The components efficiency of the integrated system is defined in Table 1.

The coal boiler is disaggregated into three components: Component #1 is a fictitious device which remove the ashes from the coal, and part of the ashes are recycled in the ash treatment process (#7). Component #2 is the combustion chamber that transform the exergy of coal without ashes into a flow of heat at adiabatic flame temperature, whose exergy is denoted by E_Q, and also produce a flow of flue gases going to stack (#6). Abatement costs for ashes landfill and combustion gases are not considered, and their formation costs are charged to coal (#1). Component #3 is the steam generator including the boiler heat exchangers and the feedwater heaters. The three stages of the turbine are aggregated into component (#4) and the exergy of the total bleeding steam is $E_B = E_4 + E_5 + E_6 + E_7 + E_9 + E_{10}$.

The condenser (#5) is a dissipative component which produces a residual flow, which cost is distributed to the turbines and steam generator proportionally to the entropy generated in each of these components.

Component #9 is a junction connecting steam produced by the natural-gas boiler (#8) with steam bleed from the steam cycle in order to produce a flow to be used in an external process. Besides, component #11 is another junction which connects clinker from the kiln (#10) with ash imported from the power plant.

Thermoeconomic Input–Output Analysis provides general relationships between the production demand and the resources cost with the efficiency and waste generation of the individual process of an energy system. It is based on the productive structure and it is represented by an input–output table called *Fuel–Product* table.

Table 2 shows the *Fuel–Product* table of the power plant, according to the productive structure described above. It includes the exergy values of the flows in the productive components, and the external interactions with the other systems. The rows represent the destination of the production of each process: as resource of other processes, as final product or as disposable waste. The first row υ_0 represents the external resources entering the system. Meanwhile the columns represent the source of the fuel of each process. The last two columns represents the waste ω_R and final production ω_S of each process. Note that, rows and columns of the fuel–table are measured in the same kind of units (exergy) and the diference between the sum of columns and rows is the exergy balance of each process, (eq. 1). It is the key point to understand the differences between the "conventional" input–output quantity model and the Thermoeconomic Approach.

Table 1: Productive structure definition

Nr	Fuel	Product
1	E_1	E_1
2	$E_1 - E_{17} - E_{18}$	$E_Q + E_{19}$
3	E_Q	$E_2 + E_3 - E_B - E_{12}$
4	$E_2 + E_3 - E_B - E_{11}$	$E_{14} + E_{15} + E_{16}$
5	$E_{11} - E_{12}$	E_{20}
6	E_{19}	E_{19}
7	$E_{17} + E_{18}$	$E_{17} + E_{18}$
8	E_{21}	E_{22}
9	$E_7 + E_{22}$	E_{23}
10	$E_{24} + E_{25}$	E_{26}
11	$E_{26} + E_{18}$	E_{27}

2.3. Results discussion

Thermoeconomic Input-Output Analysis can reveal the savings achieved in the integration as well as the origins where the savings come from. The detailed mathematical model proposed is described in Appendix A. The production costs of the integrated plant processes has been computed, using TAESS [16], by means of the equation (A.10).

Exergy distribution and waste disposal ratios are obtained from the Fuel-Product table 2, and the waste cost ratios used in the study case system are defined as:

$$\langle \mathbf{RP} \rangle = \begin{bmatrix} 0 & 0 & 0.892 & 0.108 & 0 & 0 & 0 \\ 1 & 0 & 0 & 0 & 0 & 0 & 0 \\ 1 & 0 & 0 & 0 & 0 & 0 & 0 \end{bmatrix}$$

Figure 2 compares the exergy consumption, between the isolated and the integrated systems and the potential saving of the integration. Exergy savings achieved by the integration are equal to 23.4 MW (2%), which correspond to more than € 3.5 million/year. The exergy saving for process steam is

Table 2: Fuel-Product Table of the power plant for the integrated model

	F_1	F_2	F_3	F_4	F_5	F_6	F_7	ω_R	ω_S	Total
v_0	1037.6	0	0	0	0	0	0	0	0	1037.6
P_1	0	1031.2	0	0	0	0	6.451	0	0	1037.6
P_2	0	0	757.5	0	0	38.58	0	0	0	796.1
P_3	0	0	0	410.08	62.4	0	0	0	9.22	481.7
P_4	0	0	0	0	0	0	0	0	351.56	351.56
P_5	0	0	0	0	0	0	0	49.01	0	49.01
P_6	0	0	0	0	0	0	0	38.58	0	38.58
P_7	0	0	0	0	0	0	0	5.426	1.025	6.451
Total	1037.6	1031.2	757.5	410.08	62.4	38.58	6.451	92.01	361.81	

12.08 MW (35%), and the exergy saving in clinker production is 11.84 MW (9%). The values of the resources required to obtain each final product are computed by multiplying its exergy by its unit production cost, shown in table 3.

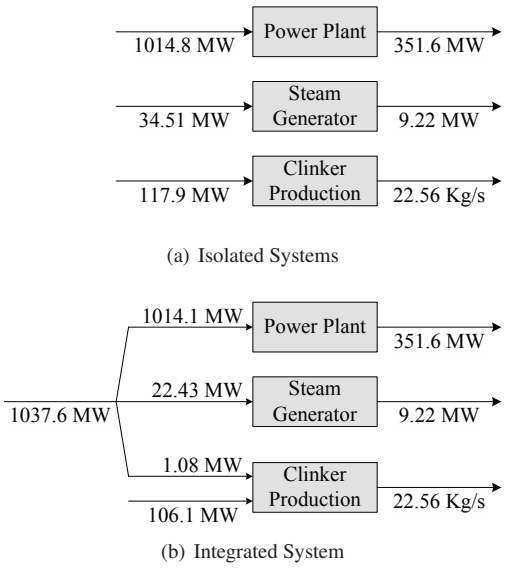

(a) Isolated Systems

(b) Integrated System

Figure 2: Resources consumption comparison, between isolated 2(a) and integrated system 2(b)

To better understand the origin of the savings caused by the integration, unit costs of the different products, shown in table 3, must be compared. The first column shows the unit costs when each plant is working independently and producing electricity, clinker and steam, meanwhile the second column shows the unit cost values when then plants are integrated.

The unit cost of the product of the ash separator is slightly greater than 1, because it includes the waste cost of ash and flue gases which are charged to this component. The costs of the combustion chamber products increase up to around 1.37 because of the irreversibility generated in the combustion. Due to heat transfer irreversibility, the cost of steam produced by the boiler increases up to 2.4. The cost of electricity (product of the turbines) increases up to more than 2.8, and the cost of the heat dissipated in the condenser is greater than 3. It can be seen that as the productive process goes forward, cost increases because of irreversibility appearing in the different components.

The cost of the product of the steam mixer decreases significantly with the integration. This reduction shows clearly the interest of the integration and how thermoeconomic analysis can help to detect integration opportunities: a key point is to substitute a given product by another with a lower cost.

The substitution of part of the clinker (which has a cost of about 4) by ash (which costs around 1) causes a reduction of the cost of the clinker mixer. Besides, the amount of ashes which were disposed of decreases, causing also a slight reduction of the cost of its product "clean coal" (1.058 to 1.056) and consequently, a reduction of the production costs of the following components, and in particular, a reduction in the electricity cost of 0.7 MW

3. Fuel Impact of Recycling Waste Analysis

In previous section the system integration potential saving, has been analyzed. Now, the fuel impact of waste recycling, without considering external integration, will be studied in detail.

Table 3: Production unit costs of the processes

Nr	Process	c_P (kW/kW)	
		Isolated	Integrated
1	Ash Separator	1.058	1.056
2	Comb. Chamber	1.370	1.368
3	Steam Generator	2.435	2.433
4	Turbines	2.887	2.885
5	Condenser	3.100	3.098
6	Stack	1.370	1.368
7	Ash Treatment	1.058	1.056
8	Natural Gas Boiler	3.743	N/A
9	Steam Mixer	3.743	2.433
10	Cement Kiln	4.213	4.213
11	Clinker Mixer	4.213	4.090

Since the production cost depends on the recycling ratios, it is possible to compute the variation of the production cost as a function of the variation of recycling ratios:

$$\Delta \mathbf{C}_{\mathrm{P}} = \langle \mathbf{P}^* \big| \, \Delta \mathbf{C}_{\mathrm{R}} \tag{2}$$

here $\Delta \mathbf{C}_{\mathrm{R}}$ represents the variation (reduction) of the waste costs charged to each component, and it is given by:

$$\Delta \mathbf{C}_{\mathrm{R}} = \frac{{}^{\mathrm{t}}\langle \mathbf{RP} \rangle \, \Delta \hat{\mathbf{G}}_{\mathrm{R}}}{\hat{\mathbf{U}} - \langle \mathbf{R}^* | \, \Delta \hat{\mathbf{G}}_{\mathrm{R}}} \mathbf{C}_{\mathrm{P}} \tag{3}$$

where $\langle \mathbf{R}^* | \equiv \langle \mathbf{P}^* | \, {}^{\mathrm{t}}\langle \mathbf{RP} \rangle$ is the residual cost operator, and then the fuel impact is given by the sum of reduction of residuals cost for all the system components:

$$\Delta F_{\mathrm{T}} = {}^{\mathrm{t}}\mathbf{u} \, \Delta \mathbf{C}_{\mathrm{R}} \tag{4}$$

If only the recycling variation of an individual component $\Delta\gamma_i = (\omega_i - \omega_i^0)/P_i$ is considered, the Sherman-Morrison-Woodbury formula [17] could be used to simplify the equation (4) as:

$$\Delta F_{\mathrm{T}} = \frac{\Delta\gamma_i \, C_{P,i}}{1 - r_{ii}^* \, \Delta\gamma_i} \tag{5}$$

here r_{ii}^* is the *i–th* diagonal element of the residual cost operator. Considering $\Delta\gamma_i \, C_{P,i} = c_{P,i} \, \Delta\omega_i$ and the updated unit cost of the recycled waste is $c_{P,i}/(1 - \Delta\gamma_i \, r_{ii}^*)$, then the unit cost of the recycled waste is the measure of the fuel impact. Since the value of r_{ii}^* is near zero (0.0066) the relationship between recycling and total fuel saving is lineal. The potential saving from the power plant point of view is 480 kJ/kg, meanwhile the total saving for the integrated plant is 5,220 kJ/kg.

4. Conclusions

Thermoeconomic analysis is proposed as a systemic methodology based on physical roots for the analysis of integrations that characterize Industrial Ecology. In addition to the main concepts and tools of Thermoeconomics, new ideas related to Industrial Ecology, such as the recycling ratios, have been introduced. Furthermore, it has been shown that Input-Output analysis appears as the common mathematical framework for both disciplines.

This formulation has been applied to a case study comprising a coal-fired power plant, a cement kiln and a gas-fired boiler producing steam. Comparison of the Fuel Product tables with and without integration shows clearly how the total resources savings are formed. Besides, the analysis of the unit costs not only shows how they are reduced due to the integration but also justifies clearly its interest. For example, it is better to bleed steam from the power plant than to produce it separately because the cost of the former is higher than that of the latter. The case of ashes is even more interesting because it is a win-win situation: reduction of cost of clinker produced, benefits for the cement plant, and reduction of the electricity cost.

This paper is a first and promising step in the application of Thermoeconomics to Industrial Ecology, which can help to solve several important problems such as the identification of possibilities of integration and efficiency improvement, quantification of benefits obtained by integration or determination of prices based on physical roots. Furthermore, all Thermoeconomic techniques developed during years for the analysis, optimization, and diagnosis of energy systems can now be applied to Industrial Ecology.

References

[1] Frosch, R. and Gallopoulos, N., 1989, Strategies for Manufacturing, *Scientific American*, 261(3), pp. 144-152.

[2] USPCSD (US President's Council on Sustainable Development), *Eco-industrial Park Workshop Proceedings*, Cape Charles, Virginia, October 17-18, 1996. http://clinton2.nara.gov/PCSD/Publications/Eco_Workshop.html.

[3] Chertow, M.R., 2007, Uncovering Industrial Symbiosis. *Journal of Industrial Ecology*, 11(1), pp. 11-30.

[4] Ayres, R. and Ayres, L., 1996, *Industrial Ecology. Towards Closing the Material Cycle*, Edward Elgar Publishing.

[5] Valero, A., Lozano, M.A. and Muñoz, M., 1886, A General Theory of Exergy Saving. Part I: On the Exergetic Cost, *Computer Aided Engineering and Energy Systems, Vol. 3: Second Law Analysis and Modeling*, ASME AES, Vol. 2-3, R.A. Gaggioli, ed, pp. 1-8.

[6] Szargut, J. and Morris, D., 1987, Cumulative Exergy Consumption and Cumulative Degree of Perfection of Chemical Processes, *Int. J. Energy Res*, 11, pp. 245-261.

[7] Valero, A., Correas, L., Zaleta, A., Lazzaretto, A., Reini, M., Verda, V., and Rangel, V.H, 2004, On the Thermoeconomic Approach to the Diagnosis of Energy System Malfunctions, *Energy*, 29 (12–15), pp. 1875-1907.

[8] Miller, R.; Blair, P., 2009 *Input-Output Analysis. Foundations and Extensions*, 2^{nd} edition, Cambridge University Press.

[9] Suh S., 2009, *Handbook of Input-Output Economics in Industrial Ecology*, Springer science, 2009.

[10] Hau, J.; Bakshi, B., 2004, Expanding Exergy Analysis to Account for Ecosystem Products and Services, *Environ. Sci. Technol.*, 38, pp. 3768-3777.

[11] Torres, C., 2009, Symbolic Thermoeconomic Analysis of Energy Systems, In *Exergy, Energy System Analysis and Optimization*, C.A. Frangopoulos, ed, Eolss Publishers, Oxford, UK, Vol.2, pp. 61-82.

[12] Uson, S., 2008, *Comparative Analysis of Causal Diagnosis Methods of Malfunctions in Power Cycles*, PhD Dissertation, Department of Mechanical Engineering, University of Zaragoza.

[13] Integrated Pollution Prevention and Control Bureau, Institute for Prospective and Technological Studies, Joint Research Centre, European Comission, 2001, *Best Available Techniques Reference Document on Lime and Cement Industries.*

[14] Valero A., Valero Al , 2010 A Thermodynamic Approach for Accounting the Earth's Mineral Capital. The Case of Bauxite–Aluminium and Limestone–Lime Chains, *Energy*, 35, pp. 229-238

[15] Torres C., Serra L. and Valero A, 1996, The Productive Structure and Thermoeconomic Theories of System Optimization, *Thermodynamics and The Design, Analysis and Improviment of Energy Systems*, A.B. Duncan, J. Fiszdon, D. O'Neal and K. Braven , eds, ASME AES 36, pp. 429-436.

[16] Perez E. and Torres C., 2007, *TAESS. Thermoeconomic Analysis of Energy System Software*. CIRCE. Centro de Investigación de Recursos y Consumos Energéticos. Available at: `http://www.exergoecology.com`

[17] Press, H., Teukolsky, S., Vetterling W., Flannery, B., *Numerical Recipes. The Art Of Scientific Computing*. 3^{th} edition, Cambridge University Press, 2007, Chap. 2.

[18] Torres C., Valero A., Rangel V., and Zaleta A., 2008, On the Cost Formation Process of the Residues, *Energy* , 33, pp. 144-152.

Appendix

A. Thermoconomics Input–Output Analysis

In this appendix a review of the Symbolic Thermoeconomics formulation is shown. For further information, see reference [11, 18]. Symbolic Thermoeconomics provides general relationships between the production demand and the resources cost with the efficiency and waste generation of the individual process of an energy system.

The relationships between the Fuels and Products of each system process can be compactly summarized in matrix notation as:

$$\begin{aligned} \mathbf{F} &= \upsilon_0 + {}^{t}\mathbf{u}\,[\mathbf{FP}] \\ \mathbf{P} &= [\mathbf{FP}]\,\mathbf{u} + \omega_R + \omega_S \end{aligned} \tag{A.1}$$

where [**FP**] is a square matrix ($n \times n$) whose elements E_{ij} represent the exergy values of the internal interactions of the Fuel–Product table. **F** and **P** are column vectors ($n \times 1$) that represent the fuel and product of each component respectively. Column vectors ω_S and ω_R ($n \times 1$) represent the exergy of primary output and the waste generated for each

component. The column vector υ_0 $(n \times 1)$ contains the exergy values of the external resources entering each component.

We use **u** to represent a column vector of 1's (with the appropriate dimension – here the number of components n). An important observation is that post-multiplication of a matrix by **u** is a column vector whose elements are the row sums of the matrix. Similarly ${}^{t}\mathbf{u}$ is a row vector of 1's and pre-multiplication of a matrix by ${}^{t}\mathbf{u}$ is a row vector whose elements are the column sums of the matrix. We also denote $\hat{\mathbf{x}}$ to represent a diagonal matrix, whose elements are the elements of the vector **x**.

Let define the *exergy distribution ratios*, $y_{ij} = E_{ij}/P_i$ as the part of the production of the $i-th$ component becoming fuel of the $j-th$ component. If we denote by $\langle \mathbf{FP} \rangle$ the square matrix $(n \times n)$ which contains the exergy distribution ratios of the system, then it verifies:

$$\langle \mathbf{FP} \rangle = \hat{\mathbf{P}}^{-1} [\mathbf{FP}], \tag{A.2}$$

Once the Fuel-Product model has been defined, it is possible to determine the exergy cost of the flows E^*_{ij} on the productive structure, and the corresponding Fuel-Product cost table $[\mathbf{FP}^*]$. In accordance with the proposed model, the resources cost of each component is given by:

$$\mathbf{C}_F = \upsilon^*_0 + {}^{t}[\mathbf{FP}^*]\,\mathbf{u} \tag{A.3}$$

where υ^*_0 is a $(n \times 1)$ vector that represents the cost of the external resources entering the component. Likewise, the cost of the products of each process, is:

$$\mathbf{C}_P = [\mathbf{FP}^*]\,\mathbf{u} + \omega^*_S + \omega^*_R \tag{A.4}$$

where ω^*_S represents the cost of the final products and $\omega_R *$ the cost of the disposed wastes.

All costs yielded by the productive process must be included in the cost of the final or primary products. Torres et al. [18] proposed a general methodology for cost allocation of wastes. The waste exergy cost that is disposed of, and the cost of the resources required in its treatment, must be allocated to the productive units that have generated them. Each residual flow has a cost formation process that must be identified to calculate the cost of all functional products correctly.

Therefore, the cost of the residues charged to each component, denoted as $\mathbf{C}_R$is written as:

$$\mathbf{C}_R = {}^{t}\langle \mathbf{RP} \rangle\, \omega^*_R, \tag{A.5}$$

where $\langle \mathbf{RP} \rangle$ is a $(n \times n)$ matrix containing the waste cost distribution ratios ψ_{ij}, which represent the portion of the waste cost assessed to each productive component.

Accordingly from the application of the Exergy Cost Theory rules, it is stated:

- The cost of external resources is a known quantity and equal to its exergy: $\upsilon^*_0 = \upsilon_0$
- The production cost of a process contains both the cost of the resources required to obtain it as well as the costs generated by disposal of the waste produced:

$$\mathbf{C}_P = \mathbf{C}_F + \mathbf{C}_R \tag{A.6}$$

- The cost of each one of the flows making up the product of a component is proportional to its exergy:

$$[\mathbf{FP}^*] = {}^{t}\langle \mathbf{FP} \rangle\, \hat{\mathbf{C}}_P \tag{A.7}$$

Combining the previous equations, it is get:

$$\mathbf{C}_P = \upsilon_0 + {}^{t}\langle \mathbf{FP} \rangle\, \mathbf{C}_P + {}^{t}\langle \mathbf{RP} \rangle\, \omega^*_R \tag{A.8}$$

The cost of the residuals generated by a component could be related with its production cost, by introducing the disposal waste ratio: $\gamma_i = \omega_{R,i}/P_i$ equation (A.8), hence is rewritten as:

$$\mathbf{C}_P = \upsilon_0 + {}^{t}\langle \mathbf{FP} \rangle\, \mathbf{C}_P + {}^{t}\langle \mathbf{RP} \rangle\, \hat{\mathbf{G}}_R \mathbf{C}_P \tag{A.9}$$

where $\hat{\mathbf{G}}_R$ is a diagonal matrix $(n \times n)$ whose elements are the disposal waste ratios of each component, and the production cost could be determined as:

$$\mathbf{C}_P = \langle \mathbf{P}^* |\, \upsilon_0 \tag{A.10}$$

where $\langle \mathbf{P}^* | \equiv \left(\hat{\mathbf{U}} - {}^{t}\langle \mathbf{FP} \rangle - {}^{t}\langle \mathbf{RP} \rangle\, \hat{\mathbf{G}}_R\right)^{-1}$ is called the *production cost matrix*.

The thermodynamic properties of the upper continental crust: Exergy, Gibbs free Energy and Enthalpy

Alicia Valero[1], *Antonio Valero*[1] *and Philippe Vieillard*[2]

[1]*CIRCE. Centro de Investigación de Recursos y Consumos Energéticos*
[2]*HYDRASA, Faculté des Sciences, Université de Poitiers*

Abstract: In this paper, the thermodynamic properties of the most abundant minerals of the upper continental crust are presented. For those substances whose thermodynamic properties are not listed in the literature, their enthalpy, Gibbs free energy and exergy are calculated with 12 different estimation methods presented in this paper, with associated errors ranging from 0 to 10%. Accordingly, the thermodynamic properties of the bulk continental crust are obtained. Finally, the chemical exergy of the continental crust is compared to the exergy of the concentrated mineral resources. The numbers obtained indicate that the chemical exergy of the crust is huge. However, only 0,001% of that amount can be effectively used by man.

Keywords: Exergy, Enthalpy, Gibbs Free Energy, Minerals.

1. Introduction

The upper continental crust is the reservoir of the main minerals and other natural resources useful for mankind. As stated in [1], a lot of effort has been placed in determining the chemical composition of the upper continental crust, but the mineralogical composition of it has been barely studied. This is due mainly to the complexity and heterogeneity of the earth's crust.

In this paper our final goal is to obtain the chemical exergy of the Earth's upper crust and to compare it with that of the concentrated minerals, i.e., with what we call mineral resources.

But for that purpose, knowing the chemical composition of the elements that compose the crust is not enough. We need to know the mineralogical composition of it. In [1], we obtained a first model of mineralogical composition of the crust. The latter will be used in this paper for obtaining the chemical exergy of the bulk upper crust.

2. Methodology

Assuming that the upper continental crust is composed by an ideal solution of substances, the average Enthalpy ($\Delta\overline{H}_f$), Gibbs free energy ($\Delta\overline{G}_f$) and Chemical Exergy ($\overline{b}_{ch}$) of each layer of the earth expressed as kJ/mole of atmosphere, hydrosphere or upper crust, are calculated as:

$$\Delta\overline{H}_f = \sum_{i=1}^{m}(x_i \cdot \Delta H_{f\,i}) \tag{1}$$

$$\Delta\overline{G}_f = \sum_{i=1}^{m} x_i \cdot (\Delta G_{f\,i} + \bar{R}T_0 ln x_i) \tag{2}$$

$$\overline{b}_{ch} = \sum_{i=1}^{m} x_i \cdot (b_{ch\,i} + \bar{R}T_0 ln x_i) \tag{3}$$

Being x_i, molar fraction of the species composing each sphere of the earth, and $\Delta H_{f\,i}$, $\Delta G_{f\,i}$ and $b_{ch\,i}$, their enthalpy, Gibbs free energy and chemical exergy in kJ/mole, respectively.

The enthalpy and Gibbs free energy of the substances are obtained either through the literature or through the estimation methods explained in the next section.

The chemical exergy of the substance ($b_{ch\,i}$) in kJ/mole is calculated with Eq. 4:

$$b_{ch\,i} = \Delta G_f + \sum_j r_{j,i} b_{ch\,j} \tag{4}$$

where $b_{ch\,j}$ is the standard chemical exergy of the elements that compose substance i. In our case we will use the chemical exergy of the elements obtained with an update of Szargut's R.E. [2] and published in [3].

Corresponding author: Alicia Valero, Email: aliciavd@unizar.es

The average enthalpy, Gibbs free energy and exergy of the continental crust, can be expressed in $mole/g$ by substituting x_i with the molar fraction ξ_i for the i constituents of the sphere. Eq. 5 relates both properties through the molecular weight of the upper continental crust which was obtained in [1] as equal to MW_{cr} = 157.7 g/mole:

$$x_i = \xi_i \cdot MW_{cr} \tag{5}$$

3. Prediction of Enthalpy and Gibbs free energy of formation of minerals

The determination of the thermodynamic properties of the substances requires the knowledge of their corresponding enthalpies and Gibbs free energies of formation. Many of these have been already estimated through empirical and semi-empirical processes[1] and are tabulated. Comprehensive compilations of the thermodynamic properties of inorganic substances can be found in Faure [4], Wagman [5], Robie et al. [6], [7] or Weast et al. [8].

Unfortunately, not all the enthalpies and Gibbs free energies of the minerals that compose the earth's upper crust are recorded in the literature. Nevertheless, many of them can be predicted satisfactorily through different semi-empirical methods. In the next sections, the estimation methods of the thermodynamic properties used to obtain the standard enthalpy and Gibbs free energy of formation of the minerals will be provided.

3.1. Calculation of ΔH_f^0 or ΔG_f^0 from s^0

If either ΔH_f^0 or ΔG_f^0 and the entropy (s^0) of the mineral under consideration are available, the unknown property can be easily calculated applying Eq. 6.

$$\Delta G_f^0 = \Delta H_f^0 - T_0 \cdot \Delta S \tag{6}$$

Where the entropy change ΔS is calculated from the standard entropy of the mineral and its constituent elements in the standard state (T_0 = 298.15 K and 1 bar), as in Eq. 7:

$$\Delta S = s^0_{mineral} - \sum s^0_{elements} \tag{7}$$

Note that this procedure does not have associated any error, since it is based on the definition of ΔG_f.

[1] Such as calorimetric or solubility measurements.

3.2. The ideal mixing model

An ideal solid solution of i components with x_i molar fractions obeys the equations:

$$\Delta H_m = 0 \tag{8}$$

$$\Delta G_m = +RT \sum x_i ln x_i \tag{9}$$

Where ΔH_m and ΔG_m, are the enthalpy and Gibbs free energy of mixing. This means that the ideal mixing will take place without any heat loss or heat production. Moreover, the different cations will be fully interchangeable [9]. The enthalpy and Gibbs free energy of formation of the solid solution is calculated then with the following equations:

$$\Delta H^0_{f,solution} = \sum_i x_i \Delta H^0_{f,i} \tag{10}$$

$$\Delta G^0_{f,solution} = \sum_i x_i \Delta G^0_{f,i} + RT \sum x_i ln x_i \tag{11}$$

The error associated to the assumption of the mineral as an ideal solid solution varies greatly with the mineral under consideration and decreases with the disorder among components. We will assume a maximum error of ±1%.

3.3. Assuming ΔG_r and ΔH_r constant

3.3.1. Thermochemical approximations for sulfosalts and complex oxides

Craig and Barton [10] developed an approximation method for estimating the thermodynamic properties of sulfosalts in terms of mixtures of the simple sulfides. The ideal mixing model does not apply correctly to most sulfosalts, because the mixtures of layers are rather ordered. The modified ideal mixing model of Craig and Barton involves a mixing term (ΔG_m) in the estimation of the Gibbs free energy of formation of the sulfosalt per gram atom of S that is added to the weighted sum of free energies of the simple sulfides:

$$\Delta G_m = (1.2 \pm 0.8)(+RT \sum x_i ln x_i) \tag{12}$$

The mixing term can be divided into two parts, one estimated from the crystal structure as an entropy change, and the reminder as a non-ideal term. The non-ideal term of this model was assumed to be constant for all sulfosalts. However, Vieillard [11]

showed that the properties of complex sulfides with respect to their simple sulfides are a function of the electronegativity difference between the cations of the sulfosalt.

The thermodynamic properties of sulfosalts (sfs) may then be calculated by adding a term (ΔH_r or ΔG_r) to the appropriately weighted sum of the enthalpies or free energies of the simple component sulfides:

$$\Delta H_{f,sfs} = \sum x_i \Delta H_{f,sulfides} + n_{S,sfs}\Delta H_r \quad (13)$$

$$\Delta G_{f,sfs} = \sum x_i \Delta G_{f,sulfides} + n_{S,sfs}\Delta G_r \quad (14)$$

The reaction term, which is analogous to the mixing term of Craig and Barton is associated to one atom of sulfur in the mineral ($n_{S,sfs}$) and is obtained from a sulfosalt for which its thermodynamic properties and those of its simple sulfides are known. The calculated reaction terms can be applied to a family of sulfosalts formed by the same cations and with partial element substitutions.

Vieillard et al. [11] demonstrated the analogy between the electronegativity scale of cations with respect to sulfur and to oxygen. They showed that the methodology of estimation of the thermodynamic properties of sulfosalts from simple sulfides can be equally applied to complex oxides able to be decomposed into simple oxides. As for sulfosalts, the reaction terms ΔH_r and ΔG_r (for this case denoted as ΔH_{ox} and ΔG_{ox}) should be obtained for an oxide of the same family of the mineral under analysis. The maximum error associated to this methodology is assumed to be ±1%.

3.3.2. The method of corresponding states

Similarly, the ΔH_r and ΔG_r can be assumed to be constant in the substitution reaction of minerals A-x and B-x into A-y and B-y, if A-x and B-y are isomorphous. The associated error is assumed to be equal to the previous method, hence ±1%.

3.4. The method of Chermak and Rimstidt for silicate minerals

The method proposed by Chermak and Rimstidt [12] predicts the thermodynamic properties (ΔG_f^0 and ΔH_f^0) of silicate minerals from the sum of polyhedral oxide and hydroxide contributions. The technique is based on the observation that silicate minerals have been shown to act as a combination of basic polyhedral units. Chermak and Rimstidt determined by multiple linear regression, the contribution of $Al_2O_3^{[4]}$, $Al_2O_3^{[6]}$, $Al(OH)_3^{[6]}$, $SiO_2^{[4]}$, $MgO^{[6]}$, $Mg(OH)_2^{[6]}$, $CaO^{[6]}$, $CaO^{[8-z]}$, $Na_2O^{[6-8]}$, $K_2O^{[8-12]}$, H_2O, $FeO^{[6]}$, $Fe(OH)_2^{[6]}$ and $Fe_2O_3^{[6]}$ to the total ΔG_f^0 and ΔH_f^0 of a selected group of silicate minerals [2]. The thermodynamic properties of the minerals are calculated with Eqs. 15 and 16:

$$\Delta H_f^0 = \sum x_i \cdot h_i \quad (15)$$

$$\Delta G_f^0 = \sum x_i \cdot g_i \quad (16)$$

Where x_i is the number of moles of the oxide or hydroxide per formula unit and h_i and g_i are the respective molar enthalpy and free energy contribution of 1 mole of each oxide or hydroxide component. The values of h_i and g_i for the different polyhedral components are listed in [12].

The errors associated to the estimated vs. experimentally measured values can reach ±1% for ΔG_f^0 and ΔH_f^0, depending on the nature of the compounds. Note that this methodology can only be applied to those minerals able to be decomposed by the oxides and hydroxides mentioned before.

3.5. The ΔO^{-2} method

The linear additivity procedures based on the ΔO^{-2} parameter were developed by Yves Tardy and colleagues [13]. The parameter ΔO^{-2}, corresponds to the enthalpy $\Delta_H O^{-2}$ or Gibbs free energy $\Delta_G O^{-2}$[3] of formation of a generic oxide $MO_x(c)$ from its aqueous ion, where z is the charge of the ion and x the number of oxygen atoms combined with one atom M in the oxide ($x = z/2$):

$$\Delta_H O^{-2} M^{z+} = \frac{1}{x}[\Delta H_f^0 MO_{x(c)} - \Delta H_f^0 M_{(aq)}^{z+}] \quad (17)$$

For hydroxides, silicates, phosphates, nitrates and carbonates involving two cations, it was found that the enthalpy and Gibbs free energy of formation of a given compound from its constituent oxides vary

[2] The brackets next to the chemical formulas of oxides and hydroxides indicate the coordination number of the polyhedral structure.

[3] The calculation of $\Delta_G O^{-2}$ is analogous to that of $\Delta_H O^{-2}$.

linearly with ΔO^{-2} and have the general expressions [14]:

$$\Delta H^0_{ox} = \alpha_H \frac{n_i \cdot n_j}{n_i + n_j}[\Delta_H O^{2-} M_i^{z_i^+}(aq) - -\Delta_H O^{2-} M_j^{z_j^+}(aq)] \quad (18)$$

Being ΔH^0_{ox} [4]:

$$\Delta H^0_{ox}[(M_i)_{n_i}(M_j)_{n_j}O_N] = \Delta H^0_f[(M_i)_{n_i}(M_j)_{n_j}O_N] - -n_i\Delta H^0_f M_i O_{x_i}(c) - -n_j\Delta H^0_f M_j O_{x_j}(c) \quad (19)$$

Where n_i and n_j are the numbers of oxygen ions linked, respectively, to the $M_i^{z_i^+}$ and $M_j^{z_j^+}$ cations; and N is the number of oxygens linked to the molecular structure of the double oxide ($N = x_i + x_j$). Parameters α_H and α_G are empirical coefficients variable from one family of compounds to another one (α_G is 0.84 for hydroxides, 1.01 for silicates, 1.15 for carbonates, 1.30 for nitrates, etc.).

Equation 18, yields a statistical deviation of 35 kJ/mole for the Gibbs free energy of formation and depends on the family of compounds. We will assume a maximum error associated to the ΔO^{2-} general method of ±1%.

3.5.1. The ΔO^{-2} method for hydrated clay minerals and for phyllosilicates

Vieillard extended the methodology described above for the prediction of hydrated clay minerals [15] and for phyllosilicates [16].

The Gibbs free energy of formation of a hydrated clay mineral or a phyllosilicate composed by n_s cations located in different crystal sites and with $n_s(n_s - 1)/2$ interaction terms is calculated as:

$$\Delta G^0_f = \sum_{i=1}^{i=n_s}(n_i)\Delta G^0_f(M_i O_{x_i}) + \Delta G^0_{ox} \quad (20)$$

The Gibbs free energy of formation from the oxides ΔG^0_{ox} is calculated with Eq. 21:

$$\Delta G^0_{ox} = -N(\sum_{i=i}^{i=n_s-1}\sum_{j=i+1}^{j=n_s} X_i X_j(\Delta_G^{2-} M_i^{z_i+}(clay) - -\Delta_G^{2-} M_j^{z_j+}(clay))) \quad (21)$$

[4]The calculation of ΔG^0_{ox} is analogous to that of ΔH^0_{ox}.

where N is the total number of O atoms of all oxides; X_i and X_j are the molar fraction of oxygen related to the cations $M_i^{z_i+}$ and $M_j^{z_j+}$ in the individual oxides $M_i O_{x_i}$ and $M_j O_{x_j}$, respectively ($X_i = (1/N)(n_i x_i)$ and $X_j = (1/N)(n_j x_j)$). Parameters $M_i^{z_i+}$(clay) and $M_j^{z_j+}$ (clay) characterize the electronegativity of cations $M_i^{z_i+}$ and $M_j^{z_j+}$ in a specific site and are calculated by minimizing the difference between experimental Gibbs free energies and calculated ones from constituent oxides. The predicted Gibbs free energy values showed an error between 0.0 and 0.6 %.

3.5.2. The ΔO^{-2} method for different compounds with the same cations

Tardy [14] showed that the Gibbs free energy of formation of a compound from its two constituent oxides calculated per one oxygen in the formula was a parabolic function of mean ΔO^{-2} compound. Subsequently, an expression for calculating the Gibbs free energy of formation of a compound C intermediate in composition to two compounds A and B, $A + B \rightarrow C$ was developed:

$$\Delta G_{ox,A+B\rightarrow C} = +\alpha(\Delta_G O^{2-} M_i^{z_i^+} - -\Delta_G O^{2-} M_j^{z_j^+}) n_C(X_i^C - X_i^A)(X_i^C - X_i^B) \quad (22)$$

where n_c designates the total number of oxygens of the compound C and X_i^A, X_i^B, X_i^C the mole fractions of oxygen that balance cation $M_i^{z_i^+}$ in compounds A, B, and C and α the correlation parameter for a given class of compounds.

3.6. Assuming ΔS_r zero

Helgeson et al. [17] showed that the entropy of formation of mineral a certain mineral can be determined, assuming that the entropy of the reaction involved in the formation of the mineral is zero (Helgeson's algorithm). Helgeson algorithm is useful when either ΔG_f or ΔH_f are known. Once the entropy of the mineral is known, ΔG_f (or ΔH_f) can be calculated with ΔH_f (or ΔG_f) through Eq. 6. The error associated to this approximation is up to 5%.

3.7. Assuming ΔG_r and ΔH_r zero

3.7.1. The element substitution method

In some cases, thermodynamic properties are available for a certain mineral (A), belonging to the same

family of the substance under consideration (B), but with partial element substitutions. In such a case, the ΔH_f^0 and ΔG_f^0 of mineral B can be calculated from mineral A, assuming that the reaction enthalpy or free energy of formation of mineral B from A is zero. This approximation increases with the magnitude of substitution and may yield to associated errors of up to 5%, although it rarely exceeds ±2%.

3.7.2. The addition method for hydrated minerals

Hydrated minerals have the ability to absorb water molecules, forming part of their crystal structure:

$$A + n \cdot H_2O \rightarrow A \cdot nH_2O$$

Usually, thermodynamic properties are available for the non-hydrated mineral. But the enthalpy and Gibbs free energy of formation of the hydrated substance can be estimated by addition of the hydration enthalpy and Gibbs free energy ΔG_{hydr}^0 or ΔH_{hydr}^0 to those of the dehydrated substance, as in Eqs. 23.

$$\begin{aligned} \Delta H_{f,A\cdot nH_2O}^0 &= \Delta H_{f,A}^0 + n \cdot \Delta H_{hydr,A}^0 \\ \Delta G_{f,A\cdot nH_2O}^0 &= \Delta G_{f,A}^0 + n \cdot \Delta G_{hydr,A}^0 \end{aligned} \quad (23)$$

If ΔG_{hydr}^0 and ΔH_{hydr}^0 are not available, one can assume that the enthalpy and Gibbs free energy of the hydration reaction are zero (as in section 3.7.1.). And hence, the properties of the liquid water molecules contained in the hydrated substance must be added in place of ΔG_{hydr}^0 and ΔH_{hydr}^0. This is not rigourously exact, as demonstrated by Vieillard and Jenkins ([18], [19], [20]) and the error associated depends on the nature of the dehydrated component[5]. We will assume an associated error of ±5%, although it rarely exceeds ±2%.

3.7.3. The decomposition method

If none of the previously described methods can be applied, the thermodynamic properties of a certain mineral can be estimated as the last resort by decomposing it into its major constituents for which the enthalpy and Gibbs free energy of formation are known. It will be assumed that the energy of reaction of the constituents to form the mineral under consideration is zero. The error associated to this methodology is significantly greater than with the substitution and addition methods, since in this case we are not dealing with partial substitutions or additions of a known mineral, but with the formation of a completely new mineral from its building blocks. The mineral under analysis will be decomposed into its most complex compounds (usually double silicates). If this is not possible, most minerals can be decomposed into its simple oxides, sulfides, carbonates, etc. We will assume that the decomposition method throws an error of up to 10%.

[5]This methodology is not applied for hydrated clay minerals and phyllosilicates. In those cases, the ΔO^{2-} method is applied.

3.8. Summary of the methodologies

The described methodologies in the previous sections, will be used for calculating the thermodynamic properties of the most abundant minerals in the earth's upper crust. Each methodology is given a number so as to specify in the next section, which methodology has been used for determining the enthalpy or free energy of formation of the minerals (see table 1). Additionally, the assumed maximum errors associated to the estimation methods ($\pm\varepsilon$) are given.

Table 1: Summary of the methodologies used to predict the thermodynamic properties of minerals

Method	Nr.	$\pm\varepsilon$, %
Calculation of ΔH_f^0 or ΔG_f^0 from s^0	1	0
The ideal mixing model	2	1
Thermochemical approximations for sulfosalts and complex oxides	3	1
The method of corresponding states	4	1
The method of Chermak and Rimstidt for silicate minerals	5	1
The ΔO^{-2} method	6	1
The ΔO^{-2} method for hydrated clay minerals and for phyllosilicates	7	0.6
The ΔO^{-2} method for different compounds with the same cations	8	1
Assuming ΔS_r zero	9	5
The element substitution method	10	5
The addition method for hydrated minerals	11	5
The decomposition method	12	10

4. Results

Table 3 shows the the thermodynamic properties of the 291 main minerals included in the crust. About a half of the properties (159) were compiled directly from the literature. The remaining were obtained with the 12 different estimation methods described in [21]. From the latter, 18 minerals were calculated

without committing any associated error. Five minerals were estimated committing a maximum error of $\epsilon < 0.6\%$. Thirty-eight minerals were estimated with an error smaller than 1%, 20 substances with $\epsilon < 5\%$, and 44 minerals with $\epsilon < 10\%$. Only the properties of 6 minerals: iridium, osmium, nickeline, polixene, sylvanite and yttrialite were not able to be estimated. Additionally, the enthalpy of formation of gersdorffite and the Gibbs free energy of smaltite are missing. Nevertheless, all together account for only $3.5 \times 10^{-6}\%$ of the continental crust.

It should be pointed out that the R.E. generates some negative exergies of the minerals. This is because we chose our R.E. based on Szargut's criterion of partial stability. According to this, among a group of reasonable abundant substances, the most stable will be chosen if they also satisfy the "earth similarity criterion". This criterium is different from that of [22] or [23], where complete stability was assumed. As a consequence, the latter R.E. do not generate any negative exergies, but the resulting environment is completely different from that of the current earth. Our chosen R.E. obeys in principle the "earth similarity criterion", but does generate some negative exergies. Hence, this leads us to question the methodology used for establishing the R.E.

4.1. The chemical exergy of the earth

With these results, we can now calculate the average standard enthalpy, Gibbs free energy and chemical exergy of the upper continental crust with Eqs. 1-3:

$$(\Delta\overline{H}^0_f)_{cr} = -1959.96 \text{ kJ/mole}$$
$$(\Delta\overline{G}^0_f)_{cr} = -1841.10 \text{ kJ/mole}$$
$$(\overline{b}^0_{ch})_{cr} = = 366.56 \text{ kJ/mole}$$

For the calculation of the absolute exergy of the continental crust, we require information about its total mass. According to [24], the earth has a mass of around 5.98×10^{24} kg. The earth's relative mass proportions of each of the earth's spheres are according to [25]: core (35.5%), mantle (67%), oceanic crust (0.072%), continental crust (0.36%), hydrosphere (0.023%) and atmosphere (0.842 ppm). The upper layer of the crust constitutes a mass of around 50% of the whole continental crust [26]. With this information we can obtain a fist approximation of the exergy of the upper continental crust (see table 2). It has been assumed that there is no mixing among the considered layers and hence the Gibbs free energy and exergy of the mixture is zero.

Table 2: Exergy of the bulk upper crust

Mass, kg	**MW, g/mole**	$\overline{b}^0_{ch}$, **kJ/mole**	$\overline{B}^0_{ch}$, **Gtoe**
1.08E+22	157.7	366.56	5.97E+08

Of course these are very rough numbers, and are subject to ulterior updates, especially when a more appropriate R.E. is found. But they are good enough, for providing an order of magnitude of the chemical exergy of our planet.

In [27] we carried out an inventory of the exergy resources of the Earth. For the case of non renewable resources, including nuclear energy, fossil fuels and non-fuel minerals, the estimation of the available exergy on Earth obtained was at least around 115000 Gtoe, from which 65% come from the not yet technologically developed fusion of deuterium and tritium. The potential exergy use of non-renewable resources was around 6000 Gtoe. Considering these figures, we can now state that the non-renewable available resources contribute to a very small fraction of the total chemical exergy of the earth: less than 0.02%. The exergy of conventional fossil fuels and non energy mineral resources, constitute only 0.001% of the upper continental crust's chemical exergy.

5. Conclusions

In this paper, the standard thermodynamic properties of the main constituents of the upper Earth's crust have been provided for the first time. That is the standard enthalpy, Gibbs free energy and chemical exergy of more than 330 natural substances.

The enthalpies and Gibbs free energies, have been obtained either from the literature, or have been calculated with the 12 estimation methods described in this paper. The exergy of the substances has been calculated with the chemical exergies of the elements, generated with a R.E. based on Szargut's methodology.

Despite of the limitations of the R.E. pointed out, it still constitutes a tool for obtaining chemical exergies. Since the mass of the earth and of its spheres is

known, we were able to calculate the absolute chemical exergy of the upper continental crust: 6.0×10^8 Gtoe. Obviously the numbers are very rough, and are subject to ulterior updates, but they are good enough, for providing an order of magnitude of the huge chemical wealth of our planet.

The wealth of our planet is enormous, but man can only take advantage of a very small part of it: the resources. With current technology, it is impossible to use the chemical exergy of dispersed substances. Non-renewable resources are considered as such, because they represent a stock of concentrated chemical exergy. Therefore, the earth's 6.0×10^8 Gtoe of chemical exergy constitutes nowadays a useless reservoir of exergy. Consequently, we should resign ourselves with a maximum of only 0.02% of that amount.

References

[1] Valero, A. and Valero, A., 2009, The crepuscular planet. part ii: A model for the exhausted continental crust, in *Proceedings of ECOS 2009*.

[2] Szargut, J., 1989, Chemical exergies of the elements, Applied Energy, vol. 32, pp. 269–286.

[3] Valero D., A. et al., 2008, Evolution of the decrease in mineral exergy throughout the 20th century. The case of copper in the US, Energy, vol. 33(2), pp. 107–115.

[4] Faure, G., 1991, *Principles and applications of Inorganic Chemistry*, MacMillan.

[5] Wagman, D. et al., 1982, *The NBS tables of chemical thermodynamic properties: Selected values for inorganic and C1 and C2 organic substances in SI units*, American Chemical Society and the American Institute of Physics for the National Bureau of Standards, New York.

[6] Robie, R. A. and Hemingway, B. S., 1995, *Thermodynamic properties of minerals and related substances at 298.15 K and 1 bar (*10^5 *Pascals) pressure and higher temperature*, U.S. Geological Survey Bulletin 2131.

[7] Robie, R. A. et al., 1978, *Thermodynamic properties of minerals and related substances at 298.15 K and 1 bar (*10^5*Pascals) pressure and at higher temperatures*, U.S. Geological Survey Bulletin 1452.

[8] Weast, R. C. et al., 1986, *CRC Handbook of Chemistry and Physics*, CRC Press.

[9] Ottonello, G., 1997, *Principles of geochemistry*, Columbia University Press, New York.

[10] Craig, J. and Barton, P., 1973, Thermochemical approximations for sulfosalts, Economic Geology, vol. 68, pp. 493–506.

[11] Vieillard, P. et al., 2006, Prediction of enthalpies of formation of sulfides and sulfosalts minerals, in *Colloque Bilan et prospective de GDR Transmet*, Nancy, 6-7 juillet 2006.

[12] Chermak, J. A. and Rimstidt, D., 1989, Estimating the thermodynamik properties (ΔG_f^0 and ΔH_f^0) of silicate minerals at 298 K from the sum of polyhedral contributions, American Mineralogist, vol. 74, pp. 1023–1031.

[13] Tardy, Y. and Garrels, R. M., 1974, A method of estimating the Gibbs energies of formation of layer silicates, Geochim. Cosmochim. Acta, vol. 38, pp. 1101–1116.

[14] Tardy, Y., 1979, Relationship among Gibbs energies of formation of compounds, Amer. Jour. Sci., vol. 279, pp. 217–224, referencia del libro Ottonello1997.

[15] Vieillard, P., 2000, A new method for the prediction of Gibbs free energies of formation of hydrated clay minerals base on the electronegativity scale, Clays & Clay Minerals, vol. 48(4), pp. 459–473.

[16] Vieillard, P., 2002, A new method for the prediction of Gibbs free energies of formation of phyllosilicates (10 A and 14 A) based on the electronegativity scale, Clays and Clay Minerals, vol. 50(3), pp. 352–363.

[17] Helgeson, H. C. et al., 1978, Summary and critique of the thermodynamic properties of the rock-forming minerals, American Journal of Science, vol. 278-A, pp. 1–229.

[18] Vieillard, P. and Jenkins, H. D. B., 1986, Empirical relationships for estimation of enthalpies of formation of simples hydrates. Part I Hydrates of alkali- metal cations, of hydrogen and of monovalent cations, Journal Chemical Research (Synopsis), pp. 444–445.

[19] Vieillard, P. and Jenkins, H. D. B., 1986, Empirical relationships for estimation of enthalpies of formation of simples hydrates. Part 2. Hydrates of alkaline-earth metal cations, Journal Chemical Research (Synopsis), pp. 446–447.

[20] Vieillard, P. and Jenkins, H. D. B., 1986, Empirical relationships for estimation of

enthalpies of formation of simples hydrates. Part 3. Hydrates of transitionmetal cations ($Cr^{2+}, Fe^{2+}, Co^{2+}, Ni^{2+}, Cu^{2+}, Zn^{2+}, Cd^{2+}$ and UO_2^{2+}), Journal Chemical Research (Synopsis), pp. 448–449.

[21] Valero D., A., 2008, Assessing world mineral deposits through the second law of thermodynamics, in *Inproceedings of the Mineral Deposit Studies Group (MDSG) conference*, Nottingham (UK).

[22] Ahrendts, J., 1980, Reference states, Energy, vol. 5, pp. 667–677.

[23] Diederichsen, D., 1999, Referenzumgebungen zur Berechnung der chemischen Exergie, Tech. rep., Technical Report, Fortschr.-Ber.VDI Reihe 19, Düsseldorf, in German.

[24] Beichner, R. J. et al., 2000, *Physics For Scientists and Engineers*, Saunders College, New York.

[25] Javoy, M., 1999, Chemical earth models, C.R. Acad. Sci. Paris, Sciences de la terre et des planètes / Earth & Planetary Sciences, vol. 329, pp. 537–555.

[26] Yoder, C., 1995, *Global Earth Physics: A handbook of physical constants*, Amercian geophysical union, chap. Astrometic and geodetic properties of the Earth and Solar system, pp. 1–31.

[27] Valero, A. and Valero, A., 2010, Inventory of the exergy resources of the earth including its mineral capital, Energy, vol. 35(2), pp. 989–995.

[28] Karzhavin, V. K., 1991, Amphiboles: thermodynamic properties, Geokhimiya, vol. 12, pp. 1724–1732.

[29] Holland, T. J. B. and Powell, R., 1998, An internally consistent thermodynamic data set for phases of petrological interest, Journal of Metamorphic Geology, vol. 16, pp. 309–343.

[30] Wolery, T. J. and Daveler, S. A., 1992, *A software package for geochemical modeling of aqueous systems*, Lawrence Livermore National Laboratory.

[31] Lynch, D., 1982, Standard free energy of formation of NiAs, Metallurgical and Materials Transactions B, vol. 13(2), pp. 285–288.

[32] Langmuir, D., 1978, Uranium solution-mineral equilibria at low temperatures with applications to sedimentary ore deposits, Geochim. et Cosmoch. Acta, vol. 42(6), pp. 547–565.

[33] Harvie, C. and Moller, J., N.and Weare, 1984, The prediction of mineral solubilities in natural waters: The Na-K-Mg-Ca-H-Cl-SO4-OH-HCO3-CO3-CO2-H2O system to high ionic strengths at 25^{o}C, Geochim. Cosmochim. Acta, vol. 48, pp. 723–751.

[34] Vieillard, P. and Tardy, Y., 1984, *Phosphate Minerals*, Springer Verlag, New York, chap. Thermochemical properties of phosphates.

[35] Komada, N. et al., 1995, Thermodynamic properties of sodalite at temperatures from 15 K to 1000 K, J Chem Thermodyn, vol. 27(10), pp. 1119–1132.

[36] Hemingway, B. et al., 1990, The thermodynamic properties of dumortierite, American Mineralogist, vol. 75, pp. 1370–1375.

Table 3: Thermodynamic properties of the upper continental crust

Mineral	**Formula**	ξ_i, **mole/g**	$\Delta H^0_{f\,i}$, **kJ/mole**	$\Delta G^0_{f\,i}$, **kJ/mole**	**Reference**	$\pm\epsilon$, %	b_{chi}, **kJ/mole**
Quartz	SiO_2	3.81E-03	-911.6	-857.2	[4]		1.0
Albite	$NaAlSi_3O_8$	5.14E-04	-3927.6	-3704.5	[4]		4.8
Oligoclase	$Na_{0.8}Ca_{0.2}Al_{1.2}Si_{2.8}O_8$	4.49E-04	-796.0	-750.9	[4]		3023.9
Orthoclase/ K-feldspar	$KAlSi_3O_8$	4.22E-04	-3977.5	-3752.1		0	-12.8
Andesine	$Na_{0.6}Ca_{0.4}Al_{1.4}Si_{2.6}O_8$	2.03E-04	-808.9	-763.7	[4]		3076.6
Opal	$SiO_2 \cdot 0,5H_2O$	1.42E-04	-1044.5	-967.9		5	9.3
Augite	$Ca_{0.9}Na_{0.1}Mg_{0.9}Fe^{2+}_{0.2}Al_{0.4}Ti_{0.1}Si_{1.9}O_6$	1.27E-04	-3201.5	-3026.8	[6]		-446.9
Labradorite	$Na_{0.5}Ca_{0.5}Al_{1.5}Si_{2.5}O_8$	9.25E-05	-815.0	-769.8	[4]		3103.2
Biotite	$K(Mg_{2.5}Fe_{0.5})(Si_3Al)O_{10}\ (OH)_{1.75}F_{0.25}$	8.80E-05	-6079.4	-5706.7		1	78.6
Calcite	$CaCO_3$	8.00E-05	-1207.7	-1129.0	[4]		11.0
Hydromuscovite/ Illite	$K_{0.6}(H_3O)_{0.4}Al_2\ Mg_{0.4}Fe^{2+}_{0.1}Si_{3.5}O_{10}(OH)_2$	7.73E-05	-5886.2	-5499.1		1	325.2
Sillimanite	Al_2SiO_5	6.15E-05	-2587.4	-2441.0	[4]		11.7
Paragonite	$NaAl_3Si_3O_{10}(OH)_2$	4.95E-05	-5932.5	-5557.6	[4]		-15.7
Nontronite	$Na_{0.3}Fe^{3+}_2(Si_{3.7}\ Al_{0.3})O_{10}(OH)_2 \cdot 4(H_2O)$	3.88E-05	-6841.0	-5447.7		0.6	738.2
Magnetite	$Fe^{3+}_2Fe^{2+}O_4$	3.43E-05	-1118.3	-1015.9	[4]		122.6
Kaolinite	$Al_2Si_2O_5(OH)_4$	3.24E-05	-4117.7	-3796.0	[4]		-9.0
Ilmenite	$Fe^{2+}TiO_3$	3.10E-05	-1237.2	-1163.5	[4]		123.7
Diaspore	$AlO(OH)$	2.95E-05	-998.1	-917.6	[4]		-1.3
Hornblende-Fe	$Ca_2Fe^{2+}_4Al_{0.75}Fe^{3+}_{0.25}\ (Si_7AlO_{22})(OH)_2$	2.78E-05	-10976.4	-10303.7			398.5
Muscovite	$KAl_3Si_3O_{10}(OH)_{1.8}F_{0.2}$	2.54E-05	-5991.3	-5616.6		1	-13.1
Titanite	$CaTiSiO_5$	2.28E-05	-2597.1	-2455.1		0	37.2
Almandine	$Fe^{2+}_3Al_2(SiO_4)_3$	2.09E-05	-5305.5	-4969.8	[4]		335.7
Graphite	C	2.01E-05	0.0	0.0	[4]		410.3
Ripidolite	$(Mg_{3.75}Fe_{1.25}Al)\ (Si_3Al)O_{10}(OH)_2(OH)_6$	2.01E-05	-8429.2	-7788.2		0.6	175.2
Epidote	$Ca_2Fe^{3+}Al_2(SiO_4)_3(OH)$	1.87E-05	-6466.1	-6076.3	[4]		43.1
C org	C	1.84E-05	N.A.	N.A.			N.A.
Hydragillite/ Gibbsite	$Al(OH)_3$	1.77E-05	-1282.2	-1155.8	[4]		-1.4
Diopside	$CaMgSi_2O_6$	1.40E-05	-3031.2	-3026.3	[4]		47.4
Beidellite	$Na_{0.33}Al_{2.33}Si_{3.67}\ O_{10}(OH)_2$	1.39E-05	-5691.6	-5317.2		1	39.4
Ankerite	$CaFe^{2+}_{0.6}Mg_{0.3}Mn^{2+}_{0.1}(CO_3)_2$	1.36E-05	-2076.8	-1923.1		10	96.6
Aegirine	$NaFe^{3+}Si_2O_6$	1.32E-05	-2585.5	-2417.2	[6]		16.5
Andalusite	Al_2SiO_5	1.25E-05	-2590.4	-2443.0	[4]		9.7
Hyperstene	$MgFe^{2+}Si_2O_6$	1.17E-05	-2757.4	-2594.6	[4]		132.2
Goethite	$Fe^{3+}O(OH)$	1.17E-05	-559.4	-489.2	[4]		9.7
Halite	$NaCl$	1.01E-05	-386.3	-384.4	[4]		14.3
Boehmite	$AlO(OH)$	9.65E-06	-988.1	-914.1	[4]		2.2
Bytownite	$Na_{0.2}Ca_{0.8}Al_{1.8}Si_{2.2}O_8$	9.08E-06	-4186.8	-3960.7	[4]		10.5
Phosphate rock	$Ca_3(PO_4)_2$	8.99E-06	-3886.6	-3878.2	[4]		32.4
Natrolite	$Na_2Al_2Si_3O_{10} \cdot 2(H_2O)$	7.82E-06	-5722.1	-5316.6	[4]		3.8
Dolomite	$CaMg(CO_3)_2$	7.63E-06	-2327.9	-2167.9	[4]		18.0
Clinochlore	$Mg_{3.75}Fe_{1.25}Al_2\ Si_3O_{10}(OH)_8$	7.33E-06	-8435.5	-7796.6		1	166.8
Montmori- llonite	$Na_{0.165}Ca_{0.084}Al_{2.33}\ Si_{3.67}O_{10}(OH)_2$	6.52E-06	-5523.8	-5354.5		1	39.6
Lawsenite	$CaAl_2Si_2O_7(OH)_2 \cdot H_2O$	6.36E-06	-4812.8	-4510.6		5	2.2
Riebeckite	$Na_2Fe^{2+}_3Fe^{3+}_2(Si_8O_{22})(OH)_2$	6.14E-06	-10087.1	-9399.5		0	318.9
Hematite	Fe_2O_3	6.05E-06	-826.1	-742.2	[4]		17.4
Sepiolite	$Mg_4Si_6O_{15}(OH)_2 \cdot 6(H_2O)$	5.67E-06	-10123.7	-9257.8	[4]		1284.5
Hydrobiotite	$(K_{0.3}Ca_{0.1})(Mg_{2.3}Fe^{3+}_{0.6}\ Al_{0.1})(Si_{2.8}Al_{1.2})\ O_{10}((OH)_{1.8}F_{0.2}) \cdot 3(H_2O)$	5.26E-06	-7362.2	-6238.9		5	46.2
Ulvöspinel	$TiFe^{2+}_2O_4$	5.21E-06	-1489.4	-1392.9		10	273.1
Distene/Kyanite	Al_2SiO_5	4.37E-06	-2593.7	-2442.0	[4]		10.7
Cummingtonite	$Mg_7(Si_8O_{22})(OH)_2$	3.73E-06	-12070.0	-11343.0	[6]		181.6
Glaucophane	$Na_2(Mg_3Al_2)Si_8O_{22}(OH)_2$	3.65E-06	-12080.6	-11346.7	[4]		-78.8
Celestine	$SrSO_4$	3.65E-06	-1454.1	-1341.6	[4]		32.4
Prehnite	$Ca_2Al_2Si_3O_{10}(OH)_2$	3.58E-06	-6197.3	-5823.0	[4]		35.7
Rutile	TiO_2	3.41E-06	-945.4	-890.1	[4]		18.3
Barite	$BaSO_4$	3.04E-06	-1470.4	-1361.9	[4]		18.8
Niter	KNO_3	2.96E-06	-495.0	-395.2	[4]		-22.3
Nitratine	$NaNO_3$	2.96E-06	-468.2	-367.1	[4]		-24.2
Pennine	$(Mg_{3.75}Fe_{1.25}Al)\ (Si_3Al)O_{10}(OH)_2(OH)_6$	2.87E-06	-8429.2	-7788.2		0.6	175.2

Continued on next page ...

Table 3: Thermodynamic properties of the upper continental crust. – continued from previous page.

Mineral	Formula	ξ_i, mole/g	$\Delta H^0_{f\,i}$, kJ/mole	$\Delta G^0_{f\,i}$, kJ/mole	Reference	$\pm\epsilon$, %	b_{chi}, kJ/mole
Actinolite	$Ca_2Mg_3Fe_2Si_8O_{22}(OH)_2$	2.82E-06	-11519.4	-10801.5		1	405.9
Pyrite	FeS_2	2.75E-06	-175.0	-163.3	[4]		1428.1
Sanidine	$K_{0.75}Na_{0.25}AlSi_3O_8$	2.67E-06	-3860.7	-3715.9		1	15.9
Hastingsite	$NaCa_2Fe^{2+}_4Fe^{3+}(Si_6Al_2O_{22})(OH)_2$	2.60E-06	-11926.3	-11343.4	[28]		289.2
Ferrosilite	$Fe^{2+}MgSi_2O_6$	2.32E-06	-2757.4	-2594.6	[4]		132.2
Zircon	$ZrSiO_4$	2.11E-06	-2034.8	-1919.5	[4]		20.0
Siderite	$Fe^{2+}CO_3$	2.08E-06	-742.3	-671.1	[4]		122.0
Spodumene	$LiAlSi_2O_6$	2.06E-06	-3056.8	-2882.9	[4]		24.6
Pigeonite	$Mg_{1.35}Fe_{0.55}Ca_{0.1}(Si_2O_6)$	1.99E-06	-1535.4	-1448.8		1	1401.1
Leucoxene	$CaTiSiO_5$	1.90E-06	-2591.6	-2454.8	[4]		37.5
Pyrrhotite	$Fe^{2+}S$	1.79E-06	-105.5	-100.5	[4]		883.6
Lepidomelane/ Annite	$KFe^{2+}_{2.5}Mg_{0.5}Fe^{3+}_{0.75}\ Al_{0.25}Si_3O_{10}(OH)_2$	1.78E-06	-4995.0	-4642.3		1	284.8
Bronzite	$MgFeSi_2O_6$	1.77E-06	-2753.4	-2585.3		0	141.5
Anhydrite	$CaSO_4$	1.73E-06	-1435.1	-1322.7	[4]		16.3
Serpentine	$Mg_3Si_2O_5(OH)_4$	1.64E-06	-4363.4	-4035.4		0	51.9
Olivine	$Mg_{1.6}Fe^{2+}_{0.4}(SiO_4)$	1.53E-06	-2083.3	-1925.0		1	95.3
Enstatite	$Mg_2Si_2O_6$	1.39E-06	-3055.5	-2919.9	[4]		59.6
Corundum	Al_2O_3	1.20E-06	-1668.9	-1563.0	[4]		31.5
Thuringite- Chamosite	$(Fe_3Mg_2Fe^{3+}_{0.5}Al^{3+}_{0.5})\,(Si_3Al)O_{10}(OH)_2$	1.14E-06	-7596.0	-6981.9		0.6	-389.8
Neptunite	$KNa_2LiFe^{2+}_{1.5}Mn^{2+}_{0.5}\ Ti_2Si_8O_{24}$	1.10E-06	-10724.6	-10061.3		10	868.9
Sphalerite	ZnS	1.02E-06	-206.1	-201.4	[4]		744.9
Analcime	$NaAlSi2O_6\Delta(H_2O)$	1.01E-06	-3310.2	-3088.5	[4]		0.8
Anorthite	$CaAl_2Si_2O_8$	9.90E-07	-4274.4	-4021.0	[4]	1	15.6
Rhodochrosite	$MnCO_3$	9.48E-07	-894.7	-817.1	[4]		83.8
Chromite	$Fe^{2+}Cr_2O_4$	8.83E-07	-1445.7	-1358.4	[4]		195.1
Gypsum	$CaSO_4 \cdot 2H_2O$	7.96E-07	-2024.0	-1798.6	[4]		16.6
Apatite	$Ca_5(PO_4)_3(OH)_{0.33}\,F_{0.33}Cl_{0.33}$	7.91E-07	-6773.4	-6386.9		5	-23.2
Staurolite	$Fe^{2+}Al_9Si_4O_{23}(OH)$	7.68E-07	-12066.8	-11215.6	[4]		269.1
Talc	$Mg_3Si_4O_{10}(OH)_2$	7.67E-07	-5907.2	-5543.0	[4]		22.6
Aragonite	$CaCO_3$	7.64E-07	-1207.9	-1128.6	[4]		11.4
Clinozoisite	$Ca_2Al_3(SiO_4)_3(OH)$	7.51E-07	-6883.9	-6483.9	[4]		53.0
Vermiculite	$Mg_3Si_4O_{10}(OH)_2 \cdot 2(H_2O)$	6.78E-07	-7018.8	-5957.2	[4]	10	1717.4
Tephroite	$Mn^{2+}_2(SiO_4)$	6.30E-07	-1733.3	-1632.1	[4]		199.3
Thomsonite	$NaCa_2Al_5Si_5O_{20} \cdot 6H_2O$	6.19E-07	-12413.7	-11543.9		1	-49.1
Zoisite	$Ca_2Al_3Si_3O_{12}(OH)$	5.68E-07	-6883.9	-5416.5	[4]		1120.4
Pyrolusite	MnO_2	5.64E-07	-520.4	-465.2	[4]		23.4
Anatase	TiO_2	5.59E-07	-940.4	-883.7	[4]		24.7
Psilomelane	$Ba_2Mn^{2+}_2Mn^{4+}_3\ O_{10} \cdot 2H_2O$	5.10E-07	-2569.1	-2347.2		1	2103.1
Nepheline	$Na_{0.75}K_{0.25}Al(SiO_4)$	5.09E-07	-2087.6	-1972.4		1	28.1
Forsterite	Mg_2SiO_4	4.95E-07	-2175.5	-2057.8	[4]		63.6
Jadeite	$NaAl_{0.9}Fe^{3+}_{0.1}(Si_2O_6)$	4.78E-07	-2990.4	-2812.1		1	-2.7
Spessartine	$Mn2 + 3Al2(SiO4)3$	4.77E-07	-5646.3	-5326.3	[29]		302.6
Monazite (Ce)	$Ce_{0.5}La_{0.25}Nd_{0.2}\ Th_{0.05}(PO_4)$	4.29E-07	-2074.0	-1943.3		10	-43.3
Tremolite	$Ca_2Mg_5Si_8O_{22}(OH)_2$	4.28E-07	-12367.8	-11639.3	[4]		73.7
Crossite	$Na_2Mg_2Fe^{2+}Al_2\ (Si_8O_{22})(OH)_2$	4.06E-07	-11600.3	-10925.8		1	133.0
Braunite	$Mn^{2+}Mn^{3+}_6SiO_{12}$	4.06E-07	-4260.0	-3944.7	[6]		325.8
Chalcopyrite	$CuFeS_2$	3.62E-07	-194.6	-195.1	[6]		1530.3
Sassolite	H_3BO_3	3.60E-07	-1095.1	-969.0	[4]		19.7
Magnesite	$MgCO_3$	3.58E-07	-1114.1	-1030.2	[4]		15.6
Ilmenorutile	$Ti_{0.7}Nb_{0.15}Fe^{2+}_{0.225}O_2$	3.22E-07	-864.6	-813.2		1	45.5
Witherite	$BaCO_3$	3.04E-07	-1217.1	-1137.6	[4]		44.1
Stilpnomelane	$K_{0.}8Fe_8Al_{0.8}5Si_{11.1}\ O_{21}(OH)8 \cdot 6H_2O$	2.77E-07	-16655.5	-15197.0		0	5459.7
Hedenbergite	$CaFe^{2+}Si_2O_6$	2.75E-07	-2842.4	-2676.1	[4]		8651.4
Hollandite	$Ba_{0.8}Pb_{0.2}Na_{0.125}\ Fe_{1.3}Al_{0.2}Si_{0.1}\ Mn^{2+}_{0.5}Mn^{4+}_6O_{16}$	2.63E-07	-4733.3	-4330.4		1	288.3
Fayalite	$Fe^{2+}_2SiO_4$	2.34E-07	-1480.9	-1369.2	[4]		246.6
Rhodonite	$Mn^{2+}SiO_3$	2.32E-07	-1321.6	-1243.1	[4]		101.7
Cristobalite	SiO_2	2.06E-07	-910.1	-855.5	[4]		2.7
Pumpellyte	$Ca_2MgAl_2(SiO_4)\,(Si_2O_7)(OH)_2 \cdot H_2O$	1.89E-07	-7148.6	-6672.5		1	57.9

Continued on next page ...

Table 3: Thermodynamic properties of the upper continental crust. – continued from previous page.

Mineral	Formula	ξ_i, mole/g	$\Delta H^0_{f\,i}$, kJ/mole	$\Delta G^0_{f\,i}$, kJ/mole	Reference	$\pm\epsilon$, %	b_{chi}, kJ/mole
Phlogopite	$KMg_3AlSi_3O_{10}F(OH)$	1.58E-07	-6292.8	-5902.2		1	128.1
Manganite	$MnO(OH)$	1.55E-07	-622.4	-557.3		10	49.4
Fluorite	CaF_2	1.44E-07	-1220.5	-1168.1	[4]		111.9
Amblygonite	$Li_{0.75}Na_{0.25}Al(PO_4)\,F_{0.75}(OH)_{0.25}$	1.29E-07	-307.1	-282.7		10	1992.6
Vesuvianite	$Ca_{10}Mg_2Al_4(SiO_4)_5(Si_2O_7)_2(OH)_4$	1.20E-07	-21175.8	-19948.7	[29]		219.0
Jacobsite	$Mn^{2+}_{0.6}Fe^{2+}_{0.3}Mg^{2+}\ Fe^{3+}_{1.5}Mn^{3+}_{0.5}O_4$	1.20E-07	-1237.4	-1137.5		5	711.5
Bastnaesite	$La(CO_3)F$	1.16E-07	-1660.9	-1527.8		5	160.8
Arfvedsonite	$Na_3Fe^{2+}_4Fe^{3+}(Si_8O_{22})(OH)_2$	1.09E-07	-11926.3	-11201.5	[28]		-1146.5
Spinel	$MgAl_2O_4$	1.07E-07	-2281.0	-2172.5	[4]		53.6
Lepidolite	$KLi_2AlSi_4O_{10}F(OH)$	1.03E-07	-6003.2	-5654.7		1	126.7
Cordierite	$Mg_2Al_4Si_5O_{18}$	9.52E-08	-9114.7	-8603.9	[4]		139.2
Kernite	$Na_2O\cdot 2B_2O_3\cdot 4H_2O$	8.99E-08	-4104.9	-3713.1		5	440.8
Pyrophyllite	$Al_2Si_4O_{10}(OH)_2$	8.93E-08	-5632.5	-5257.6	[4]		7.6
Francolite	$Ca_5(PO4)_{2.63}\ (CO_3)_{0.5}F_{1.11}$	8.68E-08	-5984.4	-5698.1		1	714.3
Orthite- Allanite	$Ca(Ce_{0.4}Ca_{0.2}Y_{0.133})\,(Al_2Fe^{3+})Si_3O_{12}(OH)$	7.81E-08	-6481.6	-6055.4		1	32.3
Pentlandite	$Fe^{2+}_{4.5}Ni_{4.5}S_8$	7.44E-08	-778.3	-766.2		10	6833.9
Ulexite	$NaCa(B_5O_6(OH)_6\cdot 5H_2O$	7.19E-08	-6762.2	-6151.5		0	2855.3
Scapolite- Marialite	$Na_4Al_3Si_9O_{24}Cl$	6.34E-08	-12197.4	-11504.2		0	22.5
Chloritoid	$Fe^{2+}_{1.2}Mg_{0.6}Mn^{2+}_{0.2}\,Al_4Si_2O_{10}(OH)_4$	6.18E-08	-6606.9	-6152.6		1	159.8
Pollucite	$Cs_{0.6}Na_{0.2}Rb_{0.1}Al_{0.9}\,Si_{2.1}O_6\cdot(H_2O)$	6.14E-08	-3297.1	-3074.2		10	10.0
Colemanite	$Ca_2B_6O_{11}\cdot 5H_2O$	5.99E-08	-6949.7	-6277.0		5	-796.8
Beryl	$Be_3Al_2Si_6O_{18}$	5.99E-08	-9006.5	-8500.4		0	56.9
Marcasite	$FeS2$	5.24E-08	-154.9	-156.6	[8]		1434.8
Grossular	$Ca_3Al_2(SiO_4)_3$	4.62E-08	-6631.1	-6281.0	[4]		65.4
Vaesite	NiS_2	4.23E-08	-134.2	-126.4	[30]		1320.6
Gedrite	$Mg_5Al_2(Si_6Al_2O_{22})(OH)_2$	4.12E-08	-12319.7	-11584.2		0	149.9
Tourmaline- Schorl	$NaFe^{2+}_3Al_6(BO_3)_3Si_6\ O_{18}(OH)_4$	4.09E-08	-14401.4	-13453.5		0	377.6
Wollastonite	$CaSiO_3$	4.08E-08	-1631.6	-1550.9	[4]		33.1
Clementite	$Fe^{2+}_3Mg_{1.5}AlFe^{3+}Si_3AlO_{12}(OH)_6$	3.81E-08	-7657.8	-7043.1		1	504.6
Cryptomelane	$K_8(Mn^{4+}_{7.5}Mn^{2+}_{0.5})\,O_{16}$	3.09E-08	-3743.6	-3432.2		1	3409.1
Kieserite	$MgSO_4\cdot(H_2O)$	3.06E-08	-1602.1	-1428.7	[5]		54.2
Arsenopyrite	$FeAsS$	2.89E-08	-41.9	-50.2	[4]		1428.0
Galena	PbS	2.79E-08	-100.5	-95.9	[4]		743.6
Murmanite	$Na_4Ti_{3.6}Nb_{0.4}(Si_2O_7)_2O_4\cdot 4(H_2O)$	2.78E-08	-9804.0	-9096.6		10	354.0
Sylvite	KCl	2.74E-08	-437.0	-410.2	[4]		18.5
Brucite	$Mg(OH)_2$	2.71E-08	-925.9	-834.8	[4]		34.9
Anthophyllite	$Mg_7Si_8O_{22}(OH)_2$	2.67E-08	-12094.6	-11396.0	[4]		128.6
Ferrocolum- bite	$Fe^{2+}Nb_2O_6$	2.40E-08	-2172.8	-2018.6		10	170.5
Covellite	CuS	2.27E-08	-53.2	-53.6	[4]		687.7
Vernadite	$Mn^{4+}_{0.6}Fe^{3+}_{0.2}Ca_{0.2}\ Na_{0.1}O_{1.5}(OH)_{0.5}\cdot 1.4(H_2O)$	2.18E-08	-637.8	-571.4		1	393.5
Thorite	$ThSiO_4$	2.13E-08	-2160.5	-2048.8		5	27.8
Nickeline	$NiAs$	2.04E-08	N.A.	N.A.			N.A.
Sapphirine	$Mg_4Al_{6.5}Si_{1.5}O_{20}$	2.04E-08	-10563.3	-9962.9	[4]		2366.3
Andradite	$Ca_3Fe^{2+}_2(SiO_4)_3$	1.96E-08	-5764.4	-5419.4	[4]		92.1
Chrysoberyl	$BeAl_2O_4$	1.80E-08	-2302.3	-2178.2	[4]		20.9
Cassiterite	SnO_2	1.73E-08	-581.1	-519.6	[4]		32.0
Violarite	$Fe^{2+}Ni_2S_4$	1.72E-08	-378.0	-368.9		1	2902.0
Todorokite	$Na_2Mn^{4+}_4Mn^{3+}_2O_{12}\cdot 3H_2O$	1.34E-08	-4037.4	-3576.5		1	742.6
Cubanite	$CuFe_2S_3$	1.33E-08	-293.7	-302.8		1	2406.7
Topaz	$Al_2(SiO_4)F_{1.1}(OH)_{0.9}$	1.29E-08	-3044.4	-2875.2		5	-11.4
Glauconite	$(K_{0.6}Na_{0.05})(Fe^{3+}_{1.3}\,Mg_{0.4}Fe^{2+}_{0.2}Al^{3+}_{0.15})\,(Si_{3.8}Al_{0.2})O_{10}(OH)_2$	1.21E-08	-5150.3	-4785.6		0.6	52.1
Garnierite	$(Ni_2Mg)Si_2O_5(OH)_4$	1.18E-08	-3494.6	-3267.1		1	25.9
Molybdenite	MoS_2	1.14E-08	-271.8	-262.8	[6]		1682.2
Clinohumite	$Mg_{6.75}Fe_{2.25}Si_4O_{16}\ (OH)_{0.5}F_{1.5}$	1.10E-08	-8966.4	-8410.0		1	613.5
Tridymite	SiO_2	1.05E-08	-909.7	-855.9	[4]		2.3
Euxenite	$Y_{0.7}Ca_{0.2}Ce_{0.1}(Ta_{0.2})_2\ (Nb_{0.7})_2(Ti_{0.025})O_6$	1.02E-08	-2671.5	-2506.3		10	136.7
Gersdorffite	$NiAsS$	9.70E-09	N.A.	-144.3	[31]		1189.5
Jarosite	$KFe^{3+}_3(SO_4)_2(OH)_6$	9.57E-09	-3521.7	-3318.7		10	208.5

Continued on next page …

Table 3: Thermodynamic properties of the upper continental crust. – continued from previous page.

Mineral	Formula	ξ_i, mole/g	$\Delta H^0_{f\,i}$, kJ/mole	$\Delta G^0_{f\,i}$, kJ/mole	Reference	$\pm\epsilon$, %	b_{chi}, kJ/mole
Humite	$Mg_{5.25}Fe^{2+}_{1.75}(SiO_4)_3\ F_{1.5}(OH)_{0.5}$	9.46E-09	-6953.6875	-6512.3		5	504.3
Scheelite	$CaWO_4$	9.28E-09	-1646.2	-1419.6	[4]		139.8
Komerupine	$Mg_{1.1}Fe_{0.2}Al_{5.7}\ (Si_{3.7}B_{0.3})O_{17.2}(OH)$	9.24E-09	-9172.9	-8624.8		1	173.8
Omphacite	$Ca_{0.6}Na_{0.4}Mg_{0.6}Al_{0.3}\ Fe_{0.1}Si_2O_6$	7.48E-09	-3075.5	-2904.3		1	38.7
Phenakite	Be_2SiO_4	7.31E-09	-2146.2	-2033.3	[4]		34.1
Hisingerite	$Fe^{3+}_2Si_2O_5(OH)_4 \cdot 2(H_2O)$	6.25E-09	-3229.6	-2895.6	[16]		1012.8
Uraninite	UO_2	5.60E-09	-1085.6	-1032.5	[4]		167.6
Malachite	$Cu_2(CO_3)(OH)_2$	5.46E-09	-1052.1	-906.0	[4]		24.3
Strontianite	$SrCO_3$	5.34E-09	-1220.9	-1140.1	[4]		34.9
Brookite	TiO_2	5.27E-09	-942.4	-821.9	[4]		86.5
Perovskite	$CaTiO_3$	5.10E-09	-1662.2	-1575.7	[4]		58.5
Yttrialite	$Y_{1.5}Th_{0.5}Si_2O_7$	4.64E-09	N.A.	N.A.			N.A.
Azurite	$Cu_3(CO_3)_2(OH)_2$	4.38E-09	-1633.3	-1447.5	[4]		39.0
Copper	Cu	3.90E-09	0.0	0.0	[4]		134.0
Pyrochlore	$NaCaNb_2O_6(OH)_{0.75}F_{0.25}$	3.47E-09	-2897.9	-2687.3		10	345.0
Bertrandite	$Be_4Si_2O_7(OH)_2$	3.38E-09	-4586.1	-4300.6		0	72.3
Aenigmatite	$Na_2Fe^{2+}_5TiSi_6O_{20}$	3.16E-09	-8184.4	-7660.9		10	-164.8
Carnotite	$K_2(UO_2)_2(VO_4)_2 \cdot 3H_2O$	2.80E-09	-4907.3	-4585.5	[32]		792.4
Palygorskite	$MgAlSi_4O_{10}(OH) \cdot 4(H_2O)$	2.77E-09	-6477.8	-5939.9		1	440.4
Dietzeite	$Ca_2(IO_3)_2(CrO_4)$	2.76E-09	-2425.4	-2148.1		10	78.7
Lautarite	$Ca(IO_3)_2$	2.76E-09	-1002.5	-839.3	[5]		71.4
Bornite	Cu_5FeS_4	2.65E-09	-334.5	-393.1	[4]		3083.0
Dawsonite	$NaAl(CO_3)(OH)_2$	2.51E-09	-1965.3	-1787.3	[4]		-0.1
Cryolite	Na_3AlF_6	2.36E-09	-3311.3	-3144.7	[4]		327.9
Orpiment	As_2S_3	1.85E-09	-169.1	-168.7	[4]		2641.2
Sulphur	S_8	1.84E-09	0.0	0.0	[4]		4858.2
Zinc	Zn	1.55E-09	0.0	0.0	[4]		339.0
Helvite	$Mn_4Be_3(SiO_4)_3S$	1.45E-09	-5843.9	-5532.4		10	1407.7
Carnallite	$KMgCl_3 \cdot 6(H_2O)$	1.45E-09	-2946.7	0.0	[33]		2611.0
Gadolinite	$Y_2Fe^{2+}Be_2(Si_2O_{10})$	1.41E-09	-5220.0	-4943.3		10	299.7
Xenotime	$YbPO_4$	1.38E-09	-1868.6	-1790.3	[34]		24.2
Nosean	$Na_8Al_6Si_6O_{24}\ SO_4$	1.29E-09	-13936.7	-13131.5		5	115.0
Wolframite	$Fe^{2+}_{0.5}Mn_{0.5}WO_4$	1.06E-09	-1246.2	-1146.4		1	120.0
Hydrosodalite	$Na_8Al_6Si_6O_{24}\ (OH)_2$	9.06E-10	-13408.5	-12678.2		5	193.1
Cerussite	$PbCO_3$	8.27E-10	-700.0	-627.5	[4]		20.9
Stibnite	Sb_2S_3	8.10E-10	-175.0	-173.7	[4]		2522.3
Greenockite	CdS	8.01E-10	-162.0	-156.5	[4]		743.9
Chalcocite	Cu_2S	6.83E-10	-79.5	-86.2	[4]		789.1
Smithsonite	$ZnCO_3$	6.36E-10	-813.3	-731.9	[4]		23.3
Blomstrandite	$U_{0.3}Ca_{0.2}Nb_{0.9}Ti_{0.8}Al_{0.1}\ Fe^{3+}_{0.1}Ta_{0.5}O_6(OH)$	4.96E-10	-2884.5	-2683.8		10	90.0
Loparite - (Ce)	$Na_{0.6}Ce_{0.22}La_{0.11}\ Ca_{0.1}Ti_{0.8}Nb_{0.2}O_3$	4.81E-10	-1430.8	-1343.6		10	181.6
Magnesioferrite	$MgFe^{3+}_2O_4$	4.40E-10	-1429.4	-1351.0	[4]		40.2
Eudyalite	$Na_4Ca_2Fe^{2+}_{0.7}Mn_{0.3}ZrSi_8O_{22}(OH)_{1.5}Cl_{1.5}$	4.30E-10	-11859.9	-11062.9		1	335.0
Sirtolite	$ZrSiO_4$	4.02E-10	-2034.8	-1919.2	[4]		20.3
Bischofite	$MgCl_2 \cdot 6(H_2O)$	3.96E-10	-2500.7	-2116.4	[4]		66.0
Tin	Sn	3.87E-10	0.0	0.0	[4]		547.6
Anglesite	$PbSO_4$	3.82E-10	-920.0	-784.5	[4]		62.9
Ramsayite	$Na_2Ti_2Si_2O_9$	3.62E-10	-4360.1	-4103.9		10	104.3
Ferrotantalite	$Fe^{2+}Ta_2O_6$	3.07E-10	-2319.3	-2163.9		10	174.5
Lead	Pb	3.05E-10	0.0	0.0	[4]		232.2
Chondrodite	$Mg_{3.75}Fe^{2+}_{1.25}(SiO_4)_2\ F_{1.5}(OH)_{0.5}$	2.93E-10	-5023.0	-4701.4		5	564.2
Arsenolite	As_2O_3	2.80E-10	-659.8	-579.1	[4]		415.0
Cinnabar	HgS	2.46E-10	-58.2	-50.7	[4]		671.3
Iotsite	FeO	2.38E-10	-272.1	-251.5	[4]		127.3
Britholite	$Ca_{2.9}Ce_{0.9}Th_{0.6}La_{0.4}Nd_{0.2}\ Si_{2.7}P_{0.5}O_{12}(OH)_{0.8}F_{0.2}$	2.18E-10	-7057.3	-6666.9		10	734.0
Sodalite	$Na_8Al_6Si_6O_{24}Cl_2$	2.05E-10	-13457.0	-12703.6	[35]		51.9
Native silver	Ag	1.94E-10	0.0	0.0	[4]		69.7
Axinite- Fe	$Ca_2Fe^{2+}Al_2BO_3\ Si_4O_{12}(OH)$	1.93E-10	-7640.4	-7180.9		10	427.3
Realgar	As_4S_4	1.40E-10	-140.3	-132.7		0	4272.6

Continued on next page ...

Table 3: Thermodynamic properties of the upper continental crust. – continued from previous page.

Mineral	Formula	ξ_i, mole/g	$\Delta H^0_{f\,i}$, kJ/mole	$\Delta G^0_{f\,i}$, kJ/mole	Reference	$\pm\epsilon$, %	b_{chi}, kJ/mole
Bismuth	Bi	1.30E-10	0.0	0.0	[4]		274.8
Bismutite	$Bi_2(CO_3)O_2$	1.19E-10	-968.0	-888.7		10	81.1
Rhabdophane	$Ce_{0.75}La_{0.25}(PO_4)\cdot H_2O$	1.03E-10	-1964.9	-1821.9		1	325.0
Bismite	$Bi2O_3$	9.91E-11	-574.3	-493.7	[4]		61.9
Bismuthinite	Bi_2S_3	9.91E-11	-143.2	-140.6	[4]		2230.8
Baddeleyite	ZrO_2	9.75E-11	-1101.3	-1043.3	[4]		38.1
Fergusonite	$Nd_{0.4}Ce_{0.4}Sm_{0.1}Y_{0.1}NbO_4$	8.08E-11	-2808.3	-2631.2		10	-717.4
Cobaltite	$CoAsS$	5.06E-11	-163.1	N.A.		1	N.A.
Smaltite	$CoAs_2$	5.06E-11	-61.5	N.A.	[5]		N.A.
Argentite	Ag_2S	4.99E-11	-29.4	-39.4	[4]		707.3
Cancrinite	$Na_6Ca_2Al_6Si_6O_{24}(CO_3)_2$	4.20E-11	-14980.9	-14136.3		10	101.8
Moissanite	SiC	3.51E-11	-62.8	-60.3	[4]		1204.1
Uranium- Thorite	$ThSiO_4$	3.18E-11	-2160.5	-2048.8		5	27.8
Powellite	$CaMoO_4$	3.05E-11	-1542.4	-1434.7	[4]		27.6
Chevkinite	$Ce_{1.7}La_{1.4}Ca_{0.8}Th_{0.1}\ Fe^{2+}_{1.8}Mg_{0.5}\ Ti_{2.5}Fe^{3+}_{0.5}Si_4O_{22}$	2.76E-11	-10499.8	-9894.5		10	1006.2
Acanthite	Ag_2S	2.74E-11	-32.4	-40.3	[4]		706.4
Lavenite	$Na_{1.1}Ca_{0.9}Mn^{2+}_{0.5}Fe^{2+}_{0.5}\ Zr_{0.8}Ti_{0.1}Nb_{0.1}(Si_2O_7)\ O_{0.6}(OH)_{0.3}F_{0.1}$	2.59E-11	-4191.1	-3925.1		10	604.8
Pyrargirite	Ag_3SbS_3	2.38E-11	-131.5	-142.2		5	2325.9
Linnaeite	Co_3S_4	1.69E-11	-307.3	-323.6	[4]		3032.2
Thorianite	ThO_2	1.56E-11	-1227.2	-1169.6	[4]		48.8
Troilite	FeS	1.19E-11	-100.5	-99.9	[4]		884.2
Microlite	$Na_{0.4}Ca_{1.6}Ta_2O_{6.6}\ (OH)_{0.3}F_{0.1}$	8.71E-12	-3208.3	-3004.3		10	315.1
Delorenzite	$Y_{0.7}Ca_{0.2}Ce_{0.12}(Ta_{0.7})_2\ (Nb_{0.2})_2(Ti_{0.1})O_{5.5}(OH)_{0.5}$	8.33E-12	-2721.2	-2549.9		10	54.6
Stephanite	Ag_5SbS_4	7.72E-12	-166.1	-184.5		5	3030.3
Naegite	$ZrSiO_4$	6.98E-12	-2034.8	-1919.2	[4]		20.3
Gold	Au	6.47E-12	0.0	0.0	[4]		51.5
Lampro- phyllite	$Na_2SrBaTi_3Si_4O_{16}(OH)F$	5.61E-12	-8401.2	-7865.3		10	892.0
Chlorargirite	$AgCl$	5.47E-12	-127.2	-109.9	[4]		22.0
Periclase	MgO	3.77E-12	-602.2	-569.5	[4]		62.1
Chrysocolla	$Cu_2Si_2O_6(H_2O)_4$	3.54E-12	-3279.4	-2964.6		10	-23.9
Freibergite	$Ag_{7.2}Cu_{3.6}Fe^{2+}_{1.2}\ Sb_3AsS_{13}$	3.52E-12	-703.2	-727.5		5	10786.0
Metacinnabar	HgS	3.17E-12	-53.6	-47.7	[4]		674.3
Vivianite	$Fe_3(PO_4)_2(H_2O)_8$	2.59E-12	-4608.4	-4428.2		10	457.4
Cooperite	$Pt_{0.6}Pd_{0.3}Ni_{0.1}S$	2.11E-12	-79.8	-73.8		1	688.3
Miserite	$KCa_2Ce_3Si_8O_{22}\ (OH)_{1.5}F_{0.5}$	2.00E-12	-11738.2	-11035.1		10	1138.1
Tortbernite	$Cu(UO_2)2(PO_4)2\cdot 8(H_2O)$	1.81E-12	-4455.9	-4129.8	[32]		151.6
Weinschenkite	YPO_4	1.68E-12	-1987.7	-1871.1		0	-35.2
Wulfenite	$PbMoO_4$	1.66E-12	-1112.9	-952.8	[4]		17.8
Loellingite	$FeAs_2$	1.30E-12	-85.7	-80.2		0	1284.7
Tennantite	$Cu_{10}Fe_2As_4S_{13}$	1.24E-12	-1968.6	-1999.6		0	9965.1
Tellurite	TeO_2	1.14E-12	-322.8	-270.3	[4]		60.0
Sylvanite	$Au_{0.75}Ag_{0.25}Te_2$	7.62E-13	N.A.	N.A.			N.A.
Nordite	$Na_{2.8}Mn^{2+}_{0.2}Sr_{0.5}Ca_{0.5}\ La_{0.33}Ce_{0.6}Zn_{0.6}\ Mg_{0.4}Si_6O_{17}$	7.20E-13	-8020.8	-7532.2		10	958.5
Calaverite	$AuTe_2$	5.71E-13	-19.0	-17.4		0	686.8
Samsonite	$Ag_4MnSb_2S_6$	5.29E-13	-444.9	-463.5		5	4817.9
Tetrahedrite	$Cu_{10}Fe_2Sb_4S_{13}$	3.47E-13	-1909.5	-1939.7		0	9797.1
Thortveitite	$Sc_{1.5}Y_{0.5}Si_2O_7$	2.71E-13	-3740.2	-3540.6		5	50.5
Tetradymite	Bi_2Te_2S	2.27E-13	-100.2	-100.6		1	1709.0
Rinkolite	$Na_2Ca_3Ce_{1.5}Y_{0.5}\ Ti_{0.4}Nb_{0.5}Zr_{0.1}(Si_2O_7)_2\ O_{1.5}F_{3.5}$	2.25E-13	-9415.1	-8808.5		10	1441.1
Alunite	$KAl_3(SO_4)2(OH)_6$	2.20E-13	-5173.2	-4652.2	[4]		127.3
Osmium	$Os_{0.75}Ir_{0.25}$	1.57E-13	N.A.	N.A.			N.A.
Iridium	$Ir_{0.5}Os_{0.3}Ru_{0.2}$	1.50E-13	N.A.	N.A.			N.A.
Dumortierite	$Al_{6.9}(BO_3)(SiO_4)_3O_{2.5}(OH)_{0.5}$	1.33E-13	-9109.0	-8568.0	[36]		108.9
Polycrase (Y)	$Y_{0.5}Ca_{0.1}Ce_{0.1}U_{0.1}\ Th_{0.1}Ti_{1.2}Nb_{0.6}Ta_{0.2}O_6$	2.46E-14	-2847.7	-2681.3		10	125.4
I-Platinum	Pt	1.54E-14	0.0	0.0	[4]		146.5
Polixene/ Tetraferro-platinum	$PtFe$	1.20E-14	N.A.	N.A.			N.A.
Boulangerite	$Pb_5Sb_4S_{11}$	2.12E-15	-1034.5	-1023.7		5	8565.5
Wohlerite	$NaCa_2Zr_{0.6}Nb_{0.4}\ Si_2O_{8.4}(OH)_{0.3}F_{0.3}$	1.27E-15	-4439.7	-4170.0		10	466.6
End of the table							

Comparison of Exergoenvironmental Analysis Using Three Different Environmental Impact Assessment Methods in a Case of a Process of Electricity Production

J. Buchgeister

Karlsruhe Institute of Technology, Institute for Technology Assessment and Systems Analysis, Karlsruhe, Germany

Abstract: The exergoenvironmental analysis has been developed in order to reveals to which extent each component of an energy conversion system is responsible for the overall environmental impact, and identifies the sources of the impact. The required values of the environmental impact are determined by applying a life cycle assessment which quantifies the environmental impact. Here the Eco-indicator 99 is chosen as a single score life cycle impact assessment (LCIA) method, but besides the Eco-indicator 99 exists different other LCIA methods in order to quantify environmental impacts.
To validate this selection of Eco-indicator 99 as LCIA method for quantifying environmental impacts in the new exergoenvironmental analysis a comparative analysis is carried out.
Based on the results of exergoenvironmental analysis for electricity production by means of SOFC with integrated allothermal biomass gasification published in [1,2] two other LCIA methods (CML 2001, IMPACT 2002) are conducted in the exergoenvironmental analysis. It will be presented the general structure, extent of considered environmental aspects, and mathematical relationship for quantifying the cause-effect chain from emissions to an environmental impact for all used LCIA methods in detail.
Furthermore as result will be shown that for all applied LCIA methods the same components (heat exchanger HX A1, gasifier, SOFC) are main relevant for the highest environmental impact. Anymore is pointed out the results of sensitivity analysis which presents various pollutants are responsible for the highest contribution of each LCIA method in relation to the total environmental impact.

Keywords: Exergoenvironmental Analysis, life cycle impact assessment.

1. Introduction

The exergoenvironmental analysis has been developed in order to reveals to which extent each component of an energy conversion system is responsible for the overall environmental impact, and identifies the sources of the impact [1,2]. The exergoenvironmental analysis consists of three steps. In the first step, a detailed exergy analysis of the considered energy conversion system is conducted. In the second step, the required values of the environmental impact are determined by applying a life cycle assessment (LCA) which quantifies the environmental impact. Here the Eco-indicator 99 is used as a single score life cycle impact assessment (LCIA) method [3]. In the third step, the environmental impact associated with each component is assigned to the product exergy streams of the component; subsequently exergoenvironmental variables are calculated and an exergoenvironmental evaluation is conducted.

In conjunction with the LCA exists besides the Eco-indicator 99 different other LCIA methods in order to quantify environmental impacts. The development of LCIA methods provide different approaches according to the given standards of DIN EN ISO 14040 and 14044 [4].

The differences are the extent of considered environmental aspects, mathematical relationship for quantifying the cause-effect chain from emissions to an impact in the environment (describing environmental mechanism).

The CML 2001 and IMPACT 2002 method are two of these different LCIA methods. The CML method has a long tradition and was applied very often in LCA [5,6]. The IMPACT method is a new one which combines elements of the Eco-indicator and CML methods [7,8].

To validate the selection of Eco-indicator 99 as LCIA method for quantifying environmental impacts in the new exergoenvironmental analysis a comparative analysis is carried out. In the following based on the results of exergo-environmental analysis for electricity production by means of SOFC with integrated allothermal

Corresponding Author: Jens Buchgeister, Email: Jens.Buchgeister@kit.edu

biomass gasification published in [1,2] the CML and IMPACT method are conducted in the exergo-environmental analysis. It will be investigated the influence of the used LCIA method on the result of exergoenvironmental analysis.

2. Methodology of the Exergoenvironmental Analysis

The structure of the exergoenvironmental analysis consists in analogy to the exergoeconomic analysis mainly of three steps. After goal and scope definition and the modeling of the energy conversion process starts the first major step: the exergy analysis. The exergy of all material and energy flows connecting the components and crossing the system boundaries as inputs and outputs is determined. To calculate exergetic efficiency of every process component k the the definition of its exergetic fuel $\dot{E}_{F,k}$ and product $\dot{E}_{P,k}$ must be carried out according to its exergetic purpose.

2.1. Determination of quantitative Environmental Impacts

In the second step quantitative environmental impacts are determined by applying the method of LCA. The LCA is an internationally established and standardized method for the analysis of the complete life cycle of products and services [6]. It analyses the consumption and emission of material flows from all process steps within the life cycle.

Based on the life cycle inventory (LCI) result the environmental impacts for various environmental impact categories are calculated by a quantitative impact assessment method. For methodological development of exergoenvironmental analysis is chosen an single-score LCIA method – the Eco-indicator 99 [3]. It is especially developed as impact assessment method to support decision-making in a design for the environment. The structure and the considered environmental aspects are displayed in figure 1.

In the resource analysis, land use analysis or fate analysis inventory data of each component of the overall system are assigned to compartments (e.g., water, soil, air) in which they could cause environmental problems. Within the following exposure and effect analysis, a classification into categories of environmental problems is performed. The categories cover the width of environmental aspects and model the environmental damages to three damage categories: human health, ecosystem quality and natural resources.

In a last step, the 3 damage categories are normalized and weighted (hierarch perspective is applied) so that consequently the result is expressed as Eco-indicator points (pts), where higher damage is represented by a higher Eco-indicator value. The characterization model for each impact category is determined in detail in [3].

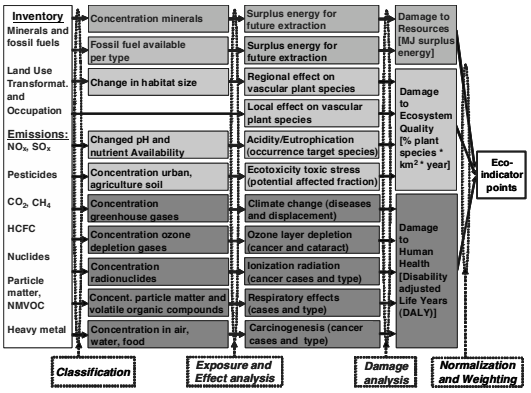

Fig. 1. Structure of the endpoint LCIA method Eco-indicator 99 (hierarch perspective).

2.2. Assigning Environmental Impacts to Exergy Streams

In the third step, the results of the LCA are assigned to the corresponding exergy streams by calculating the specific environmental impact rate of each material and energy stream b_j (expressed in eco-indicator points per exergy unit).

The latter depends on the environmental impact rate $\dot{B}_j$ and the exergy rate $\dot{E}_j$ of the jth stream:

$$b_j = \frac{\dot{B}_j}{\dot{E}_j} \qquad (1)$$

The environmental impacts associated with the supply of an input stream (e.g. the impacts of cultivation, harvest, and transport of biomass) can be calculated directly. To calculate the values for internal as well as for output streams, the functional relations among the system components have to be considered.

This is done by formulating environmental impact balances for all components k of the system:

$$\sum \dot{B}_{j,k,in} + \dot{Y}_k = \sum \dot{B}_{j,k,out} \qquad (2)$$

Basically, all environmental impacts entering a component have to exit the component associated with all output streams. Therefore, there is not only an exergy flow through the system but also a flow of environmental impacts. Besides the environmental impacts associated with incoming exergy flow also component-related environmental impacts $\dot{Y}_k$ associated with the kth component are considered. The environmental impacts that occur during the three life cycle phases construction $\dot{Y}_k^{CO}$, operation and maintenance $\dot{Y}_k^{OM}$, and disposal $\dot{Y}_k^{DI}$ constitute the component-related environmental impacts and are obtained by LCA:

$$\dot{Y}_k = \dot{Y}_k^{CO} + \dot{Y}_k^{OM} + \dot{Y}_k^{DI} \quad (3)$$

2.3. Exergoenvironmental variables

On the basis of the exergy and environmental impact rates and the specific environmental impacts of each exergy stream in the process the exergoenvironmental variables can be calculated for every process component. Only two exergoenvironmental variables will be discussed here.

Within exergy analysis, the exergy destruction of each component is calculated. The exergo-environmental analysis allows to calculate the environmental impact rate $\dot{B}_{D,k}$ associated with the exergy destruction $\dot{E}_{D,k}$ in the kth component by applying the following equation:

$$\dot{B}_{D,k} = b_{F,k} \cdot \dot{E}_{D,k} \quad (4)$$

The exergy destruction rate is multiplied by average specific environmental impacts of the exergetic fuel of the kth component $b_{F,k}$. This value is calculated based on the definition of exergetic fuel and product within exergy analysis.

The sum of the environmental impacts $\dot{B}_{TOT,k}$ of the kth component is calculated by adding the environ-mental impacts of exergy destruction $\dot{B}_{D,k}$ and the component-related environmental impacts $\dot{Y}_k$:

$$\dot{B}_{TOT,k} = \dot{B}_{D,k} + \dot{Y}_k \quad (5)$$

This exergoenvironmental variable reveals the environmental relevance of each component. The exergoenvironmental evaluation is carried out applying the exergoenvironmental variables. On basis of the evaluation of the process and its components possibilities for an improvement with respect to the environmental performance can be developed. The exergoenvironmental analysis is shown in detail in [2,9].

3. Application of Electricity Production by means of SOFC with Integrated Biomass Gasification

For an application of exergoenvironmental analysis a thermochemical process for the conversion of biomass to electricity was used. The details of the process can be found in [9]. The modeling of a

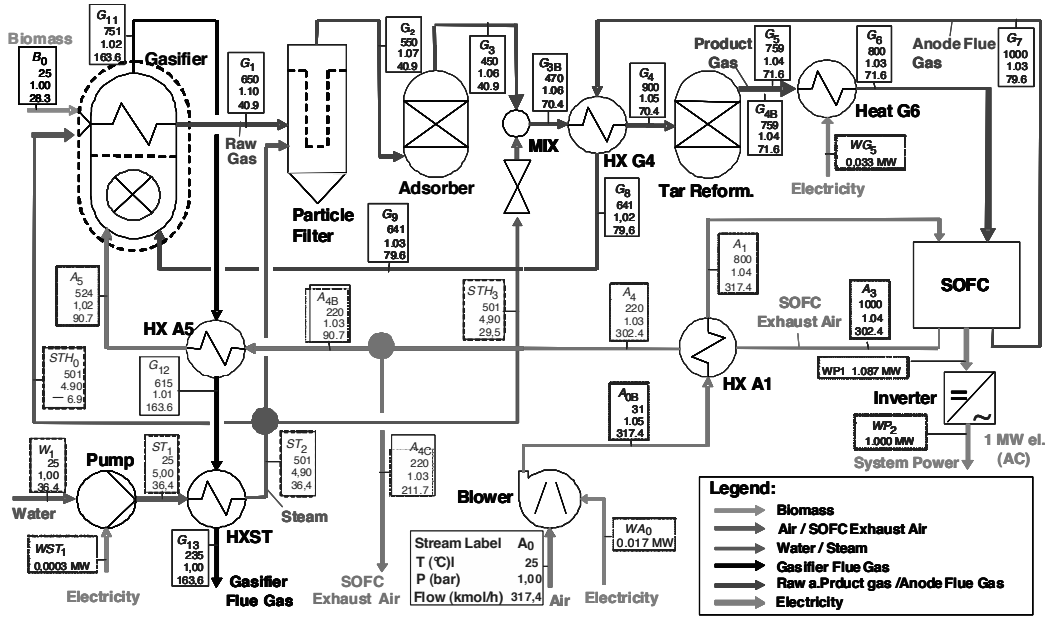

Fig. 2. Flowchart of electricity production by means of biomass conversion process.

similar process has been reported in [10,11]. Fig. 2 shows the flowchart of the process designed for electricity generation of 1 MW alternating current. In the same fig., temperatures, pressures and mol flow rates of the material streams are presented. These values were obtained by modeling and simulation of the process described below.

Biomass (wood chips) is fed to an allothermal fluidized bed gasifier (Gasifier) that is heated by an integrated burner. The flue gas of the solid oxide fuel cell (SOFC), which contains non-depleted fuel, represents the feedstock for the burner. The gasification agent is steam generated within the process. At 750°C the biomass is converted to a raw gas which mainly consists of H2, CO, CO2 and CH4. After leaving the gasifier, the raw gas enters the hot gas cleaning facility at 650°C. First it passes through a ceramic particle filter and an adsorber. Char, bed material and ash is removed in the first component, halogen and sulphur compounds are removed in the latter. Steam pulses periodically clean the particle filter. After the adsorber, steam is added to the gas in a mixer (MIX) to adjust the steam-to-gas ratio to a value of 2.5, which is necessary for tar and CH4 reforming and for preventing coke formation. Before the gas enters the tar reformer it has to be heated from 470 to 900°C to enable the reforming reaction to take place. This is realized in a heat exchanger (HX G4) by transferring heat from the hot anode flue gas (1000°C) from the SOFC to the tar laden gas. The tar is completely reformed to lower hydrocarbons in the catalytic tar reformer (Tar Reform.). The clean gas is heated to 800°C in an electric heater (Heat G6) before entering the anode side of the SOFC. Preheated air (800°C) is supplied to the SOFC at the cathode. At an operation temperature of 1000°C the fuel cell produces direct current by oxidizing hydrogen and carbon monoxide. Prior to that, methane was internally converted with steam to hydrogen and carbon monoxide. The fuel utilization factor in the SOFC is 69 %. The inverter converts the direct current to alternating current. Ambient air is fed to the air preheater HX A1 by an electric blower. Heat from the fuel cell exhaust air (1000°C) is transferred to the outside air. The exhaust air from the SOFC is partly released to the environment and partly preheated in another heat exchanger (HX A5) to about 520°C and fed to the burner, which is integrated into the gasifier. The hot stream in the heat exchanger is the flue gas from the burner that has previously heated the gasifier. The water supply of the system is provided by a pump (Pump) that pressurizes water to 5 bar. Following this, steam is generated from the water in a heat exchanger (HX ST) that transfers heat from the flue gas of the burner integrated into the gasifier. The gasifier model is based on a mass and energy balance and on the reforming reactions taking place in the gasifier. The fuel cell model was been adapted from a model for a tubular SOFC recently published in [12]. Depending on gas composition and operating conditions, the power output as well as the conditions and compositions of the exiting material flows of the SOFC can be simulated. The lifespan of all components is fixed at 100,000 h or 15 years. Only the SOFC stack has to be exchanged every 40,000 h.

3.1. Results of the Exergy Analysis

For the entire energy conversion process, the exergetic efficiency is 33.7 %. Table 1 presents the main exergetic variables of the system components. For dissipative components, there are no definitions available for exergetic product and fuel so that the particle filter is assigned to the gasifier just like the adsorber and inverter are assigned to the SOFC.

Table 1. Exergetic variables of system components.

System Component	Exergetic Efficiency [%]	Exergy Destruction [MW]
Gasifier (incl. disipative comp.)	**11.6**	**0.658**
HX G4	**94.0**	**0.015**
Tar Reform.	**23.9**	**0.068**
HEAT G6	**70.3**	**0.010**
HX A1	**80.5**	**0.265**
SOFC (incl. dissipative comp.)	**93.1**	**0.126**
HX A5	**76.5**	**0.039**
HX ST	**56.2**	**0.153**
Pump	**24.7**	**0.0**
Blower	**65.2**	**0.006**

The result shows that the gasifier, the heat exchangers HX A1 and HX ST and the SOFC are responsible for almost 80 % of the exergy destruction within the process.

3.2. Results of the Exergoenvironmental Analysis

Table 2 shows the environmental impact rates of components associated with component-related

impacts $\dot{Y}_k$ and impacts due to exergy destruction $\dot{B}_{D,k}$. The sum of both impact rates are the total environmental impacts $\dot{B}_{TOT,k}$.

Table 2. Exergoenvironmental variables of system components.

System Component	$\dot{Y}_k$ [mPts/s]	$\dot{B}_{D,k}$ [mPts/s]	$\dot{B}_{TOT,k}$ [mPts/s]
Gasifier (incl. disipative comp.)	**0.222**	**0.875**	**1.097**
HX G4	**0.008**	**0.017**	**0.025**
Tar Reform.	**0.044**	**0.070**	**0.114**
HEAT G6	**0.001**	**0.058**	**0.059**
HX A1	**0.042**	**1.461**	**1.503**
SOFC (incl. dissipative comp.)	**0.514**	**0.140**	**0.654**
HX A5	**0.003**	**0.052**	**0.055**
HX ST	**0.011**	**0.203**	**0.214**
Pump	**0.0**	**0.001**	**0.001**
Blower	**0.002**	**0.033**	**0.035**

It is obvious that the heat exchanger HX A1, the gasifier, and the SOFC are mainly relevant for the formation of environmental impact. Only the SOFC is assigned a dominant value as regards the component-related environmental impacts.

4. Comparative Investigation of Exergoenvironmental Analysis using different LCIA methods

Methodological structure of the exergoenvironmental analysis shows that a quantitative environmental assessment method in order to calculate the environmental impact is needed. As one of most used LCIA method worldwide, developed to support decision-making, and in line with economic assessment using costs as single-score indicator, is chosen the Eco-indicator 99 method. Besides the Eco-indicator exist different other used LCIA methods in LCA studies which are discussed in [13, 14]. Today the discussion which is the best LCIA method is not just solved, because the modeling of environmental impacts is under development. Therefore ISO standardization has not defined a specific LCIA method till today. However, the development of Eco-indicator 99 leads to a great discussion of main schools of approaches: endpoint or midpoint LCIA methods.

The terms midpoint and endpoint mean the location of the environmental impact category indicator. An impact category describes the relationship between the LCI results, and if possible environmental endpoint(s), i.e. the receptors that are damaged. It includes a quantitative cause-effect chain (environmental mechanism) based on an environmental model. The category indicator can be located at any point between the LCI results and the category endpoints (where the environmental effect occurs).

An example about the difference of midpoint and endpoint impact assessment is presented for the impact category stratospheric ozone depletion in figure 3.

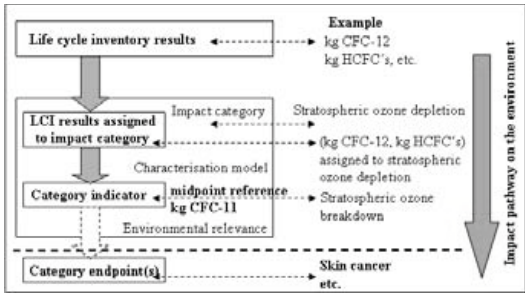

Fig. 3. Concept of category indicators according to ISO 14044 [4]

The midpoint indicator is characterized by the effect to reduce the ozone concentration in the stratosphere. Furthermore all released substances, which has an ozone depletion potential, classified in an impact category and characterized with regard to their quantitative impact in relation to a reference substance (e.g. kg CFC-11 for stratospheric ozone depletion).

In contrast to them, endpoint indicators assess not the potential of an environmental impact, but the actual damage resulting from the reduced stratospheric ozone concentration. The resulting effect is an increasing of ultraviolet B (UV-B) radiation that consequently leads to an increase of skin cancer for humans and therefore damages to the expectation of life years. Moreover an increasing of UV-B radiation has also an harmful impact on plants and animals. But at the moment it is not possible to quantify these impacts on plants and animals too.

4.1. The CML 2001 method

The CML 2001 method is a classical agent of a midpoint life cycle impact assessment method. It is developed by the Institute of Environmental Science (CML) of Leiden University. The CML has a long tradition in the methodological development of LCIA [5,6]. The general structure

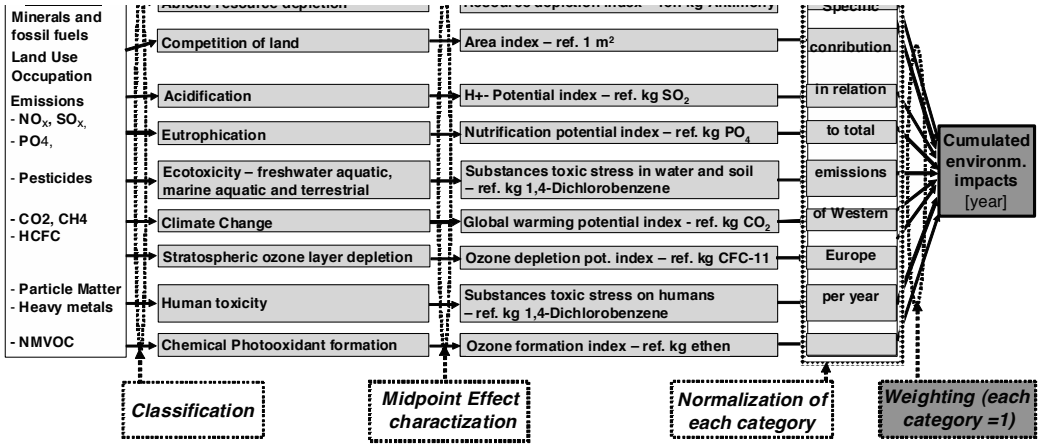

Fig. 4. General structure and model of the life cycle impact assessment method – CML 2001

and model of the CML method (baseline impact categories) is presented in fig. 4. In contrast to the endpoint structure of the Eco-indicator 99 each impact category is characterized by an midpoint indicator. For each midpoint indicator a reference substance is defined in order to quantify the impact of a classified emission in relation to the reference substance.

Usually the CML method is finished after the normalization of each impact category whereby the result shows an environmental profile of different 9 baseline impact categories. The step of normalization calculates the specific magnitude of impact category result of the investigated system in relation to an reference information. In the case of CML method as spatial reference value the total emission of Western Europe per year is selected. Subsequently the normalized result of an impact category has the unit year.

To use the CML method in exergoenvironmental analysis quantifying the environmental impact the weighting of each impact category has to integrate in the model. For this reason each impact category was equally weighted and can be cumulative added to the total environmental impact.

4.2. The IMPACT 2002 method

The LCIA method IMPACT 2002 proposes an implementation of a combined midpoint/damage approach, linking all types of inventory results via 12 midpoint categories to 4 damage categories [7,8]. The general structure and model of IMPACT 2002 is shown in figure 5. All midpoint scores are expressed in units of a reference substance and related to the four damage categories human health, ecosystem quality, resources, and climate change. To use IMPACT 2002 method in exergo-environmental analysis in order to quantify the environmental impact a weighting of four damage categories have to integrate in the model structure.

Similar to CML 2001 each damage category was equally weighted. The result of IMPACT 2002 is expressed in units of person * year (=points).

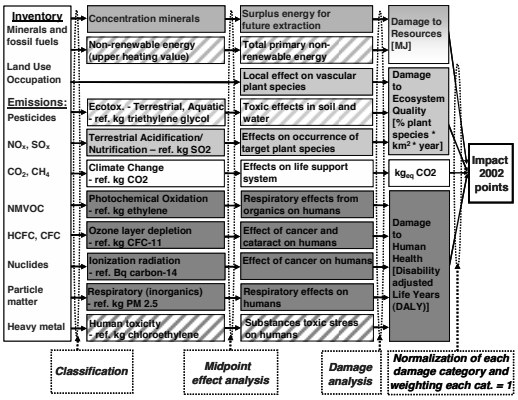

Fig. 5. Structure and model of the midpoint/endpoint LCIA method IMPACT 2002.

In contrast to the Eco-indicator 99 method the impacts of greenhouse gases are separated in the additional damage category climate change. Furthermore for human toxicity and eco-toxicity new environmental models were developed and for non-renewable energy carriers the total primary energy content is accounted. All of these differences to the Eco-indicator 99 method are marked by hatched areas in figure 5.

In figure 6 the total environmental impact rate $\dot{B}_{TOT,k}$ for Eco-indicator 99 is presented (table 2).

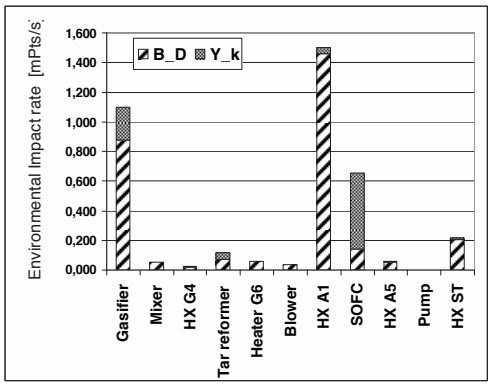

Fig. 6. Sum of environmental impact rate $\dot{B}_{TOT,k}$ of Eco-indicator 99

This result is compared to figure 7 which shows the result of total environmental impact rate for the CML 2001 and IMPACT 2002 methods. Both figures look very similar. Especially the same components (Heat exchanger HX A1, Gasifier and SOFC) are mainly relevant for the formation of environmental impacts for all methods.

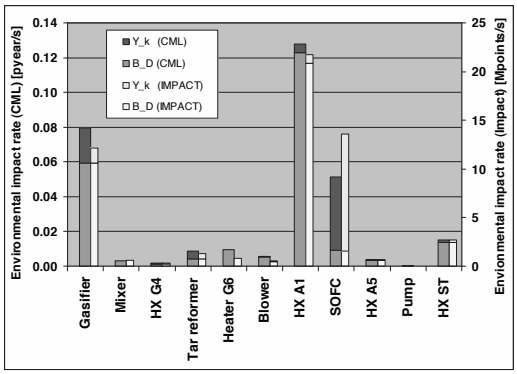

Fig. 7. Sum of environmental impact rate $\dot{B}_{TOT,k}$ of CML 2001 and IMPACT 2002 LCIA method

A difference is that the total environmental impact rate of the SOFC accounting with the IMPACT 2002 method has a higher value than the gasifier.

More information about the differences provide figure 8 which presents the percentage of environmental impact of all input streams and system components in relation to the total environmental impact associated with the final product for all applied LCIA methods. It shows that the supply of biomass has the highest environmental impact for all methods but the values varies from 58.7 % (Eco-indicator) to 45.0 % (IMPACT) and to 33.5 % (CML).

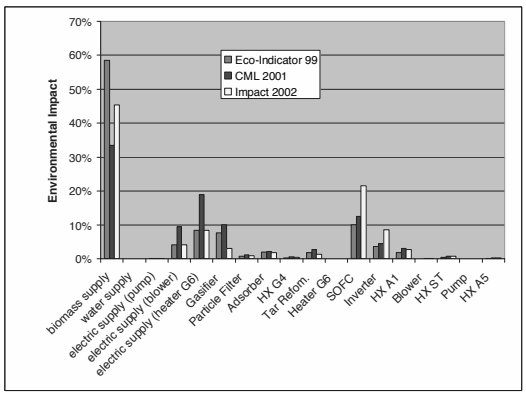

Fig. 8. Percentage of total environmental impact of input streams and system components

One reason for the highest impact of biomass supply of all used LCIA methods can be explained by the high effort for the transport of the biomass that is transported about a distance of 50 km. Additionally the impact of land occupation especially land transformation which is only included in the Eco-indicator 99 method contributes to the highest value.

On the other hand the values for the electrical supply of the Blower and Heater G6 are clearly higher for the CML method during both others methods show similar values. The reason for this result is the high impact of hydrogen fluoride (HF) by the CML method. This pollutant is produced especially in fossil power plants which have the main contribution in the used EU electricity mix.

Other divergences between the results of the different used LCIA methods can be explained in parts by the differences in their applied environmental models. That leads to the result that different pollutants cause the highest environmental impact. For the Eco-Indicator has the highest contribution the particles PM 2.5. During for the CML method hydrogen fluoride (HF) and for the IMPACT method dioxin (TCDD) is responsible for the highest impact.

5 Conclusion

It can be conclude that the application of the two used LCIA methods CML 2001 and Impact 2002 instead of the Eco-indicator 99 has a small influence on the calculated exergoenvironmental

variables $\dot{B}_{TOT,k}$, $\dot{B}_{D,k}$ and $\dot{Y}_k$ (the same components) are relevant for the highest impact.

Nomenclature

$\dot{B}_j$ environmental impact rate of the j-th material or energy stream, (Eco-indicator 99) Points/s

b_j specific (exergy-based) environmental impact of the j-th material or energy stream, (Eco-indicator 99) Points/GJ

$\dot{E}_j$ exergy rate of the jth stream, GJ

$\dot{Y}$ component-related environmental impact rate associated with the life cycle of the component, (Eco-indicator 99) Points/s

Subscripts and superscripts

D destruction

F fuel

in input

j j-th material or energy stream of the energy conversion system

k k-th component of the energy conversion system

P product

TOT total (with reference to the component)

CO construction

DI disposal

OM operation, maintenance

References

[1] Meyer L. et al., 2007, Formation of environmental impacts in energy conversion process revealed by a novel Exergoenvironmental Analysis, Proceedings of ASME Conference 2007, Seattle, USA, IMECE2007-42210.

[2] Meyer, L, Tsatsaronis, G., Buchgeister, J., Schebek, L., 2009, Exergoenvironmental Analysis for Evaluation of the Environmental Impact of Energy Conversion Systems, Energy, 34(1), 75-89.

[3] Goedkoop, M, Spriensma, R., 2000, The Eco-indicator 99: A damage oriented method for life cycle impact assessment. Methodology Report, Amersfoort, Netherlands, Available at: www.pre.nl.

[4] International Organization for Standardization (ISO), 2006, Environmental Management - LCA. European Standard EN ISO 14040 and 14044, Geneva, Switzerland.

[5] Heijungs, R. et al., 1992, Environmental life cycle assessment of products. Guide and Backgrounds, Centre of Environmental Science, Leiden, Netherland.

[6] Guinée, J. B. (ed.)., 2001, LCA, An Operational Guide to the ISO Standards; LCA in Perspective; Guide; Operational Annex to Guide, Centre for Environmental Science, Leiden University, Netherland.

[7] Jolliet, O., Margni, M., Charles, R., Humbert, S., Payet, J., Rebitzer, G., Rosenbaum, R., 2003, IMPACT 2002+: A New Life Cycle Impact Assessment Methodology, Int. Journal of LCA, 8(6), 324-330.

[8] Humbert, S., Margni, M., Jolliet, O., 2004, IMPACT 2002: User Guide, Draft for version 2.0, Industrial Ecology & Life Cycle Systems Group, GECOS, Swiss Federal Institute of Technology Lausanne (EPFL), Switzerland, Available at: http://www.epfl.ch/impact

[9] Meyer, L., 2006, Exergiebasierte Untersuchung der Entstehung von Umweltbelastungen in Energieumwandlungsprozessen auf Komponentenebene: Exergoökologische Analyse, Universität Darmstadt, Germany, Dissertation (PhD) (in German).

[10] Panopoulos, K. D. et al., 2006, High temperature solid oxide fuel cell integrated with novel allothermal biomass gasification: Part I: Modelling and feasibility study, Journal of Power Sources, 159(1), 570-585.

[11] Panopoulos, K. D. et al., 2006, High temperature solid oxide fuel cell integrated with novel allothermal biomass gasification: Part II: Exergy Analysis, Journal of Power Sources, 159(1), 586-594.

[12] Zhang, W et al., Simulation of a tubular solid oxide fuel cell stack using AspenPlus unit operation models, 2005, Energy Conversion and Management, 46(2), 181-196.

[13] Udo de Haes, H. A. et al., 2002, Life Cycle Impact Assessment – Striving towards best practice, Society of Environmental Toxicology and Chemistry (SETAC), (USA).

[14] Jolliet, O. et al., 2004, The LCIA Midpoint-Damage Framework of the UNEP/SETAC Life Cycle Initiative, Int. Journal of LCA, 9(6), 394 – 404.

Application of the Thermoecological Cost for Sustainability Assessment of Coupled Technologies of Biomass Co-firing in Cogeneration Technologies

Jaroslaw Zuwala[a]*, Andrzej Ziebik*[b]

[a] *Institute for Chemical Processing of Coal, Zamkowa 1, 41-803 Zabrze, Poland, Central Mining Institute, Plac Gwarkow 1, 40-166 Katowice, Poland*
[b] *Institute of Thermal Technology, Konarskiego 11, 44-101 Gliwice, Poland*

Abstract: The paper presents the application of thermoecological cost methodology as a sustainability measure for biomass co-firing technologies coupled with co-generation of electricity and heat. For both kinds of fuels: fossil fuel (hard coal) and biomass (willow chips) the value of thermoecological cost has been calculated. These parameters have then been used for the evaluation of the thermoecological cost for electricity and heat generated in CHP plant with a backpressure turbine. The change of these values along with the increasing energy share of biomass in the combusted blend has been analyzed. It was observed that biomass addition leads to the decrease of the thermoecological cost of electricity and heat generated in co-firing processes.

Keywords: Biomass co-firing, Cogeneration, Sustainable Development, Thermoecological cost.

1. Introduction

The striving for minimization of non-renewable energy resources consumption is crucial from the sustainable mankind development point of view.

Useful products, including final energy carriers such as electricity and heat are generated as results of power, technological and transport processes implementation, creating a network of interdependences. Consequently, they should be burdened not only with the direct consumption of chemical energy in the processes of fuel combustion in utility boilers ("upstream"), but also with indirect energy consumption in the transmission of final energy carriers, energy consumption in fuels transport and their extraction from the deposit as well as with energy consumption in the manufacture of machines and equipment used in each of the aforementioned stages ("downstream").

As long as biomass use is regarded (e.g. in the process of co-firing, a very popular technology across Europe and USA [1]) all the manufacturing process stages from its acquisition until processing to the final physical form prior to use should be considered. A diversified approach should be used here depending on biomass origin (e.g. forest residue biomass or dedicated short rotation coppices).

Many European countries have already implemented incentive mechanisms for renewable energy (feed-in tariffs or certificates of origin). For the case of biomass use in some cases the amount of financial support varies depending on generation technology (biomass combustion, direct co-firing systems, gasification etc.) and the origin of biomass combusted [14].

However none of the existing incentive systems was found to be based on the assessment of real environmental benefits or burdens resulting from the full life cycle of biomass co-firing implementation.

The use of exergy as a measure for the natural resources depletion and accounting for environmental burdens was proposed by a few authors [2-3,6-8]. The concept of thermoecological cost expressing the cumulative consumption of non-renewable exergy has been developed in [11]. Its application for the assessment of environmental impact of technological processes was proposed in [7].

The authors of this paper propose the methodological approach for the application of thermoecological cost of biomass co-firing in backpressure turbine based cogeneration plant as tool for sustainability assessment of renewable energy generated in co-firing process of coal and biomass. The model has been built and the simulation was carried out for the variable

composition of coal and biomass blend and both cogeneration process energy carriers: electricity and heat.

2. Thermo-ecological cost of electricity and heat in CHP plant

Different natural resources are characterized by different quality [3]. According to [8], the thermoecological cost is defined as the cumulative consumption of non-renewable exergy connected with the manufacturing of a particular product with additional inclusion of the consumption resulting from the necessity of compensation of environmental losses caused by the release of harmful substances to the environment. Thermo-ecological cost of a by-product of a main process should be evaluated basing on the avoided expenditures. This means that a by product should be burdened with the amount of energy avoided in the substituted process due to the use of a by-product.

Thermoecological cost can be determined by solving the set of thermo-ecological cost balance equation (1) [3]:

$$\rho_i + \sum_i \left(f_{ij} - a_{ij}\right)\rho_i - \sum_r a_{rj}\rho_r = \sum_s b_{sj} + \sum_k p_{kj}\zeta_k \qquad (1)$$

In this paper, the thermoecological cost will be evaluated for energy carriers like fuels and products of biomass co-firing cogeneration system based on a backpressure CHP plant.

2.1. Base assumptions

For the coal fired CHP plant with a backpressure turbine the following input data can be assumed:

- $\sigma = 0.4$;
- $\eta_{Eb} = 0.85$;
- $\eta_{me} = 0.95$;
- $\eta_{E\,CHP\,G} = 0.8374$;
- $\varepsilon_{el} = 0.11$;
- $\varepsilon_{th} = 0.025$;
- $\eta_{tt} = \eta'_{tt} = 0.9$;
- $\eta_{ht} = 0.85$ (traditional heat distribution network);
- $\eta_{E\,ut\,N} = 0.36$;
- $\eta_{E\,el\,CHP\,G} = 0.4045$;
- $\eta_{E\,h\,CHP\,G} = 1.4643$;

In the calculations the following data concerning the values of thermoecological cost of primary fuels and basic emissions were used basing on [7]:

- ρ_c =1.13 MJ/MJ,
- ρ_{ng} = 0.9 MJ/MJ,
- ρ_{do} = 1.1 *MJ/MJ*,
- ζ_{SO2} = 45 *MJ/kg*, ζ_{NOx} = 45 *MJ/kg*, $\zeta_{p.m.}$ = 9.3 *MJ/kg*,
- σ_c=0.0175 *MJ/MJ*
- σ_{ng}=0.0038 *MJ/MJ*
- σ_{do}=0.0131 *MJ/MJ*

For the regarded case of a backpressure turbine CHP plant fired with biomass and coal blend the methodology of determination of cumulative energy consumption indices for final products of the cogeneration process is presented based on the example of a CHP with a back-pressure turbine (Fig. 1).

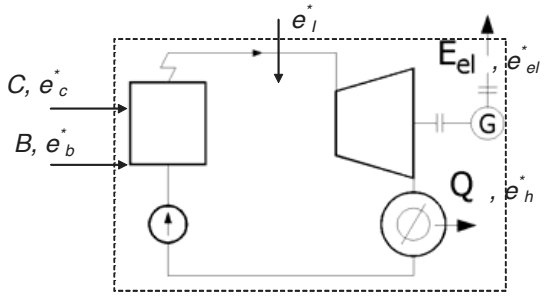

Fig.1 CHP plant with back-pressure turbine – calculation layout [12]

Hard coal used as a fuel in biomass co-firing plant comes from underground resources and is burdened with upstream unit energy consumption of e_c^* . Also biomass used for co-firing can originate from the different resources. Depending on the length of its production and supply chain, the different values of cumulative energy consumption indices can be estimated. For the present analysis use of biomass coming from dedicated willow plantation is assumed and it is burdened with the cumulative energy consumption of e_b^*.

2.2 Thermoecological cost of electricity and heat co-generated in coal fired CHP plant.

Gross thermoecological cost indicator for electricity from a CHP can be calculated as follows:

$$\rho_{el\,CHP\,G} = \frac{E_{ch\,el\,CHP} \cdot \left(\rho_f + \rho_{em} + \rho_{CO_2} + \rho_I\right)}{E_{el\,CHP\,G}} \quad (2)$$

The CO_2 removal cost method may be used for approximate evaluation of CO_2 emission thermoecological cost indicator: $\rho_{CO2} = p_{CO2} \cdot \sigma_{CO2}$, where: p_{CO2} – CO_2 emission volume, σ_{CO2} – 4.4 *MJ/kg* – thermoecological cost of CO_2 removal.

However in further considerations, the component related to CO_2 emission as well as the investment components have not been taken into account. Cardle-to-the-grave type life cycle analysis always takes into account the investment component resulting from the extra expenditures for the installation manufacturing. However, it was found in that the energy consumption in the process of manufacturing and erection of 1.2 GW_{el} utility plant results in consumption of primary energy resources equal to 13.5 PJ. At the same time, the co-firing installation manufacturing and construction in Polish conditions takes only 9.4 TJ (maximal output of the line: 15% biomass on energy basis [10]).

Taking the above into consideration it can be obtained:

$$\rho_{el\,CHP\,G} = \frac{\rho_f + \rho_{em}}{\eta_{E\,el\,CHP\,G}} \text{ and } \rho_{em} = \sigma_c \quad (2)$$

where the partial efficiency of electricity generation in CHP plant can be defined as:

$$\eta_{E\,el\,CHP\,G} = \frac{E_{el\,CHP\,G}}{E_{ch\,el\,CHP}} \quad (3)$$

Substituting numerical values to (2) the following can be obtained:

$\rho_{el\,CHP\,G} = 2.8368$

The thermoecological cost indicator for electricity generated in a CHP at customer's (net value):

$$\rho_{el\,CHP} = \frac{\rho_{el\,CHP\,G}}{\left(1-\varepsilon_{el}\right)\cdot\eta_{tt}} = 3.5416\frac{MJ}{MJ} \quad (4)$$

For comparison, the average thermoecological cost indicator for the national power system amounts to 3.6 *MJ/MJ*.

The gross thermoecological cost for heat production in a CHP (fuel ρ_f and emission ρ_{em} components) can be expressed as:

$$\rho_{h\,CHP\,G} = \frac{E_{ch\,h\,CHP} \cdot \left(\rho_f + \rho_{em}\right)}{Q} \qquad \rho_{em} = \sigma_c \quad (5)$$

$$\rho_{h\,CHP\,G} = \frac{\rho_f + \rho_{em}}{\eta_{E\,h\,CHP\,G}} = 0.7837\frac{MJ}{MJ} \quad (6)$$

The thermoecological cost for heat generated in a CHP at customer's (net value) is equal to:

$$\rho_{h\,CHP_0} = \frac{\rho_{h\,CHP\,G}}{\left(1-\varepsilon_{th}\right)\cdot\eta_{ht}} = 0.9456\frac{\mathrm{MJ}}{\mathrm{MJ}} \quad (7)$$

2.3 Thermoecological cost of willow biomass chips

For energy crops coming from dedicated plantations, like willow, the following stages of its manufacturing and transport can be named [12-13]: planting, harvesting, storage (with natural seasoning), transport. The following consumption of diesel oil in these individual periods was estimated as: planting: 126.6 MJ/t b.c (biomass chips), harvesting: 97.7 MJ/t b.c., transport and storage: 68 MJ/t b.c. This makes the total diesel oil consumption for all the stages at 292 MJ/t (b.c.).

The thermoecological cost resulting from the above estimated diesel oil consumption:

$\rho_{b.c.\,do} = E_{ch\,do}\,(\rho_f + \rho_{em}) = 325\ MJ/t\ b.c.$ (8)

An assumption was made that the consumption of cumulative energy burdening cuttings and shoots at the amount of 93 MJ/t b.c. results also from the diesel oil consumption. Hence:

$\rho_{b.c.\,cs} = 93(1.1 + 0.0131) = 103.5\ MJ/t\ b.c.$

Steel wire for plantation fencing is burdened with cumulative energy consumption of 96 MJ/t b.c. An assumption was made that in this case the ratio of cumulative exergy consumption to cumulative energy consumption amounts to 1.2 [11]. Then an assumption was made that the thermoecological cost burdening the steel wire is equal to cumulative exergy consumption:

$\rho_{b.c.\,sw} = 1.2 \cdot 96 = 115.2\ MJ/t\ b.c.$

The cumulative energy consumption related to fence maintenance chemicals amounts to *34 MJ/t b.c*. An assumption was made that the cumulative exergy consumption is the same (like for diesel oil) and that the thermoecological cost is equal to the cumulative exergy consumption:

$\rho_{b.c.\,fen} = 34\ MJ/t\ b.c.$

The agrochemical components results from fertilizers and herbicide consumption for the certain plantation cycles. It amounts to 242 MJ/t b.c. An assumption was made that the agrochemical component is burdened primarily with the natural gas consumption. Therefore:

$$\rho_{b.c.f\&h} = E_{ch\,ng}\,(\rho_f + \rho_{em}) = 218.7\ MJ/t\ b.c. \quad (9)$$

Therefore, the thermoecological cost (operational component) of naturally dried biomass chips:

$$\rho_{b.c.} = 796.4\ MJ/t\ b.c. \quad (10)$$

The thermoecological cost for naturally dried biomass chips referred to chemical unit of biomass (LHV=12.725 GJ/kg, [11])

$$\rho_{b.c.} = \frac{796.4}{12\,725} = 0.0626\ MJ/MJ$$

As it was assumed earlier in the assumptions, the calculated value of the thermoecological cost indicator for naturally dried biomass does not comprise the investment component and the CO_2 emission component.

The emission component of naturally dried willow chips should be taken basing on the real emission data from willow biomass combustion (e.g. as described in [4] where emission indices for coal/biomass co-firing were measured to be as follows: $p_{NOx} = 0.0966\ g/MJ$, $p_{SO2} = 0.2973\ g/MJ$, $p_{p.m.} = 0.016\ g/MJ$.). The data from industrial scale co-firing involve the effects which on the (like the auto-desulphurisation effect caused by alkali metals contents in biomass ash, causing higher desulphurization ratio than resulting from the lower sulphur content in biomass).

For the case described in [4], the total emission component of thermoecological cost of coal and biomass blend (willow share of 4.4% energy basis) can be calculated from the following equation:

$$\sigma = p_{NOx}\cdot\zeta_{NOx} + p_{SO2}\cdot\zeta_{SO2} + p_{p.m.}\cdot\zeta_{p.m.} = 0.0179\ MJ/MJ \quad (11)$$

An assumption can be made that the calculated thermoecological cost of emission for biomass (willow chips) co-firing remains valid also in the case of changes in biomass energy fraction in the blend considered in the paper.

In the present analysis, the biomass preparation stages (e.g. grinding, drying, pelletisation) were not considered due to the fact, that in co-firing cases studies with biomass energy share up to 20% (as considered in this paper) mostly raw biomass is combusted. Biomass of a better quality is most often used in the high-share biomass co-firing installations, with the co-firing ratio up to 60% on energy basis [10]. For biomass path including more stages than considered above, all the thermoecological cost components should be included in the analysis.

2.4 Dependence of thermoecological cost burdening the heat production in a CHP on the biomass share in the co-fired blend

The thermoecological cost indicator burdening the heat production in a CHP in the case of biomass co-firing (12) and coal only combustion (13) is covered by the equations:

$$\rho_{hCHP} = \frac{\rho_f + \sigma}{\eta_{E\,hCHPG}\cdot\left[1-\varepsilon_{th}\right]\cdot\eta_{ht}} \quad (12)$$

$$\rho_{hCHP0} = \frac{\rho_c + \sigma_c}{\eta_{E\,hCHPG\,0}\cdot\left(1-\varepsilon_{th0}\right)\cdot\eta_{ht0}} \quad (13)$$

After dividing by sides (efficiency of heat transmission remains on the same level for coal and blends combustion) the following equation is obtained:

$$\frac{\rho_{hCHP}}{\rho_{hCHP0}} = \frac{\rho_c + \sigma}{\rho_c + \sigma_c}\cdot\frac{\eta_{E\,hCHPG\,0}\cdot\left(1-\varepsilon_{th0}\right)}{\eta_{E\,hCHPG}\cdot\left[1-\varepsilon_{th}\right]} \quad (14)$$

including biomass energy share in the blend expressed with "b" it can be written:

$$\rho_f = (1-b)\cdot\rho_c + b\cdot\rho_{b.c.} \quad (15)$$

In the considered range of biomass energy fraction in the combustible blend (up to 20%) it is possible to assume that:

$$\sigma \cong \sigma_c \quad (16)$$

Taking into account (16) and assuming that biomass is not additionally dried in a CHP (which results in the assumption of heat auxiliaries' consumption indicator constancy) the following can be obtained:

$$\frac{\rho_{hCHP}}{\rho_{hCHP0}} = \frac{(1-b)\cdot\rho_c + b\cdot\rho_{b.c.} + \sigma_c}{\rho_c + \sigma_c}\cdot\frac{\eta_{E\,hCHP0}}{\eta_{E\,hCHPG}} \quad (17)$$

Substituting the relationship for gross partial energy efficiency of heat production the following is obtained:

$$\frac{\rho_{h\,CHP}}{\rho_{h\,CHP0}} = \frac{(1-b)\cdot\rho_c + b\cdot\rho_{b.c.} + \sigma_c}{\rho_c + \sigma_c} \cdot \frac{\eta_{E\,h\,CHPG0}}{\eta_{E\,h\,CHPG}} \cdot \frac{1-\sigma\cdot\left[\frac{\eta_{E\,CHPG}}{\eta_{E\,el\,CHPG0}} - 1\right]}{1-\sigma\cdot\left[\frac{\eta_{E\,CHPG}}{\eta_{E\,el\,CHPG0}} - 1\right]} \tag{18}$$

from where:

$$\frac{\rho_{h\,CHP}}{\rho_{h\,CHP0}} = \frac{(1-b)\cdot\rho_c + b\cdot\rho_{b.c.} + \sigma_c}{\rho_c + \sigma_c} \cdot \frac{\eta_{E\,b0}}{\eta_{E\,b}} \tag{19}$$

Simplified relationship (19) can be written with the assumption that the same empirical relationships are binding in the case of substituted utility plant and the CHP plant regarded. In such a case, the last term of formula (18) takes the value equal to 1. Introducing to relationship (19) the numerical values ρ_{wk}=1.13 *MJ/MJ*; $\rho_{b.c.}$=0.0626 *MJ/MJ*; σ_c=0.0175 *MJ/MJ* and empirical relationships for the ratio of efficiencies of coal and biomass-blend fired boiler [5] the following is obtained:

$$\frac{\rho_{h\,CHP}}{\rho_{h\,CHP0}} = \frac{1-0.9302\cdot b}{1-0.1515\cdot b} \tag{20}$$

also:

$$\rho_{h\,CHP0} = 0.9456 \tag{21}$$

Further on, the change of the thermoecological cost of heat generated in CHP plant along with the increasing biomass share in the blend can be obtained. The relation can be presented graphically in the Fig. 1.

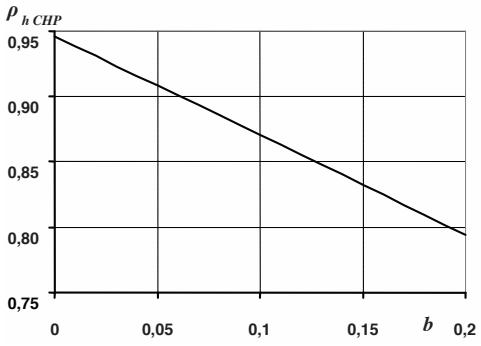

Fig 1 Thermoecological cost for heat vs. biomass energy fraction in the co-fired blend

It can be noted that with the increasing biomass share in the blend, the thermoecological cost for heat decreases. An assumption that the thermoecological cost indicator for biomass does not depend on the moisture content in biomass (only natural drying was applied) is however binding.

2.5 Dependence of thermoecological cost indicator burdening the electricity production in a CHP on the biomass energy fraction in the combustible blend

Because electricity production in cogeneration leads to avoiding the production of certain amount of electricity in utility plant, again an allocation rule of avoided fuel input can be applied.

The thermoecological cost indicator burdening the electricity production in a CHP in the case of biomass co-firing (22) and hard coal only combustion is covered by the equations:

$$\rho_{el\,CHP} = \frac{\rho_f + \sigma}{\eta_{E\,el\,CHPG}\cdot\left[1-\varepsilon_{el}\right]\cdot\eta_{tt}} \tag{22}$$

$$\rho_{el\,CHP0} = \frac{\rho_c + \sigma_c}{\eta_{E\,el\,CHPG0}\cdot\left(1-\varepsilon_{el0}\right)\cdot\eta_{tt0}} \tag{23}$$

After dividing by sides the following is obtained:

$$\frac{\rho_{el\,CHP}}{\rho_{el\,CHP0}} = \frac{\rho_f + \sigma}{\rho_c + \sigma_c} \cdot \frac{\eta_{E\,el\,CHPG0}\cdot\left(1-\varepsilon_{el0}\right)}{\eta_{E\,el\,CHPG}\cdot\left[1-\varepsilon_{el}\right]} \tag{24}$$

where relationships (15) and (16) are still valid.

Hence:

$$\frac{\rho_{el\,CHP}}{\rho_{el\,CHP0}} = \frac{(1-b)\cdot\rho_c + b\cdot\rho_{b.c.} + \sigma_c}{\rho_c + \sigma_c} \cdot \frac{\eta_{E\,el\,CHPG0}\cdot\left(1-\varepsilon_{el0}\right)}{\eta_{E\,el\,CHPG}\cdot\left[1-\varepsilon_{el}\right]} \tag{25}$$

It must be borne in mind that along with the increasing biomass share in the blend, the energy efficiency changes and so do the auxiliaries indicators. Basing on biomass trial test results, this has been proved in [5] where the empiric correlations for different biomass and different base fuels were evaluated. The dependence of the partial electricity generation efficiency in CHP plant on the energy efficiency of utility plant can be written as:

$$\frac{\eta_{\mathrm{E\,el}\,CHP\,G}}{\eta_{\mathrm{E\,el}\,CHP\,G0}} = \frac{\eta_{\mathrm{E}\,ut\,\mathrm{N}}}{\eta_{\mathrm{E}\,ut\,\mathrm{N0}}} \cdot \frac{1-\varepsilon_{\mathrm{el0}}}{1-\varepsilon_{\mathrm{el}}}$$

also, the utility energy efficiency depends on

$$\frac{\eta_{\mathrm{E}\,ut\,\mathrm{N}}}{\eta_{\mathrm{E}\,ut\,\mathrm{N0}}} = \frac{1-\varepsilon'_{\mathrm{el}}}{1-\varepsilon'_{\mathrm{el0}}} \cdot \frac{\eta'_{\mathrm{E}\,b}}{\eta'_{\mathrm{E}\,b0}}$$

the following is obtained:

$$\frac{\rho_{\mathrm{el}\,CHP}}{\rho_{\mathrm{el}\,CHP\,0}} = \frac{(1-b)\cdot\rho_c + b\cdot\rho_{b.c.} + \sigma_c}{\rho_c + \sigma_c} \cdot \frac{\eta'_{\mathrm{E}\,b0}}{\eta'_{\mathrm{E}\,b}} \cdot \frac{1-\varepsilon'_{\mathrm{el0}}}{1-\varepsilon'_{\mathrm{el}}} \qquad (26)$$

Introducing to relationship (26) the numerical values $\rho_c = 1.13$ *MJ/MJ*; $\rho_{b.c.} = 0.0626$ *MJ/MJ*; $\sigma_c = 0.0175$ *MJ/MJ* and empirical relationships for the ratio of energy efficiency and electrical auxiliaries' indicator for a substitute (equivalent) condensing power plant, coal and biomass-blend fired, the following is obtained:

$$\frac{\rho_{\mathrm{el}\,CHP}}{\rho_{\mathrm{el}\,CHP\,0}} = \frac{1-0{,}9302\cdot b}{(1-0.1515\cdot b)\cdot(1+1.1852\cdot b^2-0.3747\cdot b)} \qquad (27)$$

also:

$$\rho_{\mathrm{el}\,CHP\,0} = 3.5416\frac{J}{J} \qquad (28)$$

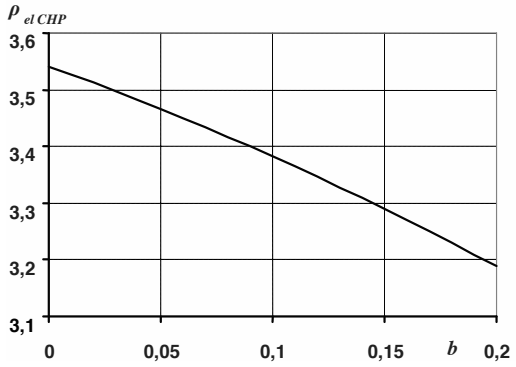

Fig. 2 Dependence of thermoecological cost indicator burdening the electricity production in CHPs on the biomass energy fraction in the blend.

Fig. 2 presents the influence of biomass energy fraction in a combustible blend and the moisture content in biomass on the thermoecological cost indicator for electricity generated in a CHP. Also in this case, an assumption that the thermoecological cost indicator for biomass chips does not depend on the moisture content in biomass is valid.

3. Conclusions

As it was suggested in the report [9], the environmental taxes (on the example of carbon tax) along with the proper tax reforms could influence the individual country's economy. Analogically, it can be assumed that the reform of Polish green energy support system could enhance the development biomass and biomass-bound industries.

The methodology of thermoecological cost was applied to analyze the impact of biomass co-firing implementation on environmental burdens. In the calculations the empiric correlations of boiler auxiliaries' change and boiler energy efficiency along with the increasing share of biomass in the co-fired blend were used.

The simulation results described in the paper showed that the addition of biomass to the co-fired blend leads to the decrease of the thermoecological cost of direct energy carriers in the CHP plant.

The partial substitution of coal with biomass leads to the decrease of upstream cumulative energy consumption for generation and supply of 1MJ of chemical energy of fuels combusted in utilities boilers. Along with the increasing biomass share in the blend, the thermoecological cost of electricity and heat drops down up to 16% (heat) and up to 10% (electricity) for energy share of biomass in the blend of 20%.

As it was assumed, only the operational component of thermoecological cost was taken into consideration. However the co-firing plant building phase is also burdened with energy consumption and harmful emissions release to the environment.

The analysis has not considered the investment component related to the manufacture of machines and equipment for the needs of expansion of fuel storage, preparation and feeding for the needs of biomass co-firing, what may be of some importance at biomass shares exceeding 20%. As it was proved, at lower shares this component will have probably a negligible influence on the computations result.

Nomenclature:

ρ_i – thermo-ecological cost of the i-th and j-th products, J/kg,
ρ_r – specific thermoecological cost of the r-th imported good (raw material or half-product), J/kg,
a_{rj} – coefficient of the consumption of the r-th imported product per unit of the j-th product, kg/kg,
b_{sj} – exergy of the s-th non-renewable natural resource extracted from the nature in the considered process per unit of i-th product.
p_{kj} – the amount of k-th aggressive component of waste products disposed to the environment per unit of the j-th product, kg/kg
ζ_K – cumulative exergy consumption of non-renewable resources for compensation of the results of the emission per unit of the k-th waste product, J/kg
a_{ij}, f_{ij} – coefficients of consumption and coefficients of by-production of the i-th product per unit of the j-th major product, kg/kg.
$E_{ch\,el\,ec}$ - coal chemical energy consumption in a CHP,
$E_{el\,ec\,B}$ - gross electricity generation in a CHP,
ρ_{pal} - fuel component of the thermoecological cost,
ρ_{em} - emission component (SO_2, NO_x, p.m.) of the thermoecological cost referred to unit of fuel chemical energy,
ρ_{CO_2} - component related to CO_2 emission referred to unit of fuel chemical energy,
ρ_{inw} - investment component referred to unit of fuel chemical energy,
C, e_h^* - coal consumption and cumulative energy consumption index burdening its acquisition and delivery,
B, e_b^* - biomass (willow chips originating from a plantation) consumption and the cumulative energy consumption index burdening the chips production,
e_I^* - investment component of the cumulative energy consumption in the CHP production process,
Q, e_h^* - gross heat production and the cumulative energy consumption index burdening the heat production,
E_{el}, e_{el}^* - gross electricity production and the cumulative energy consumption index burdening the electricity production.
σ - cogeneration factor,
η_{Eb} - energy efficiency of CHP boiler,–
η_{me} - electromechanical efficiency of the turbine set,
$\eta_{E\,CHP\,G}$ - gross energy efficiency of a CHP plant,
ε_{el} - CHP electric auxiliary services factor,
ε_{th} - CHP thermal auxiliary services factor,
$\eta_{tt} = \eta'_{tt}$ - efficiencies of electricity transformation and transmission for the CHP and substituted utility were assumed on identical level,
η_{ht} - heat transmission efficiency,
$\eta_{E\,ut\,N}$ - net power efficiency for electricity generation in substituted utility,
$\eta_{E\,el\,CHP\,G}$ - gross partial efficiency for electricity generation in cogeneration,
$\eta_{E\,h\,CHP\,G}$ - gross partial efficiency for heat generation in cogeneration.
ρ_c - thermoecological cost indicator for hard coal,
ρ_{ng} - thermoecological cost indicator for natural gas (domestic and imported – on the average),
ρ_{do} - thermoecological cost indicator for diesel oil,
$\zeta_{SO2}, \zeta_{NOx}, \zeta_{p.m.}$ - thermoecological cost indicator for gaseouos hazardous substances and particulate matter,
$\sigma_c, \sigma_{ng}, \sigma_{do}$ - thermoecological cost of emission referred to chemical energy unit of the for hard coal, natural gas and diesel oil,

Indexes:
CHP - relating to the CHP plant,
0 - relating to the plant with coal only combustion (without biomass),
b.c. - biomass chips,
ut` - condensing utility (substituted).

References

- Journals:

[1] Al-Mansour, F., Zuwala, J.: An evaluation of biomass co-firing in Europe. Biomass and Bioenergy 34 (2010), pp. 620-629

[2] Szargut, J., , Ziebik, A., Stanek, W., Depletion of the non-renewable natural exergy resources as a measure of the ecological cost, Energy Conversion and Management 43 (2002) pp. 1149–1163

[3] Szargut, J., Stanek, W. Influence of the pro-ecological tax on the market prices of fuels and electricity. Energy 33 (2008) pp. 137–143

[4] Ziebik, A., Zuwala, J., Sciazko, M.: Energy and ecological effectiveness of biomass co-firing in CHP plants. Archives of Thermodynamics Vol. 30 (2009), pp. 29-44

[5] Zuwala J. Influence of biomass co-firing on the operational parameters of utility plants. Energetyka Vol. 2 (2010) (in Polish)

- Books and monographs:

[6] Valero, A., 1998, Thermoeconomics as a conceptual basis for energy-ecological analysis. In: Ulgiati S, editor. Advances in energy studies. Energy flows in ecology and economy. Roma: Musis; p. 415–44.

[7] Stanek, W., 2009, Methodology of thermal processes ecological assessment by exergy analyses (in Polish). Silesian University of Technology, ISBN 978-83-7335-560-6

[8] Szargut, J., Morris, D, Steward, F., 1988; Exergy analysis of thermal, chemicals and metallurgical processes. New York: Hemisphere Publishing Corporation.

[9] Repetto, R., Dower, R.C., Jenkins, R., Geoghegan, J., 1992; Green Fees: How a Tax Shift Can Work for the Environment and the Economy. World Resources Institute ISBN 0-915825-76-7

[10] Zuwala, J.; Energy and ecology optimization of the structure of power unit with biomass co-firing and cogeneration of electricity and heat. Central Mining Institute, Katowice, 2010 (in press)

- Conference Proceedings and Electronic publications:

[11] Szargut, J. Depletion of the unrestorable natural energy resources as a measure of the ecological cost. In: Ishida M, Tsatsaronis G, Moran MJ, Katzoka H, editors. Proceedings of ECOS'99. Tokyo: Tokyo Institute of Technology; 1999. p. 42–5.

[12] Zuwala, J., Ziebik, A.,; Analysis of Accumulated Energy Consumption In The Process Of Acquiring and Co-Firing Biomass in Heat and Power Plants. Proceedings of Coal Gen Europe Conference & Exhibition, 1-4 Sept., 2009 Expo Silesia, Sosnowiec – Katowice, Poland.

- Theses and technical reports:

[13] Elsayed, M.A., Mattthews, R., Mortimer, N.D.: Carbon and energy balances for a range of biofuel options. DTI Report No. B/B6/00784/REP URN03/836,

[14] Zuwala, J., et. al. Co-firing technology state-of-the-art study. Report prepared in the framework of EU Project Co-firing – from research to practice: technology and biomass supply know – how promotion in Central and Eastern Europe. Project no.: 038479 Project acronym: COFITECK. Available at: http://www.cofiteck.eu/index.php?option=com_content&task=blogcategory&id=23&Itemid=48

Acknowledgments:

The authors would like to express their gratitude to the Ministry of Science and Higher Education for co-financing the research described in the paper in the framework of the projects:
No. PBZ/MNiSW/07/2006/55, carried out in Central Mining Institute in Katowice (J. Zuwala),
No. N R06 0004 06/2009 "CHP STRATEGY (A. Ziebik).

Application of genetic algorithm in optimization of heat exchanger network of the Fluid Catalytic cracking unit

Amirmahyar Azizi Yeganeh[a], Majid Amidpour[a], Gholamreza Salehi[a] ,Yousef Shamsaei[a]

[a] *K.N.Toosi University of Technology, Tehran, Iran*

Abstract: Regarding the ever increasing importance of energy costs in chemical units, employing methods of energy conservation and specifically, using heat recovery and heat exchanger networks has become very common in these units. However, in spite of the extensive research done on synthesis of heat exchanger networks, up to now a comprehensive formulation free from simplifying assumptions for solution of the problem has not been presented. On the other hand, in the majority of provided viewpoints, the issue of synthesis of heat exchanger networks has been considered in an abstract manner, neglecting the interconnection between the network and the process. One way to optimize a heat exchanger network is using the genetic algorithm. Genetic algorithms employ principles of natural selection for finding the optimum formula for prediction or adjustment of patterns and are usually a good choice for fitness-based prediction and optimization.

Keywords: Heat exchanger network, gen, chromosome, DNA.

1. Introduction

One of the prominent challenges involving chemical units is their massive energy consumption, since a major portion of costs of production deals with energy, reaching up to one third of the whole production cost in some cases. On the other hand, regarding the escalation of fuel costs and the extensive competition in global markets for reducing the finished cost of the product, employing energy economy methods in design of new units has become very common.

The issue of synthesis of heat exchanger networks involves heating and cooling process streams using heat integration. This means wherever possible, hot process streams are sued to heat cold process streams and cold streams are used to cool hot streams. This results in lower consumption of hot and cold utilities. Besides, the issue of quantity of heat exchangers should also be considered to reduce capital costs along with operational costs.

The concept of heat exchanger network design was first put forward by Broeck in 1944 [6] Later in 1969 [7], heat exchanger network synthesis was defined as designing the heat exchanger network using the data related to hot and cold process streams, including input and target temperatures, heat capacities, temperatures, costs of utilities and costs of heat exchangers, so that capital and operational costs are minimum.

In some engineering issues it is possible to use methods related to the gradient of the objective function but in many problems, it is either impossible or complicated to use these methods. In some cases the search space is discontinuous and in other cases, although the space is continuous, local optima prevent obtaining the global optimum.

Genetic algorithm has an accidental nature. It starts the search from a special point and continues the accidental search until it reaches a global optimum.

Another issue is that other mathematical methods usually result in a special formula or procedure for solving the problem, while smart methods are general recipes which can be used for every problem.

In this work try to show the application of genetic algorithm optimizer with a computer programming in the typical heat exchanger network of FCC (Fluid Catalytic Cracking) unit in a refinery process and then evaluate the results with the real condition of the unit.

2. Genetic Algorithm

Genetic algorithm starts from a formula. Each member of the population is tested against a set of data and the fittest ones are chosen. These fittest individuals mate together (exchanging DNA elements) and mutate (accidental change of DNA members) and through a large number of generations, evolve towards the fittest individuals which correspond the most accurate formulae for the optimal point.

Similar methods such as neural networks are also nonlinear and parametric but the genetic algorithm is attractive specially because its final answer is visible for the user and in order to increase the confidence about the results, it can be tested using statistical formulae.

The genetic algorithms technology is subject to constant development and improvement. Generally, solutions are shown as sets of 1s and 0s; there are also other ways of representation, though.

The evolution starts from a completely accidental set of entities and repeats in next generations. In each generation, the fittest are chosen.

A solution for the problem at hand is shown as a set of parameters which are called chromosomes. Chromosomes are usually shown as a simple set of data. Other data structures can also be used, however.

First, a multiple of properties are generated in an accidental manner for producing the first generation. In any generation, each of these properties is evaluated using a fitness function and a number is assigned to its fitness.

The next step is creating the next generation and then connecting chromosomes and mutation.

Genetic algorithms have a constant, small mutation probability which is usually a small number like 0.01 or smaller. This is actually the probability of accidental mutation of chromosomes of the offspring.

The process results in a new generation of chromosomes which are different from the old generation. The whole process is repeated for the next generation, pairs are chosen for mating, the population of the third generation is formed and so on. This procedure is iterated until we get to the last generation.

The following are the ending conditions of a genetic algorithm:

- Reaching a preset number of generations
- Depleting of the dedicated resource (calculation time, money)
- Finding an individual who satisfies the required minimum criteria
- Reaching the highest degree of fitness where no more improvement happens upon iteration

2.1. Advantages of genetic Algorithm

The first and the most important advantage of genetic algorithms is that they are basically parallel, while the majority of other algorithms are not parallel and can only search the search space in one direction at a time and if a found solution is a local optimum or a subset of the main solution, all the path to this solution should be put away and the search started from the beginning, while a genetic algorithm (GA) has several start points, searches the search space in several directions at a time and if one of these directions fails to obtain a result, the rest of them carry on with more resources. GAs are very advantageous for problems which have a large solution space since they have a parallel nature and are capable of evaluating several solutions at the same time. Problems with these characteristics are called non linear. In a linear problem, the fitness of each element is independent and any change in any part has a direct effect on the entire system. However, only few of real world problems are linear. In nonlinear problems, when a change happens in a part of the problem it can have a non uniform effect on the entire system, or changing a few elements can have a large effect on the whole system. Fortunately, the parallel nature of the GA solves this problem in a short time. For instance, for solving a 1000 digit linear problem, there are 2000 possible solutions but for solving a nonlinear problem, there are up to 21000 solutions.

Another advantage of genetic algorithms which might at the first glance seem a disadvantage is that GAs know nothing about the problem they are solving and that is why they are called 'blind watchmakers'. They make accidental changes in their solution candidates and then, evaluate them using a fitness function. This enables the method to start solving the problem with an unbiased frame of mind and its accidental decisions open all the ways towards the problem. Whereas the problems which are limited by information have to make decisions through comparison and that

results in loosing a large number of novel solutions.

Another advantage of genetic algorithms is that they can change several parameters simultaneously. A great proportion of real world problems can not be limited to one characteristic and should be viewed multilaterally. GAs are very effective in solving these sorts of problems and this is actually a result of their parallel nature. They can find two or three solutions for a single problem, each of them found by considering one of the parameters.

2.2. Limitation of genetic algorithms

One of the problems with this method is the question of how to write the fitness operator so that it results in the best solution for the problem. If this fitness operator is not chosen well, the algorithm might find no solution for the problem or mistakenly solve another problem. Moreover, in order to choose the proper function for fitness, other parameters like population, mutation rate, crossover, strength and type of selection must also be considered.

Another problem is that there might be a chromosome with a large distance from other individuals of its generation (high fitness). This chromosome might be seen to early and lead the solution to a local optimum. This usually happens in small populations. Methods such as Scaling and Ran Tournament selection overcome this problem.

3. Process Data

The first step to extract process data is calculating the heat transfer between hot and cold streams and utilities. The following equation can be used to calculate this quantity [5]:

Heat transfer from hot streams to cold streams:

$$Q = UAF_t\Delta T_{LM} \quad (1)$$

Overall heat transfer coefficient:

$$U = \frac{1}{\frac{A}{h_{in}A_{in}} + R_{f,in} + R_{wall} + R_{f,out} + \frac{A}{h_{out}A_{out}}} \quad (2)$$

Average logarithmic temperature difference:

$$\Delta T_{LM} = \frac{(T_{h,out} - T_{c,in}) - (T_{h,in} - T_{c,out})}{\ln(\frac{T_{h,out} - T_{c,in}}{T_{h,in} - T_{c,out}})} \quad (3)$$

Hot fluid's thermal load:

$$Q_h = M_h C_{p,h}(T_{h,out} - T_{h,in}) \quad (4)$$

Cold fluid's thermal load:

$$Q_c = M_c C_{p,c}(T_{c,out} - T_{c,in}) \quad (5)$$

The data that need to be gathered for each flow include: T_s , supply temperature or T_{in} input temperature, $T_,$ target temperature or T_{out} output temperature, M (mass flow rate), C_p, specific heat, h, film heat transfer coefficient, R_f fouling coefficient, R: the transferred heat load.

Input temperatures, fouling factor and mass flow rate are taken from documents such as the flow diagram of the process and mass balance data. In order to accurately calculate physical properties of flows (viscosity, density and heat transfer coefficient), film heat transfer coefficient and the amount of heat transferred are taken into account as follows:

The rating of the heat exchanger is carried out by a heat exchanger design software using data sheets of heat exchangers and the required values are extracted.

As a first stage of methods of network based synthesis, the suitable network to be synthesized is chosen. After choosing the proper network, the problem is formulated and the result of this formulation is usually a Mixed Integer Nonlinear Programming (MINLP). In the next stage, the optimum network is obtained by solving this model using optimization methods.

4. Methodology

The methodology is presented in two stages.

In the first stage, ΔT_{min} is calculated using the genetic algorithm for the heat exchanger network (HEN). The concepts related to the first stage are taken from heat recovery analysis (pinch) [1]. By having $\Delta T_{min,}$ the optimum values for cold and hot utility consumption and location of the pinch point are calculated. The pinch point divides the problem into two regions, above pinch and below pinch. The HEN structure is determined separately for each region.

In the next stage, the objective function is constructed and constraints are clearly specified. Since the objective function is nonlinear, another genetic algorithm is used to optimize it. Thermodynamic concepts are used to find the best heat exchanger network and finally two optimized heat exchanger networks for above and below the pinch point are obtained and connected to each

other at the pinch point. The final optimum network is designed such that it yields minimum utility consumption besides minimum annual cost.

4.1. Optimizing ΔT_{min}

As noted earlier, in order to find ΔT_{min}, the total cost function is constructed as the sum of annual energy costs and capital costs.

At this stage, the HEN has not yet been analyzed. Later, heat transfer surface area of the heat exchangers should be optimized as far as possible. This surface area is obtained after optimizing ΔT_{min} for hot and cold process streams via the composite curve diagram for temperature versus enthalpy.

The composite curve diagram is divided to different intervals and the minimum surface area is calculated using (6) proposed in [4].

$$A_{\min} = \sum_{j}^{interval} \left(\frac{1}{\Delta T_{LM,i}}\right)\left\{\sum_{i}^{Stream} \frac{q_i}{h_i}\right\}_j \quad (6)$$

Where j is the the enthalpy interval, i is the number of streams in each interval and $\Delta T_{LM,i}$ is the logarithmic mean temperature difference for the stream i in the interval j, q_i and h_i are the heat available or necessary and the individual heat transfer coefficient for the stream i in the interval j. For each value of ΔT_{min}, different values are obtained for A_{min} and hot and cold utilities. Consequently, different values are found for the total cost function which depends on these costs. Annual energy cost and capital cost and the total cost are obtained using (7), (8) and (9), respectively [1].

$$C_{Energy} = C_{HU}.HU + C_{CU}.CU \quad (7)$$

$$C_{Capital} = (A + B.A^{C}_{\min}).\frac{(1+i)^t}{t} \quad (8)$$

$$C_{Global} = C_{Energy} + C_{Capital} \quad (9)$$

Where C_{HU} is the cost of hot utility in \$/kw/year, C_{cu} is the cost of cold utility, HU is the consumption of hot utility and Cu s the consumption of cold utility both in kW, and a, b, and c are constants pending on the equipments. i is the interest rate, t is the life time of the industrial unit in years, and costs are calculated in \$/year.

The optimum value of ΔT_{min} is found by minimizing equation (6), which represents the cost of HEN. Thus, the objective function which needs to be minimized is equation (6).

A genetic algorithm is used to optimize this nonlinear objective function.

5. Synthesis the heat exchanger network.

The minimum utility cost is found by calculating values of hot and cold utilities which s in turn found from the previous analysis and the optimum $\Delta T_{min.}$ The minimum capital cost is found through finding the best combination of process streams in heat transfer facilities like heat exchangers, heaters and coolers.

In order to find an ideal heat exchanger network, it is adequate to satisfy the following constraints [2]:

1- Heat is only transferred from the hot stream to the cold stream and the temperature of the hot stream must be higher than that of the cold stream.(according to 11)
2- The value of ΔT_{min} must not be violated at the output of any of the heat exchangers (hot or cold)
3- The lowest utility consumption must be assumed constant in the first stage (in accordance with 12).
4- Every subset of the network must have a minimum number of heat exchangers.

The objective function is nonlinear and we have both equality and inequality constraints which are shown in the following [1]:

Minimize C_{Global} subject to:

$$(T_{h,in})_k > (T_{c,out})_k$$

$$(T_{h,out})_k > (T_{c,in})_k \quad (10)$$

Where K=1,..., the number of heat transfer equipments.

$$|(T_{h,in})_k - (T_{c,out})_k| \geq f.\ \Delta T_{min}$$

$$|(T_{h,out})_k - (T_{c,in})_k| \geq f.\ \Delta T_{min} \quad (11)$$

$$HU \leq HU_{min}$$

$$CU \leq CU_{min} \quad (12)$$

$$U_{min} = N-1 \quad (13)$$

Where K represents heat exchanger, heater or cooler, $T_{h,in}$ and $T_{h,out}$ are inlet and outlet temperatures of the hot heat exchanger, $T_{c,in}$ and $T_{c,out}$ are inlet and outlet temperature for the cold heat exchanger, f is the clearance factor for constraints of ΔT_{min}, HU_{min} and CU_{min} are minimum consumptions for hot and cold utilities, U_{min} represents

the minimum number of heat transfer equipments, N represents the number of process streams plus the number of utility streams.

6. A brief description of the process of the fluid catalytic cracking unit (FCCU)

The cracking catalytic unit cracks heavy molecules of the gas oil cut to more expensive, high octane gasoline, in the proximity of the power-shaped catalyst Alumina-silica and in a temperature between 500 °C and 530 °C. The feed stock for the fluid catalytic cracking unit is heavy gas oil which is obtained from atmospheric and vacuum distillation columns and the coke unit. Globally there are about 350 FCC units in operation which have been installed by a number of different companies.

In addition to gasoline, some other side products are also produced in catalytic cracking units. These include:

- Dry gas: It is usually sweetened and then, consumed as fuel for the refinery itself.
- Liquid gas (LPG): It is a combination of propane and propylene which is consumed in petrochemical units.
- B.B: A mixture of butane and butene which is the feed of the alkylation unit
- Light gasoil: After sweetening it is taken to product storage tanks of the refinery.
- Slurry oil: It is used in wax and asphalt industries.

6.1. Heat recovery targeting & simulation methodology

Regarding the existing data about heat exchangers in the FCCU and lack of price data for hot and cold utilities, for some of these data (such as interest rate and heat transfer coefficient) hypothetical values are assumed which are close to reality. Composite curves, Ground composite curves (GCCs) and heat exchanger network are analyzed using the software ASPEN PINCH®. ΔT_{min} of the process is calculated to be 27 °C.

6.2. Simulation the network

The large amount of heat production during catalyst reforming in the regenerator which is caused by burning of the coke deposited on the catalyst in the reactor, provides the heat necessary for evaporation of the feed and also cracking of heavy feed molecules to light products. Therefore, two main sources of thermal energy in catalytic cracking unit are flue gas flows leaving the reduction column at the temperature of approximately 700 °C and reactor product vapors at the temperature of 500 °C. Since there is a need to cool output gases of the reactor in the separation column, the heat at the bottom of this column is used to preheat the feed and also to produce saturated vapor, so that using circulating flows and products of the column, makes up the furnace heat demand. The flue gas hot stream is used for producing power and hot steam.

Composite curves of energies of flows illustrate the existence of threshold phenomenon which means there is no need for hot thermal energy in the unit. On the other hand, the cold utility curve in the composite curve shows that 64200 kg/hr hot steam is produced at the temperature of 382°C from water at the temperature of 107°C. The requirement for cooling water is MW 83.31 from a total of 125.19 MW cold energy requirement of the process, while the total heat transfer between cold and hot stream of the process is 67.64 MW.

Data presented below are extracted from a typical FCC unit in Iran.

Table 1. Data of hot and cold streams of the FCC unit

Item	Name	T_{in}(°C)	T_{out}(°C)	MC_p	Stream
1	Overhead	138	40	0.91	hot
2	H.N. Circulation	171	143	0.40	hot
3	LCO Circulation	219	182	0.38	hot
4	LCO Circulation2	219	166	0.42	hot
5	Lean Oil	166	40	0.04	hot
6	LCO Product	208	50	0.07	hot
7	HCO Circulation	319	228	0.29	hot
8	Bottom Circulation	366	271	0.35	hot
9	Flue Gas	712	288	0.15	hot
10	Bottom Product	366	66	0.02	cold
11	Feed	60	232	0.31	cold
12	DEC3 Reboiler	183	200	1.55	cold
13	Stip. Reboiler	115	149	0.99	cold
14	Rich Oil	60	124	0.05	cold
15	Strip FE.	40	60	0.51	cold
16	DEC4	183	38	0.20	hot

	Bottom				
17	DEC4 Overhead	65	48	1.49	hot
18	DEC4 Product	48	40	0.05	hot
19	Cop. Int.	72	40	0.29	hot
20	Cop. Dis.	66	40	0.79	hot

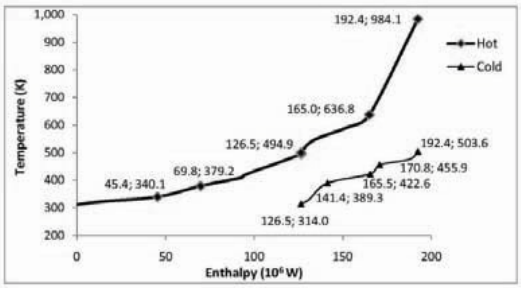

Fig. 1. Composite curves of FCCU (CC)

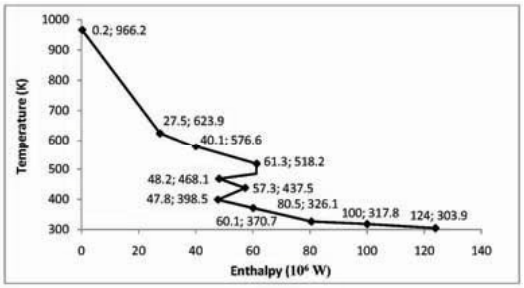

Fig. 2. Grand Composite curve of FCCU (GCC)

7. Generating the code & optimization using genetic algorithm

In this section, the effort is made to validate the results obtained from Aspen, by empirical relationships which are implemented n the MATLAB environment. These results are in fact $A_{\min}$ (minimum heat transfer surface area). Finally codes are written in the genetic algorithm toolbox of MATLAB and a new method is presented for finding hot and cold utility requirements of the unit through minimizing energy costs.

Evaluation of minimum energy requirement, followed by estimation of hot and cold utility requirements are carried out using the genetic algorithm which is very interesting, once compared to the optimized results of Aspen and empirical observations.

7.1. Calculating $A_{\min}$

Minimum heat transfer area is obtained using the equation (6), the different parts of which have been described in previous sections.

This relationship is implemented in MATLAB®. The obtained value of $A_{\min}$ is 650.6669 m^2.

Next, we try to estimate the number of hot and cold utilities required for the heat exchanger network for a value of $\Delta T_{\min} = 27\,^{\circ}C$. This task is done by writing codes in genetic algorithm toolbox of MATLAB and through minimization of global energy using the equations (7), (8) and (9).

Numerical values are as follows:

$C_{HU} = 7$ \$/KW/Year

$C_{CU} = 5$ \$/KW/Year

$a = 0$

$b = 1200$

$c = 0.57$

$i = 0.03$

$t = 20$ Year

$A_{\min} = 650.67 m^2$

$C_{Capital} = 59812.11$ \$

And HU and CU, hot and cold utility requirements respectively, are unknowns which are evaluated by minimization of costs through genetic algorithm.

The results of genetic algorithm for 20, 50 and 100 members are as follows:

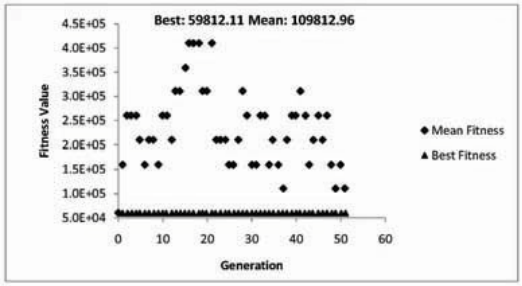

Fig. 3. The results for 20 members and 51 births in which the values of HU and CU are 0.25168 and 0.28325 respectively.

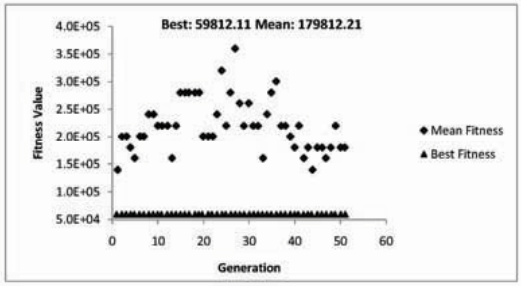

Fig. 4. Results for 20 members and 51 births in which HU and CU are 0.6483 and 0.22384 respectively.

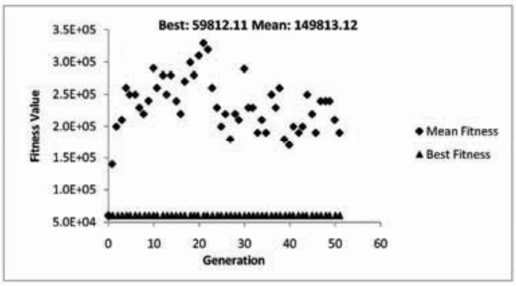

Fig. 5. Results for 100 members and 51 births in which the values of HU and CU are 0.95013 and 0.58279 respectively.

Composite curves of the hot and cold streams of the heat exchanger network of the FCC unit are constructed using Aspen Pinch simulator.
After simulation and targeting, the results are as follows:

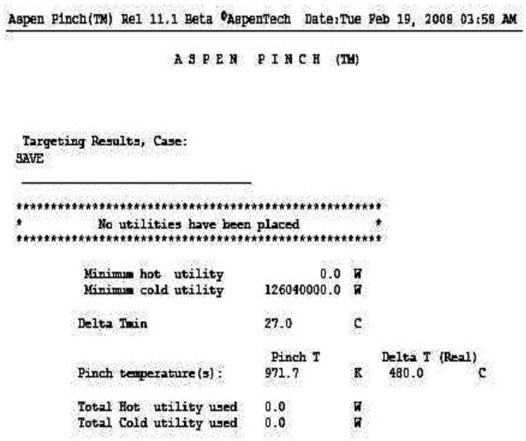

```
Aspen Pinch(TM) Rel 11.1 Beta ©AspenTech  Date:Tue Feb 19, 2008 03:58 AM

                    A S P E N   P I N C H  (TM)

 Targeting Results, Case:
SAVE

*****************************************************
*          No utilities have been placed            *
*****************************************************

        Minimum hot  utility              0.0  W
        Minimum cold utility    126040000.0  W

        Delta Tmin                 27.0        C

                                  Pinch T           Delta T (Real)
        Pinch temperature(s):     971.7      K      480.0       C

        Total Hot  utility used   0.0        W
        Total Cold utility used   0.0        W
```

Fig. 6. Targeting results calculated by Aspen pinch simulator software

It is observed that in the three solutions obtained form genetic algorithm, hot and cold utility values are smaller than 1, which corresponds with results of Aspen Pinch simulation and also empirical results. Therefore, we can conclude that one can get good results for simulation of different process units using genetic algorithms

Conclusion

As a conclusion, the unique features of this research can be expressed as follows: The presented viewpoint employs simultaneous group synthesis to correctly consider the trade-off between operational and capital costs.

Because of the network nature of the adopted viewpoint, increasing the number of streams enlarges the dimensions of the problem in an uncontrollable manner and consequently the design will become less effective.

Heat exchanger network synthesis using thermal analysis and then optimizing with genetic algorithm is very effective and leads to getting better results than the other works with different methodologies.

Using GA toolbox in MATLAB software after running the related code, gives us trusted value for the hot & cold utility needed in the network.

Nomenclature

a utility constant

A area, m^2

b utility constant

c utility constant

C cost, \$/year

C_p specific heat, J/(kg K)

h heat transfer coefficient, W/(m^2 ºC)

i benefit ratio

K Utility index(Heater, Cooler or Heat Exchanger)

M mass flow rate, kg/s

R transferred heat load, kW

R_f fouling coefficient

t plant life, year

T temperature, °C

U overall heat transfer coefficient, W/(m^2 ºC)

q_i and h_i heat available for stream i, kW

Subscripts and superscripts

c cold stream

CU cold utility

h hot stream

HU hot utility

in inlet

min minimum

out outlet

s supply

References

[1] M.A.S.S Ravagnani., et al., Heat exchanger network synthesis and optimization using genetic algorithm, Applied Thermal Engineering 25 (2005) 1003-1017.

[2] Smith, R., Chemical process design and integration, 1995, McGraw-Hill, Inc, New York.

[3] Linnhoff, B. and Hindmarsh, E., 1983, The pinch design method for heat exchanger networks, Computers and chemical engineering 38 (5) 745-763.

[4] Linnhoff, B. and Towsend, D.W., 1984, Surface area for heat exchanger networks, IChemE Annual Re. Mtg Bath.

[5] Kakac, S. and Hongtan, L. 2002, Heat Exchangers, selection , rating and thermal design, CRC Press, USA.

[6] Broeck, H.T. 1944 Economic selection of exchanger sizes, Ind Eng Chem *36* (1) .

[7] Masso. and Rudd. 1969, Develop a network of countercurrent heat exchangers with minimum annual costs,

A macro-level multi-objective model with uncertain data for sustainability studies

Carla Oliveira[a], Carlos Henggeler Antunes[a,b],

[a] INESC Coimbra, Rua Antero de Quental 199, 3030-030 Coimbra, Portugal
[b] Department of Electrical Engineering and Computers,
University of Coimbra, Polo II, 3030-030 Coimbra, Portugal,

Abstract: A multi-sectoral economy-energy-environment model is proposed to perform a prospective analysis of the changes in the economic structure and the energy system resulting from different policies, as well as to assess the corresponding environmental impacts, providing decision support in policy making. The model is a top-down macro-economic multi-objective model, which allows taking into account the energy carriers associated with primary supplies, conversion and transformation processes. The demand for energy services is disaggregated by economic sectors and may be disaggregated by specific functions within a sector. The model allows to explore the effects of new less energy-intensive or carbon-intensive technologies on the total system costs, changes in fuel and technology mix, and the levels of greenhouse gases and other emissions. This is done in the model framework by considering pollutant/energy coefficients defined as intervals, which capture the uncertainty associated with new processes and/or technologies. This type of analysis is of outstanding importance for understanding the role of technology in carbon mitigation efforts and other energy system planning studies at a macro level.

Keywords: Economy-energy-environment interactions, Multi-objective linear programming, Multi-sectoral models, uncertainty handling.

1. Introduction

Portugal is faced with great challenges regarding the policies to achieve the targets that have been imposed both for the energy and environmental sectors, without neglecting the economic and social issues associated with those policies. Thus, the use of adequate tools, which allow obtaining sound information in order to facilitate decision-making, is of capital importance. Multi-sectoral economy-energy-environment (ME3) models provide the ability to perform a prospective analysis of the changes in the economic structure and the energy system, as well as to assess the corresponding environmental impacts, resulting from distinct policies for decision support in policy making. This type of models may combine bottom-up technology approaches with top-down macro-economic models, in which industries, commodities, consumers and government expenditures, as well as foreign trade and investment, are disaggregated. These models allow taking into account the energy carriers associated with primary supplies (e.g. mining, petroleum extraction), conversion and processing processes (e.g. power plants, refineries) and end-use demand for energy services (e.g. automobiles). Moreover, the demand for energy services may be disaggregated by sector (i.e. residential, industrial, transportation and commercial) and by specific functions within a sector (e.g. residential air conditioning, heating, lighting, hot water). In the framework of ME3 models, optimization models are mainly dedicated to decision-making on the choice of technology, given an objective function (generally the minimization of operational and fixed costs) and some constraints on technological availability. These models identify the technologies that should be chosen to optimize the objective function, subject to the satisfaction of the constraints. A representative example is MARKAL - Market allocation model - for energy policy [6] and EFOM - Energy Flow Optimization model [16]. Since the sustainable development concept is inherently a multidimensional one, multicriteria methods provide a suitable framework for dealing with the conflicting axes of evaluation underlying sustainability problems

([10]; [7]). In particular, multiple objective linear programming (MOLP) models based on the linear inter/intra industrial linkages of production can be used to study the interactions between the four main pillars of sustainable development: economy, energy, social and environmental concerns (see [1]; [2]; [3]; [8]; [11]). Within these models, the specification of new less energy or carbon-intensive technologies allows to explore the effects of these choices on the total system costs, changes in fuel and technology mix, and the levels of greenhouse gases and other emissions. However, in most real-world situations, these coefficients are not exactly known because data is scarce, difficult to obtain or estimate and the system being modeled might be subject to changes. Therefore, these mathematical programming models for decision support must take explicitly into account the handling of the uncertainty associated with the coefficients. This can be done in this modeling framework, for instance, by considering pollutant/energy coefficients defined as intervals (see [12,13]), with bounds that cope with more or less intensive carbon/energy technologies. That is, uncertainty is captured through coefficients that are unknown but bounded, which is generally more realistic in this setting than assuming probability (as in stochastic programming) or possibility (as in fuzzy programming) distributions. This kind of analysis is of outstanding importance for understanding the role of technology in carbon mitigation efforts and other energy system planning settings. In this context, an MOLP ME3 model with interval coefficients is proposed, which allows assessing economy-energy-environment impacts of distinct policies, based on the levels of activity of the economic sectors.

2. A MOLP ME3 model

A comprehensive MOLP model to deal with E3 interactions has been proposed previously [11]. However, some noteworthy modifications have been further included: changes consistent with the European System of Accounts (ESA95); 80 (real and artificial) activity branches; volume and price components of the economy; interval coefficients for the energy use within the coefficients matrix, as well as in other constraints (namely on pollutant coefficient emissions); emissions not just arising from the combustion processes but also from other sources; consideration of the acidification equivalent potential (AEP) and the tropospheric ozone potential (TOP), besides the global warming potential (GWP).

2.1. Constraints

The model includes two types of constraints: coherence constraints and defining constraints. The first set of constraints is based on Input-Output (I-O) analysis and they guarantee that intermediate consumption and final demand of goods or services of each activity sector cannot exceed the total amount available from national production and competitive imports of that same good or service:

$$\mathbf{A}\mathbf{x}+\mathbf{a}_{cptf}\ (cptf)+\mathbf{a}_{csf}(csf)+\mathbf{a}_{g}(g)+\mathbf{a}_{gfcf}(gfcf)+\mathbf{a}_{sc}(sc)+ +\mathbf{a}_{aldv}(aldv)+\mathbf{a}_{exp}(expstcif)\leq\mathbf{x}+\mathbf{imp}^{c}, \quad (1)$$

A is the interval technical coefficients matrix (product-by-product) and each of its elements, a_{ij}, is the amount of good or service i needed to produce a unit of good or service j; **x** is the vector of total output for each activity branch; $\mathbf{a}_{cptf}$ is the interval vector with the weight of each good or service aimed at household consumption on the total household consumption; cptf is the total consumption of the resident and non-resident households on the territory; $\mathbf{a}_{csf}$ is the interval vector with the weight of each good or service aimed at the consumption of non-profit institutions serving households (NPISH) on the total NPISH consumption; csf is the total consumption of the NPISH; $\mathbf{a}_{g}$ is the interval vector with the weight of each good or service aimed at public consumption on the total public consumption; g is the total public consumption; $\mathbf{a}_{gfcf}$ is the interval vector with the weight of each good or service aimed at gross fixed capital formation (GFCF) on the total GFCF; gfcf is the total GFCF; $\mathbf{a}_{sc}$ is the interval vector with the weight of each good or service aimed at changes in inventories on the total changes in inventories; sc is the total changes in inventories; $\mathbf{a}_{aldv}$ is the interval vector with the weight of each good or service aimed at acquisitions less disposals of valuables (ALDV) on the total ALDV; aldv is the total ALDV; $\mathbf{a}_{exp}$ is the interval vector with the weight of each good or service aimed at exports at CIF (cost, insurance and freight) prices on the total exports (excluding tourism); expstcif is the total exports at purchasers' CIF prices (excluding tourism); $\mathbf{imp}^{c}$ is the vector of competitive imports, where the

elements which correspond to non-energy goods or services have null value.

The defining constraints, including economic, social and environmental indicators, are described in detail in [13]. The economic indicators include several consumption representations: the households' consumption on the territory, the residents' (households and NPISH) consumption and, finally, the tourism imports. In what concern foreign trade, it is possible to obtain total exports and imports at constant FOB (free on board) prices, exports at constant purchasers' prices, total exports and imports including tourism and total imports at CIF prices. The employment level for each activity branch is obtained by dividing the output by the corresponding expected labor gross productivity for each branch. GDP is computed according to the production approach and to the expenditure approach. GDP at current prices is obtained from the distinct components of GDP at constant prices according to the expenditure approach, which are multiplied by the corresponding deflators. Other economic indicators such as disposable income of households and NPISH, the public debt and the public administration's global balance are also obtainable.

The environmental sphere of the model considers several kinds of emissions: CO2 and non-CO2 emissions from fuel combustion; fugitive emissions; emissions from industrial processes, from solvent and other products use, from agriculture activities, from waste management and from waste water handling. CO2 emissions from fuel combustion are easily obtained from the I-O table, where the total fuel use is the total amount of fuel production plus imports. The emission factors used in the computation of other pollutant emissions are highly dependent on the technology used. In this case a tier 2 methodology has been used whenever possible, with data from the National Program for Emission Ceilings and the National Inventory Report. Finally, it is important to mention that the economic and environmental defining constraints with interval coefficients have been imposed with interval (upper/lower) bounds.

2.2. Objective functions

The allocation of energy resources should be made having in mind that the energy sector is a part of the economic system as a whole and that energy planning requires the consideration of economic, social, energy and environmental objectives. In this way, the model herein proposed considers the following objective functions: maximization of GDP (gdp), a measure of economic performance; maximization of the total level of employment (emp), a measure of social well-being; minimization of GWP (gwp), measured through the emission of green house gases (GHG); minimization of energy imports (eimp), a measure of the country's foreign energy dependency.

$$\max Z_1 = \text{gdp}. \quad (2)$$

$$\max Z_2 = \text{emp}. \quad (3)$$

$$\min Z_3 = \text{gwp}. \quad (4)$$

$$\min Z_4 = \text{eimp} \quad (5)$$

Further details about the MOLP model may be seen in [11, 13].

3. An interactive method for interval MOLP

The interactive approach used to obtain compromise solutions to the MOLP model based on I-O analysis with interval coefficients is based on [12]. The interactive nature of the algorithmic approach to compute solutions is very important in this policy support setting, by providing the decision maker (DM) with the means to explore not just the trade-offs at stake in different regions of the search space between the competing objectives but also his/her own preferences.

Without loss of generality, the MOLP problem with interval coefficients is given by:

$$\max Z_k(\mathbf{x}) = \sum_{j=1}^{n} \left[c_{kj}^L, \quad c_{kj}^U\right] x_j \text{ , } k = 1, \ldots, p, \quad (6)$$

$$\text{s.t. } \sum_{j=1}^{n} \left[a_{ij}^L, \quad a_{ij}^U\right] x_j \leq \left[b_i^L, \quad b_i^U\right], \; i = 1, \ldots, m,$$

$$x_j \geq 0, \; j = 1, \ldots, n,$$

where $\left[c_{kj}^L, \quad c_{kj}^U\right]$, $\left[a_{ij}^L, \quad a_{ij}^U\right]$ and $\left[b_i^L, \quad b_i^U\right]$, k = 1, …, p, j = 1, …, n, and i = 1, …, m, are closed intervals.

The method starts by defining two surrogate deterministic problems, by considering the minimization of the worst possible deviation of the interval objective functions from their corresponding interval ideal solutions (see [9]) and considering threshold levels on the constraints (see [15]). The interval ideal solutions are computed

considering both the extreme versions of the objective functions and of the feasible region [5]. Hence, the surrogate problem is:

$$\min \max_{k=1,\ldots,p} \lambda_k D_k(\mathbf{x}), \quad (7)$$

$$\text{s.t. } \sum_{j=1}^{n}(a_{ij}^{L} + \alpha_i(a_{ij}^{U} - a_{ij}^{L}))x_j \le b_i^{U} - \alpha_i(b_i^{U} - b_i^{L}),$$

$i = 1, \ldots, m,$

$x_j \ge 0, j = 1, \ldots, n,$

where $D_k(\mathbf{x}) = |[Z_k^{L^*} - Z_k^{U}(\mathbf{x}), Z_k^{U^*} - Z_k^{L}(\mathbf{x})]|$, $Z_k^{L^*}$ is the optimum with the worst set of coefficients and $Z_k^{U^*}$ is the optimum with the best set of coefficients for $Z_k(\mathbf{x})$. $Z_k^{U}(\mathbf{x})$ and $Z_k^{L}(\mathbf{x})$ are the upper and lower bounds of $Z_k(\mathbf{x})$, respectively, and λ_k is a coefficient to take into account the different orders of magnitude of the objective function values. The expanded pay-off table (containing the individual optimal solutions for each objective function) is composed of two parts: one for $\alpha_i = 0$ ($\forall_i$, i.e. the broadest feasible region) and another for $\alpha_i = 1$ ($\forall_i$, i.e. the narrowest feasible region).

Let $\varepsilon_k = Z_k^{L^*} - Z_k^{U}(\mathbf{x})$ and $\varepsilon_k = \varepsilon_k^{+} - \varepsilon_k^{-}$, $\varepsilon_k^{+}, \varepsilon_k^{-} \ge 0$. In order to obtain the first compromise solution, the DM starts by considering the most constraining feasible region. Let the first compromise solutions be given by $\mathbf{x}^{1U'}$ and $\mathbf{x}^{1U''}$, which are obtained from the two surrogate deterministic problems obtained from (6), according to pessimistic or optimistic stances, in case the DM wants to minimize the upper bound or the lower bound of the worst possible deviation, respectively. If this compromise solution is satisfactory, then the algorithm stops and the solution $\mathbf{x}^{1U'}$ or $\mathbf{x}^{1U''}$ is chosen; otherwise, the algorithm proceeds. The other compromise solutions are given by $\mathbf{x}^{m} = \mathbf{x}^{mU'}$ and/or $\mathbf{x}^{mU''}$. The interactive phases are described next.

For each compromise solution obtained, the following data is shown to the DM:

1) $Z_k(\mathbf{x}^m)$, $m[Z_k(\mathbf{x}^m)] = \frac{(Z_k^{U}(\mathbf{x}^m) + Z_k^{L}(\mathbf{x}^m))}{2}$ (the centre of the interval) and $w[Z_k(\mathbf{x}^m)] = Z_k^{U}(\mathbf{x}^m) - Z_k^{L}(\mathbf{x}^m)$ (the width of the interval);

2) $d(Z_k^*, Z_k(\mathbf{x}^m)) = \text{Max}\ (|Z_k^{L} * - Z_k^{L}(\mathbf{x}^m)|, |Z_k^{U} * - Z_k^{U}(\mathbf{x}^m)|)$, $k = 1, \ldots, p$, and the "acceptability index" (see [14]) of $Z_k(\mathbf{x})$ being inferior to Z_k^*, $A\ (Z_k(\mathbf{x}^m) \prec Z_k^*) = \frac{(m[Z_k^{L^*}] - m[Z_k(\mathbf{x}^m)])}{(\frac{w[Z_k^{L^*}]}{2} + \frac{w[Z_k(\mathbf{x}^m)]}{2})}$. When A $(Z_k(\mathbf{x}^m) \prec Z_k^*)$ and $d(Z_k^*, Z_k(\mathbf{x}^m))$ are close to zero, $Z_k(\mathbf{x}^m)$ is closer to Z_k^*.

3) The achievement rate of $Z_k(\mathbf{x}^m)$ and $Z_k(\mathbf{x}^m)$ with respect to Z_k^*. The achievement rate is $tc_k^{L} = 1 - \frac{(Z_k^{L^*} - Z_k^{L}(\mathbf{x}^m))}{(Z_k^{L^*} - m_k^{L})}$, with respect to $Z_k^{L}(\mathbf{x}^m)$, and $tc_k^{U} = 1 - \frac{(Z_k^{U^*} - Z_k^{U}(\mathbf{x}^m))}{(Z_k^{U^*} - m_k^{U})}$, with respect to $Z_k^{U}(\mathbf{x}^m)$, where m_k^{L} and m_k^{U} are the worst optimum values obtained in the expanded pay-off table. The closer the values of tc_k^{L} and tc_k^{U} are to 1 the closer the DM is to meet its aspiration level Z_k^*. In general, $0 < tc_k^{U} < 1$; however, tc_k^{L} may be greater than 1, namely when α_i is relaxed. In this situation, a value greater than 1 corresponds to a deviation from the goal considered and not to an improvement of the achievement rate solution.

4) The impact of different values for α_i on the compromise solution.

After providing this information to the DM, he/she is asked to reveal his/her satisfaction regarding the solution being analyzed. If the DM is not yet satisfied with the solution obtained, then the algorithm proceeds. The DM is then asked to choose the objective function he/she wishes to improve. If the problem obtained with the additional constraints has an empty feasible region, then information is provided on the amount he/she should relax the different objective reference values, in order to restore feasibility [4]. In this phase the DM can also choose the objective function(s) he/she is willing to relax in order to improve the other objective function(s) and solve the problem with the additional constraints. The impacts of different thresholds on the constraints on the compromise solution may also be shown, allowing the DM to analyse distinct solutions with different coefficient settings. The exhaustiveness of the solution search process depends on the DM, who may decide to end the procedure when he/she considers to have gathered enough information about the solution structure and trade-offs that are at stake between the contending objectives.

4. Some illustrative results

In order to obtain the compromise solutions which best suit the DM's preference structure, the analysis begins by computing the individual optima of each objective function with the best and worst case scenarios, respectively. The solutions obtained are given by

x_k^{β}, k = 1, 2, ..., 4 and β = 0, 1.

Let us suppose that the solution search process is driven by a DM who begins by considering the model formulation that minimizes the upper bound of the worst possible deviation (that is, adopting a conservative stance). In order to obtain a global overview of the model with this formulation four coefficient settings are considered in the analysis. The solutions obtained according to these settings are briefly characterized as follows (see Fig. 1). Solution $\mathbf{x}^{1U''}$, obtained with $\alpha_i = 1$ (for all i, where α_i is the threshold level of constraint i; the higher this value the more tightened the feasible region is), allows achieving the worst optimum of GWP and energy imports. Solution $\mathbf{x}^{2U''}$, obtained with $\alpha_i = 0.8$ (for all i), allows improving the upper bounds on the environment and energy objectives. The interval objective functions regarding energy and environmental concerns and the corresponding interval ideal solutions are now closer. On the other hand, the economic and social axes of evaluation have lower values, having in the last situation both achievement rates with negative values. Solution $\mathbf{x}^{3U''}$, obtained with $\alpha_i = 0.5$ (for all i), allows improving the upper bounds of the environmental and energy objectives, regarding the two solutions previously analyzed. Nevertheless, the economic and social axes of evaluation are worsened. Solution $\mathbf{x}^{4U''}$, obtained with $\alpha_i = 0$ (for all i), allows improving the upper and lower bounds of GDP, regarding the previous solutions, being closer to its interval ideal solution. On the other hand, the level of employment reaches its worst optimum value, leading to an improvement of both achievement rates.

Admitting that the DM does not consider any of the solutions obtained so far as satisfactory, the quest for new solutions continues. Suppose that the DM wants to evaluate what would happen if he/she adopts a more optimistic stance. Hence, new solutions are obtained by considering three coefficient settings with the following thresholds on the constraints: 1, 0.5 and 0, corresponding to $\mathbf{x}^{1U'}$, $\mathbf{x}^{2U'}$ and $\mathbf{x}^{3U'}$, respectively (see Fig. 2). Solution $\mathbf{x}^{1U'}$ is the one with the best environmental results and the worst energy, economic and social results (within this new group of solutions); solution $\mathbf{x}^{2U'}$ allows obtaining the worst environmental outcomes (particularly in what concerns to AEP, TOP and to GWP with the most favorable version of the coefficients setting) and the worst performance of the public global balance, but the best economic and social effects; solution $\mathbf{x}^{3U'}$ is the one which allows the best performance for the public global balance and the worst values for GWP in its less favorable version and the lower level of energy imports.

Suppose that the DM wishes to analyze the solutions obtained by combining situations more/less favorable in the scope of the energy coefficients settings (reduction/increase of the energy consumption/efficiency coefficients) with the environmental and economic coefficients at their central values within the intervals. Solution $\mathbf{x}^{4U'}$ and solution $\mathbf{x}^{5U'}$ are obtained with the most and less favorable version of energy consumption coefficients, respectively. The results obtained in these solutions indicate that the reduction of the energy consumption coefficients leads to a positive impulse on the economic growth and on the employment in a more energy efficient way, that is, with a lower requirement for energy imports.

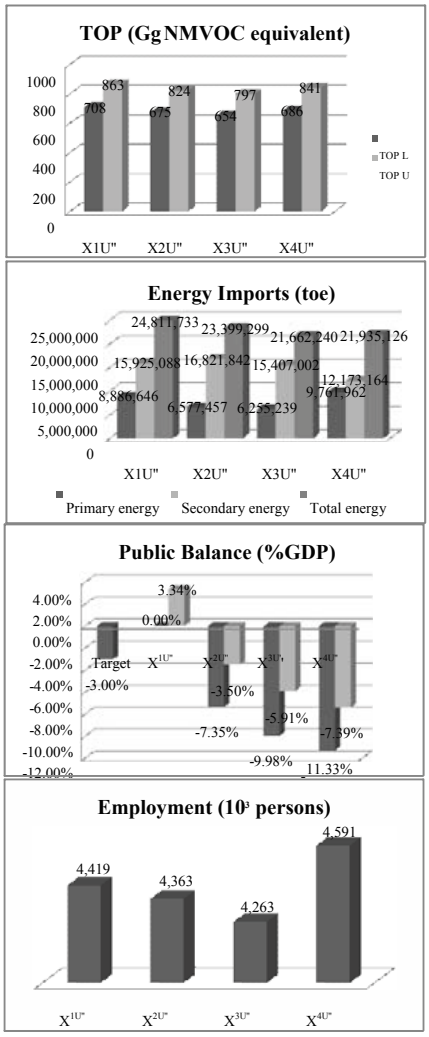

Fig. 1. Some illustrative results obtained with a conservative stance.

Let us now suppose that the DM wants to review his/her solution search process, by adopting once more a conservative stance, but imposing inferior values (reservation levels) to the lower bounds of GDP, GWP and energy imports with the coefficients setting of solution $\mathbf{x}^{3U''}$. Hence, the following constraints are added to the model:

$Z_1^L(\mathbf{x}) \geq 120\,000,$

$Z_3^L(x) \geq -76\,022,$

$Z_4^L(x) \geq -18\,881,$

in which L refers to the lower bound of each objective function.

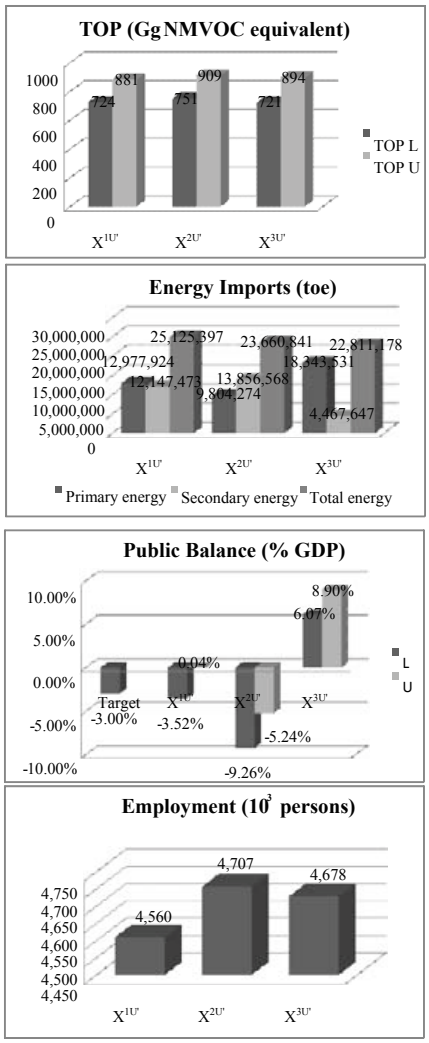

Fig. 2. Some illustrative results obtained with an optimistic stance

With this coefficient setting, the additional constraints lead to an empty feasible region. Hence, an elastic LP problem is solved to restore feasibility and a new solution ($\mathbf{x}^{5U''}$) is obtained. Thus, regarding solution $\mathbf{x}^{3U''}$ there is a slight improvement of the lower bound of GDP, of the level of employment (which has the same value of its worst optimum), of the upper bound of GWP and of the upper bound of energy imports. Notice that this solution is not dominated from the point

of view of the achievement rates of the objective functions (the same might be said about $\mathbf{x}^{4U''}$), since it corresponds to higher outcomes on the environmental and energy plans. On the other hand, the best results of GWP and energy imports are obtained when compared to the other solutions analyzed so far (see Fig. 3).

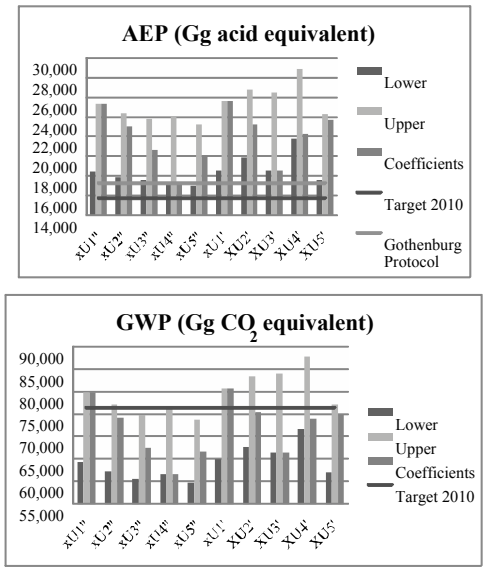

Fig. 3. Ranges of variation of GWP and AEP in the solutions analyzed.

The solution search process stops when the DM considers to have gathered enough information on the problem to grasp the solution structure associated with different trade-offs between the multiple axes of evaluation that are at stake.

All the solutions obtained indicate the need to reduce the energy intensity of the economy in order to overcome the deficit regarding the Kyoto Protocol fulfillment. Then again, it might be said that the improvement of energy efficiency is not enough to attain the necessary emissions reduction in order to achieve the targets imposed on the acidifying substances, being necessary to operate substantial changes namely on the electricity generation sector.

5. Final remarks

Traditionally the multi-sectoral modeling approach has omitted any sources of uncertainty. Inter/intra industrial linkages have generally been viewed as static and deterministic. This paper proposes a MOLP ME3 model, which allows the analysts/DMs to assess E3 impacts, based on the levels of activity of industrial sectors, in a situation of uncertain data modeled through interval coefficients. The aim is to provide information regarding robust solutions, that is, non-dominated solutions attaining desired levels for the objective functions across a set of plausible scenarios. By analyzing globally the solutions obtained with a more or less conservative stance of the DM we can conclude that, in general, the former allows obtaining better results for the energy and environmental objectives, and the latter allows attaining better outcomes for the economic and social concerns.

The development of economic-energy-environment integrated models is a challenging topic, because of their methodological, computational and mathematical complexity. Therefore, the need arises to combine approaches and models, reconcile results and work on a synthesis of partial conclusions. Hence, research is currently underway in order to couple top-down and bottom-up approaches to improve previous analysis tools developed so far.

References

[1] Antunes, C. H., et al., 2002, A study of the interactions between the energy system and the economy using TRIMAP. In. D. Bouyssou et al. (Eds.), Aiding Decisions with multiple criteria - Essays in Honor of Bernard Roy, pp. 407–427, Kluwer Academic Publishers.

[2] Borges, A., C. H. Antunes, 2003, A fuzzy multiple objective decision support model for energy-economy planning, European Journal of Operational Research, 145(2), pp. 304–316.

[3] Cho, J.–C., 1999, The economic-energy-environmental policy problem: An application of the interactive multi-objective decision method for Chungbuk Province, Journal of Environmental Management, 56(2), pp. 119–131.

[4] Chinneck, J., E. Dravnieks, 1991, Locating minimal infeasible constraint sets in linear programs, ORSA Journal on Computing, 3(2), pp. 157–168.

[5] Chinneck, J., K. Ramadan, 2000, Linear programming with interval coefficients, Journal of the Operational Research Society, 51 (2), 209–220.

[6] Fishbone, L., et al., 1983, User's Guide for MARKAL, BNL 51701, Brookhaven National Laboratory, Upton.

[7] Giampietro, M., et al., 2006, Integrated assessment and energy analysis: Quality assurance in multi-criteria analysis of sustainability, Energy, 31(1), pp. 59-86.

[8] Hsu, G., F.–Y. Chou, 2000, Integrated planning for mitigating CO2 emissions in Taiwan: a multi-objective programming approach, Energy Policy, 28 (8), pp.519–523.

[9] Inuiguchi, M., Y. Kume, 1991, Goal programming problems with interval coefficients and target intervals, European Journal of Operational Research, 52(3), 345–360.

[10] Munda G., 2005, Multi-Criteria Decision Analysis and Sustainable Development. In: Figueira, J., Greco, S., Ehrgott, M. (Eds.), Multiple Criteria Decision Analysis: The State of the Art Surveys. Springer Science, Business Media Inc., New York, pp. 953-986.

[11] Oliveira, C., C. H. Antunes, 2004, A multiple objective model to deal with economy-energyenvironment interactions, European Journal of Operational Research, 153(2), pp. 370–385.

[12] Oliveira, C., C. H. Antunes, 2009, An interactive method of tackling uncertainty in interval multiple objective linear programming", Journal of Mathematical Sciences, vol. 161(6), pp. 854-866.

[13] Oliveira, C., C. H. Antunes, 2009, Energy-environment sustainability - a multi-objective approach with uncertain data, INESC Coimbra Research Report, no. 4. Available at http://www.inescc.pt/documentos/4_2009.pdf

[14] Sengupta, A., T. Pal, 2000, On comparing interval numbers, European Journal of Operational Research, 127(1), pp. 28–43.

[15] Urli, B., R. Nadeau, 1992, An interactive method to multi-objective linear programming problems with interval coefficients, INFOR, 30(2), 127–137.

[16] Van der Voort, E., et al., 1995, Energy Supply Modelling Package EFOM-12C, European Commission, DG-XII, EUR 8896 EN/II, Brussels.

Acknowledgments: This research has been partially supported by the Portuguese Foundation for Science and Technology under Project Grant PTDC/ENR/64971/2006 "Multi-objective Models in Energy Efficiency Evaluation Problems".

Advanced Exergetic Analysis of a Steam Methane Reforming System for Hydrogen Production

Alicia Boyano[a], Ana-Maria Blanco-Marigorta[b], Tatiana Morosuk[a], George Tsatsaronis[a]

[a] *Institute for Energy Engineering, Technische Universität Berlin, Germany*
[b] *Department of Process Engineering, University of Las Palmas de Gran Canaria, Spain*

Abstract: Steam methane reforming (SMR) is one of the most promising processes for the production of hydrogen. Therefore, the overall thermodynamic efficiency of this process is of particular importance. The thermodynamic inefficiencies in a thermal system are related to exergy destruction and exergy loss. However, a conventional exergetic analysis cannot evaluate the mutual interdependencies among the system components nor the real potential for improving the energy conversion system being considered. One of the tools under development for the improvement of energy conversion systems from the thermodynamic viewpoint is the advanced exergetic analysis. In this paper, the avoidable part of the exergy destruction is estimated and the interactions among components of the overall system are evaluated in terms of endogenous and exogenous exergy destruction. The assumptions required for these calculations are discussed in detail, especially for those components that are typically used in chemical processes. Results of this paper suggest options for increasing the thermodynamic efficiency of hydrogen production by steam-methane reforming.

Keywords: Steam methane reforming (SMR), hydrogen production, conventional exergetic analysis, advanced exergetic analysis.

1. Introduction

The continuously increasing demand for energy, and concerns about greenhouse gas emissions have increased the interest in the efficient and cost effective generation and use of hydrogen. Hydrogen is produced industrially mainly through steam reforming of natural gas, coal gasification, water electrolysis, and as a by-product of naphtha reforming. The steam/methane reforming (SMR) process is one of the most widespread ways for producing hydrogen from natural gas [1-2]. Therefore, improvements of this process are highly desired.

In a previous study [3], a conventional exergetic analysis of this hydrogen production process was carried out. However, such an analysis cannot evaluate the mutual interdependencies among the system components nor the real potential for improving the energy conversion system being considered.

The purpose of this work is to develop a better understanding of the formation of thermodynamic inefficiencies in an SMR process for hydrogen production [3, 4] by means of an advanced exergetic analysis. In this study, the thermodynamically most relevant system components of the total process are identified and information about possibilities for improving the overall thermodynamic efficiency is provided.

2. SMR process: Modeling and simulation

The conceptual design of an SMR process shown in [3] is used to demonstrate the application of advanced exergetic analysis to an energy-intensive chemical reaction process.

The flow diagram of the SMR system is given in Figure 1. The hydrogen production process includes two reactants: methane and pure water. This process consists of compressing natural gas from atmospheric pressure to 10 bar to decrease the size of downstream equipment and to take advantage of the increased reaction rates and driving forces seen at higher pressures. The natural gas is then heated. Steam is produced by preheating and vaporizing pure water in several heat exchangers: Methane-stream heat exchanger ($HX\text{-}CH_4$), shift-reactor heat exchanger (HX-SHIFT), pre-shift heat exchanger (HX-B), and exhaust-gas-stream heat exchanger (HX-A). Steam is needed also to avoid carbon depositions during the endothermic reforming reaction and to be used as a chemical reactant in the water- gas shift

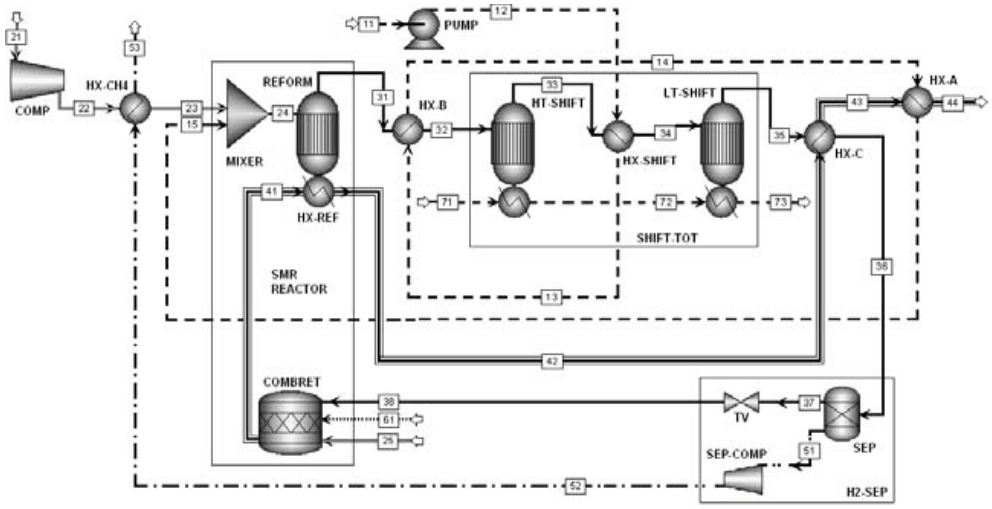

Fig.1. Schematic of a SMR plant for hydrogen production:
..... – air; ═══ – CH4; — · — · — – H2;
═══ – exhaust gases; ━━━ – syngas; - - - - - – water.

reaction. The steam and methane streams are combined and fed to the steam methane reformer. This reactor contains a nickel-based catalyst where the following reactions take place:

$$CH_4 + H_2O \rightarrow CO + 3H_2 \quad (1)$$
$$CO + H_2O \rightarrow CO_2 + H_2 \quad (2)$$

The reforming reaction (1) is highly endothermic.

For the analysis, the reformer is modelled using the following components:

- A methane/steam mixer (MIXER) providing stream (stream 24),
- A reformer (REFORM), and
- A combustion chamber (COMBRET) of retentate (stream 38) and methane (stream 25) with air (stream 61) to provide the thermal energy required for the endothermic reforming reaction, and a heat exchanger to transfer the thermal energy from the exhaust gas stream (stream 41) to the reforming reactor (HX-REF).

The heat of reaction is supplied by the exhaust gases provided by the combustion of (a) additional methane, and (b) the retentate stream, i.e. the stream resulted after hydrogen separation. The resulting synthesis gas is cooled through a heat exchanger to enter first the high temperature reactor (HT-SHIFT) and then the lower temperature reactor (LT-SHIFT). In both reactors, the reaction occurs over a promoted nickel catalyst to increase the amount of H_2 while decreasing the CO (Equation 2). The next step is to heat up the gas stream before the hydrogen enters the separation unit. The hydrogen separation unit is modeled as a metallic membrane able to separate the hydrogen with a high efficiency and a purity of 100% [3,4].

The analysis presented in this paper uses the main system component models: A chemical equilibrium model for the reactor components and a detailed heat integration to perform exergy analysis. Heat integration is an essential part of this study because an optimal performance of a SMR system depends largely on the amount of methane required by the system.

The following parameters are assumed for the analysis [3]:

- The input rate of methane entering the reforming reactor was set to 1 kmol/s of CH_4, to produce 2.67 kmol/s of H_2.
- Air composition: O_2 – 21 mol %, N_2 – 79 mol %.
- Water gas shift reactors: T_{33} =350ºC; p_{33} =10.13 bar, and T_{35} =200ºC; p_{35} =10.13 bar.
- H_2 separator: The efficiency amounts to 90%, the purity of H_2 is 99%.
- Reformer: T_{31} =700ºC; p_{31} =10.13 bar. The

steam/methane molar ratio is equal to 3.2 [4] so that no carbon deposition takes place.

- Other parameters for equipment: η_{COMP} =70%; η_{PUMP} =85%; the chemical conversion of the fuel in the COMBRET is equal to 97%. The effectiveness of heat exchangers is equal to 90% and it is assumed that there are no pressure losses across the heat exchangers.

The ASPEN plus software [5] was used to model the SMR system (the mass flow rate, temperature, pressure and chemical composition of all streams). The designs of the main components as well as the engineering design parameters are based on data published in [6]. Methane was used to simulate natural gas feedstock.

All exergy values are calculated using for the reference environment T_0=298.15K, p_0=1.013, and Ahrendts' model (model I in [7]) for calculating standard molar chemical exergy values.

Table 1 shows the main results of simulation including the values of the chemical and physical exergies.

3. Conventional exergetic analysis

The exergetic analysis is the best approach for evaluating energy conversion systems from the thermodynamic viewpoint [7,8]. The exergy analysis provides a powerful tool for assessing the quality and quantity of a resource. An exergy analysis identifies the location, magnitude and sources of thermodynamic inefficiencies in an energy conversion system. In a conventional exergetic evaluation, the following variables are used [8]: (a) exergy destruction rate within the k th plant component $\dot{E}_{D,k} = \dot{E}_{F,k} - \dot{E}_{P,k}$ (exergy balance for the k th component); (b) exergetic efficiency of the k th plant component $\varepsilon_k = \dfrac{\dot{E}_{P,k}}{\dot{E}_{F,k}}$; and of the overall system $\varepsilon_{tot} = \dfrac{\dot{E}_{P,tot}}{\dot{E}_{F,tot}}$; and (c) exergy destruction ratio for the k th plant component $y_k = \dfrac{\dot{E}_{D,k}}{\dot{E}_{F,tot}}$.

The following definitions of exergy of fuel and exergy of product for SMR plant components were used [7,8]:

Table 1. Thermodynamic data of streams for the SMR plant.

Stream, j	Material stream	$\dot{m}_j$ (kg/s)	p_j (bar)	T_j (°C)	$\dot{E}_j^{CH}$ (MW)	$\dot{E}_j^{PH}$ (MW)	$\dot{E}_j$ (MW)
11	Water	57.649	25	1.013	0.04	0.14	0.18
12	Water	57.649	25	10.13	0.09	0.14	0.23
13	Water	57.649	149	10.13	5.89	0.14	6.03
14	Water *)	57.649	180	10.13	32.08	0.14	32.22
15	Water	57.649	500	10.13	71.69	0.14	71.83
21	CH_4	16.043	25	1.013	0.01	824.40	824.41
22	CH_4	16.043	238	10.13	7.95	824.40	832.35
23	CH_4	16.043	400	10.13	12.49	824.40	836.89
25	CH_4	1.925	25	10.13	0.00	98.92	98.92
31	Syngas	73.691	700	10.13	105.80	921.00	1026.80
32	Syngas	73.691	350	10.13	61.08	921.00	982.08
33	Syngas	73.691	350	10.13	60.89	920.30	981.19
34	Syngas	73.691	200	10.13	47.76	920.30	968.06
35	Syngas	73.691	200	10.13	46.18	916.00	962.18
36	Syngas	73.691	450	10.13	70.65	916.00	986.65
38	Syngas	68.351	447	1.013	28.76	296.60	325.36
41	Exhausted gases	220.298	1341	1.013	270.20	21.27	291.47
42	Exhausted gases	220.298	749	1.013	116.50	21.27	137.77
43	Exhausted gases	220.298	587	1.013	81.80	21.27	103.97
44	Exhausted gases	220.298	272	1.013	29.44	21.27	50.71
52	H_2	5.340	450	1.013	12.54	623.30	635.84
53	H_2	5.340	342	1.013	7.88	623.30	631.18
61	Air	150.022	25	1.013	0.00	0.89	0.89
71	Water	4.200	25	1.013	0.00	–	0.00
72	Water	4.200	102	1.013	0.20	–	0.20
73	Water	4.200	113	1.013	2.37	–	2.37

*) Vapor fraction is equal to 0.555 kg/kg.

- Pump: $\dot{E}_{F,PUMP} = \dot{W}_{PUMP}$
  and $\dot{E}_{P,PUMP} = \dot{E}_{12} - \dot{E}_{11}$
- Compressor: $\dot{E}_{F,COMP} = \dot{W}_{COMP}$
  and $\dot{E}_{P,COMP} = \dot{E}_{22} - \dot{E}_{21}$
- Heat exchangers: $\dot{E}_{F,HX} = \dot{E}_{hot,in} - \dot{E}_{hot,out}$
  and $\dot{E}_{P,HX} = \dot{E}_{cold,out} - \dot{E}_{cold,in}$
- Reformer: $\dot{E}_{F,REFORM} = \dot{E}_{41} - \dot{E}_{42}$
  and $\dot{E}_{P,REFORM} = \dot{E}_{31} - \left(\dot{E}_{23} + \dot{E}_{15}\right)$
- Combustion chamber:
  $\dot{E}_{F,COMBRET} = \dot{E}_{25} + \dot{E}_{38}$
  and $\dot{E}_{P,COMBRET} = \dot{E}_{41} - \dot{E}_{61}$
- Hydrogen separator:
  $\dot{E}_{F,H2-SEP} = \dot{W}_{H2-SEP} + \dot{m}_{38}\left(e^{PH}_{36} - e^{PH}_{38}\right)$
  $\dot{E}_{P,H2-SEP} = \dot{E}^{CH}_{52} + \dot{E}^{CH}_{37} - \dot{E}^{CH}_{36} + \dot{m}_{52}\left(e^{PH}_{52} - e^{PH}_{36}\right)$
- Water-gas-shift reactors:
  $\dot{E}_{F,SHIFT} = \left[\left(\dot{m}^{CO}_{in} e^{CO}_{in} - \dot{m}^{CO}_{out} e^{CO}_{out}\right) + \left(\dot{m}^{H2O}_{in} e^{H2O}_{in} - \dot{m}^{H2O}_{out} e^{H2O}_{out}\right) + \left(\dot{m}^{CH4}_{in} e^{CH4}_{in} - \dot{m}^{CH4}_{out} e^{CH4}_{out}\right) + \left(\dot{m}^{CO2}_{out} e^{CO2}_{out} - \dot{m}^{CO2}_{in} e^{CO2}_{in}\right)\right]^{CH}$
  and
  $\dot{E}_{P,SHIFT-TOT} = \left(\dot{m}^{H2}_{in} e^{CH,H2}_{in} - \dot{m}^{H2}_{out} e^{CH,H2}_{out}\right) + \left(\dot{E}_{water,out} - \dot{E}_{water,in}\right)$.

The exergetic balance for the overall system is $\dot{E}_{F,tot} = \dot{E}_{P,tot} + \sum_k \dot{E}_{D,k} + \dot{E}_{L,tot}$. The exergy losses of the overall SMR system are equal to the sum of exergy of exhaust gases and exergy difference between outlet and inlet streams of the cooling water of the SHIFT-TOT, $\dot{E}_{L,tot} = \dot{E}_{44} + \left(\dot{E}_{73} - \dot{E}_{71}\right)$.

The exergetic efficiency of the overall SMR system is

$$\varepsilon = \frac{\dot{E}_{P,tot}}{\dot{E}_{F,tot}} = \frac{\dot{E}_{53}}{\left(\dot{E}_{11} + \dot{E}_{21} + \dot{E}_{61} + \dot{E}_{25} + \dot{W}_{COMP} + \dot{W}_{PUMP} + \dot{W}_{H2-SEP}\right)} \quad (3)$$

The exergetic efficiency of the overall SMR plant is 67%. The data obtained from the conventional exergetic analysis of the SMR system (Table 2) show that the combustion chamber has the highest exergy destruction value followed by the hydrogen separation unit, the reformer and some heat exchangers. The exergy destruction is mainly due to the chemical reaction that takes place in the combustion chamber.

Table 2. Results obtained from the conventional exergetic analysis of the SMR plant ($\dot{E}_{L,tot}$ = 53.08 MW).

Component	$\dot{E}_{F,k}$ (MW)	$\dot{E}_{P,k}$ (MW)	$\dot{E}_{D,k}$ (MW)	y_k (%)	ε_k (%)
COMBRET	424.30	290.60	133.70	14.25	68.49
H2-SEP	41.56	11.42	30.14	3.21	27.48
REFORM	153.80	118.10	35.70	3.81	76.78
HT-SHIFT	9.39	8.67	0.72	0.08	92.33
HX-SHIFT	13.12	5.80	7.32	0.78	44.20
LT-SHIFT	63.43	59.69	3.73	0.40	94.11
HX-A	52.35	39.61	12.74	1.36	75.66
HX-B	44.69	26.19	18.50	1.97	58.60
HX-C	34.68	24.47	10.21	1.09	70.55
HX-CH4	4.66	4.54	0.12	0.01	97.43
COMP	8.70	7.95	0.75	0.08	91.31
PUMP	0.06	0.05	0.01	<0.01	90.78
Overall system	**937.90**	**631.20**	**253.60**	**27.04**	**67.30**

4. Advanced exergetic analysis

The conventional exergetic analysis, however, does not provide any information with respect to (a) the potential for improving the overall system and the single components, and (b) the interactions among the components. To answer these questions, the advanced exergetic analysis was developed.

The real thermodynamic inefficiencies in an energy conversion system are related to exergy destruction and exergy loss. Exergy destruction is caused by effects such as chemical reactions, heat transfer through a finite temperature difference, mixing of matter of different compositions or states, unrestrained expansion and friction. At any given state of technological development, some exergy destruction within a system component will always be unavoidable due to physical and economical constraints [9-12]. For this reason, the development of an advanced exergetic analysis for evaluating chemical process where the unavoidable and avoidable parts of the exergy destruction are calculated, can be of value for improving the overall system performance.

The methodology for splitting the exergy destruction into unavoidable/avoidable parts is presented in [9-14]. An approach for estimating the avoidable part of the exergy destruction associated with each system component of a SMR system is already discussed in detail [3, 13]. Table 3 shows the parameters used for calculating the unavoidable exergy destruction within components of the SMR system. The values of $\dot{E}_{D,k}^{UN}$ and $\dot{E}_{D,k}^{AV}$ are given in Table 4.

The interactions among different components of the same system can be estimated and the quality of the conclusions obtained from an exergetic analysis can be improved, when the exergy destruction in each (important) system component is split into endogenous/exogenous parts. The methodology for splitting the exergy destruction into endogenous/exogenous parts can be found in [11, 12, 14, and 15]. An approach for estimating the endogenous part of the exergy destruction associated with each system component of a SMR system is discussed in this paper for the first time.

For splitting the exergy destruction into endogenous and exogenous parts, we need to define the so-called *theoretical operation conditions* for each component. Using the theoretical operating conditions, we can achieve:

- For pumps and compressors, $\dot{E}_{D,k}^{T} = 0$;
- For heat exchangers, the only possible condition is $\dot{E}_{D,k}^{T} = min$, with $\Delta T^{T} = 0$;
- For components where a chemical reaction occurs (SHIFTs, REFORM and CC), the condition $\dot{E}_{D,k}^{T} = 0$ ($\varepsilon_k^T = 1$) can be achieved only through fulfilling the exergy balance for the component ($\dot{E}_{F,k}^{T} = \dot{E}_{P,k}^{T}$), and by ignoring the mass and the energy balances [15].

The so-called *hybrid processes* (only one component is real, i.e. operates with its real efficiency, while all other components operate in a theoretical way) are employed to split the exergy destruction into endogenous and exogenous parts. In a hybrid process, the exergy destruction within the component being considered represents the endogenous exergy destruction for this component. The step-by-step introduction of irreversibilities in each system component enables us to calculate the endogenous exergy destruction within each component [11, 12, and 15].

The thermodynamic data for the theoretical and the hybrid operating conditions are given in Table 3. Note that

- the HX-A does not exist for the theoretical and, therefore, hybrid operation conditions, because $T_{14}^{T} > T_{43}^{T}$. For the reformer, $T_{14}^{T} = T_{15}^{T}$ and $T_{14}^{H} = T_{15}^{H}$,
- the assumption $\varepsilon_k^H = \varepsilon_k^R$ is used for the hybrid operation conditions for the HT-SHIFT, LT-SHIFT, REFORM and CC, and
- the chemical composition of the syngas and also the chemical conversion for the theoretical and the hybrid operation conditions remain the same as for the real operation conditions.

The values of $\dot{E}_{D,k}^{EN}$ and $\dot{E}_{D,k}^{EX}$ are given in Table 4.

By combining the two concepts of splitting the exergy destruction, we obtain

- the unavoidable endogenous part of the exergy destruction ($\dot{E}_{D,k}^{UN,EN}$), which cannot be reduced because of technical limitations for the k th component,
- the unavoidable exogenous part of the exergy destruction ($\dot{E}_{D,k}^{UN,EX}$) that cannot be reduced because of technical limitations in the remaining components of the overall system for the given structure,
- the avoidable endogenous part of the exergy destruction ($\dot{E}_{D,k}^{AV,EN}$), which can be reduced by improving the efficiency of the k th component, and finally
- the avoidable exogenous part of the exergy destruction ($\dot{E}_{D,k}^{AV,EX}$) that can be reduced by improving the efficiency of the remaining components and of course by improving the efficiency in the k th component.

The methodology for splitting the exergy destruction into the above mentioned parts has been discussed in detail in [11, 12, 14, and 15]. The values of the four above mentioned parts of the exergy destruction within components of the SMR system are given in Table 4.

For the compressor, pump, HX-A, HX-CH4 and hydrogen separator, the concept of splitting the exergy destruction into endogenous/exogenous parts is not applied because of the followings:

- Small values of the total and the unavoidable part of the exergy destruction within compressor,

Table 3. Key design parameters at design-point (real operation conditions), and for calculating the unavoidable and the endogenous exergy destructions.

Component	Parameter, unit	Design-point	To calculate the unavoidable exergy destruction		To calculate the endogenous exergy destruction		
			Unavoidable thermodynamic inefficiency	$\left(\frac{\dot{E}_D}{\dot{E}_P}\right)_k^{UN}$	Theoretical conditions	Hybrid conditions	$\dot{E}_{P,k}^{EN}$
COMP	η_s (-)	0.85	0.93	0.0445	1.0	0.85	7.560
PUMP	η_s (-)	0.85	0.93	0.0755	1.0	0.85	0.048
HX-A	ΔT (K)	25*)	15*)	0.0412	–	–	–
HX-B	ΔT (K)	25*)	15*)	0.0626	$T_{14}^T = T_{31}^R$	$T_{14}^H = T_{15}^H = T_{15}^R$	39.130
HX-C	ΔT (K)	25*)	15*)	0.0145	$T_{36}^T = T_{42}^T$	$T_{36}^H = T_{36}^R$	22.990
HX-CH4	ΔT (K)	25*)	15*)	0.0218	$T_{23}^T = T_{52}^T$	$T_{23}^H = T_{15}^H$	21.320
HT-SHIFT	T (°C)	350	300	0.0807	$T_{32}^T = T_{32}^R$ $T_{33}^T = T_{33}^R$	$T_{32}^H = T_{32}^R$ $T_{33}^H = T_{33}^R$	7.348
	χ (mol %)				$\chi_{33}^T = \chi_{33}^R$	$\chi_{33}^H = \chi_{33}^R$	
HX-SHIFT	ΔT (K)	25*)	15*)	0.2057	$T_{13}^T = T_{34}^T$	$T_{13}^H = T_{13}^R$	4.905
LT-SHIFT	T (°C)	200	150	0.0620	$T_{34}^T = T_{34}^R$ $T_{35}^T = T_{35}^R$	$T_{34}^H = T_{34}^R$ $T_{35}^H = T_{35}^R$	68.255
	χ (mol %)				$\chi_{35}^T = \chi_{35}^R$	$\chi_{35}^H = \chi_{35}^R$	
REFORM	Mixer	Base case	Isothermal Isobaric	0.2703	$T_{31}^T = T_{31}^R$ $T_{23}^T = T_{15}^T$ (to avoid irreversibilities within mixing) $T_{41}^T = T_{41}^R$ $T_{42}^T = T_{31}^T$ (for ΔT_{min}=0 in HX-SHIFT) $\chi_{31}^T = \chi_{31}^R$ CH_4 conversion = 1	$T_{31}^T = T_{31}^R$ $T_{41}^T = T_{41}^R$ $\chi_{31}^H = \chi_{31}^R$	114.599
	$\dot{m}_{41}$ (kg/s)	220.3	350				
	T_{41} (°C)	1340	1340				
	T_{31} (°C)	700	800				
	S/M (-)	3.2	3.2				
	CH_4 conversion	0.8323	0.9073				
H2-SEP	H_2 Separation efficiency (%)	90	99	0.5847	Separation efficiency 100 % $\dot{m}_{52}^T = \chi_{H2,36}^T \cdot \dot{m}_{36}^T$	Separation efficiency 90 % $\chi_{52}^H = \chi_{52}^R$	18.496
	$\dot{W}_{H2-SEP}$ (MW)	4.79	6.00				
COMBRET	Air excess (%)	20	5	0.3420	$\frac{\dot{m}_{air}}{\dot{m}_{fuel}} = real$ $\dot{m}_{25}^T = 0$ $\chi_{41}^T = \chi_{41}^R$	$\frac{\dot{m}_{air}}{\dot{m}_{fuel}} = real$ $\dot{m}_{25}^T = 0$ $\chi_{41}^H = \chi_{41}^R$	286.390
	T_{41} (°C)	1341	1460				
	Heat duty (MW)	12500	0				

*) ΔT refers to the average thermodynamic temperature within a heat exchanger.

pump and HX-CH4 demonstrate that the SMR system cannot be significant improved through decreasing irreversibilities within these three component.

- HX-A does not exist when the SMR system is simulated at theoretical operation conditions.
- Hydrogen separator is simulated as a "black box" according to information obtained from [4]. At least three processes take place within this component (Figure 1). In this way, the exergy destruction should be spit into endogenous/ exogenous part for each sub-components of the H2-SEP.

5. Results and discussions

For all components we have $\dot{E}_{D,k}^{EN} > \dot{E}_{D,k}^{EX}$, which shows that the interconnections among the components of the SMR system are not very strong. In addition, we have $\dot{E}_{D,k}^{UN} > \dot{E}_{D,k}^{AV}$ for COMPRET, REFORM, HT-SHIFT and LT-SHIFT, i.e. there is not a large potential for improving these components, because the irreversibilities within these components are caused by chemical reactions. For heat exchangers on the other side we obtain $\dot{E}_{D,k}^{UN} < \dot{E}_{D,k}^{AV}$. These components can be improved by decreasing the temperature difference within them.

The conclusions about the improvement of the components based on the value of $\dot{E}_{D,k}^{AV,EN}$ are as follows: The SMR process can be improved by improving the combustions chamber (highest priority), and three heat exchangers (HX-B, HX-SHIFT, and HX-A).

6. Conclusions

In this study a SRM process has been analyzed by means of an advanced exergetic method for chemical process. This analysis is based on previous methods applied to thermal systems, in which no chemical reactions take place, and is able to identify the endogenous/exogenous and unavoidable/avoidable exergy destruction of each component pointing out the components with the highest improvement potentials.

When chemical reactions are present in an energy conversion process, the definition of the best operating conditions should take into account not only the most favorable thermodynamic conditions to drive the chemical reaction (such as temperature, pressure or reactant concentrations) but also possible catalyst deactivation, coke deposition and other factors that decrease the total conversion and consequently the exergetic efficiency of this type of components.

The data provided by the advanced exergetic analysis will be used in advanced exergoeconomic and exergoenvironmental analyses, in order to determine the avoidable costs and environmental impact and the best way to improve the overall SMR system performance from the economic and ecological viewpoints.

Table 4. Splitting the exergy destruction within the k th component of the SMR system.

Component	$\dot{E}_{D,k}^{EN}$ [MW]	$\dot{E}_{D,k}^{EX}$ [MW]	$\dot{E}_{D,k}^{UN}$ [MW]	$\dot{E}_{D,k}^{AV}$ [MW]	Splitting $\dot{E}_{D,k}^{real}$ [MW]			
					$\dot{E}_{D,k}^{UN}$ [MW]		$\dot{E}_{D,k}^{AV}$ [MW]	
					$\dot{E}_{D,k}^{UN,EN}$	$\dot{E}_{D,k}^{UN,EX}$	$\dot{E}_{D,k}^{AV,EN}$	$\dot{E}_{D,k}^{AV,EX}$
COMBRET	131.76	1.94	99.38	34.32	97.94	1.44	33.82	0.50
H_2 SEP	–	–	6.68	23.46	–	–	–	–
REFORM	34.66	1.04	31.92	3.78	30.96	0.96	3.70	0.08
HT-SHIFT	0.61	0.11	0.70	0.02	0.59	0.11	0.02	0
HX-SHIFT	7.11	0.21	1.19	6.13	1.01	0.18	6.10	0.03
LT-SHIFT	4.27	-0.54	3.70	0.03	4.23	-0.53	0.04	0.01
HX-A	–	–	1.63	11.11	–	–	–	–
HX-B	17.22	1.28	1.64	16.86	2.45	-0.81	14.77	2.09
HX-C	7.25	2.96	0.35	9.86	0.33	0.02	6.92	2.94
HX-CH_4	–	–	0.10	0.02	–	–	–	–
COMP	–	–	0.35	0.40	–	–	–	–
PUMP	–	–	0.004	0.006	–	–	–	–

Acknowledgement

The authors wish to thank the European Union for the financial support within the Framework of the INSPIRE Network (MRTN CT-2005-019296 - INSPIRE). A. Boyano is indebted to TU-Berlin and the Institute for Energy Engineering for her post-doctoral position.

Nomenclature

$\dot{E}$	exergy rate [W]
j	j th stream
k	k th component [-]
m	mass [kg]
p	pressure [Pa]
$\dot{Q}$	heat (W)
T	temperature [K]
$\dot{W}$	power (W)
y	exergy destruction ratio [%]

Greek symbols

ε	exergetic efficiency [%]
η	isentropic efficiency [-]
χ	molar concentration [%]

Subscripts

D	refers to exergy destruction
F	fuel
P	product
tot	refers to the total system

Superscripts

AV	avoidable
CH	chemical exergy
EN	endogenous
EX	exogenous
PH	physical exergy
UN	unavoidable

Supercripts

CO	refers to CO mass fraction in a mixture
CO_2	refers to CO_2 mass fraction in a mixture
CH_4	refers to CH_4 mass fraction in a mixture
CH	chemical
H_2O	refers to H_2O mass fraction in a mixture
H_2	refers to H_2 mass fraction in a mixture
H	hybrid conditions
PH	physical
R	real conditions
T	theoretical conditions

Subscripts

D	exergy destruction
F	exergy of fuel
j	j th stream
k	k th component
P	exergy of product
0	reference state

Abbreviations

COMBRET	combustion chamber using retenate stream and methane as fuel
COMP	compressor
HT-SHIFT	high-temperature water-gas-shift reactor
HX	heat exchanger
H2-SEP	hydrogen separation unit
LT-SHIFT	low-temperature water-gas-shift reactor
MIXER	mixer
PUMP	pump
REFORM	reformer
SEP	separator
SMR	steam methane reforming
TV	throttling valve

References

[1] Rosen M.A., 1991, Thermodynamic investigation of hydrogen production by steam-methane reformation. *Int J Hydrogen Energy*, Vol. 16, No.3, pp. 207-217.

[2] Yang Y.C., Lee B.J., Chun Y.N., 2009, Characteristics of methane reforming using gliding arc reactor *Energy – The International Journal,* Vol. 34, pp. 172-177.

[3] Boyano A., Blanco-Marigorta A.M., Morosuk T., Tsatsaronis G., 2010, Exergoenvironmental analysis of a steam methane reforming process for hydrogen production. Submitted to *Energy – The International Journal*.

[4] Simpson A.P., Lutz A.E., 2007, Exergy analysis of hydrogen production via steam methane reforming, *Int. J. Hydrogen Energy*, Vol. 32, pp. 4811-4820.

[5] *Aspen Plus*, 2007, User Guide- Vol. 1 and 2-Release x.

[6] Twigg M.V., ed., 1989, *Catalyst handbook*, 2nd Edition, Wolfe Publishing Ltd.

[7] Bejan A., Tsatsaronis G., Moran M., 1996, *Thermal design and optimization*, John Wiley and Sons, USA.

[8] Tsatsaronis G., Cziesla F., 2002, *Thermoeconomics*. In: Enclyclopedia of Physical Science and Technology, 3rd ed. Academic Press, Vol. 16, pp. 659-680.

[9] Tsatsaronis G., Park M.H., 2002, On avoidable and unavoidable exergy destructions and investment costs in thermal systems, *Energy Conversion and Management*, Vol. 43, pp.1259–1270.

[10] Cziesla F., Tsatsaronis G., Gao Z., 2006, Avoidable thermodynamic inefficiencies and costs in an externally fired combined cycle power plant, *Energy Int. J.*, Vol. 31, Nos.10–11, pp. 1472–1489.

[11] Tsatsaronis G., Morosuk T., 2008, A general exergy-based method for combining a cost analysis with an environmental impact analysis. Part I. *Proceedings of the ASME International Mechanical Engineering Congress and Exposition,* Boston, USA, 2008, files IMECE2008-67218.

[12] Tsatsaronis G., Morosuk T., 2008, A general exergy-based method for combining a cost analysis with an environmental impact analysis. Part II. *Proceedings of the ASME International Mechanical Engineering Congress and Exposition*, Boston, USA, 2008, files IMECE2008-67219.

[13] Boyano A., Tsatsaronis G., Morosuk T., Blanco-Marigorta A.M., 2009, Advanced exergetic analysis of chemical processes, *Proceedings of the ASME International Mechanical Engineering Congress and Exposition*, Lake Buena Vista, USA, Paper IMECE2009-10463.

[14] Morosuk T., Tsatsaronis G., Naw R., Omar M.N.B., 2010, Advanced Exergetic Analysis of a Refrigeration System for Liquefaction of Natural Gas. *Paper submitted to the ECOS-2010*.

[15] Morosuk T., Tsatsaronis G., 2009, Advanced Exergy Analysis for Chemically Reacting Systems – Application to a Simple Open Gas-Turbine System, *Int. J. of Thermodynamics*, Vol. 12, No. 3, pp. 105-111.

Environmental Assessment of Power Systems: Integrating LCA and Operational Requirements

Ruben Ramalho[a] and Tiago Domingos[a]

[a] Environment and Energy Section, DEM, and IN+, Center for Innovation, Technology and Policy Research, Instituto Superior Técnico, Lisboa, Portugal

Abstract: The environmental superiority of electricity generation technologies/systems over competing options is preferentially determined through the use of the life-cycle assessment (LCA) methodology. In this paper, the LCA approaches commonly used are challenged and a new one is proposed. Currently, most LCA approaches do not consider operational *reliability* and the essential requirements for power systems to attain it (e.g. ancillary services) thus neglecting the intrinsic differences between generation technologies' operational features. The approach proposed here focuses on how *reliability* requirements should be properly taken into account in the LCA methodology to ensure a fair and realistic comparison between each generation technology, and how the inclusion of the former influences the environmental merit of the latter. An example is presented for wind power implementation in the Portuguese power system (addressing the greenhouse gas (GHG) emissions), considering its operational problems of generation unpredictability and inflexibility to meet load variations. Several possible scenarios were considered to face these problems, namely wind backed up by pumping hydro, batteries and gas-fired power plants. The obtained results ranged between 46% to 9 times higher than literature LCA values, confirming that the inclusion of reliability requirements leads to significant changes in the final LCA results.

Keywords: Environmental assessment, Generation technologies, Life-cycle assessment, Operational requirements, Power systems, Wind power.

1. Introduction

Life cycle assessment (LCA) is an officially recognized and standardized tool to support decisions based on environmental criteria [1,2] that has been widely applied to electricity generation technologies over the past few years. The comparative analysis of power generation systems can be essentially focused on three different perspectives corresponding to different functional units (FUs): installed capacity (kW), electrical energy produced (kWh), and provision of a specific energy service (e.g. load balancing). On the one hand, comparisons based on the installed capacity are common but often stated to be inappropriate due to the natural discrepancies between the availability and capacity factors of each technology [3]. On the other hand, studies based on energy services are extremely rare, possibly due to notion that the FU should reflect the direct service itself that is provided to consumers, and not the means to achieve it. Finally, the kWh is presented as the best base for comparisons [3] and thus it is the FU overwhelmingly privileged in the literature. Notwithstanding this, one should remark that this prevailing *status-quo* does not necessarily take into consideration the concept of *reliability* of electricity supply and the full complex requirements needed to ensure it (e.g. ancillary services). In fact, most existing LCA studies are carried out by comparing directly generation technologies without imposing any constraints on them, therefore neglecting their different technical features to respond single-handed to all power system essential requirements. Generation technologies are not necessarily true operational replacements, and thus, such an assumption leads to unfair and unrealistic comparisons that can provide inaccurate results to decision makers. Moreover, it should be also highlighted that the FU of any LCA study must be by definition based on the consumers' standard requirements for the quality of the service that is being assessed [1,2]. To be completely accurate, the final consumers' actual requirement is more than a "general kWh" from the electricity sector: they require a reliable kWh, when demanded, to ensure their comfort at every time. Currently, one can find a general trend

Ruben Ramalho, ruben.s.ramalho@ist.utl.pt

in the results for most of conducted LCAs with such approach, which is clearly in favour of renewable energy technologies [4]. However, it must be determined if neglecting *reliability* leads to significant changes in the final environmental merit of electricity generation technologies, and, if so, by how much.

This shortcoming has been pointed out a small number of times throughout the literature [3], although without its proper importance or at least without exploring its relevance to an extent worth mentioning. The very few efforts that have been made to overcome it led to simplistic approaches that provide, in the best case scenario, scarce and limited assessments. For instance, [5] solved it by simply excluding from analysis any generation technology that is not capable of responding to short-term variations in demand by itself. Other studies have opted to group technologies according to their short-term flexibility (e.g. inflexible technologies serve exclusively for the base load) and establish the comparisons only within the group's competing options. One should note that both methodological approaches falsely narrow down the comparison possibilities because they do not consider all the technical solutions (including future ones) to deal with the operational differences between generation technologies. Yet, another approach has been suggested by [3] and more recently by [6]: rather than compare each technology by itself, a set of additional equipment should be included in the original generation technology so that it could actually fulfill the requirements to allow a fair and more realistic comparison between competing alternatives. However, the authors did not specify which requirements should be considered, neither what equipment needs to be included (other than batteries for load-balancing). Moreover, they do not provide any suggestion on how to determine them either.

Most recently, [7] highlighted the potential that has remained undiscovered regarding the interaction between LCA and several other fields of scientific research. Yet, it is now clear that another potential synergy remains to be properly explored: the integration of power systems reliability assessment tools to determine what requirements and resulting backup equipment must be included. This paper intends to provide a significant contribution to explore it, first, by analyzing what operational variables should be taken into account, second, by designing a possible approach to deal with it and finally by presenting a small case-study. The case study focused on the load-balancing issues regarding the wind power technology in the Portuguese power system (PPS), considering greenhouse gas (GHG) emissions.

2. Proposed Approach

2.1. *Reliability* - A criterion for rigorous comparisons

Considering what was previously mentioned, we propose the *reliable kWh* as a rigorous FU for LCA studies that are intended to support power system planning decisions. However, reliability is a rather complex concept and its inclusion into the FU demands profound changes in the current LCA approaches for electricity generation technologies.

According to [8,9] reliability encompasses two attributes of the power system (Fig. 1.): (i) (generation) Adequacy, which represents its ability to meet the aggregate power and energy requirements of consumers in all regions at all times; and (ii) (operational) Security, which describes the power system's ability to withstand disturbances (contingencies) such as accidental electric short circuits, unanticipated losses of system components and critical load conditions.

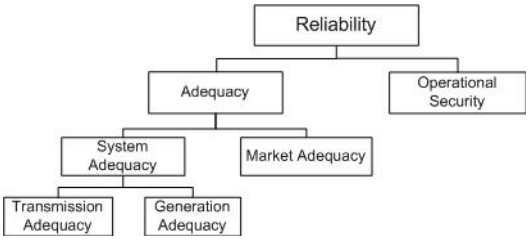

Fig. 1. Schematic of reliability attributes [9].

The notion of adequacy includes simultaneously the correct dimensioning of the physical system itself and a proper electricity market structure in force to explore it. It is primarily concerned with active load balancing dynamics to meet demand's daily and seasonal variations, and comprises both the generation technologies and the transmission/distribution equipment. Generation adequacy is traditionally measured in terms of the operational reserves' availability throughout the year and can be verified by specific adequacy indicators. The notion of security, in contrast, is more related to complex operational aspects, or more specifically to some ancillary services such

as controlling frequency and voltage values within the required ranges in all situations. Security is typically characterized through contingency analysis and dynamic stability assessments and is provided by means of protection devices and operation standards and procedures [9]. Preferentially, both adequacy and operational security should be verified. So, instead of comparing directly every generation technology, we propose to integrate backup equipment in those technologies that are not capable of providing the full operational requirements (adequacy and security) by themselves. The resulting combination (hereafter designated as *Operational Technology System*, OTS) must ensure the same reliability as other "stand-alone" systems (e.g., gas-fired thermal power plants). The OTS comprises the three following main components:

I. *Main Technology*, which is the technology intended to be implemented, regardless of its ability to meet by itself the full operation requirements;

II. *Regulation Technologies*, composed by the additional backup technologies to meet all major operational requirements for the secure/reliable use of the implemented technology - ensuring generation adequacy and operational security. The major operational requirements that should ideally be verified by the OTS to ensure adequacy and security can be easily identified in the power system operation literature, namely in [8] and [9], as well as in every operation procedure handbook of worldwide system operators (SOs):
   - Controllable generation, i.e., the ability to provide energy flexibly to satisfy minute-to-minute demand needs (a.k.a *dispatchable*).
   - Operating reserve, i.e., the ability to immediately correct unforeseen load imbalances. It must include reserve capacity to increase and decrease.
   - Black-start capability, i.e., the ability to recover from grid shocks and blackouts within acceptable time and without assistance from the electrical grid.
   - Voltage and frequency control, i.e., to supply the generated energy within the range of values required by the grid.

III. *Transmission capacity*, i.e. equipment (substations, transformers, lines, underground cables, etc.) strictly imposed by the implementation of the main technology - ensuring transmission adequacy.

It is worth mentioning that, as far as we know, LCA studies have never considered or even mentioned the different transmission and distribution requirements of each technology. This assumption, sometimes avoided by using the kWh measured at the entrance to the grid, is for evident reasons wrongfully taken in some cases. For instance, wind farms installed in remote places require a completely different amount and type of transmission equipment than microgeneration PV's installed in the urban distribution grid. The boundaries to be considered for the FU, i.e. the physical point of where the *reliable kWh* will be measured, must be at the consumers' plug.

2.2. The need to assess the complete power system

The design of an OTS for every single generation technology that provides a complete and equivalent operational capability may not be feasible due to unavoidable technical limitations to correct all its intrinsic reliability gaps. In fact, all generation facilities depend on one another, whether they are "must-run" systems like nuclear energy, intermittent renewable technologies or reliable thermal power plants, because they all are at least subject to unforeseen problems, and thus they all rely on the remaining facilities available in the power system to keep ensuring the supply. Furthermore, the power system in which the *main technology* with operational gaps is to be implemented might still have enough backup technologies so that its introduction does not necessarily impose the increase of new backup capacity, but only increases its use. If every main technology has its own *regulation technology* and *transmission equipment* dimensioned to deal specifically with its gaps, the final outcome would certainly lead to redundancy of the regulation and transmission capacities of the resulting power system. So, rather than try to assemble OTSs that fulfill single-handedly all the reliability requirements by themselves, it is the entire power system's structural changes induced by the implementation of the main technology that should be compared. Backup technologies should be determined by the extra amount demanded by the comparative power system scenarios that each main technology leads to. As a result, regulation

technologies and other backup equipment are determined specifically for each power system's unique conditions, and depend on the total amount of the main technology that will be installed.

The dispatch model in force (which depends on the existing market structure and economic competiveness of the remaining generation technologies) plays here a very important role.

To make a fair comparison between the alternative main technologies, it must be imposed that the comparison between their resulting power systems must have an approximately equivalent reliability throughout the year, measured by standard adequacy/security indicators, namely the Coverage Index, Remaining Capacity and Adequacy Reference Margin.

3. Case study: wind power

3.1. Main technology

Wind power technology is a perfect example to highlight the concerns around the reliability issue, since due to its very own operational gaps and high penetration in worldwide power systems over the past years, has become one of the most cited and studied subject among developers, network planners and system operators (SOs) [10,11,14,15,16]. The following case study applies the proposed LCA approach to the large scale implementation of wind power in the Portuguese Power System (PPS) in the next years, to reach a total capacity of 3750 MW by 2010 and 5100 MW in 2013 according to current government goals. To determine the operational constraints and feasible solutions for the *Regulation technologies* and *Transmission capacity,* several studies were gathered.

3.2. Regulation technologies

3.2.1. Controllable generation and operating reserve

Wind power is an intermittent generation source driven by weather conditions and thus with unpredictable behaviour both for generation timing and output power. To deal with it the SO currently relies on short-term weather forecasts. However, this forecast is never a certainty and forecast errors will occur. The average error with existing forecast tools for a single wind farm is between 10% and 20% of the installed wind power capacity for a forecast horizon of 36 hours. In the best case scenario considering smoothing effects, scaling up to aggregated wind power of a whole area can result in a drop of the error below 10% [16].

In Portugal, the maximum unforeseen loss of wind power has already reached the equivalent value of the largest conventional thermal group (400 MW). Moreover, [12] estimated the PPS's imbalances for 2010 and 2015 and stated that the large scale implementation of wind power sources is potentially more problematic in the case of power surges, since to maximize the use of renewable production it may be necessary to remove thermal groups from the grid if all regulation reserve to decrease (including storage capacity) runs out. In many simulations, there was a reduction of the primary reserve and an increase of the probability of failure in starting the shut down groups. In this way, balance difficulties will become more common and achieve higher values, particularly for positive imbalances. These numbers stress the importance of adequate backup balancing capacity to support wind power, especially if the current EU directive [13] remains in force, imposing that all energy produced by renewable sources must be privileged by the SO.

Numerous technologies can be used to deal with such balancing needs: the first and privileged option to perform these tasks is to resort to flexible pumping hydro technology (PHS) with considerable storage capacity because it can potentially face single-handedly both positive and negative imbalances [14-16]. If not possible, gas-fired thermal units with advantageous start-up and shutdown characteristics are a logical way of balancing intermittent generation [16]. However, hydro capacity is limited by geophysical reasons, and thermal facilities might face serious problems in handling large positive imbalances, therefore other large scale storage technologies are also taking their first steps in becoming serious balancing options with particular relevance to positive imbalances. Redox flow batteries (namely vanadium redox batteries [VRB] and Polysulphide Bromide Batteries) and compressed air energy storage [CAES] are currently the frontline options for energy management. However, CAES systems require caverns with very particular geophysical features and thus are limited by existing natural availability [17]. Redox flow batteries are then the main contender. Moreover, several authors have in fact emphasized that this is most likely the best alternative to pair with wind power technology both for load balancing and economic criteria, and

in particular for Portugal; [18] pointed them out (specifically VRB) as the most profitable option for wind park investors.

One can find other possible approaches to face wind power intermittency. For instance [11] proposed a solution relying on the installation of generation dispatch centres (acting as generation aggregation agents) and the adoption of a hierarchical control architecture which, through the combination of wind parks with excess capacity with an optimized grid connection, could significantly decrease imbalance problems. However, such unconventional approaches are still under trial and have not yet proved their full capability.

3.2.2. Voltage and frequency control and black-start capability

Besides being a non-controllable generation technology, wind power usually sets other operational problems:

- It does not provide voltage and frequency control – in fact it may have a negative effect due to its intermittency;
- It does not have black-start capability.

For Portugal the need for these requirements was also verified [10] according to a study carried to assess the connection of the programmed wind power capacity to the PPS during 2010-2013: wind power must be mandatorily equipped in the future with additional control equipment (such as flexible AC transmission systems devices) to have *ride-through fault capability* and it must also start contributing to voltage and frequency control by request of the SO. Two possible solutions can be used to solve this last gap: by integrating specific technical components in the wind parks or by resorting to the remaining generation technologies thus imposing their increase as well.

3.3. Transmission capacity

According to [10], in the existing plan to achieve the capacity goals for 2010 and 2013, most of renewable (wind and hydro) will be located in remote places and scattered throughout large areas with very small demand. In order for the local power surplus to be transported to large consumption centres, additional transmission capacity is identified, namely: new underground-cables and inner network inside the wind parks, new 400 and 220 kV lines, new 400 and 220 kV substations and new phase-shifter transformers. Therefore, a very significant amount of additional transmission equipment must be implemented to allow wind technology integration. Nonetheless, the total amount that is indeed strictly induced by wind was impossible to determine.

3.4. General composition of the OTS

The resulting OTS that would derive from the implementation of wind power should ideally be composed by:

Table 1. Possible OTS components for wind power.

Main technology	2 MW Wind Turbines	
Regulation technologies	Controllable generation and Operating Reserves	- PHS - VRB - Thermal spinning reserves
	Black-start capability and voltage and frequency control	- Direct control devices - Backed up by other operating reserves
Transmission capacity	- Phase shifter transformers - Additional transmission lines (…).	

The quantification of certain backup components proved to be difficult. Thus, due to lack of data and for simplifying purposes, the only component considered for the calculations in the exemplifying OTSs are related to load balancing problems, i.e., ensure a controllable generation and guarantee operational reserves both for positive and negative imbalances.

3.5. Scenarios

3.5.1. Imbalance scenarios

Considering the mentioned future imbalance problems where positive imbalances are prominent, the OTSs were developed to face the following imbalance scenarios.

- Negative imbalances

The negative imbalances considered are related to periods when the real wind power production is lower than what has been previously forecasted. Considering that forecast errors for large wind installed capacity can vary between 10% and 20% as previously mentioned, it was assumed an equal distribution of that error between positive and negative imbalances (unbiased error). Thus, two cases for annual energy shortage during negative imbalances were analyzed: 5% (510 GWh) and 10% (1020 GWh) of total wind annual production, which corresponds to an average of 1.4 GWh/day and 2.8 GWh/day respectively. However, because imbalances are not equally distributed throughout

the days, the maximum shortage was assumed to be ten times bigger than the daily average, i.e. 14 GWh/day for the 5% scenario and 28 GWh/day for the 10% scenario. The maximum instant power drop was considered to be equal to 800 MW - twice the biggest drop already registered in the PPS with around half of the targeted 5100 MW installed capacity.

- Positive imbalances

The positive imbalances are related to periods when wind power generation exceeds the load requirements even after all possible corrective actions were taken by the SO, thus jeopardizing the security/reliability of the PPS. Two scenarios for positive imbalances were assumed: 10% (1020 GWh) and 20% (2040 GWh) of wind annual production. The 10% scenario assumptions are consistent with the PPS imbalance forecast values for the year 2015 considering dispatch intervention [18]. The highest overload induced by wind was assumed to reach 1000 MW and the maximum amount of energy produced during the biggest imbalance, was assumed to be 10 times higher than the daily average – 28 GWh. The 20% scenario of wind annual production intends to represent a critical scenario where the highest overload reached 2000 MW. The maximum amount of energy produced during the biggest imbalance was 55 GWh (also considering a factor of 10 on the daily average).

3.5.2. OTS scenarios

The considered OTS scenarios are as follows:

I. Wind exclusively backed up by PHS

This represents the OTS best case scenario, in which pumping hydro storage (PHS) systems with the adequate features (storage capacity and output power) can solve single-handedly positive and negative imbalances by transferring the energy generated during the void periods to peak periods.

An unconstrained availability of the hydrologic resources regardless of the seasonal variations was assumed. For scenarios where the stored energy is not enough to cover wind generation shortages, it was assumed that the PHS would still have enough available capacity to deal with this.

II. Wind backed up by VRB

This OTS scenario intends to represent the situations in which the positive and negative imbalances can be solved just with VRB systems. Negative imbalances are exclusively resolved through the transfer of energy stored during positive imbalances and therefore this scenario is only a feasible solution to imbalance scenarios where positive imbalances are higher than negative imbalances.

III. Wind backed up by energy storage capacity and thermal spinning reserves

This OTS scenario represents the situations in which the positive imbalances are solved through energy storage systems and the negative imbalances need the help of thermal facilities. This only applies to imbalance scenarios where negative imbalances are larger than or equal to positive imbalances, i.e., when stored energy is not enough to cover wind generation shortages. This scenario is carried out both for PHS and VRB systems, which are dimensioned to meet the maximum power and energy produced during positive imbalance periods. In either case, the environmental impact of their life-cycle accounted for the same reasons previously mentioned.

The thermal technologies considered are gas-fired: the 250 MW open cycle gas turbine (250 GT) and the 400 MW combined cycle gas turbine (400 CCGT) which are according to [19] the best options for the PPS.

IV. Wind exclusively backed up by thermal spinning reserves

This OTS stands for the worst case scenario in which there is no storage capacity and therefore the wind technology shuts down during positive imbalance, leading to the waste of that energy amount. For negative imbalances, the same gas-fired facilities considered previously are called to cover them.

The OTS dimensioning was carried out to meet power and energy capacity requirements for each imbalance scenario considered previously. The power of the OTS was defined with the objective of absorbing/providing the highest instantaneous power imbalances, considering both positive and negative imbalances.

The features of the technologies used are fully described in *Appendix A*. Furthermore, the description of each OTS scenario for every imbalance scenario can be found in the tables presented in *Appendix B*.

4. Results and Discussion

A summary of the results obtained for the life-cycle GHG emissions of each OTS is represented

by the best and worst case scenarios in Fig.2 (the full results are presented in Appendix C).

The first inference to be drawn is that the inclusion of backup technologies to support generation technologies in order for them to behave within acceptable reliability requirements does lead to significant changes in the final LCA results achieved by existing approaches. The obtained results for all the OTSs and imbalance scenarios were considerably different from the literature values for the 2 MW wind turbine LCA, even for wind exclusively backed up by PHS. The difference in life-cycle GHG emission values ranged from a minimum of 5 gCO_{2eq}/kWh (46% of the literature value) for the PHS' OTS, to 88 g CO_{2eq}/kWh (9 times higher than the literature value) for the worst case scenario represented by wind shutdown during positive imbalances, and a 250 MW GT built specifically to cover energy shortages. Furthermore, the obtained results for the assessed OTSs have only included backup technologies for load balance problems, neglecting completely all the other backup technologies mentioned such as induced transmission equipment, "ride-through-fault" capability equipment, and frequency and voltage control devices, whose inclusion is more than likely to accentuate even further the differences between the results from current approaches and the approach proposed here. The obtained results for the assessed case study corroborate the argument that by including the necessary backup equipment into the LCA technology analysis, the information about its environmental superiority over competing options can change, or at least be substantially inaccurate. Choices between generation technologies based on environmental criteria should not fail to take this into account.

Regarding specifically the environmental performance of GHG emissions for the assessed OTSs, it was found that even in the worst case scenario wind technology trend still presents a better performance than the best thermal facility asset (CCGT) and thus no doubts seems to arise from its environmental superiority over thermal technologies, even if not all required regulation technologies were considered. Anyhow, for other environmental impact categories the outcome could be different.

A particular emphasis should be given for the OTS regarding the VRB storage system: the results reveal that besides being an extremely valuable asset for wind power operation, it also presents relatively low GHG emissions during its life-cycle, even in scenarios where a share of negative imbalance needs to be covered with gas-fired thermal technology. Moreover, since its implementation is not dependent on geophysical conditions, providing easy-to-build and flexible storage features, it is a serious alternative to the PHS system if decision-makers' criteria rely on combining operational benefits with good performance in GHG emissions.

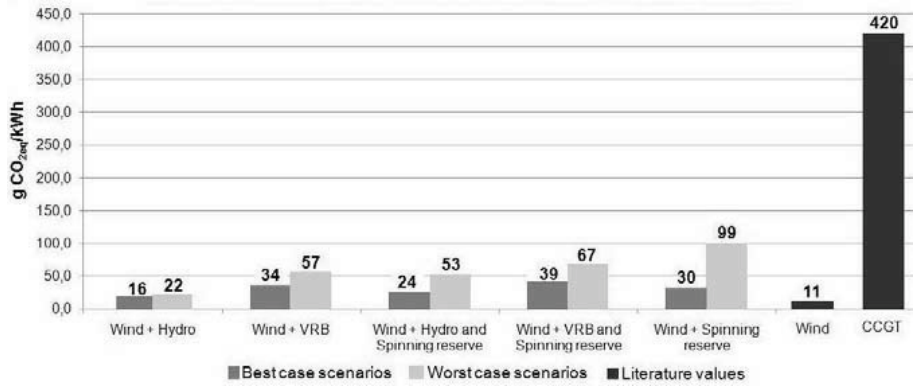

Fig. 2. Life-cycle GHG emissions results for OTSs considering the best and worst case scenario[1]

[1] Best case scenario stands for the lowest imbalance situation solved by resorting to remaining facilities already existing; Worst case scenario represents the situations for the highest load imbalance and that require the construction of additional regulation technologies' capacity).

References

[1] ISO14040, 1997, Environmental Management – Life Cycle Assessment – Principles and Framework, International Organisation for Standardization.

[2] Rebitzer, G., et al., 2004, Life Cycle assessment: part 1: framework, goal and scope definition, inventory analysis, and applications, Environment International Journal, 30(5), pp. 701–20.

[3] Gagnon, L., et al., 2002, Life-cycle Assessment of Electricity Generation Options: The Status of Research in Year 2001, Energy Policy, 30, pp. 1267-1278.

[4] Varun, et al., 2009, LCA of Renewable Energy for Electricity Generation Systems – A Review, Renewable and Sustainable Energy Reviews, 13, pp. 1067-1073.

[5] Weidema, B., et al., 1999, Marginal Production Technologies for Life Cycle Inventories, International Journal of LCA, (4), pp.48-56.

[6] Mathiesen, B., et al., 2009, Uncertainties Related to the Identification of the Marginal Energy Technology in Consequential Life Cycle Assessments, Journal of Cleaner Production, 17, pp. 1331–1338.

[7] Frischknecht, R. and Wolfram, K., 2009, Meeting the NEEDS of European Environmental Sustainability Assessment, ESU-Services Ltd.

[8] UCTE, 2004, UCTE Operation handbook, Union for the Coordination of Transmission of Electricity (UCTE).

[9] Euroelectric, 2004, Security of Electricity Supply - Discussion Paper, Working Group Security of Electricity Supply.

[10] Estanqueiro, A., et al, 2008, How to Prepare a Power System for 15% of Wind Energy Penetration: the Portuguese Case Study, Wind Energy, 11, pp. 75-84.

[11] EWEA, 2005, Large Scale Integration of Wind Energy in the European Power Supply: Analysis, Issues and Recommendations, European Wind Energy Association.

[12] Faias, S., et al, 2007, Forecasting the Impact of Increasing Integration of Renewable Sources in the Power Unbalance During Peak and Off-peak Hours, *International Conference on Power Engineering, Energy and Electrical Drives*.

[13] Directive 2001/77/EC of the European Parliament and of the Council of 27 on the Promotion of Electricity Produced From Renewable Energy Sources in the Internal Electricity Market, European Union Council, 2001.

[14] Milborrow, D., 2004, The Real Cost of Integrating Wind, Windpower Monthly, 20, pp. 35-39.

[15] Leonhardand W. and Grobe E., 2004, Sustainable Electrical Energy Supply With Wind and Pumped Storage – A Realistic Long-term Strategy or Utopia?, *IEEE Power Eng. Soc. General Meeting*, pp.1221–1225.

[16] Luickx, P., et al, 2008, Considerations on the Backup of Wind Power: Operational Backup - A working paper, Kuleuven Energy Institute.

[17] Ibrahim, H., et al, 2007, Energy Storage Systems - Characteristics and Comparisons, Renewable & Sustainable Energy Reviews, 1, pp. 1221–1250.

[18] Faias, S., et al, 2008. Evaluation of Energy Storage Devices for Renewable Energies Integration: Application to a Portuguese Wind Farm, *5th International Conference on the European Electricity Market.*

[19] REN, 2005, Perspectivas de Evolução do Sistema Electroprodutor Português: Período 2006-2025, Technical Report, REN - Rede Eléctrica Nacional, S. A., (in Portuguese).

[20] REN, 2009, REN - Centro de Informação, http://www.centrodeinformacao.ren.pt/PT/InformacaoExploracao/Paginas/DiagramadeProduçãoEólica.aspxx, [Online website].

[21] Martínez, E., et al., 2009, Life Cycle Assessment of a Multi-megawatt Wind Turbine, Renewable Energy, 34, pp. 667-673

[22] Commission of the European Communities, 2007, Energy Sources, Production Costs and Performance of Technologies for Power Generation, Heating and Transport, Second Strategic Energy Review, Brussels.

[23] Denholm, P. and Kulcinski G., 2004, Life Cycle Energy Requirements and Greenhouse Gas Emissions From Large Scale Energy Storage Systems, Energy Conversion & Management, 45, pp. 2153-2172.

Appendix A – Data and general assumptions

Table A.1. Capacity factor of wind power technology in the PPS for the years 2007 and 2008 [20].

Year	*2007*	*2008*
Installed capacity [MW]	2048	2624
Net annual production [GWh]	4012	5694
Net annual production by MW [GW_l/MW]	1.9	2.2
Capacity factor [%]	22	25

Based on these values the capacity factor considered for wind power technology was 23%.

Table A.2. Features of wind power and natural gas thermal facilities considered [19, 21, 22].

Technology	*2 MW Wind Turbine*	*400MW CCGT*	*250MW GT*
MW_{net}	-	392	249
Net efficiency considered [%]	-	58	38
Total annual availability [%] / [GWh/MW]	-	93 / 8.0	96 / 8.4
Annual capacity factor considered [%]	23	85 (Maximum)	85 (Maximum)
Average annual production [GWh] / [GWh/MW]	4 / 2.0	2919 / 7.3	1854 / 7.4
Operation emissions [g CO_{2eq}/kWh]	0	350	530
Total indirect emissions [ton CO_{2eq}]	880	5.108×10^6	5.100×10^6
Expected Life-time (years)	20	25	25

Table A.3. Features of pumping hydro system (PHS) and vanadium redox battery system (VRB) considered [23].

Storage technology system	*PHS*	*VRB*
GHG Emissions of construction and decommissioning stages [ton CO_{2eq}/MWh storage capacity]	35.7	261
Operation & Maintenance emissions [g CO_{2eq}/GWh]	1.8	3.3
Efficiency [%]	78	83
Expected life-time (years)	60	20

Appendix B – Scenarios description

Table B.1. Scenarios description for wind exclusively backed up by PHS (Wind + Hydro).

Imbalance scenarios (% of wind annual production)		*PHS features*		*OTS Net supply (GWh)*	
Positive imbalance	Negative imbalance	Storage capacity (GWh)	Nominal power (MW)	Directly from wind	From PHS
20	10 and 5	55	2000	8160	2040
10	10	28	1000	9180	1020
10	5				785

Table B.2. Scenarios description for wind exclusively backed up by VRB (Wind + VRB).

Imbalance scenarios (% of wind annual production)		*VRB features*		*OTS Net supply (GWh)*	
Positive imbalance	Negative imbalance	Storage capacity (GWh)	Nominal power (MW)	Directly from wind	From VRB
20	10 and 5	55	2000	8160	1693
10	5	28	1000	9180	847

Table B.3. Scenarios description for wind backed up by storage energy systems and thermal reserves (Wind + Hydro and Spinning Reserve or Wind + VRB and Spinning Reserve)

Energy storage technology	*Energy storage features*		*OTS Net supply (GWh)*		
	Storage capacity (GWh)	Nominal power (MW)	Directly from wind	From storage system	From thermal spinning reserve
PHS	28	1000	9180	785	235
VRB				847	173

Table B.4. Scenarios description for wind exclusively backed up by thermal spinning reserves.

Imbalance scenarios (% of wind annual production)		*OTS Net supply (GWh)*		*Energy loss due to positive imbalance (GWh)*
Positive imbalance	Negative imbalance	Directly from wind	From thermal spinning reserve	
20	10	9180	1020	2040
	5		510	
10	10	8160	1020	1020
	5		510	

Appendix C – Results for all scenarios

Table C.1. Life-cycle GHG emissions for wind backed up by PHS for all imbalance scenarios.

Positive imbalance (% of wind annual production)	*Negative imbalance (% of wind annual production)*	*Life-cycle GHG emissions (gCO_{2eq}/kWh)*
20	10 and 5	22
10	10 and 5	16

Table C.2. Life-cycle GHG emissions for wind backed up by VRB for all imbalance scenarios.

Positive imbalance (% of wind annual production)	*Negative imbalance (% of wind annual production)*	*Life-cycle GHG emissions (gCO_{2eq}/kWh)*
20	10 and 5	57
10	5	34

Table C.3. Life-cycle GHG emissions for wind backed up by storage systems and thermal facilities for 10% positive imbalance and 10% negative imbalance scenario – i.e. the imbalance scenarios where the stored energy is not enough to cover wind generation shortages.

Backup storage technology	*Backup thermal technology*	*Construction of dedicated thermal facility*	*Life-cycle GHG emissions (gCO_{2eq}/kWh)*
PHS	400MW CCGT 250MW GT	x	24 28
	400MW CCGT 250MW GT	✓	49 53
VRB	400MW CCGT 250MW GT	x	39 42
	400MW CCGT 250MW GT	✓	64 67

Table C.4. Life-cycle GHG emissions for wind backed up by storage systems and thermal facilities for all imbalance scenarios.

Positive imbalance (%)	*Negative imbalance (%)*	*Construction of dedicated thermal facility*	*Life-cycle GHG emissions (gCO_{2eq}/kWh)*	
			400MW CCGT	250MW GT
20	10	x ✓	51 79	71 99
	5	x ✓	34 63	44 74
10	10	x ✓	46 71	64 89
	5	x ✓	30 56	40 66

A Comparative Sustainability Assessment of Combined Heat and Electricity Supply by Cogeneration and Heat Pump Systems for Switzerland

Christian Bauer[a], Warren Schenler[a], and Stefan Roth[b]

[a] *Paul Scherrer Institut, Villigen, Switzerland*
[b] *Axpo Holding AG, Baden, Switzerland*

Abstract: The Energy Trialog process in Switzerland was a cooperative discussion between representatives of industry, academia and society. This paper reports on a study prepared for the Trialog by a cooperative effort between the Paul Scherrer Institute (PSI) and Axpo Holding AG (Axpo). The purpose of this study was to conduct a systems comparison of different technologies providing a fixed ratio of heat and electricity from decentralized and centralized technologies. Decentralized cogeneration systems based on internal combustion engines providing both heat and electricity were compared with electric, ground-loop heat pumps plus additional electricity from several generation sources, including natural gas, hydroelectric, nuclear and the average Swiss electricity supply mix. This analysis was performed for installations ranging in size from individual households to large commercial facilities. The system comparison is based on a wide range of sustainability-related criteria covering environmental, economic and social concerns. Results for differently sized systems were aggregated to find the total impacts of providing equal amounts of total heat and electricity to the Swiss system. These indicators were then used to conduct a multi-criteria decision analysis of the different supply technologies, combining the indicator values with generic preference profiles.

Keywords: Combined heat and power generation, Life cycle analysis (LCA), Multi-Criteria Decision Analysis (MCDA), Sustainability assessment.

1. Introduction

Based on the current trend [1], Swiss electricity consumption is expected to grow in the next decades, while decreases are expected in both domestic generation (due to shut-down of the older nuclear reactors) and stipulated imports, creating a gap between consumption and generation. Increased use of decentralized electricity generation is one possible means to close this gap. Although the political consensus is that renewable energy carriers need to play a more important role in the Swiss energy supply, the potential of decentralized renewable electricity generation from wind turbines, solar panels, or small hydropower is limited by resource availability and/or cost. As a consequence, natural gas should also be considered as an energy carrier for decentralized use, usually for combined heat and power (CHP) generation. Such CHP plants are commercially available in a wide range of sizes with electric capacities between a few kW_{el} and several MW_{el} and are commonly sized to provide the building heat demand. The simultaneously generated electricity can either be used internally, i.e. in the same building, or fed back into the electricity network. However, heat pumps combined with electricity from centralized power plants can fulfill the same demands, and therefore the performance of decentralized CHP systems should be evaluated against heat pumps and centralized electric supply options.

2. Goal and scope

The goal of the work presented in this paper is a comparative technology assessment evaluating the sustainability of selected decentralized natural gas based CHP units compared to heat pumps combined with electricity generation in large scale power plants. This paper concisely summarizes the more comprehensive report [2] published in the framework of "Energietrialog Schweiz," a common initiative of policy, science and economic stakeholders with the goal of developing consistent and sustainable strategies for the Swiss energy system in the next decades. The comparative evaluation is based on a large set of sustainability indicators and carried out for three size categories: single family houses, multi-family

Corresponding Author: Christian Bauer, Email: christian.bauer@psi.ch

houses, and large commercial buildings like shopping centers or offices, taking into account the specific characteristics of CHP units with different capacities. This study only addresses installations in new buildings, not as part of renovation of old buildings. The impacts of decentralized power generation on the costs of electricity networks, system services and costs to customers are investigated on a qualitative level.

3. Methodology

3.1 Technology & system characterization

In addition to CHP units of different sizes using current technology, the assessment also includes combinations of ground loop heat pumps with electricity supply from centralized power plants and the Swiss electricity supply mix, including yearly average imports and exports [3] via the grid. The various options considered are summarized in Table 1. A 50 kW_{el} CHP plant is selected as the reference technology determining the ratio of heat to electricity to be supplied by all systems. This ratio is 1.8:1, i.e. all systems must supply 1.8 kWh_{th} of heat and 1 kWh_{el} of electricity in the comparison. This means that CHP units with a ratio above 1.8:1, i.e. generating proportionately more heat and less electricity than the 50 kW_{el} CHP plant must be supplemented with electricity from the grid – the Swiss supply mix in this analysis. This applies only to the 2 kW_{el} CHP unit (number 1 in Table 1). CHP plants with a ratio below 1.8:1, i.e. generating proportionately less heat and more electricity than the 50 kW_{el} CHP plant, need a supplemental heat source. Four different options are considered: a natural gas boiler, a heat pump, a solar collector supported by a natural gas boiler, and a wood pellet boiler (Table 1: numbers 3 and 4). In the case of centralized electricity generation, the heat pump is combined with electricity from a natural gas combined cycle (CC) power plant, a nuclear, or a hydro power plant, or the Swiss supply mix (Table 1: numbers 5 to 8). In these cases, total power consumption consists of two parts: first to run the heat pump which must supply 1.8 units of heat, and second 1 unit of electricity to meet the ratio of heat to electricity supply of 1.8:1. The 2 kW_{el} CHP unit is assumed to cover the heat demand for single family houses, the 50 kW_{el} CHP plant for multi-family houses, and both the 160 kW_{el} and the 1 MW_{el} CHP unit for commercial buildings. These three application areas are compared separately. The capacities of the heat pumps are adjusted according to the respective heat demand. Characteristics of the individual technologies are summarized in Table 2. It is assumed that CHP units are mainly operated for heat supply during winter, when their electricity production can help to meet the higher power demand.

Table 1. Reference technology and system combinations analyzed [2].

#	Technology (combination) for heat & electricity supply	Electricity source	(Supplemental[a]) heat source
Decentralized			
1	CHP 2 kW_{el} + electricity from the grid	CHP 2 kW_{el}, additional: Swiss supply mix	
2	CHP 50 kW_{el}	CHP 50 kW_{el}	
3a	CHP 160 kW_{el} + gas boiler	CHP 160 kW_{el}	gas boiler
3b	CHP 160 kW_{el} + heat pump	CHP 160 kW_{el}	heat pump
3c	CHP 160 kW_{el} + gas boiler + solar collector	CHP 160 kW_{el}	gas boiler + solar collector
3d	CHP 160 kW_{el} + wood pellet boiler	CHP 160 kW_{el}	wood pellet boiler
4a	CHP 1 MW_{el} + gas boiler	CHP 1 MW_{el}	gas boiler
4b	CHP 1 MW_{el} + heat pump	CHP 1 MW_{el}	heat pump
4c	CHP 1 MW_{el} + gas boiler + solar collector	CHP 1 MW_{el}	gas boiler + solar collector
4d	CHP 1 MW_{el} + wood pellet boiler	CHP 1 MW_{el}	wood pellet boiler
Centralized			
5	Heat pump + natural gas CC power plant	Natural gas CC power plant	Heat pump (electricity from natural gas CC plant)
6	Heat pump + nuclear power plant	Nuclear power plant	Heat pump (elec. from nuclear)
7	Heat pump + hydro power plant	Hydro power plant	Heat pump (elec. from hydro)
8	Heat pump + electricity from the grid	Swiss supply mix	Heat pump (supply mix CH)

[a] Supplementary in case of the 160 kW_{el} and 1 MW_{el} CHP units with a ration of heat vs. electricity generation below 1.8:1.

Table 2. Reference technologies, system combinations and technology characteristics as considered in this study.

Technology	Data source[h]	Electric efficiency	Thermal efficiency	Electricity generation	Heat generation	External electricity	External heat	Lifetime [years]	Operating time [h/a]
CHP 2 kW_{el}	[4]	0.25	0.65	0.69	1.80	0.31	0	20	2000
CHP 50 kW_{el}	[4]	0.30	0.54	1	1.80	0	0	20	4000
CHP 160 kW_{el}	[4]	0.32	0.55	1	1.72	0	0.08	20	4000
CHP 1 MW_{el}	[4]	0.38	0.44	1	1.16	0	0.64	20	4000
natural gas CC power plant	[5]	0.58	-	1.46[c]	-	0	1.8	36	5000
nuclear power	[6]	0.31	-	1.46[c]	-	0	1.8	40	7400
hydro power	[7]	n.a.	-	1.46[c]	-	0	1.8	120	3213
gas boiler	[5]	-	1.02	-	[c]	-	-	20	1250
heat pump[a]	[8]	-	3.9[b]	-	[d, e]	-	-	20	1250[f] 4000[g]
gas boiler + solar collector	[9]	-	1.02 (gas)	-	[c]	-	-	25	950 (gas)
wood pellet boiler	[10]	-	0.85	-	[c]	-	-	15	1250

[a] Either used as supplemental heating system for CHP units or as heating system in combination with electricity from centralized power plants.
[b] Ratio of heat production to electricity consumption.
[c] Thereof: 0.46 units of electricity for the heat pump generating 1.8 units of heat.
[d] For use as supplemental heating system: Amount of heat generation is determined by the CHP unit.
[e] For use as heating system combined with electricity from centralized power plants: 1.8.
[f] As additional heat source for CHP units.
[g] As main heat source in combination with electricity from centralized power plants.
[h] For technology specification.

Besides the capacities, the CHP units differ in terms of engine type: the 50 kW_{el} and the 1 MW_{el} plants are lean-burn engines, while the 2 kW_{el} and the 160 kW_{el} units are equipped with three-way catalysts, mainly reducing NO_x emissions. Sensitivity analyses in the result section show the impact of the different engine technologies on the overall results of the Multi-Criteria Decision Analysis (MCDA). Figure 1 shows the heat supply profiles of the different CHP plants over the year, peaking in winter. The area below the lines – depending on the CHP characteristics – corresponds to the total yearly heat generation. The 160 kW_{el} and 1 MW_{el} units need supplemental heating systems (Table 1) in order to comply with the system requirements, i.e. to match the heat supplied by the 50 kW_{el} plant. In reality, such supplemental heating systems are operated for at least 1250 hours per year for economic reasons. In order to comply with this requirement the thermal capacities of the supplemental systems are set to be 300% of the thermal capacities of the respective CHP units. The amount of heat produced, but not needed to meet the supply of the 50 kW_{el} plant is not included within the system boundaries of the assessment. This assumption mainly affects the system costs, i.e. the economics of the systems.

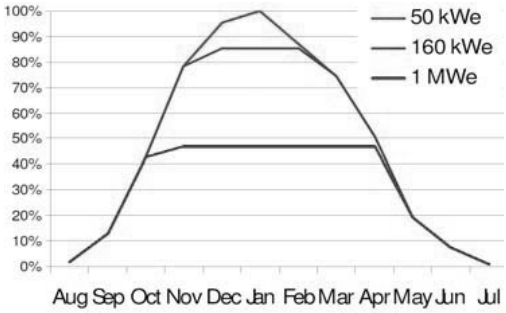

Fig. 1. Heat supply of CHP units according to the heating period. The 2 kW_{el} unit matches the 50 kW_{el} line [2].

3.2 Sustainability indicators

The comparative sustainability assessment of the combined systems for heat and electricity supply is based on selected environmental, economic, and social indicators, determined for each system. The indicators are summarized in Table 3, together with the sources of the methodologies for quantification and the respective weighting factors for the MCDA.

Table 3. Sustainability indicators, "standard profile" weighting factors, and methods used for quantification [2].

	Indicator	Unit	Weighting factor	Source
1	ENVIRONMENT		0.33	
1.1	Resources		0.2	
1.1.1	Fossil primary energy	MJ-eq./(1.8kWh heat+1kWh electricity)	0.6	[12]
1.1.2	Uranium	MJ-eq. /(1.8kWh heat+1kWh electricity)	0.1	[12]
1.1.3	Metal ores	kg(Sb.-eq)/(1.8kWh heat+1kWh electricity)	0.3	[13]
1.2	Climate change		0.4	
1.2.1	Greenhouse gas emissions	kg(CO_2-eq.)/(1.8kWh heat+1kWh electricity)	1.00	[14]
1.3	Impact on ecosystems		0.2	
1.3.1	Ecosystem quality	(PDF*m^2*a)/(1.8kWh heat+1kWh electricity)	1.00	[15]
1.4	Waste		0.2	
1.4.1	Non radioactive waste	kg/(1.8kWh heat+1kWh electricity)	0.3	[11]
1.4.2	Radioactive waste	kg/(1.8kWh heat+1kWh electricity)	0.7	[11]
2	SOCIAL ASPECTS		0.33	
2.1	Impacts on human health		0.6	
2.1.1	Normal operation: reduction of life expectancy	(YOLL[a])/(1.8kWh heat+1kWh electricity)	0.8	[b]
2.1.2	Severe accidents[c]: fatalities	(Number of fatalities)/(1.8kWh heat+1kWh el.)	0.2	[16]
2.2	Perceived risks		0.2	
2.2.1	Risk aversion: max. fatalities	Max. credible number of fatalities in accidents	0.7	[d]
2.2.2	Confinement time for critical waste	Relative measure, proportional to quantity of radioactive waste	0.3	[11]
2.3	Quality of life		0.2	
2.3.1	Negative impacts on the landscape	Relative measure	0.5	[e]
2.3.2	Freight traffic	tkm/(1.8kWh heat+1kWh electricity)	0.5	[11]
3	ECONOMY		0.33	
3.1	National economy		0.15	
3.1.1	Employment	(Number of jobs directly created)/(1.8kWh heat+1kWh electricity)	1.00	[17]
3.2	Impacts on customers		0.5	
3.2.1	Energy costs for the customer	CHF/(1.8kWh heat+1kWh electricity)	1.00	[18-21]
3.3	Security and flexibility of supply		0.35	
3.3.1	Autonomy of supply	Ordinal scale depending on renewable/non renewable energy carrier and origin of supply	0.25	[17]
3.3.2	Volatility of fuel costs	Relative scale: costs of primary energy vs. energy costs for the customer	0.25	[17]
3.3.3	Marginal costs for the consumer	Sum of costs of fuel, electricity, and variable O&M costs	0.25	[17]
3.3.4	Flexibility of energy generation: benefit for the overall energy system	Contribution to energy system stabilisation: ability of the system to follow the demand	0.25	[17]

[a] Years of Life Lost.
[b] Location specific impact pathway approach, based on LCA results after [11].
[c] Accidents are categorized as "severe" in case of more than five fatalities per accident.
[d] Based on historical data and probabilistic calculations in case of nuclear.
[e] based on expert judgement.

3.2.1 Environmental indicators

All environmental indicators are based on LCA and calculated using the ecoinvent LCA database [11]. The selection of indicators is intended to cover the main environmental concerns of today's society: depletion of non-renewable resources, impacts of climate change and on ecosystems, and waste disposal.

3.3.2 Social indicators

The social indicators cover objective elements like impacts on human health and subjective aspects like risk aversion and impacts on

landscape quality. They include complete energy chains, either mostly using LCA calculations for the objective indicators, or applying a life cycle philosophy for subjective indicators.

3.2.3 Economic indicators

The economic indicators include aspects directly quantified in monetary terms like energy costs for the consumer, and system aspects with indirect impacts due to the economic performance of the systems like employment rates and the flexibility of energy generation.

3.3 Impact of decentralized generation on the power grid and system aspects

The main aspect in this respect is the currently existing "hidden" subsidy of decentralized electricity generation: operators are not required to pay the fixed costs of the network infrastructure (metering, network capital and operation, system services, see Fig. 2) associated with their own electricity consumption, independently of the infrastructure use.

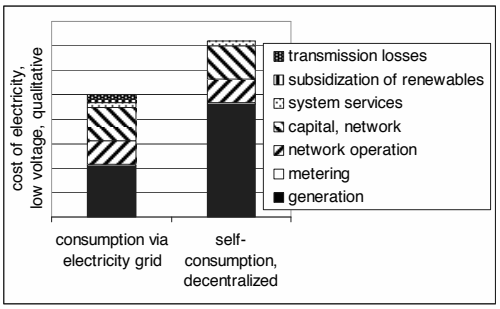

Fig. 2. Qualitative scheme of electricity costs for small customers today; only the generation costs have to be paid for the own electricity consumption by operators of decentralized plants [2].

These costs contribute about 50% to total electricity prices for small customers. A higher market penetration of decentralized systems would no longer allow such cross-subsidies.

3.4 Weighting and aggregation of indicators

The MCDA, i.e. the aggregation of the specific indicators into a single "sustainability index", is based on the weighted sum approach [17]; higher scores (with 100 as the maximum) indicate better performance. The weights of the single indicators in the "standard weighting profile" shown in Table 3, were chosen by the authors and reflect their estimation of the specific significance of the different aspects for the development of a sustainable energy system as well as a kind of consensus in the current political debate on sustainable development. The focus in this weighting profile is on objective and scientifically supported impacts, rather than on subjective elements like perception of environmental and social issues. Although the weighting profile reflects a consensus among the authors, it remains subjective. However, the advantage of the transparent weighting process is that it allows different stakeholders to set their own specific weighting profiles, based on their individual value judgments and preferences.

4. MCDA results and discussion

4.1 Standard weighting profile

Figures 3-5 show the MCDA results for single family, multi-family and commercial buildings, respectively, applying the standard weighting profile for the aggregation of the indicators. In interpreting the results, it is important to keep in mind that due to the MCDA method the scores of the systems can only be compared within one building category, and not between different building classes. Independently of the size of the buildings, the combinations of heat pumps and electricity from hydro or nuclear power plants show the best performances, i.e. the highest scores. Mainly due to the comparatively high installation costs of the small 2 kW_{el} CHP unit, this CHP option scores below all options with "heat pump + centralized power generation" in single family houses. However, this pattern changes with increasing size of the CHP units, as they become economically more competitive. In the case of multi-family houses, the "clean" CHP plant performs slightly better than the heat pump combined with electricity from natural gas CC plants. The impact of the CHP technology (whether equipped with a 3-way-catalyst or not) is also important for the performance of the CHP units for commercial buildings: despite higher costs, the 160 kW_{el} unit with the catalyst scores better than the 1 MW_{el} plant. Since the amount of heat to be supplied by the supplementary heating system is very small for the 160 kW_{el} unit, its impact on the overall results is

negligible. However, this impact becomes important for the 1 MW_{el} plant: the pellet boiler is the worst option for supplemental heat mainly due to particulate and NO_x emissions from wood combustion.

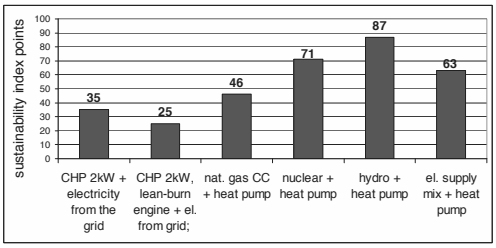

Fig. 3. MCDA results for single family houses, standard weighting profile.

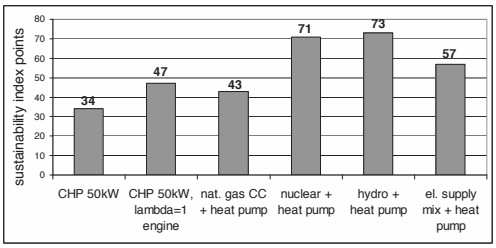

Fig. 4. MCDA results for multi family houses, standard weighting profile.

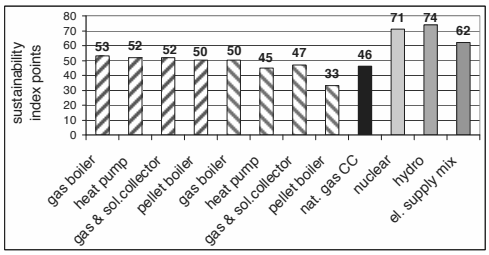

Fig. 5. MCDA results for commercial buildings, standard weighting profile.

4.2 Sensitivity: environmental focus

This sensitivity analysis, shown in Figures 6-8, is performed with modified weights on the first indicator level: instead of equally weighting the three categories of environment, social aspects, and economy, the weighting factors are 0.8, 0.1, and 0.1, respectively. Compared to the standard weighting profile, this results in better performances by the 2 kW_{el} and 50 kW_{el} CHP units, since their high costs have much less impact on the overall results. The gap between natural gas fueled systems and clean electricity from hydropower is also increased by this profile.

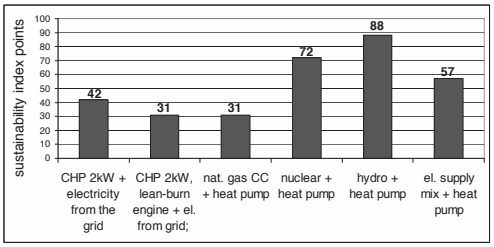

Fig. 6. MCDA results for single family houses, weighting with environmental focus.

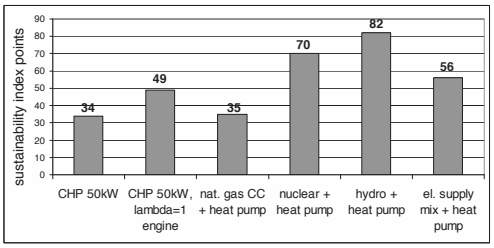

Fig. 7. MCDA results for multi family houses, weighting with environmental focus.

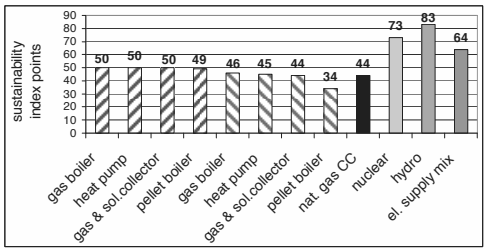

Fig. 8. MCDA results for commercial buildings, weighting with environmental focus.

4.3 Sensitivity: social focus

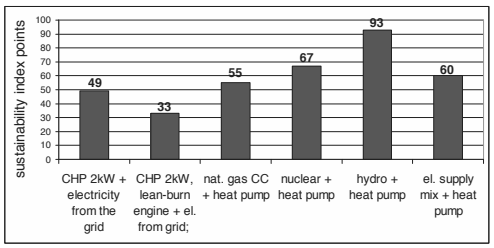

Fig. 9. MCDA results for single family houses, weighting with social focus.

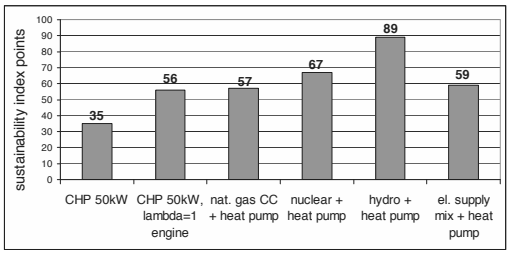

Fig. 10. MCDA results for multi family houses, weighting with social focus.

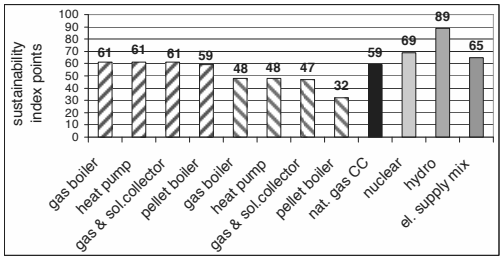

Fig. 11. MCDA results for commercial buildings, weighting with social focus.

Focusing on social aspects with modified weights on the first indicator level (0.1:0.8:0.1 for environment, social aspects and economy, respectively) results in higher importance of perceived risks and therefore in a worse performance by the nuclear option (Figures 9-11). The CHP units without exhaust gas treatment are penalized for their high emissions of air pollutants with negative impacts on human health.

4.4 Sensitivity: economic focus

An economic focus with a distribution of first level weights of 0.1:0.1:0.8 for environment, social aspects and economy, respectively, (Figures 12-14) results in clearly worse performance by the expensive CHP units, especially the 2 kW_{el} plant. It scores worse than all heat pump options for single family houses by far. The CHP plants are also penalized in multi-family buildings. Since hydro power is the most expensive option for centralized power generation and nuclear power the cheapest, the combination "heat pump + hydro power" scores worse than with the standard weighting profile, while the performance of "heat pump + nuclear" improves, resulting in the top ranking for multi-family and commercial buildings.

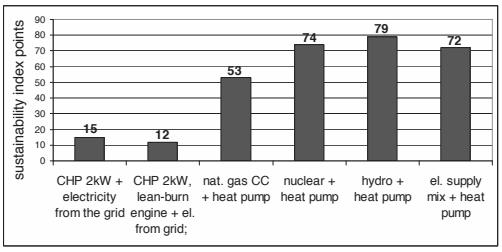

Fig. 12. MCDA results for single family houses, weighting with economic focus.

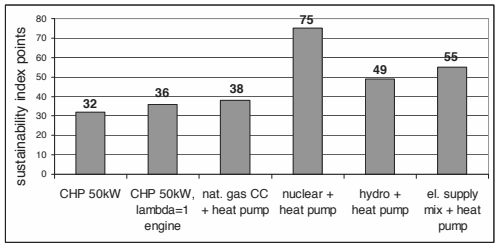

Fig. 13. MCDA results for multi family houses, weighting with economic focus.

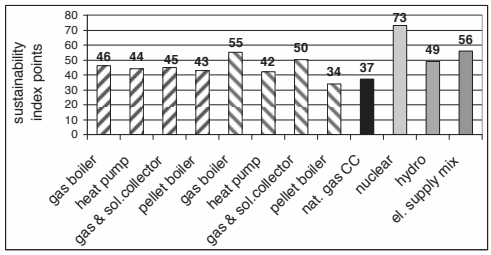

Fig. 14. MCDA results for commercial buildings, weighting with economic focus.

5. Conclusions

This sustainability assessment of selected systems for heat and electricity supply, using either CHP plants fueled by natural gas with supplemental heating systems, or heat pumps combined with centralized power generation, allows the following main conclusions based on the indicator weighting profiles presented:

- Given the current political boundary conditions, combining heat pumps with electricity from hydro power plants is the most sustainable option, even if system costs are slightly higher than for other options.
- Combining heat pumps with nuclear power allows energy supply at low costs with very

low greenhouse gas emissions and impacts on human health. However, it remains a controversial issue due to perceived risks.

- "Clean" CHP technologies, i.e. those with low air pollutant emissions should be used.
- Small CHP units for single family houses are not economically competitive and were thus evaluated as worse than heat pumps.
- Current electricity supply costs favor decentralized CHP units compared to centralized power plants: Although operating CHP units requires the availability of the electricity network, the consumer does not have to pay for fixed costs of system services associated with the fraction of electricity consumed by the producer. These cross subsidies would no longer be possible with a major share of decentralized power generation in the energy system.

References

[1] Bundesamt für Energie (BFE), 2009, Schweizerische Elektrizitätsstatistik 2008, BFE, Berne.

[2] Bauer, C., et al., 2009, Systemvergleich von Strom- und Wärmeversorgung mit zentralen und dezentralen Anlagen, Paul Scherrer Institut (PSI), Villigen & Axpo Holding AG, Baden, Switzerland.

[3] Frischknecht, R., et al., 2007, Strommix und Stromnetz, ecoinvent report No. 6-XVI, v2.0, Swiss Centre for Life Cycle Inventories, Dubendorf, Switzerland.

[4] Heck, T., 2007, Wärme-Kraft-Kopplung, ecoinvent report No. 6-XIV, v2.0, PSI, Villigen, Switzerland.

[5] Faist Emmenegger, M., et al., 2007, Erdgas, ecoinvent report No. 6-V, v2.0, Swiss Centre for Life Cycle Inventories, Dubendorf, Switzerland.

[6] Dones, R., et al., 2007, Kernenergie, ecoinvent report No. 6-VII, v2.0, PSI, Villigen, Switzerland.

[7] Bauer, C., et al., 2007, Wasserkraft, ecoinvent report No. 6-VII, v2.0, PSI, Villigen, Switzerland.

[8] Heck, T., 2007, Wärmepumpen, ecoinvent report No. 6-X, v2.0, PSI, Switzerland.

[9] Jungbluth, N., 2007, Sonnenkollektoranlagen, ecoinvent report No. 6-XI, v2.0, Swiss Centre for Life Cycle Inventories, Dubendorf, Switzerland.

[10] Bauer, C., 2007, Holzenergie, ecoinvent report No. 6-IX, v2.0, PSI, Villigen, CH.

[11] ecoinvent, 2008, The ecoinvent LCA database, v2.0, Swiss centre for Life Cycle Inventories, URL: http://www.ecoinvent.org

[12] Frischknecht, R., et al., 2007, Implementation of Life Cycle Impact Assessment Methods, ecoinvent report No. 3, v2.0. Swiss Centre for Life Cycle Inventories, Dubendorf, Switzerland.

[13] Guinée, J. B., 2001, LCA; An operational guide to the ISO standards; Parts 1 & 2, Centre of Environmental Science, Leiden, The Netherlands.

[14] IPCC, Intergovernmental Panel on Climate Change, 2007, Climate Change 2007: The Physical Science Basis, Cambridge University Press, Cambridge, UK.

[15] Goedkoop, M., and Spriensma, R., 2000, The Eco-indicator 99: A damage oriented method for life cycle impact assessment, PRé Consultants, Amersfoort, Netherlands.

[16] Burgherr, P. and Hirschberg, S., 2008, A comparative analysis of accident risks in fossil, hydro and nuclear energy chains, Human and Ecological Risk Assessment, 14(5), pp. 947 - 973.

[17] Roth, S., et al., 2009, Sustainability of electricity supply technology portfolio, Annals of Nuclear Energy 36(2009), pp. 409–416.

[18] Ganter, U., et al., 2001, Perspektiven der zukünftigen Strom- & Wärmeversorgung für die Schweiz, PSI report no. 01-12, PSI, Villigen, Switzerland.

[19] Eicher H., et al., 2003, Technologie-Monitoring. Bundesamt für Energie, Berne, Switzerland.

[20] Heck, T. and Bauer, C., 2005, Ausgewählte Indikatoren zu Wärmekraftkopplungsanlagen, PSI, Villigen, Switzerland.

[21] Online databases on CHP units, URL: http://www.minibhkw.de/minibhkw-plan/update.html and http://www.bhkw-infozentrum.de/service/download.html

An Environmental Analysis of Electricity Consumption in Built Environments

T.M. Lai [a], W.M. To [a], W.C. Lo [b], H.K. Lam [c]

a Macao Polytechnic Institute, Macao SAR, People's Republic of China
b Hong Kong Polytechnic University, Hong Kong SAR, People's Republic of China
c The University of Hong Kong, Hong Kong SAR, People's Republic of China

Abstract: Electricity is considered as an inseparable part of our modern life. In built environments, the demands for electricity are much greater and more intense. In 2008, electricity consumption amounted to 5,856 kWh per capita in Hong Kong and the electricity productivity of Hong Kong was US$5.27 GDP per kWh, a very high level in the world. However, high productivity comes at a cost – poor perceived environmental quality. This study examines the environmental impacts of electricity consumption in Hong Kong, using greenhouse gases as a basis for impact analysis. Since Hong Kong imports some percentage of electricity from a nuclear power plant in a nearby area, the imported electricity causes an illusion of low emission per unit of electricity consumed and transfers hidden environmental burdens from the electricity consumption destination (Hong Kong) to the electricity generation region (Shenzhen). However, Hong Kong will also be adversely affected by those hidden burdens because of the proximity effect in long run. Moreover, we estimate the extent of the environmental impacts from a global perspective. In realizing that Hong Kong imports fuels from overseas and emissions along fuel life cycles have yet to be taken into account, we suggest that pollution indices from utilities companies and government departments need be adjusted accordingly.

Keywords: Electricity Generation & Consumption, Greenhouse Gases Emission, Life Cycle Approach.

1. Introduction

Electricity is considered as an inseparable part of our modern life. Its production and consumption affect a city's economic development, and more importantly the quality of life. In Asia, population in cities has grown rapidly over the past decades, mostly due to the baby boom in the 1950s and 1960s and people migrating from rural areas to urban areas since 1970s. According to the Census and Statistics Department of Hong Kong Special Administrative Region, population increases from 2.24 millions in 1950 to 6.99 millions in 2008 in Hong Kong. During the same period of time, electricity consumption grew several times faster than the growth of population to 40,929 million kWh in 2008. It is because people primarily used electricity for lighting and businesses had a wide range of fuels to choose from in the 1950s. Nowadays, people have all sorts of electrical appliances and businesses in Hong Kong are service-based and commercial buildings, shopping malls, hotels, etc. utilize a significant amount of electricity for lighting, heating, ventilating, air-conditioning, plumbing, vertical transporting, and powering IT backbones. However, a price has to be paid. People living in Hong Kong has witnessed the deterioration of air quality over the past ten years. Visibility is getting poor year after year, most notably in autumn and winter when humidity is relatively low [1]. Hong Kong is covered by haze almost continuously between October and March. It has been recognized that the generation of electricity contributes significantly to the inventory of major air pollutants in Hong Kong [2]. In addition, greenhouse gases emission is also an important issue that should be studied thoughtfully, especially in considering its effect on global climate change. For this reason, this study examines the environmental impact of electricity consumption in Hong Kong using greenhouse gases as a basis for impact analysis.

The reminder of the paper is structured as follows. Section 2 describes the growth of electricity consumption, change in economic structure and GDP in Hong Kong between 2000 and 2008. From that, we estimate per capita electricity consumption and per capita productivity based on the amount of electricity consumed in 2008. Section 3 presents the Incremental Backward Life Cycle Analysis methodology and illustrates how this methodology can be utilized to

Corresponding Author: T.M. Lai, Email: tmlai@ipm.edu.mo

obtain a more complete picture about emissions of greenhouse gases and other pollutants from the fuels used in Hong Kong power companies. Section 4 describes the data sources and presents the analyzed results. Finally, a conclusion and managerial implications are given in Section 5.

2. Electricity Consumption and GDP

The relationship between electricity consumption and GDP has been the subject of intense research over the past three decades. In 1978, Kraft and Kraft [3] pioneered the study of the causal relationship between electricity consumption and economic growth using data over the 1947-1974 period in the U.S. They found evidence of a unidirectional causality running from gross national product to electricity consumption. Since then, numerous empirical studies [4-11] have been carried out to investigate the relationship between electricity (or energy) consumption and economic growth. Murray and Nam [4], Lee [8], Wolde-Rufael [9], and Yoo [10] found that there are diverse causality between electricity/energy consumption and economic growth in different countries. There were in general long-run and short-run causalities running from energy consumption to GDP in developing countries (see Lee [8] and Wolde-Rufael [9]) but mixed causalities in most other countries. The conflicting results might arise due to different data set and different countries' characteristics. Besides, the results also depend on different econometric methodologies used with the same country (Soytas and Sai [7]). All and all, these studies, Lai et al. [12] and Ferguson et al. [13] who studied electricity consumption and economic development in over 100 countries supported that there is strong correlation between economic growth and electricity consumption.

Hong Kong is a services center in Asia and an international finance center that had the largest total funds raised through new IPOs in 2009. It (as a former British colony) used to be a major manufacturing center for light industrial goods in the 1960s and 1970s because of its low labor cost. Hong Kong transformed to a commercial and trading center in the 1980s when manufacturers started moving their labor-intensive operations to mainland China. Over the past two decades, Hong Kong has transformed itself as an international finance center, emphasizing its strong link between East and West and a gateway to mainland China. In the past couple of years, Hong Kong has benefited significantly from the Individual Visit Scheme (IVS) and its Close Economic Partnership Arrangement (CEPA) with mainland China. Under the IVS, 0.27 billion residents in 49 Mainland cities are allowed to visit Hong Kong in their individual capacity. In 2008, Hong Kong attracted over 29 million visitors and most of them were people from mainland China. Electricity consumption grew by 12.8 percent between 2000 and 2008. More specifically, the net electricity consumption increased by 4813 million kWh in Hong Kong's commercial sector between 2000 and 2008. Figure 1 shows Hong Kong's electricity consumption and per capita GDP from 2000 to 2008.

As population in Hong Kong was 6.99 million in 2008, one can estimate that per capita electricity consumption was 5,856 kWh. The electricity productivity of Hong Kong was US$5.27 GDP per kWh, a very high level in the world (c.f. the electricity productivity of the US was US$3.76 GDP per kWh while that of its leading ten states was about US$6.10 GDP per kWh in 2005 [14]).

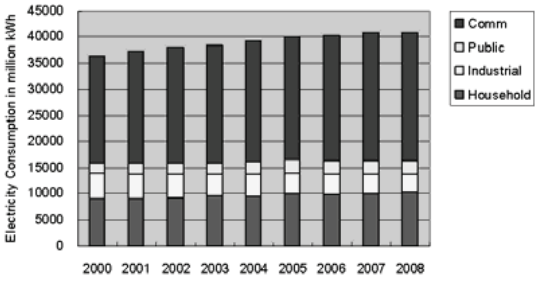

(a) Hong Kong's Electricity Consumption

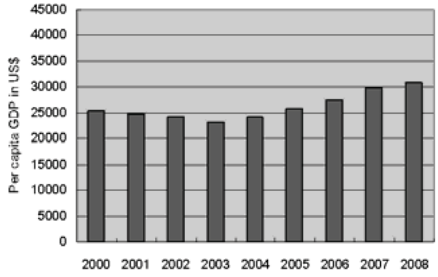

(b) Hong Kong's GDP

Figure 1(a) and (b) Hong Kong's electricity consumption and GDP from 2000 to 2008

3. Incremental Backward Life Cycle Approach

Life cycle analysis (LCA; also known as "life cycle assessment") is defined as a technique for assessing the environmental aspects and potential impacts associated with a product, process or service by compiling an inventory of relevant energy and material inputs and environmental releases; evaluating the potential environmental impacts associated with identified inputs and releases; and interpreting the results to help decision-makers make a more informed decision [15]. It is a systematic, phased approach and consists of four components: goal definition and scoping, inventory analysis, impact assessment, and interpretation [15]. The central idea of LCA is to investigate the entire life cycle of a product, system or service "from cradle to grave", with all different energy and material flows that are relevant for that product, system or service delivery. However, a comprehensive LCA of electricity generation and consumption would be too complex and require a multi-level approach to identify and quantify indirect resource consumption and pollutant emissions from all sorts of plants, machineries, and processes in different spatial locations and temporal scales. The major disadvantage of comprehensive LCA is the fact that uncertainty increases with the number of layers, i.e. analysis boundaries [16]. Ney and Schnoor [16] suggest applying an incremental approach to balance the advantages and disadvantages associated with the coverage (cost) and certainty. They developed an Incremental Life Cycle Approach to quantify greenhouse gas benefits from substitution of bioenergy fuel for fossil fuel in electricity generation. Following their idea, our study focuses on emissions of greenhouse gases and other pollutants due to electricity consumption in Hong Kong. As two or more fuels are used to generate electricity in Hong Kong's power plants, we use an Incremental Backward Life Cycle Approach[1] to identify the major (direct) emission sources of the "Well-to-Electricity" process. In this sense, we quantify the direct emission of gaseous pollutants from the extraction, transportation, refining, storage, and combustion of fuels. Although we know that all plants and machineries have embedded energy and produced gaseous pollutants indirectly, we ignore these indirect emissions because of the calculation

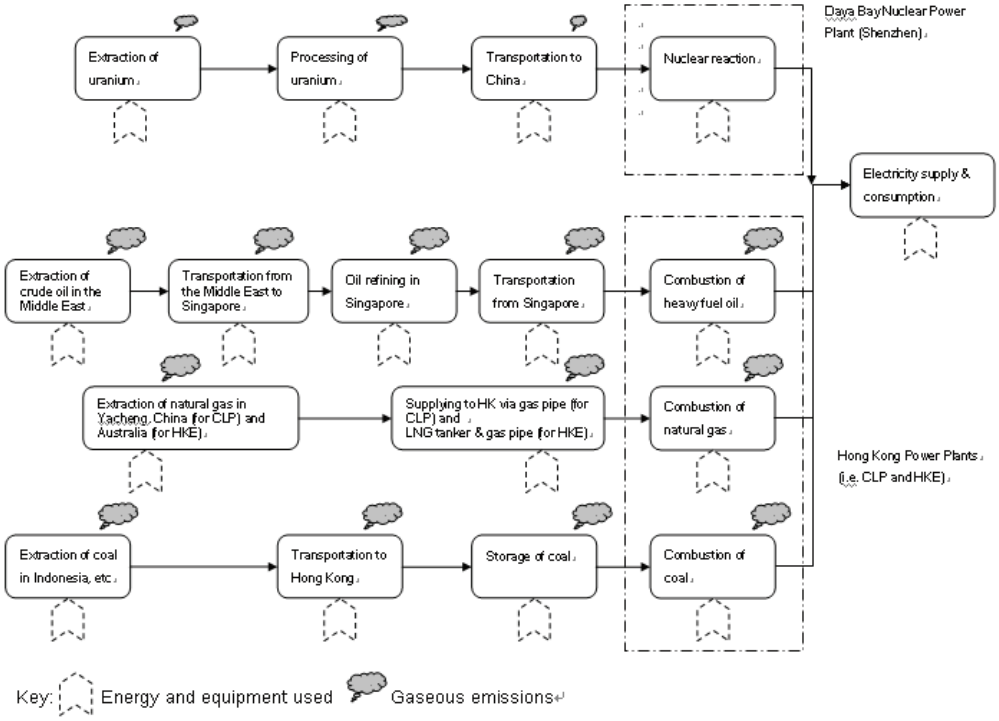

Figure 2 Fuel life cycle for electricity generation & consumption in Hong Kong (2008)

of these emissions requires an infinite expansion of system boundaries and carries a high degree of uncertainties.

Figure 2 illustrates the fuel life cycles for producing electricity in Hong Kong. From this figure, the operating greenhouse gases and other air pollutant emissions along the paths of fuel life cycles are identified.

4. Data Sources and Results

Fuel data were gathered from the Census and Statistics Department of Hong Kong, the annual reports, and the social and environmental reports of power and energy companies in Hong Kong and Shenzhen. Table 1 shows fuel consumption for generating electricity in Hong Kong for the period of 2002 to 2008 (no data were available from Hong Kong Electric for 2000 and 2001). In 2008, the majority of electricity generated was made by burning coal (around 73 percent), supplemented by burning natural gas (over 26 percent) and oil (less than 1 percent).

4.1. Emissions of gaseous pollutants during the "Well-to-Electricity" process

Fossil fuel production, transportation, refining and combustion results in emissions of carbon dioxide (CO_2), methane (CH_4), nitrous oxide (N_2O), nitrogen oxides (NO_x), sulfur oxides (SO_x), and particulate matters (PM). The amount of these emissions depends primarily on the extraction method, refining method, transport mode, storage method, the efficiency of combustion, and post-processing treatment of flue gases. According to the Intergovernmental Panel on Climate Change (IPCC), CO_2, CH_4, and N_2O are greenhouse gases that have a profound effect on global warming. The global warming potentials (GWP) of CH_4 and N_2O relative to CO_2 are shown in Table 2.

Greenhouse Gas	Symbol	GWP (for 100 yrs)
Carbon dioxide	CO_2	1
Methane	CH_4	25
Nitrous oxide	N_2O	298

Table 2. Global warming potentials (GWP) relative to CO_2

* Adopted from "Changes in Atmospheric Constituents and in Radiative Forcing"- IPCC Fourth Assessment Report (AR4), 2007

4.1.1. Emissions from oil production, transportation, refining and combustion

Most oil fields contain both crude oil and natural gas. When the oil is extracted from underground, natural gas is also pumped to the surface. If the gas cannot be collected and sold economically (as the case in the Middle East), it must be flared and CO_2 and small quantity of unburned hydrocarbons, including CH_4, are produced. By taking flaring, venting of CH_4, and emissions due to the combustion of fossil fuels by machineries in the oil fields into consideration, the US Department of Energy [18] reported that greenhouse gas emissions range from 13.6 kg CO_2E/bbl of crude oil (for Saudi Arabia) to 16.5 or 19.5 kg CO_2E/bbl of crude oil (for Kuwait or Iraq respectively) while 1 barrel of crude oil has a mass of 138.8 kg. From that, one can determine that greenhouse gas emission from crude oil extraction ranges from 95.54 to 137.69 kg CO_2E/tonne of crude oil. Al-Hamad and Khan [19] calculated the total emissions from flaring in Kuwait oilfields. They estimated that emission factors were 0.51 kg SO_2 and 0.02 kg NO_2 per tonne of crude produced in 2005.

Crude oil is transported from the Middle East to Singapore and the refining oil products including heavy fuel oil and diesel/gas oil are transported from Singapore to Hong Kong by oil tankers (mostly Aframax-type tankers). According to the latest study on pollutant emission statistics for the world commercial fleet [20], burning of marine diesel fuels generate a significant amount of greenhouse gases and other air pollutants. Psaraftis and Kontoves [20] report that Aframax oil tankers generate 5.63 g CO_2, 0.12 g SO_2, and 0.15 g NO_x per tonne-km. By knowing the distances between the Middle East and Singapore and between Singapore and Hong Kong to be 3702 and 1460 nautical miles (or 6871 and 2710 km) respectively and quantities of heavy fuel oil and diesel oil consumed in power plants on a yearly basis, we can estimate the yearly CO_2, SO_2, and NO_x emissions due to transportation of crude oil and refined products.

Oil refining requires energy and combustion of fossil fuels. Babusiaux and Pierru [21] used a linear-programming approach in which mass balance and market constraint were taken into consideration simultaneously. They showed that

0.017 tonne of CO_2 would be generated in producing 1 tonne of heavy fuel oil while 0.027 tonne of CO_2 would be generated in producing 1 tonne of diesel oil. The European Commission [22] carried out a survey and reported that emission factors of refineries are 0.03 to 6 kg SO_2, 0.06 to 0.7 kg NO_x, and 0.01 to 3 kg PM per tonne of crude processed.

Combustion of oil products generates CO_2, CH_4, N_2O, and other pollutants such as SO_2, NO_x, and PM. The IPCC [23] states that emission factors of heavy fuel oil are 77400 kg CO_2/TJ, 3 kg CH_4/TJ, and 0.6 kg N_2O/TJ while the net calorific value (NCV) of heavy fuel oil is 40.4 TJ/kT. Emission factors of diesel/gas oil are 74100kg CO_2/TJ, 3 kg CH_4/TJ, and 0.6 kg N_2O/TJ while the NCV of diesel/gas oil is 43.0 TJ/kT. Emission of SO_2, NO_x, and PM depends heavily on the pollution control equipment installed in power plants. According to the information published by power companies in Hong Kong, emission factors of these pollutants are not available separately for the combustion of oil products. Power companies quantify emissions of SO_2, NO_x, and PM in terms of kg/kWh generated/sales.

4.1.2. Emissions from coal production, transportation, and combustion

Pressure reduction during coal mining results in the release of methane stored in coal-bed. The amount of stored methane depends on the depth and type of coals [24]. Generally speaking, deeper mines have higher methane content. Hong Kong imports coals from Indonesia in which surface mining techniques have been adopted. The IPCC [23] states that the emission factors for surface mining are 0.3 to 2.0 m^3 CH_4 per tonne of coal for extraction (average 1.2 m^3 $tonne^{-1}$) and 0 to 0.2 m^3 CH_4 per tonne of coal for processing.

Coal is transported by Post-Panamax-type bulk carriers from PT Indonesia Bulk Terminal located on the South Western tip of Pulau Laut to Hong Kong. The distance between these two locations is about 4000 km. Psaraftis and Kontoves [20] report that a Post-Panamax bulk carrier generates 4.92 g CO_2, 0.11 g SO_2, and 0.14 g NO_x per tonne-km.

Coal is burnt in Hong Kong power plants to generate electricity. The IPCC [23] states that emission factors of coal are 94600 kg CO_2/TJ, 1 kg CH_4/TJ, and 1.5 kg N_2O/TJ while the net calorific value (NCV) of coal is 25.8 TJ/kT.

4.1.3 Emissions from natural gas production, transportation, and combustion

Raw natural gas is a mixture of methane (major component), ethane, propane and higher hydrocarbons, carbon dioxide and nitrogen. When natural gas is being liquefied for export at LNG, CO_2 is stripped and vented at natural gas processing facility with a small amount of CH_4. According to the Australian study on the projections of fugitive greenhouse gas emissions, the CO_2 content of raw North West Shelf gas is 2.5% on a volume or molecular basis. Venting of all CO_2 content gives rise to 70 kg CO_2 and 0.68 – 0.76 kg CH_4 per tonne of LNG produced. Flaring at natural gas processing plant is normally associated with the burning of volatile hydrocarbons arising from various activities. The amount of gas flared at natural gas processing plant is relatively small comparing with venting and normally ignored in most studies.

Natural gas is transported from the processing facility located on North West Shelf in Australia to the Guangdong LNG Terminal in Shenzhen by LNG carriers. The distance between these two locations is 2770 nautical miles (approx. 5141 km). Psaraftis and Kontoves [20] report that a LNG carrier generates 12.72 g CO_2, 0.28 g SO_2, and 0.35 g NO_x per tonne-km. In Hong Kong, one of its power companies – CLP Power imports natural gas via a 780-km subsea pipeline from the Yacheng gas field off Hainan Island. The transmission loss for this pipeline system is assumed to be 2000$m^3$$CH_4$/km/yr ([23], Table 4.2.8).

When natural gas is burnt in Hong Kong power plants, CO_2, CH_4, and N_2O are generated as by-products of electricity generation. The IPCC [23] states that emission factors of natural gas are 56100 kg CO_2/TJ, 1 kg CH_4/TJ, and 0.1 kg N_2O/TJ while the net calorific value (NCV) of natural gas is 48.0 TJ/kT.

4.2. Greenhouse gases emissions due to the consumption of electricity in Hong Kong

Table 3 shows that 28.83 million tonne of CO_2, 345 tonne of CH_4, and 385 tonne of N_2O were generated in Hong Kong power plants in 2008. By converting CH_4 and N_2O to CO_2-equivalent using GWP, greenhouse gas emissions amounted to

28.95 million tonne of CO_2-equivalent in Hong Kong power plants. In addition, there were 211 kilotonne of CO_2 for fuel transport and 370 kilotonne of CO_2-equivalent for fuel extraction and processing. In total, the fuel life cycle for Hong Kong power plants produced 29.53 million tonne CO_2-equivalent greenhouse gases. As the plants generated 37990 million kWh in 2008, emission factor of the plants was 777.4 g/kWh using the incremental backward LCA approach. However, Hong Kong imported a portion of electricity from a nuclear power plant in Shenzhen with almost zero (12kg/MWh) CO_2-equivalent greenhouse gases emissions. By taking the net imported electricity, emission factor due to the consumption of electricity in Hong Kong would be 724.8 g/kWh. These two values are 3.5 to 11 percent higher than the one (700 g/kWh) claimed by the Hong Kong Government.

5. Conclusion and Implications

The demand for electricity in built environments has been growing rapidly in the past decades. The consumption of electricity in Hong Kong's commercial sector grew by 22 percent between 2000 and 2008. In 2008, the electricity productivity of Hong Kong was US$5.27 GDP per kWh, making Hong Kong to be one of the highest in the world. However, such a high productivity comes at a cost – poor environmental quality. By adopting a holistic view of fuel life cycle in this study, we found that the emission factor of power plant was 777.4 g/kWh in Hong Kong. However, Hong Kong imported electricity from a nuclear power plant in Shenzhen. By taking the net imported electricity and the associated greenhouse gases emissions into consideration, emission factors due to the consumption of electricity would be 724.8 g/kWh in Hong Kong. We also found that greenhouse gases emissions due to the extraction, transportation, processing of fossil fuels contributed to 2 – 6 percent of the overall greenhouse gases emissions.

The Kyoto Protocol on climate change for combating global warming was extended to Hong Kong as a special administrative region of People's Republic of China. Recently, the Government has publicized the importance of energy savings and subsidized new initiatives for energy development, and reduction of greenhouse gases emissions. Certainly, when a city is being developed, more and more energy would be used unavoidably so as to support economic development. In order to minimize the harmful effects due to greenhouse gases emissions during the energy generation, transportation and production, clean and renewable energies, such as wind, solar and tidal energies, should be explored. Unfortunately, some technologies of renewable energies are expensive due to special material adopted and relevant patents. As a result, research in renewable energy, energy-saving in building design, and energy-efficiency analysis [25] should be promoted in order to improve the efficiency of renewable energies and to reduce the costs associated with the production of relevant renewable materials.

Note:

[1] The word "*Backward*" has a special meaning because Hong Kong has no primary energy resources and rely entirely on the fuels imported from elsewhere. As a result, a backward information tracking was undertaken to identify that the majority of crude oil imported to Singapore comes from the Middle East [17], and natural gas via Guangdong province from Australia. On the other hand, Hong Kong imports fuels from Indonesia (for 94.5 percent coal used in 2008), Australia (for natural gas via Shenzhen LNG terminal for Hong Kong Electric (HKE) only and for 1.3 percent coal used in 2008), China (for natural gas from Hainan province for China Light & Power (CLP) only and 4.2 percent coal used in 2008), and the Middle East (for heavy fuel oil and diesel/gas oil via oil refineries in Singapore).

References

1. Lam, C.Y., and Lau, K.H., 2005, Scientific Background of Haze and Air Pollution in Hong Kong, presented in the 13th Annual Conference of Hong Kong Institution of Science (Made in Hong Kong II - Science for Better Health & Environment), The Hong Kong Polytechnic University, Hong Kong, China, 29 October 2005
2. HKEPD, 2008, Hong Kong Air Pollutant Emission Inventory, the Environmental Protection Department of the Hong Kong Special Administrative Region, URL: http://www.epd.gov.hk/epd/english/environmentinhk/air/data/emission_inve.html

3. Kraft, J., and Kraft, A., 1978, On the relationship between energy and GNP, Journal of Energy and Development 3:401-403.
4. Murry, D.A., and Nan, G.D., 1996, A definition of the gross domestic product – electrification interrelationship, Journal of Energy and Development 19(2):.275-283.
5. Yang, H.Y., 2000, A note of the causal relationship between energy and GDP in Taiwan, Energy Economics 22:309-317.
6. Aqueel, A., and Butt, M.S., 2001, The relationship between energy consumption and economic growth in Pakistan, Asia-Pacific Development Journal 8(2):101-109.
7. Soytas U., and Sari R., 2003, Energy consumption and GDP: causality relationship in G-7 countries and emerging markets, Energy Economics 25:33-37.
8. Lee, C.C., 2005, Energy consumption and GDP in developing countries: A cointegrated panel analysis, Energy Economics 27:3, 415-427.
9. Wolde-Rufael, Y., 2006, Electricity consumption and economic growth: a time series experience for 17 African countries, Energy Policy 34:1106-1114.
10. Yoo, S.H., 2006, The causal relationship between electricity consumption and economic growth in the ASEAN countries, Energy Policy 34:3573-3582.
11. Meherara, M., 2007, Energy consumption and economic growth: The case of oil exporting countries, Energy Policy 35:2939–2945.
12. Lai, T.M., To, W.M., Lo, W.C. and Choy, Y.Z., 2008 Modeling of Electricity Consumption in the Asian Gaming and Tourism Center – Macao SAR, People's Republic of China, Energy 33(5):679-688.
13. Ferguson, R, Wilkinson, R. and Hill, R., 2000, Electricity use and economic development, Energy Policy 28:923-934.
14. Natalie Mims, N., Bell, M. and Doig, S., 2009, *Assessing the Electric Productivity Gap and the U.S. Efficiency Opportunity*, Rocky Mountain Institute, US.
15. EPA, 2006, *Life Cycle Assessment: Principles and Practice*, US Environmental Protection Agency, Report No. EPA/600/R-06/060.
16. Ney, R.A. and Schnoor, J.L., 2002, Incremental life cycle analysis: using uncertainty analysis to frame greenhouse gas balances from bioenergy systems for emission trading, Biomass and Bioenergy 22:257-269.
17. Kannan, R., Tso, C.P., Osman, R. and Ho, H.K., 2004, LCA-LCCA of oil fired steam turbine power plant in Singapore, Energy Conversion and Management 45:3093-3107.
18. DOE, 2009, An Evaluation of the Extraction, Transport and Refining of Imported Crude Oils and the Impact on Life Cycle Greenhouse Gas Emissions, US National Energy Technology Laboratory, Report No.DOE/NETL-2009/1362.
19. Al-Hamad, K.K. and Khan, A.R., 2008, Total emissions from flaring in Kuwait oilfields, American Journal of Environmental Sciences 4(1):31-38.
20. Psaraftis, H.N. and Kontovas, C.A., 2009, CO_2 emission statistics for the world commercial fleet, WMU Journal of Maritime Affairs 8(1):1-25.
21. Babusiaux, D. and Pierru, A., 2007, Modelling and allocation of CO2 emissions in a multiproduct industry: The case of oil refining, Applied Energy 84:828-841.
22. EC, 2003, Integrated Pollution Prevention and Control (IPPC) - Reference Document on Best Available Techniques for Mineral Oil and Gas Refineries, The European Commission, February 2003.
23. IPCC, 2006, 2006 IPCC Guidelines for National Greenhouse Gas Inventories, edited by S. Egglestrom, L. Buendia, K. Miwa, T. Ngara, K. Tanabe, IPCC National Greenhouse Gas Inventories Programme, IGES, Hayama, Japan.
24. Wuebbles, D.J., and Hayhoe, K., 2002, Atmospheric methane and global change, Earth Science Reviews 57:177-210.
25. To, W.M., Yu, T.W., Lai, T.M. and Li, S.P., 2007, Characterization of commercial clothes dryers based on energy-efficiency analysis, International Journal of Clothing Science and Technology, 19(5):277-290.

Year	Hong Kong							China	
	Hong Kong Electric				CLP Power			Nuclear plant	
	Coal $\times 10^3$ tonne	Light gas oil $\times 10^3$ tonne	Heavy fuel oil $\times 10^3$ tonne	Natural gas $\times 10^3$ tonne	Coal $\times 10^3$ tonne	Gas/diesel oil $\times 10^3$ tonne	Natural gas $\times 10^3$ tonne	Imported electricity $\times 10^6$ (kWh)	Exported electricity $\times 10^6$ (kWh)
2000					2887	29	1940	10203	1181
2001					3188	30	1988	10355	1581
2002	4136	8	6	0	3901	32	1936	10182	2175
2003	4168	6	5	0	5948	39	1237	10397	3008
2004	4242	5	5	0	5171	47	1787	9837	3087
2005	4327	5	5	0	5618	28	1786	11001	4498
2006	4088	5	6	98	5769	26	1780	10897	4528
2007	3646	5	4	279	6961	20	1324	10959	4035
2008	3747	5	6	260	5952	24	1614	11297	3553

Table 1. Fuel consumption for generating electricity in Hong Kong for the period 2000 – 2008

				Combustion			**Transport**	**Extraction and Processing**	
	Fuel Type	Used in*	kT	CO_2 (tonne)	CH_4(tonne)	N_2O(tonne)	CO_2 (tonne)	CO_2/CO_2E (tonne)	CH_4 (tonne)
Hong Kong	Heavy fuel oil	HKE & CLP	6	18762	0.7	0.1	324	802	
	Diesel/gas oil	HKE & CLP	29	92403	4	0.7	1564	4165	
	Natural gas (China)	CLP	1614	4346179	77	8	1560	112980	1162
	Natural gas (Australia)	HKE	260	700128	13	1	17002	18200	187
	Coal	HKE & CLP	9699	23672155	250	375	190100		7997
	Overall CO_2E			***28953045***					
							210550	***369811***	
Shenzhen	Nuclear			0					
	Overall CO_2E			***0***				***135564*****|	

Table 3. Greenhouse gases emissions due to electricity consumption in Hong Kong in 2008.

* HKE and CLP stand for "Hong Kong Electric" and "CLP Power", respectively.

** Canadian Energy Research Institute indicates that nuclear emits 12 kg CO_2/MWh due to the mining, processing, and transport of nuclear fuel. (from www.cna.ca/english/pdf/studies/ceri/CNAEconomicReport08.pdf)

Examples of Application of Exergy Analysis for the Evaluation of Ecological Effects in Thermal Processes

Wojciech Stanek

Institute of Thermal Technology, Silesian University of Technology, Gliwice, Poland

Abstract: Unfavourable influence of human activity on the natural environment can be divided into two groups: depletion of limited non-renewable resources and rejection of harmful substances. The depletion of non-renewable resources should be minimized to keep them for future mankind (sustainable development). Exergy can be applied as measure of the quality of natural resources. The influence of human activities on the depletion of natural resources can be evaluated by means of the calculus of cumulative consumption of exergy of non-renewable natural resources (thermo-ecological cost). The paper presents selected applications of the theory of hermoecological cost developed by Szargut.

Keywords: Exergy, Non-Renewable Resources Depletion, Sustainability, Thermo-Ecological Cost.

1. Introduction

Our civilization is based mainly on the non-renewable resources of fuels. The depletion of natural non-renewable resources is accelerated by an increasing consumption level of society. From the economic point of view the increase of consumption level is the base for further development. There are many examples of ancient civilizations that collapsed because they had exhausted local natural resources, for example the act of cutting off forests in Easter Islands, the depletion of fresh water in Central America, the depletion of agricultural area in South-East Asia. At present, the symptoms of depletion of natural resources can be also observed. It results in the increase of price of primary energy carriers. Some experts state that in the future non-renewable resources can be replaced by the renewable ones.

However, sober thinking leads to the conclusion that our economy will depend on the non-renewable natural resources of fuels. For this reason we should minimize depletion of fuel resources. The economic criterion is opposite to this statement. Still, to optimize design and operation of different systems, basic economic criterion is used. However, the ecological criterion should become more important.

2. Concept of the Thermo-Ecology

Fig.1 presents schematically simplified diagram of chain of production processes.

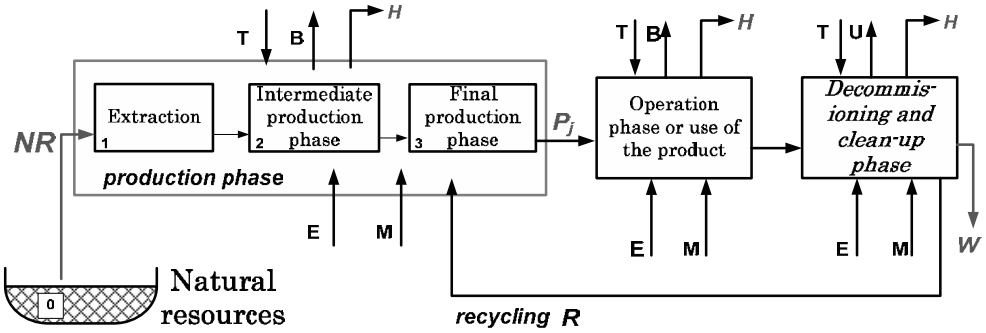

Fig. 1. Diagram of production chain.

Final production phase is preceded with so called intermediate production phase delivering semi-finished products to the main process. Final production phase delivers products or systems that are used or operated according to their life-time. Then, they can be decommissioned and some parts can be recycled and used in production again. Analyzing back-wards nets of interconnected processes, we always reach a preliminary stage which is extraction of resources from nature, even if some of processes are based on renewable resources. The interconnections between processes or between process and environment are represented by flows of *M*-materials, *E*-energy, *B*-by products, *T*-transportation needs, *H*-harmful substances. The aim of thermoecology is to express the total expenditure resulting from these flows and express them as consumption of natural resources taken from nature in a common unit taken into account different quality of different resources. As different resources and products are consumed in each of mentioned steps of power plant lifetime we have to take common measure that let us to compare all of these unfavourable effects. For this purpose we can apply exergy [2],[3],[5],[6],[9],[11].

2.1. Thermo-Ecological cost

According to J. Szargut [5],[6] the thermo-ecological cost is defined as cumulative consumption of non-renewable exergy connected with the fabrication of a particular product including additionally the consumption resulting from the necessity of compensation of environmental losses caused by rejection of harmful substances to the environment. The index of operational thermo-ecological cost can be determined by solving a set of thermoecological cost balance presented in Fig. 2.

The equation of the balance of thermo-ecological cost takes the following form:

$$\rho_j + \sum_i \left(f_{ij} - a_{ij}\right)\rho_i - \sum_r a_{rj}\rho_r = \sum_s b_{sj} + \sum_l z_{lj}\sigma_l + \sum_k p_{kj}\zeta_k \quad (1)$$

This set should comprise all the branches of domestic economy. However, it would be difficult to solve such problem. For this reason in practical calculation only strongly connected production processes are taken into account [4]. The results of calculations of the thermoecological cost have been presented for example in [4],[7].

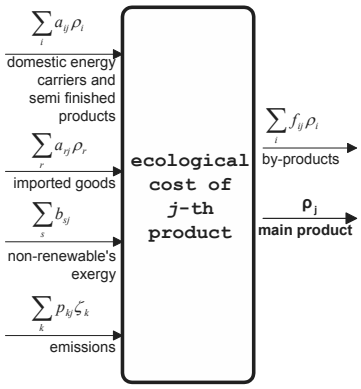

Fig. 2. Balance of thermo-ecological cost.

It is worth introducing index of sustainability into the thermoecological cost analyses:

$$r_i = \frac{\rho_i}{b_i} \quad (2)$$

Such an index expresses the ratio of thermoecological cost of the useful *i*th product related to its specific exergy. The lower index of sustainability is the better results are obtained from the ecological point of view. We pay less cumulative exergy of natural resources per unit of exergy of particular useful products. Aspirations for decreasing the sustainability index should be, of course, justifiable from the economic point of view.

Table 1 and 2 presents calculation results of thermoecological cost as well as a sustainability index of the main fuels utilized within the domestic energy management and selected semi-products.

Table 1. Thermoecological cost of fuels.

Energy carrier	b_{ch}	ρ	r
	MJ/um	MJ/um	MJ/MJ
Hard coal [1]	26.2	27.2	1.04
Coke[1]	31.8	46,1	1.45
Natural gas[2]	821.6	710.3	0.86
Natural gas[2] (domestic)	821.6	835.7	1.02
Natural gas[2] (import)	821.6	619.9	0.75
Coke-oven gas[2]	380.0	356.5	0.94

)[1] um = kg,)[2] um = kmol, b_{ch} – specific chemical exergy

Results presented in table 1 confirm that besides fuels most commonly used in domestic energy management, the coke is characterized by relatively high value of thermoecological cost and sustainability index. For this reason the utilization of coke should be minimized as far as possible.

Table 2. Thermoecological cost of fuels.

Energy carrier	b_{ch}	ρ	r
	MJ/um	MJ/um	MJ/MJ
Pig iron[1]	8.7	28.7	3.30
Oxygen[2]	3.4	153.0	45.0
Cement[1] (Portland)	1.8	10.8	6.00
Amonia[1]	19.8	40.5	2.04
Sulphur acid[1]	1.7	14.5	8.53
Aluminium[1]	33.0	190.6	5.77

)[1] um = kg,)[2] um = kmol

Table 2 shows that semi-products are burdened by relatively high values of the sustainability factor. Mainly, it results mainly from accumulation of fuel consumption in the inter-connected processes that lead to semi-products. Among the products included in table 2, oxygen is burdened by the highest value of factor *r*. It should be taken into account, for example, when we consider oxy-combustion.

2.2. Life cycle assessment (LCA)

The Thermo Ecological Life Cycle Assessment (TELCA) based on methodology, described in previous section, comprises the following phases:

1. Construction Phase encompasses project, extraction of raw materials, semi-finished products fabrications, transport expenditures in the construction phase. All these expenses influence the final thermoecological cost burdening the final useful consumptive product. This phase has a significant contribution in case of processes that are based on renewable sources of energy. For instance, in case of wind power plant thermoecological cost results mainly from expenses in construction phase.

2. Operational phase is defined as a period of time between an end of construction phase and a beginning of decommissioning phase. In processes utilising non-renewable resources, this phase is predominant in the cumulative consumption of natural resources, mainly energy carriers.

3. Decomissioning phase of plant concerns the period at an end of installation's life. In this phase, thermoecological cost results from expenditures for develop remains of system and for example some expenditures for reclamation of terrain.

General form of the objective function in case of thermoecological cost minimisation taking into account life – time of a product has been formulated by J. Szargut and is presented in [6] and applied for example investigation in work of Szargut and Stanek [7]. This function has the following form:

$$\Theta_{LCA} = \tau_n \left(\sum_j \dot{G}_j \rho_j + \sum_k \dot{P}_k \zeta_k - \sum_u \dot{G}_u \rho_i s_{iu} \right) + \frac{1}{\tau} \left(\sum_m G_m \rho_m (1 - u_m) + \sum_r G_r \rho_r \right) \quad (3)$$

The presented formula expresses the yearly thermoecological cost of investigated useful product with inclusion whole life time (TH-LCA) of this product. Equation (3) can be also applied to optimize construction and operational parameters of different resources intensive systems. In this case:

$$\Theta \rightarrow \min. \quad (4)$$

should be fulfilled.

2.3. Thermoecological assesment of rejection of harmful substances

Fig. 3 presents the connections between *j* – th productive process and rejections of harmful substance to the natural environment.

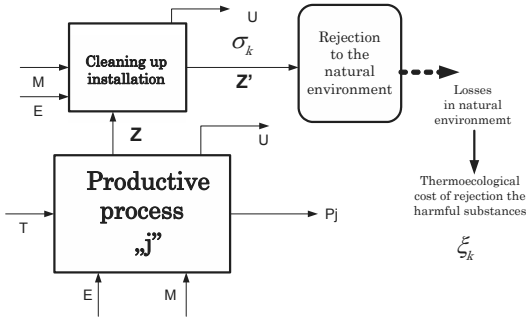

Fig. 3. Rejection of harmful substances to natural environment.

Symbols in Fig. 3 concern: *E* – energy, *M* – raw materials or semi-finished products, *U* – by-products, *T* – transport, P_j – main product of *j*-th productive process, ***Z*** – harmful waste products

generated in *j*-th productive process transferred to cleaning up installation, ***Z'*** – harmful waste products rejected to natural environment.

From thermoecological point of view, this chain (Fig. 3) can be divided into two characteristic stages. The first stage encompasses the thermoecological cost resulting from the necessity of cleaning of harmful products of *j* – th productive process while the second stage is the rejection of harmful substance *k* to the natural environment. The environmental losses are caused by both of such phases. The first phase requires some exergy expenditure of natural resources to clean up of the stream ***Z*** (abatement cost [8]). The rejection of harmful substance causes environmental losess in the fields of human health, useful industrial and other manufactured products (machines, buildings, transportation equipment) and losses in agriculture and forestry. All of such losses require some additional resources expenditure to compensate them.

Thermoecological cost resulting from rejection of harmful substances to natural environment can be evaluated by means of monetary indices of harmful impacts w_k [4],[6]:

$$\zeta_k = \frac{Bw_k}{GDP + \sum_k P_k w_k} \tag{5}$$

Besides the thermoecological cost of harmful substances we can distinguish so-called "abatement cost" of harmful substances. Such cost expresses the energy and m aterial expenditures resultion from operation of cleaning-up installations. It can be obtained from the following simplified formula:

$$\sigma_k = \frac{\sum_j G_{jk}\rho_j - \sum_u G_{uk}s_{iu}\rho_i}{G_k} \tag{6}$$

Basing on thermoecological cost index ζ_k and abatament cost σ_k the sustainability factor for clearing installation can be defined as:

$$r_k = \frac{\sigma_k}{\zeta_k} \tag{7}$$

Table 3 presents calculation results of thermoecological cost ζ_k ,abatament cost σ_k and the sustainability factor for main pollutants.

Table 3. Comparison of abatement and thermoecological cost

Harmful substance	Abatement cost MJ/kg	Thermoeco--logical cost MJ/kg	Sustaina-bility %
CO_2	4.4	= =	= =
SO_2	17.5	45.0	38.0
NO_x	26.0	45.0	58.0
dust	0.5	9.5	5.0

Cleaning of waste product is profitable when the sustainability index is less than 1. Presented results show that cleaning of flue gases from dust using electrostatic precipitator is relatively high efficient from ecological point of view in comparison with other pollutants taken into account. Because it is impossible to determine thermoecological cost of CO_2 by means of monetary indices of harmful impact (eq. 5) only the method of abatement cost can be applied as an approximate method of evaluation of thermoecological cost of rejection of CO_2 to the natural environment.

3. Examples of application of Thermo-Ecology

The presented theory of thermoecological cost can be applied to solve the following problems [6]:

1) Influence of operational parameters of energy and technological systems upon depletion of non-renewable natural resources,

2) selection of kind of technology that ensures minimal consumption of non-renewable natural resources,

3) optimisation of design and operational parameters to ensure minimum depletion of natural resources,

4) evaluation of harmful impacts of waste products,

5) investigation of the influence of interregional exchange upon depletion of domestic natural resources,

6) evaluation of the ecological harmfulness of particular useful goods in their whole life time (thermo-ecological life cycle analysis),

7) comparison of sustainability of different useful products,

8) determination of pro-ecological tax replacing existing PIT and VAT.

3.1. TH-LCA of useful heat

In the paper thermoecological cost of selected heat sources, taking whole life cycle has been determined. The results are as follow [12]:

Solar collector 0.6 MJ_{ex}/MJ_q,

Water boiler fed with gas 1.05 MJ_{ex}/MJ_q, (η_{Ek} = 90%)

Water boiler fired with coal 1.44 MJ_{ex}/MJ_q, (η_{Ek} = 80%)

Central heating in polish condition (without cogeneration) 1.3 MJ_{ex}/MJ_q,

Cogeneration In polish condition 0.94 MJ_{ex}/MJ_q, (η_{CHP}=0.85).

The presented results confirmed the favourable influence of cogeneration on savings of non - renewable natural resources.

Fig. 4 presents the structure of thermo-ecological cost of useful heat in the case of the boiler fired with gas in the case of solar collector [12].

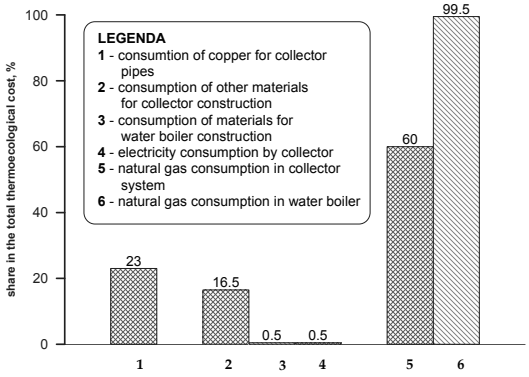

Fig. 4. Structure of the thermoecological cost in whole life cycle – hot water

In the case of heat production in a boiler in a structure of thermoecological cost consumption of gas dominance – 99.5%. For this reason in systems based on the consumption of non-renewable fuels, we can estimate thermoecological indices basing mainly on fuel consumption, in these cases operational thermoecological cost dominates (Eg.1). In the case of production of hot water in collector installation, it is necessary to take into account all life cycle (Eq. 3). The share of thermoecological cost of materials for construction of collector reaches 39.5%. 23% represent thermoecological cost of copper tubes. The share of consumption of gas in peak heater reaches 60%. Taking into account only operational part of thermoecological cost of systems, using partly renewable resources, is not acceptable.

3.2. Thermo-Ecological optimization

Existence of only minimum possibility of exhaustion of natural non-renewable resources, the minimisation of depletion of this resources should become more and more important criterion during constructing and operating of any system. Minimisation if thermo-ecological cost can concern both operational and constructional parameters. Thermodynamic optimization can be done in local or global scale [1],[6]. In this chapter it will be shown that local optimization (minimization of entropy generation or internal exergy losses) can lead to wrong conclusion. For this purpose, the blast furnace has been investigated. Coke is the basic fuel for blast-furnace. However this fuel is characterised by relatively high index of thermo-ecological cost (Table 1). Coke can be partly replaced in blast-furnace by injection of pulverized coal. The effect of replacement of coke by coal is presented in Fig. 5.

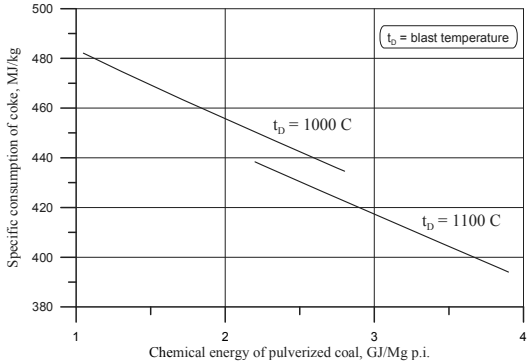

Fig. 5. Specific consumption of coke in blast furnace

Blast furnace is characterized by rather high exergy efficiency reaching 70%. Such high exergy efficiency can be obtained because processes of mass and heat exchange have counter-current character in the blast furnace. Injection of cold coal destroy this phenomena and leads of course to decrease of blast furnace exergy efficiency. This effects is presented in Fig. 6

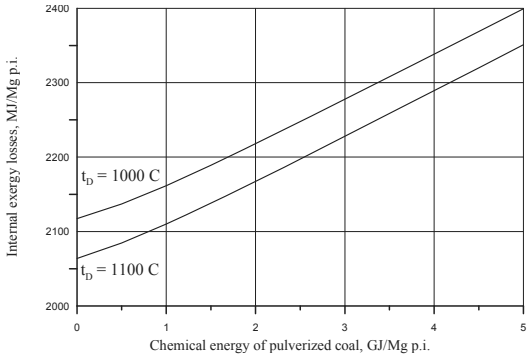

Fig. 6. Internal exergy losses in blast furnace

Taking into account the criterion of local minimisation of thermoecological cost we reach from Fig. 6 the conclusion that the injection of coal is not-favourable. However, this conclusion is wrong conclusion. Fig. 7 shows clearly that the thermo-ecological cost decreases with the increasing amount of injected coal. We reach the savings in natural non-renewable resources not locally but in other point of complex systems of processes connected with blast process. The consumption of coke with rather sustainability index has been replaced by coal of relatively lower sustainability index.

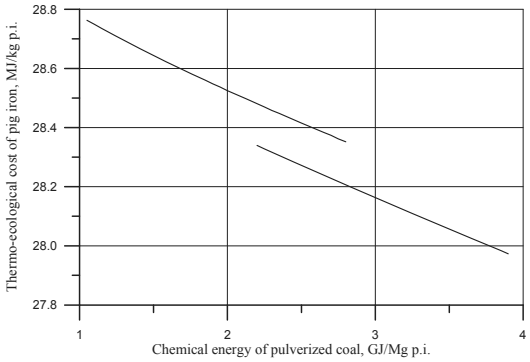

Fig. 7. Influence of injection of pulverised coal into blast furnace on the thermoecological cost of pig iron

Presented results of thermoecological analysis show clearly that in the presented minimization entropy generation criterion is not correct. In systems with strong connections between particular processes the cumulative calculus should be taken into account. Taking into account minimization of non-renewable resources consumption, a criterion similar to thermo-ecological cost presented in this paper is necessary.

4. Summary

In this paper the theory of thermoecological cost is presented and discussed. Example calculations illustrating possibilities of thermoecology have been included. The author showed selected results of calculation of thermoecological cost and sustainability factor of fuels and non-energetic material. The sustainability factor has been useful for selection of production technology. Presented results confirmed that coke should be eliminated as far as possible. Additionally the application of thermoecological cost to evaluation of the whole life cycle has been additionally presented and selected results has been included. This part shows that it is necessary to take into account the LCA methodology when we analyse processes based on consumption of renewable resources. The problem of application of thermoecological cost for minimization of depletion of non-renewable resources has been presented. Example results of calculation of thermoecological cost of pig iron. In this part, it is stated and confirmed that local optimization does not always lead to correct conclusion.

Nomenclature

a_{ij} coefficient of the consumption of the *i*-th product per unit of the *j*-th major product

a_{rj} coefficient of the consumption of the *r*-th imported product per unit of the *j*-th major product

b_i specific exergy of the *i*th good

b_{sj} exergy of the *s*th non-renewable natural resource immediately consumed in the process under consideration per unit of the *j*th product

B exergy extracted per year from the domestic non-renewable natural resources

f_{ij} coefficient of by-production of the *i*-th product per unit of the *j*-th major product

GDP Gross Domestic Product

$\dot{G}_j$ nominal flow rate of the *j*th major product

$\dot{G}_u$ nominal flow rate of the useful uth by-product

G_m consumption of mth material or energy carrier used for construction of installation

p_{kj} amount of the kth aggressive component of waste products rejected to the environment per unit of the jth product

P_k annual amount of kth waste product

$\dot{P}_k$ nominal flow rate of the kth deleterious waste product rejected to the environment

r_i sustainability index of ith good

s_{iu} replacement ratio in units of the ith replaced product per unit of the uth by-product

u_m expected recovery factor of the mth material

w_k monetary factor of harmfulness of kth substances

z_{lj} amount of the lth aggressive component of waste products entering the cleaning installation

Greek letters

ρ_i thermo-ecological cost of the ith product

ρ_m thermoecological cost of mth material or energy carrier used for construction of installation

ρ_r specific thermoecological cost of the rth imported good

η_{Ek} boiler energy efficiency

η_{CHP} - energy efficiency of CHP plant

τ nominal life time of installation

τ_n annual operation time with nominal capacity

ζ_k cumulative exergy consumption of non-renewable resources due to the emission of unit of the kth waste product

σ_k cumulative exergy consumption of non-renewable resources due to the removing of kth aggressive product from wastes

References

[1] Bejan A., Tsatsaronis G., Moran M. J., Thermal design and optimisation. J. Wiley, 1996.

[2] Finneveden G., Ostlund P.: Exergies of natura resources in life-cycle assessment and other applications, Energy, Vol. 22, No. 9, 1997.

[3] Sciubba, E. Beyond thermoeconomics? The concept of Extended Exergy Accounting and its application to the analysis and design of thermal systems. Exergy Int. J., Vol.1., 2001.

[4] Stanek W. Iterative evaluating method of the ecological cost of imported goods. Proc. of ECOS'01, Istanbul 2001, 575-80.

[5] Szargut J., Zięb ik A., Stanek W.: Depletion of the Unrestorable Natural Exergy Resources as a Measure of the Ecological Cost, Energy, Conversion and Management 42, 2002..

[6] Szargut J. Exergy method, technical and ecological applications. Southampton, Boston: WIT Press, 2005.

[7] Szargut J., Stanek W.: Thermo-ecological optimization of a solar collector. Energy 32 (2007) 584–590

[8] Valero A., Botero E., An assessment of the Earth's clean fossil exergy capital based on Exergy Abatement Cost. Proc. Conf. ECOS'2002, Berlin

[9] Valero A., Botero E. An exergetic assessment of natural mineral capital (1): Reference environment, a thermodynamic model for s degradated, Proc. Conf. ECOS 2002, Berlin

[11] Wall, G., Gong M. On exergy and sustainable development, Exergy Int. J., Vol.1., 2001.

[12] Stanek W.. Method of evaluation of ecological effects in thermal processes with the application of exergy analysis. Silesian University of Technology Press, 2009 (in Polish).

Acknowledgments

The paper has been prepared within the RECENT project (**RE**search **C**enter for **E**nergy and **N**ew **T**echnologies) supported by 7th Framework Programme, Theme 4, Capacities.

The Condenser Product and Residues Allocation in Thermoeconomics

Julio Mendes da Silva[a], José Santos[b], Silvio Oliveira Jr[a]

[a] *Polytechnic School, University of São Paulo, São Paulo, Brazil*
[b] *Department of Mechanical Engineering, Federal University of Espírito Santo, Espírito Santo, Brazil*

Abstract: The product of the condenser is an important point in the discussions related to thermoeconomic methodologies. Although there has been an advance in the development of criterion to quantify the product of the condenser, this subject is still opened. In a Rankine Cycle, the condenser is usually aggregated to the steam turbine, so it is not necessary to calculate its product. When a disaggregated model is important, such as in diagnosis or local optimization applications, it becomes necessary to include the negentropy flows in order to define the condenser's product. This paper proposes a new method to calculate the condenser product, taking into consideration that the condenser is the component responsible for the steam expansion from the atmospheric pressure down to the saturation pressure, thus it is responsible for part of the power provided by the steam turbine. This new method used to calculate the condenser product is described, applied to a cogeneration steam cycle and compared to the most wide-spread methodologies, and to different forms of residue allocation. By using this new approach, the costs obtained for the plant's products are exactly the same costs obtained when the condenser is aggregated to the steam turbine but with the advantage that all components are disaggregated and no negentropy flow is required.

Keywords: Condenser Product, Dissipative Component, Residues Allocation, Thermoeconomics.

1. Introduction

The main purpose of a thermoeconomic analysis is to appropriately allocate the production and financial costs such as maintenance, operation, fuel and capital costs, to the plant's products taking the exergy of the streams as basis for this distribution.

The exergy is considered by most of authors the best basis for rational cost allocation because differently from energy, it takes into consideration the quality of the energy present in the streams.

This kind of analysis is especially important in cases where a plant that produces more than one product, such as in a steam and electricity cogeneration, has to determine the prices of its products based on the costs of the products. This kind of situation may occur when the plant's consumers are insiders to the company [1] or when it is a law imposition as may happen to some state-owned plants in monopoly regime.

To implement a thermoeconomic analysis in an energy system it is necessary to define the fuel and the product of each component. As the condenser of a Rankine cycle is a dissipative component, it is not possible to quantify its product in terms of exergy as done for most of the components of thermal cycles, called productive components. In any energy system, in the same manner that there are productive components, there also exist dissipative components, whose utility lies in interacting with other components, which in some cases allows the system to have a higher production or a better efficiency.

To solve this problem some methodologies make use negentropy (entropy decrease multiplied by environmental temperature) as fictitious flows (E&S Model) or as exergy component flows (H&S Model) to define the product of the condenser. Others aggregate the condenser to the steam turbine so that the product of the composition can be defined as the electricity generated by the steam turbine.

The method here proposed considers, that the product of the condenser is the electricity generated by the expansion of the steam in the steam turbine, from environmental pressure down to condensing pressure. In this paper, this

Corresponding Author: Julio Mendes da Silva, Email: jams@usp.br

method is applied to a cogeneration Rankine cycle and the cost of the products are compared to the costs obtained using the most wide-spread methodologies and different forms of residue allocation.

2. Cycle Description

The cycle used to test the proposed method and compare it to the others methodologies is a simple cogeneration Rankine cycle that produces 48.18 (MW) of electric power and 5.2 (kg/s) of steam at 4000 (kPa), see fig. 1. Part of the produced steam goes to a hypothetical external process (stream 8) and returns to the cycle (stream 9) with the same parameters as condensed water (stream 10). The exhausting gas has to be treated before disposal into atmosphere, so a gas treatment component was added to the cycle. In order to completely condensate the steam exiting the turbine (stream 4) a condensing system is needed. The condensing system is composed by a cooling tower a circulating pump and also a vacuum pump (ejectors may be used instead) to keep the condensing pressure low. The condensing system will be treated as a single component. All the exergy and monetary costs regarding the cooling tower make up water were considered negligible. The cooling tower, vacuum pump and circulating pump electricity consumption were considered together as the electric consumption of the condensing system. The thermodynamic properties of each stream are depicted together with exergy in table 1. The fuel considered is pure methane; the isentropic efficiency is 0.85 for pumps and steam turbine and the boiler's thermal efficiency was considered 0.9. The power consumption in the condensing system is 97.8 (kW).

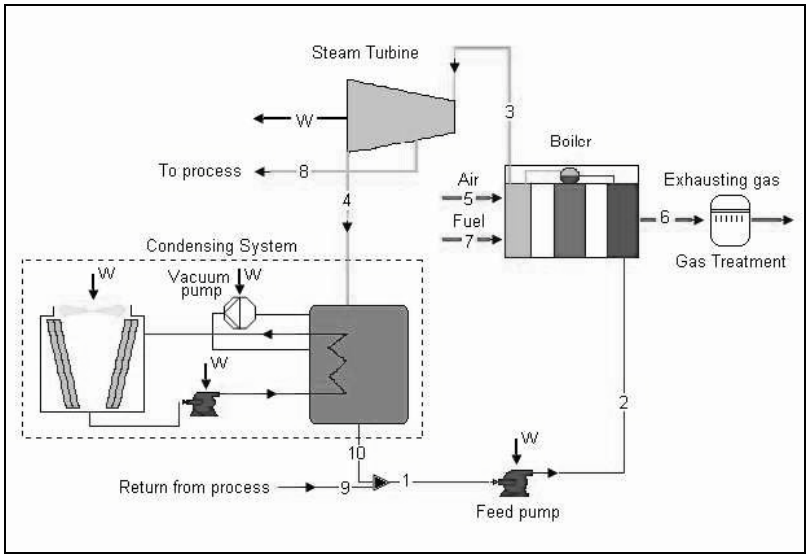

Fig. 1. Cogeneration Rankine cycle used to test the proposed method and compare it the others methodologies.

Table 1. Numerical values of the thermodynamic properties of each stream of the cycle.

Stream (i)	mi [kg/s]	Ti [C]	Pi [kPa]	hi [kJ/kg]	si [kJ/kg-K]	bi [kJ/kg]	Bi [kW]	LHV [kJ/kg]	x [%]
0 (Environment)		25.00	101.33	104.84	0.37	-	-	-	-
1	52.00	51.56	13.33	215.85	0.72	4.64	241.14	-	-
2	52.00	52.09	6,700.00	223.81	0.73	11.50	598.00	-	-
3	52.00	485.00	6,700.00	3,377.74	6.77	1,363.58	70,906.16	-	-
4	46.80	51.56	13.33	2,360.00	7.33	181.01	8,471.21	-	0.90
5	83.57	25.00	101.33	298.45	6.86	0.00	0.00	-	-
6	87.22	159.78	101.33	121.49	0.34	45.56	3,973.28	-	-
7	3.64	25.00	101.33	-	-	51,978.13	189,360.77	50,020.00	-
8	5.20	411.70	4,000.00	3,241.05	6.81	1,216.32	6,324.85	-	-
9	5.20	51.56	13.33	215.85	0.72	4.64	24.11	-	-
10	46.80	51.56	13.33	215.85	0.72	4.64	217.03	-	-

3. Applied Methodologies

Most of the methodologies used in this work have different criteria for residues costs allocation and on the treatment of the dissipative component. The following methods were applied:

REX: this method considers that the function of the condenser is the thermal exergy disposal to atmosphere. Thus, the costs regarding the exergy released to atmosphere in condensing process are distributed to the components weighted by exergy increase in the working fluid. The costs related to the exhausting gas treatment are, in all methods, allocated to the component where this residue is generated: the boiler. In fig. 2 the arrows indicate that the costs of the condensing system has been apportioned to boiler and to feed water pump, that are the components responsible for exergy increase, while the costs regarding exhausting gas treatment are allocated to the boiler. This kind of residues treatment was used by [2] to allocate the residues costs in a combined cycle power plant.

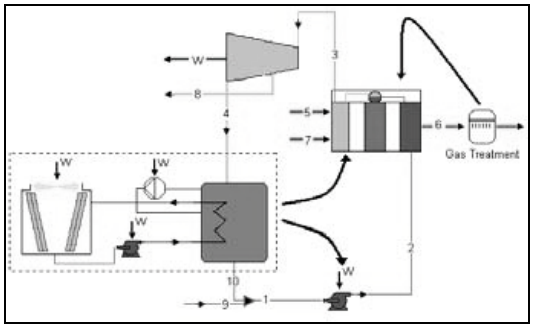

Fig. 2. Condenser treatment and residues allocation in REX method.

RET: this method does not define the product of the condensing system. However the costs associated to the condensing process should be the apportioned to the components according to the entropy increase in each component. Thereby fig. 3 shows that in RET method, the costs regarding the condensing system have been distributed to steam turbine, boiler and feed water pump weighted by the entropy increase in each one of these components. This method, for condensing system costs allocation using entropy as a weighting factor, was suggested by [3].

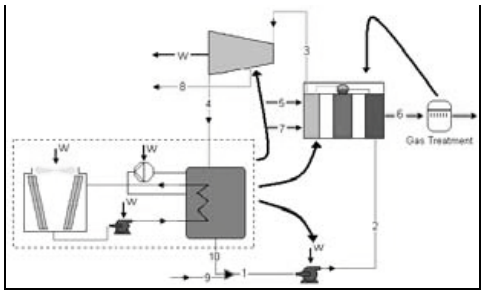

Fig. 3. Condenser treatment and residues allocation in RET method.

REL: this is one of the most used methodologies. It considers that the function of the condenser is to assist the steam turbine in power generation. Thus the steam turbine and the whole condensing system are considered as single component as shown in fig. 4. In this case all the costs regarding condensing process are directly allocated to the electricity generated by the steam turbine, which is the component served by the condensing system. This approach was suggested by [4]. The main disadvantage of this method is that several equipments are involved by the control volume forming a single component, and in some cases the study of a disaggregated model is of considerable importance as in local optimization and detailed diagnosis applications.

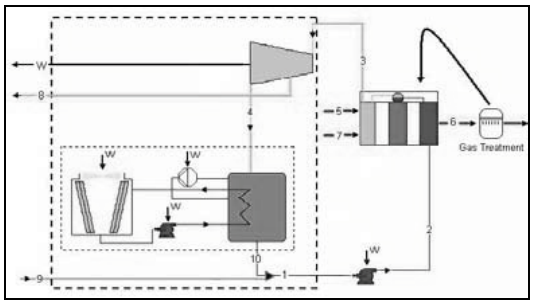

Fig. 4. Condenser treatment and residues allocation in REL method.

RNG (E&S): this method makes use of negentropy as a fictitious flow in order to define a product to the condensing system. The productive structure, that graphically represents the costing equations used, is shown in fig. 5. According to this methodology the condenser produces a fictitious flow called negentropy, defined by (1) as the entropy variation between

condenser input and output multiplied by environmental temperature. The product of the condensing system is apportioned to the components responsible for the entropy increase in the working fluid: feed water pump, boiler and steam turbine. This method was suggested by [5] and was also used by [6]. According to this method the negentropy that comes from the external process has the same unit cost as the negentropy generated by condensing system.

$$NG = To \cdot (S_4 - S_{10}) \quad (1)$$

RNG (H&S): this method also makes use of negentropy but as an exergy component flow. As negentropy is indeed part of exergy, in order to avoid double penalty in the components that increase the entropy as well as double reward in the components that decrease entropy, the productive structure proposed by this method has the same structure shown in fig. 5, however using enthalpy and negentropy (H&S) instead of exergy and negentropy (E&S). Thus the flows representing exergy (B) in fig. 5, according to RNG (H&S) method will represent enthalpy. This method was proposed by [7]. As this method considers that negentropy is part of the exergy flow, the negentropy that comes from the external process has the same unit cost as the enthalpy that goes to the external process.

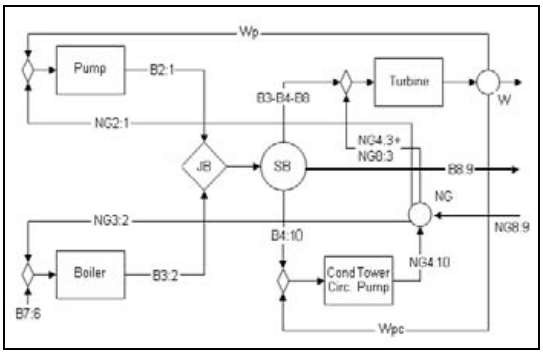

Fig. 5. Productive structure of the cycle graphically describing RNG (E&S) costs equations.

Proposed Methodology: the proposed method is based on the fact that without the condensing system it would be possible to expand the high pressure steam (stream 3) only down to atmospheric pressure. In order to condensate the steam that leaves the steam turbine, at a pressure near atmospheric pressure, a simple component such as the tank shown in fig. 6 (or any dissipative system without vacuum devices), could be used to dissipate the energy released during the condensation to environment, ensuring that only liquid water goes to the pump. Therefore the electricity generated by the steam turbine from atmospheric pressure down to condensing pressure is due to condensing system even though it is generated in the steam turbine.

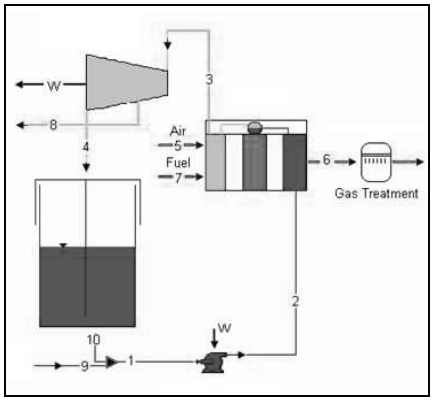

Fig. 6. Steam cycle using a tank to condensate the steam before going to feed water pump.

Since the costs related to condensing system are much lower than the costs associated to the steam turbine, the cost of electricity generated from the expansion attained by condensing system, based on the condensing system costs, is usually smaller then the cost of the electricity obtained by the steam expansion from high pressure steam down to atmospheric pressure. That's why this kind of system is used rather than a more powerful steam turbine that condensates the steam in a regular tank, as in fig. 6.

The following equations are the proposed equations for fuel exergy allocation in the streams. In these equations B means exergy, c are the unknown unit exergy costs that are been calculated, W means power, while W_T means power produced by steam turbine (expansion down to atmospheric pressure) and W_C means power attained by condensing system by expansion from atmospheric pressure down to condensing pressure.

$$c_2 \cdot B_2 = c_1 \cdot B_1 + c_{W_M} \cdot W_{F.PUMP} \quad (2)$$

$$c_3 \cdot B_3 = c_2 \cdot B_2 + c_5 \cdot B_5 - c_6 \cdot B_6 + c_7 \cdot B_7 \quad (3)$$

$$c_{W_T} \cdot W_T = c_3 \cdot B_3 - c_8 \cdot B_8 - c_4 \cdot B_{4INT} \quad (4)$$

$$c_{W_C} \cdot W_C = c_4 \cdot B_{4INT} - c_{10} \cdot B_{10} + c_{W_M} \cdot W_{C.SYSTEM} \quad (5)$$

By using the control volume around the feed water pump, fig. 1, (2) is obtained. To obtain (3) and (4) the control volume was considered around boiler and steam turbine respectively, (5) is regarding the condensing system products and fuels. According to (6) and (7) the air and exhausting gas unit exergy costs were considered zero.

$$c_5 = 0 \quad (6)$$

$$c_6 = 0 \quad (7)$$

In order to obtain a solution to the equation system 6 more equations are necessary once there are 12 unknown variables (C_1 to C_{10}, except for C_7 that is the fuel unit exergy cost, plus C_{WT}, C_{WC} and C_{WM}). By choosing a control volume around the junction of the process return and the condensate, fig. 1, (8) can be obtained.

$$c_1 \cdot B_1 = c_{10} \cdot B_{10} + c_9 \cdot B_9 \quad (8)$$

Equations (9), (10), (11) and (12) can be obtained using the fuel principle (criterion used in proposal F), as suggested by [3]. The fuel principle considers that the cycle exergy consumers, such as steam turbine and condensing system, make use of part of the exergy present in the stream that gets into the component to generate the component's products while the stream's remaining exergy, that pass through the component and goes out has the same unit exergy cost as the stream that gets in. Thus the unit exergy cost of streams 3, 4, 8, 9 and 10 are considered the same.

$$c_4 = c_3 \quad (9)$$

$$c_8 = c_3 \quad (10)$$

$$c_9 = c_3 \quad (11)$$

$$c_{10} = c_3 \quad (12)$$

This criterion is not always reasonable. In some cases as in refrigeration cycles the product of the expander is the cooling effect (thermal exergy) at the expense of a give reduction in the mechanical exergy, while the electricity is only a useful by-product, as considered in [8]. Another example is when a steam pressure reduction is necessary in order to deliver steam at proper pressure to an important process. In this case the electricity may also be considered as a useful by-product. If the chosen criterion indicated that the steam turbine extraction (stream 8) is also a turbine's product then (13) and (14) should be used instead of (10) and (11). This criterion is known as equality principle (criterion used in proposal E) and according to this approach the unit exergy cost of the extraction is equal to the unit exergy cost of the electricity generated by the steam turbine as suggested in [1].

$$c_8 = c_{W_T} \quad (13)$$

$$c_9 = c_{W_T} \quad (14)$$

Equation (15) is used to obtain the mean unit exergy cost for the whole power generated in the plant.

$$c_{W_M} = \frac{c_{W_T} \cdot W_T + c_{W_C} \cdot W_C}{W_T + W_C} \quad (15)$$

4. Results and Discussion

The seven different methods (REX, RET, REL, RNG (E&S), RNG (H&S), proposal F and proposal E) were applied to the cycle described in section 2. The results of the methodologies based on the physical structure are shown in table 2 while the results of the methods based on productive structure are shown in table 3. It can be seen in table 4, that the unit exergy costs of each product of the cycle (electricity and steam) obtained using the proposal F and REL methods are exactly the same. This happens because in both cases all the costs regarding condensing system are directly allocated to the electricity. This equality can be proved by the substitution of (4) and (5) into (15) what will result in an equation which is equivalent to (16) used to calculate the electricity unit exergy cost in REL method. However the proposed method defines the product of the condenser thus the unit exergy cost of stream 4 can be calculated.

$$c_W \cdot W_T = c_3 \cdot B_3 - c_8 \cdot B_8 - c_{10} \cdot B_{10} + c_W \cdot W_{C.SYSTEM} \quad (16)$$

Table 2.Unit exergy cost of each cycle stream calculated using REX, RET, REL and the proposed methods (kJ/kJ)

Stream	REX	RET	REL	PROPOSAL F	PROPOSAL E
1	3.06	3.03	2.70	2.70	2.70
2	3.91	3.71	3.58	3.58	3.58
3	3.06	3.03	2.70	2.70	2.70
4	3.06	3.03	-	2.70	2.70
5	0.00	0.00	0.00	0.00	0.00
6	0.00	0.00	0.00	0.00	0.00
7	1.00	1.00	1.00	1.00	1.00
8	3.06	3.03	2.70	2.70	3.03
9	3.06	3.03	2.70	2.70	2.70
10	3.06	3.03	2.70	2.70	2.70
Electricity cost	3.55	3.56	3.60	3.60	3.56

Table 3.Unit exergy cost of each cycle stream calculated using RNG (E&S) and RNG (H&S) methods (kJ/kJ)

Stream	RNG E&S	RNG H&S
Pump Product	4.23	4.01
Boiler Product	3.07	3.03
Cond. Product	0.28	3.31
B/H	3.07	3.03
From Process (9)	3.35	6.06
Electricity cost	3.61	3.56

Table 4.Deviation of the unit exergy cost of the products of the cycle regarding the average values of all methods (kJ/kJ)

Method	Steam	Electricity	Steam Deviation	Elect. Deviation
REX	3.06	3.55	3.96%	-0.63%
RET	3.03	3.56	2.90%	-0.52%
REL	2.70	3.60	-8.33%	0.63%
Proposal F	2.70	3.60	-8.33%	0.63%
Proposal E	3.03	3.56	2.67%	-0.49%
RNG E&S	3.07	3.61	4.23%	0.88%
RNG H&S	3.03	3.56	2.90%	-0.52%
Average	**2.95**	**3.58**		

5. Monetary application

In order to calculate the monetary cost of the streams it is necessary to know the production and financial costs regarding each cycle's component. Thus, table 5 was build up considering typical Brazilian market prices for the components of the cycle depicted in section 2 and its necessary services (O&M), at a Є/R$ ratio of 2.6, an interest rate of 10% per year and an amortization period of 10 years.

Table 5. Costs related to components and fuel

Component	Cost	Unit
Boiler	523.97	Є/h
Steam Turbine	366.78	Є/h
Cond. System	104.79	Є/h
Pump	52.40	Є/h
Fuel	0.0377	Є/kWh

In table 6 it can be seen that the lowest cost of electricity is obtained in proposal E method once that part of the steam turbine costs is apportioned to steam. The second lowest electricity cost method is obtained using REX method because none of the costs regarding condensing process is directly allocated to steam turbine. The opposite can be seen in REL and in proposal F methods where the whole cost of condensing system is directly allocated to the generated electricity. However the highest cost of electricity is calculated by the methodology (E&S) that makes use of negentropy as a fictitious flow. This happens because a strong penalty is applied to the components that increase entropy such as the steam turbine, directly affecting the electricity cost. Besides that, the negentropy produced by the external process (NG8:9) was defined as having the same monetary unit cost of the negentropy produced by the condensing system (NG4:10), see fig.4. If this cost were considered zero the electricity cost would decrease for this methodology.

The monetary unit cost regarding the external process return (stream 9) was considered the same monetary unit cost of the steam turbine extraction (stream 8), based on the argument that the external process only consumes part of the exergy present in the extraction (F principle). Because of this consideration and taking into account that the cost of stream 9 changes according to the used methodology, the net cost of the steam that goes to the external process is calculated by stream 8 (exergy or enthalpy) minus stream 9 (exergy or enthalpy plus negentropy if applied). The resulting total cost (electricity plus steam) will be the same for all methods and it is equal to the sum of the costs described in table 5, considering the fuel multiplied by its respective exergy. That means that the monetary output is equal to its input.

Table 6.Deviation of the monetary cost of the products of the cycle regarding the average of all methods (€/h)

Method	Steam*	Electricity	Stream 8	Stream 9	Steam Deviation	Elect. Deviation
REX	1,844.59	17,771.86	1,852.10	7.51	6.18%	-0.60%
RET	1,825.04	17,791.40	1,832.48	7.43	5.05%	-0.49%
REL	1,617.49	17,998.96	1,624.07	6.59	-6.90%	0.67%
Proposal F	1,617.49	17,998.96	1,624.07	6.59	-6.90%	0.67%
Proposal E	1,862.69	17,753.76	1,869.27	6.59	7.22%	-0.70%
RNG E&S	1,570.14	18,046.31	1,857.05	286.91	-9.62%	0.93%
RNG H&S	1,823.71	17,792.74	5,087.08	3,263.38	4.97%	-0.48%
Average	**1,737.31**	**17,879.14**	**2,249.45**	**512.14**		

6. Conclusion

A new method was developed to define the product of condensing systems in steam cycles. This method was applied to a hypothetical cogeneration Rankine cycle and the costs of the cycle's products (electricity and steam) were compared to the results obtained using the most wide-spread methodologies, as well as different forms of residue allocation. The results show that the proposed method provides the same results obtained using the method that aggregate the condenser to the steam turbine. However the proposed method has the advantage that no aggregation is needed and no negentropy flow is required to determine the product of the condensing system. Therefore this approach can be useful in application where a highly disaggregated model is required, such as in local optimization and detailed diagnosis. Furthermore the proposed method shows the product of condensing system from a more practical point of view.

Nomenclature

B Extensive Exergy [kJ/s]
b Specific Exergy [kJ/kg]
c Unit exergy costs [kJ/kJ]
E&S Exergy and Negentropy
F Fuel principle
h Specific Enthalpy [kJ/kg]
H&S Enthalpy and Negentropy
m Mass flow [kg/s]
E Equality principle
REL Residues allocated to Electricity.

RNG Residues allocated using Negentropy

REX Residues allocated based on Exergy increase

RET Residues allocated based on Entropy increase

s Specific Entropy [kJ/kg-K]

S Extensive Entropy [kJ/ K]

T Temperature [K]

W Power [kW]

Subscripts

C Produced in Condenser

CSYSTEM Consumed by Condensing system

FPUMP Feed water pump

INT Intermediary

M Mean Value

W Power

T Turbine

TOWER Cooling tower

VACUUM Vacuum pump

References

[1] Gaggioli, R. A., and El-Sayed, Y. M, 1987, Critical Review of Second Law Costing Methods. *IV International Syposium on Second Law Analysis of Thermal Systems*, New York. ASME, pp 59-73 (ASME book I00236)

[2] Torres, et al. 2008, On the Cost Formation Process of the Residues, *Energy*, vol. 33, pp 144-152.

[3] Lazzaretto, A., and Tsatsaronis, G., 2006, SPECO: A Systematic and General Methodology for Calculating Efficiencies and Costs in Thermal Systems, *Energy*, pp 1257 - 1289

[4] Lozano, M. A., and Valero, A, 1993, Theory of Exergetic Cost, *Energy*, vol. 18, nº9, pp 939-960.

[5] Frangopoulos, C., 1987, Thermo-Economic Functional Analysis and Optimization, *Energy*, vol. 12. n 7, pp 563-571

[6] Erlach, B. et al., 1999, Structural Theory as a Standard for Thermoeconomics, *Energy Conversion and Management*, 40, pp 1627-1649.

[7] Santos, J. C. S., et al., 2009, On the Negentropy Application in Thermoeconomics: a fictitious or an exergy component flow?, *Int. J. of Thermodynamics,* 12 (4), pp. 163-176.

[8] Kotas, T. J., 1985, The Exergy Method of Thermal Plant Analysis, *Krieger Publishing Company*, Malabar, Florida.

Acknowledgments: The authors would like to thank CNPq and ANP for the financial support.

Methods for complex energy system design under uncertainty

Matthias Dubuis [a], *Francois Marechal* [a]

[a] *LENI-EPFL, Lausanne, Switzerland*

Abstract: The main issue in energy conversion system design is to define interconnected equipments (their type, size and operating conditions) in order to propose a system that provides, in a given context, energy services considering available resources and technologies. The optimal design is characterized by a set of decisions that define the investment (process design) to be done.
This optimization procedure involves the modelization of the whole process. The most of time, models are built on fixed parameters. However in real-case application, they are uncertain.
In many cases, a basic sensitivity analysis is performed in order to study the influence of uncertain parameters one by one. However, this approach covers only a small part of the uncertain parameters domain. Then, two ways to include uncertainty in optimization have been studied. First, a Monte-Carlo simulation strategy has been applied. In this case, a Monte Carlo method is used to generate randomly values of the uncertain parameters. Their influence on solution is computed after optimization. This allows one to study uncertain parameters sensitivity on the calculated performances. Secondly, stochastic optimization has been performed. Here the uncertain parameters are randomly generated when evaluating the model during the optimization procedure. This allows one to generate a Pareto set and compare the results obtained with the results obtained applying the optimization using the mean values of the uncertain parameters. This allows one to study the impact uncertain parameters on the optimal decision set.
In conclusion, methods have developed to evaluate influence of uncertainty on the solution of a process, on the optimization procedure and on control variable has been demonstrated. However, the presented approach are highly time and memory consuming.

Keywords: Uncertainty, Process design, optimization

1. Introduction

Design under uncertainty has been receiving increasing attention over the last years. New methods and specific algorithms are designed for each kind of application. Process synthesis problems present a division of decision variables types into two substantially different families: design variables that describe the choice on the plant construction and operating variables that control the operation of the plant. This leads naturally to two-stage programming strategies with the operating variables acting as second stage ones. The following papers propose formulations and resolution schemes for process synthesis problems. Acevedo and Pistikopoulos [1] define a two-stage mixed integer non linear programming (MINLP) formulation with integration schemes for the computation of the expectancy of the objective function, this formulation includes the notion of feasibility i.e. the plant ability to operate under uncertain external conditions. Pistikopoulos and Ierapietrou have suggested further improvement of this formulation including feasibility [14]. Following these works, Rooney and Biegler have designed a method to include the correlations between uncertain parameters defining joint confidence regions [15]. However the proposed resolution scheme requires the linearization of the problem. Early software implementation of uncertainty analysis in a chemical processes modeling software has been performed by Diwekar and Rubin [4]. The software presented the capabilities to study the propagation of the uncertainties on the process flowsheet using sampling techniques. The access to such high performance sampling techniques has led to the definition of Stochastic annealing [12]. While most of the stochastic optimization resolution schemes are based on deterministic optimization methods, stochastic annealing uses the heuristic combinatorial optimization technique of simulated annealing to solve the optimization problem. Much work has been accomplished on the development of efficient sampling techniques to re-

Corresponding author: Dubuis Matthias, Email: matthias.dubuis@epfl.ch

duce computational time of stochastic optimization problems resolutions [5]. The recent application of such techniques to optimization of hybrid fuel cell systems is of interest for the present project as it proposes a multi-objective optimization framework [18]. Stochastic optimization techniques can also be used to evaluate and optimize the flexibility of a plant e.g. its ability of feasible operation under uncertain parameters. Much work is done to improve flexibility of processes as this extends the operation time of a plant. Several mathematical definitions of flexibility exist, Straub and Grossmann have proposed to take into account the measure of the probability of feasible operation [17]. Pistikopoulos and Grossmann have also proposed to increase flexibility in retrofit design [13]. Another approach of flexibility is addressed by robust optimization. As Bertismas and Sim [2] explain this method aims at designing solution approaches that are immune to data uncertainty. This is done by adding strong constraints in the optimization problem formulation. Linke and Kokossis [11] take into account robustness with heuristic optimization techniques for reaction/separation systems .

For stochastic programming problems, the book of [3] has been used as a reference.

2. Problem formulation

The concepts presented in this paragraph consider specifically the problem of process design under uncertainty. The formalism has been mainly developed for mathematical programming formulation in [7], [8], [9] and [6]. Design problems are generally formulated as constrained optimization problems, the form of which is:

$$\begin{aligned} &\min_{x} \ f(x) \\ &s.t\ h(x) = 0 \\ &\quad g(x) \leq 0 \end{aligned} \tag{1}$$

The objective function $f(x)$ is typically the cost of the system to be minimized or the efficiecny that has to be maximized. The constraints $h(x) = 0$ represent the equations of the model. The inequality constraints $g(x)$ define the feasibility domain of the process design. The inequality constraints represents limits applied to the process equipments or limits imposed by the regulation.

The variables x represent the state variables of the system, these include the calculated values, the model parameters and the decisions variables of the problem.

In order to express the design under uncertainty problem, the variables x are classified in the following categories:

- **Decision variables** z: the variables whose value will be adapted in order to minimize the objective function. The definition of the decision variable set results from the degree of freedom analysis. The decision variables may be separated into:
  - **Design variables**, z_v: continuous variables characterizing the design, these indicate for example the size of the equipment
  - **Design decisions**, z_d: integer variables characterizing the design, indicating the selection of a technology for example
  - **Operating variables**, z_o: describe the operation of the plant such as pressures, temperatures, or flow rates
- **Parameters**, θ: the models parameters are not considered as variables *i.e.* they are not able to adapt to operating condition, and they can not be imposed when optimizing the system. They are divided in two groups:
  - **Certain parameters**,θ_c wich are constant for a given design.
  - **Uncertain parameters**, θ_u which can vary independently of any decision.
- **Dependent variables**, d: are resulting from the resolution of the equality constraints $h(z_v, z_d, z_o, d, \theta) = 0$ once the value of the decision variables is fixed so that [8]:

$$\begin{aligned} h(z_v, z_d, z_o, d, \theta) = 0 &\rightarrow d = h^*(z_v, z_d, z_o, \theta) \\ f(z_v, z_d, z_o, d, \theta) &\rightarrow f(z_v, z_d, z_o, \theta) \\ g(z_v, z_d, z_o, d, \theta) &\rightarrow g(z_v, z_d, z_o, \theta) \end{aligned} \tag{2}$$

Without distinguishing between the different types of decision variables (i.e. $z = \{z_v, z_d, z_o\}$), the problem of equation (1) is therefore restated as:

$$\begin{aligned} &\min_{z} \ f(z, \theta) \\ &s.t.\ g(z, \theta) \leq 0 \end{aligned} \tag{3}$$

2.1. Design under uncertainty

In most of the cases, the uncertainties are considered by plant are overdesign. The size of the equipment is considered with enough margin to guarantee

the feasibility of the design. There might be ad-hoc analysis that can be applied in order to check the flexibility and robustness of a design [8].
The transformation of problem of equation (3) into a deterministic equivalent is not unique, and will reflect the philosophy adopted to handle uncertainty. We present below several formulations of deterministic equivalents for design problems. For sake of simplicity of notation, we consider that there are no correlations on the uncertain parameters and that the binary variables are included in z.

2.1.1. Expected value minimization

If no distinction is made between the design and the operating variables, the problem of the expected value minimization can be solved:

$$\min_{z} \; E(\theta_u) \{ f\left(z, h^*(z,\theta), \theta\right) | g\left(z, h^*(z,\theta), \theta\right) \leq 0 \} \tag{4}$$

This formulation does not take into account the fact that the operating conditions can be adapted during operation.

2.1.2. Optimization on worst case

The objective function can be optimized on the worst case using a min-max strategy:

$$\begin{aligned} &\min_{z} \; \max_{\theta_u} \; f(z, h^*(z,\theta), \theta) \\ &s.t. \; g(z, h^*(z,\theta), \theta) \leq 0 \end{aligned} \tag{5}$$

Here also, no advantage is taken from the fact that the operating conditions can be adapted.

2.1.3. Stochastic programming

The principle of the formulation is to take advantage of the fact that operating variables can compensate uncertain parameters. This leads to a two-stage stochastic programming considers the expected value of the cost as the objective function (first stage optimization), allowing control with operating variables (second stage optimization):

$$\begin{aligned} &\min_{z_v, z_d} \; E(\theta) \{ \min_{o} \; f(z_v, z_d, h^*(z_v, z_d, z_o, \theta), \theta) \\ &s.t. \; g(z, h^*(z_v, z_d, z_o, \theta), \theta) \leq 0 \} \end{aligned} \tag{6}$$

The resolution of this problem requires the computation of the expected value. This can be a difficult task, especially if there is no simple analytical form of the model. The expected value is therefore often computed by sampling the space of the uncertain parameters and approximating the integral by a weighted sum. This is similar to the scenario approach explained below.

One problem that appears in stochastic method is that it runs the model for each sample what can imply very long time of calculation. Some method have been developped [16] to avoid this by sample reweighting and to transform a MINLP in MILP.

3. Studied system

A Solid Oxyd Fuel Cell coupled with a gas turbine has been modeled as presented in [10]. The system includes:

- Fuel processing, to produce syngas through partial oxydation or steam to methane reforming.
- Fuel cell (SOFC).
- The post-combustion to burn the fuel left in the fuel cell outlet.
- The gas turbine to recover energy from post-combustion.

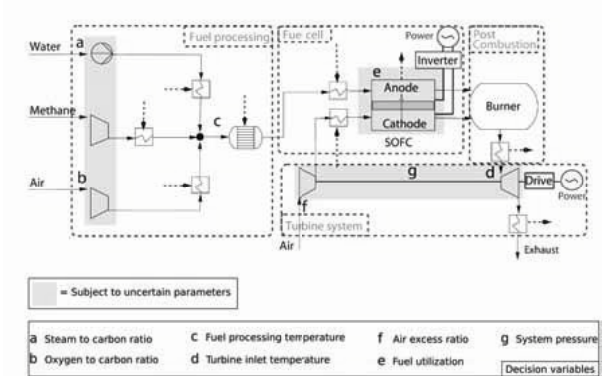

Figure 1: Simplified scheme of the SOFC-gas turbine system

4. Methods for optimal design under uncertainty

4.1. Introduction

In many cases, a basic sensitivity analysis is performed in order to study the influence of uncertain parameters one by one.However, this approach covers only a small part of the uncertain parameters domain. Then, three ways to include uncertainty in optimization have been studied:

1. Monte-Carlo simulation strategy(in grey in figure 2): In this case, the Monte Carlo method is used to generate randomly values of the uncertain parameters. The Monte Carlo simulation is applied a postertiori on one or more points of the Pareto set $z_{opt}(\hat{\theta_u})$. This allows one to study uncertain parameters sensitivity on the calculated performances $Y\left(z_{opt}(\hat{\theta_u}), h^*\left(z_{opt}(\hat{\theta})\right), \theta\right)$.
2. Stochastic optimization (in grey dotted line in figure 2): In this case the uncertain parameters are randomly generated when evaluating the model. This allows one to generate a Pareto set $z_{opt}(\theta)$ and compare the results obtain in comparison with the results obtained applying the optimization using the mean values of the uncertain parameters . This allows one to study the impact uncertain parameters on the optimal decision set.
3. Multi-period computation (in black dotted line in figure 2): In this case, scenarios of appearance of the uncertain parameters are generated using sampling methods. The probability of appearance is considered in the analysis as the equivalent period duration during which the process will see the value of the uncertain parameters. This allows to include in the design procedure every possible realization of the uncertain parameters and therefore propose flexible designs.

4.2. Monte-Carlo simulation

The first way of assessing the influence of the uncertain parameters is to calculate the performances of optimal Pareto set $z_{opt}(\hat{\theta})$ calculated for the most probable value of the uncertain parameters ($\hat{\theta}$) using a Monte-Carlo simulation applied on the uncertain parameters (θ). For each member of the Pareto set ($z_{opt,i}(\hat{\theta})$) the system performances are recalculated for randomly generated realisation of the uncertain parameters set (θ). By this way, we obtain for each member of the Pareto set the values of the performances of the system calculated by $Y(z_{opt,i}(\hat{\theta}), h^*(z_{opt,i}(\hat{\theta})), \theta)$. This calculates for each set of decision variables in the Pareto set a cloud of performances that represents the influence of uncertainties of a given design.
However, it has been shown [**?**] that this approach have some defaults:

- Uncertainy are considered in the optimization procedure *a posteriori*
- Optimization is already a huge computing task. Recomputing clouds containing enough points

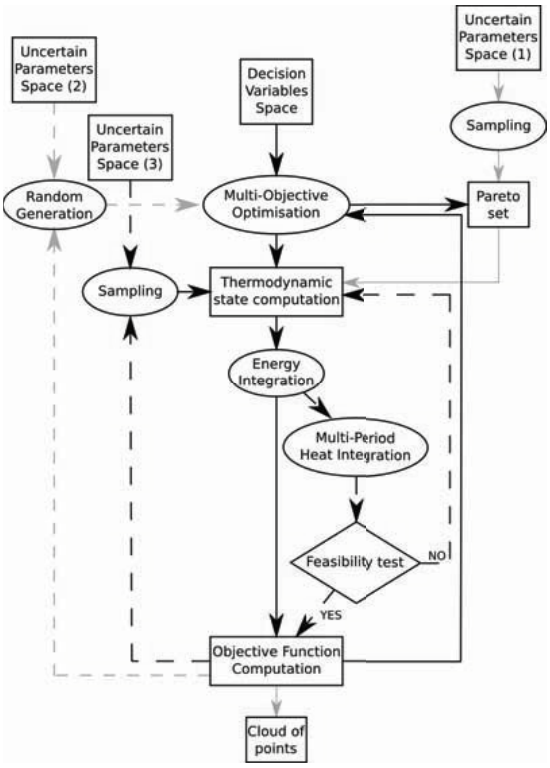

Figure 2: Method algorithm

to be representative of the uncertain parameters space becomes almost infeasible.

- Due to surjective nature of the problem, it becomes hard to extrapolate the value of a performance to appear.

This last point underlines the problem of representativity. If Y is the objectives corresponding to the set of uncertain parameters $\theta_u^1 = [\theta_{u,1}...\theta_{u,n}]$, and if two of these parameters $\theta_{u,l}^1$ and $\theta_{u,m}^1$ have opposite effect on the objectives, new values $\theta_{u,l}^2$ and $\theta_{u,m}^2$ can be defined so that the objectives doesn't change:

$$Y_1 = Y_2 \Rightarrow f(z_1, \theta_c^1, \theta_u^1, o_1) = f(z_1, \theta_c^1, \theta_u^2, o_1)$$
$$s.t.\ \theta_u^2 = [\theta_{u,1}^1, ..., \theta_{u,l}^2, \theta_{u,m}^2, ..., \theta_{u,n}^1] \tag{7}$$

Then if $\theta_{u,m}$ and $\theta_{u,n}$ are discrete, the probablility to get given perfomances for a fix design is:

$$p_{tot} = \sum_{i=1}^{n_s} p(\theta_u^i) \quad | \quad Y_i = Y_s \tag{8}$$

Whith n_s, the number of set θ_u leading to objectives Y_s. In case of continuous variables, the sum in

equation (8) is expressed as an integral. The question of reprentativity becomes then more important. However, it is possible to formulate the problem of sampling as a multi-objectives problem using representativity and sample size as performance indicator [19]. Despite this approach, monte-carlo simulation remains highly time and memory consuming.

4.3. Stochastic optimization

The method that has been defined is represented in figure 3. A classical evolutionary algorithm generate randomly decision variables, send them to the model and calculate the corresponding objectives. This is done several times so that all the calculated points constitute a generation. The best elements (*i.e.* those with the best objectives) of this generation (parents) are used to generate decision variables of the next generation (children). In order to include uncertainty in the optimization procedure, at each iteration, uncertain parameters are picked randomly in their possible range.

First, a conventional approach has been used

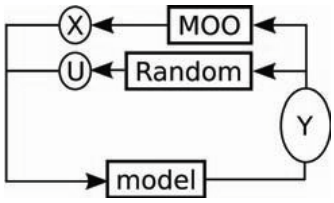

Figure 3: Stochastic optimization

(in black in figure 4). In that case, each uncertain parameters have been used at their most probable value $\hat{\theta_u}$, giving the perfomances $Y(z_{opt}(\hat{\theta_u}), h^*(z_{opt}(\hat{\theta_u})), \hat{\theta_u})$. The shape of each point (square, triangle, circle, diamond) represents the different clusters.

The Pareto curve represented in white is the one calculated with the method described in figure 3. It appears that this "random" optimization gives better results since some uncertain parameters (like efficiency) will lead to better performances than the conventional approach can reach.

Both problems have been solved with the same number of evaluation (10^4). Due to the stochastic nature of the problem the Pareto set obtained by stochastic optimization is less "converged" than the one of the conventional approach using $\hat{\theta}$.

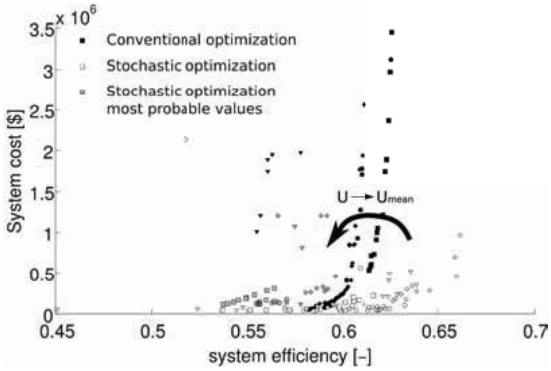

Figure 4: Comparison of "classical" (in black) and stochastic (in grey) multi-objective optimization

There is two different ways of comparing the solutions obtained with this procedure. The first one is to apply the Monte Carlo simulation as presented in section 4.2. on the reference Pareto set. This apporach is time consuming and will not necessarily lead to comparable results due to the stochastic nature of the method.

The second way of comparing the results is to recompute the Pareto front ($z_{opt}(\theta)$) obtained by the stochastic optimisation using the most probable realization of the uncertain parameters, i.e.calculate $Y(z_{opt}(\theta), h^*(z_{opt}(\theta)), \hat{\theta})$. This third Pareto curve is presented on figure 4 under reference "Stochastic optimization most probable values"

It can be seen that the stochastic optimisation leads to a Pareto that is worse than the one obtained by the conventional approach. This explains by the fact that some the members of the Pareto set have been selected based on randomly selected events. The difference between the two curves shows the impact of the uncertain parameters on the expected design performances.

In process engineering design, the expected result concern the specification of the investment in terms of equipments selection, their corresponding sizes and the interconnections. It is therefore interesting to analyze if the incorporation of uncertainty in the optimization procedure changes the decisions that will be taken. This can be done by comparing the values of design decisions between the two Pareto sets. As an example, figure 5 shows that design decisions may differ from one case to the other. In the Pareto set of the conventional design method, the fuel cell design pressure is decreased when the ef-

ficiency is increasing. This is not the case for the stochastic Pareto set for which the operating pressure of the fuel cell should remain high if we consider the uncertainties.

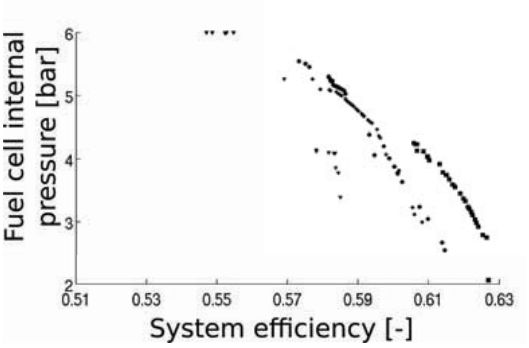

(a) "Conventional" optimization

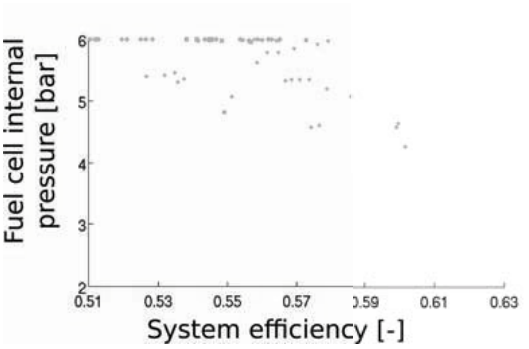

(b) Stochastic optimization

Figure 5: Fuel cell operating pressure in the hybrid system

5. Conclusion and further work

In this paper, methods have been studied to include uncertainties in an energy system design procedure. Limits of the monte-carlo simulation have been exposed. They are mainly the problem of surjectivity, the fact that its computation is highly time and memory consuming and the separation of optimization and uncertainties in the procedure.
Then, a stochastic problem has been formulated so as to include uncertainties in the optimization. It has been shown that uncertainties leads to different decision and that they leads to worst performances when computing the stochastic solution with $\hat{\theta_u}$ instead of θ_u.

The previously presented method allows one designing processes for a given randomly generated realisation of the uncertain parameters. In reality, one could consider that some of the uncertain parameters have a given probability to appear over a typical period of the process, which can be a cyclic phenomenon like for the temperature in a whole year or a lifetime. In the presented example it may concern:

- the efficiency of an equipment that can be influenced by the equipment production process.
- the material degradation that leads to degradation of the expected performances with time
- the market cost that have seasonal variations as well as market rules related variations.
- the energy services demands for example the heat/electricity demand for a cogeneration system

Then, the range of each uncertain parameter $[\theta_u - \sigma_1, \theta_u + \sigma_2]$ can be sampled in N part θ_u^i. Each θ_u^i correspond to a given probability $p(\theta_u^i)$ with $\sum_{i=1}^{N} p(\theta_u^i) = 1 - \varepsilon$. This can be translated as follow: A typical period t_{tot} can be devided in N period so that the variable θ_u will spend a time t_i at a state θ_u^i. This time is given by:

$$\frac{t_{tot}}{t_i} = \frac{1}{p(\theta_u^i)} \tag{9}$$

It becomes then possible to define a problem formulation to optimize the control strategy with operating variables z_o for each optimal point z^j ($j = [1, n]$]) of the Pareto.

$$\min_{z_o^i} \sum_{i=1}^{N} p(\theta_u^i) \cdot t_{tot} \cdot f(z_v^i, z_d^i, z_o^i, \theta_u^i) \tag{10}$$

Nomenclature

z	decision variables
z_v	design variables
z_d	decision variables
z_o	operating variables
d	dependent variables
Y	vector of objectives value
n_s	number of different uncertain variables set that leads to same perfomances
N	number of period
n	number of point in the Pareto

Greek Letters

θ_c certain parameters of the model

θ_u uncertain parameters of the model

$\hat{\theta}_u$ most probable value of θ_u

Subscripts and superscripts

opt optimal, *i.e.* corresponding to solution proposed in the Pareto curve

References

[1] J. Acevedo and E. N. Pistikopoulos. Stochastic optimization based algorithms for process synthesis under uncertainty. *Computers & Chemical Engineering*, 22(4-5):647–671, 1998.

[2] D. Bertismas and M. Sim. The price of robustness. *Operations Research*, 52(1):35–53, 2004.

[3] John R. Birge and Francois Louveaux. *Introduction to Stochastic Programming*. Operations Research. Springer, 1997.

[4] U. M. Diwekar and E. S. Rubin. Stochastic modeling of chemical processes. *Computers & Chemical Engineering*, 15(2):105–114, 1991.

[5] Y. Fu and U. M. Diwekar. An efficient sampling approach to multiobjective optimization. *Annals of Operations Research*, 132(1-4):109–134, 2004.

[6] I. E. Grossmann and K. P. Halemane. Decomposition strategy for designing flexible chemical-plants. *Aiche Journal*, 28(4):686–694, 1982.

[7] I. E. Grossmann and R.W.H Sargent. Optimum design of chemical plants with uncertain parameters. *Aiche Journal*, 24(6):1021–1028, 1978.

[8] I. E. Grossmann and David A. Straub. Recent developments in the evaluation and optimization of flexible chemical processes. In *COPE91*, page 41. Elsevier, 1991.

[9] K. P. Halemane and I. E. Grossmann. Optimal process design under uncertainty. *Aiche Journal*, 29(3):425–433, 1983. Times Cited: 114 Article English Cited References Count: 11 Qt999.

[10] Diego Larrain, Francois Marechal, Nordhal Autissier, and Daniel Favrat. Methodology for computer aided desing of sofc repeat element. 2004.

[11] P. Linke and A. Kokossis. On the robust application of stochastic optimisation technology for the synthesis of reaction/separation systems. *Computers & Chemical Engineering*, 27(5):733–758, 2003.

[12] L. Painton and U. M. Diwekar. Stochastic annealing for synthesis under uncertainty. *European Journal of Operational Research*, 83(3):489–502, 1995.

[13] E. N. Pistikopoulos and I. E. Grossmann. Optimal retrofit design for improving process flexibility in linear-systems. *Computers & Chemical Engineering*, 12(7):719–731, 1988.

[14] E. N. Pistikopoulos and M. G. Ierapetritou. Novel-approach for optimal process design under uncertainty. *Computers & Chemical Engineering*, 19(10):1089–1110, 1995.

[15] W. C. Rooney and L. T. Biegler. Incorporating joint confidence regions into design under uncertainty. *Computers & Chemical Engineering*, 23(10):1563–1575, 1999.

[16] Y. Shastri and U. M. Diwekar. An efficient algorithm for large scale stochastic nonlinear programming problems. *Computers & Chemical Engineering*, 30(5):864–877, 2006.

[17] D. A. Straub and I. E. Grossmann. Design optimization of stochastic flexibility. *Computers & Chemical Engineering*, 17(4):339–354, 1993.

[18] Karthik Subramanyan, U. M. Diwekar, and Amit Goyalb. Multi-objective optimization for hybrid fuel cells power system under uncertainty. *Journal of Power Sources*, 132:99–112, 2004.

[19] Z. Wuillemin, D. Demierre, H. Becker, M. Dubuis, V. Chenaux, and L. Girardin. Optimisation d'un plan d'expérience à l'aide d'un algorithme génétique: Application à un modèle de pertes pour microturbine. Technical report, LENI-EPFL, Lausanne, 2009.

Mixed Integer Linearized Exergoeconomic (MILE) method for energy system synthesis and optimization

Mauro Reini[a], *Dario Buoro*[b]

[a] *Dept. Of Mechanical Engineering, University of Trieste, Italy*
[b] *Dept. of Energy and Turbomachinary, University of Udine, Italy*

Abstract: The aim of paper is to present an energy system optimization method, based on the Fuel Impact Formula, able to overcome typical limitations of previous formulations. In particular, the methodology allows time dependent production levels to be considered and on-off operation and presence-absence of any component to be modelled by means of binary decision variables and inequality constraints. These often happen if the synthesis and operation of Combined Heat and Power (CHP) systems are considered at the same time. Moreover, the effect of replacing actual not linear thermodynamic inputs-output relations of each component with linear, or even proportional ones, is highlighted in the paper. Finally, an example of application is shown, dealing with a multi-component DH and CHP system in the tertiary sector.

Keywords: Optimization, thermoechonomics, cogeneration, district heating network.

1 Introduction

A deeper integration among energy systems is expected to significantly contribute to reducing primary energy consumption, as well as global pollutant emissions and the energy costs for final users. Examples of this trend may be found in Combined Plants (gas + steam, engine + Rankine, etc.), District Heating (DH) networks with multiple thermal sources, Combined Heat and Power (CHP) and Combined Heat Cool and Power (CHCP) systems. Integrated DH and CHP are of particular interest and are widely discussed in Literature [1-9]. In practical application, the advantage of energy integration can be actually obtained only if the structure (synthesis) and the management of the whole system are carefully optimized.

Synthesis and operation optimization of integrated multi-component energy systems generally require a binary variable set to be introduced to describe the existence/absence and the on/off operation status of components and energy connections inside the model. Besides these, other continuous variables have to be introduced for modelling the energy and material flows exchanged among components, as well as other possible design options.

In addition to this complex variable set, the variation of the thermal demands of the final users has also to be taken into account. Thus, a Mixed Integer Non Linear Programming (MINLP) problem has generally to be solved for obtaining the optimal synthesis and operation of the integrated system, with a high computational effort.

The computational effort can be reduced if the whole problem is decomposed in a set of (smaller) sub-problems. In this way, each sub-problem can be solved dealing with a reduced number of independent variables, even if a certain degree of approximation in the optimal solution has to be accepted. Moreover, an iterative procedure has to be defined and many problems have to be solved, than only one [Michael b, c]. The solution would be easier obtained if the problem could be described with sufficient precision by means of a linear model, even if additional variables had to be introduced for consider strong non-linear relations among energy and material flows [1-3,7-9].

On the other hand, information about the cost formation process of internal flows and of final products is very useful when dealing with complex energy systems design and optimization [10-13]. In fact, knowing the cost formation process allows identifying how and where the energy and economic resources are consumed by the system, to obtain the final products. Optimization just consists in selecting the structure and the operation strategy for the whole system allowing the energy user demands to be satisfied, with a minimum consumption of energetic and economic resources.

Different kind of internal costs have been defined in the ambit of Thermoeconomics (marginal, average, shadow costs); relations among them are widely discussed in Literature [14-17]. The aim of the paper is to propose an optimization method that takes advantage from the

Corresponing Author: Mauro Reini, e-mail: reini@units.it

information contained in the cost formation process and possibly from the linear formulation of the model, allowing the problem to be decomposed consistently with the physical structure of integrated DH and CHP systems and with the energy demands of the final users.

In 1994 a complete differential versions of the Fuel Impact and the Cost Impact Formulae (FaCIF) [18, 19] were presented in the frame of the Exergy Cost Theory. The next year, it was proven that these formulae can be used to define both a thermodynamic or thermoeconomic optimization procedure and hypotheses were explicitly stated, under which the procedure is analogous to other methods, named "Functional Analysis", presented during the 80s [20, 21]. In particular, Impact Formula based optimization procedure also allows the whole problem to be decomposed into sub-problem, each one having a reduced number of decision variables. Nevertheless, Impact Formula based optimization procedures were affected by the following limitations: i) Design load level only is taken into account; ii) Binary decision variables are not explicitly considered; iii) Proportional inputs-output relations are assumed a priori to be consistent with component thermodynamic models.

The aim of Mixed Integer Linearized Exergoeconomic (MILE) optimization method is to overcome these limitations, allowing the Impact Formula based optimization procedure to be applied also in cases where variable load operation has to be considered, or where on-off operation and presence-absence of any component have to be modelled by means of binary decision variables.

2 Fuel impact formula revised

To fix ideas, let's first consider a steady state operation of a multi-component energy system, keeping in mind in the following that its Total Fuel (F_T) has to be regarded as the whole consumed energetic and/or economical resources. FaCIF is based on the so called Productive Structure (PS) of the plant, where components are connected by flows describing their productive relations with other components and with the outside the plant. In the PS each component is regarded, at local level, as an autonomous production unit, having one output flow named Product or *Function* and one or more input flows named Fuels or internal resources. In other words, a sort of *local model* of each component has to be isolated from the whole plant thermodynamic model and has to be expressed in analytic form.

Each flow E_i describing *productive relations* among components has to be defined on the basis of heat, work and mass flow rates and of thermodynamic conditions of working fluids inside the plant. From a mathematical point of view, the choice of the analytic formulation is free and is left to the Analyst. If exergy flows were used to describe the productive relations inside the system, additional information could be obtained about losses inside each control volume and about distance from reversibility of each energy conversion process [14, 15, 22, 23]. Nevertheless, the definition of a linear model can be simplified sometimes by using energy flows based descriptions.

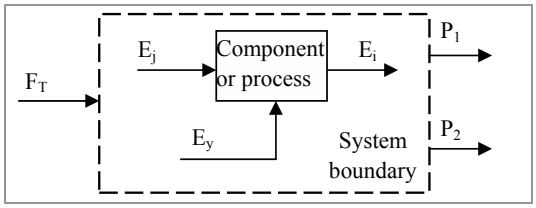

Figure 1: The local model of a generic single-product component.

Let's suppose that the global model of the whole system is available. In this model each exergy / energy or cost flows in the PS (E_i) can be expressed as a function of an independent variables set ($\boldsymbol{\tau}_T$), made with all continuous or binary independent variables necessary to describe the behaviour of the specific component (or control volume) obtaining that flow as a Product.

The *local model* of a general single-product component (see figure 1) can be first formulated as shown in the left hand side below, by operating a simple variable change, i.e. by identify the Product as one of the local independent variables:

$$E_i = f_i(\tau_i) = f_i(\tau_1, \tau_{T-1}) \Rightarrow f_i^{-1}(E_i, \tau_{T-1})$$
$$E_j = f_j(\tau_T) = f_j(f_i^{-1}(E_i, \tau_{T-1}), \tau_{T-1}) \Rightarrow$$
$$E_j = f_j^{+}(E_i, \tau_{T-1})$$
$$E_y = f_y(\tau_T) = f_y(f_i^{-1}(E_i, \tau_{T-1}), \tau_{T-1}) \Rightarrow$$
$$E_y = f_y^{+}(E_i, \tau_{T-1}) \quad (1)$$

The hypothesis that a component has to have one and only one Product is widely applied in Literature. The choice of a single outgoing flow, representing the purpose, or the *Product* of the component, makes easier the economic interpretation of the PS. The problem of multi-product components can be summarised in the following two cases:

In the first case the apparent second product is an outgoing flow from a control volume having its main product, but the second product is not independent for

the main one, i.e. the two products depend on the same degree of freedom of the component. In this case the second product is a sub-product or a residue, according if its production implies a reduction, or an increase of total fuel consumption, respectively, at global level. The cost formation process of by-products and residue in the ambit of the ECT is discussed in [24, 25]. The heat cogenerated by an internal combustion engine can be regarded as an example of sub-product (when it is supplied to thermal users), or of residue (when it is not). Then, sub-product and residue have to be dealt with as they were local resources (with negative or positive cost, respectively), even if the flow direction is from the inside to the outside the control volume.

In the second case, inside the multi-product component an internal PS could be defined, where each sub-component obtains only one product [14].

The previous local model formulation, expressing local resources as well as sub-product and residue vs. the local product, can be linearized, with the aim of building a linear constraint set for the optimization problem, obtaining the Local Linear Model (LLM).

$$E_j = \mu_{ij}(\tau_{T-1}, E_i)E_i + \theta_j(\tau_{T-1}, E_i)$$
$$E_y = \mu_{iy}(\tau_{T-1}, E_i)E_i + \theta_y(\tau_{T-1}, E_i) \quad (2)$$

In these relations the coefficients of the linearizations are regarded as functions of the product too. This is the general case. But, if the production level variations are restricted inside an interval where a specific linear relation is acceptable, the linearization coefficients can be regarded being independent from the production level of the component. This property of the LLM is expected to be an important advantage in the application of the MILE optimization procedure, described in the following. Thus, recollecting the LLMs of all components and nodes (junctions and branches), the minimum resource consumption (energetic and/or economic) can be obtained as the solution of the following MILP problem (expressed in matrix form):

$$\text{min. } F_T = {}^{t}\mathbf{c}_e \cdot \mathbf{E} \quad (3)$$
$$\mathbf{E} = {}^{t}\mathbf{M}\mathbf{E} + \mathbf{Q} + \boldsymbol{\omega} \quad (4)$$
$$\mu_{ij} = f_{ij}(\tau_{T-1}) \quad (5)$$
$$\theta_i = g_i(\tau_{T-1}) \quad (6)$$

Where $\mathbf{c}_e$ and $\boldsymbol{\omega}$ are vectors containing the unit cost of external resources and the amount of the required final products, respectively, as it is common used in the Thermoeconomic Literature.

M is a square matrix and **Q** is a vector containing the linearization coefficients μ and θ, respectively, where these latter depend on both continuous and binary independent variables of the system. In both the ECT [15] and the Structural Theory of Thermoeconomics (ST) [28] an equation very close to Eq. 4 is presented. In particular, vector **Q** is assumed to be always null, while matrix **M** is named **K**, or $|\mathbf{EG}\rangle$. In the ambit of Thermoecomics Eq. 4 has always one solution only, because the productive relations (analogous to eq. 1, 2), jointly with the fixed values of all independent external products of the system, they completely define the state of the system, once that the coefficients μ (or μ and θ, if the latter is not forced to be zero) have been calculated consistently with the thermodynamic model of the system (see, for instance, [15]).

The situation may be quite different in an optimization problem, because different internal flows arrangements may be possible, even if all coefficients in the productive relations are constants, and finding the best arrangement is exactly the optimization object. On the other hand, when the optimal solution were calculated, the corresponding state of the system would be identified, as well as all internal flows and final products. Taking into account the linear nature of the problem, the optimal solution has to be a vertex of the feasible polyhedron, inside the domain region (see, for instance, [27]). In effect, additional constraints have to operate in the optimization problem: they are the inequality constraints that are certainly required, in order to limit the range inside which the linear productive relations are valid. In the optimal solution, *active* inequality constraints have to be sufficient to make defined the state of the system, all internal flows and final products. Therefore, the LLMs of all components and nodes (Eq. 4) would be still valid, provided that the rows of the matrix **M,** which express the magnitude of flows subject to the optimization, were replaced by the active inequality constraints.

Also note that actual active constraints can be usually known only when the problem is already solved. But this apparent contradiction can be overcame, because the complete definition of matrix **M** could be carried out when a local sub-problem were solved, not the complete optimization problem. This is consistent with the target of the paper, that is to define a proper decomposition of the whole problem and with the perspective of using an iterative, heuristic procedure.

Let's finally introduce the production level variation with time. In Literature this issue is usually dealt with by properly discretizing the demands curves, so that the production level can be regarded as constant in each time interval. This approach is applied also in the MILE optimization method. In some cases this may lead to the favourable situation that each time interval can be

solved independently from the others (reaching the so called time decomposition, see, for instance [28]). But this is not the general case, because all independent variables expressing the existence / absence of components and connections certainly couple many time intervals.

On the basis of previous consideration, the whole MILP problem can be formulated as:

$$\min. F_T = \sum_{h=1}^{h=H} {}^t\mathbf{c}_e(h)\,\mathbf{E}(h) \quad (7)$$

$$\mathbf{E}(h) = {}^t\mathbf{M}\mathbf{E}(h) + \mathbf{Q} + \boldsymbol{\omega}(h) \quad (8)$$

$$E_i \le P_{\max i}(h) \quad (9)$$

$$E_i \ge P_{\min i}(h) \quad (10)$$

$$\mu_{ij} = f_{ij}(\tau_{T-1}, h) \quad (11)$$

$$\theta_i = g_i(\tau_{T-1}, h) \quad (12)$$

Let's suppose that a feasible solution were available (when dealing with energy systems integration, a feasible solution can be easily obtained by considering autonomous systems). A variation in the objective function F_T can be expressed rearranging the total derivative of eq. 7, taking into account linearization coefficients behaviour (eq. 11, 12) and recalling that matrix **M** has to be integrated with active inequality constraints only, in order to allows the calculation of flows in vector **E**. Except for the latter warning, the procedure is very similar to that presented in [14], where additional details can be found. In this way the revised formulation of the FaCIF is obtained:

$$dF_T = \sum_{h=1}^{h=H}\left[{}^t\mathbf{E}(h)\cdot d\mathbf{M}(\tau_T, h)\cdot\boldsymbol{\lambda}(h) + {}^t\boldsymbol{\lambda}(h)\cdot d\mathbf{Q}(\tau_T, h) + \sum_n^{n_u}\lambda_u(h)\cdot d\omega_u(h)\right] \quad (13)$$

$$\boldsymbol{\lambda}(h) = \left[\mathbf{U}_D - \mathbf{M}_{(\tau_T,h)}\right]^{-1}\cdot\mathbf{c}_e(h) \quad (14)$$

Eq. 14 corresponds to the structural cost formulation, obtained by Valero – Lozano – Serra [29] through a lagrangian procedure, when a single time interval is considered and vector **Q** is equal to zero.

In Literature it has been demonstrated [14, 29, 30, 31] that the dual (called also marginal, or shadow) costs of the flows **E** do coincide with the structural costs (**k***), under the hypotheses of using not only the same thermodynamic and cost model, but also the same Productive Structure. It can be analogously demonstrated that costs $\boldsymbol{\lambda}$ in Eq. 14 are the dual costs of the restrictions expressed by Eq. 8. Note that this is consistent with the KKT conditions [32], when active constraints only have a positive Lagrange multiplier and concur to the system state definition. Therefore costs $\boldsymbol{\lambda}$ too have to be regarded as the dual (or marginal, or shadow) costs of flows **E.** This apparent inconsistency of different cost with the same meaning can be easily explained: the structural costs (**k***) are the dual costs obtained when the unit resources consumptions are kept constant, even if this were not consistent with possible inequality constraints, while the dual costs $\boldsymbol{\lambda}$ are obtained keeping constant the linearization coefficients and taking active inequality constraints into account. This latter kind of costs is expected to be much more stable in the neighbourhood of a feasible solution. Moreover, if constraints in Eq. 8 are actual linear with respect of all flows **E**, the dual costs $\boldsymbol{\lambda}$ have constant values and they may change only if independent variable ($\boldsymbol{\tau}_T$), or active inequality constraints, vary.

On the other hand, the structural costs (**k***) can be calculated from a single state of the system, while the dual costs $\boldsymbol{\lambda}$ can be obtained only through an actual linearization of the cost and energy model.

3 Mile optimization method

Putting Eq. 13 in scalar form is the key for a complete disaggregation of the whole model. Without losing generality, let's think the time profiles of the final products (**ω**) to be unchanged. The total fuel variation now appears as a triple summation, on components and nodes (*i*), local resources consumed by each component (*y*) and time intervals (*h*):

$$dF_T = \sum_{h}^{time}\sum_{y}^{resource}\sum_{i}^{comp.}\lambda_{iy}(h)\cdot \left[d\mu_{iy}(\tau_{T-1}, h)\cdot E_i(h) + d\theta_{iy}(\tau_{T-1}, h)\right] \quad (15)$$

Note that the variations of the linearization coefficients depend on both continuous and binary independent variables of the whole system and are still affected by active inequality constraints, as well as the costs $\boldsymbol{\lambda}$. Nevertheless, the hope is that a set of independent variables affect mainly (if not only) a set of component, or of time intervals. To fix ideas, let's go on taking into account a problem decomposed in two sub-set of components, being straightforward the extension to three or more sub-set. Since the two sub-set are part of a unique integrated system, there will be some productive relations (E_i) coupling the two sub-set each other.

Step1. Define a feasible solution for the whole system, and calculate the production relations $\mathbf{E}^0$.

Step 2. Than active inequality constraints are known and costs $\boldsymbol{\lambda}$ can be calculated. Moreover, a sensitivity analysis can be performed by varying the production level of the coupling flows (for each time interval), so that the relation λ_i vs. E_i can be obtained for each coupling flow. In this step, a preliminary re-arrangement of time intervals, which allows that all similar situations are dealt with as they were the identical repetition of a typical time interval, may be

crucial for a proper calculation of costs $\boldsymbol{\lambda}$. In the following case study, a typical day of operation has been introduced in order to reduce the number of independent variables and to enhance the effect on the objective function of a variation in the production level related to a specific time interval.

Step 3. With the costs $\boldsymbol{\lambda}$ obtained in the previous step, Eq. 15 can be decomposed in two independent summations, each of them corresponds to an optimization problem of the following kind (subscript A refer to sub-set A):

$$\min. F_T = \sum_{h=1}^{h=H} {}^t\boldsymbol{\lambda}_A(\mathbf{E}_A, h) \cdot [\mathbf{E}_A(h) - \mathbf{E}_A^0(h)] \quad (16)$$

$$\mathbf{E}_A(h) = {}^t\mathbf{M}_A\mathbf{E}_A(h) + \mathbf{Q}_A + \boldsymbol{\omega}_A(h) \quad (17)$$

$$\lambda_{Ai} = f_{Ai}(E_i, h) \quad (18)$$

$$E_i \le P_{\max i}(h) \quad (19)$$

$$E_i \ge P_{\min i}(h) \quad (20)$$

$$\mu_{ij} = f_{ij}(\tau_{T-1}, h) \quad (21)$$

$$\theta_i = g_i(\tau_{T-1}, h) \quad (22)$$

From these optimizations, a different production level is obtained for each sub-set of components ($\mathbf{E}^1$). Note that Eq. 18 is expected to be a discontinuous function, because the cost λ_{Ai} could vary if a different set of inequality constraints became active, or if binary decision variables changed, as the production level E_i increases / decreases. To avoid discontinuous, not-linear functions (or their complex multi-linear approximations, where additional binary variables could be used) Eq. 18 can be replaced by a constant value of the cost λ_{Ai}, obtained as an average value over a proper interval for the production level E_i. This second option has been adopted in the case study.

Step 4. Each sub-set is re-optimized, taking the new production level into account. In this way, a new feasible solution is obtained and the iteration starts again from Step 2. The iterations can stop when feasible solutions obtained in two subsequent steps 4 are quite close, or when the objective function F_T becomes stable.

4 The applied model formulation

The optimization of a district heating network is grounded on a basic concept: the optimal design can be determined only knowing the realistic operation conditions that result from an hourly optimization of each unit. Depending on the price of energy (electric energy and gas) and on the energy loads, the optimal design of units and grid influence each other.

The MILE method allows the whole optimization problem to be decomposed in two, or more, sub problems, each of that related to a sub-set of components. In this case it allows solving with separately the problem related to the optimization of each CHP units and the optimization of the district heating network. In this way, solving problems with a lot of units and possible connections between buildings will be possible, reducing the computational effort with respect to the simultaneous solution of the whole problem [1].

To do this, making two different models is necessary that optimize first each isolated CHP unit, and then the heating network. The two models are reported in the following.

4.1 Unit optimization

In this section the description of independent variables and constraints of model that allows optimizing the design and managing of CHP unit shows, in figure 2, is given. The input parameters required from the model are the electrical demands that have to be supplied to the users, the thermal demands that have to be supplied to thermal nodes, the coefficients that express the performance curves of the CHP unit and the boiler, the cost of electric energy and gas and the capital costs of CHP unit. For simplifying the definition of a linear model, energy has been use to quantify production flows.

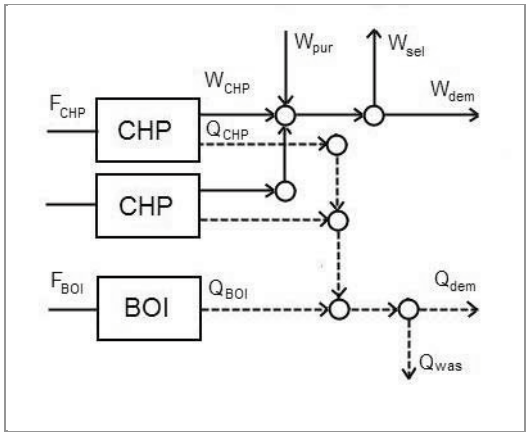

Figure 2: Scheme of CHP unit

4.1.1 Independent variables

The model independent variables represent the existence/absence ("**X**"), the hourly on/off ("**y**") and hourly load ($\mathbf{W_{CHP}}$) of each CHP Unit, the amount of hourly purchase electric energy ($\mathbf{W_{pur}}$) from the grid, and of wasted thermal energy ($\mathbf{Q_{was}}$). Obviously **X** and **y** are binary variables set, while the remaining are

continuous ones. Assuming to consider only 24 time interval and 2 CHP groups, the model has already 146 independent variables, or degrees of freedom, per final user. Those independent variables have to be multiplied for number of users. In the following the index *h, j,* and *k* indicate generic hour, CHP unit, and user respectively.

4.1.2 Objective function and constraints

The amortization factor used to define the capital annual cost is expressed by:

$$fa = \frac{(1+ir)^n}{(1+ir)^n-1} \quad (22)$$

The sum of capital costs are the costs of installed CHP groups unit only and is expressed by:

$$C_{inv} = \sum_k \sum_j (C_{CHP\ j,k} \cdot X_{j,k}) \quad (23)$$

In this case study, the purchase of boiler hasn't to be considered, assuming that they are already installed c/o in each user.

Maintenance cost of CHP groups is supposed proportional to annual amount of electric energy produced, and is expressed by:

$$C_{main} = \sum_k \sum_j \sum_h (W_{CHP\ h,j,k} \cdot f_{main}) \quad (24)$$

About the set of equality constraints represented by equation 17, only the main energy balances are reported below.

Electric balance:

$$W_{sel\ h,k} = \sum_j W_{CHP\ h,j,k} + W_{pur\ h,k} - W_{dem\ h,k} \quad (25)$$

Thermal balance:

$$Q_{BOI\ h,k} = \sum_j Q_{CHP\ h,j,k} - Q_{was\ h,k} - Q_{dem\ h,k} \quad (26)$$

Other equality constraints express relation of fuel consumption (F_{CHP}, F_{BOI}) vs. component load, relation between sub-products (Q_{CHP}) and main products (W_{CHP}), and so on, for each component.

The operating cost is express by:

$$C_{ope} = \sum_k \left(\sum_h \sum_j (F_{CHP\ h,j,k} \cdot CF_{CHP}) + F_{BOI\ h,k} \cdot CF_{BOI} + W_{pur\ h,k} \cdot C_{pur\ h,k} - W_{sel\ h,k} \cdot C_{sel\ i,k} \right) \quad (26)$$

The objective function to minimize, results as the sum of capital costs, maintaining costs and operating costs:

$$C_{year} = fa \cdot C_{inv} + C_{main} + C_{ope} \quad (27)$$

The inequality constraints represent in equation 19 ensure the physical feasibility of the problem. They also describe the operating field of CHP group and boiler, they enforce that CHP_j won't be able to start if it doesn't exist. Moreover, each independent variable has to be positive (more details about model can be found in [1].

$$W_{CHP\ min} \cdot y_{h,j,k} \leq W_{CHP\ h,j,k} \leq W_{CHP\ min} \cdot y_{h,j,k} \quad (28)$$

$$X_{j,k} \geq y_{h,j,k} \quad (29)$$

The hourly dual costs of thermal energy can be known only after minimizing the objective function. They are obtained keeping unchanged the electrical demands and varying the thermal ones. This operation has been made for every hour, for obtaining the trend of every dual cost, in every time interval. The trend of dual costs and the thermal demands are the link with the model that optimizes the district heating cooling network.

As an example, Figure 3 shows the trend of the thermal product dual cost for a CHP unit, like that shown in figure 2, in one time interval. In the area 1 no one CHP group is switched on and the thermal demand is supplied by boiler. In the area 2 group CHP_1 is switched on and some thermal energy is wasted. Reaching the limits of area 3, all thermal energy from group CHP_1 is used so that the further thermal load must be supplied by boiler. In area 4 both CHP groups are in operation and some heat is wasted. In area 5 all heat supplied by CHP groups is used and some electric energy is sold to the electric grid, reducing the heat dual cost. In the last area, both CHP groups work at full load and further thermal production may be obtained from the boiler only. Note that the previous considerations are affected by electric demand that has to be supplied to the final user. A map similar to figure 3 can be obtained for each thermal product and each time interval.

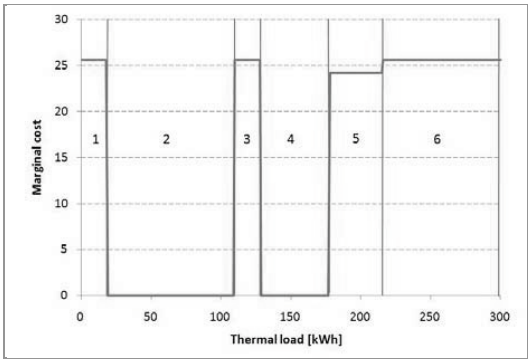

Figure 3: Marginal cost vs CHP unit thermal load in a time interval

4.2 DH-Network optimization

In this section the model that optimizes the district heating network is reported. The input parameters necessary to optimize this are the thermal demands that have to be supplied to the user, the marginal cost trends of each thermal products and the costs of the thermal network. Obviously, the latter depends on the distance among buildings. Figure 4 shows the scheme of three users that can be connected each other by a thermal network.

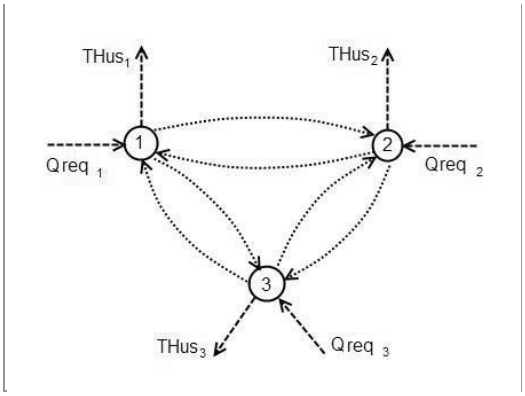

Figure 4: Scheme of the optimization problem of a DH network, with three nodes only, as separated from the CHP units

4.2.1 Independent variables

The model independent variables represent the existence/absence of each pipelines (**r**), the hourly thermal flows that have to be required from users ($\mathbf{Q_{req}}$), the hourly flows through each pipeline ($\mathbf{Q_{flow}}$) and the corresponding maximum flow ($\mathbf{D_{pip}}$). In this case only **r** are binary variables while the remaining are continuous ones.

4.2.2 Objective function and constraints

The amortization factor used to define the capital annual cost is similar to eq. 22, even if different amortization time for machines and network can be considered. The cost of grid per unit length is obtaining by summing a fixed cost (F1), related to the excavation, and a cost proportional to the size of the pipeline (according to a coefficient F2):

$$C_{pip\,k,v} = F1 \cdot r_{k,v} + F2 \cdot D_{pip\,k,v} \quad (30)$$

The cost of thermal flow can be expressed by:

$$C_{flow\,i,k} = \int_0^{Qreq} \lambda_{h,k}(Q_d) \cdot dQ_d \quad (31)$$

Then, the objective function to minimize is:

$$C_{net} = \sum_k \left(\sum_v C_{pip\,k,v} \cdot l_{k,v} + \sum_h C_{flow\,h,k} \right) \quad (32)$$

The main equality constraint that has to be introduced is the balance of each node:

$$Q_{req\,h,k} + Q_{flow\,h,k,v} - TH_{us\,h,k} - Q_{flow\,h,v,k} \cdot p_{v,k} = 0 \quad (33)$$

Where **p** express the thermal losses in each pipeline and are calculated through:

$$p_{k,v} = \frac{\delta \cdot l_{k,v}}{1000} \quad (34)$$

The main inequality constraints reported below express that thermal energy conveyed by a pipeline, in each time interval, has to be lower than its design maximum thermal flow, whereas the latter has to be included between a maximum and a minimum possible values.

$$Q_{flow\,h,k,v} \leq D_{pip\,k,v} \quad (35)$$

$$Dmin \cdot r_{k,v} \leq D_{pip\,k,v} \leq Dmax \cdot r_{k,v} \quad (36)$$

Optimizing this model the lay-out of district heating network and the new thermal demands ($\mathbf{Q_{dem}}$) are obtained. In the next iteration, $\mathbf{Q_{dem}}$ are the new input value for the CHP units optimization.

5 Case study

The previous model has been applied to a tertiary sector real case, that considers a theatre, a library and a primary school located in the centre of a north-east Italy small town. Hourly thermal and electrical demands, supplied by current owners, are shown in Figure 5 and Figure 6 for a typical mid-season day, that is the considered the typical day. Thermal losses among the district heating have been taken into account introducing a constant factor δ (eq. 34), that represent a percentage of lost flow during the switch, per unit length. A prudential factor of 15% has been considered in the model.

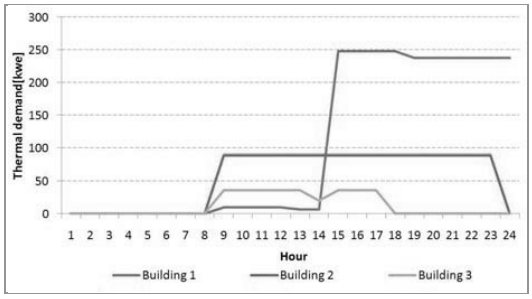

Figure 5: Thermal demand curves of considered users

Table 1 represents gas and electricity cost rates, machine capital costs, maintenance machine cost and cost coefficients (F1, F2) for the thermal network. According to Italian legislation, different values of prices for gas supplying microturbines and boilers have been assumed.

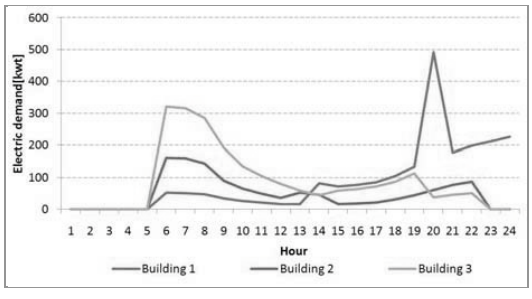

Figure 6: Electric demand curves of considered users

Bought and sold electric energy prices have been considered to be fixed. Installation and balance of plant cost per machine is supposed to decrease with the rise of installed machines number inside the same unit. Then, the first machine installed in a CHP unit is more expensive than the second one. The considered CHP groups are gas microturbines, model Capstone C60.

The optimization procedure has been carried out by a commercial software that allows solving each sub-problem. The control of the output is necessary to verify the convergence of the iterative procedure.

Table 1: Considered costs in the case study

Electric energy purchase cost (*CBUY*)	0.170	[€/kWh]
Sold electric energy price (*CSEL*)	0.044	[€/kWh]
Integration boiler fuel cost (CF_{BOI})	0.59	[€/m^3]
µTG fuel cost (CF_{CHP})	0.39	[€/m^3]
1st machine capital cost	120.000	[€]
2nd machine capital cost	90.000	[€]
Maintenance cost (G)	0,01	[€/kWh]
Fixed cost of excavation (F1)	270,63	[€/m]
Cost proportional to diameter (F2)	0,179	[€/m^3]

As introduced above, implementing the whole trend of marginal cost related to each thermal user demand would involve other binary variables, getting more complicated the problem and implying more computational efforts. The solution proposed by the authors is to calculate the marginal costs only near the operation point, without taking into account all possible range of variation. The proper interval has to be properly chosen to promote the convergence of the iteration procedure.

The marginal costs and the possible values for the thermal flows required by the network, in the interval $[Q_{dem}; Q_{dem}+\Delta Q]$, can be expressed as:

$$\lambda_{h,k} = \frac{C_{year}\left(Qdem_{h,k}+\Delta Q\right)-C_{year}\left(Qdem_{h,k}\right)}{\Delta Q} \quad (37)$$

$$Q_{req\ h,k} \in \left\{Q_{dem\ h,k}; Q_{dem\ h,k}+\Delta Q\right\} \quad (38)$$

In this case study, positive and negative ΔQs have to be assumed, involving two different λ for each hour and each thermal product. The latters can be simultaneously taken into account by introducing a multi-linear cost formulation, which implies only one addition binary variable. Doing this also the cost of thermal flow in the objective function (eq. 31) has to be changed:

$$C_{flow\ h,k} = \lambda_{h,k\ Q_{req}} \cdot \left(Q_{dem\ h,k} - Q_{req\ h,k}\right) \quad (39)$$

The iteration procedure is composed by steps that have to be followed to obtain the optimal solution.

Step 0

In this step the traditional cost is calculated. It can be obtained optimizing the model of CHP units, forcing that no-one CHP group is installed and assuming that $\mathbf{Q_{dem\ h,k}} = \mathbf{TH_{us\ h,k}}$. This cost will be considered as reference for the results presented below.

Step 1

In this step the optimization of CHP units is done. In the first iteration it is necessary to consider $\mathbf{Q_{dem\ h,k}} = \mathbf{TH_{us\ h,k}}$. In the further iteration $\mathbf{Q_{dem\ h,k}}=\mathbf{Q_{req\ h,k}}$, that will be obtained by the optimization DH-Network. The most significant results of this step are a new value of the objective function and the number of installed machines. The value of objective function has to be compared with the previous value, inferring if the problem is converging, or not.

Step 2

Starting with the solution of Step 1, the marginal costs $\boldsymbol{\lambda_{h,k}}$ of each the thermal demand $\mathbf{Q_{dem\ h,k}}$ can be calculated, after deciding the proper value of ΔQ. The previous $\boldsymbol{\lambda_{h,k}}$ and $\mathbf{Q_{dem\ h,k}}$ have to be compared with the current ones. If the they are different, a new solution will be find, if they are not, a previous solution has to be refined by diminishing the value of ΔQ.

Step 3

In this step the optimization of the DH-Network is done. Optimizing the DH-Network model, the optimal lay out and the cost of the network, and the new thermal requests for the CHP units are carried out. This new request $\mathbf{Q_{req\ i,k}}$ will be the input for the next step.

Step 4

Each CHP unit can be re-optimized taken into account a new production level request $\mathbf{Q_{req\ i,k}}$. Than the procedure can start again as in the Step 1.

Following the steps reported above, the results shown in Table 2 can be found. The iteration 0 concerns the conventional solution, the second is obtained for isolated users and since iteration 2 the network is introduced. Until iteration 4 the value of ΔQ is kept equal to 50 kWh, while in the further iteration its value is diminished, allowing to refine the solution.

Note that the integration between CHP groups and thermal district network allows diminishing the number of the installed machines and the total annual cost. More details about the energy and economic benefits of DH-CHP integrated systems for a case similar to that shown in this paper, can be found in [1].

Tabella 2: Main results of optimization performed with MILE method

			Iter. 0	Iter. 1	Iter. 2	Iter. 3	Iter. 4	Iter. 5	Iter. 6
CHP units opt.	Number of CHP group	unit 1	/	2	2	2	2	2	2
		unit 2	/	1	1	1	1	1	1
		unit 3	/	1	0	0	0	0	0
	Annual capital cost [€]		/	47.905	35.130	35.130	35.130	35.130	35.130
	Operative cost [€]		392.255	318.937	322.220	313.468	311.169	310.690	310.266
Network opt.	Pipeline maximum thermal flow [kW]	us. 1-us. 2	/	0	0	50	100	99	98
		us. 2-us. 3	/	0	50	102	141	141	141
		us. 3-us. 1	/	0	0	0	0	0	0
	Annual capital cost [€]		/	0	4.895	7.259	7.451	7.449	7.448
Value of ΔQ [kWh]			/	0	50	50	50	30	5
Annual cost [€]			392.255	366.842	362.245	355.857	353.751	353.270	352.844

It is interesting notice that more than 92% of the possible reduction in the total annual cost has yet obtained at iteration 3, that means after a couple of optimization of the DH Network.

Figure 7 shows the convergence of total annual cost (objective function of the whole problem) in subsequent iteration of the MILE method. The dashed line represents the actual optimum obtained by solving the global problem without any decomposition. Also the amount of heat exchanged flows and the load level of CHP groups are quite close in the two approaches.

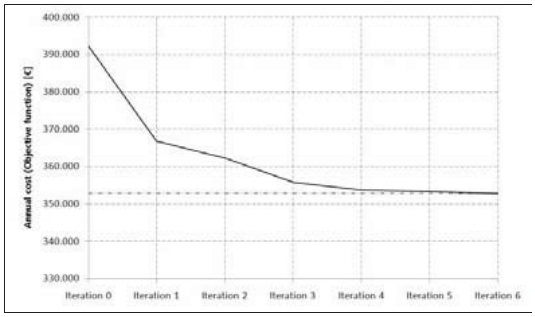

Figure 7: Convercence of total annual cost in subsequent iteration of MILE method

6 Conclusion and perspectives

This formulation is based on an actual linearization of the Fuel-Product relations for system components, so that proportional approximations of the same relations have not assumed a priori to be consistent with component thermodynamic models. Moreover, inequality constraint and binary decision variables can be explicitly considered. Thanks to these new features, the FaCIF had been used as a starting point in the formulation of the MILE optimization method of energy systems. In the ambit of this optimization method, the typical thermoeconomic information about the cost formation process of internal flows and final products is explicitly available. On the bases of both Impact Formulation and thermoeconomic costs information the whole problem can be decomposed into sub-problems, each one having a reduced number of decision variables.

The MILE optimization method has been applied to the synthesis and operation optimization of multi-component DH and CHP systems in the tertiary sector, highlighting the advantages of decomposing the global optimization problem. In fact, according with cost formation process, the whole system is decomposed in two stages in series: the production of electrical and thermal energy inside the CHP units and the heat distribution to the final users through the DH-Network. In this way, the MILE optimization method can achieve the global optimum by means of an iterative procedure.

The expectation is that the reduced computational effort required by each sub-problem will allow dealing with much bigger problems, so that various technological options, various sizes of components, additional time interval and /or additional final users could be taken into account.

As an example, a simple DH and CHP systems, with three CHP units and three final users only, has been optimized. The results show that a very good approximation of the global optimum solution can be obtained in very few interactions. In particular, more than the 92% of the possible annual cost reduction has been obtained by performing two optimizations only of the sub-problem related to the DH-Network alone.

7 Nomenclature

C_{chp}	CHP capital cost [€]
c_e	Cost of external input [€]
C_{fboi}	Integration boiler fuel cost [€/m^3]
CF_{chp}	CHP fuel cost [€/m^3]
C_{flow}	Cost of Thermal flow [€]

CHCP	Cogenerated heat cooling and power
CHP	Cogenerated heat and power
C_{inv}	Capital costo f installed CHP [€]
C_{main}	Maintenance cost [€]
C_{net}	Total cost of network (Objective func.) [€]
C_{ope}	Operating cost [€]
C_{pip}	Cost of grid per unit lenght [€/m]
C_{pur}	Electrical energy purchase cost [€/kWh]
C_{sel}	Sold electrical energy price [€/kWh]
C_{year}	Annual cost (Objective function) [€]
DH	District Heating
D_{min}, D_{max}	Minimum/maximum pipeline heat flow [kW]
E	Energy/Exergy flow
E	Vector of Energy/Exergy flow
f, g	Generic function
F1, F2	Network cost parameter
fa	Amortization factor
FaCIF	Fuel and Cost Impact Formula
F_{boi}	Integration boiler fuel consumption [m^3]
F_{chp}	CHP fuel consumption [m^3]
f_{main}	Maintenance coefficient [€/kWh]
Ft	Objective function
h	index related to time interval
h, j, k, v	Generic index
i, j	Generic index
l	Lenght of each pipeline [m]
M	Matrix of coefficients mi
MILE	Mixed Integer Linearized Exergoechonomics
MILP	Mixed Integer Linear Programming
MINLP	Mixed Integer Non Linear Programming
n	Number of year
P	Product
p	District heating pipeline thermal losses [kWh]
Q	Matrix of coefficients teta
Q_{boi}	Integration boiler thermal energy [kWh]
Q_{chp}	Cogenerated thermal energy [kWh]
Q_{dem}	Thermal CHP unit demand [kWh]
Q_{flow}	Flow through each pipeline [kWh]
Q_{pip}	Maximum flow of a related pipeline [kWh]
Q_{req}	Thermal CHP unit demand [kWh]
Q_{was}	Dissipated thermal energy [kWh]
r	Binary variables related to heating pipelines
T	Total variable number
TH_{us}	Thermal energy demand of final user[kWh]
U_d	Identity matrix
W_{chp}	CHP produced electrical energy [kWh]
$W_{chp\ min,max}$	Minimum CHP electrical production [kWh]
W_{dem}	Electric energy demand of final user[kWh]
W_{pur}	Purchased electrical energy [kWh]
W_{sel}	Sold electrical energy [kWh]
X, y	Binary variables related to μTG
δ	cooling pipeline per unit length [km^{-1}]
λ	Dual cost
λ	Vector of dual cost
μ, θ	Linear coefficients
ω	Vector of final products
τ	Independent variable

8 Bibliography

1- Casisi M., Pinamonti P., Reini M., "Optimal lay-out and operation of CHP distributed generation systems" *Energy,* Volume: 34, Issue: 12, December, 2009, pp. 2175-2183.

2- Casisi M., Castelli L., Pinamonti P., Reini M., "Effect of different economic support policies on the optimal definition and operation of a CHP and RES distributed generation systems", *ASME paper Gt2008-50353*, *proc.* ASME TURBO EXPO 2008,June 9-13,Berlin, Germany.

3- Buoro D., Casisi M., Pinamonti P., Reini M., "Optimal lay-out and operation of a district heating and cooling distributed trigeneration systems", In press ASME TURBO EXPO 2010, Glasgow, 13-17 June 2010

4- Lozano MA, Ramos JC, Carvalho M, Serra L. "Structure optimization of energy supply systems in tertiary sector buildings", Energy and Buildings 41 (2009) 1063-1065;

5- Oyarzabal, B., von Spakovsky, Ellis, M. W., 2004, "Application of a Decomposition Strategy to the Optimal Synthesis/Design of a PEM Fuel Cell Cogeneration System for Multi-Unit Residential Applications", Journal of Energy Resources Technology, ASME transactions, vol. 126, pp 30-39, March, N.Y., N.Y;

6- Muñoz, J.R., von Spakovsky, M.R., 2001, A "Decomposition Approach for the Large Scale Synthesis/Design Optimization of Highly Coupled, Highly Dynamic Energy Systems", International Journal of Applied Thermodynamics, March, vol. 4, no. 1.

7- Ito K., Akagi S."An optimal planning method for a marine heat and power generation plant by considering its operational problem", Int. Journal of energy research, Vol. 10, 1986.

8- Horii S., Ito K., Suzuki Y.: "A computer aided planning (CAP) system for the gas engine co-generation plant", Int. J. of energy research, Vol. 11, 1987.

9- Yokoyama R, Ito K., Kamimura K., Miyasaja F.: "Development of a General purpose optimal operational planning system for energy supply plants", J. of energy resources technology Vol. 116 Dec. 1994.

10- Gaggioli RA. "Second law analysis for process and energy engineering". In efficiency and costing. ACS Symposium Series 1983;235:3–50.

11- El-Sayed YM, Gaggioli RA. "A critical review of second law costing methods" Parts I and II. ASME Journal of Energy Research Technology 1989;111:1–15.

12- El-Sayed YM. "The thermoeconomics of energy conversions". Pergamon; 2003.

13- El-Sayed YM, Tribus M. "The strategic use of thermoeconomic for systems"

14- Reini M., Lazzaretto A., Macor A.(1995): "Average Structural and Marginal Costs as Result of a Unified Formulation of the Thermoeconomic Problem", Proc. of Int. Conf. Second Law Analysis of Energy System Towards the 21-st Century, E. Sciubba, M. J. Moran Eds, Esagrafica Roma. Roma, 5-7 July 1995.

15- Lozano MA, Valero A. "Theory of the exergetic cost. Energy" 1993;18:939–60.

16- Serra L, Lozano MA, Valero A, Torres C. "On average and marginal costs in thermoeconomics". In: Proceedings of ECOS'95, Istanbul, Turkey, July 11–15, 1995, pp. 99–112.

17- Lazzaretto A, Tsatsaronis G. Speco: "A systematic and general methodology for calculating efficiencies and costs in thermal systems". Energy 2006; 31;

18- Reini M. (1994) (in Italian), "Analisi e Sviluppo dei Metodi Termoeconomici per lo studio degli Impianti di Conversione dell'Energia", Ph.D. Thesis, University of Padova (Italy), Department of Mechanical Engineering.

19- Lozano M. A., Bartolome J. L., Valero A. and Reini M. (1994). "Thermoeconomic Diagnosis of Energy Systems", Proceedings of the third Florence World Energy Research Symposium, Florence, Italy, July 6-8, 1994, pp. 149-156.

20- Frangopoulos C. A. (1987). "Thermoeconomic Functional Analysis and Optimization", Energy - The Int. J. 7, pp.563-571.

21- Spakovsky von M. R., Evans R. B. (1987) "The Optimal Design and Performance of Thermal System and their Components", Analysis and Design of Advanced Energy System Fundamentals, A.E.S. vol.3-1, A.S.M.E., N.Y., pp.1-18.

22- Tsatsaronis G, Winhold M. "Exergoeconomic analysis and evaluation of energy conversion plants". Energy 1985;10:69–80.

23- Lazzaretto A, Tsatsaronis G. Speco: "A systematic and general methodology for calculating efficiencies and costs in thermal systems" Energy 2006;31: 1257–86.

24- Reini, M., Taccani, R., (2004), "On the Thermoeconomic Approach to the Diagnosis of Energy System Malfunctions The Role of the Fuel Impact Formula", Int. J. Thermodynamics, Vol. 7, No. 2, pp. 61-72.

25- Torres C., Valero A., Rangel V., Zaleta A. (2008): "On the cost formation process of the residues", Energy 33 pp. 144–152.

26- Pike R. W. (1986) "Optimization for engineering systems", Van Nostrand Reinhold (New York).

27- Frangopoulos, C.A., von Spakovsky, M. R., Sciubba, E., 2002, A "Brief Review of Methods for the Design and Synthesis Optimization of Energy Systems", International Journal of Applied Thermodynamics, ICAT, Istanbul, Turkey, December, vol. 5, no. 4.

28- Valero A., Lozano M.A. Serra L (1993), "Structural Theory of Thermoeconomics". Proc. of ASME AES v.30, Book N° H00874, 1993.

29- Lazzaretto A., Macor A., 1994, "Marginal and Average Costs in Engineering Functional Analysis", proceedings of the third Florence World Energy Research Symposium, Florence, July 1994.

30- Serra L., Lozano M. A., Valero A., Torres C. (1995), "On average and marginal costs in thermoeconomics, Proc. ECOS'95. Efficiency, Costs, Optimization, Simulation and Environmental Impact of Energy Systems". Eds. A. Gogus, A. Ozturk and G. Tsatsaronis, pp. 428-435, Istanbul, Turkey

31- Von Spakovsky MR, Evans RB. "The foundations of engineering functional analysis". In: Proceedings of FLOWERS´ 90, Florence, Italy, May 28–June 1, 1990, pp. 445–72.

32- Wikipedia, *The Karush-Kun-tuker conditions*, consulted Feb. 26, 2010: http://en. wikipedia.org/wiki/K ar ush %E 2%80% 93Kuhn%E2 %80%93Tucker_conditions

Critical Flow of Dense Gases – Modeling and Experimental Validation

Jan Górski [a], *Sławomir Rabczak* [b]

[a] *AGH University of Sciences and Technology, Cracow, Poland*
[b] *Rzeszow University of Technology, Rzeszow, Poland*

Abstract: The critical mass flow of dense gases strongly depends on real gas effects. In the present work the detailed assessment of the critical flow conditions and the limiting mass velocity in the flow of refrigerants has been experimentally verified. Critical flow function C^* data for R-410A and R-507A have been predicted based on *Martin–Hou* equation of state. The computational study was provided by implementation of theoretical model [1] for one dimensional (1D) and non-linear gas dynamic problems. This model, with the corrections for the boundary layer (BL) displacement thickness, gives a better prediction of the critical flow function than classical approach. Appropriate sonic flow conditions have been executed in the pressurized closed loop system by using ISO 9300 critical Venturi nozzle. Measurements of critical mass flow for dense superheated vapour of R-410A carried out on laboratory test stand confirmed the accuracy of the model and its physical significance. A main goal of the investigations is a set of charts $C^*(T_0, p_0)$ and tables developed for an assumed range of stagnation temperature T_0 and pressure p_0 in the upstream fluid-flow.

Keywords: refrigerant flow measurements, critical flow function, Venturi nozzles.

1. Introduction

Growing energy consumption associated with local environmental and operating problems of electric, heating and cooling power systems have lead to an increase of the interest in refrigerants not applied for the broader scale so far. Solutions utilizing low-temperature or waste energy sources in low boiling point applications are being introduced more and more commonly in the various energy conversion systems. Main group so mentioned low boiling agents are organic refrigerants as propane, butane and inorganic substances (carbon dioxide) or whole range of ozone depletion free CFC replacements.

Detailed data referring to the estimation of their critical flow characteristics are not available for many of them, particularly in the high pressures area (used e.g. in transcritical cycles). The implementation of an ideal gas model to the process calculations in real compressible fluid can lead to large discrepancies between measured and predicted values of state parameters. There is currently the development of a class of methods involving the application of fundamental equations of state (EOS) not only within applied process thermodynamics but also in the numerical fluid flow analysis [2].

At the principal study and qualitative examination of any physical processes the most useful and still popular is a simple *van der Waals* (*vdW*) model. A main weakness of such approach is a poor quantitative level of the obtained particular numerical results. More sophisticated methods are involving the application of multi-parameter EOS's and special computer routines for the calculation of the necessary parameters. In an engineering practice the most popular and well known equations of state are the *Martin-Hou* (*MH*) and the modified *Benedict-Webb-Rubin* (*MBWR*) EOS [3]. These EOS's have been widely applied and actually used for pure new refrigerants and refrigerant blends, for example R-134a, R-407C, R-410A and R-507.

The main purpose of this work is to deliver useful tools and data for the prediction of the critical (sonic) conditions in a compressible and high-density flow of gases or vapours. Based on refrigerant R-410A (a near azeotropic blend) source data [4] an experimental verification of the theoretical results were performed.

a) Jan Górski, E-mail: jagorski@agh.edu.pl

In the present work authors propose an effective tool for the prediction of the critical flow of vapour-phase refrigerants and high-density technical gases proving its usefulness and correctness on the basis of experimental results.

2. RESEARCH PROBLEM

A critical or sonic nozzle is a device to measure the mass flow with only the nozzle supply conditions making use of flow choking phenomenon at the throat [5]. An accurate prediction of the mass flow rate and the critical flow function is of practical importance since the mass flow rate is essentially associated with limiting the working gas consumption or the accidental release flow rates from pressurized gas systems. Critical pressure ratio should be known to establish the operating conditions for safety and design the expansion valves in the high-pressure refrigeration units and Organic Rankine Cycle (ORC) systems, measuring natural gas flows and many other applications [6,7].

According to classical 1D gas dynamics, the mass flow rate is a function of the pressure and temperature at upstream stagnation conditions, the diameter of nozzle throat and specific heats ratio. This phenomenon is one of the unique features of compressible internal flows. In the compressible flow with a sufficiently high backpressure ratio, the flow is choked at minimum cross section A_* and the mass flow rate reaches its maximum value. At the critical pressure ratio the flow is no longer dependent on pressure change downstream and flow the mass flow is determined only by fluid upstream stagnation conditions.

In the one-dimensional (1D) steady isentropic flow ($s_0 = s_* = idem.$) an energy equation is simply given by

$$h_0 = h + \frac{w^2}{2} = h_* + \frac{a_*^2}{2} = idem. \qquad (1)$$

For the sonic flow conditions at Mach Number Ma=1, the flow velocity equals to sound speed $w=a_*$, and the static parameters correspond to the critical ones ($T= T^*$, $p = p^*$, $h = h^*$, $a = a^*$). All complete relations in a compressible critical flow of the perfect gases can be found anywhere in the classical gas dynamics lectures. The critical mass flow $\dot{m}_*$ and related critical flow functions are respectively

$$\dot{m}_* = C^* \cdot \frac{A_* p_0}{\sqrt{RT_0}}, \qquad (2)$$

$$C^* = \frac{\dot{m}_* \sqrt{RT_0}}{A_* p_0}, \quad \text{or} \quad \Psi^* = \frac{\dot{m}_*}{A_* \sqrt{p_0 \rho_0}} = \sqrt{\frac{C^*}{z}}. \qquad (3)$$

The calculated theoretical values may differ from the experimental data and an actual mass flow $\dot{m}_*^{\exp}$ should be corrected. Considering the well-known discharge coefficient C_d, it is possible to account for the three dimensional (3D) effects C_{3D}, non-isentropic process C_γ and viscous (boundary-layer) phenomena C_{BL}, see [8]

$$C_d = \dot{m}_*^{\exp} / \dot{m}_*, \quad \text{and} \quad C_d = C_{3D} \cdot C_\gamma \cdot C_{BL}. \qquad (4)$$

For sufficiently high Reynolds numbers and the steady uniform flow, the discharge coefficient approaches unity, indicating that the 1D inviscid model is valid for prediction of the maximum mass flow. For low Reynolds numbers the discharge coefficient reduces considerably below unity. This is due to the boundary layer growth in the flow through the sonic nozzle. For a small critical nozzle, the Reynolds number can be low, and in this case the prediction of the mass flow rate is not straightforward since it depends on downstream pressure variations, even under the condition of the critical pressure ratio.

2. CRITICAL ISENTROPIC FLOW

According to ideal gas dynamics, in the steady 1D flow, the flow rate is a function of the pressure ratio and of the gas properties. The problem of the critical flow peculiarities in the dense gases was previously treated by many authors [9-11]. For CFC refrigerants R-12, R-22 and R-502, the theoretical analysis is presented in [11]. In the monograph [1], a unified approach for the analysis of the thermal-flow processes for arbitrary real gas EOS was proposed. The method of *Virial Compressibility Derivatives* (VCD), gives a clear results which can be directly related to the ideal gas model.

In the case of 1D dense gas steady flow, the well-known relations presented in classical books on gas dynamics are in general invalid. It is caused by strong variation of physical constants and all

thermal and caloric properties involved in the calculation of the process. As is shown in [1], it is possible to find the analogous parameters to the isentropic flow of real gases, similar to ideal gas flow. The approximate relations between critical and stagnation parameters in the sonic flow can be shortly expressed [1]

$$\frac{T^*}{T_0} \cong \left(\frac{2}{\chi+1}\right)^{\frac{\Phi}{\chi-1}}, \frac{\rho^*}{\rho_0} \cong \left(\frac{2}{\chi+1}\right)^{\frac{1}{\chi-1}}, \quad (4)$$

$$\frac{p^*}{p_0} = \beta^* \cong \left(\frac{2}{\chi+1}\right)^{\frac{k}{\chi-1}}, \quad \text{where}$$

$$\Phi = \frac{\rho}{T}\left(\frac{\partial T}{\partial \rho}\right)_s = \frac{z_T}{\bar{c}_v}, \; k = \frac{\rho}{p}\left(\frac{\partial p}{\partial \rho}\right)_s = \gamma\frac{z_v}{z}, \quad (5)$$

$$\chi = k + \frac{\rho}{k}\left(\frac{\partial k}{\partial \rho}\right)_s = 2\Gamma - 1, \quad \text{and}$$

$$z = \frac{p}{\rho RT}, z_v = z - v\left(\frac{\partial z}{\partial v}\right)_T = z + \rho\left(\frac{\partial z}{\partial \rho}\right)_T, \quad (6)$$

$$z_T = z + T\left(\frac{\partial z}{\partial T}\right)_v, \; \gamma = \frac{c_p}{c_v}, \; \bar{c}_v = \frac{c_v}{R}.$$

In equations (4) and (5) the *Grüneisen parameter* Φ and the generalized isentropic exponent χ (corresponding to the fundamental derivative Γ) are introduced. Other important factors are: the specific heat ratio γ, isentropic exponent k, compressibility factor and VCD derivatives z_T and z_v [1]. These parameters can be simply found from an EOS, usually given by $p = p(T, v)$. For a perfect gas case, all factors in equations (4) –(6) take the values of well-known constants

$$z = z_T = z_v = 1, \; \chi = k = \gamma, \; \Phi = R/c_v, \quad (7)$$

as well as the critical flow function and ratio of local sonic state parameters would only depend on the specific heat ratio. In a real gas case all the above mentioned parameters are functions of temperature and pressure, see the reciprocal of β^*, Figure 1.

The calculation results of the critical pressure ratio in an isentropic flow of real gases for refrigerant R-410A shows a strong influence of both the stagnation temperature and stagnation pressure.

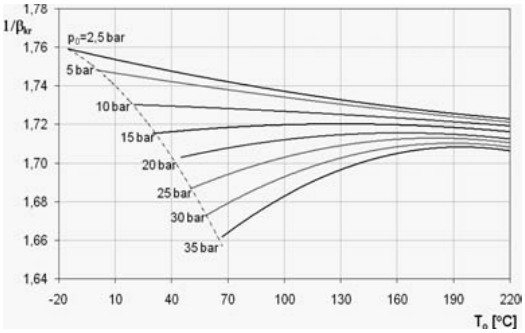

Fig.1. Critical pressure ratio for vapour of R-410A.

Assuming the isentropic exponent k = 1.125 for R-410A at the normal conditions, in an ideal gas case the corresponding value of $p_0/p^* = 1/\beta^*$ = 1.726. From the Figure 1, this parameter can vary between 1.67 and 1.75, and an even wider range is closer to the saturation line (x = 1).

Using *Martin-Hou* EOS and the equations (1)-(6), the critical flow factor C^* was calculated for dense refrigerant vapour over the range 300 to 500 K and 0 to 4 MPa (excluding areas where condensation occurs). The calculation procedures are iterative but fast convergent. It begins by making an initial estimate of the throat conditions, i.e. temperature, pressure and density. It is found from relations (4) and initial values of coefficients (5). In the next iteration step, all data corresponding to the mean values of parameters from (5), allow to calculate and obtain new results much closer to final ones. The end of the iterative procedure is only limited by the assumed and acceptable discrepancies for the enthalpy and entropy equalities (1).

3. EXPERIMENTAL TESTS

A main goal of this work was an experimental verification of theoretical results and to compare data from laboratory tests to the computational ones. An original test–bench has been developed, to attain the sonic conditions in a closed refrigeration circuit [12]. This facility is operating based on critical Venturi nozzles (CVN). Superheated vapours of refrigerants R-410A and R-507A were used as working media. Based on the computational study the selection of two ISO-9300 Venturi Nozzles [5], with the throat diameter d = 0,8 and 1 mm was made. The critical nozzle of 0,8 mm diameter, was used for the upper range of stagnation pressures p_0 > 1.5 MPa. At the smaller

pressures, a 1 mm throat nozzle was taken in order to preserve the heat capacity of flow-calorimeter. In a low pressure range, a 1 mm throat CVN has been used in order to preserve the limited heat capacity of flow-calorimeter.

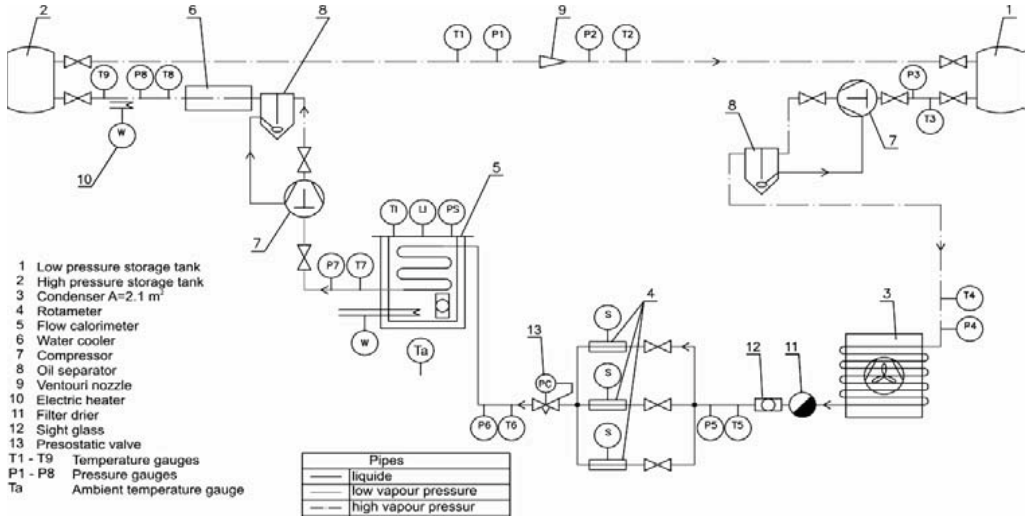

Fig. 2. Schema of test – bench for measurement of critical flow function, [12].

A steady-state flow calorimeter method was applied for selective measuring thermal and flow parameters of refrigerant blends. Principal schema of the meter circuit and instrumentation is shown in the Fig. 2. Circulating tested refrigerant, in the main measuring line (high pressure vapour), flows between two pressure vessels: high – DCR0487s Danfoss (1), and low pressure – DCR0967s (2). In this pipeline the critical Venturi nozzle (9), thermocouples (T1, T2 – type Pt100) and the pressure gauges (P1, P2 – type AKS Danfoss) were installed. Vessels (1) and (2) serve as the pressure buffers, whereas the required conditions for the demanded stagnation temperature and pressure level in the installation were assured by two compressors ML80TB (7), water cooler HE1.0 Danfoss (3), 2,1 sq.m condenser (6), 1 kW electric heater (10) and control valves. For keeping the suitable pressure in the system a pressostatic expansion valve PZ Fach (13) was operating on the high pressure side. Fluid conditions on the low-pressure side (liquid refrigerant) have been forced by 1 kW flow calorimeter PP51 (class 0,5) with R-134a as the secondary fluid (5). Three calibrated rotameters DK37E Krohne (4), installed on the liquid side of cooling circuit, assure the control of the fluid mass flow and maintain the energy balance of the flow calorimeter. The stable conditions, required for the measurements were obtained after 3 to 4 hours. The uncertainty of the temperature close to the critical nozzle (T1/T2 gauges) was ±0,1 K, and the pressure ±0.5% (P1/P2 gauges, see Fig. 2). Less important temperature and pressure data in the remaining points were measured with a smaller accuracy (±0,3 K and ±1 % respectively). The operating conditions of the proposed test loop were limited up to $p_0 \leq 35$ bar and $T_0 \leq 110$ ^{0}C, behind the refrigerant saturation line in order to avoid two–phase flow in the main pipeline. The equipment components and gauges used for the measurements allowed to obtain a maximum uncertainty level below 1,7%. During test–bench operation the data were collected in a computer storage with the sequence of 1 second interval. Stabilised conditions in the circuit have been reached after about 4 to 5 hours, and the data were collected to obtain the critical mass flow and critical flow function. The operating conditions of the test loop were limited up to $p_0 \leq$ 3.5 MPa and $T_0 \leq$ 110 ^{0}C in superheated vapour area in order to avoid two–phase flows in the main circuit. The principal view of the circuit loop is presented in Figure 3. All of the main components are insulated by the polyethylene foam.

4. RESULTS AND DISCUSSION

In 2006, authors obtained experimental data on the critical function for R-410A vapour at sixteen

points and compared C^* to the previously found theoretical results.

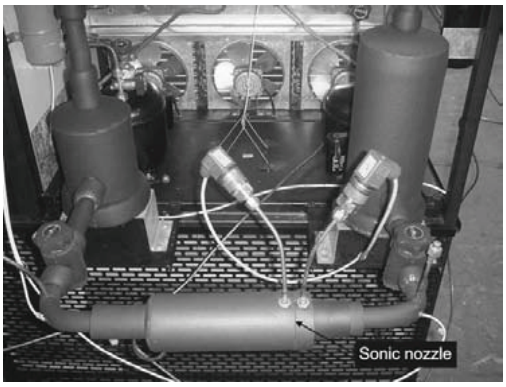

Fig. 3. View on the sonic nozzle on test – bench, [12].

Figure 4 presents a comparison of theoretical results for the critical flow function to the experimental stand data for R-410A refrigerant superheated vapour. Obtained experimental data are in a close agreement with computations based on the *M-H* equation of state.

The average discrepancy between theoretical and experimental results is less then 1,0%. It confirms that the new analytical model is valid and formulated in accordance to the real physical phenomena. All experimental points in the Figure 4 take into consideration the boundary layers corrections.

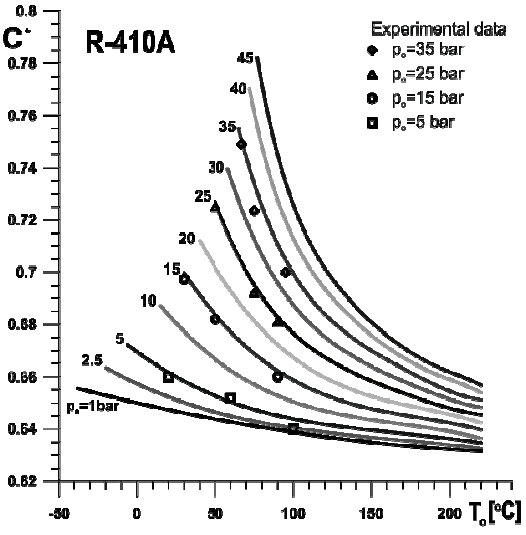

Fig.4. Critical flow function vs. stagnation parameters - theoretical and experimental data, [12].

The boundary-layer displacement thickness δ^* was calculated by using model [13] and the formula

$$\frac{2\delta^*}{d} = 0,001309 + 1,72169\frac{1}{\sqrt{Re}}. \qquad (8)$$

Figure 5 shows the correlation of boundary-layer thickness referred to the nozzle throat in the range corresponding to the experiment conditions (Re = $2\cdot10^5$ to $1.2\cdot10^5$). As one can notice, the flow is developed and turbulent in all the analysed cases.

The boundary-layer thickness strongly increases due to *Reynolds Number* for $Re < 6\cdot10^5$. At the higher Reynolds Numbers, the *BL* displacement thickness for the selected two nozzles, are in a narrow range. The replacement of the nozzle throat diameter from 0,8 to 1,0 mm, causes only an approximately 0,58 μm change in the *BL* displacement-thickness. Comparable results were obtained in [6-8].

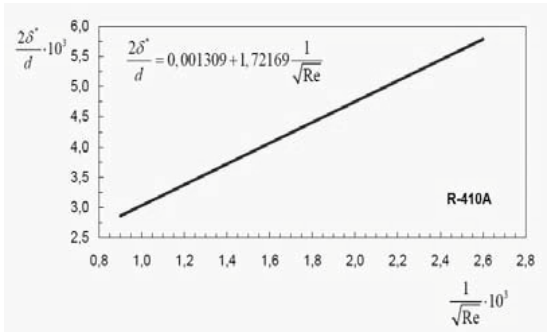

Fig. 5. Boundary-layer displacement thickness versus Reynolds Number, [12]

5. CONCLUSIONS

The paper compares results of computational analysis of the critical nozzle flow to the experimental data. The validity of the analytical results has been confirmed by research tests. The final results of the work are summarised:

1. The critical flow function for refrigerants strongly depends on the upstream stagnation conditions.
2. The computation results for R-410A are in a satisfactory agreement with experimental data.
3. The proposed approximation of critical flow conditions in the real and dense gases is better than other comparable methods.

4. The perfect gas model is not applicable in the flow of superheated vapour of refrigerants when stagnation pressure exceeds 0.5 MPa.
5. The boundary-layer at the throat of sonic nozzle is turbulent and affects the critical flow function.
6. Other theoretical results have been actually developed for R-22, R-123, R-125, R-134a, R-143a, R-152a, R-227, R-404A, R-407C, R-410A, R-507 and CO_2. The measurements of critical flow conditions will be done in the nearest future.

NOMENCLATURE

A^*	nozzle throat area [m^2]
a	speed of sound [m/s]
C^*	critical flow function [-]
C_d	discharge coefficient [-]
c_p, c_v	specific heats [J/kg K]
d	nozzle throat diameter [mm]
h	specific enthalpy [kJ/kg K]
k	isentropic exponent [-]
Ma	Mach Number [-]
$\dot{m}$	mass flow [kg/s]
p	pressure [Pa]
R	gas constants [J/kg K]
Re	Reynolds Number [-]
s	specific entropy [J/kgK]
T	temperature [K]
v	specific volume [m^3/kg]
w	gas velocity [m/s]
z	compressibility factor [-]
z_T, z_v	VCD's, equation (6) [-]
β^*	critical pressure ratio [-]
Γ	fundamental derivative, equation (5) [-]
γ	specific heats ratio [-]
δ^*	BL displacement-thickness [mm]
ρ	density [kg/m^3]
χ	generalized exponent, equation (5) [-]
Φ	Grüneisen parameter, equation (5) [-]
Ψ^*	critical flow function, equation (5) [-]

Indices

0	stagnation state
*	critical flow (Ma = 1)
s	isentropic
T	isothermal
v	isochoric

REFERENCES

[1] Górski, J., 1997, *Modeling of Real Gas Properties and its Thermal-Flow Processes,* (in Polish). Rzeszow, Oficyna Wyd. PRz.

[2] Thompson P.A., and Sullivan D.A., 1977, Simple Predictions for the Sonic Conditions in a Real Gas, ASME Jour. Fluids Eng.; 99(1), pp. 217-225.

[3] Span,R., 2000, *Multiparameter Equations of State: An Accurate Source of Thermodynamic Property Data*. Springer Verlag, Berlin.

[4] Annon, DuPont™, Suva refrigerants, URL: http://www2.dupont.com/Refrigerants/en_US/ products/ Suva/index.html.

[5] Standard ISO 9300:2005, Measurement of Gas Flow by Means of Critical Flow Venturi Nozzles.

[6] Johnson, R.C., 1971, Real Gas Effects in the Flow of Methane and Natural Gas Through Critical Flow Nozzles. *NASA-TM-X-52994*.

[7] Annon, 1997, Sonic Nozzles for Mass Flow Measurement and Reference Nozzles for Thrust Verification, *AGARD AR- 321*.

[8] Johnson, A.N., 2000, Numerical Characterization of the Discharge Coefficient in Critical Nozzles, Ph.D. Dissertation, Pennsylvania State University, College Station, PA.

[9] Leung J.C., and Epstein M., 1988, A Generalized Critical Flow Model for Nonideal Gases, *AIChE J*., 34 (9), pp. 1568-1572.

[10] Bober W., and Chow W.L., 1977, Nonideal Isentropic Flow Through Converging-Diverging Nozzles, *ASME J. Fluids Eng*., 112(4), pp. 455 -460.

[11] Shumann, S.P., 1990, Real Gas Critical Flow Factors for R12, R22 and R502, *ASHRAE Transactions*, 96(2), pp. 329-336.

[12] Rabczak, S., 2007, Thermal Equations of State in the Flow Analysis of New Refrigerants, (in Polish), PhD Dissertation, Fac. of Environmental Engineering, Warsaw University of Technology.

[13] Geropp, D., 1971, Laminare Grenzschichten in ebenen und Rotationssymmetrischen Lavalduesen, *Deutsche Luft- und Raumfahrt Forschungsbericht*, pp.71-90.

Thermodynamics at the Nano-Scale

Altug Sisman

Energy Institute, Istanbul Technical University, Istanbul, Turkey

Abstract: At the nano scale, the wave character of particles becomes important and changes the thermodynamic behavior of matter considerably. Therefore, thermodynamic effects which are negligible at the macro scale must be taken into account at the nano scale. To predict and examine the thermodynamic behavior and properties of nano systems, the wave character of particles should be considered. One way to do this is to use statistical and quantum mechanics to construct the mathematical models which properly estimate the thermodynamic properties of matter at the nano scale. In this study, the thermodynamic properties of ideal monatomic gases confined in nano structures are discussed by considering the wave character of gas atoms. Some thermodynamic behaviors, which are never observed in the macro systems, are presented. The results could lead to some new thermodynamic processes, cycles and nano engines.

Keywords: Thermodynamics at nano scale, Quantum size effects, Quantum surface energy.

1. Introduction

The capabilities of today's nano technology allow us to manufacture nano structures, devices and even machines. In particular, nano heat engines are of current interest [1-4]. Therefore, thermodynamics at the nano scale has become an interesting research subject in recent years [5-16]. In quantum mechanics, it is well known that particles have a wave character characterized by the de Broglie wave length, $\lambda = h/mv$ where h is Planck's constant, m and v are the particle mass and velocity, respectively. Mean de Broglie wave length ($\overline{\lambda}$) of gas atoms are on the order of nanometers or sub-nanometers depending on the temperature. For an Helium-4 gas, for example, $\overline{\lambda} \cong 0.036$ nm for 300 K. The wave character of particles can be neglected as long as the sizes of the domain, where the particles are confined, and the interparticular mean distance are much longer than $\overline{\lambda}$. Therefore, classical mechanics and classical statistics, which are based on the particle nature of atoms, are sufficient for macro systems at high temperature and/or low density. If the temperature is low enough and/or density is high enough, the interparticular mean distance becomes on the order of $\overline{\lambda}$ and quantum statistics (Bose and Fermi statistics) must be used instead of the classical (Maxwellian). Thus, momentum or energy spectrum of particles is assumed to be continuous (the assumption of the classical mechanics) as long as the system size is large enough in comparison to $\overline{\lambda}$. When this is not the case, the discreet nature of the momentum or energy spectrum of particles must be considered. This is the case for nano systems.

The discreet nature of the momentum values of the particles makes some important mathematical treatments invalid. In statistical thermodynamics, for example, all thermodynamic properties of an ideal gas are calculated by using the partition function which is a summation over all possible momentum values of a single particle [17,18]. In macro systems, the summation operation is replaced by integration since the momentum values can be assumed to be continuous. When they are not, this substitution is not possible since the momentum is a discreet spectrum. In this case, one of the most important corrections for the thermodynamic properties comes from the exclusion of the zero momentum values of particles confined in a finite size domain due to their wave character. In other words, particles cannot move parallel to the domain boundaries. This exclusion of surface modes results in unavoidable quantum surface energy which is completely negligible for macro domains. However, it contributes considerably to the thermodynamic properties in domains [9].

Another important correction comes from the probability density which represents the probability of finding a particle in a differential volume element for given spatial coordinates. In classical mechanics, the probability density is homogenous at thermodynamic equilibrium and is

$1/V$ for all particles confined in a domain of volume V. On the other hand, in quantum mechanics, it is given by $|\psi_r|^2$ for a particle in quantum state (or momentum state) r. $|\psi_r|^2$ is obtained from the solution of the Schrödinger equation and it is not a homogenous quantity. Therefore, the density distribution is not homogenous even in thermodynamic equilibrium. The inhomogeneity of the density occurs mainly near the boundaries of the domain. The thickness of this inhomogeneous region is on the order of $\overline{\lambda}$ and so it is negligible for macro systems while it becomes important for nano systems [12].

As a result of the discreet nature of the momentum values of particles and the inhomogeneous probability density, thermodynamic behaviors are substantially changed at the nano scale. Some corollaries of thermodynamics at this scale can be summarized as follows:

- The size and shape of a system affect the thermodynamic state functions,
- The pressure of an ideal gas becomes a tensorial quantity instead of a scaler and depends on direction in an anisometric confinement domain,
- Unavoidable quantum surface energy appears even for ideal gases,
- The additivity rule for extensive quantities breaks down,
- Size difference itself becomes a driving force for gas diffusion,
- Thermosize effects appear similar to thermoelectric or thermomolecular effects,
- The density distribution becomes inhomogeneous and a quantum boundary layer near to the domain boundaries arises,
- Even density oscillations occur in the case of a Fermi gas, such as helium-3, under low temperature or high density conditions,
- Lateral forces arise even at thermodynamic equilibrium.

These new behaviors lead to some new thermodynamic processes and allow us to design some completely new devices and heat engines at the nano scale. In the following sections, the thermodynamic properties of ideal monatomic gases confined in nano structures are discussed to understand how the thermodynamic behavior of such systems changes.

2. Thermodynamics under quantum size effects

2.1 Quantum surface energy

If the discreet nature of momentum values of particles is considered, free energy of an ideal monatomic Maxwell gas is given as [9,12]

$$F = -Nk_bT\ln\left(\frac{n_q}{n_{cl}}\right) + Nk_bT\frac{\lambda_{th}}{2}\frac{A}{2V} \qquad (1)$$

where N is the total number of particles confined in volume V, n_{cl} is the classical number density of particles defined by $n_{cl} = N/V$, n_q is the quantum density given by $n_q = 1/\lambda_{th}^3$, λ_{th} is thermal de Broglie wave length of particles given by $\lambda_{th} = h/\sqrt{2\pi m k_b T}$ and A is the area of the surface bounding the volume. The first term represents the conventional bulk free energy while the second one represents the quantum surface energy, which appears due to the wave character of the particles. The necessary condition for using Maxwell statistics is that $n_q >> n_{cl}$. Therefore the magnitude of the logarithmic term in (1) is much bigger than unity. On the other hand, the term $\lambda_{th}A/V$ is completely negligible for macro systems since V/A is much greater than λ_{th} at the macro scale. However, the contribution of the quantity $\lambda_{th}A/V$ to the free energy becomes appreciable for nano domains. For a given temperature and density of the gas, the second term in equation (1) is proportional to the surface area while the first term is proportional to the volume of the domain. Therefore, the second term represents the quantum surface energy and is zero in the classical limit as Planck's constant goes to zero.

2.2 Inhomogeneous density, quantum boundary layer and effective density

In order to better understand the origin of quantum surface energy, it is necessary to examine the local density distribution of a gas confined in a finite domain. For an ideal Maxwell gas, density is defined by considering the wave character of particles as [12]

$$n(x) = \sum_r n_r(x) = N \frac{\sum_r \exp(-\varepsilon_r/k_bT)\,|\psi_r(x)|^2}{\sum_r \exp(-\varepsilon_r/k_bT)} \quad (2)$$

where ε_r and ψ_r are the energy eigenvalue and eigenfunction of a given quantum state r. ε_r and ψ_r are obtained from the solution of the , Fig. 1, shows the dimensionless density distribution, n/n_{cl}, of an ideal Maxwell gas confined in a rectangular domain. The solid curve represents the true density while the dashed one represents the thickness of the boundary layer.

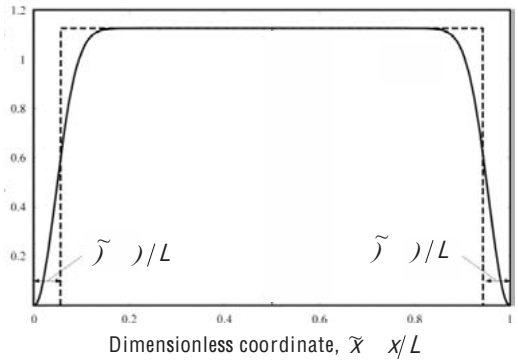

Fig.1 Dimensionless density distribution of an ideal Maxwell gas in a rectangular domain in one direction.

It is seen that density is not homogenous within a layer near to the boundaries. This layer has been called quantum boundary layer since the thickness of the layer $\delta = \lambda_{th}/4$ goes to zero in the classical limit when P . understood that the wave character of the particles keep them away from the boundaries. Therefore the density in the inner part of the domain is higher than the classical one, $n_{cl} = N/V$. In other words, particles occupy an effective volume which is smaller than the geometric one. Consequently, the effective density is higher than the classical one. Effective density can easily be determined as [12]

$$n_e = \frac{N}{V - \delta A} = n_{cl}\frac{1}{1 - \frac{\delta A}{V}}. \quad (3)$$

If the effective density is used instead of the classical density in the expression for bulk free energy, then the second term of (1) can directly be obtained from the first one. It is possible to express the second term of (2) as $nk_bT(-\delta A)$ which is the mechanical work done against the gas pressure to evacuate the region of thickness δ. Therefore, the origin of the quantum surface energy, the second term in (2), is explained by the inhomogeneous density distribution.

For ideal Fermi and Bose gases, the dimensionless density is calculated by [16]

$$\tilde{n}(\tilde{x}) = \frac{n(x)}{n_{cl}} = \frac{\sum_r |\psi_r(x)|^2 \exp(-\varepsilon_r/k_bT)}{\frac{1}{V}\sum_r \exp(-\varepsilon_r/k_bT)}. \quad (4)$$

Fig. 2 shows the dimensionless density distributions of ideal Fermi, Bose, and Maxwell gases versus to the dimensionless coordinate, $\tilde{x} = x/L$. In a Fermi gas, the quantum boundary layer is very thin and there is a density oscillation. In contrast, the thickness of the quantum boundary layer is very large in a Bose gas.

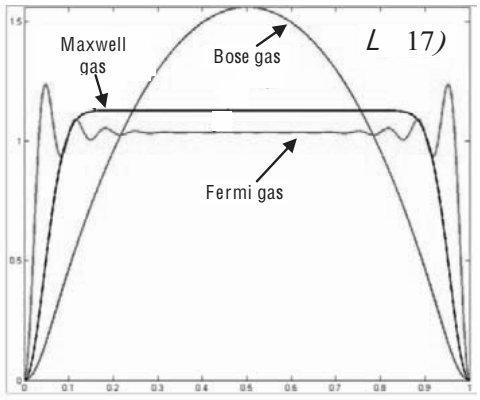

Fig.2 Dimensionless density distributions of ideal Fermi, Bose, and Maxwell gases in a 1D domain. ε_F/k_bT is chosen as 5 for the degenerate Fermi gas and 0.01 for the degenerate Bose gas while the size of the domain L 17) to make the differences between the curves clear enough.

2.3 Non-additivity, anisotropic pressure and lateral forces

Due to the unavoidable existence of the quantum surface energy, the additivity rule of extensive quantities breaks down. Since V/A represents an effective size of the domain and also depends on the domain shape, the thermodynamic state functions, like

the free energy, depend on the size and shape of the system in addition to two independent intensive quantities like temperature and density. The pressure of a gas confined in an anisometric rectangular domain of dimensions $L_x \neq L_y \neq L_z$, is determined from [8]

$$p_{xx} = -\frac{1}{L_y L_z}\left(\frac{\partial F}{\partial L_x}\right)_{N,T} = nk_bT + nk_bT\frac{2\delta}{L_x} \quad (5)$$

$$p_{yy} = -\frac{1}{L_x L_z}\left(\frac{\partial F}{\partial L_y}\right)_{N,T} = nk_bT + nk_bT\frac{2\delta}{L_y} \quad (6)$$

$$p_{zz} = -\frac{1}{L_x L_y}\left(\frac{\partial F}{\partial L_z}\right)_{N,T} = nk_bT + nk_bT\frac{2\delta}{L_z}. \quad (7)$$

Therefore, even the pressure of an ideal gas can be anisotropic in an anisometric domain. In other words, pressure is not a scalar quantity but a tensorial quantity.

Furthermore, lateral forces appear at nano scale. If a rectangular box is separated into two parts by a movable wall of infinitesimal thickness, as shown in Fig. 3, the system tries to minimize the quantum surface energy and causes a lateral force, τ, acting on the movable wall in the vertical direction parallel to this wall. This lateral force is determined by

$$\tau = \left(\frac{\partial F}{\partial L_s}\right)_{N,V} = nk_bT2\delta L_y \quad (8)$$

It is understood that the movable wall has an effective thickness of 2δ. For the box filled by He-4 at 300 K and 10^5 Pa, the lateral force is about 25 pN when L_y=10 μm.

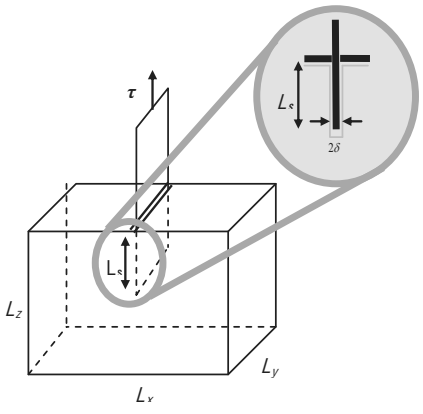

Fig.3 Lateral force acting on a movable and infinitesimally thin wall.

2.4 Diffusion due to size difference

The chemical potential is determined by using equation (1) so that [8]

$$\mu = -\left(\frac{\partial F}{\partial N}\right)_{T,V,A} = -k_bT\ln\left(\frac{n_q}{n_{cl}}\right) + k_bT\delta\frac{A}{V}. \quad (9)$$

It is clear that the second term results from the second term in equation (1) and it is due to the exclusion of the zero momentum values of particles confined in a finite size domain. The second term can also directly be obtained from the first term, the conventional term, if the effective density given by equation (3) is used for the density, instead of the classical one. If one small and one large rectangular box, I and II, respectively, are connected to each other by a permeable wall, mutual thermodynamic equilibrium requires the equality of both temperature and chemical potential across the boxes. Therefore, if the second term is negligible as it would be if both boxes were large, the equality of chemical potentials would require the equality of classical densities, $n_{cl}^{I} = n_{cl}^{II}$. This is a trivial result for the macroscopic domains. On the other hand, in the nano domains, the equality of chemical potentials requires $n_{cl}^{I} < n_{cl}^{II}$. This is an unusual result caused by the second term in equation (9) for the case of a small and a large box. The ratio of the densities is given by

$$\frac{n_{cl}^{II}}{n_{cl}^{I}} \cong 1 + \delta\left(\frac{A_I}{V_I} - \frac{A_{II}}{V_{II}}\right). \quad (10)$$

Therefore, if n_{cl}^{I} is forced to be equal to n_{cl}^{II}, a diffusion process is induced due to the size difference. This diffusion has been called "size dependent diffusion" [8]. This quantum effect may be used for isotropic enrichment since δ depends on the inverse square root of atomic mass. If $(V/A)_{II} >> (V/A)_I = 10\,\text{nm}$, equation (10) predicts a 7900 ppm concentration difference for a He-4 gas and 9100 ppm for a He-3 at 30 K. Therefore, the concentration of He-3 in box-II is higher than that in box-I.

2.5 Thermosize effects

To show the existence of thermosize effects, a monatomic ideal gas is confined in a rectangular box which is separated into macro and nano parts and kept thermally in contact with high (T_H) and low (T_L) temperature reservoirs, as shown in Fig.

4. On the low temperature side, there is no separator and the gas can flow between point 2 and point 3. In contrast, this is not allowed on the high temperature side. Therefore, the net particle flux is zero in steady state. In the macro part, the minimum size of the box is much bigger than δ while this condition is not fulfilled in the nano part. In other words, the second term of equation (9) is negligible in the macro part while it is not in the nano part. It should be noted that equation (9) is valid also for local equilibrium condition [8]. In the nano part, local equilibrium is maintained by particle-wall collisions although it is maintained by particle-particle collisions in the macro part. Therefore, the chemical potential gradients due to the temperature gradient are different in each box although the local chemical potentials on the cold side should be equal. As a result, there is a chemical potential difference on the hot side. This difference can drive a gas flow if the disconnected parts on the high temperature side are connected to each other. Consequently, the temperature gradient and size difference together cause a driving force for gas flow from region 1 to region 4 and begin a gas circulation between the domains, which is able to produce work. Isothermal gas flow under a chemical potential difference causes heat exchange between the working gas and its environment. These effects, which are similar to thermoelectric effects, are called thermosize effects [8].

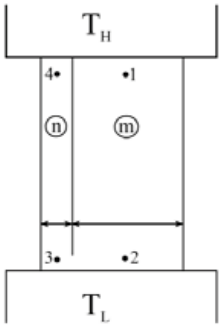

Fig. 4. Schematic view of a possible device based on thermosize effects. n and m indicate nano and macro parts, respectively. T_L and T_H represent low and high temperature reservoirs.

5. Conclusion

The size and shape of a system become independent variables of the thermodynamic state functions at the nano scale. These new variables change a system's thermodynamic behavior substantially and cause some new thermodynamic behaviors and processes which are not observed in macro systems. The results could be used to design some new thermodynamic processes, cycles, and nano engines. In order to make robust verification of these effects, a molecular simulation based on many body Schrödinger equation is necessary before any experimental verification.

References

[1] Goddard III W A, Brenner D W, Lyshevski S E and Iafrate G J (Editors), 2003, *Handbook of Nanoscience, Engineering, and Technology*, 2nd ed., CRC Press, Boca Raton, Chaps. 1

[2] Cui, L. and Brisson, JG., 2005, MEMS-Type Rankine Cycle Machines, Journal of Engineering for Gas Turbines and Power, 127, pp. 683-692.

[3] Epstein, AH., 2004, Millimeter-Scale, Micro-Electro-Mechanical Systems Gas Turbine Engines, Journal of Engineering for Gas Turbines and Power, 126, pp. 205-226.

[4] Kribus, A., 2004, Heat Transfer in Miniature Heat Engines, Heat Transfer Engineering, 25(4), pp. 1-3.

[5] Molina, M. I., 1996, Ideal Gas in a Finite Domain, American Journal of Physics, 64(4), pp. 503-505.

[6] Pathria, R. K., 1998, American Journal of Physics, An Ideal Quantum Gas in a Finite-Sized Container, 66(12), pp. 1080-1085.

[7] Dai, WS., and Xie, M., 2003, Quantum Statistics of ideal gases in confined space, Physics Letters A, 311, pp. 340-346.

[8] Sisman, A., and Muller, I., 2004, The Casimir-like size effects in ideal gases, Physics Letters A, 320(5-6), pp. 360-366.

[9] Sisman, A., 2004, Surface Dependency in Thermodynamics of Ideal Gases, Journal of Physics A: Mathematical and Geneneral, 37, pp. 11353-11361.

[10] Dai, W. S. and Xie, M., 2004, Geometry Effects in Confined Space, Physical Review E, 70, pp.016103.

[11] Pang, H., Dai, WS., and Xie, M., 2006, The difference of boundary effects between Bose and Fermi systems, Journal of Physics A: Mathematical and Geneneral, 39, pp. 2563-2571.

[12] Sisman, A., Ozturk, Z. F. and Firat C., 2007, Quantum Boundary Layer: A Non-Uniform Density Distribution of an Ideal Gas in Thermodynamic Equilibrium, Physics Letters A, 362(1), pp. 16-20.

[13] Nie, W., and He, J., 2008, Performance analysis of a thermosize micro/nano heat engine, Physics, Letters A, 372(8), pp. 1168-1173.

[14] Nie, W., He, J., and Du, J., 2009, Performance characteristic of a Stirling refrigeration cycle in micro/nano scale, Physica A 388(4), pp. 318-324.

[15] Firat, C. and Sisman, A., 2009, Universality of the Quantum Boundary Layer for a Maxwellian Gas, Physica Scripta, 79(6), pp. 065002.

[16] Ozturk, Z. F. and Sisman, A., 2009, Quantum Size Effects on the Thermal and Potential Conductivities of Ideal Gases, Physica Scripta, 80(6), pp. 065402.

[17] Reif, F., 1965, *Fundemantals of Statistical and Thermal Physics*, McGraw-Hill.

[18] Pathria R. K., 1996, *Statistical Mechanics*, Butterworth-Heinemann, Woburn.

Acknowledgments: This work is supported by Scientific and Technological Research Council of Turkey, TUBITAK, under contract number 105T086 and by Istanbul Technical University Scientific Research Program.

ENTROPY GENERATION MINIMIZATION IN RECTANGULAR MICROCHANNELS WITH FULLY AND NON-FULLY DEVELOPED CONDITIONS

C. A. Rubio-Jimenez[a], A. Hernandez-Guerrero[a],
V. H. Rangel-Hernandez[a], J. L. Zuñiga-Cerroblanco[a]
[a] Apartado Postal 215A
Apartado Postal 215A, Zip Code 36885
Salamanca, Guanajuato, Mexico

Abstract: The present work shows an analytical study about the entropy generation trend in the operation of rectangular microchannels. A specific number of microchannels are used for heat sinks arrangements. These arrangements are designed to dissipate very high heat fluxes. A specific fluid in a laminar regime for this scale is used as the working fluid. The thermal and hydrodynamic behaviors for both fully and non-developed conditions are considered. A constant heat flux is applied to the bottom wall of the heat sink. A specific part of this heat flux is supplied into each channel section. A Three-side heating condition is considered in the channels section. Entropy generation variation with channel aspect ratio, Reynolds number and total heat flux supplied into the system are presented. The Bejan number for both fully and non-fully developed conditions is calculated as well.

Keywords: Rectangular Microchannels Heat Sinks. Entropy Generation Minimization Method, Bejan Number.

1. Introduction

The current era is known as the information age. The information must be process and carry out faster. Thus, devices with large capability to process it are required. High-tech electronic devices are currently used for this proposal. Large quantity of resources had been focused in different areas of their development. One area is the cooling systems. Currently, heat sink systems are used for cooling these devices. In the last two decades, rectangular microchannel heat sinks manufactured on a silicon substrate have been deeply studied since they are a good alternative for the new generation of electronic cooling systems. New materials, geometrics, sizes, configuration, etc. have been studied [1-12]. Nevertheless, only a few quantity of research peoples had been focused to determinate the quantity of energy which is lost and wasted in the system.

Typically a heat sink system requires two things: a geometrical arrangement and a specific working fluid. A microchannel heat sink is no exception. This is a defined geometrical arrangement (typically a specific quantity of channels that are placed in parallel) and a quantity of specific fluid is passing through each channel. These involve two phenomena: heat transfer from the solid domain to the fluid domain and fluid motion. The entropy generation associated with the heat transfer and the frictional factors is a good parameter to determine the capability that a heat sink has for transferring heat to a cooling medium. A governing equation of the entropy generation is obtained by applying first and second law of thermodynamics as well as energy and mass balances. As a result, this governing equation is a function of the geometrical parameters, fluid and solid properties, etc. [19].

Some researchers have applied this technique to determine the behavior of a specific system. In some cases, an optimal configuration can be obtained [13-16,19]. Nevertheless, this technique has not been strongly applied to microchannel heat sinks. This work shows a methodology for obtaining the entropy generation in this kind of heat sinks, formed by rectangular channels. One important contribution is to obtain equations for the entropy generation considering that the fluid enters the channels with fully developed or with non-developed condition.

2. Problem Description

A typical rectangular microchannel heat sink is considered for the study. This arrangement is formed by 100 rectangular microchannels

Corresponding Author: A. Hernandez-Guerrero, e-mail: abelh@salamanca.ugto.mx

manufactured over a specific material substrate. A plate of adiabatic material is placed over this manufactured arrangement. Figure 1 shows a sketch of the heat sink. A constant heat flux is supplied on the bottom wall of the device. The total width, height and length of the heat sink are W_{hs}, H_{hs} and L_{hs}, respectively. The shadowed part represents the fluid domain. A specific fluid is passing through the system. Due to the symmetry that the arrangement presents, a part of the total heat sink is cut in order to reduce the analysis complexity. This process generates a cut cell formed by both solid and fluid domains. Figures 2 and 3, respectively. The solid cut cell and fluid channel dimensions are width W_{cell} and $W_{channel}$, and height H_{cell} and $H_{channel}$, respectively. Each cell contains a full channel and the middle of the space between channels ($S_{channels}$) at each side. Heat, $\dot{Q}_{cell}$, is supplied on the bottom wall of the solid cut cell. This heat is a proportional part of the total heat supplied on the device. A similar consideration is taken into account for the fluid domain. A proportional heat, $\dot{Q}_{channel}$, is supplied into the fluid channel from the channel solid walls. A proportional part of the total mass flow, $\dot{m}_{channel}$, is passed through each channel, as well.

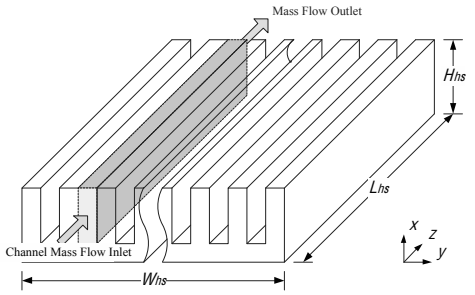

Figure 1. Heat sink arrangement formed by 100 rectangular microchannels.

Since this analysis tries to evaluate the behavior of the entropy generated by the fluid motion (hydrodynamic phenomenon) and thermal energy motion (thermodynamic phenomenon) present in the system, a good approach is to consider only the fluid domain behavior. Thus, a differential volume control ($W_{channel}$ x $H_{channel}$ x dz) is taken for the analysis, see Figure 4. In this case, it is considered that three heat fluxes, q_1'', q_2'' and q_3'', are flowing into the control volume (three-side heating channel assumption.) Each wall has a proportional part of $\dot{Q}_{channel}$ (this is a function of the area of the channel wall.) The four side (upper wall) of the control volume does not have a heat flux since it is considered as an adiabatic boundary wall (the adiabatic plate). T is the environmental temperature near the device boundary. The mean temperature (bulk temperature) is adjusted as $T+\Delta T$.

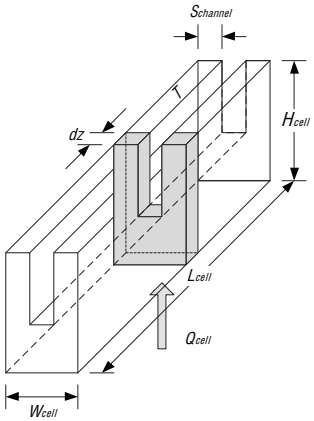

Figure 2. Solid domain of the heat sink cut cell to analyze.

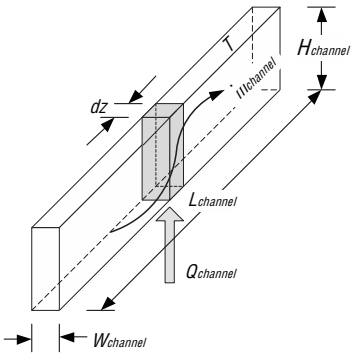

Figure 3. Fluid domain of the heat sink cut cell to analyze.

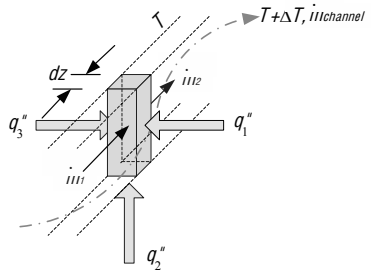

Figure 4. Differential control volume of the fluid considered for the analysis.

3. Analysis

The continuity, first and second law of thermodynamics equations and the Tds relationships are applied to the control volume to obtain an equation able to calculate the total entropy generation in the system.

3.1. Continuity equation application

Since it is considered that the system is in steady state and there is not accumulation of fluid into the channel, the Equation (1) is obtained.

$$m_{channel} = m_1 = m_2 \tag{1}$$

3.2. First Law of the Thermodynamics application

Applying the first law of thermodynamics with the given assumptions, the quantity of thermal energy in the process is equal to the product of the enthalpy variation and the mass flow passing into the control volume (Equation (2).)

$$Q_{cv} = m_{channel}\, dh \tag{2}$$

3.3. Second Law of the Thermodynamics application

Applying the second law of thermodynamics to the differential control volume, the ratio of entropy generation for the system is obtained. This is affected by the entropy variation and the thermal energy thrown to the environment. Equation (3) shows this. The derivative of this equation respect to the *z*-axis (channel length), provides the gradient of entropy generation.

$$\dot{S}_{gen} = m_{channel} ds - \frac{Q_{cv}}{T + \Delta T} \tag{3}$$

$$\frac{\dot{S}_{gen}}{dz} = m_{channel} \frac{ds}{dz} - \frac{1}{T + \Delta T} \frac{Q_{cv}}{dz} \tag{4}$$

3.4. Tds relationship

From the Tds relationship shown in Equation (5), it is possible to obtain the enthalpy gradient along the *z*-axis as a function of the entropy gradient and pressure variation along the same direction, Equation (6).

$$Tds = dh - vdP \tag{5}$$

$$\frac{dh}{dz} = T\frac{ds}{dz} + \frac{1}{\rho}\frac{dP}{dz} \tag{6}$$

3.5. Model generation

Substituting Equations (2) and (4) in Equation (6), an expression for the entropy generation gradient along the flow direction as a function of the thermal energy, pressure variation and environmental temperature in the system is obtained. These parameters can be obtained by experimental study of these devices, see Equation (7). In order to reduce the complexity of this equation, it is possible to consider that the temperature variation ΔT is much smaller than the net environmental temperature. Thus, Equation (7) can be rewritten as:

$$\frac{S_{gen}}{dz} = \left(\frac{1}{T} - \frac{1}{T + \Delta T}\right)\frac{Q_{cv}}{dz} - \frac{m_{channel}}{\rho T}\frac{dP}{dz} \tag{7}$$

$$\frac{S_{gen}}{dz} = \frac{\Delta T}{T^2}\frac{Q_{cv}}{dz} - \frac{m_{channel}}{\rho T}\frac{dP}{dz} \tag{8}$$

As it was previously mentioned, the heat flux that is flowing into each cut cell is a proportional part of the total heat flux supplied into the channel, see Equation (9).

For this kind of arrangements, a good approach is to assume the system as a pin fins heat sink [20]. The thermal efficiency can be calculated by Equation (10). The part of total heat flux supplied on the system which arrives to the channel can be calculated by Equation (11)

$$q''_{cell} = \frac{q''_{total}}{N_{cells}} \tag{9}$$

$$\eta_f = \frac{\tanh(mH_{channel})}{mH_{channel}} \tag{10}$$

$$q''_{channel} = \eta_f q''_{cell} = \eta_f \frac{q''_{total}}{N_{cells}} \tag{11}$$

The m parameter is calculated by Equation (12). The $S_{channels}$ is taken as the half of channel width, $W_{channel}$.

$$m = \sqrt{\frac{2h_{convection}}{k_s S_{channels}}} \tag{12}$$

Under this consideration, the heat flux entering to the differential control volume can be calculated by Equation (13). This is a function of the total heat flux supplied into the system, geometrical parameters, thermal properties and the convective

coefficient in the flow. The total heat in the control volume is given by Equation (14).

$$q''_{cv} = \frac{1}{L_{channel}} \int_0^{L_{channel}} \eta_f \frac{q''_{total}}{N_{cell}} dz \tag{13}$$

$$\frac{Q_{cv}}{dz} = Pw_{channel} q''_{cv} = \eta_f \frac{(2H_{channel} + W_{channel})}{N_{cell}} q''_{total} \tag{14}$$

Substituting the last equation in Equation (8) the gradient of entropy generation as a function of the total heat flux supplied into the system is obtained.

$$\frac{S_{gen}}{dz} = \frac{\Delta T}{T^2} \eta_f \frac{(2H_{channel} + W_{channel})}{N_{cell}} q''_{total} - \frac{m_{channel}}{\rho T} \frac{dP}{dz} \tag{15}$$

4. Fully and Non-Fully Developed Flow Conditions

4.1. Fully developed flow consideration

There are two conditions that consider the case of fluid flowing through a channel with specific cross section areas: fully developed and non-developed flow conditions. The first one involves that the fluid at the channel inlet has both temperature and velocity profiles (fully developed both thermal and hydrodynamic boundary layers) and keep them along the channel. Thus, the entropy generation involves uniquely a convective coefficient and friction factor along the channel length. The total entropy generation can be calculated by Equation (16) for these considerations. The minus sign in the ΔP term is due to the fact that the pressure is decreasing in the flow direction.

$$S_{gen} = \frac{\Delta T}{T^2} \eta_f \frac{(2H_{channel} + W_{channel})L}{N_{cell}} q''_{total} - \frac{m_{channel}}{\rho T} \Delta P_{fd} \tag{16}$$

Using the Stanton number definition (Equation (17)), Equation (16) can be rewritten in terms of the Nusselt number. Also, the pressure drop can be expressed as a function of the Poiseuille and Reynolds number. Equation (18) shows this.

$$\frac{Nu_{fd,3s} k_f}{D_h} = \frac{q''_{channel}}{\Delta T} \tag{17}$$

$$\Delta P_{fd} = -\frac{2(f\,\mathrm{Re})\mu V_{mean} L_{channel}}{D_h^2} \tag{18}$$

Thus, the entropy generation equation can be rewritten to include those dimensionless parameters, resulting Equation (19). The channel aspect ratio, α, is defined as the quotient between the channel width and the channel height, $W_{channel}/H_{channel}$.

$$S_{gen} = 2\alpha \frac{(\alpha+2) H^2_{channel} L_{channel}}{(\alpha+1) Nu_{fd,3s} k_f T^2} \left(\eta_f \frac{q''_{total}}{N_{cell}} \right)^2 + \frac{m_{channel}}{\rho T} \left[\frac{(f\,\mathrm{Re})\mu V_{mean} L_{channel} (\alpha+1)^2}{2 H^2_{channel} \alpha^4} \right] \tag{19}$$

Since the analysis considers rectangular channels with three-side heating and fully developed flow, it is necessary to use adequate Nusselt and Poiseuille number correlations for having successful approaches of the entropy generation in this kind of systems. The fully developed Nusselt number for three-side heated rectangular ducts had been compiled from various sources. Equation (20) shows the most adequate correlation [20]. This considers that a side is larger than other one, being one of these smaller sides not-heated. Shah and London [17] provide Equation (21) to calculate the Poiseuille number for a rectangular channel under the same consideration of channel aspect ratio. Table 1 shows the constant values. Equation (19) is developed for analyzing a single channel. Thus, the total entropy generation in the system is given by Equation (22)

$$Nu_{fd,3s} = \frac{A_1 + A_2\alpha + A_3\alpha^2}{1 + A_4 + A_5\alpha + A_6\alpha^2} \tag{20}$$

$$f\,\mathrm{Re} = 24\,(1 + B_1\alpha + B_2\alpha^2 + B_3\alpha^3 + B_4\alpha^4 + B_5\alpha^5) \tag{21}$$

$$S_{gen,total} = N_{channels} S_{gen} \tag{22}$$

4.2. Non-developed flow consideration

A non-developed flow consideration involves that the fluid is entering to the channel with constant temperature and velocity profiles. These profiles develop until a defined profile is reached due to heat and friction on the channel walls. The boundary layer developments involve an increment of the fluid friction with channel walls and with itself, as well as larger temperature gradients between them. Thus, four phases or

phenomena can be observed (two for thermal effects and two for hydrodynamic effects.) The entropy generation calculation requires considering all of those effects:

$$S_{gen} = S_{gen,therm} - S_{gen,hydro} = S_{gen,therm,fd} + S_{gen,therm,nd} - S_{gen,hydro,fd} - S_{gen,hydro,nd} \quad (23)$$

The hydrodynamic inlet length required for developing the hydrodynamic boundary layer is the well-accepted Equation (24) [18,20]. The thermal inlet length required for developing the thermal boundary layer is expressed by Equation (25). Phillip [2] mentioned that $c=0.1$ is an adequate value for rectangular channels.

$$\frac{L_h}{D_h} = 0.05\,\mathrm{Re} \quad (24)$$

$$\frac{L_t}{D_h} = c\,\mathrm{Re}\,\mathrm{Pr} \quad (25)$$

Thus, the entropy generation given by each part of the analysis (fully and non-developed sections for both thermal as hydrodynamic condition) can be calculated by Equations (26-28), respectively.

$$S_{gen,therm,nd} = \int_0^{Lt} \frac{\Delta T}{T^2}\eta_f \frac{(2H_{channel}+W_{channel})}{N_{cell}} q''_{total}\,dz \quad (26)$$

$$S_{gen,therm,fd} = \int_{Lt}^{L_{channel}} \frac{\Delta T}{T^2}\eta_f \frac{(2H_{channel}+W_{channel})}{N_{cell}} q''_{total}\,dz \quad (27)$$

$$S_{gen,hydro} = S_{gen,hydro,fd} + S_{gen,hydro,nd} = \frac{\dot{m}_{channel}}{\rho T}\Delta P_{nd} \quad (28)$$

At the inlet section of the channel where the fluid presents a non-developed condition, it is required to use a Nusselt number correlation for this effect. In an analogous form to Equation (17), the Stanton number for this condition can be expressed as:

$$\frac{Nu_{nd,3s}k_f}{D_h} = \frac{q''_{channel}}{\Delta T} \quad (29)$$

Integrating and grouping Equations (26) and (27), and substituting Equations (29), the equation for calculating the total thermal entropy generation as a function of the Nusselt numbers for fully and non-developed conditions and channel aspect ratios is obtained.

$$S_{gen,therm} = 2\alpha\frac{(\alpha+2)H^2_{channel}}{(\alpha+1)k_f T^2}\left(\eta_f \frac{q''_{total}}{N_{cell}}\right)^2 * \left(\frac{L_t}{Nu_{nd,3s}} + \frac{L-L_t}{Nu_{fd,3s}}\right) \quad (30)$$

The Nusselt number correlation for fully developed condition is given by Equation (20). For non-developed condition and three-side heating configuration the scheme shown in Equation (31) is suggested by Phillips [2]. The $Nu_{fd,4s}$ is given by Equation (32).

$$Nu_{nd,3s}(x^*,\alpha) = Nu_{nd,4s}(x^*,\alpha)\frac{Nu_{fd,3s}(x^*,\alpha)}{Nu_{fd,4s}(x^*,\alpha)} \quad (31)$$

$$Nu_{fd,4s} = \frac{C_1 + C_2\alpha + C_3\alpha^2}{1 + C_4 + C_5\alpha + C_6\alpha^2} \quad (32)$$

Kandlikar [20] presents a data-table to obtain the $Nu_{nd,4s}$ for different entrance regions and channel aspect ratios. Table 1 shows the values for constants C_1 to C_6.

The pressure drop equation for non-developed conditions is based on Equation (18). Some terms are added to consider all the quantity of pressure drop due to friction and developing region effects. The incremental pressure defect, $K(x)$, is the parameter used to consider these effects:

$$\Delta P_{nd} = -\frac{2(f\,\mathrm{Re})\mu V_{mean} x}{D_h^2} + K(\infty)\frac{\rho V^2_{mean}}{2} \quad (33)$$

Equation (33) expresses it. The Poiseuille number is calculated, as it was previously shown. In a global way, the incremental pressure defect is taken as a constant parameter, $K(\infty)$, known as Hagenbach's factor. Steinke and Kandlikar [11] present a correlation to calculate it for rectangular channels.

$$K(\infty) = D_1 + D_2\alpha + D_3\alpha^2 + D_4\alpha^3 + D_5\alpha^4 + D_6\alpha^5 \quad (34)$$

Thus, the entropy generation due to the fluid pressure drops is obtained substituting Equation (33) in Equation (28):

$$S_{gen,hydro} = \frac{\dot{m}_{channel}}{\rho T}\left[\frac{(f\,\mathrm{Re})\mu V_{mean} x(\alpha+1)^2}{2H^2_{channel}\alpha^4} + K(\infty)\frac{\rho V^2_{mean}}{2}\right] \quad (35)$$

The total entropy generation in the channel is the sum of both thermal and hydrodynamic entropy generation. The total entropy generation in the system is calculated in a similar way that Equation (22).

Finally, the Bejan number, Be, is a good parameter to determine what phenomenon is the larger

generator of losses in a specific thermodynamic system. This number is given by the ratio between the thermal entropy generation and the total entropy generation [19]. This number varies in the range 0 to 1.

$$Be = \frac{S_{gen,therm}}{S_{gen}} \tag{36}$$

A Be near zero indicates that the system has the larger losses due to the fluid motion. A Be near 1 indicates that the thermal energy that is not used by the system is larger and must be taken into account. A Be near 0.5 indicates the system is balanced, that is, the energy losses, thermal and hydrodynamically, are similar.

The entropy generation equations obtained for both conditions are evaluated in order to observe their behavior. Table 2 shows the properties of the fluid which is considered for flowing through the channels. The thermal conductivity of the solid, k_s, is considered as 300 W/m-K.

Table 1. Constant parameters for correlations.

	A	B	C	D
1	8.2313	-1.3553	8.2313	0.6796
2	-2.295	1.9467	1.9349	1.2197
3	2.2389	-1.7012	-2.295	3.3089
4	2.0263	0.9564	0.92381	-9.5921
5	0.29805	-0.2537	7.928	8.9089
6	0.0065322	--	0.0033937	-2.9959

Table 2. Fluid properties values.

Property	Value
Thermal conductivity, k_f	0.6069 W/m-K
Viscosity, μ	889.9x10^{-6} kg/m-s
Density, ρ	997 kg/m^3
Prandtl number, Pr	6

5. Results

5.1. Results for fully developed flow consideration

A heat sink arrangement formed by 100 rectangular microchannels was used for evaluating Equation (22). The Reynolds number of the fluid at the channel inlet is 100. The total heat flux supplied to the bottom wall of the heat sink is 100 W/cm^2. The environmental temperature is taken as 300 K. The channel height was evaluated with three constant values (20 μm, 100 μm and 200 μm.) These values are taken in order to get channel hydraulic diameters into the range of microchannel classification [3]. The total entropy generation in the system for these conditions is shown in Figure 5. This presents a larger decrement when the channel aspect ratio and channel hydraulic diameter are increased. For a channel with $H_{channel}$=200 μm and α values larger than 0.8, the entropy generation is kept almost constant. This is due to the thermal entropy generated at this conditions and dimensions takes large effect (Figure 7.) Thus, this curve section can be considered as an optimal zone for these conditions. Under this tendency, the same behavior of the total entropy generation occurs when the channel height is decreased, but the minimum point occurs for channel aspect ratios larger than 1.

The behavior of the total entropy generation is larger affected by the hydrodynamic entropy generation for lower channel heights and channel aspect rations (Figure 6.) It is possible to observe almost the same behavior with different order of magnitude. The lower value is near 10^{-7}. This generation is affected directly by the pressure drop which is affected inversely by the channel hydraulic diameter. This means, the pressure drop diminishes for larger channel hydraulic diameter due to the friction between the fluid and the channel walls is diminished. The fluid velocity is lesser for large hydraulic diameter since the Reynolds number is kept for all cases. This reduces the friction effects as well.

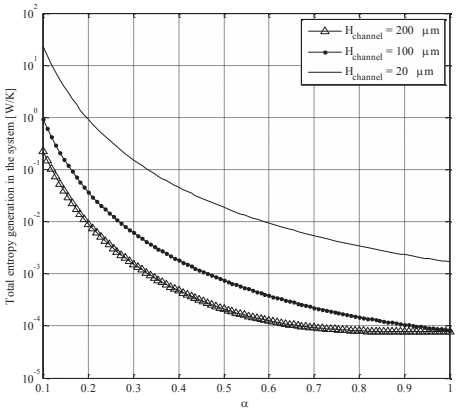

Figure 5. Variation of total entropy generation in the system against channel aspect ratio.

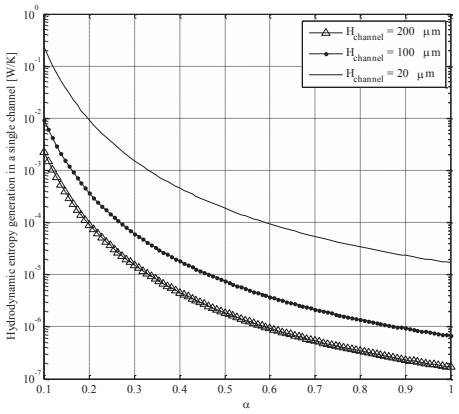

Figure 6. Variation of hydrodynamic entropy generation in a single channel against channel aspect ratio.

On the other hand, the thermal entropy generation presents a larger impact in the total entropy generation for large channel heights and channel aspect ratios (Figure 7.) In this figure it is possible to observe that the larger value is around 10^{-6}. This tendency is due mainly to the Nusselt number performance for this condition. When the channel aspect ratio is increased, the Nusselt number decreases drastically until α values near 0.4. After this, the decrement is smoother since the heat transfer area is lesser for smaller α values, and the convective coefficient is increased as well. It is important to emphasize that this parameter affects inversely the thermal entropy generation, this means, for larger Nusselt numbers, the system becomes more efficient, reducing the thermal losses (thermal entropy generation.) Thus, one idea emerges: the larger entropy generation for smaller channels with lower channel aspect ratios is generated by hydrodynamic effects; however for larger channels with larger channel aspect ratios, the thermal effects present a larger impact in the total entropy generation.

Figures 8 and 9 present the variation of the total entropy generation against the channel height for the same heat sink arrangement with a channel aspect ratio of 0.5. In Figure 8 it is presented the behavior for different Reynolds numbers and Figure 9 for different heat fluxes. Results agree with the previously mentioned. It is generated a clear increment of this generation when the Reynolds number increases. When the heat flux increases, there is not a large difference in the total entropy generation. Also, in these figures it is possible to observer that the entropy generation decreases when the channel height increases. Thus, another important sentence can be mentioned: for a specific channel aspect ratio, the minimum total entropy generation is obtained for larger channel hydraulic diameter.

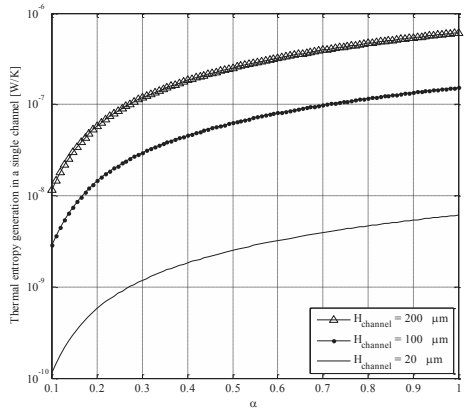

Figure 7. Variation of thermal entropy generation in a single channel against channel aspect ratio.

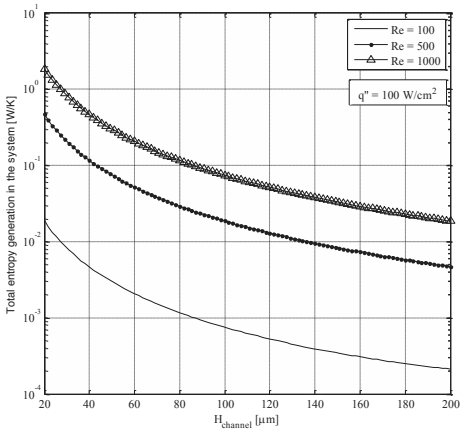

Figure 8. Variation of total entropy generation in the system against $H_{channel}$ for different Reynolds numbers.

Finally, the Bejan number can be calculated for the system with fully developed condition. It is possible to observe from Equation (36) that the Bejan number is almost zero for smaller channel hydraulic diameter and aspect ratios; and near 0.8 for larger channel hydraulic diameters and aspect ratios. This means that the system has a good

thermal development when the arrangement is formed by microchannel with channel hydraulic diameters near nanochannels, nevertheless large part of energy is lost for the fluid motion. An optimal performance under these conditions can be observed for channel aspect ratio upper 0.8 and channel height near 200 μm.

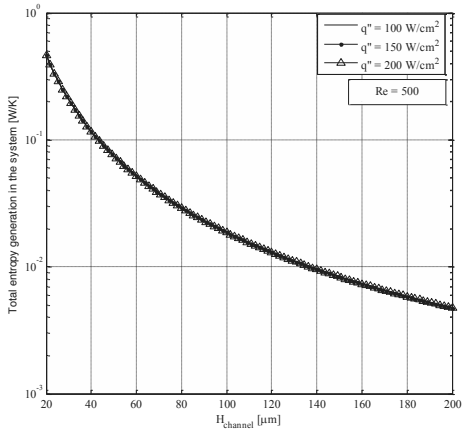

Figure 9. Variation of total entropy generation in the system against $H_{channel}$ for different total heat fluxes.

5.2. Results for non- developed flow consideration

Figure 10 shows the variation of the total entropy generation with the channel aspect ratio. The conditions mentioned in the results for fully developed condition are used for calculating this generation under this condition. The same channel heights (10 μm, 100 μm and 200 μm) are used. The curves present a similar behavior that Figure 5, however, the total entropy generation in this calculus was lightly larger than in the fully developed condition for lower channel aspect ratios and channel heights. This agrees with theory. It is not observe a minimum point or asymptotic behavior in curves. Figure 11 presents the hydrodynamic entropy generation. This shows a similar behavior that Figure 6 with the same lightly increment. The Hagenbach's factor, which involves all the energy losses due to the development of the hydrodynamic boundary layer, is the main guilty of this variation. Since this is only added linealy to the quantity of the entropy generation (Equation (35)), the difference between both conditions is kept along the variation of channel aspect ratio for this entropy generation.

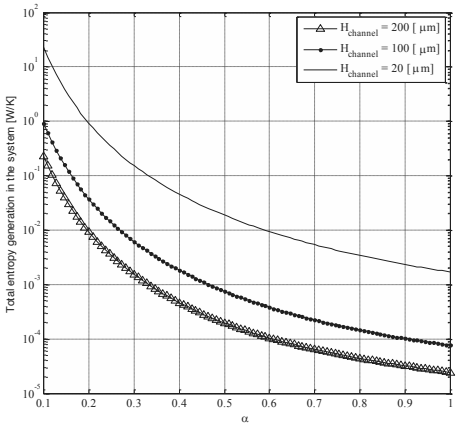

Figure 10. Variation of total entropy generation in the system against channel aspect ratio.

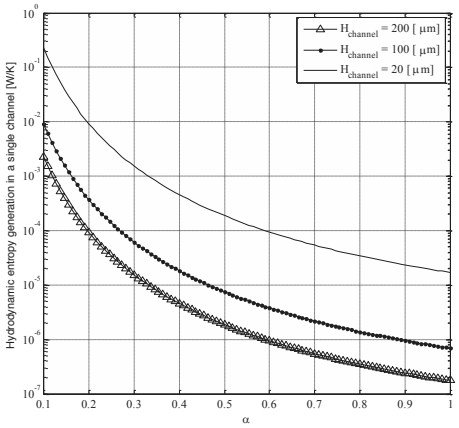

Figure 11. Variation of hydrodynamic entropy generation in a single channel against channel aspect ratio.

Figure 12 shows the thermal entropy generation for different channel aspect ratios using the same channel heights. The thermal entropy generated in these cases is lower than Figure 7. This agrees with theory. Since the Nusselt number is larger for the non-fully developed condition, there is a large capability of the fluid to dissipate heat (absorb heat from channel walls.) This makes more efficient the heat dissipation and the thermal energy is better managed in the process, reducing thermal losses. One important observation is that the thermal inlet length required for developing the thermal boundary layer is not achieved into the channel for a configuration $H_{channel}$=200 μm and α

values upper to 0.73. This is due to the study considers that the heat sink has a length of 0.01 m.

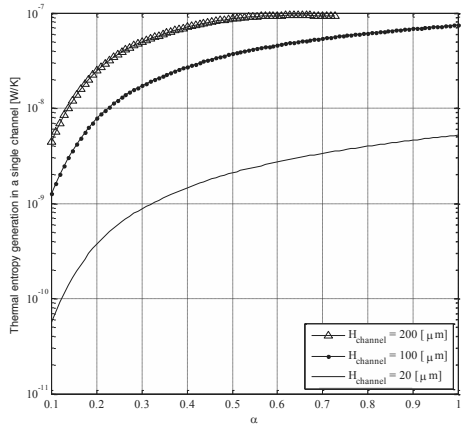

Figure 12. Variation of thermal entropy generation in a single channel against channel aspect ratio.

Figures 13 and 14 show the total entropy generated for different channel heights with a channel aspect ratio of 0.5. Figure 13 presents the results obtained for different Reynolds numbers and Figure 14 for different total heat fluxes. Results show a similar tendency that the results previously presented for fully developed condition. The total entropy generation is clearly affected by the Reynolds number. However, the heat supplied on the system does not affect in an important way the total entropy generation. The hydrodynamic and thermal inlet lengths required for developing both boundary layers for large channels was not reached into the channel due to the fluid velocity. Thus, curves are cut at some channel height. Comparing Figure 8 with Figure 13, it is possible to observe that the hydrodynamic entropy generation for non-developed condition is lightly larger than the obtained for fully developed condition for lower channel aspect ratios and Reynolds numbers due to the fluid friction increases when it is developing. Also, comparing Figures 9 and 14, it is possible to observe that the thermal entropy generation is larger for fully developed condition. This behavior is mainly due to the Nusselt number. For non-developed condition this number is larger, producing a better thermal development of the device.

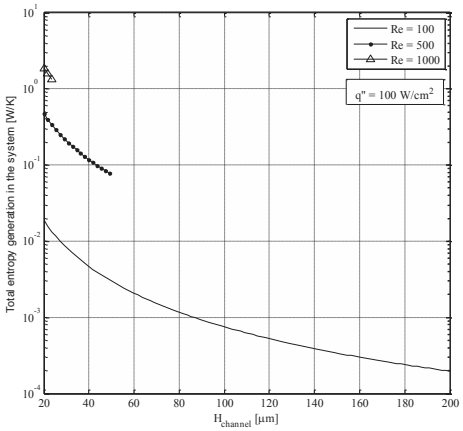

Figure 13. Variation of total entropy generation in the system with $H_{channel}$ for different Reynolds numbers.

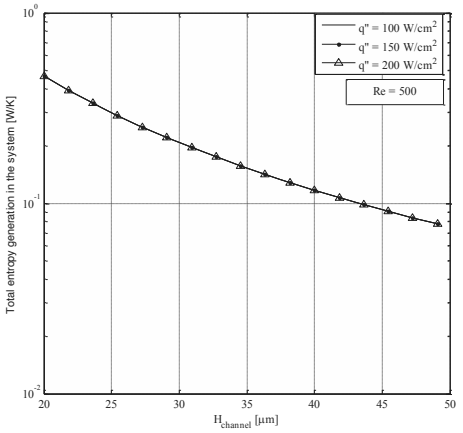

Figure 14. Variation of total entropy generation in the system with $H_{channel}$ for different total heat transfer.

The Bejan number can be calculated for the system with non-developed condition. From Equation (36) it is possible to observe that the Bejan number is almost zero for smaller channel hydraulic diameter and aspect ratios; and near 0.3 for larger channel hydraulic diameters and aspect ratios. This means, the large entropy generation in the system is caused by hydrodynamic effects, affecting seriously at each channel aspect ratios. An optimal point is not observed clearly.

6. Conclusions

Two equations to calculate the total entropy generation in a microchannel heat sink considering the both thermal and hydrodynamic effects with fully and non-developed fluid inlet conditions were obtained. Results show that the entropy generation at small channel hydraulic diameters and low channel aspect ratios is caused mainly by hydrodynamic effects for both conditions. For large hydrodynamic diameters and channel aspect ratios, under fully developed condition, thermal effects have significant influence in the entropy generation due to the Nusselt variation. Arrangement with these considerations and non-developed inlet flow are affected more seriously by hydrodynamic effects. The Bejan numbers obtained for each condition ratifies the observation in curves. It is possible to obtain a Bejan number near 0.8 and 0.3 for fully and non-developed conditions, respectively.

References

[1] Tuckerman, D.B., Heat transfer microstructures for integrated circuits, PhD Thesis, Stanford, CA, Stanford University, 1984.

[2] Phillips, R. J., Microchannel heat sinks, Advances in Thermal Modeling of Electronic Components and Systems, NewYork, NY: Hemisphere Publishing Corporation, 1990, Chapter 3.

[3] Gad-el-Hak, M., The fluid mechanics of microdevices, J. Fluid. Eng., 121, 7–33, 1999.

[4] Xu, B., Ooi, K. T., Wong, N. T., and Choi, W. K., Experimental investigation of flow friction for liquid flow in microchannels, Int. Com. Heat Mass Trans., 27(8), 1165–1176, 2000.

[5] Judy, J., Maynes, D., and Webb, B. W., Characterization of frictional pressure drop for liquid flows through microchannels, Int. J. Heat Mass Trans, 45, 3477–3489, 2002.

[6] Tu, X. and Hrnjak, P., Experimental investigation of single-phase flow and pressure drop through rectangular microchannels, ASME ICMM2003-1028, April 24–25, 257–267, 2003.

[7] Baviere, R., Ayela, F., Le Person, S., and Favre-Marinet, M., 2004, An experimental study of water flow in smooth and rough rectangular microchannels, ASME ICMM2004-2338, Rochester, NY USA, June 17– 19, 221–228, 2004.

[8] Garimella, S. V., and Singhal, V., Single-phase flow and heat transport and pumping considerations in microchannel heat sinks, Heat Trans. Eng., 25(1), 15–25, 2004.

[9] Kandlikar, S. G. and Grande, W. J., Evaluation of single-phase flow in microchannels for high flux chip cooling – thermohydraulic performance enhancement and fabrication technology, Heat Trans. Eng., 25(8), 5–16, 2004.

[10] Kandlikar, S. G. High heat flux removal with microchannels – A roadmap of challenges and opportunities, Heat Trans. Eng., 26(8), 2005.

[11] Steinke, M. E. and Kandlikar, S. G., Review of single-phase liquid heat transfer in microchannels, ASME ICMM2005-75114, Toronto, Canada, June 13–15, 2005.

[12] Sobhan C. B., Arimboor, K., Abraham, T., Anoop, P. S., Peterson, G. P., "Microchannels Optimization for Heat Dissipation from a Solid Subtrate", ECOS 2006, Vol. 1 A4, 2006.

[13] Abbassi, A., Entropy generation analysis in a uniform heated previous microchannel heat sink, Int. J. Heat Mass Trans, 50, 1932-1947, 2007.

[14] Li, J., Peterson, G. P., "3-Dimensional Numerical optimization of Silicon-Based High Performance Parallel Microchannel Heat Sink with Liquid Flow", International Journal of Heat and Mass Transfer, Vol. 50, 2007.

[15] Jankowski, T. A. Minimizing entropy generation in internal flows by adjusting the shape of the cross-section, Int. J. Heat Mass Trans. 52, 3439-3445, 2009.

[16] Hung, Y. M., A comparative study of viscous dissipation effect on entropy generation in single-phase liquid flow in microchannels, Int. J Heat Mass Trans, 50, 1026-1035, 2009.

[17] Shah, R. K. and London, A. L., Laminar Flow Forced Convection in Ducts, Supplement to Advances in Heat Transfer, New York: Academic Press, 1978.

[18] Kakac, S., Shah, R. K., and Aung, W., Handbook of Single-Phase Convective Heat Transfer, New York: John&Wiley and Sons, Inc., 1987.

[19] Bejan, A., Kulacki, F. A., Entropy Generation Minimization: The Method Of Thermodynamic Optimization Of Finite-size Systems And Finite-time Processes (mechanical Engineering Series), 1996 CRC Press LLC

[20] Kandlinkar, S., Garimella, S., Li, D., Colin, S., King, M.R., Heat Transfer and Fluid Flow in Minichannels and Microchannels Elsevier Publishers, 2006.

Improvement and Automation of a Single Sinker Densimeter for the Determination of (p, ρ, T) Properties of Mixtures of Gases Related with Biogas

María E. Mondéjar, José J. Segovia, Miguel A. Villamañán, Rosa M. Villamañán, M. Carmen Martín and César R. Chamorro

Escuela de Ingenierías Industriales, Valladolid, Spain

Abstract: Accurate reference equations of state for pure gases and mixtures are required to optimize the gas transport and storage systems, and also, to increase the efficiency of the industrial processes in which these gases are involved. Reliable (p, ρ, T) measurements are essential for the development of these equations.

A single sinker densimeter with a magnetic suspension coupling has been modified and optimized for the measurement of accurate gas (p, ρ, T) properties over the range 250-400 K and 0-20 MPa. It is based on Archimedes's Principle and measures both pure gases and mixtures densities. Several modifications have been made to improve the measurement procedure. In first place the original sinker has been replaced by a double in volume silicon sinker to increase the density resolution. In second place the temperature measurement procedure has been improved and thermal isolation of the cell has been increased. In third place a new pressure transducer has been added to the existing one.

To test the effectiveness of these modifications density measurements on Nitrogen were performed in the whole temperature and pressure ranges of the equipment. Mixtures of components of Biogas are planned to be measured as a contribution to develop and test its equations of state.

Keywords: Biogas, Density measurements, Nitrogen, (p, ρ, T) data, Single sinker densimeter.

1. Introduction

Nowadays the development of new alternative fuels is taking relevance as it is needed to decrease the external energy dependence of our countries. Among these renewable fuels biogas is intended to play an important part whether using it as a substitute of natural gas or by injecting it into the natural gas grid. To optimize the exploitation, storage and use of this resource an accurate gas phase behavior description of it is essential. This description is mainly determined by the equation of state of the gas.

The need of an accurate description of the natural gas behavior in the early 90's brought about the development of the AGA8-DC92 equation of state which was internationally accepted as a standard for the calculation of natural gas properties in the gas phase. Later the GERG-2004 equation of state [1] was developed to increase the accuracy and widen the range of application of the previous one.

In the same way, the growing utilization of biogas makes necessary to develop a multiparameter equation of state for biogas in order to describe with sufficient precision its thermodynamic behavior in a wide range of temperatures and pressures and for different compositions. For this purpose accurate pressure-density-temperature (p, ρ, T) data both for pure components and binary mixtures are of great importance. Binary mixtures data are also of special relevance because there is a lack of this kind of data and they are necessary to study the molecular interaction which takes place in the mixture.

The single sinker densimeter with a magnetic suspension coupling is a very accurate density-measuring method for gases that was developed in the early 90's by Wagner's group [2]. It is based on the Archimedes's principle whereby a solid body in a fluid displaces a volume of fluid which weight is equal to the buoyancy force exerted by the fluid upon the body. Density is then determined by the following relation

$$\rho = \left(m_{s,vacuum} - m_{s,fluid}\right)/V_s(T,p), \qquad (1)$$

where $\left(m_{s,vacuum} - m_{s,fluid}\right)$ is the buoyancy force calculated as the difference between the sinker mass in vacuum and the sinker mass in the fluid, and $V_s(T,p)$ is the sinker volume as a function of the fluid temperature and pressure.

The main novelty of this densimeter is the magnetic coupling between the balance and the sinker support so that the pressurized measuring cell is completely isolated from the balance. This fact allows a wide range in temperature and pressure to be covered.

Our single sinker densimeter is suitable for operation for densities in the range (0 to 2000) kg m^{-3} over a temperature range of (233 to 523) K and pressure range up to 20 MPa. Several modifications have been carried in order to improve the measurement method and to reduce the measuring uncertainty on density. The overall uncertainty in density ρ after these modifications is estimated to be (1.1 10^{-4} ρ + 1.9 10^{-3} kg m^{-3}) (coverage factor k=2). This single sinker densimeter was used previously to perform (p, ρ, T) measurements of binary mixtures of methane and nitrogen at different compositions. These experimental data [3], together with speed of sound data performed for the same mixtures by our group [4], among a huge number of experimental data for pure components and mixtures contributed to the development of the GERG-2004 equations of state for natural gas [1].

2. Experimental

In order to improve the measuring process and to reduce the overall uncertainty several modifications were carried out on our single sinker densimeter. In first place the old titanium sinker was replaced by a new silicon sinker in order to increase the balance resolution and to reduce the measuring uncertainty. A complete study of the temperature and pressure dependence of sinker volume was made. In second place both temperature and pressure measuring procedures were improved by the addition of new temperature probes and pressure transducers. Moreover the cell insulation was increased and a temperature homogeneity and stability study was made. A description of the initial state of experimental setup is given in [3].

2.1. Change of sinker

The old titanium sinker (volume $V_s \approx 13 cm^3$ and mass $m_s \approx 60 g$) was replaced by a new silicon sinker (volume $V_s \approx 26 cm^3$ and mass $m_s \approx 60 g$) in order to improve the balance resolution (10^{-5} g). This new sinker has the same mass as the old one but doubles its volume so that for a same temperature and pressure conditions the silicon sinker experiments the double buoyancy force than the titanium one. When the buoyancy force is bigger it is measured by the balance with higher accuracy due to its resolution and this fact is transferred to the final density measurement.

2.1.1. T, p – influence on sinker volume

The sinker volume is variable and depends on the temperature and the pressure of the fluid surrounding it. This dependence is given by the following relation

$$V_s(T,p) = V_{s0}[1 + 3\alpha\Delta T - 3\Delta p(1-2\nu)/E], \quad (2)$$

where V_{s0} is the calibration volume of the sinker calibrated at CEM (Centro Español de Metrología) , α the thermal expansion coefficient, ν the Poisson's coefficient and E the Young's modulus. Both temperature and pressure gradients are respect to the calibration conditions. These are given in Table 1.

Table 1. Calibration conditions of the silicon sinker.

Magnitude	Value
Volume, V_{s0}	26.444 cm^3
Temperature	294.45 K
Pressure	93.417 kPa

To determine the volume variation of the new silicon sinker a research on its mechanical and thermal properties was made. Due to the anisotropy of the silicon several hypothesis were accounted.

In first place the thermal expansion coefficient was taken as a function of temperature following the relation [5],

$$\alpha(T) = \left(3.725\left(1 - e^{-5.88\,10^{-3}(T-124)}\right) + 5.548\,10^{-4}T\right)10^{-6} \quad (3)$$

which is valid in the range (120-1500) K.

Mechanical properties were obtained as functions of the second order elastic constants C_{11}, C_{12} and C_{44}. The average values for these constants were estimated by considering the material as isotropic and they depend on temperature as indicated in (4),(5) and (6) [6],

$$\left(\frac{1}{C_{11}}\right)\frac{dC_{11}}{dT} = -9.4\,10^{-5}K^{-1} \quad (4)$$

$$\left(\frac{1}{C_{12}}\right)\frac{dC_{12}}{dT} = -9.8\,10^{-5}K^{-1} \quad (5)$$

$$\left(\frac{1}{C_{44}}\right)\frac{dC_{44}}{dT} = -8.3\,10^{-5}K^{-1} \quad (6)$$

The room temperature values of these constants are C_{11}=1.6564 10^{11} Pa, C_{12}=0.6394 10^{11} Pa and C_{44}=0.7951 10^{11} Pa [7]. Thus, Young's modulus

and Poisson's coefficient can be calculated by using the Voigt average as indicated in (7) and (8)

$$E = 2(C_{44} - H/5)(1 + \nu), \quad (7)$$

$$\nu = \frac{C_{12} - H/5}{2(C_{12} + C_{44} - 2H/5)}, \quad (8)$$

where $H=2C_{44}+C_{12}-C_{11}$ is the anisotropy factor. Once calculated, the expressions obtained for E and ν when fitting them to a linear regression in the range (250-400) K are those shown in (9) and (10)

$$E = 1.6681\ 10^5 - 1.4494\ 10^2\ T \quad (9)$$

$$\nu = 0.21788 - 2.3748\ 10^{-5}\ T \quad (10)$$

Finally, the volume relation for the silicon sinker is obtained by substituting relations (3) and (9, 10) in expression (2).

2.2. Improvement on temperature procedure measurement

Initially a single temperature probe (Rosemount model 162D) was used to measure the cell temperature. Nonetheless the temperature distribution in the cell was unknown and temperature gradients could exist between different points of the cell. Thus, two more PRT-25 probes (Minco model S1059PJ5X6) were added to the existing one. They are now placed surrounding the cell in a radial and an axial way so that Minco's probes were diametrically opposed while Rosemount's probe was above one of the others. Thus, temperature homogeneity in both directions could be studied.

The probes were connected to an AC resistance bridge (Automatic Systems Laboratory model F700). To reduce the temperature measuring uncertainty the internal resistor of the bridge was replaced by a calibrated resistor (Tinsley model 5685A, 25Ω).

To avoid heat flows between the measuring cell and the ambient guaranteeing the temperature stability different isolation slides were added to the cell. Immediately in contact with the cylinder covering the cell silicone foam insulation (250 kg m^{-3}) was disposed. This foam is suitable to work in the range (213-473) K. Over it a casing with polyethylene insulation (Armaflex) for the range (203-383) K was disposed.

Pipes between the gas cylinder and the measuring cell and conduits for the thermostatic bath oil were also insulated.

Once temperature probes were added and cell insulation was improved a study about the cell temperature homogeneity and stability was made.

Thermal homogeneity is defined as the maximum difference between the temperature values on two different points of an isothermal medium. To study the thermal homogeneity in the measuring cell the temperature values for each probe were analyzed and compared in the range (250-400) K. This study yielded that the maximum difference between the temperature values measured by each probe take place when the cell temperature is far removed from the environment temperature. This is due to the fact that bigger heat losses occur when a bigger temperature gradient exists. Moreover, the temperature gradient is bigger in the axial than in the radial direction. This fact is negligible since the Rosemount's probe is nearer the electromagnet place than the measuring cell. Hence temperature homogeneity in the cell can be considered as acceptable since the maximum temperature gradients are lower than the temperature measuring uncertainties of the probes, which are shown in Table 2.

Table 2. Temperature probes uncertainties in mK at different calibration points.

Probe	Temperature uncertainty (mK)
Rosemount	12
Minco 712	8
Minco 713	8

Thermal stability is defined as the maximum temperature variation during a period of time in an isothermal medium. To study the thermal stability in the measuring cell the average value of the temperature measured by the Minco's probes was analyzed during a period of time similar to that needed for a complete density measurement.

Table 3. Maximum temperature gradients in mK yielded by the study.

Gradient	Value (mK)
Maximum temperature gradient in the radial direction	6.8
Maximum temperature gradient in the axial direction	8.9
Maximum temperature gradient in a measuring period	5

Results yielded that the maximum difference between the initial and the final temperature of the cell during the measuring time took place also when this temperature was far removed from the environment temperature. However this difference

resulted to be lower than the measuring uncertainty of the probes.

Main results of the temperature homogeneity and stability study are shown in Table 3.

2.3. Improvement on pressure procedure measurement

Initially pressure was measured using a Paroscientific absolute pressure transducer (Paroscientific model 43KR-HHT-101) which operated in the range (0-20) MPa. However this pressure transducer was not accurate enough at low pressures (below 2 MPa). To cover all the pressure range with a low uncertainty a new

Paroscientific absolute pressure transducer (Paroscientific model 2300A-101) for the range (0-2) MPa was added. Both transducers were calibrated against a dead weight gauge (traceable to international standards) at our calibration facility. Pressure measuring uncertainties for both transducers are shown in Table 4.

Table 4. Pressure measuring uncertainties of the transducers.

Pressure transducer	Uncertainty
Paroscientific model 43Kr-HHT-101	$7.5\ 10^{-4}\ p+6.86\ 10^{-4}$
Paroscientific model 2300A-101	$6\ 10^{-4}\ p+5.8\ 10^{-5}$

3. Results

To check the accuracy of the single-sinker densimeter nitrogen (p, ρ, T) measurements were performed in the homogeneous gas region along seven different isotherms at temperatures between 250 and 400 K, and pressures up to 20 MPa. The experimental results were compared with the reference equation of state for nitrogen developed by Span et al. [8].

The nitrogen used for the measurements was supplied by Alphagaz (Air Liquid), Spain, with a certified mole fraction purity of $x(N_2) \geq 0.999999$ {impurities: $x(H_2O) \leq 0.5\ 10^{-6}$, $x(O_2) \leq 0.1\ 10^{-6}$, $x(C_nH_m) \leq 0.1\ 10^{-6}$, $x(CO) \leq 0.1\ 10^{-6}$, $x(CO_2) \leq 0.1\ 10^{-6}$, $x(H_2) \leq 0.1\ 10^{-6}$}. The experimental (p, ρ, T) results for nitrogen are listed in Table 5 together with the relative deviations from the densities obtained from the reference equation of state for nitrogen reported by Span et al. [8]. (p, ρ, T) measured data are also shown as a plot in Fig. 1.

Relative deviations for each measured point are shown in Fig. 2. All measurements have a relative deviation below 0.02 percent which is the estimated uncertainty of the equation of state for nitrogen in the working range of temperature and pressure.

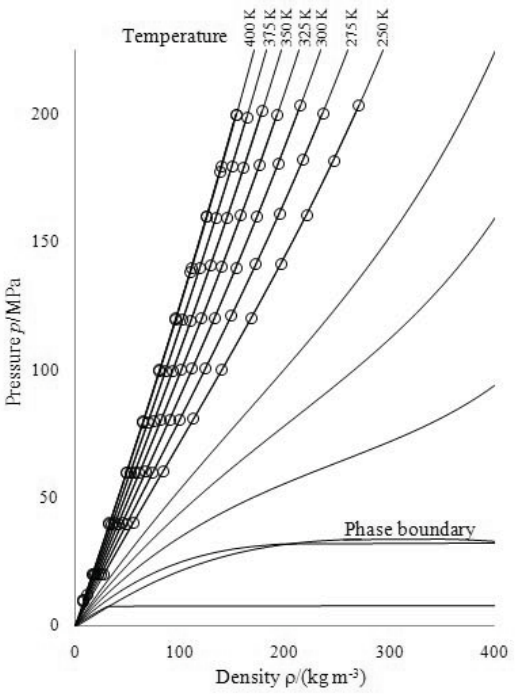

Fig. 1. Survey of the (p, ρ, T) surface of nitrogen measured with the single-sinker densimeter: ○ measured point.

Both sinker volume and mass were previously calibrated in the Centro Español de Metrología, CEM, whereas temperature and pressure transducers were calibrated at our own calibration facility. All measurements are traceable to international standards. The uncertainty in temperature is estimated to be 5.7 mK and the uncertainty in pressure is estimated to be $7.5\ 10^{-4}\ p+4.0\ 10^{-4}$ in the range (2-20 MPa) and $6.0\ 10^{-4}\ p+5.8\ 10^{-5}$ in the range (0-2 MPa). Thus, the overall uncertainty in density is estimated to be ($1.1\ 10^{-4}\ \rho + 1.9\ 10^{-3}$ kg m^{-3}).

Table 5. (p, ρ, T) results for nitrogen and comparison with densities (ρ_{calc}) obtained with the reference equation of state for nitrogen by Span et al. [8].

T/K	p/MPa	ρ/(kg m^{-3})	10^2 (ρ− ρ_{calc})/ ρ_{calc}
		250 K isotherm	
250,015	20,3096	271,521	0,006
250,011	18,1706	247,133	0,004
250,011	16,0568	221,461	0,002
250,010	14,1270	196,751	0,002
250,012	12,0313	168,705	0,000
250,013	9,98981	140,439	0,000
250,009	8,07095	113,310	-0,005
250,012	6,03689	84,3056	-0,004
250,006	4,00768	55,4689	-0,006
250,009	1,98597	27,1564	0,000
		275 K isotherm	
275,020	19,9403	235,969	0,004
275,020	17,8621	214,438	0,004
275,024	16,0267	194,541	0,007
275,023	14,0211	171,910	0,006
275,020	12,0092	148,371	0,000
275,017	10,0169	124,389	0,002
275,020	8,00918	99,6989	0,000
275,018	6,00173	74,6924	0,000
275,014	3,99985	49,6374	0,000
275,013	1,99762	24,9054	-0,001
		300 K isotherm	
299,936	20,3095	215,440	0,006
299,941	18,0778	194,580	0,006
299,950	16,0093	174,403	0,005
299,950	13,9924	154,000	0,003
299,954	12,0280	133,492	0,003
299,959	10,0390	112,168	0,002
299,957	8,04186	90,2957	0,000
299,956	6,03708	67,9893	0,000
299,954	4,00241	45,1222	0,000
299,952	1,98111	22,3146	0,003
		325 K isotherm	
324,971	19,9664	193,263	0,005
324,973	17,9972	176,335	0,006
324,971	16,0133	158,681	0,005
324,972	14,0046	140,225	0,005

Table 5. Continued

T/K	p/MPa	ρ/(kg m^{-3})	10^2 (ρ− ρ_{calc})/ ρ_{calc}
324,975	12,0017	121,274	0,003
324,973	9,98872	101,736	0,003
324,974	8,02754	82,2803	-0,002
324,971	5,97222	61,5310	-0,006
324,970	3,98061	41,1593	-0,003
324,972	1,18993	12,3347	0,000
		350 K isotherm	
349,932	20,0944	178,806	0,000
349,941	17,9046	161,408	-0,001
349,940	15,9061	144,999	-0,005
349,939	14,0669	129,470	-0,003
349,935	11,9142	110,787	-0,006
349,938	9,97072	93,4927	-0,003
349,940	7,99363	75,5087	-0,013
349,936	5,96474	56,7158	-0,013
349,939	3,99351	38,1727	-0,011
349,939	1,99345	19,1363	0,000
		375 K isotherm	
374,957	19,8369	163,963	0,002
374,958	17,9184	149,751	0,001
374,957	15,9261	134,570	0,000
374,959	13,9648	119,210	0,000
374,957	11,9392	102,931	-0,002
374,956	9,95426	86,5943	0,000
374,957	7,96134	69,8274	-0,004
374,956	5,98854	52,9077	-0,011
374,957	3,98711	35,8157	-0,010
374,957	1,99714	18,0409	-0,001
		400 K isotherm	
400,030	19,9786	154,016	0,000
400,029	17,9468	139,944	0,000
400,031	15,9775	125,926	0,000
400,029	13,9637	111,214	0,000
400,031	11,9938	96,4609	0,000
400,030	9,98197	81,0376	-0,002
400,032	7,98816	65,4192	-0,002
400,029	5,99146	49,4645	-0,005
400,027	3,98587	33,1519	-0,005
400,026	1,99611	16,7135	-0,002

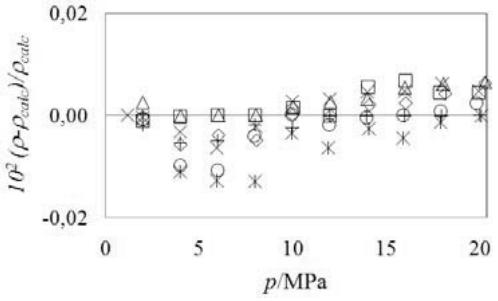

Fig. 2. Relative density deviations of experimental (p, ρ, T) values and calculated densities (ρ_{calc}) of nitrogen from the equation of state of Span et al. [8]:◇ 250 K; □ 275 K; △ 300 K; × 325 K; ∗ 350 K; ○ 375 K; + 400 K.

4. Discussion

A complete set of (p, ρ, T) measurements on nitrogen over the whole ranges of temperature and pressure of our single sinker densimeter was made to check its accuracy. Experimental results show an agreement with values obtained from the equation of state for nitrogen of Span et al. [8] to within less than 0.02 percent in density.

Both the temperature and pressure measuring uncertainties were reduced by the improvement of the measuring procedures. The overall uncertainty in density was also reduced due to the modifications that were made on the densimeter. Differences between measuring uncertainties before and after these modifications are shown in Table 6.

Table 6. Measuring uncertainties before and after the improvements.

Magnitude	Units	Estimated uncertainty
	Before	
Temperature	mK	8
Pressure	MPa	$7.5\ 10^{-4}$ p+$4.0\ 10^{-4}$
Density	kg m^{-3}	$1.5\ 10^{-4}$ ρ+$3.8\ 10^{-3}$
	After	
Temperature	mK	5.7
Pressure (2-20 MPa)	MPa	$7.5\ 10^{-4}$ p+$6.86\ 10^{-4}$
Pressure (0-2 MPa)	MPa	$6\ 10^{-4}$ p+$5.8\ 10^{-5}$
Density	kg m^{-3}	$1.1\ 10^{-4}$ ρ+$1.9\ 10^{-3}$

Therefore, the correct operation of the single sinker densimeter in measuring gas densities and its high accuracy were proved.

As a conclusion, the high accuracy measuring method presented on this paper was enhanced by doing several modifications. Improvements on temperature and pressure measuring procedures resulted in a reduction in both temperature and pressure measuring uncertainties. The change of the sinker implied a reduction in the overall uncertainty in density. Thus, more accurate measuring data are expected to be measured.

Several mixtures of biogas components are planned to be measured with this method to contribute to the development of new accurate equations of state.

Nomenclature

E Young's modulus, MPa

m mass, kg

p pressure, MPa

V volume, m^3

T temperature, K

x mole fraction

Greek symbols

α thermal expansion coefficient, K^{-1}

ν Poisson's coefficient

ρ density, kg m^{-3}

Subscripts and superscripts

s sinker

0 calibration conditions

calc density value from the equation of state

References

[1] Kunz, O., Klimeck, R., Wagner, W., Jaeschke, M. The GERG-2004 wide-range reference equation of state for natural gases. To be published as GERG Technical Monograph. Fortschr.-Ber. VDI, VDI-Verlag, Düsseldorf, 2007.

[2] Klimeck, J., Kleinrahm, R. and Wagner, W., 1998, An accurate single-sinker densimeter and measurements of the (p, ρ, T) relation of argon and nitrogen in the temperature range from (235 to 520) K at pressures up to 30 MPa, J. Chem. Thermodynamics, 30, pp. 1571-1588.

[3] Chamorro, C.R., et al., 2006, Measurement of the (pressure, density, temperature) relation of two (methane + nitrogen) gas mixtures at temperatures between 240 and 400 K and pressures up to 20 MPa using an accurate single-sinker densimeter, JJ. Chem. Thermodynamics, 38, pp. 916-922.

[4] Estela-Uribe, J.F., et al., 2006, Speeds of sound in {(1-x)CH4+ xN(2)} with x=(0.10001, 0.19999, and 0.5422) at temperatures between 170 K and 400 K and pressures up to 30 MPa, JJ. Chem. Thermodynamics, 38, pp. 929-937.

[5] Okada, Y., and Tokumaru, Y., 1984, J. Appl. Phys. (USA), vol.56 no.2, pp. 314-320.

[6] Landolt-Bornstein, 1979, *Numerical Data and Functional Relationships in science and Technology*, Ed. K. H. Hellwidge, Springer-Verlag, Germany, Vol. 17 and 22.

[7] Hall, J. J., 1967, Phys. Rev. (USA), vol.161, pp. 756.

[8] Span, R., et al., 2000, A reference quality thermodynamic property formulation for nitrogen, J. Phys. Chem. Ref. Data, 29(6), pp. 1361-1433.

Acknowledgments: Support for this work came from the Programa Nacional de Formación de Profesorado Universitario (FPU) of the Spanish Ministry of Science and Innovation, project ENE2006-133 of the Spanish Ministry of Science and Innovation and from the Junta de Castilla y León reference GR152.

Effects of Particle-Wall Interactions on the Thermodynamic Behavior of Gases at the Nano Scale

Coskun Firat, Altug Sisman

Istanbul Technical University, Energy Institute

Abstract: The thermodynamic behavior of gases confined in nano structures is considerably different than those in macro ones due to the effects of both particle-wall interactions and the wave character of particles. The homogeneous density distribution of a gas at thermodynamic equilibrium is disturbed by these effects. Because of particle-wall interactions, the local density of a gas changes drastically near the domain boundaries. Also, the wave character of the particles causes an inhomogeneous density distribution, especially near the boundaries. Consequently, the apparent density (number of particles over the domain volume) is different than the real one. All the density-dependent thermodynamic properties are affected by the inhomogeneity in the density distribution. Therefore, it is important to consider these effects on local density to analyse the thermodynamic behaviors of gases confined in nano structures. The detailed analysis of these effects on local density also gives a base of knowledge for the experimental verification of quantum size effects on local density due to the wave character of particles. In this study, the density distributions of classical (Maxwellian) and quantum (both Fermi and Bose) gases are calculated and investigated by considering both particle-wall interactions and quantum size effects. The results can be used for experimental verification of quantum size effects on gas density as well as the modeling of nano heat engines.

Keywords: Quantum size effects, density distribution, Lennard-Jones potential, thermodynamic properties

1. Introduction

Today, especially in parallel to progress in semiconductor technology, the development of nanotechnology makes the mechanical systems and structures at the micro/nano scale possible. Mechanical structures at the micro/nano scale such as gas turbines, pumps, mixers, heat exchangers, valves, etc., bring the following topics into consideration: how do the thermodynamic properties of gases at the nano scale differ, how can they be modeled, how can one make use of these differences, and how new devices and technologies can be developed at this scale. In this perspective, the subject of quantum size effects (QSE) on the thermodynamics of gases at the micro/nano scale is a new research area and has many potential applications from the technologies of genetics, space, and energy to military ones [1-8].

At the nano scale, the thermodynamic properties (TP) of gases differ from those at macro scales. One of the reasons for this difference is the QSE, which become important when the thermal de Broglie wavelength of particles (λ_T) is not negligible in comparison with the characteristic length of the system ($L=V/A$, V volume, A surface area). In such a case, the continuum approximation for the energy eigenvalues of particles becomes invalid and the discrete nature of energy eigenvalues causes QSE, which are noticeable at the nano scale. QSE make the thermodynamic state functions depend on the geometry (shape) and size of the system, and QSE causes some new and interesting behaviors, which are not observed at the macro scale. Some of them are anisotropic gas pressure, gas diffusion due to size and geometry differences, thermosize effects like thermoelectric effects and the disappearance of the additivity of extensive quantities [9-16].

The homogeneous density distribution of a gas at thermodynamic equilibrium is disturbed by the wave character of particles. All the density dependent thermodynamic properties are affected by the inhomogeneity in the density distribution [17-19].

The density distribution is disturbed also by particle-wall interactions. The interactions occurring between the gas particles and the particles of the walls cause local density changes near the boundaries and, therefore, another size effect appears besides the quantum size effects. The modeling of the change in local density due to particle-wall interactions as well as the wave

Corresponding Author: Altug Sisman, Email: sismanal@itu.edu.tr

character of particles allows one to distinguish these different effects on the density distribution from each other. Therefore, model results provide a basis for an experimental verification of quantum size effects on the thermodynamic properties of gases at the nano scale. In this study, for this purpose, the local density changes in both classical (Maxwellian) and quantum (Fermi and Bose) gases are calculated and examined by considering particle-wall interactions and QSE. To consider QSE, energy eigenvalues and eigenfunctions of particles are obtained by solving the Schrödinger equation. For different temperatures, local density changes due to only particle-wall interactions are compared to the density changes due to both QSE and particle-wall interactions.

The common function used for the interaction potential for particle-wall interactions is the Lennard-Jones, LJ (12-6), potential [20-21]. Therefore, in this study, the LJ (12-6) potential is used for the calculations. Here, the local density distribution of a gas (e.g., He) confined in a rectangular box with wall of, e.g., Si, and having dimensions of L_x, L_y and L_z is investigated. The wall-gas interaction is represented by the LJ. In a rectangular domain, 3D results can be expressed by the production of 1D results for each direction. Therefore, in this study, a one-dimensional problem is discussed. One-dimensional problems are not only simplified problems. In fact, in nano systems, often only one of the dimensions is at a nano scale and therefore, the system can be examined by reducing the problem to a one-dimensional problem.

2. Particle-wall interaction in a 1D domain

In this section, density distributions of both classical (MB) and quantum (FD and BE) gases are investigated under a LJ (12-6) potential in the 1D and 2D domains.

2.1 Lennard-Jones (12-6) interaction potential

For a 1D confinement domain, the LJ (12-6) potential function can be written as follows [20-21]:

$$U(x)=4\varepsilon_{LJ}\left[\left(\frac{r_0}{x}\right)^{12}-\left(\frac{r_0}{x}\right)^{6}\right]+4\varepsilon_{LJ}\left[\left(\frac{r_0}{L-x}\right)^{12}-\left(\frac{r_0}{L-x}\right)^{6}\right] \quad (1)$$

where the parameters r_0 and ε_{LJ} are the characteristic constants in unit length and energy, respectively, L is the domain size and x refers to the position in the domain.

Instead of using the numerical values of the parameters used in the calculations directly, the purpose there is to obtain generalized conclusions by using their dimensionless values. Thus all lengths are divided by the domain length, L and all energies are divided by k_bT to obtain the dimensionless values. In this case, the dimensionless LJ (12-6) potential can be written as follows:

$$\widetilde{U}(\widetilde{x})=\frac{4}{\widetilde{T}}\left[\left(\frac{\widetilde{r}_0}{\widetilde{x}}\right)^{12}-\left(\frac{\widetilde{r}_0}{\widetilde{x}}\right)^{6}\right]+\frac{4}{\widetilde{T}}\left[\left(\frac{\widetilde{r}_0}{1-\widetilde{x}}\right)^{12}-\left(\frac{\widetilde{r}_0}{1-\widetilde{x}}\right)^{6}\right] \quad (2)$$

In this expression, the dimensionless function and variables are defined as $\widetilde{U}(\widetilde{x})=U(\widetilde{x})/k_bT$, $\widetilde{r}_0=r_0/L$, $\widetilde{x}=x/L$, $\widetilde{T}=T/T_{LJ}$ with $T_{LJ}=\varepsilon_{LJ}/k_b$, and k_b equals to the Boltzmann constant. The dimensionless interaction potential between the wall and gas atoms confined in a one-dimensional domain (for L=L_x=1 nm) is given in Fig. 1.

In this study, helium gas confined in a domain made of silicon is considered. The LJ parameters for the He-Si interaction are r_0=0.2855 nm, ε_{LJ}=0.2413 kJ mol^{-1} , and T_{LJ}=29 K [22].

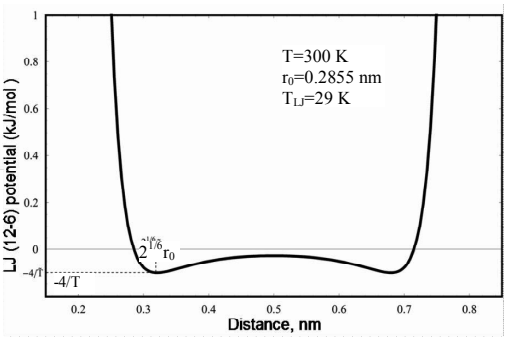

Fig. 1. Dimensionless LJ(12-6) potential function for the He-Si interaction.

2.2 Derivation of the density distribution equations

For Fermi (FD) and Bose (BE) gases, the local density obtained by using dimensionless energy eigenvalues $\tilde{\varepsilon}_r$ and eigenfunctions $\psi_r(\tilde{x})$, which are the solutions of Schrödinger equation for the LJ potential, is expressed as follows [17-19]:

$$\begin{pmatrix}\text{FD}\\ \text{BE}\end{pmatrix} \quad n(\tilde{x}) = \sum_r \frac{|\psi_r(\tilde{x})|^2}{\exp(-\Lambda+\tilde{\varepsilon}_r)\pm 1} \tag{3}$$

where $\Lambda = \mu/k_bT$, is the dimensionless chemical potential in the absence of the LJ potential and is a (global) constant which is independent of the position.

The domain integral of equation (3) is equal to the total number of particles. Thus the apparent density (classical density) is written as follows:

$$\begin{aligned}\begin{pmatrix}\text{FD}\\ \text{BE}\end{pmatrix} \; n_{cl} &= \frac{N}{L} = \frac{1}{\tilde{L}}\int_0^{\tilde{L}} n(\tilde{x})d\tilde{x} \\ &= \frac{1}{\tilde{L}}\sum_r \int_0^{\tilde{L}} \frac{|\psi_r(\tilde{x})|^2 d\tilde{x}}{\exp(-\Lambda+\tilde{\varepsilon}_r)\pm 1} \\ &= \frac{1}{\tilde{L}}\sum_r \frac{1}{\exp(-\Lambda+\tilde{\varepsilon}_r)\pm 1}\end{aligned} \tag{4}$$

Here, it should be noted that the integral of $|\psi_r(\tilde{x})|^2$ is equal to one. Remembering that all the lengths are divided by the domain size, the dimensionless density for both Fermi and Bose gases is written as follows ($\tilde{L}=1$):

$$\begin{pmatrix}\text{FD}\\ \text{BE}\end{pmatrix} \tilde{n}(\tilde{x}) = \frac{n(\tilde{x})}{n_{cl}} = \frac{\sum_r \frac{|\tilde{\psi}_r(\tilde{x})|^2}{\exp(-\Lambda+\tilde{\varepsilon}_r)\pm 1}}{\sum_r \frac{1}{\exp(-\Lambda+\tilde{\varepsilon}_r)\pm 1}} \tag{5}$$

In this equation, the eigenfunctions are also in dimensionless form. The dimensionless Schrödinger equation can be written as follows [23]:

$$-\frac{d^2\tilde{\psi}}{d\tilde{x}^2} + \left(\frac{\pi}{\alpha}\right)^2 \tilde{U}\tilde{\psi} = \left(\frac{\pi}{\alpha}\right)^2 \tilde{\varepsilon}\tilde{\psi} \tag{6}$$

In this expression, $\tilde{\varepsilon} = \varepsilon/k_bT$ and $\alpha = L_c/L$ where $L_c = h/\left(2\sqrt{2mk_bT}\right)$ is half of the most probable de Broglie wavelength and m is the mass of a particle.

For a potential function given by equation (2), equation (6) cannot be solved analytically. The Eigenfunctions and eigenvalues can be obtained only by numerical methods. By using the numerical solution of the Schrödinger equation, the dimensionless local density distribution of a gas confined in a one dimensional domain is obtained.

In order to determine how much the local density distribution changes due to the existence of QSE, the distribution is calculated first by considering only the LJ potential and then by including the QSE.

To calculate the former, the classical probability is used instead of the quantum probability density to calculate the density distribution in the absence of QSE. Thus, a continuous approximation for the energy eigenvalues is used, i.e., $\tilde{\varepsilon} \to \tilde{\varepsilon}_0 + \tilde{U}(\tilde{x}) = (\alpha i)^2 + \tilde{U}(\tilde{x})$ where i is a continuous quantity running from zero to infinity. Integration over i is used to calculate the summation, so that equations (3) and (4) are rewritten as follows, respectively;

$$\begin{aligned}\begin{pmatrix}\text{FD}\\ \text{BE}\end{pmatrix} n(\tilde{x}) &= \frac{1}{\tilde{L}}\int_0^{\infty} \frac{di}{\exp\left[-\Lambda+(\alpha i)^2+\tilde{U}(\tilde{x})\right]\pm 1} \\ &= \mp\frac{\sqrt{\pi}}{2\alpha\tilde{L}} Li_{1/2}\left[\mp\exp\left[\Lambda_L(\tilde{x})\right]\right]\end{aligned} \tag{7}$$

$$\begin{pmatrix} \text{FD} \\ \text{BE} \end{pmatrix} n_{cl} = \frac{N}{L} = \frac{1}{\tilde{L}} \int_0^{\tilde{L}} n(\tilde{x}) d\tilde{x} = \mp \frac{\sqrt{\pi}}{2\alpha \tilde{L}} \int_0^{\tilde{L}} Li_{1/2}\left[\mp \exp\left[\Lambda_L(\tilde{x})\right]\right] d\tilde{x} \quad (8)$$

where $\Lambda_L(\tilde{x}) = \Lambda - \tilde{U}(\tilde{x})$ and $Li_{1/2}$ is the poly-logarithmic function.

The dimensionless density distribution in the absence of QSE is thus,

$$\begin{pmatrix} \text{FD} \\ \text{BE} \end{pmatrix} \tilde{n}(\tilde{x}) = \frac{n(\tilde{x})}{n_{cl}} = \frac{Li_{1/2}\left[\mp \exp\left[\Lambda_L(\tilde{x})\right]\right]}{\int_0^1 Li_{1/2}\left[\mp \exp\left[\Lambda_L(\tilde{x})\right]\right] d\tilde{x}} \quad (9)$$

In the case of Bose gas, $\Lambda_L(\tilde{x}) = \Lambda - \tilde{U}(\tilde{x}) < 0$, and therefore, the upper limit for the zero-dimensional global chemical potential is of the form $\Lambda < -1/\tilde{T}$. In the Maxwell-Boltzmann (MB) limit, equation (9) simplifies to,

$$(\text{MB})\ \tilde{n}(\tilde{x}) = \frac{\exp\left[\Lambda_L(\tilde{x})\right]}{\int_0^1 \exp\left[\Lambda_L(\tilde{x})\right] d\tilde{x}} = \frac{\exp\left[-\tilde{U}(\tilde{x})\right]}{\int_0^1 \exp\left[-\tilde{U}(\tilde{x})\right] d\tilde{x}} \quad (10)$$

2.3 Investigation of the density distribution for classical and quantum gases

The dimensionless local density distributions of a $_2He^4$ gas confined in a one-dimensional domain made of silicon material, 1 nm in length, are given in Fig. 2, 3 and 4 for the case of MB statistics for different temperatures. The red curves in the figures show the density distribution with QSE calculated according to equation (5) and the blue curves show the densities without QSE calculated according to equation (10).

As can be seen in Figs. 2, 3 and 4, the contribution of QSE to the density distribution is negligible at high temperatures, while at low temperatures it causes a considerable difference. Both densities with and without QSE decrease to zero rapidly at the limit $\tilde{r}_0$. Thus, there is a boundary layer due to the repulsive part of the LJ potential. This layer may be called the LJ boundary layer, and it is about $\tilde{r}_0$ in thickness. In addition, the negative peaks of the LJ potential lead to the LJ peaks in density. However, it is seen that total boundary layer becomes thicker due to the presence of QSE. The wave character of the particles drives the gas towards the inner regions of the domain and, therefore, the LJ peaks decrease.

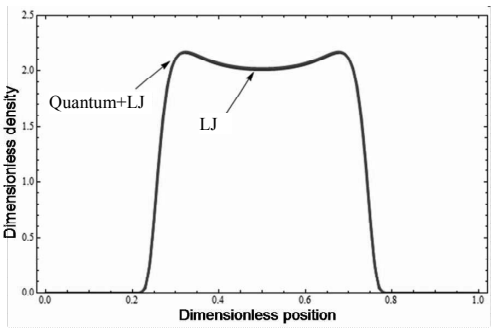

Fig. 2. The dimensionless local density distribution of a Maxwellian gas in a one-dimensional domain with, α=0.045 and T=300 K.

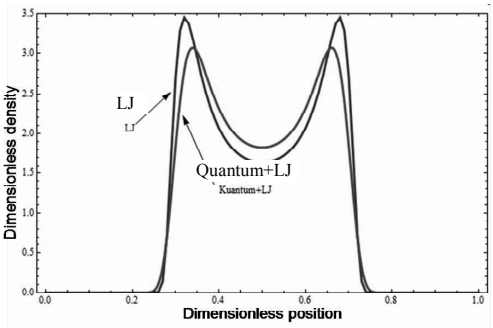

Fig. 3. The dimensionless local density distribution of a Maxwellian gas in a one-dimensional domain with α=0.14 and T=30K.

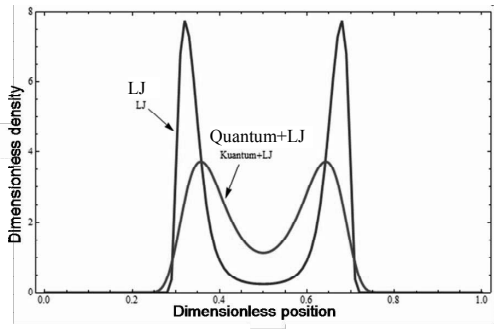

Fig. 4. The dimensionless local density distribution of a Maxwellian gas in a one-dimension domain with α=0.35 and T=5K.

In Fig. 5, the local density distribution of a MB gas confined in a square domain, (1 nm^2), subject to LJ potential is given for 300 K. Because T_{LJ}=30 K, it can be seen that the LJ peaks are weakened at 300 K. In addition, the 2D distribution is obtained by multiplying the 1D distribution for each direction given in Fig. 2.

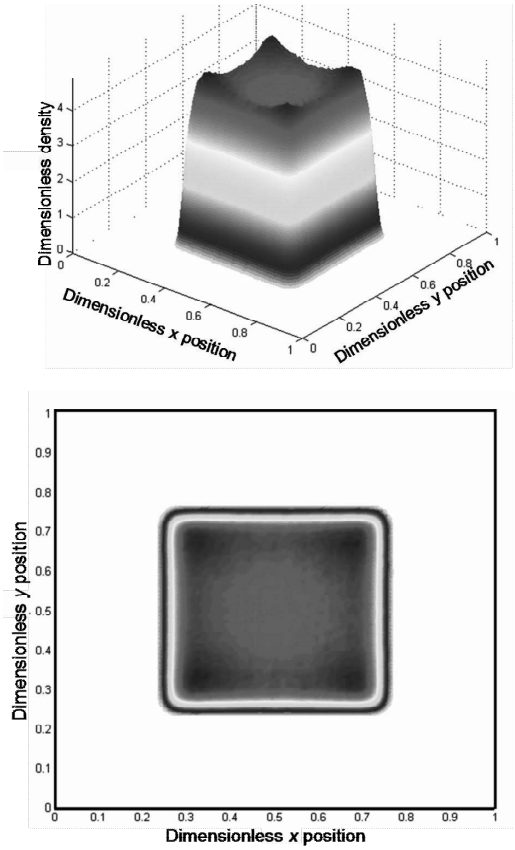

Fig. 5. The dimensionless local density distribution of a Maxwellian gas in a square domain subject to the LJ potential (^{4}He and Si wall interaction), with α=0.045 and T=300 K.

In Figs. 6, 7 and 8, the local density distribution of a degenerate Fermi gas is given at different temperatures.

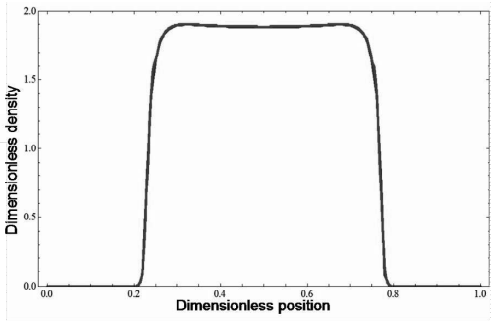

Fig. 6. The dimensionless local density distribution of a Fermi gas in a one-dimension subject to the LJ potential (^{3}He and Si wall interaction), with α=0.045, T=300 K, and Λ=5.

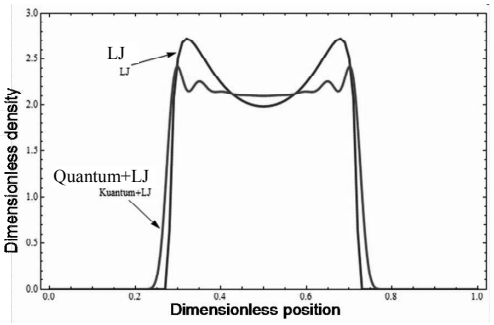

Fig. 7. The dimensionless local density distribution of a Fermi gas in a one-dimension domain subject to the LJ potential (^{3}He and Si wall interaction) with α=0.14, T=30 K, and Λ=5.

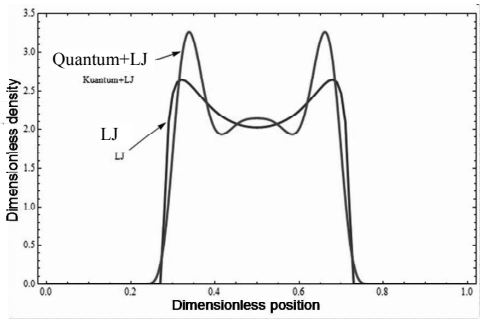

Fig. 8. The dimensionless local density distribution of a Fermi gas in a one-dmension domain subject to the LJ potential (^{3}He and Si wall interaction) with α=0.35, T=5 K, and Λ=5.

In Figs. 9 and 10, the local density distribution, with QSE of a degenerate Fermi gas confined in a square domain subject to the LJ potential is given for 30 K and 5 K, respectively. It is clearly seen that the Friedel oscillations are dominant at 5 K,

that the LJ peaks still exist, and that large peaks occur in the distribution due to overlapping with the first peak of Friedel oscillations and the LJ peak [24].

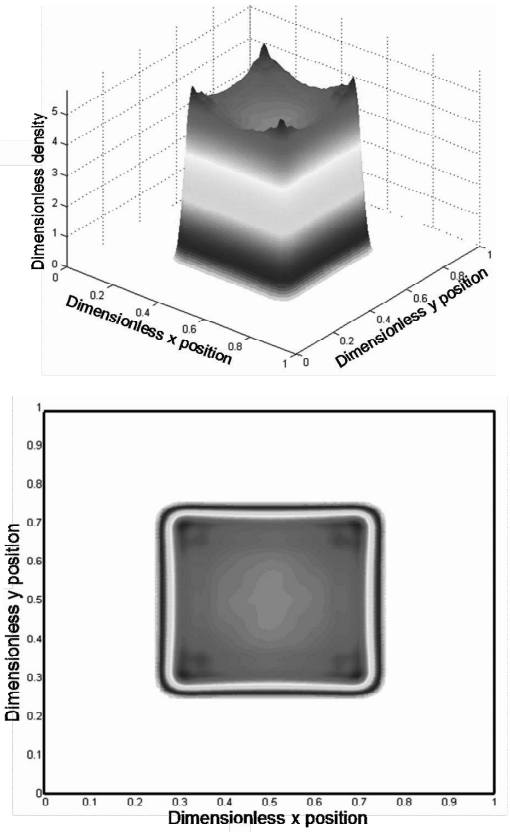

Fig. 9. The dimensionless local density distribution of a Fermi gas in a square-shaped domain subject to the LJ potential (^{3}He and Si wall interaction) with α=0.14, T=30 K, and Λ=5.

In Figs. 11, 12 and 13, the local density distributions of a degenerate Bose gas are given at different temperatures. In a Bose gas, the LJ peaks seem to be stronger in the absence of QSE even at 300 K relative to those with QSE and become even more so as the temperature decreases. The reason for this is the tendency of Bose particles to be in the same quantum state with the lowest energy. In addition, the QSE disturb the particle distribution by making the mid-point of the domain as a preferred region. Since the total particle number is conserved, the LJ peaks are weakened.

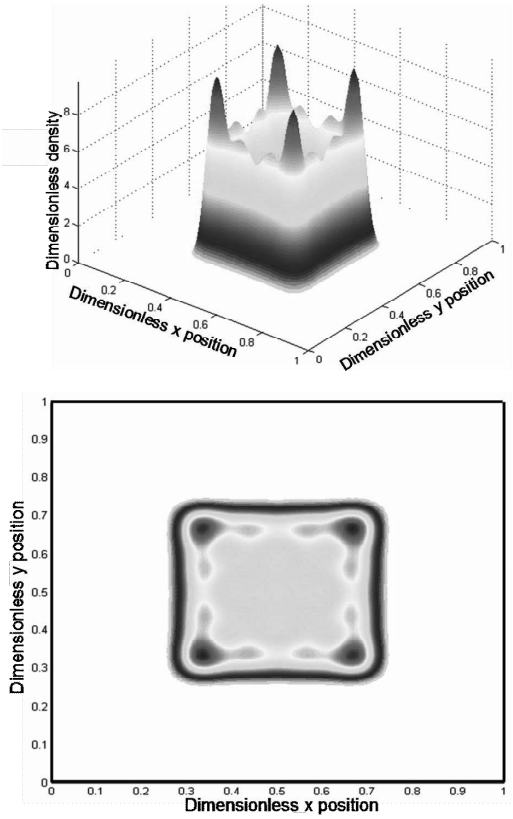

Fig. 10. The dimensionless local density distribution of a Fermi gas in a square-shaped domain subject to the LJ potential (^{3}He and Si wall interaction) with α=0.35, T=5 K, and Λ=5.

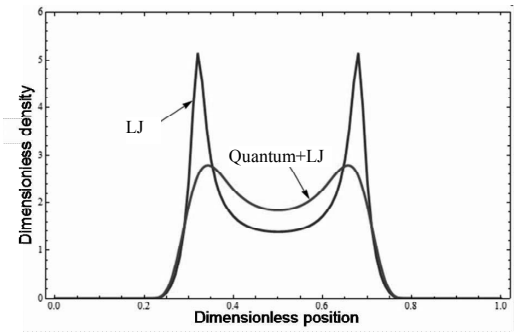

Fig. 11. The dimensionless local density distribution of a Bose gas in a 1D domain subject to the LJ potential (He-4 and Si wall interaction) with α=0.045, T=300 K, and Λ=-0.11.

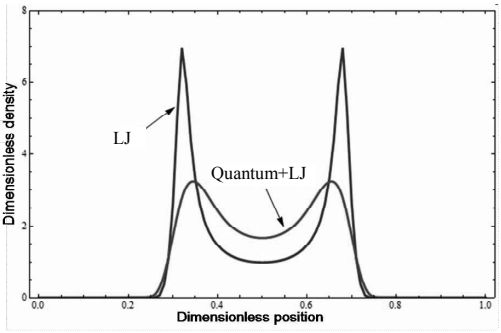

Fig. 12. The dimensionless local density distribution of a Bose gas in a 1D domain subject to the LJ potential (^{4}He and Si wall interaction) with α=0.14, T=30 K, and Λ=-1.11.

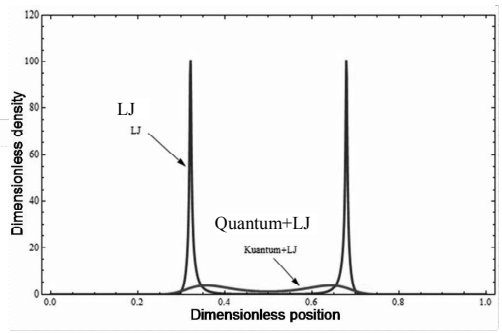

Fig. 13. The dimensionless local density distribution of a Bose gas in a 1D domain subject to the LJ potential (^{4}He and Si wall interaction) with α=0.35, T=5 K, and Λ=-6.14.

In Figs. 14 and 15 the local density distribution, with QSE, of a degenerate Bose gas confined in a square domain subject to the LJ potential is given for 30 K and 5 K, respectively. It is observed that the LJ peaks continue to be the preferred region in the case of the Bose gas. It is clearly seen that QSE cause the distribution to be much smoother and force the particles to be accumulated the inner region of the domain.

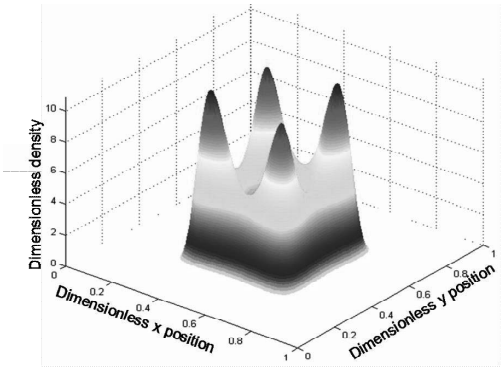

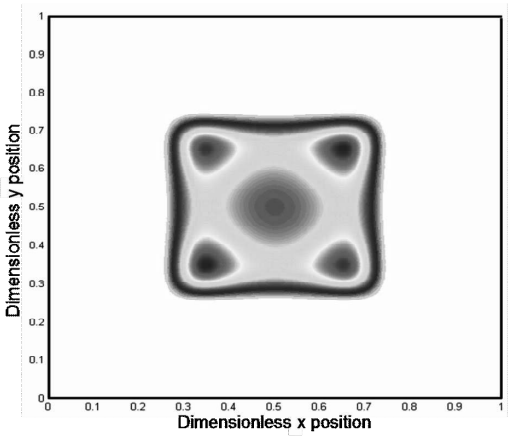

Fig. 14. The dimensionless local density distribution of a Bose gas in a square-shaped domain subject to the LJ potential with α=0.14, T=30 K, and Λ=-1,11

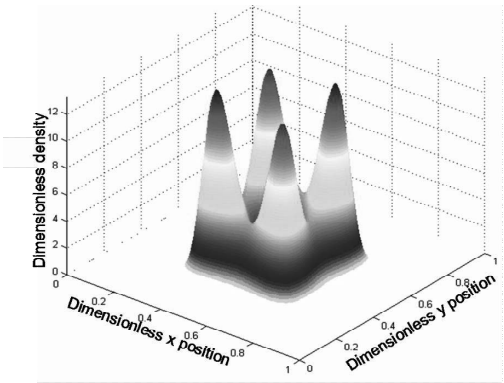

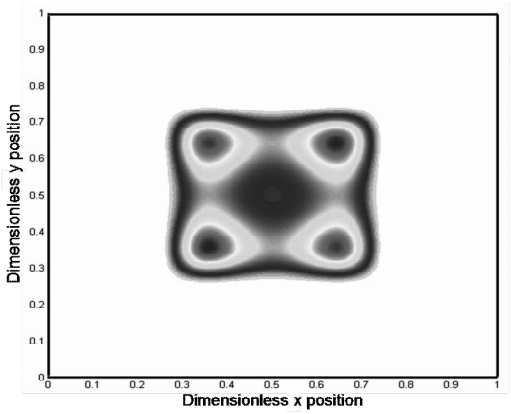

Fig. 15. The dimensionless local density distribution of a Bose gas in a square-shaped domain subject to the LJ potential (^{4}He and Si wall interaction) with α=0.35, T=5 K, and Λ=-6,14.

Conclusion

In this study, the local density distribution in 1D and 2D for both classical (MB) and quantum (FD and BE) gases subject to a LJ (12-6) interaction potential are examined by considering the existence of QSE. Both density distributions with and without QSE decrease to zero rapidly before the limit $\widetilde{r}_0$. Thus, there is a boundary layer with thickness $\widetilde{r}_0$ due to the LJ potential which is called here the LJ boundary layer. In addition, the negative peaks of the LJ potential lead to the LJ peaks in density. However, it is seen that the boundary layer observed in density becomes thicker due to the existence of QSE and drives the gas towards the inner regions of the domain with the result that the LJ peaks reduce.

All of the density-dependent thermodynamic properties are thus, affected by the inhomogeneity in the density distribution. Therefore, it is important to consider these effects on local density to analyze the thermodynamic behaviors of gases confined in nano structures. A detailed analysis of these effects on local density also provides a basis for the experimental verification of QSE on local density due to the wave character of particles.

Acknowledgements

This work is supported by The Scientific and Technological Research Council of Turkey, TUBITAK, under contract number 105T086 and the Istanbul Technical University Scientific Research Program.

References

[1] Kang, J. W., Hwang, H. J., Lee, J.H. and Lee, H. J., 2004, Fluidic gas-driven carbon-nanotube motor: Molecular dynamics simulations, *J. Korean Phys. Society*, 45, 573-576.

[2] Kang, J. W., and Hwang, H. J., 2004, Nanoscale carbon nanotube motor schematics and simulations for micro electro-mechanical machines, *Nanotechnology*, 15, 1633-1638.

[3] Moriarty, P., 2001, Nanostructured materials, *Rep. Prog. Phys*. 64, 297–381.

[4] Terrones, M., Kamalakaran, R., Seeger, T. and Rühle, M., 2000, Novel nanoscale gas containers: encapsulation of N2 in CN*x* nanotubes, *Chem. Commun*, 2335-2336.

[5] Cumings, J. and Zettl, A., 2000, Low-Friction Nanoscale Linear Bearing Realized from Multiwall Carbon Nanotubes, *Science*, 289, 602-604.

[6] Hoummady, M. and Fujita, H., 1999, Micromachines for nanoscale science and technology, *Nanotechnology*, 10, 29–33.

[7] Lijima, S. and Ichihashi, T., 1993, Single-shell carbon nanotubes of 1-nm diameter, *Nature*, 363, 603-605.

[8] Lijima, S., 1991, Helical Microtubules of graphitic carbon, *Nature*, 354, 56-58.

[9] Molina, M. I., 1996, Ideal gas in a finite container, *Am.J.Phys.*, 64, 503-505.

[10] Gutierrez, G. and Yanez, J. M., 1997, Can an ideal gas feel the shape of its container?, *Am. J. Phys.*, 65, 739-743.

[11] Pathria, R. K., 1998, An ideal quantum gas in a finite-sized container, *Am. J. Phys.*, 66, 1080-1085.

[12] Dai W.S. and Xie M., 2003, Quantum statistics of ideal gases in confined space, *Phys. Lett. A,* 311, 340-346.

[13] Sisman, A. and Müller, I., 2004, The Casimir-like size effects in ideal gases, *Phys. Lett. A*, 320, 360-366.

[14] Dai W.S. and Xie, M., 2004, Geometry effects in confined space, *Phys. Rev. E,* 70, 016103-1.

[15] Sisman, A., 2004, Surface dependency in thermodynamics of ideal gases, *J.Phys. A: Math. Gen.*, 37, 11353-11361.

[16] Pang, H., Dai,W.S. and Xie, M., 2006, The difference of boundary effects between Bose and fermi systems, *J. Phys. A: Math. Gen*., 39, 2563-2571.

[17] Sisman, A., Ozturk, Z.F., and Firat, C., 2007, "Quantum boundary layer: a non-uniform density distribution of an ideal gas in thermodynamic equilibrium", *Phys. Lett. A*, 362, pp.16-20.

[18] Firat, C., Sisman, A., and Ozturk, Z.F., 2010, "Thermodynamics of gases in nano cavities", *Energy*, 35, 814-819.

[19] Firat, C., Sisman, A., 2009, "Universality of quantum boundary layer for a Maxwellian gas*"* , *Physica Scripta*, 79:6, 065002(1-5).

[20] Hirschfelder, J. O., Curtiss, C. F. And Bird, R. B., 1954, Molecular Theory of Gases and Liquids, John Wiley & Sons, New York.

[21] Israelachvili, J. N., 1992, Intermolecular and Surface Forces, Academic Press, London.

[22] Nagy, L. T., Tunega, D. and Liska, M., 1996, Modeling of interaction properties of surfaces of phyllosilicates: A theoretical forecast of adsorption isotherms of noble gases at the talc surface, *Int. J. Quantum Chem.*, 57, 843-849.

[23] Griffiths, D. J., 1995, Introduction to Quantum Mechanics, Prentice Hall, New Jersey.

[24] Tüttő, I. and Zawadowski, A., 1985, Quantum theory of local perturbation of the charge-density wave by an impurity: Friedel oscillations, *Phys.Rev.B*, 32, 2449-2470.

Investigation of Controllability of heat integrated separation systems for a multicomponent stream

Kazem Hasanzadeh[a], Ata Arvani[a], Gholam Reza Salehi[a], Majid Amidpour[a]

[a] *Center of Integration KN Toosi University of Technology, Tehran, Iran*

Abstract: The understanding of the dynamic behavior of distillation columns has received considerable attention due to the fact that distillation is one of the most widely used unit operations in chemical process industries. Heat integrated distillation sequences can provide significant energy savings with respect to the operation of sequences based on conventional distillation columns. They exhibit a complex structure, with heat-integrations, that appear to affect their controllability properties. One potential solution to this problem has been suggested through the operation of heat integrated distillation sequences under conditions that do not provide minimum energy consumption, but this work proves that the process under conditions of minimum energy consumption can operate with the best controllability properties. In this work, we analyze the dynamic behavior of heat integrated distillation sequences. The control analysis properties are analyzed with the application of the Minimum Singular Value (MRI), Condition Number (CN) and Relative Gain Array (RGA), which are frequency-dependant indices. The results show that the controllability of best heat integrated distillation column, Distributed (C1&C3-R2) sequence which has the minimum total annual cost, is more than other sequences.

Keywords: Distillation, Sequence, Condition Number, Singular Value.

1. Introduction

Certainly, the distillation is the most widely applied separation technology and will continue as an important process for the foreseeable future because there seems not to be another industrially viable alternative around. Although distillation is generally recognized as one of the best developed chemical processing technologies there are still many barriers that could, when overcome, secure the position of the distillation and even make it more attractive for use in the future. The main disadvantage of the distillation is its high-energy requirements. Appropriate integration of the distillation column with the overall process can result in significant energy savings, but the scope for this is often limited. Rev et al. (2001) provide a comprehensive study on the energy saving for ternary systems. Separation configurations, internal thermal coupling and external heat-integration are explored. The design, optimization, and control of such energy-integrated distillation columns require engineering experience and knowledge, which represent a challenge to the researches [1-6]. In practice, the economic potential of such energy-integrated schemes has already been recognized, but their control properties have not been studied to the same degree. Since dynamic behavior and control of these heat integrated sequences is also important recent efforts have contributed to the understanding of dynamic properties of these sequences [7-15]. Some works studied the control for three different heat-integration configurations: feed-split, light-split forward(integration), and light-split reverse [16-17]. The understanding of the control properties of columns with heat-integrations for the separation of multicomponenet mixtures is an extremely important issue because many times designs with economic incentives conflict with their operational characteristics. Two of the most important controllability indexes are the MRI and CN, which derive from the singular value decomposition of the transfer function (linear model). The relative gain array (RGA) is also typically used to study the controllability of distillation systems. In this work, these controllability indexes are used to select the best control structures, as well as to compare the controllability of the different distillation arrangements for separating a multicomponent stream

Corresponding Author: Reza Salehi, rezasalehi@kntu.ac.ir

2. Basic equations and methods

Controllability was analyzed through Minimum Singular Value (MRI), Condition Number (CN) and Relative Gain Array (RGA), which are frequency-dependant indices. The MRI is the smallest singular value of the open-loop transfer function. It is the poorer gain of the process (poorer sensitivity), which corresponds to specific input and output directions. The set of manipulated variables that gives the largest MRI over the frequency range of interest is preferred. Open-loop dynamic responses to step changes around the assumed operating point were obtained through the use of commercial software. Transfer function matrices (G) were then collected for each arrangement, and they were subjected to singular value decomposition (SVD):

$$G = V \sum W^{H}, \quad (1)$$

Where $\sum = diag(\sigma_1,...,\sigma_n)$ and $\sigma_i =$ singular value of $G = \lambda^{1/2}(GG^{H})$, $V = (v_1,...,v_n)$ matrix of left singular vectors, and $W = (w_1,...,w_n)$ matrix of right singular vectors. The most important controllability index is CN, which derive from the singular value decomposition of transfer function. The CN is the ratio of the maximum singular value (σ^*) to the minimum singular value (σ_*), typically used for the selection of the best set of manipulated variables (condition number = γ^*):

$$\gamma^* = \frac{\sigma^*}{\sigma_*}$$

It provides a numerical indication of the sensitivity balance in a multivariable system. Large CNs indicate unbalanced sensitivity and also sensitivity to changes in process parameters. Therefore, sets of manipulated variables with small CNs over the frequency range of interest are preferred. RGA is a matrix that determines the interaction among control loops in a multivariable process, and it is frequently used to select the control pairing. Each element of the RGA is defined as the ratio of the open-loop gain for a selected output when all loops in the process are open to its open-loop gain when all of the other loops are closed. Pairings that have RGA close to the unity matrix at frequencies around the bandwidth are preferred. All the MRI, CN, and RGA depend on the frequency, and for this reason, they will be evaluated in the frequency domain. These parameters provide a qualitative assessment of the theoretical control properties of the alternative designs. The system with higher minimum singular values and lower condition numbers are expected to show the best dynamic performance under feedback control. A full MRI analysis should cover a sufficiently complete range of frequencies. For this initial analysis of the integrated schemes to the conventional configurations, we simply estimated the SVD properties for each separation system at zero frequency. Such analysis should give some preliminary indication of the control properties of each system around the nominal operating point. To compare the controllability of the different distillation arrangements, their controllability indexes are analyzed. In Figures 6-9, the MRI and CN for all possible composition control structures of all of the arrangements are plotted in the frequency domain.

3. Case study

In this work, the controllability of different distillation sequences for the separation of six basic component mixtures is compared. The process examined in this paper, is the separation of a multi-component flow to four categories of products with a purity of 0.99. The intake flow has a temperature of 59.3 oC, a pressure of 1785 kPa and a flow rate equal to 1355 kmole/hr. Compositions of process intake flow and products are shown in table 1. The initial process is illustrated in figure 1-A and it is regarded as a reference case for other states. Simulations are carried out using the comercial software and two models, Shortcut and Rigorous, are employed for simulating the columns. Structures are simulated and are shown in figures 1-5. According to the considered methods, the Distributed(C1&C3-R2) sequence shows the best controllability parameters between the all structures.

Table 1 Feed and product specifications

Product Product groups	Feed Components	Feed Xi (mol fraction)
1	A: C3H6	0.4538
2	B: C3H8	0.2912
3	C1: C4H8 C2: C4H10	0.1541 0.0359
4	D1: C5H12 D2: C6H14	0.0419 0.0137

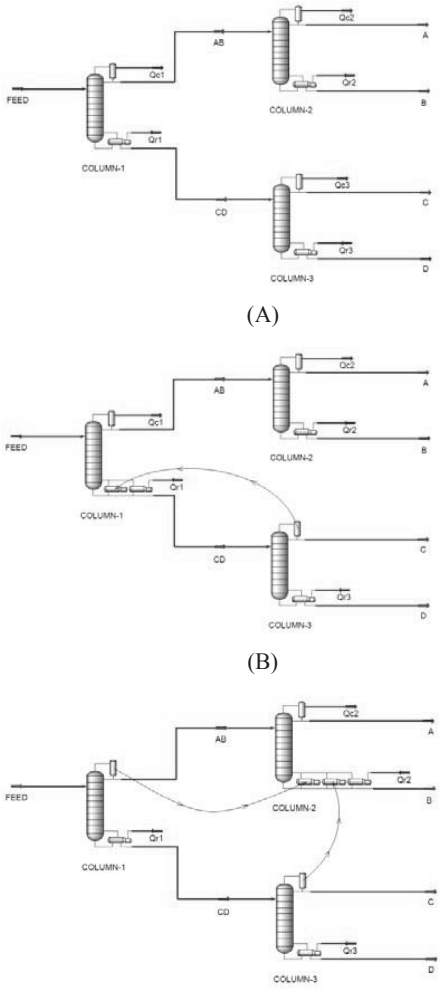

(A)

(B)

(C)

Fig. 1. Distributed sequences

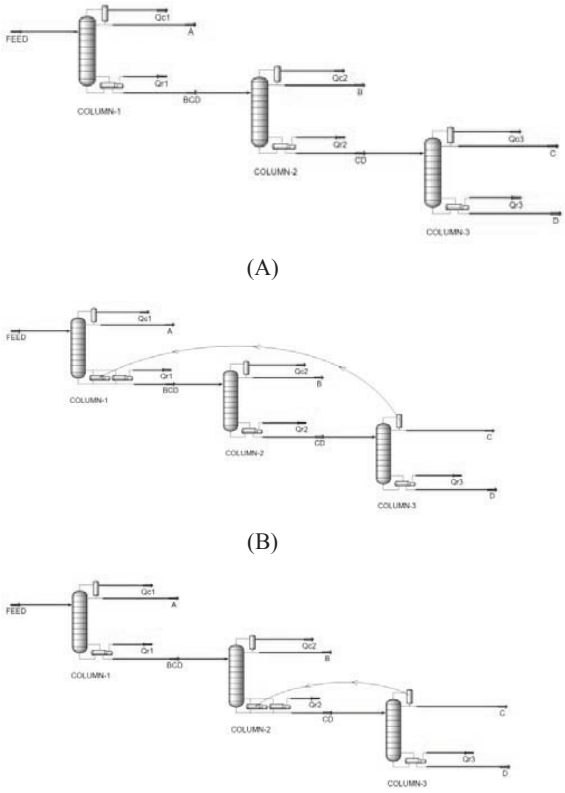

(A)

(B)

(C)

Fig. 2. Direct sequences

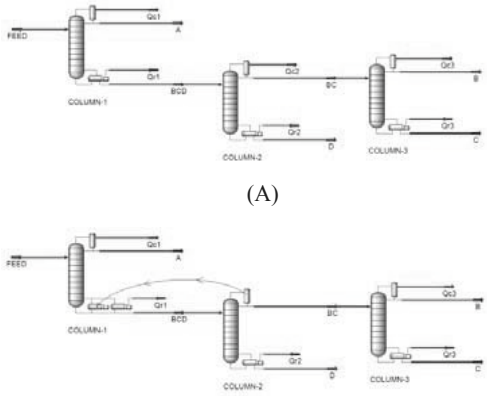

(A)

(B)

Fig. 3. Direct-Indirect sequences

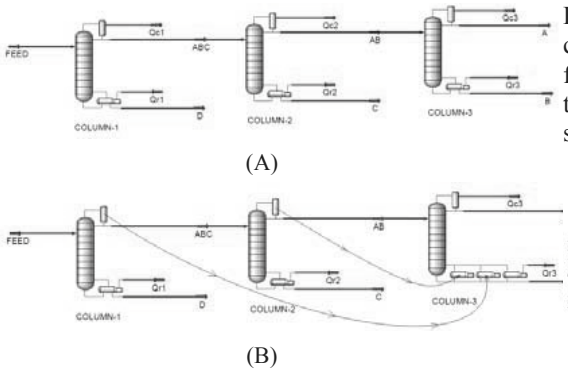

Fig. 4. Indirect sequences

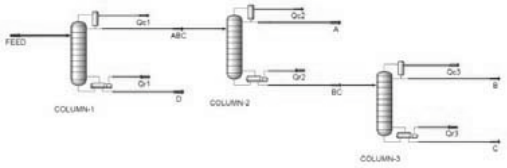

Fig. 5. Indirect-Direct sequence

4. MRI and CN analysis

The MRI technique (SVD technique) requires transfer function matrices, which are generated by implementing step changes in the manipulated variables of the optimum design of the distillation sequences and registering the dynamic responses of the six products. It can be mentioned that for a system with a single input and a single output, the zeros and poles of the transfer function give important information in order to evaluate the fully controllability of the system, but for multivariable systems, the SVD analysis provides the theoretical control properties. For the distillation sequences presented in this work, six controlled variables were considered, i.e., the product composition A, B, C1, C2, D1, D2. Similarly, six manipulated variables were defined. After the optimum designs were obtained, open-loop dynamic simulations were obtained in order to obtain the transfer function matrix. Matlab Programming software is used to find the transfer function and demonstrate the changes of control properties to frequencies.

Figure 6 and 7 demonstrate the minimum singular values at low and intermediate frequencies. In general, lower values of the condition number and higher values of the minimum singular value are preferred. Therefore, it can be expected that the Distributed(C1&C3-R2) system exhibit better control properties than the other sequence under feedback control and they are better conditioned to the effect of disturbances than the other distillation schemes.

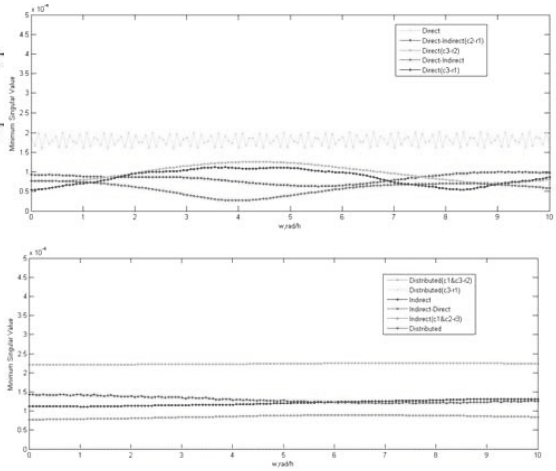

Fig. 6. Minimum Singular Values at low frequencies

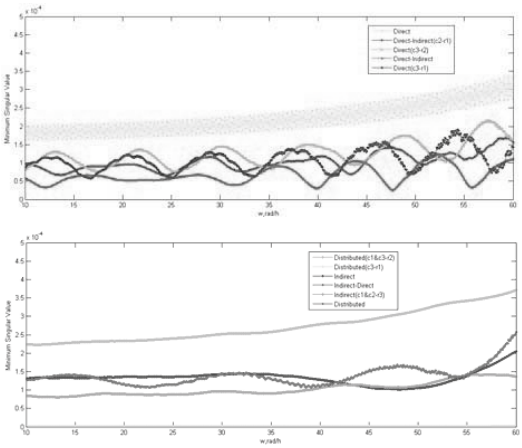

Fig. 7. Minimum Singular Values at intermediate frequencies

Figure 8 demonstrates the minimum singular values at high frequencies. Figure 8 demonstrates that the Distributed(C1&C3-R2) system has the higher values of minimum singular value at high frequencies. As a result, Distributed(C1&C3-R2) system has the highest singular values for the whole frequency range when it compared with all arrangements.

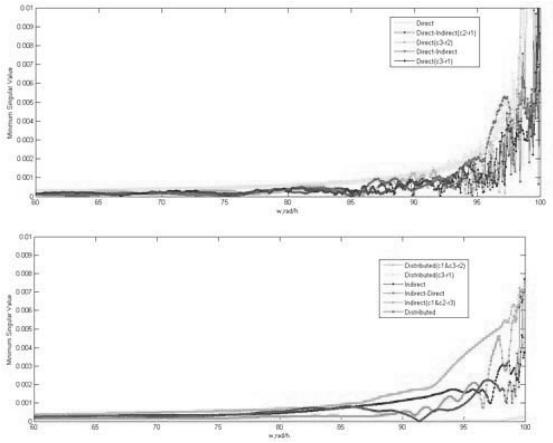

Fig. 8. Minimum Singular Values at high frequencies

Figure 9 and 10 demonstrate the condition numbers at low and intermediate frequencies. These two figures demonstrate that the Distributed(C1&C3-R2) system has the lower values of the condition number.

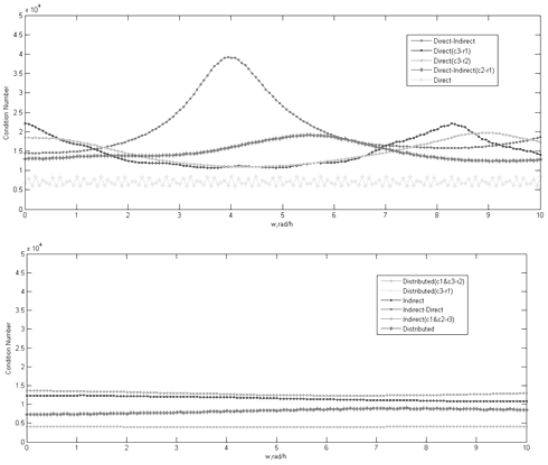

Fig. 9. Condition Numbers at low frequencies

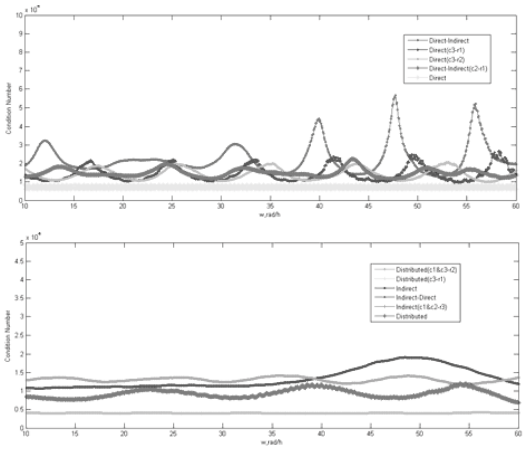

Fig. 10. Condition Numbers at intermediate frequencies

Figure 11 demonstrates the condition numbers at high frequencies. Figure 11 demonstrates that the Distributed(C1&C3-R2) system has the lower values of condition numbers at high frequencies. As a result, Distributed (C1&C3-R2) system has the lowest condition numbers for the whole frequency range when it compared with all arrangements.

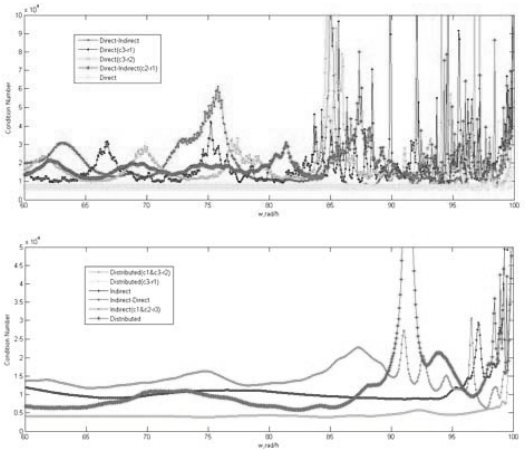

Fig. 11. Condition Numbers at high frequencies

It can be seen that the Distributed(C1&C3-R2) system has smaller CN and higher values of minimum singular value at high frequencies than other structures. Therefore, according to the controllability index, the controllability of the Distributed(C1&C3-R2) system is better.

5. RGA analysis

RGA has also been considered as the controllability index. It has also been used to select appropriate pairings. The relative gain arrays (RGA) were obtained for the best controllable sequence founded with SVD and CN analyses. For the Distributed(C1&C3-R2) sequence, the relative gain arrays are indicated in matrix below.

$$\Lambda = G \times (G^{-1})^T = \begin{bmatrix} 0.5746 & -0.4276 & 0.4635 & -0.3138 & 0.1728 & 0.0553 \\ 0.0813 & 1.0792 & 0.1457 & -0.6359 & -0.1458 & -0.2658 \\ 0.1506 & -0.3758 & 1.0519 & 0.0486 & 0.0511 & 0.0475 \\ -0.3263 & -0.8502 & 0.7897 & 1.2885 & -0.7855 & -0.7849 \\ -0.0281 & -0.5529 & 0.3275 & 0.3254 & 1.3256 & 0.3240 \\ -0.0984 & -0.6216 & 0.4388 & 0.4361 & 0.4353 & 1.4339 \end{bmatrix}$$

There are six controlled variables (composition A, B, C1, C2, D1, and D2) and six manipulated variables. According to the RGA, the pairing showing the lowest interaction for the Distributed(C1&C3-R2) sequence is (RR2-xA, BU2-xB, RR3-xC1, RR3-xC2, BU3-xD1, BU3-xD2), where xA is A molar purity, xB is B molar purity, xC1 is C1 molar purity, xC2 is C2 molar purity, xD1 is D1 molar purity, xD2 is D2 molar purity, RR2 is reflux ratio of column 2, BU2 is boil up ratio of column 2, RR3 is reflux ratio of column 3, and BU3 is boil up ratio of column 3. In the first row, we can see that composition A should be controlled by manipulating reflux ratio of column 2; the second row of the relative gain array suggests that a good pairing is composition B and the heat duty of column 2; in the third row the control loop for composition C1 should be made by manipulating reflux ratio of column 3; the fourth row indicates a pairing between the composition C2 and the reflux ratio of column 3; the fifth row indicates that the composition D1 should be controlled by manipulating the heat duty of column 3; finally the last row indicates that a good pairing is composition D2 and heat duty of column 3. It is important to note that the relative gain array of matrix shows diagonal control loop pairing.

6. Conclusions

Upon analysis of the MRI, CN, and RGA in the frequency domain, the controllabilities of the column sequences, the columns with or without heat-integration are compared for a given separation problem. According to the Minimum Singular Value analysis (MRI) the best controllable sequences are ranked as, Distributed(C1&C3-R2) (figure 1-C), Direct (Figure 2-A), Distributed (figure 1-A), Indirect (Figure 4-A), Indirect (C1&C2-R3) (Figure 4-B), Direct-Indirect(C2-R1) (Figure 3-B), Direct-Indirect (Figure 3-A), Indirect-Direct (Figure 5), Direct(C3-R2) (Figure 2-C), Direct(C3-R1) (Figure 2-B), and Distributed(C3-R1) (Figure 1-B).

According to the CN analysis the best controllable sequences are ranked as, Distributed(C1&C3-R2) (figure 1-C), Direct (Figure 2-A), Distributed(figure 1-A), Direct-Indirect (Figure 3-A), Indirect (Figure 4-A), Indirect (C1&C2-R3) (Figure 4-B), Direct-Indirect(C2-R1) (Figure 3-B), Indirect-Direct (Figure 5), Direct(C3-R2) (Figure 2-C), Direct(C3-R1) (Figure 2-B), and Distributed(C3-R1) (Figure 1-B).

The MRI and CN methods show almost the same results about the controllability of considered sequences. According to them, the Distributed(C1&C3-R2) sequence (figure 1-C) has the maximum of controllability among the all sequences and It means that this sequence has the minimum cost of control systems. RAG analysis also showed that the appropriate pairings with the lowest interaction for the Distributed(C1&C3-R2) sequence is (RR2-xA, BU2-xB, RR3-xC1, RR3-xC2, BU3-xD1, BU3-xD2). The Distributed(C1&C3-R2) sequence also has the minimum total annual cost, according to former researches [18], thus, this sequence is the best configuration for heat integrated separation system in considered case study. Taking into account all three controllability indexes at the frequency range of interest, it is concluded that the Distributed(C1&C3-R2) sequence has a better controllability properties than the other sequences. This result is very important because it indicates this sequence operated at optimal operating conditions has the best controllability and the lower energy consumption of all of the arrangements. It proves that the heat-integrated sequence with the minimum energy consumption can operate by the best controllability properties.

References

[1] Rev, E., Emtir, M., Szitkai, Z., Mizsey, P., Fonyo, Z., (2001). Energy saving of integrated and coupled distillation systems. Computers and Chemical Engineering 25, 119.

[2] Bildea, C. S., and Dimian, A. C. (1999). Interaction between design and control of a heat integrated distillation system with prefractionator. Trans IchmE., 77,597.

[3] Fisher, W. R., Doherty, M. F. and Douglas, J. M. (1988). The interface between design and control. Industrial Engineering and Chemistry Research, 27, 597.

[4] Grossmann, I. E. and Morarri, M. (1984). Operability, resiliency, and flexibility process design objectives for a changing world, Proc. of the 2nd Int. Conf. On Foundation of Computer Design, Austin, Texas, pp. 931.

[5] Hernandez, S. and Jimenez, A. (1999). Controllability analysis of thermally coupled distillation systems. Industrial Engineering and Chemistry Research, 38, 3957.

[6] Jimenez, A., Hernandez, S., Montoy, F. A., and Zavala Garcia, M. (2001). Analysis of control properties of conventional and non-conventional distillation sequence. Industrial Engineering and Chemistry Research, 40, 3757.

[7] Luyben, W. L. (1990). Process modeling, simulation and control for chemical engineering. McGraw-Hill Inc., New York.

[8] Mizsey, P., Hau, N. T., Benko, N., Kalmar, I. and fonyo, Z. (1998). Process control for energy integrated distillation schemes. Computer and Chemical Engineering, 22, 427.

[9] Doukas, N. P.; Luyben, W. L. (1981). Control of an Energy-Conserving Prefractionator/ Sidestream Column Distillation System. Ind. Eng. Chem. Process Des. Dev., 20, 147-153.

[10] Luyben, W. L. Practical Distillation Control; Van Nostrand Reinhold: New York, (1992).

[11] Skogestad, S. (1997). Dynamics and Control of Distillation Columns: A Tutorial Introduction. Trans. Inst. Chem. Eng., Part A, 75.

[12] Abdul Mutalib, M. I.; Smith, R. (1998). Operation and Control of Dividing Wall Distillation Columns. Part I: Degrees of Freedom and Dynamic Simulation. Trans. Inst. Chem. Eng., 76, 308.

[13] Lin, S.W. and Yu, C.C., (2004). Interaction between design and control for recycle plants with heat-integrated separators, Chem Eng Sci, 59: 53.

[14] Tyreus, B.D. and Luyben, W.L., (1976). Dynamics and control of heat integrated distillation columns, Chem Eng Prog, 72(9): 59.

[15] Weitz, O. and Lewin, D.R., (1996). Dynamic controllability and resiliency diagnosis using steady state process flowsheet data, Comput. Chem. Eng, 20, 325.

[16] Chiang, T.P., Luyben, W.L., (1988). Comparison of the dynamic performance of three heat-integrated distillation configurations. Industrial and Engineering Chemistry Research 27, 99.

[17] Han, M., Park, S., (1996). Multivariable control of double-effect distillation configurations. Journal of Process Control 6, 247.

[18] Hasanzadeh, K.; Salehi, R.; Amidpour, M.; Omidkhah, M. R. “Design of heat integrated distillation column sequences for the olefin separation process”, submitted in Chemical Engineering journal.

Heat Integration of a ketone-benzol dewaxing process

Hui Chen[a], *Xiao Feng*[b]

[a] *Department of Chemical Engineering, Xi'an Jiaotong University, Xi'an 710049, China*
[b] *Faculty of Chemical Science and Engineering, China University of Petroleum, Beijing 102249, China*

Abstract: Solvent dewaxing process is an energy-intensive process, and so optimizing its entire heat exchanger network is an important approach for saving energy and improving the energy efficiency. In this paper, the pinch technology is used to analyze and optimize the heat exchanger network of a ketone-benzol dewaxing process. The unreasonable heat exchange matches are found, all of which are coolers above the pinch. Based on the pinch analysis and considering the existing heat exchanger network structure, the retrofit scheme with a short payback period is proposed.

Keywords: Energy-saving, Pinch technology, Heat exchanger network, Ketone-benzol dewaxing process

1. Introduction

With the development of society, energy consumption is increasing seriously, and so improving energy efficiency is a main task of industries. Statistical studies show that the average energy efficiency in China is merely 32%[1], which is 10% lower than that in developed countries. Increasing the energy efficiency can significantly enhance the competitiveness of enterprises and improve the environment. Therefore, energy conservation is an important approach for achieving sustainable development for the states or enterprises. Among the many energy-saving approaches (e.g. process modifications), heat exchanger network (HEN) optimization[2] can not only be used for process retrofit to eliminate the system "bottleneck" [3], but also guide the optimization of unit operations to increase production, save energy and reduce the cost.

The ketone-benzol dewaxing process is the traditional and widely-used process in the production of lubricating oil and paraffin. There are totally 23 sets[4] of dewaxing plants in the two major oil companies, Sinopec and PetroChina, in which 19 sets using the solvent dewaxing processes. Moreover, the majority solvent is the mixture of methyl ethyl ketone and toluene. However, the original design of some ketone-benzol dewaxing processes is unreasonable, and some retrofit on ketone-benzol dewaxing processes may not fully use the waste heat or has some unreasonable the heat exchange matches. Thus, analysis and optimization of HEN for the process is meaningful for energy conservation.

The ketone-benzol dewaxing process is an energy-intensive process, and so many studies have been focused on how to reduce the energy consumption in the process. The production system of the ketone-benzol dewaxing process is a complex system constituted of a number of sub-systems. Up to date, the research on improving the energy efficiency of the ketone-benzol dewaxing process has been focused on certain sub-systems, and the same even for the heat exchanger network. For the crystallization sub-system, the optimization of the system was conducted by Huang via the energy system integration technology[5-6], and the "bottleneck" in the sub-system was figured out by Zheng[7], both of which can be used to guide the reduction of the expensive refrigeration utility. For the de-oiling sub-system, the heating utility was reduced by optimizing its heat exchanger network[6]. For the solvent recovery sub-system, the analysis and optimization of the energy utilization reached a certain energy-saving effect[8-10]. However, those efforts can be considered as local optimization, which can not achieve the maximum of energy-saving potential. If the whole system can be taken as a whole, more energy-saving effect can be obtained.

In this paper, the HEN for the whole system of the ketone-benzol dewaxing process is analyzed based on pinch technology[11-13]. The appropriate matches between hot and cold streams

Corresponding Author: Xiao Feng, Email: xfeng@cup.edu.cn

in the whole system are identified. Compared with present researches, this work can achieve more effective energy conservation.

2. Brief description of a certain ketone-benzol dewaxing process

In this paper, a ketone-benzol dewaxing process in an oil refinery is taken as a case study. The selected solvent is the mixture of methyl ethyl ketone (MEK) and toluene. The refinery was designed in 1990 and practically operated in 1997, with its processing capacity of 35 million ton per year. The processing capacity reached 420,000 tons per year after the retrofit on 2005.

The ketone-benzol dewaxing process can be divided into four sub-systems, which are refrigeration, crystallization, vacuum filtration and solvent recovery sub-systems. The simplified flow sheet is illustrated as shown in Figure 1.

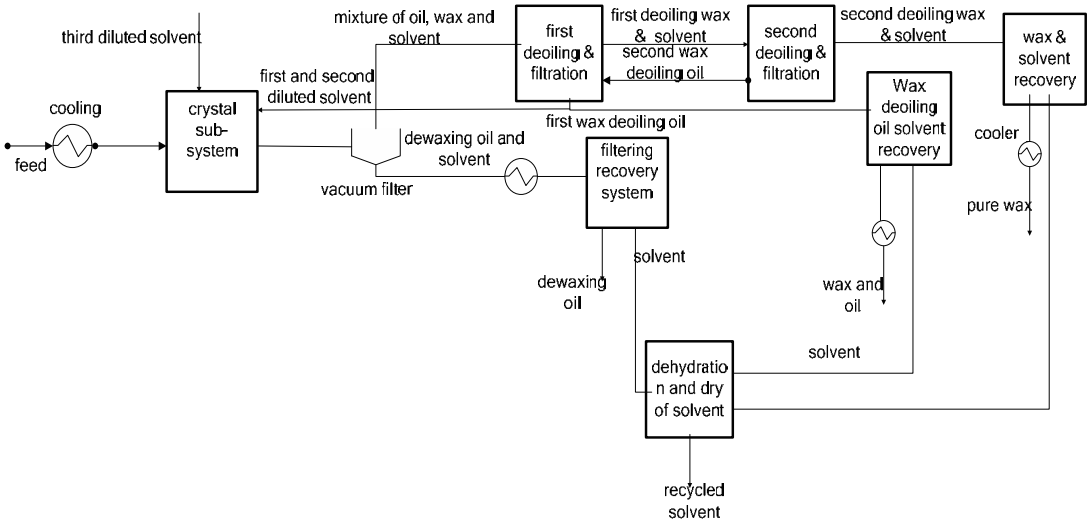

Fig.1. Simplified flow sheet of the ketone-benzol dewaxing process

1. Refrigeration sub-system

In the refrigeration sub-system, high-pressure liquid ammonia goes through the throttling valve and is endothermic vaporized into low-pressure gas ammonia. Then it is pressurized by an ammonia compressor into high-pressure gas ammonia, which is condensed and cooled into high-pressure liquid state, which is ready for cycle usage. This process is used to provide refrigeration duty and can be considered as the refrigeration utility. Thus, the refrigeration sub-system is not included in Figure 1.

2. Crystallization sub-system

In the sub-system, wax is cooled and precipitated from the raw materials in an easy filtration form of crystal. In the raw material cooling crystallization process, the pre-cooled solvent is added several times. The cold-point temperature of the solvent is determined by the variety of the raw materials.

3. Vacuum filtration sub-system

The mixture of the raw materials and solvent from the crystallization process goes into the vacuum filter, in which oil and wax are separated. This sub-system consists of dewaxing filtration process and de-oil filtration process.

4. Solvent recovery sub-system

In the solvent recovery sub-system, because there are great differences in boiling points among solvent, oil and wax, the solvent can be fully recovered by heating, flash evaporation, condensation and cooling. Based on the azeotrope feature of methyl ethyl ketone and water, water can be removed by heating, distillation, condensation and cooling in this process.

3. Analysis of the existing HEN

3.1. Stream data extraction

For the existing HEN of the whole ketone-benzol dewaxing process, 25 hot streams and 14 cold streams are extracted, and the detailed information is shown in Tables 1 and 2, respectively.

Table 1. Cold stream data.

Stream code	Stream name	Inlet temp. /℃	Outlet temp. /℃	Heat load /kW
c1	wax deoiling oil	16.2	21.3	46.51
c2	dewaxed oil, solvent	8	90.8	8734.95
c3	wax deoiling oil	16.2	30.7	383.72
c4	wax, solvent	42.3	106	2673.63
c5	wax, solvent	105.3	125.5	1508.15
c6	wax, solvent	125.9	178.8	1861.29
c7	wax deoiling oil, solvent	30.7	90.9	4482.59
c8	wax deoiling oil, solvent	93.7	125.2	2402.34
c9	wax deoiling oil, solvent	122.8	181	2573.28
c10	wax deoiling oil, solvent	174.8	175.5	139.54
c11	dewaxed oil, solvent	87.8	121.8	5816.33
c12	dewaxed oil, solvent	120.2	179.9	6780.29
c13	dewaxed oil, solvent	178.3	179.4	168.61
c14	wax, solvent	173.7	175.1	222.10

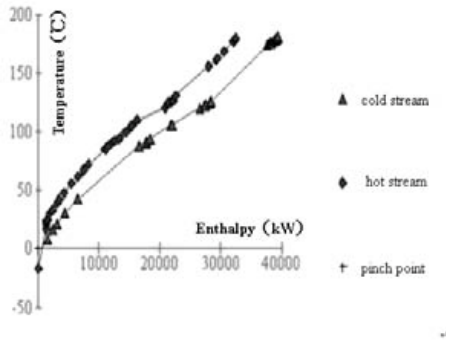

Fig.2. Composite curves

3.2. Pinch calculation

In this paper, the minimum approach temperature difference is set to be 10 ℃, based on considering energy recovery, heat transfer area, retrofit cost and stable operation[3]. According to pinch technology, the average pinch temperature is calculated to be 13℃, which means that at the pinch point, hot stream temperature is 18℃, while the cold stream is 5℃. In addition, the required minimum heating utility is obtained as 6715.17kW, while the minimum cooling utility is 1501.97kW. However, in the current HEN, the heating utility is 11745.1kW and the cooling utility is 6530.84 kW. Therefore, the energy-saving potential is 5029kW, accounting for 42.8% of the current heating utility and 77% of the existing cooling utility. The composite curves are shown in Figure 2. Figure 3 shows the grand composite curve.

Table 2. Hot stream data.

Stream code	Stream name	Inlet temp. /℃	Outlet temp /℃	Heat load /kW
H1	solvent	32	-24.1	1593.04
H2	solvent	33	26	383.72
H3	solvent	105	72	1353.85
H4	solvent	168.3	21	545.94
H5	solvent	126.7	39	929.08
H6	wax	155.6	86	405.24
H7	solvent	176.6	130.5	1216.29
H8	solvent	125.3	125	619.19
H9	solvent, steam	161.5	24.2	2132.58
H10	solvent	93.6	91	451.17
H11	solvent	95	24.5	1113.61
H12	solvent	123.1	85	1777.92
H13	solvent	162.7	90.9	275.82
H14	solvent	178.5	104	2211.65
H15	dewaxed oil	179.8	47.7	1703.50
H16	solvent	87.3	30	3615.15
H17	solvent	179.1	130	5483.76
H18	solvent	110	32	2997.70
H19	solvent	120.3	110	3232.58
H20	solvent	26	23.5	104.65
H21	Inert gas	105	24	77.91
H22	Inert gas	109	42	55.81
H23	Inert gas	24	-17	39.54
H24	Inert gas	42	23	16.28
H25	raw material	67	56	244.19

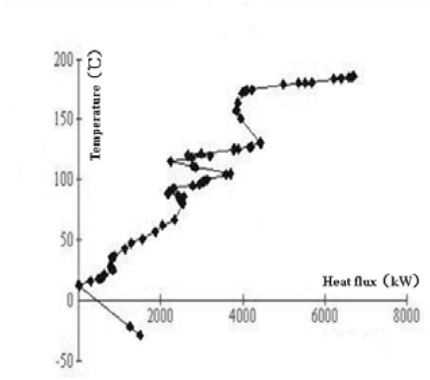

Fig.3. Grand composite curve

3.3. Analysis of pinch rule violations

According to the three principles of pinch technology (no cooling utility exists above the pinch, no heating utility locates under the pinch and no heat transfer crosses the pinch), by analyzing the existing HEN, the pinch rule violations are identified, all of which are the coolers above pinch, as shown in Table 3.

The total unreasonable heat duty is calculated as 5038.03kW, accounting for 42.9% of the current heating utility and 77.1% of the existing cooling utility. There is a small difference between this result and that from pinch calculation. It is because the minimum approach temperature difference in the existing HEN is less than the selected minimum one.

4. Retrofit of HEN

Unlike the design of a new HEN, in the retrofit of the existing HEN, the restrictions of the present structure should be fully considered and simultaneously more waste heat should be recovered on the premise of fewer changes in the HEN to enhance economic effect.

In the plant, there are a large number of coolers with unreasonable heat exchange in the current HEN. To recover more heat with fewer changes, the coolers with large heat duty are prior to be re-matched. Moreover, this paper considers the retrofit for the overall HEN, including the sub-systems such as crystallization, filtration and solvent recovery. So the following constrains should be taken into account.

1. Practical factors such as distribution and position of heat exchangers and distance among sub-systems should be considered.

Table 3. Pinch rule violations of the heat exchange network

cooler	stream	temperature (℃)		unreasonable heat load (kW)
		inlet	outlet	
cooler 1	wax and oil	67	56	244.19
	water	25	32	
cooler 5	solvent	26	23.5	104.65
	ammonia	-12	-12	
cooler 6/1	inert gas	105	24	77.91
	water	28	32	
cooler 6/2	inert gas	109	42	55.81
	water	25	32	
cooler 7/1-2	ammonia	-27.5	-27.5	5.78
	inert gas	24	8	
cooler 7/3	ammonia	-12	-12	16.28
	inert gas	42	23	
cooler 10	solvent	84	44	1534.9
	dry gas	13	19.7	
cooler 11	dewaxed oil	44	32	461.63
	wet air	6	9.04	
cooler 12	oil	92	47.7	572.1
	water	25	32	
cooler 19	solvent	100	92	12.79
	dry gas	13	19.7	
cooler 20	solvent	92	21	115.12
	wet air	6	9.04	
cooler 21	solvent	100	75	266.28
	dry gas	13	19.7	
cooler 22	solvent	75	39	380.24
	wet air	6	9.04	
cooler 23	wax deoiling oil	105.5	86	113.37
	water	25	32	
cooler 24	solvent	62	27	106.98
	dry gas	13	19.7	
cooler 25	solvent	27	24.2	8.14
	wet air	6	9.04	
cooler 26	solvent	80	25	868.61
	wet air	6	9.04	
cooler 27	solvent	25	24.5	8.14
	wet air	6	9.04	
cooler 28	wax	114.5	90.9	85.12
	water	25	32	

2. The ketone-benzol plant adopts two kinds of heat exchange medium, one of which is the mixture of MEK, and the other is dewaxing oil. The heat exchange between two sub-systems should be avoided in case process streams are polluted when liquid leakage occurs in heat exchangers.

Based on the considerations mentioned above, the following retrofit strategies have been proposed and the HEN after retrofit is shown in Fig. 4. Because the unreasonable cooled hot streams locate at low temperature area, in order to recover energy, many streams may have to be re-matched.

1. Cooler 10 is removed. Cooler 10 is originally used for cooling the hot stream H18, the temperature of which decreases from 84 ℃to 44 ℃. Now a new heat exchanger E2 is added, where hot stream H18 exchanges heat with a branch of the cold stream C2. The temperature of the branch of C2 increases from 21.9 ℃ to 41.8 ℃. In this way, 1534.9 kW of cooling utility is saved.
2. Cooler 11 is removed. Cooler 11 is formerly used to cool the hot stream H18, the temperature of which decreases from 44 ℃ to 32 ℃. Now a new heat exchanger E1 is added, where hot stream H18 exchanges heat with a branch of the cold stream C2. The temperature of the branch of C2 increases from 17.5 ℃ to 27.9 ℃. In this way, 461.63 kW of cooling utility is saved.
3. Cooler 12 is removed. Cooler 12 is originally used for cooling the hot stream H15, which makes the stream's temperature decreases from 92 ℃ to 47.7 ℃. Now a new heat exchanger E3 is added, where hot stream H15 exchanges heat with a branch of the cold stream C2. The temperature of the branch of C2 increases from 21.9 ℃ to 41.8 ℃. In this way, 572.1 kW of cooling utility is saved.
4. In the three steps above, the recovery energy is all used for heating the cold stream C2. Hence, several changes of heat exchange matches have been taken along the cold stream C2 and its downstream streams. First, by reducing the temperature difference of heat exchangers, the temperature levels for heat exchangers 11, 12 and 13 are adjusted in sequence while keeping the current heat loads unchanged, to make sure the cold stream C2 matches with the hot stream with lower temperature level. Besides, the cold stream C2 in the high temperature range exchanges heat with hot stream H19 through heat exchanger 14. Then a new heat exchanger E4 is added, where cold stream C2 exchanges heat with hot stream H19. The hot stream H19 in the high temperature range exchanges heat with cold stream C11 by heat exchanger 14, whose area needs to be changed. The cold stream C11 originally exchanges heat with H17 via heat exchanger 16. Now the temperature level for heat exchanger 16 is adjusted and its heat load is changed from 5483.7kW to 2915.13kW. Finally, the hot stream H17 exchanges heat with cold stream C12 via a newly added heat exchanger E5. The heat exchanger 17 which is used for heating the cold stream C12 is removed. Hence total 2568.63kW of heating utility for heating cold stream C12 can be saved, which equals the amount of energy recovered by removing the three coolers 10, 11, 12.
5. The heat load of cooler 26 is decreased, where the hot stream H11 is currently cooled from 80 ℃ to 25 ℃ and now it will be cooled from 40 ℃ to 25 ℃. To do that, a new heat exchanger E6 is added, in which the hot stream H11 is cooled by cold stream C7. In this way, 631.7kW of cooling utility can be saved. The cold stream C7 matched the hot stream H9 by heat exchanger 30 originally. Now the temperature level and heat exchange area of the heat exchanger 30 are changed and its heat load is reduced to be 631.7kW. A new heat exchanger E7 is added and heat exchanger 36 for heating cold stream C9 is removed, which makes the hot stream H9 in the high temperature range be cooled by cold stream C9. In this way, 631.7kW of heating utility for heating the cold stream C9 can be recovered

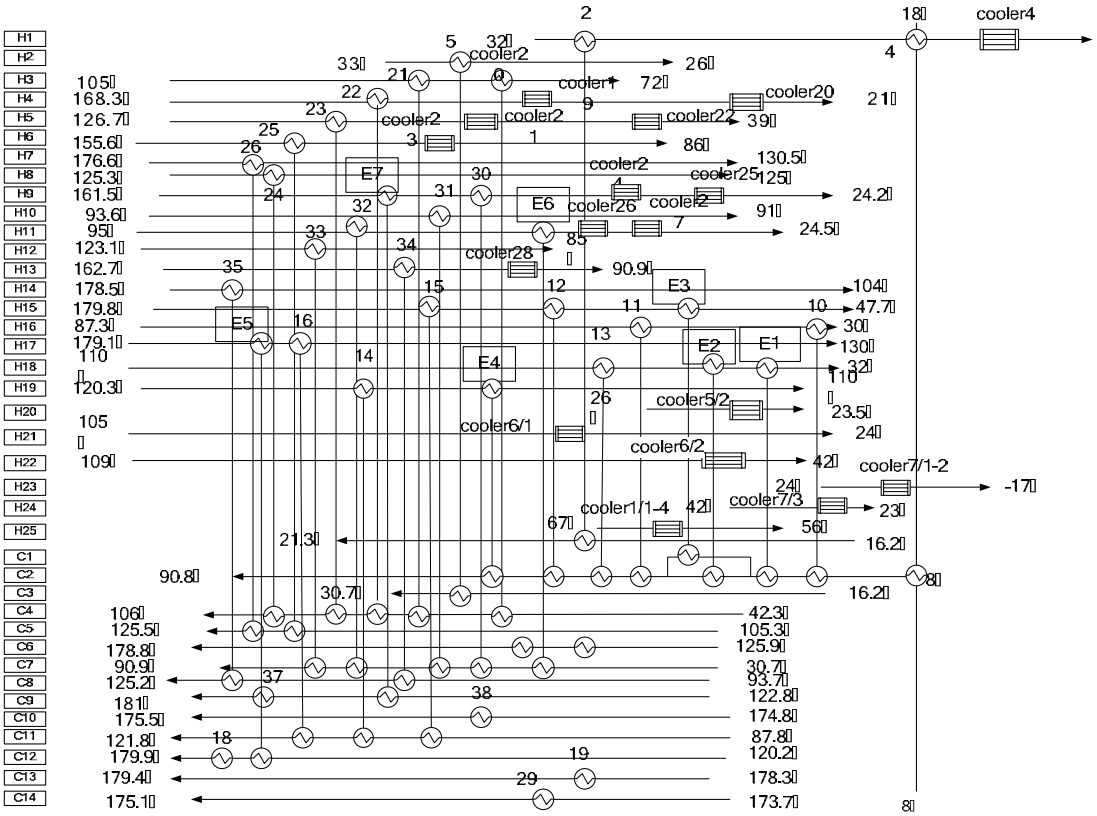

Fig. 4. HEN after retrofit

After the retrofit above, 3200.3kW of heating utility can be recovered, which equals to save 5.74t·h^{-1} of steam based on the given latent heat 2005.1kJ·kg^{-1}. The annual saved amount of steam can be calculated as 45.9 thousand tons according to 8,000 operation hours per year. The local cost for steam is given as 50 RMB per ton. The annual saved steam cost can be obtained as 2.2974 million RMB. In addition, 24.295kg·s^{-1} of recirculating cooling water can be saved. The annual cost of saved recirculating water is calculated as 349.8 thousand RMB based on its price of 0.5 RMB per ton.

Seven new heat exchangers (E1, E2, E3, E4, E5, E6, E7) need to be added, and areas of two heat exchangers (heat exchanges 12 and 13) need to be adjusted, while other heat exchangers are kept the same as before. Heat transfer coefficient in this system is 450W•m^{-2}•℃ $^{-1}$ [14]. The investment cost is obtained as 4.3196 million RMB based on Equation (1) [3].

$$Y = 13 \times (8600 + 670\ A^{0.83}) / 10000 \text{ (RMB)} \quad (1)$$

where Y is the capital cost, RMB, and A represents the heat transfer area, m^2. The cost of piping, instrumentation, control systems and so on are included in the coefficient 13. So the payback period is only 1.63 years (= 431.96/264.72).

5. Conclusions

In this paper, the HEN of the whole ketone-benzol dewaxing process, including the crystallization, vacuum filtration, and solvent recovery sub-systems, is analyzed and optimized based on pinch technology. According to pinch analysis, the energy-saving potential in the overall HEN is about 5029kW, accounting for 42.8% of the current heating utility and 77% of the existing cooling utility. Moreover, the unreasonable energy usage is figured out. Retrofit strategies are proposed by considering the current network structure and constraints. After the retrofit, 3200 kW of heating and cooling utility can be recovered, which accounts for 27.2% of the current heating utility and 49% of the current

cooling utility. The payback period is only 1.6 years.

References

[1] Zhang, L., 2002, Strategic adjustment of China's energy supply, China Construction News sunlight energy(Chinese), 24(12), pp. 7-9.

[2] Panjeshahi, M. H. et al., 2008, Retrofit of ammonia plant for improving energy efficiency, Energy, 33(1), pp. 46-64.

[3] Feng, X., 2004, *Principles and technology of chemical energy conservation* (in Chinese), Chemical Industry Press, Beijing, China.

[4] Shui,T., 1997, *Modern production technology of Lubricating Oil* (in Chinese), Sinopec Press, Beijing, China.

[5] Huang, M., et al., 2006, Optimization and application of the heat-exchanger network in dewaxing system, Petrochemical Design, (Chinese) 23(4), pp. 54~56.

[6] Huang, M., et al., 2009, Optimization of energy saving in ketone-benzol dewaxing &deoiling system, Lubricating Oil(Chinese), 24(2), pp. 15-22.

[7] Zheng, Z., 2006, The effect analysis of energy conservation measure on mek-toluene dewaxing unit, Chemical Engineering of Oil and Gas(Chinese), 35(2), pp. 125-126.

[8] Miao, Q. 2002, Energy conservation renovation for unit separating wax from oil by toluene-ketone, Chemical Engineering of Oil and Gas (Chinese), 31(3), pp. 128-131.

[9] Tian, H, 2002, Analysis of energy use of ketone-benzone dewaxing and deoil, Chemical Engineering of Oil and Gas(Chinese), 31(6), pp. 310-315.

[10] Zhang, W., et al., 2001, The application of pinch technology in the heat exchanging of recycle system of ketone-benzol dewaxing unit, Petrochemical Technology(Chinese), 8(2), pp. 99-102.

[11] Linnhoff, B. and Hindmarsh, E., 1983, The pinch design method for heat exchanger networks, Chemical Engineering Science, 38(5), pp. 745~763.

[12] Kralj, K.A., 2009, Estimating the maximum possible internal heat integrations of individual process, Energy, 34(9), pp. 1372-1377.

[13] Yoon, S., et al., 2007, Heat integration analysis for an industrial ethylbenzene plant using pinch analysis, Applied Thermal Engineering, 27(5-6), pp. 886-893.

[14] He, C. and Feng, X., 2001, *Principles of Chemical Engineering*, Science Press, Beijing, China.

Acknowledgments

Financial supports provided by the National Natural Science Foundation of China under Grant No. 50876079 and 20936004 are gratefully acknowledged.

Increasing of heat integration in separation system of olefin plants

Kazem Hasanzadeh[a], *Gholam Reza Salehi*[a], *Majid Amidpour*[a]

[a] *Center of Integration KN Toosi University of Technology, Tehran, Iran*

Abstract: This paper presents an industrial case-study: the synthesis of heat-integrated distillation systems applied to the light ends separation section of olefin and gas process plants. The distillation systems presented in this work employ heat-integration principles to significantly reduce the heat requirements compared to the traditional simple column train. The work started from the simulation of the existing plant, by which the parameters of the system were identified. Then the possible sequences of simple columns with sharp splits were identified for the considered application, and all columns of the configurations were designed and the heat-integrated configuration was also considered. In order to verify the examined distillation systems, all simple and complex configurations were simulated by rigorous numerical models. On the basis of the numerical simulations, the energy requirements for each configuration were evaluated. A rating of different plants was then performed, based on the total annual cost, allowing identifying the best plant configuration. A heat-integrated configuration showed the best performances for the considered separation.

Keywords: Distillation, Sequence, Heat Integration, TAC.

1. Introduction

Distillation is the most widely used separation technique in the petrochemical and chemical process industries for the separation of fluid mixtures despite its high energy requirement. Significant energy saving can be reached by the use of complex distillation arrangements such as the side-stripper, the side-rectifier, the thermal (internal) column coupling (also known as petlyuk system), the (external) energy integration (also known as energy integrated distillation system) and the heat pumping techniques [1-3].

The energy saving in distillation is an essential field of the chemical engineering research since the early 1970; appropriate integration of the distillation columns with the overall process often results in a significant reduction of the energy consumption in many cases. The classical design of a Nomenclature distillation system for a multicomponent separation uses only the simple columns.

Each of the simple columns in a multicomponent distillation configuration receives a feed and performs a sharp split between two adjacent components of the feed mixture. Meanwhile, each of the simple columns produces a top product with a condenser and a bottom product with a reboiler. Thus, in any case of the simple column configuration for an n-component mixture, it needs n - 1 simple columns with n - 1 condensers and n - 1 reboilers [4, 5]. The simple column configurations for multicomponent distillation are simple and easy to design and operate. Because the number of separation sequences increases dramatically when the number of components in the feed mixture increases, a considerable number of works have been conducted on optimal synthesis of simple column configurations for an n-component distillation [4-7]. Thompson and King reported the following formula to calculate the number of all simple configurations [8]:

$$S_n = \frac{[2(n-1)]!}{n!(n-1)!} \quad (1)$$

The task for the design of a heat integrated simple column configuration consists of searching for the possible heat matches among all of the condensers and reboilers of the simple columns. Large numbers of works have been done for the synthesis of the optimal heat integrated simple column configurations since the work by Rathore et al [9-16]. This paper considers the heat integrated distillation systems for a chemical

Corresponding Author: Reza Salehi, rezasalehi@kntu.ac.ir

process in order to minimize the total annual costs. The plant configuration considered in our case shown in (figure 1-A). This configuration can be classified as a distributed sequence and can be represented by the following separation task: AB/CD; A/B; C/D. Other four simple column configurations are possible for this separation, the direct (A/BCD; B/CD; C/D) sequences (Figure 2-A) and the direct-indirect (A/BCD; BC/D; B/C) sequences (Figure 3-A), the indirect (ABC/D; AB/C; A/B) sequences (Figure 4-A) and the indirect-direct (ABC/D; A/BC; B/C) sequence (Figure 5).

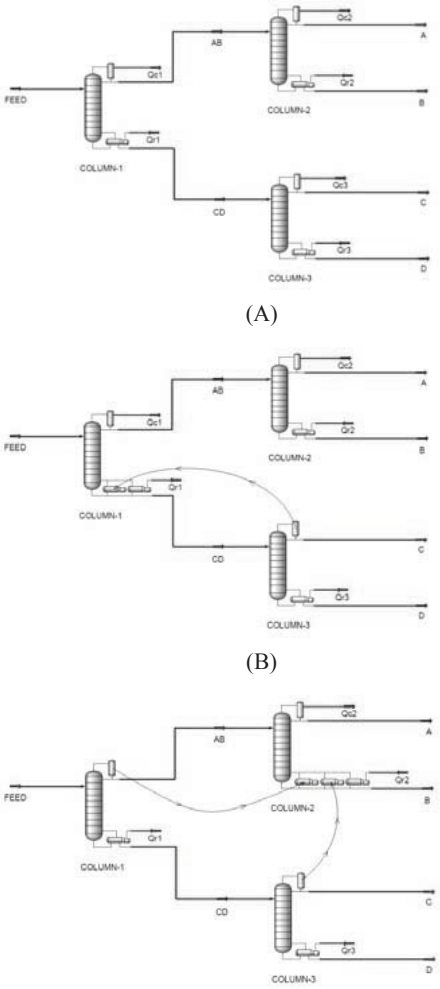

(A)

(B)

(C)

Fig. 1. Distributed sequences

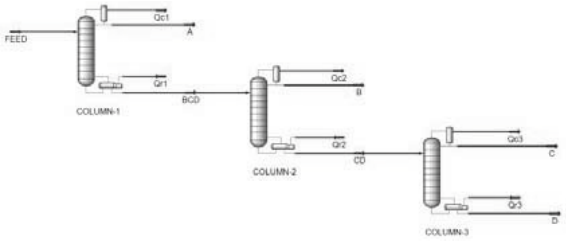

(A)

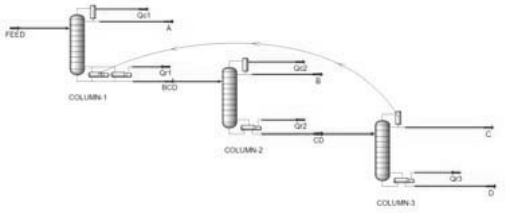

(B)

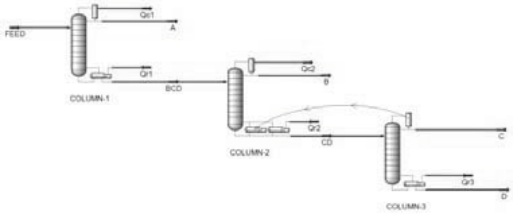

(C)

Fig. 2. Direct sequences

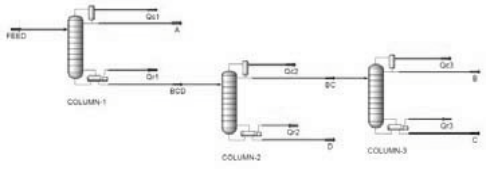

(A)

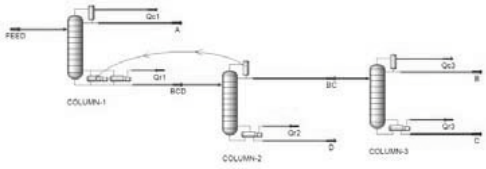

(B)

Fig. 3. Direct-Indirect sequences

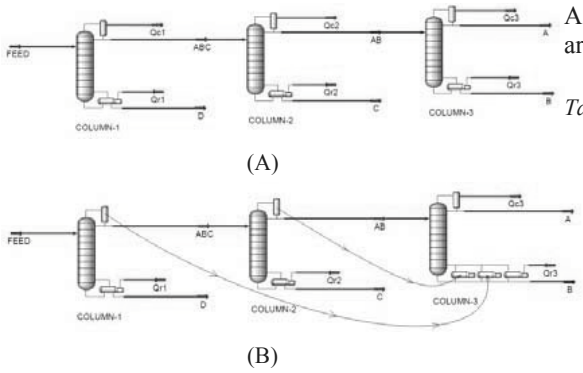

Fig. 4. *Indirect sequences*

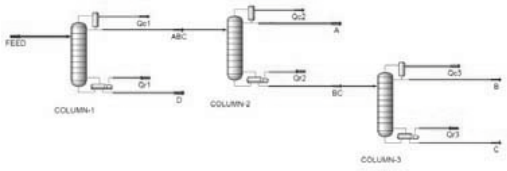

Fig. 5. Indirect-Direct sequence

2. Case study

The process examined in this paper, is the separation of a multi-component flow to four categories of products with a purity of 0.99. The intake flow has a temperature of 59.3 oC, a pressure of 1785 kPa and a flow rate equal to 1355 kmole/hr. Compositions of process intake flow and products are shown in table 1. The initial process is illustrated in figure 1-A and it is regarded as a reference case for other states. Simulations are carried out using the software HISYS and two models, Shortcut and Rigorous, are employed for simulating the towers. The governing equations for simulating the columns are NRTL equations.

The TAC function is optimized using the optimizer of HYSYS software. The method SQP is used to minimize TAC function. Different arrangements have been obtained for the process with heat integration satisfying the constraints of the problem. These arrangements are shown in figures 1-5. In this paper, first all possible states for arrangement of columns in separation of the process intake flow are simulated and then attempts are made for optimization and heat integration of columns. Utility costs are shown in table 2[16]. Equations related to installation and start up costs of columns is provided in appendix A [17]. Results of design and optimization of arrangements are shown in table 3A-E.

Table 1- Feed and product specifications

Product groups	Feed Components	Feed Xi (Mol Fraction)
A	C2H4	0.0001
	C3H4	0.0047
	C3H6	0.4538
B	C3H8	0.2912
	C4H4	0.0003
C	C4H6	0.0011
	C4H8	0.1541
	C4H10	0.0359
D	C5H12	0.0419
	C6H14	0.0137
	C7H16	0.0031

Table. 2. Utility costs

Utility	Temperature Level (° C)	Values
LP-steam ($/ton)	158	13
MP-steam ($/ton)	200	16
HP-steam ($/ton)	250	20
Cooling water ($/ton)	35-45	0.082

Table. 3. A- Optimal schemes for Primary Distributed and Distributed (C3-R1)

Description	Primary Distributed			Distributed (C3-R1)		
	C1	C2	C3	C1	C2	C3
Pressure (kpa)	2989	2220	1042	2365	2113	651
Diameter (m)	3.41	4.92	1.72	6.29	2.39	1.68
Reflux ratio	0.77	8.62	0.74	8.95	1.21	0.65
Actual plates	43	167	44	176	42	41
Total actual plates	254			259		
Heating rate (kJ/h)	78498124			100110119		
Cooling rate (kJ/h)	82738403			105533811		
HX duty (kJ/h)	32886838			-		
Steam cost ($/yr)	3326005			4224193.8		
C.W cost ($/yr)	1298478.3			1656224.4		
Operat. cost ($/yr)	4624483.2			5880418.2		
Capital cost ($/yr)	525335.21			554833.01		
TAC ($/yr)	5149818.4			6435251.2		
Op. cost saving (%)	27.51			7.83		
Capital saving (%)	30.78			26.89		
TAC saving (%)	27.86			9.85		

Table 3. B- Optimal schemes for Distributed (C1&C3-R2) and Direct

Description	Distributed (C1&C3-R2)			Direct		
	C1	C2	C3	C1	C2	C3
Pressure (kpa)	2989	2220	1042	2365	2113	651
Diameter (m)	3.41	4.92	1.72	6.29	2.39	1.68
Reflux ratio	0.77	8.62	0.74	8.95	1.21	0.65
Actual plates	43	167	44	176	42	41
Total actual plates	254			259		
Heating rate (kJ/h)	78498124			100110119		
Cooling rate (kJ/h)	82738403			105533811		
HX duty (kJ/h)	32886838			-		
Steam cost ($/yr)	3326005			4224193.8		
C.W cost ($/yr)	1298478.3			1656224.4		
Operat. cost ($/yr)	4624483.2			5880418.2		
Capital cost ($/yr)	525335.21			554833.01		
TAC ($/yr)	5149818.4			6435251.2		
Op. cost saving (%)	27.51			7.83		
Capital saving (%)	30.78			26.89		
TAC saving (%)	27.86			9.85		

Table 3. D- Optimal schemes for Direct-Indirect and Direct-Indirect (C2-R1)

Description	Direct-Indirect			Direct-Indirect (C2-R1)		
	C1	C2	C3	C1	C2	C3
Pressure (kpa)	2080	1307	1854	2024	2740	1717
Diameter (m)	6.27	2.37	1.83	6.27	2.42	1.9
Reflux ratio	8.9	0.31	1	8.89	0.37	1.13
Actual plates	174	44	42	174	49	46
Total actual plates	260			269		
Heating rate (kJ/h)	109826812			96202845		
Cooling rate (kJ/h)	113397355			99389758		
HX duty (kJ/h)	-			14648275		
Steam cost ($/yr)	4634066			4414348.8		
C.W cost ($/yr)	1779633.1			1559801		
Operat. cost ($/yr)	6413699.2			5974149.8		
Capital cost ($/yr)	639173.17			701488.26		
TAC ($/yr)	7052872.3			6675638		
Op. cost saving (%)	-0.53			6.36		
Capital saving (%)	15.78			7.57		
TAC saving (%)	1.2			6.48		

Table 3C- Optimal schemes for Direct (C3-R1) and Direct (C3-R2)

Description	Direct (C3-R1)			Direct (C3-R2)		
	C1	C2	C3	C1	C2	C3
Pressure (kpa)	2414	1969	1698	2313	1839	2667
Diameter (m)	6.29	2.38	1.71	6.28	2.37	1.74
Reflux ratio	8.97	1.2	0.73	8.93	1.18	0.78
Actual plates	174	40	44	176	40	49
Total actual plates	258			265		
Heating rate (kJ/h)	94211676			96031322		
Cooling rate (kJ/h)	96995376			97473954		
HX duty (kJ/h)	7832094			7279755.3		
Steam cost ($/yr)	4127335.1			4238147.6		
C.W cost ($/yr)	1522224.1			1529734.8		
Operat. cost ($/yr)	5649559.2			5767882.4		
Capital cost ($/yr)	550778.59			578258.09		
TAC ($/yr)	6200337.8			6346140.5		
Op. cost saving (%)	11.44			9.59		
Capital saving (%)	27.42			23.8		
TAC saving (%)	13.14			11.1		

Table 3 E- Optimal schemes for Indirect (C1&C2-R3) and Indirect-Direct

Description	Indirect (C1&C2-R3)			Indirect-Direct		
	C1	C2	C3	C1	C2	C3
Pressure (kpa)	2585	2986	2169	1844	2296	1912
Diameter (m)	3.2	2.71	4.92	3.18	5.01	1.89
Reflux ratio	0.25	0.72	8.61	0.22	8.69	1.12
Actual plates	51	49	168	48	167	44
Total actual plates	268			259		
Heating rate (kJ/h)	82072805			117517206		
Cooling rate (kJ/h)	83029960			120136244		
HX duty (kJ/h)	48112352			-		
Steam cost ($/yr)	4003977.4			5307057.3		
C.W cost ($/yr)	1303053.9			1885391.8		
Operat. cost ($/yr)	5307031.3			7192449		
Capital cost ($/yr)	607282.93			525144		
TAC ($/yr)	5914314.3			7717593		
Op. cost saving (%)	16.81			-12.74		
Capital saving (%)	19.98			30.8		
TAC saving (%)	17.15			-8.11		

This table shows that the arrangement Distributed (C1&C3-R2) (figure 1-C) with a TAC optimization of 27.86% represents a better result in comparison to other states. Arrangements Indirect(C1&C2-R3), with a TAC optimization of

17.15%, Direct(C3-R1) with an optimization of 13.14%, Direct(C3-R2) with an optimization of 11.1%, Direct with an optimization of 9.85%, Direct-Indirect(C2-R1) with an optimization of 6.48%, Distributed(C3-R1) with an optimization of 4.8%, Direct-Indirect with an optimization of 1.2% respectively, represented better result compared to the initial arrangement. The arrangements Indirect and Indirect-Direct increased the TAC 17.31% and 8.11% respectively.

The Distributed arrangement of the initial process is considered as the reference of comparison for other arrangements (Figure 1-A)

In the arrangement Distributed (C1&C3-R2), as can be seen in table 3-B and figure 2, by increasing pressures of columns 1 and 3 and creating the proper temperature difference, the heat output of these towers is transferred to the reboiler of column 2 and thus cooling costs of condensers 1 and 3 are eliminated and the heating of the reboiler of column 2 is considerably reduced. This has resulted in reduction of operational costs to an amount of 27.51% compared to the reference case. The results, illustrates the degree of heat integration in 62.86^{o}C and temperature change of the columns relative to the reference state. In this state, the reboilers of all towers are fed with LP steam which lowers the cost of consumption of steam in reboilers. Moreover, new designs of columns and heat exchangers have decreased initial costs to an amount of 30.78%. In the end, TAC has decreased by 27.86%. Among the reasons involving in high efficiency of this arrangement is separation of products of groups A and B in tower number 2, and away from the products of groups C and D. Products A and B are primarily propane and propylene. Because their relative volatilities are close to each other, their separation is difficult. Their molar percentages while entering the process is high compared to other compounds which have caused the heat consumption, height and diameter of column 2 to be higher than other columns in the process. One can say that in this arrangement, as a result of separation of products A and B in one column and also in the intermediate columns of the process, better conditions have been provided for the possibility of better heat integration and lower annual costs.

3. Conclusions

The obtained results show that the best arrangements were the ones in which two products A and B with high and close –to-each other values of relative volatility were separated in one column. On the other hand, because their molar percentages are high compared to other products, this column is preferred to be one of the primary or intermediate columns. For example in the state Indirect(C1&C2-R3), since products A and B are separated in column 3 and are present with high molar percentages in columns 1 and 2, the heat consumption of these columns have become more than that of columns 1 and 3 in the case Distributed(C1&C3-R2) and consequently the operational costs have increased. Because products A and B are separated in one column, only in cases Distributed(C1&C3-R2) and Indirect(C1&C2-R3) one can bring about two different heat integrations between condensers and reboilers of different columns. Low temperature difference inside the columns increases the freedom in changing columns' temperatures and heat integration of the column. The temperature difference in one column depends on the value of volatility of the components inside that column and molar percentages of these components in the intake flow of the column. Since molar percentages of components A and B are high, being respectively 45% and 29% of the process intake flow and also because of the proximity of their relative volatilities, the temperature difference of the columns which separate A from BCD and the columns which separate A from B are low. It can be deduced that in order to select arrangements with low temperature difference in columns, relative volatilities and molar percentages of the components should be investigated from the very beginning.

From the table 3,A-E it can be seen that the sum of costs related to consumption of steam and cold water in TAC has an order of 10E6 while the sum of initial costs of columns and heat exchangers is of the order 10E5. Consequently, it can be said that in designing the arrangements, one needs to increase the number of heat integrations and the amount of transferred heat since the amount of decrease of operational costs will be considerably higher than the increase of initial costs. Therefore, the chosen arrangements should be the ones which

provide the possibility of more heat integration in the process.

In the all table 3 it can be seen that the sum of costs of the cold water is a number of the order 10E5 but the sum of the costs of the steam is a number of the order 10E6. This is to say that more attention should be paid to temperature reduction and heat consumption of reboilers in the optimization procedure of columns.

By examining the initial costs we can come up with this conclusion that it is better to keep a higher value for the minimum temperature difference in the condensers of the columns which exchange a large amount of heat with cold water, so that their finished costs are lowered. The obtained results can be summarized as follows:

1- Choosing arrangements which provide the possibility for largest amounts of integration with high heat transfer potential
2- Separation of components with close volatilities in one column and away from the other components
3- Separation of components with high molar percentages in primary or intermediate columns
4- Keeping the heat of reboilers lower, and lowering consumption of expensive MP and HP steams
5- Investigating the values of volatilities and molar percentages of the components of the intake flow in order to choose arrangements with lower temperature differences in columns
6- Separation of ultra light and ultra heavy components in separate columns in order to lower the temperature difference between the condenser and the reboiler of the column.
7- Keeping higher the minimum temperature difference in condensers which have high heat loads.

The optimum state can be easily found considering the above conditions and that way, many of the arrangements will be eliminated in the primary stages of optimization of columns.

Nomenclature

S_n number of all simple configurations

N number of components

$M\&S$ Marshal and swift index

D Diameter of column

A Area of exchanger, m^2

H Height of column, m

References

[1] Petlyuk, F. B., Platonov, V. M., & Slavinskii, D. M. "Thermodynamically Optimal method of separating multicomponent mixtures." *International Chemical Engineering, 5* (1965) 555.

[2] Emtir, M.; Rev, E.; Fonyo, Z., "Rigorous Simulation of Energy Integrated and Thermally Coupled Distillation Schemes for Ternery Mixture", *Applied Thermal Engineering*, 21 (2001) 1299-1317.

[3] Rev, E., Emtir, M., Szitkai, Z., Mizsey, P., Fonyo, Z. "Energy savings of integrated and coupled distillation systemes." Computer and Chemical Engineering 25 (2001) 119–140.

[4] Thompson, R. W.; King, C. J. "Systematic Synthesis of Separation Schemes." *AIChE J*. 1972, *18*, 941.

[5] Freshwater, D. C.; Henry, B. D. "The Optimal Configuration of Multicomponent Distillation Trains". *Chem. Eng*. 1975, *301*, 533.

[6] Seader, J. D.; Westerberg, A. W. "A Combined Heuristic and Evolutionary Strategy for the Synthesis of Simple Separation Sequences." *AIChE J*. 1977, *23*, 951.

[7] Nadgir, V. M.; Liu, Y. A. "Studies in Chemical Process Design and Synthesis: Part V: A Simple Heuristic Method for Systematic Synthesis of Initial Sequences for Multicomponent Separations." *AIChE J*. 1983, *29*, 926.

[8] C.J. King, "Separation Processes," second ed., McGraw-Hill, New York, 1980.

[9] Rathore, R. N. S.; Wormer, K. A. V.; Powers, G. J. "Synthesis Strategies for Multicomponent Separation Systems with Energy Integration. " *AIChE J*. 1974, *20*, 940.Rathore, R. N. S.; Wormer, K. A. V.; Powers, G. J. "Synthesis Strategies for Multicomponent Separation Systems with Energy Integration. " *AIChE J*. 1974, *20*, 940.

[10] Andrecovich, M. J.; Westerberg, A. W. "A Simple Synthesis Method Based on Utility Bounding for Heat-integrated Distillation Sequences." *AIChE J.* 1985, *31*, 363.

[11] Kattan, M. K.; Douglas, P. L. "A New Approach to Thermal Integration of Distillation Sequences." *Can. J. Chem. Eng*. 1986, *64*, 162.

[12] Dhallu, N. S.; Johns, W. R. "Synthesis of Distillation Trains with Heat Integration."

Inst. Chem. Eng., Symp. Ser. 1988, *109*, 22-43.

[13] Isla, M. A.; Cerda, J. "A Heuristic Method for the Synthesis of Heat-integrated Distillation Systems. " *Chem. Eng. J.* 1988, 38, 161 - 177

[14] Schuttenhelm, W.; Simmrock, K. H. "Knowledge Based Synthesis of Energy Integrated Distillation Columns and Sequences." *Inst. Chem. Eng., Symp. Ser.* 1992, *128*, A461.

[15] Sobocan, G.; Glavic, P. "A Simple Method for Systematic Synthesis of Thermally Integrated Distillation Sequences." *Chem. Eng. J.* 2002, *89*, 155.

[16] Mascia, M.; Ferrara, F.; Vacca, A.; Tola, G.; Errico, M. "Design of Heat Integrated Distillation Systems for a Light Ends Separation Plant. ", *Applied Thermal Engineering*, 2007, 27, 1205-1211

[17] Errico, M.; Rong, B.; Tola, G.; Turunen, I., "A method for systematic synthesis of multicomponent distillation systems with less than N-1 columns," *Chemical Engineering and Processing*, 2009.

[18] Chem. Eng. 2009.

Appendix A. Cost estimation

A.1. Distillation columns

The total cost of a distillation column can be considered as a sum of the costs of column shell and trays. The number of stages and the diameter values obtained from the Aspen simulations can be utilized in the following correlations. All the correlations are valid for carbon steel construction and are updated from mid-1968 to 2009 utilizing the Marshall and Swift cost index [18].

• Column shell

$$\$ = \left(\frac{M\ \&\ S}{280}\right)(937.61)D^{1.066}H^{0.802} \quad \text{(A.1)}$$

$$H = (N-1)\times 0.6 + 6.0 \quad \text{(A.2)}$$

The correlation (A.1) is valid for a pressure less than 345 kPa; otherwise a correction factor must be applied. The column height is evaluated considering 0.6m as tray spacing and 6.0m as disengagement.

• Column trays

Considering sieve trays, the following correlation has been utilized.

$$\$ = \left(\frac{M\ \&\ S}{280}\right)(97.24)D\ H^{0.802}$$

(A.3)

A.2. Heat exchangers

The heat exchanger cost evaluation is based on the heat exchanger area evaluated utilizing the usual design formula:

$$A = \frac{Q}{U\ \Delta T_M}$$

(A.4)

Mean values of 1800 kJ/ (m2 h ◦C) and 2100 kJ/(m2 h ◦C) for the overall heat transfer coefficient for condensers and reboilers are assumed respectively. Assuming shell and tube, floating head and carbon steel construction the cost correlation is as follows:

$$\$ = \left(\frac{M\ \&\ S}{280}\right)(474.67)A^{0.65}$$

(A.5)

The reported correlation is valid for design pressure less than 1034.2 kPa and an exchange area range between $18.6 < A < 464.5$m2.

A.3. Annual capital cost

The capital cost (purchase plus installation cost) is annualized over a period which is often referred to as plant life time.

Annual capital cost = Capital cost / Plant life time

TAC = Annual operating cost + Annual capital cost

Operating cost was assumed just utility cost (steam and cooling water).

- Plant lifetime = 10 years
- Operating hours = 8000 h/year

Retrofit of Heat Exchanger Network of Crude Fractionation Unit

Kitipat Siemanond[a], Suppanit Srathongniam[a] , Kitisak Junlobol[b] , and Sira Nukulkit[c]

[a] *The Petroleum and Petrochemical College, Chulalogkorn University, Bangkok, Thailand*
[b] *PTT-AR Public Company Limited, Rayong, Thailand*
[c] *Department of Civil Engineering, Chulalogkorn University, Bangkok, Thailand*

Abstract: This study is to develop a mathematical programming model of heat exchanger network (HEN) retrofit called stage model (Yee and Grossmann, 1990) and apply it to the crude preheating train of a refinery in Thailand to reduce the energy consumption at the furnace and cooler. From pinch analysis, the composite curves of the base case show the retrofit potential at the heat recovery approach temperature (HRAT) about 33.5 ^{o}C. The retrofit design of the crude preheating train is done by applying the stage model, resulting in 14.5 % and 67.7 % energy saving at the furnace and cooler, respectively, with additional exchanger area of 9,610 m^2. After that, the retrofit design of HEN with multiple crude types; light and heavy ones, is done to find the optimal HEN for the refinery.

Keywords: Pinch analysis, Mathematical programming, Heat exchanger network retrofit.

1. Introduction

The crude fractionation unit, as shown in Figure 1, is one of the largest energy-consuming units in a refinery, having a complex heat exchanger network (HEN) of crude preheating train which transfers heat from hot-product and pump-around streams to the crude oil feed.

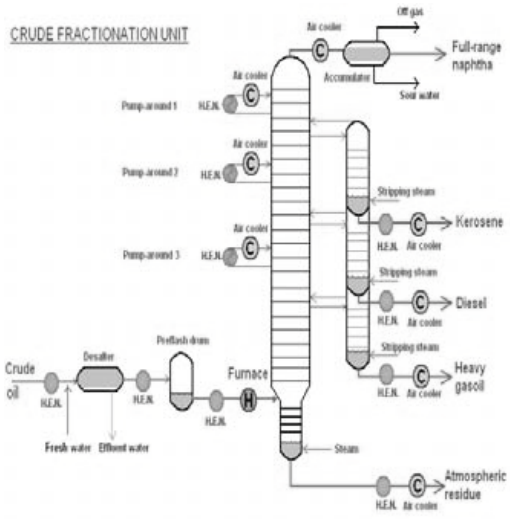

Fig. 1 Crude fractionation unit.

By preheating the crude, this HEN reduces fuel consumption in the crude furnace. In the 1970s, pinch technology, or process heat integration, which assists the design of an efficient HEN by the use of composite curves (T-Q diagram), as shown in Figure 2, was developed. This technology has enabled a theoretical approach to design an optimal HEN and find retrofit potential of the process. The composite curves consist of hot and cold composite lines presenting the relationships between temperature (T) and heat content (Q) for heat sources and sinks in the system. A pinch point of two lines indicates a heat recovery approach temperature (HRAT) or a thermodynamic constraint on heat exchange. Shifting the cold composite curve to the left improves heat recovery, or energy saving, by increasing the heat-exchanger area. Due to the energy crisis, a refinery in Thailand is trying to save the energy usage. The energy

efficiency of the crude preheating HEN can be improved by modifying the existing HEN.

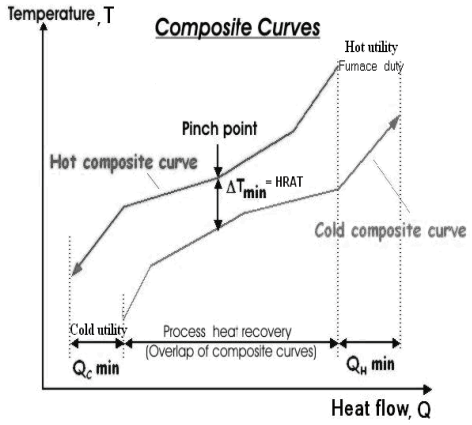

Fig. 2. Composite curves.

There are two kinds of HEN design; grassroots and retrofit design. The grassroots design of HEN is to do new design of HEN for the process. The retrofit design of HEN is to modify the existing HEN with exchanger relocation to gain more heat recovery and save utility usage. However, the results of HEN retrofit is the HEN design with minimal modification to reduce utility usages of the existing process.

2. Literature Survey

Grossmann et al. (1987) and Gundersen (1990,1991) provide comprehensive reviews of the existing retrofit techniques. The retrofit technique by Linnhoff & Tjoe (1985) using pinch technology or thermodynamic method applies targeting procedures to energy-area trade offs which subsequently translate into investment savings plots. Yee and Grossmann (1984) proposed assignment-transshipment models for structural modifications and a two-stage approach (Yee & Grossmann,1987). Ciric and Floudas (1989) proposed a retrofit strategy using a decomposition method.Asante and Zhu (1996) introduce an automated approach for HEN retrofit featuring minimal topology modifications. Briones and Kokossis (1998) use the hypertargets or conceptual programming approach for retrofitting industrial heat exchanger networks.

3. Stage Model

The stage model is based on the stage-wise superstructure representation proposed by Yee et al. (1990). The structure is shown in Figure 3. Within each stage of superstructure, possible exchanger between any pair of hot and cold streams can occur. Heater and coolers are placed at the end of cold and hot streams, respectively. The objective function of the model is to minimize the duty of heater, cooler and number of exchangers under the constraint functions of energy balance, thermodynamics, logical, and retrofit constraints.

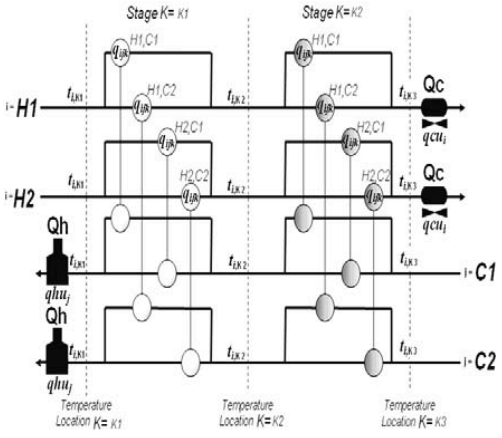

Fig. 3. Two-stage model structure.

The target temperatures and flow rate of hot and cold process streams are fixed and the stage-

Corresponding Author: Kitipat Siemanond, Email: kitipat.s@chula.ac.th

model will design HEN into two stages (K1 and K2) with the minimum utility usages and number of exchangers for fixed EMAT (Exchanger Minimum Approach Temperature). The constraints and objective function are

Overall heat balance for each stream.

$$(TIN_i - TOUT_i)F_i = \Sigma \quad \Sigma \quad (q_{ijk} + qcu_i) \quad i \in HP \quad \text{.....(1)}$$
$$k \in ST \quad j \in CP$$

$$(TOUT_j - TINj)F_j = \Sigma \quad \Sigma \quad (q_{ijk} + qhu_j) \quad j \in CP \quad \text{.....(2)}$$
$$k \in ST \quad i \in HP$$

Heat balance at each stage.

$$(t_{i,k} - t_{i,k+1})Fi = \Sigma \quad q_{ijk} \quad k \in ST, \; i \in HP \quad \text{.....(3)}$$
$$j \in CP$$

$$(t_{j,k} - t_{j,k+1})Fj = \Sigma \quad q_{ijk} \quad k \in ST, \; j \in CP \quad \text{.....(4)}$$
$$i \in HP$$

Assignment of superstructure inlet temperatures.

$$TIN_i = t_{i,1} \quad \text{.....(5)}$$

$$TIN_j = t_{j,NOK+1} \quad \text{.....(6)}$$

Feasibility of temperatures.

$$t_{i,k} \geq t_{i,k+1} \quad k \in ST, \; i \in HP \quad \text{.....(7)}$$

$$t_{j,k} \geq t_{j,k+1} \quad k \in ST, \; j \in CP \quad \text{.....(8)}$$

$$TOUT_i \leq t_{i,NOK+1} \quad i \in HP \quad \text{.....(9)}$$

$$TOUT_j \geq t_{j,1} \quad j \in CP \quad \text{.....(10)}$$

Hot and cold utility load.

$$(t_{i,NOK+1} - TOUT_i) Fi = qcu_i \quad i \in HP \quad \text{.....(11)}$$

$$(TOUT_j - t_{j,1}) F_j = qhu_j \quad j \in CP \quad \text{.....(12)}$$

Logical constraints.

$$q_{ijk} - \Omega z_{ijk} \leq 0 \quad i \in HP, \; j \in CP \; , \; k \in ST \quad \text{.....(13)}$$

$$qcu_i - \Omega zcu_i \leq 0 \quad i \in HP \quad \text{.....(14)}$$

$$qhu_j - \Omega zhu_j \leq 0 \quad \text{.....(15)}$$

$$z_{ijk}, z_{cui}, zhu_j = 0,1 \quad \text{.....(16)}$$

Calculation of approach temperatures.

$$dt_{ijk} \leq t_{i,k} - t_{j,k} + \Gamma(1 - z_{ijk}) \quad k \in ST, \; i \in HP, \; j \in CP \quad \text{.....(17)}$$

$$dt_{ijk+1} \leq t_{i,k+1} - t_{j,k+1} + \Gamma(1 - z_{ijk}) \quad k \in ST, \; i \in HP, \; j \in CP \quad \text{.....(18)}$$

$$dtcu_i \leq t_{i,NOK+1} - TOUT_{CU} + \Gamma(1 - zcu_i) \quad i \in HP \quad \text{.....(19)}$$

$$dthu_j \leq TOUT_{HU} - t_{j,1} + \Gamma(1 - zhu_j) \quad j \in CP \quad \text{.....(20)}$$

The temperature between the hot and cold streams at any point of any exchanger will be at least EMAT:

$$dt_{ijk} \leq \text{EMAT} \quad \text{.....(21)}$$

Objective function.

The objective function is to minimize utility cost and capital cost

$$\Sigma CCU \, qcu_i + \Sigma \, CHU \, qhu_j + \Sigma \; \Sigma \; \Sigma \; CF_{ij} z_{ijk}$$
$$i \in HP \quad j \in CP \quad i \in HP \; j \in CP \; k \in ST$$
$$+ \Sigma \, CF_{i,CU} \, zcu_{ijk} + \Sigma \, CF_{j,HU} \, zhu_j + \Sigma \; \Sigma \; \Sigma \; Carea \; q_{ijk} \quad \text{.....(22)}$$
$$i \in HP \quad j \in CP \quad i \in HP \; j \in CP \; k \in ST$$

Nomenclature

HP = set of hot process streams

F = heat capacity flow rate

CP = set of cold process streams

U = overall heat transfer coefficient

ST = set of stage no.

CCU = unit cost for cold utility = 400 $/ kw

CHU = unit cost of hot utility = 100 $/ kw

CF = fixed cost for exchanger = 4000 $/exchanger unit

C area = linearized variable (area) cost for exchanger = *46.5* $/ kw

TIN = inlet temperature of stream

TOUT= outlet temperature of stream

β = exponent for area cost

NOK = total number of stages

Ω = upper bound for heat exchange

Γ = upper bound for temperature difference

dt_{ijk}= temperature approach of match (*i,j*) at temperature location *k*

$dtcu_i$= temperature approach of match-hot stream *i* and cold utility

$dthu_j$ = temperature approach of match-cold stream *j* and hot utility

q_{ijk} = heat exchanged between hot process stream *i* and cold process stream *j* in stage *k*

qcu_i = heat exchanged between hot stream *i* and cold utility

qhu_j = heat exchanged between hot stream and cold stream *j*

$t_{i,k}$ = temperature of hot stream *i* at hot end of stage *k*

$t_{j,k}$ = temperature of cold stream *j* at hot end of stage *k*

z_{ijk} = binary variable to denote existence of match (*i,j*) in stage *k*

z_{cui} = binary variable that cold utility exchanges heat with stream i

z_{huij} = binary variable that hot utility exchanges heat with stream *j*

4. Crude Preheating Train

For this study, crude preheating train is a heat exchanger network (HEN) with a furnace used

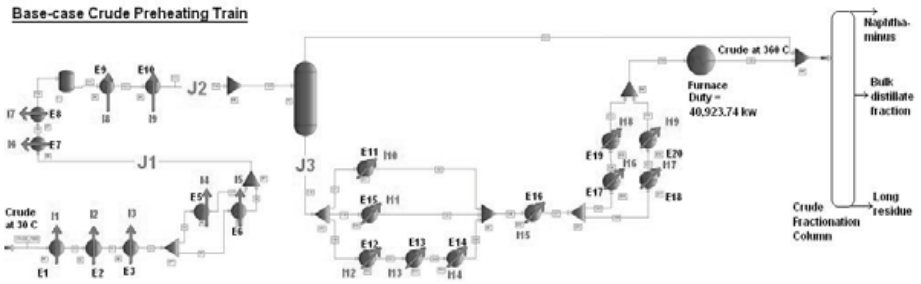

Fig. 4. Base-case crude preheating train from PRO-II simulation.

to heat the crude from temperature of 30 ^{o} C to 360 ^{o}C or more. This HEN contains 19 process-to-process exchangers; E1, E2, E3, E5, E6,E7, E8, E9, E10, E11, E12,E13, E14, E15, E16, E17, E18, E19, and 20, to transfer heat from 19 hot process streams; I1 to I19, to heat the cold crude stream; divided into three parts; J1, J2, and J3. For the furnace, it requires heat duty of 40,923.9 kw to preheat the crude before entering the fractionation column to produce products; naphtha-minus, bulk distillate fraction, and long residue, as shown in Figure 4. The base-case HEN of crude preheating train can be represented by the grid diagram as shown in Figure 5 and the details of each exchanger from the base case; recovered heat, (Q), area, overall heat transfer coefficient (U), and logarithm mean temperature difference (LMTD), are shown in Table 1.

Exchanger No.	Q (kw)	Area (m2)	LMTD (C)	U (kw/m2/C)
E1	14152	440	72.76840806	0.442
E2	12091	228	114.7850687	0.462
E3	7930	321	87.66518752	0.2818
E5	2907	70	83.8961039	0.495
E6	5678	146	83.81554086	0.464
E7	10680	311	70.25876209	0.4842
E8	5554	242	50.14291725	0.4577
E9	10476	441	55.98657092	0.4243
E10	10578	940	31.41857634	0.36817
E11	10624	600	40.9024409	0.4329
E12	4160	183	52.53579948	0.4327
E13	2690	162	40.01189945	0.415
E14	1180	147	38.04366348	0.211
E15	16350	1509	37.13156292	0.2918
E16	18820	1374	38.24227141	0.36817
E17	2013	125	39.05893767	0.4123
E18	1230	98.2	44.40077366	0.2821
E19	10174	1424	34.76721616	0.2055
E20	6360	1028	36.95800734	0.1674

Overall area =	9789.2	m2
Overall recovery Q =	153547	kw
Number of exchangers :	19	

Table 1. Detail of all exchangers of the base case.

5. Retrofit Potential

Pinch analysis (1970s) is applied to find the retrofit potential of the crude preheating train by using the composite curves of hot and cold process streams as shown in Figure 6. It shows that this base-case HEN has minimum temperature difference (HRAT) of 33.5 ^{o}C and the scope of energy saving on furnace duty is not more than 8,793 kw. To reduce the energy usage of crude furnace, more exchanger area is needed for the base-case HEN.

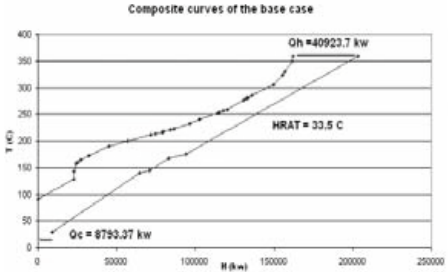

Fig.6. The composite curves of the base case.

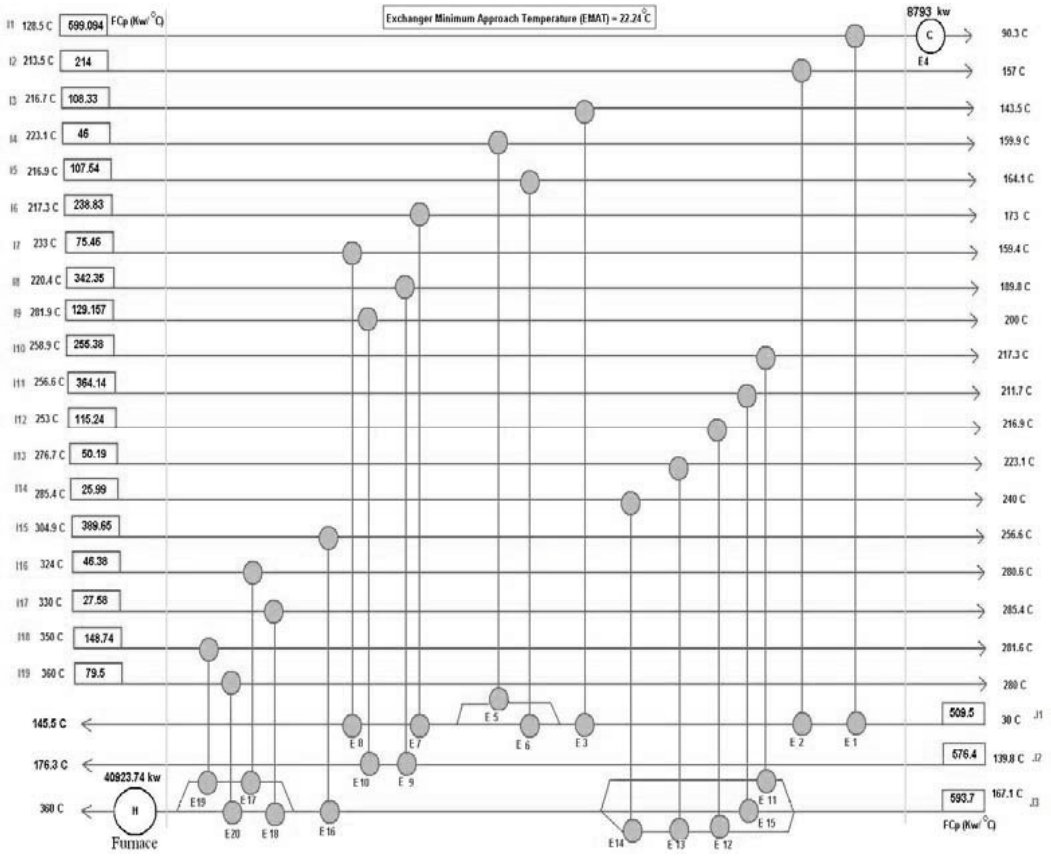

Fig. 5. The grid diagram of the base case.

6. Retrofit Design of HEN

The stage model by Yee and Grossmann (1990) is applied, using 20 stages, to retrofit the base-case HEN. There are three splitting sections; located at stage no. 5, 10, and 15. The other stages are for additional/removal exchanger area or new exchangers needed after retrofitting. The model using MILP (Mixed Integer Linear Programming) to minimize the total cost of furnace, cooler duties and the fixed/variable costs of exchanger, resulting in the optimal HEN with the retrofit structure.

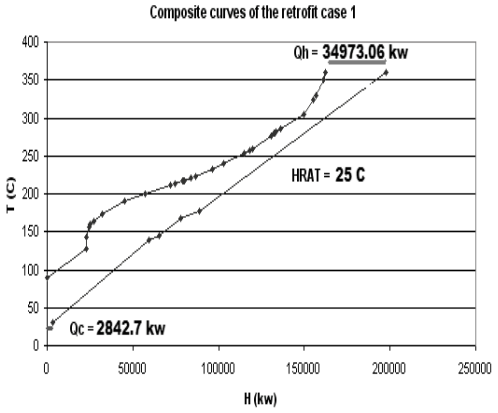

Fig.8. The composite curves of the retrofit case.

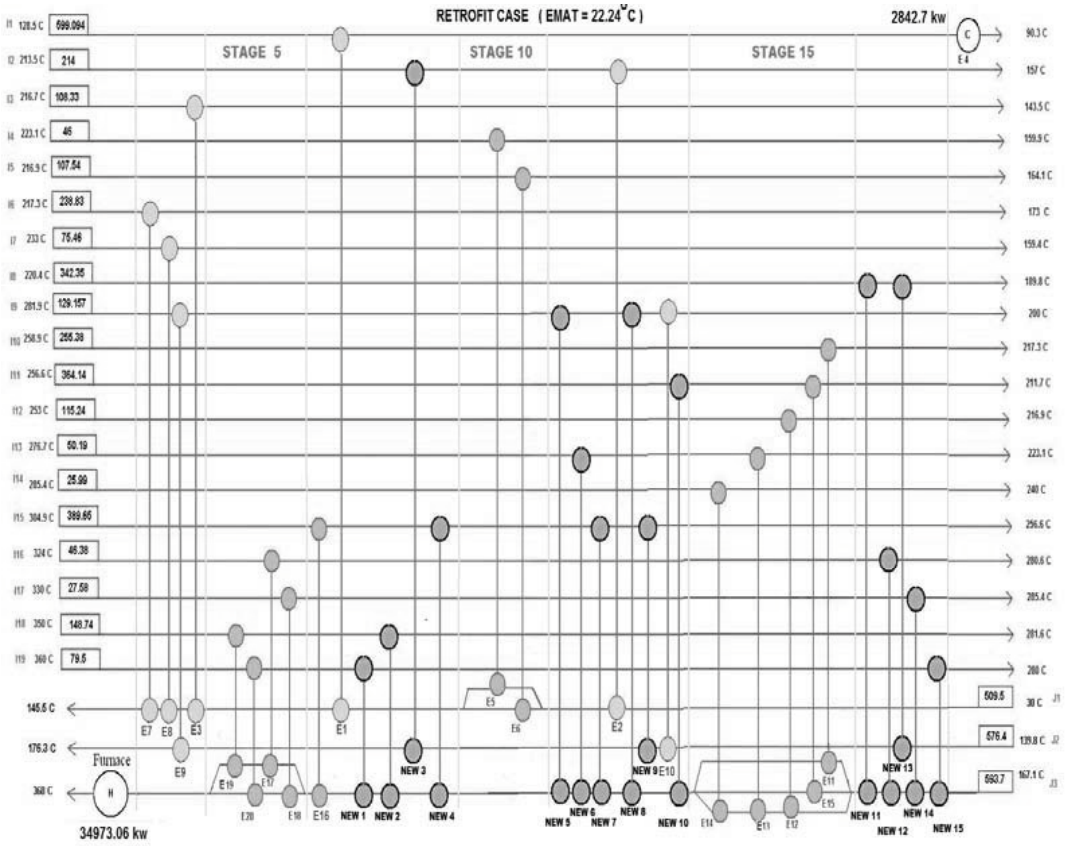

Fig.7. The grid diagram of the retrofit case.

For this study, the costs of utility and exchangers are assumed. For utility costs, they are $100 and $400 per kilowatt of hot and cold utility, respectively. For exchanger costs, the fixed cost is $4000 per unit and the variable cost is $46.5 per kilowatt of heat recovery by process-to-process exchanger. The retrofit-case HEN is generated by stage model, as shown in Figure 7, resulting in the reduced HRAT of 25 ^{o}C, as shown in the composite curves of Figure 8. It consumes less furnace duty than the base case; about 34,973 kw by adding more exchanger area of 9,610 m^2, as shown in Table 2a and 2b.

Exchanger No.	Q (kw)	Area (m2)	LMTD (C)	U (kw/m2/C)
E1	20042.701	1370.6	33.08	0.442
E2	6155.456	98.57	135.17	0.462
E3	7929.756	401.16	70.15	0.2818
E5	2907.2	42.04	139.70	0.495
E6	5678.112	87.9	139.22	0.464
E7	10580.169	368.75	59.26	0.4842
E8	5553.856	167.49	72.45	0.4577
E9	6789.327	400.65	39.94	0.4243
E10	7110.946	253.9	78.19	0.35817
E11	10623.808	700	35.06	0.4329
E12	14896.385	1188.8	28.96	0.4327
E13	4160.164	180.97	55.39	0.415
E14	2137.855	205.7	49.26	0.211
E15	1179.946	54.5	74.20	0.2918
E16	6701.345	746.03	25.08	0.35817
E17	1160.008	86.8	32.41	0.4123
E18	855.282	86.71	34.97	0.2821
E19	7587.368	1096.45	33.67	0.2055
E20	4850.37	693.24	41.80	0.1674

Overall area =	8230.26	m2
Overall recovery Q =	126900.054	kw
Number of exchangers =	19	

Table 2a Detail of 19 old exchangers from the retrofit case.

New Exchanger No.	Q (kw)	Area (m2)	LMTD (C)	Assumed U (kw/m2/C)
New1	1036.089	376.78	27.50	0.1
New2	2586.448	915.32	28.26	0.1
New3	5935.544	1498.05	39.62	0.1
New4	6917.528	2748.32	25.17	0.1
New5	1972.802	709.92	27.79	0.1
New6	552.329	204.84	26.96	0.1
New7	4821.942	1983.97	24.30	0.1
New8	1494.21	563.65	26.51	0.1
New9	379.379	36.76	103.20	0.1
New10	1453.501	631.88	23.00	0.1
New11	2863.08	1194.62	23.97	0.1
New12	852.884	70.87	120.34	0.1
New13	823.502	163.11	50.49	0.1
New 14	374.786	30.26	123.86	0.1
New15	473.541	41.01	115.47	0.1

Overall area =	11169	m2
Overall recovery Q =	32537.565	kw
Number of new exchangers	15	

Table 2b Detail of 15 new exchangers from the retrofit case.

The retrofit results include the relocation of the base-case exchangers, the addition of fifteen new exchangers with area of 11,169 m^2, and the additional/removal area of the existing exchangers.

7. Conclusion

In the face of global energy crisis, most refinery in Thailand are desirous of improving energy efficiency by trying to reduce energy consumption or saving fuel usages at the crude furnace of the crude preheating train. For this study of a refinery, the HEN retrofit with applying 20-stage model is carried out by relocating some existing exchangers and adding fifteen new exchangers to the base-case HEN, resulting in the 14.5% energy saving at the furnace, and 67.7% energy saving at a cooler of pump-around as shown in Table 3.

		HRAT	Utilities (kW)			
	EMAT (°C)	(°C)	Furnace	Saving (%)	Cooler	Saving (%)
Base Case	22.24	33.5	40923.74	.	8793	-
Retrofit Case	22.24	25	34973.06	**14.54%**	2842.7	**67.67%**

Table 3. Comparisons of energy usages between the base case and retrofit case.

This retrofit technique can also be applied to the crude fractionation unit with different crude types; light and heavy ones. The retrofit results will be the optimal HEN of crude preheating train for both crude types.

8. References

[1] Linnhoff, B. and Hindmarsh, E. (1983). The pinch design method for heat exchanger networks. Chemical Engineering Science, 38, 745-763.

[2] Yee, T. F. and Grossmann, I. E. (1990). Simultaneous optimization models for heat integration – II. Heat exchanger network synthesis. Computers and Chemical Engineering, 14(10), 1165-1184.

[3] Bagajewicz, Miguel and Soto, J. (2001). Rigorous procedure for the design of conventional atmospheric crude fractionation units. Part II: Heat Exchanger Networks. Industry and Engineering Chemistry Research, 40(2), 627-634.

Acknowledgments: Authors would like to thank PTT-AR Public Company Limited for the data support. In addition, we would like to acknowledge with thanks the valuable contribution of Prof. Miguel Bagajewicz in educating us mathematical programming, GAMS. Finally, we would like to express our gratitude to the Government Budget, the Petroleum and Petrochemical College, Chulalongkorn University, and Center for Petroleum, Petrochemical, and Advanced Materials for funding support.

Strategy for sustainable energy matrix conversion based on exergy life cycle analysis: A case study.

M. A. Rubio Rodríguez [a], V. K. Verma [b], S. Bram [b, c], J. De Ruyck [b], P. Roque Díaz [a].

[a] *Universidad Central "Marta Abreu" de Las Villas, Santa Clara, Cuba*

[b] *Vrije Universiteit Brussel (VUB),Brussels, Belgium*

[c] *Erasmushogeschool Brussel, Brussel, Belgium*

Abstract: Scientists and policymakers are searching for alternatives for the current energy transformation systems to address the problems of environmental pollution and resource scarcity and depletion. The questions are: how environmentally friendly and sustainable are the available alternatives and which of them will ensure a major improvement in environmental quality at lowest economic cost? To answer some of these questions, the present work proposes a method where a sustainability indicator based on exergy life cycle data complemented with concepts from classical monetary investment assessment. This approach allows for the determination of an investment hierarchy by comparing alternative energy conversion routes in terms of their concerned environmental contribution and their natural resource indirect cost. The aim of this work is to highlight the convenience of a quite different exergy indicator, based on indirect exergetic cost and environmental exergetic cost. Four approaches are at the base of this investigation: the cumulative exergy consumption (CExC) from Szargut [1] and its implementation as a Life Cycle Assessment (LCIA) on the Ecoinvent database; the zero-exergy emission approach from Cornelissen [2] also used by Sciubba's Extended Exergy Accounting [3]; the renewability concept from Dewulf [4-5] and Ocaña [6]; and the indirect exergy concept, defined as the additional exergy needed from the technosphere to drive a transformation energy route as proposed by Wall [7]. Important concepts that were followed in this paper are the concept of energy route or energy path, and the philosophy behind a System Perturbation Analysis from Bram [8]. A case study is presented using data from the Ecoinvent database (v2.01 2007) to investigate the alternatives for petrol driven cars. The alternative energy routes assessed were methanol from biomass synthetic gas and biogas. All three energy routes for personal transport were compared to find out the most sustainable route with the lowest indirect exergy cost.

Keywords: Energy system, energy route, energy sustainability, LCA, ELCA.

1. Introduction

Mankind is realizing that dependence on fossil fuels can no longer be sustained. Consequently many studies have been performed to plan the way back to the usage of renewable energy sources [7, 9-14]. Care must however be taken to go for alternatives which offer the highest degree of sustainability in order to use the limited resources in an optimal way.

One trend has been the search for a sustainability function that might be applied in parallel with a classical economic function. First there is the category of indicators and indexes, integrated or not, which represent a state of economic, social and environmental development in a defined region, often the national level [15-17], secondly there are those product-related assessment tools with the focus on the material and/or energy flows of a product or service from a life cycle perspective [6, 17-18]. Within the frame of the second approach, present work has been developed.

A wide collection of those product-related assessment tools are implemented on Ecoinvent data base [19]. Some of these assessment tools are CML 2001, eco-indicator 99, ecological-footprint, and some others like cumulative exergy demand and cumulative energy demand. All these indexes are also formed by subcategories which are calculated using linear weight functions. These assessments aim to quantify specific environmental troubles as well as the total impact. The main disadvantage of these assessments is the use of weight function which is obtained by subjective procedures like experts opinions.

On the other hand exergy life cycle based indicators have been proposed not only as a measure for economic losses and dematerialization, but for waste

Corresponding Author: M. A. Rubio Rodríguez, Email: manuelrr@uclv.edu.cu

accounting and ecotoxicity as well. The reason for this is that exergy embodied in resources, products, and waste materials, has the potential to cause change in both the industrial environment and the natural ecosystem [5]. The advantages of use exergy as measurement of environmental impact are widely recognized [2, 5]. But the use of the exergy entering the technosphere as base of net exergy efficiency and the no distinction between renewable and nonrenewable primary resources bear to a contradiction due to fact that "energy sources cannot convert as much of the available energy to useful energy as nonrenewable do" [20]. So an increment in the renewability share of primary resources could be canceled by a decrease of net exergy efficiency, despite the fact that probably it would be preferable to decrease the use of nonrenewable resources in spite of an efficiency decrement.

This investigation aims at demonstrating the convenience of a quite different exergy indicator, based on indirect exergetic cost and environmental exergetic cost, when it is necessary to assess the exergetic sustainability of energy transformation strategies to different final services or commodities. This new perspective would contribute to later elaborate a new optimization function for energy matrixes.

2. Methodology

2.1. Background

The present sustainability measuring procedure for alternative energy transformation routes is based on four approaches: Szargut's cumulative exergy consumption (CExC) [1], Zero-exergy emission from Cornelissen [2, 21], Dewulf's renewability idea [4] and the indirect exergy consumption approach from Wall [22].

The first approach was the cumulative exergy consumption (CExC) from Szargut [1] and its implementation as a Life Cycle Assessment (LCIA) on the Ecoinvent database [23]. In order to quantify the life cycle exergy demand of a product, Cumulative Exergy Demand (CExD) is defined as the sum of exergy of all resources required to provide a service or product [24].

The second approach is the Zero-exergy emission from Cornelissen also used by Sciubba's Extended Exergy Accounting [2-3]. The present work addressed the accounting of pollution impact based on exergy approach, which was used also by Dewulf [4]. The essence of this idea is that: "the potential environmental impact of an effluent is represented by the cumulative amount of exergetic resources that must be consumed to attain an ideal, zero-impact disposal of both the effluent itself and the equipment that handles it".

On the issue of sustainability measuring Dewulf's works and Ocaña´s PhD thesis [6] will be used as reference [4-5]. From both authors exergy accounting idea has been retained also the notion of renewability index and efficiency as important factors on sustainability issues.

Finally the indirect exergy concept proposed by Wall will be applied. This exergy would be the part of the CExD which is not directly transformed to obtain the final energy service [7].

An important concept that will be followed along this paper, used in Bram's work [8], is the concept of energy route or energy path. This route or path was defined as all transformations necessary to convert a primary natural resource into a final service or commodity. For instance it is the path from crude oil under ground as joules of exergy, to transported passengers as passenger-kilometer, or the route from energy in the wind as joules, to electricity served at consumer as watt-hour.

2.2. Exergetic costs of sustainability

It was possible to define four exergetic cost function for an energy transformation route, taking into account the life cycle exergy consumption and the exergy neutralization cost.

The first one was based on Dewulf's idea [4] about a renewability parameter:

$$k_F=(CExD_F)/(Fm) \quad [J/fu] \qquad (1)$$

Where k_F is the fossil exergetic cost in joule of fossil cumulative exergy, $CExD_F$ is the fossil part of CExD and Fm is a proper functional magnitude chosen as a final desired product or service, for instance passengers-kilometer, tons-kilometer, kWh, etc; and fu is the corresponding functional unit.

The same concept was used by Ocaña [6] to create a fossil exergy consumption index for a system, but it accounted only for the exergy of energy flows in the assessed system lacking of the life cycle approach of the CExD concept which considered the cumulative amount of exergy "embodied" in the product or service by the successive contribution of each step in the production chain [5].

The second exergetic cost was based on the CExD of renewable resources. This is similar to the previous but accounting for the renewable portion of the CExD, thus the expression is:

$$k_R=(CExD_R)/(Fm) \quad [J/fu] \qquad (2)$$

Where, as it was said, $CExD_R$ is the renewable part of the life cycle exergy demand in resources. Consequently if both exergy costs are summed one

obtains the cumulative exergy demand due to the consumption of all natural resources chargeable to a final service (k).

$k_C=k_F+k_R$ *[J/fu]* (3)

It would be valuable also to account for externalities due to the pollutants emission and associated environmental consequences. Thus an expression to calculate an exergetic cost due to zero exergy impact of an energy transformation chain is:

$k_P=\Sigma(m_i*y_i)/(Fm)$ *[J/fu]* (4)

Where m_i is the mass of each computable pollutant emitted during the life cycle of the energy route assessed and y_i would be the exergy mitigation cost or Zero-exergy cost for each pollutant [21, 25].

In spite of the lack of this term to be proportional to the real magnitude of environmental impact, it is obvious that $k_P=0$ implies a non polluting scenario or technology.

At this point it was proposed by the authors to account for the exergetic cost of non-sustainability in order to later assess the energy routes which imply the larger reduction in terms of environmental impact. Hence there is the possibility to group just the zero impact exergetic cost k_P and the fossil exergetic cost k_F. The new category could be called environmental exergetic cost. This environmental cost represents the nonsustainability and it would be part of the sustainability concept that is supported in this work:

$k_I=k_F+k_P$ *[J/fu]* (5)

This term accounts for cumulative exergy from fossil fuels and that of zero impact cost, both during the life cycle of one functional unit of final energy route. It is important to remark that the environmental exergetic cost k_I embodies the influence of the life cycle efficiency because an increment of the efficiency without any other change, obviously decreases environmental exergetic cost k_I.

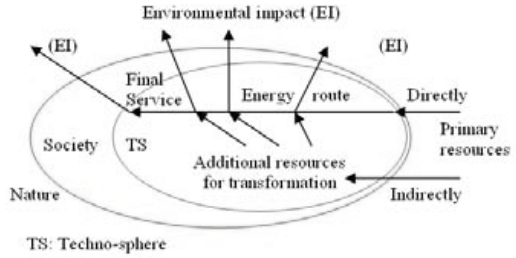

Figure 1 Energy route model

An idea supported by the authors, which is similar to that from Wall [7], is represented in Figure 1. The additional primary resources are those which indirectly enter the considered system during the transformation process of a primary resource, which itself is directly related with the supply of an energy service either inside the techno-sphere or the society.

According to the concepts presented above, the category that will be called indirect exergetic cost (k_T) was obtained by subtracting the exergy of the primary resource directly related with the energy route itself from the CExC accounted for the route, that is:

$k_T=k_C - B_{PR}/Fm$ *[J/fu]* (6)

where B_{PR} is the exergy of the primary resource directly related with the energy route. The expression above is proposed by the authors based on Wall's ideas [7], but intended to be used with the data supply by the Ecoinvent data base.

2.3. Assessing alternative energy routes

A cardinal problem today is the assessment of substituting current fossil based energy routes by other more sustainable alternatives. It is also convenient to know how much each alternative route contributes to the sustainability and which of them are the most suitable to be implemented independently of the final service or product.

The environmental exergetic cost (k_I) was defined previously in this work as a measure of the impact on sustainability of a certain energy route. So it was defined the variation in terms of this indicator when it is decided to assess an alternative route:

$\Delta k_I=k_I^0-k_I$ *[J/fu]* (7)

Where k_I is the environmental exergetic cost of the alternative route and k_I^0 is of the current one or an appropriated base to be used, a positive value of Δk_I implies a reduction in the environmental impact of the alternative route. Consequently the alternative routes showing a positive Δk_I will be superior to the current one and that with the highest variation would be the most advantageous. It should be keep in mind that alternatives are needed also for coproducts if they are generated along the energy route, leading to a complete balance when the base alternative is substituted by the assessed one [8].

Finally, it was expressed Δk_I in proportion to the realized exergetic cost reduction, which leads to the following sustainability index:

$S_{IC}= \Delta k_I/k_T$ (8)

S_{IC} represents joules of exergy potentially avoided in terms of "environmental impact" per joule of exergy invested in terms of the natural resources which can be chosen where to invest.

The indicator proposed represents the gain or loss in terms of environmental impact (k_I) when an energy transformation route is substituted by an alternative

one, divided by the indirect cost of the alternative. So it is possible to assess routes which contribute with the highest reduction of environmental impact at the lowest indirect exergetic cost of the alternative option. This indirect exergetic cost represents the exergy added in the route to drive it. Thus indirect exergy cost is cumulative exergy supposed already stored inside technosphere that like money should be administrated.

This indicator is the major contribution of this work and successfully embodies three important concepts that should be present on an index which aims at expressing sustainability improvements. First, the decrement in using nonrenewable resources used during the life cycle of the assessed services, products or commodities. Second, the efficiency using renewable and nonrenewable resources which indirectly contribute to the energy route. And finally the proposed indicator includes the influence of abatement exergy cost of the pollutants emitted to the environment. Since the net exergy efficiency is not part of the indicator and the indicator is proportional to the reduction of environmental impact and inversely proportional to the indirect exegetic cost, the contradiction stated in the introduction is not expressed on the indicator proposed.

3. Case study: replacing gasoline by methanol or biogas for transport

The present approach is used to analyze whether so called sustainable alternative fuels would really be a viable way to enhance environmental sustainability. Biofuels are widely treated in the literature [26-27], and they are seen as a way to improve CO2 balance and avoid fossil fuel dependence. Cars driven by methanol and biogas from biowaste are considered as alternatives for gasoline. The life cycle data base used was Ecoinvent [23, 28], and all data were processed by means of software developed for this purpose.

It should be reminded that Ecoinvent is a life cycle data base which includes all resources from *cradle to grave* including infrastructure. Ecoinvent is built up on statistical linear models. All assumptions (efficiencies, infrastructure useful life hours, etc), and the way the information was gathered and processed, can be found in [28].

The base case chosen in this sample was transportation by personal petrol car, and the selected process in the Ecoinvent data base was the 6590 named: transport, passenger car, petrol, EURO5. The LCA sumary for this service is shown in Table 1.

Table 1 LCA summary for petrol passenger car base case

Process or assessment name	Unit	Value
transport, passenger car, petrol EURO5	pkm	1
CO2, fossil	kg	1,59E-01
nitrogen oxides	kg	1,86E-04
sulphur dioxide	kg	2,74E-04
non-renewable exergy resources fossil	MJ-Eq	2,49E+00
non-renewable exergy resources nuclear	MJ-Eq	3,70E-01
renewable exergy resources, kinetic (in wind), converted	MJ-Eq	2,71E-03
renewable exergy resources, sola converted	MJ-Eq	5,10E-05
renewable exergy resources potential (in barrage water) converted	MJ-Eq	7,28E-02
non-renewable exergy resources primary forest	MJ-Eq	7,61E-06
renewable exergy resources, biomass	MJ-Eq	8.10E-03
renewable material resources, water	MJ-Eq	7,94E-02
non-renewable material resources metals	MJ-Eq	3,01E-02
non-renewable material resources minerals	MJ-Eq	6,16E-03

The primary exergy which in this case is the crude oil to produce the gasoline consumed to obtain one passenger-kilometer (pkm), was 1,489 MJ-Eq.

Exergy removal costs for CO2, SO2 and NOx. were taken from Cornelissen [21]. 90% of SO2 abatement would cost 57 MJ/kg, 80% abatement of NOx 16 MJ/kg, and 90% abatement of CO2 3 MJ/kg on the base of removal by compression and storage in empty gas field. The exergetic cost to remove this pollutants is not 100% because this is information from real technologies and in practice it is no possible to achieve a higher removal.

Table 2 ELCA and zero-exergy emission for petrol passenger car base case.

Concept	Unit	Value
k_F	MJ-Eq/pkm	2,892
k_R	MJ-Eq/pkm	0,1630
k_C	MJ-Eq/pkm	3,055
B_{PR}	MJ-Eq/pkm	1,489
k_T	MJ-Eq/pkm	1,566
k_P	MJ-Eq/pkm	0,4964

With these primary data and the specific zero-exergy cost of the pollutants accounted (carbon dioxide equivalent, sulphur dioxide and nitrogen oxides) the non renewable exergy demand, renewable exergy

demand, indirect exergy demand and the cumulative zero-exergy emission were calculated, everything per passenger-kilometer and shown in Table 2.
The same procedure was applied to the other two alternatives, methanol and methane fueled cars. The methanol was supposed to be obtained from biomass synthetic gas and the methane from biowaste anaerobic digestion. The results are presented in Table 3 and Table 4.

Table 3 ELCA summary for methanol alternative.

Concept	Unit	Value
k_F	MJ-Eq/pkm	1,602
k_R	MJ-Eq/pkm	5,705
k_C	MJ-Eq/pkm	7,308
B_{PR}	MJ-Eq/pkm	5,415
k_T	MJ-Eq/pkm	1,893
k_P	MJ-Eq/pkm	0,1718

Chart 1 compares k_F, k_R, k_C, B_{PR}, k_T and k_P. Savings in terms of non-renewable resources (k_F), correspond to 45% for methanol alternative and 38% for the methane alternative. The abatement exergy (kP) would be also reduced by 65% and 63% respectively. Primary exergy (B_{PR}) is 3,6 times higher in the case of methanol alternative and 1,5 times higher in the case of methane, comparing with the petrol base case, but these are renewable sources. Indirect exergy (k_T) which represents the cost in terms of natural resources to drive the alternative routes is 21% higher in the case of methanol option and 31% in the case of methane.
Equation 8 yields the exergy potentially avoided representing non-renewable resources and pollution abatement per megajoule of indirect exergy for each alternative (S_{IC}). The value for methanol alternative is 0,85 and for methane alternative is 0,69. So this means it is possible to obtain higher improvement on sustainability in the case of methanol with the same amount of resources.

Table 4 ELCA summary for methane from biowaste alternative.

Concept	Unit	Value
k_F	MJ-Eq/pkm	1,796
k_R	MJ-Eq/pkm	2,449
k_C	MJ-Eq/pkm	4,245
B_{PR}	MJ-Eq/pkm	2,195
k_T	MJ-Eq/pkm	2,050
k_P	MJ-Eq/pkm	0,1838

The two alternatives for the use of fossil oil discussed in the previous section can also be compared with another one not related with transport but with any other service or product, and maybe such alternative will lead to a higher reduction of environmental impact when using the same amount of indirect exergy.

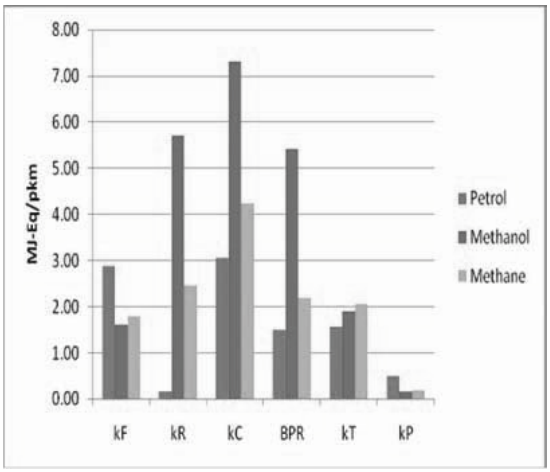

Chart 1: ELCA comparison among petrol, methanol and methane alternatives.

This means that the same resources put on substituting heat from natural gas by heat from wood pellets burning for example would ensure a higher reduction in terms of environmental impact than those assessed alternative concerning transport. Hence, a possible strategy can be that alternatives which will contribute with the highest environmental improvement at the lowest resources cost should be implemented first.
Something to be considered is that this analysis was carried out using a datasets which was obtained on the base of actual statistics and it corresponds to the current Swiss energy transformation matrix. Hence it is a fact that these results are consistent only for small perturbation of the actual Swiss energy matrix. In the case of an intended optimization of the energy transformation system with large perturbation on the system, it will be necessary to elaborate a flexible LCA model to account for influence of the alteration on the whole energy matrix. This complementary analysis would be suitable since major energy matrix perturbations could lead to dissimilar results.
There are other issues to be addressed when the energy matrix is assessed as a whole and the interactions of routes inside it become an important influence. The substitution of products by those byproducts generated on the alternative assessed routes is one of those interactions. This question has been already addressed by the SPA [8]. Another major issue is the influence downstream on a route of other routes and its alternatives, which would lead to a different S_{IC} depending on the sequence of the evaluation of all alternative routes. This fact would bear to an optimization of the substitution strategy to take an energy matrix to the sustainability.

4. Conclusions

The indicator proposed in this paper successfully accomplished the purpose of conserving the advantages of exergy indicators to measure the technosphere metabolism, its simplicity and in addition it successfully embodies three sustainability criteria: exergy efficiency of non-renewable resources, indirect resources cost (part of the economic cost) and the abatement exergy of pollution.

A comparison among alternatives strategies to petrol personal car was carried out. Results showed that substituting petrol driven cars by methanol ones from wood synthetic gas, generates and environmental benefit of 0,85 MJ of exergy in terms of non-renewable natural resources and pollutants abatement, per MJ of cumulative indirect exergy used to drive the alternative. In the case of biogas from biowaste it results in a benefit of 0,69 MJ per MJ of indirect exergy.

Nomenclature

CExC	Cumulative exergy consumption
CExD	Cumulative exergy demand
EI	Environmental impact
ELCA	Exergy life cycle assessment
LCA	Life cycle assessment
LCI	Life cycle impact
LCIA	Life cycle impact assessment
SPA	System perturbation analysis
k	Cumulative exergetic cost
S_{IC}	Sustainability index

Subscripts

F	Nonrenewable
R	Renewable
P	Pollution abatement
I	Cost due to fossil resources and pollution abatement
T	Indirect exergetic cost

References

[1] Szargut, J., 2005, Exergy Method Technical and ecological Applications, Boston: WIT Press, 162.

[2] Cornelissen, R.L. and G.G. Hirs, 2002, The value of the exergetic life cycle assessment besides the LCA, Energy Conversion and Management, **43**(9): p. 1417-1424.

[3] Sciubba, E., 2003, Cost analysis of energy conversion systems via a novel resource-based quantifier, Energy, **28**(5): p. 457-477.

[4] Dewulf, J., et al., 2000, Illustrations towards quantifying the sustainability of technology, Green Chemistry, **2**.

[5] Dewulf, J., et al., 2008, Exergy: its potential and limitations in environmental science and technology, Environmental science & technology, **42**(7): p. 2221-2232.

[6] Ocaña, V.S., 2006, Procedimiento para la valoración de la sostenibilidad energético-ambiental de estrategias energéticas, in *Ingeniería mecánica*, UCLV: Santa Clara.

[7] Wall, G., 2002, Conditions and tools in the design of energy conversion and management systems of a sustainable society, Energy Conversion and Management, **43**: p. 14.

[8] Bram, S., J. De Ruyck, and D. Lavric, 2009, Using biomass: A system perturbation analysis, Applied Energy, **86**(2): p. 194-201.

[9] Böhringer, C., 1998, The synthesis of bottom-up and top-down in energy policy modeling, Energy Economics(20): p. 233-248.

[10] Haurie. MARKAL-LITE An energy environment model to assess urban sustainable development policies. 2002; Available from: http://ecolu-info.unige.ch/recherche/sutra/contributions/markal-lite_02.pdf.

[11] Loken, E., 2007, Use of multicriteria decision analysis methods for energy planning problems, Renewable and Sustainable Energy Reviews, **11**(7): p. 1584-1595.

[12] Lund, H., et al., 2007, Two energy system analysis models: A comparison of methodologies and results, Energy(32): p. 948-954.

[13] Messner, S. and L. Schrattenholzer, 2000, MESSAGE–MACRO: linking an energy supply model with a macroeconomic module and solving it iteratively, Energy(25): p. 267-282.

[14] Pohekar, S.D. and M. Ramachandran, 2004, Application of multi-criteria

decision making to sustainable energy planning-A review, Renewable and Sustainable Energy Reviews, **8**(4): p. 365-381.
[15] Belli., M. and E. Sciubba., 2007, Extended Exergy Accounting as a general method for assessing the primary resource consumption of social and industrial systems, International Journal of Exergy, **4**(4): p. 421 - 440
[16] Chen, G.Q. and Z.H. Qi, 2007, Systems account of societal exergy utilization: China 2003, Ecological Modelling, **208**(2): p. 102-118.
[17] Ness, B., et al., 2007, Categorising tools for sustainability assessment, Ecological Economics, **60**(3): p. 498-508.
[18] Chen, B. and G.Q. Chen, 2007, Modified ecological footprint accounting and analysis based on embodied exergy-a case study of the Chinese society, Ecological Economics, **61**(2): p. 355-376.
[19] Frischknecht, R., et al., 2007, Implementation of Life Cycle Impact Assessment Methods. ecoinvent report No. 3 v2.0, Swiss Center for Life Cycle Inventories: Dubendorf.
[20] Koroneos, C., T. Spachos, and N. Moussiopoulos, 2003, Exergy analysis of renewable energy sources., Renewable Energy(28): p. 295-310.
[21] Cornelissen, R.L., 1997, Thermodynamics and sustainable development. The use of exergy analysis and the reduction of irreversibility., universiteit Twente.
[22] Wall, G. and M. Gongb, 2001, On exergy and sustainable development—Part 1: Conditions and concepts, Exergy, **1**(3): p. 18.
[23] Frischknecht, R. and G. Rebitzer, 2005, The ecoinvent database system: a comprehensive web-based LCA database, Journal of Cleaner Production, **13**(13-14): p. 1337-1343.
[24] Bosch, M.E., et al., 2007, Applying Cumulative Exergy Demand (CExD) Indicators to the ecoinvent Database.
[25] Sciubba, E., S. Bastianoni, and E. Tiezzi, 2008, Exergy and extended exergy accounting of very large complex systems with an application to the province of Siena, Italy, Journal of Environmental Management, **86**(2): p. 372-382.
[26] De Ruyck J., et al., 2006, Liquid Biofuels in Belgium in a global bio-energy context, B.A. Policy, Editor, BSP VUB UCL: Brussels. p. 138.
[27] Gnansounou, E., et al., 2009, Life cycle assessment of biofuels: Energy and greenhouse gas balances, Bioresource Technology, **100**(21): p. 4919-4930.
[28] Spielmann, M., et al., 2007, Transport services. Ecoinvent report No. 14, Swiss Centre for Life Cycle Inventories: Dubendorf.

Acknowledgments: This work was supported by VLIR program through the project: Environmental education and development of clean technologies. And it also results from the collaboration between Vrije Universiteit Brussel and Universidad Central ‘Marta Abreu’ de Las Villas.

Improvement of Airlift Pump Performance Based on the Exergy Analysis

S. Ghanbarzadeh [a,b], P. Hanafizadeh [a,b], P. Gholampour[a], and H. Shams [a],M. H. Saidi [a]

[a] *Multiphase Flow Research Group*
Center of Excellence in Energy Conversion
School of Mechanical Engineering
Sharif University of Technology
Tehran, Iran, P.O.BOX: 11155-9567
[b] *Iranian National Elite Foundation*

Abstract: Airlift systems (ALS) are widely used in various fields such as petroleum and oil extracting industries. As gas-liquid two phase flow is the main part of the flow through these systems, the analysis of such systems accompanies with problems of two phase flow modeling. However, exergy analysis could be a simple method for modeling of airlift systems. In the present study, an analytical model based on thermodynamic principles has been implemented on each phase to analyze the performance of airlift systems. The experimental data were collected at a large scale multiphase flow test rig for the airlift pump with 6m height and diameter of 50 mm. Finally, irreversibility terms, energy destruction, flow availability and entropy generation were estimated by this method.

Keywords: Airlift system, Multiphase Flow, Exergy Analysis, Entropy Generation, Availability

1. Introduction

Airlift pump systems have a vertical pipe which compressed air is injected at the bottom of it. These pipes have a head of liquid or mixture of liquid and solid that is desired to be pumped. The injected air constructs a set of bubbles in vertical pipe which transfer the liquid or solid media to the upper level aiding buoyancy effect. Airlift Pump is a unique technology due to its simple structure, but it has some weak points like weak suction and unstable flow rate. This pump has a low efficiency in comparison with ordinary pumping systems. The possibility of using air lift pumps in special applications like pumping corrosive, abrasive, radioactive and chemical fluids is a great advantage of these pumps. Since no moving parts exist in this kind of pump, no lubrication would be needed. Therefore, the maintenance of these pumps is very simple and the operating costs are low. Due to simplicity of construction, reliability and low maintenance costs of airlift pumps, these systems are widely used in the mines, oil industries, bioreactors and nuclear power plants. Most studies on airlift pumps are concerned with its applications.

Airlift pump was invented by German mining engineer, Carl Loescher, in 1797 [1]. Developing the performance of these pumps has remained a great interest of researchers up to now. Various analyses are found in the literature, which have tried to simulate the behaviour of airlift pumps. Kato et al. [2] studied an airlift pump experimentally for solid particles and proposed a model based on the momentum equation. Parker et al. [3] used an airlift pump for aerating warm water ponds. Apazidis [4] considered influence of bubble expansion on the performance and stability of an airlift pump. Wicomb et al. [5] used an airlift system for perfusion storage of the isolated heart. Parker and Suttle [6] designed an airlift system for aquaculture applications. Chisti [7] derived the theoretical equations for airlift loop reactors which described the relation between superficial gas velocity and liquid circulation velocity. Reinemann et al. [8] experimentally considered the effect of tube diameter on the performance of 3-25 mm airlift pumps. Zenz [9] used various correlations to simulate airlift pumps. De Chachard and Delhaye [10] proposed a model to predict pressure gradient for slug flow in the airlift pump. Margaris and Papanikas [11] introduced a pseudo liquid which is formed by liquid and solid phase for analyzing a three phase flow airlift pump. Nenes et al. [12] simulated an airlift pump numerically for deep water well. A linear stability method was proposed by de Cachard and Delhaye [13] to consider the stability of small diameter airlift pumps. White [14] considered application of airlift pumps in the absorption refrigeration cycles. Kumar et al. [15] considered augmentation of airlift pumps performance with tapered

pipe experimentally. Abed [16] used a mathematical model to find operational criteria for performance of airlift pumps. The performance of a small airlift system used for transporting Alumina particles of 3 mm diameter was experimentally investigated by Fujimoto et al. [17]. Samaras and Margaris [18] found a new flow regime map which is appropriate for airlift pump performance and regime transition. Kassab et al. [19] developed a theoretical model based on the control volume approach to predict airlift pump performance in three phase flow. Darbandi et al. [20] developed a numerical approach to simulate two phase flow in the airlift pumps. Kassab et al. [21] evaluated the performance of a pump experimentally and introduced a theoretical model to optimize the operating parameters of the pump. Most of the work mentioned above analyzed the ALS regarding the nature of two phase flow and its governing equations. No previous publication has been found on exergy analyses of ALS, but there are various research works which have been noticed in the literature about exergy analysis of other systems like vortex tube systems [22] (Saidi and Yazdi 1999), PEFC fuel cell systems [23, 24] (Saidi et al. 2005 and Delsman et al. 2006) and magneto hydrodynamic (MHD) plasma generators [25] (Saidi and Montazeri 2007).

Considering the mixing process of two phases and energy dissipation during the procedure in the airlift pump riser pipe due to friction between the phases, a method considering this loss, could be useful to find an optimum efficiency in the ALS. Various parameters such as: inlet gas pressure, inlet mass fraction and diameter of gas injection device, are effective in mixing of phases and as a result they would affect pump performance. Therefore, in this paper a novel approach based on exergy analysis has been developed to consider the effect of energy dissipating parameters on the behavior of airlift pumps. Considering second law of thermodynamics, the entropy generation, availability and performance of the pump were achieved. Also this model was used to optimize efficiency of airlift pump regarding the performance parameters**.**

2. Experimental setup

The experiments in this study were carried out in large scale two phase flow test rig at the school of mechanical engineering, Sharif University of Technology. The experimental apparatus is shown schematically in Fig. 1. The air and purified water are used as the gas and liquid phases in all the experiments. Water supply is a tank with an adjustable head. Water flow rate is measured by calibrated magnetic flow meter [Siemens MAG5100] with an accuracy of ±0.5%. The compressed air has been continuously fed by the compressor [Atlas-Copco GA210] up to 6 bar continuously. The air flow rates have been set and filtered by the Wilkerson filter and regulator and measured by calibrated Gas Turbine flow meter [Omega-FTB934] with an accuracy of ±1%. Air and water would be mixed together in the plenum made of acrylic glass and placed at the bottom of the riser pipe. Compressed air is injected into the plenum by the porous stainless steel plate with 108 holes of 0.5 mm diameter. The overall height and inside diameter of the riser pipe are 6m and 50 mm, respectively. In order to be capable of visual observation of the two phase flow patterns, the riser pipe has been chosen from transparent acrylic glass. Air and water flow upward through the riser and would be separated in the separation tank above the riser.

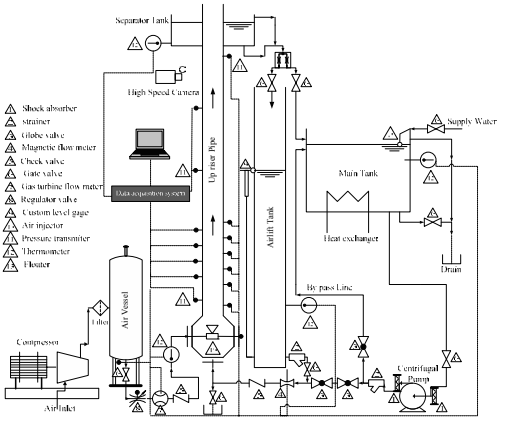

Fig.1. Schematic of two phase flow test rig

Air is discharged to atmosphere and water returns to main tank or to airlift tank, depending on test application, and then it would be circulated in the loop. Applying several combinations of submergence ratios, level of water in the airlift tank can be changed. In this system work both done and lost, therefore water temperature may be changed during different processes and pumping cycle, although these changes are very small but in our approach using exergy analysis these changes play an important role. Accurate, fast response and calibrated thermocouples were installed in test loop with accuracy of 0.1^{o}C and their locations are visible in Fig.1. 16 transmitters [Indumart, PTF106] with an accuracy of 0.3% full scale were installed at different positions along the riser pipe to measure the pressure. All the above instruments have a special kind of signal;

these signals are scaled and fed for a rapid and wide band data acquisition card [National Instrument, PCI-6255]. Recorded data are stored for further post processing. A high speed digital camcorder [Casio, F1] of 1200 fps at a height of 5m on the riser is responsible for Visualization, flow regime identification and flow recording.

3. Method of Analyzing

In this paper exergy method has been chosen to analyze the behavior of the airlift pump. So, the riser pipe has been considered as a control volume, and then first and second laws of thermodynamic have been implemented on it. Fig. 2 illustrates schematic of control volume. The first law of thermodynamic for control volume can be written in the following form

$$\dot{Q}_{C.V} + \sum \dot{m}_i \left(h_i + \frac{V_i^2}{2} + gZ_i \right) = \frac{dE_{C.V}}{dt} + \sum \dot{m}_e \left(h_e + \frac{V_e^2}{2} + gZ_e \right) + \dot{W}_{C.V} \quad (1)$$

Considering adiabatic steady state flow with no interchange of heat and work in the control volume and neglecting variation of kinematic energy, the eq.1 can be simplified as

$$\sum \dot{m}_i (h_i + gZ_i) = \sum \dot{m}_e (h_e + gZ_e) \quad (2)$$

Implementing this equation for assumed control volume results in

$$\dot{m}_{a\_in}(h_{a\_in} + gZ_{a\_in}) + \dot{m}_{w\_in}h_{w\_in} = \dot{m}_{a\_out}(h_{a\_out} + gZ_{a\_out}) + \dot{m}_{w\_out}(h_{w\_out} + gZ_{w\_out}) \quad (3)$$

Considering air as an ideal gas with constant specific heat, assuming equal temperature for air and water at outlet and dividing equation 3 by water mass flow rate, gives

$$C_{p\_a}y(T_{a\_in} - T_{a\_out}) + yg(Z_{a\_in} - Z_{a\_out}) = C_w(T_{w\_out} - T_{w\_in}) + gZ_{w\_out} \quad (4)$$

The second law of thermodynamic for control volume can be written as

$$\frac{dS_{C.V}}{dt} + \sum \dot{m}_e s_e - \sum \dot{m}_i s_i = \int_0^t \frac{\dot{Q}_{C.V}}{T} dt + \dot{S}_{gen} \quad (5)$$

In the absence of heat transfer in control volume and assuming steady state conditions, this equation reduces to

$$\sum \dot{m}_e s_e - \sum \dot{m}_i s_i = \dot{S}_{gen} \quad (6)$$

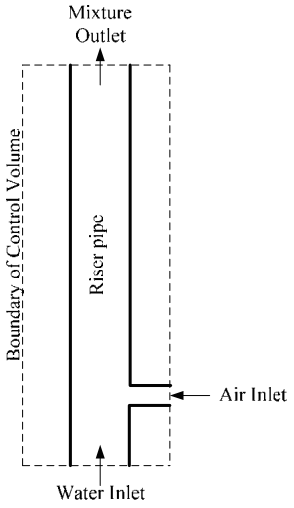

Fig.2. Schematic of control volume

Implementing this formula for ALS's riser pipe and rearranging, gives

$$\dot{S}_{gen} = \dot{m}_a(s_{a\_out} - s_{a\_in}) + \dot{m}_w(s_{w\_out} - s_{w\_in}) \quad (7)$$

Assuming air as an ideal gas with constant specific heat, it follows that

$$\dot{S}_{gen} = \dot{m}_a \left(C_{p\_a} ln \frac{T_{a\_out}}{T_{a\_in}} - Rln \frac{P_{a\_out}}{p_{a\_in}} \right) + \dot{m}_w C_w ln \frac{T_{w\_out}}{T_{w\_in}} \quad (8)$$

The entropy generation could be found from equation 8 if temperature of the outlet phases is known. We can find the outlet temperature from the equation 4. Also the irreversibility can be related to the change in the availability as

$$\dot{I}_{C.V} = \left(\sum \dot{m}_i \Psi_i - \sum \dot{m}_e \Psi_e \right) + \sum \left(1 - \frac{T_0}{T_j} \right) \dot{Q}_{C.V,j} - \dot{W}_{C.V}^{ac} \quad (9)$$

In the absence of heat transfer and actual work the rate of irreversibility is seen to be equal to the rate of destruction of availability which is also proportional to the entropy generation.

$$\dot{I}_{C.V} = \left(\sum \dot{m}_i \Psi_i - \sum \dot{m}_e \Psi_e \right) = T_0 \dot{S}_{gen\_C.V} \quad (10)$$

where, applying the definition of exergy or flow availability,

$$\psi = (h - T_0 s + gZ) - (h_0 - T_0 s_0 + gZ_0) \quad (11)$$

Equation 10 can be written for up-riser of airlift as below

$$\dot{I}_{C.V} = \left(\dot{m}_{a\_in}\Psi_{a\_in} + \dot{m}_{w\_in}\Psi_{w\_in}\right) - \left(\dot{m}_{a\_out}\Psi_{a\_out} + \dot{m}_{w\_out}\Psi_{w\_out}\right) \quad (12)$$

The exergy of inlet air can be defined as

$$\psi_{a\_in} = \left(h_{a\_in} - h_{a\_0}\right) - T_0\left(s_{a\_in} - s_{a\_0}\right) + g\left(Z_{a\_in} - Z_0\right) \quad (13)$$

It would be noticed that using assumption of constant specific heat and ideal gas for air transform equation 13 to

$$\psi_{a\_in} = C_{p\_a}\left(T_{a\_in} - T_0\right) - T_0\left(C_{p\_a} ln\frac{T_{a\_in}}{T_0} - Rln\frac{P_{a\_in}}{p_0}\right) + g\left(Z_{a\_in} - Z_0\right) \quad (14)$$

utilizing equation 11 and assuming constant specific heat for inlet water, we have

$$\psi_{w\_in} = C_w\left(T_{w\_in} - T_0\right) - T_0\left(C_w ln\frac{T_{w\_in}}{T_0}\right) + g\left(Z_{w\_in} - Z_0\right) \quad (15)$$

As $P_{out} = P_{atm} = P_0$ then term of $ln\frac{P_{a\_out}}{p_0}$ in the exergy of outlet air will be zero. Consequently, the exergy of air at the exit would be given by

$$\psi_{a\_out} = C_{p\_a}\left(T_{a\_out} - T_0\right) - T_0\left(C_{p\_a} ln\frac{T_{a\_out}}{T_0}\right) + g\left(Z_{a\_out} - Z_0\right) \quad (16)$$

Similarly, the exergy of outlet water can be expressed as

$$\psi_{w\_out} = C_w\left(T_{w\_out} - T_0\right) - T_0\left(C_w ln\frac{T_{w\_out}}{T_0}\right) + g\left(Z_{w\_out} - Z_0\right) \quad (17)$$

3.1. Efficiency

For the device which does not involve the input our output work, like airlift up-riser pipe, the second law efficiency is defined in term of ratio of input to output availability. Thus, for this case from the second law efficiency definition, we can state the efficiency of airlift as

$$\eta_{2nd\ law} = \frac{\dot{m}_{a\_out}\psi_{a\_out} + \dot{m}_{w\_out}\psi_{w\_out}}{\dot{m}_{a\_in}\psi_{a\_in} + \dot{m}_{w\_in}\psi_{w\_in}} \quad (19)$$

But this kind of efficiency is typically defines for devices which include heat transfer between the inlet and outlet flows. Therefore, it seems that the second law efficiency is not appropriate for remarking the state of efficiency for ALS. Since the main goal in airlift pump is related to the outlet water mass flow rate and the main source of energy is in the inlet air mass flow rate, combining the first and second law efficiency can lead us to define a new efficiency for airlift systems. In this study we have defined the efficiency of ALS as

$$\eta_{airlift} = \frac{\dot{m}_w(\psi_{w_{out}} - \psi_{w_{in}})}{\dot{m}_{a\_in}\psi_{a\_in}} \quad (20)$$

In some literature, efficiency of ALS is described as the ratio of outlet water flow rate to the inlet air flow rate. This efficiency is defined as

$$\eta_{old} = \frac{\dot{m}_{w\_out}}{\dot{m}_{a\_in}} \quad (21)$$

The main disadvantage of such a definition is that efficiency is not between 0 and 1, but the new definition of efficiency for an ALS is in the range mentioned.

4. Result and Discussion

The main flow regimes identified in the gas–liquid vertical upward pipe are bubble, slug, churn, annular and mist flow [26]. In the bubbly flow the gas phase is distributed as bubbles in the continuous liquid phase. Increase of gas phase cause the coalescence of bubbles and the slug flow forms in the pipe. The slugs are approximately in size of the diameter of the pipe with the round heads. The large bubble in the slug flow break down and churn flow is constructed. The churn flow is the oscillatory regime which varies with time. Having more increase in gas rate, annular flow appears. In the annular flow the continuous gas phase exists at the centre of the pipe and the liquid films are formed at the pipe wall. The annular flow in which the gas phase is accompanied by the separate tiny droplets would be called mist. In the airlift system the bubbly flow regime cannot lift the water perfectly due to the low buoyant force exerted by the air bubbles. The main flow regimes which are detected by flow visualization with high speed camcorder (1200 fps) in the ALS are slug, churn and annular which are shown in Fig. 3.

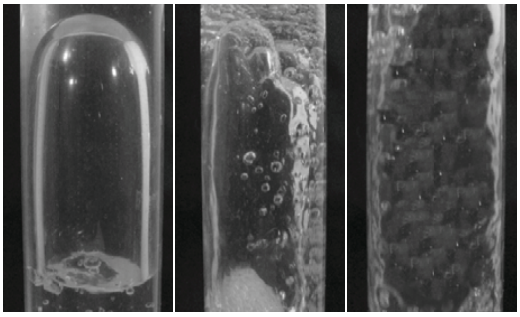

slug churn annular

Fig.3. Picture of three main flow regimes which are detected in the airlift pump

Fig. 4 shows the efficiency of airlift pump which is defined by the equation 20, in terms of injected air flow rate for different submergence ratios of 0.34, 0.42, 0.5, 0.58 and 0.67. As noticed in this figure, two major trends exist for efficiency of the pump. High submergence ratios have a descending procedure and low submergence ratios have ascending and descending trend. The reason can be described by two phase flow patterns related to these submergence ratios. The start point of the submergence ratio of 0.58 and 0.67 are in the region of slug flow pattern and the start points of other low submergence ratios are located in the region of churn flow. Thus, it can be conclude that the best flow pattern for the airlift pump is the slug flow regime. Moreover, Fig. 4 shows that the increase of submergence ratio increases the efficiency of the ALS. This concept is completely in accordance with the physics of the problem, because in high submergence ratios the amount of augmentation of water is lower and consequently less power is needed for lift water.

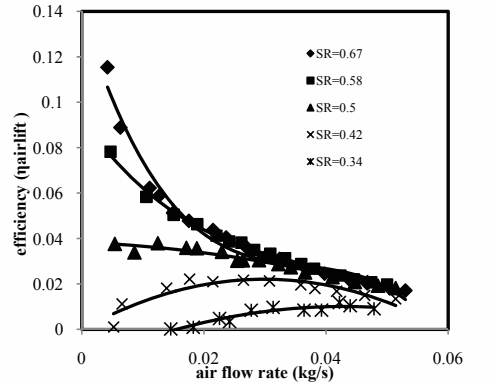

Fig.4. Efficiency of airlift pump in terms of air flow rate for different submergence ratio

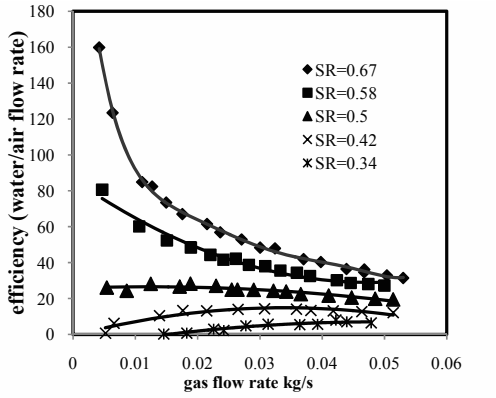

Fig.5. Old definition of efficiency for airlift pump in terms of air flow rate for different submergence ratio

Fig. 5 illustrates the efficiency of ALS which is used in the most literature. The comparison between Fig. 4 and Fig. 5 shows that the overall behaviours of curves in both figures have the same form. Two major trends which are impressed in Fig. 4 are repeated in Fig. 5. The main blind spot of the old efficiency is the range of it. It shown in Fig. 5 the quantity of efficiency crosses 100, which is in contradiction with the concept of efficiency. Fig. 6 depicts the second law efficiency of the airlift pump defined by the equation 19 in terms of injected air flow rate. As expected, this efficiency cannot exactly predict the behaviour of the pump. The facts observed in Fig. 6 are the same as Fig. 4 and Fig. 5. Again in this figure, lower submergence ratios have lower efficiency.

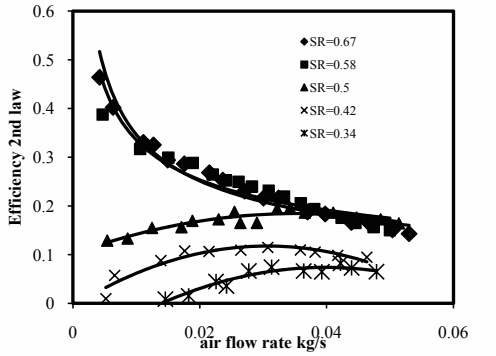

Fig.6. Second law efficiency of airlift pump in terms of air flow rate for different submergence ratios

Fig. 7 depicts entropy generation in terms of air inlet pressure. These results are for different submergence ratios of 0.25 to 0.75.

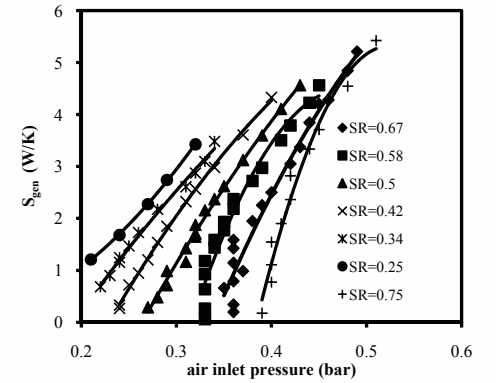

Fig.7. Entropy generation in airlift pump in terms of air inlet pressure for different submergence ratios

It is obviously seen that for constant submergence ratios, enhancing inlet pressure, increases the rate of entropy generation in pump. As seen in the figure, slips

of curves are very high and therefore the entropy generated in the ALS is completely dependent on the injected air pressure. Since the entropy generation has reverse relation to the efficiency, in the constant submergence ratios, pumps are preferred to work in the minimum possible pressure. Variation of airlift pump entropy generation in terms of level of water submerged in the up-riser pipe is shown in Fig. 8. As it can be seen, entropy generation reduces with increase in submergence ratio. As a result, it will be prospected that the pump working in the high submergence ratio enjoys higher efficiency. This conclusion is indicated in the efficiency diagram (Fig. 4).

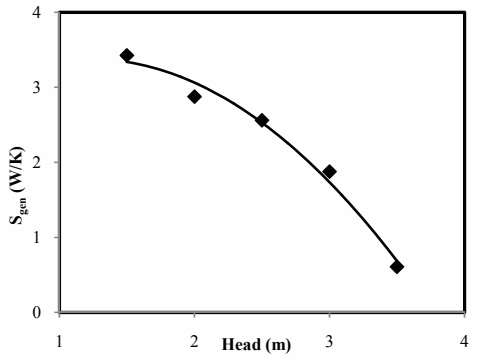

Fig.8. Entropy generation in airlift pump in terms of water head

The airlift entropy generation is demonstrated in terms of injected air flow rate and two phase flow regimes in Fig. 9. As shown in Fig. 9-a, increase in air flow rate enhances the generated entropy.

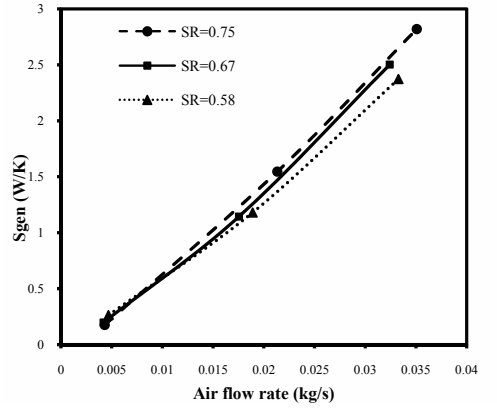

(a) entropy generation in terms of air flow rate for different submergence ratios

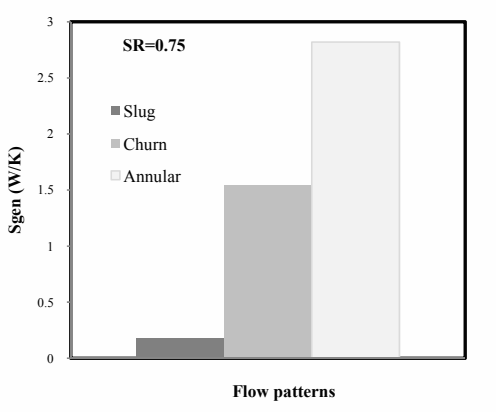

(b) entropy generation in different flow patterns for submergence ratio of 0.75

Fig.9. Entropy generation for different flow patterns, a) entropy generation in terms of air flow rate b) submergence ratio of 0.75

Fig. 9- b shows that the minimum entropy generation happens in the slug flow regime. It can be concluded then that the best suitable flow regime for function of the ALS from the viewpoint of entropy generation, is slug flow regime. The least entropy generation in slug flow regime can be attributed to the fact that the mixing of two phases in this regime is less than the churn and annular flow regimes; hence, the pump has the lowest entropy generation and thus will contain the highest efficiency.

5. Error analysis

In the experimental work in order to have meaningful conclusion from the data it is important to analyze data. To do this, it is vital to understand that all measurements are subject to the uncertainties. The main part of the experimental procedure is the error analysis and for valid conclusion the error of measured quantities must be indicated. The uncertainty of the variable F, which is a function of n independent variable X_i (experimentally measured data), is calculated by

$$U_F^2 = \left(\frac{\partial F}{\partial X_1}\right)^2 U_{X_1}^2 + \left(\frac{\partial F}{\partial X_2}\right)^2 U_{X_2}^2 + \cdots + \left(\frac{\partial F}{\partial X_n}\right)^2 U_{X_n}^2 \quad (22)$$

$$F = fun(X_1, X_2, \ldots, X_n)$$

where, U_{X_i} is uncertainty of measured variable X_i. On the other hand, it is the accuracy of means used to measure X_i. In the above equation, the variable X_i is an independent variable and also the uncertainties of

variable are independent of each other. The Eq. 22 can be summarized as

$$U_F^2 = \sum_1^n \theta_i^2 U_{X_i}^2 \quad (23)$$

where, θ_i is defined by the partial derivation of F as a sensibility factor. The main parameters considered in this paper are efficiency and entropy generation. These two parameters are functions of following measured variables

$$\eta_{airlift} = fun(\dot{m}_a, \dot{m}_w, \psi_{a\_in}, \psi_{w\_in}, \psi_{w\_out}) \quad (24)$$

$$\dot{S}_{gen} = fun(\dot{m}_a, \dot{m}_w, T_{a\_in}, T_{w\_in}, T_{out}, P_{a\_in}) \quad (25)$$

where, $\dot{m}_a$ was measured by turbine flow meter with accuracy of 1%, $\dot{m}_w$ was measured by magnetic flow meter with accuracy of 0.5%, all temperatures were measured by thermocouple with accuracy of 0.1 ^{o} C and the pressure transmitter with accuracy of 0.3% were used to measure pressure. T_{out} is calculated from Eq. 4, so the amount of its uncertainty must be calculated before being used in the Eq. 24. It can be easily seen from Eq. 4 that the outlet temperature is a function of the variables below

$$T_{out} = fun(\dot{m}_a, \dot{m}_w, T_{a\_in}, T_{w\_in}, T_{out}, P_{a\_in}) \quad (26)$$

The uncertainties of measured and calculated variables are summarized in Table 1. The derivative and their values for three main flow regimes in the airlift pump (slug, churn and annular) are summarized in Tables 2-4 in the appendix.

Table 1 uncertainty of variables

Quantity	Amount of uncertainty	Approximate error
Efficiency	±0.02	20%
Flow availability (gas and water)	±0.82 and 5.05	0.05% and0.5%
Rate of entropy generation	±0.24	10%

6. Conclusion

An exergy analysis was used for considering the effect of some parameters on the performance of the airlift systems. The experimental data for this purpose were collected from the airlift with diameter of 50 mm and length of 6 m. The results were used to investigate both the entropy generation and efficiency in the ALS. It was observed that the flow regime in the up-riser pipe has the main role in the efficiency of the pump and it was concluded that the best flow regime for airlift pump is the slug flow regime. It was also seen that, the lower entropy generation happened in the lower inlet air pressure and flow rate. In addition, it was demonstrated that using high submergence ratio decrease the entropy generation and hence increases the efficiency of the ALS.

Reference

[1] Castro, W.E., Zielinski, P.B., and Sandifer, P.B., 1975, Performance characteristics of airlift pumps, World Mari Culture Society Meeting, 6, pp. 451-460.

[2] Kato, H., Miyazawa, T., Tiyama, S., and Iwasaki, T., 1975, A study of an air-lift pump for solid particles, Bull. JSME, 18-(117), pp. 286–294.

[3] Parker, N.C., Suttle, M.A., and Fitzmayer K., 1984, Total gas pressure and oxygen and nitrogen saturation in warm water ponds aerated with airlift pumps. Aquacultural Engineering, 3, pp.91-102.

[4] Apazidis N., 1985, Influence of bubble expansion and relative velocity on the performance and stability of an airlift pump. Int. J. Multiphase Flow, 11, pp. 459-479.

[5] Wicomb, W.N., Cooper, D.K., and Novitzky, D., 1985, An airlift pump device for low pressure perfusion storage of the isolated heart. Cryobiology; 22(5), pp. 401-408.

[6] Parker, N.C., and Suttle, M.A., 1987, Design of airlift pumps for water circulation and aeration in aquaculture. Aquacultural Engineering, 6, pp. 97-110.

[7] Chisti, M. Y., 1989, Airlift bioreactors. London: Elsevier Applied Science.

[8] Reinemann, D. J., and Parlange, J. Y., 1990, Timmons M. B. Theory of small diameter airlift pumps. Int. J. Multiphase Flow, 16 (1), pp. 113-122.

[9] Zenz, F.A., 1993, Explore the potential of air-lift pumps and multiphase systems. Chem. Eng. Prog., 89(8), p. 51.

[10] De Cachard, F., and Delhaye, J. M., 1996, A slug-churn model for small-diameter airlift pumps. Int. J. Multiphase Flow, 22 (4), pp. 627-649.

[11] Margaris, D.P., and Papanikas, D.G., 1997, A generalized gas-liquid-solid three-phase flow analysis for airlift pump design. Journal of Fluids Engineering; 119, pp. 995-1002.

[12] Nenes, A., Assimacopoulos, D., Markatos, N., and Mitsoulis E., 1997, Simulation of airlift pumps for

deep water wells. Int. J. Multiphase Flow, 23 (7), p. 58.

[13] De Cachard, F., and Delhaye, J. M., 1998, Stability of small diameter of airlift pumps, Int. J. Multiphase Flow, 24 (1), pp. 17-34.

[14] White, S.J., 2001, Bubble design and performance, Georgia Institute of Technology.

[15] Kumar, E.A., Kumar, K.R.V., and Ramayya A.V., 2003, Augmentation of airlift pump performance with Tapered upriser pipe- an experimental study. IE (I) Journal-MC; 84, pp. 114-119.

[16] Abed, K.A., 2003, Operational criteria of performance of Airlift Pumps. IE (I) Journal-MC; 84, pp. 1-6.

[17] Fujimoto, H., Nagatani, T., and Takuda, H., 2005, Performance characteristics of a gas–liquid–solid airlift pump. Int. J. Multiphase Flow, 31, pp. 1116-1133.

[18] Samaras, V.C., and Margaris, D.P., 2005, Two-phase flow regime map for air-lift pump vertical upward gas–liquid flow. International Journal of Multiphase flow; 31, pp. 757–766.

[19] Kassab, S.Z., Kandil, H.A., Warda, H.A., and Ahmedb, W.H., 2007, Experimental and analytical investigations of airlift pumps operating in three-phase flow. Chemical Engineering Journal, 131, pp. 273–281.

[20] Darbandi, M., Saidi, M. H., Hanafizadeh P., 2007. A numerical approach to simulate two-phase flow in airlift pumps. The international conference on computational methods, ICMM2007, Hiroshima, Japan.

[21] Kassab, S. Z., Kandil, H. A., Warda, H. A., and Ahmed, W. H., 2009, Air-lift pumps characteristics under two-phase flow conditions. Int. J. Heat and Fluid Flow, 30, pp. 88-98.

[22] Saidi, M.H., Allaf Yazdi, M.R., 1999, Exergy model of a vortex tube system with experimental results. Energy; 24, pp. 625–632.

[23] Saidi, M.H., Ehyaei, M.A., and Abbasi, A., 2005, Optimization of a combined heat and power PEFC by exergy analysis. Journal of Power Sources; 143, pp. 179–184.

[24] Delsman, E.R., Uju, C.U., Croon, M.H.J.M. de, Schouten, J.C., Ptasinski, K.J., 2006, Exergy analysis of an integrated fuel processor and fuel cell (FP-FC) system. Energy; 31(15), pp. 3300-3309.

[25] Saidi, M.H., and Montazeri, A., 2007, Second law analysis of a magneto hydrodynamic plasma generator. Energy, 32, pp. 1603–1616.

[26] Taitel, Y., Barnea, D., Dukler, A.E., 1980, Modeling flow pattern transitions for steady upward gas–liquid flow in vertical tubes. AIChE J., 26, pp. 345–354.

Acknowledgment

This research was funded by Iran Supplying Petrochemical Industries Parts, Equipment and Chemical Design Corporation (SPEC) as a joint research project with Sharif University of Technology (project no. KPR-8628077). The contribution is greatly appreciated.

Appendix

In this part, partial detail of error analysis is presented. As we know, in two phase flows, flow properties strongly relate to flow pattern; therefore, error analyses were done for three main flow regimes and the significant difference is obvious. The average of errors in three different patterns was calculated and considered as the amount of final error.

Table 2 example of error analysis for entropy generation in three flow regimes

	$\frac{\partial \dot{S}_{gen}}{\partial \dot{m}_a}$	$\frac{\partial \dot{S}_{gen}}{\partial \dot{m}_w}$	$\frac{\partial \dot{S}_{gen}}{\partial T_{a\_in}}$	$\frac{\partial \dot{S}_{gen}}{\partial T_{w\_in}}$	$\frac{\partial \dot{S}_{gen}}{\partial T_{out}}$	$\frac{\partial \dot{S}_{gen}}{\partial p_{a\_in}}$	$\sum_1^n \theta_i^2 U_{\bar{x}_i}^2$	Error amount
Slug	96.17	-18.10	-0.0014	-1.36	1.36	3.17	0.011	0.10
Churn	96.90	-23.67	-0.0071	-2.14	2.15	15.30	0.071	0.27
Annular	105.30	-22.25	-0.012	-2.57	2.58	23.97	0.13	0.36
Average							0.071	0.24

Table 3 example of error analysis for flow availability in three flow regimes

		$\frac{\partial \psi_{a\_in}}{\partial T_{a\_in}}$	$\frac{\partial \psi_{a\_in}}{\partial p_{a\_in}}$	$\frac{\partial \psi_{a\_in}}{\partial Z_{a\_in}}$	$\frac{\partial \psi_{w\_in}}{\partial T_{w\_in}}$	$\frac{\partial \psi_{w\_in}}{\partial Z_{w\_in}}$	$\frac{\partial \psi_{a\_out}}{\partial T_{out}}$	$\frac{\partial \psi_{a\_out}}{\partial Z_{a\_out}}$	$\frac{\partial \psi_{w\_out}}{\partial T_{out}}$	$\frac{\partial \psi_{w\_out}}{\partial Z_{w\_out}}$
Slug		7.99	2.19	-9.81	58.34	-9.81	9.63	-9.81	40.46	-9.81
Churn		6.66	2.14	-9.81	61.08	-9.81	8.97	-9.81	37.70	-9.81
Annular		5.34	2.04	-9.81	63.81	-9.81	9.96	-9.81	41.84	-9.81
$\sum_{1}^{n} \theta_i^2 U_{X_i}^2$	**Slug**	0.65			34.05		0.94		16.38	
	Churn	0.45			37.32		0.82		14.22	
	Annular	0.30			40.73		1.02		17.52	
Average amount of error		0.67			6.11		0.96		4.00	

Table 4 example of error analysis for efficiency of airlift pump in three flow regimes

	$\frac{\partial \eta_{airlift}}{\partial \dot{m}_a}$	$\frac{\partial \eta_{airlift}}{\partial \dot{m}_w}$	$\frac{\partial \eta_{airlift}}{\partial \psi_{a\_in}}$	$\frac{\partial \eta_{airlift}}{\partial \psi_{w\_in}}$	$\frac{\partial \eta_{airlift}}{\partial \psi_{w\_out}}$	$\sum_{1}^{n} \theta_i^2 U_{X_i}^2$	Error amount
Slug	-903.26	4.00	-1.51e-4	-8.72e-4	8.72e-4	1.9e-3	0.044
Churn	-53.47	0.73	-4.76e-5	-3.02e-4	3.02e-4	1.6e-4	0.013
Annular	-10.41	0.20	-1.66e-5	-2.4e-4	2.4e-4	1.9e-5	0.004
average						6.9e-4	0.020

Entropy generation and local exergy losses in steady state and transient heat conduction processes

Zygmunt Kolenda [a], Jacek Latkowski [b] and Adam Holda [a]

[a] *AGH-University of Science and Technology, Krakow, Poland*
[b] *Department of Mathematics, The British School, Warsaw, Poland*

Abstract: On the basis of minimum entropy generation and minimum of exergy losses, new formulation of the boundary and initial-boundary value problems of heat conduction with the first kind boundary conditions are proposed. Two independent approaches are presented, first as the Euler-Lagrange variational formulation and second on classical minimization procedure. It is shown that entropy generation and local exergy losses minimization are always possible by introducing additional heat sources.

Key Words: entropy generation, exergy losses, minimization

1. Introduction

The problem of entropy generation minimization has been engaging a good deal of attention during last decades. The problem is also known in literature as thermodynamic optimization and was formulated for the first time by Bejan [1]. The measure of energy dissipation in irreversible processes, according to the Second Law of Thermodynamics, is the increase of entropy production. Gouy-Stodola's theorem states that destroyed exergy is directly proportional to the entropy production and the amount of entropy production is the measure of degree of irreversibility in the system [2, 4]. The core of entropy production minimization centers on searching for methods of conducting the process, so with the known constraints and boundary conditions, entropy production and exergy losses are minimized. Analytical solution of the linear boundary and initial-boundary problems are presented. To simplify mathematical considerations, linear and 1-D problems will be analysed.

2. Problem Formulation

2.1. Boundary value problems

According to the thermodynamics of irreversible processes [4], entropy generation at steady state is at minimum. Introducing expression for local entropy generation

$$\dot{S}_{gen} = \dot{S}_{gen}(T, T_{x_i}) = \frac{d_i s}{d\tau} = \frac{k(T)}{T^2}\left(grad\, T\right)^2 \quad (1)$$

where $T=T(x_i)$ and T_{x_i} denotes gradient components $\partial T / \partial x_i$, the problem can be formulated in the following way: find such a function $T=T(x_i)$ *which while satisfying boundary conditions minimizes simultaneously integral*

$$\dot{S}_{gen,t} = \int_{\Omega} \dot{S}_{gen}(T, T_{x_i}) d\Omega \quad (2)$$

over the whole domain Ω. Here, $\dot{S}_{gen}$ represents global entropy production of the process. Using variational calculus, this special function T_{x_i} for which $\dot{S}_{gen}$ reaches minimum, satisfies the Euler equation [4]

$$\frac{\partial \dot{S}_{gen}}{\partial T} - \sum_i \frac{\partial}{\partial x_i}\left(\frac{\partial \dot{S}_{gen}}{\partial T_{x_i}}\right) = 0 \quad (3)$$

Consider one dimensional (1 D) problem of heat conduction in plane wall with first kind boundary conditions shown in Figure 1.
Local entropy generation is $\sigma(T, T_{x_i}) = \frac{k}{T^2(x)}\left(\frac{dT(x)}{dx}\right)^2$ and its global value to be minimizes is given by integral

Corresponding Author: Zygmunt Kolenda, Email: kolenda@agh.edu.pl

$$\dot{S}_{gen,t} = \int_0^1 \frac{k(T)}{T^2(x)} \left(\frac{dT(x)}{dx} \right)^2 A\,dx \qquad (4)$$

where A is unit surface area perpendicular to the heat flux vector (A – $1m^2$). This fact should be taken into consideration in the dimensions of consecutive equations.

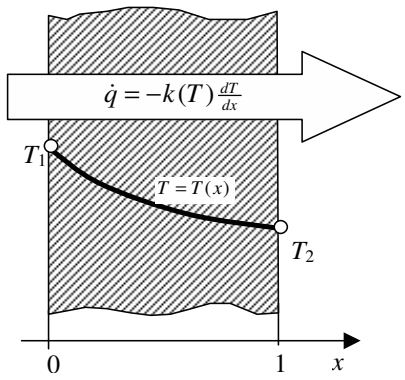

Boundary Conditions:

$x = 0$ $T(0)=T_1$
$x = 1$ $T(1)=T_2$

Fig. 1. Heat conduction through a plane-wall.

Assuming k is constant, (3) becomes in the final form

$$\frac{d^2T}{dx^2} - \frac{1}{T}\left(\frac{dT}{dx} \right)^2 = 0 \qquad (5)$$

and is different from Laplace heat conduction equation

$$\frac{d^2T}{dx^2} = 0$$

For boundary conditions of the first kind, $T(0) = T_1$ and $T(1) = T_2$, solution to (5) is

$$T(x) = T_1 \left(\frac{T_2}{T_1} \right)^x \qquad (6)$$

Using (6), it is easy to show that the law of energy conservation in classical form is not satisfied as $div\,\dot{q}(x) \neq 0$. Further calculations lead to the next confusing result that

$$div\left(\frac{\dot{q}(x)}{T(x)} \right) = div(\dot{s}) = 0$$

Explanation comes directly from (5). Interpreting its second term as the additional internal hear source

$$\dot{q}_v(x) = -\frac{k}{T}\left(\frac{dT}{dx} \right)^2 < 0 \qquad (7)$$

it is easy to prove that the first law of thermodynamics is satisfied and entropy increase of the whole process is positive and equal to

$$\dot{S}_{gen,t} = -\int_0^1 \frac{\dot{q}_v(x)}{T(x)} dx = k\left(\ln \frac{T_2}{T_1} \right)^2 > 0$$

The same result has been obtained by Bejan [1] using a different mathematical approach. Also, the same results come from entropy balance equation

$$\dot{S}_{gen}(x) + \dot{S}_v = \frac{d}{dx}\left(\frac{\dot{q}(x)}{T(x)} \right) \qquad (8)$$

where $\dot{S}_v$ represents internal entropy generation rate as the result of internal heat source. Equation (8) takes explicit form (k-constant)

$$\dot{S}_{gen}(x) + \dot{S}_v = \frac{k}{T^2}\left(\frac{dT}{dx} \right)^2 - \frac{k}{T}\frac{d^2T}{dx^2} \qquad (9)$$

Introducing equation (7) derived from previous variational principle

$$\dot{q}_v(x) = -\frac{k}{T}\left(\frac{dT}{dx}\right)^2 \tag{10}$$

the entropy internal generation rate is:

$$\dot{S}_v(x) = \frac{\dot{q}_v(x)}{T(x)} = -\frac{k}{T^2}\left(\frac{dT}{dx}\right)^2 \tag{11}$$

Because

$$\dot{S}_{gen}(x) = \frac{k}{T^2}\left(\frac{dT}{dx}\right)^2$$

equation (9) becomes

$$\frac{d^2T}{dx^2} - \frac{1}{T}\left(\frac{dT}{dx}\right)^2 = 0 \tag{12}$$

which is the same as (5) obtained with variational calculus.

2.2. Initial boundary value problem

For 1-D problem, global entropy generation rate is given by the integral

$$\dot{S}_{gen,t} = \int_0^1\int_0^\infty \frac{1}{T^2}\left(\frac{dT}{dx}\right)^2 dx d\tau \tag{13}$$

T=T(x,τ) with the integral constraint describing entropy change with time of the system (state function not path function)

$$\Delta s = \int_0^1\int_0^\infty \frac{\rho c_p}{T}\frac{\partial T}{\partial \tau} dx d\tau = C \tag{14}$$

where C is constant and its value is the same both for reversible and irreversible path. Variational calculus requires the function

$$K(x,\tau) = \frac{k}{T^2}\left(\frac{\partial T}{\partial x}\right)^2 + \lambda\frac{\rho c_p}{T}\frac{\partial T}{\partial \tau} \tag{15}$$

to satisfy Euler-Lagrange equation

$$\frac{\partial K}{\partial T} - \frac{\partial}{\partial x}\left(\frac{\partial K}{\partial T_x}\right) = 0 \tag{16}$$

where λ is a Lagrange multiplier [3].
After calculation we have

$$k\frac{d^2T}{dx^2} - \frac{k}{T}\left(\frac{dT}{dx}\right)^2 = \rho c_p\frac{\partial T}{\partial \tau} \tag{17}$$

where term

$$\dot{q}_v(x) = -\frac{k}{T}\left(\frac{dT}{dx}\right)^2$$

represents again the additional heat source. Equation (17) can also be derived using entropy balance equation

$$\dot{S}_{gen}(x,\tau) + \dot{S}_v(x) = \frac{d}{dx}\left(\frac{\dot{q}_v}{T}\right) + \frac{\partial s}{\partial \tau} \tag{18}$$

Introducing from definitions

$$\dot{S}_{gen}(x,\tau) = \frac{k}{T^2}\left(\frac{dT}{dx}\right)^2$$

$$\dot{S}_v(x) = \frac{\dot{q}_v(x)}{T(x)} = -\frac{k}{T^2}\left(\frac{dT}{dx}\right)^2$$

$$\frac{\partial}{\partial x}\left(\frac{\dot{q}}{T}\right) = k\frac{d^2T}{dx^2} - \frac{k}{T}\left(\frac{dT}{dx}\right)^2$$

$$s(x,\tau) = \rho c_p \ln T(x,\tau)$$

$$\frac{\partial s}{\partial \tau} = \frac{\rho c_p}{T}\frac{\partial T}{\partial \tau}$$

equation (18) becomes in the final form

$$k\frac{d^2T}{dx^2} - \frac{k}{T}\left(\frac{dT}{dx}\right)^2 = \rho c_p\frac{\partial T}{\partial \tau} \tag{19}$$

which is identical with (17) derived with variational calculus.

3. Analytical solution of the initial value problems

Consider 1-D initial-boundary value problem – *heat conduction equation*

$$k\frac{d^2T}{dx^2}-\frac{k}{T}\left(\frac{dT}{dx}\right)^2=\rho c_p\frac{\partial T}{\partial \tau},\qquad T=T(x,\tau)$$

and after assuming $\frac{k}{\rho c_p}=1$

$$\frac{d^2T}{dx^2}-\frac{1}{T}\left(\frac{dT}{dx}\right)^2=\frac{\partial T}{\partial \tau} \tag{20}$$

where x, τ and $T(x,\tau)$ are dimensionless variables.
boundary and initial conditions

x=0, τ>0, $T(0,\tau)$=1
x=1, τ>0, $T(1,\tau)$=1
xε(0,1), τ=0, $T(x,0)=f(x)$ (21)

Using new variable

$Y=Y(x,\tau)=\ln T(x,\tau)$

initial boundary value problem takes the form

$$\frac{\partial^2 Y}{\partial x^2}=\frac{\partial Y}{\partial \tau}$$
$Y(0,\tau)$=o
$Y(1,\tau)$=0
$Y(x,0)=\ln f(x)=f_1(x)$ (22)

The solution of (22) is [5,6]

$$Y(x,\tau)=\sum_{n=1}^{\infty}a_n\sin n\pi x\exp(-n^2\pi^2\tau)$$

where

$$a_n=2\int_0^1 f_1(x)\sin n\pi x dx$$

Finally

$$T(x,\tau)=\exp\left[\sum_{n=1}^{\infty}a_n\sin n\pi x\exp(-n^2\pi^2\tau)\right] \tag{23}$$

For comparison purposes, the solution of the classical initial value problem

$$\frac{d^2T}{dx^2}=\frac{\partial T}{\partial \tau}$$
x=0, τ>0, $T(0,\tau)=T_1$
x=1, τ>0, $T(1,\tau)=T_2$
xε(0,1), τ=0, $T(x,0)=f(x)$ (24)

takes the form [5,6]

$$T(x,\tau)=T_1+(T_2-T_1)x$$
$$+\frac{2}{\pi}\sum_1^{\infty}\frac{T_2\cos n\pi-T_1}{n}\sin n\pi x\exp(-n^2\pi^2\tau)$$
$$+2\sum_1^{\infty}\sin n\pi x\exp(-n^2\pi^2\tau)\int_0^1 f(x)\sin n\pi x dx$$

Local entropy generation rate is

$$\dot{S}_{gen}=\frac{k}{T^2}\left(\frac{\partial T}{\partial x}\right)^2$$

and its global value

$$\dot{S}_{gen,t}=\int_0^1\int_0^{\infty}\frac{k}{T^2}\left(\frac{\partial T}{\partial x}\right)^2 dxd\tau$$

Local exergy losses $\delta\dot{B}$ can easily be calculated from Gouy-Stodola law so that

$$\delta\dot{B}=T_2\dot{S}_{gen}=T_2\frac{k}{T^2}\left(\frac{\partial T}{\partial x}\right)^2$$

and

$$\delta\dot{B}_t=T_2\int_0^1\int_0^{\infty}\frac{k}{T^2}\left(\frac{\partial T}{\partial x}\right)^2 dxd\tau$$

All calculation can be done using solution (23).

Conclusion

Minimization of entropy generation and equivalently exergy losses in steady state and transient heat conduction processes can easily be achieved by introducing additional heat sources which must be practically used. Many examples are discussed by Bejan [2]. The most important conclusion is that the minimization of entropy generation can also be used in the case of transient problems.

Nomenclature

$\dot{B}$ exergy flux, W

c_p specific heat capacity under constant pressure, J/kgK

k heat conduction coefficient, W/(mK)

$\dot{q}$ heat flux, W/m^2

$\dot{q}_v$ intensity of internal heat source, W/m^3

T temperature, K, also dimensionless

s specific entropy , kJ/kgK

x Cartesian coordinates

$\dot{S}_{gen}, \dot{S}_{gen,t}$ - local and global intensity of entropy generation rate

ρ density of solid, kg/m^3

τ time, s or Fourier number

References

[1] Bejan A., 1979, A General variational principle for thermal insulation system design, Int. J Heat Mass Transfer, 22, 217-227

[2] Bejan A., 1996, *Entropy generation minimization* Chapter 6, Boca Raton, Florida (USA), CRC Press

[3] Margenau H., Murphy GM., 1959 *The mathematics principles of physics and chemistry,* Chapter 6, D. Van Nostrand Co. Ins.

[4] Prigogine I., 1955 *Introduction to thermodynamics of irreversible processes,* Springfield, Ill., C. Thomas Publisher

[5] Bejan A., 1993, *Heat Transfer* , John WileySons, Inc, New York

[6] Carslaw H.S., and Jaeger J.C., 1959, *Conduction of heat in solids*, Clarendon Press, Oxford

Acknowledgments:

This research was supported by the Polish Ministry of Science and Higher Education (grant AGH No. 10.10.210.182).

Gas Diffusion at the Nano Scale

Z. Fatih Ozturk and Altug Sisman

Istanbul Technical University, Energy Institute, Istanbul, Turkey

Abstract: The thermodynamic and transport properties of gases confined at the nano scale are considerably different than those at the macro scale. At the nano scale, quantum size effects (QSE) become important and changes the behavior of gases. In this study, the diffusion coefficients of monatomic Fermi and Bose gases are analytically derived by considering QSE. The influence of QSE and quantum degeneracy on the diffusion coefficients are examined separately to analyze these effects individually. The variations of the ratio of diffusion coefficients of He3 and He4 gases with the concentration of He3 are analyzed for both low and high density conditions. It is seen how shape and size affect the diffusion process at the nano scale.

Keywords: Quantum size effects, nano scale diffusion, quantum potential.

1. Introduction

There has been a great deal of interest in understanding the electric, optic, thermodynamic and transport properties of nano scale systems in recent years. In these systems, size induced quantum confinement plays an important role affecting electron transport in thin films [1] and metallic nano wires [2-4], the transport properties of gases and water in carbon nano tubes [5,6,7], the density distributions of ideal gases [8], the optical properties of small metals [9,10], the thermodynamic properties of gases confined in nano structures [11] and the transport properties of gases in nano channels [12].

At the nano scale, the wave character of particles becomes important and modifies some fundamental quantities such as the probability density, the momentum components and the momentum spectrum of the particles. Quantum size effects (QSE) arise due to these modifications. Furthermore, in statistical mechanics, the infinite volume approximation is often used and infinite sums are replaced by integrals. However, when the size of the domain is scaled down to the nanometer, the thermal de Broglie wavelength of particles becomes comparable with the dimensions of the domain. In this case, infinite sums cannot be replaced by integrals and some more precise formulas, like Poisson's formula, must be used. In this case, results show that the shape and size of the domain affect the transport and thermodynamics properties of the system. Finite size effects on the thermodynamic properties of ideal Maxwellian and quantum gases have been examined in the literature [13-16].

The classical and quantum mechanical descriptions use the particle and wave character of matter, respectively. There are some differences between these two viewpoints and the classical results differ considerably from those obtained by using quantum mechanics at the nano scale. From the classical viewpoint, the probability density of particles confined in a domain is constant. From the quantum mechanical viewpoint, however, the probability density is not homogeneous even at thermodynamic equilibrium and particle density goes to zero near the boundaries if the boundaries are impenetrable. In other words, due to the wave character of matter, the particle feels the boundaries when the distance between the particle and the boundary is on the order of the thermal de Broglie wave length. This behavior can also be modeled by introducing an effective quantum potential which keeps the particle away from the boundaries [12]. In the absence of an external potential field, chemical and effective quantum potentials together affect the particle distribution. In the inner part of the domain, the effective quantum potential is negligible even though it is very high near the boundaries. The inhomogeneous density region near the boundaries has been called a quantum boundary layer [7] whose thickness has been found independent of the domain shape for an ideal Maxwellian gas [11].

In this study, the diffusion coefficients of monatomic Fermi and Bose gases in a rectangular transport domain are analytically derived by considering QSE. To solve the problem analytically, mixtures of ideal monatomic gases with different concentrations of He3 and He4

Corresponding Author: Altug Sisman, Email: sismanal@itu.edu.tr

confined in large containers connected with a rectangular nano channel is considered. In the transport direction, the nano channel is assumed to be much longer than the thermal de Broglie wave length and the mean free path of the gas particles. Thus, QSE can be neglected only in the transport direction. The diffusion process inside the channel is supposed to be carried out at constant temperature and pressure. The particle flux due to the density gradient at constant temperature and pressure is derived for Fermi and Bose gases by considering QSE. It is shown how the shape and size of the transport domain affect the diffusion processat the nana scale and how this behavior can in particular be used to enhance the isotropic enrichment for light elements.

2. Derivation of diffusion coefficient

The equilibrium distribution function of Fermi and Bose gases can be written in a closed form as

$$f_0^s = \frac{|\psi_w(\mathbf{x})|^2}{\exp\left[\left(\varepsilon_w - \mu^s\right)/k_b T\right] \pm 1} \tag{1}$$

where ε_w and ψ_w are the energy eigenvalue and the wave eigenfunction of a particle in quantum state *w,* respectively, μ^s is the chemical potential of species s (s=He4, He3), k_b is Boltzmann's constant, T is the temperature and the upper (lower) sign is used for a Fermi (Bose) gas. By considering the rectangular geometry and infinite potential representation for the boundaries, eigenvalues and wavefunctions are obtained by solving the Schrödinger equation. Therefore, $\varepsilon_w / k_b T$ in (1) is written as

$$\frac{\varepsilon_w}{k_b T} = \frac{\varepsilon_{ijk}}{k_b T} = (\alpha_1 i)^2 + (\alpha_2 j)^2 + (\alpha_3 k)^2 \tag{2}$$

where $\alpha_1 = L_c / L_1$, $\alpha_2 = L_c / L_2$, $\alpha_3 = L_c / L_3$, the length $L_c = h / \sqrt{8 m^s k_b T}$ is one half of the most probable de Broglie wavelength of the particles, h is Planck's constant, m^s is the rest mass of a gas particle of specie s , and L_1, L_2 and L_3 are the sizes of the rectangular domain. By introducing an effective quantum potential, the quantum mechanical probability density, $|\psi(x)|^2$, is replaced by the classical probability density $1/V$. Thus the equilibrium distribution function is expressed as

$$f_0^s = \frac{1}{V} \frac{1}{\exp\left[\left(\varepsilon_w - \mu_q^s\right)/k_b T\right] \pm 1} \tag{3}$$

where $\mu_q^s = \mu^s - \varphi^s$ and φ is the effective quantum potential [12]. Under the relaxation time approximation for the steady state case, the particle flux in direction 1 is given by

$$J_1^s = -\sum \tau v_1^2 \frac{\partial f_0^s}{\partial x_1} \tag{4}$$

where v_1 is the velocity of the particle in direction 1 and τ is the relaxation time. Since the sizes of the domain in the transverse directions are much smaller than the mean free path of the particles, the relaxation time is determined by $\tau = L_g / v$ where L_g is the geometric mean free path of the particles defined in terms of the volume V and surface area A, i.e., $L_g = 2V / A$. If (2) and (3) are used in (4) and the summation in (4) is calculated with the Poisson summation formula, the diffusive particle flux is derived as

$$J_1^s = -\frac{4 L_g n}{3} \frac{k_b T}{\sqrt{2\pi m^s k_b T}} \left(\frac{Li_1}{Li_{1/2}} \right)_s \times \left[\frac{1 - \frac{3\sqrt{\pi}}{8} \left(\alpha_2 + \alpha_3\right) \frac{Li_{1/2}}{Li_1}}{\frac{1}{\sqrt{\pi}} \left(\alpha_2 + \alpha_3\right) \frac{Li_0}{Li_{1/2}}} \right]_s \frac{\partial c^s}{\partial x_1} \tag{5}$$

where c^s is the concentration of the species s defined by $c^s = n_s / n$, n_s and n are the species and total number density of particles, respectively, and Li is the polylogarithm function with an exponential argument $\mp \exp\left(\mu_q^s / k_b T\right)$. The details of the non-equilibrium distribution function in terms of driving forces are given in reference [12]. It should be noted that $\sum_s c^s = 1$ and the chemical potentials of He3 and He4 can be expressed in terms of the He3 concentration c^{He3} and the total density n, $\mu_q^{He3}\left(c^{He3}, n\right)$ and $\mu_q^{He4}\left(1 - c^{He3}, n\right)$. By using (5), the normalized diffusion coefficient of species s is written as

$$D_s = \frac{1}{\sqrt{m^s}}\left(\frac{Li_1}{Li_{1/2}}\right)_s \left[\frac{1-\frac{3\sqrt{\pi}}{8}\left(\alpha_2+\alpha_3\right)\frac{Li_{1/2}}{Li_1}}{1-\frac{1}{\sqrt{\pi}}\left(\alpha_2+\alpha_3\right)\frac{Li_0}{Li_{1/2}}}\right]_s \quad (6)$$

The normalization is done by dividing the diffusion coefficient by

$$\frac{4L_g n}{3}\frac{k_b T}{\sqrt{2\pi k_b T}}.$$

Here, the mixture consists of He3 and He4 gases which obey Fermi-Dirac and Bose-Einstein statistics, respectively. If the first and second brackets of (6) are represented by QD and SE, respectively, the dimensionless ratio of the diffusion coefficients of He3 to He4 is obtained as

$$\hat{D} = \frac{D_{He3}}{D_{He4}} = \sqrt{\frac{m_{He4}}{m_{He3}}}\frac{QD_{He3}}{QD_{He4}}\frac{SE_{He3}}{SE_{He4}} \quad (7)$$

(7) can be rewritten as

$$\hat{D} = \frac{D_{He3}}{D_{He4}} = \hat{D}_{cl}\hat{D}_{QD}\hat{D}_{SE} \quad (8)$$

where $\hat{D}_{cl} = \sqrt{m_{He4}/m_{He3}}$, $\hat{D}_{QD} = QD_{He3}/QD_{He4}$ and $\hat{D}_{SE} = SE_{He3}/SE_{He4}$. Therefore, $\hat{D}_{cl}$, $\hat{D}_{QD}$ and $\hat{D}_{SE}$ represent the influences of mass, degeneracy and size effects on diffusion, respectively. Before to examining the variation of $\hat{D}_{QD}$ and $\hat{D}_{SE}$ versus c^{He3} and n, it is better to define the dimensionless total number density of particles as $\tilde{n} = n/n_q$ where n_q is the quantum density given by $n_q = 1/\lambda_{th}^3$ and $\lambda_{th} = 2L_c/\sqrt{\pi}$. During the calculations, the relation between the alpha values of He3 and He4 is used and is given by

$$\alpha_i^{He4} = \sqrt{m_{He3}/m_{He4}}\,\alpha_i^{He3}. \quad (9)$$

3. Results

Fig. 1 shows the variation of the influence of weak quantum degeneracy on the diffusion coefficients ratio at low density conditions ($\tilde{n} = 0.1$) where Maxwellian statistics is valid. It seems that the diffusion coefficient of He3 increases more than that of He4 with increasing values of c^{He3}. The opposite behaviour is seen in Fig. 2 for high density conditions ($\tilde{n} = 2$). It is seen that the variation of $\hat{D}_{QD}$ with c^{He3} becomes stronger for higher values of the total density.

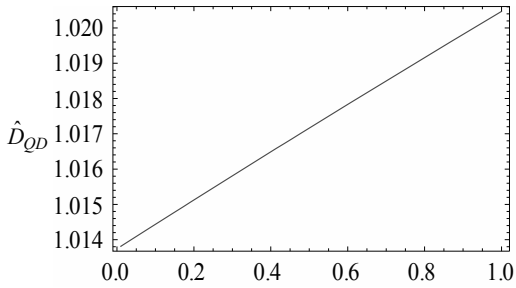

Fig. 1. Variation of $\hat{D}_{QD}$ vs c^{He3} for $\tilde{n} = 0.1$.

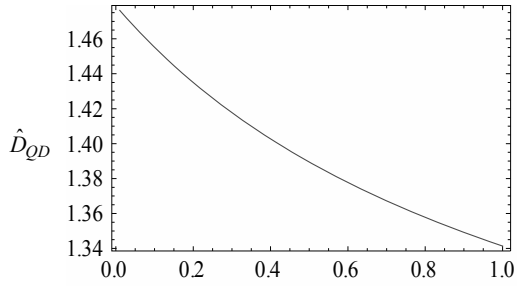

Fig. 2. Variation of $\hat{D}_{QD}$ vs c^{He3} for $\tilde{n} = 2$.

The influence of QSE on the diffusion coefficient ratio at low density conditions ($\tilde{n} = 0.1$) is shown in Fig. 3 for $\alpha = \alpha_2^{He3} = \alpha_3^{He3} = 0.2$. It is seen that the ratio is nearly constant, at 0.99. On the other hand, in Fig. 4, the variation of $\hat{D}_{SE}$ for high density conditions ($\tilde{n} = 2$) is much greater than that in Fig. 3. In addition, $\hat{D}_{SE}$ goes to unity with increasing c^{He3}. The de Broglie wave length decreases with increasing c^{He3} and the influence of QSE on the diffusion coefficient ratio decreases.

In the Maxwell limit, the ratio of the polylogarithm functions in (6) goes to unity. Substituting (9) into (6) and using $m_{He3}/m_{He4} = 3/4$, $\hat{D}_{QD}$ and $\hat{D}_{SE}$ simplify to $\hat{D}_{QD} = 1$ and

$$\hat{D}_{SE} = \frac{1-\alpha^{He3}\left(\frac{3\sqrt{\pi}}{4}+\frac{\sqrt{3}}{\sqrt{\pi}}\right)}{1-\alpha^{He3}\left(\frac{2}{\sqrt{\pi}}+\frac{3\sqrt{3\pi}}{8}\right)} \quad (10)$$

where $\alpha_2^{He3} = \alpha_3^{He3} = \alpha^{He3}$ is used for simplicity. For $\alpha^{He3} = 0.2$, $\hat{D}_{SE} = 0.9901$ which agrees with Fig. 3.

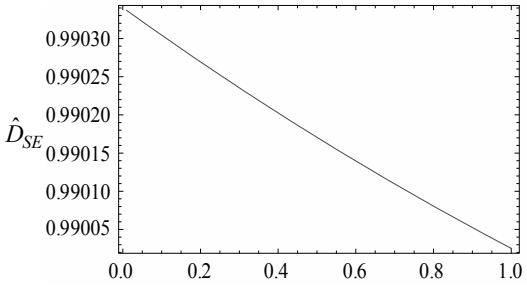

Fig. 3. Variation of $\hat{D}_{SE}$ vs to c^{He3} for $\tilde{n} = 0.1$ and $\alpha = \alpha_2^{He3} = \alpha_3^{He3} = 0.2$.

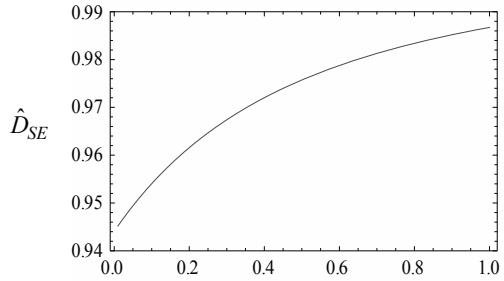

Fig. 4. Variation of $\hat{D}_{SE}$ vs to c^{He3} for $\tilde{n} = 2$ and $\alpha = \alpha_2^{He3} = \alpha_3^{He3} = 0.2$.

Conclusion

Fig. 3 and Fig. 4 show that $\hat{D}_{SE}$ is different than unity especially for high density condition. It means that the diffusion coefficients of He3 and He4 are different due to QSE. QSE depends on the de Broglie wave length which is inversely proportional to the square root of particle mass. Therefore, QSE in the diffusion process can be used for the isotropic enrichment of especially light elements and supplements the classical method based on the mass dependency of diffusion coefficients. Furthermore, Fig.1 and Fig. 2 show that the diffusion coefficients of He3 and He4 are different also due to quantum degeneracy. This difference becomes higher especially when the total density is high and He3 concentration is low. Therefore, the influence of quantum degeneracy on the diffusion process can also be used for isotropic enrichment. The quantum degeneracy effect on diffusion provides a more effective way for the separation of isotopes.

References

[1] Trivedi, N. and Ashcorft, N. W., 1988, Quantum Size Effects in Transport Properties of Metallic Films, Physical Review B, 38(17), pp. 12298-12309.

[2] Liu, K., Chien, C. L. and Searson, P. C.,1998, Finite Size Effects in Bismuth Nanowires, Physical Review B, 58(22), pp.1468114684.

[3] Arora, V. K., 1981, Quantum Size Effects in Thin-Wire Transport, Physical Review B, 23(10), pp. 5611-5612.

[4] Barati, M. and Sadeghi, E., 2001, Study of Ordinary Size Effect in the Electrical Conductivity of Bi Nanowires, 12, pp. 277-280.

[5] Jakobtorweihen, S., Keil, F. J., and Smit, B., 2006, Temperature and Size Effects on Diffusion in Carbon Nanotube, Journal of Physical Chemistry B, 110, pp. 16336-16336.

[6] Skoulidas, A. I., Ackerman, D. M., Johnson, J. K. and Sholl, D. S., 2002, Rapid Transport of Gases in Carbon Nanotubes, Physical Review Letters, 89(18), pp. 185901.

[7] Striole, A., 2006, The Mechanism of Water Diffusion in Narrow Carbon Nanotubes, Nano Letters, 6(4), pp. 633-639.

[8] Sisman, A., Ozturk, Z. F. and Firat C., 2007, Quantum Boundary Layer: A Non-Uniform Density Distribution of an Ideal Gas in Thermodynamic Equilibrium, Physics Letters A, 362(1), pp. 16-20.

[9] Oleshko, V. P., 2008, Size Confinement Effects on Electronic and Optical Properties of Silver Halide Nanocrystals as Probed by Cryo-EFTEM and EELS, Plasmonics, 3, pp. 41-46.

[10] Wood, D. M. and Ashcroft, N. W., 1982, Quantum Size Effects in the Optical Properties of Small Metallic Particles, Physical Review B, 25(10), pp. 6255-6274.

[11] Firat, C. and Sisman, A., 2009, Universality of the Quantum Boundary Layer for a Maxwellian Gas, Physica Scripta, 79(6), pp. 065002.

[12] Ozturk, Z. F. and Sisman, A., 2009, Quantum Size Effects on the Thermal and Potential Conductivities of Ideal Gases, Physica Scrpita, 80(6), pp. 065402.

[13] Sisman, A., 2004, Surface Dependency in Thermodynamics of Ideal Gases, Journal of Physics: Math. And Gen., 37, pp. 11353-11361.

[14] Dai, W. S. and Xie, M., 2004, Geometry Effects in Confined Space, Physical Review E, 70, pp.016103.

[15] Molina, M. I., 1996, Ideal Gas in a Finite Domain, American Journal of Physics, 64(4), pp 503-505.

[16] Pathria, R. K., 1998, American Journal of Physics, An Ideal Quantum Gas in a Finite-Sized Container, 66(12), 1080-1085.

Acknowledgments: This work is supported by the Scientific and Technological Research Council of Turkey, TUBITAK, under contract number 105T086 and by the Istanbul Technical University Scientific Research Program.

Second-law analysis of laminar slip-flow boundary layer heat transfer over a flat-plate

Mortaza Yari[*]*, Sanaz Mirzaparikhany*

Faculty of Engineering, University of Mohaghegh Ardabili,
Ardabil 179, Iran

Abstract: The purpose of this work is to investigate the entropy generation in a flow over a flat plate with slip-flow boundary layers. Steady state and laminar flow is considered with different forms of thermal boundary conditions: constant heat flux and the constant temperature at the wall. The effects of viscous dissipation, the velocity slip and the temperature jump at the wall are taken into consideration. The velocity and temperature profiles are obtained numerically and used to compute the entropy generation rate. The present numerical results, for the case without viscous dissipation effect are compared with those available in the literature, and an excellent agreement is observed. The effects of the slip (rarefaction) parameter, Brinkman number, and dimensionless temperature difference on velocity and temperature profiles, entropy generation rate are discussed. Moreover these results are compared simultaneously for two forms of thermal boundary conditions at the wall. Entropy generation is shown to decrease with an increase in rarefaction parameter, while increasing Brinkman number, dimensionless temperature difference and Prandtl number results in increasing entropy generation. For low rarefaction parameter, entropy generation in the wall with constant temperature at the wall is less than entropy generation in wall with constant heat flux. Also Entropy generation for both thermal boundary conditions, close together with an increase in rarefaction parameter.

Keywords: laminar boundary layer; second law; Knudsen number; slip-flow; temperature jump

1. Introduction

Entropy generation is associated with thermodynamic irreversibility, which is common in all types of heat transfer processes.

Different sources are responsible for generation of entropy like heat transfer across finite temperature gradient, characteristic of convective heat transfer, viscous effect etc. Bejan [1, 2] focused on the different reasons behind entropy generation in applied thermal engineering. Generation of entropy destroys available work of a system. Therefore, it makes a good engineering sense to focus on irreversibility of heat transfer and fluid flow process and try to understand the function of entropy generation mechanism [2]. Second law analysis focusing on entropy generation and its minimization been playing a dominant role in recent times to understand the irreversibility in applied engineering and transport processes.

Fluid flow and heat transfer at microscale have attracted an important research interest in recent years due to the rapid growth of novel techniques applied in MEMS (microelectromechanical systems) and biomedical applications such as drug delivery, DNA sequencing, and bio-MEMS. Readers may refer to recent excellent reviews related to transport phenomena in microchannels by Ameel et al. [3], Ho and Tai [4], Palm [5], Obot [6], Rostami et al. [7], Gad-el-Hak [8], Guo and Li [9-10] and Morini [11].

Recently, Marques et al. [12] analyzed the Couette flow with slip and jump boundary conditions. The steady plane Couette flow is analyzed within the framework of the five field equations of mass, momentum and energy for a Newtonian viscous heat conducting ideal gas in

Corresponding author: Mortaza Yari, E-mail: myari@uma.ac.ir

which slip and jump boundary conditions are considered. Haddad et al. [13] investigated numerically the entropy generation due to steady laminar forced convection fluid flow through parallel plate microchannel. The effect of Knudsen, Reynolds, Prandtl, Eckert numbers and nondimensional temperature difference on entropy generation within the microchannel is discussed. Aydin and Avci [14] studied laminar forced convective heat transfer of a Newtonian fluid in a micropipe by taking the viscous dissipation effect, the velocity slip and the temperature jump at the wall into account. Hydrodynamically and thermally fully developed flow case is examined. Two different thermal boundary conditions are considered: the constant heat flux (CHF) and the constant wall temperature (CWT). Aydin and Avci [15] examined laminar forced convective heat transfer of a Newtonian fluid in a microchannel between two parallel plates analytically. The viscous dissipation effect, the velocity slip and the temperature jump at the wall are included in the analysis. Both hydrodynamically and thermally fully developed flow case is examined. Two different thermal boundary conditions are considered: the constant heat flux (CHF) and the constant wall temperature (CWT). Hooman [16] presented the closed form solutions for fully developed temperature distribution and entropy generation due to forced convection in microelectromechanical systems (MEMS) in the slip-flow regime, for which the Knudsen number lies within the range $0.001<Kn<0.1$. Two different cross-sections are analyzed, being microducts and micropipes, with the effects of viscous dissipation being included. Barkhordari and Etemad [17] performed numerical simulations to study flow and thermal fields of non-Newtonian fluids in circular microchannels. The flow is considered to be slip, axisymmetric, steady, incompressible, laminar, and power law model is used to characterize the behaviour of the non-Newtonian fluid. The constant wall heat flux and constant wall temperature are employed as thermal boundary conditions. Sun et al. [18] investigated the steady-state convective heat transfer for laminar, two-dimensional, incompressible rarefied gas flow in the thermal entrance region of a tube under constant wall temperature, constant wall heat flux, and linear variation of wall temperature boundary conditions, by the finite-volume finite difference scheme with slip flow and temperature jump conditions. Avci and Aydin [19] are applied the second-law analysis of thermodynamics to the two different microgeometries: microtube and microducts, between two parallel plates. Hydrodynamically and thermally fully developed slip-flow with constant properties is examined Using the previously obtained velocity and temperature profiles, a parametric study is carried out to determine the combined effects of the Brinkman number, Knudsen number on the entropy generation. Avci and Aydin [20] studied and presented an analytical solution to forced convective heat transfer in hydrodynamically and thermally fully developed slip-flows of viscous dissipation gases in annular microducts between two concentric micro cylinders. Two different cases of the thermal boundary conditions are considered: uniform heat flux at the outer wall and adiabatic inner wall (Case A) and uniform heat flux at the inner wall and adiabatic outer wall (Case B). Hooman [21] presented superposition approach to investigate forced convection in microducts of arbitrary cross-section, subject to H1 and H2 boundary conditions, in the slip-flow regime with further complication of a temperature jump condition assumption. It was shown that applying an average slip velocity and temperature jump definition, one can still use the no-slip/no-jump results with some minor modifications. Yari [22] presented the first and second laws of thermodynamics analysis for laminar forced convective heat transfer of a Newtonian fluid in a microchannel between parallel plates for Coette-Poiseuille. Hydrodynamically and thermally fully developed flow with constant properties is examined. Entropy generation is shown to decrease with an increase in Kn while increasing Br and Br/Ω results in increasing entropy generation. Yari [23] in another work investigated the entropy generation in a micro-annulus flow. Fully developed laminar flow is considered with uniform heat flux at the walls. The viscous dissipation effect, the velocity slip and the temperature jump at the wall were taken into consideration. The velocity and temperature profiles are obtained analytically and used to compute the entropy generation rate. Entropy generation was shown to decrease with an increase in Kn while increasing Br, Br/Ω and r^* results in increasing entropy generation.

The effect of slip flow on the flat plate thermal boundary layer characteristics has received limited attention. In the recent papers, Martin and Boyd [24] and Aziz [25] considered the thermal boundary layer over an isothermal and constant flux flat plate in the presence of slip flow. In these analysis they took into account the effect of slip parameter K (a function of x, direction along the plate) in transforming the momentum equation and found that the stream function and consequently the y (direction normal to the plate) component of the velocity v also depends on the variation of the similarity variable f with respect to K. With this modification, the similarity equation for the hydrodynamic boundary layer became a partial differential equation instead of the classical Blasius ordinary differential equation. With the introduction of temperature jump condition, the transformed energy equation also became a partial differential equation.

There is a lack of information in the literature regarding the second-law analysis and entropy generation for laminar boundary layer fluid flow and heat transfer over a flat-plate taking viscous dissipation effect, slip velocity and temperature jump into account.

2. Analysis

In this analysis the following assumptions were done:

- The flow is considered to be: Steady, laminar flow having constant properties (i.e. thermal conductivity and the thermal diffusivity of the fluid are considered to be independent of temperature).
- No significant gradient of pressure in the x direction, and that velocity gradient in the x direction are small in compare to velocity gradient in the y direction.
- The axial heat conduction in the fluid and in the wall is assumed to be negligible.

Two different forms of the thermal boundary Conditions are applied, which are shown in Fig. 1. In the following, these two different cases are treated separately.

2.1 Hydrodynamic aspects

The first-order slip velocity for a cylindrical geometry can be expressed as [24-25]:

$$u_s = -\frac{2-F}{F}\lambda\frac{\partial u}{\partial y}\Big|_{y=0} \qquad (1)$$

Where u_s is the slip velocity, λ the mean free path, and F is the momentum accommodation factor which is close to unity for most of the gas solid couples used in engineering applications and taken so herein. Similarly, temperature jump for a cylindrical geometry can be expressed as [24-25]:

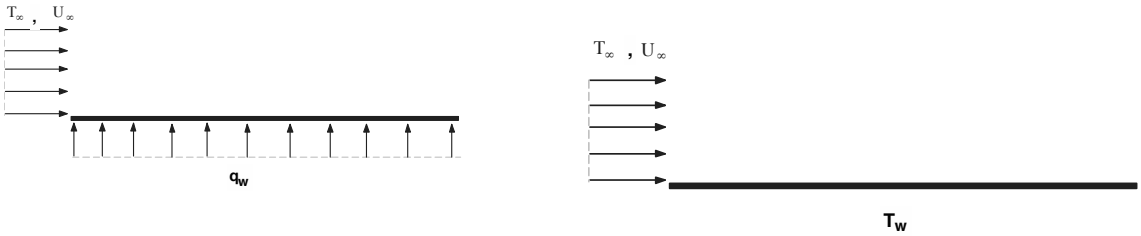

Figure 1: Geometry and schematic diagram of flow domain: (a) Case A, (b) Case B

$$T_s - T_w = -\frac{2-F_t}{F_t}\frac{2\gamma}{1+\gamma}\frac{\lambda}{Pr}\frac{\partial T}{\partial y}\Big|_{y=0} \quad (2)$$

Where γ is the specific heat ratio, Pr is the Prandtl number of the fluid, T_s is the temperature of the gas at wall, T_w the wall temperature, and F_t is the thermal accommodation factor, which depends on the gas and surface material. Particularly for air, it assumes typical values near unity [24-25]. For the rest of the analysis, F and F_t will be shown by F. By imposing these two effects into the boundary conditions as slip velocity and temperature jump, the Navier-Stokes equations become applicable for the slip flow regime.

As shown in Fig. 1, flow over a flat-plate can be described as consisting of a uniform external flow region and a boundary layer of finite thickness.

Based on assumptions that noted in section 2, the equations of continuity and conservation of momentum, simplify into the boundary layer equations given as [26-27]:

$$\frac{\partial u}{\partial x} + \frac{\partial v}{\partial y} = 0 \quad (3)$$

$$u\frac{\partial u}{\partial x} + v\frac{\partial u}{\partial y} = \frac{\mu}{\rho}\frac{\partial^2 u}{\partial y^2} \quad (4)$$

By using the following non-dimensional parameters:

$$\eta = \frac{y}{x}\sqrt{Re_x} \quad (5)$$

Where the dependent variable $f(\eta)$ is defined as:

$$\frac{u}{u_\infty} = f'(\eta) \quad (6)$$

$$f = \frac{\psi(x,y)}{u_\infty\sqrt{\nu x/u_\infty}} \quad (7)$$

From the definition of stream function, the equations (3) and (4) can be written as:

$$\frac{v}{u_\infty} = \frac{1}{2\sqrt{Re_x}}(f'\eta - f) \quad (8)$$

$$2f''' + ff'' = 0 \quad (9)$$

Referring to the above equations, the slip conditions and the free stream-merge condition:

$$f'(\infty) = 1 \quad (10)$$

$$f'(0) = \frac{2-F}{F}Kn_x\sqrt{Re_x}f''(0) = Kf''(0) \quad (11)$$

Where the local Knudsen number and the local Reynolds number are defined as:

$$Kn_x = \frac{\lambda}{x} \quad (12)$$

$$Re_x = \frac{u_\infty x}{\nu} \quad (13)$$

And

$$K = \frac{2-F}{F}Kn_x\sqrt{Re_x} \quad (14)$$

It should be noted that, the slip (rarefaction) parameter, K is a function of x and as a consequence the solution of Eq. (9) subjected to the boundary condition (10), (11) for fixed values of K would locally similar [24-25].

2.2 First-law analysis

The steady-state energy equation for laminar boundary layer flow over a flat-plate with

constant fluid properties, including heat dissipation, can be written as [26-27]

$$u\frac{\partial T}{\partial x}+v\frac{\partial T}{\partial y}=\frac{k}{\rho C_p}\frac{\partial^2 T}{\partial y^2}+\frac{\mu}{\rho C_P}\left(\frac{\partial u}{\partial y}\right)^2 \quad (15)$$

By introducing the following non-dimensional temperature [26-27]

$$\theta=\frac{T_w-T}{T_w-T_0} \quad (16)$$

The Eq. (15) for different forms of thermal boundary conditions: constant heat flux and constant temperature at the wall can be written as:

$$T_w=\text{const.}\longrightarrow \theta''+\frac{Pr}{2}f\theta'-Br\,f''^2=0$$

$$q_w=\text{const.}\longrightarrow \theta''+\frac{Pr}{2}(f\theta'-f'\theta+f')-Brf''^2=0 \quad (18)$$

Where,

$$Br=\frac{\mu u_\infty{}^2}{k(T_w-T_0)} \quad (19)$$

Thermal boundary conditions in the dimensionless form may be written as:

$$\theta(0)=\frac{2-F_t}{F_t}\frac{2\gamma}{\gamma+1}\frac{k}{Pr}\theta'(0) \quad (20)$$

$$\theta(\infty)=0 \quad (21)$$

And Nusselt number is defined as:

$$Nu_x=\frac{h_x}{k(T_w-T_0)}=\theta'(0)\sqrt{Re_x} \quad (22)$$

2.3 Second-law analysis

According to Bejan [28], the volumetric rate of entropy generation is defined as

$$\dot{S}'''_{gen}=\frac{K}{T^2}\nabla T^2+\frac{\mu}{T}\phi \quad (23)$$

In a two-dimensional convection laminar boundary layer flow and heat transfer situation, the local entropy generation rate yields

$$\dot{S}'''_{gen}=\frac{K}{T_0{}^2}\left(\frac{\partial T}{\partial y}\right)^2+\frac{\mu}{T_0}\left(\frac{\partial u}{\partial y}\right)^2 \quad (24)$$ where

T_0 is the absolute reference temperature [29]. The dimensionless form of entropy generation rate is entropy generation number (N_s) and it is equal to the ratio of the actual entropy generation to the characteristics entropy transfer rate [2].

By using the non-dimensional quantities, the equation (24) can be written as:

$$N_s=\frac{\dot{S}'''_{gen}}{S_{G,C}}=Re_x\left(\theta'^2+\frac{Br}{\phi}f''^2\right)=N_H+N_F \quad (25)$$

Where ϕ is the dimensionless temperature difference, $S_{G,C}$ is the characteristics entropy generation rate respectively, and is defined as

$$S_{G,C}=\frac{(T_w-T_0)^2k}{T_0{}^2x^2} \quad (26)$$

On the right-hand side of Eq. (25), the first term (N_H) accounts for entropy generation due to heat transfer in normal direction to the x axis and the last term (N_F) is the fluid friction contribution to entropy generation.

The rate of the entropy generation due to heat transfer, N_H, to the total entropy generation, N_s is called the Bejan number, Be:

$$Be=\frac{N_H}{N_H+N_F} \quad (27)$$

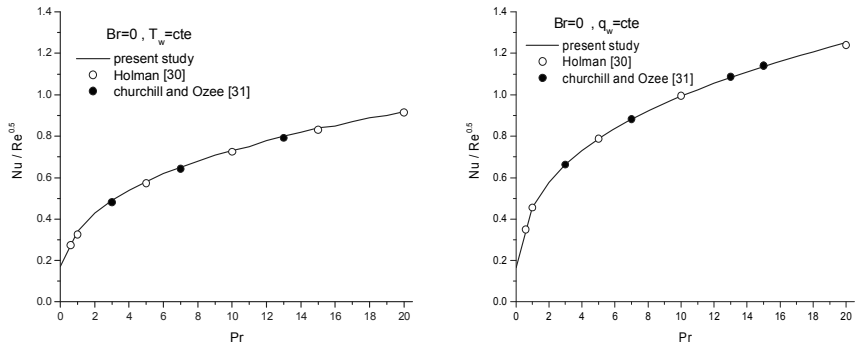

Figure2: *Values of* $\mathrm{Nu}/\mathrm{Re}^{0.5}$ *for present study and the available results from [30-31] at different values of Pr for constant heat flux and Constant wall temperature*

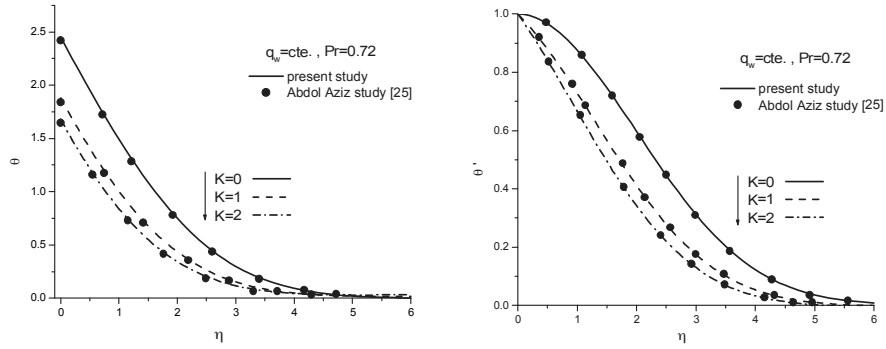

Figure 3: *Dimensionless temperature and temperature gradient distributions for present study and the available results from the [25] at different values of K.,for (a) case A and (b) case B*

2.3 Analysis validation

In order to validate the present numerical model, the numerical simulation results have been compared with the available numerical and experimental data for simplified cases from Ref. [25, 30-31] which are given in Figs. 2 and 3. As seen, an excellent agreement is obtained.

3. Results and discussion

In this study, we investigate the interactive effects of the brinkman number and Knudsen number on the entropy generation for flow over a flat plate with different forms of thermal boundary conditions: constant heat flux and the constant temperature at the wall. Note that K=0 represent the macro-scale case, while K > 0 hold for the micro-scale case. Br=0 represent the case without the effect of the viscous dissipation.

Fig. 4 illustrates the dimensionless velocity and fig.5 illustrates velocity gradient profiles obtained from Eq. (9) for different value of K number. As the flow becomes more rarefied, the slip velocity, $f'(0)$, increases and so does the x component of the velocity for any value of η, while decreases the velocity gradient profiles in the boundary layer.

Similarly, Fig.6 shows dimensionless temperature profiles and Fig.7 shows temperature gradient at different value of K, Br for prandtl number of 0.72 and for the both boundary conditions. The temperature value at η=0, represent the dimensionless value of the temperature jump. Increasing K results in an increase the temperature profiles in the boundary layer and temperature jump at the wall. The viscous dissipation behaves like an energy source that changes the temperature profile. For both cases, the increasing viscous dissipation will result in decreasing temperature profile and temperature jump at the wall. Also viscous dissipation severely distorts the temperature gradient.

Note that temperature profiles in the boundary layer and temperature gradient for wall with constant temperature is less than those for wall with constant heat flux.

Fig.8 and Fig.9 show the influence of Br/φ on the entropy generation at K=0, 1 and 5 for constant heat flux and constant wall temperature. This parameter determines the relative importance of viscous effect. As seen, increasing Br/φ result in increasing entropy generation while increasing K results in decreasing entropy generation; moreover entropy generation for wall with constant temperature is less than these results for wall with constant heat flux that with increasing K results for these boundary conditions close together As rarefaction parameter, K increases the velocity gradient and temperature gradient decreases, therefore entropy generation due to both fluid friction and heat transfer decreases.

Moreover, entropy generation number reduces to minimum in the region of the annual where the velocity and temperature magnitude are maximum. Another point worthy of comment is that, the entropy generation spatial variation is similar to the temperature profile because that temperature gradient is paramount than velocity gradient and velocity gradient by coefficient of Br/φ due to entropy generation.

4. Conclusion

This work was undertaken to understand the entropy generation in micro-scale flow and how it varies with the K, Br and Br/φ. This study could be used to optimize the design of micro-scale device by minimizing the entropy generation rate. Therefore, the purpose of this paper is to investigate the entropy generation in flow over a flat plate with two different thermal boundary conditions: constant heat flux and the constant temperature at the wall. The viscous dissipation, the velocity slip and the temperature jump have been included in the numerically analysis. The velocity and temperature profiles are obtained numerically and used to compute the entropy generation rate.

The effects of K, Br and Br/φ on velocity, temperature profiles, entropy generation rate are discussed.

The following conclusions can be summarized from this study:

1. Entropy generation rate decreases as K increases while increasing of Br and Br/φ lead to an increase in entropy generation.

2. In low K, the wall with constant temperature produced the least entropy generation.

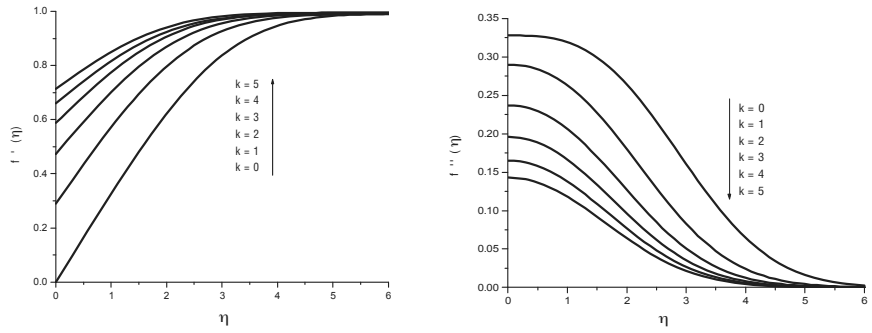

Figure 4 *Dimensionless velocity and velocity gradient distributions at different value of K*

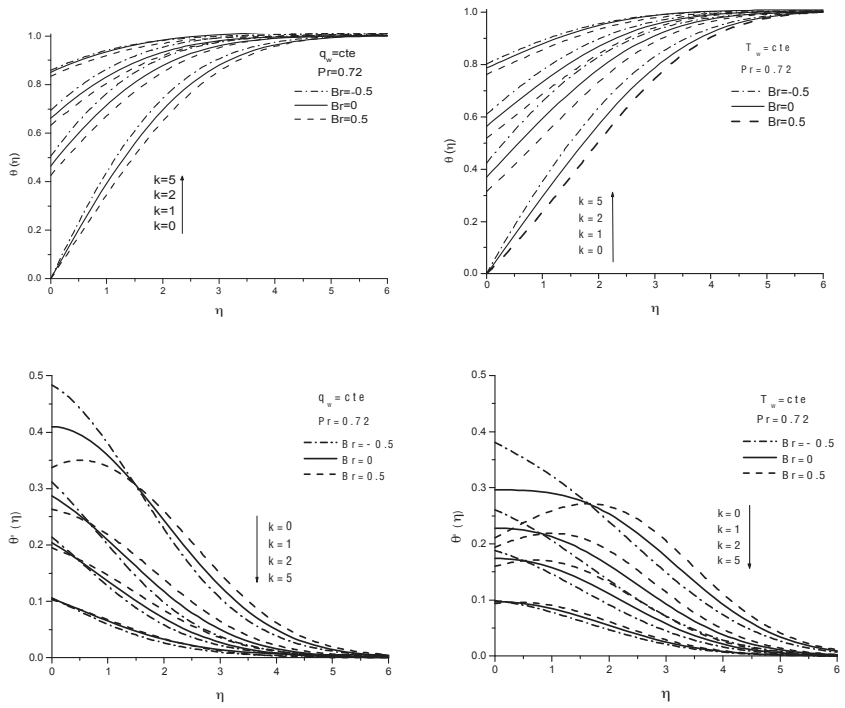

Figure 6 *Dimensionless temperature and temperature gradient distributions at different value of K and Br for case (a) , (b)*

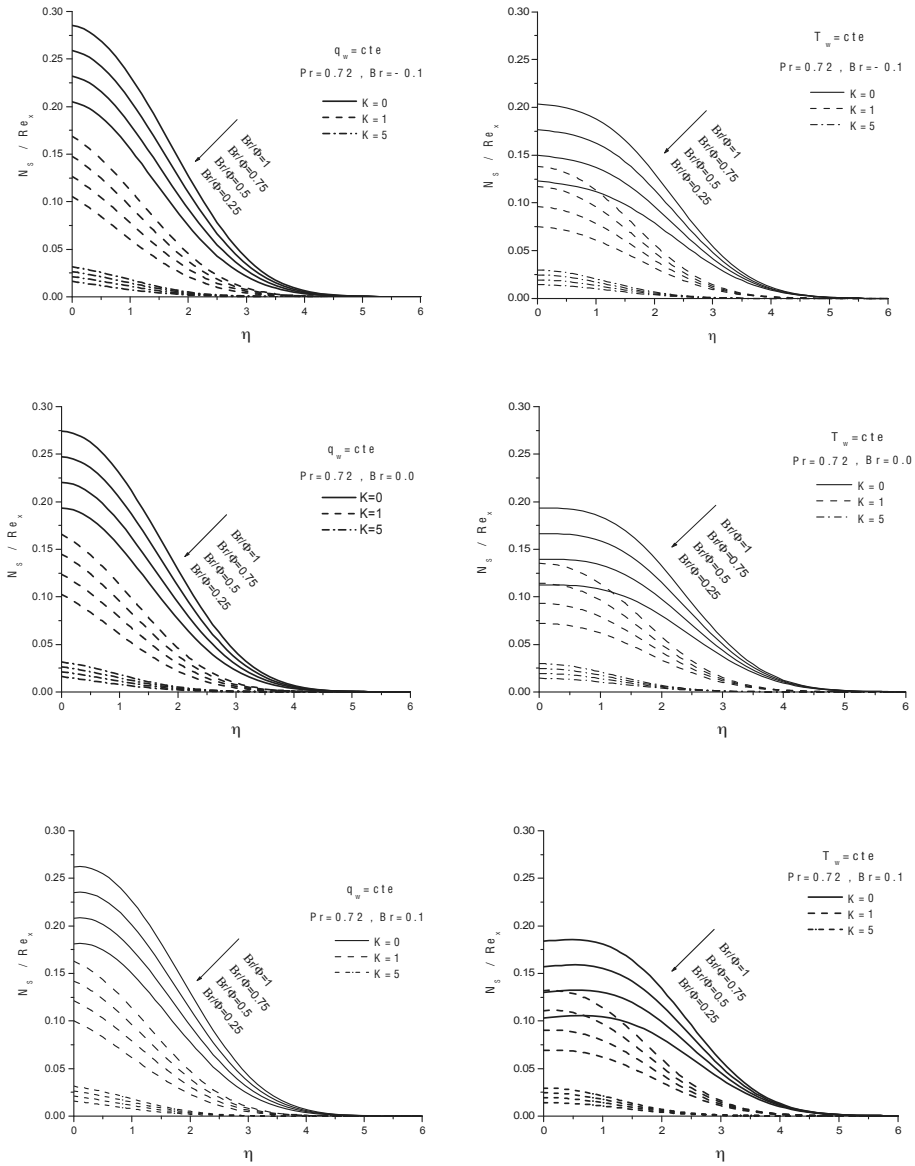

Figure 8 *Values of* N_S / Re_x *at different value of K and Br/φ for constant heat flux*

References

[1] A. Bejan, 1982, Second-law analysis in heat transfer and thermal design, *Heat Transfer*, 15 p.p.1-58

[2] A. Bejan, 1996, Entropy generation minimization, CRC Press, Boca Raton, NY

[3] T.A. Ameel, X.M. Wang, R.F. Barron, R.O. Warrington, 1997, Laminar forced convection in a circular tube with constant heat flux and slip flow, *Microscale Thermophysics* 1 (4) p.p.303-320.

[4] C.M. Ho, C.Y. Tai, 1998, Micro-electro-mechanical systems (MEMS) and fluid flows, *Annual. Rev. Fluid Mech*., 30 p.p. 579-612.

[5] A.A. Palm, 2001, Heat transfer in microchannels, *Microscale Thermophysical Engineering* , 5 p.p.155-175.

[6] N.T. Obot, 2002, Toward a better understanding of friction and heat/mass transfer in microchannels- A literature review, *Microscale Thermophysical Engineerin*g, 6 p.p.155-173.

[7] A.A. Rostami, A.S. Mujumdar, N. Saniei, 2002 , Flow and heat transfer for gas flowing in microchannels: *a review, Heat Mass Transfer*, 38 p.p.359-367.

[8] M. Gad-el-Hak, 2001, Flow physics in MEMS, *Mech. Ind*., 2 p.p.313-341.

[9] Z.Y. Guo., Z.X. Li, 2003, Size effect on single-phase channel flow and heat transfer at micro scale, *International Journal of Heat and Mass Transfe*r, 46 p.p. 59-149.

[10] Guo Z.Y., Li Z.X. 2003, Size effect on single-phase channel flow and heat transfer at micro scale, *International Journal of Heat and Fluid Flow,* 24 pp. 284-298.

[11] G.L. Morini, 2004, Single-phase convective heat transfer in microchannels: a review of experimental results, *International Journal of Thermal Sciences*, 43 p.p.631-651.

[12] W. Marques Jr, G.M. Kremer, F.M. Sharipov, 2000, Couette flow with slip and jump boundary conditions, *Continuum Mech. Thermodynamic*, 12 p.p.379-386.

[13] O. Haddad, M. Abuzaid, M. Al-Nimr, 2004 , Entropy generation due to laminar incompressible forced convection flow through parallel plates microchannel, *Entropy*, 6 (5) p.p.413-426.

[14] O. Aydin, M. Avci, 2006, Heat and fluid flow characteristics of gases in micro pipes, *International Journal of Heat and Mass Transfer,* 49 p.p.1723-1730.

[15] O. Aydin, M. Avci, 2007, Analysis of laminar heat transfer in micro-poiseuille flow, *International Journal of Thermal Sciences*, 46 p.p. 30-37.

[16] K. Hooman, 2007, Entropy generation for Microscale forced convection: effects of different thermal boundary conditions, velocity slip, temperature jump, viscous dissipation, and duct geometry, *International Communications in Heat and Mass Transfer*, 34 p.p.945-957.

[17] M. Barkhordari, S.G. Etemad, 2007, Numerical study of slip flow heat transfer of non-Newtonian fluids in circular microchannels, *International Journal of Heat and Fluid Flow*, 28 p.p. 1027-1033.

[18] W. Sun, S. Kakac, A.G. Yazicioglu, 2007, A numerical study of single-phase convective heat transfer in micro tubes for slip flow, *International Journal of Thermal Sciences* ,46 p.p. 1054-1094.

[19] M. Avci, O. Aydin, 2003, Second-law analysis of heat and fluid flow in micro scale geometries, *International Journal of Exergy,* 4 (3) p.p.286-301.

[20] M. Avci, O. Aydin, 2008, Laminar forced convection slip-flow in a micro-annulus between two concentric cylinders, *International Journal of Heat and Mass Transfer*, 51 p.p. 3460-3467.

[21] K. Hooman, 2008, A superposition approach to study slip-flow forced convection in straight microchannels of uniform but arbitrary

cross-section, *International Journal of Heat and Mass Transfer*, 51 p.p.3753–3762.

[22] M. Yari, 2009, Entropy generation analysis for Couette–Poiseuille flow through parallel-plates microchannel, *International Journal of Exergy*, 6(6) p.p. 809-825.

[23] M. Yari, 2009, Second-law analysis of flow and heat transfer inside a micro annulus, *International Communications in Heat and Mass Transfer* , 36 p.p. 78–87.

[24] MJ. Martin, ID. Boyd, 2006 , Momentum and heat transfer in laminar boundary layer with slip flow, *Journal of Thermophysics Heat Transfer*, 20(4) p.p. 710–9.

[25] A. Aziz, 2010, Hydrodynamic and thermal slip flow boundary layers over a flat plate with constant heat flux boundary condition, *Commun Nonlinear Sci Number Simulat* , 15 p.p.573–580.

[26] H. Patrick, O. Osthuizen and D. Naylor, 2005, An introduction to convective heat transfer analysis, McGraw-Hill

[27] W. Kays., M. Grawford, B. Weigand, 2005 , Convection heat and mass transfer, Mc Graw-Hill, NY.

[28] A. Bejan, 2004, Convection heat transfer, John Wiley and Sons ed., NY.

[29] S. Mahmud, R.A. Fraser, 2003, The second law analysis in fundamental convective heat transfer problems, *International Journal of Thermal Sciences*, 42 p.p.177-186.

[30] J. P. Holman, 2005, Heat transfer, McGraw-Hill

[31] S.W. Churchill, H. Ozee, 1973, Correlations for laminar forced convection in flow over isothermal flat plate and in developing and developed flow in an isothermal tube, *Journal of Heat Transfer,* 95 p.p. 46

Pressure Drop Consideration in Targeting and Design of Heat Exchanger Networks with Different Types of Heat Exchangers

M.H. Panjeshahi[a], *J. Dashtbani*[b] *and H.R. Fallahi*[c]

[a] *Department of Chemical Engineering, University of Tehran, Tehran, Iran*
[b] *Department of Chemical Engineering, University of Tehran, Tehran, Iran*
[c] *Petro Hitech Co., Tehran, Iran*

Abstract: In the synthesis of heat exchanger networks, estimation of minimum area and energy requirement (targeting stage) plays an important role, since it allows the prediction of investment requirement ahead of design. On the other hand, Heat exchanger networks in chemical and process industries often require different heat transfer devices. The economic implications of such network designs are often very significant; therefore, it is important that the performance of such networks be reliably determined before their actual designs. Also, it is necessary to use actual values for heat transfer coefficients in targeting stage and this will be practicable by using stream allowable pressure drops in this stage as in detail design.

In this paper, we have developed a new method for area targeting and design of heat exchanger networks in grass-roots design based on Pinch Technology, which allows area and capital cost targets to take into account of differences in exchanger types and consideration of streams allowable pressure drops in calculation of realistic heat transfer coefficients instead of assumed ones. This method enables the designer to determine match-wise heat transfer coefficients in different exchangers in the network. The method is capable to estimate the distribution of the heat transfer surface areas and the total number of heat transfer units amongst different exchanger types in the network and take into account the effect of this distribution in problem economic. It allows using real cost law for each individual exchanger without having to change them. Therefore, the method would be able to predict the correct optimum ΔT_{min} necessary to initialize a design and consequently able to direct the designer to the optimum energy and capital costs in design stage.

The method has been applied to a case study, consisting of Shell & Tube and Plate-Fin heat exchangers, and the results proved to be much better and more reliable compare to the existing methods.

Keywords: Pinch technology, Heat exchanger network, Area targeting, Pressure drop consideration, Plate-fin heat exchanger, Sell-and-tube heat exchanger.

1. Introduction

Over the last few decades and particularly after the energy crisis of the 1970s, heat exchanger networks (HENs) synthesis has shown fast and outstanding improvements. Several methods have been developed for the design of HENs as part of synthesis of a chemical process. In general, the design methods for HEN can be divided into two major approaches. One uses the Pinch point concepts, and the other one make use of mathematical programming methods.

The synthesis of HEN by means of Pinch Technology has two steps: namely, targeting and design. In targeting stage, the minimum energy (energy cost) and area requirements (capital cost) are determined prior to design [1,2]. Until 1990, most of the works done on networks capital cost targets have assumed that the networks have a "uniform" exchanger specification, that is, all the exchangers in the network are assumed to be of the same type, and consequently all obey the same cost law.

Indeed, the real networks don't usually consist of exchangers with "uniform" specifications, and process streams may require special or expensive exchangers. Similarly, although the shell-and-tube heat exchangers (STHE) are still the most commonly used heat transfer devices in the process industries today, the need for more efficient heat exchangers lead the designers toward compact heat exchangers such as plate-and-fin heat exchangers (PFHE) or other ones. Differences in exchanger types have to be recognized at the

Corresponding Author: Panjeshahi M. H., mhpanj@ut.ac.ir

targeting stage. Failure to do this, could lead to a capital cost target which may be very different from the actual network capital cost; and result of this could be a wrong capital-energy trade-off that leading to the selection of the non-optimum ΔT_{min} for network design initialization. The consequence of this is that, a non-optimal design maybe obtained [3, 4].

For solving this, a few Pinch-based design methods have been reported, such as Hall et al., 1990, Jegede and Polly, 1992 [3,4]. Also, recently Serna-gonzalez and et al., 2007, presented a targeting method based on diverse pinch concept and different cost laws [5]. But similar to common methods in targeting stage, they have applied assumed heat transfer coefficients. In the context of mathematical programming methods, Colberg and Morari (1990) develop a non-linear program formulation for HEN with non-uniform exchanger specification. Their method had the advantages of considering unequal heat transfer coefficient effects in area targeting [6]. But, in all of above mentioned methods, the allowable pressure drop of streams ignored.

However, most published design methods don't take into account the pressure drop aspect. Polly and Panjeshahi, 1991, pointed out that the delay in considering pressure drops can lead to two serious problems. Firstly, actual stream pressure drop in detail design may be much higher than allowable pressure drops. Thus the conceptual design has to be rejected and the network has to be redesigned. The tedious procedure of trial and error is inevitable. Conversely, the actual pressure drops may be much lower than the allowable values. These will lead to more surface area being installed than necessary and so result in incorrect capital-energy trade-off in determination of the optimum value for ΔT_{min} In whichever case, neglecting of pressure drop will lead to non-optimal design in terms of both total cost and pressure drop constraints. They proposed a method and used pressure drop correlation in the form of $\Delta P = K.A.h^m$ [7].

The aim of this paper is to develop a new area (or capital cost) targeting procedure for a network with "non-uniform" heat exchanger types and considering allowable stream pressure drops in determination of match-wise heat transfer coefficients in different exchangers in the network.

2. Relationship between Pressure Drop, Heat Transfer Coefficient, and Heat Exchanger Area

In the case where pressure drop and film heat transfer coefficient of streams appears a function of velocity, there will be a relationship between the area of heat exchanger, pressure drop and heat transfer coefficient.

Shell-and-Tube Heat Exchanger:

The shell-and-tube heat exchanger is the most common of various types of unfired heat transfer equipment used in industry. It is consist of a bundle of tubes that is placed in a shell. Its shape makes it well suited to pressure operation.

For the case of fluid flowing inside the tubes of an exchanger, the best and suitable relationship is [1,7,8]:

$$\Delta P_t = K_t.A.h_t^{3.5} \quad (1)$$

Where, K_t is a constant solely dependent on physical properties, volumetric flow rate, and the heat exchanger system.

For a fluid flowing inside the shell of *STHE*, there are several relationships. Some of them are simple and some of them are too complex, but the best and accurate one is a relationship that proposed by Panjeshahi, based on Bell-Delaware method. The relationship is [7,8,9]:

$$\Delta P_s = K_s.A.h_s^{4.412} \quad (2)$$

Similarly, in this equation, K_s is a constant solely dependent on physical properties, volumetric flow rate, and the heat exchanger system.

Plate-fin Heat Exchanger

A plate-fin heat exchanger (PFHE) is a type of compact exchanger that consists of a stack of alternate flat plates called parting sheets and corrugated fins brazed together as a block. It has some advantages over other forms of heat exchangers, only limited by operating fluid temperatures and pressures. These advantages are: very close temperature approaches and high thermal effectiveness, large heat transfer area per unit volume (1000 m^2/m^3 typical), low weight per unit transfer and possibility of heat exchange between many process streams [10]. In the last decade by improving the construction technology of Plate-and-Fin heat exchangers; application of

these exchangers beside the other usual heat exchangers like *STHE*, has increased.

The key to the derivation of the design procedure based upon fullest use of pressure drop for this exchanger is the development of a thermo-hydraulic model. This model, should relates the pressure drop of a specific stream to the total exchanger heat transfer area or volume and to the heat transfer coefficient of that side of the exchanger. This model has been derived for volume of this heat exchanger previously [11]. But, for more compatible result with other exchanger results, we should have this model for heat transfer area. The heat transfer performance for a large number of compact surfaces can be correlated in terms of Reynolds number. The correlating expressions take the form of $j = a.\mathrm{Re}^{-b}$ [11]. By combining the correlation with Stanton and J Colburn Factor relations, we have below general relation for Nusselt number [12]:

$$Nu = a.Re^{(1-b)}.Pr^{1/3} \quad (3)$$

By substituting Nu, Re and Pr definitions in secondary surface channel and solving for the heat transfer coefficient h, yields:

$$h = k_1 u^{(1-b)} \quad (4)$$

Where

$$k_1 = a.(\frac{\rho d_h}{\mu})^{(1-b)}.(\frac{\lambda}{d_h}).\mathrm{Pr}^{1/3}$$

Eq. (4) gives the heat transfer coefficient as a function of physical properties, mass flow rate and velocity in channel.

A similar procedure can be applied to derive an expression that relates pressure drop to velocity, physical properties. An expression that represents the pressure drop a cross the core of a heat exchanger (generally in channel and tube) is

$$\frac{\Delta P}{l} = 2 . f . \frac{\rho .u^2}{d_h} \quad (5)$$

For most secondary surfaces, the values of the friction factor f within a range of Reynolds numbers between 500 and 10,000 can be correlated in terms of the Reynolds number in a similar way as the heat transfer data given by Eq. (8)[12]. The expression is as follows

$$f = x . \mathrm{Re}^{-y} \quad (6)$$

Combining Eqs 5 and 6 gives:

$$\Delta P = 2x .(\frac{\rho d_h}{\mu})^{-y} . \frac{\rho}{d_h} . l u^{(2-y)} \quad (7)$$

Using hydraulic diameter and volumetric flow rate (υ) definitions in secondary surface and substituting l with A in this equation gives:

$$\Delta P = k_2 . A u^{(1-y)} \quad (8)$$

Where

$$k_2 = x .(\frac{\rho d_h}{\mu})^{-y} . \frac{\rho}{2\upsilon}$$

Finally by can substituting U from Eq. (4) in (8):

$$\Delta P = K . A . h^{(\frac{3-y}{1-b})} \quad (9)$$

Where K is:

$$K = \frac{k_2}{k_1^{(\frac{3-y}{1-b})}}$$

The constant of the Eq. (9), *K,* is dependent of fin type that is used in *PFHE*. By selecting fin type in this exchanger and having physical properties and volumetric flow rate of stream, the value of the *K* is determined. This relationship is used for both sides of *PFHE*.

3. Targeting through Conventional Assumed-h Method

In Pinch technology method, after the determination of energy requirements of the process, on the basis of the thermodynamic and heat transfer constrains of problem (for specified ΔT_{min}) hot and cold composite curves are drawn and the minimum area required by the network at the same ΔT_{min}, is determined [13].

In the case of network with different types of exchanger, Jegede and Polly (1992) proposed a method for area targeting [4]. Their method uses match dependent coefficients, h_{ij} and h_{ji}, between the pair of streams to determine A_{ij} of matches between streams. Sum of these areas gives the total area within the intervals. By repeating this procedure over all enthalpy intervals in the composite curves, the total area of the network can be projected as given by below equation:

$$A_{\min} = \sum_{k=1}^{K} \frac{1}{\Delta T_{LM,k}} \sum_{i=1}^{I} \sum_{j=1}^{J} q_{ijk} \left(\frac{1}{h_{ij}} + \frac{1}{h_{ji}} \right) \quad (10)$$

This method is capable to determine area contribution of exchangers that are exist in the network.

4. New Method for Area and Capital Cost Targeting

As mentioned, conventional methods use assumed-h coefficients in targeting stage, but in new proposed method we have used allowable pressure drops of streams for determining h-values of streams in each match. For this, we combined Jegede method for different types of heat exchanger and Panjeshahi method for pressure drop consideration in HEN. So because of the dependency of h-values of each match to heat exchanger type, pressure drop and physical properties of streams, therefore we can determine the correct values for heat transfer coefficients by this new method.

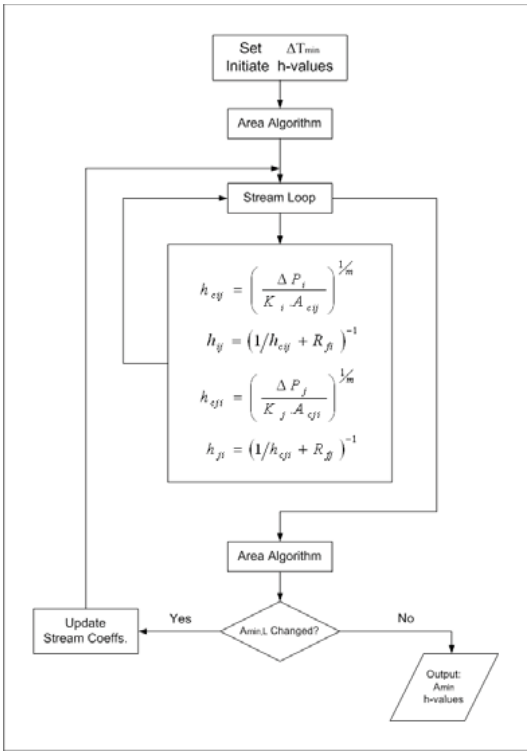

Fig. 1. New area targeting procedure

In proposed method, the first step is developing an "Exchanger Classification Table". In this table the type of the exchangers for each pair of streams in network is specified. In second step, after establishing of composite curves, streams of each enthalpy intervals are specified. Now by using spaghetti model and exchanger classification table, type of exchanger for each mach in spaghetti model is specified, and third step is calculating contact area for each match. In this stage for contact area calculation, a suitable method for each type of exchangers should be used.

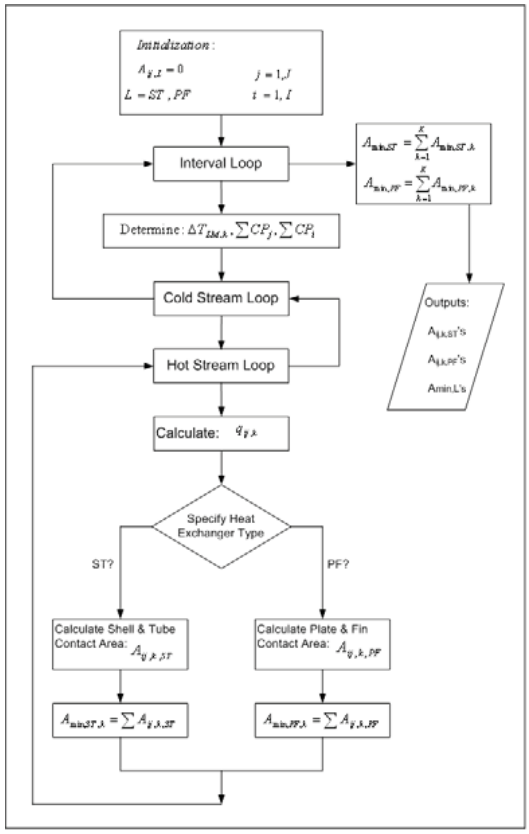

Fig. 2. Area algorithm of new area targeting procedure

The new procedure for area targeting is fully outlined in figure 1 and 2. For starting calculation we assume some values for heat transfer coefficients, *h*, for each streams (*i* and *j*) in each match. Amount of heat load between streams *i* and *j* in each interval (for each match) is calculated by using below equation:

$$q_{ij,k} = CP_i \times \Delta T_{LM} \times \frac{CP_j}{\sum CP_j} \quad (11)$$

Next step is determination of the required area of each match in each interval and this is done by applying area equation of each type of exchanger and initial values for heat transfer coefficients. Proper equations are as below:

For shell-and-tube heat exchanger:

$$A_{ij,k,ST} = \frac{q_{ij,k}}{\Delta T_{LM,k}.F_T}\left(\frac{1}{h_{ij,ST}} + \frac{d_o}{d_i}\frac{1}{h_{ji,ST}}\right) \quad (12)$$

And for plate-fin heat exchanger:

$$A_{C,ij,k,PF} = \frac{q_{ij,k}}{\Delta T_{LM,k}.F_T}\left(\frac{1}{\eta_c h_{c,ij,PF}} + \frac{\alpha_c}{\alpha_h}\frac{1}{\eta_h h_{h,ji,PF}}\right) \quad (13)$$

$$\frac{A_{C,ij,k,PF}}{A_{h,ji,k,PF}} = \frac{\alpha_c}{\alpha_h} \quad (14)$$

In equation (12), d_i and d_o are inner and outer diameter of tubes in shell-and-tube heat exchanger and in equation (13) α and η refer to compactness factor of fin that is used in plate-fin exchanger and fin efficiency respectively.

In each interval, total area for each type of exchanger is calculated separately. By applying this method to all intervals and summing the results of contact areas, the minimum required area of each exchanger type in the network is determined. Now by using these values for contact areas of each match, allowable pressure drop of streams and pressure drop relationships for each type of exchanger, gives new value for heat transfer coefficients of streams in each match. After adding fouling resistance of streams to heat transfer coefficients area algorithm is repeated until the results are converged [12].

For unit targeting we have used Jegede and Polly's (1992) method. In this method, unit targeting is done for above and below Pinch point, separately. The minimum number of units for maximum energy recovery, $N_{u,mer,L}$, for each type of exchanger, L, is given by:

Table 1. Process and stream data for case study

Stream	T_{in} (ºC)	T_{out} (ºC)	ρ (kg/m^3)	Cp (J/kgºC)	μ (cP)	k_f (W/mºC)	ΔP (kPa)	R_f (m^2/kWºC)	CP (kW/ºC)
H1	160	45	697	5480	0.31	0.11	60	0.14	300
H2	230	100	1.234	998.6	0.024	0.034	50	0.11	100
H3	175	80	0.684	1802.8	0.015	0.054	50	0.11	150
Hot Ut.	330	280	1000	6000	2	0.11	---	0.18	---
C1	85	220	464	2000	0.16	0.11	50	0.14	250
C2	160	240	570	1590	0.3	0.11	40	0.14	150
C3	90	150	1.881	657.2	0.022	0.031	40	0.11	100
C4	55	115	1.2	1000	0.027	0.04	20	0.11	60
Cold Ut.	10	30	1000	4187	1	0.61	---	0.18	---

Table 2. Economic data for case study

Hot Ut. Cost: 110$/kW.yr Cold Ut. Cost: 10$/kW.yr	Plant life time: 5 year Interest rate: 15%
Shell-and-Tube Area Cost: $30800+750A^{0.81}$ Plate-and-Fin Area Cost: $30000+1900A^{0.83}$	
Annualization Factor: $i(i+1)^N / \{(i+1)^N - 1\}$	

$$N_{u,mer,L} = (N_a - 1)\left(\frac{V_{La}}{V_a}\right) + (N_b - 1)\left(\frac{V_{Lb}}{V_b}\right) \quad (15)$$

Where the subscripts a and b denote the regions above and below the Pinch point, respectively. N is the number of hot and cold streams (including utilities), V_L is the number of spaghetti matches of exchanger type L and V is the total number of spaghetti matches.

Finally, the capital cost for an exchanger type L can be estimated with equation:

$$C_{CAP,L} = N_{u,mer,L}\left[a_L + b_L\left(A_L / N_{u,mer,L}\right)^{C_L}\right] \quad (16)$$

Where a_L, b_L and c_L are capital cost constants for the exchanger type L.

The target for total annualized capital cost is given by:

$$C_{CAP} = \sum_{L=1}^{N_{type}} (C_{CAP,L}).(K_{fL}) \quad (17)$$

Where N_{type} and K_{fL} are total number of exchanger type and annualization factor for exchanger type L, respectively.

5. Pre-optimization and Synthesis of HEN

By repeating the targeting procedure over a range of ΔT_{min} and finding the total annual cost (operating and capital cost), the optimum ΔT_{min} can be obtained ahead of design. For any selected ΔT_{min}, the total utility requirements (and hence cost) can be determined by proper method for the problem [14]. The capital cost target can be obtained as demonstrated in previous section. Finally, the total annual cost target can be calculated by:

$$TAC = (Q_{H\min}.C_H) + (Q_{C\min}.C_C) + C_{CAP} \quad (18)$$

The optimum value for ΔT_{min} is obtained where the TAC is minimized. Now by using pinch design rules, design of the network for selected ΔT_{min} can be accomplished.

6. Application of the New Procedure to an Example

The procedure has been applied to solve an example recently considered by Panjeshahi and Khoshgard (2006) [15]. Process and stream data, and economic data of problem are presented in table1and 2.

In this case study, our strategy is using *PFHE* for gas streams and *STHE* for liquid streams. Also, PFHE has a priority to *STHE* where we can apply both type of exchangers. Therefore, for *gas-gas* and *gas-liquid* matches we should use *PFHE* and for *liquid-liquid* matches we should use *STHE*. Table3 shows *Stream Classification Table* for this case.

Targeting results with new procedure are given in Table 4a and 4b. Targeting is done for 4 conditions: only STHE, only PFHE, using both exchangers (all condition with pressure drop consideration) and assumed h-values (conventional method with 500 and 200 W/m^2 ºC for liquid and gas streams, respectively)

Table 3. Stream classification table for case study

	Hot streams			
Cold Streams	H1	H2	H3	Hot Ut.
C1	STHE	PFHE	PFHE	STHE
C2	STHE	PFHE	PFHE	STHE
C3	PFHE	PFHE	PFHE	PFHE
C4	PFHE	PFHE	PFHE	PFHE
Cold Ut.	STHE	PFHE	PFHE	---

As indicated in Table 4b, for base case that we used PFHE and STHE, the optimum value for ΔT_{min} is 15 ºC and corresponding total annualized cost is 3,803,064 $/yr. Having the optimum value for ΔT_{min}, now we can do initial and detail design of problem. These steps are done for the problem and the results are presented in figures 2, 3 and Table 5.

During refinement and optimization of the initial design, two exchangers were eliminated and this caused that total area for network decreased and energy requirement of network increased. Now we can compare the results of final design with targeting. Table 6 shows the comparison between targeting and final design. It is obvious that the results of targeting with new method have the least difference with final design.

Table 4. Result of targeting for 4 conditions and comparison of them

Condition	$\Delta T_{\min,opt}$ (ºC)	Energy Cost ($/yr)	Area Cost ($/yr)	Number of Units	TAC ($/yr)	Differences (%)
Only STHE	7	2404846	697944	10	3102790	-18.4
Only PFHE	16	2746846	1502593	11	4249438	+11.8
STHE & PFHE (base case)	15	2704746	1098219	3+8	3803064	0.0
Assumed-h	24.3	3095255	1859991	11	4955246	30.3

Table 5. Energy and area targeting for 4 conditions

Condition	PFHE Area (m^2)	STHE Area (m^2)	Hot Ut. (kW)	Cold Ut. (kW)
Only STHE	0	10079.3	19507.7	25900.0
Only PFHE	7254.1	0	22707.7	29100.0
STHE & PFHE (base case)	4638.7	1393.7	22007.7	28400.0
Assumed-h	2716.6	9208.9	25261	31653

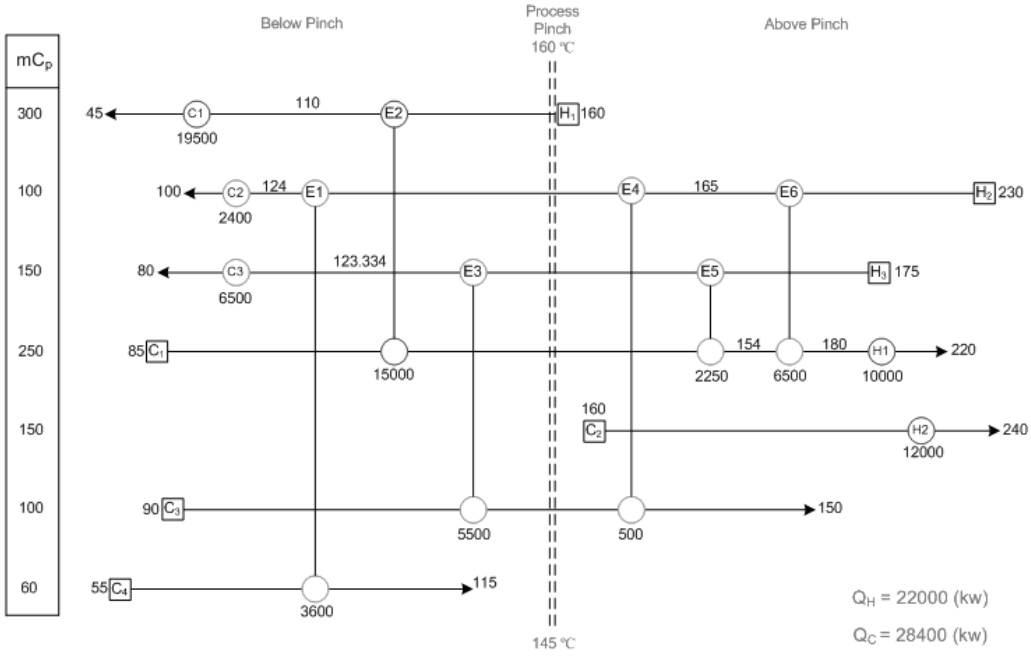

Fig. 3. Initial network design for base case condition (ΔT_{min}=15 °C)

Table 6. Result of network after detail design

	Value	Annualized Cost ($/yr)
PFHE Area	4186.1 m^2	778,132
STHE Area	1352.8 m^2	132,989
Hot Ut.	23750 KW	2,612,500
Cold Ut.	30150 KW	301,500
Total Annualized Cost ($/yr):		**3,825,121**

Table 7. Comparison of targeting with final design

Case	TAC ($/yr)	Differences (%)
Final Design	3825121	---
New Method	3803064	+0.58
Only STHE	3102789	-18.4
Only PFHE	4249438	+11.7
Assumed-h	4955246	+30.3

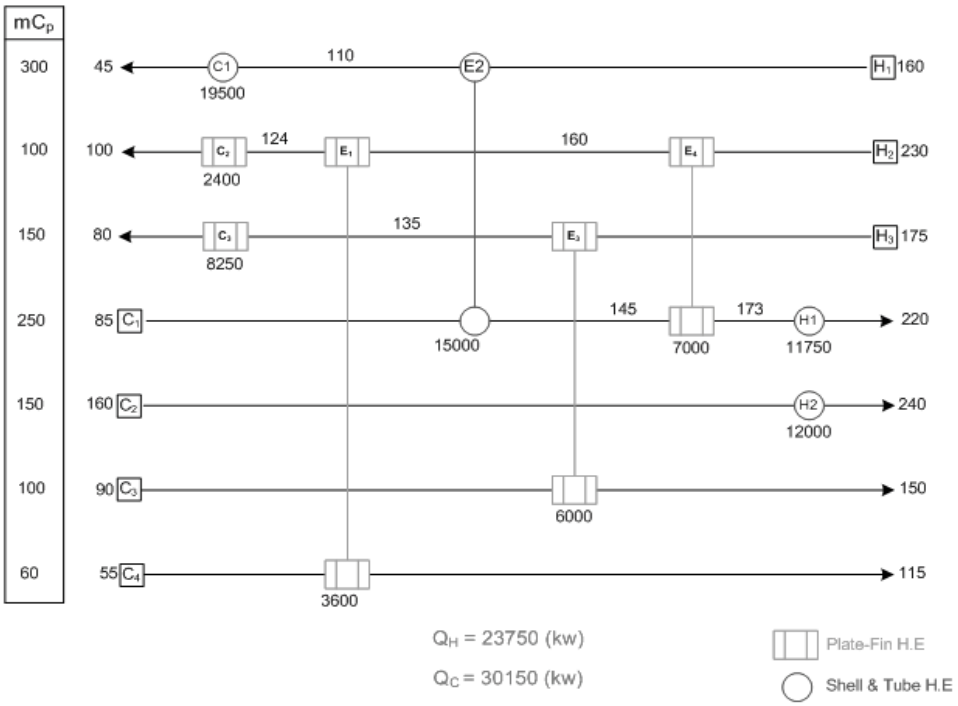

Fig. 4. Final network design

7. Conclusion

In this paper, a new method for targeting and design of heat exchanger networks for Grassroots design have been presented, by taking different exchanger types into account and also considering stream allowable pressure drops. By calculation of the real heat transfer coefficients, we could determine match-wise heat transfer coefficients in different exchangers and distribute the total area of the network amongst different units.

Application of the method to a case study, consisting of Shell-and-Tube and Plate-and-Fin heat exchangers, showed that the new method (both targeting and design procedures) enables the designer to find optimum and realistic solutions when dealing with mixed exchanger-type problems. Also, the comparisons between the results of the targeting and design stages seem to be in a good agreement, which in turn represents the accuracy of the procedures.

Nomenclature

A heat transfer area, m^2

a, b, constants of heat exchanger cost law

a coe cient in heat transfer vs. Re correlation

b exponent in heat transfer vs. Re correlation

C cold streams

C_C unit cost for cold utility, $/(kWyear)

C_{cap} annualized capital cost, $

C_H unit cost for cold utility, $/(kWyear)

Cp heat capacity (J/kg °C)

CP heat capacity-flowrate, W/°C

d_h hydraulic diameter, m

f friction factor

F_T correction factor of ΔT_{LM}

H Hot streams

h heat transfer coefficient, $W/(m^2°C)$

HEN Heat exchanger network

i interest rate, %

j Colburn factor ($StPr^{2/3}$)

K_{fl} annualization factor

K constant in pressure drop equation

l exchanger length, m

m exponent of heat transfer coefficient in pressure drop equation

m° mass flowrate, kg/s
Nu Nusselt number
Pr Prandtl number
PFHE plate-fin heat exchanger
ΔP pressure drop
ΔT temperature difference, °C
ΔT_{LM} Logarithmic mean temperature difference, °C
ΔT_{min} minimum approach difference, °C
q heat load, W
R_f thermal resistance due to fouling, $(m^2°C)/W$
Re Reynolds number
R_W wall thermal resistance, $(m^2°C)/W$
St Stanton number
STHE shell-and-tube heat exchanger
TAC total annualized cost
T temperature, °C
u velocity, m/s
Ut. Utility
V number of matches in spaghetti model
x coefficient in friction factor vs. Re correlation (Eq.(6))
y exponent in friction factor vs. Re correlation (Eq.(6))

Greek symbols

α total heat transfer area of one side of exchanger to total exchanger volume, m^2/m^3
λ fin thermal conductivity, W/(m°C)
μ viscosity, kg/(ms)
ρ Density (kg/m^3)
η fin temperature effectiveness
υ volumetric flowrate, m^3/s
k fluid thermal conductivity, W/(m°C)

Subscripts and superscripts

1 side 1 of exchanger
2 side 2 of exchanger
a, b above and below pinch respectively
C cold side of exchanger
h hot side of exchanger
i index of hot stream
j index of cold stream
k index of interval
L index of exchanger type
mer maximum energy recovery
min minimum value
opt optimum value
PF plate-fin
S shell side of shell-and-tube heat exchanger
ST shell-and-tube
t Tube side of shell-and-tube heat exchanger
W wall conditions

References

[1] Panjeshahi, M.H., Pressure Drop Consideration in Process Integration, Ph.D. Thesis, UMIST, Manchester, UK, 1992.

[2] Fallahi, H.R., Pressure Drop Optimization in Process Integration, Ph.D. Thesis, Tehran University, Tehran, Iran, 1999.

[3] Hall, S. G., Ahmad, S. and Smith, R., 1990, Capital Cost Target for Heat Exchanger Networks Comprising Mixed Materials of Construction, Pressure Ratings and Exchanger Types, Comput Chem Engng, 14(3), pp. 319-335.

[4] Jegede, F. and Polley G. T., 1992, Capital Cost Targets for Networks with Non-uniform Heat Exchanger Specifications, Copmut Chem Engng, 16(5), pp. 477-495.

[5] Serna-Gonzalez, M., Jimenez-Gutierrez, A. and Ponce-Ortega, J. M., 2007, Targets for Heat Exchanger Network Synthesis with Different Heat Transfer Coefficient and Non-Uniform Exchanger Specifications, Chemical Engineering Research and Design, 85(A10), pp. 1447-1457.

[6] Colberg, R.D. and Morari., 1990, Area and Capital Cost Targets for Heat Exchanger Network Synthesis with Constrained Matches and Unequal Heat Transfer Coefficients, Comput Chem Engng, 14(1), pp. 1-22.

[7] Polly, G.T. and Panjeshahi, M.H., 1991, Interfacing Heat Exchanger Network Synthesis and Detailed Heat Exchanger Design, Transactions of the Institution of Chemical Engineers, 69(A), pp. 445-457.

[8] Zhu, X.X. and Nie, X.R., 2002, Pressure Drop Considerations for Heat Exchanger Network

Grassroots Design, Comput Chem Engng, 26(12), pp. 1661-1676.

[9] Polley, G.T., Panjeshahi, M.H. and Picon Nunez, M., 1991, Rapid Design Algorithm for Shell-and-Tube and Compact Heat Exchangers, Transactions of the Institution of Chemical Engineers, 69(A), pp. 435-444.

[10] Hesselgreaves J.E., 2001, *Compact Heat Exchangers Design, Selection and Operation*, 1st ed., Elsevier Ltd., Oxford, Chap. 2.

[11] Picon-Nunez, M., Polley, G.T., Torres-Reyes, E. and Gallegos-Nunez, E., 1999, Surface Selection and Design of Plate-fin Heat Exchangers, Applied Thermal Engineering, 19(9), pp. 917-931.

[12] Dashtbani, J., Pressure Drop Consideration in Heat Exchanger Networks With Different Types of Heat Exchangers' M.Sc. Dissertation, Tehran University, Tehran, Iran, 2009.

[13] Smith, R., 2005, *Chemical Process Design and Integration*, 1st ed., John Wiley & Sons Ltd., New York.

[14] Kemp Ian. C., 2007, *Pinch Analysis and Process Integration*, 2nd ed., Elsevier Ltd., Chaps. 2,4,6.

[15] Panjeshahi, M.H. and Khoshgard, A., 2006, Heat Exchanger Networks Targeting and Design with Unequal Heat Transfer Coefficient Regarding Allowable Pressure Drop of Streams, Heat Transfer Eng. 27(9), pp. 36-43.

Acknowledgments:

The authors would like to express their gratitude for financial support from Iran Fuel Conservation Organization (IFCO) throughout this research work.

Using Technology in the Classroom for Multidisciplinary Instruction on Environmental Impacts and Sustainability of Energy Systems

Melissa C. Lott, David M. Wogan and Michael E. Webber

The University of Texas, Austin, USA

Abstract: This paper examines the use of technology in and out of the classroom to improve understanding of the complexities of sustainability topics for an audience comprised of students from many different fields of study and at many different levels (freshmen through Ph.D.). Four technologies were deployed in three multidisciplinary university course settings: large-format first year undergraduate lecture, small-format first year undergraduate seminar, and a large-format graduate student lecture. The technologies that were deployed include: 1) An original interactive website that teaches the environmental and economic tradeoffs of power choices, 2) Interactive radio-frequency remote clickers, 3) Blogging and online discussion in response to current events, and 4) Student development of original multi-media podcasts based on their individual research. We found that the interactive website and podcasts were particularly popular among the students. While the results gathered to date are far from conclusive about the pedagogical value of technology in and out of the classroom for instruction on sustainability, the preliminary conclusions are that the four forms of teaching technology that were examined in this manuscript offer more value than detriment, and can serve as useful complements to a traditional lecture.

Keywords: Multidisciplinary education, sustainability, energy systems, classroom technology

1. Introduction

Issues related to environmental impacts and sustainability of energy systems are inherently multidisciplinary, bringing together natural sciences, engineering, economics, culture and policy. However, most instruction in university settings in the United States for these topics is organized along traditional academic disciplines. Bringing together the different disciplines for coherent instruction remains a challenge for instructors. To overcome this educational challenge, four technologies were deployed in three multidisciplinary university course settings: large- format first year undergraduate lecture, small-format first year undergraduate seminar, and a large-format graduate student lecture. The technologies that were deployed include:

1. An original interactive website that teaches the environmental and economic tradeoffs of power choices
2. Interactive radio-frequency remote clickers
3. Blogging and online discussion in response to current events
4. Student development of original multi-media podcasts based on their individual research

To determine the pedagogical value of these approaches, a variety of methods were used to collect data about the student attitudes toward the use of technology. Firstly, course evaluations were used to obtain quantitative and qualitative assessments about the use of these technologies as teaching tools. Secondly, pre- and post-surveys of the students were used to gauge perspectives on the teaching value of the interactive websites, clickers, blogging and podcasts. Thirdly, web-based diagnostic tools were used to collect data on web traffic, click-throughs, and user duration while interacting with the websites.

This manuscript includes a description of how these four technologies were deployed, original first-cut analysis about the efficacy of these technologies based on data, feedback, and usage statistics gathered from students, and recommendations for incorporating these approaches into curriculum design for multidisciplinary instruction on environmental impacts and sustainability of energy systems.

Corresponding Author: Melissa C. Lott, Email: mclott@mail.utexas.edu

2. Courses

Three multidisciplinary courses were developed at the University of Texas at Austin to explore the topic of environmental impacts and sustainability of energy systems. The courses were multidisciplinary in student composition (people from many different disciplines enrolled) and content (topics including engineering, economics, policy, media, journalism and sociology were integrated into the lectures). That is, engineering concepts about energy were taught to non-engineers (to improve their understanding about the scientific fundamentals that underpin the energy system), while non-engineering concepts (policy, economics, culture, history) were taught to engineers so they would understand how to devote their problem-solving skills to society's largest energy and environmental challenges. In addition, these courses were taught for a variety of levels, from incoming Freshmen to Ph.D. students). The four aforementioned technologies were used in these three courses to help with the learning process.

2.1 First year undergraduate courses

Two courses were developed for first year undergraduate students, at least one of which has been taught each long academic semester for the past two years.

2.1.1 Large-format lecture

A large-format multidisciplinary course in lecture format was developed for first year undergraduate students, almost exclusively from non-STEM (Science, Technology, Engineering, and Mathematics) majors at the university. This course has consisted of approximately 85-100 students since its inaugural year in Spring 2009. The class subject matter includes energy, environment, and society. In this course, students explore how energy impacts our environment and how it fits into our societal structure. Topics include the history of energy, power generation, energy in the media, and transportation fuels among others. Weekly discussions in groups of 15-19 students are lead by graduate students in engineering who serve as teaching assistants.

2.2.2 Small-format seminar

A small-format course in seminar style, with an interactive, discussion-oriented format that includes project-oriented assignments was developed for first year undergraduate students, about evenly mixed from STEM and non-STEM fields. This course has consisted of approximately 15 students per semester since it was first taught in Fall 2007.

2.2 Graduate student course

A large-format graduate student course was first taught in the spring semester of 2008 and is now in its third year. This lecture course has an annual enrolment that has grown from 66 to 114 students. While senior-level undergraduates are eligible to enroll in this course it predominantly consists of graduate students. These students come from a wide mix of backgrounds, primarily majoring in engineering, public policy, business and geosciences.

3. Technologies Deployed

Four technologies were used in different combinations in- and out-of-class to enhance the educational objectives of the three courses described above.

3.1 Original teaching website

The Texas Interactive Power Simulator (TIPS) is an interactive online teaching and learning tool developed at the University of Texas at Austin for use by the general public and courses at the university. The website was available for use globally, without restriction, so that students could explore the website as a self-taught learning environment. [1-3] The TIPS website was used in conjunction with a custom-designed companion homework assignment for the first year undergraduate large-format lecture course.

The homework assignment required students to interact with the online tool to individually explore and learn the economic and environmental tradeoffs of different fuels and power generation technologies. This assignment and the website allowed students to virtually change the fuels used in Texas to supply electricity to homes and businesses. Afterwards, TIPS generates graphs, charts, and pictograms to quantitatively and qualitatively communicate the economic and environmental differences for today's nominal power generation and the new variations that the students selected. Students typically spent 20-30 minutes with the website to complete the homework assignment. [2, 4]

3.2 Radio-frequency remote clickers

Remote clickers are a technology that allows students to participate in class by anonymously answering questions provided by the instructor. [5] These questions can serve as a way of taking roll, quizzing students about reading assignments, and to gauge general reactions to different topics or ideas. The clicker remote control devices contain multiple buttons (different answer choices, A through E) and a radio transmitter that allow students to answer questions and transmit their selections to the instructor's computer.

Clickers were used primarily to foster interaction during class sessions. At different points throughout a lecture, a presentation slide is shown with a question and up to 5 possible answers. Students then select their answer on their clickers, which are then transmitted to the instructor's computer. The student's responses can be anonymously displayed to the class to show aggregate results, but individual responses are available to the instructor to assess individual performance.

3.3 Blogging current events

A course blog (short for "weblog") was created to provide students with an opportunity to share ideas about current events in energy- and policy-related topics of their choice. This blog provided an online forum for discussion of classroom topics to enhance the students' learning and critical thinking skills. [6] The blogging was available for worldwide viewing, but only class participants could post and comment. Wordpress and Google's Blogger platforms were chosen as vehicles for students to create blog posts (original entries, plus comments on others) and accommodate a large number of authors. Students were encouraged to create posts that analyzed current events and topics related to energy, technology and policy and also foster online discussions of these topics. Student blog posts have included original content and analyses in addition to images, videos, and text from the internet and other sources.

3.4 Multi-media podcasts

Podcasting is a technology that combines a digital media file (typically containing audio and/or video) with a syndicated distribution method (i.e., and RSS or syndicated feed) for publication to the internet. Podcast files can contain audio, images, videos, and internet links and can be played back in web browsers, on a personal computer, or on portable devices such as an Apple iPod or iPhone. [7, 8] Student-produced podcasts were individually created on topics of their choosing and were published to the iTunes Store for worldwide viewing and downloading. In 2008, the podcasts from this class were featured in the iTunes Store Educational Technology section. [9]

A video podcasting assignment was used in the graduate student lecture course as a tool for students to instruct others on an energy- and policy-related topic of their choice. The podcasting required the instructors to have significant familiarity and skill-level with computers; encoding and hosting a larger number of podcasts; and providing adequate feedback and attention to each student's podcast.

Table 1. Four technologies were used for three different classes, as noted below.

Technology \ Course	1st Year Undergraduate Seminar	1st Year Undergradaute Lecture	Graduate Lecture
Interactive website	X	X	
Classroom clickers			X
Blogging	X		X
Podcasts			X

4. Data

Data were collected regarding student response to each of the four technologies used in the three courses via quantitative and qualitative course evaluations, custom-designed pre- and post-surveys, and web-based diagnostic tools.

4.1 Original teaching website

The Texas Interactive Power Simulator (TIPS) was used in both of the first year undergraduate courses predominantly as a self-teaching aide for introducing the students to the Texas electricity system and to illustrate economic and environmental tradeoffs of different changes to that system. The students had little to no background in energy technology or energy policy at the onset of the course. They were given a companion homework assignment consisting of 7 questions the required information provided on the TIPS website. [2] The assignment was developed by the instructors and teaching assistants for the

course using questions that would guide the students through all sections of the website including embedded data sheets that contained extensive background information with citations for fuels and technologies. Seven questions were asked, from each of the following learning modules:

1. Electricity generation mix (3 questions)
2. Impacts and tradeoffs (3 questions)
3. Term definitions (1 question)

This distribution of questions forced the students to explore all aspects of the tool including the main interface, pop-up information bubbles and fuel-technology datasheets. The students were given one week to complete the assignment. After completing the homework assignment, they were given a survey about their impressions of the website. The survey was not targeted at evaluating the specific knowledge that the students gained while using the website, but instead was geared toward impressions and observations that the students developed during website use. The survey questions sought to reveal student perceptions about the website's objectivity, credibility, and educational usefulness.

4.2 Radio-frequency remote clickers

A survey was given at the end of the course to ascertain the usefulness of remote clickers for making the course material engaging.

4.3 Blogging about current events

Students in the graduate student lecture course and freshman seminar course were required to publish blog entries on a variety of technical and policy topics related to energy and the environment. In various iterations, students were required to publish two to three original blog posts and provide three to six comments to their peers' posts throughout the semester. The combination of posting and commenting allowed for discussion to develop for different topic areas between the students and instructors and became a vehicle for forcing students to read current events while developing their research and writing skills.

Pre- and post-blog surveys were administered in the graduate course to assess student's impressions of the strengths and shortcomings of blogging as a useful platform for expressing technical ideas.

4.4 Multi-media podcasts

Surveys were administered before and after students had been exposed to creating podcasts to gauge their familiarity with podcasts in an educational setting. Student responses provided insight into the usefulness of podcasts as a medium for instructing the general public on technical and topics. Responses also provided data regarding students' preferences on podcasting versus traditional writing assignments (i.e. term papers).

5. Analysis

The datasets constructed from survey responses were used to determine the pedagogical value of these technologies.

5.1 Original teaching website

The survey responses were analyzed to gain insight into the student response to the TIPS website and its approach to communicating lessons in the interdisciplinary field of the tradeoffs of power generation. The surveys were mostly quantitative (simple questions, with multiple choices), though with an opportunity for respondents to qualitatively elaborate on their answers.

5.1.1 Student response to TIPS

Seventy-six percent of students who used the Texas Interactive Power Simulator said that they liked using the tool and eighty-two percent expressed a desire to have more tools like it to use to understand energy concepts. Ninety-three percent of respondents believed that the Texas Interactive Power Simulator is a valuable learning tool for those interested in the tradeoffs of electricity generation.

Seventy-six percent of users liked using the Texas Interactive Power Simulator website. Of the twenty-four percent who did not enjoy using the site, frequent comments included a lack of enjoyment due to the website layout and lack of clarity of information presented. One anonymous respondent specifically commented that they "couldn't figure out how to use the chart… couldn't figure out how to use it." Of those who liked using the TIPS website, frequent comments included a surprise at how easily they grasped new concepts and gained knowledge on the current state of the Texas electricity generation landscape. Comments such as "I can't believe we use so much natural gas" and "the environmental effects

were easy to see… I had no idea nuclear used a lot of water" were included in responses to the survey.

5.1.2 Credibility

Because of the politically-charged environment that is the context in which sustainability is taught in the United States, it was determined that assessing the credibility of the website would be valuable. A distinct majority (95%) of the respondents believed the website to be credible.

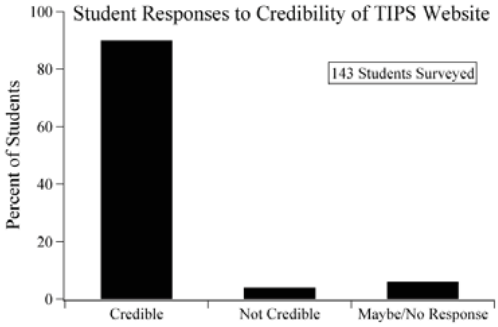

Fig. 1. Ninety percent of students surveyed responded "yes" to the question "Do you believe that the [TIPS] website is credible?"

Specific comments regarding website credibility included "I believe this website was credible because it included lots of citations and data" as well as "this website belongs to The University of Texas at Austin, so I believe it must be credible." Those who were uncertain as to the credibility of the website credited their uncertainty with the general technical structure of the tool itself as indicated by the comment "I couldn't use the tool easily and so couldn't decide if it was credible" and "the information was hard to find, so it might not be credible." In subsequent informal discussions with the students, it was apparent that having the University of Texas at Austin as the website creator produced a large effect on the perception of credibility of the site. Future studies using students at other institutions of higher learning can test a potential bias of those enrolled at the University of Texas.

Though not directly tested there was a strong indication from the students that a non-academic website creator (for example, an oil company) would have elicited more skepticism as to credibility. Future work might test student perspectives about the relative credibility of industrial versus academic websites in the context of teaching sustainability concepts.

5.1.3 Understanding gained

Ninety-three percent of those surveyed thought it was a useful tool for specifically teaching lessons on the economic and environmental tradeoffs of electricity generation methods in the state of Texas.

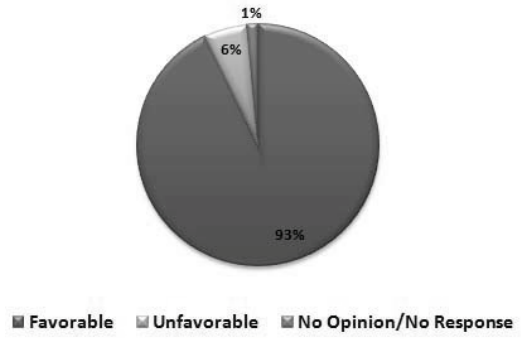

Fig. 2. Of the 143 students surveyed, ninety-three percent responded "yes" when asked if they believed that "TIPS was useful in illustrating the environmental and economic tradeoffs of electricity generation methods in Texas."

5.1.3 Desire for future learning

Of the students surveyed, eighty-two percent said that they would want more online learning tools like the Texas Interactive Power Simulator for topics related to energy and the environment. When asked what they learned while using the simulator via the website, the list was diverse. Many respondents expressed surprise at learning key facts such as the current amount of wind generation in the state of Texas, the fuel classifications (renewable vs. non-renewable) for the fuel types, and the variation in water use between different fuels.

5.2 Radio-frequency remote clickers

The remote clickers proved to be a helpful learning tool for fifty-four percent of the students surveyed, while forty-two percent of the remaining students were indifferent to their usage. Very few students, however, found the remote clickers to be distracting. The anonymous nature of the remote clickers allowed ninety-seven percent of the students to feel comfortable answering questions related to course material, their opinions on current events, and other questions that they might not be comfortable answering in front of their peers. When asked if they responded and participated in class more with the use of a clicker, fifty-two percent of the students responded that

they respond more frequently with a clicker while forty-six percent of the students responded the same amount as they would have without the clickers.

5.3 Blogging about current events

Sixty-nine percent of the students responded that the blog posting and commenting assignments enhanced their learning of the course material. Only thirteen percent found that the blogging requirements did not enhance their learning. When asked if blogs are a reasonable forum to discuss technical and/or complicated information, sixty-two percent responded they believed blogs are a reasonable forum. These responses suggest that overall, blogging, commenting, and engaging in an online discourse with their peers about technical and course-related issues was a useful experience and enhanced their learning.

5.4 Multi-media podcasts

In order to gauge feedback about the students' experiences with podcasts, the students in the graduate lecture course were first asked about their familiarity with podcasts. Before starting the podcast assignment, two-thirds of the students surveyed responded that they were familiar with podcasts, while eighteen percent of the students had never listened to a podcast. Only two percent of students had created a podcast prior to the assignment while approximately twenty-eight percent of the students surveyed had listened to podcasts that included course materials for a class.

5.4.2 Educational Benefit of using podcasts

In anticipation of creating the podcasts, the students overwhelmingly responded that they believed podcasts would be a convenient way to learn from their peers. Students anticipated podcasts as being convenient to view, enhancing support for their individual learning preferences, a new way to learn from their classmates, and an opportunity to link out-of-class material with what they learned in class. After creating the podcasts, however, approximately two-thirds of the students responded that they learned more from writing a traditional research paper than from creating the podcast. With that said, the responses were divided: when given a hypothetical choice to write a traditional research paper or create a podcast (in actuality, for this graduate course, students were required to write a paper and create a podcast), fifty-four percent of students said they would rather create a podcast, and forty-five percent said they wanted to write a report.

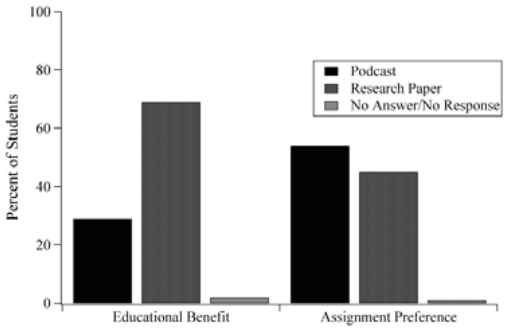

Fig. 3. Survey results indicated mixed feelings regarding the educational benefit of podcasting versus research papers and student preference of podcasting versus research papers.

This result might be explained by the different learning preferences of students. The graduate level course in which these podcasts were produced contained a mix of backgrounds and experiences. Both undergraduate and graduate students preferred writing a paper to creating a podcast by seventy-six to twenty-nine percent and seventy-four to twenty-six percent, for graduate and undergraduate students respectively. However, preferences were divided along education backgrounds. Engineering and Business students preferred writing a traditional report, while students from the Geological Sciences and Public Affairs were evenly divided between podcasts and papers. These results suggest that students in the more analytical fields of Business and Engineering prefer a more analytical approach to their learning while students in Public Affairs and the Geosciences are open to alternative approaches, such as creating podcasts.

5.4.3 Podcasting as a medium to convey technical information

Eighty-one percent of the students responded that podcasts are a reasonable medium to convey complicated and/or technical information. The number of students with this opinion increased from sixty-nine percent in the pre-survey (prior to creating the podcast). Possible explanations for the increase in the students' opinion are that the students became more familiar with the mechanics of researching and creating a podcast. Also, the students' attitudes could have changed viewing podcasts from their peers.

5.4 Four technologies comparison

As shown below in Figure 4, survey responses to each of the four technologies revealed that the TIPS website and podcasting technologies were the most popular amongst students. The least popular technology was the remote clicker, with a much more mixed response from students.

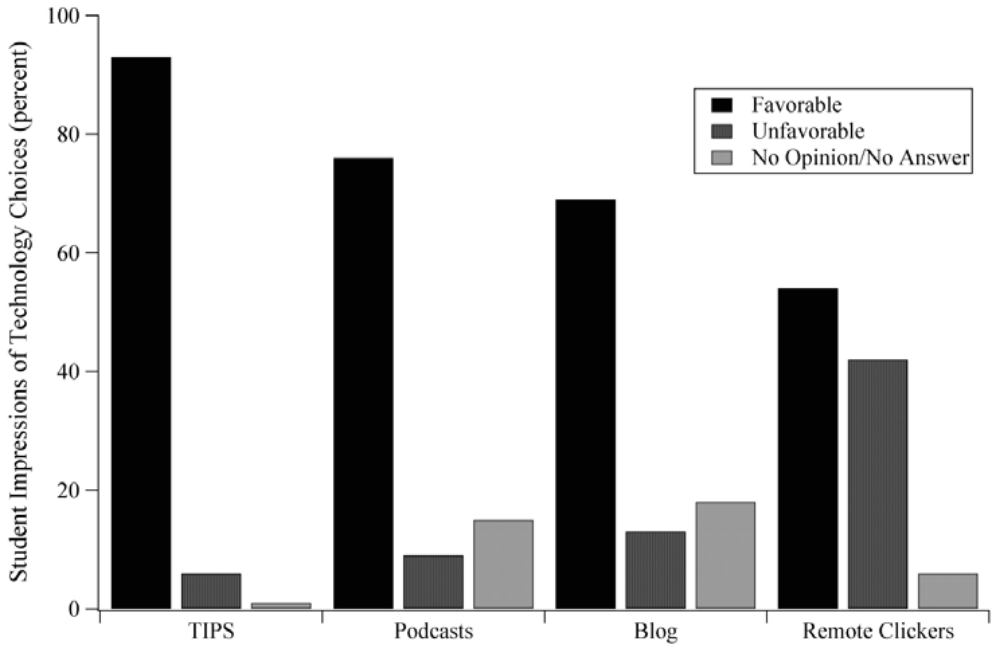

Fig. 4. Survey results showed that the TIPS website and podcasting technologies were the most popular among students taking the three multidisciplinary courses. The least popular technology used was the remote clickers.

5. Conclusion

The survey results, course evaluations, anecdotal feedback, and web-traffic data all point towards the mixed opportunity presented by the use of technologies for direct instruction on these multidisciplinary topics. They reveal the challenges in creating a comprehensive multidisciplinary curriculum on the environmental impacts and sustainability of energy systems. They also indicate that the use of these technologies is very promising, and help to convey complicated topics to a broader audience with mixed academic backgrounds.

While the process of refining a curriculum dedicated to teaching sustainability will be iterative and evolve over the years, it is clear that a variety of approaches can be deployed. At the University of Texas at Austin, a multidisciplinary learning environment was used in conjunction with the four different technologies to convey the complicated and interwoven subject matter related to energy and the environment. While the results gathered to date are far from conclusive about the pedagogical value of technology in and out of the classroom for instruction on sustainability, the preliminary conclusions are that the four forms of teaching technology that were examined in this manuscript offer more value than detriment, and can serve as useful complements to a traditional lecture. Data will continue to be gathered in subsequent semesters in order to firm up these conclusions.

References

[1] Lott, M., et. al., 2009, Analyzing Tradeoffs in Electricity Choices Using the Texas Interactive Power Simulator (TIPS). *Proc. 3rd Annual International Conference on Energy Sustainability*. San Francisco, CA. pp. ES2009-90135

[2] Lott, M., et. al. 2009, Using the Texas Interactive Power Simulator for Direct Instruction. *Proc. ASEE Annual Meeting*. Austin, TX. pp 2009-525.

[3] Lott, M.C. a. (2009). The Texas Interactive Power Simulator – an Analytical Tool for Direct Instruction & Informing Public Policy Decisions. *2009 ASEE Gulf Southwest Conferece.* Baylor Univeristy, Waco: ASEE.

[4] Google Analytics. http://www.google.com/analytics

[5] Gallaga, Omar. Four innovations changing the way kids learn: Some subtle technologies used in central Texas schools help teachers, students and parents better connect. *Austin American-Statesman*. Sept. 19, 2009. Retrieved from http://www.statesman.com/life/content/life/stories/other/2009/09/19/0919techclassroom.html

[6] Richardson, Will. New Jersey High School Learns the ABCs of Blogging. *THE Journal: Transforming Education through Technology*. June 2005, Vol. 32 Issue 11, p 40.

[7] Campbell, G. There's Something in the Air: Podcasting in Education. 2005. Educause Review, 40(6). pg.32.

[8] Dew, Kristin. Why Academia Digs iTunes. *BusinessWeek*. June 5, 2006, Issue 2987, p14.

[9] Apple Corporation. Education: Mobile Learning and iTunes U. http://www.apple.com/education/mobile-learning/

Acknowledgments: The authors would like to thank the co-instructors for the first year courses discussed in this course, Dr. Philip Schmidt, Dr. David Allen, and Dr. Thomas Edgar. They would also like to acknowledge Dr. Carey King and the Faculty Innovation Center at the University of Texas at Austin for their work on the TIPS website.

AUTHOR'S INDEX

KEYWORD'S INDEX

ecos 2010

SPONSORS

ÉCOLE POLYTECHNIQUE FÉDÉRALE DE LAUSANNE

Schweizerische Eidgenossenschaft
Confédération suisse
Confederazione Svizzera
Confederaziun svizra

Office fédéral de l'énergie OFEN

INSTITUTIONAL PARTNERS

Lausanne

canton de vaud
LIBERTÉ ET PATRIE

TECHNICAL PARTNERS

ALPIQ

ecleer

HOLDI GAZ

BG
Ingénieurs Conseils
Ingenieure & Berater
Consulting Engineers

SUPPORTING ORGANIZATION

ASME
SETTING THE STANDARD

International centre for applied thermodynamics
ICAT
1997